antioxidants

Special Issue Reprint

Oxidative Stress in Aquatic Organisms

Edited by
Bo Liu, Changyou Song and Cunxin Sun

www.mdpi.com/journal/antioxidants

MDPI

Oxidative Stress in Aquatic Organisms

Oxidative Stress in Aquatic Organisms

Editors

Bo Liu
Changyou Song
Cunxin Sun

MDPI • Basel • Beijing • Wuhan • Barcelona • Belgrade • Manchester • Tokyo • Cluj • Tianjin

Editors

Bo Liu
Chinese Academy of Fishery Sciences
Wuxi, China

Changyou Song
Chinese Academy of Fishery Sciences
Wuxi, China

Cunxin Sun
Chinese Academy of Fishery Sciences
Wuxi, China

Editorial Office
MDPI
St. Alban-Anlage 66
4052 Basel, Switzerland

This is a reprint of articles from the Special Issue published online in the open access journal *Antioxidants* (ISSN 2076-3921) (available at: https://www.mdpi.com/journal/antioxidants/special_issues/Oxidative_Stress_Aquatic_Organisms).

For citation purposes, cite each article independently as indicated on the article page online and as indicated below:

LastName, A.A.; LastName, B.B.; LastName, C.C. Article Title. *Journal Name* **Year**, *Volume Number*, Page Range.

ISBN 978-3-0365-8186-6 (Hbk)
ISBN 978-3-0365-8187-3 (PDF)

Cover image courtesy of Changyou Song

Contents

About the Editors

Bo Liu

Bo Liu, Ph.D., professor, doctoral supervisor, is a senior scientist in the field of aquaculture nutrition of China and Jiangsu Province Agriculture Research System; Chief Scientist of Conventional Freshwater Aquatic Animal Nutrition and Feed Innovation Team, CAFS; and Director of the Aquatic Diseases and Feed Research Department, FFRC. He is also a member of the Aquaculture Technology Discipline Committee of CAFS and a member of the Aquatic Animal Nutrition and Feed Professional Committee of the Chinese Fisheries Society. His current research interests include aquaculture nutrition and epigenetic regulation; stress-related signaling pathways and the development of functional feed for aquatic animals; and research on new Chinese herbal medicines and microbial preparations. To this point, he has presided more than 13 scientific projects, including International Foundation of Science (IFS), Natural Science Foundation of China, sub-project of National Key R&D Program of China, Jiangsu Province Natural Science Foundation, and Jiangsu Province Sanxin Engineering Projects. He has published more than 100 papers as the first or corresponding author, won 9 provincial and ministerial prizes of China, and been authorized for 14 national invention patents.

Changyou Song

Changyou Song earned his Ph.D. in aquaculture nutrition at Nanjing Agricultural University in 2019, and have worked as a joint-training Ph.D., majoring in muscle regeneration in Purdue University during 2017–2019. Currently, Changyou Song is an associate research fellow working in the Freshwater Fisheries Research Center, Chinese Academy of Fishery Sciences. Changyou's research interest is to improve the nutrient and flavor value of editable parts of aquatic animals, especially by means of nutritional regulatory approach and various external factors control of the living surroundings. Specifically, overall metabolism, lipid development, as well as muscle regeneration are the main research focus. Changyou has participated in over 20 scientific projects, trained 9 master or Ph.D. students, and has published more than 60 scientific papers, including 18 papers as the first or corresponding author.

Cunxin Sun

Cunxin Sun, Ph.D., master's supervisor, and associate research fellow, is a member of the senior personnel of Chinese Academy of Fishery Sciences. He is mainly engaged in research on the nutritional requirements and metabolism of freshwater prawns and crabs, development of microecological preparations, and quality regulation of aquatic animal. He has presided over Natural Science Foundation of China and Jiangsu Province, Postdoctoral Foundation of China, and Agricultural Independent Innovation Fund of Jiangsu Province. He has co-authored more than 60 papers, won 2 provincial and ministerial prizes of China, and been authorized for 7 national patents.

antioxidants

MDPI

Editorial

Oxidative Stress in Aquatic Organisms

Changyou Song [1,2], Cunxin Sun [1,2], Bo Liu [1,2,*] and Pao Xu [1,2,*]

[1] Key Laboratory of Freshwater Fisheries and Germplasm Resources Utilization, Ministry of Agricultural and Rural Affairs, Freshwater Fisheries Research Center, Chinese Academy of Fishery Sciences, Wuxi 214081, China; songchangyou@ffrc.cn (C.S.); suncx@ffrc.cn (C.S.)
[2] Wuxi Fisheries College, Nanjing Agricultural University, Wuxi 214081, China
* Correspondence: liub@ffrc.cn (B.L.); xup@ffrc.cn (P.X.)

Oxidative stress mainly refers to the imbalance between reactive oxygen species production and antioxidant defense systems in organisms [1]. Excessive oxidative stress can induce cell and tissue damage, mainly manifested as DNA hydroxylation, protein denaturation, lipid peroxidation and cell apoptosis [2]. In the past few decades, aquaculture has developed rapidly and has become the fastest growing food production sector for humans. Oxidative stress is ubiquitous in aquatic animals. In general, endogenous and exogenous factors are the main elements that induce oxidative stress, including temperature, oxygen, life history, nutrition, food deprivation, and industrial and agricultural pollutants [3]. In accordance with other animals, aquatic organisms have evolved complex mechanisms to resist oxidative stress. Therefore, uncovering the causes of oxidative stress, elucidating the underlying physiological mechanisms and developing antioxidant strategies are of great importance for the development of aquaculture.

In this Special Issue, 28 original scientific research papers are published, all of which highlight the most recent advances in all aspects of oxidative stress response in aquatic animals, including the generation process, the response mechanism and the resistant approaches. Papers in this Special Issue provide an updated overview of the advances in oxidative stress research, with advanced molecular approaches in both living organisms and habitats of aquatic animals.

Taxonomically, these papers cover freshwater fish (*Carassius auratus* [4], *Monopterus albus* [5], *Ictalurus punctatus* [6], *Megalobrama amblycephala* [7], *Micropterus salmoides* [8], *Lateolabrax maculatus* [9–12], *Carassius gibelio* [13,14], *Aplodinotus grunniens* [15], *Pangasianodon hypophthalmus* [16], *Danio rerio* [17], and hybrid grouper [18]), marine fish (*Scophthalus maximus* [19]), crustaceans (*Macrobrachium rosenbergii* [20–22], *Litopenaeus vannamei* [23–25], *Penaeus monodon* [26], *Scylla paramamosain* [27], and *Eriocheir sinensis* [28]), and molluscs (*Crassostrea hongkongensis* [29], *Trachinotus ovatus* [30], and *Pacific abalone* [31]). Meanwhile, these papers reveal several endogenous and exogenous factors that induce oxidative stress, such as environmental factors (water hardness [4], chronic hyperthermia [6], acute hypoxic stress [10], acute ammonia nitrogen [12], hypothermia [15], low salinity [23], and ammonia-N-stress [26]), nutritional factors (high carbohydrate levels [5], oxidized lipids [7], high-fat diet [12,20], and lipopolysaccharide [29,31]), essential or heavy metals (Zn [4], cadmium [13,27], Cu^{2+} [28], and polyinosinic–polycytidylic acid sodium salt [31]), pathogenic bacteria or virus (aflatoxin B1 and cyprinid herpesvirus 2 [14], water bubble disease (WBD) [21], *Vibrio harveyi* [29,31], and *Streptococcus agalactiae* [30]), and feeding practices (stocking density [8], transport stress [11]). Therapeutically, some papers have also explored some medicines or immunostimulants to resist oxidative stress, such as herbal medicine (mulberry leaf flavonoids [5], emodin [7], berberine [17], *Sophora flavescens* root extract [19], and tea tree oil [22]), nutritional stimulants (*Atractylodes macrocephala* polysaccharide [9], taurine alleviates [13], histamine [16,18], vitamin E [20], β-Glucan [23], krill oil [24], and zinc [25]), antibiotics (florfenicol and ofloxacin [21]), and feeding administration (feed restriction [6]). Additionally, the full length of antioxidant genes was also

Citation: Song, C.; Sun, C.; Liu, B.; Xu, P. Oxidative Stress in Aquatic Organisms. *Antioxidants* **2023**, *12*, 1223. https://doi.org/10.3390/antiox12061223

Received: 29 May 2023
Accepted: 31 May 2023
Published: 6 June 2023

cloned to analyze their functional responses to oxidative stress, such as glutaredoxin [26] and catalase [31].

To uncover the relationship between oxidative stress inducers and response mechanisms, tissue or cell morphology, antioxidant and immunity enzymes and related gene expression, metabolic homeostasis, and cell fate related autophagy and apoptosis, as well as mortality, have been extensively studied in these papers. Mechanically, some key molecular signaling processes were studied, such as Nrf2 signaling [7,9,22,27], Notch signaling [7], PPAR signaling [8], MAPK signaling [10], NF-κB signaling [15,20,30], Relish-Imd signaling [22], TLR2-MyD88-NF-κB [28], and epigenetic regulator m6A methylation [17]. Additionally, the regulation of gut microbiota on oxidative stress resistance was also investigated in some papers [5,10,11,14,24,25]. A brief summary of each paper is shown below for reference.

Specifically, in freshwater fish, Choi et al. [4] investigated the toxicity stress of Zn and water hardness in *C. auratus*. They found that high water hardness can influence the absorption of Zn, and alleviating the hardness levels can reduce the toxicity stress caused by Zn. Shi et al. [5] found that 300 mg/kg mulberry leaf flavonoids (MLF) can alleviate the negative effects of high-carbohydrate-induced low growth performance, glucose metabolism disorder, liver oxidative damage and intestinal microbiota disturbance in *M. albu*, and that the relief of MLF is dose-related. Lu et al. [6] investigated the effects and mechanisms of feed restrictions on improving chronic, heat-induced (27 to 31 °C) liver peroxidation and damages in channel catfish (*I. punctatus*). They concluded that 2.5% body weight/day is recommended to improve antioxidant capacity and liver health during the summer season. Song et al. [7] studied the therapeutic mechanism of emodin on metabolic and oxidative disorders induced by dietary oxidized fish oil in *M. amblycephala* liver. Their results indicate that oxidative stress blocked the crosstalk between Notch and Nrf2 signaling, while emodin rescued Notch-Nrf2 interaction to ameliorate oxidative stress. The crosstalk between Notch and Nrf2 signaling might be the potential therapeutic target for emodin to ameliorate oxidative stress and metabolic disorder in the liver. Jia et al. [8] focused on the effects of stocking density on fish health in integrated rice–fish farming systems. They indicate that a high density (HD, 120 g/m^3) inhibited growth and caused physiological responses, oxidative stress, and abnormal hepatic lipid metabolism in *M. salmoides*. Dong et al. [9] revealed that 400–4000 mg/kg *Atractylodes macrocephala* polysaccharide (AMP) could improve growth performance and antioxidant activity, as well as nutrient absorption in largemouth bass. Specifically, Nrf2 signaling was involved in the regulation. Song et al. [10] showed that hypoxia caused oxidative stress, exfoliation of the intestinal villus epithelium, and villus rupture, and increased cell apoptosis in largemouth bass (*M. salmoides*). Mechanically, MAPK signaling pathway and inflammatory related microbiota played an important role under hypoxic stress. Wang et al. [11] indicated that transport stress resulted in oxidative stress, and altered innate immune responses and affected the gut microbial compositions, mainly among proteobacteria, firmicutes, cyanobacteria and spirochaetes in juvenile largemouth bass. Dong et al. [12] revealed that the potent endoplasmic reticulum stress (ERs) inhibitor 4-PBA could decrease the peroxidation content and attenuated ERs induced by high-fat diet (HFD) and acute ammonia nitrogen. Xu et al. [13] revealed that taurine (1%) alleviates cadmium-induced endoplasmic reticulum stress via autophagy and apoptosis in gibel carp (*C. gibelio*), demonstrating the potential use of taurine in the mitigation of heavy metal toxicity in aquatic organisms. Xue et al. [14] investigated the defensive ability of gibel carp exposed to aflatoxin B1 (AFB1) by challenging it with cyprinid herpesvirus 2 (CyHV-2) infection. Their results indicate that AFB1 may increase the susceptibility of *C. gibelio* to CyHV-2 infection, and thus amplify the viral outbreak to endanger ecological safety in an aquatic environment. Chen et al. [15] revealed that acute hypothermia (10 °C for 8 d) induced oxidative stress, immunosuppression, mitochondrial enlargement, nucleoli aggregation, lipid droplet accumulation, metabolism, programmed cell death, and disease. Interactively, apoptosis and inflammation in immune organs were correlated with antioxidation and immunity suppression induced by hypothermia exposure. Liu et al. [16]

indicated that high dietary histamine (480 mg/kg) decreases intestinal immunity and antioxidant capacity, inducing digestive tract oxidative damage and ultimately decreasing the growth of striped catfish (*P. hypophthalmus*). Zhang et al. [17] revealed that Berberine (BBR) ameliorates cellular oxidative stress, apoptosis and autophagy induced by lipid metabolism disorder by mediating Camk1db m6A methylation through the targeting of the Camk1db/ERK pathway in zebrafish-hepatocyte. Zhang et al. [18] revealed that high levels of histamine (≥404.12 mg/kg) were detrimental to the digestive physiology function and muscle quality of hybrid grouper (*Epinephelus fuscoguttatus* ♀× *Epinephelus lanceolatus* ♂), although it did compromise its growth performance.

Accordingly, in marine fish, Hou et al. [19] indicated that 0.1–0.2% *Sophora flavescens* root extract (SFE) improved the growth performance, antioxidant activity and disease resistance against *Edwardsiella tarda* in *S. maximus*.

Moreover, in crustaceans, Sun et al. [20] found that 600 mg/kg dietary vitamin E alleviated hepatopancreas oxidative stress and apoptosis induced by high fat diet (13% dietary lipid in the diet) in *M. rosenbergii*, and that the NF-κB/NO signaling pathway was the antioxidant target for oxidative stress. Zhao et al. [21] demonstrated how antibiotic florfenicol and ofloxacin prevent *Citrobacter freundii*-induced water bubble disease (WBD) in giant freshwater prawns, *M. rosenbergii*, evidenced by improved antioxidant capacity, immune-related gene expression, and the anti-lipopolysaccharide factor in hepatopancreas. Liu et al. [22] reported that 100 mg/kg tea tree oil (TTO) could alter the hepatopancreatic lipid metabolism by affecting the antioxidant–autophagy axis in *M. rosenbergii*. The relish-Imd pathway functions significantly in the regulation. Qiao et al. [23] suggested that dietary β-glucan (0.1–0.2%) markedly increased growth performance and alleviated the negative effects of low-salinity stress by contributing to the activity of biochemical enzymes and enriching carbohydrate metabolism. Liang et al. [24] indicated that Krill oil is a suitable dietary phospholipid source to improve antioxidant capacity and innate immunity and establish the intestinal immune barrier by increasing the richness of Fusibacter, promoting the growth of Pacific white shrimp *L. vannamei*. Yang et al. [25] revealed that organic zinc had a higher bioavailability to improve zinc homeostasis, antioxidant capacity, immune response, glycolysis and intestinal microbiota, and was therefore a more beneficial zinc resource than inorganic zinc in white shrimp (*L. vannamei* Boone, 1931). Fan et al. [26] identified a novel glutaredoxin (PmGrx2) in *P. monodon*. They cloned the full length and indicated that PmGrx2 is involved in redox regulation and plays an important role in resistance to ammonia-N-stress. Cheng et al. [27] revealed that cadmium exposure increased H_2O_2 production, lipid peroxidation and tissue damage in mud crabs, but decreased the activity of SOD and catalase CAT, and caused lipid peroxidation and tissue damage. With Nrf2 knockdown, antioxidant capacity was decreased, leading to aggravated hepatotoxicity and cell injury. Feng et al. [28] revealed that Cu^{2+} exposure decreased antioxidative capacity and immunity, promoted lipid peroxidation and induced apoptosis, autophagy and ER stress in Chinese mitten crab (*E. sinensis*); the toxicity may be implicated following the activation of the ERK, AMPK, and TLR2-MyD88-NF-κB pathways.

Additionally, in molluscs, Ma et al. [29] suggested that post-spawning-phase male Hong Kong oysters *C. hongkongensis* have a more significant energy metabolic response and a greater ability to cope with oxidative stress under *Vibrio harveyi* and lipopolysaccharide (LPS) infection than female oysters, which provides prospects for oyster farming or oyster disease in natural seas. Gao et al. [30] investigated the effects of Streptococcus agalactiae infection on the immune and antioxidant regulatory mechanisms of golden pompano (*T. ovatus*). Results showed that *S. agalactiae* could activate TNF-α/NF-κB signaling in the liver to induce defense and immune responses. Hossen et al. [31] cloned the full length of catalase (Hdh-CAT) and found Hdh-CAT was induced by thermal stress, H_2O_2 induction, starvation, cadmium and immune challenges with Vibrio, lipopolysaccharides and polyinosinic–polycytidylic acid sodium salt in *P. abalone*.

We would like to acknowledge the authors that have contributed to this Special Issue "Oxidative Stress in Aquatic Organisms". These papers offer fresh perspectives on

expanding knowledge and research possibilities in the creation of antioxidant resistance in aquaculture.

Funding: This paper was funded by the National Natural Science Foundation of China (32172990, 32002404); the Central Public-interest Scientific Institution Basal Research Fund, CAFS (2021XT0702, 2020TD59, 2022XT0401); the Central Public-interest Scientific Institution Basal Research Fund, Freshwater Fisheries Research Center, CAFS (2023JBFM11); the China Agriculture Research System of MOF and MARA (CARS-48); the Jiangsu Agriculture Industry Technology System (JATS[2022]514); and the Jiangsu Agricultural Science and Technology Independent Innovation Fund (CX(22)3077).

Conflicts of Interest: The authors declare no conflict of interest.

References

1. Song, C.Y.; Liu, B.; Ge, X.; Li, H.; Liu, B.; Xu, P. miR-34a/Notch1b mediated autophagy and apoptosis contributes to oxidative stress amelioration by emodin in the intestine of teleost *Megalobrama amblycephala*. *Aquaculture* **2022**, *547*, 737441. [CrossRef]
2. Hoseinifar, S.H.; Yousefi, S.; Van Doan, H.; Ashouri, G.; Gioacchini, G.; Maradonna, F.; Carnevali, O. Oxidative Stress and Antioxidant Defense in Fish: The Implications of Probiotic, Prebiotic, and Synbiotics. *Rev. Fish. Sci. Aquac.* **2020**, *29*, 198–217. [CrossRef]
3. Ahmed, I.; Reshi, Q.M.; Fazio, F. The influence of the endogenous and exogenous factors on hematological parameters in different fish species: A review. *Aquac. Int.* **2020**, *28*, 869–899. [CrossRef]
4. Choi, C.Y.; Li, Z.; Song, J.A.; Park, Y.-S. Water Hardness Can Reduce the Accumulation and Oxidative Stress of Zinc in Goldfish, *Carassius auratus*. *Antioxidants* **2022**, *11*, 715. [CrossRef]
5. Shi, Y.; Zhong, L.; Fan, Y.; Zhang, J.; Zhong, H.; Liu, X.; Shao, C.; Hu, Y. The Protective Effect of Mulberry Leaf Flavonoids on High-Carbohydrate-Induced Liver Oxidative Stress, Inflammatory Response and Intestinal Microbiota Disturbance in *Monopterus albus*. *Antioxidants* **2022**, *11*, 976. [CrossRef] [PubMed]
6. Lu, Q.; Gong, Y.; Xi, L.; Liu, Y.; Xu, W.; Liu, H.; Jin, J.; Zhang, Z.; Yang, Y.; Zhu, X.; et al. Feed Restriction Alleviates Chronic Thermal Stress-Induced Liver Oxidation and Damages via Reducing Lipid Accumulation in Channel Catfish (*Ictalurus punctatus*). *Antioxidants* **2022**, *11*, 980. [CrossRef]
7. Song, C.; Liu, B.; Li, H.; Tang, Y.; Ge, X.; Liu, B.; Xu, P. Protective Effects of Emodin on Oxidized Fish Oil-Induced Metabolic Disorder and Oxidative Stress through Notch-Nrf2 Crosstalk in the Liver of Teleost *Megalobrama amblycephala*. *Antioxidants* **2022**, *11*, 1179. [CrossRef]
8. Jia, R.; Wang, L.; Hou, Y.; Feng, W.; Li, B.; Zhu, J. Effects of Stocking Density on the Growth Performance, Physiological Parameters, Redox Status and Lipid Metabolism of *Micropterus salmoides* in Integrated Rice & Fish Farming Systems. *Antioxidants* **2022**, *11*, 1215.
9. Dong, B.; Wu, L.; Chen, Q.; Xu, W.; Li, D.; Han, D.; Zhu, X.; Liu, H.; Yang, Y.; Xie, S.; et al. Tolerance Assessment of Atractylodes macrocephala Polysaccharide in the Diet of Largemouth Bass (*Micropterus salmoides*). *Antioxidants* **2022**, *11*, 1581. [CrossRef]
10. Song, Z.; Ye, W.; Tao, Y.; Zheng, T.; Qiang, J.; Li, Y.; Liu, W.; Xu, P. Transcriptome and 16S rRNA Analyses Reveal That Hypoxic Stress Affects the Antioxidant Capacity of Largemouth Bass (*Micropterus salmoides*), Resulting in Intestinal Tissue Damage and Structural Changes in Microflora. *Antioxidants* **2023**, *12*, 1. [CrossRef]
11. Wang, Q.; Ye, W.; Tao, Y.; Li, Y.; Lu, S.; Xu, P.; Qiang, J. Transport Stress Induces Oxidative Stress and Immune Response in Juvenile Largemouth Bass (*Micropterus salmoides*): Analysis of Oxidative and Immunological Parameters and the Gut Microbiome. *Antioxidants* **2023**, *12*, 157. [CrossRef] [PubMed]
12. Dong, Y.; Li, L.; Xia, T.; Wang, L.; Xiao, L.; Ding, N.; Wu, Y.; Lu, K. Oxidative Stress Can Be Attenuated by 4-PBA Caused by High-Fat or Ammonia Nitrogen in Cultured Spotted Seabass: The Mechanism Is Related to Endoplasmic Reticulum Stress. *Antioxidants* **2022**, *11*, 1276. [CrossRef] [PubMed]
13. Xu, W.; Li, H.; Wu, L.; Jin, J.; Han, D.; Zhu, X.; Yang, Y.; Liu, H.; Xie, S. Taurine Alleviates Cadmium-Induced Toxicity via Genetically Specific Strategies in Two Strains of Gibel Carp (*Carassius gibelio*). *Antioxidants* **2022**, *11*, 1381. [CrossRef]
14. Xue, M.; Fu, M.; Zhang, M.; Xu, C.; Meng, Y.; Jiang, N.; Li, Y.; Liu, W.; Fan, Y.; Zhou, Y. Aflatoxin B1 Induced Oxidative Stress and Gut Microbiota Disorder to Increase the Infection of Cyprinid Herpesvirus 2 in Gibel Carp (*Carassius auratus* gibelio). *Antioxidants* **2023**, *12*, 306. [CrossRef]
15. Chen, J.; Li, H.; Xu, P.; Tang, Y.; Su, S.; Liu, G.; Wu, N.; Xue, M.; Yu, F.; Feng, W.; et al. Hypothermia-Mediated Apoptosis and Inflammation Contribute to Antioxidant and Immune Adaption in Freshwater Drum, *Aplodinotus grunniens*. *Antioxidants* **2022**, *11*, 1657. [CrossRef] [PubMed]
16. Liu, Y.; Fu, X.; Huang, H.; Fan, J.; Zhou, H.; Deng, J.; Tan, B. High Dietary Histamine Induces Digestive Tract Oxidative Damage in Juvenile Striped Catfish (*Pangasianodon hypophthalmus*). *Antioxidants* **2022**, *11*, 2276. [CrossRef]
17. Zhang, M.; Liu, J.; Yu, C.; Tang, S.; Jiang, G.; Zhang, J.; Zhang, H.; Xu, J.; Xu, W. Berberine Regulation of Cellular Oxidative Stress, Apoptosis and Autophagy by Modulation of m6A mRNA Methylation through Targeting the Camk1db/ERK Pathway in Zebrafish-Hepatocytes. *Antioxidants* **2022**, *11*, 2370. [CrossRef]

18. Zhang, Y.; Zhou, H.; Liu, Y.; Zhu, L.; Fan, J.; Huang, H.; Jiang, W.; Deng, J.; Tan, B. Dietary Histamine Impairs the Digestive Physiology Function and Muscle Quality of Hybrid Grouper (*Epinephelus fuscoguttatus*♂ × *Epinephelus lanceolatus*♀). *Antioxidants* **2023**, *12*, 502. [CrossRef]
19. Hou, Y.; Gao, X.; Shi, X.; Dong, N.; Yue, T.; Zhang, P.; Liu, H. Dietary Supplementation of *Sophora flavescens* Root Extract Improved the Growth Performance, Antioxidant Capacity, Innate Immunity, and Disease Resistance against Edwardsiella tarda Challenge in Turbot (*Scophthalmus maximus*). *Antioxidants* **2023**, *12*, 69. [CrossRef]
20. Sun, C.; Shan, F.; Liu, M.; Liu, B.; Zhou, Q.; Zheng, X.; Xu, X. High-Fat-Diet-Induced Oxidative Stress in Giant Freshwater Prawn (*Macrobrachium rosenbergii*) via NF-κB/NO Signal Pathway and the Amelioration of Vitamin E. *Antioxidants* **2022**, *11*, 228. [CrossRef]
21. Zhao, C.; Wen, H.; Huang, S.; Weng, S.; He, J. A Novel Disease (Water Bubble Disease) of the Giant Freshwater Prawn *Macrobrachium rosenbergii* Caused by *Citrobacter freundii*: Antibiotic Treatment and Effects on the Antioxidant Enzyme Activity and Immune Responses. *Antioxidants* **2022**, *11*, 1491. [CrossRef] [PubMed]
22. Liu, M.; Zheng, X.; Sun, C.; Zhou, Q.; Liu, B.; Xu, P. Tea Tree Oil Mediates Antioxidant Factors Relish and Nrf2-Autophagy Axis Regulating the Lipid Metabolism of *Macrobrachium rosenbergii*. *Antioxidants* **2022**, *11*, 2260. [CrossRef] [PubMed]
23. Qiao, Y.; Zhou, L.; Qu, Y.; Lu, K.; Han, F.; Li, E. Effects of Different Dietary β-Glucan Levels on Antioxidant Capacity and Immunity, Gut Microbiota and Transcriptome Responses of White Shrimp (*Litopenaeus vannamei*) under Low Salinity. *Antioxidants* **2022**, *11*, 2282. [CrossRef] [PubMed]
24. Liang, X.; Luo, X.; Lin, H.; Han, F.; Qin, J.G.; Chen, L.; Xu, C.; Li, E. Growth, Health, and Gut Microbiota of Female Pacific White Shrimp, *Litopenaeus vannamei* Broodstock Fed Different Phospholipid Sources. *Antioxidants* **2022**, *11*, 1143. [CrossRef] [PubMed]
25. Yang, J.; Wang, T.; Lin, G.; Li, M.; Zhang, Y.; Mai, K. The Assessment of Dietary Organic Zinc on Zinc Homeostasis, Antioxidant Capacity, Immune Response, Glycolysis and Intestinal Microbiota in White Shrimp (*Litopenaeus vannamei* Boone, 1931). *Antioxidants* **2022**, *11*, 1492. [CrossRef] [PubMed]
26. Fan, R.; Li, Y.; Yang, Q.; Jiang, S.; Huang, J.; Yang, L.; Chen, X.; Zhou, F.; Jiang, S. Expression Analysis of a Novel Oxidoreductase Glutaredoxin 2 in Black Tiger Shrimp, *Penaeus monodon*. *Antioxidants* **2022**, *11*, 1857. [CrossRef]
27. Cheng, C.; Ma, H.; Liu, G.; Fan, S.; Guo, Z. Mechanism of Cadmium Exposure Induced Hepatotoxicity in the Mud Crab (*Scylla paramamosain*): Activation of Oxidative Stress and Nrf2 Signaling Pathway. *Antioxidants* **2022**, *11*, 978. [CrossRef]
28. Feng, W.; Su, S.; Song, C.; Yu, F.; Zhou, J.; Li, J.; Jia, R.; Xu, P.; Tang, Y. Effects of Copper Exposure on Oxidative Stress, Apoptosis, Endoplasmic Reticulum Stress, Autophagy and Immune Response in Different Tissues of Chinese Mitten Crab (*Eriocheir sinensis*). *Antioxidants* **2022**, *11*, 2029. [CrossRef]
29. Ma, L.; Lu, J.; Yao, T.; Ye, L.; Wang, J. Gender-Specific Metabolic Responses of *Crassostrea hongkongensis* to Infection with *Vibrio harveyi* and Lipopolysaccharide. *Antioxidants* **2022**, *11*, 1178. [CrossRef]
30. Gao, J.; Liu, M.; Guo, H.; Zhu, K.; Liu, B.; Liu, B.; Zhang, N.; Zhang, D. ROS Induced by Streptococcus agalactiae Activate Inflammatory Responses via the TNF-α/NF-κB Signaling Pathway in Golden *Pompano Trachinotus* ovatus (Linnaeus, 1758). *Antioxidants* **2022**, *11*, 1809. [CrossRef]
31. Hossen, S.; Sukhan, Z.P.; Kim, S.C.; Hanif, M.A.; Kong, I.-K.; Kho, K.H. Molecular Cloning and Functional Characterization of Catalase in Stress Physiology, Innate Immunity, Testicular Development, Metamorphosis, and Cryopreserved Sperm of Pacific Abalone. *Antioxidants* **2023**, *12*, 109. [CrossRef] [PubMed]

antioxidants

MDPI

Article

High-Fat-Diet-Induced Oxidative Stress in Giant Freshwater Prawn (*Macrobrachium rosenbergii*) via NF-κB/NO Signal Pathway and the Amelioration of Vitamin E

Cunxin Sun [1,2], Fan Shan [2], Mingyang Liu [2], Bo Liu [1,2,*], Qunlan Zhou [1,2], Xiaochuan Zheng [1] and Xiaodi Xu [2]

[1] Key Laboratory of Freshwater Fisheries and Germplasm Resources Utilization, Ministry of Agriculture and Rural Affairs, Freshwater Fisheries Research Center, Chinese Academy of Fishery Sciences, Wuxi 214081, China; suncx@ffrc.cn (C.S.); zhouql@ffrc.cn (Q.Z.); zhengxiaochuan@ffrc.cn (X.Z.)

[2] Wuxi Fisheries College, Nanjing Agricultural University, Wuxi 214081, China; 15261865196@163.com (F.S.); 2018813045@njau.edu.cn (M.L.); 2021213005@stu.njau.edu.cn (X.X.)

* Correspondence: liub@ffrc.cn; Tel.: +86-0510-8555-6101

Abstract: Lipids work as essential energy sources for organisms. However, prawns fed on high-fat diets suffer from oxidative stress, whose potential mechanisms are poorly understood. The present study aimed to explore the regulation mechanism of oxidative stress induced by high fat and the amelioration by vitamin E (VE) of oxidative stress. *Macrobrachium rosenbergii* were fed with two dietary fat levels (LF 9% and HF 13%) and two VE levels (200 mg/kg and 600 mg/kg) for 8 weeks. The results showed that the HF diet decreased the growth performance, survival rate and antioxidant capacity of *M. rosenbergii*, as well as inducing hypertrophied lipid droplets, lipophagy and apoptosis. A total of 600 mg/kg of VE in the HF diet alleviated the negative effects induced by HF. In addition, the HF diet suppressed the expression of toll-dorsal and imd-relish signal pathways. After the relish and dorsal pathways were knocked down, the downstream iNOS and NO levels decreased and the MDA level increased. The results indicated that *M. rosenbergii* fed with a high-fat diet could cause oxidative damage. Its molecular mechanism may be attributed to the fact that high fat suppresses the NF-κB/NO signaling pathway mediating pro-oxidant and antioxidant targets for regulation of oxidative stress. Dietary VE in an HF diet alleviated hepatopancreas oxidative stress and apoptosis.

Keywords: high fat diet; oxidative stress; NF-κB; vitamin E; *Macrobrachium rosenbergii*

Citation: Sun, C.; Shan, F.; Liu, M.; Liu, B.; Zhou, Q.; Zheng, X.; Xu, X. High-Fat-Diet-Induced Oxidative Stress in Giant Freshwater Prawn (*Macrobrachium rosenbergii*) via NF-κB/NO Signal Pathway and the Amelioration of Vitamin E. *Antioxidants* **2022**, *11*, 228. https://doi.org/10.3390/antiox11020228

Academic Editor: Stanley Omaye

Received: 28 December 2021
Accepted: 24 January 2022
Published: 25 January 2022

1. Introduction

For a long time, China's aquaculture industry has been steadily pursuing growth and using high-protein feeds in intensive development, which has led to a series of problems, such as a decline in flesh quality, immunosuppression, and water eutrophication. As a more environmentally friendly nutrient than protein, fat has been shown to have significant protein-sharing effects [1,2]. Therefore, developing high-fat diets in the field of aquafeeds has broad application prospects. However, in current production practices, long-term feeding with high fat diets has led to problems such as oxidative stress and immunosuppression in cultured aquatic animals [3,4]. Vitamin E (VE) is a fat-soluble vitamin that can maintain the stability of the phospholipid bilayer of the cell membrane through antioxidant effects. When free radicals attack the biofilm, VE can undergo a redox reaction with the oxygen-containing groups of ROS to block the generation of peroxides. Studies have shown that VE can significantly enhance specific immunity and anti-stress effects in *Macrobrachium nipponense* [5] and *Palaemonetes argentinus* [6]. In addition, VE has a particular alleviating effect on oxidative stress caused by oxidized fat and high-fat diets [3,7]. Given this, it is crucial to study the mechanism of oxidative stress in organisms induced by high-fat diets and evaluate the amelioration of VE.

For farmed fish, oxidative stress damage induced by the long-term feeding of high-fat diets is manifested by a surge in inflammatory factors, decreased activity of antioxidant

enzymes, abnormal mitochondrial metabolism, and increased apoptosis rate, which seriously affect growth performance, stress tolerance, and pathogen sensitivity [3,8]. Further research found that oxidative stress is mainly induced by the long-term free fatty acid level, which exceeds the metabolic capacity of the body, and leads to an increase in ROS production in the adipose tissue. On the other hand, adipose tissue oxidative stress induces abnormal cytokine production in fat. These two pathways form a vicious cycle in the body that aggravates lipid metabolism disorders and oxidative stress damage [9–11]. Fish and shrimp differ greatly in lipid digestion and metabolism. The major difference between shrimp and fish is that crustaceans do not produce bile and cannot use bile salts in fat digestion and metabolism [12]. Besides, fish accumulate fat in the hepatocyte, the adipose tissues in the abdominal cavity, and between the skin and flesh, while shrimp deposit fat mainly in the hepatocyte, which indicates an shrimps' inability to tolerate and utilize higher dietary fat levels [13]. In the crustacean species, the haemolymph is an essential component of the immunological barrier system and nutrient exchange, which also performs wide functions, such as cellular and biochemical transport, oxygen exchange, and osmotic pressure regulation. The hepatopancreas is the primary organ responsible for the synthesis and degradation of fat, and performs digestion, enzyme secretion, and the excretion of waste materials, which is analogous to the liver in vertebrates. However, studies on haemolymph and hepatopancreas response, as well as oxidative stress induced by high-fat diets in crustaceans, have rarely been reported, with most research focusing on fish species. According to these limited studies, only malondialdehyde and antioxidant enzymes were measured in the hepatopancreas of crustaceans fed high-fat diets [14,15]. The regulatory mechanism of oxidative stress induced by high fat is yet to be determined.

As a critical transcription factor regulating inflammatory response, NF-κB has been shown to be closely related to immune regulation, cell cycle regulation, tumor metastasis, and apoptosis in vertebrates [16,17]. Dorsal and relish are two homologous proteins of NF-κB found in mollusks and crustaceans [18,19]. The main upstream and downstream factors of NF-κB in shrimp have also been determined. The stimulatory and inhibitory roles of NF-κB in ROS regulation have been investigated in vertebrates [20]. However, the studies of the NF-κB signaling pathway in shrimp mainly focus on the immune response to bacteria or viruses [21–24]. Few studies focus on oxidative stress regulation, which is yet to be further explored and verified.

The giant freshwater prawn *Macrobrachium rosenbergii* has been widely cultivated in China and worldwide. Its output in China was about 161,888 tons in 2020, with an increase of 15.96% over the previous year [25]. In the process of breeding, *M. rosenbergii* generally has high feed protein (> 40%) and high density of breeding, which causes significant feed waste and water eutrophication [26]. Therefore, this species can be used as an ideal model for developing high-fat diets and exploring the mechanism of oxidative stress in invertebrates. In view of this, the present study aimed to evaluate the molecular mechanism of oxidative stress induced by high-fat diets in *M. rosenbergii* and the amelioration of VE. The results will shed more light on the molecular mechanism of oxidative stress induced by nutrients, and also provide a reference for the development and application of high-fat feed.

2. Materials and Methods

2.1. Experimental Ingredients and Diets

Four experimental diets were formulated in this study, including two levels of fat and VE. LF/200 VE included 9% fat and 200 mg/kg VE, LF/600 VE included 9% fat and 600 mg/kg VE, HF/200 VE included 13% fat and 200 mg/kg VE, an HF/600 VE included 13% fat and 600 mg/kg VE. The formulation and proximate composition of the experimental diets are presented in Table 1. Fish meal, casein, and gelatin served as the protein sources; fish oil was supplemented as the lipid source; and α-starch and dextrin were used as the carbohydrate source.

Table 1. Formulation and proximate composition of the experimental diets.

	LF/200VE	LF/600VE	HF/200VE	HF/600VE
Ingredients%				
Fish meal [1]	22.00	22.00	22.00	22.00
Casein [2]	24.00	24.00	24.00	24.00
Gelatin [1]	6.00	6.00	6.00	6.00
α-starch [3]	20.00	20.00	20.00	20.00
Dextrin [3]	5.00	5.00	5.00	5.00
Fish oil [1]	6.00	6.00	10.00	10.00
Soybean oil [1]	0.00	0.00	0.00	0.00
Rapeseed oil [1]	0.00	0.00	0.00	0.00
Microcystalline cellulose [4]	5.00	5.00	1.00	1.00
Carboxymethyl cellulose [4]	3.00	3.00	3.00	3.00
Bentonite [1]	1.53	1.49	1.53	1.49
Soybean lecithin (50%) [1]	2.00	2.00	2.00	2.00
Cholesterol [1]	0.30	0.30	0.30	0.30
Ecdysone (2%) [5]	0.10	0.10	0.10	0.10
DMPT [5]	0.05	0.05	0.05	0.05
Choline chloride [5]	1.00	1.00	1.00	1.00
Vitamin premix [5]	1.00	1.00	1.00	1.00
Vitamin E [1]	0.02	0.06	0.02	0.06
Mineral premix [5]	1.00	1.00	1.00	1.00
Calcium dihydrogen phosphate [1]	2.00	2.00	2.00	2.00
Proximate composition %				
Crude protein	40.90	40.90	40.90	40.90
Crude lipid	9.58	9.58	13.28	13.28
Gross energy (MJ/kg)	15.80	15.80	17.38	17.38

Notes: [1] Obtained from Wuxi Tongwei feedstuffs Co., Ltd., Wuxi, China; [2] obtained from Hulunbeier Sanyuan Milk Co., Ltd., Inner Mongolia, China; [3] obtained from Yinhe Dextrin Co., Ltd., Zhengzhou, China; [4] obtained from Yifeng Food Additives Co., Ltd., Shanghai, China; [5] obtained from Jiangsu Fuyuda Food Products Co., Ltd., Yangzhou, China.

All the ingredients were ground through a 60 mm mesh. The fine powder was carefully weighed, then lipid sources and 30% water were added to the mixture, which was further blended to ensure homogeneity. A laboratory pelletizer (Guangzhou Huagong Optical Mechanical and Electrical Technology CO. LTD, Guangzhou, China) was used for the pelletizing process. The diet diameter was 1.5 mm. After drying in the laundry drier, the feeds were offered to prawns.

2.2. Prawns and the Feeding Trial

Juvenile prawns were provided by Zhejiang Southern Taihu Lake freshwater aquatic seed industry CO. LTD (Huzhou, China). After two weeks of acclimation, prawns of similar size (0.24 ± 0.001 g) were randomly distributed into 12 concrete tanks (2.0 m × 1.5 m × 0.8 m) at a rate of 50 prawns per tank. Four experimental diets were randomly allotted to prawns with triplicate tanks. All prawns were fed three times daily at 7:00, 12:00, and 17:30 for 56 days, and the feeding rate was 2–5% of body weight. Feces and molts were removed by siphoning the tanks. During the feeding trial, the average water temperature was 30 ± 0.4 °C; continuous aeration was supplied to each tank to maintain the dissolved oxygen above 50 mg/L; pH was 7.6–8.0, and total ammonia nitrogen level was above 0.02 mg/L. Total ammonia nitrogen and nitrite were kept < 0.2 and 0.005 mg/L, respectively.

2.3. Sample Collection

At the end of the feeding period, prawns were fasted for 24 h to empty the digestive tract. The hemolymphs from five prawns were randomly sampled from the cardiocoelom per tank. Alsever's solution was used as the anticoagulant at a ratio of 1:1 with haemolymph. Hemolymph samples were collected into anticoagulation tubes, then centrifuged at 2000× *g*

4 °C for 10 min. Hepatopancreas was stored in 4% paraformaldehyde for apoptosis measurement and 2.5% glutaraldehyde for ultrastructure study. Furthermore, the remaining hepatopancreases were quickly removed and stored at −80 °C for subsequent analysis.

2.4. Ultrastructure Study

Electron microscopy samples were fixed with 2.5% glutaraldehyde for 24 h, then fixed with 1% osmium tetroxide for 1 h and stored at 4 °C. The sections were embedded in epoxy resin Epon 812, cut into 70 nm-thick sections by RMC PowerTomeXL microtome, stained with uranyl acetate and lead citrate, and examined under a transmission electron microscope (Hitachi H-7650, Tokyo, Japan).

2.5. Apoptosis Detection

Hepatocyte apoptosis was determined by Lu et al.'s methods [27], the terminal deoxynucleotidyl transferase-mediated dUTP-biotin nick end labeling (TUNEL) assay followed the protocol of the apoptosis detection kit (Nanjing Jian-Cheng Bioengineering Institute, Nanjing, China). The positive cell nucleus was dyed brown-yellow granules. The DNase1-treated tissue was used as the positive control. The reaction without TdT enzyme was used as the negative control.

2.6. Biochemical and Antioxidative Parameters in Hemolymph

Total cholesterol (TC), total triglycerides (TG), alanine aminotransferase (ALT) and aspartate aminotransferase (AST) were determined by an automatic hemolymph biochemical analyzer (Mindray BS-400, Shenzhen, China), as described by Wangari et al. [28]. Inducible nitric oxide synthase (iNOS), superoxide dismutase (SOD), glutathione peroxidase (GPx) and anti-superoxide anion (ASA) activity, as well as malonaldehyde (MDA) nitric oxide (NO) content in hemolymph were detected using a commercially available assay kit (Nanjing Jiancheng Bioengineering Institute, Nanjing, China) according to the manufacturer's instructions.

2.7. RNA Isolation and RT-qPCR Analysis

Total RNA was isolated using RNAiso Plus (Takara Co. Ltd., Tokyo, Japan), and then purified with RNase-Free DNase (Takara Co. Ltd., Tokyo, Japan) to avoid genomic DNA amplification. The purity and concentration of RNA were measured using a NanoDrop (DN-1000, Thermo Scientific, Waltham, MA, USA). After normalizing the concentration of the RNA samples, cDNA was generated from 500 ng DNase-treated RNA using ExScriptTM RT-PCR kit, according to the manufacturer's instructions (Takara Co. Ltd., Tokyo, Japan).

The cDNA samples were analyzed by real-time quantitative detector (BIO-RAD, Hercules, CA, USA) using a SYBR Green II Fluorescence Kit (Takara Co. Ltd., Tokyo, Japan). The fluorescent qPCR reaction solution consisted of 10 μL SYBR® premix Ex TaqTM, 0.4 μL ROX Reference Dye II, 0.4 μL PCR forward primer (10 μM), 0.4 μL PCR reverse primer (10 μM), 2.0 μL RT reaction (cDNA solution), and 6.8 μL dH2O. All RT-qPCR primers were designed using Primer 5 software and listed in Table 2. The thermal profile was 95 °C for 30 s, followed by 40 cycles of 95 °C for 5s and 60 °C for 30 s, followed by a melt curve analysis of 15 s from 95 to 60 °C, 1 min for 60 °C, and then up to 95 °C for 15 s. Control reactions were conducted with non-reverse transcribed RNA to determine the level of background or genomic DNA contamination, respectively. In all cases, genomic DNA contamination was negligible. β-actin was selected as the housekeeping gene to normalize our samples because of its stable expression in the present study. The reaction was carried out in three duplicates of each sample. Values for the threshold (CT) from the treated and control tissue templates were compared, and the $2^{-\Delta\Delta CT}$ method was used as the relative quantification calculation method.

Table 2. Sequences of the primers used in the study.

Gene	GenBank Acc. No.	Primer Sequences (5′–3′)	Length (bp)	Purpose	Reference
T7-*relish*	KR827675.1	TAATACGACTCACTATAGGGATCA TCATGAGGCGGAAAAG	40	RNAi	
		TAATACGACTCACTATAGGGTG GCATGTAGGTGAAATCCA	40		
T7-*dorsal*	KX219631.1	TAATACGACTCACTATAGGGCA AGTGTTCCTCGAAGGCTC	40	RNAi	
		TAATACGACTCACTATAGGGA ACTTCACCAATTTGTCCGC	40		
relish	KR827675.1	GATGAGCCTTCAGTGCCAGA CCAGGTGACGCCATGTATCA	20 20	RT-qPCR	
dorsal	KX219631.1	TCAGTAGCGACACCATGCAG CGAGCCTTCGAGGAACACTT	20 20	RT-qPCR	
imd		CGACCACATTCTCCTCCTCCC TTCAGTGCATCCACGTCCCTC	21 21	RT-qPCR	[24]
toll	KX610955.1	TTCGTGACTTGTCGGCTCTC GCAGTTGTTGAAGGCATCGG	20 20	RT-qPCR	
β-actin	AY651918.2	TCCGTAAGGACCTGTATGCC TCGGGAGGTGCGATGATTTT	20 20	RT-qPCR	

2.8. Knock-Down of Relish and Dorsal In Vivo Expression by RNA Interference

To determine the duration and efficiency of gene knock-down of silencing, *M. rosenbergii* were divided into four groups. The first group was a blank group and PBS was injected; the second group was the negative control group and 1.5 μg/g dsGFP was injected; the third group was the dorsal group and 1.5 μg/g dsdorsal was injected; the fourth group was the relish group and 1.5 μg/g dsrelish was injected. Hepatopancreases were harvested at 1 d, 4 d, 7 d, and 10 d after injection. The efficiency of gene knock-down was monitored using RT-qPCR analysis with primers T7-*relish* and T7-*dorsal*. β-actin expression analysis was used as an internal control. The optimum time point of gene silencing was found to be at 4 d after dsRNA injection, and the duration is 7 days after injection. In all of the following experiments, the prawns were therefore injected with dsRNA consecutive 4 day intervals. This knockdown assay was carried out with three replicates.

In total, 12 prawns from the LF/200VE and 36 prawns from the HF/200VE were divided into 4 groups for intramuscular injection. LF/200VE group was injected with 1.5 μg/g dsGFP; HF/200VE group was injected with 1.5 μg/g dsGFP; dsdorsal and dsrelish, respectively. After 24 h of injection, the first group was fed the basal diet, and the other groups were fed with the high-fat diet for 2 weeks. After feeding trial, the hemolymph and hepatopancreases were sampled for analysis.

2.9. Calculations and Statistical Analysis

The growth parameter was calculated as follows:

- Weight gain rate (WGR, %) = $(W_t - W_0) \times 100/W0$.
- Specific growth rate (SGR, % day^{-1}) = $(LnW_t - LnW_0) \times 100/day$.
- Feed conversion ratio (FCR) = feed consumption (g)/Weight gain (g).
- Survival rate (SR, %) = initial number/final number × 100
- Where W_0 and W_t are initial and final body weight.

Data were subjected to two-way analysis of variance (ANOVA) to investigate the growth performance, hemolymph parameters and mRNA expression, after testing the homogeneity of variances with the Levene test. If significant ($p < 0.05$) differences were found, Duncan multiple range test was used to rank the means. Analyses were performed using the SPSS program v16.0 (SPSS Inc., Michigan Avenue, Chicago, IL, USA) for Windows. All data were presented as means ± S.E.M (standard error of the mean).

3. Results

3.1. Growth Performance

As shown in Figure 1, dietary fat and VE level had significant effects on the growth performance and survival rate of *Macrobrachium rosenbergii*, and the interaction of dietary fat and VE levels was significant ($p < 0.05$). In the prawns fed LF diets, different dietary levels of VE had no significant effect on SR, WGR, SGR, and FCR ($p > 0.05$). In the prawns fed with 200VE diets, SR, WGR, and SGR decreased significantly with increasing dietary fat level ($p < 0.05$), and FCR increased significantly ($p < 0.05$). In the prawns fed with HF diets, SR, WGR, and SGR increased significantly with increasing dietary VE levels ($p < 0.05$), and FCR reduced significantly ($p < 0.05$).

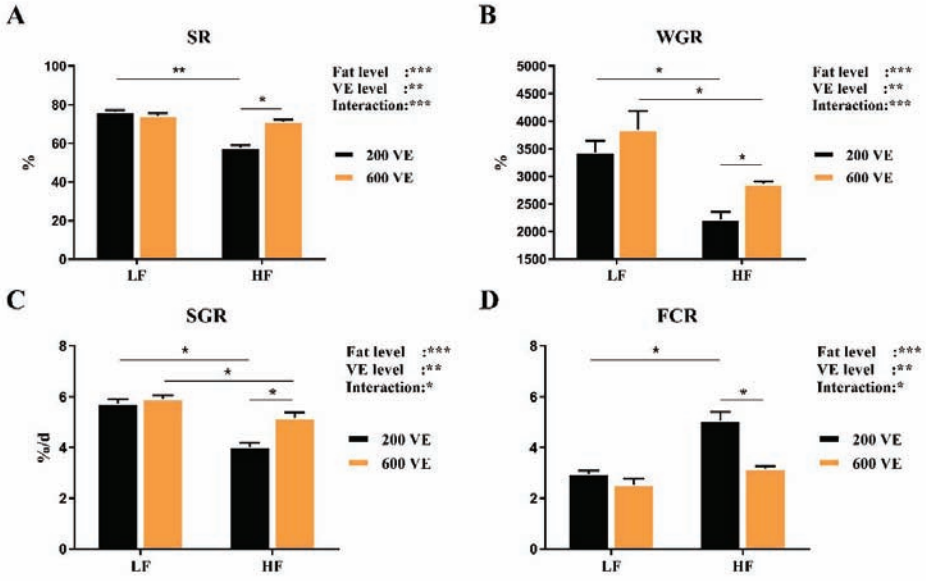

Figure 1. Growth performance and feed utilization of *Macrobrachium rosenbergii* fed with different dietary fat and VE levels. (**A**) survival rate (SR, %) of *M. rosenbergii* fed with different dietary fat and VE levels; (**B**) Weight gain rate (WGR, %) of *M. rosenbergii* fed with different dietary fat and VE levels; (**C**) specific growth rate (SGR, %/day) of *M. rosenbergii* fed with different dietary fat and VE levels; (**D**) feed conversion ratio (FCR) of *M. rosenbergii* fed with different dietary fat and VE levels. Values are means ± SEM. ***: $p < 0.001$, **: $p < 0.01$, *: $p < 0.05$. WGR = (final weight − initial weight) × 100/initial weight; SGR = (Ln final weight − Ln initial weight) × 100/day; FCR = feed consumption (g)/weight gain (g); SR = final number of prawns/initial number of prawns.

3.2. Hemolymph Biochemistry Parameters

As shown in Figure 2, hemolymph AST and TC were significantly affected by dietary fat levels ($p < 0.05$), TC was significantly affected by dietary VE levels, and AST and TG were significantly affected by the interaction of dietary fat and VE levels ($p < 0.05$). In prawns fed LF diets, the levels of dietary VE showed no significant effect on the levels of ALT, AST, TC, and TG ($p < 0.05$). In the prawns fed 200VE diets, ALT, AST, TC, and TG levels increased significantly with increasing dietary fat levels ($p < 0.05$). In the prawns fed HF diets, ALT, AST, TC, and TG levels decreased significantly with increasing dietary VE levels ($p < 0.05$).

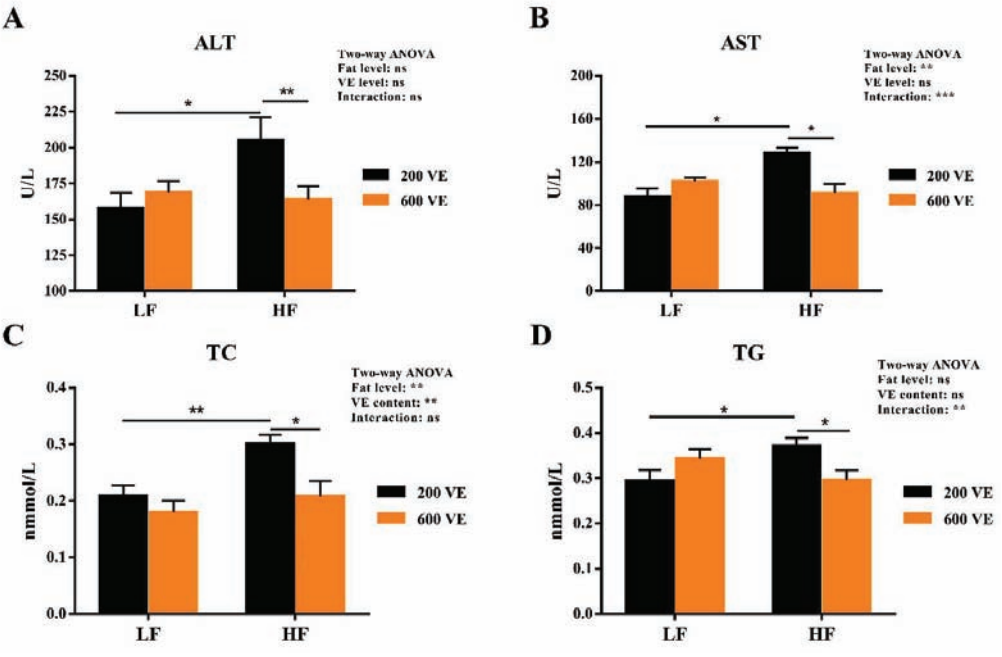

Figure 2. Hemolymph biochemistry parameters of *Macrobrachium rosenbergii* fed with different dietary fat and VE levels. (**A**) hemolymph alanine aminotransferase (ALT) activity of *M. rosenbergii* fed with different dietary fat and VE levels; (**B**) hemolymph aspartate aminotransferase (AST) activity of *M. rosenbergii* fed with different dietary fat and VE levels; (**C**) hemolymph total cholesterol (TC) content of *M. rosenbergii* fed with different dietary fat and VE levels; (**D**) hemolymph total triglycerides (TG) content of *M. rosenbergii* fed with different dietary fat and VE levels. Values are means ± SEM. ***: $p < 0.001$, **: $p < 0.01$, *: $p < 0.05$, ns: $p < 0.05$.

3.3. Hepatopancreas Ultrastructure and Apoptosis

The prawn hepatopancreas ultrastructure pictures are presented in Figure 3. The prawns fed the LF diets exhibited normal ultrastructures with round and clear nuclei; fewer lipid droplets were visible. The 600 VE group exhibited increased endoplasmic reticulum compared with the 200 VE group. Nevertheless, the prawns fed the HF diet showed hypertrophied lipid droplets in the cytoplasm, and lipophagy was observed. A total of 600 VE in the HF diet led to alleviated hepatic lipid accumulation with fewer droplets surrounding the centered nucleus compared with the 200 VE group.

The apoptosis of the hepatopancreatic cells is shown in Figure 4. The cells with stained brown nuclei were considered in a state of apoptosis and were counted to calculate the hepatopancreatic apoptosis cell ratio. Three paraffin sections were used for the TUNEL assay in each group. In the prawns fed LF diets, apoptotic cells were about 16–17% of the total hepatocytes (Figure 4A,B). In the hepatopancreases from the prawns fed the HF/200 VE diet, the apoptotic cells were about 30% of the total hepatocytes, which was significantly higher than in those fed LF/200 VE diet ($p < 0.05$) (Figure 4C). The 600 VE addition significantly decreased the ratio of apoptosis cells compared with 200 VE in the HF groups ($p < 0.05$) (Figure 4D).

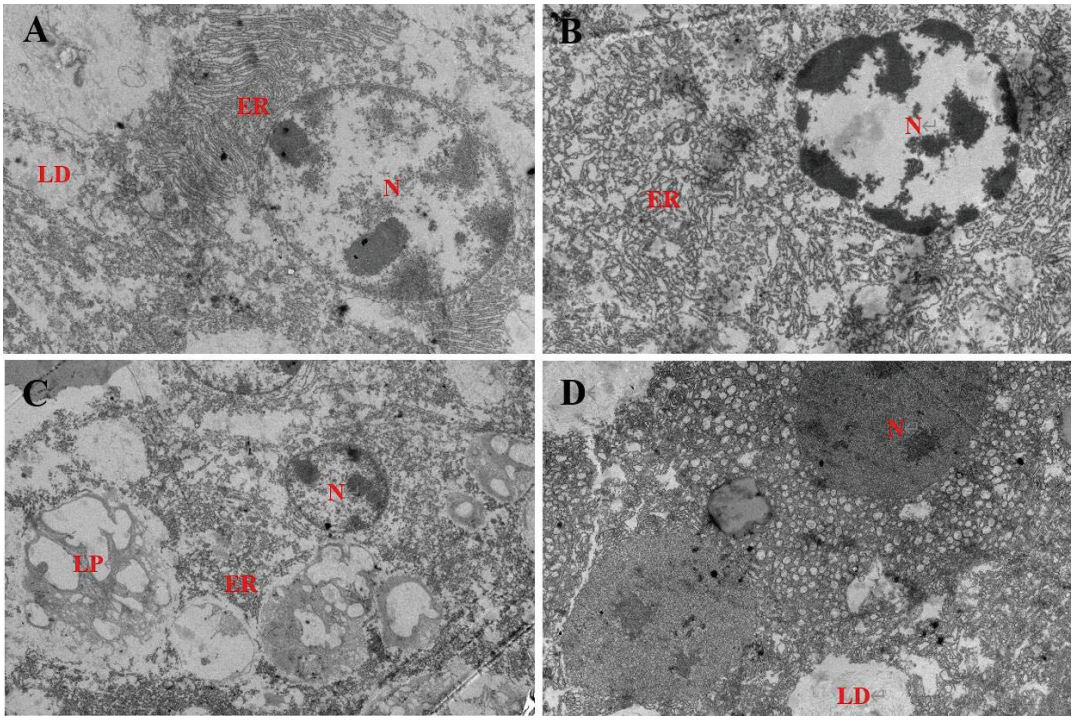

Figure 3. Transmission electron microscope images of *Macrobrachium rosenbergii* hepatocyte ultrastructure (2500×) fed with different dietary fat and VE levels. (**A**) prawns fed diet including 9% fat and 200 mg/kg VE; (**B**) prawns fed diet including 9% fat and 600 mg/kg VE; (**C**) prawns fed diet including 13% fat and 200 mg/kg VE; (**D**) prawns fed diet including 13% fat and 600 mg/kg VE. N: nucleus; LD: lipid droplet; ER, endoplasmic reticulum; LP, lipophagy.

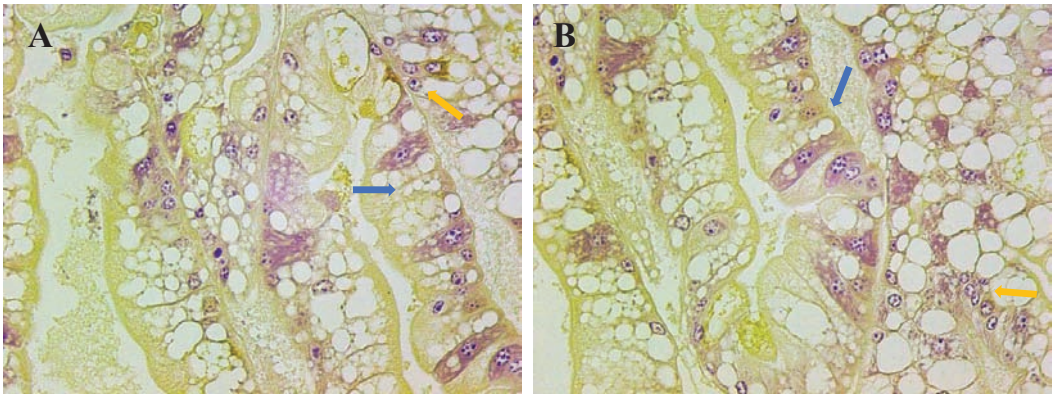

Figure 4. *Cont*.

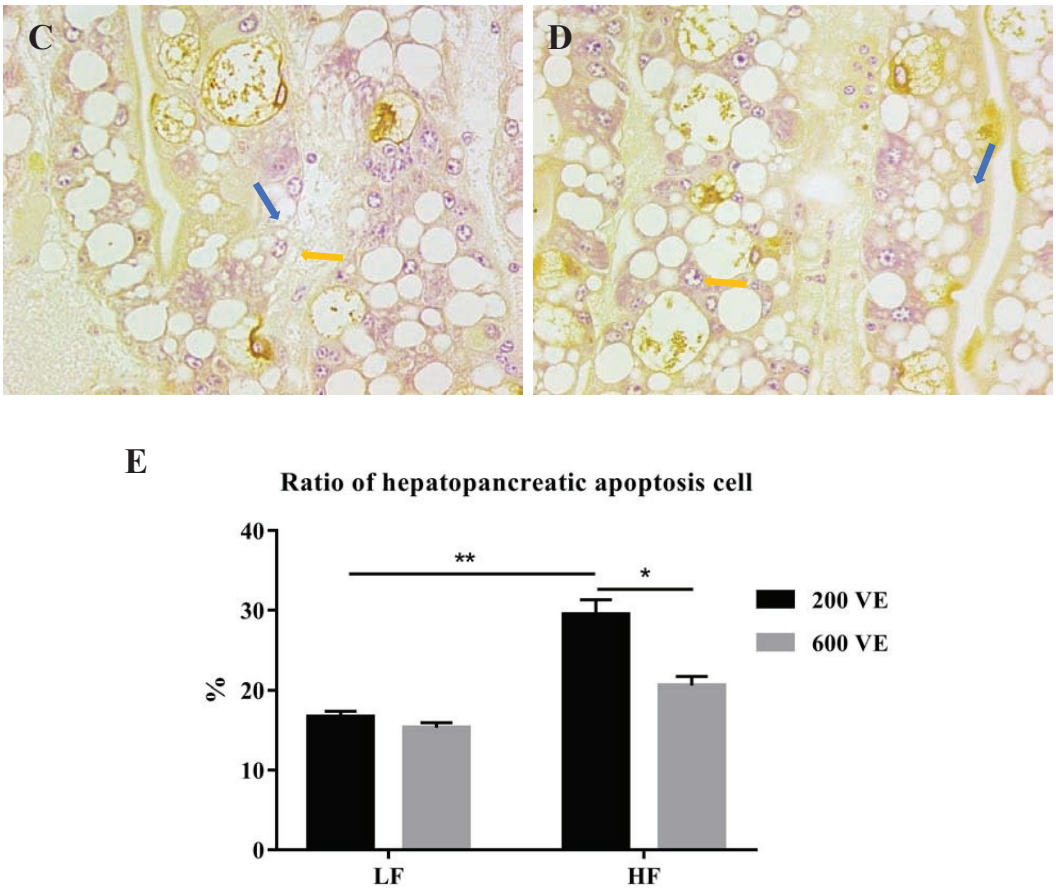

Figure 4. Hepatocyte apoptosis of *Macrobrachium rosenbergii* fed with different dietary fat and VE levels. (**A**) prawns fed diet including 9% fat and 200 mg/kg VE; (**B**) prawns fed diet including 9% fat and 600 mg/kg VE; (**C**) prawns fed diet including 13% fat and 200 mg/kg VE; (**D**) prawns fed diet including 13% fat and 600 mg/kg VE; (**E**) ratio of hepatopancreatic apoptosis cells ($n = 3$). Blue arrow: normal cells; yellow arrow: apoptotic cells. **: $p < 0.01$, *: $p < 0.05$.

3.4. Hemolymph Antioxidant Capacity

The hemolymph antioxidant indexes are shown in Figure 5. SOD, GPX, and ASA were significantly affected by dietary fat levels ($p < 0.05$), GPx was significantly affected by dietary VE levels, and SOD was significantly affected by the interaction of dietary fat and VE ($p < 0.05$). In prawns fed LF diets, dietary levels of VE had no significant effect on the levels of SOD, GPx, ASA, and MDA ($p < 0.05$). In the prawns fed 200VE diets, the SOD, GPx, and ASA activities were significantly reduced when the dietary fat level was increased, while the MDA content was significantly increased ($p < 0.05$). In the prawns fed HF diets, the GPx activity was significantly increased and the MDA level was significantly decreased when the VE level was increased ($p < 0.05$).

The hemolymph iNOS activity and NO content are shown in Figure 6. The iNOS and NO were significantly affected by dietary fat levels ($p < 0.05$) and iNOS was significantly affected by the interaction of dietary fat and VE ($p < 0.05$). In the prawns fed 200 VE diets, the iNOS and NO levels were significantly reduced when the dietary fat level was increased ($p < 0.05$). In prawns fed the same fat-level diets, VE levels showed no significant difference in iNOS activity or NO content ($p < 0.05$).

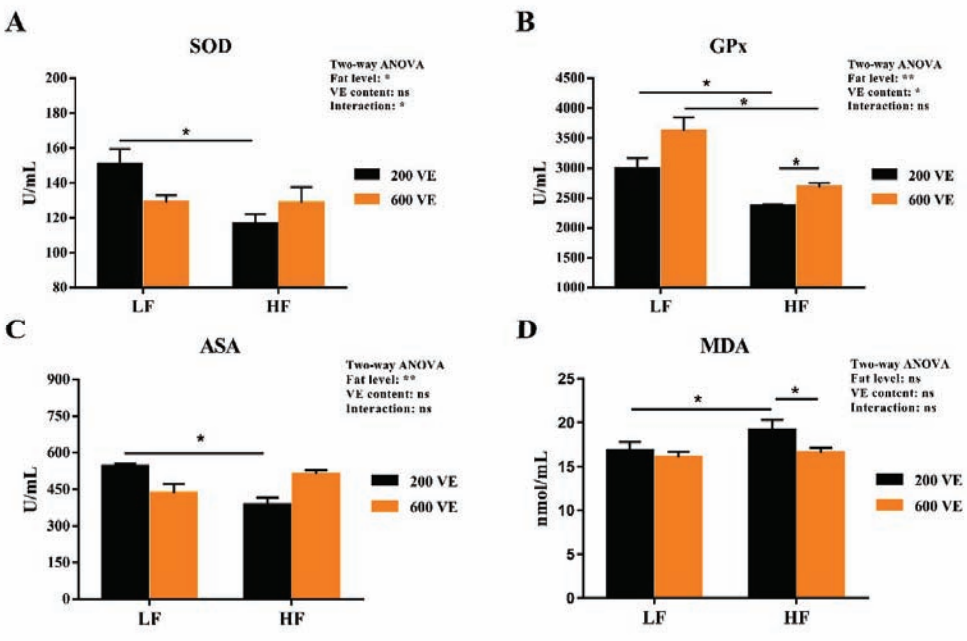

Figure 5. Hemolymph oxidative status of *Macrobrachium rosenbergii* fed with different dietary fat and VE levels. (**A**) hemolymph superoxide dismutase (SOD) activity of *M. rosenbergii* fed with different dietary fat and VE levels; (**B**) hemolymph glutathione peroxidase (GPx) activity of *M. rosenbergii* fed with different dietary fat and VE levels; (**C**) hemolymph anti-superoxide anion (ASA) activity of *M. rosenbergii* fed with different dietary fat and VE levels; (**D**) hemolymph malonaldehyde (MDA) content of *M. rosenbergii* fed with different dietary fat and VE levels. Values are means ± SEM. **: $p < 0.01$, *: $p < 0.05$, ns: $p < 0.05$.

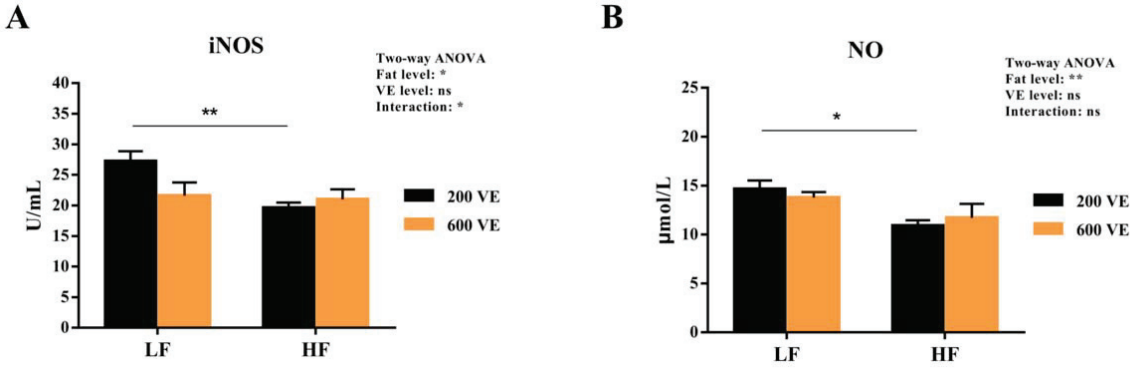

Figure 6. Hemolymph iNOS activity and NO content of *Macrobrachium rosenbergii* fed with different dietary fat and VE levels. (**A**) hemolymph inducible nitric oxide synthase (iNOS) activity of *M. rosenbergii* fed with different dietary fat and VE levels; (**B**) hemolymph nitric oxide (NO) content of *M. rosenbergii* fed with different dietary fat and VE levels. Values are means ± SEM. **: $p < 0.01$, *: $p < 0.05$, ns: $p < 0.05$.

3.5. Hepatopancreas NF-κB Signal Pathway Expression

The hemolymph gene expression of the NF-κB signal pathway expression is shown in Figure 7. *Imd*, *relish*, *toll*, and *dorsal* expression were significantly affected by dietary fat

levels ($p < 0.05$), *Imd*, *relish*, *dorsal* expression was significantly affected by dietary VE levels ($p < 0.05$), and the interaction of dietary fat and VE showed no significant difference in NF-κB signal pathway expression ($p > 0.05$). In the prawns fed LF diets, dietary 600 VE significantly inhibited the expression of *imd* and *dorsal* compared with 200 VE ($p < 0.05$). In the prawns fed 200 VE diets, dietary HF significantly inhibited the expression of *imd*, *relish*, *toll*, and *dorsal* compared with LF ($p < 0.05$). In the prawns fed HF diets, dietary 600 VE significantly inhibited *imd* and *relish* expression compared with 200VE ($p < 0.05$). No significant difference was observed in the expression of *toll* or *dorsal* ($p > 0.05$).

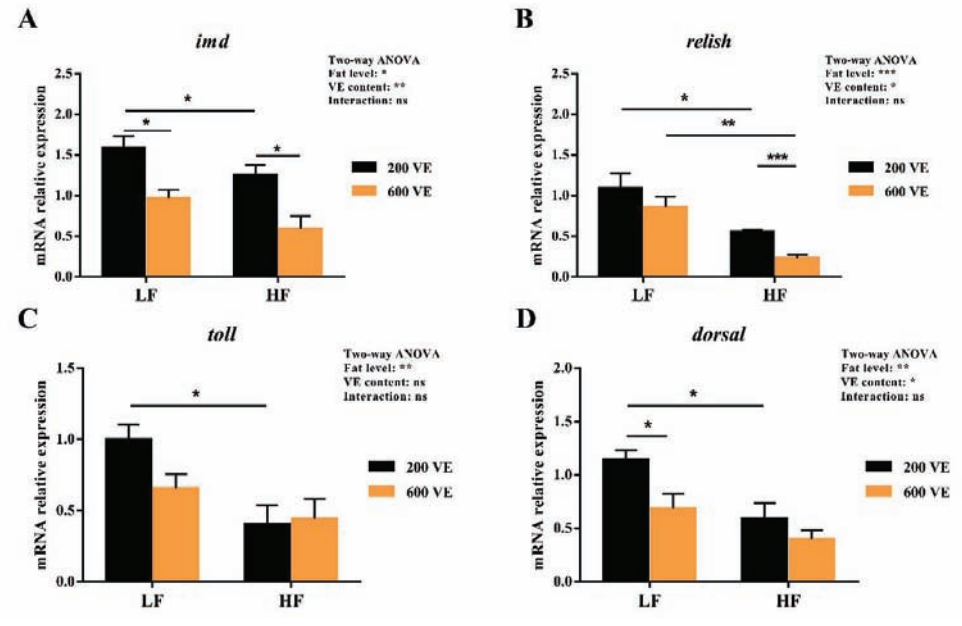

Figure 7. Relative expression of NF-κB signal pathway in hepatopancreas. (**A**) relative expression of *imd* in hepatopancreas; (**B**) relative expression of *relish* in hepatopancreas; (**C**) relative expression of *toll* in hepatopancreas; (**D**) relative expression of *dorsal* in hepatopancreas. Values are means ± SEM. ***: $p < 0.001$, **: $p < 0.01$, *: $p < 0.05$, ns: $p < 0.05$.

3.6. In Vivo Knock-Down of Relish and Dorsal by RNA Interference

A relish and dorsal knock-down experiment was performed to further characterize the role of NF-κB in the antioxidative process induced by dietary HF. As shown in Figure 8A,B, *relish* and *dorsal* expression reduced significantly at 4d–7d post-injection of *relish*- and *dorsal*-specific dsRNA ($p < 0.05$). After a two-week in vivo knock-down of *relish* and *dorsal* by RNA interference, the expression of *dorsal* was suppressed by the *dorsal* dsRNA injection ($p < 0.05$) (Figure 8C), and the expression of *relish* was suppressed by the *relish* dsRNA injection ($p < 0.05$) (Figure 8D).

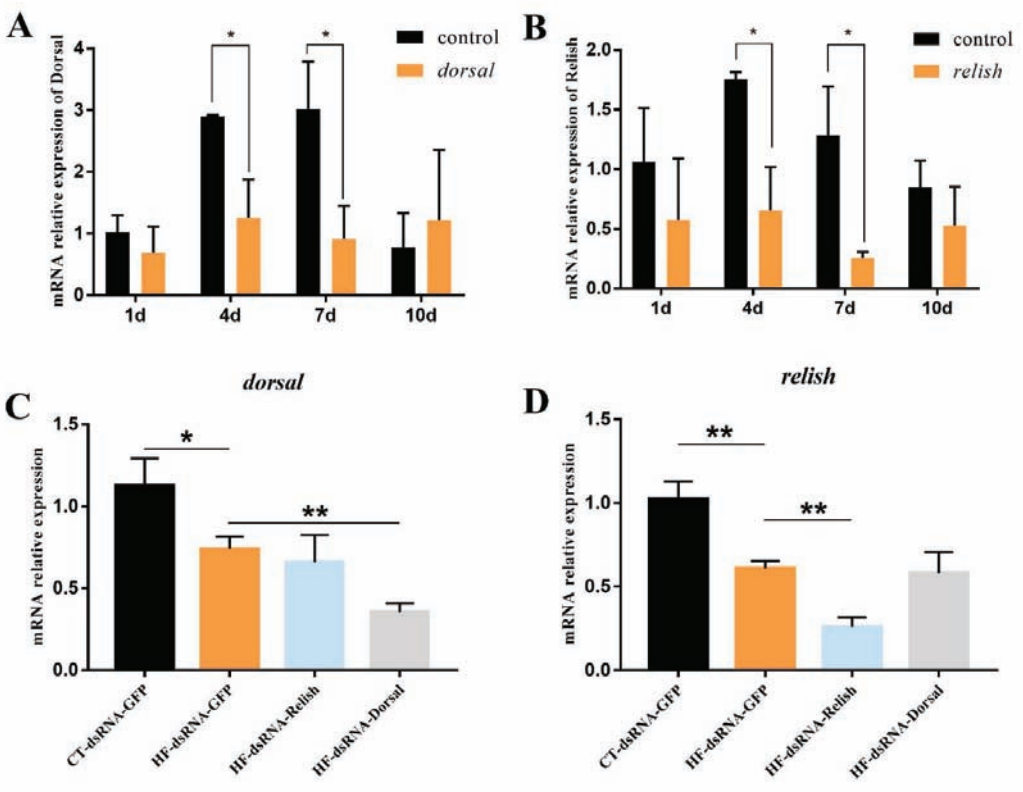

Figure 8. Knock-down of *relish* and *dorsal* in vivo expression by dsRNA-mediated RNA interference. (**A**) Time-course study of *dorsal* expression in hepatopancreas after RNA interference; (**B**) Time-course study of *relish* expression in hepatopancreas after RNA interference; (**C**) *dorsal* expression in *M. rosenbergii* fed with high-fat diet after RNA interference; (**D**) *relish* expression in *M. rosenbergii* fed with high-fat diet after RNA interference. Values are means ± SEM. **: $p < 0.01$, *: $p < 0.05$.

3.7. Hemolymph Antioxidant Capacity after NF-κB Suppression

As shown in Figure 9, the iNOS activity and NO content in the hemolymph of *M. rosenbergii* fed with the HF diet significantly decreased ($p < 0.05$). A further decline in the iNOS and NO levels was observed when the expression of *relish* and *dorsal* was suppressed ($p < 0.05$). Hemolymph ASA activity and MDA content are showed in Figure 10. Compared with the control group, the HF group's MDA content significantly increased and its ASA activity significantly decreased ($p < 0.05$). In the prawns fed HF diet, *relish* and *dorsal* suppression further increased the MDA content and decreased the ASA activity ($p < 0.05$).

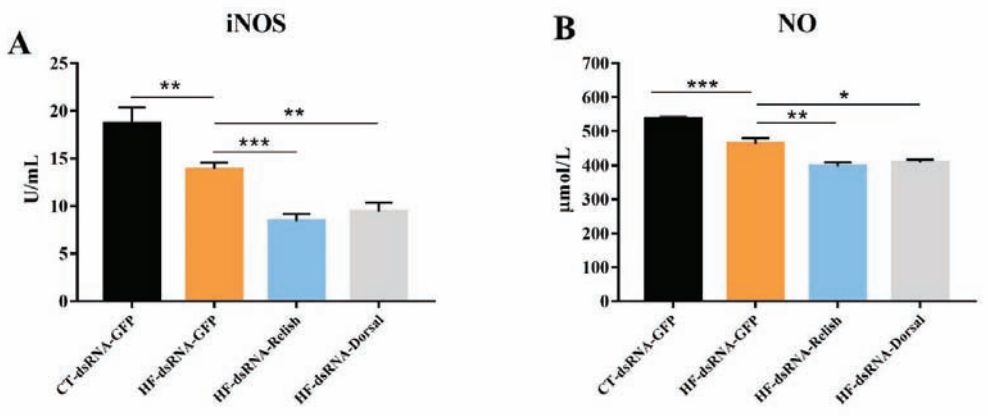

Figure 9. Hemolymph iNOS activity and NO content of *Macrobrachium rosenbergii* after knock-down by dsRNA-mediated RNA interference. (**A**) Hemolymph inducible nitric oxide synthase (iNOS) activity of *M. rosenbergii* after RNA interference; (**B**) Hemolymph nitric oxide (NO) content of *M. rosenbergii* after RNA interference. Values are means ± SEM. ***: $p < 0.001$, **: $p < 0.01$, *: $p < 0.05$.

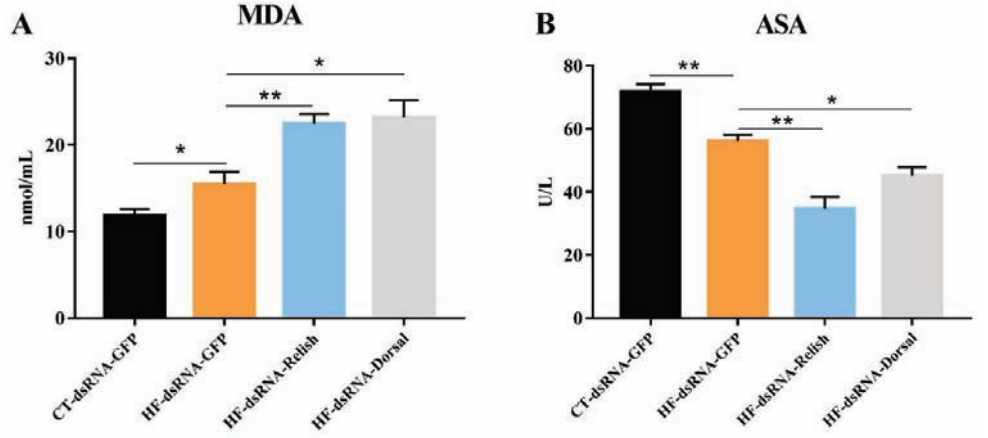

Figure 10. Hemolymph ASA activity and MDA content of *Macrobrachium rosenbergii* after knock-down by dsRNA-mediated RNA interference. (**A**) Hemolymph anti-superoxide anion (ASA) activity of *M. rosenbergii* after RNA interference; (**B**) Hemolymph malonaldehyde (MDA) content of *M. rosenbergii* after RNA interference. Values are means ± SEM. **: $p < 0.01$, *: $p < 0.05$.

4. Discussion

Physiological conditions limit carnivorous fish's demand for and utilization of fat. The long-term intake of high amounts of fat will accumulate in the body, leading to obstacles in fat transport, affecting body tissue fat, and reducing body fat deposition and fat metabolism by regulating lipid metabolism. Improving fish health has become one of the feasible means. In this study, the high-fat diet reduced the growth performance and survival rate of *M. rosenbergii*. Similar results were also observed in spotted seabass (*Lateolabrax maculatus*) [29], Pacific white shrimp (*Litopenaeus vannamei*) [14], largemouth bass (*Micropterus salmoides*) [30], and blunt snout bream (*Megalobrama amblycephala*) [31]. The reason for this might be the damaged antioxidant capacity, stress and disease resistance induced by dietary high fat. The previous studies pointed out that a high-fat diet could induce aberrant hepatic lipid secretion, reduce mortality rates and worsen the adverse

effects of antibiotics by activating oxidant stress and endoplasmic reticulum stress [32–34]. This is also supported by the fact that high fat reduced the survival rate of *M. rosenbergii* in the present study. VE supplementation alleviated the growth inhibition induced by high fat levels in the present study, which was also confirmed in turbot (*Scophthalmus maximus*) [3]. Previous studies found that VE could alleviate high-fat-diet-induced hepatic oxidative stress and hypoimmunity to keep health and growth, while VE deficiency inhibited fat metabolism and induced lipid peroxidation [3,35]. The above results suggested that VE may be beneficial for maintaining the growth and health of prawns by reducing lipid metabolism disorder and the oxidative stress induced by high-fat diets.

Haemolymph biochemical indicators are important in diagnosing the health of aquatic animals. ALT and AST are sensitive biomarkers for hepatopancreas injury, and the TC and TG content can reflect lipid metabolism. In this study, the increase in the hemolymph ALT and AST activities of *M. rosenbergii* fed with a high-fat diet indicated the impaired function and metabolism of the hepatopancreas. Similar results were also observed in blunt snout bream [27] and grass carp (*Ctenopharyngodon idella*) [36]. The increase in hemolymph TC and TG in high fat group also indicated lipid metabolic disturbances and disorders because high serum TG and TC are significant risk factors related to fatty liver that can result in oxidative stress and decrease disease resistance. The present study found that extra dietary VE reduced the hemolymph levels of TG and TC, as well as ALT and AST activities in prawns fed an HF diet. The previous study demonstrated that the appropriate amounts of dietary VE improve the metabolic health of the liver in grass carp juveniles [37]. This was further supported by the fact that the VE requirement of aquatic animals increases as the fat content of feed increases [38]. These findings suggested that extra VE supplementation may contribute to the hepatopancreas health benefits of *M. rosenbergii*.

The hepatopancreas is the main organ responsible for the absorption and storage of the ingested substances. In the present study, the HF diet caused excessive lipid droplet accumulation in the hepatopancreas, which was also widely reported in other aquatic species [27,29,39]. In addition, the high-fat diet also induced hepatopancreas lipophagy and apoptosis. Lipophagy is the selective autophagy of lipid droplets degraded by lysosomes, which is associated with the regulation of lipid metabolism [40]. Existing evidence shows that high-fat diets can induce endoplasmic reticulum stress, autophagy, and apoptosis [41]. These pathologies may also cause the abnormal secretion of lipoproteins and lipid peroxidation, leading to a vicious circle. The results obtained here are still highly significant for human beings, although there are huge differences in the physiological structure of aquatic and terrestrial animals. In mice, high-fat diets could induce dyslipidemia and non-alcoholic fatty liver disease (NAFLD) [42,43]. Nutritional liver disease in shrimp has not yet been clearly defined, but the apoptosis and steatosis of the hepatopancreas found in prawns fed high levels of fat in the present study were similar to the NAFLD symptoms in humans. Nevertheless, these deformities can be relieved by extra VE supplementation. According to previous studies, VE can protect cells against lipid peroxidation and attenuate hepatic steatosis and mitochondrial damage [44]. VE could ameliorate apoptosis and autophagy induced by stress and disease in mammals [45–47]. Thus, based on histological and TUNEL apoptosis observation, the lipid-lowering effect of VE may be attributed to the attenuation of apoptosis and autophagy induced by high-fat diets. Similar results were also found in rats [48], indicating that *M. rosenbergii* can serve as a model for developing drugs for NAFLD.

Oxidative stress damage refers to the excess reactive oxygen species (ROS) production stimulated by factors such as the environment and nutrition, which breaks the redox equilibrium and ultimately leads to cell and tissue damage. In the present study, the HF diet reduced hemolymph ASA activity and increased MDA content. Similar results were also observed in largemouth bass (*Micropterus salmoides*) [49] and *M. amblycephala* [8]. This indicates that excess fat might induce oxidative stress damage and lipid peroxidation as MDA is the main component of lipid peroxide, which damages cell structures and functions [3]. In addition, the antioxidant enzyme system composed of SOD and GPx can

remove excessive free radicals, reducing the damage by lipid peroxidation. The inhibition of the SOD and GPx activities in the HF group further supported the notion that excess fat induced oxidative stress. Nevertheless, VE improved GPx activities and reduced MDA content in the prawns fed the high-fat diet. This might due to the fact that VE has a significant effect of enhancing specific immunity and anti-oxidants by undergoing a redox reaction with the oxygen-containing groups of ROS to block peroxide production [50]. The ameliorative effect of VE on oxidative stress and hypoimmunity induced by a high-fat diet and oxidized oil also supported these results [3,51]. NO generated by iNOS could inhibit lipid peroxidation, which relies on its ability to eliminate oxygen free radicals [52]. The inhibition of hemolymph iNOS and NO in prawns fed with high fat also indicated the oxidative damage induced by excess fat, which is supported by the results in mussels [53] and *L. vannamei* [54]. However, VE showed no significant effect on iNOS and NO. As a non-enzymatic oxidant, VE halts lipid peroxidation by donating its phenolic hydrogen to peroxyl radicals, forming tocopherol radicals [55]. This may partly explain the reason of the invalidation of VE on iNOS and NO levels.

In general, the activation of transcription factors NF-κB is an indispensable step for increasing iNOS activity, which subsequently induces the release of NO [56]. In the present study, the expression of *imd-relish* and *toll-doral*, two major homologs of the components of NF-κB signal pathways, were inhibited by dietary high fat. It is speculated that both the *imd-relish* and the *toll-doral* signal pathway were suppressed by oxidative stress, which further reduced the production of NO, forming a vicious circle. A previous study also supported the notion that oxidative stress induced by high fat could inhibit the expression of the toll signal pathway [3]. However, VE only decreased *imd-relish* expression in the HF group. The regulation of VE in high-fat diets might attribute to the production of anti-microbial peptides as *relish* translocates into the nucleus to activate the expression of antibacterial peptide genes after stimulation [57]. To further verify the effect of the regulation of NF-κB on oxidative stress induced by high levels of fat, *relish* and *dorsal* expression were knocked down, respectively. The levels of iNOS and NO were suppressed, while MDA content increased and ASA activity decreased after relish and dorsal knock-down. The results above suggested that dietary high fat induced oxidative stress via the suppression of the NF-κB/NO signal pathway. Some research supported the notion that the NF-κB signal pathway also plays a crucial regulatory role in NAFLD induced by high-fat diets [58,59]. In vertebrates, NF-κB is activated by high-fat diets to induce inflammation. Nevertheless, crustaceans lack inflammatory cytokines. The different regulation of NF-κB in crustaceans and vertebrates still requires further in-depth studies.

5. Conclusions

The present study investigated the growth performance and oxidative status of *M. rosenbergii* fed different fat and VE levels, and revealed the molecular regulatory mechanism in response to a high-fat diet. In the present study, VE ameliorated the growth retardation and oxidative stress induced by a high-fat diet. A putative mechanism that could explain our results is shown in Figure 11. The high-fat diet caused excessive lipid deposition in *M. rosenbergii*, which further induced hepatopancreas lipophagy, apoptosis, and lipid peroxidation, resulting in oxidative stress damage. The *toll-dorsal* and *imd-relish* signaling pathways were inhibited by the high fat levels, which mediated pro-oxidant targets (iNOS and NO) and antioxidant targets (SOD and GPx) for the negative feedback regulation of oxidative stress. Dietary VE supplementation combined with the high-fat diet alleviated hepatopancreas oxidative stress and apoptosis. The reason for this may be related to the antioxidant properties of VE and the activation of the antioxidant enzyme system.

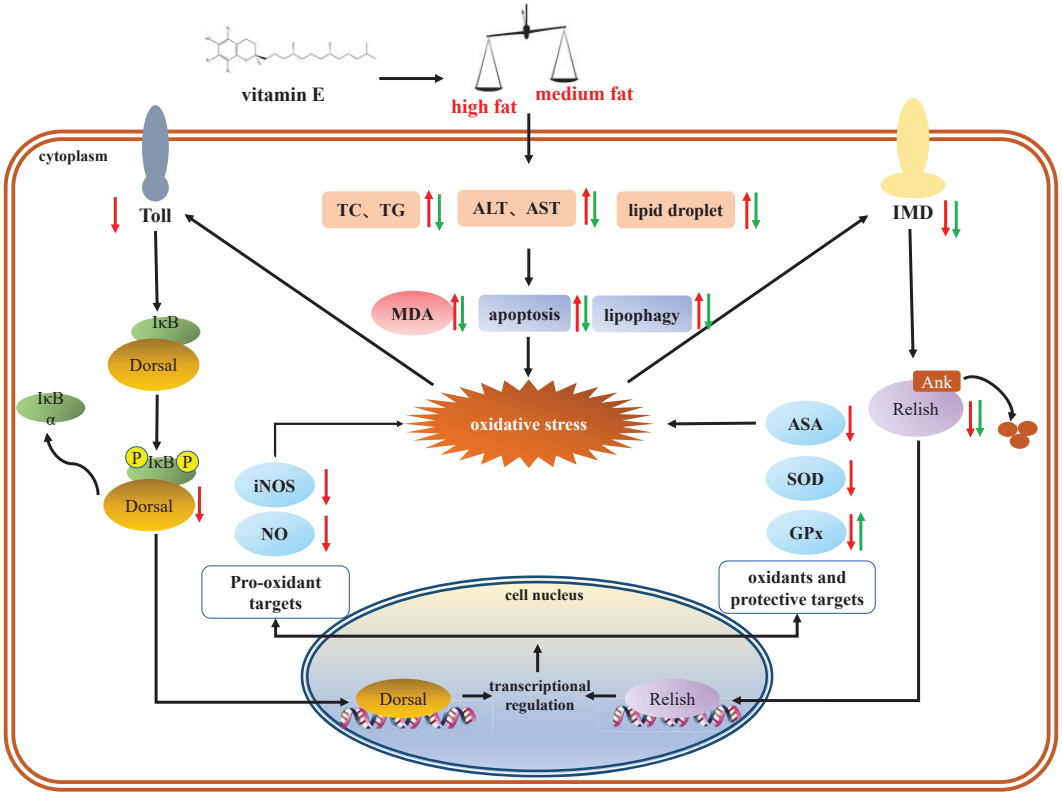

Figure 11. NF-κB/NO signaling mechanism in response to dietary high fat and VE. The red arrows indicate the effects of high fat; the green arrows indicate the effects of VE.

Author Contributions: The author contributions were as follows: C.S. contributed in the areas of experimental design, sampling, data analysis, and write-up; B.L., Q.Z. and X.Z. contributed to the experimental design and manuscript review; F.S. and M.L. contributed to feeding and cultivating of experimental prawns, sampling, and statistics and X.X. contributed to feed production, feeding of prawns, and sampling. All authors have read and agreed to the published version of the manuscript.

Funding: This work is supported by the Project of National Key R&D Program of China (2019YFD0900200), the National Natural Science Foundation of China (32002404), the Natural Science Foundation of Jiangsu Province for Youths (BK20180172), China Agriculture Research System of MOF and MARA (CARS-48), Central Public-interest Scientific Institution Basal Research Fund, CAFS (2020TD59). All the funders had no role in the design, analysis or writing of this article.

Institutional Review Board Statement: The care and use of animals followed Animal Research Institute Committee guidelines of Nanjing Agricultural University, China. This study has been approved by the Committee of the Animal Research Institute of Nanjing Agricultural University, China (SYXK (Su) 2019-0136, approved 21 May 2017).

Informed Consent Statement: Not applicable.

Data Availability Statement: Data is contained within the article.

Acknowledgments: The authors would acknowledge Zhejiang Southern Taihu Lake freshwater aquatic seed industry CO. LTD for the contribution of juvenile prawns and the administration in the feeding trial.

Conflicts of Interest: The authors declare no conflict of interest.

References

1. Méndez-Martínez, Y.; García-Guerrero, M.U.; Arcos-Ortega, F.G.; Martínez-Córdova, L.R.; Yamasaki-Granados, S.; Pérez-Rodríguez, J.C.; Cortés-Jacinto, E. Effect of different ratios of dietary protein-energy on growth, body proximal composition, digestive enzyme activity, and hepatopancreas histology in *Macrobrachium americanum* (Bate, 1868) prawn juveniles. *Aquaculture* **2018**, *485*, 1–11. [CrossRef]
2. Zhang, N.N.; Ma, Q.Q.; Fan, W.J.; Xing, Q.; Zhao, Y.L.; Chen, L.Q.; Ye, J.Y.; Zhang, M.L.; Du, Z.Y. Effects of the dietary protein to energy ratio on growth, feed utilization and body composition in *Macrobrachium nipponense*. *Aquac. Nutr.* **2017**, *23*, 313–321. [CrossRef]
3. Jia, Y.; Jing, Q.; Niu, H.; Huang, B. Ameliorative effect of vitamin E on hepatic oxidative stress and hypoimmunity induced by high-fat diet in turbot (*Scophthalmus maximus*). *Fish Shellfish Immunol.* **2017**, *67*, 634–642. [CrossRef]
4. Lu, K.; Wang, L.; Zhang, D.; Liu, W.; Xu, W. Berberine attenuates oxidative stress and hepatocytes apoptosis via protecting mitochondria in blunt snout bream *Megalobrama amblycephala* fed high-fat diets. *Fish Physiol. Biochem.* **2017**, *43*, 65–76. [CrossRef] [PubMed]
5. Li, Y.; Fan, B.; Huang, Y.; Wu, D.; Zhang, M.; Zhao, Y. Effects of dietary vitamin E on reproductive performance and antioxidant capacity of *Macrobrachium nipponense* female shrimp. *Aquac. Nutr.* **2018**, *24*, 1698–1708. [CrossRef]
6. Griboff, J.; Morales, D.; Bertrand, L.; Bonansea, R.I.; Monferrán, M.V.; Asis, R.; Wunderlin, D.A.; Amé, M.V. Oxidative stress response induced by atrazine in *Palaemonetes argentinus*: The protective effect of vitamin E. *Ecotoxicol. Environ. Saf.* **2014**, *108*, 1–8. [CrossRef]
7. Mourente, G.; Dıaz-Salvago, E.; Bell, J.G.; Tocher, D.R. Increased activities of hepatic antioxidant defence enzymes in juvenile gilthead sea bream (*Sparus aurata* L.) fed dietary oxidised oil: Attenuation by dietary vitamin E. *Aquaculture* **2002**, *214*, 343–361. [CrossRef]
8. Lu, K.L.; Xu, W.N.; Liu, W.B.; Wang, L.N.; Zhang, C.N.; Li, X.F. Association of mitochondrial dysfunction with oxidative stress and immune suppression in blunt snout bream *Megalobrama amblycephala* fed a high-fat diet. *J. Aquat. Anim. Health* **2014**, *26*, 100–112. [CrossRef] [PubMed]
9. Essick, E.E.; Sam, F. Oxidative stress and autophagy in cardiac disease, neurological disorders, aging and cancer. *Oxid. Med. Cell. Longev.* **2010**, *3*, 168–177. [CrossRef]
10. Jiang, S.; Du, P.; An, L.; Yuan, G.; Sun, Z. Anti-diabetic effect of *Coptis Chinensis* polysaccharide in high-fat diet with STZ-induced diabetic mice. *Int. J. Biol. Macromol.* **2013**, *55*, 118–122. [CrossRef] [PubMed]
11. Furukawa, S.; Fujita, T.; Shimabukuro, M.; Iwaki, M.; Yamada, Y.; Nakajima, Y.; Nakayama, O.; Makishima, M.; Matsuda, M.; Shimomura, I. Increased oxidative stress in obesity and its impact on metabolic syndrome. *J. Clin. Investig.* **2004**, *114*, 1752–1761. [CrossRef] [PubMed]
12. Cherif, S.; Fendri, A.; Miled, N.; Trabelsi, H.; Mejdoub, H.; Gargouri, Y. Crab digestive lipase acting at high temperature: Purification and biochemical characterization. *Biochimie* **2007**, *89*, 1012–1018. [CrossRef] [PubMed]
13. Council, N.R. *Nutrient Requirements of Fish and Shrimp*; National Academies Press: Pittsburgh, PA, USA, 2011.
14. Xu, C.; Li, E.; Liu, Y.; Wang, S.; Wang, X.; Chen, K.; Qin, J.G.; Chen, L. Effect of dietary lipid level on growth, lipid metabolism and health status of the Pacific white shrimp *Litopenaeus vannamei* at two salinities. *Aquac. Nutr.* **2018**, *24*, 204–214. [CrossRef]
15. Zhao, J.; Wen, X.; Li, S.; Zhu, D.; Li, Y. Effects of dietary lipid levels on growth, feed utilization, body composition and antioxidants of juvenile mud crab *Scylla paramamosain* (Estampador). *Aquaculture* **2015**, *435*, 200–206. [CrossRef]
16. D'Ignazio, L.; Bandarra, D.; Rocha, S. NF-κB and HIF crosstalk in immune responses. *FEBS J.* **2016**, *283*, 413–424. [CrossRef]
17. Meyerovich, K.; Fukaya, M.; Terra, L.F.; Ortis, F.; Eizirik, D.L.; Cardozo, A.K. The non-canonical NF-κB pathway is induced by cytokines in pancreatic beta cells and contributes to cell death and proinflammatory responses in vitro. *Diabetologia* **2016**, *59*, 512–521. [CrossRef]
18. Jiang, Y.S.; Wu, X.Z. Characterization of a Rel\NF-κB homologue in a gastropod abalone, *Haliotis diversicolor supertexta*. *Dev. Comp. Immunol.* **2007**, *31*, 121–131. [CrossRef]
19. Li, F.; Wang, L.; Zhang, H.; Zheng, P.; Zhao, J.; Qiu, L.; Zhang, Y.; Song, L. Molecular cloning and expression of a Relish gene in Chinese mitten crab *Eriocheir sinensis*. *Int. J. Immunogenet.* **2010**, *37*, 499–508. [CrossRef]
20. Morgan, M.J.; Liu, Z.G. Crosstalk of reactive oxygen species and NF-κB signaling. *Cell Res.* **2011**, *21*, 103–115. [CrossRef]
21. Arockiaraj, J.; Avin, F.A.; Vanaraja, P.; Easwvaran, S.; Singh, A.; Othman, R.Y.; Bhassu, S. Immune role of MrNFκBI-α, an IκB family member characterized in prawn *M. rosenbergii*. *Fish Shellfish Immunol.* **2012**, *33*, 619–625. [CrossRef]
22. Huang, X.; Wang, W.; Ren, Q. Dorsal transcription factor is involved in regulating expression of crustin genes during white spot syndrome virus infection. *Dev. Comp. Immunol.* **2016**, *63*, 18–26. [CrossRef] [PubMed]
23. Srisuk, C.; Longyant, S.; Senapin, S.; Sithigorngul, P.; Chaivisuthangkura, P. Molecular cloning and characterization of a Toll receptor gene from *Macrobrachium rosenbergii*. *Fish Shellfish Immunol.* **2014**, *36*, 552–562. [CrossRef]
24. Shi, Y.R. Study on Sequences Analysis and Function of IMD and Relish in IMD Signal Pathway in *Macrobrachium rosenbergii*. Master's Thesis, Nanjing Normal University, Nanjing, China, 2016.
25. Fishery Bureau of Ministry of Agriculture of the People's Republic of China. *China Fishery Statistics Yearbook 2021*; China Agriculture Press: Beijing, China, 2021.
26. Paul, P.; Rahman, M.A.; Mer, M.; Hossain, M.; Islam, M.S.; Mondal, S.; Haq, M.M. Effect of stocking density on the growth and production of freshwater prawn (*Macrobrachium rosenbergii*). *Int. J. Fish. Aquac. Sci.* **2016**, *6*, 77–86.

27. Lu, K.L.; Xu, W.N.; Li, J.Y.; Li, X.F.; Huang, G.Q.; Liu, W.B. Alterations of liver histology and blood biochemistry in blunt snout bream *Megalobrama amblycephala* fed high-fat diets. *Fish. Sci.* **2013**, *79*, 661–671. [CrossRef]
28. Wangari, M.R.; Gao, Q.; Sun, C.; Liu, B.; Song, C.; Tadese, D.A.; Zhou, Q.; Zhang, H.; Liu, B. Effect of dietary *Clostridium butyricum* and different feeding patterns on growth performance, antioxidant and immune capacity in freshwater prawn (*Macrobrachium rosenbergii*). *Aquac. Res.* **2021**, *52*, 12–22. [CrossRef]
29. Dong, Y.Z.; Xia, T.; Lin, J.B.; Wang, L.; Song, K.; Zhang, C.X. Quercetin attenuates high-fat diet-induced excessive fat deposition of spotted seabass (*Lateolabrax maculatus*) through the regulatory for mitochondria and endoplasmic reticulum. *Front. Mar. Sci.* **2021**, *8*, 746811. [CrossRef]
30. Yin, P.; Xie, S.; Zhuang, Z.; He, X.; Tang, X.; Tian, L.; Liu, Y.; Niu, J. Dietary supplementation of bile acid attenuate adverse effects of high-fat diet on growth performance, antioxidant ability, lipid accumulation and intestinal health in juvenile largemouth bass (*Micropterus salmoides*). *Aquaculture* **2021**, *531*, 735864. [CrossRef]
31. Zhou, W.; Rahimnejad, S.; Lu, K.; Wang, L.; Liu, W. Effects of berberine on growth, liver histology, and expression of lipid-related genes in blunt snout bream (*Megalobrama amblycephala*) fed high-fat diets. *Fish Physiol. Biochem.* **2019**, *45*, 83–91. [CrossRef]
32. Limbu, S.M.; Ma, Q.; Zhang, M.L.; Du, Z.Y. High fat diet worsens the adverse effects of antibiotic on intestinal health in juvenile Nile tilapia (*Oreochromis niloticus*). *Sci. Total Environ.* **2019**, *680*, 169–180. [CrossRef]
33. Sink, T.D.; Lochmann, R.T.; Goodwin, A.E.; Marecaux, E. Mortality rates in golden shiners fed high-fat diets with or without a dairy-yeast prebiotic before challenge with *Flavobacterium columnare*. *N. Am. J. Aquac.* **2007**, *69*, 305–308. [CrossRef]
34. Cao, X.F.; Dai, Y.J.; Liu, M.Y.; Yuan, X.Y.; Wang, C.C.; Huang, Y.Y.; Liu, W.B.; Jiang, G.Z. High-fat diet induces aberrant hepatic lipid secretion in blunt snout bream by activating endoplasmic reticulum stress-associated IRE1/XBP1 pathway. *Biochim. Biophys. Acta Mol. Cell Biol. Lipids* **2019**, *1864*, 213–223. [CrossRef] [PubMed]
35. Qiang, J.; Wasipe, A.; He, J.; Tao, Y.F.; Xu, P.; Bao, J.W.; Chen, D.J.; Zhu, J.H. Dietary vitamin E deficiency inhibits fat metabolism, antioxidant capacity, and immune regulation of inflammatory response in genetically improved farmed tilapia (GIFT, *Oreochromis niloticus*) fingerlings following *Streptococcus iniae* infection. *Fish Shellfish Immunol.* **2019**, *92*, 395–404. [CrossRef] [PubMed]
36. Liu, G.; Yu, H.; Wang, C.; Li, P.; Liu, S.; Zhang, X.; Zhang, C.; Qi, M.; Ji, H. Nano-selenium supplements in high-fat diets relieve hepatopancreas injury and improve survival of grass carp *Ctenopharyngodon Idella* by reducing lipid deposition. *Aquaculture* **2021**, *538*, 736580. [CrossRef]
37. Li, J.; Liang, X.F.; Tan, Q.; Yuan, X.; Liu, L.; Zhou, Y.; Li, B. Effects of vitamin E on growth performance and antioxidant status in juvenile grass carp *Ctenopharyngodon idellus*. *Aquaculture* **2014**, *430*, 21–27. [CrossRef]
38. Lin, Y.H.; Shiau, S.Y. Dietary vitamin E requirement of grouper, *Epinephelus malabaricus*, at two lipid levels, and their effects on immune responses. *Aquaculture* **2005**, *248*, 235–244. [CrossRef]
39. Wang, L.; Xu, B.; Sagada, G.; Ng, W.K.; Chen, K.; Zhang, J.; Shao, Q. Dietary berberine regulates lipid metabolism in muscle and liver of black sea bream (*Acanthopagrus schlegelii*) fed normal or high-lipid diets. *Br. J. Nutr.* **2021**, *125*, 481–493. [CrossRef]
40. Liu, C.; Liao, J.Z.; Li, P.Y. Traditional Chinese herbal extracts inducing autophagy as a novel approach in therapy of nonalcoholic fatty liver disease. *World J. Gastroenterol.* **2017**, *23*, 1964–1973. [CrossRef]
41. Ling, S.C.; Wu, K.; Zhang, D.G.; Luo, Z. Endoplasmic reticulum stress-mediated autophagy and apoptosis alleviate dietary Fat-induced triglyceride accumulation in the intestine and in isolated intestinal epithelial cells of yellow catfish. *J. Nutr.* **2019**, *149*, 1732–1741. [CrossRef]
42. Uetake, Y.; Ikeda, H.; Irie, R.; Tejima, K.; Matsui, H.; Ogura, S.; Wang, H.; Mu, S.; Hirohama, D.; Ando, K.; et al. High-salt in addition to high-fat diet may enhance inflammation and fibrosis in liver steatosis induced by oxidative stress and dyslipidemia in mice. *Lipids Health Dis.* **2015**, *14*, 6. [CrossRef]
43. Sarna, L.K.; Sid, V.; Wang, P.; Siow, Y.L.; House, J.D.; Karmin, O. Tyrosol attenuates high fat diet-induced hepatic oxidative stress: Potential involvement of cystathionine β-synthase and cystathionine γ-lyase. *Lipids* **2016**, *51*, 583–590. [CrossRef]
44. Rasool, M.; Malik, A.; Saleem, S.; Ashraf, M.A.B.; Khan, A.Q.; Waquar, S.; Zahid, A.; Shaheen, S.; Abu-Elmagd, M.; Gauthaman, K.; et al. Role of oxidative stress and the identification of biomarkers associated with thyroid dysfunction in schizophrenics. *Front. Pharmacol.* **2021**, *12*, 646287. [CrossRef] [PubMed]
45. Kaur, S.; Bansal, M.P. Protective role of dietary-supplemented selenium and vitamin E in heat-induced apoptosis and oxidative stress in mice testes. *Andrologia* **2015**, *47*, 1109–1119. [CrossRef] [PubMed]
46. Khorramabadi, K.M.; Talebi, A.R.; Sarcheshmeh, A.A.; Mirjalili, A. Protective effect of vitamin E on oxidative stress and sperm apoptosis in diabetic mice. *Int. J. Reprod. Biomed.* **2019**, *17*, 127–134. [CrossRef] [PubMed]
47. Zhao, Y.; Zhang, W.; Jia, Q.; Feng, Z.; Guo, J.; Han, X.; Liu, Y.; Shang, H.; Wang, Y.; Liu, W.J. High dose vitamin E attenuates diabetic nephropathy via alleviation of autophagic stress. *Front. Physiol.* **2019**, *10*, 1939. [CrossRef] [PubMed]
48. Asrullah, M.; Arsanti Lestari, L.; Helmyati, S.; Farmawati, A. Effect supplementation of mung bean sprouts (*Phaseolus radiatus* L.) and vitamin E in rats fed high fat diet. *KnE Life Sci.* **2019**, *4*, 36–46. [CrossRef]
49. Xie, S.; Yin, P.; Tian, L.; Yu, Y.; Liu, Y.; Niu, J. Dietary supplementation of astaxanthin improved the growth performance, antioxidant ability and immune response of juvenile largemouth bass (*Micropterus salmoides*) fed high-fat diet. *Mar. Drugs* **2020**, *18*, 642. [CrossRef] [PubMed]
50. Cheng, C.H.; Guo, Z.X.; Wang, A.L. Growth performance and protective effect of vitamin E on oxidative stress pufferfish (Takifugu obscurus) following by ammonia stress. *Fish Physiol. Biochem.* **2018**, *44*, 735–745. [CrossRef] [PubMed]

51. Gao, J.; Koshio, S.; Ishikawa, M.; Yokoyama, S.; Mamauag, R.E.P.; Han, Y. Effects of dietary oxidized fish oil with vitamin E supplementation on growth performance and reduction of lipid peroxidation in tissues and blood of red sea bream *Pagrus major*. *Aquaculture* **2012**, *356–357*, 73–79. [CrossRef]
52. Sun, C.; Liu, B.; Zhou, Q.; Xiong, Z.; Shan, F.; Zhang, H. Response of *Macrobrachium rosenbergii* to vegetable oils replacing dietary fish oil: Insights from antioxidant defense. *Front. Physiol.* **2020**, *11*, 218. [CrossRef]
53. Belavgeni, A.; Dailianis, S. The role of phosphatidylinositol-3-OH-kinase (PI3-kinase) and respiratory burst enzymes in the [omim][BF4]-mediated toxic mode of action in mussel hemocytes. *Fish Shellfish Immunol.* **2017**, *68*, 144–153. [CrossRef]
54. Duan, Y.; Dong, H.; Wang, Y.; Li, H.; Liu, Q.; Zhang, Y.; Zhang, J. Intestine oxidative stress and immune response to sulfide stress in Pacific white shrimp *Litopenaeus vannamei*. *Fish Shellfish Immunol.* **2017**, *63*, 201–207. [CrossRef] [PubMed]
55. Carocho, M.; Ferreira, I.C.F.R. A review on antioxidants, prooxidants and related controversy: Natural and synthetic compounds, screening and analysis methodologies and future perspectives. *Food Chem. Toxicol.* **2013**, *51*, 15–25. [CrossRef] [PubMed]
56. Pautz, A.; Art, J.; Hahn, S.; Nowag, S.; Voss, C.; Kleinert, H. Regulation of the expression of inducible nitric oxide synthase. *Nitric Oxide Biol. Chem.* **2010**, *23*, 75–93. [CrossRef]
57. Shi, Y.R.; Jin, M.; Ma, F.T.; Huang, Y.; Huang, X.; Feng, J.L.; Zhao, L.L.; Chen, Y.H.; Ren, Q. Involvement of relish gene from *Macrobrachium rosenbergii* in the expression of anti-microbial peptides. *Dev. Comp. Immunol.* **2015**, *52*, 236–244. [CrossRef] [PubMed]
58. Zhao, W.; Yan, Y.; Xiao, Z.; Wang, M.; Xu, M.; Wang, Z.; Wang, Y.; Zhuang, Z.; Yang, D.; Chen, G.; et al. Bicyclol ameliorates nonalcoholic fatty liver disease in mice via inhibiting MAPKs and NF-κB signaling pathways. *Biomed. Pharmacother.* **2021**, *141*, 111874. [CrossRef]
59. Liu, P.; Wu, P.; Yang, B.; Wang, T.; Li, J.; Song, X.; Sun, W. Kaempferol prevents the progression from simple steatosis to non-alcoholic steatohepatitis by inhibiting the NF-κB pathway in oleic acid-induced HepG2 cells and high-fat diet-induced rats. *J. Funct. Foods* **2021**, *85*, 104655. [CrossRef]

antioxidants

MDPI

Article

Water Hardness Can Reduce the Accumulation and Oxidative Stress of Zinc in Goldfish, *Carassius auratus*

Cheol Young Choi [1,*], Zhongze Li [1], Jin Ah Song [2] and Young-Su Park [3]

[1] Division of Marine BioScience, Korea Maritime and Ocean University, Busan 49112, Korea; lzzz@g.kmou.ac.kr
[2] Marine Bio-Resources Research Unit, Korea Institute of Ocean Science and Technology, Busan 49111, Korea; jinah@kiost.ac.kr
[3] Department of Nursing, Catholic University of Pusan, Busan 46252, Korea; yspark@cup.ac.kr
* Correspondence: choic@kmou.ac.kr

Abstract: We investigated the changes in toxicity stress in goldfish, *Carassius auratus*, under exposure to different concentrations of Zn and water hardness for 14 days. We analyzed the changes in water hardness and Zn accumulation after exposure. To investigate the stress levels, the expression of metallothionein, caspase-3 activity, NO activity, and total antioxidant capacity were detected. Terminal deoxynucleotidyl transferase dUTP nick end labeling (TUNEL) assays were also performed to measure apoptosis in the liver. The results showed that compared to the control group, a more significant difference in the accumulation of Zn in body stress markers (metallothionein, caspase-3 activity, NO activity, and total antioxidant capacity) were observed with increasing Zn concentration and exposure time. Notably, at the same Zn concentration and exposure time, lower stress levels were discovered in the samples under harder water conditions. Finally, the TUNEL assay showed that Zn accumulation caused apoptosis and high water hardness could reduce the apoptosis. In conclusion, we found that high water hardness can influence the absorption of Zn, and alleviating the hardness levels can reduce the toxicity stress caused by Zn.

Keywords: antioxidant; apoptosis; goldfish; toxicity stress; water hardness; zinc

Citation: Choi, C.Y.; Li, Z.; Song, J.A.; Park, Y.-S. Water Hardness Can Reduce the Accumulation and Oxidative Stress of Zinc in Goldfish, *Carassius auratus*. *Antioxidants* **2022**, *11*, 715. https://doi.org/10.3390/antiox11040715

Academic Editors: Bo Liu, Changyou Song and Cunxin Sun

Received: 20 February 2022
Accepted: 2 April 2022
Published: 5 April 2022

Publisher's Note: MDPI stays neutral with regard to jurisdictional claims in published maps and institutional affiliations.

1. Introduction

Industrialization has led to the occurrence of various pollutants, as industrial wastes containing high concentrations of heavy metals are discharged into the aquatic ecosystem, increasing their concentrations in the environment [1,2]. Pollution caused by heavy metals has been a concern for several decades. Most aquatic organisms are directly or indirectly affected by the chemical composition of water [3]. Moreover, most heavy metals, including essential and non-essential elements, are not biodegradable and accumulate in the fish body because of their long biological half-life [4]. Bioaccumulated heavy metals act as stressors to aquatic organisms and inhibit the synthesis of proteins and nucleic acids, causing various metabolic, biochemical, physiological, and histological changes [5,6].

Among various heavy metals, Zn is an essential trace element in the body for the synthesis of cellular enzymes [7]. However, when fish are exposed to high concentrations of Zn, toxic responses, such as the destruction of various protein structures, are induced in their bodies [8,9]. According to a previous study [10], the concentration of Zn increased to a high level around the world from the 1970s (0.23 ± 0.47 mg/L) to the 2010s (0.48 ± 1.38 mg/L). Excess heavy metals may release reactive oxygen species (ROS) and reactive nitrogen species (RNS), leading to oxidative stress [11]. In particular, representative ROS include H_2O_2, OH-, and O_2- while RNS include NO and NO_2 [12]. When the concentrations of ROS and RNS are high in the body, peroxidation of proteins, lipids, and nucleic acids occurs and sometimes apoptosis is induced [12].

When an organism is poisoned with heavy metals, including Zn, metallothionein (MT) is activated in the body as a detoxification mechanism. MT serves to offset the

toxicity of heavy metals by combining with various heavy metals, such as copper, Zn, and Hg [13,14]. Additionally, MT plays a role in inducing an antioxidant response to remove excess ROS [15]. The antioxidant response mainly occurs in the liver, and the ROS that is not removed through the antioxidant response process is known to cause inflammation. Typical examples of genes causing inflammation include nitric oxide synthase (iNOS) and cyclooxygenase-2 (COX-2) [16,17]. When a fish is exposed to a toxic environment, the expression of iNOS, which is involved in NO production, is induced in the fish body. Nitric oxide (NO) is a representative oxidative substance. The excessive production of iNOS causes apoptosis by promoting oxidation of cells and excessive induction of NO [18]. Enzymes involved in apoptosis include caspase (cysteinyl aspartate-specific proteinase), of which, caspase-3 plays a role as an enzyme that catalyzes cell protein degradation and apoptosis [19].

The water quality of an aquatic environment, determined by parameters, including pH, water temperature, oxygen content, and hardness, is very important for the survival of aquatic organisms [20]. Among these indicators, hardness can be defined by the amount of polyvalent cations but most often by the concentration of Ca^{2+} and Mg^{2+}, which are commonly present in the natural environment [21]. Therefore, hardness can generally be measured by the concentration of $CaCO_3$ in water. Usually, water containing 0−90 mg/L $CaCO_3$ is considered soft water, 90−350 mg/L as hard water, and >350 mg/L as very hard water. A previous study [22] reported that water hardness had an effect on the metabolic activity of the South American catfish, *Rhamdia quelen*. Another study [23] showed that the growth rate of the common snook, *Centropomus undecimalis*, was the highest in the test group containing water with 100 mg/L $CaCO_3$ hardness. Furthermore, a study on the degree of acute toxicity through the survival rate of fish exposed to various heavy metals reported that the higher the water hardness, the higher the lethal concentration (LC50) for heavy metals [24]. These results suggest that the toxicity of heavy metals can be inhibited by increasing the water hardness. A study by Baldisserotto [20] reported that Ca^{2+} inhibits the absorption of heavy metals by reducing the penetration of heavy metals into the gills. Alsop [25] reported that the amount of Zn^{2+} dissolved in water decreased as the hardness increased when $ZnSO_4$ was added to the hardness test plots of various concentrations.

Generally, compared to seawater, fresh water has low ionic strength, which increases the saturation concentration of external pollutants, and thus, increases the risk of heavy metal (such as Zn) contamination [26].

Therefore, the possibility of reducing toxic stress in fish must be investigated by controlling the water hardness caused by Zn.

In our study, we selected a species of goldfish, *Carassius auratus*, which is a freshwater fish mainly used for toxicity evaluation due to its low sensitivity to toxic substances, and exposed it to various concentrations of Zn and water hardness, to determine the stress factors and the degree of apoptosis. According to a previous study [27], the water hardness in Korea river is around 50~90 mg/L, which is soft water and the hardness can thus be increased. In addition, we analyzed the effects of these two parameters (Zn concentration and hardness) on the physiological response of goldfish to examine the extent to which hardness reduces the toxicity of Zn.

2. Materials and Methods

2.1. Experimental Fish

Goldfish, *C. auratus* (n = 384, body length 6.8 ± 0.8 cm, and mass 12.4 ± 2.1 g), were purchased from Choryang aquarium (Busan, Korea), acclimatized for 1 week, and divided into control and experimental groups. They were maintained in tanks filled with 300 L of fresh water in the laboratory (16 fish per tank). Four fishes from each replicate treatment group were randomly sampled at each time period. All experimental conditions had two replicates to ensure consistency. The freshwater temperature was maintained at 19.5 ± 1 °C with aeration and the feeding was stopped 24 h before the experiment. We used these vertebrates (goldfish) according to the animal study protocol approved by the Institutional

Animal Care and Use Committee of Korea Maritime and Ocean University (Approved protocol no # KMOU IACUC 2022-02).

2.2. Zn and Water Hardness Treatment and Sampling

Goldfish in the experiment were exposed to Zn ($ZnSO_4$, 83265, Sigma, St. Louis, MO, USA) concentrations of 0, 0.5, 1, and 3 mg/L and water hardness by adding $CaCO_3$ (239216, Sigma, St. Louis, MO, USA). The concentration of Zn was set according to previous studies [8,28], which showed that a Zn concentration higher than 6.0 mg/L could lead to the death of the goldfish while 1.0 mg/L of Zn could cause oxidative stress. The control group for the water hardness was 90 mg/L $CaCO_3$, according to the hardness value of running water in Busan, Korea detected using a water hardness pure water meter (PWH-303, Lutron, China). We considered 3 conditions of water hardness: soft water (S) (90 mg/L of $CaCO_3$), hard water (H) (270 mg/L of $CaCO_3$), and very hard water (V) (450 mg/L of $CaCO_3$). For convenience, the experimental groups were named as follows according to the concentration of Zn (in brackets): in the soft water (S) group: Zn 0 + S (0 mg/L, control) Zn 0.5 + S (0.5 mg/L), Zn 0.5+ S (1.0 mg/L), and Zn 3.0 + S (3.0 mg/L); in the hard water (H) group: Zn 0 + H (0 mg/L), Zn 0.5 + H (0.5 mg/L), Zn 0.5+ H (1.0 mg/L), and Zn 3.0 + H (3.0 mg/L); and in the very hard water (V) group: Zn 0 + V (0 mg/L), Zn 0.5 + V (0.5 mg/L), Zn 0.5+ V (1.0 mg/L), and Zn 3.0 + V (3.0 mg/L). During this time, water hardness was detected and recorded daily. Before sampling, all the fish were anesthetized using clove oil (C8392, Sigma, St. Louis, MO, USA). Blood was collected rapidly from the caudal vein using a 1 mL syringe coated with heparin. Plasma samples were separated by centrifugation (4 °C at 12,000 × *g* for 12 min). Prior to analysis, the samples were stored at −80 °C and part of the liver samples was stored at 18–20 °C in 10% formalin. During the experiment, the mortality rate was 0% in all experiment groups.

2.3. Zn Accumulation in Fish Body

The fish were added to 60% NO and 2% of NO with 5 ppm of Au and decomposed at 100–150 °C for more than 12 h. Then, the mixture was filtered using Whatman No. 4 (WHA1004125, Sigma, St. Louis, MO, USA) filter paper and diluted using 2% nitric acid to a final volume of 50 mL. All samples were detected using an optical emission spectrometer (ICP-OES; Optima 2000DV, Perkin Elmer, Waltham, MA, USA) at an absorbance of 213.856 nm.

2.4. Expression of the Metallothionein Gene and iNOS mRNA

Total RNA was extracted from the liver using TRI Reagent® (TR188, Molecular Research Center, Inc., Cincinnati, OH, USA), according to the manufacturer's instructions. The purity of all the RNA samples was determined by the ratio of their absorbance at 260 and 280 nm (A260/A280), which was confirmed to be between 1.8 and 2.0. Total RNA (2 µg) was reverse-transcribed to complementary DNA (cDNA) using an oligo-(dT)15 anchor and M-MLV reverse transcriptase (RT0015, Takara, Japan) according to the manufacturer's protocol. All the synthesized cDNA was diluted by 1:100 and stored at −20 °C. The relative expressions of MT, iNOS, and β-actin were measured by real-time quantitative polymerase chain reaction (qPCR). The qPCR primers were designed according to the known sequences at NCBI (Table 1). qPCR amplification was conducted by a Bio-Rad iCycler iQ multicolor real-time PCR detection system (Bio-Rad, USA), and the iQ SYBR green supermix (Bio-Rad, USA), according to the manufacturer's instructions. As an internal control, the experiments used β-actin (accession no. LC383464) after evaluation by Bestkeeper from 3 reference genes, including β-actin, GAPDH (accession no. KT985226.1), and ribosomal protein S18 (RPS18, accession no. XR_003291850.1). The highest correlation among them was used as the internal control gene. All data were expressed as changes with respect to the corresponding calculated β-actin cycle threshold (ΔCt) levels. The calibrated

ΔCt value (ΔΔCt) for each sample and internal control (β-actin) was calculated using the following equation:

$$\Delta\Delta Ct = 2^{-(\Delta Ct\ sample - \Delta Ct\ internal\ control)} \quad (1)$$

Table 1. Primers used for qPCR amplification.

Genes (Accession No.)	Forward Primer	Reverse Primer
Metallothionein (X97271.1)	5′-TTA ACT GTG CCA CCT GC-3′	5′-AGG AAT TGC CCT TAC ACA CG-3′
iNOS (AY904362.1)	5′-AAG TCG TTT GCA TGG AGG AC-3′	5′-GGT GTC TAA GGT TGT TCA GG-3′
β-actin (LC382464)	5′-TTC CCT TGC TCC TTC CAC CA-3′	5′-TGG AGC CAC CAA TCC AGA CA-3′

All the results for MT and iNOS mRNA in the target genes were the relative values between the target gene and internal control (β-actin).

2.5. NO Activity and Total Antioxidant Capacity (TAC) in Plasma and Caspase-3 Activity in Liver

The NO activity was measured by an assay kit (BM-NIT-200 BIOMAX Inc, Seoul, Korea) according to the manufacturer's protocol and the absorbance was measured at 450 nm. The assay kit can detect both NO_2- and NO_3- to calculate the total activity of NO, which is one species of RNS. TAC was measured using an assay kit (BM-TAC-200 BIOMAX Inc, Seoul, Korea) according to the manufacturer's protocol and the absorbance was measured at 540 nm. TAC was measured based on the Trolox equivalent antioxidant capacity and the assay is based on the reduction of copper (II) to copper (I) by antioxidants, which reflects the level of ROS. The caspase-3 activity in the liver was detected using an enzyme-linked immunosorbert assay kit (MBS012786, Mybiosource Inc., San Diego, CA, USA) according to the manufacturer's protocol.

2.6. MT mRNA In Situ Hybridization

The MT sequence for the in situ hybridization probe was designed for the forward primer 5′-ATG GAT CCC TGC GAT TGC GC-3′ and reverse primer 5′-TCA TTG ACA GCA GCT GGA GC-3′ (Accession no. X9727.1), amplified using PCR, and ligated to a pGEM-T easy vector (A137A, Promega, Madison, WI, USA). Furthermore, the anti-sense was confirmed by sequencing, and plasmid DNA was amplified using PCR, with the antisense and T7 primer (5′-TAA TAC GAC TCA CTA TAG GG-3′). Digoxigenin (DIG)-labeled probes were created using a DIG RNA Labeling Mix (Merck, Darmstadt, Germany) and the PCR products using the anti-sense primer and T7 RNA polymerase were used as the antisense labeling probes.

The liver tissue of the groups (control, Zn 3.0 + S, Zn 3.0 + H, and Zn 3.0 + V) exposed for 7 days were stored in 4% paraformaldehyde (PFA) and in 30% sucrose to prevent frostbite before sectioning. Sections were hybridized with hybridization buffer (containing 5 mL of deionized formamide, 2.5 mL of 20× saline sodium citrate (SSC), 100 μL of 0.1% Tween-20, 92 μL of 1 M citric acid (pH 6.0), and DEPC-H_2O up to a total volume of 20 mL), spiked with yeast total RNA (50 μL) and the RNA probe, and kept overnight at 65 °C.

For hybridization signal detection, tissue sections were first incubated with a blocking solution (10% calf serum in 1× PBS containing 0.1% Tween 20 (PBST)) for 1 h at 20 °C, followed by overnight incubation at 4 °C with an alkaline phosphatase-conjugated anti-digoxigenin antibody (1:2000 in blocking solution; Roche, Basel, Switzerland). After a series of washing steps (6 times for 15 min each, in PBST at room temperature) and rinsing in alkaline Tris buffer, consisting of 1 M Tris at pH 9.5, 1 M $MgCl_2$, 5 M NaCl, and 10% Tween-20 (3 times for 5 min each at room temperature), color imaging was performed using a labeling mix (1 mL of alkaline Tris buffer, 4.5 μL of nitroblue tetrazolium, and 3.5 μL of 5-bromo-4-chloro-3-indolyl phosphate disodium salt), which was sprayed over the sections.

Then, the sections were kept in a dark and humid chamber for at least 8 h to develop color. The slides were washed with PBST, fixed with 4% PFA for 1 h, mounted with Aquamount (Aqua Polymount, Warrington, PA, USA), and covered with a slip. A stereomicroscope (Eclipse Ci, Nikon, Tokyo, Japan) was used to capture the images.

2.7. Terminal Transferase dUTP Nick End Labeling (TUNEL) Assay

A TUNEL assay was performed on the Zn 3.0 S, Zn 3.0 H, and Zn 3.0 V groups on day 14. Samples of liver were washed and fixed in 10% formalin using an ApopTag® Peroxidase In Situ Apoptosis Detection Kit (S7100, Sigma, St. Louis, MO, USA) following the manufacturer's specifications. Finally, all the slides were observed using an optical microscope (Eclipse Ci). Brown cells that could be observed indicated apoptosis.

2.8. Statistical Analysis

All data were analyzed using SPSS version 25.0 (IBM SPSS Inc., Armonk, NY, USA). For all parameters analyzed, a three-way ANOVA followed by Tukey's post-hoc test was performed to compare the differences among the different Zn concentrations, water hardness levels, and exposure times of the samples, and the effects of the interaction among the three factors are shown in Table 2. The significance level was set higher than 95% ($p < 0.05$). The measured values are expressed as the means ± standard deviations (SDs).

Table 2. Interaction effects of Zn concentration and water hardness.

Time		Accumulation	MT	iNOS	NO	TAC	Caspase-3
Day 0	F	0.002	0.000	0.000	0.000	0.000	0.000
	p	0.998	1.000	1.000	1.000	1.000	1.000
Day 3	F	4.256	2.658	9.661	3.225	1.985	2.065
	p	0.045 *	0.084	0.010 *	0.052	0.152	0.149
Day 7	F	5.226	15.68	16.52	2.226	2.336	4.658
	p	0.032 *	0.002*	0.002 *	0.068	0.114	0.041 *
Day 14	F	29.28	28.10	5.662	9.658	3.521	7.632
	p	<0.001 *	<0.001 *	0.030 *	0.010 *	0.050 *	0.024 *

The symbol "*" indicates a significant difference.

3. Results

3.1. Changes in Water Hardness

No significant changes were observed in the hardness levels of the water with increasing exposure times in the experiment. After measuring the water hardness daily, we found that the soft water, hard water, and very hard water groups at various Zn concentrations retained the water hardness levels of approximately 90, 270, and 450 mg/L $CaCO_3$, respectively.

3.2. Changes in Zn Accumulation in Fish

Zn accumulation was significantly affected by the exposure time, Zn concentration, water hardness, and all their interactions (Table 2). An increase in Zn accumulation occurred in the fish body after they were exposed to Zn (Table 3). The Zn 3.0 group showed a significantly higher accumulation than the other groups. After 14 days, the accumulation of Zn reached the highest level. Zn 3.0 + S reached 113.53 ppm, which was almost 300% of the value after 3 days of exposure. However, on day 14, the same Zn concentration groups, at higher water hardness levels, showed a significant decrease in Zn accumulation, with 90.07 (299% of Zn 0 + H) and 60.96 (249% of Zn 0+ V) ppm for Zn 3.0 + H and Zn 3.0 + V, respectively.

Table 3. Zinc accumulation in the fish body (ppm).

Time	Hardness	Zn 0	Zn 0.5	Zn 1.0	Zn 3.0
Day 0	Soft	22.10 ± 1.54^{a1}	21.91 ± 0.98^{a1}	21.54 ± 1.66^{a1}	22.10 ± 1.55^{a1}
	Hard	22.00 ± 1.01^{a1}	23.05 ± 1.39^{a1}	21.80 ± 1.26^{a1}	21.75 ± 1.65^{a1}
	Very hard	23.10 ± 1.18^{a1}	22.65 ± 1.25^{a1}	22.56 ± 0.99^{a1}	22.25 ± 1.54^{a1}
Day 3	Soft	22.18 ± 1.49^{a1}	32.22 ± 2.22^{b2}	$37.18 \pm 2.21^{b2**}$	$40.22 \pm 2.69^{b2**}$
	Hard	23.28 ± 1.95^{a1}	29.09 ± 1.96^{b2}	30.87 ± 1.96^{b2}	$34.45 \pm 2.26^{b3*}$
	Very hard	23.79 ± 1.89^{a1}	28.58 ± 2.01^{b2}	28.91 ± 1.55^{b2}	29.09 ± 1.14^{b2}
Day 7	Soft	24.18 ± 1.22^{a1}	$41.27 \pm 2.14^{c2**}$	$48.57 \pm 2.15^{c3*}$	$57.39 \pm 3.00^{c4**}$
	Hard	23.99 ± 1.36^{a1}	$36.15 \pm 1.54^{c2*}$	$48.48 \pm 2.44^{c3*}$	$49.60 \pm 2.54^{c3*}$
	Very hard	23.14 ± 0.78^{a1}	$33.12 \pm 1.33^{c2\alpha}$	41.88 ± 2.01^{c3}	40.33 ± 1.96^{c3}
Day 14	Soft	23.47 ± 0.95^{a1}	$45.33 \pm 1.92^{d2**}$	$69.05 \pm 3.24^{d3**}$	$113.53 \pm 5.94^{d4**}$
	Hard	$30.12 \pm 1.12^{b1*}$	$40.97 \pm 2.01^{d2*}$	$54.54 \pm 2.94^{d3*}$	$90.07 \pm 5.69^{d4*}$
	Very hard	24.48 ± 1.77^{a1}	35.96 ± 1.87^{c2}	47.59 ± 2.11^{d3}	60.96 ± 4.36^{d4}

Different letters indicate significant differences among goldfish exposed to the same Zn concentration and water hardness level. Different numbers indicate significant differences among goldfish exposed to different Zn concentrations at the same water hardness levels and for the same duration. The symbol "*" and "**" represent statistical significance ($p < 0.05$ and $p < 0.01$, respectively) among goldfish exposed to different water hardness levels at the same Zn concentration and for the same duration. Values are mean ± SD ($n = 4$).

3.3. Changes in MT mRNA Expression in the Liver

mRNA expression of the metallothionein gene was significantly affected by exposure time, Zn concentration, water hardness, and their interactions. The overall mRNA expression of the MT gene in the liver increased with increasing Zn concentration and exposure duration at the same water hardness level (Figure 1). Notably, at the same Zn concentration and exposure duration but increasing water hardness levels, the MT mRNA expression decreased (on day 14, the expression for Zn 3.0 + S and Zn 3.0 + V were 1.79 ± 0.19, 325% of Zn 0 + S and 1.10 ± 0.09, 199% of Zn 0 + V, respectively). Furthermore, no significant difference was observed between all the control groups with different water hardness levels and no Zn (0.46 ± 0.05).

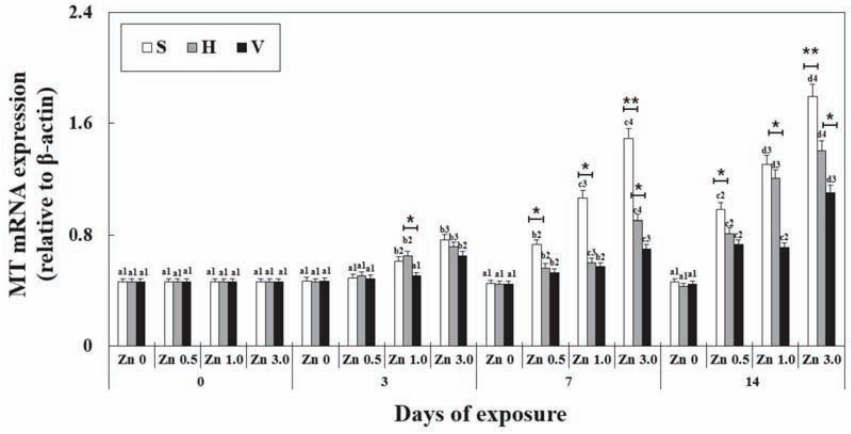

Figure 1. Changes in the mRNA expression of the metallothionein gene measured for 14 days. Different letters indicate significant differences among goldfish exposed to the same Zn concentration and water hardness. Different numbers indicate significant differences among goldfish exposed to different Zn concentrations at the same water hardness level and for the same duration. The symbol "*" and "**" represent statistical significance ($p < 0.05$ and $p < 0.01$, respectively) among goldfish exposed to different water hardness levels at the same Zn concentration and for the same duration. Values are mean ± SD ($n = 4$).

3.4. MT mRNA Expression in Liver Using In Situ Hybridization

The mRNA expression of the metallothionein gene in liver was detected by in situ hybridization (Figure 2). In the figure, the dark area (black arrow) indicates the MT mRNA expression in the cytoplasm. The control showed no signal while the Zn-exposed groups expressed MT mRNA. Moreover, Zn 3.0 + S showed more signal than Zn 3.0 + H and Zn 3.0 +V, and the signal in Zn 3.0 + V was less than Zn 3.0 + H.

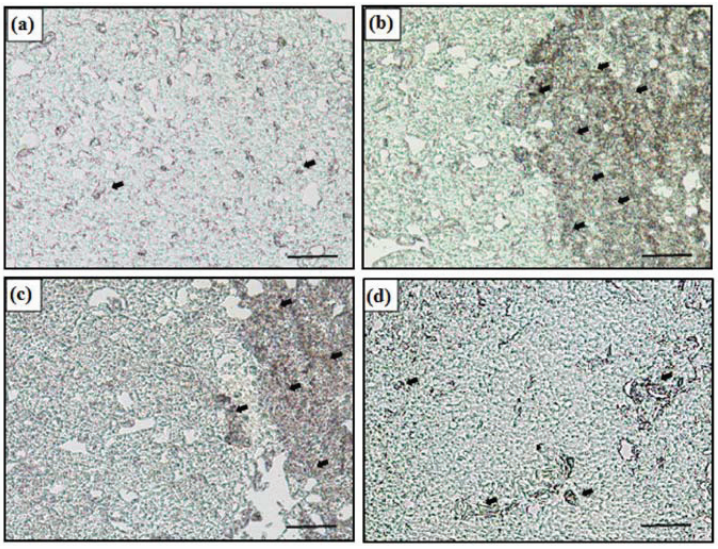

Figure 2. In situ hybridization of control and Zn 3.0 in 7 days. (**a**) Control, (**b**) Zn 3.0 + S, (**c**) Zn 3.0 + H, and (**d**) Zn 3.0 + V. The dark area (black arrow) indicates the mRNA expression of the metallothionein gene in the liver (Scale bars = 200 μm).

3.5. Changes in iNOS mRNA Expression in the Liver

iNOS mRNA expression was significantly affected by exposure time, Zn concentration, water hardness, and their interactions (Table 2). The changes in iNOS mRNA expression in the liver showed a similar tendency to MT (Figure 3). After 7 days in Zn 3.0 + S, the expression was 1.66 ± 0.2, which was 5 times that of the control (0.3 ± 0.04) at the same exposure time. At the same Zn concentration and exposure time, the increasing hardness of water decreased iNOS mRNA expression (2.02 ± 0.2 in Zn 3.0 + S, 578% of Zn 0 + S and 1.00 ± 0.1 in Zn 3.0 + V, 287% of Zn 0 + V on day 14). iNOS mRNA expression increased with the increasing concentration of Zn at the same water hardness environment and the same exposure duration.

3.6. Changes NO Activity and TAC in Plasma

NO activity and TAC were significantly affected by exposure time, Zn concentration, water hardness, and their interactions (Table 2). At the same water hardness level, the NO activity increased with the increase in exposure time and Zn concentration. An increase in the NO activity with time occurred in the soft water group, and reached the highest among all the experimental groups (129.23 ± 9.8 μM). However, in the hard water and very hard water groups, the increase in NO activity was slower than that in the soft water groups, and the activity even became constant in Zn 3.0 + V between day 7 (44.21 ± 5.6 μM) and 14 (50.12 ± 4.9 μM). The TAC increased similar to the NO activity but not as rapidly, with less significant differences compared to the NO activity (Figure 4). Similar to the other stress factors in the experiment, TAC in the Zn 3.0 + S group exhibited the highest value (840.0 ± 70.0 μM, 426% of Zn 0 + S on day 14).

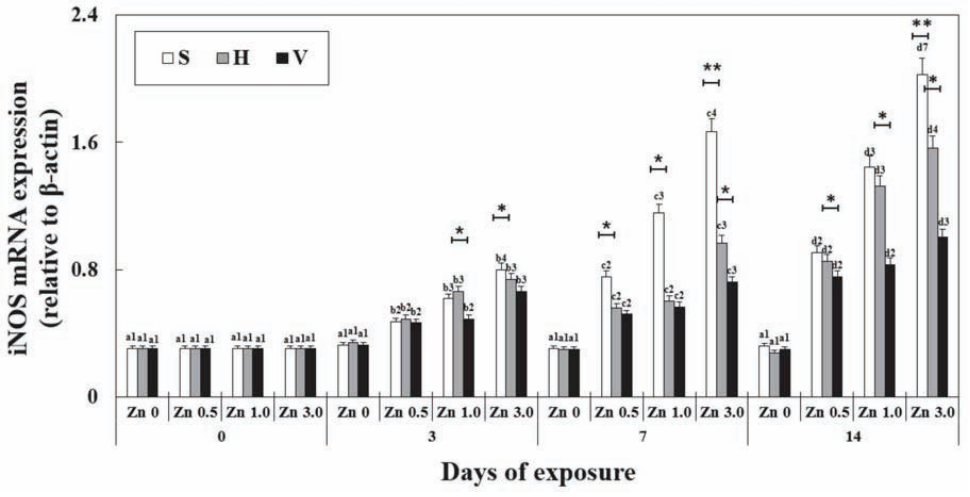

Figure 3. Changes in the mRNA expression of iNOS measured for 14 days. Different letters indicate significant differences among goldfish exposed to the same Zn concentration and water hardness for different exposure times ($p < 0.05$). Different numbers indicate significant differences among goldfish exposed to different Zn concentrations at the same water hardness level and for the same duration. The symbol "*" and "**" represent statistical significance ($p < 0.05$ and $p < 0.01$, respectively) among goldfish exposed to different water hardness levels at the same Zn concentration and for the same duration. Values are mean ± SD ($n = 4$).

3.7. Changes in Caspase-3 Activity in the Liver

The caspase-3 activity was significantly affected by the exposure duration, Zn concentration, water hardness, and their interactions (Table 2). A significant increase in caspase-3 activity in the liver was observed in the Zn-exposed groups from day 7 with the increase in the Zn concentration at the same water hardness level (Figure 5). On the 14th day, Zn 3.0 + S reached the highest expression among the groups in the experiment (42.12 ± 0.8 pmol/mL) and with the increase in the water hardness, the other groups showed a significant decrease in caspase-3 activity (37.22 ± 0.9 of Zn 3.0 + H, 88% of Zn 3.0 + S and 29.88 ± 1.0 of Zn 3.0 + V, 71 of Zn 3.0 + S). In all of the Zn 0 groups, no significant difference in caspase-3 activity occurred with the change in the water hardness levels.

3.8. TUNEL Assay

The results of the TUNEL assay are shown in Figure 6 and the brown cells indicate the presence of apoptotic cells (Figure 6a–d). After 14 days, the Zn-exposed groups showed significantly more apoptotic cells than the control (7.11 ± 0.6%), and Zn 3.0 + S (21.14 ± 1.6%) showed more apoptosis than any other group. According to the results for Zn 3.0 + H (14.22 ± 1.0%) and Zn 3.0 + V (9.9 ± 0.7%), the numbers of apoptotic cells decreased with the increase in the water hardness (Figure 6e).

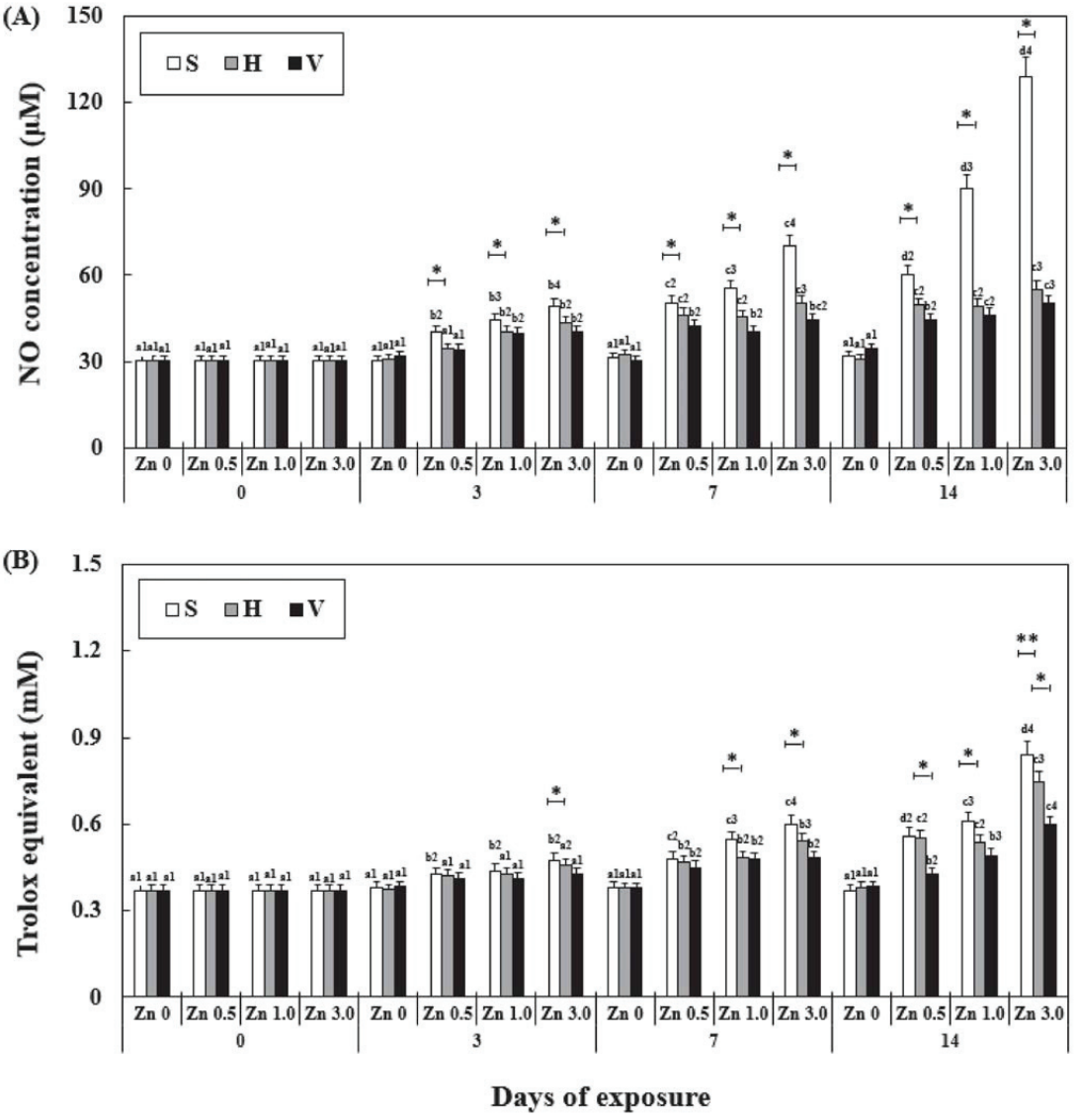

Figure 4. Changes in the NO (**A**) activity and TAC (**B**) measured for 14 days. Different letters indicate significant differences among goldfish exposed to the same Zn concentration and water hardness for different exposure times ($p < 0.05$). Different numbers indicate significant differences among goldfish exposed to different Zn concentrations at the same water hardness level and for the same duration. The symbol "*" and "**" represent statistical significance ($p < 0.05$ and $p < 0.01$, respectively) among goldfish exposed to different water hardness levels at the same Zn concentration and for the same duration. Values are mean ± SD ($n = 4$).

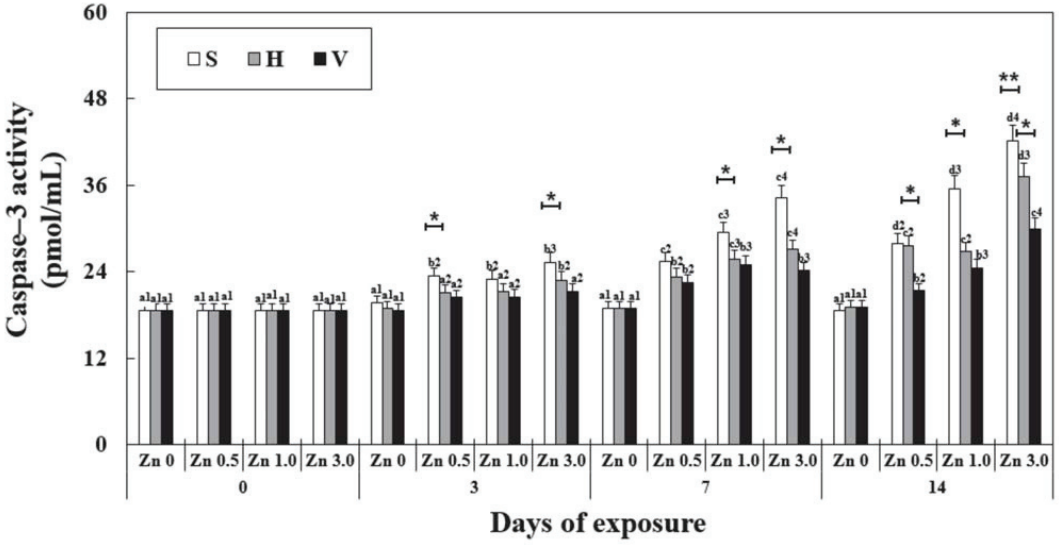

Figure 5. Changes in the activity of caspase-3 measured for 14 days. Different letters indicate significant differences among goldfish exposed to the same Zn concentration and water hardness for different exposure times ($p < 0.05$). Different numbers indicate significant differences among goldfish exposed to different Zn concentrations at the same water hardness level and for the same duration. The symbol "*" and "**" represent statistical significance ($p < 0.05$ and $p < 0.01$, respectively) among goldfish exposed to different water hardness levels at the same Zn concentration and for the same duration. Values are mean ± SD ($n = 4$).

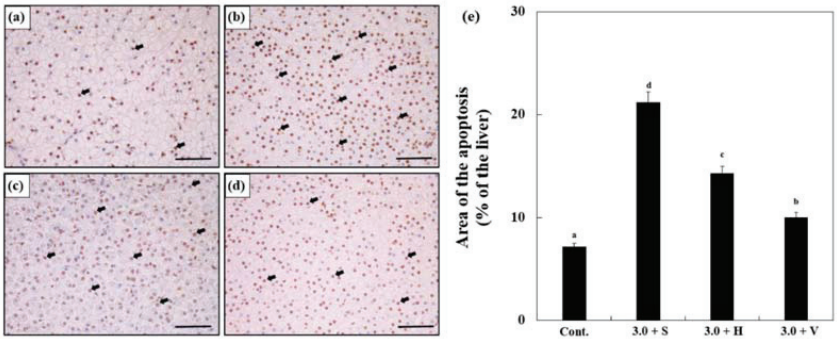

Figure 6. Images from a terminal deoxynucleotidyl transferase dUTP nick end labeling (TUNEL) assay using the liver cells of goldfish in the experiment for (**a**) control, (**b**) Zn 3.0 + S, (**c**) Zn 3.0 + H, and (**d**) Zn 3.0 + V. Brown cells indicate apoptotic cells. Scale bars = 200 μm. (**e**) Quantification of TUNEL assay images of the liver cells of goldfish exposed to different Zn concentrations and water hardness levels, which are indicated by the changes in the areas of apoptosis relative to the tissue area (%). Different letters indicate significant differences among goldfish exposed to different Zn concentrations and water hardness levels for the same duration. ($p < 0.05$). Values indicate means ± SD ($n = 4$).

4. Discussion

Although Zn is an essential trace element in the fish body, high concentrations of Zn cause histological abnormalities, such as epithelial cell proliferation, necrosis, and mucus secretion [29]. However, previous research has reported that the lethal concentration (LC_{50})

for the exposure of fish to heavy metals (including Zn) increased as the water hardness level increased [24]. Based on this finding, our research hypothesized that an increase in the water hardness could reduce the Zn toxicity stress generated in the body, and conducted a study to reveal this using the antioxidant measurement method.

Therefore, in this study, after exposing goldfish to various concentrations of Zn and various water hardness levels for 14 days, we aimed to determine whether water hardness affected the reduction in Zn toxicity by comparing the experimental groups.

During the entire experimental period, no significant changes were observed in the water hardness levels set at the beginning of the experiment. The results indicated that Ca^{2+} ions in the water did not decrease, and that Zn^{2+} ions did not significantly affect the change in the hardness of the water. However, the degree of Zn accumulation in the body increased as the exposure time elapsed with the increasing concentration of Zn. In contrast, as the water hardness increased, the degree of Zn accumulation in the body tended to decrease.

Alsop and Wood [25] reported that the concentration of Zn^{2+} dissolved in the water decreased as the hardness of water increased. Hogstrand et al. [30] reported that Ca^{2+} and Zn^{2+} absorbed into the body decreased in the experimental group injected with $CaCl_2$ as compared to the control injected with NaCl in rainbow trout, *Oncorhynchus mykiss*.

As these findings are similar to the results of this study, we inferred that in higher water hardness groups, the Ca^{2+} ions present in large amounts in water not only reduced the solubility of Zn but also reduced its degree of absorption as Zn^{2+} is absorbed via the same pathway as Ca^{2+} ions through the gills.

In addition, the expression levels of MT and iNOS mRNA could determine the degree of change in toxic stress in the goldfish body based on the hardness and Zn exposure levels. On comparing hardness and similar Zn exposure time periods, the expression of the metallothionein gene and iNOS mRNA tended to increase in the high-concentration Zn experimental groups. Moreover, in the same experimental groups with the same Zn concentration, the expression levels were observed to increase as the hardness of water decreased. Furthermore, at the same water hardness level, the expression of MT and iNOS mRNA increased as the Zn concentration increased. According to a study by Khodadoust and Ahmad [14], when medaka, *Oryzias javanicus*, was exposed to Cd, a higher concentration of Cd showed higher expression levels of MT mRNA. In addition, Khan et al. [31] reported that the expression of NOS increased as a result of exposure to various heavy metals present in batteries in a fish species, *Oreochromis niloticus*.

Consistent with the findings of previous studies, our study showed that the expression of the metallothionein gene and iNOS mRNA increased according to exposure to external heavy metals and toxic substances. Although Zn induced toxicity in the fish body, the toxic stress in the body was assumed to be reduced by Ca^{2+} ions by inhibiting the absorption of Zn into the body.

In addition, the in situ hybridization results visually confirmed the mRNA expression of the metallothionein gene within the liver tissue of goldfish and showed that MT was expressed in the liver cytoplasm, with the lowest MT mRNA expression observed in the experimental groups treated with very hard water at the same Zn concentration. Macirella et al. [32] reported that after exposing *Denio rerio* to two different concentrations of Hg, MT expression was confirmed by in situ hybridization. They [32] also found that that MT mRNA expression was higher at a higher concentration of Hg exposure than that in the control, which occurred to protect against oxidation, and denatured the cells of proteins due to the toxicity of heavy metals. This was consistent with the results of our study. Goldfish, when exposed to Zn, activated a cell-protecting mechanism by increasing MT to alleviate the toxicity caused by heavy metals. The expression of the metallothionein gene in the liver cytoplasm of goldfish may have reduced because the very hard water environment reduced the effect of toxicity on heavy metals.

In this study, the NO and TAC activities, which are representative oxidative stress indicators, were also measured to confirm the level of toxic substances that are generated in the body after exposure to various concentrations of Zn and hardness. We observed that

the NO and TAC activity values did not significantly change with the change in hardness in the Zn 0 experimental groups. However, as the exposure time increased, the NO and TAC activities increased, and we observed that the NO and TAC activities decreased as the hardness increased among the high Zn concentration groups, whereas the NO and TAC activities increased as the Zn concentration increased. A previous study reported that the activity of various antioxidant proteins in the body were inhibited when goldfish were exposed to Zn concentrations of 0.1 and 1.0 mg/L [9]. Romano et al. [33] reported that no significant change was observed in the growth rate and metabolic activity of largemouth bass, *Micropterus salmoides*, at concentrations of 50 L to 600 mg/L, that is, for soft water to very hard water.

Comparing the results of this study with those of the previous study [33], in the general freshwater environment without an additional supply of heavy metals, a change in the hardness value within 450 mg/L does not evidently have a significant effect on the stress response of the fish. In addition, under the water quality environment in which a 0.1 mg/L or higher concentration of Zn is present, Zn inhibited the antioxidant activity of *C. auratus* in vivo to increase the activity of RNS and ROS but suppressed Ca^{2+} ions in breeding water from being absorbed into the net. This consequently reduced the stress index of NO and TAC. To confirm the actual degree of apoptosis in the experimental section, caspase-3 activity was observed and a TUNEL assay was performed. Similar to the pattern of change in the previous stress indicators, the higher the Zn concentration, the higher the degree of caspase-3 activity and cell death. Zhao et al. [34] reported that exposing zebrafish *D. rerio* to 0–120 mg/L ZnO significantly increased the apoptosis in fish as the concentration of ZnO increased. Mo et al. [35] also reported that when HepG2 cells were exposed to Zn^{2+}, caspase-3 activity and apoptosis were increased via the increase in ROS in the cells.

Based on the previous studies, Zn may have induced the generation of free radicals, such as RNS and ROS, in the fish in this study, thereby increasing the degree of apoptosis. However, under the experimental conditions (hard and very hard water) with a high concentration of Ca^{2+} ions dissolved in water, the degree of caspase-3 activity and apoptosis decreased, and the higher the hardness, the higher the observed effect of apoptosis. Therefore, we conclude that a higher hardness level of water is effective in reducing the toxicological effect on Zn.

5. Conclusions

When goldfish were exposed to more than 0.1 mg/L of Zn, a toxic stress response was induced, but it was confirmed that this toxic stress was significantly reduced as the water hardness increased. Thus, we considered that Ca^{2+} ions in the water play an effective role in reducing heavy metals absorbed into the fish body.

Moreover, to reduce the toxic stress that fish may be subjected to when exposed to heavy metal-contaminated environments, the appropriate hardness environment for various fish species must be studied further. In addition, investigating whether other water quality environmental factors, such as water temperature and pH, can reduce heavy metal toxicity through the ion absorption pathway of fish is valuable in this context.

Author Contributions: Conceptualization, C.Y.C.; Writing—Original Draft, Supervision, Z.L.; Writing—Formal Analysis, Methodology, J.A.S.; Investigation, Data curation, Y.-S.P.; Review and Editing. All authors have read and agreed to the published version of the manuscript.

Funding: This research was supported by Korea Institute of Marine Science & Technology Promotion (Grant number 20170392).

Institutional Review Board Statement: The animal study protocol was approved by the Institutional Animal Care and Use Committee of Korea Maritime and Ocean University (Approved protocol no # KMOU IACUC 2022-02).

Informed Consent Statement: Not applicable.

Data Availability Statement: All relevant data are within the manuscript.

Conflicts of Interest: The authors declare no conflict of interest.

References

1. Luoma, S.N. Bioavailability of trace metals to aquatic organisms—A review. *Sci. Total. Environ.* **1983**, *28*, 1–22. [CrossRef]
2. Dane, H.; Sisman, T. A morpho-histopathological study in the digestive tract of three fish species influenced with heavy metal pollution. *Chemosphere* **2020**, *242*, 125212. [CrossRef]
3. Gillis, P.L.; Mitchell, R.J.; Schwalb, A.N.; McNichols, K.A.; Mackie, G.L.; Wood, C.M. Sensitivity of the glochidia (larvae) of freshwater mussels to copper: Assessing the effect of water hardness and dissolved organic carbon on the sensitivity of endangered species. *Aquat. Toxicol.* **2008**, *88*, 137–145. [CrossRef]
4. Kim, J.; Kim, S.; Lee, S. Differentiation of the toxicities of silver nanoparticles and silver ions to the Japanese medaka (*Oryzias latipes*) and the cladoceran *Daphnia Magna*. *Nanotoxicology* **2008**, *5*, 208–214. [CrossRef]
5. Bertin, G.; Averbeck, D. Cadmium: Cellular effects, modifications of biomolecules, modulation of DNA repair and genotoxic consequences (a review). *Biochimie* **2006**, *88*, 1549–1559. [CrossRef] [PubMed]
6. Abdel-Warith, A.A.; Younis, E.M.; Al-Asgah, N.A.; Wahbi, O.M. Effect of zinc toxicity on liver histology of Nile tilapia, *Oreochromis niloticus*. *J. Lit. Sci.* **2011**, *6*, 3760–3769. [CrossRef]
7. Kozlowski, H.; Janicka-Klos, A.; Brasun, J.; Gaggelli, E.; Valensin, D.; Valensin, G. Copper, iron and zinc ions homeostasis and their role in neurodegenerative disorders (metal uptake, transport, distribution and regulation). *Coord. Chem. Rev.* **2009**, *253*, 2665–2685. [CrossRef]
8. Qu, R.; Feng, M.; Wang, X.; Qin, L.; Wang, C.; Wang, Z.; Wang, L. Metal accumulation and oxidative stress biomarkers in liver of freshwater fish *Carassius auratus* following in vivo exposure to waterborne zinc under different pH values. *Aquat. Toxicol.* **2014**, *150*, 9–16. [CrossRef]
9. Faheem, M.; Lone, K.P. Oxidative stress and histopathologic biomarkers of exposure to bisphenol-A in the freshwater fish, *Ctenopharyngodon idella*. *Braz. J. Pharm. Sci.* **2018**, *53*, 1–9. [CrossRef]
10. Li, Y.; Zhou, Q.; Ren, B.; Luo, J.; Yuan, J.; Ding, X.; Yao, X. Trends and health risks of dissolved heavy metal pollution in global river and lake water from 1970 to 2017. *Rev. Environ. Contam. Toxicol.* **2019**, *251*, 1–24. [CrossRef]
11. Pisoschi, A.M.; Pop, A. The role of antioxidants in the chemistry of oxidative stress: A review. *Eur. J. Med. Chem.* **2015**, *97*, 55–74. [CrossRef]
12. Lushchak, V.I. Environmentally induced oxidative stress in aquatic animals. *Aquat. Toxicol.* **2011**, *101*, 13–30. [CrossRef]
13. Viarengo, A.; Burlando, B.; Cavaletto, M.; Marchi, B.; Ponzano, E.; Blasco, J. Role of metallothionein against oxidative stress in the mussel *Mytilus galloprovincialis*. *Am. J. Physiol-Reg. I.* **1999**, *277*, R1612–R1619. [CrossRef]
14. Khodadoust, D.; Ahmad, I. Metallothionein-like protein levels in Java Medaka fish (*Oryzias javanicus*) exposed to different concentrations of cadmium. *Walailak. J. Sci. Technol.* **2014**, *11*, 883–893. [CrossRef]
15. Sevcikova, M.; Modra, H.; Slaninova, A.; Svobodova, Z. Metals as a cause of oxidative stress in fish: A review. *Vet. Med. Sci.* **2011**, *56*, 537–546. [CrossRef]
16. Akarasereenont, P.; Bakhle, Y.S.; Thiemermann, C.; Vane, J.R. Cytokine-mediated induction of cyclo-oxygenase-2 by activation of tyrosine kinase in bovine endothelial cells stimulated by bacterial lipopolysaccharide. *Brit. J. Pharmacol.* **1995**, *115*, 401–408. [CrossRef]
17. Ramadori, G.; Armbrust, T. Cytokines in the liver. *Eur. J. Gastroenterol. Hepatol.* **2001**, *13*, 777–784. [CrossRef]
18. Lirk, P.; Hoffmann, G.; Rieder, J. Inducible nitric oxide synthase-time for reappraisal. *Curr. Drug. Targets. Inflamm. Allergy.* **2002**, *1*, 89–108. [CrossRef]
19. Porter, A.G.; Jänicke, R.U. Emerging roles of caspase-3 in apoptosis. *Cell. Death. Differ.* **1999**, *6*, 99–104. [CrossRef]
20. Tyagi, S.; Sharma, B.; Singh, P.; Dobhal, R. Water quality assessment in terms of water quality index. *J. Am. Water. Resour. Assoc.* **2013**, *1*, 34–38. [CrossRef]
21. Baldisserotto, B. Water pH and hardness affect growth of freshwater teleosts. *Braz. J. Vet. Res. Anim. Sci.* **2011**, *40*, 138–144.
22. Golombieski, J.I.; Koakoski, G.; Becker, A.J.; Almeida, A.P.G.; Toni, C.; Finamor, I.A.; Baldisserotto, B. Nitrogenous and phosphorus excretions in juvenile silver catfish (*Rhamdia quelen*) exposed to different water hardness, humic acid, and pH levels. *Fish. Physiol. Biochem.* **2013**, *39*, 837–849. [CrossRef]
23. Michelotti, B.T.; Passini, G.; Carvalho, C.; Salbego, J.; Mori, N.C.; Rodrigues, R.V.; Cerqueira, V.R. Growth and metabolic parameters of common snook juveniles raised in freshwater with different water hardness. *Aquaculture.* **2018**, *482*, 31–35. [CrossRef]
24. Kiyani, V.; Hosynzadeh, M.; Ebrahimpour, M. Investigation acute toxicity some of heavy metals at different water hardness. *Int. J. Adv. Biol. Biomed. Res.* **2013**, *1*, 134–142.
25. Alsop, D.; Wood, C.M. Metal uptake and acute toxicity in zebrafish: Common mechanisms across multiple metals. *Aquat. Toxicol.* **2011**, *105*, 385–393. [CrossRef]
26. Rani, S.; Gupta, R.K.; Rani, M. Heavy metal induced toxicity in fish with special reference to zinc and cadmium. *Int. J. Fish. Aquat. Stud.* **2015**, *3*, 118–123.
27. Houri, D.; Koo, C.M. Water quality evaluation of PET bottled water by mineral balance in the Northeast Asian region: A case study of South Korea. *Yonago Acta Med.* **2015**, *58*, 115.

28. Huo, J. Acute toxicity of zinc to goldfish and its accumulation and distribution in the body. *Shanghai. Environ. Sci.* **1996**, *15*, 42–43. [CrossRef]
29. Hollis, L.; Hogstrand, C.; Wood, C.M. Tissue-specific cadmium accumulation, metallothionein induction, and tissue zinc and copper levels during chronic sublethal cadmium exposure in juvenile rainbow trout. *Arch. Environ. Contam. Toxicol.* **2001**, *41*, 468–474. [CrossRef]
30. Hogstrand, C.; Verbost, P.M.; Bonga, S.E.; Wood, C.M. Mechanisms of zinc uptake in gills of freshwater rainbow trout: Interplay with calcium transport. *Am. J. Physiol. -Regul. Integr. Comp. Physiol.* **1996**, *270*, R1141–R1147. [CrossRef]
31. Khan, M.S.; Javed, M.; Rehman, M.T.; Urooj, M.; Ahmad, M.I. Heavy metal pollution and risk assessment by the battery of toxicity tests. *Sci. Rep.* **2020**, *10*, 16593. [CrossRef] [PubMed]
32. Macirella, R.; Guardia, A.; Pellegrino, D.; Bernabò, I.; Tronci, V.; Ebbesson, L.O.; Brunelli, E. Effects of two sublethal concentrations of mercury chloride on the morphology and metallothionein activity in the liver of zebrafish (*Danio rerio*). *Int. J. Mol. Sci.* **2016**, *17*, 361. [CrossRef] [PubMed]
33. Romano, N.; Egnew, N.; Quintero, H.; Kelly, A.; Sinha, A.K. The effects of water hardness on the growth, metabolic indicators and stress resistance of largemouth bass *Micropterus salmoides*. *Aquaculture* **2020**, *527*, 735469. [CrossRef]
34. Zhao, X.; Ren, X.; Zhu, R.; Luo, Z.; Ren, B. Zinc oxide nanoparticles induce oxidative DNA damage and ROS-triggered mitochondria-mediated apoptosis in zebrafish embryos. *Aquat. Toxicol.* **2016**, *180*, 56–70. [CrossRef]
35. Mo, J.; Lin, D.; Wang, J.; Li, P.; Liu, W. Apoptosis in HepG2 cells induced by zinc pyrithione via mitochondrial dysfunction pathway: Involvement of zinc accumulation and oxidative stress. *Ecotoxicol. Environ. Saf.* **2018**, *161*, 515–525. [CrossRef]

antioxidants

MDPI

Article

The Protective Effect of Mulberry Leaf Flavonoids on High-Carbohydrate-Induced Liver Oxidative Stress, Inflammatory Response and Intestinal Microbiota Disturbance in *Monopterus albus*

Yong Shi [1], Lei Zhong [1], Yuding Fan [2], Junzhi Zhang [1], Huan Zhong [1], Xiang Liu [1], Chuang Shao [1] and Yi Hu [1,*]

[1] Hunan Research Center of Engineering Technology for Utilization of Distinctive Aquatic Resource, Hunan Agricultural University, Changsha 410128, China; shiyong@stu.hunau.edu.cn (Y.S.); zhonglei@hunau.edu.cn (L.Z.); zhjun123@hunau.edu.cn (J.Z.); zhonghuan@hunau.edu.cn (H.Z.); dreaml@stu.hunau.edu.cn (X.L.); shaoc@stu.hunau.edu.cn (C.S.)

[2] Yangtze River Fisheries Research Institute, Chinese Academy of Fishery Sciences, Wuhan 430223, China; fanyd@yfi.ac.cn

* Correspondence: huyi0231@hunau.edu.cn; Tel.: +86-138-7591-0605

Abstract: An 8-week feeding trial with high-carbohydrate- and 100, 200 and 300 mg/kg mulberry leaf flavonoids (MLF)-supplemented diets (HCF1, HCF2 and HCF3, respectively) was conducted to evaluate the protective effect of MLF on oxidized high-carbohydrate-induced glucose metabolism disorder, liver oxidative damage and intestinal microbiota disturbance in *Monopterus albus*. The results showed that HC diets had significant negative effects on growth, glucose metabolism, liver antioxidant and immunity, as well as intestinal microbiota, in comparison to CON diets. However, WGR and SR in the HCF3 group dramatically increased compared to the HC group. With the increase of MLF in the HC diet, the activities of glycolysis and antioxidant enzymes in the liver tended to increase, while the changes of gluconeogenesis-related enzyme activities showed the opposite trend and significantly changed in the HCF3 group. Additionally, MLF supplementation dramatically increased the mRNA expression involved in glycolysis, antioxidative enzymes and anti-inflammatory cytokines in comparison with the HC group. Furthermore, gluconeogenesis and pro-inflammatory cytokine genes' expression dramatically decreased. Furthermore, the proportion of *Clostridium* and *Rhodobacter* in the HC group dramatically declined, and the proportion of *Lactococcus* dramatically increased, compared to the HC group. In addition, 300 mg/kg MLF supplementation significantly improved the species composition and homeostasis of intestinal microbiota. These results indicate that MLF can alleviate the negative effects of low growth performance, glucose metabolism disorder, liver oxidative damage and intestinal microbiota disturbance caused by HC diets, and the relief of MLF is dose-related.

Keywords: rice field eel; plant extract; immunity; antioxidant; intestinal health

Citation: Shi, Y.; Zhong, L.; Fan, Y.; Zhang, J.; Zhong, H.; Liu, X.; Shao, C.; Hu, Y. The Protective Effect of Mulberry Leaf Flavonoids on High-Carbohydrate-Induced Liver Oxidative Stress, Inflammatory Response and Intestinal Microbiota Disturbance in *Monopterus albus*. *Antioxidants* **2022**, *11*, 976. https://doi.org/10.3390/antiox11050976

Academic Editor: Min Xue

Received: 11 April 2022
Accepted: 12 May 2022
Published: 16 May 2022

1. Introduction

With the decrease of fishmeal output and the increase in price, the production of a cost-effective diet (cost and effective) has attracted much attention [1]. At present, the mainstream strategy is to achieve a protein-saving effect in diets by supplementing carbohydrate and lipid. Compared with lipid sources, carbohydrates have a price advantage. Studies have shown that, by reducing the protein content in diets and filling it with energy substances (such as carbohydrates), the nitrogen excretion of aquatic animals can be reduced, thereby reducing water environmental pollution and reducing the cost of breeding [2,3].

Compared to terrestrial animals, aquatic animals have poorer utilization of carbohydrates [4]. Further studies have confirmed that carnivorous fish have weaker blood

sugar clearance and glucose absorption capacity and thus, lower starch utilization capacity. Therefore, carnivorous fish have the lowest utilization of sugar compared with other fish [5]. Studies have shown that adding an appropriate carbohydrate into the diet can not only improve the growth performance but also antioxidant capacity in brook trout (*Salvelinus fontinalis*) [6]. However, when fish are fed excessive carbohydrate diets, it can lead to reduced growth performance, a low survival rate, physiological metabolism disorder and inflammatory response [7]. For example, when largemouth bass (*Micropterus salmoides*) and turbot (*Scophthalmus maximus* L.) were fed high-carbohydrate diets, there were negative effects such as reduced growth and disturbance of glucose metabolism [8,9]. In addition, high-carbohydrate diets induced high expression of proinflammatory factors in the head kidney of largemouth bass [10] and inhibited antioxidant enzyme activities (including CAT, SOD and GPx) in large largemouth bass [11]. Chinese perch (*Siniperca chuatsi*) fed with high-carbohydrate diets had disturbed intestinal microbiota [12]. Based on this, numerous studies have shown that feed additives are potential means to alleviate glucose metabolism disorders, oxidative stress and inflammation in fish. In particular, plant extracts have become a research hotspot as feed additives due to their various biological activities.

Mulberry (*Morus alba* L.) leaf is considered an excellent Chinese herbal medicine and contains many natural active substances, including flavonoids, polyhydroxyalkaloids, iminosugars, stilbenes, chlorogenic acids and benzofurans [13,14]. Therefore, mulberry leaf extract has attracted great attention in medicine. In clinical medicine, mulberry leaf extract has a variety of pharmacological effects, such as antibacterial, anti-inflammatory, antioxidant, anticancer and hypolipidemic effects, as well as promoting lipid metabolism, hypoglycemia and so on [13,15]. Similarly, dietary mulberry leaf extract supplementation alleviated high-fat-diet-induced lipid deposition, oxidative damage and inflammation in mice [16]; regulated intestinal microbiota homeostasis in pigs [17]; and improved growth, nutrient digestibility and meat quality in piglet and chicken broilers [18,19]. At present, mulberry leaf extract is also used as a high-quality additive in aquatic diets. Studies have reported that dietary mulberry leaf extract or leaves can improve growth performance and intestinal microbiota homeostasis in crucian carp (*Carassius carassius*) [20] and enhance antioxidant capacity and immune function in largemouth bass [21].

Flavonoids are one of the main functional components of mulberry leaves, accounting for about 1–3% of the dry matter of mulberry leaves. Mulberry leaf flavonoids enhanced glucose metabolism and mitochondrial function through activating AMPK-PGC1α signaling pathways, alleviated liver and kidney injury and improved antioxidant capacity in type 2 diabetes [22,23]. In addition, Zhong et al. found that mulberry leaf flavonoids can alleviate high-fat-induced lipid dysmetabolism induced through intestinal microbiota in mice [24]. In aquatic animals, studies have indicated that dietary mulberry leaf flavonoids can improve growth performance and resistance to nitrite exposure in tilapia (*Oreochromis niloticus*) [25], promote intestinal mucosal morphology and regulate the diversity of intestinal microbiota in *Litopenaeus vannamei* [26]. Therefore, the potential benefits of mulberry leaf flavonoids as additives in high-carbohydrate diets deserve further study.

Rice field eels, a carnivorous fish with high nutritional value, are widely cultivated in China. Studies have shown that the carbohydrate content in the optimal diet for rice field eel growth is 24–33% [27]. In this study, rice field eel was used as the research object to test the hypothesis that mulberry leaf flavonoids can ameliorate the negative effects caused by high-carbohydrate diets. Our objective was to evaluate the growth performance, glucose metabolism, liver antioxidant capacity and intestinal microbiota of rice field eel to determine whether mulberry leaf flavonoids have beneficial effects on fish fed high-carbohydrate diets and to provide a basis for the application of mulberry leaf flavonoids in high-carbohydrate diets.

2. Materials and Methods

2.1. Animals, Experimental Design, Diet Preparation and Culture Conditions

Rice field eel juveniles were obtained from Xihu Farm, Changde, China. The acclimatization method was consistent with our previous research [28]. After this, 900 healthy rice field eel juveniles (initial weight 14.97 ± 0.06 g) randomly allocated to five diets (three cages per dietary treatment, 60 fish per cage): CON diets (20% corn starch); HC diets (40% corn starch); or HC diets supplemented with 100, 200 and 300 mg/kg mulberry leaf flavonoids (HCF1, HCF2 and HFC3, respectively) (Table 1). The mulberry leaf flavonoids (purity > 85%, total flavonoids) were provided by Sericulture and Agricultural Products Processing Institute of Guangdong Academy of Agricultural Sciences. Diet preparation was the same as in a previous study [28]. The breeding experiment lasted for 8 weeks, and the feeding amount was 3–5% of body weight once a day (17:00–18:30 h). Water conditions including pH (7.3 ± 0.2), temperature (28.6 ± 2.2 °C), dissolved oxygen (6.3 ± 0.4 mg/L) and ammonia nitrogen (0.12 ± 0.04 mg/L) were measured.

Table 1. Formulation and proximate composition of the experimental diets (%, dry matter).

Ingredients	CON	HC	HCF1	HCF2	HCF3
Fish meal [a]	40.00	40.00	40.00	40.00	40.00
Wheat gluten [a]	14.46	14.46	14.46	14.46	14.46
Corn starch [a]	20.00	40.00	40.00	40.00	40.00
Microcrystalline cellulose [a]	20.50	0.50	0.49	0.48	0.47
Fish oil [a]	2.00	2.00	2.00	2.00	2.00
Choline [a]	0.50	0.50	0.50	0.50	0.50
Premix [b]	1.00	1.00	1.00	1.00	1.00
$Ca(H_2PO_4)_2$ [a]	1.50	1.50	1.50	1.50	1.50
Antioxidants [a]	0.01	0.01	0.01	0.01	0.01
Mold inhibitor [a]	0.03	0.03	0.03	0.03	0.03
Mulberry leaf flavonoids [c]	0.00	0.00	0.01	0.02	0.03
Proximate composition (%)					
Crude protein	43.86	43.72	44.04	43.87	43.79
Crude lipid	5.86	5.93	5.82	5.79	5.87
Ash	10.85	11.03	10.94	10.72	10.83

[a] Provided by Hunan Aohua Agriculture and Animal Husbandry Technology Co. Ltd. (Changde, China). [b] Provided by MGO Ter Bio-Tech (Qingdao, China). Composition consistent with previous studies [28]. [c] Provided by Sericulture and Agricultural Products Processing Institute of Guangdong Academy of Agricultural Sciences.

2.2. Sample Collection

After the feeding trial, fish were collected after 24 h of fasting. All fish were euthanized (MS-222 at 100 μg/mL). Serum collection was consistent with previous studies [29]. Liver samples (3 fish per cage) were collected and stored at −80 °C. The intestinal contents of three fish per cage were also collected and stored at −80 °C until further analysis of intestinal microbiota.

2.3. Chemical Analysis

The measurement methods of crude lipid, crude protein and ash in diets were consistent with previous studies [29].

2.4. Serum Biochemical Indices Analysis

Glucose (GLU), triacylglycerol (TG), total cholesterol (TC), high-density lipoprotein cholesterol (HDL-C) and low-density lipoprotein cholesterol (LDL-C) were enzymolyzed, respectively, to produce H_2O_2, which could generate red benzoquinone imine under the catalytic action of peroxidase. The products had characteristic absorption peaks at 505, 510, 510, 546 and 546 nm, respectively, and the contents of GLU, TG, TC, HDL-C and LDL-C could be determined by the change in the absorbency value.

Alanine aminotransferase (ALT) and aspartate aminotransferase (AST), respectively, catalyze the transamination reaction to produce pyruvate, which can react with 2,4-dinitrophenylhydrazine to produce 2,4-dinitrophenylhydrazone, which is brownish red under alkaline conditions. The products had characteristic absorption peaks at 510 nm, and the activities of ALT and AST could be determined by the change in the absorbency value.

2.5. Liver Glucose Metabolism and Antioxidant Indices Analysis

The levels of reactive oxygen species (ROS), pyruvate kinase (PK), glucokinase (GK), glucose-6-phosphatase (G-6-Pase), phosphoenolpyruvate carboxykinase (PEPCK), fructose-1.6-bisphosphatase (FBPase) and phosphofructokinase (PFK) in each sample were measured using Elisa kits [30]. The detection method for catalase (CAT), glutathione (GSH), and superoxide dismutase (SOD) levels in the liver were the same as in the previous study [29]. The glutathione peroxidase (GPx) activity in the liver was spectrophotometrically measured at 412 nm.

2.6. Total RNA Extraction, Reverse Transcription and Real-Time PCR

The procedures of total RNA extraction, reverse transcription and qRT-PCR were performed, using methods previously used in our laboratory [31]. The amplification efficiency of all genes was approximately equal and ranged from 0.95 to 1.10. The relative expression level of genes was calculated by the formula $E = 2^{-\Delta\Delta CT}$ [32]. Gene primer sequences were designed by Primer Premier 5.0 (Table 2). The internal reference gene was ribosomal protein L-17 (*rpl-17*) [33].

Table 2. Primers used for mRNA quantitative real-time PCR.

Gene	Forward Sequences (5′→3′)	Reverse Sequences (5′→3′)	Accession No.
gk	AAGCCATCGTATCCCACC	GGGTCCCAGTCCATAGTGT	XM_020620531.1
pk	CCGCCAAGGGACTGTTT	CCACTGGTGGTAAGGACTATG	XM_020617665.1
fpk	AGCATAGGAGCAGACACCG	CACAGAATCCACCCATAGTC	XM_020594803.1
g6pd	CCACCCACTGTCTACCA	GGCTCTGCACCATTTCT	XM_020610610.1
pepck	CTGTGACGGCTCTGACG	ATACATGGTGCGACCTTTC	XM_020621224.1
g6pase	GGTATGAGGGTCTGTTTAGC	GACAGCCACCCAGATGA	XM_020616553.1
fbpase	GCTGCGGTTGCTGTATG	TTCTTGGCGTGTTTATGG	XM_020585913.1
gsk3β	GGTGTTGTCTACCAGGCTAA	CAATGGTCCAACTTCCTCA	XM_020609458.1
gys	CGGCTGCCAGGTTTATT	GCCCAGGATGAGCGAGT	XM_020608327.1
nrf2	CTTCAGACAGCGGTGACAGG	GCCTCATTCAGTTGGTGCTT	XM_020596409.1
keap1	AGCCTGGGTGCGATACGA	CAAGAAATGACTTTGGTGGG	XM_020597068.1
sod	AGCTGGCTAAGTTCTCATTCAC	GCAGTAACATTGCCCAAGTCT	XM_020598413.1
cat	GTCCAAGTCTAAGGCATCTCC	CTCCTCTTCGTTCAGCACC	XM_020624985.1
gpx1	GTTCACCGCCAAACTCTT	TTCCCATTCACATCTACCTT	XM_020607739.1
gpx8	GTCCACTTACGGTGTTACCT	ATGGGCTCGTCAGTTCTC	XM_020593975.1
il-1β	GAGATGTGGAGCCCAAACTT	CTGCCTCTGACCTTCTGGACTT	KM113037.1
il-8	TACTGGTTCTGCTTACTGTCGC	CAAATCTTTTGCCCATCCCT	XM_020597077.1
il-12β	CAAGTCAGTTGCCAAAATCC	CCAAGCAGCTCAGGGTCT	XM_020594580.1
il-10	TTTGCCTGCCAAGTTATGAG	CATTTGGTGACATCGCTCTT	XM_020593225.1
tgf-β1	AACCCACTACCTCACTACCCG	GCCGAAGTTGGAAACCCT	XM_020605575.1
nf-κb	ACCCTACCGTGACACTAACCT	TGCCGTCTATCTTGTGGAAT	XM_020616319.1
tlr-3	TATTTAGAGCCATACAGGG	CACAATCAAGAACGCACA	XM_020614353.1
tlr-7	ATCCTCACGACTTCCCTC	TTTCTTTCATCACCCACT	XM_020596482.1
rpl-17	GTTGTAGCGACGGAAAGGGAC	GACTAAATCATGCAAGTCGAGGG	109952565

2.7. Intestinal Microbiota Analysis

In this study, the Illumina platform was used for the paired-end sequencing of community DNA fragments. The DADA2 method was used for sequence denoising [34]. Vsearch (V2.13.4_linux_x86_64) was used for clustering. Sequence data analyses were mainly performed using QIIME2 and R packages (v3.2.0). Alpha diversity indices, such as Chao1, observed species, Shannon diversity index, Simpson index and Good's coverage, were

calculated using the table in QIIME2 and visualized as box plots. Species analysis at the phylum and genus level was the same as in our previous study [31].

2.8. Statistical Analysis

All data (mean ± SE) were analyzed by one-way ANOVA. After testing for homogeneity of variances, Duncan multiple comparisons were performed. p values less than 0.05 were considered significant differences. All graphs were drawn using Graphpad software (San Diego, CA, USA). SPSS 24.0 software (New York, NY, USA) was used for all statistical analysis.

3. Results

3.1. Growth and Morphology Parameters

No significant differences were showed in final weight, VSI, CF or FCR ($p > 0.05$) (Table 3). The rice field eel fed HC diets had significantly lower WGR and SR than those fed CON and HCF3 diets ($p < 0.05$). Dietary 300 mg/kg mulberry leaf flavonoids significantly decreased HSI compared to the HC group ($p < 0.05$).

Table 3. Effects of dietary mulberry leaf flavonoids on the growth performance of *Monopterus albus* fed high-carbohydrate diets (mean ± S.E.).

	CON	HC	HCF1	HCF2	HCF3	*p*-Value
Initial weight (g)	14.96 ± 0.12	14.97 ± 0.24	15.11 ± 0.12	14.96 ± 0.02	15.01 ± 0.03	0.919
Final weight (g)	36.56 ± 0.94	33.08 ± 1.02	34.96 ± 0.60	35.58 ± 1.50	37.13 ± 0.70	0.112
WGR	144.26 ± 4.47 ^{a}	120.92 ± 3.27 ^{b}	131.41 ± 3.57 ^{ab}	137.82 ± 9.71 ^{ab}	147.37 ± 4.24 ^{a}	0.046
SR	91.11 ± 2.78 ^{a}	77.78 ± 3.38 ^{b}	77.22 ± 2.00 ^{b}	81.66 ± 3.33 ^{ab}	88.33 ± 2.89 ^{a}	0.023
FCR	1.39 ± 0.06	1.67 ± 0.07	1.52 ± 0.04	1.47 ± 0.10	1.36 ± 0.04	0.051
HSI	3.44 ± 0.15 ^{ab}	3.92 ± 0.07 ^{a}	3.63 ± 0.08 ^{ab}	3.49 ± 0.13 ^{ab}	3.32 ± 0.24 ^{b}	0.048
VSI	15.73 ± 0.71	17.22 ± 0.81	18.00 ± 1.28	15.65 ± 1.88	17.68 ± 1.07	0.533
CF	9.00 ± 0.32	10.20 ± 0.49	9.80 ± 0.66	10.00 ± 0.32	10.00 ± 0.55	0.465

Note: In the same row values with different small letter superscripts mean significant difference ($p < 0.05$). Weight gain rate (WGR, %) = (final body weight − initial body weight)/initial body weight × 100; survival rate (SR, %) = final number of fish/initial number of fish × 100; feed-conversion rate (FCR) = total amount of the feed consumed/(final body weight − initial body weight); hepatosomatic index (HSI, %) = liver weight/whole body weight × 100; viserosomatic index (VSI, %) = visceral weight/whole body weight × 100; Condition factor (CF, g/cm^3) = 100 × whole body weight/(body length)^3.

3.2. Serum Biochemical Indices

The rice field eel fed HC diets had significantly higher AST, ALT, TG, TC, GLU and LDL-C concentrations than those fed CON diets ($p < 0.05$) (Table 4). However, feeding the rice field eel mulberry leaf flavonoids (100, 200 and 300 mg/kg) markedly decreased serum AST, ALT, TG, TC, GLU and LDL-C concentrations ($p < 0.05$). Dietary 200 and 300 mg/kg mulberry leaf flavonoids significantly increased HDL-C concentration compared to the HC group ($p < 0.05$).

3.3. Carbohydrate Metabolism Enzyme Activity

No significant differences were shown in liver PK concentration ($p > 0.05$) (Figure 1). Compared with the CON and HC groups, PEPCK activity in the HCF1, HCF2 and HCF3 groups was significantly decreased ($p < 0.05$). HC diets significantly increased liver PFK activity and decreased liver PEPCK, FBPase and G-6-Pase concentrations compared to the CON group ($p < 0.05$). However, feeding the rice field eel mulberry leaf flavonoids (100, 200 and 300 mg/kg) markedly decreased liver PEPCK activity ($p < 0.05$). Dietary 200 and 300 mg/kg mulberry leaf flavonoids also significantly increased GK and PFK concentrations compared to the HC group ($p < 0.05$). FBPase and G-6-Pase concentrations in the HCF3 treatment were markedly low than those in the HC group ($p < 0.05$).

Table 4. Effects of dietary mulberry leaf flavonoids on serum biochemical indices of rice field eel (*Monopterus albus*) fed high-carbohydrate diets (mean ± S.E.).

	CON	HC	HCF1	HCF2	HCF3	*p*-Value
AST (U/L)	3.45 ± 0.09 ^{d}	7.86 ± 0.26 ^{a}	3.68 ± 0.04 ^{d}	5.47 ± 0.23 ^{b}	4.90 ± 0.10 ^{c}	<0.001
ALT (U/L)	3.75 ± 0.07 ^{c}	9.18 ± 0.41 ^{a}	4.21 ± 0.28 ^{bc}	4.44 ± 0.2 ^{bc}	4.99 ± 0.31 ^{b}	<0.001
GLU (mg/dL)	38.72 ± 1.31 ^{c}	51.96 ± 1.88 ^{a}	42.11 ± 1.74 ^{bc}	43.71 ± 0.91 ^{b}	40.52 ± 0.80 ^{bc}	<0.001
TG (mmol/L)	0.40 ± 0.01 ^{b}	0.56 ± 0.01 ^{a}	0.40 ± 0.00 ^{b}	0.39 ± 0.00 ^{b}	0.41 ± 0.01 ^{b}	<0.001
TC (mmol/L)	2.72 ± 0.03 ^{b}	3.16 ± 0.07 ^{a}	2.34 ± 0.04 ^{c}	2.44 ± 0.08 ^{c}	2.36 ± 0.09 ^{c}	<0.001
LDL-C (mmol/L)	3.22 ± 0.03 ^{b}	6.30 ± 0.42 ^{a}	3.31 ± 0.27 ^{b}	2.74 ± 0.27 ^{b}	2.86 ± 0.16 ^{b}	<0.001
HDL-C (mmol/L)	3.00 ± 0.01 ^{b}	3.08 ± 0.05 ^{b}	3.40 ± 0.05 ^{b}	4.49 ± 0.09 ^{a}	4.28±0.31 ^{a}	<0.001

Note: In the same row, values with different small letter superscripts mean significant difference ($p < 0.05$). Aspartate aminotransferase (AST), alanine aminotransferase (ALT), glucose (GLU), triacylglycerol (TG), total cholesterol (TC), low-density lipoprotein cholesterol (LDL-C), high-density lipoprotein cholesterol (HDL-C).

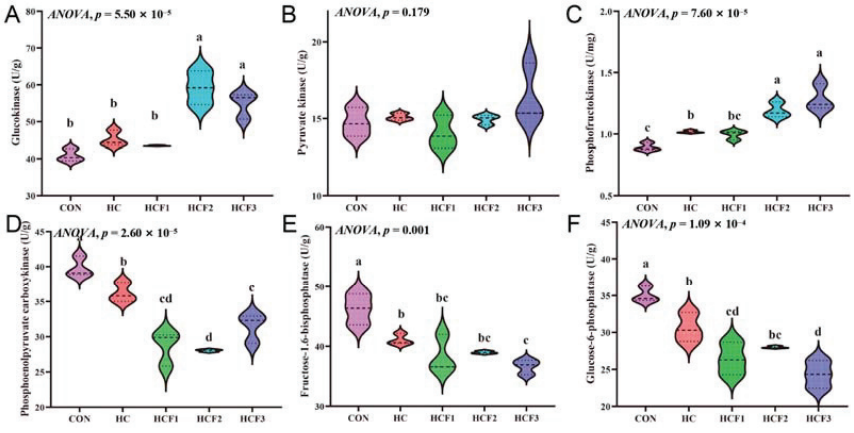

Figure 1. Influences of dietary mulberry leaf flavonoids on carbohydrate metabolism enzymes activities in liver in rice field eel fed on a high-carbohydrate diet. (**A**) Glucokinase, GK; (**B**) Pyruvate kinase, PK; (**C**) Phosphofructokinase, PFK; (**D**) Phoenolpyruvate carboxykinase, PEPCK; (**E**) Fructose-1.6-bisphosphatase, FBPase; (**F**) Glucose-6-phosphatase, G-6-Pase. Different letters show a significant difference ($p < 0.05$).

3.4. Genes Expression of Carbohydrate Metabolism

No significant differences were shown in the mRNA expression of liver *pepck* ($p > 0.05$) (Figure 2). HC diets significantly upregulated the mRNA expression of *fpk*, *g6pd* and *gys* compared to the CON group ($p < 0.05$), with downregulated gene expression of *g6pase*, *fbpase*, and *gsk3β* ($p < 0.05$). Furthermore, 100, 200 and 300 mg/kg mulberry leaf flavonoid supplementation in HC-fed rice rield eel significantly downregulated the mRNA expression of *g6pase* and *gys*, as well as upregulated the mRNA expression of *fpk* and *gsk3β* ($p < 0.05$). The HCF3 group significantly reduced the mRNA expression of *fbpase* and increased the mRNA expression of *gk*, *pk* and *g6pd* compared to the HC group ($p < 0.05$).

3.5. Antioxidant Indices in the Liver

No significant differences were showed in liver SOD and GSH concentrations ($p > 0.05$) (Figure 3). The rice field eel fed HC diets had significantly higher ROS content and lower CAT and GPx activities than those fed CON diets. However, feeding the rice field eel mulberry leaf flavonoids (100, 200 and 300 mg/kg) markedly decreased liver ROS content and increased liver GPx activity ($p < 0.05$), which was similar to results from the CON group ($p > 0.05$). Dietary 200 and 300 mg/kg mulberry leaf flavonoids also significantly increased CAT activity compared to the HC group ($p < 0.05$).

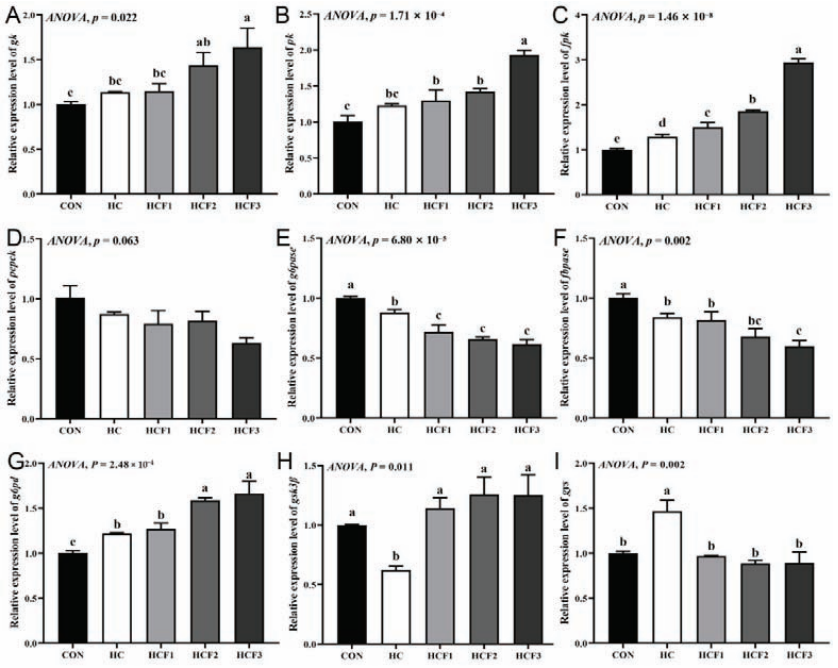

Figure 2. Influences of dietary mulberry leaf flavonoids on carbohydrate metabolism relative genes expression in liver in rice field eel fed on a high-carbohydrate diet. (**A**) *gk*; (**B**) *pk*; (**C**) *fpk*; (**D**) *pepck*; (**E**) *g6pase*; (**F**) *fbpase*; (**G**) *g6pd*; (**H**) *gsk3β*; (**I**) *gys*. Different letters show significant difference ($p < 0.05$).

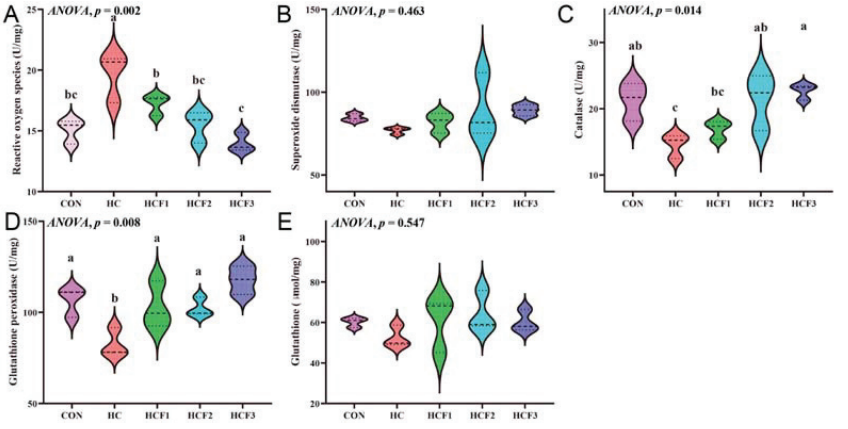

Figure 3. Influences of dietary mulberry leaf flavonoids on antioxidant enzymes activities in the liver of rice field eel fed on a high-carbohydrate diet. (**A**) Reactive oxygen species, ROS; (**B**) Superoxide dismutase, SOD; (**C**) catalase, CAT; (**D**) Glutathione peroxidase, GPx; (**E**) Glutathione, GSH. Different letters show a significant difference ($p < 0.05$).

3.6. Genes Expression of Liver Antioxidant

The rice field eel fed HC diets had significantly higher mRNA expression of *keap1* and lower mRNA expression of *gpx1*, *gpx8*, *cat*, *sod* and *nrf-2* than those fed CON diets ($p < 0.05$) (Figure 4). However, feeding the rice field eel mulberry leaf flavonoids (100, 200 and 300 mg/kg) markedly decreased liver *keap1* mRNA expression and increased *sod* and

nrf-2 mRNA expression ($p < 0.05$), which was similar to the CON group ($p > 0.05$). Dietary 200 and 300 mg/kg mulberry leaf flavonoids also significantly increased *gpx1*, *gpx8* and *cat* mRNA expression compared to the HC group ($p < 0.05$).

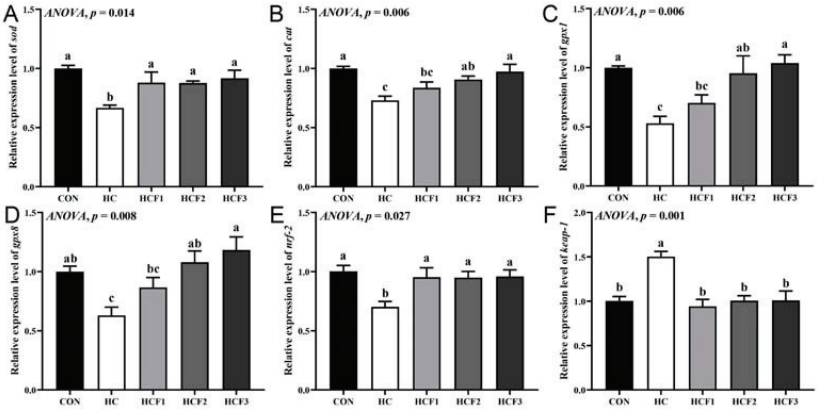

Figure 4. Influences of dietary mulberry leaf flavonoids on antioxidant-related genes' expression in the liver of rice field eels fed on a high-carbohydrate diet. (**A**) *sod*; (**B**) *cat*; (**C**) *gpx1*; (**D**) *gpx8*; (**E**) *nrf-2*; (**F**) *keap1*. Different letters show a significant difference ($p < 0.05$).

3.7. Gene Expression Related to the Liver Damage

The rice field eel fed HC diets had significantly higher mRNA expression of *il-1β*, *il-12β*, *tlr-3*, *tlr-7* and *nf-κb* and lower mRNA expression of *il-10* and *tgf-β1* than those fed CON diets ($p < 0.05$) (Figure 5). The supplementation of 100–300 mg/kg mulberry leaf flavonoids remarkably downregulated *il-1β*, *il-12β*, *tlr-3*, *tlr-7* and *nf-κb* mRNA expression compared to the HC group ($p < 0.05$). *il-10* mRNA expression in the HCF2 and HCF3 groups and *tgf-β1* mRNA expression in the HCF3 group were remarkably downregulated compared to the HC diet ($p < 0.05$). With the increase in the mulberry leaf flavonoid supplemental level, the mRNA expression of *tgf-β1* and *il-10* showed an increasing trend, while the mRNA expression of *il-1β*, *tlr-3* and *tlr-7* showed a decreasing trend.

Correlation analysis revealed that the mRNA transcription level of *nf-κb* was significantly ($p < 0.05$) positively correlated with that of the mRNA transcription levels of *il-10* and *tgf-β1* and negatively correlated with that of the mRNA transcription levels of *il-1β*, *il-8*, *il-12β*, *tlr-3* and *tlr-7* (Figure 6).

3.8. Intestinal Microbiota Analysis

3.8.1. Diversity Analysis

No significant differences were showed in the Simpson index ($p > 0.05$) (Figure 7). HC diets significantly decreased Chao1, Shannon and observed species indexes in comparison with the CON group ($p < 0.05$). A total of 300 mg/kg mulberry leaf flavonoid supplementation significantly increased the Chao1, Shannon and observed species indexes in comparison with the HC group ($p < 0.05$).

3.8.2. Microbial Composition

The tree diagram shown that no significant differences were shown in dominant intestinal microbiota at the phylum level ($p > 0.05$), mainly including *Firmicutes* and Proteobacteria (Figure 8A). The rice field eel fed HC diets had significantly higher abundance of Lactococcus and lower abundance of *Clostridium* and *Rhodobacter* than those fed CON diets ($p < 0.05$) (Figure 8B,C). The supplementation of 300 mg/kg mulberry leaf flavonoids remarkably decreased the abundance of *Lactococcus* and increased the abundances of *Clostridium* and *Rhodobacter* in comparison with the HC group ($p < 0.05$), without reaching the CON group.

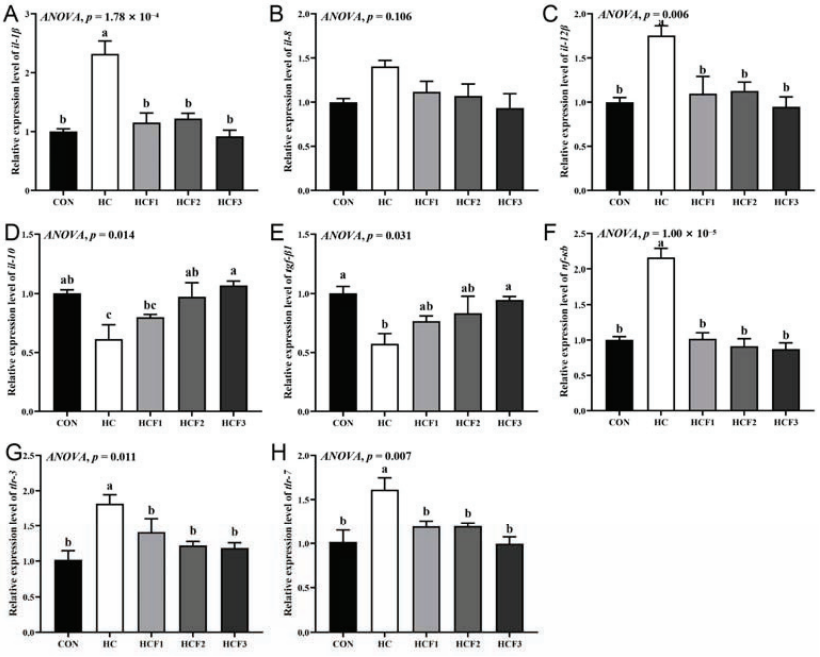

Figure 5. Influences of dietary mulberry leaf flavonoids on inflammation-related genes' expression in the liver of rice field eel fed on a high-carbohydrate diet. (**A**) *il-1β*; (**B**) *il-8*; (**C**) *il-12β*; (**D**) *il-10*; (**E**) *tgf-β1*; (**F**) *nf-κb*; (**G**) *tlr-3*; (**H**) *tlr-7*. Different letters show a significant difference ($p < 0.05$).

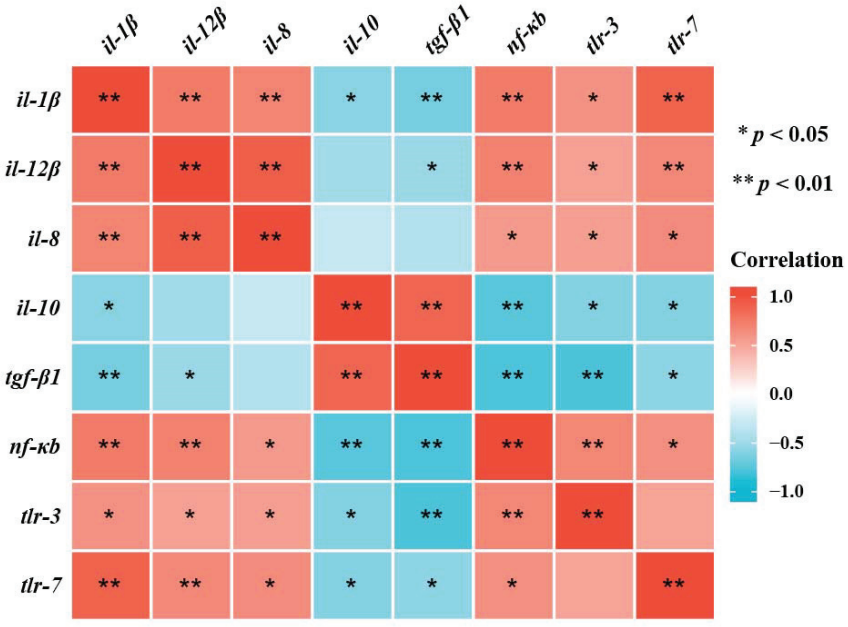

Figure 6. Correlative analysis of liver-inflammation-related gene expression. * $p < 0.05$, ** $p < 0.01$.

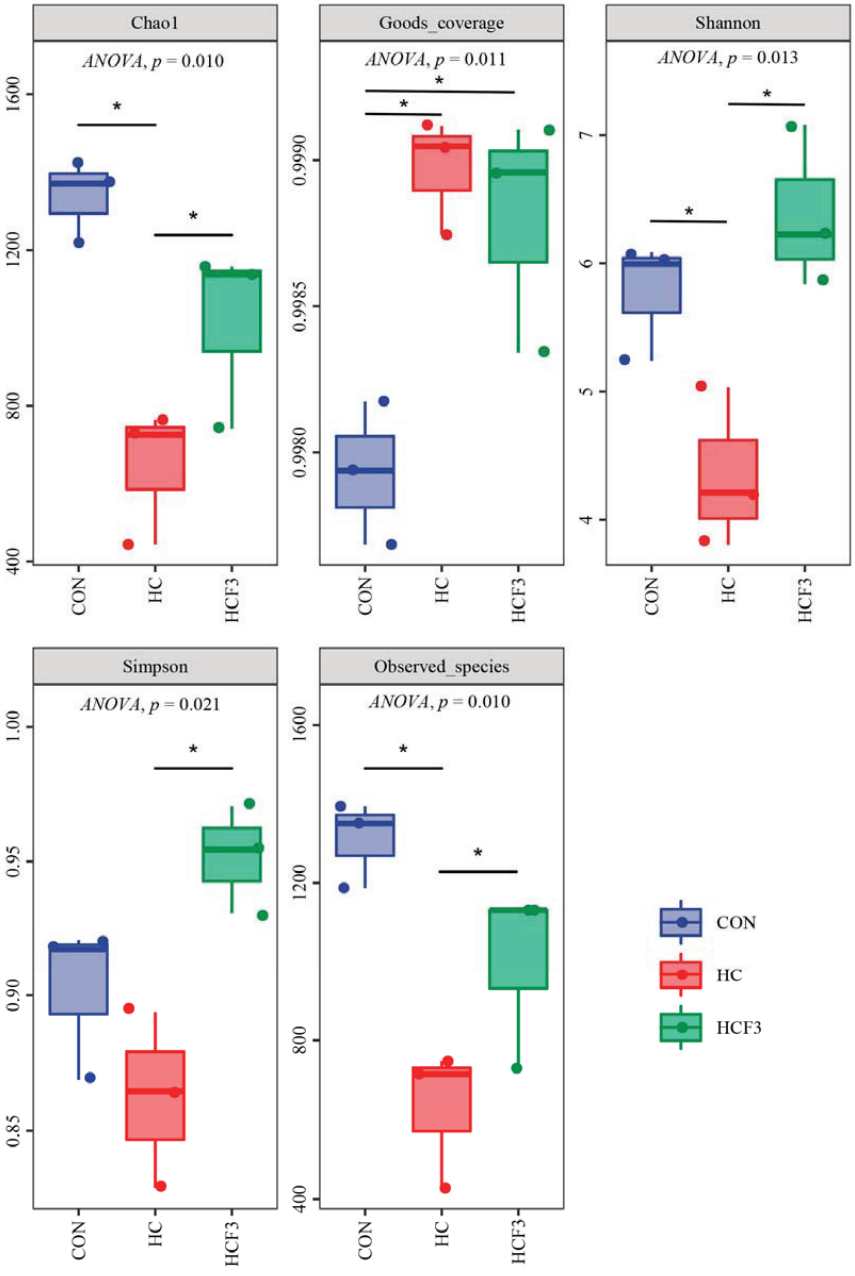

Figure 7. Influences of dietary mulberry leaf flavonoids on the alpha-diversity of intestinal microbiota in rice field eel fed a high-carbohydrate diet. * indicates a significant difference between groups ($p < 0.05$).

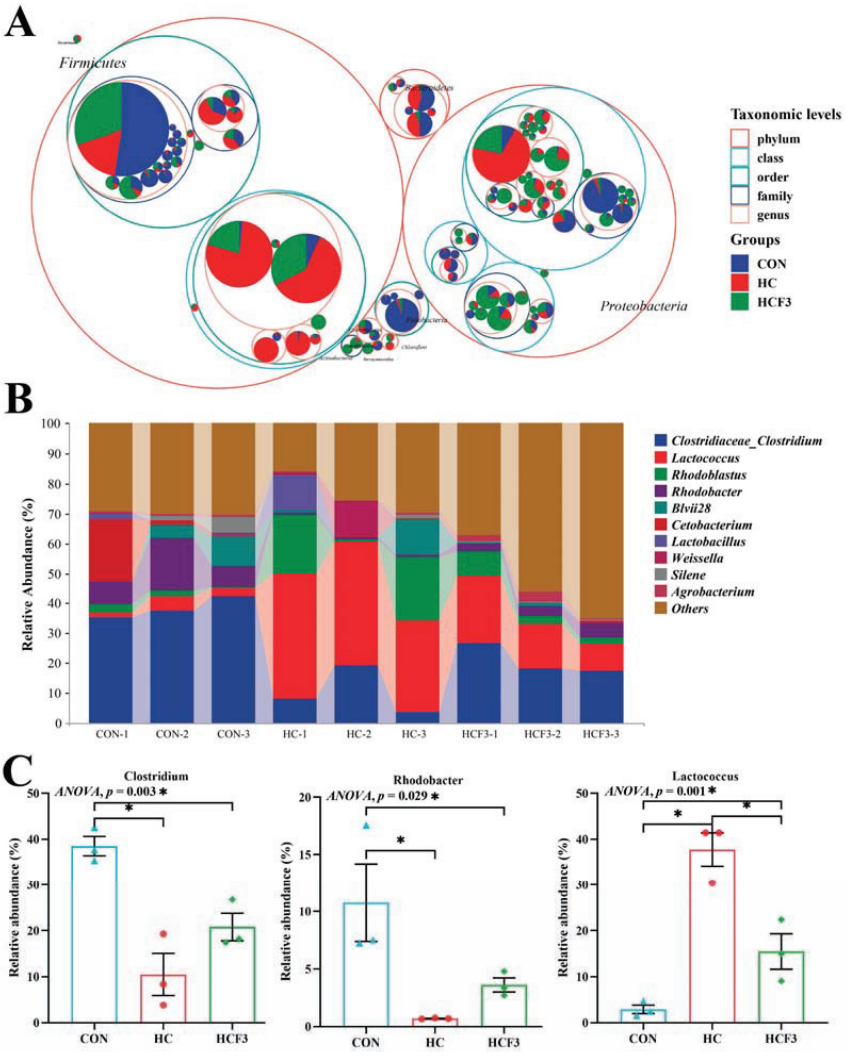

Figure 8. Effects of dietary mulberry leaf flavonoids on the intestinal microbial composition of rice field eel (*Monopterus albus*) fed high-carbohydrate diets. (**A**) Classification hierarchy tree diagram (The largest circle represents phylum level, and the decreasing circle represents class, order, family, genus and species in descending order). (**B**) Species abundance at the genus level (Top 10), (**C**) showing significant variations of the relative abundance of intestinal microbiota at the genus level. * indicates a significant difference between groups ($p < 0.05$).

4. Discussion

The appropriate dietary carbohydrate content can improve the growth performance of kelabau (*Osteochilus melanopleurus*) [35]. However, HC diets significantly decreased the growth performance of *Lateolabrax japonicus* [36], cobia (*Rachycentron canadum* L.) [6], hybrid grouper [37] and largemouth bass [38]. The results of this study demonstrated that rice field eels fed a HC diet had a significantly reduced weight-gain rate. The main reason for this may be their low carbohydrate-utilization capacity; studies have shown that carnivorous fish are natural diabetic patients [5]. Functional additives are a common method for improving carbohydrate utilization in aquatic animals. The flavonoids of *Alnus*

glutinosa can improve the growth performance of mutton sheep by promoting the secretion of growth hormone and insulin-like growth factor-1 in the serum [39]. Similarly, dietary mulberry leaf flavonoids improved the growth performance of tilapia [25]. Flavonoids from *Allium mongolicum Regel* have also been found to improve the growth performance in juvenile northern snakehead fish (*Channa argus*) [40]. This study also demonstrated that supplementation of diets with 300 mg/kg mulberry leaf flavonoids significantly improved the weight-gain rate of the HC-diet-fed rice field eel, which was similar to results from the CON group. This indicates that mulberry leaf flavonoids increased growth performance in rice field eels.

High serum-glucose content has previously been found in largemouth bass and tilapia fed high-carbohydrate diets [38,41]. In this study, long-term feeding of HC diets significantly increased serum GLU content in rice field eels. However, liver tissue plays an important role in regulating blood glucose homeostasis [42]. Several important pathways are involved in this regulation, such as gluconeogenesis and glycolysis, in which G-6-Pase, FBPase and PEPCK activities are restriction enzymes in the gluconeogenesis pathway, and PFK, PK and GK are the limiting enzymes in the glycolysis pathway [43]. This study showed that rice field eel fed HC diets had significantly higher PFK and GK concentrations and lower FBPase, G-6-Pase and PEPCK concentrations than those fed CON diets. In addtion, the mRNA expression of *fpk*, *gk*, *fbpase*, *g6pase* and *pepck* were the same as their enzyme activity changes. Similar results were seen in blunt snout bream (*Megalobrama amblycephala*) [41] and largemouth bass [10].

Mulberry leaf is a Chinese medicinal supplement that is widely used to regulate blood glucose [44]. Flavonoids, one of the main active ingredients in mulberry leaves, have the potential to treat type II diabetes [23,45]. In this study, the addition of mulberry leaf flavonoids, especially at the higher level (300 mg/kg), remarkably downregulated the transcriptional levels of *fbpase* and *g6pase* and upregulated the transcriptional levels of *fpk*, *pk* and *gk* of HC-diet-fed fish, and the corresponding enzyme activity results were consistent with them. Some studies have reported that Gys plays a very important role in the final stage of catalyzing glycogen synthesis during carbohydrate metabolism, and *gys* mRNA expression is negatively correlated with *gsk3β* [46]. This study showed that compared to the CON diet, the HC diet induced significantly lower liver *gsk3β* mRNA expression and higher *gys* mRNA expression. However, the addition of mulberry leaf flavonoids to HC diets reversed this trend. Thus, these results indicate that mulberry leaf flavonoids reduced serum-glucose content by promoting glycolysis and inhibiting the gluconeogenesis pathway.

According to previous studies, excessive carbohydrate intake can cause severe physiological stress, such as oxidative stress and inflammation [47,48]. In this study, high-carbohydrate diets induced relatively high levels of serum ALT and AST activity; liver ROS content; and liver *il-1β*, *il-8* and *il-12β* mRNA expression levels compared to the CON group. In contrast, the hepatic activities of CAT, GPx and liver *il-10* and *tgf-β1* mRNA expression levels were relatively low. These findings indicate that long-term feeding of a HC diet causes oxidative stress and induces inflammation in rice field eels. The above conclusions can be supported by the following reasons: first, studies have shown that a decrease in antioxidant enzyme (such as GPx, CAT and SOD) activity and an increase in ROS content are the symbolic signals of oxidative damage in fish [49–51]; Second, evidence of high-carbohydrate diet-induced liver inflammatory damage was supported by the increase in serum AST and ALT activities, which is an important marker of liver damage [52], as well as *il-1β* and *il-8*, which are the main pro-inflammatory factors [53].

The alleviation of the HC-diet-induced oxidative stress and inflammatory response imperative is improved by the application of carbohydrates in aquatic feed. The flavonoids in mulberry leaves are natural antioxidants, which can significantly increase SOD, CAT and CPx activities and significantly reduce MDA content, thereby improving antioxidant capacity and reducing oxidative stress [54]. Moreover, flavonoids are known to be effective immune enhancers [55]. In this study, the addition of mulberry leaf flavonoids, especially

at the higher level (300 mg/kg), significantly increased hepatic CAT and GPx activities, as well as the liver *il-10* and *tgf-β1* mRNA expression levels of HC-diet-fed fish, while decreasing serum AST and ALT activities; liver MDA content; and liver *il-1β*, *il-8* and *il-12β* mRNA expression levels. These findings indicate that dietary mulberry leaf flavonoid supplementation enhances antioxidant capacity and alleviates inflammation in the liver of rice field eels fed high-carbohydrate diets. According to previous studies, dietary flavonoid supplementation can significantly enhance antioxidant ability (such as CAT, SOD and GPx) in farmed tilapia [25] and reduce significant the chromium-induced upregulation of pro-inflammatory factors (such as *tnf-α* and *il-1β*) in *Ctenopharyngodon idella* [56]. Furthermore, dietary flavonoids from *Allium mongolicum Regel* can reduce Se-accumulation in organs, decrease oxidative stress, increase immune response and regulate immune-related signaling molecules following Se exposure in *Channa argus* [57]. In the same way, the excellent antioxidant properties of mulberry leaf flavonoids are derived from their ability to directly scavenge ROS by providing a hydrogen atom or single-electron transfer and immediately chelate free radicals [58]. In this study, dietary mulberry leaf flavonoid supplementation significantly decreased ROS content. This further supports the antioxidant capacity of mulberry leaf flavonoids.

Antioxidant capacity and inflammatory responses in animals are regulated by the Nrf2/Keap1 and NF-κB/TLRs signaling pathways, respectively [31,59]. A previous study showed that high-carbohydrate diets induce oxidative damage and inflammatory responses by influencing the Nrf2 and NF-κB signaling pathways in blunt snout bream [60]. *keap1* inhibits the expression of antioxidant genes by inhibiting the nuclear translocation of *nrf2* [61]. This study showed that HC diets remarkably upregulated the transcriptional levels of *keap1*, *nf-κb*, *tlr-3* and *tlr-7* in the liver, whereas the transcriptional level of *nrf2* was downregulated. These findings indicate that high-carbohydrate diets lead to oxidative stress and inflammation by activating the NF-κB signaling pathway and inhibiting the Nrf2 signaling pathway. Subsequently, the addition of mulberry leaf flavonoids to HC diets remarkably downregulated the transcriptional levels of *keap1*, *nf-κb*, *tlr-3* and *tlr-7* in the liver, whereas the transcriptional level of *nrf2* was upregulated. Furthermore, correlation analyses showed that the transcriptional level of *nf-κb* was negatively correlated with the mRNA expression levels of *il-1β*, *il-8*, *il-12β*, *tlr-3* and *tlr-7*, and positively correlated with the mRNA expression levels of *il-10* and *tgf-β1*. This suggests that mulberry leaf flavonoids inhibited the NF-κB signaling pathway to protect high-carbohydrate-induced inflammatory response in rice field eels. Similar studies have been conducted on flavonoids extracted from other plants. For example, flavonoids extracted from *Barnebydendron riedelii* can enhance antioxidant capacity by inhibiting the Nrf2 signaling pathway [62], and flavonoids extracted from cocoa can alleviate the inflammatory response by inhibiting the NF-κB signaling pathway [63]. These results indicate that plant flavonoids could effectively enhance the antioxidant capacity and inhibit inflammation via the Nrf2/Keap1 and NF-κB/TLRs signaling pathways in rice field eels fed HC diets.

Numerous studies have shown that the intestinal microbiota plays a beneficial role for the host in diabetes, oxidative damage and inflammatory responses [64,65]. Alpha-diversity (Chao1, Shannon and observed species index) is an important indicator for judging the species richness of intestinal microbiota. In this study, the rice field eel fed HC diets had significantly lower Chao1, Shannon and observed species indices than those fed CON diets, and similar results were found in Nile tilapia and Chinese perch [12,41]. These results indicate that fish fed HC diets for a long time showed reduced diversity of intestinal microbiota.

In addition, we also found that HC-diet feeding remarkably increased the abundance of *Lactococcus* and reduced the abundance of *Clostridium* and *Rhodobacter* in rice field eels. However, *Clostridium* is able to promote the production of butyrate, a short-chain fatty acid that scavenges oxygen and free radicals and enhances host antioxidant immunity [66–68]. *Lactococcus*, a globular gram-positive anaerobe, causes adverse host reactions, including inflammatory responses and low growth rates [69,70]. *Rhodobacter* gram-negative bacteria

have been used to produce terpenes, which have various biological functions [71]. However, in this study, HC diets resulted in a significant decrease in *Clostridium* and *Rhodobacter*, which may reduce their metabolites and lead to physiological disorders. However, the specific metabolites involved require further study. These results may indicate that oxidative stress and inflammatory responses induced by high-carbohydrate diets are closely related to intestinal microbiota homeostasis.

Flavonoids interact with intestinal microbiota, which can participate in the transforming flavonoids in vivo. For example, *Clostridium* participates in the metabolism of flavonoids in vivo and has a stronger physiological function [26]. Flavonoids also support the growth of normal bacteria, inhibit the proliferation of harmful bacteria and regulate the intestinal microecological balance [72]. Previous research has confirmed that *Cyclocarya paliurus* flavonoids can positively regulate the composition and function of intestinal microbiota disturbed by host circadian disturbances, thus improving the intestinal microecological balance in mice [73]. The present study also showed that 300 mg/kg mulberry leaf flavonoid supplementation in HC diets caused no significant difference in Chao1, Shannon and observed species compared to that in the CON group. Furthermore, the supplementation of 300 mg/kg mulberry leaf flavonoids remarkably decreased the abundance of *Lactococcus* and increased the abundance of *Clostridium* and *Rhodobacter* in comparison with the HC group. In pre-weaned calves, dietary mulberry leaf flavonoids can reduce the number of diarrhea days after *Escherichia coli* K99 infection, effectively regulate the intestinal microbiota and improve intestinal health [74]. These findings indicate that mulberry leaf flavonoids could restore the intestinal microbiota dysbiosis induced by HC diets. Furthermore, the enhancement of the antioxidant capacity and anti-inflammatory capacity of mulberry leaf flavonoids is closely related to the regulation of the intestinal microbiota of rice field eels. However, the specific regulatory mechanism requires further study.

5. Conclusions

We have shown that HC-diet feeding had an adverse effect on growth, carbohydrate metabolism, liver antioxidant, immune capacity and intestinal microbiota. However, dietary mulberry leaf flavonoid supplementation increased growth performance in rice field eels. In addition, mulberry leaf flavonoids increased carbohydrate metabolism, enhanced liver immune and antioxidant capacity and regulated intestinal microbiota homeostasis in eels fed HC diets. The optimal addition amount of mulberry leaf flavonoids was 300 mg/kg.

Author Contributions: Conceptualization, Y.H.; software, Y.S.; validation, Y.S., L.Z., Y.F. and Y.H.; formal analysis, Y.S. and X.L.; data curation, Y.S. and L.Z.; writing—original draft preparation, Y.S.; writing—review and editing, Y.H.; visualization, Y.S. and C.S.; investigation, J.Z., H.Z. and X.L.; project administration, L.Z. and Y.H. All authors have read and agreed to the published version of the manuscript.

Funding: This research was funded by National Natural Science Foundation of China, grant number 32172986, and the National Key R&D Program of China, grant number 2019YFD0900200.

Institutional Review Board Statement: This study was approved by the Hunan Agricultural University Animal Care and Use Committee (430364 and 28 May 2020).

Informed Consent Statement: Not applicable.

Data Availability Statement: All data generated or analyzed during this study are included in this published article.

Acknowledgments: We thank Kai Xie, Yong Guo, Feng Shen and Tuo Chen for their help in diet production and sampling.

Conflicts of Interest: The authors declare no conflict of interest.

Abbreviations

WGR: weight-gain rate; SR: survival rate; FCR: feed-conversion rate; HSI: hepatosomatic index; VSI: viserosomatic index; CF: condition factor; AST: aspartate aminotransferase; ALT: alanine aminotransferase; GLU: glucose; TG: triacylglycerol; TC: total cholesterol; LDL-C: low-density lipoprotein cholesterol; HDL-C: high-density lipoprotein cholesterol; ROS: reactive oxygen species; PK: pyruvate kinase; GK: glucokinase; G-6-Pase: glucose-6-phosphatase; PEPCK: phosphoenolpyruvate carboxykinase; FBPase: fructose-1.6-bisphosphatase; PFK: phosphofructokinase; CAT: catalase; GSH: glutathione; SOD: superoxide dismutase; GPx: glutathione peroxidase.

References

1. FAO. *The State of World Fisheries and Aquaculture (SOFIA)*; Food and Agriculture Organization of the United Nations: Rome, Italy, 2018.
2. Hatlen, B.; Grisdale-Helland, B.; Helland, S.J. Growth, feed utilization and body composition in two size groups of Atlantic halibut (*Hippoglossus hippoglossus*) fed diets differing in protein and carbohydrate content. *Aquaculture* **2005**, *249*, 401–408. [CrossRef]
3. Asaduzzaman, M.; Wahab, M.; Verdegem, M.; Adhikary, R.; Rahman, S.; Azim, M.; Verreth, J.A.J. Effects of carbohydrate source for maintaining a high C: N ratio and fish driven re-suspension on pond ecology and production in periphyton-based freshwater prawn culture systems. *Aquaculture* **2010**, *301*, 37–46. [CrossRef]
4. Stone, D.A.J. Dietary carbohydrate utilization by fish. *Rev. Fish. Sci.* **2003**, *11*, 337–369. [CrossRef]
5. Kamalam, B.S.; Medale, F.; Panserat, S. Utilisation of dietary carbohydrates in farmed fishe: New insights on influencing factors, biological limitations and future strategies. *Aquaculture* **2017**, *467*, 3–27. [CrossRef]
6. Zhang, Q.; Chen, Y.; Xu, W.; Zhang, Y. Effects of dietary carbohydrate level on growth performance, innate immunity, antioxidant ability and hypoxia resistant of brook trout *Salvelinus fontinalis*. *Aquac. Nutr.* **2021**, *27*, 297–311. [CrossRef]
7. Ren, M.; Ai, Q.; Mai, K.; Ma, H.; Wang, X. Effect of dietary carbohydrate level on growth performance, body composition, apparent digestibility coefficient and digestive enzyme activities of juvenile cobia, *Rachycentron canadum* L. *Aquacult. Res.* **2011**, *42*, 1467–1475. [CrossRef]
8. Zhang, Y.; Xie, S.; Wei, H.; Zheng, L.; Liu, Z.; Fang, H.; Xie, J.; Liao, S.; Tian, L.; Liu, H.; et al. High dietary starch impaired growth performance, liver histology and hepatic glucose metabolism of juvenile largemouth bass, *Micropterus salmoides*. *Aquac. Nutr.* **2020**, *26*, 1083–1095. [CrossRef]
9. Liu, D.; Zhang, Y.; Pan, M.; Yang, M.; Li, X.; Fu, Y.; Gao, W.; Zhang, W.; Mai, K. Interactive effects of dietary biotin and carbohydrate on growth performance and glucose metabolism in juvenile turbot *Scophthalmus maximus* L. *Aquaculture* **2021**, *540*, 736752. [CrossRef]
10. Liu, Y.; Liu, N.; Wang, A.; Chen, N.; Li, S. Resveratrol inclusion alleviated high-dietary-carbohydrate-induced glycogen deposition and immune response of largemouth bass, *Micropterus salmoides*. *Br. J. Nutr.* **2022**, *127*, 165–176. [CrossRef]
11. Ma, H.J.; Mou, M.M.; Pu, D.C.; Lin, S.M.; Chen, Y.J.; Luo, L. Effect of dietary starch level on growth, metabolism enzyme and oxidative status of juvenile largemouth bass, *Micropterus salmoides*. *Aquaculture* **2019**, *498*, 482–487. [CrossRef]
12. Zhang, Y.; Liang, X.F.; He, S.; Chen, X.; Wang, J.; Li, J.; Zhu, Q.; Zhang, Z.; Li, L.; Alam, M.S. Effects of high carbohydrate diet-modulated microbiota on gut health in Chinese Perch. *Front. Microbiol.* **2020**, *11*, 575102. [CrossRef] [PubMed]
13. Lim, S.H.; Choi, C.I. Pharmacological properties of *Morusnigra* L. (Black Mulberry) as a promising nutraceutical resource. *Nutrients* **2019**, *11*, 437. [CrossRef] [PubMed]
14. Wen, P.; Hu, T.; Linhardt, R.J.; Liao, S.; Wu, H.; Zou, Y. Mulberry: A review of bioactive compounds and advanced processing technology. *Trends. Food. Sci. Technol.* **2019**, *83*, 138–158. [CrossRef]
15. Sarkhel, S. Nutrition importance and health benefits of mulberry leaf extract: A review. *J. Pharmacog. Phytochem.* **2020**, *9*, 689–695.
16. Peng, C.H.; Lin, H.T.; Chung, D.J.; Huang, C.N.; Wang, C.J. Mulberry Leaf extracts prevent obesity-induced NAFLD with regulating adipocytokines, inflammation and oxidative stress. *J. Food Drug Anal.* **2018**, *26*, 778–787. [CrossRef]
17. Zhao, X.; Li, L.; Luo, Q.; Ye, M.; Luo, G.; Kuang, Z. Effects of mulberry (*Morusalba* L.) leaf polysaccharides on growth performance, diarrhea, blood parameters, and gut microbiota of early-weanling pigs. *Livest. Sci.* **2015**, *177*, 88–94. [CrossRef]
18. Fan, L.; Peng, Y.; Wu, D.; Hu, J.; Shi, X.; Yang, G.; Li, X. Dietary supplementation of *Morus nigra* L. leaves decrease fat mass partially through elevating leptin-stimulated lipolysis in pig model. *J. Ethnopharmacol.* **2020**, *249*, 112416. [CrossRef]
19. Simol, C.F.; Tuen, A.A.; Khan, H.H.A.; Chubo, J.K.; King, P.J.H.; Ong, K.H. Performance of chicken broilers fed with diets substituted with mulberry leaf powder. *Afr. J. Biotechnol.* **2012**, *11*, 16106–16111.
20. Zhu, W.; Xiao, S.; Chen, S.; Xu, Q.; Yang, Z.; Liu, J.; Lan, S. Effects of fermented mulberry leaves on growth, serum antioxidant capacity, digestive enzyme activities and microbial compositions of the intestine in crucian (*Carassius carassius*). *Aquac. Res.* **2021**, *52*, 6356–6366. [CrossRef]
21. Xv, Z.C.; He, G.L.; Wang, X.; Shun, H.; Chen, Y.J.; Lin, S.M. Mulberry leaf powder ameliorate high starch-induced hepatic oxidative stress and inflammation in fish model. *Anim. Feed Sci. Technol.* **2021**, *278*, 115012. [CrossRef]

22. Meng, Q.; Qi, X.; Fu, Y.; Chen, Q.; Cheng, P.; Yu, X.; Sun, X.; Wu, J.; Li, W.; Zhang, Q.; et al. Flavonoids extracted from mulberry (*Morus alba* L.) leaf improve skeletal muscle mitochondrial function by activating AMPK in type 2 diabetes. *J. Ethnopharmacol.* **2020**, *248*, 112326. [CrossRef] [PubMed]
23. Zhang, L.; Su, S.; Zhu, Y.; Guo, J.; Guo, S.; Qian, D.; Ouyuan, Z.; Duan, J. Mulberry leaf active components alleviate type 2 diabetes and its liver and kidney injury in db/db mice through insulin receptor and TGF-β/Smads signaling pathway. *Biomed. Pharmacother.* **2019**, *112*, 108675. [CrossRef] [PubMed]
24. Zhong, Y.; Song, B.; Zheng, C.; Zhang, S.; Yan, Z.; Tang, Z.; Kang, X.; Duan, Y.; Li, F. Flavonoids from mulberry leaves alleviate lipid dysmetabolism in high fat diet-fed mice: Involvement of gut microbiota. *Microorganisms* **2020**, *8*, 860. [CrossRef] [PubMed]
25. Yang, J.; Chen, B.; Huang, Y.; Cao, J.; Wang, G.; Sun, Y.; Chen, X. Effects of dietary mulberry leaf flavonoids on growth performance, body composition, antioxidant indices and resistance to nitrite exposure of genetic improvement of farmed Tilapia (*Oreochromis niloticus*). *Chin. J. Anim. Nutr.* **2017**, *29*, 3403–3412.
26. Wang, Y.; Chen, B.; Cao, J.; Huang, Y.; Wang, G.; Peng, K. Effects of mulberry leaf flavonoids on intestinal mucosal morphology and intestinal flora of *Litopenaeus vannamei*. *Chin. J. Anim. Nutr.* **2020**, *32*, 1817–1825.
27. Yang, D.; Chen, F.; Li, D.; Liu, B. Requirements of nutrients and optimum energy protein ratio in the diet for *Monoterus albus*. *J. Fish. China* **2000**, *3*, 259–262.
28. Shi, Y.; Zhong, L.; Ma, X.; Liu, Y.; Tang, T.; Hu, Y. Effect of replacing fishmeal with stickwater hydrolysate on the growth, serum biochemical indexes, immune indexes, intestinal histology and microbiota of rice field eel (*Monopterus albus*). *Aquac. Rep.* **2019**, *15*, 100223. [CrossRef]
29. Shi, Y.; Zhong, L.; Zhong, H.; Zhang, J.; Che, C.; Fu, G.; Hu, Y.; Mai, K. Taurine supplements in high-fat diets improve survival of juvenile *Monopterus albus* by reducing lipid deposition and intestinal damage. *Aquaculture* **2022**, *547*, 737431. [CrossRef]
30. Shi, Y.; Zhong, L.; Zhong, H.; Zhang, J.; Liu, X.; Peng, M.; Fu, G.; Hu, Y. Taurine supplements in high-carbohydrate diets increase growth performance of *Monopterus albus* by improving carbohydrate and lipid metabolism, reducing liver damage, and regulating intestinal microbiota. *Aquaculture* **2022**, *554*, 738150. [CrossRef]
31. Shi, Y.; Zhong, L.; Liu, Y.L.; Zhang, J.Z.; Lv, Z.; Li, Y.; Hu, Y. Effects of dietary andrographolide levels on growth performance, antioxidant capacity, intestinal immune function and microbioma of rice field eel (*Monopterus albus*). *Animals* **2020**, *10*, 1744. [CrossRef]
32. Livak, K.J.; Schmittgen, T.D. Schmittgen, Analysis of relative gene expression data using Real-Time Quantitative PCR and the $2^{-\triangle\triangle CT}$ Method. *Methods* **2001**, *25*, 402–408. [CrossRef] [PubMed]
33. Hu, Q.; Guo, W.; Gao, Y.; Tang, R.; Li, D. Reference gene selection for real-time RT-PCR normalization in rice field eel (*Monopterus albus*) during gonad development. *Fish Physiol. Biochem.* **2014**, *40*, 1721–1730. [CrossRef] [PubMed]
34. Callahan, B.J.; Mcmurdie, P.J.; Rosen, M.J.; Han, A.W.; Johnson, A.J.; Holmes, S.P. Dada2: High-resolution sample inference from illumina amplicon data. *Nat. Methods* **2016**, *13*, 581–583. [CrossRef] [PubMed]
35. Susanto, A.; Hutabarat, J.; Anggoro, S. The effects of dietary carbohydrate level on the growth performance, body composition and feed utilization of juvenile kelabau (*Osteochilus melanopleurus*). *Aquac. Aquar. Conserv. Legis.* **2020**, *13*, 2061–2070.
36. Peng, K.; Wang, G.; Zhao, H.; Wang, Y.; Mo, W.; Wu, H.; Huang, Y. Effect of high level of carbohydrate and supplementation of condensed tannins on growth performance, serum metabolites, antioxidant and immune response, and hepatic glycometabolism gene expression of *Lateolabrax japonicus*. *Aquac. Rep.* **2020**, *18*, 100515. [CrossRef]
37. Li, S.; Li, Z.; Zhang, J.; Sang, C.; Chen, N. The impacts of dietary carbohydrate levels on growth performance, feed utilization, glycogen accumulation and hepatic glucose metabolism in hybrid grouper (*Epinephelus fuscoguttatus* ♀× *E. lanceolatus* ♂). *Aquaculture* **2019**, *512*, 734351. [CrossRef]
38. Lin, S.M.; Shi, C.M.; Mu, M.M.; Chen, Y.J.; Luo, L. Effect of high dietary starch levels on growth, hepatic glucose metabolism, oxidative status and immune response of juvenile largemouth bass, *Micropterus salmoides*. *Fish Shellfish Immunol.* **2018**, *78*, 121–126. [CrossRef]
39. Qi, S.; Wang, T.; Chen, R.; Wang, C.; Ao, C. Effects of flavonoids from *Allium mongolicum Regel* on growth performance and growthrelated hormones in meat sheep. *Anim. Nutr.* **2017**, *3*, 33–38.
40. Li, M.; Zhu, X.; Tian, J.; Liu, M.; Wang, G. Dietary flavonoids from *Allium mongolicum Regel* promotes growth, improves immune, antioxidant status, immune-related signaling molecules and disease resistance in juvenile northern snakehead fish (*Channa argus*). *Aquaculture* **2019**, *501*, 473–481. [CrossRef]
41. Xu, R.; Li, M.; Wang, T.; Zhao, Y.W.; Shan, C.J.; Qiao, F.; Chen, L.Q.; Zhang, W.B.; Du, Z.Y.; Zhang, M.L. *Bacillus amyloliquefaciens* ameliorates high-carbohydrate diet-induced metabolic phenotypes by restoration of intestinal acetate-producing bacteria in Nile Tilapia. *Br. J. Nutr.* **2022**, *127*, 653–665. [CrossRef]
42. Enes, P.; Panserat, S.; Kaushik, S.; Oliva-Teles, A. Nutritional regulation of hepatic glucose metabolism in fish. Fish. *Physiol. Biochem.* **2009**, *35*, 519–539. [CrossRef] [PubMed]
43. Han, M.; Cao, X.; Zhao, C.; Yang, L.; Yin, N.; Shen, P.; Zhang, J.; Gao, F.; Ren, Y.; Liang, D.; et al. Assessment of glycometabolism impairment and glucose variability using flash glucose monitoring system in patients with adrenal diseases. *Front. Endocrinol.* **2020**, *11*, 544752. [CrossRef] [PubMed]
44. Kim, J.Y.; Ok, H.M.; Kim, J.; Park, S.W.; Kwon, S.W.; Kwon, O. Mulberry leaf extract improves postprandial glucose response in prediabetic subjects: A randomized, double-blind placebo-controlled trial. *J. Med. Food.* **2015**, *18*, 306–313. [CrossRef] [PubMed]

45. Ren, C.; Zhang, Y.; Cui, W.; Lu, G.; Wang, Y.; Gao, H.; Huang, L.; Mu, Z. A polysaccharide extract of mulberry leaf ameliorates hepatic glucose metabolism and insulin signaling in rats with type 2 diabetes induced by high fat-diet and streptozotocin. *Int. J. Biol. Macromol.* **2015**, *72*, 951–959. [CrossRef] [PubMed]
46. Cross, D.A.; Alessi, D.R.; Cohen, P.; Andjelkovich, M.; Hemmings, B.A. Inhibition of glycogen synthase kinase-3 by insulin mediated by protein kinase B. *Nature* **1995**, *378*, 785–789. [CrossRef]
47. Zhou, C.P.; Ge, X.P.; Liu, B.; Xie, J.; Miao, L.H. Effect of high dietary carbohydrate on the growth performance and physiological responses of juvenile Wuchang bream, *Megalobrama amblycephala*. *Asian Australas. J. Anim. Sci.* **2013**, *26*, 1598–1608. [CrossRef]
48. Xu, X.; Chen, N.; Liu, Z.; Gou, S.; Yin, J. Effects of dietary starch sources and levels on liver histology in largemouth bass, *Micropterus salmoides*. *J. Shanghai Ocean Univ.* **2016**, *25*, 61–70.
49. Dinu, D.; Marinescu, D.; Munteanu, M.C.; Staicu, A.C.; Costache, M.; Dinischiotu, A. Modulatory effects of deltamethrin on antioxidant defense mechanisms and lipid peroxidation in *Carassius auratus gibelio* liver and intestine. *Arch. Environ. Contam. Toxicol.* **2010**, *58*, 757–764. [CrossRef]
50. Ramalingam, M.; Kim, S.J. Reactive oxygen/nitrogen species and their functional correlations in neurodegenerative diseases. *J. Neural Transm.* **2012**, *119*, 891–910. [CrossRef]
51. Sies, H. Oxidative stress: From basic research to clinical application. *Am. J. Med.* **1991**, *91*, 31–38. [CrossRef]
52. Mehra, L.; Hasija, Y.; Mittal, G. Therapeutic potential of alpha-ketoglutarate against acetaminophen-induced hepatotoxicity in rats. *J. Pharm. Bioallied Sci.* **2016**, *8*, 296–299. [PubMed]
53. Rymuszka, A.; Adaszek, Ł. Pro- and anti-inflammatory cytokine expression in carp blood and head kidney leukocytes exposed to cyanotoxin stress-an in vitro study. *Fish Shellfish Immunol.* **2012**, *33*, 382–388. [CrossRef] [PubMed]
54. Cao, G.; Sofic, E.; Prior, R.L. Antioxidant and prooxidant behavior of flavonoids: Structure-activity relationships. *Free Radic. Biol. Med.* **1997**, *22*, 749–760. [CrossRef]
55. Liskova, A.; Samec, M.; Koklesova, L.; Samuel, S.M.; Zhai, K.; Al-Ishaq, R.K.; Abotaleb, M.; Nosal, V.; Kajo, K.; Ashrafizadeh, M.; et al. Flavonoids against the SARS-CoV-2 induced inflammatory storm. *Biomed. Pharmacother.* **2021**, *138*, 111430. [CrossRef] [PubMed]
56. Zhao, L.; Yuan, B.D.; Zhao, J.L.; Jiang, N.; Zhang, A.Z.; Wang, G.Q.; Li, M.Y. Amelioration of hexavalent chromium-induced bioaccumulation, oxidative stress, tight junction proteins and immune-related signaling factors by *Allium mongolicum Regel* flavonoids in *Ctenopharyngodon idella*. *Fish Shellfish Immunol.* **2020**, *106*, 993–1003. [CrossRef]
57. Li, M.Y.; Guo, W.Q.; Guo, G.L.; Zhu, X.M.; Niu, X.T.; Shan, X.F.; Tian, J.X.; Wang, G.Q.; Zhang, D.M. Effect of sub-chronic exposure to selenium and Allium mongolicum Regel flavonoids on *Channa argus*: Bioaccumulation, oxidative stress, immune responses and immune-related signaling molecules. *Fish Shellfish Immunol.* **2019**, *91*, 122–129. [CrossRef]
58. Banjarnahor, S.D.S.; Artanti, N. Antioxidant properties of flavonoids. *Med. J. Indones.* **2015**, *23*, 239–244. [CrossRef]
59. Shi, Y.; Hu, Y.; Wang, Z.; Zhou, J.; Zhang, J.; Zhong, H.; Fu, G.; Zhong, L. The protective effect of taurine on oxidized fish-oil-induced liver oxidative stress and intestinal barrier-function impairment in juvenile *Ictalurus punctatus*. *Antioxidants* **2021**, *10*, 1690. [CrossRef]
60. Xu, C.; Liu, W.B.; Remø, S.C.; Wang, B.K.; Shi, H.J.; Zhang, L.; Liu, J.D.; Li, X.F. Feeding restriction alleviates high carbohydrate diet-induced oxidative stress and inflammation of Megalobrama amblycephala by activating the AMPK-SIRT1 pathway. *Fish Shellfish Immunol.* **2019**, *92*, 637–648. [CrossRef]
61. Jung, K.A.; Kwak, M.K. The Nrf2 system as a potential target for the development of indirect antioxidants. *Molecules* **2010**, *15*, 7266–7291. [CrossRef]
62. Baraka, S.M.; Saleh, D.O.; Ghaly, N.S.; Melek, F.R.; El Din, A.A.G.; Khalil, W.K.B.; Said, M.M.; Medhat, A.M. Flavonoids from Barnebydendron riedelii leaf extract mitigate thioacetamide-induced hepatic encephalopathy in rats: The interplay of NF-κB/IL-6 and Nrf2/HO-1 signaling pathways. *Bioorg. Chem.* **2020**, *105*, 104444. [CrossRef] [PubMed]
63. Goya, L.; Sarriá, B.; Ramos, S.; Mateos, R.; Bravo, L. Effect of cocoa and its flavonoids on biomarkers of inflammation: Studies of cell culture, animals and humans. *Nutrients* **2016**, *8*, 212. [CrossRef] [PubMed]
64. Fan, Y.; Pedersen, O. Gut microbiota in human metabolic health and disease. *Nat. Rev. Microbiol.* **2021**, *19*, 55–71. [CrossRef]
65. Wastyk, H.C.; Fragiadakis, G.K.; Perelman, D.; Dahan, D.; Merrill, B.D.; Yu, F.B.; Topf, M.; Gonzalez, C.G.; Treuren, W.V.; Han, S.; et al. Gut-microbiota-targeted diets modulate human immune status. *Cell* **2021**, *184*, 4137–4153. [CrossRef] [PubMed]
66. Hamer, H.M.; Jonkers, D.; Venema, K.; Vanhoutvin, S.; Troost, F.; Brummer, R. The role of butyrate on colonic function. *Aliment. Pharmcol. Ther.* **2008**, *27*, 104–119. [CrossRef] [PubMed]
67. Hong, J.; Jia, Y.; Pan, S.; Jia, L.; Li, H.; Han, Z.; Cai, D.; Zhan, R. Butyrate alleviates high fat diet-induced obesity through activation of adiponectin-mediated pathway and stimulation of mitochondrial function in the skeletal muscle of mice. *Oncotarget* **2016**, *7*, 56071–56082. [CrossRef]
68. Aalamifar, H.; Soltanian, S.; Vazirzadeh, A.; Akhlaghi, M.; Morshedi, V.; Gholamhosseini, A.; Torfi Mozanzadeh, M. Dietary butyric acid improved growth, digestive enzyme activities and humoral immune parameters in Barramundi (*Lates calcarifer*). *Aquac. Nutr.* **2020**, *26*, 156–164. [CrossRef]
69. Teuber, M. The genus Lactococcus. In *The Genera of Lactic Acid Bacteria*; Springer: Boston, MA, USA, 1995; Volume 2, pp. 173–234.
70. Vendrell, D.; Balcázar, J.L.; Ruiz-Zarzuela, I.; de Blas, I.; Gironés, O.; Múzquiz, J.L. Lactococcus garvieae in fish: A review. *Comp. Immunol. Microbiol. Infect. Dis.* **2006**, *29*, 177–198. [CrossRef]

71. Hage-Hülsmann, J.; Klaus, O.; Linke, K.; Troost, K.; Gora, L.; Hilgers, F.; Wirtz, A.; Santiago-Schübel, B.; Loeschcke, A.; Karl-Erich Jaeger, K.E.; et al. Production of C20, C30 and C40 terpenes in the engineered phototrophic bacterium Rhodobacter capsulatus. *J. Biotechnol.* **2021**, *338*, 20–30. [CrossRef]
72. Murota, K.; Nakamura, Y.; Uehara, M. Flavonoid metabolism: The interaction of metabolites and gut microbiota. *Biosci. Biotechnol. Biochem.* **2018**, *82*, 600–610. [CrossRef]
73. Song, D.; Ho, C.T.; Zhang, X.; Wu, Z.; Cao, J. Modulatory effect of Cyclocarya paliurus flavonoids on the intestinal microbiota and liver clock genes of circadian rhythm disorder mice model. *Food Res. Int.* **2020**, *138*, 109769. [CrossRef] [PubMed]
74. Bi, Y.; Yang, C.; Diao, Q.; Tu, Y. Effects of dietary supplementation with two alternatives to antibiotics on intestinal microbiota of preweaned calves challenged with *Escherichia coli* K99. *Sci. Rep.* **2017**, *7*, 5439. [CrossRef] [PubMed]

antioxidants

MDPI

Article

Mechanism of Cadmium Exposure Induced Hepatotoxicity in the Mud Crab (*Scylla paramamosain*): Activation of Oxidative Stress and Nrf2 Signaling Pathway

Changhong Cheng, Hongling Ma, Guangxin Liu, Sigang Fan and Zhixun Guo *

Key Laboratory of South China Sea Fishery Resources Exploitation & Utilization, Ministry of Agriculture and Rural Affairs, South China Sea Fisheries Research Institute, Chinese Academy of Fishery Sciences, Guangzhou 510300, China; chengchanghong09@163.com (C.C.); maling.5679@163.com (H.M.); Guangxin_liu1988@163.com (G.L.); fansigang@scsfri.ac.cn (S.F.)
* Correspondence: guozhixun1@163.com

Abstract: Cadmium, one of the most toxic heavy metals, can cause severe oxidative damage to aquatic animals. However, the mechanism whereby the mud crabs respond to cadmium exposure remains unclear. This study investigated the effects of cadmium exposure on oxidative stress and histopathology changes and evaluated the role of the Nrf2 signaling pathway in regulating responses to cadmium-induced hepatotoxicity were investigated in mud crabs. Mud crabs were exposed to 0, 0.01, 0.05, and 0.125 mg/L cadmium for 21 d. The present results indicated that cadmium exposure increased hydrogen peroxide (H_2O_2) production, lipid peroxidation and tissue damage, but decreased the activity of superoxide dismutase (SOD) and catalase (CAT), and caused lipid peroxidation and tissue damage. The results of an integrated biomarker index analysis suggested that the toxicity of cadmium was positively related to cadmium concentration. The expression levels of the Nrf2 signaling pathway (Nrf2, metallothionein, and cytochrome P450 enzymes) were up-regulated after cadmium exposure. Silencing of Nrf2 in vivo decreased antioxidant gene (SOD, CAT, and glutathione S-transferase) expression, suggesting that Nrf2 can regulate antioxidant genes. Knocking down Nrf2 in vivo also significantly decreased the activity of SOD and CAT after cadmium exposure. Moreover, silencing of Nrf2 in vivo enhanced H_2O_2 production and the mortality rates of mud crabs after cadmium exposure. The present study indicated that cadmium exposure induced hepatotoxicity in the mud crab by increasing H_2O_2 content, which decreased the antioxidant capacity, leading to cell injury. In addition, the Nrf2 is activated to bound with antioxidant response element, initiating the expression of antioxidant enzyme genes during cadmium induced hepatotoxicity in the mud crabs.

Keywords: *Scylla paramamosain*; Nrf2 signaling pathway; oxidative stress; hepatotoxicity

Citation: Cheng, C.; Ma, H.; Liu, G.; Fan, S.; Guo, Z. Mechanism of Cadmium Exposure Induced Hepatotoxicity in the Mud Crab (*Scylla paramamosain*): Activation of Oxidative Stress and Nrf2 Signaling Pathway. *Antioxidants* **2022**, *11*, 978. https://doi.org/10.3390/antiox11050978

Academic Editors: Bo Liu, Changyou Song and Cunxin Sun

Received: 13 April 2022
Accepted: 11 May 2022
Published: 17 May 2022

1. Introduction

Heavy metal pollution in aquatic environments has serious harmful effects on living organisms. Heavy metals from mine wastes, fertilizer use, and industrial waste are the main sources of pollution in the aquatic environment. Heavy metals can be easily accumulated in organisms, which might ultimately affect human health [1]. Among these heavy metal pollutants, cadmium is a nonessential heavy metal that has high toxic effects on the health of humans and the environment. In natural surface water, the level of cadmium concentration is very low. However, a high level of cadmium concentration in many areas of China can reach as high as 100–900 μg/L [2]. The toxicity of cadmium can harm development and reproduction, decrease growth and survival, and damage tissues and organs [3–5]. Although many reports have shown the toxic effects of cadmium on aquatic animals, the mechanisms involved are not well understood.

It has been reported that reactive oxygen species (ROS) can be induced by cadmium exposure, which might cause oxidative stress, leading to damage to macromolecules, such

as DNA and proteins [6,7]. To prevent the formation of ROS, organisms develop an antioxidant system, which consists of antioxidant enzymes. Nrf2 is a basic leucine zipper nuclear transcription factor that plays a key role in response to various environmental pollutants [8]. It is responsible for regulating the expression of a variety of antioxidant genes [9]. Therefore, activation of the Nrf2 signaling pathway can regulate antioxidant and detoxification cellular responses [10]. Nrf2 might participate in host defense during antibacterial immunity response [11]. Many studies have also shown that the activation of the Nrf2 pathway could protect against hepatotoxicity induced by heavy metal pollution [12,13]. However, the role and the regulatory mechanism of the Nrf2 signaling pathway in crustaceans against cadmium exposure still need further study.

Cytochrome P450 enzymes (CYPs) are a hemoglobin superfamily that plays a crucial role in the degradation and detoxification of xenobiotics. Activation of CYPs is involved in responses to oxidative stress [14]. A previous study showed that cadmium exposure could induce the expression of CYPs [15]. In addition, CYPs have been used as a sensitive biomarker for heavy metal exposure [16]. Metallothionein (MT) is a low molecular weight protein that contains cysteine. MT is also involved in transporting various metals [17]. It plays an important role in the detoxification of metals and the scavenging of free radicals [18]. The induction of MT expression has been widely applied as a biomarker for the toxicity of heavy metals [19].

Mud crab (*Scylla paramamosain*) is an important commercial crustacean that is widely distributed in the warm temperate zones of Southeast Asia. It has become more and more popular in Chinese markets due to its high quality and fast growth. It is also exposed to various pollutants due to its habitat and diet. Therefore, understanding the mechanisms of detoxification might lead to the development of ways to protect mud crabs against environmental stressors. In this study, the effects of cadmium exposure on the antioxidant system and resulting histopathological alterations were investigated. To understand the Nrf2 signaling pathway in cadmium-induced hepatotoxicity in mud crabs, mRNA levels of Nrf2, CYP2, and MT after cadmium exposure were examined. Furthermore, we used RNAi technology to determine the function of the Nrf2 signaling pathway in response to cadmium exposure. This study will help us to understand the defense mechanism of crustaceans against environmental stress.

2. Materials and Methods

2.1. Mud Crabs

Mud crabs (51 ± 3 g) were collected from a mud crab farm (Taishan, China) and acclimated in tanks with circulating seawater (5 ppt salinity) at 25 ± 1 °C. During the acclimation period, they were fed a commercial diet twice a day.

2.2. Cadmium Exposure

Cadmium chloride was obtained from Sigma (Sigma, St. Louis, MO, USA). In our preliminary experiments, we found that 96 h LC50 of cadmium on mud crabs was approximately 10 mg/L. A stock solution of cadmium chloride (1 g/L) was used as a source of cadmium and was subsequently diluted to the desired concentrations. In the present study, groups of mud crabs were treated with 0 (control), 0.01 (1/1000 96 h-LC50), 0.05 (1/200 96 h-LC50), or 0.125 (1/200 96 h-LC50) mg/L Cd^{2+}. Each group included three tanks, and each tank contained 20 mud crabs. The water was changed daily. Water samples were acidified with HNO_3. Cadmium concentrations in water were quantified with ICP-OES (Optima 8300, Perkin Elmer Instruments, Waltham, MA, USA) [20]. Water quality parameters were as follows: salinity 5 ppt, temperature 25 ± 1 °C, and total ammonia < 0.05 mg/L. After 21 days of challenge, nine mud crabs from the control group and each cadmium treatment group were sampled. Hepatopancreas tissues were collected for the oxidative stress study.

2.3. Measurement of Oxidative Stress Parameters

Six hepatopancreas tissues from each group were homogenized in a homogenization buffer. After tissue homogenization, cell suspensions were centrifuged at 3000× *g* for 15 min. Finally, the supernatants were collected for the analyses of biochemical parameters. The measurement of superoxide dismutase (SOD), catalase (CAT), total antioxidant capacity (T-AOC), hydrogen peroxide (H_2O_2), and malondialdehyde (MDA) was performed using the corresponding assay kits (Nanjing Jiancheng Bioengineering Institute, Nanjing, China) according to the manufacturer's protocols. SOD and CAT were analyzed according to the method of Jia et al. [21]. H_2O_2 content was measured according to the method of Lin et al. [22]. MDA content was assayed according to the method of Ohkawa et al. [23] using the thiobarbituric acid reactive species assay at 532 nm. T-AOC was determined by the reduction of a ferric tripyridyltriazine complex to ferrous tripyridyltriazine [24].

2.4. Comprehensive Toxicity Assessment

An integrated biological responses version 2 (IBRv2) analysis was used to assess the toxicity of cadmium as described by Sanchez et al. [25]. An IBRv2 value was calculated based on biomarkers, including SOD, CAT, T-AOC, H_2O_2, and MDA. An IBRv2 value can provide a better understanding of the harmful effects of cadmium exposure.

2.5. Histopathologic Investigation

Six hepatopancreas tissues from each group were immediately fixed in 10% formaldehyde, embedded in paraffin, and stained with hematoxylin and eosin. Then, the stained sections were viewed under a light microscope (Olympus, Tokyo, Japan).

2.6. Quantitative Real-Time PCR (qRT-PCR) Analysis

Total RNA was extracted from the hepatopancreas using RNAiso Plus reagent (Takara, Dalian, China) according to the manufacturer's recommendations. The quality of the RNA was verified by agarose electrophoresis. Single-strand cDNA was synthesized using a PrimeScriptTM reverse transcriptase kit (Takara, Dalian, China). A qRT-PCR was performed to measure the expression of Nrf2, CYP2, and MT (Table S1). The qRT-PCR was carried out in a Qtower96G real-time system (Jena, Germany) using SYBR Green. The reaction mixtures were 20 μL, containing 2 μL of diluted cDNA sample (50 ng/μL), 10 μL 2 × SYBR Premix Ex Taq, and 0.4 μL each of primer (10 μM) and 7.6 μL dH_2O. The qRT-PCR conditions were as follows: 94 °C for 10 min, then 45 cycles at 95 °C for 30 s or 60 °C for 30 s. 18S rRNA was utilized as a reference gene. All qRT-PCRs were performed at least in triplicate. The relative expression of each gene was determined via the $2^{-\Delta\Delta CT}$ method [26].

2.7. Nrf2 Silencing in Mud Crabs

For gene knockdown experiments, double-stranded RNA Nrf2 and green fluorescent protein (GFP) were amplified by PCR using gene-specific primers (Table S1). DsNrf2 and dsGFP were synthesized using the Transcription T7 Kit (Promega, Madison, WI, USA) following the manufacturer's protocol. Sixty mud crabs were separated into two groups. One group was injected with 50 ug dsNrf2, and the other group was injected with an equivalent of dsGFP. At 48 h after injection, six hepatopancreas tissues from each group were sampled for RNA extraction. To explore the functions of Nrf2, the mRNA expressions of antioxidant enzyme genes (SOD, CAT, GST, and Gpx3) were investigated in both the Nrf2-silenced group and the control (dsGFP) group. A qRT-PCR was performed as described above.

2.8. Cadmium Exposure in Nrf2-Silenced Mud Crabs

To understand the effects of cadmium exposure on mud crabs after Nrf2 gene silencing, 120 mud crabs were injected with dsNrf2 and dsGFP, respectively. At 48 h after injection, both groups were acutely exposed to 2.5 mg/L cadmium (1/4 96 h-LC50). Six hepatopancreas tissues from each group were collected at 0, 6, 12, and 24 h after cad-

mium exposure. Then, these hepatopancreas tissues were used to measure SOD, CAT, T-AOC, and H_2O_2. Measurements of these oxidative stress parameters were detected as described in Section 2.3. Meanwhile, the numbers of dead mud crabs in both the Nrf2-silenced group and the control group were recorded after cadmium exposure.

2.9. Statistical Analysis

The experimental data were presented as means ± standard deviation. For all analyses, Levene and Shapiro–Wilk tests were used to verify the homogeneity and normality of variances, respectively. Differences between groups were analyzed using a one-way ANOVA followed by Duncan's multiple range tests in SPSS 18.0 software (SPSS; Chicago, IL, USA). A p-value < 0.05 was considered a significant difference.

3. Results

3.1. Oxidative Stress and IBRv2 after Cadmium Exposure

As shown in Figure 1A, SOD activity did not change in the treatment with 0.01 mg/L cadmium and significantly decreased in the treatments with 0.05 and 0.125 mg/L cadmium. CAT activity significantly decreased in the treatments with 0.01, 0.05, and 0.125 mg/L cadmium when compared with that in the control group (Figure 1B). T-AOC level was not significantly affected by cadmium exposure (Figure 1C). H_2O_2 content in the treatments with 0.05 and 0.125 mg/L cadmium was significantly higher than that in the control group (Figure 1D). Cadmium exposure strongly enhanced the levels of MDA in the 0.01, 0.05, and 0.125 mg/L cadmium treatments when compared with that in the control group. The highest levels of MDA were observed in the 0.05 and 0.125 mg/L cadmium treatments.

Based on the above-described oxidative stress biomarkers, IBRv2 values were calculated (Figure S1). IBRv2 values were positively correlated with cadmium concentrations. The highest IBRv2 value was 7.76 in the 0.125 mg/L cadmium group.

3.2. Histopathological Changes after Cadmium Exposure

Histopathological changes after cadmium exposure are shown in Figure 2. The hepatopancreas tissues of the control group displayed a normal histological appearance (Figure 2A). However, these hepatopancreas tissues showed some signs of cell border diffusion and cytoplasmic vacuolization when exposed to 0.01 mg/L cadmium (Figure 2B). In addition, some signs of cell abscission and cell lysis were observed in the 0.05 and 0.125 mg/L cadmium treatments (Figure 2C,D).

3.3. Effects of Cadmium Exposure on the Expression of Nrf2, CYP2, and MT

As shown in Figure 3A, the expression level of Nrf2 significantly increased after cadmium exposure. The highest expression level of Nrf2 was observed in the 0.05 mg/L cadmium treatment. The transcription level of CYP2 significantly increased in the treatments with 0.01, 0.05 and 0.125 mg/L cadmium (Figure 3B). The expression level of MT in the treatments with 0.01, 0.05, and 0.125 mg/L cadmium was significantly higher than that in the control group (Figure 3C).

3.4. The Expression of Genes Related to Antioxidants after Knockdown of Nrf2

To understand the possible mechanism of Nrf2 in regulating antioxidant-related genes in mud crabs, Nrf2 was knocked down by the injection of Nrf2 dsRNA. The expression levels of Nrf2, SOD, GST, CAT, and Gpx3 are shown in Figure 4. The transcription level of Nrf2 in the dsNrf2 group at 48 h significantly decreased by 84% when compared with that in the control group. The expression levels of SOD, CAT, and GST in the dsNrf2 group were significantly lower than those in the dsGFP group after dsRNA injection. Compared to the control group, the change in Gpx3 showed no significant difference in the dsNrf2 group after dsRNA injection.

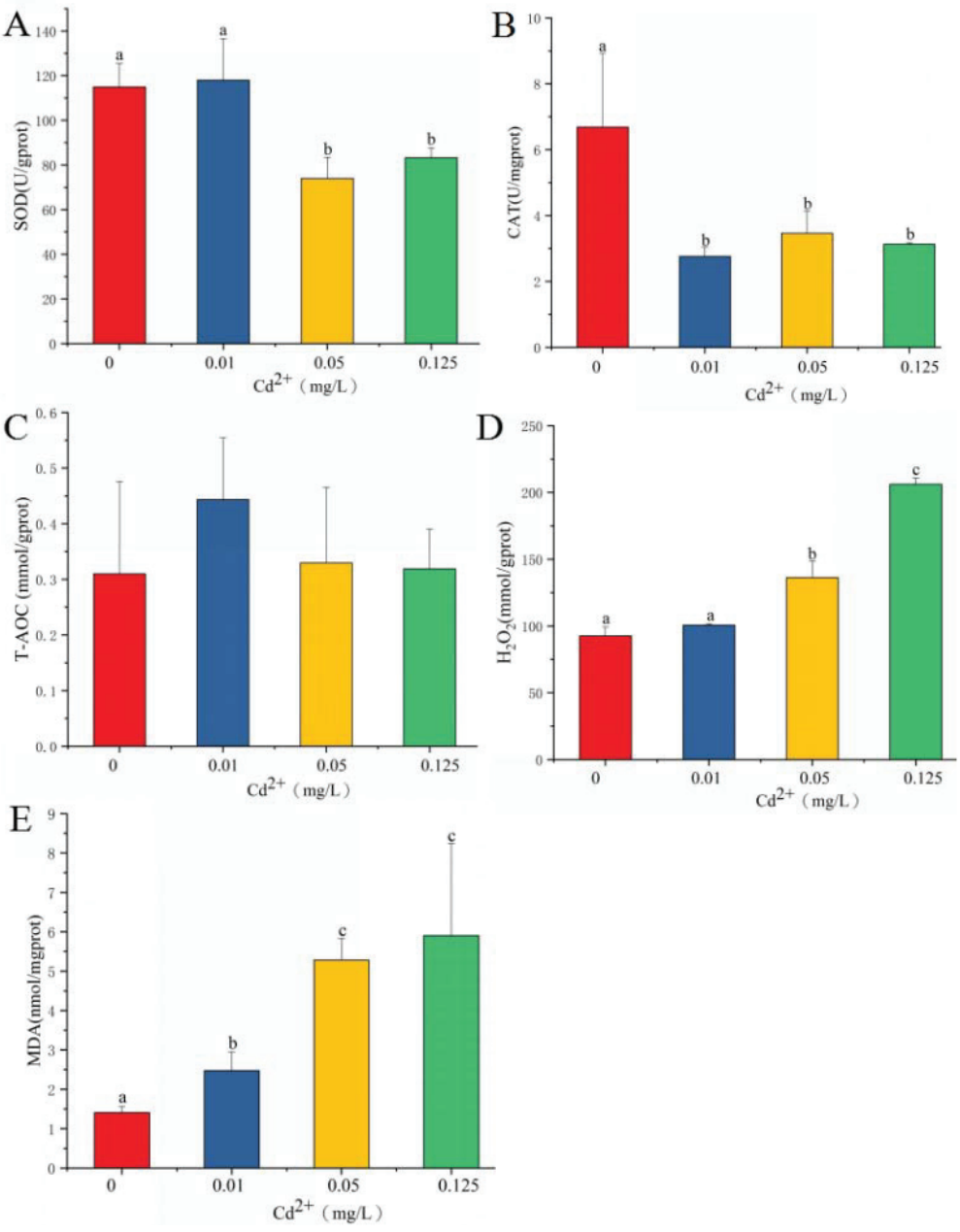

Figure 1. SOD (**A**), CAT (**B**), T-AOC (**C**), H_2O_2 (**D**), and MDA (**E**) after cadmium exposure. Values are expressed as the mean ± SD. Different letters reflect significant differences between the control group and the cadmium treatment groups ($p < 0.05$).

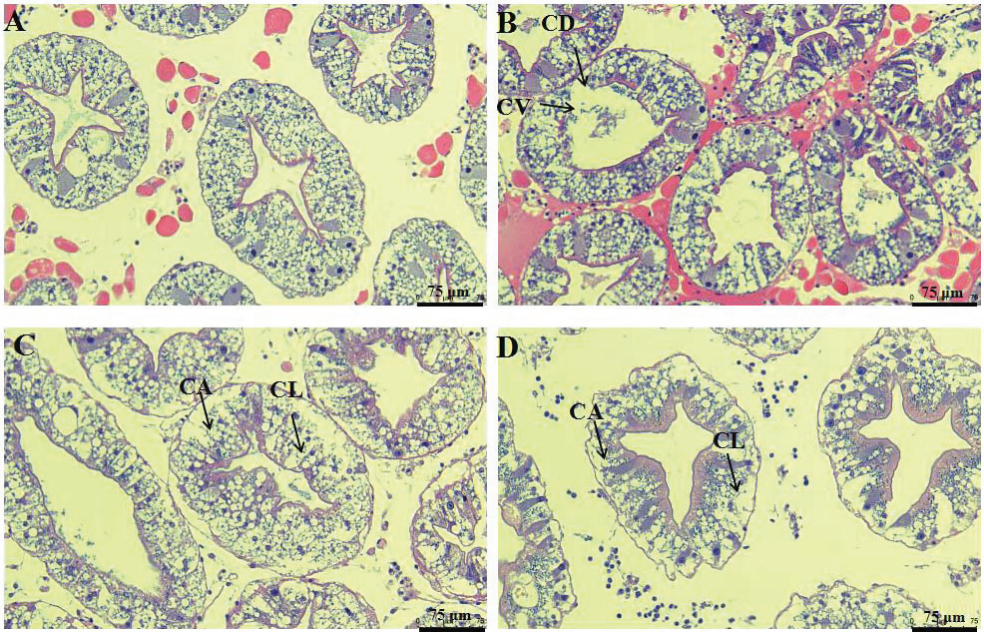

Figure 2. Histological changes after cadmium exposure: (**A**) control group; (**B**) 0.01 mg/L cadmium treatment group; (**C**) 0.05 mg/L cadmium treatment group; (**D**) 0.125 mg/L cadmium treatment group. Cell abscission (CA); Cytoplasmic vacuolization (CV); Cell border diffusion (CD); Cell lysis (CL).

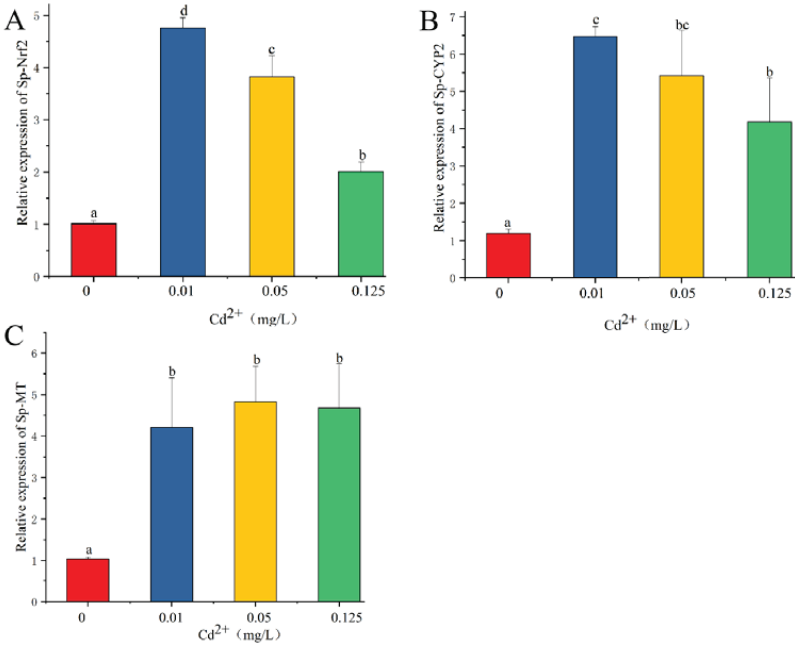

Figure 3. Effects of cadmium exposure on the expression levels of Nrf2 (**A**), CYP2 (**B**), and MT (**C**). Values are expressed as the mean ± SD. Different letters reflect significant differences between the control group and the cadmium treatment groups ($p < 0.05$).

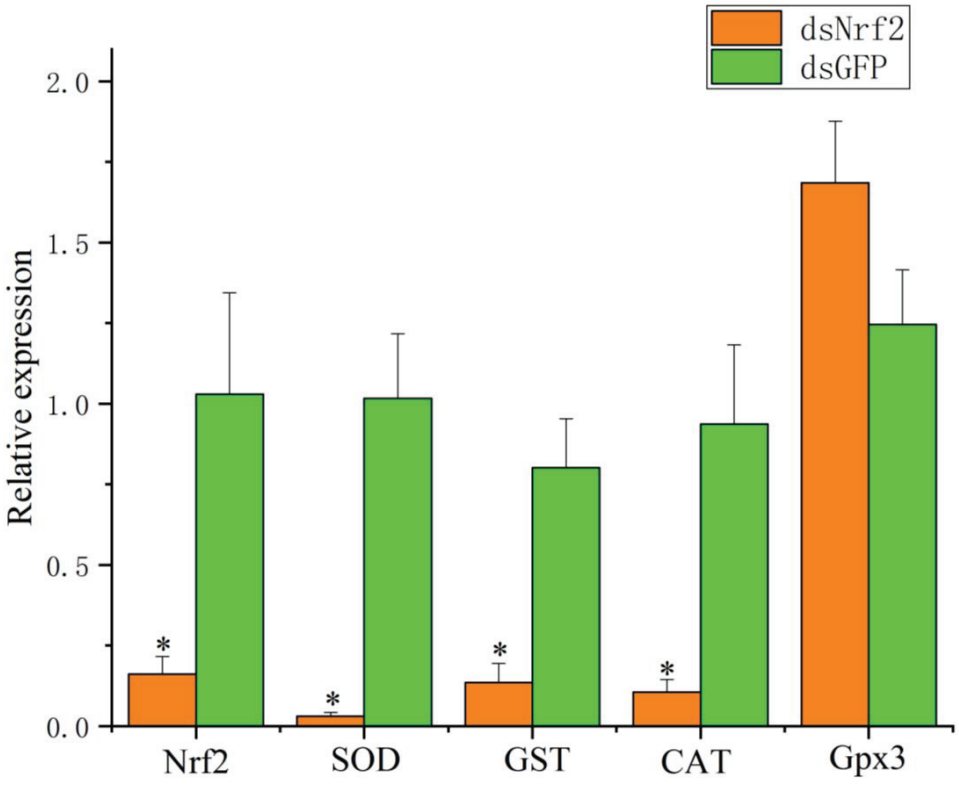

Figure 4. Expression levels of Nrf2, SOD, GST, CAT, and Gpx3 at 48 h after dsRNA injection. Values are expressed as the mean ± SD. Asterisks reflect significant differences between the dsNrf2 group and the dsGFP group (* $p < 0.05$).

3.5. Effects of Nrf2-Interfered on Oxidative Stress Biomarkers after Cadmium Exposure

As shown in Figure 5A, SOD activity in the control group significantly decreased at 6 and 12 h after cadmium exposure. SOD activity in the dsNrf2 group was significantly lower than in the dsGFP group at 0, 6, and 24 h after cadmium exposure. CAT activity in the control group significantly decreased at 12 h after cadmium exposure. CAT activity was lower at 0 and 6 h after cadmium exposure in the dsNrf2 group than in the control group (Figure 5B). T-AOC levels in both the dsNrf2 group and the dsGFP group did not change after cadmium exposure (Figure 5C). H_2O_2 content in the control group significantly increased from 6 to 24 h after cadmium exposure. H_2O_2 content was higher at 0 and 24 h after cadmium exposure in the dsNrf2 group than in the control group (Figure 5D).

3.6. The Mortality of Mud Crabs after Cadmium Exposure

The survival rates of mud crabs in the dsNrf2 group and dsGFP group after cadmium exposure are shown in Figure 6. Cumulative mortality of mud crabs was 87% in the dsNrf2 group and 63% in the control group at 60 h after cadmium exposure. Therefore, knocking down Nrf2 in vivo significantly decreased the survival rate of mud crabs after cadmium exposure.

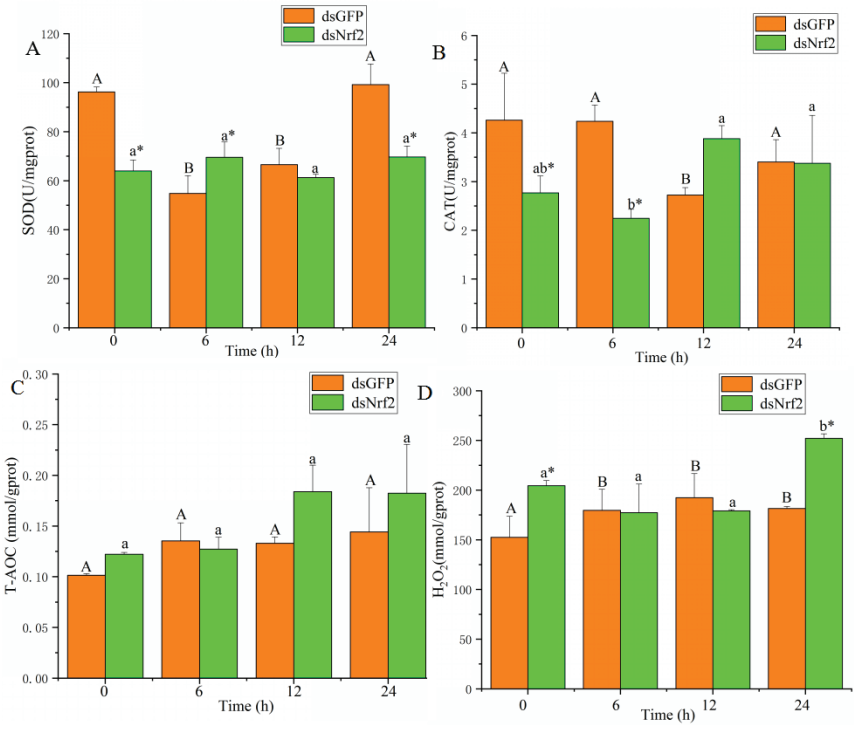

Figure 5. SOD (**A**), CAT (**B**), T-AOC (**C**), and H_2O_2 (**D**) in the dsNrf2 group and the dsGFP group after cadmium exposure. Values are expressed as the mean ± SD. Significant differences between the dsNrf2 group and the dsGFP group at each time are indicated by asterisks. Times in each group that have different letters were significantly different (* $p < 0.05$).

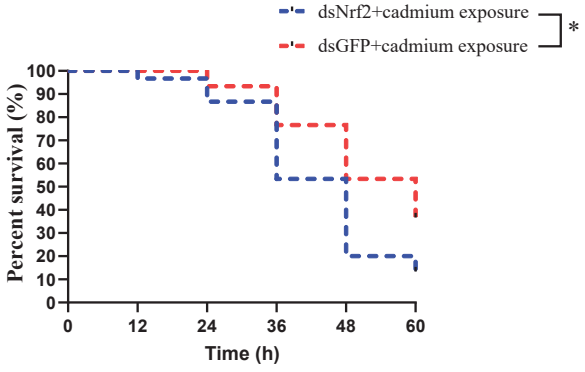

Figure 6. The percentage survival of mud crabs in the dsNrF2 group and dsGFP group (the dsGFP group was used as the control) after cadmium exposure. Asterisks reflected significant differences between the dsNrf2 group and the dsGFP group.

We also demonstrated a plausible mechanism of the Nrf2 signaling pathway in cadmium-induced hepatotoxicity in mud crabs (Figure 7).

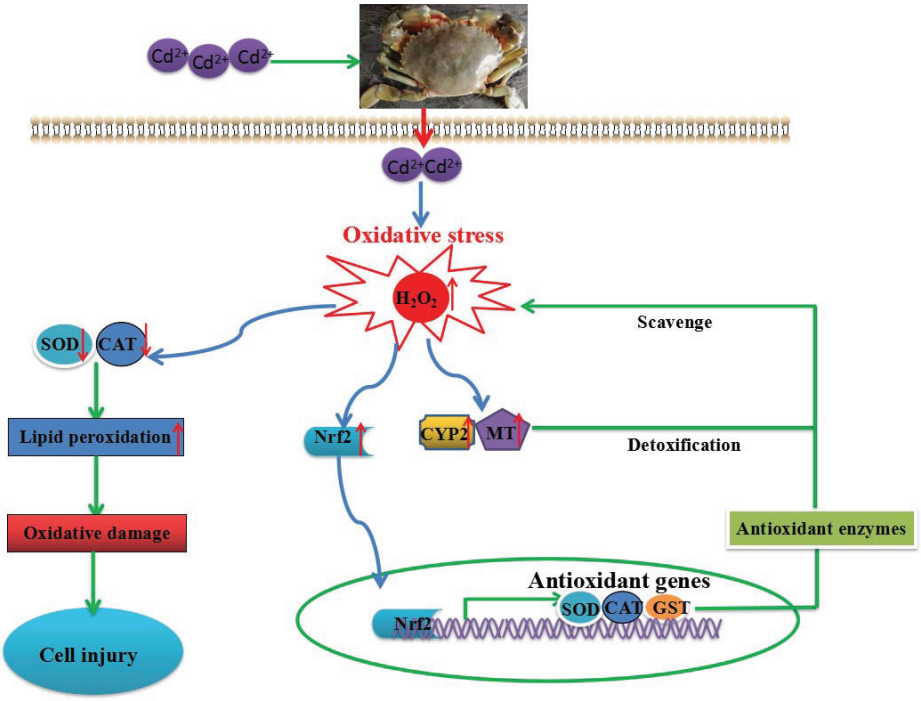

Figure 7. The molecular mechanism of the Nrf2 signaling pathway in cadmium-induced hepatotoxicity in mud crabs.

4. Discussion

Cadmium, one of the most toxic heavy metals, has negative effects on aquatic animals. However, the mechanisms of detoxification and antioxidant defense against cadmium exposure in crustaceans are still unclear. The Nrf2 signaling pathway is a master regulator of cellular responses by playing a crucial role in cellular detoxification against environmental stresses. In this study, we investigated the mechanism of the Nrf2 signaling pathway in response to cadmium stress in mud crabs.

Acute or chronic exposure to cadmium is mainly evident in the hepatopancreas. Excessive cadmium can damage hepatopancreas function. Cadmium is considered the inducer of ROS, causing oxidative stress [27]. Our study suggested that chronic exposure to 0.05 and 0.125 mg/L of cadmium induced H_2O_2 (a major by-product of ROS) production. The overproduction of ROS can promote protein and DNA damage. The antioxidant system is considered the first line of defense to remove surplus ROS. SOD and CAT are the most important antioxidant enzymes for scavenging superoxide and hydroxyl radicals. A previous study showed that cadmium suppressed the antioxidant enzyme activities and damaged the antioxidant defense system [7]. We found that chronic cadmium exposure decreased the activities of SOD and CAT and increased H_2O_2 content. This result indicated that a reduction in antioxidant capacity could cause lipid peroxidation. MDA is the end-product of lipid peroxidation. Elevated MDA levels have been reported in *Eriocheir sinensis* after cadmium exposure [22]. Similar results were also observed in this study, suggesting that chronic exposure to cadmium can cause severe oxidative damage. The tissue damage induced by cadmium was also marked by histopathological changes. Zhang et al. [20] reported that cadmium exposure caused obvious histological changes, including tubule lumen dilatation and epithelium vacuolization, in *Procambarus clarkii*. Our study found that histological changes after cadmium exposure included signs of cell lysis and abscission, suggesting that cadmium could damage the normal cellular structure and affect normal

physiological function. Moreover, the IBRv2 analysis also provided supporting evidence that the toxicity of cadmium is positively related to cadmium concentration.

The toxicity of cadmium is involved in the induction of host defenses. CYPs are monooxygenases that play a protective role in organisms against oxidative damage. A previous study reported that the mRNA levels of CYPs in common carp were increased after cadmium exposure, suggesting the activation of detoxification [15]. Our results showed that CYP2 was induced after cadmium exposure, indicating that detoxification is involved in cadmium-induced toxicity in mud crabs. MT, a group of ubiquitous low-molecular-weight proteins, is a promising candidate for heavy metal detoxification. MT is involved in the transport and storage of metals [17]. It can scavenge ROS through the oxidation of cysteine thiol groups. Activation of MT is involved in detoxification after heavy metal exposure [28]. The present study showed that the expression level of MT was strongly induced by cadmium exposure, which can alleviate the toxicity of cadmium.

Nrf2, a central regulator of cellular responses, plays a crucial role in coping with oxidative stress. The lack of Nrf2 can cause hepatic lipid peroxidation and hepatic injury [29]. Under normal physiological conditions, Nrf2 expression is controlled by Keap1. Under oxidative stress, Nrf2 is uncoupled from Keap1 and accumulated in the nucleus, which is bound with the antioxidant response element, initiating the expression of antioxidant enzyme genes [30]. Activated Nrf2 can mediate some signaling proteins to regulate innate immune responses, apoptosis, antioxidant function, and drug metabolism [9]. Dong et al. [31] reported that cadmium exposure activated Nrf2, which promoted antioxidant gene transcription. A previous study showed that Nrf2 activation prevented cadmium-induced acute liver injury [32]. The present study found that the transcription level of Nrf2 was up-regulated after cadmium exposure, suggesting that Nrf2 was activated to protect mud crabs against hepatopancreas damage induced by cadmium.

To further explore the regulation of the Nrf2 signaling pathway in mud crabs, we knocked down Nrf2 by injecting dsRNA. The expression levels of Nrf2 and some antioxidant enzyme genes, including SOD, CAT, and GST, significantly decreased in the Nrf2-interfered group when compared with the control group. Wang et al. [33] reported that after knocking down Nrf2 expression in clams, antioxidant gene expression was changed. Furthermore, we found that knocking down Nrf2 in mud crabs significantly reduced the activities of SOD and CAT and increased H_2O_2 content. All of these results suggest that Nrf2 is required for the induction of antioxidant defense genes.

To verify the function of Nrf2 involving in antioxidant defense against cadmium stress, we investigated the effects of Nrf2 silencing on the antioxidant enzymatic activities, H_2O_2 contents and cumulative mortality rates of mud crabs after cadmium exposure. The present study showed that H_2O_2 content in the Nrf2-interfered group was much higher than that in the control group at 24 h after cadmium exposure. These results might be evidence that knocking down Nrf2 inhibited gene expression as an antioxidant defense. Accumulation of ROS can damage cells, leading to cell death. The present study showed that the mortality of mud crabs in both the Nrf2-interfered and the control group significantly increased after cadmium exposure. This result is consistent with that obtained in a previous study [34]. The high mortality might be associated with higher H_2O_2 content and serious cell death after cadmium exposure. Moreover, after knocking down Nrf2, the mortality of mud crabs significantly increased after cadmium exposure. These results are attributed to that Nrf2 silencing may impair the antioxidant modulation of the mud crab exposed to cadmium. Therefore, all these results further confirm that the Nrf2 signaling pathway plays a vital role in mechanisms of detoxification and antioxidant defense against oxidative damage induced by cadmium exposure.

5. Conclusions

The present study demonstrated a plausible mechanism of the Nrf2 signaling pathway in cadmium-induced hepatotoxicity in mud crabs (Figure 7). The results showed that cadmium exposure increased H_2O_2 content and decreased antioxidant capacity, causing

severe tissue damage. In addition, the Nrf2 signaling pathway and detoxification were activated in cadmium-induced hepatotoxicity, which suggests they have essential roles in cadmium exposure. RNAi technology was used to investigate the antioxidant defense mechanisms of the Nrf2 signaling pathway. Knocking down Nrf2 in vivo significantly decreased the antioxidant capacity and increased the mortality of mud crabs after cadmium exposure. This study provided a novel insight into mechanisms of detoxification and antioxidant defense against cadmium exposure in crustaceans.

Supplementary Materials: The following supporting information can be downloaded at: https://www.mdpi.com/article/10.3390/antiox11050978/s1, Figure S1: IBRv2 values following biomarkers (SOD, CAT, MDA, T-AOC, and H_2O_2) in a gradient of cadmium exposure affection: (A) 0.01 mg/L cadmium treatment group; (B) 0.05 mg/L cadmium treatment group; (C) 0.125 mg/L cadmium treatment group. IBRv2 values were compared with the control group; Table S1: Primer sequences of all genes used in this study.

Author Contributions: Conceptualization, C.C.; methodology, C.C., H.M. and Z.G.; software, C.C.; formal analysis, G.L.; investigation, S.F. and G.L.; validation, Z.G.; resources, Z.G.; data curation, C.C.; writing—original draft preparation, C.C.; writing—review and editing, C.C.; supervision, Z.G.; project administration, Z.G.; funding acquisition, C.C. and Z.G. All authors have read and agreed to the published version of the manuscript.

Funding: This research was supported by the Key-Area Research and Development Program of Guangdong Province (2021B0202040001), the National Natural Science Foundation of China (32002380), the China Agriculture Research System of MOF and MARA (CARS-48), and Guangzhou Municipal Science and Technology Project (No. 202206010138).

Institutional Review Board Statement: All experimental protocols and methods in this study were approved by the Animal Care and Use Ethics Committee in the South China Sea Fisheries Research Institute (202100321m).

Informed Consent Statement: Not applicable.

Data Availability Statement: Data are contained within the article and Supplementary Materials.

Conflicts of Interest: The authors declare no conflict of interest.

References

1. Yi, Y.; Yang, Z.; Zhang, S. Ecological risk assessment of heavy metals in sediment and human health risk assessment of heavy metals in fishes in the middle and lower reaches of the Yangtze River basin. *Environ. Pollut.* **2011**, *159*, 2575–2585. [CrossRef] [PubMed]
2. Deng, G.; Li, M.; Li, H.; Yin, L.Y.; Li, W. Exposure to cadmium causes declines in growth and photosynthesis in the endangered aquatic fern (*Ceratopteris pteridoides*). *Aquat. Bot.* **2014**, *112*, 23–32. [CrossRef]
3. Sellin, M.K.; Kolok, A.S. Cadmium exposures during early development: DO they lead to reproductive impairment in fathead minnows? *Environ. Toxicol. Chem.* **2006**, *25*, 2957–2963. [CrossRef] [PubMed]
4. Mebane, C.A.; Hennessy, D.P.; Dillon, F.S. Developing acute-to-chronic toxicity ratios for lead, cadmium, and zinc using rainbow trout, a mayfly, and a midge. *Water Air Soil Pollut.* **2008**, *188*, 41–66. [CrossRef]
5. Zhang, Y.; Li, Z.; Kholodkevich, S.; Sharov, A.; Chen, C.; Feng, Y. Effects of cadmium on intestinal histology and microbiota in freshwater crayfish (*Procambarus clarkii*). *Chemosphere* **2020**, *242*, 125105. [CrossRef]
6. Cheng, C.H.; Ma, H.L.; Deng, Y.Q.; Feng, J.; Jie, Y.K.; Guo, Z.X. Oxidative stress, cell cycle arrest, DNA damage and apoptosis in the mud crab (*Scylla paramamosain*) induced by cadmium exposure. *Chemosphere* **2021**, *263*, 128277. [CrossRef]
7. Duan, Y.F.; Wang, Y.; Huang, J.H.; Li, H.; Dong, H.B.; Zhang, J.S. Toxic effects of cadmium and lead exposure on intestinal histology, oxidative stress response, and microbial community of Pacific white shrimp *Litopenaeus vannamei*. *Mar. Pollut. Bull.* **2021**, *167*, 112220. [CrossRef]
8. Cho, H.Y.; Reddy, S.P.; Kleeberger, S.R. Nrf2 defends the lung from oxidative stress. *Antioxid. Redox Sign.* **2006**, *8*, 76–87. [CrossRef]
9. Ma, Q. Role of nrf2 in oxidative stress and toxicity. *Annu. Rev. Pharmacol. Toxicol.* **2013**, *53*, 401–426. [CrossRef]
10. Osburn, W.O.; Kensler, T.W. Nrf2 signaling: An adaptive response pathway for protection against environmental toxic insults. *Mutat. Res.* **2008**, *659*, 31–39. [CrossRef]
11. Wang, Y.; Duan, Y.F.; Huang, J.H.; Wang, J.; Zhou, C.P.; Jiang, S.G.; Lin, H.Z.; Zhang, Z. Characterization and functional study of nuclear factor erythroid 2-related factor 2 (Nrf2) in black tiger shrimp (*Penaeus monodon*). *Fish Shellfish Immun.* **2021**, *119*, 289–299. [CrossRef] [PubMed]

12. Wang, L.; Gallagher, E.P. Role of Nrf2 antioxidant defense in mitigating cadmium-induced oxidative stress in the olfactory system of zebrafish. *Toxicol. Appl. Pharmacol.* **2013**, *266*, 177–186. [CrossRef] [PubMed]
13. Jiang, W.D.; Liu, Y.; Jiang, J.; Wu, P.; Feng, L.; Zhou, X.Q. Copper exposure induces toxicity to the antioxidant system via the destruction of Nrf2/ARE signaling and caspase-3-regulated DNA damage in fish muscle: Amelioration by myo-inositol. *Aquat. Toxicol.* **2015**, *159*, 245–255. [CrossRef] [PubMed]
14. Uno, T.; Ishizuka, M.; Itakur, T. Cytochrome P450 (CYP) in fish. *Environ. Toxicol. Pharmacol.* **2012**, *34*, 1–13. [CrossRef]
15. Sun, J.X.; Wang, S.C.; Cao, Y.R.; Wang, S.T.; Li, S. Cadmium exposure induces apoptosis, inflammation and immunosuppression through CYPs activation and antioxidant dysfunction in common carp neutrophils. *Fish Shellfish Immun.* **2020**, *99*, 284–290.
16. Cao, X.; Bi, R.; Song, Y. Toxic responses of cytochrome P450 sub-enzyme activities to heavy metals exposure in soil and correlation with their bioaccumulation in *Eisenia fetida*. *Ecotoxicol. Environ. Saf.* **2017**, *144*, 158–165. [CrossRef]
17. Isani, G.; Carpen, E. Metallothioneins, unconventional proteins from unconventional animals: A long journey from nematodes to mammals. *Biomolecules* **2014**, *4*, 435–457. [CrossRef]
18. Babula, P.; Masarik, M.; Adam, V.; Eckschlager, T.; Stiborova, M.; Trnkova, L.; Skutkova, H.; Provaznik, I.; Hubalek, J.; Kizek, R. Mammalian metallothioneins: Properties and functions. *Metallomics* **2012**, *4*, 739–750. [CrossRef]
19. Yen Le, T.T.; Zimmermann, S.; Sures, B. How does the metallothionein induction in bivalves meet the criteria for biomarkers of metal exposure? *Environ. Pollut.* **2016**, *212*, 257–268.
20. Zhang, Y.; Li, Z.; Kholodkevich, S.; Sharov, A.; Feng, Y.; Ren, N.; Sun, K. Cadmium-induced oxidative stress, histopathology, and transcriptome changes in the hepatopancreas of freshwater crayfish (*Procambarus clarkii*). *Sci. Total Environ.* **2019**, *666*, 944–955. [CrossRef]
21. Jia, R.; Han, C.; Lei, J.L.; Liu, B.L.; Huang, B.; Huo, H.H.; Yin, S.T. Effects of nitrite exposure on haematological parameters, oxidative stress and apoptosis in juvenile turbot (*Scophthalmus maximus*). *Aquat. Toxicol.* **2015**, *169*, 1–9. [CrossRef] [PubMed]
22. Lin, Y.; Huang, J.J.; Dahms, H.U.; Zhen, J.J.; Ying, X.P. Cell damage and apoptosis in the hepatopancreas of *Eriocheir sinensis* induced by cadmium. *Aquat. Toxicol.* **2017**, *190*, 190–198. [CrossRef] [PubMed]
23. Ohkawa, H.; Ohishi, N.; Yagi, K. Assay for lipid peroxides in animal tissues by thiobarbituric acid reaction. *Anal. Biochem.* **1979**, *95*, 351–358. [CrossRef]
24. Fraga, C.G.; Oteiza, P.I.; Galleano, M. In vitro measurements and interpretation of total antioxidant capacity. *Biochim. Biophys. Acta-Gen. Subj.* **2014**, *2*, 931–934. [CrossRef]
25. Sanchez, W.; Burgeot, T.; Porcher, J.M. A novel "Integrated Biomarker Response" calculation based on reference deviation concept. *Environ. Sci. Pollut. Res.* **2013**, *20*, 2721–2725. [CrossRef]
26. Livak, K.J.; Schmittgen, T.D. Analysis of relative gene expression data using real time quantitative PCR and the $2^{-\Delta\Delta CT}$ method. *Methods* **2001**, *25*, 402–408. [CrossRef]
27. Xia, L.P.; Chen, S.H.; Dahms, H.U.; Ying, X.P.; Peng, X. Cadmium induced oxidative damage and apoptosis in the hepatopancreas of Meretrix meretrix. *Ecotoxicology* **2016**, *25*, 959–969. [CrossRef]
28. Zhou, L.; Li, M.; Zhong, Z.S.; Chen, H.; Wang, X.C.; Wang, M.X.; Xu, Z.; Cao, L.; Lian, C.; Zhang, H.; et al. Biochemical and metabolic responses of the deep-sea mussel *Bathymodiolus platifrons* to cadmium and copper exposure. *Aquat. Toxicol.* **2021**, *236*, 105845. [CrossRef]
29. Copple, I.M.; Goldring, C.E.; Jenkins, R.E. The hepatotoxic metabolite of acetaminophen directly activates the Keap1-Nrf2 cell defense system. *Hepatology* **2008**, *48*, 1292–1301. [CrossRef]
30. Sara, B.; Cullinan, J.D.; Jin, J.P.; Wade, J.; Alan, D. The Keap1-BTB protein is an adaptor that bridges Nrf2 to a Cul3-based E3 ligase oxidative stress sensing by a Cul3-Keap1 ligase. *Mol. Cell Biol.* **2004**, *24*, 8477–8486.
31. Dong, W.X.; Liu, G.; Zhang, K.L.; Tan, Y.; Zou, H.; Yuan, Y.; Gu, J.H.; Song, R.L.; Zhu, J.; Liu, Z.P. Cadmium exposure induces rat proximal tubular cells injury via p62-dependent Nrf2 nucleus translocation mediated activation of AMPK/AKT/mTOR pathway. *Ecotoxicol. Environ. Saf.* **2021**, *214*, 112058. [CrossRef] [PubMed]
32. Wu, K.C.; Liu, J.J.; Klaassen, C.C. Nrf2 activation prevents cadmium-induced acute liver injury. *Toxicol. Appl. Pharmacol.* **2012**, *263*, 14–20. [CrossRef] [PubMed]
33. Wang, H.D.; Pan, L.Q.; Xu, R.Y.; Si, L.G.; Zhang, X. The molecular mechanism of Nrf2-Keap1 signaling pathway in the antioxidant defense response induced by BaP in the scallop *Chlamys farreri*. *Fish Shellfish Immun.* **2019**, *92*, 489–499. [CrossRef] [PubMed]
34. Peng, T.; Wang, W.N.; Gu, M.M.; Xie, C.Y.; Xiao, Y.C.; Liu, Y.; Wang, L. Essential roles of Cdc42 and MAPK in cadmium-induced apoptosis in *Litopenaeus vannamei*. *Aquat. Toxicol.* **2015**, *163*, 89–96. [CrossRef] [PubMed]

antioxidants

MDPI

Article

Feed Restriction Alleviates Chronic Thermal Stress-Induced Liver Oxidation and Damages via Reducing Lipid Accumulation in Channel Catfish (*Ictalurus punctatus*)

Qisheng Lu [1,2,†], Yulong Gong [1,†], Longwei Xi [1,2], Yulong Liu [1,2], Wenjie Xu [1], Haokun Liu [1], Junyan Jin [1], Zhimin Zhang [1], Yunxia Yang [1], Xiaoming Zhu [1], Shouqi Xie [1,2,3] and Dong Han [1,2,4,*]

1 State Key Laboratory of Freshwater Ecology and Biotechnology, Institute of Hydrobiology, Chinese Academy of Sciences, Wuhan 430072, China; luqisheng@ihb.ac.cn (Q.L.); gongyl@ihb.ac.cn (Y.G.); xilw@ihb.ac.cn (L.X.); liuyulong@ihb.ac.cn (Y.L.); xuwenjie@gdou.edu.cn (W.X.); liuhaokun@ihb.ac.cn (H.L.); jinjunyan@ihb.ac.cn (J.J.); zhangzm@ihb.ac.cn (Z.Z.); yxyang@ihb.ac.cn (Y.Y.); xmzhu@ihb.ac.cn (X.Z.); sqxie@ihb.ac.cn (S.X.)
2 College of Advanced Agricultural Sciences, University of Chinese Academy of Sciences, Beijing 100049, China
3 The Innovative Academy of Seed Design, Chinese Academy of Sciences, Wuhan 430072, China
4 Hubei Engineering Research Center for Aquatic Animal Nutrition and Feed, Wuhan 430072, China
* Correspondence: hand21cn@ihb.ac.cn
† These authors contributed equally to this work.

Abstract: Caloric restriction is known to suppress oxidative stress in organ systems. However, whether caloric/feed restriction alleviates chronic thermal stress in aquatic animals remains unknown. Here, we set up three feeding rations: 3% BW (3% body weight/day), 2.5% BW (restricted feeding, 2.5% body weight/day) and 2% BW (high restricted feeding, 2% body weight/day), to investigate the effects and mechanism of feed restriction on improving chronic heat-induced (27 to 31 °C) liver peroxidation and damages in channel catfish (*Ictalurus punctatus*). The results showed that, compared to 3% BW, both 2.5% BW and 2% BW significantly reduced the liver expressions of hsc70, hsp70 and hsp90, but only 2.5% BW did not reduce the growth performance of channel catfish. The 2.5% BW and 2% BW also reduced the lipid deposition (TG) and improved the antioxidant capacity (CAT, SOD, GSH and T-AOC) in the liver of channel catfish. The heat-induced stress response (plasma glucose, cortisol and NO) and peroxidation (ROS and MDA) were also suppressed by either 2.5% BW or 2% BW. Moreover, 2.5% BW or 2% BW overtly alleviated liver inflammation and damages by reducing endoplasmic reticulum (ER) stress (BIP and Calnexin) and cell apoptosis (BAX, Caspase 3 and Caspase 9) in the liver of channel catfish. In conclusion, 2.5% body weight/day is recommended to improve the antioxidant capacity and liver health of channel catfish during the summer season, as it alleviates liver peroxidation and damages via suppressing lipid accumulation under chronic thermal stress.

Keywords: thermal stress; oxidative damage; liver health; feed restriction; channel catfish

Citation: Lu, Q.; Gong, Y.; Xi, L.; Liu, Y.; Xu, W.; Liu, H.; Jin, J.; Zhang, Z.; Yang, Y.; Zhu, X.; et al. Feed Restriction Alleviates Chronic Thermal Stress-Induced Liver Oxidation and Damages via Reducing Lipid Accumulation in Channel Catfish (*Ictalurus punctatus*). *Antioxidants* **2022**, *11*, 980. https://doi.org/10.3390/antiox11050980

Academic Editors: Bo Liu, Changyou Song and Cunxin Sun

Received: 26 April 2022
Accepted: 15 May 2022
Published: 17 May 2022

1. Introduction

Temperature is a crucial environmental factor that strictly affects the metabolism, immunology and stress state of fish [1,2]. Aquatic animals suffer temperature fluctuations in their aquatic environments. As ectotherms, the body temperature of fish is closely influenced by the temperature of the surrounding water [3]. In summer, aquaculture species usually experience a high-temperature period for 2–3 months. The suitably higher water temperatures are beneficial for maximizing growth performance and improving the immune systems in aquaculture species [4]. However, the persistent extremely high temperature deteriorates due to a chronic thermal stress, which usually leads to tissue oxidative damages and metabolism disorders in cultured fish [5,6]. When the temperature rises above the threshold for one species, it may cause physiological disturbances and

even lead to fish death [7]. High temperature-induced thermal stress in cultured fish has been an obvious threat for the development of aquaculture. Therefore, exploring the available strategies is imperative for mitigating the negative effects of thermal stress on cultured fish.

As a regular approach, food restriction has been investigated to improve health spans in different organisms by enhancing their antioxidant and immunology capacities [8,9]. A previous study showed that food restriction increased the survival of rodents by altering the activities of antioxidant enzymes and reducing free radical damages in various tissues [10]. Importantly, food restriction reduced the food frequency-induced increase in mitochondrial oxidative stress and apoptosis in the central nervous system [11]. A recent study in humans also demonstrated that sustained food restriction activated a core transcriptional program that promoted the immune system and reduced inflammation [8]. Moreover, food restriction imitated vitamin E in the promotion of insulin secretion and glycemic homeostasis, which was speculated to be involved in antioxidant effects [12]. These studies indicate that food restriction is an effective experimental intervention for enhancing antioxidant capacity and attenuating oxidative stress. Consequently, appropriate feed restriction may be one of the potential solutions for alleviating high temperature-induced thermal stress and peroxidation in cultured aquatic animals.

Stressors such as high-temperature, excessive food intake and high stocking density can cause oxidative stress induced by the accumulation of reactive oxygen species (ROS) [13–15], which leads to lipid peroxidation, protein carboxylation and nucleic acid damage [16]. As a consequence, oxidative stress negatively regulates the growth performance [17,18] and the immune system in fish [19]. Therefore, investigations for improving the antioxidation capacity and health state of aquaculture fish have become more and more popular. In recent years, efforts to reduce peroxidation and stress by dietary adjustment [20], feed additives [21,22] and feeding strategies [23] have successfully improved the antioxidation systems of fish. Feed restriction was one of the feeding strategies that contributed to the skeletal muscle growth [24] and lipid consumption [25] in fish. Interestingly, feed restriction also mitigated high carbohydrate-induced oxidative stress and inflammation via motivating the AMPK-SIRT1 pathway [26]. That study determined the possibility of improving antioxidation and anti-stress capacities through feed restriction. However, whether feed restriction alleviates the chronic high temperature-induced oxidative stress and its underlying regulation mechanisms remains unanswered.

Channel catfish (*Ictalurus punctatus*) originates from North America and has become one of the most popular cultured catfish species. The production of channel catfish exceeded 390,000 tons with an increase of 3.34% over recent years worldwide [27]. However, thermal stress and oxidative stress have been major challenges for the health and survival of cultured channel catfish during the summer season. Therefore, we set out to investigate the effects and mechanism of feed restriction on the alleviation of high temperature-induced oxidative stress and liver damages of channel catfish. Using three feeding rations (3% BW, 2.5% BW and 2% BW), we confirmed the positive effects and regulation mechanism of appropriate feed restriction on the antioxidant capacity of cultured channel catfish under thermal stress. These findings provide a feasible solution for alleviating high temperature-induced thermal stress and peroxidation in cultured aquatic animals.

2. Materials and Methods

2.1. Ethics Statement

Procedures related to animal treatments in this study were conducted strictly according to the Guiding Principles for the Care and Use of Laboratory Animals and were approved by the Institute of Hydrobiology, Chinese Academy of Sciences (Approval ID: IHB 2013724).

2.2. Channel Catfish and Feeding Trial

Juvenile channel catfish were provided by Wuhan Dabeinong Technology Co., Ltd. (Wuhan, China). All fish were cultured in an experimental system with commercial feed for 2 weeks to adapt to the experimental conditions. Before the feeding trial, fish were fasted for 24 h for gastric emptying. Then, 80 channel catfish (initial weight: 35.5 ± 0.1 g) were randomly selected, weighed and assigned into each floating net cage. Six replicates were randomly distributed for each group. During the experiment, fish were fed twice a day (08:30 and 16:30). Commercial feed (crude protein, 35.5%; crude lipid, 9.0%; moisture, 9.6%; ash, 10.4%) (Wuhan Dabeinong Technology Co., Ltd., Wuhan, China) was used for feeding the fish. The daily feeding rations of each floating net cage were 3% BW (3% body weight/day), 2.5% BW (restricted feeding, 2.5% body weight/day) and 2% BW (high restricted feeding, 2% body weight/day), respectively. The 3% BW is considered an approximate satiation according to the previous studies [22,28]. The feeding trial lasted for 13 weeks. The whole experiment was carried out in a natural environment. Throughout the whole trial, the water temperature was detected by a thermometer everyday, the dissolved oxygen content of the water was maintained at 6.4 ± 0.5 mg/L, and the ammonia-N content of the water was lower than 0.5 mg/L.

2.3. Sample Collection

After a 24-h fasting, growth performance was calculated, and the fish were anesthetized with MS-222 (80 mg/L, Sigma Aldrich Co. LLC., St. Louis, MO, USA) before sampling [29]. Three fish were randomly taken from each floating net cage for tail vein blood collection, which was collected in a 1.5 mL centrifuge tube moistened with 0.2% sodium heparin and centrifuged at 3500 rpm for 10 min. Then, the supernatant was collected and stored at −80 °C. Another three fish from each floating net cage were quickly dissected on ice, and liver tissue was removed, placed onto enzyme-free tinfoil and put in liquid nitrogen before storing at −80 °C.

2.4. Determination of Growth Parameters

The weight gain rate (WG), specific growth rate (SGR), feed efficiency (FE), feeding rate (FR), survival rate (SR), hepatosomatic index (HSI), viscerosomatic index (VSI) and condition factor (CF) were calculated as follows:

WG (%) = (final body weight − initial body weight)/initial body weight × 100

SGR (%/d) = [Ln (final body weight) − Ln (initial body weight)]/days × 100

FE (%) = (final body weight − initial body weight)/dry feed intake × 100

FR (%BW/d) = dry feed intake/[days × (initial body weight + final body weight)/2] × 100

SR (%) = final number of fish/initial number fish × 100

HSI (%) = liver weight/whole body weight × 100

VSI (%) = visceral weight/whole body weight × 100

CF (g/cm^3) = whole body weight/$(\text{body length})^3$ × 100

2.5. Biochemical and Antioxidative Parameters

Glucose, alanine aminotransferase (ALT), malondialdehyde (MDA) and the cortisol content (ELISA) in plasma were assayed by commercial assay kits (Nanjing Jiancheng Bioengineering Institute, Nanjing, China, Catalog: A154-1-1, C009-2-1, A003-1-2 and H094). The measurement of liver enzyme activity needed experimental pretreatment. Physiological saline was added to the liver samples as weight (g): volume (mL) = 1:9. After centrifugation, the supernatant was taken out for subsequent enzyme activity analysis. Protein concentrations in the liver homogenates were determined by the Coomassie brilliant blue method (Beyotime, Shanghai, China, P0006). The activities of catalase (CAT), reduced glutathione (GSH) and superoxide dismutase (SOD), as well as the total antioxidant capacity (T-AOC), the content of malondialdehyde (MDA), the nitric oxide (NO) content and the lipid peroxide (LPO) content in the liver samples were determined

by enzymatic colorimetric methods (Nanjing Jiancheng Bioengineering Institute, Nanjing, China, Catalog: A007-1-1, A006-2-1, A001-3-2, A015-2-1, A003-1-2, A013-2-1 and A106-1-2). Plasma and liver ROS contents were determined by a fish ELISA kit (Wuhan MSK Biological Technology Co., Ltd., Wuhan, China, 69-86537).

2.6. Detection of Lipid Metabolism-Related Enzyme Activity in Liver

The content of liver acetyl-CoA carboxylase (ACC), lipoprotein lipase (LPL) and carnitine palmitoyltransferase 1A (CPT1A) were detected by enzyme-linked ELISA, provided by MSK Biological Technology Co., Ltd. (Wuhan, China, Catalog: 69-47369, 69-20008 and 69-22482). Triglycerides (TG) and lipase (LPS) in the liver samples were measured through colorimetric methods according to the manufacturer's instructions (Nanjing Jiancheng Bioengineering Institute, Nanjing, China, Catalog: A110-1-1 and A054-1-1).

2.7. Apoptosis Detection

The activities of Caspase 3 and Caspase 9 in the liver samples were determined following the protocol for apoptosis detection kits (Beyotime, Shanghai, China, Catalog: C1116 and C1158). The protein concentration in the sample to be tested was detected by the Bradford method (Beyotime, Shanghai, China, P0006), and the enzyme activity units of Caspase 3 and Caspase 9 contained in a unit weight protein of the sample were calculated.

2.8. Tissue Total RNA Extraction and RT-qPCR Analysis

Total RNA from the liver tissue was isolated with TRIzol Reagent (Ambion Life Technologies, Carlsbad, CA, USA), following the product manual, and the quality was tested according to the method of Sun et al. [30]. Reverse transcription was performed using M-MLV First-Strand Synthesis Kit (Invitrogen, Shanghai, China), and the cDNA was stored at −20 °C for real-time quantitative PCR (RT-qPCR) analysis.

The real-time quantitative PCR was performed on the LightCycle® 480 II system to determine the amplification efficiency in a pre-experiment and to make standard curves using internal reference and target genes. Light Cycle 480 SYBR Green I Master Mix (Roche, Basel, Switzerland) was used to determine the expression levels of target genes. The fluorescent qPCR reaction solution included 3 μL of LightCycle® 480 SYBR® Green I Master, 0.24 μL of PCR forward primer (10 μM), 0.24 μL of PCR reverse primer (10 μM), 2.0 μL of RT reaction (cDNA solution) and 0.52 μL of dH_2O. In this study, there was no difference in the expression of β-actin among the three treatments. After analysis, it was chosen as an internal reference for normalization. The qPCR primers were designed using the National Center for Biotechnology Information (NCBI) primer BLAST service. The primers used for RT-qPCR are shown in Table 1. The thermal profile was as follows: 95 °C for 5 min, followed by 45 cycles at 95 °C for 10 s, 60 °C for 20 s and 72 °C for 10 s. Each sample was run in duplicate, and the results were calculated with the means. The expression of each target gene for the different treatment groups was expressed relative to the 3% BW group, and the expression levels of the target genes were calculated by the $2^{-\Delta\Delta CT}$ method [31].

Table 1. Primers used for gene expressions assay by real-time PCR.

Target Genes	Forward (5′-3′)	Reverse (5′-3′)	Accession Numbers
aco	AGACCTGAACTTTCTGTCCCG	GCTGGACACCATAGGGATGAA	XM_017482134.1
acad9	CTGAAAAGAGTGGCCGATACA	CGTCATTGTTCTCTGGGGAAT	XM_017450491.1
acadvl	CTGTGCGATTGACTTGTATGC	CTCTACCACAGCTGCAGAAAT	XM_017472293.1
acads	TCACTCAGCTTGCAGGATTAC	ATGACTGCTTAGCTGGGAAAG	XM_017489904.1
atf4	GATTCTGATGGCTGACACCTT	GGTCAAAATCACTGAGGTCGA	XM_017482287.1
atf6	AGGAGTTTGAGGTGATGATGC	TCTACTCCAATTGCTGACACG	XM_017455892.1
bip	GAGACAGGCCAAGATTGAGAG	TTCTGAGTTGGAGCCTGATTG	XM_017460312.1
cpt1a	ACCACATCCCAATCTGCCTG	CCTGAAGTGAGCAAGCTGGA	XM_017485733.1
caspase3	GTGTGTGTGATCCTAAGCCAT	CAAATCTGTTCCACGACAAGC	NM_001201081.1
caspase8	TATGAGGAAGAGGACACGGAA	CGCAATGAGGAAATCTGCATC	XM_017480625.1
caspase9	TGCTTCCTCTGAAACCAACAA	GATCTGAATCGTCTCTCCAGC	XM_017487604.1
caspase10	ACGTGGAGTTCTTCTGTGATG	AGCTGTTCGAGGTTCTTACAC	XM_017470757.1
dgat	AAGAAATTCCCCGGGATCAAG	ACAGGAGGTAATCGATGGAGT	NM_001201076.1
eif2	CATTCTTGGAGGTTCAGAGGG	CATTCAAACGTGCCATCCAAA	XM_017468034.1
fasn	CTGGTCAGAGCAACTACGGTT	CTACATCACCGATAGCACCCC	XM_017483746.1
hsc70	CAAGATCAGTGACGAGGACAAG	GGTTACAGACTTTCTCCAGTTCC	XM_017489684.1
hsp70	CTTGATGTTACCCCTCTGTCTCT	TCAGAGTAGGTGGTGAAAGTCTG	NM_001200273.1
hsp90	ATCTGAAGGAGGATCAGACAGAG	CGCTCCTTCTCTACAAAGAGTGT	NM_001329313.1
lpl	CTGGACGGTTACTGGCATGT	GGCAGCTGAGGTTGGGTAAT	XM_017478439.1
mt	CTGCAAATGCTCAAACTGCCA	AGCACTTGGAATCGCAGGTAT	NM_001200077.1
perilipin	GGACATTGACCATTGCTCGC	ACCTCGCGTGTTTATGAGCA	XM_017472797.1
pparα	TCCGCAAGCCTTTCAGTGAT	AGCAAGGTGTCATCAGGGTG	XM_017494485.1
perk	GCAGCAAAACATTCGTGTGTA	TGGTACGATTCGGTCTCTGTA	XM_017455330.1
pdi8	GAATGAACCGAGGCGATATGA	CAAACCACATTTCCCAGCATC	XM_017482284.1
scd	GTTTGGACGTGTGGAAATGAC	TGTGTATGTTGAAGCTGAGGG	XM_017464581.1
srebp1c	ACTGGCTGCAAGGAGATGAC	TGTCTCTGAACAGGCTGCTG	XM_017452596.1
xbp1	TCTGGTCAGGAAAGAGAAGGT	AGCTCTGGTTCAATGATGTCC	XM_017452343.1
β-actin	GGATCTGTATGCCAACACTGT	CAGGTGGGGCAATGATCTTAA	XM_017454668.1

Note: aco, acyl-CoA oxidase 1; acad9, acyl-CoA dehydrogenase family member 9; acadvl, acyl-CoA dehydrogenase, very long chain; acads, acyl-CoA dehydrogenase, C-2 to C-3 short chain; atf4, activating transcription factor 4; atf6, activating transcription factor 6; bip, 78 kDa glucose-regulated protein; caspase3, caspase 3; caspase8, caspase 8; caspase9, caspase 9; caspase10, caspase 10; cpt1a, carnitine palmitoyltransferase 1A; dgat, diacylglycerol O-acyltransferase 2; eif2, GCN1 activator of EIF2AK4; fasn, fatty acid synthase; hsc70, heat shock cognate 71 kDa protein; hsp70, heat shock protein 70; hsp90, heat shock protein 90; lpl, lipoprotein lipase; mt, metallothionein; pdi8, protein disulfide isomerase family A member 8; perilipin, perilipin; perk, estrogen receptor 1; pparα, peroxisome proliferator activated receptor alpha; scd, stearoyl-CoA de-saturase; srebp1c, sterol regulatory element binding transcription factor 1; xbp1, X-box binding protein 1; β-actin, actin beta.

2.9. Protein Extraction and Western Blot Analysis

The liver samples were cell lysed by RIPA lysis buffer (Beyotime, Shanghai, China, P0013B) containing a protease inhibitor cocktail and phosphatase inhibitor cocktail (Roche, Basel, Switzerland). The lysates were sonicated and homogenized on ice, centrifuged at 13,000× *g* at 4 °C for 20 min, and the supernatant was collected for later analysis. The sample protein concentrations were determined according to the instructions of the BCA Protein Quantification Kit (Beyotime, Shanghai, China, P0012) and adjusted to a consistent protein concentration for all liver samples using 50% RIPA lysis buffer. After determination of the protein quantity, an equal volume of 5 × sample loading buffer was added and boiled at 100 °C for 5 min. Proteins (20 mg) were loaded into the wells of sodium dodecyl sulfatepolyacrylamide gel electrophoresis (SDS-PAGE gels) and then transferred to polyvinylidene fluoride (PVDF) membranes. The membranes were blocked for 1 h at room temperature by using 5% skimmed milk in TBST buffer (20 mM Tris-HCl, 150 mM sodium chloride, 0.1% Tween 20, pH 7.5) and were then incubated at 4 °C for 12 h using the following specific primary antibodies: Calnexin Antibody (ET1611-86, HUABIO, Hangzhou, China), BIP Antibody (3183S, Cell signaling, Danvers, MA, USA), BAX Antibody (ET1603-34, HUABIO, Hangzhou, China) or β-Actin (4970S, Cell signaling, Danvers, MA, USA). After washing, membranes were incubated with a secondary antibody, Anti-rabbit lgG (7074P2, Cell signaling, Danvers, MA, USA), at room temperature for 2 h. Wherein, β-Actin was used as an internal reference protein. The bands were imaged by ImageQuant LAS 4000mini (GE Healthcare Life Sciences) and quantified using Image J software (National Institutes of Health, Bethesda, MD, USA) [32].

2.10. Hematoxylin and Eosin (H&E) Staining

There were six replicates in each treatment group, and samples of the liver tissues were isolated and kept in 4% paraformaldehyde for 24 h. After that, the samples were dehydrated in gradient alcohol dehydration, impregnated with methyl salicylate, embedded in paraffin and cut into 5 μm by a Leica RM 2135 slicing machine (Leica Company, Wetzlar, Germany) followed by H&E staining [33]. The morphological structure of the liver tissues was observed and imaged with a Zeiss microscope (Axioplan-2 imaging, Oberkochen, Germany). The number of macrophages was counted manually.

2.11. Statistical Analysis

All data were compared by a one-way analysis of variance (ANOVA) and differences between the groups were tested by Duncan's multiple-range test. All results are expressed as the "mean ± SEM (standard error of the mean)" of four or six replicates, and all statistical analyses were performed using SPSS 22.0 (IBM, Armonk, NY, USA). Differences were considered significant at $p < 0.05$.

3. Results

3.1. Feed Restriction (2.5% BW) Suppressed the Thermal Stress Response of Liver without Causing Growth Retardation

During the entire feeding trial, the water temperature gradually increased from 27 °C to 31 °C in the first 8 weeks, and then it was stable at around 30 °C for the remaining 5 weeks (Figure 1A). The total feed intake and the feeding rate significantly decreased among the 3% BW, 2.5% BW and 2% BW groups ($p < 0.05$) (Figure 1B; Table 2). Compared to those of the 3% BW group, the final body weight, weight gain rate (WG) and specific growth rate (SGR) all significantly decreased in the 2% BW group ($p < 0.05$), while there was no obvious decrease in those of the 2.5% BW group ($p > 0.05$) (2). Moreover, the feeding efficiencies (FE) significantly increased both in the 2.5% BW and 2% BW groups ($p < 0.05$) (Table 2). Moreover, the hepatosomatic index (HSI) and condition factor (CF) both significantly decreased in the 2.5% BW group ($p < 0.05$), while the HSI and viscerosomatic index (VSI) both significantly decreased in the 2% BW group ($p < 0.05$) (Table 3). Importantly, we found that the transcription levels of the liver heat shock proteins, heat shock cognate 70

(*hsc70*), heat shock protein 70 (*hsp70*) and heat shock protein 90 (*hsp90*), were all significantly down-regulated by either the 2.5% BW or 2% BW feeding ration ($p < 0.05$) (Figure 1C–E). These data indicate that the appropriate feed restriction (2.5% BW) suppresses the thermal stress response of liver tissues without causing negative effects on the growth performance in channel catfish under a high water temperature.

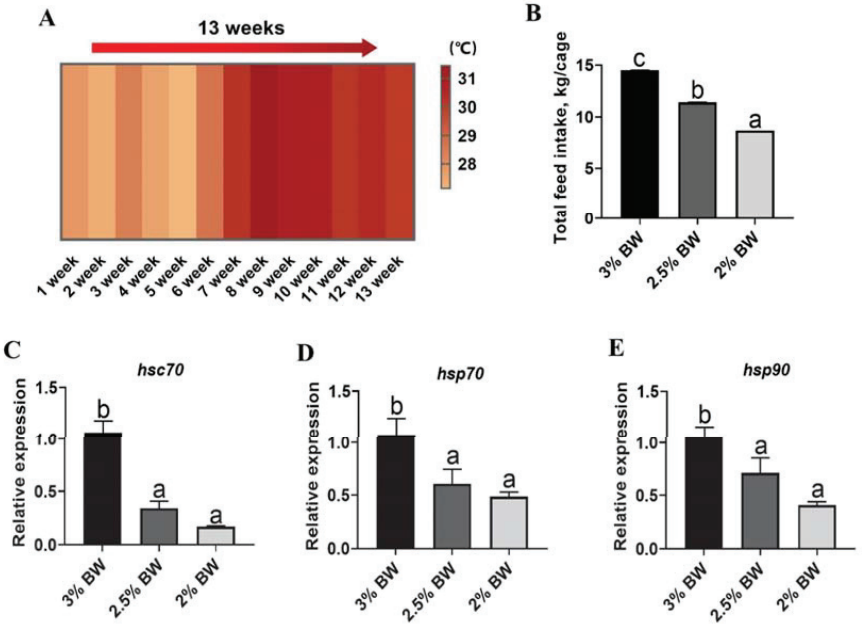

Figure 1. Feed restriction suppressed the heat stress response in livers of channel catfish. (**A**) Water temperature during feeding trial; (**B**) total feed intake during feeding trial; (**C**) liver transcription level of *hsc70*; (**D**) liver transcription level of *hsp70*; (**E**) liver transcription level of *hsp90*. Each data point represents the means ± SEM of six replicates. Significance was evaluated by a one-way ANOVA ($p < 0.05$), followed by Duncan's multiple range tests. Values marked with different letters (a, b and c) are significantly different between the treatment groups.

Table 2. Effects of feed restriction on the growth performance of channel catfish (*Ictalurus punctatus*).

	3% BW	2.5% BW	2% BW	*p*-Value
IBW, g	35.50 ± 0.06	35.50 ± 0.06	35.50 ± 0.05	$p > 0.05$
FBW, g	99.86 ± 1.04 ^{b}	97.56 ± 1.55 ^{b}	83.84 ± 0.67 ^{a}	$p < 0.05$
WG, %	181.28 ± 2.83 ^{b}	174.81 ± 4.24 ^{b}	136.33 ± 1.82 ^{a}	$p < 0.05$
SGR, %/d	1.15 ± 0.01 ^{b}	1.11 ± 0.01 ^{b}	0.99 ± 0.03 ^{a}	$p < 0.05$
FE, %	73.82 ± 1.29 ^{a}	84.91 ± 1.59 ^{b}	87.93 ± 0.78 ^{b}	$p < 0.05$
FR, %BW/d	3.02 ± 0.05 ^{c}	2.48 ± 0.03 ^{b}	2.04 ± 0.02 ^{a}	$p < 0.05$
SR, %	98.96 ± 0.50	99.25 ± 0.50	98.75 ± 0.68	$p > 0.05$

Note: Data indicate the mean values of six replicates per treatment. Mean values with different superscripts in a row are significantly different (one-way ANOVA, $p < 0.05$). IBW, initial body weight; FBW, final body weight; WG, weight gain rate; SGR, specific growth rate; FE, feed efficiency; FR, feeding rate; SR, survival rate.

Table 3. Effects of feed restriction on the physical index of channel catfish (*Ictalurus punctatus*).

	3% BW	2.5% BW	2% BW	*p*-Value
HSI, %	1.47 ± 0.05^{b}	1.14 ± 0.10^{a}	1.17 ± 0.05^{a}	$p < 0.05$
VSI, %	8.43 ± 0.41^{b}	8.01 ± 0.17^{ab}	7.45 ± 0.20^{a}	$p < 0.05$
CF, g/cm^3	1.40 ± 0.05^{b}	1.26 ± 0.04^{a}	1.32 ± 0.04^{ab}	$p < 0.05$

Note: Data indicate the mean values of six replicates per treatment. Mean values with different superscripts in a row are significantly different (one-way ANOVA, $p < 0.05$). HSI, hepatosomatic index; VSI, viscerosomatic index; CF, condition factor.

3.2. Feed Restriction Reduced Liver Lipid Accumulation and β-Oxidation

Feed restriction usually reduces lipid deposition by suppressing lipogenesis and promoting lipolysis [25]. Here, we found that the hepatic triglyceride (TG) content significantly decreased in the 2.5% BW and 2% BW groups ($p < 0.05$) (Figure 2A). Accordingly, the transcription levels of key lipogenesis-related genes, *pparα*, *srebp1c*, *dgat*, *fasn* and *scd*, all significantly down-regulated in both the 2.5% BW and 2% BW groups ($p < 0.05$) (Figure 2B). Moreover, the protein concentration of the crucial lipogenesis enzyme, Acetyl CoA carboxylase (ACC), also decreased under feed restriction ($p < 0.05$) (Figure 2C). Unexpectedly, the transcription levels of key lipolysis-related genes, *perilipin*, *lpl*, *aco*, *cpt1a*, *acad9*, *acadvl* and *acads*, almost all down-regulated in both the 2.5% BW and 2% BW groups ($p < 0.05$) (Figure 2D). Furthermore, the protein concentrations of the crucial lipolysis enzymes, Lipase (LPS), Lipoprotein lipase (LPL) and Carnitine palmitoyltransferase 1A (CPT1A), all significantly decreased in the 2% BW group ($p < 0.05$), but only CPT1A significantly decreased in the 2.5% BW group compared to the 3% BW group (Figure 2E–G). These data mean that feed restriction reduces liver lipid accumulation via suppressing lipogenesis and decreasing the fatty acid β-oxidation in the channel catfish under a high water temperature.

3.3. Feed Restriction Enhanced Liver Antioxidant Capacity and Improved Thermal Stress State

Decreased lipid accumulation may contribute to more intensive antioxidant and anti-stress systems in the liver. Hence, we detected the liver antioxidant capacity, stress state and peroxidation degree of the channel catfish under a high water temperature. We found that the activity of the liver-crucial anti-oxidase, catalase (CAT), significantly increased in the 2% BW group ($p < 0.05$) (Figure 3A), while the activity of another crucial anti-oxidase, superoxide dismutase (SOD), significantly increased in both the 2.5% BW and 2% BW groups ($p < 0.05$) (Figure 3B). Moreover, the content of liver-reduced glutathione (GSH) showed a significant increase in the 2.5% BW group ($p < 0.05$), but not in the 2% BW group (Figure 3C). Accordingly, the total antioxidant capacity (T-AOC) of the liver was significantly elevated in both the 2.5% BW and 2% BW groups ($p < 0.05$) (Figure 3D). Interestingly, the transcription level of liver metallothionein (*mt*) also increased in both the 2.5% BW and 2% BW groups ($p < 0.05$) (Figure 3E). We further detected the stress state and peroxidation degree in the livers of channel catfish. We found that the levels of plasma glucose and plasma cortisol both significantly decreased in the 2.5% BW and 2% BW groups ($p < 0.05$) (Figure 4A,B). Nonetheless, the content of liver nitric oxide (NO) only reduced in the 2% BW group ($p < 0.05$) (Figure 4C). Furthermore, the contents of the liver and plasma reactive oxygen species (ROS) and malondialdehyde (MDA) both significantly decreased in the 2.5% BW and 2% BW groups ($p < 0.05$) (Figure 4D–G). These data indicate that feed restriction enhances the liver antioxidant capacity and improves the oxidative stress state of channel catfish under a high water temperature.

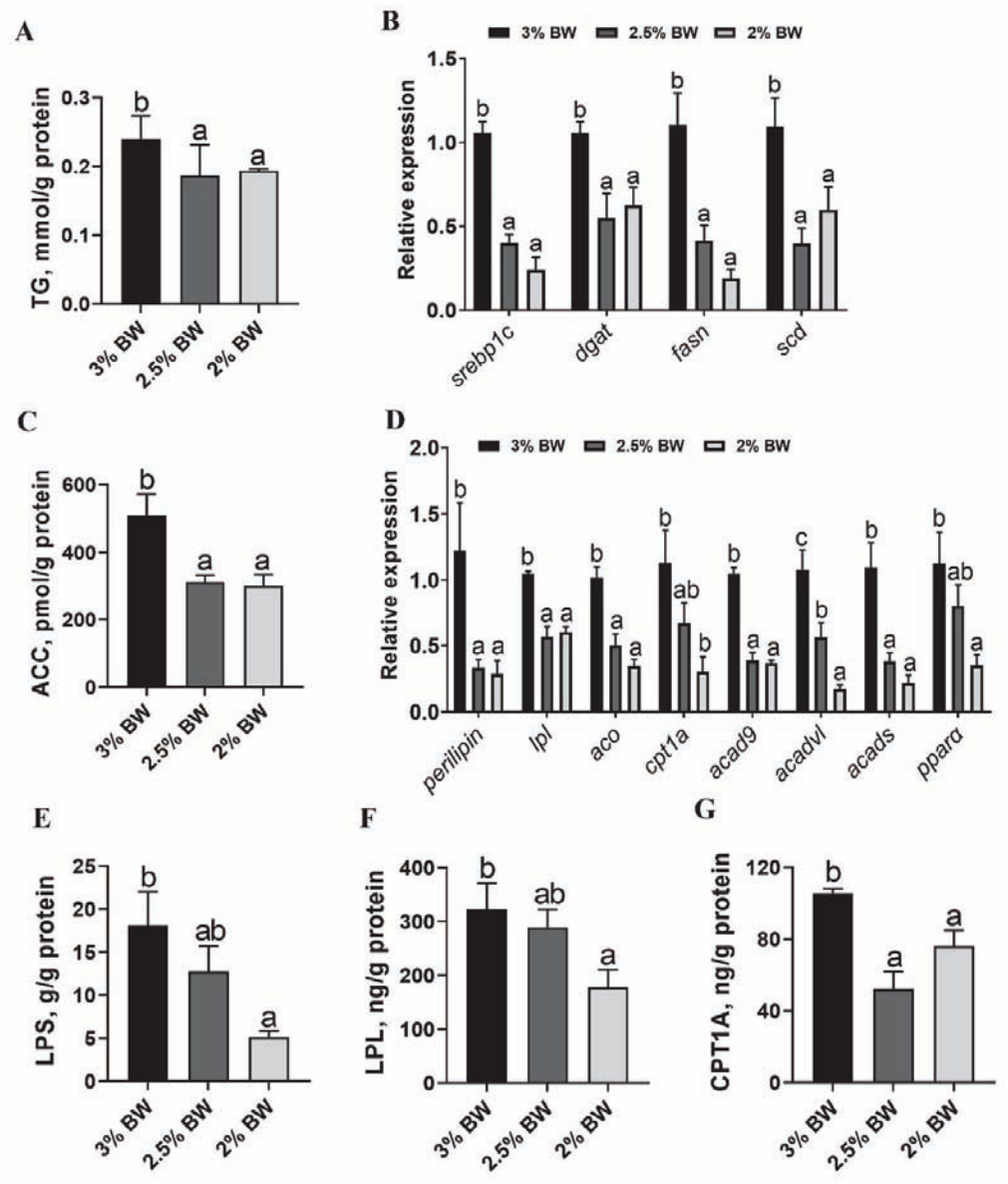

Figure 2. Feed restriction reduced the lipid accumulation and β-oxidation in the liver of channel catfish. (**A**) Triglyceride (TG) content of liver; (**B**) liver transcription levels of lipogenesis-related genes; (**C**) acetyl CoA carboxylase (ACC) content of liver; (**D**) liver transcription levels of lipolysis-related genes; (**E**) lipase (LPS) content of liver; (**F**) lipoprotein lipase (LPL) content of liver; (**G**) carnitine palmitoyltransferase 1A (CPT1A) content of liver. Each data point represents the mean ± SEM of six replicates. Bars assigned different superscripts (a, b and c) are significantly different ($p < 0.05$).

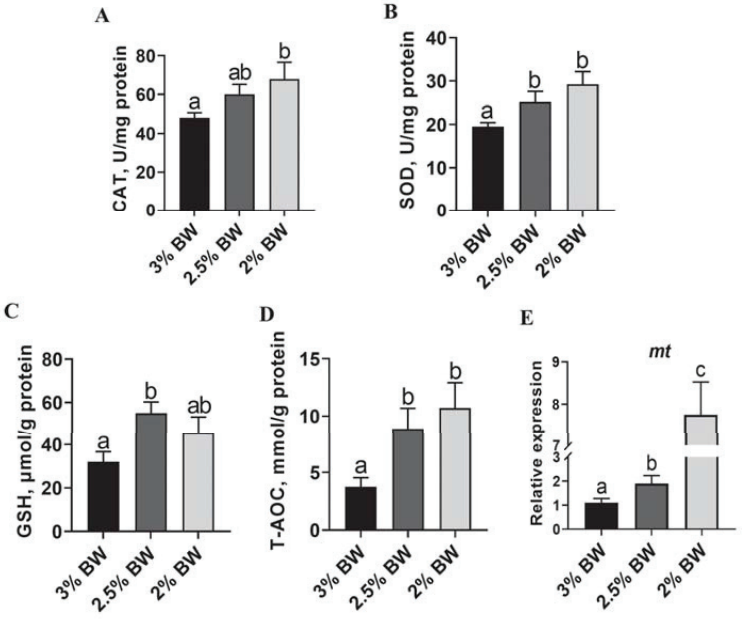

Figure 3. Feed restriction enhanced the liver antioxidant capacity of channel catfish. (**A**) Catalase (CAT) content of liver; (**B**) superoxide dismutase (SOD) content of liver; (**C**) reduced glutathione (GSH) content of liver; (**D**) total antioxidant capacity (T-AOC) of liver; (**E**) liver transcription level of metallothionein (*mt*). Each data point represents the means ± SEM of six replicates. Bars assigned different superscripts (a, b and c) are significantly different ($p < 0.05$).

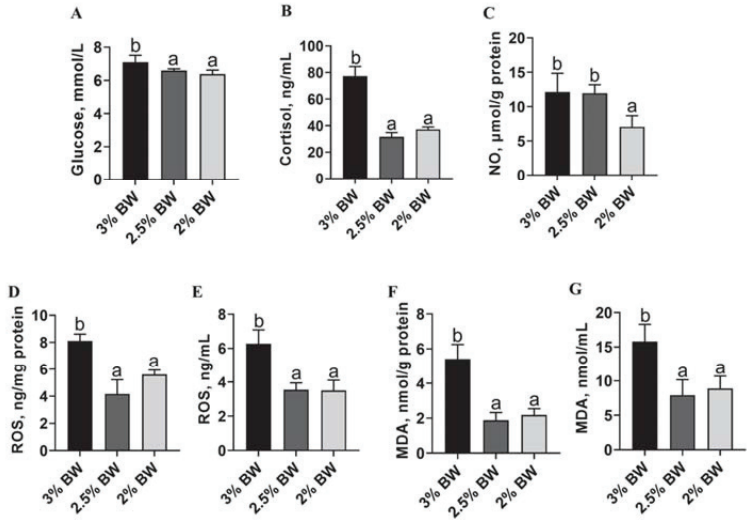

Figure 4. Feed restriction improved thermal stress and peroxidation state in channel catfish. (**A**) Plasma glucose level; (**B**) plasma cortisol level; (**C**) nitric oxide (NO) content of liver; (**D**) reactive oxygen species (ROS) of liver; (**E**) plasma ROS level; (**F**) malondialdehyde (MDA) content of liver; (**G**) MDA content of plasma. Each data point represents the means ± SEM of six replicates. Bars assigned different superscripts (a, b) are significantly different ($p < 0.05$).

3.4. Feed Restriction Mitigated the Heat-Induced ER Stress and Apoptosis in Liver

Since the antioxidant capacity and stress state are closely related to cell ER stress and apoptosis, we further determined the ER stress and apoptosis state in the livers of channel catfish. The results showed that the protein levels of the ER stress makers Calnexin and BIP both significantly reduced in the liver of the 2.5% BW and 2% BW groups ($p < 0.05$) (Figure 5A–C). The transcription levels of ER stress-related genes almost decreased in the 2.5% BW and 2% BW groups ($p < 0.05$), except for activating transcription factor 4 (*atf4*) and activating transcription factor 6 (*atf6*) in the 2% BW group (Figure 5D). For the apoptosis state, we found that the protein levels of BAX significantly reduced in the liver of the 2.5% BW and 2% BW groups ($p < 0.05$) (Figure 6A,B). We further detected the transcription level and activity of the liver Caspase family. The results showed that the transcription levels of *caspase 3*, *caspase 8*, *caspase 9* and *caspase 10* all significantly down-regulated in the 2.5% BW and 2% BW groups ($p < 0.05$) (Figure 6C). Moreover, we found the activities of hepatic Caspase 3 and Caspase 9 also significantly decreased in the 2.5% BW and 2% BW groups ($p < 0.05$) (Figure 6D,E). These data mean that feed restriction mitigates the heat-induced ER stress and apoptosis in the liver of channel catfish under a high water temperature.

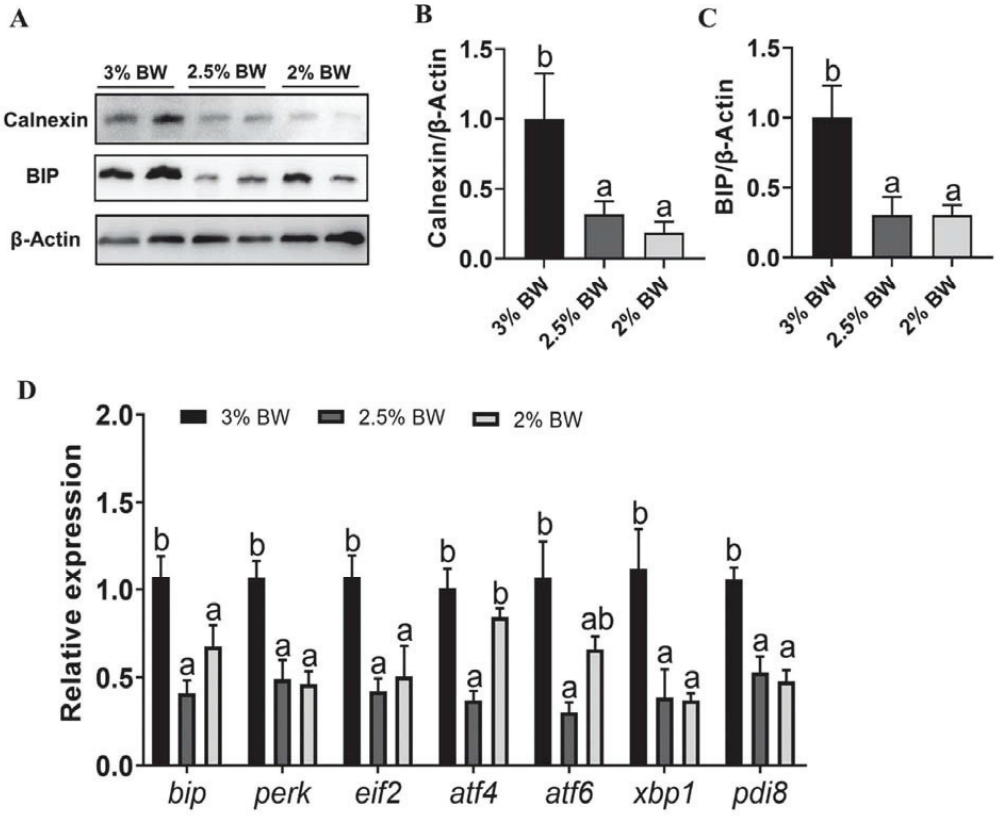

Figure 5. Feed restriction mitigated the chronic thermal stress-induced ER stress in liver of channel catfish. (**A**) Liver Calnexin and BIP protein levels; (**B**) quantification of Calnexin protein level; (**C**) quantification of BIP protein level; (**D**) liver transcription levels of ER stress-related genes. Gels were loaded with 20 mg total protein per lane. Each data point represents the means ± SEM of four replicates (**B**,**C**) or six replicates (**D**). Bars assigned different superscripts (a, b) are significantly different ($p < 0.05$).

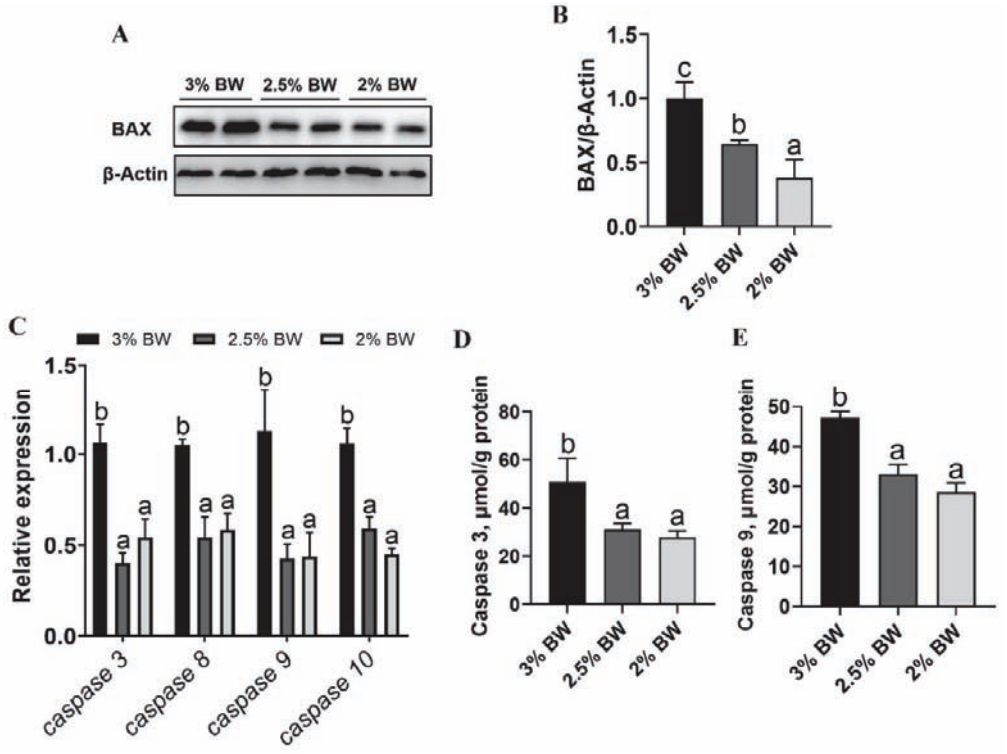

Figure 6. Feed restriction reduced the chronic thermal stress-induced apoptosis in liver of channel catfish. (**A**) Liver BAX protein level; (**B**) quantification of BAX protein level; (**C**) liver transcription levels of apoptosis-related genes; (**D**) Caspase 3 content of liver; (**E**) Caspase 9 content of liver. Each data point represents the means ± SEM of four replicates (**B**) or six replicates (Figure 5C–E). Bars assigned different superscripts (a, b and c) are significantly different ($p < 0.05$).

3.5. Feed Restriction Alleviated Heat-Induced Liver Inflammation and Damages

Given that ER stress and apoptosis ultimately impair liver health, we further evaluated liver inflammation and damages. The results showed that the liver histology of the 2.5% BW and 2% BW groups was better than that in the 3% BW group (Figure 7A), and the number of macrophages significantly decreased in the 2.5% BW and 2% BW groups ($p < 0.05$) (Figure 7A,B). Importantly, the level of plasma alanine aminotransferase (ALT) and the content of hepatic lipid peroxidation (LPO) both significantly reduced in the 2.5% BW and 2% BW groups ($p < 0.05$) (Figure 7C,D). These data indicate that feed restriction alleviates heat-induced liver inflammation and damages in the channel catfish under a high water temperature.

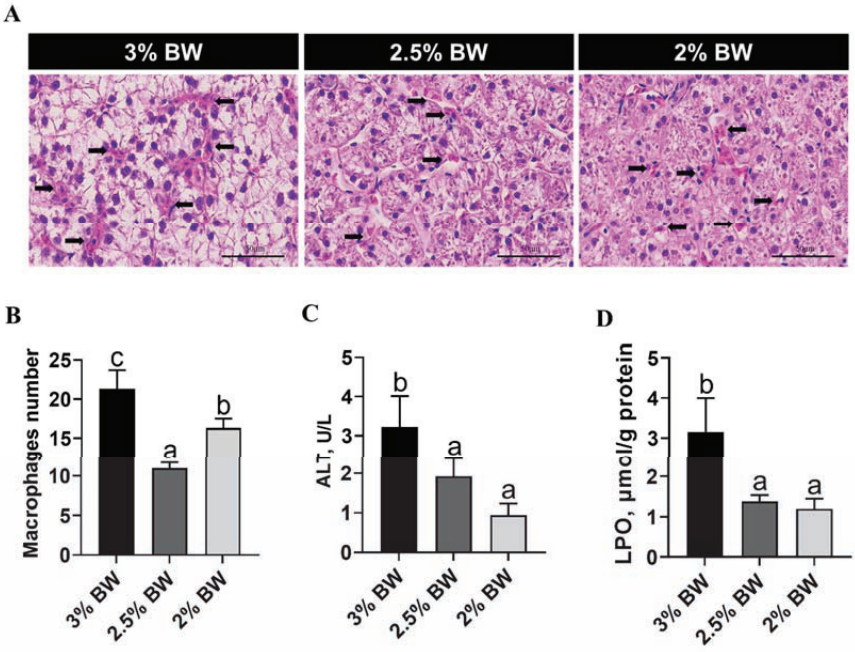

Figure 7. Feed restriction alleviated chronic thermal stress-induced liver inflammation and damages in channel catfish. (**A**) Histological images of liver in channel catfish (H&E stain, arrows indicate macrophages); (**B**) macrophages number; (**C**) plasma alanine aminotransferase (ALT) level; (**D**) lipid peroxidation (LPO) content of liver. Each data point represents the means ± SEM of six replicates. Bars assigned different superscripts (a, b and c) are significantly different ($p < 0.05$).

4. Discussion

In China, aquaculture species usually experience a high-temperature period for 2–3 months in summer season. The persistent high temperature deteriorates to a chronic thermal stress, which results in oxidative damages and metabolism disorders in cultured fish [5,6]. Previous studies showed that caloric restriction was an effective approach for reducing oxidative stress [11,34]. Thus, we investigated the effects and potential mechanism of feed restriction on improving thermal stress-induced peroxidation and damages in channel catfish. In the present study, we found that the 2.5% BW feeding ration suppressed the thermal stress response in the liver without causing negative effects on the growth performance of channel catfish under a high water temperature. We further demonstrated that feed restriction enhanced the liver antioxidant capacity and improved the stress state of the channel catfish; that was supposed to be involved in reduced lipid accumulation in liver. Moreover, we found that feed restriction mitigated the heat-induced liver ER stress and apoptosis, which ultimately alleviated liver inflammation and damages of the channel catfish under a high water temperature (Figure 8). Therefore, the present study demonstrated that appropriate feed restriction (2.5% body weight/day) alleviates liver peroxidation and damages via suppressing lipid accumulation in the liver of channel catfish under chronic thermal stress.

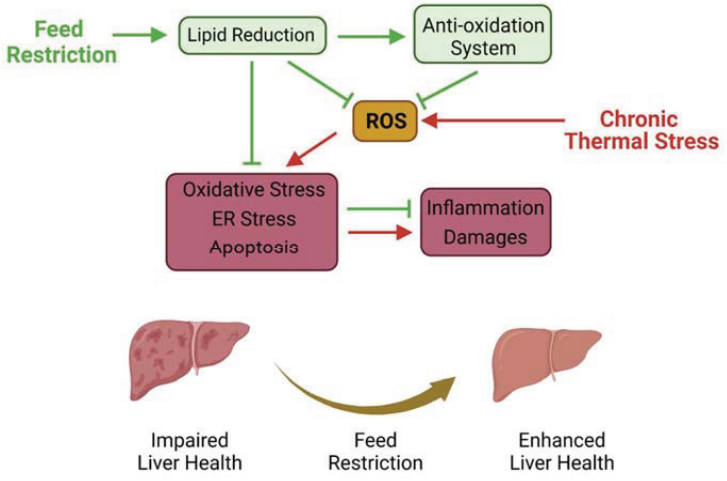

Figure 8. Proposed working model depicting the regulation mechanism of feed restriction alleviating chronic thermal stress-induced liver inflammation and damages in channel catfish.

Heat shock proteins (HSPs) are a highly conserved family of cellular proteins present in all organisms [35], including fish [36], which are the primary mediators of thermotolerance. HSPs play a role in correcting protein misfolding and defending against the accumulation of immature polypeptides under stress, while protecting cells from protein toxicity and promoting cell growth until conditions improve [37]. Studies on fish also suggested a clear link between thermal stress and heat shock proteins [38]. Here, we found that feed restriction reduced the expression level of HSPs (*hsc70*, *hsp70* and *hsp90*) in the liver of channel catfish under a high water temperature. These results mean the feed restriction can possibly suppress thermal stress in channel catfish. This is similar to a study in blunt snout bream (*Megalobrama amblycephala*), which showed that feed restriction mitigated high carbohydrate-induced oxidative stress [26]. Likewise, the expression of *hsp70* in carp (*Cyprinus carpio*) and rainbow trout (*Oncorhynchus mykiss*) was directly proportional to the transportation pressure [39]. However, feed restriction increased the expression levels of *hsc70* and *hsp70* in the gill tissue of green sturgeon (*Acipenser medirostris*) under heat stress [40]. We suppose that this was due to the excessive feed restriction (12.5% of optimum feeding ration) in that study. In view of the results obtained in this study, the decrease in HSPs may reflect a reduced stress experienced by channel catfish under elevated temperatures. Further investigations should provide more evidence for the relationships between feed restriction and thermal stress in other fish species.

The underlying mechanism for feed restriction to improve thermal stress remains unclear. Lipid accumulation correlated with systemic oxidative stress [41], and obesity was thought to be a state of chronic oxidative stress [42]. Moreover, HSPs not only function as a housekeeper and cell protector, but also as a companion for lipid metabolism [36,37]. Therefore, we speculate that improved thermal stress is involved in the decreased lipid deposition, since the feed restriction reduced the liver lipid accumulation and the CF value of channel catfish, which were consistent with a study in grass crap (*Ctenopharyngodon idella*) [25]. A previous study also illustrated that decreased lipid deposition alleviated heat stress in the liver of broilers [43]. Inversely, heat stress was proven to promote lipid accumulation by inhibiting the AMPK-PGC-1α pathway in preadipocytes [44]. Thus, an appropriate feed restriction is beneficial for maintaining the total lipid homeostasis in the thermal stress state. Furthermore, increased β-oxidation induces mitochondrial dysfunction and elevates the generation of ROS and MDA [45]. Here, we found that feed restriction enhanced the liver antioxidant capacity (CAT, SOD, GSH and T-AOC) and improved the oxidative stress state (glucose, cortisol, ROS and MDA) of the channel catfish. A previous study showed that the

non-alcoholic fatty liver disease (NAFLD) was involved in the decreased antioxidant capacity and increased oxidation stress induced by accumulation of lipids in the liver [46,47]. In fish, a high-fat diet induced an over-deposition of lipids in liver, which also impaired the antioxidant capacity and caused ROS damages [48,49]. Importantly, feed restriction or caloric restriction ameliorated the oxidative stress via reducing lipid accumulation in the liver [34,50]; the same is true in fish [26,51]. However, a study showed that feed restriction (lower than 75% satiation) decreased antioxidant capacity and triggered oxidative stress in sobaity (*Sparidentex hasta*) and yellowfin seabream (*Acanthopagrus latus*) [52]. We speculate that this is due to the excessively low feeding level, and the feeding experiment was not in a thermal condition in that study. Hence, we think feed restriction improved the stress state and enhanced the antioxidant capacity through a reduction in the lipid accumulation in the liver of channel catfish under a high water temperature.

It is known that thermal stress and peroxidation induce ER stress and apoptosis [53–55], which ultimately cause tissue damages. Various forms of cellular stress induce misfolding events and then lead to the aggregation of proteins within endoplasmic reticulum, causing ER stress [56]. Here, we found the biomarkers of ER stress (Calnexin, BIP, *perk* and *atf6*) all downregulated in the feed restriction groups. These data indicate that feed restriction can reduce thermal stress-induced ER stress, which is consistent with a study in rodents [50]. Apoptosis is a form of programmed cell death regulated by the Caspases family, and the activated Caspases can induce apoptosis to remove damaged cells in tissues [57]. Here, we found that the members of the Caspases family and BAX protein were suppressed by feed restriction, which indicated that feed restriction can alleviate thermal stress-induced cell apoptosis in the liver of channel catfish. However, a study demonstrated that short-term caloric restriction increased liver apoptosis, which was not associated Caspase levels [58]. We attribute to that study that it is not a thermal stress-induced liver apoptosis; there may exist a different regulation mechanism. Moreover, ER stress and apoptosis are closely related to tissue inflammation and damages [59,60]. Notably, the thermal stress-induced liver inflammation and damages were well improved by the feed restriction in the present study. Given these results, we propose that feed restriction alleviates heat-induced liver inflammation and damages via mitigating ER stress and apoptosis in the channel catfish under a high water temperature.

5. Conclusions

Taken together, the present study demonstrated that an appropriate feed restriction alleviated liver peroxidation and damages via suppressing lipid accumulation in the liver of cultured fish under chronic thermal stress (Figure 8). Given the growth performance, antioxidant capacity and stress state, 2.5% body weight/day was recommended to improve the liver health of channel catfish in the summer season. These findings first highlight the feasibility of feed restriction on enhancing the antioxidant and anti-stress capacities of fish suffering from thermal stress and lay the foundation for research into health care improved by feeding strategies in aquaculture.

Author Contributions: Conceptualization, D.H.; investigation and validation, Q.L., Y.G., Y.L., L.X. and W.X.; methodology, H.L. and Y.Y.; writing—original draft preparation, Y.G. and Q.L.; writing—review & editing, J.J., Z.Z., X.Z. and S.X.; D.H. had primary responsibility for the final content. All authors have read and agreed to the published version of the manuscript.

Funding: This research was funded by the National Key R&D Program of China (2018YFD0900400), China Agriculture Research System of MOF and MARA (CARS-46), the National Natural Science Foundation of China (U21A20266, 32061133009, 31972771, 31972805, 31672670) and the Fund Project in State Key Laboratory of Freshwater Ecology and Biotechnology (2019FBZ02, 2019FBZ05).

Institutional Review Board Statement: All animal experiments were conducted according to the Guiding Principles for the Care and Use of Laboratory Animals and were approved by the Institute of Hydrobiology, Chinese Academy of Sciences (Approval ID: IHB 2013724).

Informed Consent Statement: Not applicable.

Data Availability Statement: All data generated or analyzed during this study are included in this article.

Acknowledgments: The authors wish to thank Guanghan Nie and Guangxin Wang for their excellent technical assistance in these studies.

Conflicts of Interest: The authors declare no conflict of interest.

References

1. Mahanty, A.; Mohanty, S.; Mohanty, B.P. Dietary supplementation of curcumin augments heat stress tolerance through upregulation of nrf-2-mediated antioxidative enzymes and hsps in *Puntius sophore*. *Fish Physiol. Biochem.* **2017**, *43*, 1131–1141. [CrossRef] [PubMed]
2. Wang, Y.; Li, C.; Pan, C.; Liu, E.; Zhao, X.; Ling, Q. Alterations to transcriptomic profile, histopathology, and oxidative stress in liver of pikeperch (*Sander lucioperca*) under heat stress. *Fish Shellfish Immunol.* **2019**, *95*, 659–669. [CrossRef] [PubMed]
3. Narum, S.R.; Campbell, N.R.; Meyer, K.A.; Miller, M.R.; Hardy, R.W. Thermal adaptation and acclimation of ectotherms from differing aquatic climates. *Mol. Ecol.* **2013**, *22*, 3090–3097. [CrossRef] [PubMed]
4. Gradil, A.M.; Wright, G.M.; Speare, D.J.; Wadowska, D.W.; Purcell, S.; Fast, M.D. The effects of temperature and body size on immunological development and responsiveness in juvenile shortnose sturgeon (*Acipenser brevirostrum*). *Fish Shellfish Immunol.* **2014**, *40*, 545–555. [CrossRef]
5. Roychowdhury, P.; Aftabuddin, M.; Pati, M.K. Thermal stress-induced oxidative damages in the liver and associated death in fish, *Labeo rohita*. *Fish Physiol. Biochem.* **2021**, *47*, 21–32. [CrossRef]
6. Forgati, M.; Kandalski, P.K.; Herrerias, T.; Zaleski, T.; Machado, C.; Souza, M.; Donatti, L. Effects of heat stress on the renal and branchial carbohydrate metabolism and antioxidant system of Antarctic fish. *J. Comp. Physiol. B* **2017**, *187*, 1137–1154. [CrossRef]
7. Dahlke, F.T.; Wohlrab, S.; Butzin, M.; Pörtner, H.O. Thermal bottlenecks in the life cycle define climate vulnerability of fish. *Science* **2020**, *369*, 65–70. [CrossRef]
8. Spadaro, O.; Youm, Y.; Shchukina, I.; Ryu, S.; Sidorov, S.; Ravussin, A.; Nguyen, K.; Aladyeva, E.; Predeus, A.N.; Smith, S.R.; et al. Caloric restriction in humans reveals immunometabolic regulators of health span. *Science* **2022**, *375*, 671–677. [CrossRef]
9. Anderson, R.M.; Le Couteur, D.G.; de Cabo, R. Caloric restriction research: New perspectives on the biology of aging. *J. Gerontol. A Biol. Sci. Med. Sci.* **2017**, *73*, 1–3. [CrossRef]
10. Xia, E.; Rao, G.; Van Remmen, H.; Heydari, A.R.; Richardson, A. Activities of antioxidant enzymes in various tissues of male Fischer 344 rats are altered by food restriction. *J. Nutr.* **1995**, *125*, 195–201.
11. Gültekin, F.; Nazıroğlu, M.; Savaş, H.B.; Çiğ, B. Calorie restriction protects against apoptosis, mitochondrial oxidative stress and increased calcium signaling through inhibition of TRPV1 channel in the hippocampus and dorsal root ganglion of rats. *Metab. Brain Dis.* **2018**, *33*, 1761–1774. [CrossRef]
12. Venturini, P.R.; Thomazini, B.F.; Oliveira, C.A.; Alves, A.A.; Camargo, T.F.; Domingues, C.; Barbosa-Sampaio, H.; do Amaral, M. Vitamin E supplementation and caloric restriction promotes regulation of insulin secretion and glycemic homeostasis by different mechanisms in rats. *Biochem. Cell Biol.* **2018**, *96*, 777–785. [CrossRef]
13. Li, J.; Xue, B.; Cheng, X.; Hu, J.; Hu, J.; Tian, J.; Li, F.; Yu, X.; Li, B. TiO_2 NPs alleviates high-temperature induced oxidative stress in silkworms. *J. Econ. Entomol.* **2018**, *111*, 879–884. [CrossRef]
14. Ma, J.; Hampl, J.S.; Betts, N.M. Antioxidant intakes and smoking status: Data from the continuing survey of food intakes by individuals 1994–1996. *Am. J. Clin. Nutr.* **2000**, *71*, 774–780. [CrossRef]
15. Sun, H.; Wang, W.; Li, J.; Yang, Z. Growth, oxidative stress responses, and gene transcription of juvenile bighead carp (*Hypophthalmichthys nobilis*) under chronic-term exposure of ammonia. *Environ. Toxicol. Chem.* **2014**, *33*, 1726–1731. [CrossRef]
16. Guo, C.; Sun, L.; Chen, X.; Zhang, D. Oxidative stress, mitochondrial damage and neurodegenerative diseases. *Neural Regen. Res.* **2013**, *8*, 2003–2014.
17. Long, S.; Dong, X.; Tan, B.; Zhang, S.; Xie, S.; Yang, Q.; Chi, S.; Liu, H.; Deng, J.; Yang, Y.; et al. Growth performance, antioxidant ability, biochemical index in serum, liver histology and hepatic metabolomics analysis of juvenile hybrid grouper (♀*Epinephelus fuscoguttatus* × ♂*Epinephelus lanceolatus*) fed with oxidized fish oil. *Aquaculture* **2021**, *545*, 737261. [CrossRef]
18. Song, C.; Liu, B.; Xu, P.; Xie, J.; Ge, X.; Zhou, Q.; Sun, C.; Zhang, H.; Shan, F.; Yang, Z. Oxidized fish oil injury stress in Megalobrama amblycephala: Evaluated by growth, intestinal physiology, and transcriptome-based PI3K-Akt/NF-κB/TCR inflammatory signaling. *Fish Shellfish Immunol.* **2018**, *81*, 446–455. [CrossRef]
19. Biller, J.D.; Takahashi, L.S. Oxidative stress and fish immune system: Phagocytosis and leukocyte respiratory burst activity. *An. Acad. Bras. Cienc.* **2018**, *90*, 3403–3414. [CrossRef]
20. Chen, F.; Zhao, C.Y.; Guan, J.F.; Liu, X.C.; Li, X.F.; Xie, D.Z.; Xu, C. High-carbohydrate diet alleviates the oxidative stress, inflammation and apoptosis of *Megalobrama amblycephala* following dietary exposure to silver nanoparticles. *Antioxidants* **2021**, *10*, 1343. [CrossRef]
21. Wu, P.; Zhang, L.; Jiang, W.; Liu, Y.; Jiang, J.; Kuang, S.; Li, S.; Tang, L.; Tang, W.; Zhou, X.; et al. Dietary vitamin A improved the flesh quality of grass carp (*Ctenopharyngodon idella*) in relation to the enhanced antioxidant capacity through Nrf2/Keap 1a signaling pathway. *Antioxidants* **2022**, *11*, 148. [CrossRef] [PubMed]

22. Shi, Y.; Hu, Y.; Wang, Z.; Zhou, J.; Zhang, J.; Zhong, H.; Fu, G.; Zhong, L. The protective effect of taurine on oxidized fish-oil-induced liver oxidative stress and intestinal barrier-function impairment in juvenile *Ictalurus punctatus*. *Antioxidants* **2021**, *10*, 1690. [CrossRef] [PubMed]
23. Gao, X.Q.; Wang, X.; Wang, X.Y.; Li, H.X.; Xu, L.; Huang, B.; Meng, X.S.; Zhang, T.; Chen, H.B.; Xing, R.; et al. Effects of different feeding frequencies on the growth, plasma biochemical parameters, stress status, and gastric evacuation of juvenile tiger puffer fish (*Takifugu rubripes*). *Aquaculture* **2022**, *548*, 737718. [CrossRef]
24. Paula, T.G.; Zanella, B.; Fantinatti, B.; Moraes, L.N.; Duran, B.; Oliveira, C.B.; Salomão, R.; Silva, R.; Padovani, C.R.; Santos, V.; et al. Food restriction increase the expression of mTORC1 complex genes in the skeletal muscle of juvenile pacu (*Piaractus mesopotamicus*). *PLoS ONE* **2017**, *12*, e0177679. [CrossRef]
25. Gong, Y.; Chen, W.; Han, D.; Zhu, X.; Yang, Y.; Jin, J.; Liu, H.; Xie, S. Effects of food restriction on growth, body composition and gene expression related in regulation of lipid metabolism and food intake in grass carp. *Aquaculture* **2017**, *469*, 28–35. [CrossRef]
26. Xu, C.; Liu, W.B.; Remø, S.C.; Wang, B.K.; Shi, H.J.; Zhang, L.; Liu, J.D.; Li, X.F. Feeding restriction alleviates high carbohydrate diet-induced oxidative stress and inflammation of *Megalobrama amblycephala* by activating the AMPK-SIRT1 pathway. *Fish Shellfish Immunol.* **2019**, *92*, 637–648. [CrossRef]
27. *Fishery and Aquaculture Statistics 2018/FAO Annuaire*; Food and Agriculture Organization of the United Nations: Rome, Italy, 2020.
28. RuthEllen, C.; Vicki, S.B.; Carlos, E. Effects of dietary lipid on the hematology of channel catfish, *Ictalurus punctatus*. *Aquaculture* **1996**, *147*, 225–233.
29. Yang, B.; Wang, C.; Hu, H.; Tu, Y.; Han, D.; Zhu, X.; Jin, J.; Yang, Y.; Xie, S. Repeated handling compromises the immune suppression and improves the disease resistance in overwintering channel catfish (*Ictalurus punctatus*). *Fish Shellfish Immunol.* **2015**, *47*, 418–428. [CrossRef]
30. Sun, C.; Shan, F.; Liu, M.; Liu, B.; Zhou, Q.; Zheng, X.; Xu, X. High-fat-diet-induced oxidative stress in giant freshwater prawn (*Macrobrachium rosenbergii*) via NF-κB/NO signal pathway and the amelioration of vitamin E. *Antioxidants* **2022**, *11*, 228. [CrossRef]
31. Livak, K.J.; Schmittgen, T.D. Analysis of relative gene expression data using real-time quantitative PCR and the $2^{-\Delta\Delta C}{}_{T}$ method. *Methods* **2001**, *25*, 402–408. [CrossRef]
32. Ning, L.J.; He, A.Y.; Li, J.M.; Lu, D.L.; Jiao, J.G.; Li, L.Y.; Li, D.L.; Zhang, M.L.; Chen, L.Q.; Du, Z.Y. Mechanisms and metabolic regulation of PPARα activation in nile tilapia (*Oreochromis niloticus*). *Biochim. Biophys. Acta* **2016**, *1861*, 1036–1048. [CrossRef]
33. Liu, Y.; Lu, Q.; Xi, L.; Gong, Y.; Su, J.; Han, D.; Zhang, Z.; Liu, H.; Jin, J.; Yang, Y.; et al. Effects of replacement of dietary fishmeal by cottonseed protein concentrate on growth performance, liver health, and intestinal histology of largemouth bass (*Micropterus salmoides*). *Front. Physiol.* **2021**, *12*, 764987. [CrossRef]
34. Ensminger, D.C.; Salvador-Pascual, A.; Arango, B.G.; Allen, K.N.; Vázquez-Medina, J.P. Fasting ameliorates oxidative stress: A review of physiological strategies across life history events in wild vertebrates. *Comp. Biochem. Physiol. A Mol. Integr. Physiol.* **2021**, *256*, 110929. [CrossRef]
35. Feder, M.E.; Hofmann, G.E. Heat-shock proteins, molecular chaperones, and the stress response: Evolutionary and ecological physiology. *Annu. Rev. Physiol.* **1999**, *61*, 243–282. [CrossRef]
36. Roberts, R.J.; Agius, C.; Saliba, C.; Bossier, P.; Sung, Y.Y. Heat shock proteins (chaperones) in fish and shellfish and their potential role in relation to fish health: A review. *J. Fish Dis.* **2010**, *33*, 789–801. [CrossRef]
37. Pockley, A.G. Heat shock proteins as regulators of the immune response. *Lancet* **2003**, *362*, 469–476. [CrossRef]
38. Basu, N.; Todgham, A.E.; Ackerman, P.A.; Bibeau, M.R.; Nakano, K.; Schulte, P.M.; Iwama, G.K. Heat shock protein genes and their functional significance in fish. *Gene* **2002**, *295*, 173–183. [CrossRef]
39. Poltronieri, C.; Negrato, E.; Bertotto, D.; Majolini, D.; Simontacchi, C.; Radaelli, G. Immunohistochemical localization of constitutive and inducible heat shock protein 70 in carp (*Cyprinus carpio*) and trout (*Oncorhynchus mykiss*) exposed to transport stress. *Eur. J. Histochem.* **2008**, *52*, 191–198. [CrossRef]
40. Lee, S.; Hung, S.S.; Fangue, N.A.; Haller, L.; Verhille, C.E.; Zhao, J.; Todgham, A.E. Effects of feed restriction on the upper temperature tolerance and heat shock response in juvenile green and white sturgeon. *Comp. Biochem. Physiol. A Mol. Integr. Physiol.* **2016**, *198*, 87–95. [CrossRef]
41. Furukawa, S.; Fujita, T.; Shimabukuro, M.; Iwaki, M.; Yamada, Y.; Nakajima, Y.; Nakayama, O.; Makishima, M.; Matsuda, M.; Shimomura, I. Increased oxidative stress in obesity and its impact on metabolic syndrome. *J. Clin. Invest.* **2004**, *114*, 1752–1761. [CrossRef]
42. Vincent, H.K.; Innes, K.E.; Vincent, K.R. Oxidative stress and potential interventions to reduce oxidative stress in overweight and obesity. *Diabetes Obes. Metab.* **2007**, *9*, 813–839. [CrossRef] [PubMed]
43. Lu, Z.; He, X.; Ma, B.; Zhang, L.; Li, J.; Jiang, Y.; Zhou, G.; Gao, F. Dietary taurine supplementation decreases fat synthesis by suppressing the liver X receptor α pathway and alleviates lipid accumulation in the liver of chronic heat-stressed broilers. *J. Sci. Food Agric.* **2019**, *99*, 5631–5637. [CrossRef] [PubMed]
44. Huang, Y.; Xie, H.; Pan, P.; Qu, Q.; Xia, Q.; Gao, X.; Zhang, S.; Jiang, Q. Heat stress promotes lipid accumulation by inhibiting the AMPK-PGC-1α signaling pathway in 3T3-L1 preadipocytes. *Cell Stress Chaperones* **2021**, *26*, 563–574. [CrossRef]
45. Chen, Z.; Tian, R.; She, Z.; Cai, J.; Li, H. Role of oxidative stress in the pathogenesis of nonalcoholic fatty liver disease. *Free Radic. Biol. Med.* **2020**, *152*, 116–141. [CrossRef] [PubMed]

46. Farzanegi, P.; Dana, A.; Ebrahimpoor, Z.; Asadi, M.; Azarbayjani, M.A. Mechanisms of beneficial effects of exercise training on non-alcoholic fatty liver disease (NAFLD): Roles of oxidative stress and inflammation. *Eur. J. Sport Sci.* **2019**, *19*, 994–1003. [CrossRef]
47. Wang, Y.; Liu, B.; Wu, P.; Chu, Y.; Gui, S.; Zheng, Y.; Chen, X. Dietary selenium alleviated mouse liver oxidative stress and NAFLD induced by obesity by regulating the KEAP1/NRF2 pathway. *Antioxidants* **2022**, *11*, 349. [CrossRef]
48. Yin, P.; Xie, S.; Zhuang, Z.; He, X.; Tang, X.; Tian, L.; Liu, Y.; Niu, J. Dietary supplementation of bile acid attenuate adverse effects of high-fat diet on growth performance, antioxidant ability, lipid accumulation and intestinal health in juvenile largemouth bass (*Micropterus salmoides*). *Aquaculture* **2021**, *531*, 735864. [CrossRef]
49. Jin, M.; Pan, T.; Cheng, X.; Zhu, T.T.; Sun, P.; Zhou, F.; Ding, X.; Zhou, Q. Effects of supplemental dietary l-carnitine and bile acids on growth performance, antioxidant and immune ability, histopathological changes and inflammatory response in juvenile black seabream (*Acanthopagrus schlegelii*) fed high-fat diet. *Aquaculture* **2019**, *504*, 199–209. [CrossRef]
50. Ding, S.; Jiang, J.; Zhang, G.; Bu, Y.; Zhang, G.; Zhao, X. Resveratrol and caloric restriction prevent hepatic steatosis by regulating SIRT1-autophagy pathway and alleviating endoplasmic reticulum stress in high-fat diet-fed rats. *PLoS ONE* **2017**, *12*, e0183541. [CrossRef]
51. Escalante-Rojas, M.; Martínez-Brown, J.M.; Ibarra-Castro, L.; Llera-Herrera, R.; García-Gasca, A. Effects of feed restriction on growth performance, lipid mobilization, and gene expression in rose spotted snapper (*Lutjanus guttatus*). *J. Comp. Physiol. B* **2020**, *190*, 275–286. [CrossRef]
52. Hasanpour, S.; Oujifard, A.; Torfi Mozanzadeh, M.; Safari, O. Compensatory growth, antioxidant capacity and digestive enzyme activities of Sobaity (*Sparidentex hasta*) and yellowfin seabreams (*Acanthopagrus latus*) subjected to ration restriction. *Aquacult. Nutr.* **2021**, *27*, 2448–2458. [CrossRef]
53. Tang, Q.; Zheng, G.; Feng, Z.; Chen, Y.; Lou, Y.; Wang, C.; Zhang, X.; Zhang, Y.; Xu, H.; Shang, P.; et al. Trehalose ameliorates oxidative stress-mediated mitochondrial dysfunction and ER stress via selective autophagy stimulation and autophagic flux restoration in osteoarthritis development. *Cell Death Dis.* **2017**, *8*, e3081. [CrossRef]
54. Wang, H.F.; Wang, Z.Q.; Ding, Y.; Piao, M.H.; Feng, C.S.; Chi, G.F.; Luo, Y.N.; Ge, P.F. Endoplasmic reticulum stress regulates oxygen-glucose deprivation-induced parthanatos in human SH-SY5Y cells via improvement of intracellular ROS. *CNS Neurosci. Ther.* **2018**, *24*, 29–38. [CrossRef]
55. Xie, W.Y.; Zhou, X.D.; Yang, J.; Chen, L.X.; Ran, D.H. Inhibition of autophagy enhances heat-induced apoptosis in human non-small cell lung cancer cells through ER stress pathways. *Arch. Biochem. Biophys.* **2016**, *607*, 55–66. [CrossRef]
56. Oikonomou, C.; Hendershot, L.M. Disposing of misfolded ER proteins: A troubled substrate's way out of the ER. *Mol. Cell. Endocrinol.* **2020**, *500*, 110630. [CrossRef]
57. Li, J.; Yuan, J. Caspases in apoptosis and beyond. *Oncogene* **2008**, *27*, 6194–6206. [CrossRef]
58. Selman, C.; Kendaiah, S.; Gredilla, R.; Leeuwenburgh, C. Increased hepatic apoptosis during short-term caloric restriction is not associated with an enhancement in caspase levels. *Exp. Gerontol.* **2003**, *38*, 897–903. [CrossRef]
59. Slimen, I.B.; Najar, T.; Ghram, A.; Dabbebi, H.; Ben Mrad, M.; Abdrabbah, M. Reactive oxygen species, heat stress and oxidative-induced mitochondrial damage. A review. *Int. J. Hyperthermia* **2014**, *30*, 513–523. [CrossRef]
60. Dandekar, A.; Mendez, R.; Zhang, K. Cross talk between ER stress, oxidative stress, and inflammation in health and disease. *Methods Mol. Biol.* **2015**, *1292*, 205–214.

antioxidants

MDPI

Article

Growth, Health, and Gut Microbiota of Female Pacific White Shrimp, *Litopenaeus vannamei* Broodstock Fed Different Phospholipid Sources

Xiaolong Liang [1], Xiaolong Luo [1], Hongxing Lin [1], Fenglu Han [1], Jian G. Qin [2], Liqiao Chen [3], Chang Xu [1,*] and Erchao Li [1,*]

[1] Key Laboratory of Tropical Hydrobiology and Biotechnology of Hainan Province, Hainan Aquaculture Breeding Engineering Research Center, College of Marine Sciences, Hainan University, Haikou 570228, China; 19095134210017@hainanu.edu.cn (X.L.); luoxiaolong0618@163.com (X.L.); linhongxing688@163.com (H.L.); hanfenglu@163.com (F.H.)

[2] School of Biological Sciences, Flinders University, Adelaide, SA 5001, Australia; jian.qin@flinders.edu.au

[3] School of Life Sciences, East China Normal University, Shanghai 200241, China; lqchen@bio.ecnu.edu.cn

* Correspondence: cxu@hainanu.edu.cn (C.X.); ecli@bio.ecnu.edu.cn (E.L.)

Abstract: Phospholipids have an important antioxidant effect on animals. The effects of different dietary phospholipid sources on the growth, antioxidant activity, immunity, and gut microbiota of female broodstock of Pacific white shrimp *Litopenaeus vannamei* were investigated. Four isoproteic and isolipid semi-purified diets containing 4% soybean lecithin (SL), egg yolk lecithin (EL), or krill oil (KO) and a control diet without phospholipid supplementation were fed to female broodstock of *L. vannamei* (34.7 ± 4.2 g) for 28 days. The growth performance, antioxidative capacity, and innate immunity of the female broodstock fed phospholipid supplemented diets were improved regardless of sources compared with the control shrimp. The effects on growth and antioxidant capacity in female shrimp fed the KO diet were highest. The innate immunity of female shrimp fed the EL and KO diets were significantly higher than shrimp fed the SL diet. Dietary phospholipid supplementation increased gut microbiota diversity and richness, and the Chao1 and ACE values in the KO group were significantly higher than in the control group. The richness of Proteobacteria, *Photobacterium*, and *Vibrio* decreased, whereas the richness of Firmicutes and Bacteroidetes increased in the shrimp fed the KO diet compared with the shrimp fed the SL and EL diets. The interactions of gut microbiota in shrimp fed the KO diet were the most complex, and the positive interaction was the largest among all the treatments. The functional genes of gut microbiota in shrimp fed the KO diet were significantly enriched in lipid metabolism and terpenoid/polyketide metabolism pathways. Spearman correlation analysis showed that *Fusibacter* had significantly positive correlations with antioxidant activity (total antioxidant capacity, superoxide dismutase, glutathione peroxidase), immune enzyme activity (phenoloxidase and lysozyme), and immune gene expression (C-type lectin 3, Caspase-1). All findings suggest that dietary phospholipids supplementation can improve the growth and health status of female *L. vananmei* broodstock. Krill oil is more beneficial in improving the antioxidant capacity and innate immunity than other dietary phospholipid sources. Furthermore, krill oil can help establish the intestinal immune barrier by increasing the richness of *Fusibacter* and promote the growth of female shrimp. *Fusibacter* may be involved in iron metabolism to improve the antioxidant capacity of female shrimp.

Keywords: *Litopenaeus vannamei*; broodstock; phospholipid; antioxidant; gut microbiota

Citation: Liang, X.; Luo, X.; Lin, H.; Han, F.; Qin, J.G.; Chen, L.; Xu, C.; Li, E. Growth, Health, and Gut Microbiota of Female Pacific White Shrimp, *Litopenaeus vannamei* Broodstock Fed Different Phospholipid Sources. *Antioxidants* **2022**, *11*, 1143. https://doi.org/10.3390/antiox11061143

Academic Editors: Bo Liu, Changyou Song and Cunxin Sun

Received: 15 April 2022
Accepted: 8 June 2022
Published: 10 June 2022

1. Introduction

The Pacific white shrimp, *Litopenaeus vannamei*, is the most important shrimp species cultured globally in scale and production [1]. The continuous supplementation of healthy broodstock supports large-scale, healthy culture of *L. vannamei*. However, during the

practical culture of *L. vannamei* broodstock, diseases frequently occur and significantly limit the healthy and sustainable development of the industry [2,3]. Furthermore, the *L. vannamei* broodstock industry has suffered severe economic losses. In addition, the health status of shrimp broodstock can directly affect the activity and growth of shrimp larvae. Therefore, ensuring the health of *L. vannamei* broodstock is of great significance to the sustainable development of the shrimp culture industry worldwide.

After years of development, the *L. vannamei* broodstock industry has established a more efficient biosecurity system free of specific pathogens [4]. Improving reproductive performance is a fundamental goal of developing the shrimp broodstock industry. To ensure the maturation and quality of shrimp gonads, many fresh polychaetes and frozen squid are fed to *L. vannamei* broodstock in various hatcheries [5]. However, these polychaetes and squids have high price, unstable quality, and often carry pathogens [2,6,7]. *L. vannamei* broodstock is easily infected by these pathogens, and a series of health problems or mass death may occur. Therefore, it is necessary to develop nutritionally balanced diets for *L. vannamei* broodstock to ensure gonadal development and the health of *L. vannamei* broodstock.

Research on the nutrition of *L. vannamei* broodstock has been limited to dietary lipids, fatty acids, and vitamins. Previous studies have shown that dietary lipid levels can significantly affect *L. vannamei* ovary development, but the optimal dietary fatty acid level is inconsistent among previous studies on *L. vannamei* broodstock [8–10]. Dietary 2–3% highly unsaturated fatty acids could satisfy the normal development of *L. vannamei* ovaries [8,11]. Arachidonic acid, accounting for 4.65% of the total fatty acids in feed, can significantly improve the spawning performance and larval quality of *L. vannamei* [9]. Vitamin research has mainly been conducted with vitamin E and vitamin C. Dietary 300 mg/kg of vitamin E could significantly increase the hepatopancreas index and gonadosomatic index before eyestalk ablation and significantly shorten the days to spawning after eyestalk ablation [12]. Dietary 800 mg/kg of ascorbic acid can satisfy ovarian maturation and maintain good reproductive performance in *L. vannamei* broodstock [13]. However, dietary 1000–2000 mg/kg ascorbic acid had no significant effects on immune indexes, such as total hemolymph cell count and phenoloxidase activity in *L. vannamei* broodstock after eyestalk ablation [14]. Although some nutritional research on *L. vannamei* broodstock has been carried out, information on the effect of nutrients on the health status of *L. vannamei* is still scarce.

Polychaetes and squids are rich in lipids and highly unsaturated fatty acids and are especially high in phospholipids useful to ensure the gonadal development of aquatic animals [15]. Dietary 2% soybean lecithin can meet the needs of ovary maturation of giant freshwater prawn *Macrobrachium rosenbergii* [16]. Lecithin also can upregulate the expression of vitellogenin genes in the hepatopancreas of redclaw crayfish *Cherax quadricarinatus* [17]. The gonadal index of Chinese mitten crab *Eriocheir sinensis* fed 2.4% soybean lecithin was the highest among all the treatments [18]. In addition, as an essential nutrient for crustaceans, phospholipids play an essential role in modulating the growth and health of animals, but the dose effects of different phospholipids are different. The specific growth rate of swimming crabs *Portunus trituberculatus* fed the egg yolk lecithin-supplemented diet was significantly higher than that of *P. trituberculatus* fed the soybean lecithin diet [19]. Dietary krill oil could improve the antioxidant activity of *E. sinensis* more efficiently than dietary soybean lecithin or egg yolk lecithin [20]. However, there is no information on the regulation of phospholipids on the health status of *L. vannamei* broodstock. The supplementation of phospholipids to the feed can enhance the glutathione metabolism of female shrimp and further improve the antioxidant capacity [21].

Therefore, based on the results of previous research, this study evaluated the effects of three phospholipids (soybean lecithin, egg yolk lecithin, and krill oil) on *L. vannamei* in terms of growth, antioxidant capacity, immunity, and gut microbiota. The purpose of this study is to find a suitable phospholipid source for the culture of healthy *L. vannamei* broodstock. The results of this study contribute to diet development for *L. vannamei* broodstock.

2. Materials and Methods

2.1. Experimental Diets

According to the nutritional studies on broodstock of *L. vannamei* [9,10] and our previous research [21], four isoproteic (52.4% crude protein) and isolipidic (14.2% crude lipid) semi-purified diets involving 4% soybean lecithin (SL), egg yolk lecithin (EL), or krill oil (KO) and a control diet (Ctrl) without phospholipid supplementation were prepared (Table 1). The crude protein, crude lipid, and fatty acids were determined by Dumas combustion, Soxhlet extraction, and gas chromatograph-mass spectrometer (GC-MS), respectively. The protein was derived from fishmeal, gelatin, and casein in the feed ingredients. In addition, the oil sources in the experimental diets mainly included fish oil, cholesterol, palm oil, and three different phospholipids. The coarse materials were ground with a grinder, crushed into powder by an 80-mesh sieve, and then weighed. The processed dry ingredients were weighed and mixed thoroughly according to the proportions in the formulations of experimental diets, followed by the supplementation of oil and water, and mixed well again. Feed pellets with a diameter of 2.5 mm were extruded by a double helix plodder (CD4-1TS, Guangdong Huagongguang Mechanical and Electrical Technology Co., Ltd., Guangdong, China) and then were air-dried at room temperature. The feed pellets were sealed in plastic bags and frozen at −20 °C before use.

Table 1. Formulation (g/kg dry basis), proximate composition (%), and statistical analysis of differences for PUFAs contents of the experimental diets fed to female *L. vannamei*.

Ingredients	Experimental Diets			
	Ctrl	SL	EL	KO
Fish meal	200	200	200	200
Casein	320	320	320	320
Gelatin	80	80	80	80
Corn starch	150	150	150	150
Fish oil	10	10	10	10
Soybean lecithin	0	40	0	0
Egg yolk lecithin	0	0	40	0
Krill oil	0	0	0	40
Cholesterol	5	5	5	5
Palm oil	80	40	40	40
Butylated hydroxytoluene	1	1	1	1
Anhydrous calcium carbonate	4	4	4	4
Calcium lactate pentahydrate	4	4	4	4
Choline chloride	5	5	5	5
Inositol	0.25	0.25	0.25	0.25
Betaine	20	20	20	20
Vitamin premix [1]	10	10	10	10
Mineral premix [2]	20	20	20	20
Carboxymethyl cellulose	20	20	20	20
Cellulose	70.75	70.75	70.75	70.75
Total	1000	1000	1000	1000
Analyzed proximate composition (%)				
Moisture	7.51	7.43	7.78	7.42
Crude protein	52.33	52.15	52.50	52.47
Crude lipid	14.28	14.40	14.05	14.22
Ash	8.31	8.30	8.28	8.31
n-3 PUFAs	495.31 [a]	694.01 [c]	568.93 [b]	2335.27 [d]
n-6 PUFAs	335.62 [a]	1577.41 [d]	577.74 [c]	399.4 [b]

The [1] vitamin premix and [2] mineral premix are formulated with reference to the formulation suitable for female *L. vannamei* in our laboratory [21]. Values are means ± SE ($n = 3$) and values within a row with different superscript letters (a, b, c, d) are significantly different ($p < 0.05$).

2.2. Growth Trial and Sampling

All the female *L. vannamei* broodstock were obtained from a private company in Hainan, China. Before the experiment began, the female shrimp were acclimated in a black polypropylene barrel (diameter × height = 5.8 × 1.1 m). Subsequently, 160 shrimps

(34.7 ± 4.2 g, hepatosomatic index 6.23 ± 0.25%) were randomly divided into 16 barrels (diameter × height = 1.0 × 0.9 m, four barrels per treatment at 10 shrimp/barrel) and fed the control diet for 7 days to adapt to the experimental conditions. During the 28-day culture process, the daily feeding volume was about 5.5% of the body weight, and the daily feeding was carried out at 7:30, 10:00, 13:00, 15:00, 18:00, 21:00, and 23:30 for a total of 7 times. This breeding strategy is based on the summary of our previous work [21] and the suggestions of Arshadi et al. [22] to account for a total daily supply of 5% of wet weight biomass per day. Residual food and feces were removed by siphon twice a day, and the daily water exchange was about 50%. During the whole culture experiment, the water quality parameters were controlled as follows: temperature 28~29 °C, pH 7.8~8.4, salinity 30~32, dissolved oxygen 5~6 mg/L, ammonia nitrogen 0.10~0.30 mg/L, nitrite 0.03~0.10 mg/L, and 12 h light and 12 h dark.

After the 28 days of the experiment, the shrimp were fasted for 24 h for sample collection. After anesthesia for 10 min on ice, the shrimp in each experimental bucket were weighed and measured. The hemolymph of the shrimp was drawn from the cardiocoelom and abdomen (at the first swimming foot) with a 1-mL sterile syringe and stored for 24 h at 4 °C. The hepatopancreas and midgut were frozen in liquid nitrogen and transferred to a −80 °C freeze for subsequent analysis. Considering the individual differences of gut microflora, five shrimp were taken as a sample, with a total of 5 samples in each treatment. The growth performance-related parameters were calculated as follows:

$$\text{Survival (\%)} = (\text{Final number}/\text{Initial number}) \times 100;$$

$$\text{Condition factor (\%)} = \text{Final weight}/(\text{Body length})^3 \times 100;$$

$$\text{Weight gain (\%)} = (\text{Final weight} - \text{Initial weight})/\text{Initial weight} \times 100;$$

$$\text{Specific growth rate (\%, day}^{-1}\text{)} = [\text{In (Final weight)} - \text{In (Initial weight)}]/\text{Culture days} \times 100.$$

2.3. Antioxidant Capacity Related Parameter Assays

Eight hepatopancreases per treatment, from two shrimp per barrel, were homogenized in the pre-chilled 0.86% saline solution (1:10, *w*/*v*), at a frequency of 60 Hz at 4 °C for 30 s (Tissuelyser-24, Jingxin Technology, Shanghai, China), then centrifuged at 1500× *g* for 15 min in 4 °C (SIGMA 3-18K; Sigma, Laborzentrifugen GmbH, Osterode, German). The supernatant was collected for measuring total antioxidant capacity (T-AOC), malondialdehyde (MDA), glutathione peroxidase (GSH-Px), and superoxide dismutase (SOD) using diagnostic reagent kits (Nanjing Jiancheng Bioengineering Institute, Nanjing, China). Detailed steps of the parameter assays accorded with the instructions provided by the manufacturer.

2.4. Immunity Related Parameters Assay

Stored hemolymph samples were centrifuged at 4500× *g* at 4 °C for 10 min. The supernatant was aspirated and stored at −80 °C for later analysis. Eight serum per treatment from two shrimp per barrel were used to determine the activity of phenoloxidase (PO) and lysozyme (LZM).

Ashida's method [23] was improved by using levodopa as the substrate to determine phenoloxidase activity. We added 10 μL serum, 300 μL potassium phosphate buffer (0.1 mol/L, pH 6.0), and 10 μL L-dopa solution (0.01 mol/L) to the enzyme plate and the absorbance at 490 nm was read every 3 min. Under the experimental conditions, an increase of 0.001 per min of OD490 was regarded as a unit of enzyme activity.

The method based on Hultmark et al. [24] was improved by using *Micrococcus lysoleikticus* as a substrate to determine lysozyme activity. The substrate was prepared to a certain concentration of suspension (OD570 = 0.3~0.5) with potassium phosphate buffer (0.1 mol/L, pH 6.4). We placed 300 μL of the suspension and 5 μL of serum on the enzyme plate, determine the initial optical density at the 570 nm wavelength (A_0), then kept it for 30 min

in a water bath at 37 °C, and immediately determine the optical density at the 570 nm wavelength (A). The calculation was as follows: lysozyme activity (UL) = $(A_0 - A)/A \times 100$.

Total RNA was extracted from hepatopancreases and guts of two shrimp randomly selected from each parallel group using Trizol reagent (15596018, Invitrogen, Carlsbad, CA, USA). Analysis of total RNA concentration and quality using a NanoDrop 2000 spectrophotometer (Thermo Fisher Scientific, Waltham, MA, USA). RNA samples with an absorbance (260/280 nm) ranging from 1.8 to 2.1 were used for subsequent analysis. Total RNA (1 μg) from each sample was reverse transcribed into a final volume of 20 μL cDNA with Reverse Transcription Kit (containing dsNase) (Biosharp, Anhui, China). Quantitative real-time PCR (qPCR) was analyzed by ChanQ Universal SYBR qPCR Master Mix (Vazyme Biotech, Nanjing, China), carrying out the specific operational steps according to the manufacturer's instructions. To verify the stability of gene expression, β-actin was selected as the reference gene [25]. The relative expressions of target genes, including caspase-1 and C-type lectin 3 (CTL3), were analyzed by the $2^{-\Delta\Delta Ct}$ algorithm [26]. The program for the qPCR reaction was 95 °C for 30 s, 40 cycles at 95 °C for 10 s, and 60 °C for 30 s. The sequences of all PCR primers used in this study are given in Table 2.

Table 2. Primer-pair sequences and product size of the amplicons used for quantitative real-time PCR (qPCR).

Gene	Primer Sequence	Tm (°C)	GC%	GenBank NO
β-actin	F: GCAGTCCAACCCGAGAGGAAG R: GTGCATCGTCACCAGCGAA	61.49 57.09	62.00 58.00	XM_027364954
caspase-1	F: CGGGTAGGAAGCCCACATATCAA R: ACGGCGAAGTCAAAGCCAGAA	59.78 57.59	52.00 52.00	XM_027356206
CTL3	F: ATGTTCTTCGTGCTCCTGCTGT R: GCAGTGGTCGTAAATGTTGTG	57.80 55.63	50.00 48.00	XM_027356524

2.5. Gut Microbiota Analysis

Five mixed gut samples were randomly selected from each group to be used to detect gut microbiota. Total genomic DNA from samples was extracted using the CTAB method [27], and agarose gel electrophoresis was used to assess DNA purity and concentration. The V3-V4 region of 16S rRNA genes were amplified by PCR using universal primers 338F (5′ ACTCCTACGGGAGGCAGCA 3′) and 806R (5′ GGACTACHVGGGTWTCTAAT 3′) [28]. The library was built using the TruSeq® DNA PCR-Free Sample Preparation Kit. The library was quality controlled and then sequenced using the NovaSeq6000 (Illumina, San Diego, CA, USA), and bioinformatics analysis of intestinal microbes (microbial composition, diversity, function prediction, interspecific interaction) was completed on the NovoMagic cloud platform (https://magic.novogene.com/customer/main#/tool-micro/281882104460629044 61c2e3eebf9034, accessed on 8 March 2021). The sequences obtained in this study are available in the NCBI SRA database with the accession number PRJNA820522.

2.6. Gut Microbiota and Biochemical Indexes Association Analysis

Spearman correlation analysis was performed using SPSS software (ver. 26.0; SPSS Inc., Chicago, IL, USA) to show the potential connection between gut microbiota and biochemical pathways and enzymes (such as T-AOC, MDA, GSH-Px, SOD, PO, LZM, CTL3, and caspase-1). This process did not set correlation coefficients and *p*-value thresholds. A Heatmap was used to show the correlation and statistical difference (https://software.broadinstitute.org/morpheus/). Statistical significance is indicated by * $p < 0.05$, ** $p < 0.01$.

2.7. Statistical Analysis

Data on growth performance, antioxidant capacity, and immune response analysis were performed using one-way analysis of variance (ANOVA) followed by Duncan's multiple range test to assess the significance of differences among all experimental treatments.

All data are shown as means ± SE (standard error). The student's *t*-test was used to analyze functional prediction differences between all experimental treatments and control. The value of statistical significance was regarded as $p < 0.05$. All statistical analyses were performed using the SPSS software 26th version (Armonk, NY, USA, IBM SPSS Statistics).

3. Results

3.1. Growth Performance

Relative to the control, dietary phospholipid supplementation significantly increased the weight gain and specific growth rate of female *L. vannamei* broodstock regardless of phospholipid sources, but did not affect survival and condition factor (Figure 1). There were no significant differences in all the growth-related parameters among the SL, EL, and KO groups, although the shrimp fed dietary krill oil showed the highest value for these parameters.

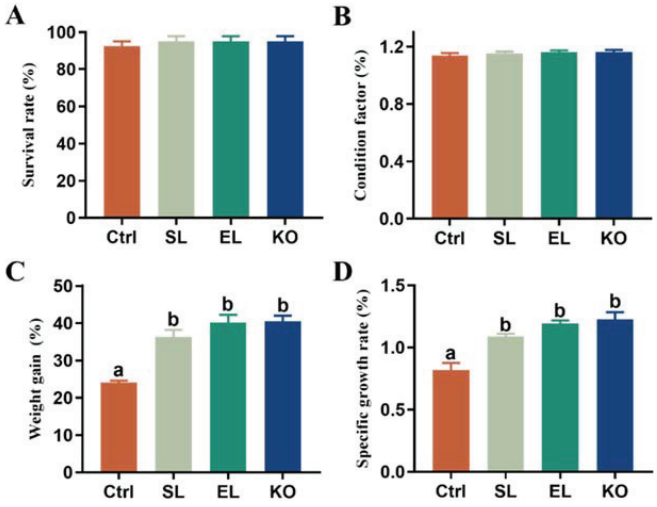

Figure 1. Growth phenotypes of female *L. vannamei* fed different experimental diets. (**A**) Survival rate. (**B**) Condition factor. (**C**) Weight gain. (**D**) Specific growth rate. The values are the mean ± standard errors ($n = 4$). Values with different superscript letters indicate significant differences ($p < 0.05$) among all the treatments.

3.2. Antioxidant Capacity

Relative to the control, dietary phospholipid supplementation significantly improved hepatopancreatic T-AOC capacity, activities of SOD and GSH-Px, and decreased the MDA contents in female *L. vannamei* broodstock, regardless of phospholipid sources (Figure 2). Among the three phospholipid-supplemented groups, shrimp fed the KO diet obtained significantly higher T-AOC capacity, activities of SOD, and GSH-Px than shrimp fed SL or EL. However, the MDA contents did not differ among the three groups.

3.3. Immune Responses

Dietary phospholipid supplementation significantly improved the activities of phenol oxidase and lysozyme and expression of C-type lectin 3 and caspase-1 in female broodstock, regardless of phospholipid sources (Figure 3). Shrimp fed EL or KO showed significantly higher phenol oxidase and lysozyme activities and expression of C-type lectin 3 and caspase-1 than shrimp fed the SL diet. Though shrimp fed the KO diet had higher immunity parameter values than shrimp fed the EL diet, a significant difference was found only for phenol oxidase activity.

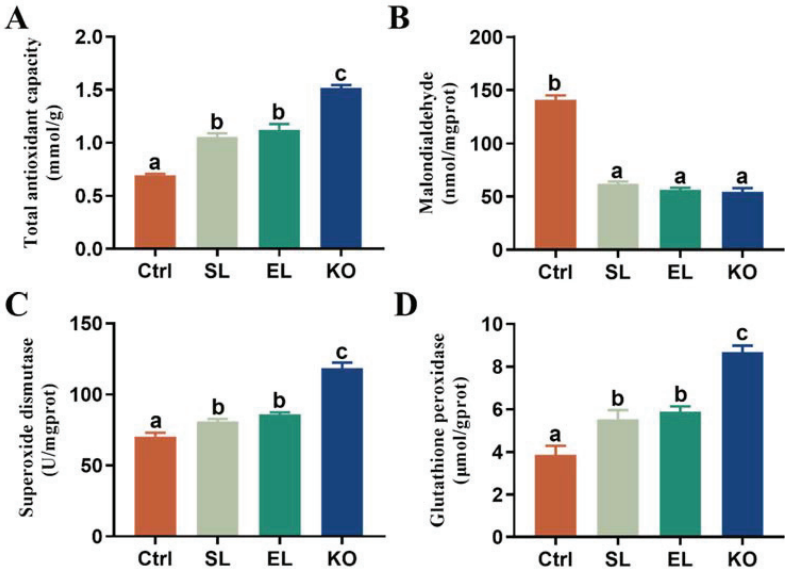

Figure 2. Hepatopancreatic antioxidant ability of female *L. vannamei* fed different experimental diets. (**A**) Total antioxidant capacity (T-AOC). (**B**) Malondialdehyde (MDA). (**C**) Superoxide dismutase (SOD). (**D**) Glutathione peroxidase (GSH-Px). The values are the mean ± standard errors (n = 4). Values with superscript different letters indicate significant differences ($p < 0.05$) among all the treatments.

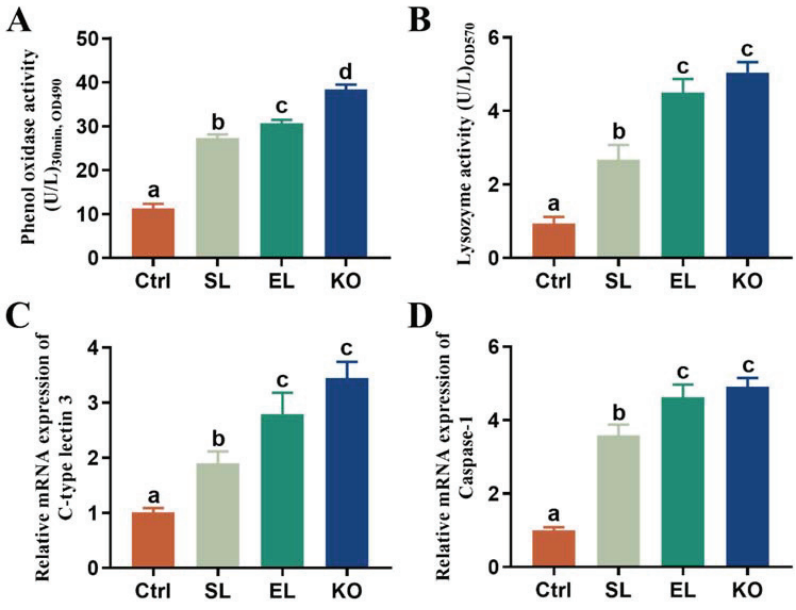

Figure 3. Immune response of female *L. vannamei* fed different experimental diets. (**A**) Phenol oxidase activity in serum. (**B**) Lysozyme activity in serum. (**C**) Relative mRNA expression of C-type lectin 3 in hepatopancreas. (**D**) Relative mRNA expression of Caspase-1 in hepatopancreas. The values are the mean ± standard errors (n = 4). Values with superscript different letters indicate significant differences ($p < 0.05$) among all the treatments.

3.4. Gut Microbiota Analysis

3.4.1. Composition of Gut Microbial Community

A total of 2,111,128 high-quality DNA sequences were obtained by gut microbial barcoding, with an average of 105,556 sequences per sample, and 56,215 valid sequences were obtained after quality control, with an average length of 425 bp. The coverage of each sample was higher than 99%. Sequence clusters with a similarity of more than 97% were regarded as belonging to the same Operational Taxonomic Units (OTUs), and 2005 OTUs were obtained. There were 163 OTUs shared among the control group and the respective phospholipid feed groups, accounting for 8.13% of the total OTUs (Figure 4A). In the horizontal direction, the number of sequences was about 6000, indicating that the sequencing was sufficient to cover most taxa in the sample, and as the number of sequences accumulated above 20,000, the rarefication curve tended to plateau, indicating that the more evenly distributed the gut microbial community (Figure 4B).

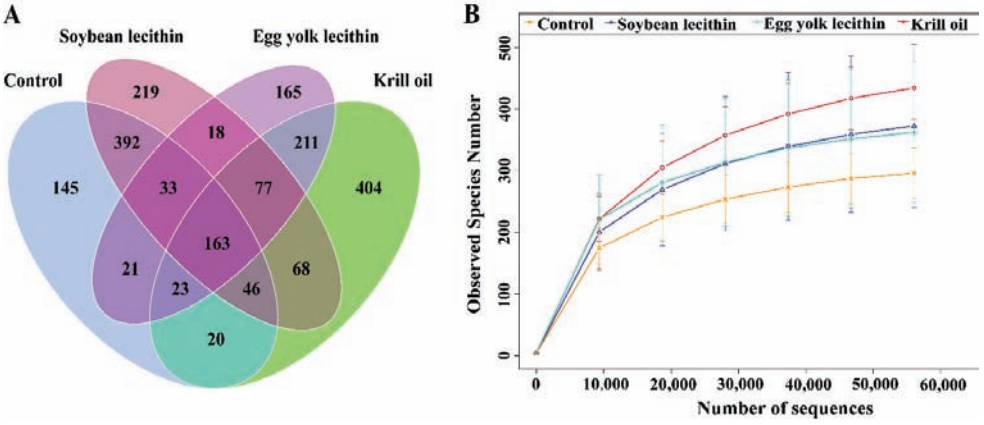

Figure 4. Gut microbial community analysis of female *L. vannamei* fed with different phospholipids. (**A**) Venn diagram indicating the number of unique and shared OTUs. (**B**) Rarefaction curve indirectly reflecting the richness of bacteria in each treatment group.

3.4.2. Diversity of Gut Microbial

The α-diversity analysis showed that Shannon and Simpson's diversity indexes were the highest for the EL and KO groups (Figure 5A,B). The richness indexes Chao 1 and ACE showed that feeding different phospholipids increased gut microbial richness, and that KO supplementation significantly improved gut microbial richness relative to the control (Figure 5C,D). Principal components analysis showed differences in gut microbial community composition among the dietary phospholipid supplementation treatments (Figure 5E).

At the phylum level, the dominant phyla in each group were Proteobacteria, Firmicutes, and Bacteroidetes, and the abundance of the Proteobacteria in the feed phospholipid group differed somewhat among treatments (Figure 6A). Among treatments, the KO group had the lowest abundance of Proteobacteria (60.28%) and the highest abundance of Firmicutes (26.07%) and Bacteroidetes (9.26%). At the genus level, the abundance of *Photobacterium* and *Vibrio* decreased slightly with dietary phospholipid supplementation, and the KO group had the lowest abundance (Figure 6B). Linear discriminant analysis effect size (LEfSe) revealed seven, six, and one biomarkers with significantly higher relative abundance in the KO, EL, and SL groups, respectively, relative to the control (Figure 6C). The phylum Bacteroidetes was significantly more abundant in the gut of shrimp fed the krill oil diet, and the genera *Spongiimonas* and *Shimia* could be regarded as biomarker taxa in the egg yolk lecithin diet. In contrast, the soybean lecithin diet had fewer biomarker taxa, with only the Family Planococcaceae (Figure 6C).

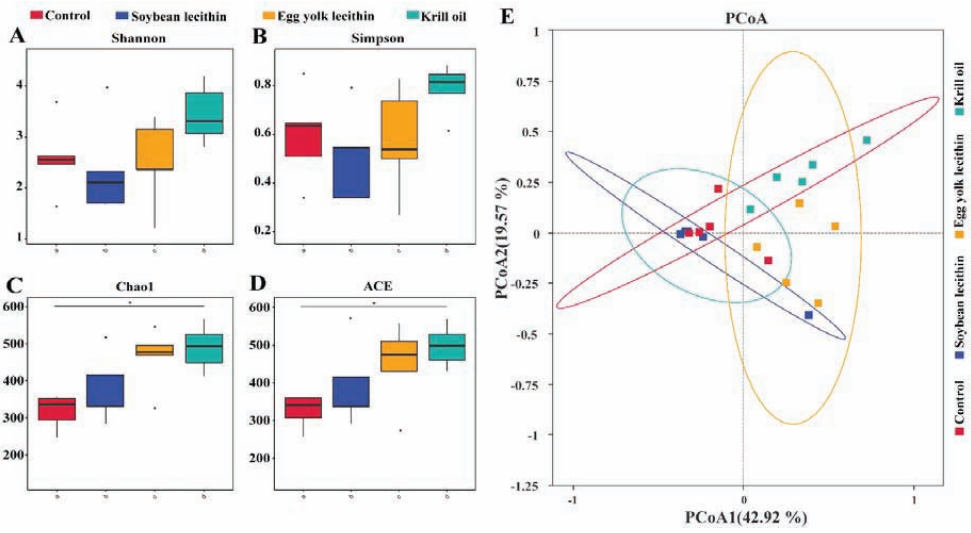

Figure 5. Diversity of gut microbial community of female *L. vannamei* fed with different phospholipids. Alpha diversity indices of bacterial communities on genus level, (**A**) Shannon, (**B**) Simpson, (**C**) Chao1, (**D**) ACE, the * $p < 0.05$ indicate significant differences. (**E**) Beta diversity, the principal coordinates analysis (PCoA) performed to evaluate the overall differences in bacterial community structure based on Bray–Curtis distance.

Comparisons of relative abundance of the top 35 genera detected in the gut of shrimp fed the respective diets were characterized by the construction of a heat map. The heat map showed that the abundance of genera was changed by different dietary phospholipids (Figure 7). In the gut microbial community of the control group, four genera [Fusobacteriota (*Hypnocyclicus*), Proteobacteria (*Ruegeria* and *Vibrio*), and Actinobacteriota (*Demequina*)] were detected. In the SL group, nine genera [Proteobacteria (*Arsenophonus*, *Citrobacter*, *Comamonas*, and *Escherichia-Shigella*), Bacteroidota (*Prevotella*), Actinobacteriota (*Cutibacterium*), and Firmicutes (*Solibacillus*, *Bacillus*, and *Lactococcus*)] were detected. In the EL group, ten genera (Firmicutes (*Lactobacillus*, *Streptococcus*, and *Faecalibacterium*), Proteobacteria (*Litorilituus*, *Sphingomonas*, *Enterococcus*, *Shimia*, and *Pseudomonas*), and Bacteroidota (*Spongiimonas* and *Xanthomarina*)) were detected. In the KO group, four genera (Firmicutes (*Staphylococcus* and *Fusibacter*), Desulfobacterota (*Gardnerella*), and Bacteroidota (*Carboxylicivirga*)) were detected.

3.4.3. Gut Microbiota Functional Prediction

The KO group had the largest number of functional OTUs, followed by the SL and EL groups (Figure 8A). The control and all treatment groups were classified into six categories at KEGG level 1: "Cellular Processes", "Environmental Information Processing", "Genetic Information Processing", "Human Diseases", "Metabolism", "Organismal Systems". Metabolism was the predominant KEGG pathway in all treatment groups (27.3%), including lipid metabolism, energy metabolism, and amino acid metabolism (Figure 8B). At KEGG level 2, relative to the control, there was a significant difference in "Aging" and "Cellular processes and signaling" in the SL and EL groups, respectively ($p < 0.05$) (Figure 8C). Further, relative to the control, the KO group had significant differences in "Lipid metabolism", "Metabolism", and "Metabolism of terpenoids and polyketides" ($p < 0.05$) (Figure 8C). At KEGG level 3, relative to the control, "Amino acid related enzymes" were significantly increased in phospholipid supplementation groups ($p < 0.05$) (Figure 8D).

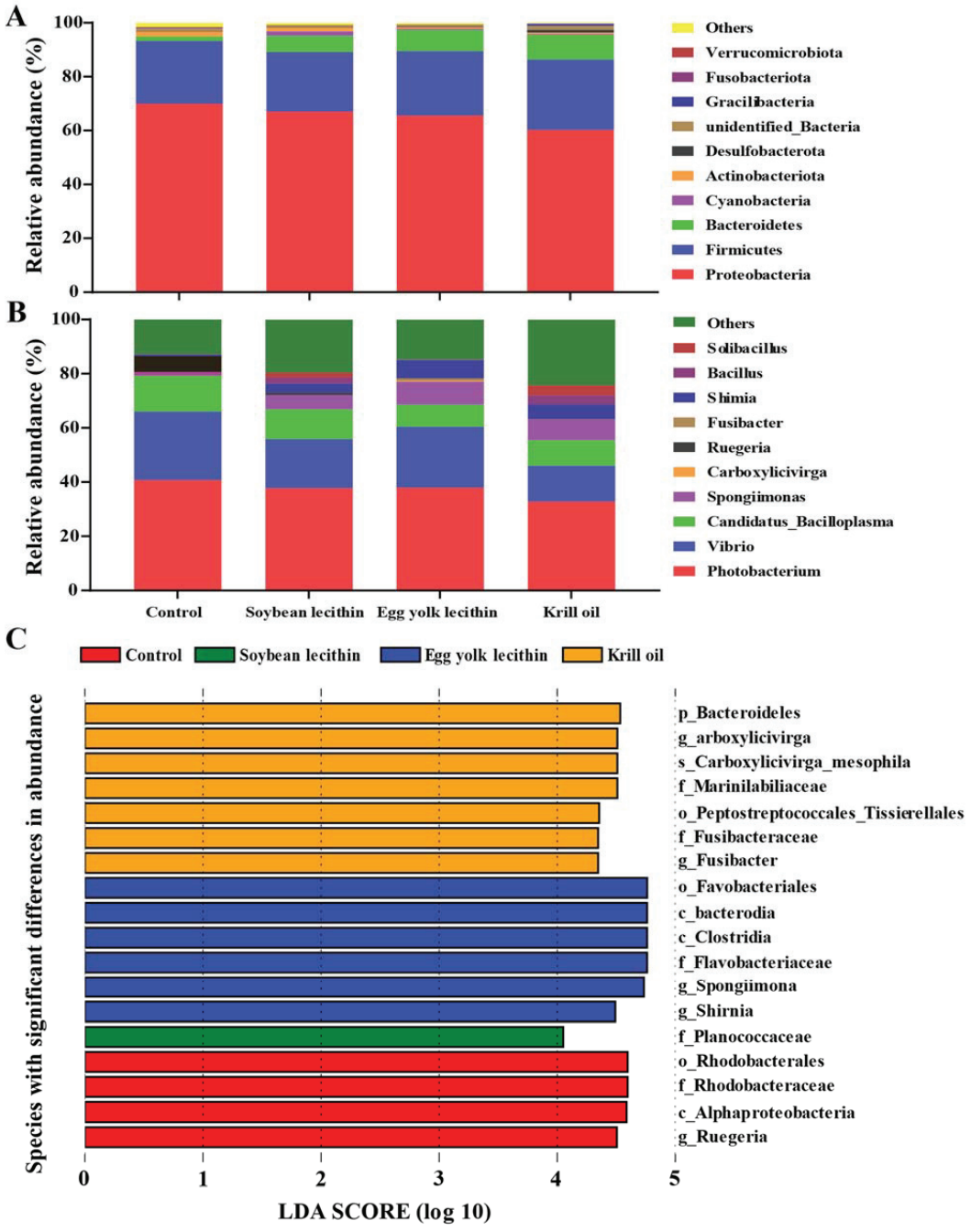

Figure 6. Gut microbial community composition of female *L. vannamei* fed with different phospholipids. Average relative abundances of dominant bacterial phyla (**A**) and genera (**B**) in the intestine. (**C**) Histogram of differentially abundant taxa identified from phylum level to genus level detected by linear discriminant analysis (LDA) effect size analysis (LEfSe; LDA > 3.5).

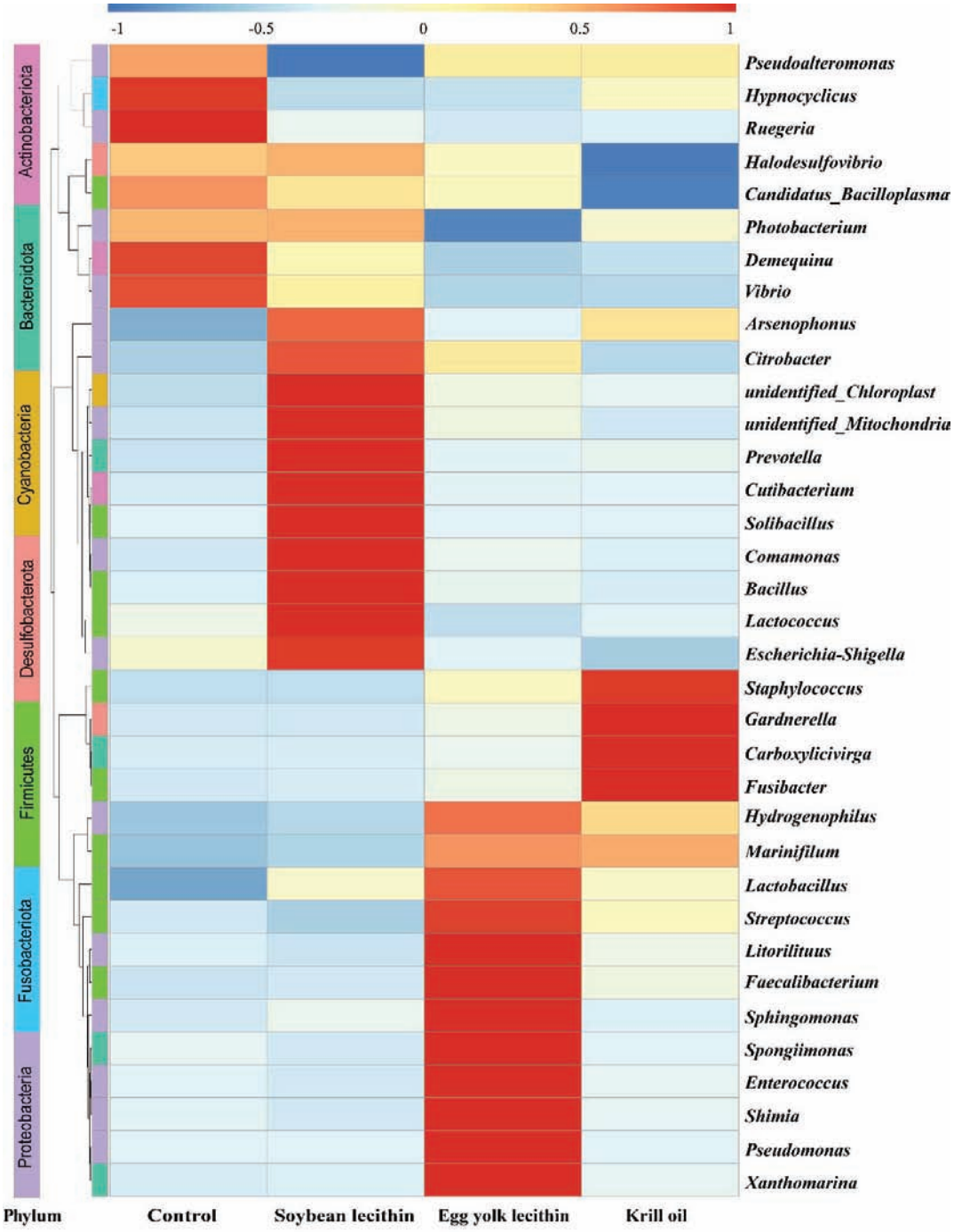

Figure 7. Genus-level composition (top 35) heat map of the gut microbiota of female *L. vannamei* fed different phospholipids. Warmer colors indicate a higher abundance of species.

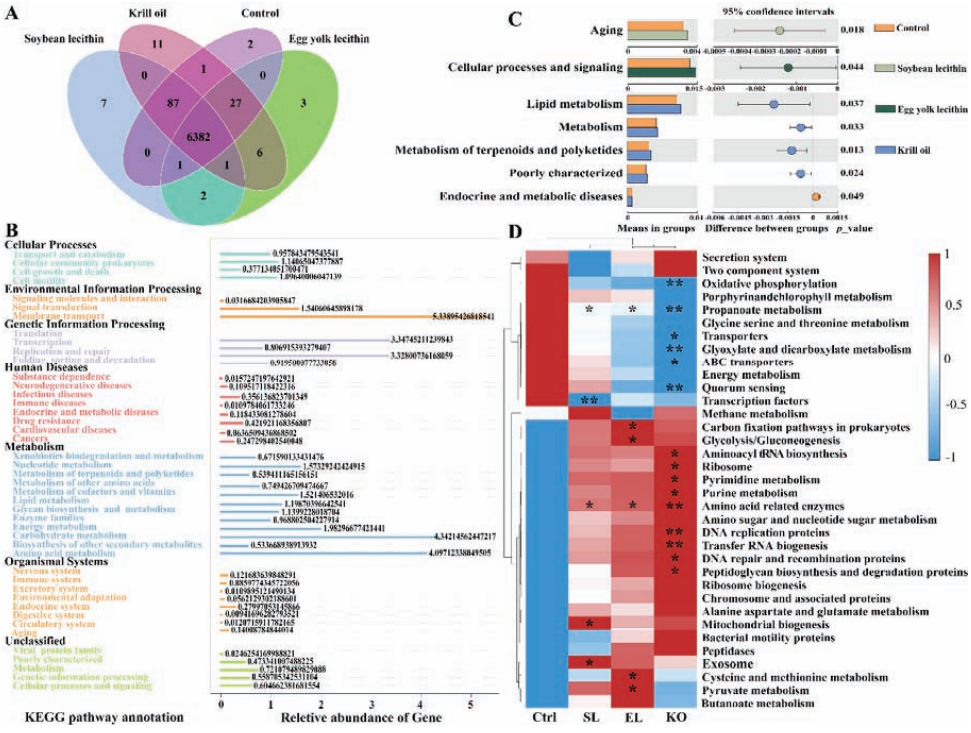

Figure 8. Effect of different phospholipids fed to female *L. vannamei* on gut microbiota function. (**A**) Venn diagram indicates the number of unique and shared OTUs of the gut microbiota. (**B**) Statistical chart of gene prediction results showing the proportion of annotated genes. (**C**) Level-2 functional prediction of gut microbial abundance in different phospholipid groups and control. (**D**) KEGG level-3 clustering heatmap of relative abundance of functions. Asterisks within the different squares indicate the significance of different phospholipid supplementations relative to the control. $p < 0.05$ represents a significant difference, and *T*-test was used for statistical analysis, and * $p < 0.05$, ** $p < 0.01$ indicate statistical significance.

3.4.4. Gut Microbiota Network

According to the analysis of the interspecies interaction network of gut microbial communities (Figure 9A,B), the control group was composed of 46 nodes and 70 edges. The network diagram for the SL group was composed of 47 nodes and 77 edges. The network diagram of the EL group was composed of 42 nodes and 84 edges. The network diagram for the KO group was composed of 45 nodes and 127 edges. Relative to the control, the number of "edges" in the network diagram for each phospholipid group increased, and the number for the KO group was the largest. In addition, the average degree and average clustering coefficient for each phospholipid group were higher than those of the control group. The analysis showed that the gut microbial community in the KO group had the most complex interspecific relationships and the greatest positive interactions.

3.5. Gut Microbiota and Biochemical Indexes Association Analysis

Results of the microbiota and biochemical indexes association analysis at the genus level are shown in Figure 10. *Carboxylicivirga*, *Halodesulfovibrio*, *Fusibacter*, *Marinifilum*, *Xanthomarina*, and *Cutibacterium* were positively correlated with T-AOC, SOD, GSH-Px, CTL3, PO, LZM, and Caspase-1, respectively, and negatively correlated with MDA ($p < 0.01$). *Ruegeria* was positively correlated with MDA and negatively correlated with T-AOC, SOD,

GSH-Px, CTL3, LZM, and Caspase-1 ($p < 0.01$). By contrast, *Arsenophonus* and *Litorilituus* were positively correlated with SOD, GSH-Px, CTL3, PO, LZM, and Caspase-1, but negatively correlated with MDA ($p < 0.05$). *Spongiimonas*, *Vibrio*, and *Comamonas* were positively correlated with LZM, and *Prevotella* and *Citrobacter* were positively correlated with Caspase-1 ($p < 0.05$). In contrast, *Demequina* was negatively correlated with GSH-Px, SOD, LZM, and Caspase-1, and *Vibrio*, *Spongiimonas*, and *Shimia* were negatively correlated with MDA ($p < 0.05$).

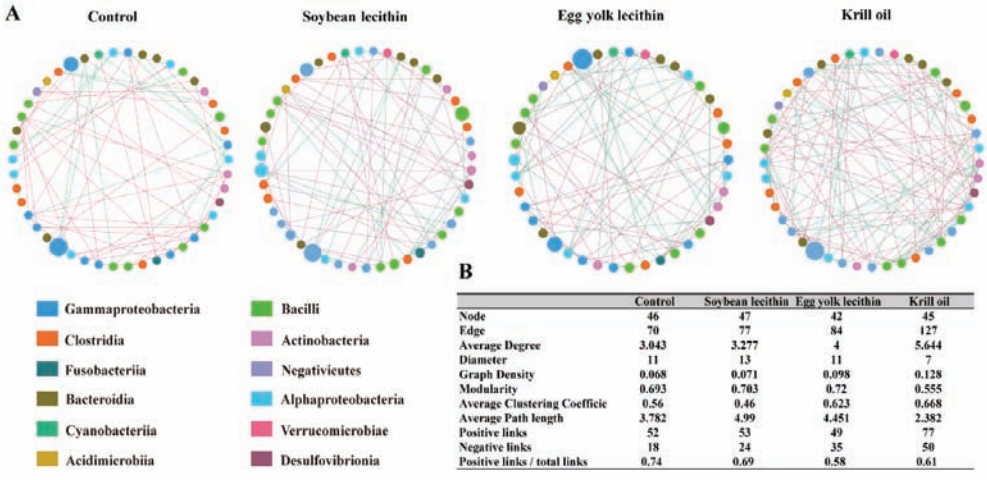

	Control	Soybean lecithin	Egg yolk lecithin	Krill oil
Node	46	47	42	45
Edge	70	77	84	127
Average Degree	3.043	3.277	4	5.644
Diameter	11	13	11	7
Graph Density	0.068	0.071	0.098	0.128
Modularity	0.693	0.703	0.72	0.555
Average Clustering Coefficie	0.56	0.46	0.623	0.668
Average Path length	3.782	4.99	4.451	2.382
Positive links	52	53	49	77
Negative links	18	24	35	50
Positive links / total links	0.74	0.69	0.58	0.61

Figure 9. Ecological interaction network analysis of gut microbial community. (**A**) Interspecies interaction network of bacteria communities for female *L. vannamei* fed with different phospholipids. Each node represents a genus. Node colors indicate genus affiliated with different classes. A green edge indicates negative correlations between two individual nodes, whereas a red edge indicates positive correlations. (**B**) Topological properties of gut microbial community networks.

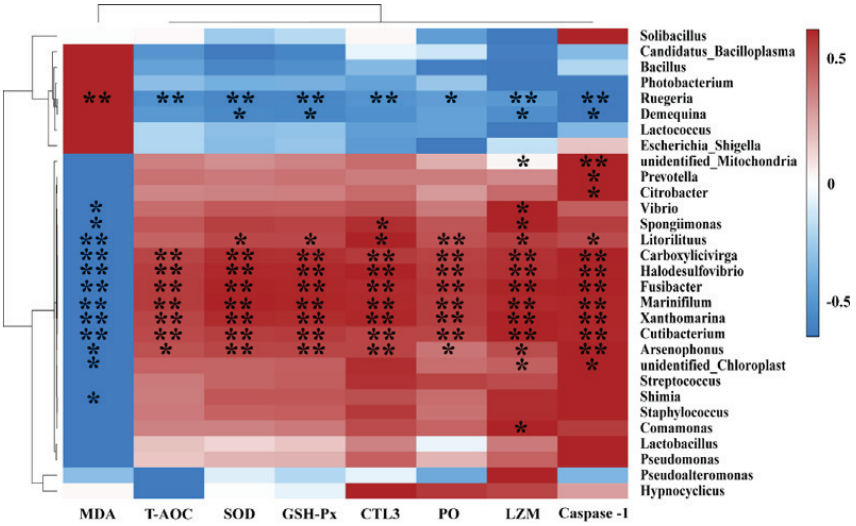

Figure 10. Correlation analysis between genera of gut microbiota and biochemical indexes. Red squares indicate positive correlations, whereas blue squares indicate negative correlations. Asterisks within the different squares indicate significance, * $p < 0.05$, ** $p < 0.01$.

4. Discussion

Maintaining the health of *L. vannamei* broodstock is particularly important for the industry's sustainable development. Studies have shown that dietary phospholipid supplementation can significantly improve the growth performance of crustaceans and fishes [29,30]. Similar results were found in this study. Adding phospholipids to diets significantly increased shrimp weight gain and specific growth rates. Further, the growth performance of shrimp fed with krill oil was better than that fed soybean lecithin and egg yolk lecithin. The same results were obtained in the study of *E. sinensis* [31]. The possible reason is that krill oil has a higher n-3 HUFA content. Studies have shown that the replacement of 50–100% soybean oil with dietary black soldier fly oil rich in n-3 HUFA has a positive effect on the growth performance and health of juvenile mirror carp (*Cyprinus carpio* var. *specularis*) [32], and the first stages of juvenile *L. vannamei* fed the diet containing 0.86 % n-3 HUFA had highest weight gain and specific growth rate [33]. Krill oil is a good source of n-3 phospholipids with high bioavailability [34], which explains how feeding krill oil can achieve the highest growth performance. The effects of phospholipids on aquatic animals vary with the phospholipids' dosages and forms [31,35], affecting the immune and antioxidant systems that are the two primary physiological mechanisms protecting the health of aquatic animals [36].

Dietary phospholipids can enhance the animal's ability to resist environmental stress and induce an antioxidant response to protect organs from oxidative damage [37,38]. The antioxidation mechanism of phospholipids can be a function of enzymatic oxidation or non-enzymatic oxidation, which is initiated by reactive oxygen species and mediated by the free radical chain reaction [39]. This study showed that the dietary phospholipids significantly increased shrimp's total antioxidant capacity (T-AOC). T-AOC is an important indicator of the antioxidant system for scavenging excessive reactive oxygen species (ROS) [40]. ROS is mainly produced in the hepatopancreas of crustaceans [41,42]. Studies have shown that the n-3 polyunsaturated fatty acids (n-3 PUFAs) in the organism are extremely easy to oxidize and induce reactive oxygen species production [42,43]. Many antioxidant enzymes are produced in an organism to reduce the detrimental effect of reactive oxygen species, including superoxide dismutase (SOD) and glutathione peroxidase (GSH-Px) [38,44]. In addition, one of the important biomarkers of oxidative stress injury has been considered to be malondialdehyde (MDA), a product of lipid peroxidation [42,43]. Dietary phospholipids can significantly increase the specific activity of superoxide dismutase (SOD) and glutathione peroxidase (GSH-Px) and reduce the content of malondialdehyde (MDA) [37,45,46]. This study confirms the view that dietary phospholipids can significantly increase the activities of SOD and GSH-Px in the hepatopancreas. Female shrimp with gonadal development accumulate much fat in the hepatopancreas, and the activities of SOD and GSH-Px are significantly increased, thereby reducing the content of MDA. As a result, dietary phospholipids can improve the oxidative pressure of excessive fat accumulation in the hepatopancreas. Our previous research has shown that differentially expressed genes could enrich glutathione metabolic pathways after feeding different phospholipid diets, confirming the hypothesis that dietary phospholipids can improve antioxidant capacity [21]. Furthermore, krill oil showed a greater antioxidant effect than soy lecithin and egg yolk lecithin. It is believed that krill oil contains an effective antioxidant, astaxanthin [47].

Due to a lack of adaptive immunity, crustaceans can only rely on innate immunity to remove pathogenic microorganisms [48], and it is the first line of defense against pathogenic infections [49]. The innate immunity of crustaceans includes cellular immunity and humoral immunity [50]. Apoptosis plays a crucial role in impeding viral propagation by eliminating infected cells [51]. Caspase-induced apoptosis can inhibit white spot syndrome virus (WSSV) infection by innate immunity in shrimp [52]. In this study, dietary phospholipids significantly up-regulated the relative mRNA expression of caspase-1 in hepatopancreas. We suggest that the diet supplemented with phospholipids can increase the relative mRNA expression of caspase-1 and induce apoptosis as appropriate to reduce the risk of WSSV infection in shrimp. Phenoloxidase (PO) [53] and lysozyme (LZM) [54]

play essential roles in the nonspecific immune system of crustaceans and can eliminate foreign pathogenic microorganisms by damaging acetaminoglycan in the cell walls of Gram-positive bacteria. Other humoral immune factors playing important roles in the immune response of crustaceans include lectins [55], which can bind to carbohydrates on the surface of pathogens and elicit antimicrobial responses in shrimp. This study shows that dietary phospholipids can enhance the activities of PO and LZM and up-regulate the expression of CTL3. Therefore, based on the study results, we suggest that the intake of phospholipid in shrimp feed can enhance the immune system to resist the invasion of pathogens.

The gut is a suitable environment for the colonization and proliferation of symbiotic microorganisms in aquatic animals [56]. The intestine is the main organ for digestion and absorption of nutrients and the largest "immune organ" of the organism [57]. The gut microbiota promotes gut health and ensures the continuous normal physiological function of the gut by constructing the first barrier against pathogens [58]. Proteobacteria, Bacteroidetes, Actinobacteria, and Firmicutes are dominant in the shrimp gut at various stages of development [59]. Similarly, in this study, the dominant bacteria in each group were Proteobacteria, Firmicutes, and Bacteroidetes, and dietary phospholipids decreased the abundance of Proteobacteria in the gut. Proteobacteria include *Rickettsiaceae* which is a pathogenic bacterium that endangers the health of shrimp [60]. Firmicutes and Bacteroidetes can participate in maintaining gut immune homeostasis and improve the health of the animals [61]. These results suggest that dietary phospholipid can benefit intestinal immune homeostasis in shrimp. By contrast, dietary krill oil induced a reduction in the abundance of Proteobacteria in this study.

Krill oil is a significant source of gut-derived endotoxin lipopolysaccharide (LPS) [62] to trigger inflammation by innate immune responses in the liver [63]. Our results show that dietary krill oil could reduce hepatopancreatic injury caused by Proteobacteria. At the genus level, *Fusibacter* is associated with iron metabolism [64], and the metabolites participate in the antioxidant and immune responses in the form of ferritin [65,66]. The present study shows that the addition of KO to the feed could increase the richness of *Fusibacter* compared to the addition of SL and EL. *Fusibacter* was positively associated with antioxidant (T-AOC, SOD, GSH-Px) and immune response (CTL3, PO, LZM, Caspase-1). The level of gene expression ferritin can be upregulated in yellowhead virus infection of *Penaeus monodon* and acute viral attack of *Chlamys farreri* [67,68]. It is hypothesized that dietary phospholipids increase the richness of *Fusibacter*, possibly by participating in iron metabolism and thus increasing the antioxidant and immune responses of female shrimp. The abundance of the microbiome is an important environmental factor affecting energy uptake and storage in the gut [69]. Gut microbes form complex ecological networks through cooperation, competition, predation, and other interactions [70]. Furthermore, excessive n-6 HUFA may interfere with gut microbial homeostasis [58]. In this study, the n-6 HUFA in the KO diet was significantly lower than those in the SL and EL groups, indicating that KO can strongly regulate the homeostasis of intestinal microbiomes. Adding KO to the feed can enhance the function of gut microbial genes, enrich the "lipid metabolism" and "energy metabolism" pathways and enhance the inter-species interactions between microorganisms. These results indicate that feed with KO can promote the stability of the gut microbial community and maintain the health of shrimp.

5. Conclusions

Adding phospholipids to the diet can improve the antioxidant capacity of *L. vannamei* broodstock and improve natural immunity to resist environmental pathogenic bacteria. Especially with krill oil as a source of phospholipids, the activities of SOD and GSH-Px in the hepatopancreas were increased, and the total antioxidant capacity of female shrimp was enhanced. In addition, the diet supplemented with krill oil could enhance the interaction of gut microbiota of female shrimp and increase the abundance of *Fusibacter* within Firmicutes. More importantly, *Fusibacter* may be involved in iron metabolism to improve the antioxidant

capacity of female shrimp. Furthermore, krill oil can help establish the gut immune barrier to enhance the immune response of female shrimp, reduce the risk of pathogenic bacteria infection and maintain the healthy growth of female shrimp.

Author Contributions: X.L. (Xiaolong Liang) was responsible for feeding experiments, sample collection and data analysis, and writing original manuscripts. X.L. (Xiaolong Luo) and H.L. were responsible for sample collection and validation of the data. X.L. (Xiaolong Liang), F.H., C.X. and E.L. were responsible for research investigation and experimental design. C.X., J.G.Q. and L.C. were responsible for reviewing and revising articles. E.L. was responsible for the overall planning of the funds and review of the manuscript. All authors have read and agreed to the published version of the manuscript.

Funding: This study was co-sponsored by the National Key R&D Program of China [2018YFD0900400] and the Research and Development Program Projects in Key Areas of Guangdong Province [2020B0202010001].

Institutional Review Board Statement: The animal experiments in this study were reviewed and approved by the Committee on the Ethics of Animal Experiments of Hainan University (HNUAUCC-2021-00119).

Informed Consent Statement: Not applicable.

Data Availability Statement: The data provided in this study have been uploaded to the NCBI database. The accession number is PRJNA820522, and the link is https://www.ncbi.nlm.nih.gov/sra/PRJNA820522 (accessed on 29 March 2022).

Acknowledgments: The author acknowledge Hainan Zhongzheng Aquatic Products Technology Co., Ltd. for the contribution of experimental sites and experimental materials and acknowledge Beijing Novogene Co., Ltd. for assistance in microbial 16S bioinformatics analysis.

Conflicts of Interest: The authors declare no conflict of interest.

References

1. Garibay-Valdez, E.; Cicala, F.; Martinez-Porchas, M.; Gómez-Reyes, R.; Vargas-Albores, F.; Gollas-Galván, T.; Martínez-Córdova, L.R.; Calderón, K. Longitudinal Variations in the Gastrointestinal Microbiome of the White Shrimp, *Litopenaeus Vannamei*. *PeerJ* **2021**, *9*, e11827. [CrossRef] [PubMed]
2. Thitamadee, S.; Prachumwat, A.; Srisala, J.; Jaroenlak, P.; Salachan, P.V.; Sritunyalucksana, K.; Flegel, T.W.; Itsathitphaisarn, O. Review of Current Disease Threats for Cultivated Penaeid Shrimp in Asia. *Aquaculture* **2016**, *452*, 69–87. [CrossRef]
3. Anderson, J.L.; Valderrama, D.; Jory, D.E. Goal 2019: Global Shrimp Production Review. *Glob. Aquac. Alliance* **2019**. Available online: https://www.aquaculturealliance.org/advocate/goal-2019-globalshrimp-production-review/ (accessed on 14 July 2020).
4. Servin Arce, K.; de Souza Valente, C.; do Vale Pereira, G.; Shapira, B.; Davies, S.J. Modulation of the Gut Microbiota of Pacific White Shrimp (*Penaeus vannamei* Boone, 1931) by Dietary Inclusion of a Functional Yeast Cell Wall-Based Additive. *Aquac. Nutr.* **2021**, *27*, 1114–1127. [CrossRef]
5. Hoa, N.D.; Wouters, R.; Wille, M.; Thanh, V.; Dong, T.K.; Van Hao, N.; Sorgeloos, P. A Fresh-Food Maturation Diet with an Adequate HUFA Composition for Broodstock Nutrition Studies in Black Tiger Shrimp *Penaeus monodon* (Fabricius, 1798). *Aquaculture* **2009**, *297*, 116–121. [CrossRef]
6. Wouters, R.; Molina, C.; Lavens, P.; Calderón, J. Lipid Composition and Vitamin Content of Wild Female *Litopenaeus vannamei* in Different Stages of Sexual Maturation. *Aquaculture* **2001**, *198*, 307–323. [CrossRef]
7. Vijayan, K.K.; Raj, V.S.; Balasubramanian, C.P.; Alavandi, S.V.; Sekhar, V.T.; Santiago, T.C. Polychaete Worms-a Vector for White Spot Syndrome Virus (WSSV). *Dis. Aquat. Org.* **2005**, *63*, 107–111. [CrossRef]
8. Wouters, R.; Piguave, X.; Bastidas, L.; Calderón, J.; Sorgeloos, P. Ovarian Maturation and Haemolymphatic Vitellogenin Concentration of Pacific White Shrimp *Litopenaeus vannamei* (Boone) Fed Increasing Levels of Total Dietary Lipids and HUFA. *Aquac. Res.* **2001**, *32*, 573–582. [CrossRef]
9. Xu, H.; Zhang, Y.; Luo, K.; Meng, X.; Luan, S.; Cao, B.; Chen, B.; Liang, M.; Kong, J. Arachidonic Acid in Diets for Early Maturation Stages Enhances the Final Reproductive Performances of Pacific White Shrimp (*Litopenaeus vannamei*). *Aquaculture* **2017**, *479*, 556–563. [CrossRef]
10. Maneii, K.; Oujifard, A.; Ghasemi, A.; Mozanzadeh, M.T. Reproductive Performance and Vitellogenin mRNA Transcript Abundance in the Hepatopancreas of Female *Litopenaeus vannamei* Fed Diets with Different Soy Lecithin Content. *Anim. Reprod. Sci.* **2019**, *211*, 106228. [CrossRef]
11. Mirheydari, S.-M.; Matinfar, A.; Emadi, H. Relation between Reproductive and Biologic Performance of *Litopenaeus vannamei* Females Broodstock Fed Different Dietary Highly Unsaturated Fatty Acid (HUFA) Levels. *World Appl. Sci. J.* **2014**, *32*, 123–132.

12. Arshadi, A.; Gharaei, A.; Mirdar Harijani, J. Effect of Dietary Vitamin E on Reproductive Performance and Vitellogenin Gene Expression in Broodstock of *Litopenaeus vannamei*. *Iran. J. Fish. Sci.* **2020**, *19*, 2475–2492.
13. Du, S.; Hu, C.; Shen, Q. Effect of Dietary Ascorbic Acid Levels on Reproductive Performance of Shrimp, *Litopenaeus vannamei* (Boone), Broodstock. *J. Shellfish. Res.* **2004**, *23*, 251–255.
14. Maggioni, D.S.; Andreatta, E.R.; Hermes, E.M.; Barracco, M.A. Evaluation of Some Hemato-Immunological Parameters in Female Shrimp *Litopenaeus vannamei* Submitted to Unilateral Eyestalk Ablation in Association with a Diet Supplemented with Superdoses of Ascorbic Acid as a Form of Immunostimulation. *Aquaculture* **2004**, *241*, 501–515. [CrossRef]
15. Corral-Rosales, D.C.; Cruz-Suárez, L.E.; Ricque-Marie, D.; Rodríguez-Jaramillo, C.; Palacios, E. Modulation of Reproductive Exhaustion Using *Ulva Clathrata* in Pacific White Shrimp *Litopenaeus vannamei* (Boone, 1931) Broodstock during Commercial Maturation. *Aquac. Res.* **2018**, *49*, 3711–3722. [CrossRef]
16. Cavalli, R.O.; Menschaert, G.; Lavens, P.; Sorgeloos, P. Maturation Performance, Offspring Quality and Lipidcomposition of *Macrobrachium rosenbergii* Females fed Increasing Levels of Dietary Phospholipids. *Aquac. Int.* **2000**, *8*, 41–58. [CrossRef]
17. Wang, L.; Zuo, D.; Lv, W.; Li, J.; Wang, Q.; Zhao, Y. Effects of Dietary Soybean Lecithin on Gonadal Development and Vitellogenin mRNA Expression in the Female Redclaw Crayfish *Cherax quadricarinatus* (von Martens) at First Maturation. *Aquac. Res.* **2013**, *44*, 1167–1176. [CrossRef]
18. Sui, L.Y.; Wu, X.G.; Wille, M.; Cheng, Y.X.; Sorgeloos, P. Effect of Dietary Soybean Lecithin on Reproductive Performance of Chinese Mitten Crab *Eriocheir sinensis* (H. Milne-Edwards) Broodstock. *Aquac. Int.* **2009**, *17*, 45–56. [CrossRef]
19. Li, X.; Wang, J.; Han, T.; Hu, S.; Jiang, Y.; Wang, C. Effect of Dietary Phospholipids Levels and Sources on Growth Performance, Fatty Acid Composition of the Juvenile Swimming Crab, *Portunus trituberculatus*. *Aquaculture* **2014**, *430*, 166–172. [CrossRef]
20. Lin, Z.; Qi, C.; Han, F.; Chen, X.; Qin, C.; Wang, C.; Wang, X.; Qin, J.; Chen, L. Selecting Suitable Phospholipid Source for Female *Eriocheir sinensis* in Pre-Reproductive Phase. *Aquaculture* **2020**, *528*, 735610. [CrossRef]
21. Liang, X.; Luo, X.; Lin, H.; Han, F.; Qin, J.G.; Chen, L.; Xu, C.; Li, E. Effects and Mechanism of Different Phospholipid Diets on Ovary Development in Female Broodstock Pacific White Shrimp, *Litopenaeus vannamei*. *Front. Nutr.* **2022**, *9*, 830934. [CrossRef] [PubMed]
22. Arshadi, A.; Yavari, V.; Oujifard, A.; Mousavi, S.M.; Gisbert, E.; Mozanzadeh, M.T. Dietary Nucleotide Mixture Effects on Reproductive and Performance, Ovary Fatty Acid Profile and Biochemical Parameters of Female Pacific Shrimp *Litopenaeus vannamei*. *Aquac. Nutr.* **2018**, *24*, 515–523. [CrossRef]
23. Ashida, M. Purification and Characterization of Pre-Phenoloxidase from Hemolymph of the Silkworm *Bombyx Mori*. *Arch. Biochem. Biophys.* **1971**, *144*, 749–762. [CrossRef]
24. Hultmark, D.; Steiner, H.; Rasmuson, T.; Boman, H.G. Insect Immunity. Purification and Properties of Three Inducible Bactericidal Proteins from Hemolymph of Immunized Pupae of *Hyalophora Cecropia*. *Eur. J. Biochem.* **1980**, *106*, 7–16. [CrossRef] [PubMed]
25. Pfaffl, M.W.; Tichopad, A.; Prgomet, C.; Neuvians, T.P. Determination of Stable Housekeeping Genes, Differentially Regulated Target Genes and Sample Integrity: BestKeeper–Excel-Based Tool Using Pair-Wise Correlations. *Biotechnol. Lett.* **2004**, *26*, 509–515. [CrossRef] [PubMed]
26. Livak, K.J.; Schmittgen, T.D. Analysis of Relative Gene Expression Data Using Real-Time Quantitative PCR and the $2^{-\Delta\Delta CT}$ Method. *Methods* **2001**, *25*, 402–408. [CrossRef]
27. Shan, L.; Li, Y.; Zheng, S.; Wei, Y.; Shang, Y. Analysis of the Bacterial Floral Structure and Diversity of Xuanwei Ham by 16S rDNA Sequencing. *J. Food Saf.* **2020**, *40*, e12800. [CrossRef]
28. Mori, H.; Maruyama, F.; Kato, H.; Toyoda, A.; Dozono, A.; Ohtsubo, Y.; Nagata, Y.; Fujiyama, A.; Tsuda, M.; Kurokawa, K.E.N. Design and Experimental Application of a Novel Non-Degenerate Universal Primer Set That Amplifies Prokaryotic 16S rRNA Genes with a Low Possibility to Amplify Eukaryotic rRNA Genes. *DNA Res.* **2014**, *21*, 217–227. [CrossRef]
29. Wang, J.T.; Han, T.; Li, X.Y.; Hu, S.X.; Jiang, Y.D.; Wang, C.L. Effects of Dietary Phosphatidylcholine (PC) Levels on the Growth, Molt Performance and Fatty Acid Composition of Juvenile Swimming Crab, *Portunus trituberculatus*. *Anim. Feed. Sci. Technol.* **2016**, *216*, 225–233. [CrossRef]
30. Feng, S.; Cai, Z.; Zuo, R.; Mai, K.; Ai, Q. Effects of Dietary Phospholipids on Growth Performance and Expression of Key Genes Involved in Phosphatidylcholine Metabolism in Larval and Juvenile Large Yellow Croaker, *Larimichthys Crocea*. *Aquaculture* **2017**, *469*, 59–66. [CrossRef]
31. Lin, Z.; Han, F.; Lu, J.; Guo, J.; Qi, C.; Wang, C.; Xiao, S.; Bu, X.; Wang, X.; Qin, J.; et al. Influence of Dietary Phospholipid on Growth Performance, Body Composition, Antioxidant Capacity and Lipid Metabolism of Chinese Mitten Crab, *Eriocheir sinensis*. *Aquaculture* **2020**, *516*, 734653. [CrossRef]
32. Xu, X.; Ji, H.; Belghit, I.; Liland, N.S.; Wu, W.; Li, X. Effects of Black Soldier Fly Oil Rich in n-3 HUFA on Growth Performance, Metabolism and Health Response of Juvenile Mirror Carp (*Cyprinus carpio* Var. *Specularis*). *Aquaculture* **2021**, *533*, 736144. [CrossRef]
33. An, W.; He, H.; Dong, X.; Tan, B.; Yang, Q.; Chi, S.; Zhang, S.; Liu, H.; Yang, Y. Regulation of Growth, Fatty Acid Profiles, Hematological Characteristics and Hepatopancreatic Histology by Different Dietary n-3 Highly Unsaturated Fatty Acids Levels in the First Stages of Juvenile Pacific White Shrimp (*Litopenaeus vannamei*). *Aquac. Rep.* **2020**, *17*, 100321. [CrossRef]
34. Kim, M.G.; Yang, I.; Lee, H.S.; Lee, J.Y.; Kim, K. Lipid-Modifying Effects of Krill Oil vs Fish Oil: A Network Meta-Analysis. *Nutr. Rev.* **2020**, *78*, 699–708. [CrossRef] [PubMed]

35. Azarm, H.M.; Kenari, A.A.; Hedayati, M. Effect of Dietary Phospholipid Sources and Levels on Growth Performance, Enzymes Activity, Cholecystokinin and Lipoprotein Fractions of Rainbow Trout (*Oncorhynchus mykiss*) Fry. *Aquac. Res.* **2013**, *44*, 634–644. [CrossRef]
36. Chen, Y.-Y.; Sim, S.S.; Chiew, S.L.; Yeh, S.-T.; Liou, C.-H.; Chen, J.-C. Dietary Administration of a Gracilaria Tenuistipitata Extract Produces Protective Immunity of White Shrimp *Litopenaeus vannamei* in Response to Ammonia Stress. *Aquaculture* **2012**, *370*, 26–31. [CrossRef]
37. Hamza, N.; Mhetli, M.; Khemis, I.B.; Cahu, C.; Kestemont, P. Effect of Dietary Phospholipid Levels on Performance, Enzyme Activities and Fatty Acid Composition of Pikeperch (*Sander lucioperca*) Larvae. *Aquaculture* **2008**, *275*, 274–282. [CrossRef]
38. Zhao, J.; Ai, Q.; Mai, K.; Zuo, R.; Luo, Y. Effects of Dietary Phospholipids on Survival, Growth, Digestive Enzymes and Stress Resistance of Large Yellow Croaker, *Larmichthys crocea* Larvae. *Aquaculture* **2013**, *410*, 122–128. [CrossRef]
39. Liu, B.; Zhao, M.; Xue, J.; Gu, Q.; Zhang, X.; Qin, S. Hydrogen Influences HDL-Associated Enzymes and Reduces Oxidized Phospholipids Levels in Rats Fed with a High-Fat Diet. *Life Sci.* **2021**, *267*, 118945. [CrossRef] [PubMed]
40. Heink, A.E.; Parrish, A.N.; Thorgaard, G.H.; Carter, P.A. Oxidative Stress among SOD-1 Genotypes in Rainbow Trout (*Oncorhynchus mykiss*). *Aquat. Toxicol.* **2013**, *144*, 75–82. [CrossRef]
41. Yu, P.; Liu, Z.; Wu, D.; Chen, M.; Lv, W.; Zhao, Y. Accumulation of Polystyrene Microplastics in Juvenile *Eriocheir sinensis* and Oxidative Stress Effects in the Liver. *Aquat. Toxicol.* **2018**, *200*, 28–36. [CrossRef]
42. Song, D.; Shi, B.; Ding, L.; Jin, M.; Sun, P.; Jiao, L.; Zhou, Q. Regulation of Dietary Phospholipids on Growth Performance, Antioxidant Activities, Phospholipid Metabolism and Vitellogenesis in Prereproductive Phase of Female Swimming Crabs, *Portunus trituberculatus*. *Aquaculture* **2019**, *511*, 734230. [CrossRef]
43. Jin, M.; Monroig, Ó.; Lu, Y.; Yuan, Y.; Li, Y.; Ding, L.; Tocher, D.R.; Zhou, Q. Dietary DHA/EPA Ratio Affected Tissue Fatty Acid Profiles, Antioxidant Capacity, Hematological Characteristics and Expression of Lipid-Related Genes but Not Growth in Juvenile Black Seabream (*Acanthopagrus schlegelii*). *PLoS ONE* **2017**, *12*, e0176216.
44. Li, Y.; Gao, J.; Huang, S. Effects of Different Dietary Phospholipid Levels on Growth Performance, Fatty Acid Composition, PPAR Gene Expressions and Antioxidant Responses of Blunt Snout Bream *Megalobrama amblycephala* Fingerlings. *Fish Physiol. Biochem.* **2015**, *41*, 423–436. [CrossRef]
45. Gao, J.; Koshio, S.; Wang, W.; Li, Y.; Huang, S.; Cao, X. Effects of Dietary Phospholipid Levels on Growth Performance, Fatty Acid Composition and Antioxidant Responses of Dojo Loach *Misgurnus anguillicaudatus* Larvae. *Aquaculture* **2014**, *426*, 304–309. [CrossRef]
46. Cai, Z.; Feng, S.; Xiang, X.; Mai, K.; Ai, Q. Effects of Dietary Phospholipid on Lipase Activity, Antioxidant Capacity and Lipid Metabolism-Related Gene Expression in Large Yellow Croaker Larvae (*Larimichthys crocea*). *Comp. Biochem. Physiol. Part B Biochem. Mol. Biol.* **2016**, *201*, 46–52. [CrossRef] [PubMed]
47. Che, H.; Li, H.; Song, L.; Dong, X.; Yang, X.; Zhang, T.; Wang, Y.; Xie, W. Orally Administered DHA-Enriched Phospholipids and DHA-Enriched Triglyceride Relieve Oxidative Stress, Improve Intestinal Barrier, Modulate Inflammatory Cytokine and Gut Microbiota, and Meliorate Inflammatory Responses in the Brain in Dextran Sodium Sulfa. *Mol. Nutr. Food Res.* **2021**, *65*, 2000986. [CrossRef]
48. Duan, Y.; Wang, Y.; Liu, Q.; Zhang, J.; Xiong, D. Changes in the Intestine Barrier Function of *Litopenaeus vannamei* in Response to PH Stress. *Fish Shellfish. Immunol.* **2019**, *88*, 142–149. [CrossRef] [PubMed]
49. Loker, E.S.; Adema, C.M.; Zhang, S.; Kepler, T.B. Invertebrate Immune Systems–Not Homogeneous, Not Simple, Not Well Understood. *Immunol. Rev.* **2004**, *198*, 10–24. [CrossRef] [PubMed]
50. Tong, R.; Pan, L.; Zhang, X.; Li, Y. Neuroendocrine-Immune Regulation Mechanism in Crustaceans: A Review. *Rev. Aquac.* **2022**, *14*, 378–398. [CrossRef]
51. Jiang, H.-F.; Chen, C.; Jiang, X.-Y.; Shen, J.-L.; Ling, F.; Li, P.-F.; Wang, G.-X. Luteolin in *Lonicera Japonica* Inhibits the Proliferation of White Spot Syndrome Virus in the Crayfish *Procambarus clarkii*. *Aquaculture* **2022**, *550*, 737852. [CrossRef]
52. Leu, J.-H.; Lin, S.-J.; Huang, J.-Y.; Chen, T.-C.; Lo, C.-F. A Model for Apoptotic Interaction between White Spot Syndrome Virus and Shrimp. *Fish Shellfish. Immunol.* **2013**, *34*, 1011–1017. [CrossRef] [PubMed]
53. Perazzolo, L.M.; Barracco, M.A. The Prophenoloxidase Activating System of the Shrimp *Penaeus paulensis* and Associated Factors. *Dev. Comp. Immunol.* **1997**, *21*, 385–395. [CrossRef]
54. Zhang, S.-C.; Xu, N. Advance in Study of Animal Lysozymes. *Period. Ocean Univ. China* **2014**, *44*, 46–51.
55. Song, F.; Chen, G.-L.; Lu, K.-C.; Fan, J.-Q.; Yan, M.-T.; He, H.-H.; Lian, Y.-Y.; Zhang, C.-Z.; Chen, Y.-H. Identification and Functional Characterization of a C-Type Lectin Gene from *Litopenaeus vannamei* That Is Associated with ER-Stress Response. *Fish Shellfish. Immunol.* **2019**, *93*, 977–985. [CrossRef]
56. Han, S.; Liu, Y.; Zhou, Z.; He, S.; Cao, Y.; Shi, P.; Yao, B.; Ringø, E. Analysis of Bacterial Diversity in the Intestine of Grass Carp (*Ctenopharyngodon idellus*) Based on 16S rDNA Gene Sequences. *Aquac. Res.* **2010**, *42*, 47–56. [CrossRef]
57. Choct, M. Managing Gut Health through Nutrition. *Br. Poult. Sci.* **2009**, *50*, 9–15. [CrossRef]
58. Miao, S.; Wan, W.; Hu, J.; Chang, E.; Zhou, Z.; Zhou, Y.; Sun, L. Dietary Arachidonic Acid Affects the Innate Immunity, Antioxidant Capacities, Intestinal Health and Microbiota in Chinese Mitten Crab (*Eriocheir sinensis*). *Aquaculture* **2022**, *548*, 737635. [CrossRef]
59. Landsman, A.; St-Pierre, B.; Rosales-Leija, M.; Brown, M.; Gibbons, W. Impact of Aquaculture Practices on Intestinal Bacterial Profiles of Pacific Whiteleg Shrimp *Litopenaeus vannamei*. *Microorganisms* **2019**, *7*, 93. [CrossRef]

60. Zhou, L.; Chen, C.; Xie, J.; Xu, C.; Zhao, Q.; Qin, J.G.; Chen, L.; Li, E. Intestinal Bacterial Signatures of the "Cotton Shrimp-like" Disease Explain the Change of Growth Performance and Immune Responses in Pacific White Shrimp (*Litopenaeus vannamei*). *Fish Shellfish. Immunol.* **2019**, *92*, 629–636. [CrossRef]
61. Kang, C.; Wang, B.; Kaliannan, K.; Wang, X.; Lang, H.; Hui, S.; Huang, L.; Zhang, Y.; Zhou, M.; Chen, M. Gut Microbiota Mediates the Protective Effects of Dietary Capsaicin against Chronic Low-Grade Inflammation and Associated Obesity Induced by High-Fat Diet. *MBio* **2017**, *8*, e00470-17. [CrossRef] [PubMed]
62. Li, X.; Liu, L.; Cao, Z.; Li, W.; Li, H.; Lu, C.; Yang, X.; Liu, Y. Gut Microbiota as an "Invisible Organ" That Modulates the Function of Drugs. *Biomed. Pharmacother.* **2020**, *121*, 109653. [CrossRef] [PubMed]
63. Koyama, Y.; Brenner, D.A. Liver Inflammation and Fibrosis. *J. Clin. Investig.* **2017**, *127*, 55–64. [CrossRef]
64. Wang, Y.; Zhang, G.; Wang, H.; Cheng, Y.; Liu, H.; Jiang, Z.; Li, P.; Wang, Y. Effects of Different Dissolved Organic Matter on Microbial Communities and Arsenic Mobilization in Aquifers. *J. Hazard. Mater.* **2021**, *411*, 125146. [CrossRef] [PubMed]
65. Orino, K.; Lehman, L.; Tsuji, Y.; Ayaki, H.; Torti, S.V.; Torti, F.M. Ferritin and the Response to Oxidative Stress. *Biochem. J.* **2001**, *357*, 241–247. [CrossRef]
66. Torti, F.M.; Torti, S.V. Regulation of Ferritin Genes and Protein. *Blood J. Am. Soc. Hematol.* **2002**, *99*, 3505–3516. [CrossRef]
67. Pongsomboon, S.; Tang, S.; Boonda, S.; Aoki, T.; Hirono, I.; Yasuike, M.; Tassanakajon, A. Differentially Expressed Genes in *Penaeus monodon* Hemocytes Following Infection with Yellow Head Virus. *BMB Rep.* **2008**, *41*, 670–677. [CrossRef] [PubMed]
68. Chen, G.; Zhang, C.; Wang, Y.; Guo, C.; Sang, F.; Wang, C. Identification and Characterization of a Ferritin Gene Involved in the Immune Defense Response of Scallop *Chlamys farreri*. *Fish Shellfish. Immunol.* **2016**, *55*, 1–9. [CrossRef] [PubMed]
69. Bäckhed, F.; Ding, H.; Wang, T.; Hooper, L.V.; Gou, Y.K.; Nagy, A.; Semenkovich, C.F.; Gordon, J.I. The Gut Microbiota as an Environmental Factor That Regulates Fat Storage. *Proc. Natl. Acad. Sci. USA* **2004**, *101*, 15718–15723. [CrossRef]
70. Deng, Y.; Jiang, Y.-H.; Yang, Y.; He, Z.; Luo, F.; Zhou, J. Molecular Ecological Network Analyses. *BMC Bioinform.* **2012**, *13*, 113. [CrossRef]

antioxidants

MDPI

Article

Gender-Specific Metabolic Responses of *Crassostrea hongkongensis* to Infection with *Vibrio harveyi* and Lipopolysaccharide

Lijuan Ma [1,2], Jie Lu [1,*], Tuo Yao [1], Lingtong Ye [3] and Jiangyong Wang [4,*]

[1] Key Laboratory of South China Sea Fishery Resources Exploitation & Utilization, Ministry of Agriculture, South China Sea Fisheries Research Institute, Chinese Academy of Fishery Sciences, Guangzhou 510300, China; 82101202453@caas.cn (L.M.); yaotuo@scsfri.ac.cn (T.Y.)
[2] Chinese Academy of Agricultural Sciences, Beijing 100081, China
[3] Key Laboratory of Aquatic Product Processing, Ministry of Agriculture and Rural Affairs, South China Sea Fisheries Research Institute, Chinese Academy of Fishery Sciences, Guangzhou 510300, China; ltye@scsfri.ac.cn
[4] School of Life Science, Huizhou University, Huizhou 516007, China
* Correspondence: lujie@scsfri.ac.cn (J.L.); wjy104@hzu.edu.cn (J.W.)

Abstract: Gender differences in the hemocyte immune response of Hong Kong oyster *Crassostrea hongkongensis* to *Vibrio harveyi* and lipopolysaccharide (LPS) infection exist. To determine if a gender difference also exists, we use a ^{1}H NMR-based metabolomics method to investigate responses in *C. hongkongensis* hepatopancreas tissues to *V. harveyi* and LPS infection. Both infections induced pronounced gender- and immune-specific metabolic responses in hepatopancreas tissues. Responses are mainly presented in changes in substances involved in energy metabolism (decreased glucose, ATP, and AMP in males and increased ATP and AMP in LPS-infected females), oxidative stress (decreased glutathione in males and decreased tryptophan and phenylalanine and increased choline and proline in LPS-infected females), tricarboxylic acid (TCA) cycle (decreased α-ketoglutarate acid and increased fumarate in LPS-infected males, and decreased fumarate in LPS-infected females), and osmotic regulation (decreased trigonelline and increased taurine in *V. harveyi*-infected males and decreased betaine in *V. harveyi*-infected females). Results suggest that post-spawning-phase male oysters have a more significant energy metabolic response and greater ability to cope with oxidative stress than female oysters. We propose that the impact of oyster gender should be taken into consideration in the aftermath of oyster farming or oyster disease in natural seas.

Keywords: *Crassostrea hongkongensis*; metabolomics; hepatopancreas; gender-based difference

Citation: Ma, L.; Lu, J.; Yao, T.; Ye, L.; Wang, J. Gender-Specific Metabolic Responses of *Crassostrea hongkongensis* to Infection with *Vibrio harveyi* and Lipopolysaccharide. *Antioxidants* **2022**, *11*, 1178. https://doi.org/10.3390/antiox11061178

Academic Editor: Erchao Li

Received: 11 May 2022
Accepted: 13 June 2022
Published: 15 June 2022

1. Introduction

Crassostrea hongkongensis is the most important, commercially valuable cultured oyster species along the South China coast [1,2]. In recent years, the commercial production of this species has been seriously affected by mass mortality during the boreal spring, possibly caused by pathogen infection and environmental stress [3,4]. Therefore, understanding the mechanisms by which oysters respond to different stresses will improve disease control in farmed populations. The genes *ChBeclin-1* [5], *ChUb*$_{L40}$ [6], *ChAkt1* [7], *Ch*DFFA [8], and p38 MAPKs [9] play important roles in the immune defense of *C. hongkongensis* against bacterial challenge. The assembled whole genome sequences of *C. hongkongensis* have recently been released [1]. Several immune-, reproduction-, and stress-related genes have been identified [10], providing the resources and opportunity of in-depth studies at the molecular level. Moreover, metabolomics has revealed that exposure to copper can disturb osmotic regulation and energy metabolism [11]. Proteomic methods to analyze differentially expressed proteins in oyster gills exposed to long-term heavy metal pollution have also

revealed most stress and immune-reactive proteins, such as heat shock proteins (HSP) and enzymes, to be significantly down-regulated [12].

Development of metabolomic techniques in aquaculture has led to more thorough investigations of shellfish immunology. Physiological and stress responses of bivalves have now been characterized using a variety of metabolomics platforms [13]. Nuclear magnetic resonance (NMR)-based metabolomics is a powerful high-throughput technique that simultaneously detects endogenous compounds representative of a biological state. The low incremental cost and short data collection time of these analyses enable robust experimental design characterized by high reproducibility and ease of sample preparation and measurement proceedings, and also allows for quantitative analysis and in vivo metabolomics studies [14–16]. NMR-based metabolomics has been used to express bivalve responses to external disturbance, such as from pathogenic bacteria [17], estrogenic mixtures [18], hepatotoxic microcystins [19], ammonia nitrogen exposure [20], and high ρCO_2 levels [21]. Proton (^{1}H) NMR-based metabolomics has identified osmotic regulation and energy metabolism in *C. hongkongensis* to be disturbed following exposure to Cu, Zn, Pb, and other metals [22,23]. These diverse applications in bivalves suggest that NMR-based metabolomics is a powerful tool for assessing the metabolic response mechanism of stressed bivalves in general, and *C. hongkongensis* in particular.

Differences in the immunological responses of *C. hongkongensis* males and females have seldom been taken into consideration [7,9]. *Vibrio harveyi* is a pathogenic bacterium isolated in our laboratory, which can cause severe vibriosis in *C. hongkongensis*. Lipopolysaccharide (LPS) is a cell wall component of Gram-negative bacteria, and injection of LPS triggers a host immune response [24]. We previously reported gender-related differences in immune responses to LPS and *V. harveyi* in hemocyte of *C. hongkongensis* [25]. Herein we use ^{1}H NMR-based metabolomics techniques to examine metabolic changes in hepatopancreas tissues of female and male *C. hongkongensis* following infection with *V. harveyi* and LPS. Our objectives are to identify gender-specific metabolic responses in this oyster following infection and to identify potential new biomarkers for evaluating its health.

2. Materials and Methods

2.1. Animals and Experimental Design

Healthy post-spawning *C. hongkongensis* (shell length 11.23 ± 0.06 cm) were obtained from a commercial farm in Taishan, Jiangmen, Guangdong Province, China. Oysters were acclimated for 7 days in aerated sand-filtered seawater at 25 °C, salinity 20 ± 1, and pH 8.1 ± 0.1, and regularly fed the algae *Isochrysis galbana* and *Chaetoceros muelleri* at a ration of 2% of tissue per dry twice daily, namely at 08:00 and 16:00. A photoperiod of 12 h light/12 h dark was applied. Low salinity water is prepared by diluting seawater with tap water and used after 2 days of aeration. No mortality occurred during the period of acclimation. After acclimation, oysters were randomly divided into 3 treatments (control, *V. harveyi*, LPS), each with 3 replicates, each replicate containing 20 oysters, in glass aquaria (48 × 28 × 21 cm) with 30 L filtered seawater, in a completely randomized design.

2.2. Challenge Experiment

The bacterium *V. harveyi* was cultivated in liquid 2216E broth at 28 °C for 14 h and centrifuged at 5000× *g* for 10 min. This bacterium was washed twice in sterile seawater before being suspended in sterile seawater at a final concentration of approximately 1 × 107 CFU/mL. LPS (from *Escherichia coli* O111: B4, Sigma-Aldrich, St. Louis, MO, USA) was dissolved in sterile seawater to a concentration of 0.5 mg/mL [25]. Control group oysters were injected with 50 µL sterile aquaculture seawater and the experimental treatment oysters were injected with either 50 µL *V. harveyi* suspension or LPS solution. After 48 h exposure, oyster gender was determined and the oyster hepatopancreas was extracted, snap-frozen in liquid nitrogen, and stored at −80 °C for subsequent metabolite extraction. Gender was determined by light-microscopic examination of mature gonad tissue: large eggs indicated female and motile sperm male.

2.3. Metabolite Extraction

Using a water/methanol method, polar metabolites were extracted from hepatopancreas tissues. In brief, 100 mg of hepatopancreas tissue and 1 mL of methanol and water (2:1) were added into a 2 mL centrifuge tube. The mixture was crushed by shaking in a sample freezing grinding machine (Luka, Guangzhou), followed by centrifugation (10 min, 12,000× *g*, 4 °C) and dried in a vacuum centrifugal concentrator. Tissue extracts were resuspended in 600 µL of phosphate buffer in D_2O, then vortexed and centrifuged (5 min, 3000× *g*, 4 °C). The supernatant (500 µL) was transferred to a 5 mm NMR tube and analyzed by NMR [26]. One-dimensional ^{1}H NMR spectra of all samples were obtained at 298K using the 1D NOESYGPPRLD pulse on the Bruker Avance III 600 MHz spectrometer, with 128 scans and a 4 s acquisition time.

2.4. Spectral Processing and Statistical Analyses

NMRProcFlow 1.3.10 (INRA UMR 1332 BFP, Bordeaux Metabolomics Facility, Villenave d'Ornon, France) [27] was used to perform PPM calibration, baseline correction, alignment, spectra bucketing, and data normalization of raw ^{1}H NMR spectra. The DSS internal standard was taken as the chemical shift reference peak (DSS = 0.0 ppm), and the spectral images within 0.66–10 ppm were integrated to remove the chemical shift region where the water peak was located (4.67–4.86 ppm). PQN (Probabilistic Quotient Normalization) was selected for normalization. NMR spectra were preprocessed using adaptive intelligent bucketing, with buckets with a signal-to-noise ratio > 3 chosen for further investigation. The end result is a 599-bucket matrix. To increase the weight of low-intensity peaks, all NMR spectra were logarithmically transformed before multivariate statistical analysis.

SIMCA 14.1 software (Umetrics, Umeå, Sweden) was used to analyze NMR spectrum datasets. Intrinsic metabolic trends and differential metabolites of *V. harveyi* or LPS exposure were determined using principal component analysis, partial least squares discriminant analysis (PLS-DA), and orthogonal partial least squares discriminant analysis (OPLS-DA). In addition, 200 permutation tests and cross-validation analysis of variance (CV-ANOVA) were used to confirm the significance of the OPLS-DA model. Differential buckets with variable importance in the projection > 1.0 determined by OPLS-DA, and p-values < 0.05 determined by two-tailed Student's t-tests were identified. Chenomx NMR Suite 8.6 professional software (Chenomx Inc., Edmonton, AB, Canada) was used to analyze the chemical shift of buckets to complete identification of main metabolites.

2.5. Systematic Statistical Metabolic Correlation and Network Analysis

The transformations and sequential chemical reactions of substrates and products involved in diverse catabolic and anabolic processes are described by metabolic pathways [28]. We screened out different metabolites and performed metabolic pathway analysis from KEGG database analysis by MetaboAnalyst 5.0 website [29], and to all the identification of the metabolites of clustering. We used the R software package to identify the KEGG pathways of enriched metabolites in different treatments and to draw correlation heat maps between metabolites and immune-related factors.

3. Results

3.1. Hepatopancreas ^{1}H NMR Spectra

NMR spectra identified 49 different metabolites (Figure 1), including energy metabolism-related metabolites (e.g., glucose, glycogen, ATP, AMP), amino acids (e.g., tryptophan, arginine, phenylalanine, proline, tyrosine) and organic osmolytes (e.g., betaine, taurine, trigonelline). The hepatopancreas ^{1}H NMR profile was dominated largely by betaine and taurine, as previously reported for oysters [30,31].

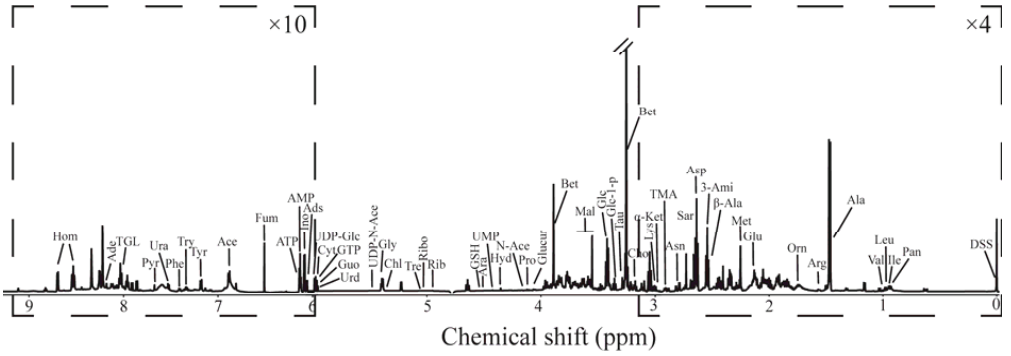

Figure 1. ^{1}H NMR spectra of *Crassostrea hongkongensis* hepatopancreas extract under infected (control) condition, with spectral regions 0.0–4.8 ppm amplified by a factor of 4, and 4.8–9.9 ppm by 10. Key: Ace, acetate; Ade, adenine; Ads, adenosine; Ala, alanine; AMP, adenosine monophosphate; Ara, arabinose; Arg, arginine; Asn, asparagine; Asp, aspartate; ATP, adenosine triphosphate; Bet, betaine; Chl, chlorogenate; Cho, choline; Cyt, cytosine; DSS, dextran sulfate sodium; Fum, fumarate; Glc, glucose; Glc-1-p, glucose-1-phosphate; Glu, glutamate; Glucur, glucuronate; Gly, glycine; GSH, glutathione; GTP, guanosine triphosphate; Guo, guanosine; Hom, homarine; Hyd, hydroxyacetone; Ile, isoleucine; Ino, inosine; Leu, leucine; Lys, lysine; Mal, malonate; Met, methionine; N-Ace, N-acetylornithine; Orn, ornithine; Pan, pantothenate; Phe, phenylalanine; Pro, proline; Pyr, pyridoxine; Rib, ribose; Ribo, riboflavin; Sar, sarcosine; Tau, taurine; TMA, trimethylamine; TGL, trigonelline; Tre, trehalose; Try, tryptophan; Tyr, tyrosine; UDP-Glc, UDP-glucose; UDP-N-Ace, UDP-N-acetylglucosamine; UMP, uridine monophosphate; Ura, uracil; Urd, uridine; Val, valine; 3-Ami, 3-aminoisobutyrate; α-Ket, α-ketoglutarate acid; β-Ala, β-alanine.

3.2. Multivariate Data Analyses

To identify metabolic differences between the control and two treatments, and between males and females, PLS-DA analysis was first performed. Treatments were well separated (Figure 2A). To analyze metabolic differences between gender, OPLS-DA was performed on NMR spectral data of males and females from all groups; a clear separation between male and female groups with reliable Q^2 values, both with p values < 0.003 calculated using CV-ANOVA (Figure 2B). We conducted 200 iterations of permutation tests to assess if models were over-fitted to demonstrate that the OPLS-DA model was reliable. Inherent biological and metabolic differences appear to exist between genders.

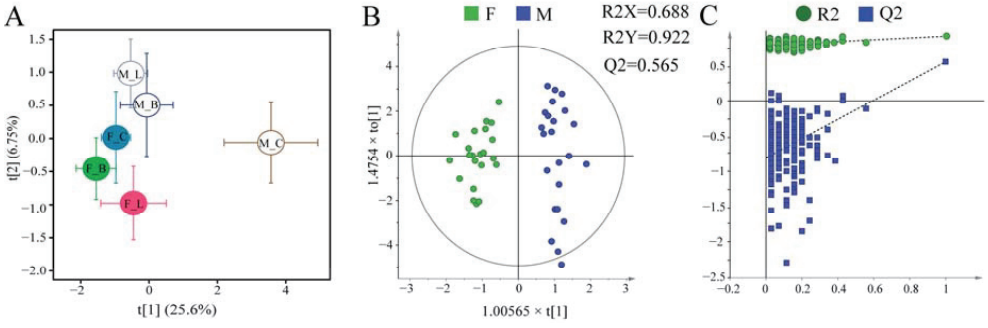

Figure 2. Multivariate statistical analysis plot based on ^{1}H NMR spectra of *C. hongkongensis* hepatopancreas tissues. (**A**) PLS-DA plots for all treatments; (**B**) OPLS-DA score plots of male and female oysters (R^2X = 68.8%, R^2Y = 0.927, Q^2 = 0.565, p < 0.003); (**C**) permutation test for the model in (**B**). Groups: F, female; M, male; C, control; B, *Vibrio harveyi* infection; L, LPS infection.

OPLS-DA score plots (left panels in Figure 3) show good separation between infected treatments and the corresponding control group for males and females. As shown in volcano maps (right panels in Figure 3) and heatmaps (Figure S1), compared with the control group, 19 metabolites were down-regulated and 1 metabolite was up-regulated in *V. harveyi*-infected females. In LPS-infected females, 14 metabolites were down-regulated and 20 metabolites were up-regulated. In *V. harveyi*-infected males, 12 metabolites were down-regulated and 16 metabolites were up-regulated, while in LPS-infected males, 15 metabolites were down-regulated and 16 metabolites were up-regulated. Table S1 provide details of these metabolites.

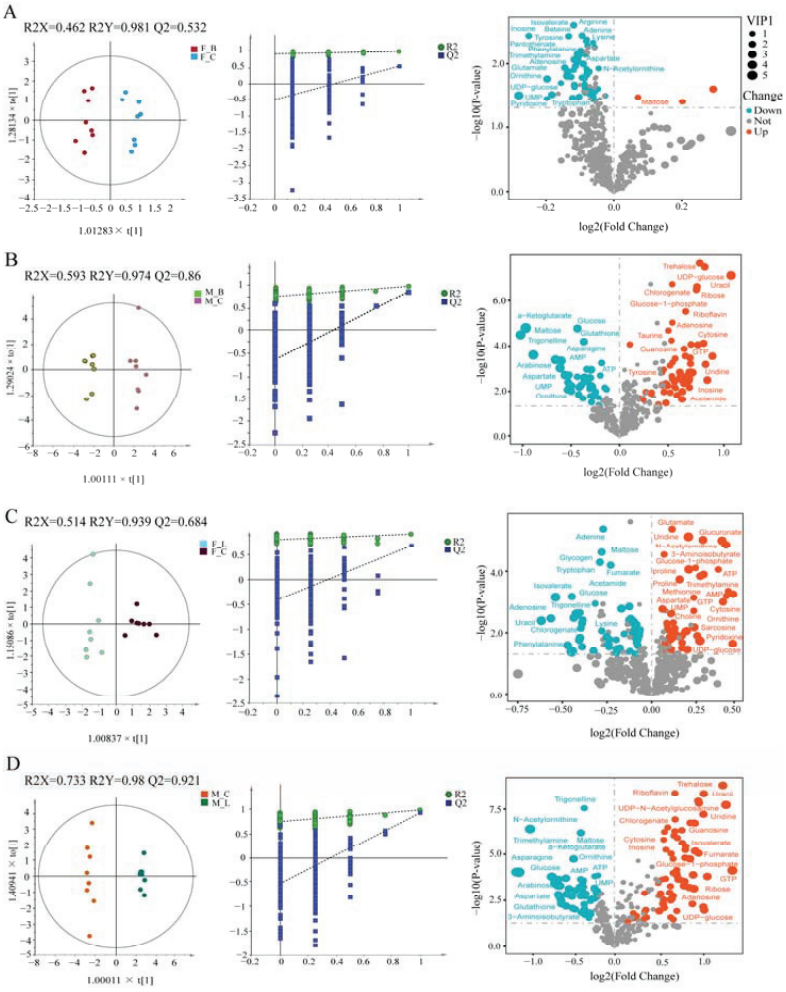

Figure 3. OPLS-DA score plots of ^{1}H NMR spectra of *C. hongkongensis* hepatopancreas extract from different paired groups (left panel) and the corresponding model permutation test chart (middle panel) and its corresponding volcano map (right panel). (**A**) F_B vs F_C. (**B**) M_B vs M_C. (**C**) F_L vs F_C. (**D**) M_C vs M_L. Groups: F, female; M, male; C, control; B, *V. harveyi* infection; L, LPS infection.

To further analyze changes in differential metabolites in *C. hongkongensis* in different treatments, an Upset diagram was prepared using R language (Figure 4). Compared with control group females, different metabolites increased in female oysters in the two treatments, but the *V. harveyi* treatment had 1 specific increased metabolite, and the LPS

group had 15 specific increased metabolites. However, six metabolites were down-regulated in both treatments, while eight metabolites were up-regulated in the *V. harveyi* treatment and five metabolites were down-regulated in the LPS treatment. Compared with the control group male oysters, in the *V. harveyi* treatment eight metabolites were commonly elevated in male oysters, with three particularly elevated, and three were particularly elevated in LPS treatment male oysters. Six metabolites were commonly down-regulated in both treatments, while the *V. harveyi* treatment had no particularly decreased metabolite, and the LPS treatment had one. These metabolites, which are only up- or down-regulated in females or males, suggest that oyster responses to either infection is gender specific. Additionally, different infections in the same gender oysters can lead to different metabolite changes, indicating that oysters are immune-specific for different stresses.

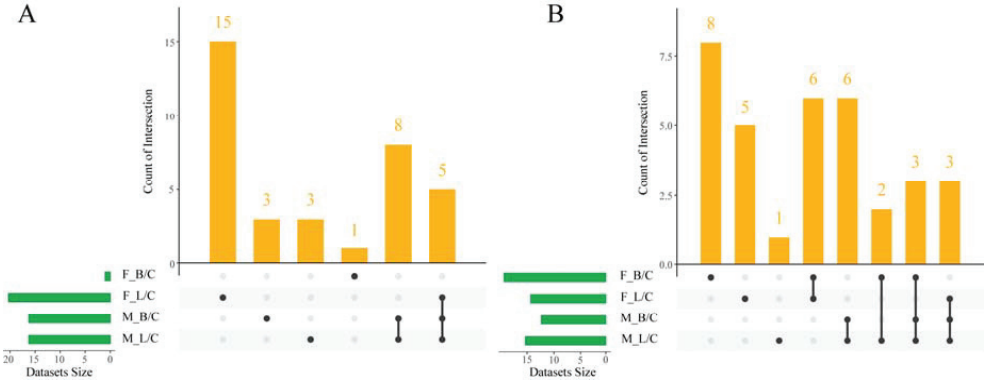

Figure 4. Upset diagram of *C. hongkongensis* hepatopancreas extracts from different paired groups. Increased metabolites (**A**), decreased metabolites (**B**). Groups: F, female; M, male; C, control; B, *V. harveyi* infection; L, LPS infection.

KEGG enrichment metabolic pathways prepared by R language clearly differ between male and female oysters (Figure 5). For example, differential metabolites in females occurred mainly in D-glutamine and D-glutamate metabolism, aminoacyl-tRNA biosynthesis and phenylalanine, and tyrosine and tryptophan biosynthesis, while males do not have these enrichment pathways. Additionally, metabolic pathways enriched by either infection in females also differ. For example, differential metabolites in oysters infected with *V. harveyi* were enriched with phenylalanine, tyrosine, and tryptophan biosynthesis and arginine and proline metabolism, while those infected with LPS were enriched with pentose and glucuronate interconversions and galactose metabolism. Based on KEGG pathway analysis, we summarize the different metabolic pathways of oyster infection in hepatopancreas tissues, mainly involving arginine biosynthesis, energy metabolism, glutathione metabolism, and other metabolic pathways (Figure 6).

A correlation network diagram (Figure 7) was used to represent Spearman's correlation coefficients between hemocyte immunological parameters and different metabolites. Changes in immunological parameters of granulocytes, including ROS and calcium levels, lysosome and mitochondrial masses, and early apoptotic, NO, phagocytic, and late apoptotic or necrotic ratios of total hemocytes in *C. hongkongensis* during immune stress, have been reported earlier [25]. Significant correlations between parameters may indicate an equilibrium or that immune stimulation in oysters simultaneously modulates parameters. Correlation analysis reveals glucose, AMP, and ATP to be positively correlated, as are proline and choline, and for phenylalanine and tyrosine to be positively correlated with ROS.

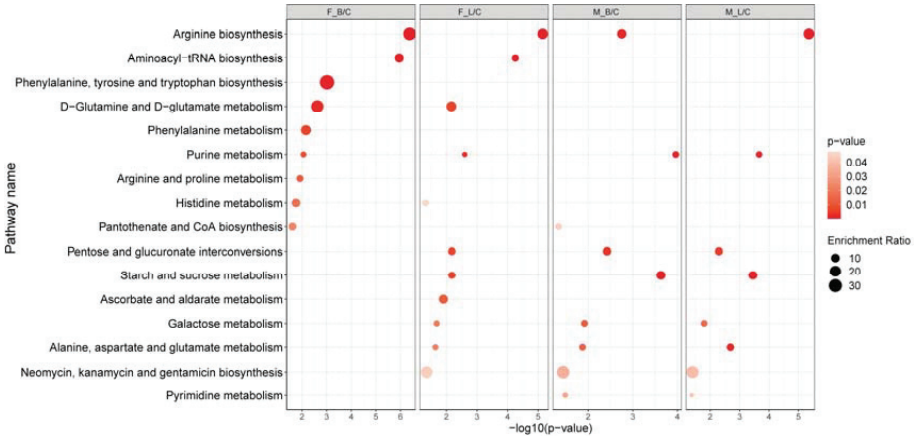

Figure 5. KEGG function analysis based on the differential metabolites from different paired groups. Pathways with p values < 0.05 are shown. Groups: F, female; M, male; C, control; B, *V. harveyi* infection; L, LPS infection.

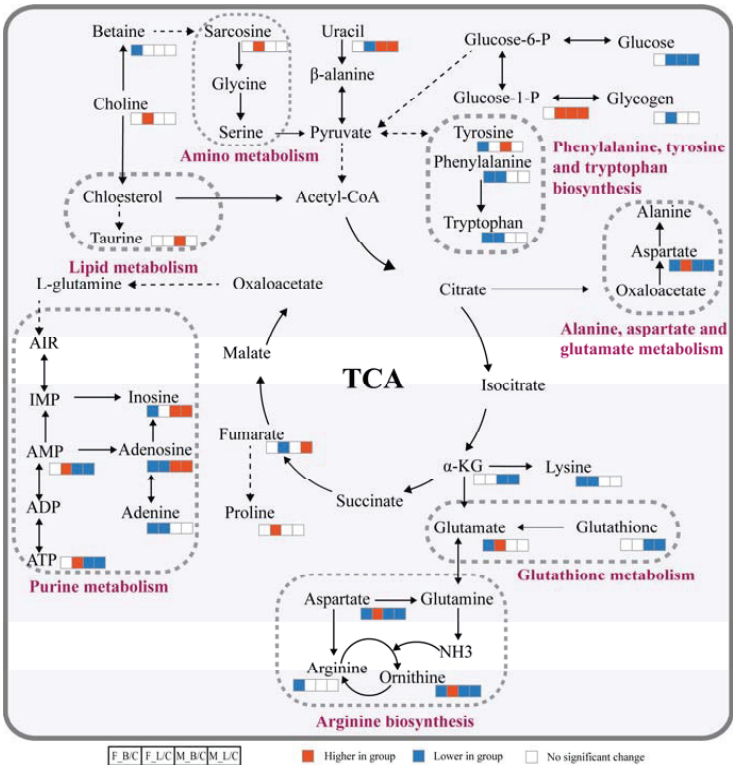

Figure 6. Molecular mechanism of the hepatopancreas response in male and female *C. hongkongensis* to *V. harveyi* and LPS infection according to KEGG. Blue (down-regulated), red (up-regulated), and white (unchanged) boxes reveal changes in levels of differential metabolites compared to controls; ellipses with different background colors indicate different interconnecting pathways. Groups: F, female; M, male; C, control; B, *V. harveyi* infection; L, LPS infection.

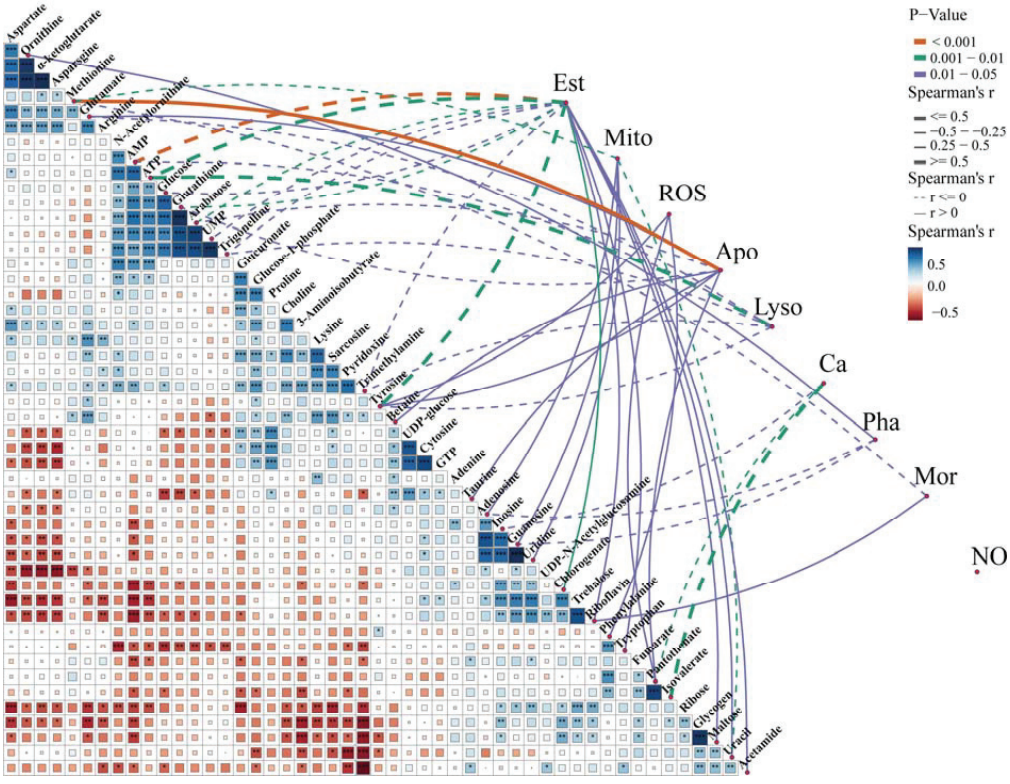

Figure 7. Differential metabolites and immune factors correlated by Spearman's correlation analysis. A color gradient denoting Spearman's correlation coefficient is shown for pairwise comparisons of metabolites. Spearman's correlation coefficients are depicted using line size and line color denotes statistical significance. Lines: dashed, positive correlation; solid, negative connection. Apo, apoptotic ratio; Ca, calcium content; Est, esterase activity; Lyso, lysosome mass; Mito, mitochondrial mass; Mor, mortality; NO, nitric oxide level; Pha, phagocytic ratio; ROS, reactive oxygen species level. *** $p < 0.001$, ** $p < 0.01$, * $p < 0.05$.

4. Discussion

Gender-specific differences in physiological response mechanisms are reported for several aquatic invertebrates when exposed to environmental stress. Using NMR-based metabolomics, gender differences have been reported for the mussel *Mytilus edulis* exposed to lower pH, higher temperature and pathogens in seawater [32], and for metabolic responses in gonads of *Perna viridis* to triazophos [33]. We previously reported gender-specific immunological responses in oyster hemocytes following exposure to *V. harveyi* and LPS. Herein, through analysis of OPLS-DA score plots (Figure 2B), we report gender differences in oysters in metabolic responses to two infections.

LPS and *V. harveyi* infection can produce ROS in female oysters [25]. Cell damage occurs when the level of ROS exceeds a cell's ability to scavenge them, eventually leading to DNA oxidative damage and abnormal protein expression, inducing inflammation and oxidative stress. We herein report proline and choline to be positively correlated, and to significantly increase after LPS infection in females. Antioxidant enzyme activity and antioxidant content are correlated with proline, and by regulating proline metabolism, damage caused by stress can be alleviated [34]. Therefore, we believe that the high expression of proline in females relieves oxidative stress induced by LPS, protecting the oysters, and that

the manner of adjustment is gender specific. As components of phospholipids, choline and phosphocholine play important roles in maintaining cell membrane integrity [35]. Therefore, an increase in female oyster hepatopancreas-tissue choline levels following LPS infection indicates that the hepatopancreas membrane is damaged by excessive ROS. In contrast, these metabolites did not change in male oysters after infection, suggesting that male oysters are more capable of coping with *V. harveyi* and LPS stress and maintaining a relatively normal metabolism. Glutathione is an important metabolite that maintains cellular redox balance [36,37] that can be used to enhance antioxidant enzyme activity and antioxidative stress capacity. Glutathione plays a vital role in cellular proliferation, maintaining intracellular redox homeostasis and protecting against oxidative damage [38,39]. In male oysters, glutathione levels decreased with *V. harveyi* and LPS infection, indicating that they mobilized more glutathione to regulate ROS levels after infection, providing further evidence that males are more capable of coping with oxidative stress.

We report phenylalanine and tryptophan levels in female oysters to decrease in both infections, and tyrosine levels following *V. harveyi* infection in female oysters to be down-regulated and in males up-regulated. Oysters are infected, with changes in aromatic amino acids being gender specific. Additionally, we report phenylalanine and tyrosine to be positively correlated with ROS. Because phenylalanine inhibits ROS-induced oxidative damage in gills of grass carp [40], we speculate that decreased phenylalanine reduces the oxidative damage of high ROS levels in female oysters, further supporting the notion that males have a stronger defense mechanism against oxidative stress than females.

In male oysters, metabolites involved in energy metabolism, glucose-1-phosphate, were up-regulated, and glucose, ATP, and AMP were down-regulated in both infections compared with control treatment levels. A decrease in glucose means that male oysters require more energy to resist infection, which will accelerate the hydrolysis of glucose within the body, and generate ATP through the glycolysis pathway and TCA cycle. The process of ATP generation is consistent with this research [41]. Coincidentally, correlation analysis revealed glucose, AMP, and ATP levels to be positively correlated. In female oysters, an increase in ATP, glucose-1-phosphate, and AMP and a decrease in glucose and glycogen occurred following LPS infection. After LPS infection, down-regulation of glucose and glycogen levels promoted the up-regulation of ATP levels. Because the breakdown of glucose and glycogen produces ATP to provide energy to fight infection, but the ATP produced is insufficient to support resistance to LPS infection, the breakdown of glycogen produces glucose-1-phosphate to provide energy. Because none of these metabolites changed after female oysters were infected with *V. harveyi*, females may use different energy metabolism strategies in response to different infections in a manner similar to how the hepatopancreas of the clam *Ruditapes philippinarum* regulates *V. anguillarum* and *V. splendidus* infections using different energy metabolism mechanisms [26]. Collectively, for the same infection conditions, male and female oysters have different energy metabolism mechanisms, indicating that their post-infection energy metabolism mechanism is gender specific. When challenged with *V. harveyi*, male and female *Mytilus galloprovincialis* mussels also induced different energy metabolic responses [42]. For both *V. harveyi* and LPS infections, metabolites involved in energy metabolism such as glucose, ATP, glucose-1-phosphate, and AMP in male oysters changed significantly, while metabolite glucose, ATP, glucose-1-phosphate, AMP, and glycogen in females only changed after LPS infection. This indicates that gender- and immune-specific energy metabolic responses were induced in *C. hongkongensis* and suggests that male oysters have a high antioxidant capacity because most of their energy is used to fight ROS caused by infection.

The TCA cycle is the primary catabolic pathway for energy production. An increase in intermediates in the TCA cycle has been reported in marine bivalves exposed to pathogens [13]. Conversely, the disruption of the TCA cycle shifts energy pathways from aerobic to anaerobic metabolism [43]. For invertebrates, anaerobic metabolism produces high levels of alanine and succinic acid as end products [44]. We found no increase in either succinic acid or alanine in oysters exposed to *V. harveyi* or LPS, suggesting that a

shift from aerobic to anaerobic metabolism did not occur. However, fumarate, an intermediate substance of the TCA cycle, decreased in LPS-infected females and increased in *V. harveyi*-infected males, and levels of α-ketoglutarate acid decreased in males in both infections. This indicates that the TCA cycle pathway of oysters in both infections is also gender specific.

Organic osmotic substances (including betaine, trigonelline, and taurine), major components of water-soluble metabolites that often play crucial roles in osmotic regulation of marine mollusks are affected by external influences [45]. Amino acids are involved in marine mollusk osmotic regulation [46]. In male oysters, taurine levels were up-regulated in the *V. harveyi* treatment, while levels of trigonelline and aspartate decreased in both infection treatments. In females, betaine and arginine levels were down-regulated in both infection treatments. In oysters, the depletion of betaine and trigonelline indicates that *V. harveyi* and LPS had disturbed osmotic regulation, as did a decrease in most amino acid levels. Increased taurine may compensate for lost betaine and trigonelline. A similar metabolic response occurred when *V. harveyi* attacked the hepatopancreas of female *M. galloprovincialis* mussels [42]. Accordingly, gender-specific responses to both infections in the oyster hepatopancreas are confirmed by differences in changes in their organic osmotic substances and amino acids.

5. Conclusions

The metabolic response of the *C. hongkongensis* hepatopancreas to *V. harveyi* and LPS infection was examined using ^{1}H NMR-based metabolomic methods. We conclude that the infection of *V. harveyi* and LPS caused gender- and immune-specific effects on oxidative stress, energy metabolism, the TCA cycle, and in osmotic regulation. The antioxidant capacity of male oysters was stronger than that of females. Overall, in terms of energy metabolism, ATP, AMP, and glucose decreased in males, while ATP and AMP increased in LPS-infected females. In terms of oxidative stress, glutathione decreased in males, and phenylalanine and tryptophan decreased in females, while proline and choline also increased in LPS-infected females. In terms of the TCA cycle, α-ketoglutarate acid decreased in males, and fumarate decreased in LPS-infected females and increased in LPS-infected males. In terms of osmotic regulation, trigonelline decreased in males, taurine increased in *V. harveyi*-infected males, and betaine decreased n *V. harveyi*-infected females. These findings help explain the response mechanisms of different oyster genders to immune stimulation and provide a reference for stress research in marine animals.

Supplementary Materials: The following supporting information can be downloaded at: https://www.mdpi.com/article/10.3390/antiox11061178/s1, Figure S1: Heat map analysis of changes in metabolites of hepatopancreas tissues in male and female oysters under *Vibrio harveyi* and LPS infection compared to control groups; Table S1: Summary of metabolic changes of oyster hepatopancreas caused by infection with *Vibrio harveyi* or LPS in different sexes.

Author Contributions: Formal analysis, writing—original draft and writing—review and editing, L.M.; formal analysis, experimental design, ideas and writing—review and editing, J.L.; experiment and obtained data, T.Y.; investigation and writing—review and editing, L.Y.; ideas, resources and writing—review and editing, J.W. All authors have read and agreed to the published version of the manuscript.

Funding: This research was funded by the China Agriculture Research System of MOF and MARA, Central Public-interest Scientific Institution Basal Research Fund, South China Sea Fisheries Research Institute, CAFS (NO.2022XK02, 2017YB22, 2020TD42, and 2021SD05), Guangdong Basic and Applied Basic Research Foundation (2021A1515110132), Fund of Key Laboratory of Aquatic Product Processing, Ministry of Agriculture and Rural Affairs, China (NYJG202106), funded by Engineering Research Center for Tropical and Subtropical Aquatic Ecological Engineering, Ministry of Education, Jinan University, China (No. 2021A0301), the Shellfish and Large Algae Industry Innovation Team Project of Guangdong Province (2021KJ146), and the Professional and Doctoral Scientific Research Foundation of Huizhou University.

Institutional Review Board Statement: The animal study protocol was approved by the Committee on Laboratory Animal Welfare and Ethics of South China Sea Fisheries Research Institute, Chinese Academy of Fishery Sciences (No. nhdf2022-05).

Informed Consent Statement: Not applicable.

Data Availability Statement: All data underlying this article are available in the main publication and in its Supplementary Material online.

Conflicts of Interest: The authors declared no conflict of interest.

References

1. Peng, J.X.; Li, Q.Z.; Xu, L.; Wei, P.Y.; He, P.P.; Zhang, X.Z.; Zhang, L.; Guan, J.L.; Zhang, X.J.; Lin, Y.; et al. Chromosome-level analysis of the *Crassostrea hongkongensis* genome reveals extensive duplication of immune-related genes in bivalves. *Mol. Ecol. Resour.* **2020**, *20*, 980–994. [CrossRef] [PubMed]
2. Zhang, Y.H.; Li, J.; Qin, Y.P.; Zhou, Y.E.; Zhang, Y.; Yu, Z.N. A comparative study of the survival, growth and gonad development of the diploid and triploid Hong Kong oyster, *Crassostrea hongkongensis* (Lam & Morton 2003). *Aquac. Res.* **2017**, *48*, 2453–2462. [CrossRef]
3. Qin, Y.P.; Li, X.Y.; Liao, Q.L.; Li, J.; Ma, H.T.; Mo, R.G.; Zhang, Y.H.; Yu, Z.N. Comparative study on the growth, survival, gonad development and trait segregation of F2 hybrids and their grandparent species (*Crassostrea ariakensis* and *C. hongkongensis*). *Aquaculture* **2021**, *541*, 736757. [CrossRef]
4. Yang, Y.; Qin, Y.P.; Zhang, A.J.; Zhou, Y.Y.; Li, J.; Liao, Q.L.; Shi, G.P.; Yu, Z.N.; Pan, Y.; Zhang, Y.H. Cloning and characterization of a novel hydrolase gene from Hong Kong oyster *Crassostrea hongkongensis*. *Aquacult. Rep.* **2022**, *23*, 101055. [CrossRef]
5. Zhou, Y.Y.; Liu, K.N.; Li, X.Y.; Qin, Y.P.; Zhang, Y.H.; Zhang, Y.; Xiang, Z.M.; Ma, H.T.; Li, J.; Yu, Z.N. Molluscan Beclin-1 is involved in the innate immune response by regulating the autophagosomes formation in *Crassostrea hongkongensis*. *Aquacult. Rep.* **2020**, *18*, 100541. [CrossRef]
6. Fu, D.K.; Zhang, Y.; Yu, Z.N. Cloning and expression analysis of a ubiquitin gene (Ub_{L40}) in the haemocytes of *Crassostrea hongkongensis* under bacterial challenge. *Chin. J. Oceanol. Limnol.* **2011**, *29*, 80–86. [CrossRef]
7. Wang, F.X.; Xiao, S.; Zhang, Y.; Zhang, Y.H.; Liu, Y.; Yan, Y.; Xiang, Z.M.; Yu, Z.N. *ChAkt1* involvement in orchestrating the immune and heat shock responses in *Crassostrea hongkongensis*: Molecular cloning and functional characterization. *Fish Shellfish Immunol.* **2015**, *47*, 1015–1023. [CrossRef]
8. Xiang, Z.M.; Qu, F.F.; Qi, L.; Ying, T.; Li, J.; Shu, X.; Yu, Z.N. Cloning and characterization of an apoptosis-related DNA fragmentation factor (DFF) from oyster, *Crassostrea hongkongensis*. *Fish Shellfish Immunol.* **2014**, *38*, 119–126. [CrossRef]
9. Qu, F.F.; Xiang, Z.M.; Zhang, Y.; Li, J.; Xiao, S.; Zhang, Y.H.; Mao, F.; Ma, H.T.; Yu, Z.N. A novel p38 MAPK indentified from *Crassostrea hongkongensis* and its involvement in host response to immune challenges. *Mol. Immunol.* **2016**, *79*, 113–124. [CrossRef]
10. Tong, Y.; Zhang, Y.; Huang, J.M.; Xiao, S.; Zhang, Y.H.; Li, J.; Chen, J.H.; Yu, Z.N. Transcriptomics analysis of *Crassostrea hongkongensis* for the discovery of reproduction-related genes. *PLoS ONE* **2015**, *10*, 0134280. [CrossRef]
11. Cao, C.; Wang, W.X. Chronic effects of copper in oysters *Crassostrea hongkonggensis* different exposure regimes as shown by NMR-based metabolomics. *Environ. Toxicol. Chem.* **2017**, *36*, 2428–2435. [CrossRef]
12. Luo, L.Z.; Ke, C.H.; Guo, X.Y.; Shi, B.; Huang, M.Q. Metal accumulation and differentially expressed proteins in gill of oyster (*Crassostrea hongkongensis*) exposed to long-term heavy metal-contaminated estuary. *Fish Shellfish Immunol.* **2014**, *38*, 318–329. [CrossRef] [PubMed]
13. Nguyen, T.V.; Alfaro, A.C. Metabolomics investigation of summer mortality in New Zealand Greenshell (TM) mussels (*Perna canaliculus*). *Fish Shellfish Immunol.* **2020**, *106*, 783–791. [CrossRef]
14. Cappello, T.; Giannetto, A.; Parrino, V.; Marco, G.D.; Mauceri, A.; Maisano, M. Food safety using NMR-based metabolomics: Assessment of the Atlantic bluefin tuna, *Thunnus thynnus*, from the Mediterranean Sea. *Food Chem. Toxicol.* **2018**, *115*, 391–397. [CrossRef] [PubMed]
15. Cappello, T.; Marco, G.D.; Conti, G.O.; Giannetto, A.; Ferrante, M.; Mauceri, A.; Maisano, M. Time-dependent metabolic disorders induced by short-term exposure to polystyrene microplastics in the Mediterranean mussel *Mytilus galloprovincialis*. *Ecotoxicol. Environ. Saf.* **2021**, *209*, 111780. [CrossRef]
16. Zitouni, N.; Cappello, T.; Missawi, O.; Boughattas, I.; Marco, G.D.; Belbekhouche, S.; Mokni, M.; Alphonse, V.; Guerbej, H.; Bousserrhine, N.; et al. Metabolomic disorders unveil hepatotoxicity of environmental microplastics in wild fish *Serranus scriba* (Linnaeus 1758). *Sci. Total Environ.* **2022**, *838*, 155872. [CrossRef]
17. Frizzo, R.; Bortoletto, E.; Riello, T.; Leanza, L.; Schievano, E.; Venier, P.; Mammi, S. NMR metabolite profiles of the bivalve mollusc *Mytilus galloprovincialis* before and after immune stimulation with *Vibrio splendidus*. *Front. Mol. Biosci.* **2021**, *8*, 686770. [CrossRef] [PubMed]
18. Islam, R.; Melvin, S.D.; Yu, R.M.K.; O'Connor, W.A.; Tran, T.K.A.; Andrew-Priestley, M.; Leusch, F.D.L.; MacFarlane, G.R. Exposure to estrogenic mixtures results in tissue-specific alterations to the metabolome of oysters. *Aquat. Toxicol.* **2021**, *231*, 105722. [CrossRef] [PubMed]

19. Yang, W.; Ye, Y.F.; Lu, K.H.; Zheng, Z.M.; Zhu, J.Y. NMR-based metabolomic responses of freshwater gastropod *Bellamya aeruginosa* to MC-producing and non MCproducing *Microcystis aeruginosa*. *J. Oceanol. Limnol.* **2022**, *40*, 260–272. [CrossRef]
20. Lu, J.; Yao, T.; Shi, S.K.; Ye, L.T. Effects of acute ammonia nitrogen exposure on metabolic and immunological responses in the Hong Kong oyster *Crassostrea hongkongensis*. *Ecotoxicol. Environ. Saf.* **2022**, *237*, 113518. [CrossRef]
21. Wei, L.; Wang, Q.; Wu, H.F.; Ji, C.L.; Zhao, J.M. Proteomic and metabolomic responses of Pacific oyster *Crassostrea gigas* to elevated ρCO2 exposure. *J. Proteom.* **2015**, *112*, 83–94. [CrossRef] [PubMed]
22. Cao, C.; Wang, W.X. Bioaccumulation and metabolomics responses in oysters *Crassostrea hongkongensis* impacted by different levels of metal pollution. *Environ. Pollut.* **2016**, *216*, 156–165. [CrossRef] [PubMed]
23. Ji, C.L.; Wang, Q.; Wu, H.F.; Tan, Q.G.; Wang, W.X. A metabolomic investigation of the effects of metal pollution in oysters *Crassostrea hongkongensis*. *Mar. Pollut. Bull.* **2015**, *90*, 317–322. [CrossRef] [PubMed]
24. Rungrassamee, W.; Maibunkaew, S.; Karoonuthaisiri, N.; Jiravanichpaisal, P. Application of bacterial lipopolysaccharide to improve survival of the black tiger shrimp after *Vibrio harveyi* exposure. *Dev. Comp. Immunol.* **2013**, *41*, 257–262. [CrossRef] [PubMed]
25. Lu, J.; Shi, Y.Y.; Yao, T.; Bai, C.M.; Jiang, J.Z.; Ye, L.T. Gender Differences in Hemocyte Immune Parameters of Hong Kong Oyster *Crassostrea hongkongensis* During Immune Stress. *Front. Immunol.* **2021**, *12*, 659469. [CrossRef]
26. Liu, X.L.; Ji, C.L.; Zhao, J.M.; Wu, H.F. Differential metabolic responses of clam *Ruditapes philippinarum* to *Vibrio anguillarum* and *Vibrio splendidus* challenges. *Fish Shellfish Immunol.* **2013**, *35*, 2001–2007. [CrossRef]
27. Jacob, D.; Deborde, C.; Lefebvre, M.; Maucourt, M.; Moing, A. NMRProcFlow: A graphical and interactive tool dedicated to 1D spectra processing for NMR-based metabolomics. *Metabolomics* **2017**, *13*, 36. [CrossRef]
28. Elliott, P.; Posma, J.M.; Chan, Q.; Garcia-Perez, I.; Wijeyesekera, A.; Bictash, M.; Ebbels, T.M.D.; Ueshima, H.; Zhao, L.C.; van Horn, L.; et al. Urinary metabolic signatures of human adiposity. *Sci. Transl. Med.* **2015**, *7*, 285ra262. [CrossRef]
29. Pang, Z.Q.; Chong, J.; Zhou, G.Y.; Morais, D.A.d.L.; Chang, L.; Barrette, M.; Gauthier, C.; Jacques, P.-E.; Li, S.Z.; Xia, J.G. MetaboAnalyst 5.0: Narrowing the gap between raw spectra and functional insights. *Nucleic Acids Res.* **2021**, *49*, W388–W396. [CrossRef]
30. Sokolov, E.P.; Sokolova, I.M. Compatible osmolytes modulate mitochondrial function in a marine osmoconformer *Crassostrea gigas* (Thunberg, 1793). *Mitochondrion* **2019**, *45*, 29–37. [CrossRef]
31. Eymann, C.; Gotze, S.; Bock, C.; Guderley, H.; Knoll, A.H.; Lannig, G.; Sokolova, I.M.; Aberhan, M.; Portner, H.O. Thermal performance of the European flat oyster, *Ostrea edulis* (Linnaeus, 1758)-explaining ecological findings under climate change. *Mar. Biol.* **2020**, *167*, 2–15. [CrossRef]
32. Ellis, R.P.; Spicer, J.I.; Byrne, J.J.; Sommer, U.; Viant, M.R.; White, D.A.; Widdicombe, S. ^{1}H NMR Metabolomics Reveals Contrasting Response by Male and Female Mussels Exposed to Reduced Seawater pH, Increased Temperature, and a Pathogen. *Environ. Sci. Technol.* **2014**, *48*, 7044–7052. [CrossRef] [PubMed]
33. Zhang, L.B.; Sun, W.; Zhang, Z.; Chen, H.G.; Jia, X.P.; Cai, W.G. Gender-specific metabolic responses in gonad of mussel *Perna viridis* to triazophos. *Mar. Pollut. Bull.* **2017**, *123*, 39–46. [CrossRef] [PubMed]
34. Zhang, D.J.; He, S.; Ming, T.H.; Lu, C.Y.; Zhou, J.; Su, X.R. A metabonomic analysis on the response of *Enterobacter cloacae* from coastal outfall for land-based pollutant under phoxim stress. *Arch. Microbiol.* **2017**, *199*, 1165–1173. [CrossRef]
35. Li, M.H.; Wang, J.S.; Lu, Z.G.; Wei, D.D.; Yang, M.H.; Kong, L.Y. NMR-based metabolomics approach to study the toxicity of lambda-cyhalothrin to goldfish (*Carassius auratus*). *Aquat. Toxicol.* **2014**, *146*, 82–92. [CrossRef]
36. Yang, C.Y.; Hao, R.J.; Du, X.D.; Wang, Q.H.; Deng, Y.W.; Sun, R.J. Response to different dietary carbohydrate and protein levels of pearl oysters (*Pinctada fucata martensii*) as revealed by GC-TOF/MS-based metabolomics. *Sci. Total Environ.* **2019**, *650*, 2614–2623. [CrossRef]
37. Tweeddale, H.; Notley-Mcrobb, L.; Ferenci, T. Effect of Slow Growth on Metabolism of *Escherichia coli*, as Revealed by Global Metabolite Pool ("Metabolome") Analysis. *J. Bacteriol.* **1998**, *180*, 5109–5116. [CrossRef]
38. Liu, J.D.; Liu, W.B.; Zhang, D.D.; Xu, C.Y.; Zhang, C.Y.; Zheng, X.C.; Chi, C. Dietary reduced glutathione supplementation can improve growth, antioxidant capacity, and immunity on Chinese mitten crab, *Eriocheir sinensis*. *Fish Shellfish Immunol.* **2020**, *100*, 300–308. [CrossRef]
39. Xia, Z.Q.; Wu, S.J. Effects of glutathione on the survival, growth performance and non-specific immunity of white shrimps (*Litopenaeus vannamei*). *Fish Shellfish Immunol.* **2018**, *73*, 141–144. [CrossRef]
40. Feng, L.; Li, W.; Liu, Y.; Jiang, W.D.; Kuang, S.Y.; Wu, P.; Jiang, J.; Tang, L.; Tang, W.N.; Zhang, Y.G.; et al. Protective role of phenylalanine on the ROS-induced oxidative damage, apoptosis and tight junction damage via Nrf2, TOR and NF-kB signalling molecules in the gill of fish. *Fish Shellfish Immunol.* **2017**, *60*, 185–196. [CrossRef]
41. Rui, L.Y. Energy Metabolism in the Liver. *Compr. Physiol.* **2014**, *4*, 177–197. [CrossRef] [PubMed]
42. Liu, X.L.; Sun, H.S.; Wang, Y.Y.; Ma, M.W.; Zhang, Y.M. Gender-specific metabolic responses in hepatopancreas of mussel *Mytilus galloprovincialis* challenged by *Vibrio harveyi*. *Fish Shellfish Immunol.* **2014**, *40*, 407–413. [CrossRef] [PubMed]
43. Nguyen, T.V.; Alfaro, A.; Arroyo, B.B.; Leon, J.A.R.; Sonnenholzner, S. Metabolic responses of penaeid shrimp to acute hepatopancreatic necrosis disease caused by *Vibrio parahaemolyticus*. *Aquaculture* **2021**, *533*, 736174. [CrossRef]
44. Sun, X.J.; Tu, K.; Li, L.; Biao, W.; Wu, L.; Liu, Z.H.; Zhou, L.Q.; Tian, J.T.; Yang, A.G. Integrated transcriptome and metabolome analysis reveals molecular responses of the clams to acute hypoxia. *Mar. Environ. Res.* **2021**, *168*, 105317. [CrossRef]

45. Lu, J.; Shi, Y.Y.; Wang, S.H.; Chen, H.; Cai, S.H.; Feng, J.H. NMR-based metabolomic analysis of *Haliotis diversicolor* exposed to thermal and hypoxic stresses. *Sci. Total Environ.* **2016**, *545–546*, 280–288. [CrossRef]
46. Li, F.; Meng, X.J.; Wang, X.Q.; Ji, C.L.; Wu, H.F. Graphene-triphenyl phosphate (TPP) co-exposure in the marine environment: Interference with metabolism and immune regulation in mussel *Mytilus galloprovincialis*. *Ecotoxicol. Environ. Saf.* **2021**, *227*, 112904. [CrossRef]

antioxidants

MDPI

Article

Protective Effects of Emodin on Oxidized Fish Oil-Induced Metabolic Disorder and Oxidative Stress through Notch-Nrf2 Crosstalk in the Liver of Teleost *Megalobrama amblycephala*

Changyou Song [1,2], Bo Liu [2], Hongxia Li [1,2], Yongkai Tang [1,2], Xianping Ge [1,2], Bo Liu [1,2,*] and Pao Xu [1,2,*]

[1] Key Laboratory of Aquatic Animal Nutrition and Health, Freshwater Fisheries Research Center, Chinese Academy of Fishery Science, Wuxi 214081, China; songchangyou@ffrc.cn (C.S.); lihx@ffrc.cn (H.L.); tangyk@ffrc.cn (Y.T.); gexp@ffrc.cn (X.G.)

[2] Wuxi Fisheries College, Nanjing Agricultural University, Wuxi 214081, China; liubo@njau.edu.cn

* Correspondence: liub@ffrc.cn (B.L.); xup@ffrc.cn (P.X.)

Abstract: Dietary oxidized lipids are key perpetrator to accumulate excessive reactive oxygen species (ROS) that induce oxidative stress for animals. Immoderate oxidative stress dysregulates cell fate, perturbs cellular homeostasis, thereby interrupts metabolism and normal growth. Therefore, a 12-week feeding trial with fish oil (FO, control group), oxidized fish oil (OF), and emodin-supplemented (OF+E) diets was conducted to evaluate the therapeutic mechanism of emodin on metabolic and oxidative resistance in *Megalobrama amblycephala* liver. Morphologically, emodin remits oxidized fish oil-induced cellular constituents damage, evidenced by lipid droplets enlargement and accumulation, mitochondria rupture, and nucleus aggregation, which were functionally related to oxidative stress, metabolism, and cell fate determination. Consecutively, glucose, lipid, and amino acid metabolism were retained under emodin stimulation. Specifically, fatty acid metabolic genes optimized fatty acid utilization and metabolism, featured as total saturated fatty acids (SFA), monounsaturated fatty acids (MUFA), and polyunsaturated fatty acids (PUFA) alternation. Physiologically, inflammation, autophagy, apoptosis, as well as antioxidant capacity were alleviated by emodin. Interactively, fatty acid metabolism was correlated with antioxidant capacity; while the crosstalk and dynamic equilibrium between apoptosis and autophagy determine the cell fate under oxidative stress amelioration. Synergistically, Nrf2 and Notch signaling were active to antioxidant defense. In particular, oxidative stress blocked the crosstalk between Notch and Nrf2 signaling, while emodin rescued Notch-Nrf2 interaction to ameliorate oxidative stress. In conclusion, these results suggest that elevated ROS levels by oxidative stress activates Notch and Nrf2 signaling but intercepts Notch-Nrf2 crosstalk to stimulate cell fate and antioxidant program; dietary emodin alleviates oxidative stress and returns overall ROS levels to a moderate state to maintain homeostatic balance. The crosstalk between Notch and Nrf2 signaling might be the potential therapeutic target for emodin to ameliorate oxidative stress and metabolic disorder in *M. amblycephala* liver.

Keywords: oxidative stress; Notch-Nrf2 crosstalk; antioxidant; metabolism; emodin; *Megalobrama amblycephala*

Citation: Song, C.; Liu, B.; Li, H.; Tang, Y.; Ge, X.; Liu, B.; Xu, P. Protective Effects of Emodin on Oxidized Fish Oil-Induced Metabolic Disorder and Oxidative Stress through Notch-Nrf2 Crosstalk in the Liver of Teleost *Megalobrama amblycephala*. *Antioxidants* **2022**, *11*, 1179. https://doi.org/10.3390/antiox11061179

Academic Editor: Stanley Omaye

Received: 11 May 2022
Accepted: 14 June 2022
Published: 15 June 2022

1. Introduction

Internal homeostasis is an important precondition for animal physiological health, growth, and reproduction maintenance. Reactive oxygen species (ROS) and reactive nitrogen species (RNS) are generated during cellular metabolism, which play important roles in internal homeostasis, cell signal transduction, cell proliferation and differentiation [1]. Generally, animals are exposed to internal or external adverse environments that could dysregulate ROS or RNS homeostasis, which trigger oxidative stress consequently. Oxidative stress is the most extensive and harmful stress among all stresses. When oxidative stress exceeds the repair capacity of the cell, oxidative damage will lead to physiological disorder,

lipid peroxidation, DNA alteration, protein degradation, immunity and growth inhibition, and even severe death [2].

Adequate energy intake and nutritional balance are important prerequisites for aquatic animal growth and reproduction. However, excessive or insufficient nutrient intake, as well as nutrient deterioration, causes an imbalance between pro-oxidants and antioxidants, which was coined as "dietary oxidative stress" [3]. Dietary oxidative stress could induce metabolic disorder and homeostasis imbalance, leading to oxidative stress and inflammatory responses [4], disrupt cellular homeostasis and cell fate turnover, thereby seriously affecting the health of aquatic animals and causing severe loss to the aquaculture industry [5]. Fat is an important nutrient and energy substance, which can provide essential fatty acids for fish, promote the absorption and utilization of fat-soluble nutrients such as vitamins, as well as maintain the stability of biofilm structure [6]. In aquaculture, fish oil and soybean oil are the most commonly used animal- and plant-based lipids. However, due to the high content of unsaturated fatty acids, they are easily to be oxidized under natural conditions. Therefore, oxidative stress caused by nutritional imbalance, especially by dietary oxidized lipids that accompanies the entire life cycle of aquatic animals, should be paid enough attention. In view of this, considering lipid oxidation-induced oxidative stress to study oxidative stress in aquatic animals, clarifying the molecular mechanism and targets of oxidative stress injury, and exploring effective stress prevention strategies are both representative and of great significance to the health development of aquaculture.

It is clear that deleterious effects of ROS are controlled by specific antioxidant systems [7]. Two potential mechanisms may be involved in increase of ROS generation by oxidized fish oil: one is the conjugation of products of metabolism with glutathione, resulting in consumption of GSH and decreasing the defense potential leading to oxidative stress [8]. Another one is the antioxidant defense system to reduce the oxidative damage, including antioxidant enzymes and signaling molecules [8]. Nowadays, attentions have been attracted to deciphering regulatory pathways in which free radicals are involved. To date, many pathways have been investigated in detail, including Nrf2/Keap1 and Notch signaling.

Nrf2 (nuclear factor, erythroid derived 2, like 2) is a nuclear transcription factor that is critical for cellular protection and cell survival [9]. Notch signaling regulates cell fate decision in animals, such as cell differentiation, survival, apoptosis, and cell cycle in both physiologic and pathologic contexts [1]. The role of Nrf2 signaling in ROS-induced oxidative stress has been well studied, and recent reports also reveal ROS could activate Notch pathway [10]. As the major effector of ROS, Nrf2 regulates a number of ARE-containing genes, including Notch1, to regulate cell fate and reduce ROS levels in the cell [10]. Meanwhile, it has been clearly shown that NICD can activate the Nrf2 pathway and Nrf2 can activate the Notch1 pathway in the liver [11]. Additionally, Notch-Nrf2 signaling was active to promote self-renewal of the liver and intestine cell by autophagy and apoptosis under ROS-induced oxidative stress [12,13]. Therefore, the crosstalk between Notch and Nrf2 is critical for liver metabolism and cell fate determination.

In recent years, dietary intake has become the main approach for stress control and prevention in aquatic animals, including probiotics, prebiotics, microbial feed additives, and natural functional feed additives [14]. These functional feed additives could improve antioxidant performance and reduce oxidative stress by chelating metal ions, regulating intestinal microorganisms, increasing antioxidant factor activity, and inhibiting ROS over-production [14]. However, the underlying molecular mechanism is still not fully investigated, which has become an urgent scientific bottleneck for oxidative stress prevention and control in aquatic animals.

Emodin is a natural anthraquinone derivative that is enriched in many widely used Chinese medicinal herbs, such as *Rheum palmatum*, *Polygonum cuspidatum*, and *Polygonum multiflorum* [15]. Emerging evidence indicates that emodin possesses a wide spectrum of pharmacological properties, including anticancer, hepatoprotective, anti-inflammatory, antioxidant, and antimicrobial activities [16]. Previously, we elucidate dietary emodin ameliorates dietary oxidized fish oil-induced oxidative stress by improving antioxidant

and immune capacity, reducing intestinal cell autophagy, and thereby rescuing the growth performance of *M. amblycephala* [17]. In particular, PPARs, Nrf2, and Notch signaling were involved in the regulation [1,17,18]. Apart from the intestine, liver is constantly exposed to environmental oxidants and therefore serves as an interesting model system to study oxidative stress. However, the regulation on metabolism and antioxidant, and the underlying mechanism between Notch and Nrf2 signaling in the liver still remains unclear.

In the present study, we investigated the systematic alternation among metabolism, immunity, and antioxidant capacity under oxidative stress in the liver of *M. amblycephala*. Meanwhile, the role of Notch and Nrf2 signaling, as well as their crosstalk in resist to oxidative stress and emodin amelioration were also identified. These results could reveal the mechanism and will provide potential therapeutic targets for emodin in aquaculture.

2. Materials and Methods

2.1. Ethics Statement

This study was approved by the Animal Care and Use Committee of Nanjing Agricultural University (Nanjing, China; protocol code: WXFC 2017-0006, approved 27 May 2017). All animal procedures were carried out in accordance with the China Laboratory Animal Care and Use Guidelines. The ethics in this experiment is the same as the ethics previously published [18].

2.2. Experimental Diets

According to our previous research, oxidized fish oil in the diet has been shown to induce oxidative stress [18], and emodin was confirmed to improve the antioxidant capacity in *M. amblycephala* [19]. Therefore, this experiment applied oxidized fish oil with a peroxide value (POV) of 375.33 mmol/kg to induce oxidative stress with the fish model of *M. amblycephala*. Specifically, isonitrogen and isoenergy (33.11% crude protein and 14.68 kJ/g energy) diets were formulated, including basal diets containing 6% fish oil (control, 6F), oxidized lipid enriched diets containing 6% oxidized fish oil (6OF), and emodin enriched diets containing 30 mg/kg emodin (6OF+E) (Table 1). All ingredients were prepared and the diets were pelleted according to the established methods [19].

Table 1. Formulation and proximate composition of experimental diets.

Ingredient/%	6F	6OF	6OF+E	Nutrition Value (%, Dry Matter)	6F	6OF	6OF+E
Casein	25.0	25.0	25.0	Dry matter, DM	92.06	92.18	92.24
Gelatin	5.0	5.0	5.0	Crude protein, CP	33.11	33.11	33.11
Fish meal	10.0	10.0	10.0	Crude lipid	7.01	7.01	7.01
Dextrin	10.0	10.0	10.0	Nitrogen Free Extract, NFE	1.00	1.06	1.09
α-starch	24.5	24.5	24.5	Ash	8.28	8.34	8.37
Fish oil	6.0	0.0	0.0	Ca	1.62	1.62	1.62
Oxidized fish oil	0.0	6.0	6.0	Total P	1.05	1.05	1.05
Microcrystalline cellulose	7.0	7.0	7.0	Lysine	2.49	2.49	2.49
Carboxymethylcellulose	5.0	5.0	5.0	Cysteine	0.92	0.92	0.92
Choline chloride	1.0	1.0	1.0	Methionine	0.19	0.19	0.19
Vitamin premix [a]	1.0	1.0	1.0	Threonine	1.34	1.34	1.34
Mineral premix [b]	1.0	1.0	1.0	Arginine	1.50	1.50	1.50
Calcium dihydrogen phosphate	2.0	2.0	2.0	Fe	33.70	33.70	33.70
Attapulgite	2.0	2.0	2.0	Gross Energy [c]	14.68	14.68	14.68
Ethoxyquin	0.5	0.5	0.5				
Total	100.0	100.0	100.0				
Emodin (mg/kg)	0.0	0.0	30.0				

Note: [a] Vitamin contents per kg diets: Vitamin A, 9000 IU; Vitamin B_1, 3.2 mg; Vitamin B_2, 10.9 mg; Vitamin B_5, 20 mg; Vitamin B_6, 5 mg; Vitamin B_{12}, 0.016 mg; Vitamin C, 50 mg; Vitamin D, 2000 IU; Vitamin E, 45 mg; Vitamin K_3, 2.2 mg; Niacin, 28 mg; Folic acid, 1.65 mg; Pantothenate, 10 mg; Choline, 600 mg. [b] Mineral contents per kg diets: $FeSO_4 \cdot 7H_2O$, 250 mg; $CuSO_4 \cdot 5H_2O$, 20 mg; $ZnSO_4 \cdot 7H_2O$, 220 mg; Na_2SeO_3, 0.4 mg; $MnSO_4 \cdot 4H_2O$, 70 mg; $CoCl_2 \cdot 6H_2O$, 1 mg; KI, 0.26 mg; [c] Energy, calculated by using standard physiological fuel values of 37.7, 16.7, and 16.7 kJ g^{-1} for protein, lipid and carbohydrate, respectively.

2.3. Experimental Animals and Rearing Conditions

The experimental fish *M. amblycephala* was generated from our research institute Freshwater Fisheries Research Center, Chinese Academy of Fishery Sciences. The experiment was conducted in fiberglass tanks (300 L each) of indoor fresh water circulation system to support equal supplemental aeration and water flow (3 L/min). Prior the feeding trail, fish were acclimated in the tank fed with the control feed for 14 days. After acclimation, fish with similar body weight (intimal average weight 5.20 ± 0.01 g) were randomly assigned to nine tanks (3 tanks for each group, 25 individuals for each tank, 225 fish in total). During the 12-week rearing experiment, fish were fed with the respective diets to near satiation four times a day (8:00, 11:00, 14:00, and 17:00). During the experiment, one-third of the water in the tank was replaced weekly, the water temperature was kept as 26 ± 1 °C, and the water quality maintained as: pH 7.6–7.8, DO > 6 mg/L, NH_3 < 0.01 mg/L.

2.4. Sample Collection

After a 12-week feeding experiment, the fish were starved for 24 h to evacuate the digestive tract contents before sampling. Nine fish in each group were taken (three fish from each tank were randomly selected) and anesthetized with tricaine mesylate (MS-222, 100 mg/L) for sampling. Blood samples were obtained from caudal vein and stored in heparin coated tubes, and then centrifuged at 4500 rpm, 4 °C for 10 min to obtain the plasma. The anesthetized fish were then dissected to remove the liver tissues on ice, immediately isolated for TEM analysis or frozen in liquid nitrogen and stored at −80 °C for subsequent analysis.

2.5. Liver Histological Ultrastructure

According to our previously established method [18], TEM was used to detect histological ultrastructure. In detail, the livers of *M. amblycephala* (3 replicates per group) were collected immediately and fixed in 2.5% glutaraldehyde for 24 h, post-fixed in 1% osmium tetroxide (OsO4) for 1 h, and stored at 4 °C till sectioning. The sections were embedded in epoxy resin Epon812, cut into thin slices (70 μm thick) with RMC PowerTome XL microtome, and stained with uranyl acetate and lead citrate. A Hitachi HT7700 transmission electron microscope (Hitachi, Tokyo, Japan) was used to observe the ultrastructure morphology.

2.6. Metabolic and Antioxidant Index Detection

Glucose content in the plasma, digestive enzyme activity of amylase, alkaline phosphatase (ALP), lipase, lipoprotein lipase (LPL), triglyceride (TG), total cholesterol (TC), and fatty acid synthetase (FAS) in the liver was determined by assay kits according to the manufacturer's protocol (provided by Nanjing Jiancheng Bioengineering Institute, Nanjing, China). In detail, glucose was detected by hexokinase method (Category No: F006-1-1), amylase was determined by starch-iodine colorimetry method (Category No: C016-1-1), ALP was determined by colorimetric method (Category No: A059-2), lipase was determined by colorimetric method (Category No: A054-1-1), LPL was determined by colorimetric method (Category No: A067-1), TG was determined by colorimetric method (Category No: A110-2), TC was determined by colorimetric method (Category No: A111-2), and FAS was determined by (Category No: A080-2-2).

Meanwhile, antioxidant capacity-related index of reactive oxygen species (ROS), total superoxide dismutase (T-SOD), inducible nitric oxide synthase (iNOS), nitric oxide (NO), reduced glutathione (GSH), glutathione peroxidase (GPx), anti-superoxide anion (ASAFR) and malondialdehyde (MDA) were all determined by assay kits according to the manufacturer's protocol (provided by Nanjing Jiancheng Bioengineering Institute, China). The category numbers of the kit were as following: ROS, E004-1; T-SOD, A001-1; iNOS, H372-1; NO, A012-1; GSH, A006-2; GPx, A005-1; ASAFR, A052-1; and MDA, A003-1.

2.7. Fatty Acid and Amino Acid Analysis

For fatty acid analysis, whole fish samples were hydrolyzed with BHT for 1.5 h, neutralized with ddH_2O and n-hexane, and centrifuged at 1000 rpm for 10 min. The supernatant

was isolated to analyze fatty acid composition by meteorological chromatography-mass spectrometer (GC-MS, Aglilent 7890B-5977A).

For amino acid analysis, whole fish samples were hydrolyzed with 6 mol/L HCl and filled with nitrogen for 24 h. The samples were applied to determine the amino acid content by liquid chromatography analyzer (Agilent-1100).

2.8. Correlation Analysis

Pearson's correlation test was performed to analyze the correlations between parameters or key genes. The significance threshold was set at a p-value < 0.05. The heatmap was created in R with the pheatmap package.

2.9. RNA Extraction and RT-PCR Analysis

Total RNA from nine livers in each group was extracted with RNAiso Plus reagent (Takara Co. Ltd., Dalian, China), and the total RNA was incubated with RNase-free DNase (Takara Co. Ltd., Dalian, China) to remove contaminated genomic DNA. Absorbance under OD 260/280 and electrophoresis (1.5% agarose) was applied to evaluate the quantity and quality of RNAs. Primers for RT-PCR was designed with primer Premier 5.0 according to the sequence we obtained with RNA-seq and synthesized by Shanghai Generay Biotechnology Co., Ltd., China (primers were shown in Table 2). RT-PCR analysis was performed using SYBR® Primix Ex TaqTM II (TliRNase Plus) kit according to the manufacturer's protocol with ABI 7500 real-time PCR system. β-actin was used as the housekeeping gene, and the relative expression was calculated using the $2^{-\Delta\Delta CT}$ method.

Table 2. Primers and sequences referred in the experiment.

Gene	Primer	Sequence (5′→3′)	Accession No.	Gene	Primer	Sequence (5′→3′)	Accession No.
LPL	F	TTACAGGCTGAGATTGACTA	KF114279.1	*AIF1*	F	GGATTTTCCTCGCACAAAAC	XM_048210652.1
	R	GAAGAACATCCACGAAAA			R	TGTCGTCTGTGGCTTCACTT	
ATGL	F	ATCCTTGTATCCCTGCTTG	KX010807.1	*CytoC*	F	GCACAAAGTCGGTCCAAATC	XM_048185968.1
	R	GTGACAGACGGAGAAAACG			R	GCTCTCTCGCCCTTCTTCTT	
CPT1	F	TACTTCCAAAGCGGTGAG	KJ141198.1	*Notch1b*	F	GCGATTATGGAAGGTGCATT	XM_048189338.1
	R	AGAGGTATTGTCCGAGCC			R	GTCGTGATACCCCTCTCTGC	
CPT2	F	CCATAGCCCACTCCGAAAC	XM_048208951.1	*DLLA*	F	TGACAACAGAAAACCCAGAGC	XM_048205545.1
	R	TGCCGCCATAAACCACAA			R	TCCCTCGCCATAGTAGTGCT	
Cox2	F	AACCCAGGACCTTACACCC	NC_010341.1	*Jag1b*	F	GTAAACGGAGGGCAGTGTGT	XM_048205450.1
	R	CCCGCAGATTTCAGAACA			R	GCGCACTTGTAGCTTCCTTC	
UCP2	F	TGGCTACAGCACAGTTGAGG	XM_048179976.1	*Jag2*	F	CTTCCTGACGTGCCTCTCTC	XM_048205375.1
	R	TGACCTCATCAAAGATGCAC			R	GTGGGCAGTTTGTCCTTGTT	
FAS	F	AGCGAGTACGGTGATGGT	KF918747.1	*Hey1*	F	GGGCTCACACCACCTACAAC	XM_048201329.1
	R	GGATGATGCCTGAGATGG			R	CCCTATTTCCATGCTCCAAG	
SREBP1	F	ACAACAGTAGCGACACCCTG	MH633449.1	*Hey2*	F	AACGGCATTTGAGAAACAGG	XM_048207495.1
	R	AGGAGCGGTAGCGTTTTTCA			R	GCTGAGGTGAGAAACCAAGC	
IL-1β	F	CGATAAGACCAGCACGACCTT	MN294974.1	*Hes1*	F	CCTGCTTTCGCTTCTGCTAC	XM_048186605.1
	R	GTTTCCGTCTCTCAGCGTCA			R	GCACTAACACCAACGGGACT	
IL-6	F	GTCCTCTGCCGGTCAAATC	KJ755058.1	*FBW7*	F	CTGAAACCGAGACCTGCCTA	XM_048197725.1
	R	CAGTCGCTGGGTCTCTTCAC			R	CTGATGACCTGTGAGCGTGT	
TNF-α	F	CTGTCTGCTTCACGCTCAAC	KU976426.1	*NOX1*	F	CTGGCTGCTCATCACAGAAG	XM_048176512.1
	R	GGTCCTGGTTCACTCTCCAA			R	CCACTATCGCTGGTCTCACA	
NF-κB	F	GGGTTTTTCATTGGTGGATG	MK315050.1	*Nrf2*	F	AAGAGCGAACGTAGCACCAG	XM_048178958.1
	R	GCAGAACTGTGGCAATCTGA			R	GCAGTGTGCTGAAGGGAGTAT	
ATG3	F	CGCCAGTTTTGAAGGAATCT	XM_048200321.1	*Keap1*	F	GAGATTCGCAGAGGAGATCGG	XM_048162397.1
	R	TTGTCTTTGGGCAGATAGGG			R	CTGGCAATGGGACAAGCTGA	
ATG7	F	ATCACACCAGGAGCGTCTTT	XM_048172227.1	*Bach1*	F	CAGCCATCATTTCCAACCTT	XM_048160868.1
	R	GGTTCATTCATCCGGTCATC			R	GAGACGCCTGACAAGAATCC	
Beclin1	F	TCGACACATCCTTCAACGTC	XM_048187618.1	*NQO1*	F	AAGCCTCTGTCCTTTGCTCC	XM_048186312.1
	R	ATGTATTTCCGAGCCACACC			R	TCTGGAGGAAGTGGTTTGCC	
Bax	F	CCCCCTCATCTTTCCATTCT	MK315043.1	*HO-1*	F	CAGGAGCAGAATGAACAGCA	KU382526.1
	R	CAAACATCCCCTTTCTTCTCC			R	CCAAAGTGATTCCCACACCT	
Casp3	F	AGATGGTGTGGGAGATGGAG	KY006115.1	*β-actin*	F	TCTGCTATGTGGCTCTTGACTTCG	AY170122.2
	R	CCAGTTGCTTGCCGTATTTT			R	CCTCTGGGCACCTGAACCTCT	
Casp8	F	TTGTCTGCTGTGTCCTCTCG	XM_048200589.1				
	R	ATCGTTCCCTTGTCCATCTG					

Note: The mRNA sequences for each gene were obtained from *M. amblycephala* transcriptome sequencing database. Primers for RT-PCR were designed using primer premier 5.0.

2.10. Statistical Analysis

To determine the variances for each parameter among different groups, data were all validated for normality and homogeneity, followed by independent samples t-test with

SPSS 25.0 (IBM, Chicago, IL, USA). Results were expressed as mean ± standard error of the mean (mean ± SEM).

3. Results

3.1. Emodin Alleviates Oxidized Fish Oil Induced Morphological Impairment in the Liver of M. amblycephala

TEM was applied to reveal the histological alternation of the liver tissue induced by dietary oxidized fish oil and emodin. In comparison with the control group (6F, Figure 1A), lipid droplets (LD) were enlarged in size and accumulated in quantity (Figure 1B, arrows in white color), mitochondria (MT) were ruptured gradually (Figure 1B, arrows in red color), and nucleolus (NC) was aggregated (Figure 1B, arrows in blue color) under oxidized fish oil (6OF). These morphological impairments indicate 6OF-induced oxidative stress, metabolic disorder, and cell fate dysregulation in the liver. Heartily, we found the structure of LD, MT, and NC was visibly rescued under emodin stimulation (6OF+E), indicating the ameliorative effects of emodin on oxidative stress, cellular metabolism, and cell fate determination (Figure 1C).

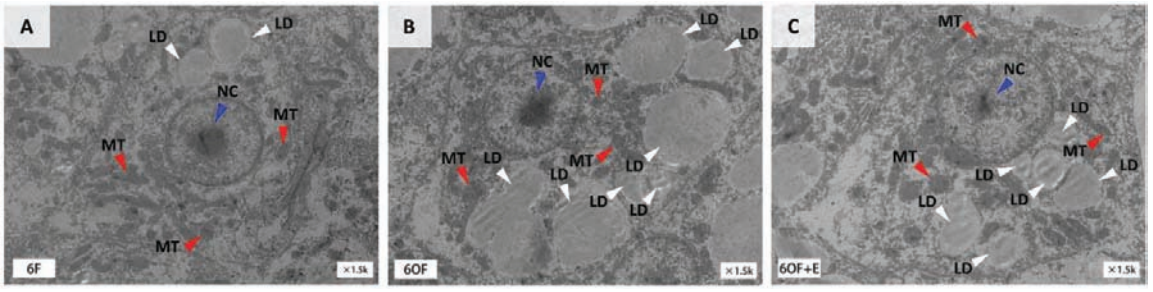

Figure 1. Emodin alleviates oxidized fish oil-induced morphological impairment in the liver of *M. amblycephala*. (**A**–**C**), Ultra-structure of the liver obtained from transmission electron microscopy (TEM), (**A**), 6% fish oil (6F); (**B**), 6% oxidized fish oil (6OF); (**C**), 6% oxidized fish oil with 30 mg/kg emodin (6OF+E). Arrows in white color represent the lipid droplets (LD), in red represent the mitochondria (MT), and in blue represent the nucleolus (NC), $n = 3$.

3.2. Emodin Alleviates Metabolic Disorder Induced by Oxidative Stress in the Liver of M. amblycephala

To reveal the metabolic alterations retrieved form the mitochondria histology, glucose, lipid, and protein metabolic-related indexes were detected with the liver tissue. Glucometabolic-related glucose content (Figure 2A) and amylase activity (Figure 2B) were inhibited by 6OF; protein metabolic-related alkaline phosphatase (ALP) activity (Figure 2C) was also inhibited by 6OF; lipid and fatty acid metabolic related lipase (Figure 2D), lipoprotein lipase (Figure 2E), triglyceride (Figure 2F), total cholesterol (TC, Figure 2G), and fatty acid synthetase (Figure 2H) were all inhibited by 6OF. However, the aberrant expression of these genes was rescued by emodin (6OF+E), and exhibited no significant difference with that in 6F ($p \geq 0.05$) (Figure 2A–H).

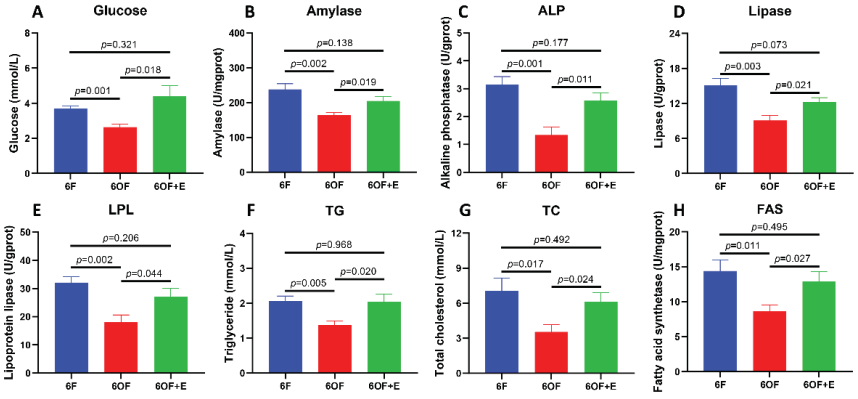

Figure 2. Emodin alleviates metabolic disorder induced by oxidative stress in the liver of *M. amblycephala*. (**A**–**G**) represent the glucose, lipid, and protein metabolic related indexes detected from the liver. (**A**), glucose; (**B**), amylase; (**C**), alkaline phosphatase (ALP); (**D**), lipase; (**E**), lipoprotein lipase (LPL); (**F**), triglyceride (TG); (**G**), total cholesterol (TC); (**H**), fatty acid synthetase (FAS). Data were analyzed by Students' *t*-test, results were indicated as mean ± SEM, $n = 9$.

3.3. Emodin Rescues Fatty Acid Metabolism under Oxidative Stress in the Liver of M. amblycephala

To further explore the potential alteration of fatty acid metabolism that is regulated by OF, fatty acid composition, fatty acid catabolism, and anabolism were analyzed. Fatty acid composition of the diet reveal saturated fatty acids (SFA) and monounsaturated fatty acids (MUFA) were significantly increased ($p < 0.05$), while the polyunsaturated fatty acids (PUFA) were significantly decreased ($p < 0.05$) after the oxidization of fish oil (Figure 3A–C, Table 3). However, the fatty acid composition from the whole fish reveal SFA exhibited no significant difference between 6F, 6OF, and 6OF+E ($p > 0.05$); MUFA in 6OF was increased, but restored to the 6F level under emodin (6OF+E); PUFA in 6OF and 6OF+E was significantly decreased ($p < 0.05$), and exhibited the same variation as that in the diet (Figure 3A–C, Table 3). These results indicate *M. amblycephala* presents positive adaptability to fatty acid metabolism under fatty acid composition alteration in the diet induced by oxidized fish oil, especially the SFA and MUFA utilization. This interesting finding inspired us to explore the fatty acid catabolic and anabolic regulation.

In the fatty acid catabolism process, we found the transcriptional expression of lipoprotein lipase (LPL, Figure 3D), adipose triglyceride lipase (ATGL, Figure 3E), carnitine palmitoyltransferase I (CPT1, Figure 3F), carnitine palmitoyltransferase II (CPT2, Figure 3G), and cyclooxygenase 2 (COX2, Figure 3H) were all inhibited by 6OF; while uncoupling protein 2 (UCP2, Figure 3I) was activated by 6OF. Meanwhile, in fatty acid anabolic process, transcriptional expression of fatty acid synthase (FAS, Figure 3J) and sterol regulatory element-binding protein 1 (SREBP1, Figure 3K) were also down-regulated under 6OF. However, results also show the expression of these key genes were restored to the control level under 6OF+E stimulation (Figure 3D–K).

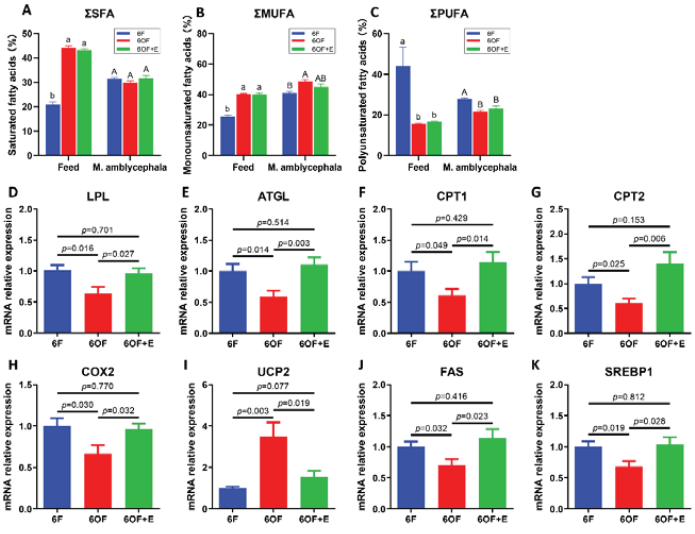

Figure 3. Emodin rescues fatty acid metabolism under oxidative stress in the liver of M. amblycephala. (**A**–**C**), fatty acid composition in the feed and M. amblycephala. (**A**), total saturated fatty acids (∑SFA); (**B**), total monounsaturated fatty acids (∑MUFA); (**C**), total polyunsaturated fatty acids (∑PUFA). (**D**–**I**), transcriptional expression of fatty acid catabolic related genes. (**D**), Lipoprotein lipase (LPL); (**E**), adipose triglyceride lipase (ATGL); (**F**), carnitine palmitoyltransferase I (CPT1); (**G**), carnitine palmitoyltransferase II (CPT2); (**H**), cyclooxygenase 2 (COX2); (**I**), uncoupling protein 2 (UCP2). (**J**,**K**), transcriptional expression of fatty acid anabolic related genes. (**J**), Fatty acid synthase (FAS); (**K**), sterol regulatory element-binding protein 1 (SREBP1). In panel (**A**–**C**), letters "a and b" represent the difference in the feed, "A and B" represent the difference in the M. amblycephala. Data were analyzed by Students' *t*-test, results were indicated as mean ± SEM, $n = 9$.

Table 3. Fatty acid composition in the diet and *M. amblycephala*.

	Feed			*M. amblycephala*		
	6F	**6OF**	**6OF+E**	**6F**	**6OF**	**6OF+E**
C12:0	0.071 ± 0.006 b	0.106 ± 0.003 a	0.120 ± 0.002 c	0.044 ± 0.002 A	0.044 ± 0.002 A	0.054 ± 0.002 A
C14:0	1.061 ± 0.035 b	2.549 ± 0.028 a	2.596 ± 0.113 a	1.584 ± 0.049 A	1.554 ± 0.031 A	1.688 ± 0.051 A
C15:0	0.132 ± 0.018 b	0.583 ± 0.139 a	0.453 ± 0.002 a	0.224 ± 0.002 A	0.235 ± 0.023 A	0.253 ± 0.031 A
C16:0	14.539 ± 0.889 b	33.132 ± 0.521 a	32.591 ± 0.341 a	21.789 ± 0.456 A	20.960 ± 0.554 A	22.351 ± 0.779 A
C17:0	0.231 ± 0.018 c	1.236 ± 0.021 a	1.099 ± 0.011 b	0.355 ± 0.020 AB	0.331 ± 0.018 B	0.437 ± 0.026 A
C18:0	4.425 ± 0.245 b	6.296 ± 0.171 a	6.072 ± 0.042 a	7.263 ± 0.152 A	6.626 ± 0.073 A	6.666 ± 0.385 A
C20:0	0.343 ± 0.025 a	0.211 ± 0.006 b	0.249 ± 0.011 b	0.103 ± 0.002 A	0.113 ± 0.008 A	0.126 ± 0.015 A
ΣSFA	**20.802 ± 1.237 b**	**44.113 ± 0.874 a**	**43.180 ± 0.521 a**	**31.362 ± 0.683 A**	**29.863 ± 0.708 A**	**31.575 ± 1.288 A**
C16:1	1.959 ± 0.034 b	12.239 ± 0.081 a	13.258 ± 0.150 a	6.604 ± 0.233 B	8.409 ± 0.121 A	8.187 ± 0.108 A
C18:1	22.940 ± 1.120 b	27.270 ± 0.156 a	26.029 ± 0.595 a	33.519 ± 0.878 B	39.298 ± 0.751 A	35.979 ± 1.721 AB
C20:1	0.311 ± 0.006 b	0.681 ± 0.047 a	0.624 ± 0.072 a	0.758 ± 0.010 B	0.960 ± 0.035 A	0.806 ± 0.061 AB
C22:1	0.150 ± 0.006 c	0.247 ± 0.010 a	0.203 ± 0.002 b	0.049 ± 0.005 A	0.022 ± 0.004 B	0.063 ± 0.008 A
ΣMUFA	**25.360 ± 1.166 b**	**40.437 ± 0.293 a**	**40.115 ± 0.818 a**	**40.930 ± 1.126 B**	**48.689 ± 0.910 A**	**45.035 ± 1.897 AB**
C18:2	10.689 ± 9.657 a	5.084 ± 0.049 b	4.978 ± 0.103 b	5.789 ± 0.051 A	4.102 ± 0.059 B	3.683 ± 0.221 B
C18:3n6	0.672 ± 0.007 a	0.390 ± 0.017 b	0.476 ± 0.015 b	0.151 ± 0.001 A	0.133 ± 0.019 A	0.141 ± 0.012 A
C18:3n3	5.167 ± 0.096 a	1.187 ± 0.062 c	1.606 ± 0.073 b	0.628 ± 0.010 A	0.408 ± 0.005 B	0.443 ± 0.025 B
C20:2	0.223 ± 0.179 a	0.063 ± 0.002 b	0.046 ± 0.003 b	0.153 ± 0.002 C	0.877 ± 0.044 A	0.548 ± 0.048 B
C20:3	0.241 ± 0.001 a	0.139 ± 0.005 b	0.131 ± 0.006 b	0.786 ± 0.015 A	0.750 ± 0.029 AB	0.658 ± 0.033 B
C20:4	1.182 ± 0.018 a	0.664 ± 0.008 b	0.754 ± 0.002 b	1.701 ± 0.058 A	1.732 ± 0.018 A	1.627 ± 0.073 A
C20:5	12.205 ± 0.061 a	5.665 ± 0.094 b	6.685 ± 0.043 b	4.776 ± 0.044 A	2.450 ± 0.202 C	3.455 ± 0.263 B
C22:3	0.118 ± 0.006 a	0.034 ± 0.002 b	0.022 ± 0.001 b	0.103 ± 0.002 A	0.147 ± 0.021 A	0.126 ± 0.015 A
C22:4	0.246 ± 0.003 a	0.090 ± 0.006 b	0.060 ± 0.006 b	0.269 ± 0.011 A	0.389 ± 0.051 A	0.350 ± 0.017 A
C22:5	0.840 ± 0.012 a	0.309 ± 0.005 b	0.247 ± 0.004 b	1.910 ± 0.064 A	1.095 ± 0.055 B	1.400 ± 0.115 B
C22:6	12.437 ± 0.021 a	1.917 ± 0.068 b	1.686 ± 0.021 b	11.449 ± 0.260 A	9.379 ± 0.161 B	10.929 ± 0.537 A
ΣPUFA	**44.020 ± 9.285 a**	**15.542 ± 0.316 b**	**16.692 ± 0.267 b**	**27.715 ± 0.517 A**	**21.462 ± 0.665 B**	**23.177 ± 1.174 B**

Note: letters "a, b, and c" represent the difference in the feed, "A, B, and C" represent the difference in the *M. amblycephala*.

3.4. Emodin Alleviates Antioxidant Capacity under Oxidative Stress in the Liver of M. amblycephala

To evaluate whether dysregulated metabolism impacts antioxidant capacity, we next evaluated the antioxidant-related parameters in the liver. 6OF significantly increased the content or activity of reactive oxygen species (ROS, Figure 4A), total superoxide dismutase (T-SOD, Figure 4B), inducible nitric oxide synthase (iNOS, Figure 4C), glutathione peroxidase (GPx, Figure 4D), anti-superoxide anion (ASAFR, Figure 4E), and malondialdehyde (MDA, Figure 4F); and significantly decreased the content of nitric oxide (NO, Figure 4G) and reduced glutathione (GSH, Figure 4H). Analogously, emodin (6OF+E) also alleviates the increased or decreased activity or content to the control level after 12-weeks stimulation ($p > 0.05$, Figure 4A–H).

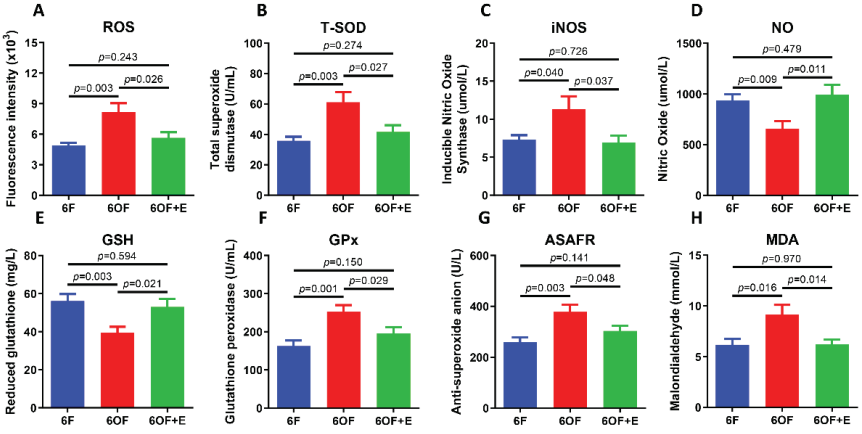

Figure 4. Emodin alleviates antioxidant disorder under oxidative stress in the liver of *M. amblycephala.* (**A**–**G**), Antioxidant related indexes. (**A**), Reactive oxygen species (ROS); (**B**), total superoxide dismutase (T-SOD); (**C**), inducible nitric oxide synthase (iNOS); (**D**), nitric oxide (NO); (**E**), reduced glutathione (GSH); (**F**), glutathione peroxidase (GPx); (**G**), anti-superoxide anion (ASAFR); (**H**), malondialdehyde (MDA). Data were analyzed by Students' *t*-test, results were indicated as mean ± SEM, $n = 9$.

To reveal the relationship between fatty acid metabolism and antioxidant capacity, a correlation analysis was conducted with Pearson analysis (Figure S1). Under oxidative stress (6OF), fatty acid metabolism-related indexes were synergistically correlated with antioxidant enzyme activities, but the correlation indexes were different with that in 6F. However, after emodin stimulation (6OF+E), the synergy was reduced with the only correlation of LPL and NO, indicating the regulation between fatty acid metabolism and antioxidant capacity were closely related to emodin stimulation.

3.5. Emodin Alleviates Inflammation, Autophagy and Apoptosis under Oxidative Stress

To uncover whether the metabolic and physiological alternation was related to immunity and cell fate determination, transcriptional expression of inflammation, autophagy, and apoptosis-related key genes were detected. Consistently, 6OF activated inflammatory response (IL-1β, IL-6, TNF-α, and NF-κB, Figure 5A–D), cellular autophagy (ATG3, ATG7, and Beclin1, Figure 5E–G), and apoptosis (Bax, Casp3, Casp8, AIF1, and CytoC, Figure 5H–L). Simultaneously, emodin (6OF+E) alleviates the expression of these genes (Figure 5A–L), and reveals emodin exerts protective effects on inflammation and cellular homeostasis under oxidative stress. Moreover, correlation analysis (shown in Figure S2) reveal inflammation factor IL-1β was associated with apoptosis factor Bax and AIF1 in 6OF; inflammation and autophagy correlation were vanished in 6OF and 6OF+E; while apoptosis and autophagy correlation were activated in 6OF (Casp9-ATG7) and 6OF+E (Casp8-ATG3,

Casp8-ATG7). These data indicate the crosstalk and dynamic equilibrium between apoptosis and autophagy determines the cell fate under oxidative stress amelioration.

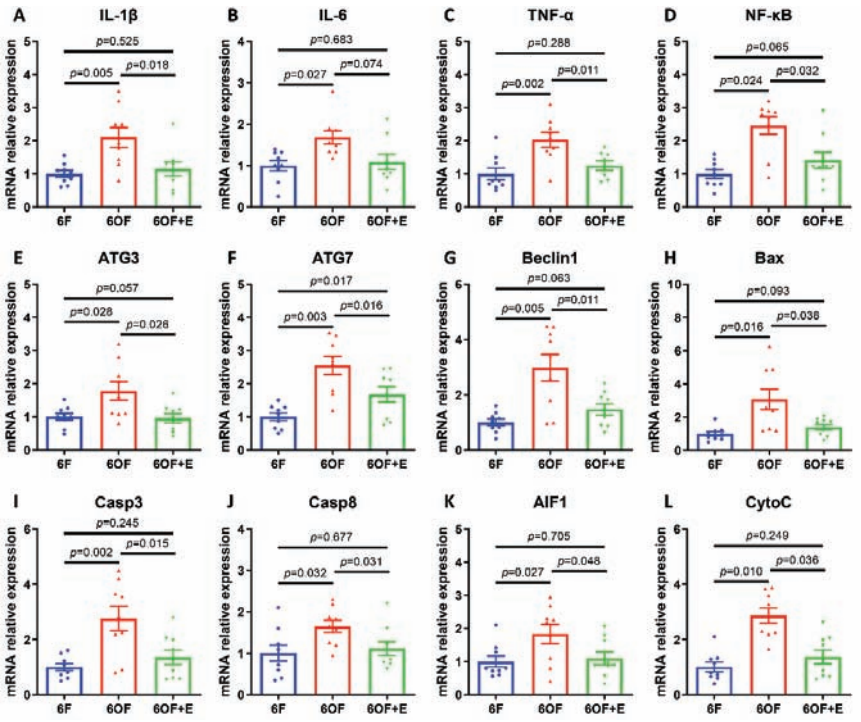

Figure 5. Emodin alleviates inflammation, autophagy, and apoptosis under oxidative stress in the liver of *M. amblycephala.* Transcriptional expression of inflammation-related (**A**–**D**), autophagy-related (**E**–**G**), and apoptosis-related (**H**–**L**) genes. (**A**), Interleukin 1 beta, (IL-1β); (**B**), interleukin 6 (IL-6); (**C**), tumor necrosis factor alpha (TNF-α); (**D**), nuclear factor kappa B (NF-κB); (**E**), autophagy-related 3 (ATG3); (**F**), autophagy-related 7 (ATG7); (**G**), Beclin1; (**H**), BCL2-Associated X (Bax); (**I**), caspase 3 (Casp3); (**J**), caspase 8 (Casp8); (**K**), apoptosis inducing factor 1 (AIF1); (**L**), cytochrome complex (CytoC). Data were analyzed by Students' *t*-test, results were indicated as mean ± SEM, $n = 9$.

3.6. Notch-Nrf2 Crosstalk Was Active to Oxidative Stress Amelioration in the Liver of M. amblycephala

According to our previous study, Notch and Nrf2 signaling function importantly in the antioxidant regulation in the intestine. In the present study, we found Notch signaling (Figure 6A) and Nrf2 signaling (Figure 6B) were all positively activated under oxidative stress (6OF), while were all restored to the control level with the administration of emodin (6OF+E). With Pearson analysis, Notch and Nrf2 signaling was confirmed to be synthetically regulated under quiescent condition (6F, Figure 6C). However, the expression of key elements in Notch and Nrf2 signaling exhibited no significant correlation under oxidative stress (6OF), indicating the crosstalk was terminated (Figure 6C). Dietary supplement with emodin (6OF+E) recovered the crosstalk, evidenced by the correlation between Jag1b-NQO1 and Hey2-Keap1 (Figure 6C).

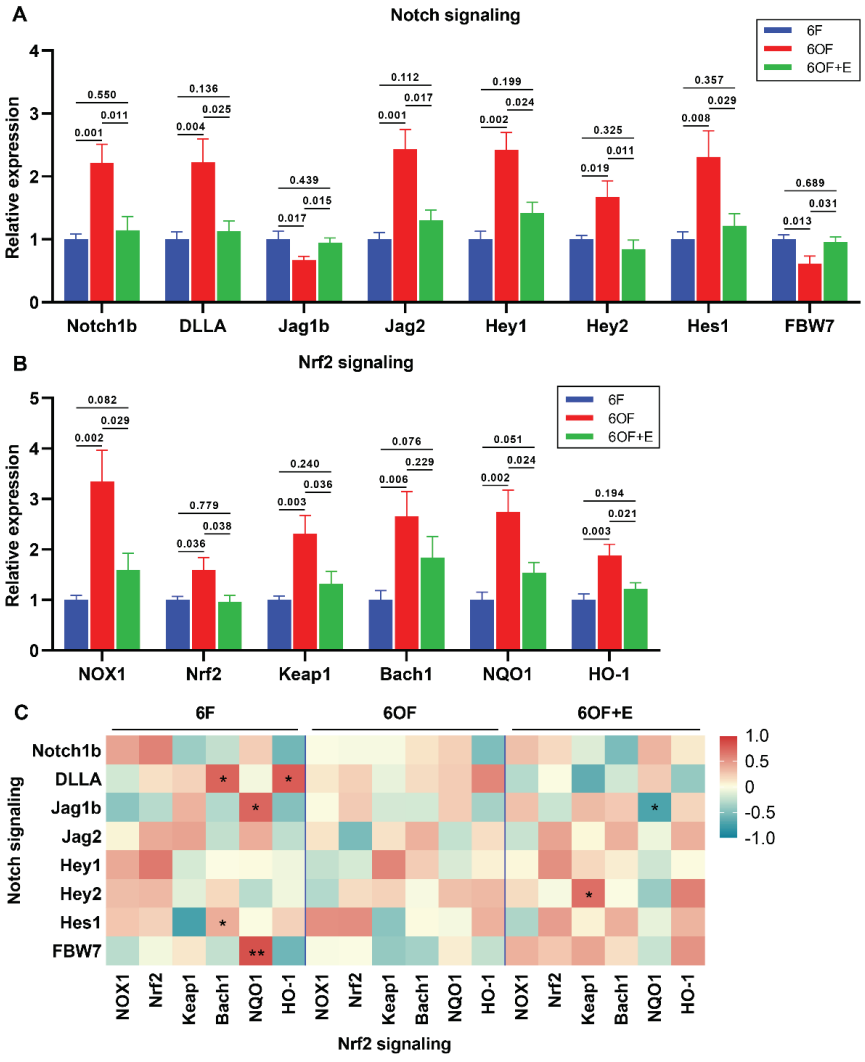

Figure 6. Notch-Nrf2 crosstalk was active to oxidative stress amelioration in the liver of *M. amblycephala*. (**A**,**B**), Transcriptional expression of key related genes under oxidative stress and emodin stimulation. (**A**), Notch signaling, Notch1b, Delta like A (DLLA), Jagged 1 beta (Jag1b), Jagged 2 (Jag2), Hairy/Enhancer of split related with YRPW motif 1 (Hey1), Hairy/Enhancer of split related with YRPW motif 2 (Hey2), hairy and enhancer of split-1 (Hes1), F-box and WD repeat domain-containing 7 (FBW7); (**B**), Nrf2 signaling, NADPH oxidase 1 (NOX1), Nuclear factor erythroid 2–related factor 2 (Nrf2), Kelch-like ECH-associated protein 1 (Keap1), BTB Domain and CNC Homolog 1 (Bach1), NAD(P)H quinone dehydrogenase 1 (NQO1), Heme oxygenase 1 (HO-1); (**C**), correlation analysis between Notch and Nrf2 signaling was retrieved from Pearson analysis. In (**C**), * represents $p < 0.05$, and ** represents $p < 0.01$. Data were analyzed by Students' *t*-test, results were indicated as mean ± SEM, $n = 9$.

3.7. Hypothetical Regulation of Notch-Nrf2 Crosstalk on Oxidative Stress Amelioration

Based on the above results, we raise the hypothetical regulation schematic of Notch-Nrf2 crosstalk under oxidative stress amelioration (Figure 7). Oxidative stress-induced ROS activates Notch1b signaling and subsequently activates Nrf2 signaling, evidenced by the

crosstalk between Notch ligands and down-stream modulators with Nrf2 key elements. Activated crosstalk of Notch-Nrf2 increased apoptosis and autophagy in the liver, which facilitates the cells to resist oxidative stress. Exhilaratingly, dietary emodin inhibited Notch-Nrf2 crosstalk to ameliorate apoptosis and autophagy, thereby alleviating oxidative stress.

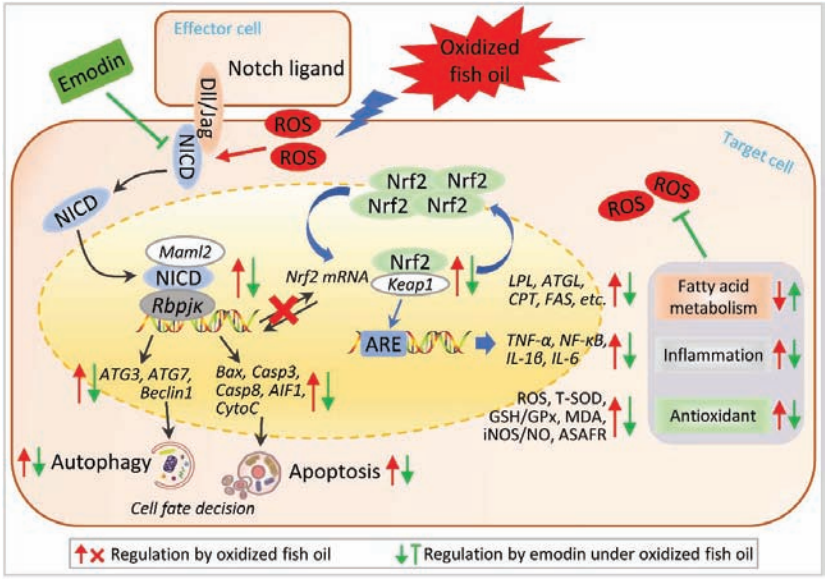

Figure 7. Hypothetical regulation of Notch-Nrf2 crosstalk on oxidative stress amelioration. Hypothetical regulation of Notch-Nrf2 crosstalk was raised based on the results in this study. Arrows in red color represent the regulation by oxidized fish oil, in blue color represent the regulation by emodin under oxidized fish oil. "×" represents oxidized fish oil blocks the co-regulation between Notch and Nrf2 signaling.

4. Discussion

Fish oil is enriched with HUFAs that could dominantly promote the growth of fish. However, fish oil is prone to oxidative rancidity, and oxidated diet is one of the most important exogenous factors leading to oxidative stress on fish [19]. Oxidative stress control and prevention have become a critical issue for aquatic animals [8]. In aquatic animals, unavoidable oxidation of dietary lipids could induce lipid peroxidation, which increases ROS production during cellular metabolism [19]. Our previous study indicates dietary oxidized lipids-induced ROS production exceeded the ability to quench the reactive species in the intestine, thereby impaired the cellular structural integrity, suppressed the immunity and antioxidant capacity of the intestine, and eventually inhibited the growth performance of *M. amblycephala* [1,17,19]. However, as the crucial organ for metabolism, immunity and antioxidant resistance, the role and underlying mechanism of liver in resisting dietary oxidized lipids remains unclear in *M. amblycephala*.

As aquatic animals contain high amounts of lipids with polyunsaturated fatty acid residues that is the substrate for oxidation, oxidative stress could induce lipid peroxidation thereby disrupting the lipid metabolism. Generally, due to the high damaging capacity and biological activity, the cellular metabolism of ROS is under fine control in quiescent conditions. However, when steady-state ROS concentration is transiently or chronically enhanced, excessive accumulation of ROS could damage cellular constituents, and disrupt metabolic and antioxidant capacity [20]. In the present study, elevated ROS reveal dietary oxidized fish oil-induced oxidative stress in *M. amblycephala* liver. Meanwhile, as the end

product of lipid peroxidation, MDA concentration was increased under 6OF, indicating dietary oxidized fish oil-induced lipid peroxidation in the liver of *M. amblycephala*.

Morphologically, cellular integrity is vital for the function of liver cells [21]. Nucleus is the control center of the cell that contains most of the genomic DNA and all of the chromosome, it maintains the integrity of genes and controls the activities of the cell by regulating gene expression [22]. Mitochondrion is the dominant organelle to produce energy through respiration that is critical for any metabolism and cellular activity [23]. Lipid droplets are lipid-rich cellular organelles to regulate the storage and hydrolysis of neutral lipids, they play a very important role in the regulation of intracellular lipid storage and lipid metabolism. Meanwhile, lipid droplets include a close association to inflammatory responses [24], lipotoxicity protection [25], as well as a platform for protein binding and degradation [26]. In the present study, TEM reveals oxidative stress-induced nucleus aggression, thereby impairing the cell fate evidenced by apoptosis and autophagy-related gene expression, indicating the metabolic disorder and cell fate determinate dysregulation in the liver.

Glucose is regarded as the major substrate for animals, and amino acids and fatty acids are also intermediates of the metabolic pathway to drive energy production [27]. Meanwhile, evidence indicate that glycolytic metabolism closely interacts with fatty acid and amino acid metabolic profiles to maintain normal cellular function, homeostasis, as well as cell fate determination [27]. It is clear that long-term administration of oxidized fish oil could induce lipid deposition in the liver [28]. In this study, oxidized fish oil led to lipid deposition in the liver, as evidenced by lipid droplets enlargement and accumulation. Similar results were also found in channel catfish [29], yellow catfish [30], loach [31], and largemouth bass [32]. In the study of channel catfish, lipid deposition in the liver induced by oxidized fish oil was originated from activated lipid synthesis [29]. However, lipid synthesis and lipolysis were both inhibited under oxidative stress in our present study, which was supported by decreased lipase, LPL, TG, TC, and FAS activity, as well as decreased lipid metabolic related gene expression of LPL, ATGL, CPT1, CPT2, COX2, FAS, and SREBP1. This contrasting result reveals there might have different regulatory mechanisms among different fishes under oxidative stress, or the regulatory mechanism was specific to different oxidative stress levels. Therefore, we suppose the oxidative stress was too severe to maintain lipid synthesis and lipolysis, thereby results in lipid deposition and inhibited lipid metabolism in our study. However, the underlying mechanism needs further investigation. Additionally, glycolytic and amino acid metabolism were also inhibited under oxidized fish oil and restored by emodin, indicating that nutrient metabolisms are closely associated with each other, and the regulation of the metabolic pathway could be important in oxidative stress resistance.

Cholesterol is a sterol type of lipid that serves as an essential structural component of animal cell membranes and a precursor for the biosynthesis of steroid hormones, bile acid, and vitamin D. Early research identifies cholesterol itself as an antioxidant that protects cells from free radical damage [33]. Interestingly, cholesterol was significantly reduced under oxidative stress in our present study. Mechanically, cholesterol was mainly synthesized from dietary lipid with fatty acid metabolism [34]. From this point of view, if the dietary lipid was oxidized to induce peroxidation for the organism, the synthesis of cholesterol will be unavoidably dysregulated. Consistently, reports indicate that oxidative damage could deplete cholesterol and disrupt cell membrane function [35,36]. Meanwhile, peroxidation-induced cellular structural impairment might be another factor to reduce cholesterol level in the liver. Additionally, it is clear that emodin could reduce cholesterol level [37,38]. In our study, cholesterol in 6OF+E was reduced in comparison with 6F, indicating ameliorative effects of emodin on oxidative stress.

Impaired lipid metabolism was reported to interact with immunity and antioxidant dysregulation [39]. iNOS-derived NO signaling plays a central role in inflammatory regulation and hepatic protection [40]. Meanwhile, interferon system was reported to induce iNOS via activating NF-κB [41]. In the present study, NF-κB, IL-1β, and IL-6 expression was

activated and iNOS content was increased under oxidized fish oil stimulation, indicating the immune system was activated, which was in accordance with that in zebrafish [42]. Antioxidant system functions importantly to remove the excessive ROS and ASAFR formation, and SOD and GPx are vital to decrease hydrogen peroxide in this process [43,44]. The present study shows that oxidized fish oil markedly increased T-SOD, GPx, and ASAFR activity, as well as ROS and MDA levels, indicating antioxidant system was activated in the liver of *M. amblycephala*. Similar studies also confirmed that oxidized fish oil dysregulates antioxidant capacity in channel fish [29] and tilapia [45].

Recent advances in physiological relevance reveal ROS acts as an important signaling molecule as well as a critical factor in cell fate determination [27]. Previous evidence suggests that ROS acts as signaling mediators linking between metabolic alteration and cell fate, such as cell cycle progression, apoptosis, and autophagy [46]. In this study, autophagy and apoptosis-related genes were all activated under oxidized fish oil stimulation, indicating prolonged oxidative stress results in apoptosis and autophagy.

Our previous reports reveal cell fate determination-related apoptosis and autophagy were closely related to Nrf2 and Notch signaling [1,17], which inspired us to uncover the relationship between apoptosis-autophagy and Nrf2-Notch signaling. Activation of Nrf2-ARE pathway protects cells from oxidative stress-induced cell death [47]. Notch signaling plays an important role in the process of cell fate determination, including cell growth, cell proliferation, and programmed death [48]. Through Notch-Nrf2 crosstalk studies, it has been clearly shown that NICD can activate the Nrf2 pathway and Nrf2 can inversely activate the Notch1 pathway in the liver [11]. Recent studies also indicate ARE is the upstream of the Notch1 major transcription start site. Furthermore, as the binding site of NICD, Rbpjκ is conserved on the promoters of Nrf2 among animal species [49]. Notch1 is one of the transmembrane Notch family receptors that drive Notch signaling, together with the Rbpjκ transcription factor [50]. Therefore, the crosstalk between Nrf2 and Notch signaling has been shown to enhance cyto-protection and maintenance of cellular homeostasis under oxidative stress, rather than as a simple on-off switch [51]. In our present study, oxidized fish oil robustly activated Nrf2 and Notch signaling, and induced aberrant Nrf2-Notch crosstalk by molecular impairment of related key genes. Under emodin stimulation, Nrf2 and Notch signaling was ameliorated and the crosstalk was restored, indicating the inhibition of Nrf2 and Notch signaling, as well as the promotion of Nrf2-Notch crosstalk plays a key role in liver development and in maintenance of hepatic function under oxidative stress. In accordance with our finding, Notch1-Nrf2 crosstalk exerts cellular protection by reducing the formation of ROS [52], promoting apoptosis and aggravating tight joint or oxidative damage [53]. Additionally, Notch or Nrf2 inhibition has been well used as a therapeutic target in the treatment of oxidative stress with different bioactive compounds, such as emodin [17], quercetin [54], and chlorogenic acid isomers [55] on Nrf2; as well as emodin [1], dibenzazepine [12], melatonin [56], and niclosamide [57] on Notch. We speculate that the ROS-Notch-Nrf2 pathway is a conserved pathway that is designed to allow cells to respond to changes in environmental levels of ROS. However, there are limited reports illustrating the breakdown of Nrf2-Notch crosstalk under oxidative stress. Presumably, a system for downregulation of this crosstalk should exist for the homeostasis maintenance, perhaps target gene products of each signaling contribute to a negative feedback mechanism for Notch and/or Nrf2 signaling regulation; the detailed mechanism requires further investigation. Our findings reveal, to our knowledge, the first observation of ROS activation and Notch-Nrf2 signaling in response to oxidative stress amelioration of *M. amblycephala*. Additionally, our study is supported by the previous report of Nrf2-Notch interaction in total liver cells [58].

To combat the adverse effects of external stress, especially the oxidative stress that could induce cellular lipid peroxidation, homeostasis imbalance, immune or antioxidant breakdown and even death, dietary implementation with functional additives has become an effective approach for stress control and prevention in aquatic animals [59]. For the characterized advantages of minor side effects and drug resistance, the medical herb

extract emodin has been widely used in clinical trial for humans and aquaculture [59]. In consistent with our previous results that emodin protects the intestine from oxidative stress impairment [1,17,18], we demonstrate emodin alleviates morphological impairment, fatty acid metabolic disorder, antioxidant disorder, and cell fate determination by targeting Notch-Nrf2 crosstalk in the liver of *M. amblycephala*. Similar functional effects of emodin was also reported in other animals [60–63].

Taken together, our study emphasizes that the loss of normal ROS-Notch-Nrf2 cellular homeostatic mechanism was associated with excessive autophagy, apoptosis, and metabolic disorder in the liver. Meanwhile, our data demonstrate a vital homeostatic mechanism that emodin prevents excessive stress injury of liver cells and allows them to respond to injury and cellular repair.

5. Conclusions

In conclusion, dietary oxidized lipid induced oxidative stress and dysregulated lipid metabolism in the liver of *M. amblycephala*. Singular activation of Nrf2 and Notch signaling, interrupted Nrf2/Notch1 crosstalk, as well as apoptosis and autophagy were involved in the regulation. Furthermore, the therapeutic Nrf2-Notch crosstalk targeting holds great promise for the treatment of oxidative stress in aquatic animals, which could promote the application of emodin from scientific research into aquaculture practice.

Supplementary Materials: The following supporting information can be downloaded at: https://www.mdpi.com/article/10.3390/antiox11061179/s1, Figure S1: Interaction analysis between fatty acid metabolism and antioxidant capacity; Figure S2: Interaction analysis among inflammation, apoptosis, and autophagy.

Author Contributions: C.S., conceptualization, methodology, validation, investigation, writing—review and editing; B.L. (Bo Liu, liubo@njau.edu.cn), validation, investigation, and data curation; H.L., formal analysis and validation; Y.T., software and formal analysis; X.G., resources; B.L. (Bo Liu, liub@ffrc.cn), methodology, writing—review and editing, supervision and funding acquisition; P.X., supervision and project administration. All authors have read and agreed to the published version of the manuscript.

Funding: This work was supported by the National Natural Science Foundation of China (32172990); the Project of National Key R&D Program of China (2019YFD0900200); the Central Public-interest Scientific Institution Basal Research Fund, CAFS (2020TD59); and the Modern Agriculture Industrial Technology System of MOF and MARA (CARS-45).

Institutional Review Board Statement: This study was approved by the Animal Care and Use Committee of Nanjing Agri-cultural University (Nanjing, China; protocol code: WXFC 2017-0006, approved 27 May 2017). All animal procedures were carried out in accordance with the China Laboratory Animal Care and Use Guidelines. The ethics in this experiment is the same as the ethics previously published [19].

Informed Consent Statement: Not applicable.

Data Availability Statement: Data is contained within the article.

Acknowledgments: The authors would like to express sincere thanks to the personnel of Freshwater Fisheries Research Center, Chinese Academy of Fishery Sciences for their kind assistance.

Conflicts of Interest: The authors declare no conflict of interest.

References

1. Song, C.; Liu, B.; Ge, X.; Li, H.; Xu, P. miR-34a/Notch1b Mediated Autophagy and Apoptosis Contributes to Oxidative Stress Amelioration by Emodin in the Intestine of Teleost *Megalobrama amblycephala*. *Aquaculture* **2022**, *547*, 737441. [CrossRef]
2. Ghosh, N.; Das, A.; Chaffee, S.; Roy, S.; Sen, C.K. Reactive Oxygen Species, Oxidative Damage and Cell Death. In *Immunity and Inflammation in Health and Disease: Emerging Roles of Nutraceuticals and Functional Foods in Immune Support*; Academic Press: Cambridge, MA, USA, 2017; pp. 45–55, ISBN 9780128054178.
3. Wu, G. Nutrition and Metabolism: Foundations for Animal Growth, Development, Reproduction, and Health. In *Advances in Experimental Medicine and Biology*; Springer: Cham, Switzerland, 2022; Volume 1354, pp. 1–24.

4. Galluccio, E.; Spadoni, S.; Fontana, B.; Bosi, E.; Piatti, P.; Monti, L.D. Long Lasting Protective Effects of Early L-Arginine Treatment on Endothelium in an in Vitro Study. *Clin. Nutr.* **2021**, *40*, 1519–1529. [CrossRef] [PubMed]
5. Chowdhury, S.; Saikia, S.K. Oxidative Stress in Fish: A Review. *J. Sci. Res.* **2020**, *12*, 145–160. [CrossRef]
6. Corsetto, P.A.; Cremona, A.; Montorfano, G.; Jovenitti, I.E.; Orsini, F.; Arosio, P.; Rizzo, A.M. Chemical-Physical Changes in Cell Membrane Microdomains of Breast Cancer Cells After Omega-3 PUFA Incorporation. *Cell Biochem. Biophys.* **2012**, *64*, 45–59. [CrossRef] [PubMed]
7. Lushchak, V.I. Free Radicals, Reactive Oxygen Species, Oxidative Stress and Its Classification. *Chem. Biol. Interact.* **2014**, *224*, 164–175. [CrossRef]
8. Lushchak, V.I. Environmentally Induced Oxidative Stress in Aquatic Animals. *Aquat. Toxicol.* **2011**, *101*, 13–30. [CrossRef]
9. He, F.; Ru, X.; Wen, T. NRF2, a Transcription Factor for Stress Response and beyond. *Int. J. Mol. Sci.* **2020**, *21*, 4777. [CrossRef]
10. Paul, M.K.; Bisht, B.; Darmawan, D.O.; Chiou, R.; Ha, V.L.; Wallace, W.D.; Chon, A.T.; Hegab, A.E.; Grogan, T.; Elashoff, D.A.; et al. Dynamic Changes in Intracellular ROS Levels Regulate Airway Basal Stem Cell Homeostasis through Nrf2-Dependent Notch Signaling. *Cell Stem Cell* **2014**, *15*, 199–214. [CrossRef]
11. Wakabayashi, N.; Chartoumpekis, D.V.; Kensler, T.W. Crosstalk between Nrf2 and Notch Signaling. *Free Radic. Biol. Med.* **2015**, *88*, 158–167. [CrossRef]
12. Ahmed, L.A.; Abd El-Rhman, R.H.; Gad, A.M.; Hassaneen, S.K.; El-Yamany, M.F. Dibenzazepine Combats Acute Liver Injury in Rats via Amendments of Notch Signaling and Activation of Autophagy. *Naunyn Schmiedebergs Arch. Pharmacol.* **2021**, *394*, 337–348. [CrossRef]
13. Dai, X.; Yan, X.; Wintergerst, K.A.; Cai, L.; Keller, B.B.; Tan, Y. Nrf2: Redox and Metabolic Regulator of Stem Cell State and Function. *Trends Mol. Med.* **2020**, *26*, 185–200. [CrossRef]
14. Hoseinifar, S.H.; Yousefi, S.; Van Doan, H.; Ashouri, G.; Gioacchini, G.; Maradonna, F.; Carnevali, O. Oxidative Stress and Antioxidant Defense in Fish: The Implications of Probiotic, Prebiotic, and Synbiotics. *Rev. Fish. Sci. Aquac.* **2020**, *29*, 198–217. [CrossRef]
15. Hsu, S.C.; Chung, J.G. Anticancer Potential of Emodin. *BioMedicine* **2012**, *2*, 108–116. [CrossRef] [PubMed]
16. Semwal, R.B.; Semwal, D.K.; Combrinck, S.; Viljoen, A. Emodin—A Natural Anthraquinone Derivative with Diverse Pharmacological Activities. *Phytochemistry* **2021**, *190*, 112854. [CrossRef] [PubMed]
17. Song, C.; Liu, B.; Xu, P.; Ge, X.; Zhang, H. Emodin Ameliorates Metabolic and Antioxidant Capacity Inhibited by Dietary Oxidized Fish Oil through PPARs and Nrf2-Keap1 Signaling in Wuchang Bream (*Megalobrama amblycephala*). *Fish Shellfish Immunol.* **2019**, *94*, 842–851. [CrossRef] [PubMed]
18. Song, C.; Liu, B.; Xu, P.; Ge, X.; Li, H.; Tang, Y.; Su, S. miR-144 Is the Epigenetic Target for Emodin to Ameliorate Oxidative Stress Induced by Dietary Oxidized Fish Oil via Nrf2 Signaling in Wuchang Bream, *Megalobrama amblycephala*. *Aquaculture* **2021**, *534*, 736357. [CrossRef]
19. Song, C.; Liu, B.; Xu, P.; Xie, J.; Ge, X.; Zhou, Q.; Sun, C.; Zhang, H.; Shan, F.; Yang, Z. Oxidized Fish Oil Injury Stress in *Megalobrama amblycephala*: Evaluated by Growth, Intestinal Physiology, and Transcriptome-Based PI3K-Akt/NF-κB/TCR Inflammatory Signaling. *Fish Shellfish Immunol.* **2018**, *81*, 446–455. [CrossRef]
20. Birnie-Gauvin, K.; Costantini, D.; Cooke, S.J.; Willmore, W.G. A Comparative and Evolutionary Approach to Oxidative Stress in Fish: A Review. *Fish Fish.* **2017**, *18*, 928–942. [CrossRef]
21. Tanabe, M.; Tamura, H.; Taketani, T.; Okada, M.; Lee, L.; Tamura, I.; Maekawa, R.; Asada, H.; Yamagata, Y.; Sugino, N. Melatonin Protects the Integrity of Granulosa Cells by Reducing Oxidative Stress in Nuclei, Mitochondria, and Plasma Membranes in Mice. *J. Reprod. Dev.* **2015**, *61*, 35–41. [CrossRef]
22. Shen, W.H.; Balajee, A.S.; Wang, J.; Wu, H.; Eng, C.; Pandolfi, P.P.; Yin, Y. Essential Role for Nuclear PTEN in Maintaining Chromosomal Integrity. *Cell* **2007**, *128*, 157–170. [CrossRef]
23. Vakifahmetoglu-Norberg, H.; Ouchida, A.T.; Norberg, E. The Role of Mitochondria in Metabolism and Cell Death. *Biochem. Biophys. Res. Commun.* **2017**, *482*, 426–431. [CrossRef] [PubMed]
24. Melo, R.C.N.; Dvorak, A.M. Lipid Body-Phagosome Interaction in Macrophages during Infectious Diseases: Host Defense or Pathogen Survival Strategy? *PLoS Pathog.* **2012**, *8*, 6. [CrossRef] [PubMed]
25. Bosma, M.; Kersten, S.; Hesselink, M.K.C.; Schrauwen, P. Re-Evaluating Lipotoxic Triggers in Skeletal Muscle: Relating Intramyocellular Lipid Metabolism to Insulin Sensitivity. *Prog. Lipid Res.* **2012**, *51*, 36–49. [CrossRef]
26. Welte, M.A. Proteins under New Management: Lipid Droplets Deliver. *Trends Cell Biol.* **2007**, *17*, 363–369. [CrossRef] [PubMed]
27. Ryu, J.M.; Lee, H.J.; Jung, Y.H.; Lee, K.H.; Kim, D.I.; Kim, J.Y.; Ko, S.H.; Choi, G.E.; Chai, I.I.; Song, E.J.; et al. Regulation of Stem Cell Fate by ROS-Mediated Alteration of Metabolism. *Int. J. Stem Cells* **2015**, *8*, 24–35. [CrossRef]
28. Tsuduki, T.; Honma, T.; Nakagawa, K.; Ikeda, I.; Miyazawa, T. Long-Term Intake of Fish Oil Increases Oxidative Stress and Decreases Lifespan in Senescence-Accelerated Mice. *Nutrition* **2011**, *27*, 334–337. [CrossRef] [PubMed]
29. Shi, Y.; Hu, Y.; Wang, Z.; Zhou, J.; Zhang, J.; Zhong, H.; Fu, G.; Zhong, L. The Protective Effect of Taurine on Oxidized Fish-Oil-Induced Liver Oxidative Stress and Intestinal Barrier-Function Impairment in Juvenile Ictalurus Punctatus. *Antioxidants* **2021**, *10*, 1690. [CrossRef]
30. Zhang, D.G.; Zhao, T.; Hogstrand, C.; Ye, H.M.; Xu, X.J.; Luo, Z. Oxidized Fish Oils Increased Lipid Deposition via Oxidative Stress-Mediated Mitochondrial Dysfunction and the CREB1-Bcl2-Beclin1 Pathway in the Liver Tissues and Hepatocytes of Yellow Catfish. *Food Chem.* **2021**, *360*, 129814. [CrossRef]

31. Zhang, Y.; Li, Y.; Liang, X.; Cao, X.; Huang, L.; Yan, J.; Wei, Y.; Gao, J. Hepatic Transcriptome Analysis and Identification of Differentially Expressed Genes Response to Dietary Oxidized Fish Oil in Loach Misgurnus Anguillicaudatus. *PLoS ONE* **2017**, *12*, e0172386. [CrossRef]
32. Xie, S.; Yin, P.; Tian, L.; Liu, Y.; Niu, J. Lipid Metabolism and Plasma Metabolomics of Juvenile Largemouth Bass Micropterus Salmoides Were Affected by Dietary Oxidized Fish Oil. *Aquaculture* **2020**, *522*, 735158. [CrossRef]
33. van Rensburg, S.J.; Daniels, W.M.U.; van Zyl, J.M.; Taljaard, J.J.F. A Comparative Study of the Effects of Cholesterol, Beta-Sitosterol, Beta-Sitosterol Glucoside, Dehydroepiandrosterone Sulphate and Melatonin on in Vitro Lipid Peroxidation. *Metab. Brain Dis.* **2000**, *15*, 257–265. [CrossRef] [PubMed]
34. Gibbons, G.F. Regulation of Fatty Acid and Cholesterol Synthesis: Co-Operation or Competition? *Prog. Lipid Res.* **2003**, *42*, 479–497. [CrossRef]
35. Jacob, R.F.; Mason, R.P. Lipid Peroxidation Induces Cholesterol Domain Formation in Model Membranes. *J. Biol. Chem.* **2005**, *280*, 39380–39387. [CrossRef]
36. Turkdogan, K.A.; Akpinar, O.; Karabacak, M.; Akpinar, H.; Turkdogan, F.T.; Karahan, O. Association between Oxidative Stress Index and Serum Lipid Levels in Healthy Young Adults. *J. Pak. Med. Assoc.* **2014**, *64*, 379–381. [PubMed]
37. Fu, X.; Xu, A.-G.; Yao, M.-Y.; Guo, L.; Zhao, L. Emodin Enhances Cholesterol Efflux by Activating Peroxisome Proliferator-Activated Receptor-γ in Oxidized Low Density Lipoprotein-Loaded THP1 Macrophages. *Clin. Exp. Pharmacol. Physiol.* **2014**, *41*, 679–684. [CrossRef]
38. Su, Z.-L.; Hang, P.-Z.; Hu, J.; Zheng, Y.-Y.; Sun, H.-Q.; Guo, J.; Liu, K.-Y.; Du, Z.-M. Aloe-Emodin Exerts Cholesterol-Lowering Effects by Inhibiting Proprotein Convertase Subtilisin/kexin Type 9 in Hyperlipidemic Rats. *Acta Pharmacol. Sin.* **2020**, *41*, 1085–1092. [CrossRef]
39. Manna, P.; Jain, S.K. Obesity, Oxidative Stress, Adipose Tissue Dysfunction, and the Associated Health Risks: Causes and Therapeutic Strategies. *Metab. Syndr. Relat. Disord.* **2015**, *13*, 423–444. [CrossRef]
40. Anavi, S.; Tirosh, O. iNOS as a Metabolic Enzyme under Stress Conditions. *Free Radic. Biol. Med.* **2020**, *146*, 16–35. [CrossRef]
41. Adams, V.; Nehrhoff, B.; Späte, U.; Linke, A.; Schulze, P.C.; Baur, A.; Gielen, S.; Hambrecht, R.; Schuler, G. Induction of iNOS Expression in Skeletal Muscle by IL-1β and NFκB Activation: An in Vitro and in Vivo Study. *Cardiovasc. Res.* **2002**, *54*, 95–104. [CrossRef]
42. Xu, H.; Yang, M.; Qiu, W.; Pan, C.; Wu, M. The Impact of Endocrine-Disrupting Chemicals on Oxidative Stress and Innate Immune Response in Zebrafish Embryos. *Environ. Toxicol. Chem.* **2013**, *32*, 1793–1799. [CrossRef]
43. Dinu, D.; Marinescu, D.; Munteanu, M.C.; Staicu, A.C.; Costache, M.; Dinischiotu, A. Modulatory Effects of Deltamethrin on Antioxidant Defense Mechanisms and Lipid Peroxidation in Carassius Auratus Gibelio Liver and Intestine. *Arch. Environ. Contam. Toxicol.* **2010**, *58*, 757–764. [CrossRef]
44. Ramalingam, M.; Kim, S.J. Reactive Oxygen/nitrogen Species and Their Functional Correlations in Neurodegenerative Diseases. *J. Neural Transm.* **2012**, *119*, 891–910. [CrossRef] [PubMed]
45. Yu, L.; Wen, H.; Jiang, M.; Wu, F.; Tian, J.; Lu, X.; Xiao, J.; Liu, W. Effects of Ferulic Acid on Growth Performance, Immunity and Antioxidant Status in Genetically Improved Farmed Tilapia (Oreochromis Niloticus) Fed Oxidized Fish Oil. *Aquac. Nutr.* **2020**, *26*, 1431–1442. [CrossRef]
46. Filomeni, G.; De Zio, D.; Cecconi, F. Oxidative Stress and Autophagy: The Clash between Damage and Metabolic Needs. *Cell Death Differ.* **2015**, *22*, 377–388. [CrossRef] [PubMed]
47. Johnson, J.A.; Johnson, D.A.; Kraft, A.D.; Calkins, M.J.; Jakel, R.J.; Vargas, M.R.; Chen, P.C. The Nrf2-ARE Pathway: An Indicator and Modulator of Oxidative Stress in Neurodegeneration. *Ann. New York Acad. Sci.* **2008**, *1147*, 61–69. [CrossRef]
48. Lai, E.C. Notch Signaling: Control of Cell Communication and Cell Fate. *Development* **2004**, *131*, 965–973. [CrossRef]
49. Wakabayashi, N.; Skoko, J.J.; Chartoumpekis, D.V.; Kimura, S.; Slocum, S.L.; Noda, K.; Palliyaguru, D.L.; Fujimuro, M.; Boley, P.A.; Tanaka, Y.; et al. Notch-Nrf2 Axis: Regulation of Nrf2 Gene Expression and Cytoprotection by Notch Signaling. *Mol. Cell. Biol.* **2014**, *34*, 653–663. [CrossRef]
50. Kojika, S.; Griffin, J.D. Notch Receptors and Hematopoiesis. *Exp. Hematol.* **2001**, *29*, 1041–1052. [CrossRef]
51. Sparaneo, A.; Fabrizio, F.P.; Muscarella, L.A. Nrf2 and Notch Signaling in Lung Cancer: Near the Crossroad. *Oxid. Med. Cell. Longev.* **2016**, *2016*, 7316492. [CrossRef]
52. Zhou, X.L.; Wu, X.; Zhu, R.R.; Xu, H.; Li, Y.Y.; Xu, Q.R.; Liu, S.; Lai, S.Q.; Xu, X.; Wan, L.; et al. Notch1–Nrf2 Signaling Crosstalk Provides Myocardial Protection by Reducing ROS Formation. *Biochem. Cell Biol.* **2020**, *98*, 106–111. [CrossRef]
53. Zhu, Y.; Wang, L.; Yu, X.; Jiang, S.; Wang, X.; Xing, Y.; Guo, S.; Liu, Y.; Liu, J. Cr(VI) Promotes Tight Joint and Oxidative Damage by Activating the Nrf2/ROS/Notch1 Axis. *Environ. Toxicol. Pharmacol.* **2021**, *85*, 103640. [CrossRef] [PubMed]
54. Ramyaa, P.; Padma, V.V. Ochratoxin-Induced Toxicity, Oxidative Stress and Apoptosis Ameliorated by Quercetin—Modulation by Nrf2. *Food Chem. Toxicol.* **2013**, *62*, 205–216. [CrossRef] [PubMed]
55. Liang, N.; Kitts, D.D. Amelioration of Oxidative Stress in Caco-2 Cells Treated with Pro-Inflammatory Proteins by Chlorogenic Acid Isomers via Activation of the Nrf2-Keap1-ARE-Signaling Pathway. *J. Agric. Food Chem.* **2018**, *66*, 11008–11017. [CrossRef]
56. Ren, B.C.; Zhang, W.; Zhang, W.; Ma, J.X.; Pei, F.; Li, B.Y. Melatonin Attenuates Aortic Oxidative Stress Injury and Apoptosis in STZ-Diabetes Rats by Notch1/Hes1 Pathway. *J. Steroid Biochem. Mol. Biol.* **2021**, *212*, 105948. [CrossRef]
57. Esmail, M.M.; Saeed, N.M.; Michel, H.E.; El-Naga, R.N. The Ameliorative Effect of Niclosamide on Bile Duct Ligation Induced Liver Fibrosis via Suppression of NOTCH and Wnt Pathways. *Toxicol. Lett.* **2021**, *347*, 23–35. [CrossRef] [PubMed]

58. Wakabayashi, N.; Shin, S.; Slocum, S.L.; Agoston, E.S.; Wakabayashi, J.; Kwak, M.K.; Misra, V.; Biswal, S.; Yamamoto, M.; Kensler, T.W. Regulation of Notch1 Signaling by Nrf2: Implications for Tissue Regeneration. *Sci. Signal.* **2010**, *3*, ra52. [CrossRef] [PubMed]
59. Tadese, D.A.; Song, C.; Sun, C.; Liu, B.; Liu, B.; Zhou, Q.; Xu, P.; Ge, X.; Liu, M.; Xu, X.; et al. The Role of Currently Used Medicinal Plants in Aquaculture and Their Action Mechanisms: A Review. *Rev. Aquac.* **2022**, *14*, 816–847. [CrossRef]
60. Wu, Y.; Tu, X.; Lin, G.; Xia, H.; Huang, H.; Wan, J.; Cheng, Z.; Liu, M.; Chen, G.; Zhang, H.; et al. Emodin-Mediated Protection from Acute Myocardial Infarction via Inhibition of Inflammation and Apoptosis in Local Ischemic Myocardium. *Life Sci.* **2007**, *81*, 1332–1338. [CrossRef]
61. Yu, Y.; Liu, H.; Yang, D.; He, F.; Yuan, Y.; Guo, J.; Hu, J.; Yu, J.; Yan, X.; Wang, S.; et al. Aloe-Emodin Attenuates Myocardial Infarction and Apoptosis via up-Regulating miR-133 Expression. *Pharmacol. Res.* **2019**, *146*, 104315. [CrossRef]
62. Park, S.Y.; Jin, M.L.; Ko, M.J.; Park, G.; Choi, Y.W. Anti-Neuroinflammatory Effect of Emodin in LPS-Stimulated Microglia: Involvement of AMPK/Nrf2 Activation. *Neurochem. Res.* **2016**, *41*, 2981–2992. [CrossRef]
63. Tian, S.L.; Yang, Y.; Liu, X.L.; Xu, Q.B. Emodin Attenuates Bleomycin-Induced Pulmonary Fibrosis via Anti-Inflammatory and Anti-Oxidative Activities in Rats. *Med. Sci. Monit.* **2018**, *24*, 1–10. [CrossRef] [PubMed]

antioxidants

MDPI

Article

Effects of Stocking Density on the Growth Performance, Physiological Parameters, Redox Status and Lipid Metabolism of *Micropterus salmoides* in Integrated Rice–Fish Farming Systems

Rui Jia [1,2,†], Long Wang [3,†], Yiran Hou [1], Wenrong Feng [1], Bing Li [1,*] and Jian Zhu [1,*]

[1] Key Laboratory of Integrated Rice–Fish Farming Ecology, Ministry of Agriculture and Rural Affairs, Freshwater Fisheries Research Center, Chinese Academy of Fishery Sciences, Wuxi 214081, China; jiar@ffrc.cn (R.J.); houyr@ffrc.cn (Y.H.); fengwenrong@ffrc.cn (W.F.)
[2] International Joint Research Laboratory for Fish Immunopharmacology, Freshwater Fisheries Research Center, Chinese Academy of Fishery Sciences, Wuxi 214081, China
[3] Wuxi Fisheries College, Nanjing Agricultural University, Wuxi 214081, China; 2020813069@stu.njau.edu.cn
* Correspondence: lib@ffrc.cn (B.L.); zhuj@ffrc.cn (J.Z.); Tel.: +86-85550535 (B.L.); +86-85550414 (J.Z.)
† These authors contributed equally to this work.

Abstract: Stocking density has been identified as one of the main factors affecting fish growth, welfare and behavior. However, few studies have focused on the effects of stocking density on fish health in integrated rice–fish farming systems. Thus, the aim of this study was to evaluate the effects of different stocking densities on the growth performance, physiological parameters, redox status and lipid metabolism of *Micropterus salmoides* in an integrated rice–fish farming system. The fish were reared at three densities: low density (LD, 40 g/m^3), medium density (MD, 80 g/m^3) and high density (HD, 120 g/m^3) for 90 days. At the end of the experiment, fish reared in the MD and HD groups showed lower growth performance than those from the LD group. The HD treatment significantly altered the physiological parameters, including glucose and lactate. Meanwhile, the HD treatment induced oxidative stress and lipid peroxidation after 90 days of farming. Furthermore, transcriptomic analysis revealed that HD treatment led to abnormal lipid metabolism. Interestingly, we found the suppression of three key pathways related to lipid metabolism, including the PPAR, insulin and adipocytokine signaling pathways, in the HD group. Overall, our data indicated that the HD treatment inhibited growth and caused physiological responses, oxidative stress and abnormal hepatic lipid metabolism in *M. salmoides* in an integrated rice–fish farming system.

Keywords: oxidative stress; physiological stress response; transcriptome; PPAR signaling pathway

Citation: Jia, R.; Wang, L.; Hou, Y.; Feng, W.; Li, B.; Zhu, J. Effects of Stocking Density on the Growth Performance, Physiological Parameters, Redox Status and Lipid Metabolism of *Micropterus salmoides* in Integrated Rice–Fish Farming Systems. *Antioxidants* **2022**, *11*, 1215. https://doi.org/10.3390/antiox11071215

Academic Editor: Stanley Omaye

Received: 18 May 2022
Accepted: 20 June 2022
Published: 21 June 2022

1. Introduction

Integrated rice–fish farming is an environmentally friendly agriculture model developed from traditional fish culture in paddies due to its environmental sustainability and food productivity [1]. In China, it is expanding rapidly and has become one of the major food production approaches, having an area of 1,793,409 ha and aquatic production of 3254 thousand tons in 2020 [2]. Integrated rice–fish farming is also considered as an ecosystem-based approach which can achieve the complementary utilization of wetland, arable land, freshwater and aquatic living resources [3]. In the system, the rice field provides potential food for fish (crab or shrimp) such as benthos, phytoplankton and zooplankton, while fish (crab or shrimp) feces can be absorbed into the soil as fertilizer [4]. Moreover, the biomass of weeds and planthoppers are effectively reduced in rice fields because of the consumption of aquatic plants, pests and insects by the farmed animals [5]. Rice–fish co-culture also alters the diversity and biomass of phytoplankton and zooplankton in the system. Phytoplankton communities and protozoan numbers are increased in rice–fish systems due to the higher availability of nutrients through fish

defecation and perturbation [6]; zooplankton and benthic invertebrates are decreased due to their utilization as food by fish in the system [7]. Furthermore, ecosystem service analyses have indicated that the value of rice–fish farming is 38% greater than that of rice monoculture [8]. Thus integrated rice–fish farming may be a sustainable alternative to rice monoculture by increasing food production, improving economic benefit and reducing environmental impact [3,9]. However, its broad practice may be limited by some existing problem, such as water management, technical and institutional constraints, adequate farming density and so on [10,11].

Stocking density has been identified as one of the main factors affecting fish growth, welfare and behavior [12]. In commercial aquaculture, the optimum stocking density of fish is set according to their physiological and biological characteristics, and the economic benefit of the farm. Numerous studies have reported that higher stocking densities inhibited the growth performance of many farmed fish, such as *Scophthalmus maximus*, *Oreochromis niloticus* and *Salmo salar* [13–15]. High stocking density is also considered to be a stress factor which may cause a negative change in physiological and biochemical parameters, reduce immunological function and increase the risk of disease outbreaks in fish [16–18]. Furthermore, a high stocking density induced oxidative stress and oxidative damage in fish [19,20]. In integrated rice–fish farming systems, the effects of stoking density on productivity, soil fertility and the environment have primarily been assessed [21]; for example, Vongvichith et al. (2018) reported that stocking density was a primary factor of fish productivity, and productivity was reduced at a higher stocking density [22]. Li et al. (2007) found that the specific growth rate (SGR) and survival rate (SR) of *Eriocheir sinensis* were significantly lower at the higher stocking density in a rice–crab co-culture system [23]. However, few studies have currently been performed on the physiological, biochemical and molecular variations of aquatic animals under different stocking densities in integrated rice–fish farming systems.

The largemouth bass (*Micropterus salmoides*) has been extensively cultured in China since its introduction in the 1980s and has become an important freshwater farmed species with a production of 619,519 tons in 2020 [24]. Pond culture is the main production method for largemouth bass [25]. In addition, it is raised in recirculating aquaculture systems and in-pond raceway systems [26,27]. The amenable stocking density of largemouth bass is different in different farming models, such as at least 0.15 kg/m^3 in ponds (12 months of farming), 6.85 kg/m^3 in land-based recirculating aquaculture systems (90 days of farming) and 4.2 kg/m^3 in in-pond raceway systems (150 days of farming) [28–30]. The adverse effects of a high stocking density on growth performance, biochemical parameters and immune response have been frequently reported in largemouth bass under various farming models [27,28]. In recent years, rice–largemouth bass co-culture, as a new farming model, has been attempted in China and has obtained a positive economic benefit [31,32]. However, the optimum stocking density of largemouth bass is still unclear, and the effects of high stocking density on growth performance, physiological response and molecular function have not been reported in this system.

In the current investigation, we aimed to evaluate the effects of stocking density on the growth performance, physiological parameters, redox status and hepatic lipid metabolism of largemouth bass in an integrated rice–fish farming system. For this purpose, the fish were raised in an integrated rice–fish farming system at three densities for 90 days. We then measured the growth performance, physiological blood parameters, antioxidant status and hepatic transcriptome. The data will provide a reference for largemouth bass farming and optimization of the rice–fish farming model.

2. Materials and Methods

2.1. Rice–Fish Farming System, Experimental Design and Sampling

The study was carried out at the experimental base of the Freshwater Fisheries Research Center (32°08′ N, 120°19′ E) belonging to a subtropical monsoon climate with an annual rainfall of 1078 mm and a mean temperature of 16–20 °C. The rice–fish farming system includes a rice planting area (1624 m^2) and a fish stocking area (0.8 m in depth, 176 m^2) (Figure S1). In the system, rice seedlings (Nangeng 5055) were transplanted in the middle of June 2021, and the rice was finally harvested in early November; the fish fingerlings were stocked on 30 July and harvested on 30 October. The management of the paddy field was performed according to the local conventional agricultural practices [33,34]. In addition to rice and fish, the rice–fish farming system contains a wide variety of other organisms, including phytoplankton, zooplankton and microorganisms. The phytoplankton (>70%) mainly include Chlorophyta, Cyanophyta and Bacillariophyta; the zooplankton (>80%) mainly consist of Rotifera, Cladocera and Protozoa; the dominant phyla of microorganisms (>75%) are Proteobacteria, Actinobacteria and Bacteroidetes.

In the experiment, three stocking densities of largemouth bass were set: low stocking density (LD, 40 g/m^3), medium stocking density (MD, 80 g/m^3) and high stocking density (HD, 120 g/m^3), and each density included three replicates. The average initial weight of the fish was 40.63 ± 0.13 g/fish. The fish were fed on a commercial pellet diet (Changzhou Haida Biological Feed Co., Ltd, Changzhou, China) which contained 47% crude protein, 5% crude lipids, 18.0% crude ash, 3.0% crude fiber, 10% water, 1.2% P and 2.7% lysine. The largemouth bass were fed two times per day, and the daily feed ration (approximately 2–3% of weight) was adjusted on their weight. During the experiment, DO and pH remained at 7.25 ± 0.32 °C and 5.8 ± 0.51 mg/L, respectively; total ammonia nitrogen and NO_2-N never exceeded 0.5 mg/L and 0.1 mg/L, respectively. Any mortality of fish was recorded during the course of the experiment.

To evaluate the growth performance, the body weight and body length were measured on 30 August, 30 September and 30 October by randomly capturing 90 individuals per group. After 90 days of farming, 36 individuals (after 24 h of fasting) were randomly obtained from each group and anesthetized immediately using 50 mg/L of tricaine methane sulfonate (MS-222, Sigma, MO, USA), and then the blood and liver tissues were collected according to regular experimental operations. The tissues from 3 fish were mixed into one sample. The plasma was separated from the blood by centrifugation (3500 r/min, 10 min) and used to detect the physiological parameters and oxidative stress indices. The liver tissue was used to measure hepatic antioxidant status and the transcriptome sequence. The fish used in the study were permitted by the Freshwater Fish Research Center, and animal welfare was taken into consideration in all experimental operations.

2.2. Growth Performance

The growth performance was assessed by evaluating the following parameters: mean body weight, mean body length, condition factor = 100 × body weight/body length^3, weight gain rate (WGR) = (average final weight—average initial weight)/average initial weight, specific growth rate (SGR) = 100 × (ln average final weight—ln average initial weight)/number of days, survival = 100 × final number of fish/initial number of fish, and feed conversion ratio (FCR) = food consumption/biomass increment.

2.3. Measurement of Physiological Parameters

Physiological parameters including glucose (Glu), total cholesterol (TC), triglyceride (TG), total protein (TP), albumin (Alb), lactate dehydrogenase (LDH), alanine aminotransferase (ALT), aspartate aminotransferase (AST), low-density lipoprotein cholesterol (LDL-c), high-density lipoprotein cholesterol (HDL-c) and alkaline phosphatase (AKP) in the plasma were measured using an automatic biochemical analyzer (BS-400, Shenzhen Mindray Bio-medical Electronics Co., LTD, Shenzhen, China). Lactate (LA) content in the plasma was detected by a colorimetric method using a commercial kit (Nanjing Jiancheng

Bioengineering Institute, Nanjing, China). The levels of heat shock protein 70 (HSP 70), complement 3 (C3) and lysozyme (LZM) in the plasma were determined by an enzyme-linked immunosorbent assay (mlbio, Shanghai, China).

2.4. Measurement of Oxidative Stress Parameters

In plasma and liver tissues, the oxidative stress parameters including total antioxidant capacity (T-AOC), glutathione peroxidase (Gpx), superoxide dismutase (SOD), catalase (CAT), glutathione (GSH) and malondialdehyde (MDA) were measured using commercial kits. Kits for T-AOC, SOD, Gpx and MDA were purchased from Suzhou Grace Biotechnology Co., Ltd. (Suzhou, China), the CAT kit was provided by Beyotime Biotechnology (Shanghai, China) and the GSH kit was ordered from Nanjing Jiancheng Bioengineering Institute. T-AOC levels were measured by the ferric reducing ability of plasma (FRAP) method, where the antioxidants reduced Fe^{3+}-tripyridine-triacridine (Fe^{3+}-TPTZ) to produce blue Fe^{2+}-TPTZ [35]. Gpx activity was detected using Cum-OOH as a substrate and 5,5′-dithiobis (2-nitrobenzoic acid) (DTNB) as a chromogenic agent [36]. SOD activity was analyzed by measuring the content of the reaction product (formazan) of water-soluble tetrazolium-8 (WST-8) and O^- [37]. CAT activity was tested by measuring the oxidation product of the decomposition of H_2O_2 under peroxidase [38]. GSH content was estimated by the DTNB method [39], MDA content was measured by the thiobarbituric acid (TBA) method [40] and hepatic protein content was tested by a bicinchoninic acid (BCA) assay [41].

2.5. Transcriptome Sequencing and Analysis

For the transcriptome study, we collected the livers of *M. salmoides* from the LD (named LL) and HD groups (named HL). Thirty-six individuals were randomly obtained from each group, and the liver tissues from 12 fish were mixed into one sample.

Total RNA of the liver tissue was separated using a Trizol reagent kit (Invitrogen, Carlsbad, CA, USA). Its quality was evaluated by an Agilent 2100 Bioanalyzer (Agilent Technologies, Palo Alto, CA, USA) and an agarose gel electrophoresis method. The RNA was enriched with Oligo(dT) beads and then used to synthesize cDNA with a commercial kit (NEB 7530, New England Biolabs, Ipswich, MA, USA). The cDNA library was constructed through size selection and PCR amplification, and the resulting cDNA library was sequenced using Illumina Novaseq6000 in Gene Denovo Biotechnology Co. (Guangzhou, China).

The raw data obtained from the sequencing machines were filtered by fastp (version 0.18.0) to obtain high-quality clean reads [42]. The clean reads were mapped to the *M. salmoides* reference genome (assembly ASM1485139v1) using HISAT2. 2.4 [43]. The transcription abundance was expressed as a FPKM (fragment per kilobase of transcript per million mapped reads) value calculated by RSEM software [44]. Relationship analysis of the samples was assessed by principal component analysis (PCA). Differentially expressed genes (DEGs) between LL and HL were analyzed by DESeq2 software [45] with a threshold (false discovery rate (FDR) < 0.05 and absolute fold change ≥ 2). The DEGs were subjected to enrichment analysis with the GO (Gene Ontology) and KEGG (Kyoto Encyclopedia of Genes and Genomes) databases. Significantly enriched GO terms and KEGG pathways were defined according to a threshold (FDR ≤ 0.05). In addition, we identified whether a set of genes in specific KEGG pathways displayed significant differences between the LL group and HL group through gene set enrichment analysis (GSEA) [46]. Raw data of the transcriptome sequences are available at the Sequence Read Archive (SRA) database (No. PRJNA838235).

2.6. Quantitative Real-Time PCR (qPCR) Analysis

Total RNA of liver tissues was extracted using RNAiso Plus reagent (Takara Biomedical Technology (Beijing) Co., Ltd, Beijing, China) and was then used to synthesize cDNA with a primeScript™ RT reagent kit (Takara, RR047A). The expression of the target gene was detected via qPCR amplification using a qPCR kit (Takara, RR820A). The relative mRNA level was calculated by the $2^{-\triangle\triangle Cq}$ method [47] using β-actin as a reference gene. The specific primers of the target genes in the study are listed in Table S1.

2.7. Statistical Analysis

All data were analyzed using SPSS version 20.0 software and expressed as means ± SEM (standard error of mean). The Shapiro–Wilk test and Levene test were used to analyze the normal distribution and variance homogeneity of these data, respectively. The difference among different stocking densities was analyzed by one-way analysis of variance (ANOVA) with LSD (least significant difference). Differences between the LL group and the HL group were assessed by Student's t-test. A p-value of <0.05 was considered statistically significant.

3. Results

3.1. Changes in Growth Performance

In this experiment, the SR was 86.38 ± 1.82%, 79.02 ± 1.08% and 76.67 ± 1.05% in the LD, MD and HD groups, respectively (Table 1). The mean body weight and mean body length of *M. salmoides* showed a rising tendency during the course of the study, and the two parameters were markedly higher in the LD group than in the MD and HD groups on 30 October ($p < 0.05$; Figure 1A,B). The condition factor value in the HD group was higher than that in LD on 30 September, while it was higher in the MD group than in the other groups on 30 October ($p < 0.05$; Figure 1C). At the end of the experiment, the FBW, WGR and SGR were higher in the LD group than in the MD and HD groups ($p < 0.05$; Table 1), but the FCR was not changed by the different stocking densities ($p > 0.05$).

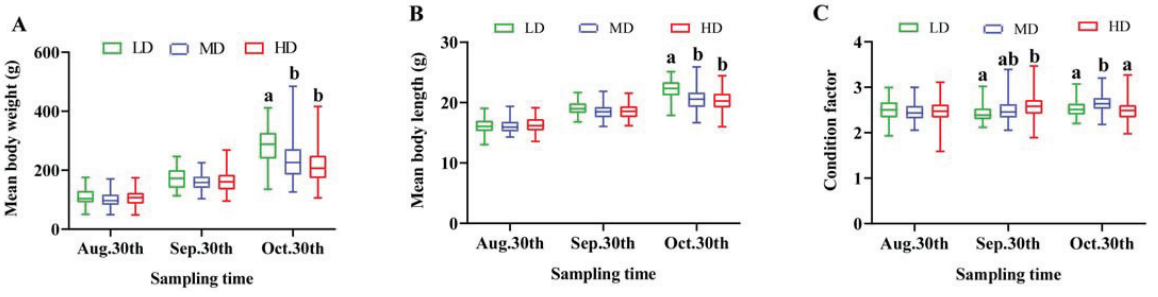

Figure 1. Mean body weight (**A**), mean body length (**B**) and condition factor (**C**) of *M. salmoides* reared at different densities in an integrated rice–fish farming system. Different letters as superscripts indicate significant differences among the different groups ($p < 0.05$). LD, low stocking density; MD, medium stocking density; HD, high stocking density.

Table 1. Growth parameters of *M. salmoides* reared at different densities in an integrated rice–fish farming system after 90 days of farming.

Parameters	LD	MD	HD
IBW (g)	40.76 ± 0.25	40.67 ± 0.21	40.43 ± 0.19
FBW (g)	278.82 ± 7.62 ^{a}	236.68 ± 7.68 ^{b}	213.81 ± 5.29 ^{b}
WGR (%)	582.67 ± 14.38 ^{a}	483.16 ± 18.07 ^{b}	429.47±12.63 ^{b}
SGR (%/d)	2.18 ± 0.024 ^{a}	2.01 ± 0.035 ^{b}	1.89 ± 0.056 ^{b}

Table 1. *Cont.*

Parameters	LD	MD	HD
SR (%)	86.38 ± 1.82 [a]	79.02 ± 1.08 [b]	76.67 ± 1.05 [b]
FCR	1.13 ± 0.019	1.12 ± 0.035	1.22 ± 0.049

Values are expressed as mean ± SEM of three replicates. For each row, means with different letters as superscripts indicate a statistical significance among different densities ($p < 0.05$). LD, low stocking density; MD, medium stocking density; HD, high stocking density.

3.2. Changes in Physiological Parameters

The physiological parameters of *M. salmoides* in the different groups are shown in Table 2. The levels of ALT, AST, LDH, AKP, TP, HDL-c, Alb, HSP70 and LZM were similar in the LD, MD and HD groups after 90 days of farming ($p > 0.05$). The Glu and LA concentrations were significantly increased in the HD group compared with the LD group ($p < 0.05$). However, the TG, TC, LDL-c and C3 levels were significantly decreased in the HD groups compared with the LD group ($p < 0.05$). In addition, compared with the LD group, the LA value was increased but the LDL-c value was lower in the MD group ($p < 0.05$).

Table 2. Physiological parameters in the plasma of *M. salmoides* reared at different densities in an integrated rice–fish farming system after 90 days of farming.

Parameters	LD	MD	HD
ALT (U/L)	4.48 ± 0.52	3.30 ± 0.39	2.84 ± 0.36
AST (U/L)	18.62 ± 2.00	17.36 ± 1.80	19.55 ± 2.37
LDH (U/L)	278.97 ± 32.07	295.08 ± 37.84	235.31 ± 23.14
AKP (U/L)	33.19 ± 1.21	33.44 ± 1.36	31.70 ± 2.35
TP (g/L)	39.49 ± 0.39	37.23 ±1.26	35.08 ± 1.65
Alb (g/L)	8.38 ± 0.60	8.86 ± 0.46	8.56 ± 0.40
Glu (mmol/L)	5.26 ± 0.20 [a]	5.64 ± 0.38 [a]	8.98 ± 0.46 [b]
LA (mmol/L)	7.51 ± 0.20 [a]	8.72 ± 0.21 [b]	9.18 ± 0.20 [b]
HSP70 (pg/mL)	49.79 ± 5.05	45.98 ± 5.02	39.06 ± 2.64
TC (mmol/L)	12.00 ± 0.26 [a]	11.07 ± 0.45 [ab]	9.40 ± 0.48 [b]
TG (mmol/L)	18.46 ± 0.94 [a]	17.71 ±0.47 [a]	13.36 ± 0.55 [b]
LDL-c (mmol/L)	3.78 ±0.12 [a]	2.94 ± 0.13 [b]	2.39 ± 0.14 [b]
HDL-c (mmol/L)	3.81 ± 0.09	3.65 ±0.17	3.57 ± 0.20
C3 (μg/mL)	9.32 ± 0.70 [a]	10.74 ± 1.22 [a]	5.75 ± 0.61 [b]
LZM (ng/mL)	32.71 ± 3.44	36.77 ± 5.63	26.77 ± 2.78

Values are expressed as means ± SEM, n = 12. For each row, means with different letters as superscripts indicate a statistical significance among different densities ($p < 0.05$). LD, low stocking density; MD, medium stocking density; HD, high stocking density.

3.3. Changes in Oxidative Stress Parameters

After 90 days of farming, the plasma T-AOC and GSH levels were significantly reduced in the HD group compared with the LD group, while the CAT and MDA levels were prominently enhanced in the HD group ($p < 0.05$; Figure 2A,C,E,F). SOD and Gpx activities in the plasma were not visibly influenced under different stocking densities ($p > 0.05$; Figure 2B,D). In the liver, the HD treatment clearly inhibited SOD activity and enhanced MDA formation compared with the LD and MD groups ($p < 0.05$; Figure 2H,L). In addition, the other oxidative stress parameters did not differ significantly in the liver among the three groups ($p > 0.05$; Figure 2G,I,J,K).

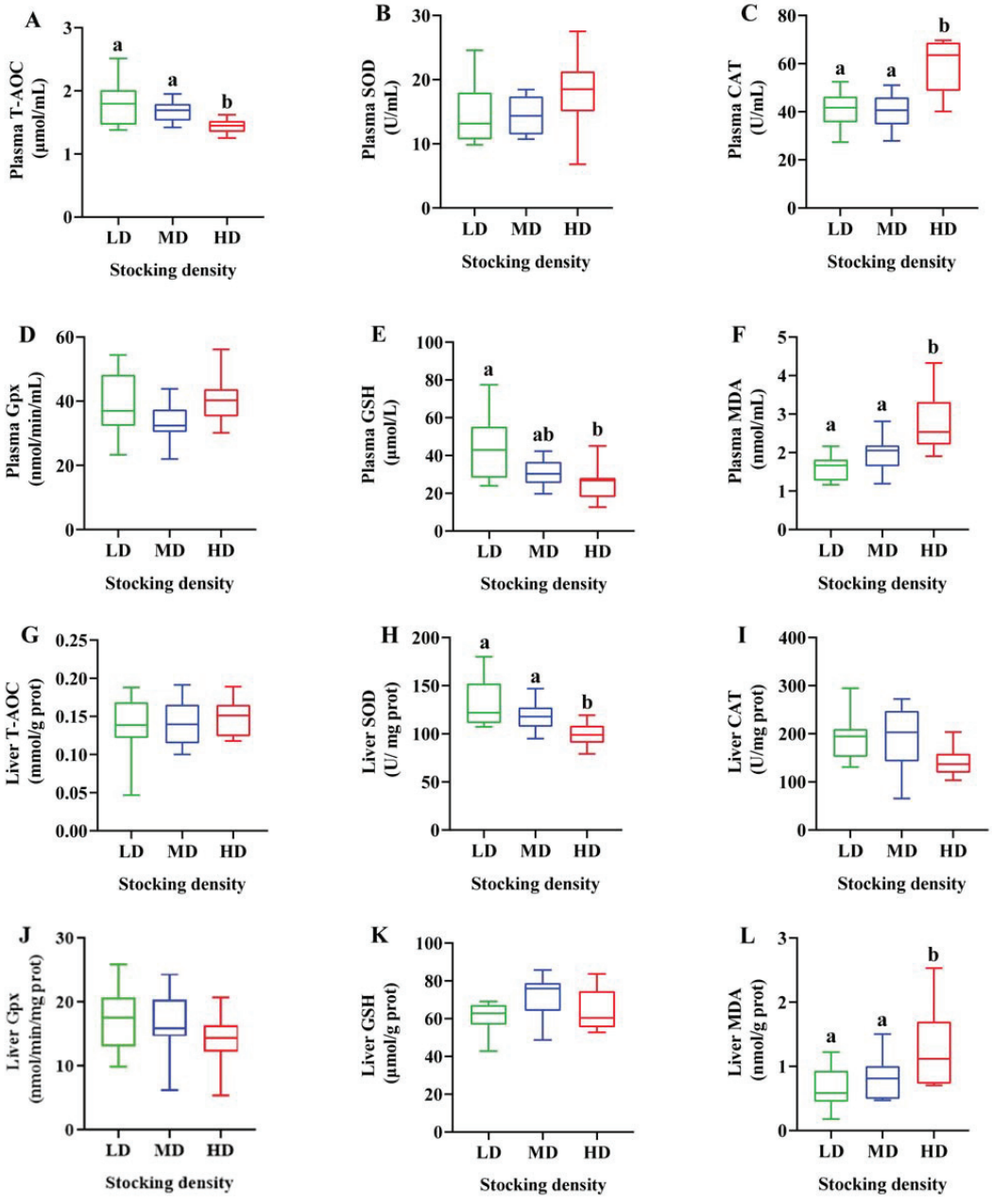

Figure 2. Antioxidative parameters in the plasma (**A**–**F**) and liver (**G**–**L**) of *M. salmoides* reared at different densities in an integrated rice–fish farming system after 90 days of farming. Values are expressed as means ± SEM, n = 12. Different letters as superscripts indicate a statistical significance among different densities ($p < 0.05$). LD, low stocking density; MD, medium stocking density; HD, high stocking density.

3.4. Transcriptome Sequencing and Analysis of DEGs

After filtering of raw reads, 40,491,348 (99.36%)—49,617,030 (98.94%) clean reads were obtained in the livers of the LL group and the HL group. The base quality score indicated that the values of Q30, Q20 and GC were 90.11–94.07%, 96.09–97.91% and 48.08–49.10%, respectively. The mapped ratio was greater than 93.36%, and 25,050 genes were identified according to alignment against the reference sequence (Table S2). According to the expression level of each gene in the samples, the PCA revealed distinct groups between the LL group and HL group (Figure 3A). After 90 days of farming, there were 150 DEGs, including 54 upregulated genes and 96 downregulated genes (Figure 3B,C).

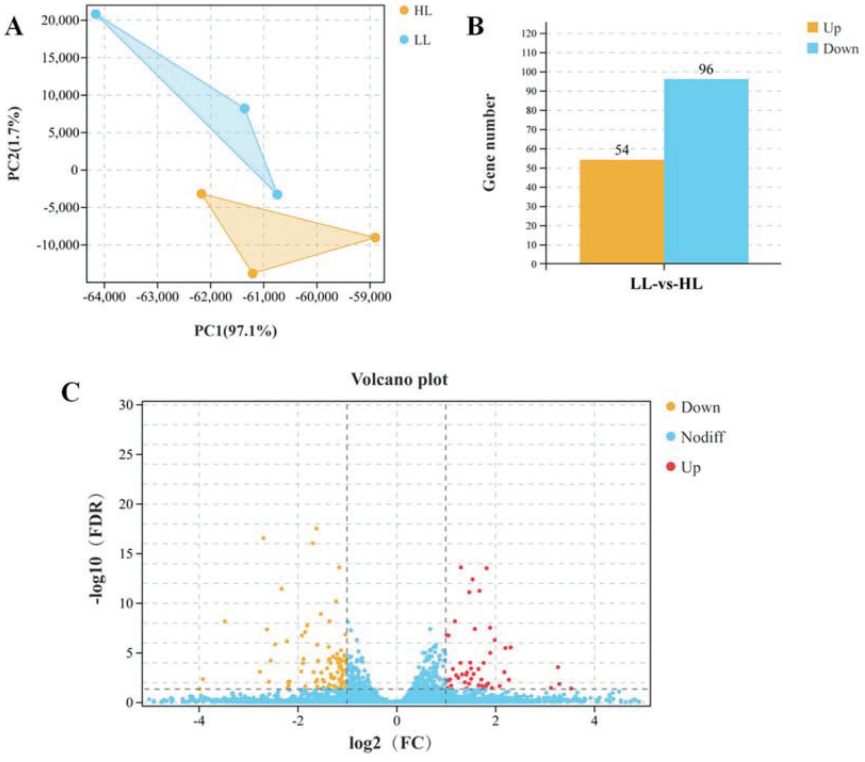

Figure 3. Differently expressed genes (DEGs) in the liver of *M. salmoides* between the low-density group (LL) and the high-density group (HL). (**A**) The correlation of samples between the LL group and the HL group. (**B**) The number of DEGs in the liver between the LL and HL groups. (**C**) Volcano plot of DEGs between the LL group and the HL group.

3.5. GO Enrichment Analysis of DEGs

For an evaluation of the biological function, we performed GO enrichment analysis on the DEGs (Figure 4). In the biological process category, the DEGs were enriched mainly in cellular processes, metabolic processes (p.adjust < 0.001), biological regulation and response to stimulus, and specifically, in single-organism metabolic processes (p.adjust < 0.001), lipid metabolic processes (p.adjust < 0.001) and the response to light stimulus (p.adjust < 0.001) (Figure 4B). In the molecular function category, two major Level 2 GO terms were binding and catalytic activity (p.adjust = 0.029). In detail, the DEGs were primarily involved in DNA photolyase activity (p.adjust = 0.002), DNA binding (p.adjust = 0.002) and monooxygenase activity (p.adjust = 0.007) (Figure 4C). In the cellular components category, organelles and membranes contained the most DEGs, and micro-

bodies (*p*.adjust = 0.028) and membrane-bounded organelles (*p*.adjust = 0.036) were the top two GO terms (Figure 4D).

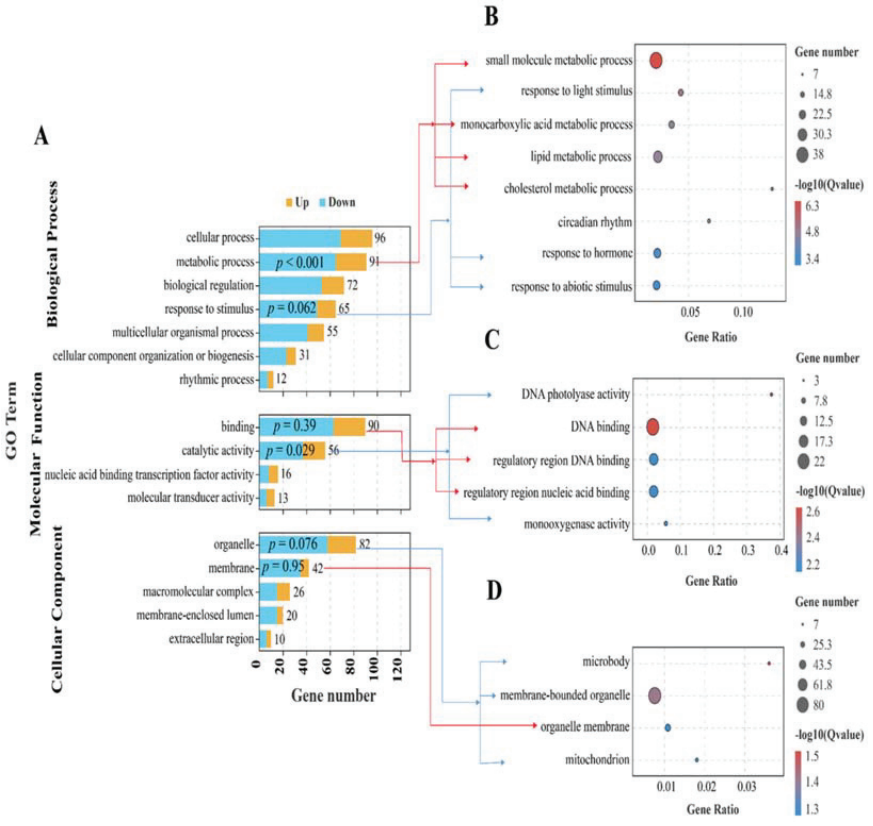

Figure 4. GO enrichment analysis for differently expressed genes (DEGs) in the livers of *M. salmoides* between the low-density group (LL) and the high-density group (HL). (**A**) GO enrichment terms pf DEGs in biological processes, molecular functions and cellular components. (**B**) Top 8 GO terms in the biological process category. (**C**) Top 5 GO terms in the molecular function category. (**D**) Top 4 GO terms in the cellular component category. *P*-values were corrected via the Benjamin–Hochberg method.

3.6. KEGG Enrichment Analysis of DEGs

To explore the key signaling pathways, the DEGs were further annotated against the KEGG database (Figure 5). The DEGs were enriched in five KEGG A classes: metabolism, organismal systems, cellular processes, genetic information processing and environmental information processing (Figure 5A). The top 10 KEGG pathways indicated that the DEGs were mainly enriched in lipid metabolism-related pathways, including the PPAR signaling pathway, steroid biosynthesis, glycerolipid metabolism and fatty acid metabolism (Figure 5B). In addition, we observed that 36 genes were enriched in the metabolic pathway (q value < 0.0001), of which 16 genes were involved in lipid metabolism (Figure 5C).

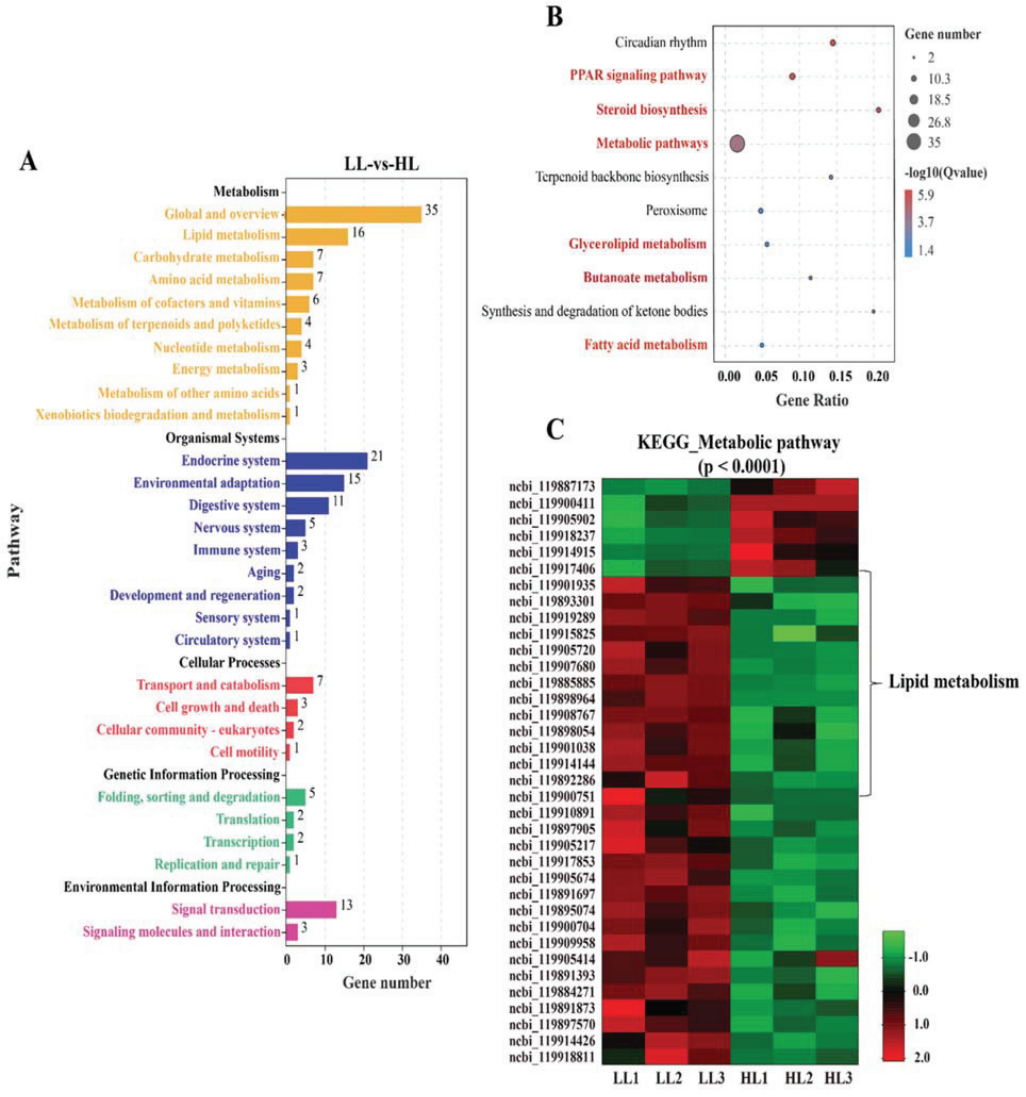

Figure 5. KEGG enrichment analysis for differently expressed genes (DEGs) in the liver of *M. salmoides* between the low-density group (LL) and the high-density group (HL). (**A**) DEG enrichment in the KEGG A Class and B Class. (**B**) The top 10 enriched KEGG pathways. (**C**) DEGs enriched in the metabolic pathway.

3.7. Changes in the PPAR Signaling Pathway and Lipid Metabolism

At the end of the experiment, the PPAR signaling pathway in the liver was considerably altered ($p < 0.0001$; Figure 6A). All altered genes showed a downregulated tendency in the HL group compared with the LL group, including the key genes *pparα*, *scd1*, *fabp3*, *lpl*, *acsl1* and *hmgcs1* (Figure 6A,B). Further, the key genes involved in the PPARα signaling pathway and lipid metabolism were verified by qPCR (Figure 6B), and the results showed that the RNA-seq data were significantly consistent with the qPCR data ($r = 0.814$, $p = 0.014$; Figure 6C).

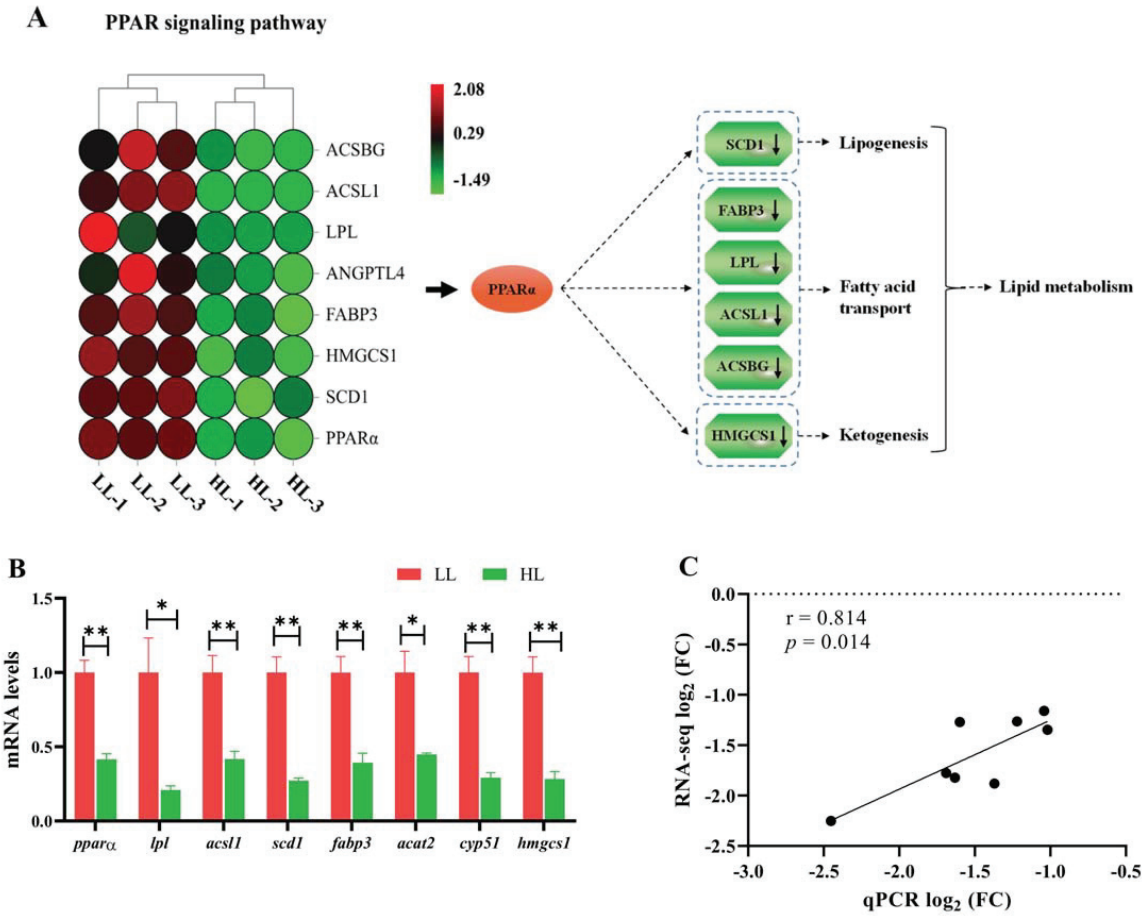

Figure 6. Changes in the PPAR signaling pathway and lipid metabolism-related genes in the liver of *M. salmoides* between the low-density group (LL) and the high-density group (HL). (**A**) DEGs in the KEGG PPAR signaling pathway and possible mechanisms regulating lipid metabolism. (**B**) Lipid metabolism-related gene expression measured by qPCR; values are expressed as means ± SEM (n = 3), * $p < 0.05$ and ** $p < 0.01$. (**C**) The correlation between the qPCR data and RNA-seq data.

3.8. Changes in Lipid Metabolism-Related Pathways

The GSEA showed significant enrichment in a range of pathways related to lipid metabolism including the PPAR signaling pathway (KO03320), the insulin signaling pathway (KO04910), the adipocytokine signaling pathway (KO04920), fatty acid metabolism (KO01212), steroid biosynthesis (KO00100) and biosynthesis of unsaturated fatty acids (KO01040) (Figure 7). The coordinated expression changes in the six pathways were significantly negatively regulated by the HL treatment. These results were consistent with the results of KEGG enrichment of the DEGs.

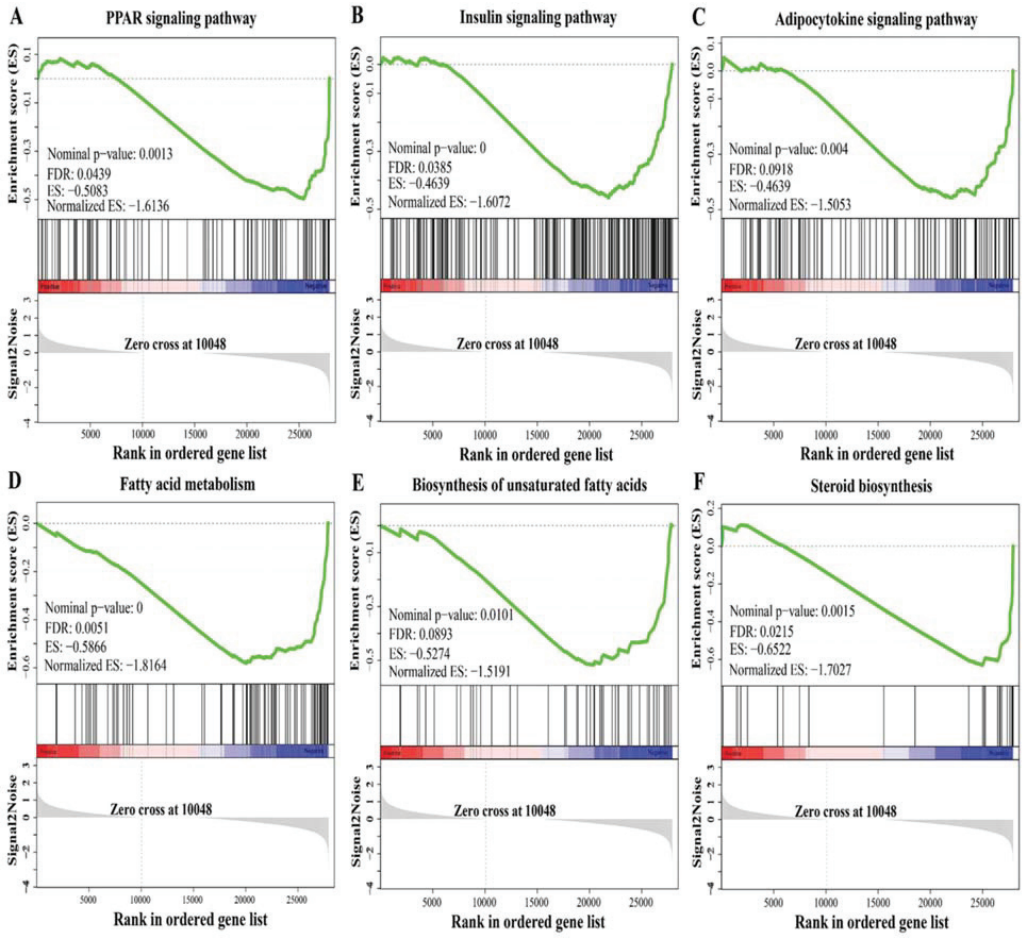

Figure 7. Changes in lipid metabolism-related pathways identified using GSEA in the liver of *M. salmoides* between the low-density group (LL) and the high-density group (HL). (**A**) PPAR signaling pathway. (**B**) Insulin signaling pathway. (**C**) Adipocytokine signaling pathway. (**D**) Fatty acid metabolism. (**E**) Biosynthesis of unsaturated fatty acids. (**F**) Steroid biosynthesis. The |Normalized ES| > 1, nominal *p*-value < 0.05 and FDR < 0.25 in each gene set were set as threshold values for statistical significance.

4. Discussion

The stocking density is a critical factor affecting the health status and production of farmed fish. Increasing the stocking density is a positive means of improving fish production and water utilization. However, an excessive stocking density may result in adverse effects for farmed fish, such as inhibiting growth performance, deteriorating water quality, and increasing mortality and disease risk. Therefore, an appropriate stocking density is required for farmed fish under different farming models. In the present study, we set out to evaluate the growth and physiological effects of different stocking densities in *M. salmoides* under an integrated rice–fish farming model, followed by assessing the underlying mechanisms via RNA-seq analysis. Accordingly, our experiment indicated that the high stocking density caused adverse changes in the growth performance, physiological responses, antioxidant status and hepatic metabolic function of *M. salmoides*.

4.1. Effect of Stocking Density on Growth Performance

Reduced growth performance is a common phenomenon for farmed fish under high stocking densities. Numerous studies have reported that the growth performance was negatively influenced in different fish species when the stocking density was above a certain value. In *Lates calcarifer*, the body weight and feed utilization efficiency were significantly decreased with an increasing stocking density (350−1750 g/m^3) after 60 days of farming [48]. In *Piaractus mesopotamicus*, the low stocking density (650 g/m^3) group had a higher final biomass, weight gain and economic profit than the high stocking density group (1300 g/m^3) after 360 days of faming [49]. Similarly, in this work, the HD and MD treatments reduced the body length, body weight, WGR and SGR of *M. salmoides* after 90 days of farming, which indicated that a density of up to 375 g/m^3 (the final density of the MD group) had an adverse impact on growth performance in the integrated rice–fish system. It is worth noting that the tolerance of *M. salmoides* to high stocking density shows obvious differences in different farming models. In a land-based recirculating aquaculture system, the growth performance of *M. salmoides* decreased when the density reached up to 23.34 kg/m^3 (65 times as high as our data) [28]. In a pond system, *M. salmoides* reared at a high stocking density (about 798 g/m^2) showed lower growth [50]. The low growth performance seemed to be related to inappropriate environmental and/or feeding conditions, the reduction in available space for individuals and the extra energy requirements induced by stress under a high stocking density [51–53].

The survival ratio is a crucial index for evaluating production and the economic benefit of farmed fish. Previous studies have shown that higher densities can cause higher mortality rates in some cultured species, such as *Platax teira* and *O. niloticus* [54,55]. In an in-pond raceway culture system, the survival of *M. salmoides* showed a downward tendency with an increasing density [56]. In the present work, we also found that the survival ratio of *M. salmoides* was significantly higher in the LD group than in the MD and HD groups. In addition, the average survival ratio (80.87%) of *M. salmoides* in the rice–fish farming system was slightly higher than that (74.47%) in pond-based production systems [57].

4.2. Effect of Stocking Density on Physiological Function

The physiological response is closely associated with the growth performance of farmed fish in aquaculture, which is commonly used to assess fish heath and to optimize management measures. High stocking density, as a chronic stressor, has been known to directly influence the physiological response of some teleost species [58,59]. Clu and LA were considered as reliable indicators for evaluating the stress response of fish. Under stress conditions, the blood Clu and LA levels were significantly increased, which agree with high energy consumption [60]. The increase in blood Glu and LA in fish is a common response to stress under high stocking densities [17]. In this study, higher plasma Glu and LA concentrations were also observed in the HD group, suggesting a physiological response to stress induced by the high stocking density. These results were supported by previous studies in *Sparus aurata*, *Solea senegalensis* and *Lates calcarife* [16,61,62]. In fish, HSP70 was also identified as a sensitivity indicator of stress, mediating protein folding and repairing. The high expression of the *hsp* 70 gene has been reported in fish farmed at a high density, as it is protective against the adverse environment [61,62]. However, in the rice–fish system, there was no significant difference in plasma HSP70 content among different stocking densities, suggesting that the current density may not have achieved stress levels that led to a change in HSP70.

In addition to Glu and LA, the TC and TG in the blood are also common parameters for the assessment of fish stress, as these are related to energy and lipid metabolism. It has been confirmed that high stocking densities affect energy reserves, consumption and reallocation to cope with the increased energy demand in fish [53]. In *Megalobrama amblycephala*, the TG and TC, as energy substrates, were markedly increased at a high stocking density [58]. Similarly, the high stocking density treatment increased the TC and TG in *Ictalurus punctatus*,

which was linked to augmented energy metabolism [63]. However, in our study, the TC and TG levels displayed a decreasing trend with increasing density. We speculated that decreased the TC and TG were linked to an abnormal lipid metabolism in the liver under HD conditions. Consistent with our data, lower levels of TG and TC were also reported in *O. mykiss* and *Trachinotus ovatus* cultured at a higher stocking density, and the authors suggested that lipid reserves were depleted in response to the increased energy demand under the stress conditions [61,64].

Abnormal immune function has been frequently reported in fish farmed at a high density. LZM and C3 are commonly used to evaluate immune status in fish after adverse stimuli. Costas et al. (2013) suggested that the decrease in plasma LZM and ACH50 displayed an impairment of the immune system in *Solea senegalensis* held at a high stocking density [65]. Liu et al. (2019) postulated that the decreased C3 and LZM indicated immune suppression in *Scophthalmus maximus* under a high stocking density [66]. Similarly, in the present work, the C3 level was decreased in the HD group after 90 days of farming, revealing that the high density had an adverse effect on the immunity of *M. salmoides*. In addition, our data showed that the GOT, GPT, AKP and LDH levels were not changed by the high stocking density, suggesting that the current density did not cause tissue damage [67].

4.3. Effect of Stocking Density on Antioxidative Status

An increasing amount of evidence has suggested that a high stocking density can induce intracellular redox imbalance, leading to oxidative stress or oxidative damage in many fish species [68,69]. In order to defend against oxidative stress, fish, similar to mammals, have developed an antioxidant defense system consisting of enzymatic antioxidants (e.g., SOD, Gpx and CAT) and non-enzymatic antioxidants (e.g., GSH, Vitamin C, carotenoids and flavonoids) [70]. It can be activated to maintain redox status under moderate oxidative stress [71]. Nevertheless, the antioxidant defense system is impaired and antioxidants are depleted under chronic or severe oxidative stress [72]. Indeed, several previous studies have shown that a high stocking density treatment decreased the levels of antioxidant parameters, such as SOD, GSH and CAT, leading to impairment of the antioxidant defense system in *O. mykiss*, *O. niloticus* and *S. maximu* [13,19,20]. Moreover, a study on *M. salmoides* farmed in an in-pond raceway system showed that high stocking density reduced hepatic SOD and CAT activity, and restrained antioxidant capacity [27]. Conversely, increased levels of the antioxidants were also observed in fish under high density, suggesting a positive response of the antioxidant defense system to stress [73,74]. Interestingly, in this study, the levels of plasma T-AOC and GSH were suppressed, but the plasma CAT activity was enhanced in HD group, suggesting a depletion of non-enzymatic antioxidants and an adaptive response to adverse conditions in plasma. Moreover, in the liver, only SOD activity was inhibited in the HD group, but the other antioxidant parameters were not significantly changed, which may indicate moderate or slight oxidative stress in the livers of *M. salmoides* reared in the HD group.

Lipid peroxidation is a vital consequence of oxidative stress, usually reflected by MDA content. Previous studies have confirmed that high stocking density as a stressor can stimulate the formation of ROS in fish [73]. Excess ROS may react with unsaturated fatty acids on cell membranes, inducing lipid peroxidation [75]. It has been reported that a large number of harmful byproducts from lipid peroxidation are capable of inactivating many cellular proteins, inducing inflammation and damaging cells or tissues [76]. In fish, increased lipid peroxidation has always attracted widespread attention under high stocking densities. We and others have found that the high stocking density treatment promoted MDA formation in the liver, blood or intestines of fish [13,19,20,77]. Similarly, increased MDA content was also observed in the plasma and liver of *M. salmoides*, indicating that the high-density treatment induced lipid peroxidation after 90 days of farming in the rice–fish farming system.

4.4. Effect of Stocking Density on Lipid Metabolism

Liver is a major lipid metabolism organ of fish, and lipid metabolism is more susceptible to environmental stressors, as it is a major energy substrate [77]. The adverse effect of a high stocking density on lipid metabolism has been widely reported in fish. Earlier studies have found that high stocking density caused a decrease in hepatic lipid content, suggesting a higher utilization of hepatic lipids under stressful conditions [78,79]. Under a high stocking density, lipid metabolic enzymes, including fatty acid synthetase, hormone-sensitive triglyceride lipase and lipoprotein lipase, were upregulated in the liver of *O. niloticus* to adapt to adverse conditions [80]. Transcriptomic analysis showed that *Ctenopharyngodon idella* farmed at a high stocking density might face issues associated with abnormal lipid metabolism [81]. Metabolomic analysis showed that lipid metabolism was repressed by a high stocking density in *Brachymystax lenok* [82]. In the current study, our data also revealed that the lipid metabolic process in the GO enrichment analysis and the lipid metabolism-related pathways in the KEGG enrichment analysis were significantly altered in the HD group, where the fatty acid metabolism, biosynthesis of unsaturated fatty acids and steroid biosynthesis tended to be suppressed in the liver of *M. salmoides*. The suppression may be harmful for the growth of *M. salmoides*, since fatty acids are essential for multiple physiological functions, such as energy production and membrane structure [83].

It was worth noting that we also found three key pathways related to lipid metabolism, including the PPAR signaling pathway, the insulin signaling pathway and the adipocytokine signaling pathway, which showed a significant difference between the LL group and the HL group. PPARα is regarded as a master regulator in lipid metabolism, which can activate its target genes (e.g., *scd*, *fabp*, and *acsl*) to mediate fatty acid transport, synthesis and oxidation, as well as lipogenesis and ketogenesis [84]. Its activation improves the symptoms of metabolic syndrome and exerts anti-inflammatory activity [85]. Ren et al. (2017) suggested that upregulation of PPARα under a high stocking density enhanced lipid mobilization and utilization in *Acipenser schrenckii* to cope with crowding stress [86], but Xu et al. (2020) found that PPARα expression was downregulated in *Takifugu rubripes* under a high density, revealing a decrease in fatty acid β-oxidation and lipid metabolism disorder [87]. In this study, downregulation of PPARα further inhibited its downstream genes, including *sce1*, *lpl*, *fabp3*, *acsl1*, *hmgcs1* and *angptl4*, indicating that the abnormal lipid metabolism in the HD group was associated with the suppression of the PPARα signaling pathway.

Growing evidence has demonstrated that the insulin signaling pathway is involved in lipid metabolism. Its activation can stimulate lipid biosynthesis [88] and regulate lipid deposition by activating lipogenesis and inhibiting fatty acid oxidation [89]. Multi-omics analyses revealed that the insulin signaling pathway was downregulated in the liver of *O. niloticus* under hypoxia stress [90]. In our work, the GSEA data were more inclined to indicate a downregulated insulin signaling pathway in the liver of *M. salmoides* under the HD treatment. In addition, the insulin signaling pathway is essential for normal glucose metabolism, and its upregulation could promote glucose metabolism [91–93]. Therefore, the downregulated insulin signaling pathway may adversely influence glucose metabolism and energy utilization in the liver.

The adipocytokine signaling pathway is a signaling cascade arising from the adipocytokines, which has been implicated in energy intake, fatty acid metabolism and insulin resistance [94]. Multi-omics analyses identified that the adipocytokine signaling pathway was related to fatty acid metabolism in *Cyprinus carpio* [95]. Microarray analysis found that the adipocytokine signaling pathway was significantly changed in *Danio rerio* under heat stress [96]. The activated adipocytokine signaling pathway might be further involved in the immune response in *Ctenopharyngodon idella* after lipopolysaccharide exposure [97]. In this study, the adipocytokine signaling pathway was negatively affected by the HD treatment, which might be a cause of hepatic lipid metabolism disorder.

4.5. Effect of Stocking Density on Welfare

Welfare is an increasing public concern in farmed fish. Accumulating evidence suggests that fish experience poor welfare under adverse conditions, accompanied by altered growth performance, physiological parameters and behavior [98]. The stress response is a common event when fish are subjected to poor welfare, and thus, physiological indicators of stress, including cortisol, glucose and lactate, are frequently used to evaluate the welfare of farmed fish [99]. A recent study also suggested that HSP 70 was a new candidate for assessing the welfare of *M. salmoides* [100]. In addition, there is a significant negative correlation between poor welfare and growth performance; therefore, the growth rate is also considered as a reliable indicator in monitoring stress and welfare [101]. Under stress conditions, energy metabolism increases to cope with abnormal physiological changes, which lead to a decrease in energy availability for growth [102]. Stocking density has been highlighted as a principal area of welfare concern in farmed fish, because they are often held at higher densities in commercial aquaculture [103]. An earlier study reported that high stocking density had the potential to adversely affect the welfare of *O. mykiss*, which was assessed by measuring population, individual, morphometric and physiological indicators [104]. A multivariate analysis showed that increasing stocking densities were associated with lower welfare score in *Salmo salar* [105]. In *Clarias gariepinus*, a high stocking density impaired welfare via decreasing growth performance and increasing skin lesions [17,106]. In line with previous studies, we also monitored the welfare through measuring the growth performance and physiological indicators (Glu, LA and HSP 70), and the data showed a poor welfare in *M. salmoides* in the HD group, reflected by a low growth rate, higher Glu and LA levels, and abnormal lipid metabolism.

5. Conclusions

In conclusion, our data indicated that the *M. salmoides* can be reared in integrated rice–fish farming systems. However, when the stocking density reached 375 g/m^3 (the final density in the MD group at the current size), the growth performance was negatively influenced. The high stocking density, as a chronic stressor, induced a physiological response and oxidative stress, which may have resulted in greater energy consumption and growth inhibition. Further, the transcriptome analysis showed that the HD treatment caused abnormal hepatic lipid metabolism via suppressing the PPAR, insulin and adipocytokine signaling pathways, which may be another potential cause of the low growth in the HD group. Thus, in a commercial integrated rice–fish farming system, improvements in strategies for managing *M. salmoides* regarding stocking density are required. This study provides a valuable reference for *M. salmoides* farming and optimization of the rice–fish farming model.

Supplementary Materials: The following supporting information can be downloaded at: https://www.mdpi.com/article/10.3390/antiox11071215/s1. Figure S1: Schematic diagram of the integrated rice–fish farming system in this study. Table S1: Specific primer sequences for qPCR in this study. Table S2: Valid data used in the transcriptome analysis.

Author Contributions: Conceptualization, writing—original draft preparation, software, R.J.; methodology, investigation, L.W.; validation, formal analysis, Y.H. and W.F.; resources, data curation, writing—review and editing, B.L.; visualization, supervision, project administration, funding acquisition, J.Z. All authors have read and agreed to the published version of the manuscript.

Funding: This research was funded by the Central Public-interest Scientific Institution Basal Research Fund, CAFS (2020TD60), the National Key R&D Program of China (2019YFD0900305) and China's Agriculture Research System of MOF and MARA, grant number (CARS-45-25).

Institutional Review Board Statement: All animals in this study were approved by the Animal Care and Use Ethics Committee of the Freshwater Fisheries (2020TD60, 15-07-2021), and all procedures were performed according to Jiangsu Laboratory's Animal Management Guidelines (014000319/2008-00079).

Informed Consent Statement: Not applicable.

Data Availability Statement: The raw data of transcriptome sequencing are available at the Sequence Read Archive (SRA) database of NCBI (No. PRJNA838235).

Conflicts of Interest: The authors declare no conflict of interest.

References

1. Guan, W.; Liu, K.; Shi, W.; Xuan, F.; Wang, W. Scientific paradigm of integrated farming of rice and fish. *Acta Ecol. Sin.* **2020**, *40*, 5451–5464.
2. NFTEC. Industrial Development Report on Integrated Rice-Fish Farming in China during "13th Five-Year". *China Fish.* **2022**, *01*, 43–52.
3. Ahmed, N.; Hornbuckle, J.; Turchini, G.M. Blue-green water utilization in rice-fish cultivation towards sustainable food production. *Ambio* **2022**. [CrossRef]
4. Lu, J.B.; Li, X. Review of rice-fish-farming systems in China—One of the Globally Important Ingenious Agricultural Heritage Systems (GIAHS). *Aquaculture* **2006**, *260*, 106–113. [CrossRef]
5. Frei, M.; Becker, K. Integrated rice-fish culture: Coupled production saves resources. *Nat. Resour. Forum* **2005**, *29*, 135–143. [CrossRef]
6. Vromant, N.; Chau, N.T.H.; Ollevier, F. The effect of rice-seeding rate and fish stocking on the floodwater ecology of the trench of a concurrent, direct-seeded rice-fish system. *Hydrobiologia* **2001**, *457*, 105–117. [CrossRef]
7. Tsuruta, T.; Yamaguchi, M.; Abe, S.-I.; Iguchi, K.I. Effect of fish in rice-fish culture on the rice yield. *Fish. Sci.* **2011**, *77*, 95–106. [CrossRef]
8. Liu, D.; Tang, R.; Xie, J.; Tian, J.; Shi, R.; Zhang, K. Valuation of ecosystem services of rice–fish coculture systems in Ruyuan County, China. *Ecosyst. Serv.* **2020**, *41*, 101054. [CrossRef]
9. Xu, Q.; Wang, X.; Xiao, B.; Hu, K. Rice-crab coculture to sustain cleaner food production in Liaohe River Basin, China: An economic and environmental assessment. *J. Clean. Prod.* **2019**, *208*, 188–198. [CrossRef]
10. Tang, J.; Li, W.; Lu, X.; Wang, Y.; Ding, X.; Jiang, J.; Tang, Y.; Li, J.; Zhang, J.; Du, J.; et al. Development Status and Rethinking of the Integrated Rice-fish System in China. *China Rice* **2020**, *26*, 1–10.
11. Ahmed, N.; Zander, K.K.; Garnett, S.T. Socioeconomic aspects of rice-fish farming in Bangladesh: Opportunities, challenges and production efficiency. *Aust. J. Agric. Resour. Econ.* **2011**, *55*, 199–219. [CrossRef]
12. Santurtun, E.; Broom, D.M.; Phillips, C.J.C. A review of factors affecting the welfare of Atlantic salmon (*Salmo salar*). *Anim. Welf.* **2018**, *27*, 193–204. [CrossRef]
13. Jia, R.; Liu, B.L.; Han, C.; Huang, B.; Lei, J. Influence of Stocking Density on Growth Performance, Antioxidant Status, and Physiological Response of Juvenile Turbot, Scophthalmus maximu, Reared in Land-based Recirculating Aquaculture System. *J. World Aquac. Soc.* **2016**, *47*, 587–599. [CrossRef]
14. Abdel-Hakim, N.; Hussein, M.; Bakeer, M.; Soltan, M. Effect of protein level and stocking density on growth performance of Nile tilapia (*Oreochromis niloticus*) cultured in tanks. *Egypt. J. Nutr. Feed.* **2001**, *4*, 763–780.
15. Liu, B.; Liu, Y.; Sun, G. Effects of stocking density on growth performance and welfare-related physiological parameters of Atlantic salmon *Salmo salar* L. in recirculating aquaculture system. *Aquac. Res.* **2017**, *48*, 2133–2144. [CrossRef]
16. Sadhu, N.; Sharma, S.R.K.; Joseph, S.; Dube, P.; Philipose, K.K. Chronic stress due to high stocking density in open sea cage farming induces variation in biochemical and immunological functions in Asian seabass (*Lates calcarifer*, Bloch). *Fish Physiol. Biochem.* **2014**, *40*, 1105–1113. [CrossRef]
17. Van de Nieuwegiessen, P.G.; Boerlage, A.S.; Verreth, J.A.J.; Schrama, J.W. Assessing the effects of a chronic stressor, stocking density, on welfare indicators of juvenile African catfish, *Clarias gariepinus* Burchell. *Appl. Anim. Behav. Sci.* **2008**, *115*, 233–243. [CrossRef]
18. Costas, B.; Aragao, C.; Mancera, J.M.; Dinis, M.T.; Conceicao, L.E.C. High stocking density induces crowding stress and affects amino acid metabolism in Senegalese sole *Solea senegalensis* (Kaup 1858) juveniles. *Aquac. Res.* **2008**, *39*, 1–9. [CrossRef]
19. Zaki, M.A.A.; Alabssawy, A.N.; Nour, A.A.M.; El Basuini, M.F.; Dawood, M.A.O.; Alkahtani, S.; Abdel-Daim, M.M. The impact of stocking density and dietary carbon sources on the growth, oxidative status and stress markers of Nile tilapia (*Oreochromis niloticus*) reared under biofloc conditions. *Aquac. Rep.* **2020**, *16*, 100282. [CrossRef]
20. Sahin, K.; Yazlak, H.; Orhan, C.; Tuzcu, M.; Akdemir, F.; Sahin, N. The effect of lycopene on antioxidant status in rainbow trout (*Oncorhynchus mykiss*) reared under high stocking density. *Aquaculture* **2014**, *418*, 132–138. [CrossRef]
21. Wu, B.L.; Chen, J.; Huang, L.; Zhang, Y.; Fang, T.; He, J.X. Dynamics of soil fertility and microbial community response to stocking density in rice-turtle co-culture. *Aquac. Rep.* **2021**, *20*, 100765. [CrossRef]
22. Vongvichith, B.; Morioka, S.; Kawamura, K.; Mori, A. Factors Influencing Fish Productivity in Rice Paddy Aquaculture: A Case Study in Vientiane Province, Central Laos. *Jpn. Agric. Res. Q.* **2018**, *52*, 359–366. [CrossRef]
23. Li, X.D.; Dong, S.L.; Lei, Y.Z.; Li, Y.G. The effect of stocking density of Chinese mitten crab *Eriocheir sinensis* on rice and crab seed yields in rice-crab culture systems. *Aquaculture* **2007**, *273*, 487–493. [CrossRef]
24. Wang, D.; Wu, F. *China Fishery Statistical Yearbook*; China Agriculture Press: Beijing, China, 2021.
25. Sun, L. Key techniques of largemouth bass under pond culture. *Sci. Fish Farm.* **2020**, *10*, 20.

26. Watts, C.; Bright, L.A.; Coyle, S.; Tidwell, J. Evaluation of Stocking Density during Second-Year Growth of Largemouth Bass, *Micropterus salmoides*, Raised Indoors in a Recirculating Aquaculture System. *J. World Aquac. Soc.* **2016**, *47*, 538–543. [CrossRef]
27. Ni, M.; Liu, M.; Lou, J.; Mi, G.; Yuan, J.; Gu, Z. Stocking density alters growth performance, serum biochemistry, digestive enzymes, immune response, and muscle quality of largemouth bass (*Micropterus salmoides*) in in-pond raceway system. *Fish Physiol. Biochem.* **2021**, *47*, 1243–1255. [CrossRef] [PubMed]
28. Wang, L.; Jia, S.P.; Guo, X.R.; Lu, K.; Zhang, L.; Gong, J.H.; Guo, X.P.; Hu, Y.J.; Cheng, T.; Shang, Q.L.; et al. Effect of stocking density on growth of largemouth bass (*Micropterus salmoides*) cultured in containers in a land-based recirculating aquaculture system (C-RAS). *Aquac. Res.* **2022**, *53*, 1518–1526. [CrossRef]
29. Wang, Y.Y.; Xu, G.C.; Nie, Z.J.; Li, Q.J.; Shao, N.L.; Xu, P. Effect of Stocking Density on Growth, Serum Biochemical Parameters, Digestive Enzymes Activity and Antioxidant Status of Largemouth Bass, *Micropterus salmoides*. *Pak. J. Zool.* **2019**, *51*, 1509–1517. [CrossRef]
30. Tidwell, J.H.; Webster, C.D.; Coyle, S.D.; Schulmeister, G. Effect of Stocking Density on Growth and Water Quality for Largemouth Bass *Micropterus salmoides* Growout in Ponds. *J. World Aquac. Soc.* **1998**, *29*, 79–83. [CrossRef]
31. Li, D. Ecological culture technology of largemouth bass in rice field. *New Countrys.* **2021**, *12*, 27.
32. Xia, H. Rice paddy cultivation techniques for largemouth bass. *Rich Peasant.* **2022**, *3*, 32–33.
33. Tao, X.; Li, B.; Yu, Z.; Hou, Y.; Wang, L.; Zhu, J. Effects of rice-crayfish integrated model on root exudates and microorganisms of rice during grain filling. *J. Fish. China* ***2021*** . Available online: http://kns.cnki.net/kcms/detail/31.1283.s.20211223.1112.006.html (accessed on 17 May 2022).
34. Zhao, Z.; Chu, C.; Zhou, D.; Wang, Q.; Wu, S.; Zheng, X.; Song, K.; Lv, W. Soil bacterial community composition in rice–fish integrated farming systems with different planting years. *Sci. Rep.* **2021**, *11*, 10855. [CrossRef] [PubMed]
35. Szollosi, R.; Varga, I.S. Total antioxidant power in some species of Labiatae (Adaptation of FRAP method). *Acta Biol. Szeged.* **2002**, *46*, 125–127.
36. Bhabak, K.P.; Mugesh, G. A Simple and Efficient Strategy To Enhance the Antioxidant Activities of Amino-Substituted Glutathione Peroxidase Mimics. *Chemistry* **2008**, *14*, 8640–8651. [CrossRef] [PubMed]
37. Li, X.; Xu, L.; Zhou, W.; Zhao, Q.; Wang, Y. Chronic exposure to microcystin-LR affected mitochondrial DNA maintenance and caused pathological changes of lung tissue in mice. *Environ. Pollut.* **2016**, *210*, 48–56. [CrossRef] [PubMed]
38. Matthews, R. Methods of Enzymatic Analysis. *J. Clin. Pathol.* **1987**, *40*, 934. [CrossRef]
39. Fan, J.; Cai, H.; Yang, S.; Yan, L.; Tan, W. Comparison between the effects of normoxia and hypoxia on antioxidant enzymes and glutathione redox state in ex vivo culture of CD34(+) cells. *Comp. Biochem. Physiol. Part B Biochem. Mol. Biol.* **2008**, *151*, 153–158. [CrossRef]
40. Ohkawa, H.; Wakatsuki, A.; Kaneda, C. Assay for lipid peroxides in animal tissues by thiobarbituric acid reaction. *Anal. Biochem.* **1979**, *95*, 351–358. [CrossRef]
41. Smith, P.K.; Krohn, R.I.; Hermanson, G.T.; Mallia, A.K.; Gartner, F.H.; Provenzano, M.D.; Fujimoto, E.K.; Goeke, N.M.; Olson, B.J.; Klenk, D.C. Measurement of protein using bicinchoninic acid. *Anal. Biochem.* **1985**, *150*, 76–85. [CrossRef]
42. Chen, S.; Zhou, Y.; Chen, Y.; Jia, G. fastp: An ultra-fast all-in-one FASTQ preprocessor. *Bioinformatics* **2018**, *34*, i884–i890. [CrossRef]
43. Kim, D.; Langmead, B.; Salzberg, S.L. HISAT: A fast spliced aligner with low memory requirements. *Nat. Methods* **2015**, *12*, 357–360. [CrossRef] [PubMed]
44. Dewey, C.N.; Li, B. RSEM: Accurate transcript quantification from RNA-Seq data with or without a reference genome. *BMC Bioinform.* **2011**, *12*, 323.
45. Love, M.I.; Huber, W.; Anders, S. Moderated estimation of fold change and dispersion for RNA-seq data with DESeq2. *Genome Biol.* **2014**, *15*, 550. [CrossRef] [PubMed]
46. Subramanian, A.; Tamayo, P.; Mootha, V.K.; Mukherjee, S.; Ebert, B.L.; Gillette, M.A.; Paulovich, A.; Pomeroy, S.L.; Golub, T.R.; Lander, E.S.; et al. Gene set enrichment analysis: A knowledge-based approach for interpreting genome-wide expression profiles. *Proc. Natl. Acad. Sci. USA* **2005**, *102*, 15545–15550. [CrossRef]
47. Livak, K.; Schmittgen, T. Analysis of relative gene expression data using real-time quantitative PCR and the 2(-Delta Delta C(T)) Method. *Methods Companion Methods Enzymol.* **2001**, *25*, 402–408. [CrossRef] [PubMed]
48. Ezhilmathi, S.; Ahilan, B.; Uma, A.; Felix, N.; Cheryl, A.; Somu Sunder Lingam, R. Effect of stocking density on growth performance, digestive enzyme activity, body composition and gene expression of Asian seabass reared in recirculating aquaculture system. *Aquac. Res.* **2022**, *53*, 1963–1972. [CrossRef]
49. Montenegro, L.F.; Cunzolo, S.; Preussler, C.A.; Hennig, H.H.; Descalzo, A.M.; Perez, C.D. Effects of stocking density on productive performance, economic profit and muscle chemical composition of pacu (*Piaractus mesopotamicus* H) cultured in floating cages. *Aquac. Res.* **2022**. [CrossRef]
50. Engle, C.R.; Stone, N.; Xie, L. Feasibility of Pond Production of Largemouth Bass, *Micropterus salmoides*, for a Filet Market. *J. World Aquac. Soc.* **2013**, *44*, 805–813. [CrossRef]
51. Hengsawat, K.; Ward, F.; Jaruratjamorn, P. The effect of stocking density on yield, growth and mortality of African catfish (*Clarias gariepinus* Burchell 1822) cultured in cages. *Aquaculture* **1997**, *152*, 67–76. [CrossRef]
52. Lupatsch, I.; Santos, G.; Schrama, J.; Verreth, J. Effect of stocking density and feeding level on energy expenditure and stress responsiveness in European sea bass *Dicentrarchus labrax*. *Aquaculture* **2010**, *298*, 245–250. [CrossRef]

53. Montero, D.; Izquierdo, M.S.; Tort, L.; Robaina, L.; Vergara, J.M. High stocking density produces crowding stress altering some physiological and biochemical parameters in gilthead seabream, *Sparus aurata*, juveniles. *Fish Physiol. Biochem.* **1999**, *20*, 53–60. [CrossRef]
54. Chiu, P.-S.; Chu, Y.-T.; Huang, C.-H.; Ho, S.-W.; Huang, J.-W.; Yeh, S.-L. Effects of stocking density on growth performance, survival and size heterogeneity of juvenile longfin batfish *Platax teira*. *Aquac. Res.* **2020**, *51*, 5269–5272. [CrossRef]
55. Garcia, F.; Romera, D.M.; Gozi, K.S.; Onaka, E.M.; Fonseca, F.S.; Schalch, S.H.; Candeira, P.G.; Guerra, L.O.; Carmo, F.J.; Carneiro, D.J. Stocking density of Nile tilapia in cages placed in a hydroelectric reservoir. *Aquaculture* **2013**, *410*, 51–56. [CrossRef]
56. Ni, J.; Wang, Y.; Xu, G.; Nie, Z.; Sun, Y.; Li, Q.; Xu, P. Effects of stocking density on growth, physiological indices and expression of GH and IGF-I genes of largemouth bass *Micropterus salmoides* in in-pond raceway culture systems. *J. Danlian Ocean. Univ.* **2020**, *35*, 805–813.
57. Quintero, H.; Roy, L.A.; Park, J.; Kelly, A.M.; Heikes, D. Evaluation of alternative pond production systems for raising largemouth bass, *Micropterus salmoides*. *J. World Aquac. Soc.* **2019**, *50*, 622–632. [CrossRef]
58. Qi, C.L.; Xie, C.X.; Tang, R.; Qin, X.; Wang, D.Y.; Li, D.P. Effect of Stocking Density on Growth, Physiological Responses, and Body Composition of Juvenile Blunt Snout Bream, *Megalobrama amblycephala*. *J. World Aquac. Soc.* **2016**, *47*, 358–368. [CrossRef]
59. Guo, H.Y.; Dong, X.Y.; Zhang, X.M.; Zhang, P.D.; Li, W.T. Survival, growth and physiological responses of juvenile Japanese flounder (*Paralichthys olivaceus*, Temminck & Schlegel, 1846) exposed to different dissolved oxygen concentrations and stocking densities. *J. Appl. Ichthyol.* **2017**, *33*, 731–739. [CrossRef]
60. Bracewell, P.; Cowx, I.G.; Uglow, R.F. Effects of handling and electrofishing on plasma glucose and whole blood lactate of Leuciscus cephalus. *J. Fish Biol.* **2004**, *64*, 65–71. [CrossRef]
61. Yang, Q.; Guo, L.; Liu, B.-S.; Guo, H.-Y.; Zhu, K.-C.; Zhang, N.; Jiang, S.-G.; Zhang, D.-C. Effects of stocking density on the growth performance, serum biochemistry, muscle composition and HSP70 gene expression of juvenile golden pompano *Trachinotus ovatus* (Linnaeus, 1758). *Aquaculture* **2020**, *518*, 734841. [CrossRef]
62. Carbonara, P.; Alfonso, S.; Zupa, W.; Manfrin, A.; Fiocchi, E.; Pretto, T.; Spedicato, M.T.; Lembo, G. Behavioral and physiological responses to stocking density in sea bream (*Sparus aurata*): Do coping styles matter? *Physiol. Behav.* **2019**, *212*, 112698. [CrossRef]
63. Refaey, M.M.; Li, D.; Tian, X.; Zhang, Z.; Zhang, X.; Li, L.; Tang, R. High stocking density alters growth performance, blood biochemistry, intestinal histology, and muscle quality of channel catfish Ictalurus punctatus. *Aquaculture* **2018**, *492*, 73–81. [CrossRef]
64. Suárez, M.D.; Trenzado, C.E.; García-Gallego, M.; Furné, M.; García-Mesa, S.; Domezain, A.; Alba, I.; Sanz, A. Interaction of dietary energy levels and culture density on growth performance and metabolic and oxidative status of rainbow trout (*Oncorhynchus mykiss*). *Aquac. Eng.* **2015**, *67*, 59–66. [CrossRef]
65. Costas, B.; Aragao, C.; Dias, J.; Afonso, A.; Conceicao, L.E.C. Interactive effects of a high-quality protein diet and high stocking density on the stress response and some innate immune parameters of Senegalese sole *Solea senegalensis*. *Fish Physiol. Biochem.* **2013**, *39*, 1141–1151. [CrossRef] [PubMed]
66. Liu, B.L.; Fei, F.; Li, X.T.; Wang, X.Y.; Huang, B. Effects of stocking density on stress response, innate immune parameters, and welfare of turbot (*Scophthalmus maximus*). *Aquac. Int.* **2019**, *27*, 1599–1612. [CrossRef]
67. Agrahar, S.; Pandey, K.C.; Gopal, K. Biochemical alteration induced by monocrotophos in the blood plasma of fish, *Channa punctatus* (Bloch). *Pestic. Biochem. Physiol.* **2007**, *88*, 268–272. [CrossRef]
68. Andrade, T.; Afonso, A.; Perez-Jimenez, A.; Oliva-Teles, A.; de las Heras, V.; Mancera, J.M.; Serradeiro, R.; Costas, B. Evaluation of different stocking densities in a Senegalese sole (*Solea senegalensis*) farm: Implications for growth, humoral immune parameters and oxidative status. *Aquaculture* **2015**, *438*, 6–11. [CrossRef]
69. Ruiz, M.A.; Betancor, M.B.; Montero, D.; Caballero, M.J.; Hernandez-Cruz, C.M.; Rosenlund, G.; Fontanillas, R.; Izquierdo, M.S. The effect of fish stocking density and dietary supplementation of vitamin C and micronutrients (Mn, Zn and Se) on the development of systemic granulomatosis in juvenile meagre (*Argyrosomus regius*). *Aquac. Res.* **2021**, *52*, 5703–5718. [CrossRef]
70. Birnie-Gauvin, K.; Costantini, D.; Cooke, S.J.; Willmore, W.G. A comparative and evolutionary approach to oxidative stress in fish: A review. *Fish Fish.* **2017**, *18*, 928–942. [CrossRef]
71. Sies, H. Oxidative stress: Oxidants and antioxidants. *Exp. Physiol.* **1997**, *82*, 291–295. [CrossRef]
72. Choi, C.Y.; Choi, J.Y.; Choi, Y.J.; Kim, B.-S.; Kim, J.-W. Effects of green wavelength light on antioxidant and non-specific immune responses of the olive flounder Paralichthys olivaceus maintained at different stocking densities. *Aquac. Eng.* **2019**, *84*, 23–28. [CrossRef]
73. Wang, X.M.; Dai, W.; Xu, M.; Pan, B.P.; Li, X.Q.; Chen, Y.T. Effects of Stocking Density on Growth, Nonspecific Immune Response, and Antioxidant Status in African Catfish (*Clarias gariepinus*). *Isr. J. Aquac. Bamidgeh* **2013**, *65*, 20667.
74. Gutteridge, J.M.C.; Halliwell, B. The measurement and mechanism of lipid peroxidation in biological systems. *Trends Biochem. Sci.* **1990**, *15*, 129–135. [CrossRef]
75. Gaschler, M.M.; Stockwell, B.R. Lipid peroxidation in cell death. *Biochem. Biophys. Res. Commun.* **2017**, *482*, 419–425. [CrossRef]
76. Hoseini, S.M.; Yousefi, M.; Mirghaed, A.T.; Paray, B.A.; Hoseinifar, S.H.; Doan, H.V. Effects of rearing density and dietary tryptophan supplementation on intestinal immune and antioxidant responses in rainbow trout (*Oncorhynchus mykiss*). *Aquaculture* **2020**, *528*, 735537. [CrossRef]
77. Zhou, W.; Rahimnejad, S.; Lu, K.; Wang, L.; Liu, W. Effects of berberine on growth, liver histology, and expression of lipid-related genes in blunt snout bream (*Megalobrama amblycephala*) fed high-fat diets. *Fish Physiol. Biochem.* **2019**, *45*, 83–91. [CrossRef]

78. Tolussi, C.E.; Hilsdorf, A.W.S.; Caneppele, D.; Moreira, R.G. The effects of stocking density in physiological parameters and growth of the endangered teleost species piabanha, *Brycon insignis* (Steindachner, 1877). *Aquaculture* **2010**, *310*, 221–228. [CrossRef]
79. Montero, D.; Robaina, L.E.; Socorro, J.; Vergara, J.M.; Tort, L.; Izquierdo, M.S. Alteration of liver and muscle fatty acid composition in gilthead seabream (*Sparus aurata*) juveniles held at high stocking density and fed an essential fatty acid deficient diet. *Fish Physiol. Biochem.* **2001**, *24*, 63–72. [CrossRef]
80. Qiang, J.; Bao, J.W.; He, J.; Tao, Y.F.; Habte-Tsion, H.M.; Xu, P. Growth, biochemical, fatty acid composition, and mRNA levels of hepatic enzymes in genetically improved farmed tilapia (GIFT, *Oreochromis niloticus*) (Linnaeus, 1758) at different stocking densities. *J. Appl. Ichthyol.* **2017**, *33*, 757–766. [CrossRef]
81. He, Y.; Yu, H.; Zhao, H.; Zhu, H.; Zhang, Q.; Wang, A.; Shen, Y.; Xu, X.; Li, J. Transcriptomic analysis to elucidate the effects of high stocking density on grass carp (*Ctenopharyngodon idella*). *BMC Genom.* **2021**, *22*, 620. [CrossRef]
82. Liu, Y.; Liu, H.B.; Wu, W.; Yin, J.S.; Mou, Z.B.; Hao, F.H. Effects of stocking density on growth performance and metabolism of juvenile Lenok (*Brachymystax lenok*). *Aquaculture* **2019**, *504*, 107–113. [CrossRef]
83. Tocher; Douglas, R. Metabolism and Functions of Lipids and Fatty Acids in Teleost Fish. *Rev. Fish. Sci.* **2003**, *11*, 107–184. [CrossRef]
84. Wang, Y.P.; Nakajima, T.; Gonzalez, F.J.; Tanaka, N. PPARs as Metabolic Regulators in the Liver: Lessons from Liver-Specific PPAR-Null Mice. *Int. J. Mol. Sci.* **2020**, *21*, 2061. [CrossRef] [PubMed]
85. Yang, Z.; Roth, K.; Agarwal, M.; Liu, W.; Petriello, M.C. The transcription factors CREBH, PPARa, and FOXO1 as critical hepatic mediators of diet-induced metabolic dysregulation. *J. Nutr. Biochem.* **2021**, *95*, 108633. [CrossRef] [PubMed]
86. Ren, Y.; Wen, H.; Li, Y.; Li, J.; He, F.; Ni, M. Effects of stocking density on lipid deposition and expression of lipid-related genes in Amur sturgeon (*Acipenser schrenckii*). *Fish Physiol. Biochem.* **2017**, *43*, 1707–1720. [CrossRef]
87. Xu, H.G.; Zhang, X.; Wei, Y.L.; Sun, B.; Jia, L.L.; Liang, M.Q. Effects of dietary phosphorus level and stocking density on tiger puffer Takifugu rubripes: Growth performance, body composition, lipid metabolism, deposition of phosphorus and calcium, serum biochemical parameters, and phosphorus excretion. *Aquaculture* **2020**, *529*, 735709. [CrossRef]
88. Zhang, J.; Liu, F. Tissue-specific insulin signaling in the regulation of metabolism and aging. *IUBMB Life* **2014**, *66*, 485–495. [CrossRef]
89. Morales, P.E.; Bucarey, J.L.; Espinosa, A. Muscle lipid metabolism: Role of lipid droplets and perilipins. *J. Diabetes Res.* **2017**, *2017*, 1789395. [CrossRef]
90. Ma, J.L.; Qiang, J.; Tao, Y.F.; Bao, J.W.; Zhu, H.J.; Li, L.G.; Xu, P. Multi-omics analysis reveals the glycolipid metabolism response mechanism in the liver of genetically improved farmed Tilapia (GIFT, *Oreochromis niloticus*) under hypoxia stress. *BMC Genom.* **2021**, *22*, 105. [CrossRef]
91. Huang, X.; Liu, G.; Guo, J.; Su, Z. The PI3K/AKT pathway in obesity and type 2 diabetes. *Int. J. Biol. Sci.* **2018**, *14*, 1483–1496. [CrossRef]
92. Hamann, I.; Petroll, K.; Hou, X.; Anwar-Mohamed, A.; El-Kadi, A.O.; Klotz, L.-O. Acute and long-term effects of arsenite in HepG2 cells: Modulation of insulin signaling. *Biometals* **2014**, *27*, 317–332. [CrossRef]
93. Zhou, C.P.; Huang, Z.; Lin, H.Z.; Wang, J.; Wang, Y.; Yu, W. Effects of dietary leucine on glucose metabolism, lipogenesis and insulin pathway in juvenile golden pompano *Trachinotus ovatus*. *Aquac. Rep.* **2021**, *19*, 100626. [CrossRef]
94. Zou, C.; Shao, J. Role of adipocytokines in obesity-associated insulin resistance. *J. Nutr. Biochem.* **2008**, *19*, 277–286. [CrossRef] [PubMed]
95. Zhang, H.Y.; Xu, P.; Jiang, Y.L.; Zhao, Z.X.; Feng, J.X.; Tai, R.Y.; Dong, C.J.; Xu, J. Genomic, Transcriptomic, and Epigenomic Features Differentiate Genes That Are Relevant for Muscular Polyunsaturated Fatty Acids in the Common Carp. *Front. Genet.* **2019**, *10*, 217. [CrossRef] [PubMed]
96. Long, Y.; Li, L.C.; Li, Q.; He, X.Z.; Cui, Z.B. Transcriptomic Characterization of Temperature Stress Responses in Larval Zebrafish. *PLoS ONE* **2012**, *7*, e37209. [CrossRef]
97. Sun, J.; Bian, C.; Ji, S.; Luo, X.; Ji, H. Greater potency of adipocytes compared with preadipocytes under lipopolysaccharide exposure in grass carp *Ctenopharyngodon idella*. *Fish Shellfish Immunol.* **2019**, *91*, 343–349. [CrossRef]
98. Barreto, M.O.; Rey Planellas, S.; Yang, Y.; Phillips, C.; Descovich, K. Emerging indicators of fish welfare in aquaculture. *Rev. Aquac.* **2022**, *14*, 343–361. [CrossRef]
99. Galhardo, L.; Oliveira, R.F. Psychological Stress and Welfare in Fish. *Annu. Rev. Biomed. Sci.* **2009**, *11*, 1–20.
100. Jia, E.; Jiang, W.; Liu, W.; Jiang, G.; Li, X.; Chi, C.; Zhang, D. Crowding stress-related protein markers: New candidates for assessing welfare of largemouth bass reared in an in-pond raceway system. *Aquaculture* **2022**, *550*, 737821. [CrossRef]
101. Zhang, Z.; Bai, Q.; Xu, X.; Guo, H.; Zhang, X. Effects of environmental enrichment on the welfare of juvenile black rockfish Sebastes schlegelii: Growth, behavior and physiology. *Aquaculture* **2020**, *518*, 734782. [CrossRef]
102. Santos, G.A.; Schrama, J.W.; Mamauag, R.; Rombout, J.; Verreth, J. Chronic stress impairs performance, energy metabolism and welfare indicators in European seabass (*Dicentrarchus labrax*): The combined effects of fish crowding and water quality deterioration. *Aquaculture* **2010**, *299*, 73–80. [CrossRef]
103. Van de Nieuwegiessen, P.G.; Olwo, J.; Khong, S.; Verreth, J.A.; Schrama, J.W. Effects of age and stocking density on the welfare of African catfish, *Clarias gariepinus* Burchell. *Aquaculture* **2009**, *288*, 69–75. [CrossRef]
104. North, B.; Turnbull, J.; Ellis, T.; Porter, M.; Migaud, H.; Bron, J.; Bromage, N. The impact of stocking density on the welfare of rainbow trout (*Oncorhynchus mykiss*). *Aquaculture* **2006**, *255*, 466–479. [CrossRef]

105. Turnbull, J.; Bell, A.; Adams, C.; Bron, J.; Huntingford, F. Stocking density and welfare of cage farmed Atlantic salmon: Application of a multivariate analysis. *Aquaculture* **2005**, *243*, 121–132. [CrossRef]
106. Hossain, M. The effects of density, light and shelter on the growth and survival of African catfish (*Clarias gariepinus* Burchell, 1822) fingerlings. *Aquaculture* **1998**, *160*, 251–258. [CrossRef]

antioxidants

MDPI

Article

Oxidative Stress Can Be Attenuated by 4-PBA Caused by High-Fat or Ammonia Nitrogen in Cultured Spotted Seabass: The Mechanism Is Related to Endoplasmic Reticulum Stress

Yanzou Dong [1], Lei Li [1], Tian Xia [1], Lina Wang [2], Liping Xiao [2], Nengshui Ding [2], Youlin Wu [2,*] and Kangle Lu [1,*]

[1] Key Laboratory of Healthy Mariculture for the East China Sea, Ministry of Agriculture and Rural Affairs, Fisheries College, Jimei University, Xiamen 361021, China; 201911908030@jmu.edu.cn (Y.D.); lileixlt@163.com (L.L.); 202011908013@jmu.edu.cn (T.X.)

[2] Key Laboratory of Swine Nutrition and Feed Science of Fujian Province, Fujian Aonong Biological Science and Technology Group Co., Ltd., Zhangzhou 363000, China; wanglina@aonong.com.cn (L.W.); xiaoliping@aonong.com.cn (L.X.); dingnengshui@aonong.com.cn (N.D.)

* Correspondence: wuyoulin@aonong.com.cn (Y.W.); lukangle@jmu.edu.cn (K.L.)

Abstract: Oxidative stress is a common phenomenon in aquaculture, which can be induced by nutritional or environmental factors. Generally, oxidative stress causes poor growth performance, metabolic dysregulation, and even the death of aquatic animals. To identify a nutritional intervention strategy, high-fat diet (HFD) feeding (Experiment I) and acute ammonia nitrogen challenge (Experiment II) tests were carried out. In Experiment I, HFD feeding significantly decreased the growth performance concomitantly with excessive fat deposition in the liver and abdomen. The addition of 4-PBA in the diet improved the excessive fat accumulation. The activities of antioxidative enzymes were suppressed, and the levels of lipid and protein peroxidation were increased, indicating that HFD feeding induced oxidative stress. The endoplasmic reticulum stress (ERs) related genes were downregulated in the HFD group. Under a transmission electron microscope (TEM), more swollen and dilated ER lumen could be observed. These results indicated that the HFD induced ERs activation. Although 4-PBA acted as a potent ERs inhibitor, as evidenced by the alleviated alterations of ERs molecules and the ER ultrastructure, the oxidative stress was also attenuated by 4-PBA. In Experiment II, dietary 4-PBA improved the tolerance to the acute ammonia nitrogen challenge, as lower mortality and serum aminotransferase activity was found. Further results showed that 4-PBA decreased the peroxidation content and attenuated ERs, thus confirming the correlation between oxidative stress and ERs. Our findings showed that dietary 4-PBA supplementation can attenuate oxidative stress induced by a HFD or acute ammonia challenge; the mechanism is related to its potent inhibition effect for ERs.

Keywords: 4-phenylbutyric acid; endoplasmic reticulum stress; oxidative stress; high-fat diet; ammonia nitrogen exposure

Citation: Dong, Y.; Li, L.; Xia, T.; Wang, L.; Xiao, L.; Ding, N.; Wu, Y.; Lu, K. Oxidative Stress Can Be Attenuated by 4-PBA Caused by High-Fat or Ammonia Nitrogen in Cultured Spotted Seabass: The Mechanism Is Related to Endoplasmic Reticulum Stress. *Antioxidants* **2022**, *11*, 1276. https://doi.org/10.3390/antiox11071276

Academic Editor: Stanley Omaye

Received: 30 May 2022
Accepted: 24 June 2022
Published: 28 June 2022

1. Introduction

Today, aquatic products are of significant nutritional interest for billions of people worldwide [1]. Furthermore, aquatic foods are regarded as ideal sources of quality protein and essential fatty acids, which could improve a range of human pathologies [2]. Over the past few decades, Chinese aquaculture production has been steadily pursuing growth, and it has become the fastest growing food production sector [3]; however, during the farming process, oxidative stress damage is ubiquitous, and it often seriously affects the growth performance, stress tolerance, and pathogen sensitivity of aquatic animals [4–6].

Oxidative stress occurs due to the disruptions between the generation of reactive oxygen species (ROS) and antioxidant defenses in living organisms [7]. Oxidative stress could cause damage to cells and tissues, and it mainly manifests as the peroxidation of

biomacromolecules and cell apoptosis [8,9]. In general, many exogenous factors can induce oxidative stress, including oxidized fat and high-fat diets, ammonia nitrogen, and so on [10–13]. Fat plays a dominant role in energy storage and supply for animals, due to its high energy density [14,15]; hence, the high-fat diet is extensively used in fish cultures for its protein-sparing effect [14,16,17]. Ammonia is the main nitrogen-based catabolic product that is released in the aquaculture system. Recently, a high-density pattern emerged in the aquaculture industry, which has become the main trigger for the overproduction of ammonia nitrogen [18]. The high-fat diet feeding, and the ammonia nitrogen compounds, can induce oxidative stress by overproducing ROS, nitric oxide, and reactive nitrogen species in fish [19]; therefore, there is a pressing need to reveal the underlying physiological mechanisms of oxidative stress induced by high-fat diet feeding and ammonia nitrogen, and to develop antioxidant strategies.

Spotted seabass (*Lateolabrax maculatus*) is a carnivorous species with a high growth speed, flesh quality, and economic value [20]. It has become the second major cultured marine fish in China, with 195,246 tons being produced in 2020 [21]. The high-fat diet is widely used in its artificial rearing, which often leads to fat deposition and oxidative stress [10]. Moreover, the stocking density of spotted seabass is often high, with a production of >100 kg/m^3; thus, it is a good model to study the oxidative stress caused by high-fat or ammonia nitrogen. Furthermore, the stress of the endoplasmic reticulum (ERs) is often found in fish that are exposed to high-fat diets or ammonia nitrogen [13,16,18,22]. The ER is also an important source of ROS, which accounts for approximately 25% of all ROS produced [23]. Recent findings showed that ERs-induced alterations in ROS production and scavenging mechanisms contribute to the worsening of oxidative stress [24]. Based on the above, the present study is conducted to evaluate the role of ERs in the process of oxidative stress and the regulation of 4-PBA on the oxidative stress of cultured fish.

2. Materials and Methods

2.1. Animals

Juvenile spotted seabass were purchased from a fish hatchery (Zhangzhou, China). Juveniles were first transported to the aquaculture system in Jimei University, and were kept in a 1500-L tank so that they could adapt to the experimental conditions for two weeks. In this period, fish were fed a Jia-kang brand commercial diet (Xiamen Jia-kang Foods Co., Ltd. Xiamen, China; 45% protein, 11% lipid) twice daily (8:00 and 17:00). The experimental conditions were maintained at the optimal water temperature (25–27 °C), pH (7.0–7.2), and level of dissolved oxygen (>6 mg/L).

2.2. Experimental Design

2.2.1. Experiment I: The High-Fat Diet Feeding Study

Two experimental diets were produced with an 11% or 17% lipid level, which is regarded as normal fat diet (NFD) and high-fat diet (HFD), respectively. Moreover, 4-phenylbutyric acid (4-PBA) was added to the diet by adding 4-PBA to the HFD at a dose of 50 mg/kg (regarded 4-PBA). The formulation and proximate composition of experimental diets are shown in Table S1. The protocols of diet production and proximate composition determination were introduced in a previous study [21].

A total of 270 healthy fish of similar sizes (13.05 ± 0.15 g) were randomly distributed into nine 200-L tanks (30 fish per tank) in a recirculating aquaculture system (RAS). Freshwater was provided with a mechanical filtration system, UV treatment, and constant aeration. Fish were fed with a NFD, HFD, and 4-BPA, and each experimental diet was hand-fed to fish from three tanks to achieve visual satiety twice daily (8:00 and 17:00). After eight weeks of feeding, the fish were euthanized with 100 mg/L MS-222 (Sigma, St. Louis, MO, USA). Then, bodyweights were measured, and liver sampling was conducted for analysis, in accordance with the method described in our recent study [10]. The experimental conditions were consistent with the conditions maintained during the acclimation period.

2.2.2. Experiment II: The Acute Ammonia Nitrogen Challenge Study

Fish from the same batch that were of similar initial sizes to the fish in Experiment I were distributed into six separate tanks (30 fish per tank). Three tanks of fish were fed a NFD and were regarded as control group, the other three were fed a NFD with 50 mg/kg 4-PBA supplementation, named the 4-PBA group. Feeding management is same as with Experiment I. After two weeks of feeding, an acute ammonia nitrogen challenge test was carried out. A stock solution of a high NH_4Cl concentration (10 g/L) was prepared and subsequently added to each tank, the ammonia nitrogen concentration was adjusted to 95 mg/L, and the 48 h LC_{50} was carried out in our preliminary test. After 48 h, serum and liver samples were conducted. During this period, the ammonia concentrations of each tank were detected by nesslerization [25] every 6 h, and adjusted with a NH_4Cl stock solution to maintain the desired concentration. One-third of the test water was replaced with fresh water every 12 h. Fish were fasting during this period.

2.3. Biochemical Assays

The contents of triglyceride (TG), protein carbonylation (PC), and malonaldehyde (MDA), and the activities of superoxide dismutase (SOD), catalase (CAT), and glutathione peroxidase (GSH-PX) were deleted in liver homogenate by using commercial kits (Nanjing JianCheng Bioengineering Institute, Nanjing, China). The activities of aspartate aminotransferase (AST) and alanine aminotransferase (ALT) were determined in serum in accordance with our recent study [26].

2.4. Liver Histology

Oil red O staining was used to evaluate fat deposition in the liver. Briefly, liver samples were fixed in a 10% formaldehyde solution for 24 h, then dehydrated in a 15% and 30% sugar solution at 4 °C. The dehydrated samples were embedded into an optimal cutting temperature (OCT) compound (Servicebio, Wuhan, China), and cut into 8 μm-thick sections using a freezing microtome (CRYOSTAR NX50, Thermo Scientific, Waltham, MA, USA). After that, sections were stained using oil red O and hematoxylin, then, they were observed and photographed under a microscope (DM5500B, Leica, Germany).

Transmission electron microscopy (TEM) analysis was conducted to observe hepatocellular ultrastructure. Samples were fixed in 2.5% glutaraldehyde solution overnight and post-fixed in osmic acid for 2 h at 4 °C. Then, the samples were dehydrated in gradient acetone solutions and embedded in epoxy resin. Ultrathin slices with a 60-nm thickness were produced, stained with uranyl acetate and lead citrate solutions, and observed under a TEM (Hitachi H-7650, Tokyo, Japan).

2.5. Gene Expression

A commercial kit (RC101-01, Vazyme Biotech Co., Ltd., Nanjing, China) was used to isolate the total RNA in the liver, according to the protocol provided by the manufacturer. Then, 1% agarose gel electrophoresis was carried out to investigate the RNA's integrity. The agarose was obtained from LABLEAD. Inc. (Beijing, China). A NanoDrop™ One spectrophotometer (Thermo Scientific, Waltham, MA, USA) was used to determine the purity at 260/280 nm. First-strand cDNA was obtained from 1 μg of the total RNA, and a commercial kit was used to achieve this (R211-01, Vazyme Biotech Co., Ltd., Nanjing, China). The residual genomic DNA was erased using a gDNA wiper.

Real-time quantitative PCR (qPCR) was conducted in accordance with the method described in our recent study [27]. The primer sequences used in the present study were shown in Table S2. The relative expression levels of target genes were normalized by *β-actin* and calculated using the $2^{-\Delta\Delta Ct}$ method.

2.6. Statistical Analysis

Statistical analysis was performed using SPSS Statistics 20. For Experiment I, one-way ANOVA and Tuckey's multiple range test were carried out to assess the differences

between three treatments. Student's *t*-test was utilized to evaluate the differences between two groups in Experiment II. Significance was set at $p < 0.05$ in both Experiment I and Experiment II, and all data were expressed as the means ± standard error (SE).

3. Results

3.1. Experiment I: The High-Fat Diet Feeding Study

3.1.1. Growth and Fat Accumulation

Fish that were fed the HFD showed a significantly lower weight gain (WG) and feed efficiency (FE) compared with fish that were fed the NFD. In addition, 4-PBA supplementation significantly improved the WG and FE (Figure 1).

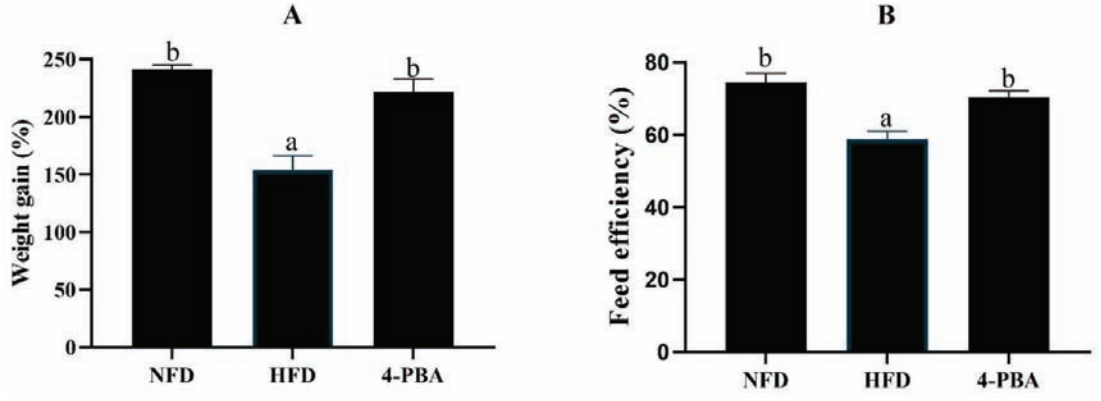

Figure 1. Weight gain (**A**) and feed efficiency (**B**) of spotted seabass (*L. maculatus*) that were fed the test diets for eight weeks. All values are exhibited as mean ± SE. The values with different superscripts (a, b) are significantly different at $p < 0.05$ (Tukey's test). Weight gain = final body weight/initial body weight; Feed efficiency = wet weight gain/dry feed fed.

Moreover, fish that were fed the HFD exhibited excessive fat deposition compared with other groups. Severe liver steatosis was observed under oil red O straining. Hepatic triacylglycerol (TAG) content was also enhanced by the HFD. Furthermore, 4-PBA supplementation significantly reduced the oil red O-stained area and TAG content of hepatocytes (Figure 2).

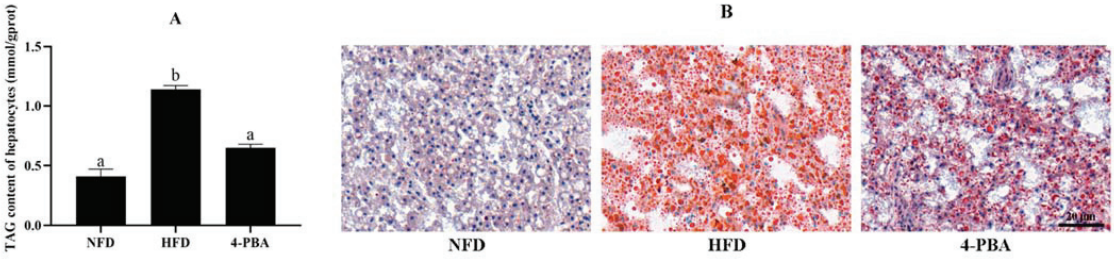

Figure 2. Hepatic TAG content (**A**) and oil red O-stained sections ((**B**) scale bar = 20 μm) of spotted seabass (*L. maculatus*) fed the test diets for eight weeks. All values are exhibited as mean ± SE. The values with different superscripts (a, b) are significantly different at $p < 0.05$ (Tukey's test).

3.1.2. Oxidative Status

In the liver, the activities/level of CAT, SOD, GPX, and T-AOC of fish that were fed the HFD significantly decreased, whereas MDA and PC content significantly increased.

The supplementation of 4-PBA dramatically elevated the activity/level of SOD, GPX, and T-AOC, and reduced the MDA and PC content (Figure 3).

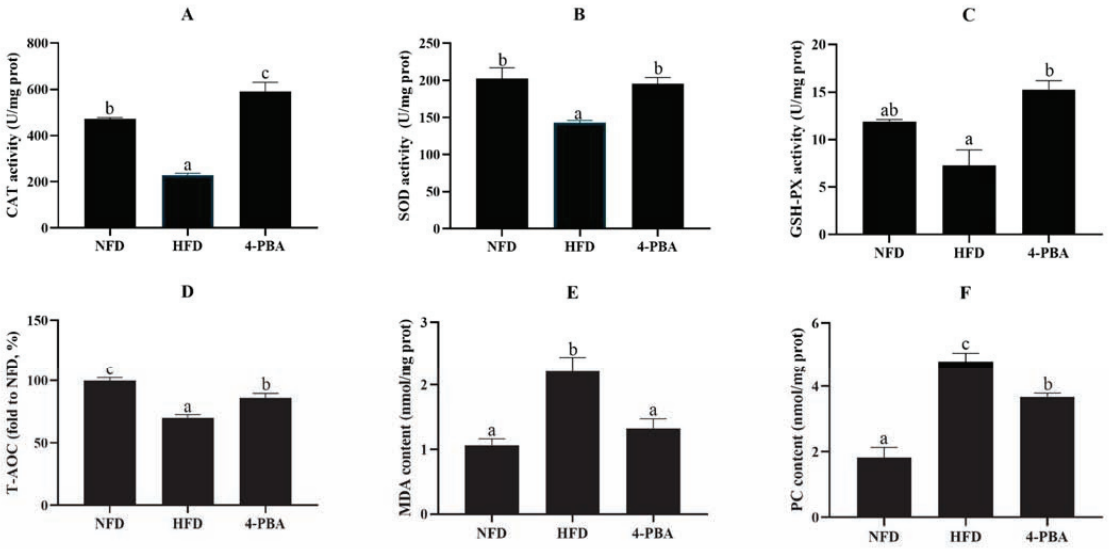

Figure 3. The activities of catalase (CAT: (**A**)), superoxide dismutase (SOD: (**B**)), glutathione peroxidase (GSH-PX: (**C**)), the level of total antioxidant capacity (T-AOC: (**D**)), and the content of malondialdehyde (MDA: (**E**)) and protein carbonylation (PC: (**F**)) in the livers of spotted seabass (*L. maculatus*) that were fed the test diets for eight weeks. All values are exhibited as mean ± SE. The values with different superscripts (a, b, c) are significantly different at $p < 0.05$ (Tukey's test).

3.1.3. Endoplasmic Reticulum Stress

The expressions of ERS-related genes (*ATF-6*, *IRE-1*, *PERK*, *EIF-2α*, *ATF-4*, *GRP78*, and *CHOP*) were significantly upregulated by HFD feeding, and the application of 4-PBA significantly downregulated the expressions of these genes. (Figure 4).

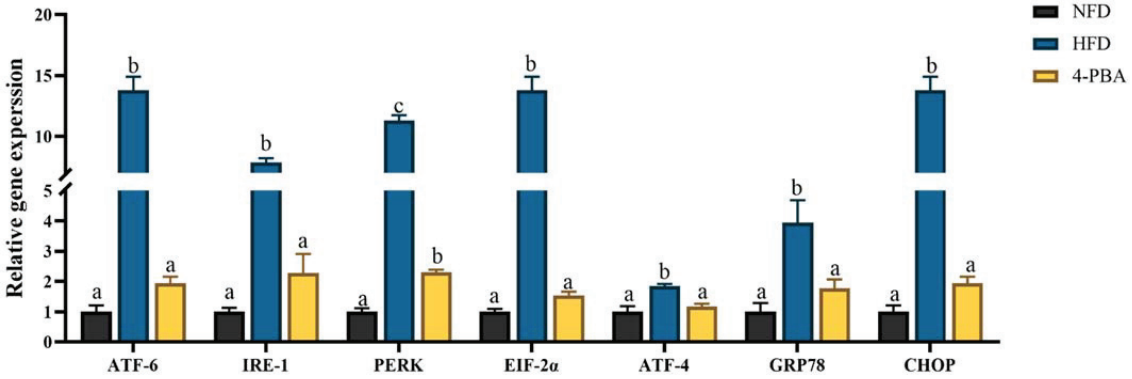

Figure 4. Relative expression levels of ERs-related genes in the livers of *L. maculatus* that were fed the test diets for eight weeks. All values are exhibited as mean ± SE. The values with different superscripts (a, b, c) are significantly different at $p < 0.05$ (Tukey's test).

Under the electron microscope, abnormalities were found in the livers of fish that were fed the HFD diet. In fish that were fed the NFD diet, the hepatocytes had stacks of rough endoplasmic reticulum (rER) that were concentrated around the nucleus and

cell membrane borders; however, there was also a widespread swelling of the ER in fish that were fed the HFD diet. More mitochondria showed matrix losses in the HFD group, whereas this phenomenon was rare in the NFD and HFD+4-PBA groups (Figure 5).

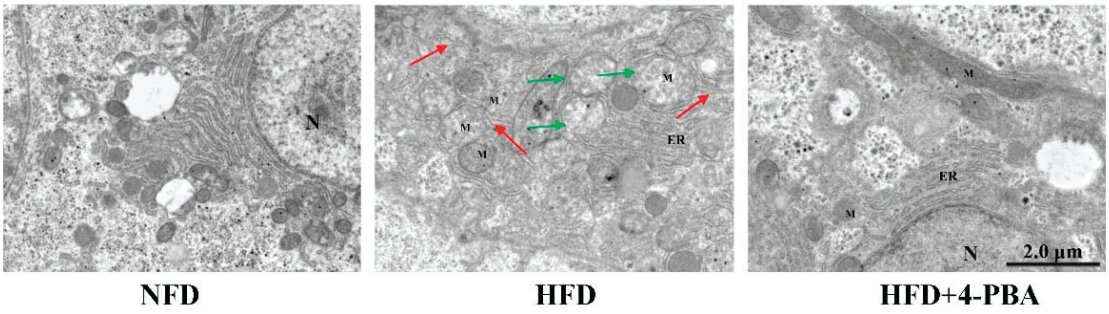

Figure 5. Hepatic transmission electron microscopy (TEM) images of *L. maculatus* that were fed the test diets for eight weeks. (N—nucleus; M—mitochondrion; green arrows—damaged mitochondria; red arrows—damaged endoplasmic reticulum).

3.2. Experiment II: The Ammonia Nitrogen Exposure Study

3.2.1. The Survival and Liver Damage of Fish

After 48 h of ammonia nitrogen exposure, the mortality of the control group was about 50%, whereas the mortality of the 4-PBA group was significantly lower. The activity of ALT in the control group is significantly higher than that of the 4-PBA group, and the activity of AST exhibited the same trend but it did not cause a significant difference (Figure 6).

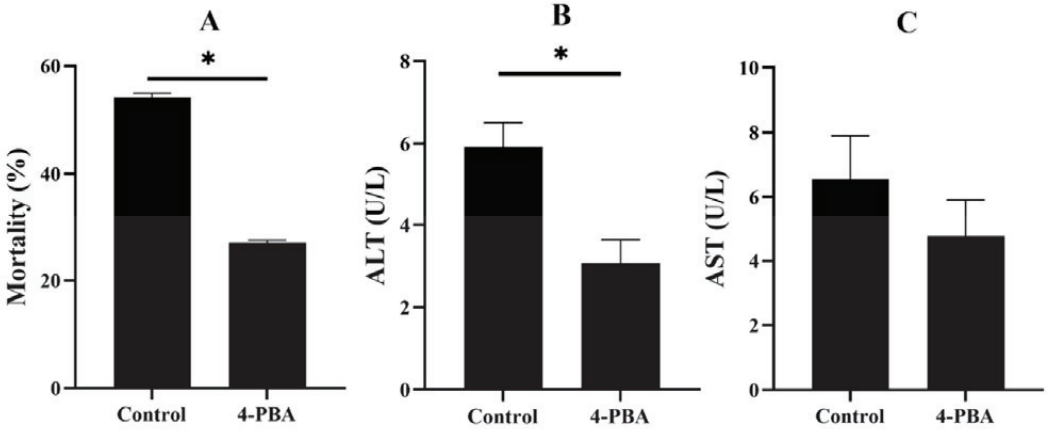

Figure 6. Mortality (**A**) and serum alanine aminotransferase (**B**) and aspartate aminotransferase (**C**) activities of *L. maculatus* after two weeks of being fed the test diets and 48 h of ammonia nitrogen exposure. All values are exhibited as mean ± SE. The values with different superscript (*) are significantly different at $p < 0.05$ (Student's *t*-test).

3.2.2. Oxidative Status

The activities/levels of SOD and T-AOC in the fish that were fed the control diet significantly decreased, compared with the 4-PBA group. Although, the content of MDA and PC were much higher in the control group than in the 4-PBA group (Figure 7).

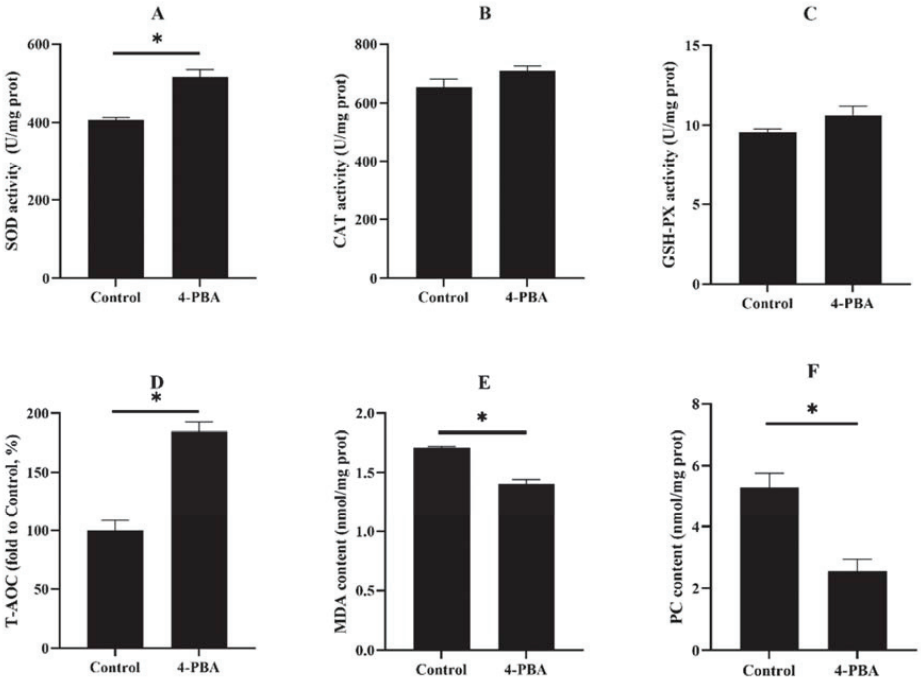

Figure 7. The activities of superoxide dismutase (SOD: (**A**)), catalase (CAT: (**B**)), glutathione peroxidase (GSH-PX (**C**)), the level of total antioxidant capacity (T-AOC: (**D**)), and the content of malondialdehyde (MDA: (**E**)) and protein carbonylation (PC: (**F**)) in the livers of *L. maculatus* after two weeks of being fed the test diets and 48 h of ammonia nitrogen exposure. All values are exhibited as mean ± SE. The values with different superscript (*) are significantly different at $p < 0.05$ (Student's *t*-test).

3.2.3. Endoplasmic Reticulum Stress

The expression levels of ERS-related genes (*CHOP*, *GRP78*, *ATF4*, *ATF6*, and *EIF-2α*) in the control group were remarkably higher than those in the 4-PBA group (Figure 8). The ultrastructural damage of the ER could be observed in both groups; however, in the control group, more ER lumens presented severe dilatation, and the ER network was fragmented (Figure 9).

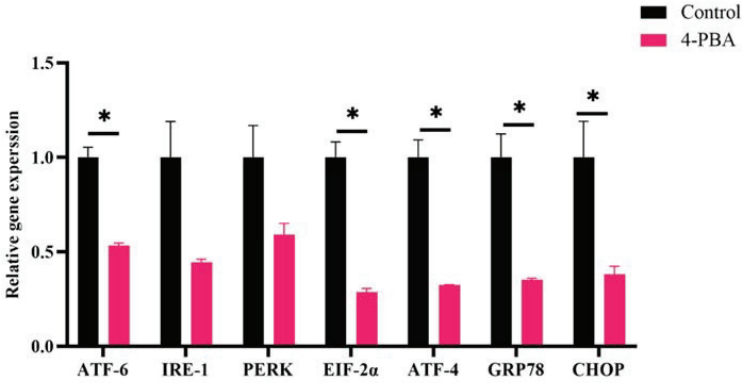

Figure 8. Relative expression levels of ERs-related genes in the livers of *L. maculatus* after two weeks of being fed the test diets and 48 h of ammonia nitrogen exposure. All values are exhibited as mean ± SE. The values with different superscript (*) are significantly different at $p < 0.05$ (Student's *t*-test).

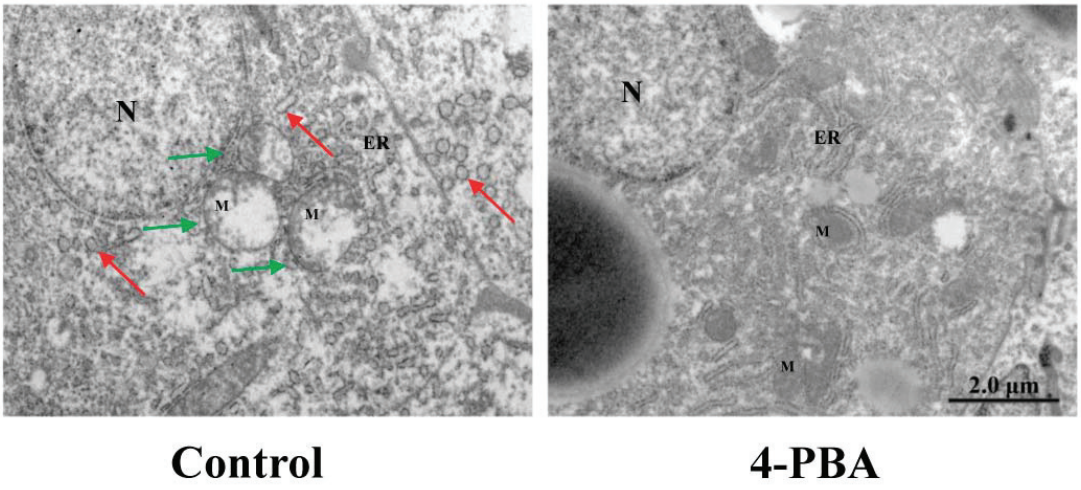

Figure 9. Hepatic transmission electron microscopy (TEM) images of *L. maculatus* after two weeks of being fed the test diets and 48 h of ammonia nitrogen exposure. (N—nucleus; M—mitochondrion; green arrows—damaged mitochondria; red arrows—damaged endoplasmic reticulum).

4. Discussion

Oxidative stress refers to the excess reactive oxygen species (ROS) production that can be stimulated by environmental and nutritional factors [28]. ROS can induce the oxidative damage of biomacromolecules and cellular membrane systems [29]. Emerging evidence also indicates that ROS often initiate the inflammation response and apoptosis [30,31].

High fat intake could cause excess fat accumulation and induce oxidative stress in fish [27,32]. Moreover, the the activities of antioxidative enzymes (CAT, SOD, and GSH-PX) decreased, and then, peroxidation occurred. In the present study, the increased MDA and PC levels indicated that HFD feeding induced oxidative stress.

The endoplasmic reticulum (ER) is composed of a complex membrane system and is susceptible to attacking ROS [33]. As the main site of protein synthesis, folding, modification, and secretion, oxidative damage to the ER often induces protein unfolding or/and misfolding [34]. The aggregation of unfolded/misfolded proteins activates endoplasmic reticulum stress (ERs) [35]. Previous studies have demonstrated that ERs activation reiles on unfolded protein response (UPR) pathways [36]. As it is downstream of UPR, CHOP plays a vital role in ERs-mediated cytotoxicity, given its contributor role to apoptosis [37]. These molecules of the UPR pathway are well accepted as biomarkers of ERs. In this study, the expressions of ERs-related genes (*ATF-6*, *IRE-1*, *PERK*, *Eif-2α*, *ATF-4*, *GRP78*, and *CHOP*) were upregulated through HFD feeding. Moreover, swollen endoplasmic reticula were observed under TEM. These results indicated that HFD feeding activated ERs. Similar results have also been reported in other fish [16,22,38] and rodent models that were fed high-fat diets [39,40]. Furthermore, 4-Phenylbutyric acid (4-PBA) has an effect on misfolded and unfolded proteins; therefore, it can be used as a specific inhibitor of ERs [41,42]. The present results showed that dietary 4-PBA significantly decreased ERs induced by a HFD.

There are many proteins involved in the synthesis and export of lipids that are folded or/and bounded at the ER. Hence, the ER also plays a key role in the homeostasis of lipid metabolism [43]. The overload of lipid metabolism leads to continuous ERs, which leads to lipid synthesis as a result of the protein metabolism in the ER [43,44]. In the present study, 4-PBA exhibited fat lowering effects that are dependent on ER metabolism remolding. The fat-lowering effect of 4-PBA also contributed to the alleviation of oxidative stress [45].

It is reported that there is an interplay between ERs and oxidative stress [23]. The overexpression of UPR components, such as CHOP and ATF4, directly contribute to ROS

synthesis in the ER [33]. Moreover, the impaired ER can translate Ca^{2+} to mitochondria through the calcium release channel and mitochondrial-associated membranes, which exaggerates the production of ROS via the electron transport chain (ETC) [46]. In the present study, the expression of *CHOP* and *ATF4* were downregulated by dietary 4-PBA. Moreover, the analysis of TEM showed that HFD-induced mitochondrial damage was also alleviated. Based on these phenomena, we postulate that 4-PBA also inhibits ROS formation in both the ER and mitochondria.

There are many factors in the aquaculture environment that can be triggers of oxidative stress [6,47]. Notably, the highly intensive aquaculture industry has boomed in recent decades, as there has been a high demand for fish products [48]. Thus, fish often suffer ammonia nitrogen stress in the highly intensive culture [12]. The high ammonia nitrogen concentration can cause serious tissue damage and high mortality, which is a high-risk factor during fish farming [49–51]. Ammonia nitrogen stress can rapidly gather in the blood and tissue of fish and act as a potent cause of oxidative stress [52]. Fish that were fed the 4-PBA supplementation diet had a lower mortality rate and serum transaminases activities after the acute ammonia nitrogen challenge. This indicates that dietary 4-PBA can improve the tolerance of fish to ammonia stress. Further analysis showed that 4-PBA can enhance antioxidative abilities and reduce the peroxidation of proteins and lipids. Moreover, 4-PBA downregulated the gene expression of UPR factors. This indicates that 4-PBA supplementation exhibits the protective effect of ER homeostasis in fish that are exposed to high ammonia nitrogen concentrations.

5. Conclusions

In summary, the present study showed that ERs played an important role in the oxidative stress induced by a HFD or stress caused by high ammonia nitrogen concentrations. Furthermore, 4-PBA can attenuate the stress of the ER and excess fat deposition caused by the HFD feeding. Moreover, the supplementation of 4-PBA can increase the tolerance of fish that have suffered ammonia stress.

Supplementary Materials: The following supporting information can be downloaded at: https://www.mdpi.com/article/10.3390/antiox11071276/s1, Table S1: Formulation and Proximate Composition of Experimental Diets; Table S2: Sequences of Primers Used for RT-qPCR.

Author Contributions: Conceptualization, K.L., L.L. and Y.D.; methodology, L.W., L.X., N.D. and Y.W.; formal analysis, Y.D., L.L. and T.X.; investigation, Y.D. and L.L.; writing—original draft preparation, Y.D.; writing—review and editing, Y.W. and K.L.; visualization, Y.D.; supervision, K.L. All authors have read and agreed to the published version of the manuscript.

Funding: This work was funded by the National Natural Science Foundation of China (32072984), the Natural Science Foundation of Fujian Province (2020J01664), and China Agriculture Research System (CARS-47).

Institutional Review Board Statement: The animal study protocol was approved by the Ethics Committee of Animal Research Institute Committee guidelines, Jimei University, China (No. 2020-29, Approval date: 15 June 2020).

Informed Consent Statement: Not applicable.

Data Availability Statement: The data presented in this study are available on request from the corresponding author.

Conflicts of Interest: K.L. has received research grants from the Fujian Aonong Biological Science and Technology Group Co., Ltd. Moreover, L.W., L.X., N.S. and Y.W. are employees of the Fujian Aonong Biological Science and Technology Group Co., Ltd.

References

1. Tigchelaar, M.; Cheung, W.W.L.; Mohammed, E.Y.; Phillips, M.J.; Payne, H.J.; Selig, E.R.; Wabnitz, C.C.C.; Oyinlola, M.A.; Frolicher, T.L.; Gephart, J.A.; et al. Compound climate risks threaten aquatic food system benefits. *Nat. Food* **2021**, *2*, 673–682. [CrossRef]
2. Golden, C.D.; Koehn, J.Z.; Shepon, A.; Passarelli, S.; Free, C.M.; Viana, D.F.; Matthey, H.; Eurich, J.G.; Gephart, J.A.; Fluet-Chouinard, E.; et al. Aquatic foods to nourish nations. *Nature* **2021**, *598*, 315–320. [CrossRef] [PubMed]
3. Wang, J.; Beusen, A.H.W.; Liu, X.; Bouwman, A.F. Aquaculture Production is a Large, Spatially Concentrated Source of Nutrients in Chinese Freshwater and Coastal Seas. *Environ. Sci. Technol.* **2020**, *54*, 1464–1474. [CrossRef] [PubMed]
4. Chen, M.; Zhou, J.; Lin, J.; Tang, H.; Shan, Y.; Chang, A.K.; Ying, X. Changes in oxidative stress biomarkers in *Sinonovacula constricta* in response to toxic metal accumulation during growth in an aquaculture farm. *Chemosphere* **2020**, *248*, 125974. [CrossRef] [PubMed]
5. Gao, J.; Koshio, S.; Ishikawa, M.; Yokoyama, S.; Mamauag, R.E.P. Interactive effects of vitamin C and E supplementation on growth performance, fatty acid composition and reduction of oxidative stress in juvenile Japanese flounder *Paralichthys olivaceus* fed dietary oxidized fish oil. *Aquaculture* **2014**, *422*, 84–90. [CrossRef]
6. Birnie-Gauvin, K.; Costantini, D.; Cooke, S.J.; Willmore, W.G. A comparative and evolutionary approach to oxidative stress in fish: A review. *Fish. Fish.* **2017**, *18*, 928–942. [CrossRef]
7. Sevcikova, M.; Modra, H.; Slaninova, A.; Svobodova, Z. Metals as a cause of oxidative stress in fish: A review. *Vet. Med.* **2011**, *56*, 537–546. [CrossRef]
8. Klaunig, J.E.; Wang, Z.; Pu, X.; Zhou, S. Oxidative stress and oxidative damage in chemical carcinogenesis. *Toxicol. Appl. Pharmacol.* **2011**, *254*, 86–99. [CrossRef]
9. Liguori, I.; Russo, G.; Curcio, F.; Bulli, G.; Aran, L.; Della-Morte, D.; Gargiulo, G.; Testa, G.; Cacciatore, F.; Bonaduce, D.; et al. Oxidative stress, aging, and diseases. *Clin. Intero. Aging* **2018**, *13*, 757–772. [CrossRef]
10. Dong, Y.-Z.; Xia, T.; Lin, J.-B.; Wang, L.; Song, K.; Zhang, C.-X. Quercetin Attenuates High-Fat Diet-Induced Excessive Fat Deposition of Spotted Seabass (*Lateolabrax maculatus*) Through the Regulatory for Mitochondria and Endoplasmic Reticulum. *Front. Mar. Sci.* **2021**, *8*, 746811. [CrossRef]
11. Gao, J.; Koshio, S.; Ishikawa, M.; Yokoyama, S.; Nguyen, B.T.; Mamauag, R.E. Effect of dietary oxidized fish oil and vitamin C supplementation on growth performance and reduction of oxidative stress in Red Sea Bream *Pagrus major*. *Aquac. Nutr.* **2013**, *19*, 35–44. [CrossRef]
12. Cheng, C.H.; Yang, F.F.; Ling, R.Z.; Liao, S.A.; Miao, Y.T.; Ye, C.X.; Wang, A.L. Effects of ammonia exposure on apoptosis, oxidative stress and immune response in pufferfish (*Takifugu obscurus*). *Aquat. Toxicol.* **2015**, *164*, 61–71. [CrossRef] [PubMed]
13. Liang, Z.; Liu, R.; Zhao, D.; Wang, L.; Sun, M.; Wang, M.; Song, L. Ammonia exposure induces oxidative stress, endoplasmic reticulum stress and apoptosis in hepatopancreas of pacific white shrimp (*Litopenaeus vannamei*). *Fish Shellfish Immunol.* **2016**, *54*, 523–528. [CrossRef]
14. Du, Z.Y.; Clouet, P.; Zheng, W.H.; Degrace, P.; Tian, L.X.; Liu, Y.J. Biochemical hepatic alterations and body lipid composition in the herbivorous grass carp (*Ctenopharyngodon idella*) fed high-fat diets. *Br. J. Nutr.* **2006**, *95*, 905–915. [CrossRef]
15. Li, Y.; Ding, W.; Li, C.-Y.; Liu, Y. HLH-11 modulates lipid metabolism in response to nutrient availability. *Nat. Commun.* **2020**, *11*, 5959. [CrossRef]
16. Cao, X.F.; Dai, Y.J.; Liu, M.Y.; Yuan, X.Y.; Wang, C.C.; Huang, Y.Y.; Liu, W.B.; Jiang, G.Z. High-fat diet induces aberrant hepatic lipid secretion in blunt snout bream by activating endoplasmic reticulum stress-associated IRE1/XBP1 pathway. *BBA Mol. Cell Biol. Lipids* **2019**, *1864*, 213–223. [CrossRef] [PubMed]
17. Xie, S.; Lin, Y.; Wu, T.; Tian, L.; Liang, J.; Tan, B. Dietary lipid levels affected growth performance, lipid accumulation, inflammatory response and apoptosis of japanese seabass (*lateolabrax japonicus*). *Aquac. Nutr.* **2021**, *27*, 807–816. [CrossRef]
18. Huang, Z.; Liang, L.; Li, N.; Li, W.; Yu, Z.; Zhang, J.; Shi, H.; Ding, L.; Hong, M. Ammonia exposure induces endoplasmic reticulum stress and apoptosis in Chinese striped-necked turtle (*Mauremys sinensis*). *Aquat. Toxicol.* **2021**, *237*, 105903. [CrossRef]
19. Seo, J.S.; Haque, M.N.; Nam, S.E.; Kim, B.M.; Rhee, J.S. Inorganic nitrogen compounds reduce immunity and induce oxidative stress in red seabream. *Fish Shellfish Immunol.* **2020**, *104*, 237–244. [CrossRef]
20. Lu, K.-L.; Cai, L.-S.; Wang, L.; Song, K.; Zhang, C.-X.; Rahimnejad, S. Effects of dietary protein/energy ratio and water temperature on growth performance, digestive enzymes activity and non-specific immune response of spotted seabass (*Lateolabrax maculatus*). *Aquac. Nutr.* **2020**, *26*, 2023–2031. [CrossRef]
21. Cai, L.-S.; Wang, L.; Song, K.; Lu, K.-L.; Zhang, C.-X.; Rahimnejad, S. Evaluation of protein requirement of spotted seabass (*Lateolabrax maculatus*) under two temperatures, and the liver transcriptome response to thermal stress. *Aquaculture* **2020**, *516*, 734615. [CrossRef]
22. Jia, R.; Cao, L.-P.; Du, J.-L.; He, Q.; Gu, Z.-Y.; Jeney, G.; Xu, P.; Yin, G.-J. Effects of High-Fat Diet on Steatosis, Endoplasmic Reticulum Stress and Autophagy in Liver of Tilapia (*Oreochromis niloticus*). *Front. Mar. Sci.* **2020**, *7*, 363. [CrossRef]
23. Ashraf, N.U.; Sheikh, T.A. Endoplasmic reticulum stress and Oxidative stress in the pathogenesis of Non-alcoholic fatty liver disease. *Free Radic. Res.* **2015**, *49*, 1405–1418. [CrossRef] [PubMed]
24. Chen, Z.; Tian, R.; She, Z.; Cai, J.; Li, H. Role of oxidative stress in the pathogenesis of nonalcoholic fatty liver disease. *Free Radic. Biol. Med.* **2020**, *152*, 116–141. [CrossRef] [PubMed]
25. Golterman, H.L. Direct nesslerization of ammonia and nitrate in fresh-water. *Ann. Limnol. Int. J. Limnol.* **1991**, *27*, 99–101. [CrossRef]
26. Zhou, W.; Rahimnejad, S.; Tocher, D.R.; Lu, K.; Zhang, C.; Sun, Y. Metformin attenuates lipid accumulation in hepatocytes of blunt snout bream (*Megalobrama amblycephala*) via activation of AMP-activated protein kinase. *Aquaculture* **2019**, *499*, 90–100. [CrossRef]

27. Dong, Y.; Xia, T.; Yu, M.; Wang, L.; Song, K.; Zhang, C.; Lu, K. Hydroxytyrosol Attenuates High-Fat-Diet-Induced Oxidative Stress, Apoptosis and Inflammation of Blunt Snout Bream (*Megalobrama amblycephala*) through Its Regulation of Mitochondrial Homeostasis. *Fishes* **2022**, *7*, 78. [CrossRef]
28. Sun, C.; Shan, F.; Liu, M.; Liu, B.; Zhou, Q.; Zheng, X.; Xu, X. High-Fat-Diet-Induced Oxidative Stress in Giant Freshwater Prawn (*Macrobrachium rosenbergii*) via NF-kappaB/NO Signal Pathway and the Amelioration of Vitamin E. *Antioxidants* **2022**, *11*, 228. [CrossRef]
29. Schieber, M.; Chandel, N.S. ROS Function in Redox Signaling and Oxidative Stress. *Curr. Biol.* **2014**, *24*, R453–R462. [CrossRef]
30. Shadel, G.S.; Horvath, T.L. Mitochondrial ROS Signaling in Organismal Homeostasis. *Cell* **2015**, *163*, 560–569. [CrossRef]
31. Zhang, J.; Wang, X.; Vikash, V.; Ye, Q.; Wu, D.; Liu, Y.; Dong, W. ROS and ROS-Mediated Cellular Signaling. *Oxidative Med. Cell. Longev.* **2016**, *2016*, 4350965. [CrossRef] [PubMed]
32. Lu, K.-L.; Wang, L.-N.; Zhang, D.-D.; Liu, W.-B.; Xu, W.-N. Berberine attenuates oxidative stress and hepatocytes apoptosis via protecting mitochondria in blunt snout bream *Megalobrama amblycephala* fed high-fat diets. *Fish Physiol. Biochem.* **2017**, *43*, 65–76. [CrossRef] [PubMed]
33. Zeeshan, H.M.A.; Lee, G.H.; Kim, H.-R.; Chae, H.-J. Endoplasmic Reticulum Stress and Associated ROS. *Int. J. Mol. Sci.* **2016**, *17*, 327. [CrossRef]
34. Xu, C.Y.; Bailly-Maitre, B.; Reed, J.C. Endoplasmic reticulum stress: Cell life and death decisions. *J. Clin. Investig.* **2005**, *115*, 2656–2664. [CrossRef]
35. Schroeder, M. Endoplasmic reticulum stress responses. *Cell. Mol. Life Sci.* **2008**, *65*, 862–894. [CrossRef]
36. Zhao, L.; Ackerman, S.L. Endoplasmic reticulum stress in health and disease. *Curr. Opin. Cell Biol.* **2006**, *18*, 444–452. [CrossRef] [PubMed]
37. Faitova, J.; Krekac, D.; Hrstka, R.; Vojtesek, B. Endoplasmic reticulum stress and apoptosis. *Cell. Mol. Biol. Lett.* **2006**, *11*, 488–505. [CrossRef]
38. Cao, X.-F.; Liu, W.-B.; Zheng, X.-C.; Yuan, X.-Y.; Wang, C.-C.; Jiang, G.-Z. Effects of high-fat diets on growth performance, endoplasmic reticulum stress and mitochondrial damage in blunt snout bream *Megalobrama amblycephala*. *Aquac. Nutr.* **2019**, *25*, 97–109. [CrossRef]
39. Wang, N.; Liu, Y.; Ma, Y.; Wen, D. Hydroxytyrosol ameliorates insulin resistance by modulating endoplasmic reticulum stress and prevents hepatic steatosis in diet-induced obesity mice. *J. Nutr. Biochem.* **2018**, *57*, 180–188. [CrossRef]
40. Li, J.; Huang, J.; Li, J.-S.; Chen, H.; Huang, K.; Zheng, L. Accumulation of endoplasmic reticulum stress and lipogenesis in the liver through generational effects of high fat diets. *J. Hepatol.* **2012**, *56*, 900–907. [CrossRef]
41. Oezcan, U.; Yilmaz, E.; Oezcan, L.; Furuhashi, M.; Vaillancourt, E.; Smith, R.O.; Goerguen, C.Z.; Hotamisligil, G.S. Chemical chaperones reduce ER stress and restore glucose homeostasis in a mouse model of type 2 diabetes. *Science* **2006**, *313*, 1137–1140. [CrossRef] [PubMed]
42. Warrell, R.P.; He, L.Z.; Richon, V.; Calleja, E.; Pandolfi, P.P. Therapeutic targeting of transcription in acute promyelocytic leukemia by use of an inhibitor of histone deacetylase. *J. Natl. Cancer. Inst.* **1998**, *90*, 1621–1625. [CrossRef] [PubMed]
43. Fu, S.; Watkins, S.M.; Hotamisligil, G.S. The Role of Endoplasmic Reticulum in Hepatic Lipid Homeostasis and Stress Signaling. *Cell Metab.* **2012**, *15*, 623–634. [CrossRef] [PubMed]
44. Fu, S.; Yang, L.; Li, P.; Hofmann, O.; Dicker, L.; Hide, W.; Lin, X.; Watkins, S.M.; Ivanov, A.R.; Hotamisligil, G.S. Aberrant lipid metabolism disrupts calcium homeostasis causing liver endoplasmic reticulum stress in obesity. *Nature* **2011**, *473*, 528–531. [CrossRef] [PubMed]
45. Halliwell, B.; Chirico, S. lipid-peroxidation—Its mechanism, measurement, and significance. *Am. J. Clin. Nutr.* **1993**, *57*, 715–725. [CrossRef]
46. Souza-Neto, F.V.; Jimenez-Gonzalez, S.; Delgado-Valero, B.; Jurado-Lopez, R.; Genty, M.; Romero-Miranda, A.; Rodriguez, C.; Nieto, M.L.; Martinez-Martinez, E.; Cachofeiro, V. The Interplay of Mitochondrial Oxidative Stress and Endoplasmic Reticulum Stress in Cardiovascular Fibrosis in Obese Rats. *Antioxidants* **2021**, *10*, 1274. [CrossRef]
47. Slaninova, A.; Smutna, M.; Modra, H.; Svobodova, Z. A review: Oxidative stress in fish induced by pesticides. *Neuroendocrinol. Lett.* **2009**, *30*, 2–12.
48. Sokolova, I.M.; Frederich, M.; Bagwe, R.; Lannig, G.; Sukhotin, A.A. Energy homeostasis as an integrative tool for assessing limits of environmental stress tolerance in aquatic invertebrates. *Mar. Environ. Res.* **2012**, *79*, 1–15. [CrossRef]
49. Wang, T.; Shan, H.-W.; Geng, Z.-X.; Yu, P.; Ma, S. Dietary supplementation with freeze-dried Ampithoe sp. enhances the ammonia-N tolerance of Litopenaeus vannamei by reducing oxidative stress and endoplasmic reticulum stress and regulating lipid metabolism. *Aquacult. Rep.* **2020**, *16*, 100264. [CrossRef]
50. Wang, T.; Yang, C.; Zhang, S.; Rong, L.; Yang, X.; Wu, Z.; Sun, W. Metabolic changes and stress damage induced by ammonia exposure in juvenile *Eriocheir sinensis*. *Ecotoxicol. Environ. Saf.* **2021**, *223*, 112608. [CrossRef]
51. Zhao, L.; Cui, C.; Liu, Q.; Sun, J.; He, K.; Adam, A.A.; Luo, J.; Li, Z.; Wang, Y.; Yang, S. Combined exposure to hypoxia and ammonia aggravated biological effects on glucose metabolism, oxidative stress, inflammation and apoptosis in largemouth bass (*Micropterus salmoides*). *Aquat. Toxicol.* **2020**, *224*, 105514. [CrossRef] [PubMed]
52. Xu, Z.; Cao, J.; Qin, X.; Qiu, W.; Mei, J.; Xie, J. Toxic Effects on Bioaccumulation, Hematological Parameters, Oxidative Stress, Immune Responses and Tissue Structure in Fish Exposed to Ammonia Nitrogen: A Review. *Animals* **2021**, *11*, 3304. [CrossRef] [PubMed]

antioxidants

MDPI

Article

Taurine Alleviates Cadmium-Induced Toxicity via Genetically Specific Strategies in Two Strains of Gibel Carp (*Carassius gibelio*)

Wenjie Xu [1,†], Hongyan Li [1,†], Liyun Wu [1,2], Junyan Jin [1,*], Dong Han [1], Xiaoming Zhu [1], Yunxia Yang [1], Haokun Liu [1] and Shouqi Xie [1,2,3]

[1] State Key Laboratory of Freshwater Ecology and Biotechnology, Institute of Hydrobiology, Chinese Academy of Sciences, Wuhan 430072, China; xuwenjie@gdou.edu.cn (W.X.); lihongyan@prfri.ac.cn (H.L.); wuliyun@ihb.ac.cn (L.W.); hand21cn@ihb.ac.cn (D.H.); xmzhu@ihb.ac.cn (X.Z.); yxyang@ihb.ac.cn (Y.Y.); liuhaokun@ihb.ac.cn (H.L.); sqxie@ihb.ac.cn (S.X.)
[2] College of Advanced Agricultural Sciences, University of Chinese Academy of Sciences, Beijing 100049, China
[3] The Innovative Academy of Seed Design, Chinese Academy of Sciences, Beijing 100101, China
* Correspondence: jinjunyan@ihb.ac.cn
† These authors contributed equally to this work.

Abstract: Our previous studies in gibel carp (*Carassius gibelio*) have shown that cadmium (Cd) exposure elicits deleterious effects depending on the genetic background, and thus we hypothesized that mitigation via nutritional intervention may vary between strains. Therefore, two gibel carp strains (the A and F strains) were fed diets supplemented with 0% or 1% taurine for 8 weeks prior to 96 h Cd exposure, and the responses of antioxidant pathways, endoplasmic reticulum (ER) stress, autophagy, and apoptosis were investigated. The results showed that taurine supplementation had no effect on the growth performance of gibel carp. After Cd exposure, histological damage to mitochondria and ER, induction of oxidative stress and antioxidant responses, occurrence of ER stress, and apoptotic signals were observed in the livers. Upon the diet effects, taurine supplementation alleviated the ER-stress-induced autophagy and apoptosis after Cd exposure and stimulated antioxidant pathways. Regarding the difference between strains, taurine played a protective role in alleviating Cd toxicity through the antioxidant response, ER stress, and autophagy in the F strain, whereas such effects were achieved by the attenuation of apoptosis in the A strain. Taken together, our results demonstrate the potential use of taurine in the mitigation of heavy metal toxicity in aquatic organisms.

Keywords: taurine; Cd exposure; strain; autophagy; apoptosis

Citation: Xu, W.; Li, H.; Wu, L.; Jin, J.; Han, D.; Zhu, X.; Yang, Y.; Liu, H.; Xie, S. Taurine Alleviates Cadmium-Induced Toxicity via Genetically Specific Strategies in Two Strains of Gibel Carp (*Carassius gibelio*). *Antioxidants* **2022**, *11*, 1381. https://doi.org/10.3390/antiox11071381

Academic Editors: Bo Liu, Changyou Song and Cunxin Sun

Received: 2 June 2022
Accepted: 14 July 2022
Published: 16 July 2022

1. Introduction

Owing to widespread environmental pollution, the diverse hazardous impacts of exposure to toxic heavy metals on living organisms are becoming a global issue of great concern [1]. Cadmium (Cd) is one of the most abundant environmental pollutants in the biosphere, and it can be both toxic and carcinogenic [2,3]. Compared to other animals, aquatic species are vulnerable to Cd toxicity via the dietborne as well as the waterborne routes [4,5]. Therefore, aquatic toxicological evaluation of the effects of Cd has been widely investigated in teleosts under chronic or acute exposure in species such as gilthead sea bream, tilapia, yellow perch, and gibel carp (*Carassius gibelio*) [6–9].

Cadmium is reported to elicit deleterious effects via neurotoxicity, immunotoxicity, induction of oxidative stress, damage to organ structure, and cellular dysfunction [2,10]. Much effort has been made to investigate the mechanism of Cd toxicity and to develop a safe therapeutic approach to mitigating the toxic effects [1]. Some chemopreventive agents such as garlic extract containing specific organosulfur compounds have been used to protect against the toxic effects of Cd in both animal models and cell lines [11,12]. Cd

exposure disrupts the cellular oxidative homeostasis [13] that is regulated by various enzymatic or non-enzymatic antioxidants. Importantly, oxidative stress and glutathione (GSH) depletion are crucial components of Cd toxicity in aquatic organisms [14]. Therefore, nutrients with antioxidant properties have been applied to ameliorate the hepatotoxicity by modulating antioxidant pathways, such nutrients include vitamin C, vitamin E, carotenoids, and selenium [1,15].

Taurine (TAU, 2-amino ethanesulfonic acid), as a semi-essential amino acid, is a derivative of a sulfur-containing amino acid that has multiple functions in fish physiology [16]. Taurine is usually supplemented as an additive in the diet of aquatic animals for the promotion of growth as well as boosting the reproduction system, immune functions, and antioxidant effects [17]. The mechanism of the antioxidant activity of taurine was reported to be associated with enhanced mitochondrial function that protects the mitochondria from excessive superoxide [18]. In addition, taurine has been considered as a promising candidate for the improvement of liver function, and it has been reported as possessing tissue protective effects in treating oxidant-induced injury [19,20]. In mammalian models, taurine has been reported to alleviate the toxic effects of copper, lead, aluminum, and cadmium [21–23]. Similarly, administration of taurine affected hepatic metabolism and reduced Cd contamination in red sea bream and catfish [16,24]. Nevertheless, the mechanisms underlying the ameliorative effects of taurine against Cd poisoning in teleost fish are still not fully elaborated.

Previous studies have shown that exposure to Cd caused different toxic effects in gibel carp (*Carassius gibelio*) A strain (CAS III) and F strain (CAS V), regardless of whether via the dietborne or waterborne routes [9,25]. Specifically, these two strains of gibel carp showed genetically based metabolic strategies in response to Cd toxicity, verifying the fact that differences in genetic background may be an important cause of metabolic differences between fish strains. To ascertain the potential of taurine in the prevention of Cd poisoning and to explore whether these effects would vary between the two strains, experiments were performed with taurine supplementation via the diet route in the present study. We assessed the liver functions of the two strains, because the liver is the center of intermediary metabolism and plays vital roles in detoxifying processes [26,27].

2. Materials and Methods

2.1. Experimental Procedures

The experimental scheme is illustrated in Figure 1. Gibel carp used in this trial were obtained from the hatchery of the Institute of Hydrobiology, the Chinese Academy of Sciences, Wuhan, Hubei, China. The healthy and uniformly sized gibel carp A (4.61 $\pm$ 0.03 g) and F (4.58 $\pm$ 0.04 g) strains were fed diets supplemented with 0% (Control) or 1% TAU for 8 weeks (Figure 1, Phase 1). Diets were formulated in the laboratory according to the procedures described by Li et al. [28]. The diet formulation and approximate composition are shown in Table 1. Therefore, four groups of fish were obtained: the A strain fed the control diet (A0), the A strain fed a 1% TAU supplemented diet (A1), the F strain fed the control diet (F0), and the F strain fed a 1% TAU supplemented diet (F1).

After the 8-week feeding trial, a challenge test was conducted with fish from each of the four groups by exposing the fish to acute waterborne Cd (11.9 mg/L) (Figure 1, Phase 2). Cd exposure was performed in a static aquarium system with continuous aeration for 96 h, with 10 fish per tank and triplicate replicates for each tank. The concentration of Cd was set based on the value shown by a preliminary experiment that identified the 96 h median lethal concentration (LC50) [25]. $CdCl_2 \cdot 2.5\ H_2O$ was added to the water by diluting a stock solution according to methods described by Li et al. [25]. During the acute exposure experiment, water in the system was refreshed daily. This experiment was implemented following the guiding principles for the care and use of laboratory animals and was approved by the Institute of Hydrobiology, Chinese Academy of Sciences.

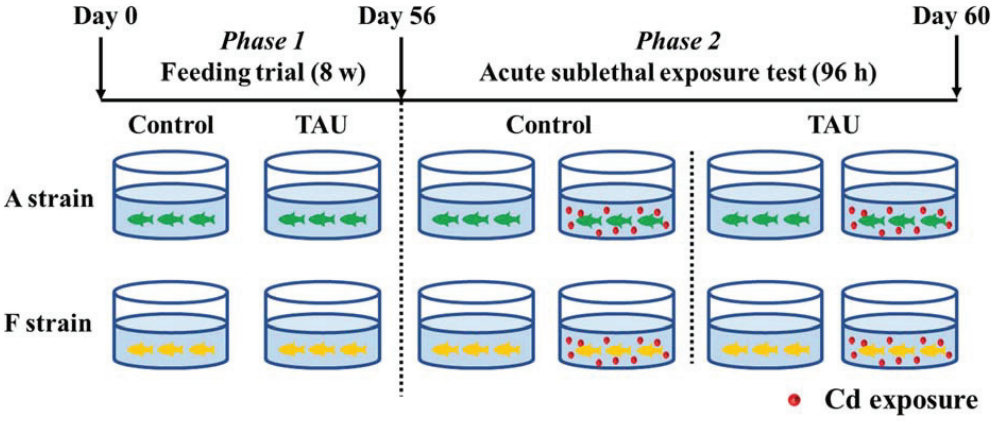

Figure 1. Experimental design. Control: control diet; TAU: diet supplemented with taurine.

Table 1. Ingredients and proximate composition of the experimental diets (g/kg).

Ingredients	Control	TAU
White fishmeal [1]	100	100
Wheat gluten	100	100
Soybean meal [2]	170	170
Rapeseed meal [2]	170	170
Fish oil	33	33
Soybean oil	33	33
Wheat flour	250	250
Taurine	0	10
Vitamin premix [3]	3.9	3.9
Choline chloride	1.1	1.1
Mineral premix [4]	50	50
CMC	30	30
Cellulose	59	59
Chemical composition (g/kg)		
Crude protein	340.5	344.0
Crude lipid	82.5	80.2
Ash	74.8	74.6
Moisture	79.3	88.1

[1] Fish meal was purchased from American Seafood Company, Seattle, Washington, USA. [2] Soybean and rapeseed meal were purchased from Coland Feed Co. Ltd., Wuhan, Hubei, China. [3] Vitamin premix (mg/kg diet): vitamin A, 1.65; vitamin D, 0.025; vitamin E, 50; vitamin K, 10; ascorbic acid, 100; thiamin, 20; riboflavin, 20; pyridoxine, 20; cyanocobalamine, 0.02; folic acid, 5; calcium pantothenate, 50; inositol, 100; niacin, 100; biotin, 0.1; cellulose, 645.2. [4] Mineral premix (mg/kg diet): NaCl, 500; $MgSO_4 \cdot 7H_2O$, 8155.6; $NaH_2PO_4 \cdot 2H_2O$, 12,500.0; KH_2PO_4, 16,000.0; $CaHPO_4 \cdot H_2O$, 7650.6; $FeSO_4 \cdot 7H_2O$, 2286.2; $C_6H_{10}CaO_6 \cdot 5H_2O$, 1750.0; $ZnSO_4 \cdot 7H_2O$, 178.0; $MnSO_4 \cdot H_2O$, 61.4; $CuSO_4 \cdot 5H_2O$, 15.5; $CoSO_4 \cdot 7H_2O$, 0.5; KI, 1.5; corn starch, 753.7.

2.2. Sample Collection

At the end of the 96 h Cd waterborne experiment, fish were anesthetized with MS-222 solution (Aminobenzoate methanesulfonate, 0.06 g/L, Sigma, St. Louis, MO, USA). The livers of two fish from each tank were dissected immediately on ice, with one part frozen in liquid nitrogen and then stored at −80 °C, and one part fixed in 2.5% glutaraldehyde solution and 4% paraformaldehyde.

2.3. Transmission Electron Microscopy (TEM) Observation

The liver samples of the two strains were dissected into 1 mm^3 cubes and then fixed immediately in 2.5% glutaraldehyde solution. The samples were then rinsed with 0.1 M phosphate buffer solution (pH = 7.4) three times (15 min each time). Postfixation was

conducted with 1% osmium tetroxide for 2 h, and then the fixed samples were washed three times with 0.1 M phosphate buffer solution (pH = 7.4). The dehydration was performed in a graded ethanol series followed by acetone. After that, samples were infiltrated with acetone:SPI-Pon 812 resin (1:1) followed by acetone:SPI-Pon 812 resin (1:2) and SPI-Pon 812 resin. Subsequently, the samples were embedded in SPI-Pon 812 resin for 48 h at 60 °C. Ultra-thin sections (80–100 nm) were stained with uranyl acetate and lead citrate. Finally, observations were conducted using a transmission electron microscope (Tecnai G2 20 TWIN, FEI, Hillsboro, OR, USA).

2.4. TUNEL Analysis

Terminal deoxynucleotidyl transferase dUTP nick end labeling (TUNEL) analyses were performed according to the procedure described by Li et al. [25]. The liver samples were fixed in 4% paraformaldehyde and then embedded in paraffin. After that, the samples were cut into 5 μm sections and deparaffinized in dimethylbenzene. The samples were dehydrated in a graded ethanol series, repaired with proteinase K, and permeabilized with Triton X-100/PBS solutions. DNA fragmentation was determined using TdT and dUTP reagents (1:9) for 2 h incubation followed by staining with 4′,6-diamidino-2-phenylindole (DAPI, 0.3 mmol/L) for 10 min. The samples were examined under a Nikon Eclipse Ti-SR inverted microscope.

2.5. Chemical and Biochemical Analyses

Cd concentrations in water samples were measured in accordance with the National Standards of the Republic of China (GB/T 7475-1987, Water quality determination of copper, zinc, lead and cadmium—atomic absorption spectrometry). In summary, sample digestion was conducted by adding hydrogen peroxide and concentrated nitric acid to the samples. After adding palladium nitrate, the samples were tested via inductively coupled plasma optical emission spectroscopy (ICP-OES, PerkinElmer Optima 8000, Waltham, MA, USA).

The activities of total antioxidant capacity (T-AOC), superoxide dismutase (SOD), reduced glutathione (GSH), glutathione peroxidase (GSH-Px), catalase (CAT), and the contents of malondialdehyde (MDA) were measured using commercial kits (Nanjing Jiancheng Bioengineering Institute, Nanjing, Jiangsu, China). The activity of caspase 3 (Casp3) in livers was tested using a commercial kit (Caspase 3 Activity Assay Kit, Be-yotime Biotechnology, Shanghai, China).

2.6. qRT-PCR Analysis

Total RNA from liver samples was extracted using TRIzol reagent (Ambion, Life Technologies, Austin, TX, USA) according to the manufacturer's instructions. The RNA integrity and purity were assessed by agarose gel electrophoresis and NanoDrop spectrophotometer determination, respectively. The cDNA was synthesized by reverse transcription using an M-MLV First-Strand Transcriptase kit (Invitrogen, Carlsbad, CA, USA). All quantitative real-time PCR (qRT-PCR) assays were performed on a LightCycler 480 System (Roche, Jena, Thüringen, Germany). The primers used for quantitative RT-PCR are shown in Table 2. The housekeeping gene *tubulin* was chosen to normalize the relative quantification of target genes according to the methods described by Pfaffl [29].

Table 2. Sequences of the primers used for qRT-PCR analysis in gibel carp.

Gene	Acronym	Prime Sequence	Amplicon Size (bp)	Accession No.
Tubulin	*tubulin*	TCCTTCAACACCTTCTTCAGTGAGAC	134	JX4135181
		AGCTGCTCAGGGTGGAACAGC		
Nuclear factor [erythroid-derived 2]-like 2	*nrf2*	CCCTTCACCAAAGACAAGCA	128	MG759384
		TTGAAGTCATCCACAGGCAG		
Kelch-like ECH-associated protein-1	*keap1*	CTCACCCCCAACTTCCTGCAG	150	MG759382
		GATGAGCTGCGGCACCTTGGG		
CNC homolog 1	*bach1*	TGGAGCGCAGGAGCTTTCGAG	98	XM_026282740
		AGTGGGGTTTGGTCGGCTGTG		
Peroxiredoxin 2	*prx2*	AGGTCATCGCTGCTTCCACCG	90	XM_026211451
		TGTTCATGGAGCCCAGGCCAC		
Heat shock protein 70	*hsp70*	CTCAACAAGAGCATCAACCCAG	155	JN006055.1
		ATGACTCCACCAGCCGTTTC		
Metallothionein	*mt*	AACTTGTTCGTCTGTGCTGG	93	XM_026230631.1
		GAGAACAACAGGGAGGTCGT		
Activating transcription factor 6	*atf6*	TGCAGGTGTATTACGCCCCTCAC	176	XM_026290872.1
		GTAATTCATAGCTGGCAGGACCAC		
Eukaryotic translation initiation factor 2A	*eif2a*	AGCTGCCAAAGAACGGCCCCATT	226	XM_026230526.1
		CAAACTTCCATCTGCCCTCTCAG		
Inositol-requiring protein-1α	*ire1*	GCGACCTTTCCTGCCTTACT	253	XM_026218282.1
		AGTCTCCTGTTTGGACAGCG		
X-box-binding protein 1	*xbp1*	CATCTACACCAAACCCACCGA	264	MN852578
		CATCCAGAGTCACTGTACGCA		
Eukaryotic translation initiation factor 2-alpha kinase 3	*perk*	TGCCATCAAGAGGATCCGTCTGC	122	XM_026224076.1
		CCTGCCAAGCATTGAAGTAACGG		

Table 2. *Cont.*

Gene	Acronym	Prime Sequence	Amplicon Size (bp)	Accession No.
Activating transcription factor 4	*atf4*	CAGCCGAGAGATCCGCTATC	215	XM_026260813.1
		GATGAGCCCCTTACTGGACG		
DNA damage-inducible transcript 3 protein	*chop*	ACCACTCCTCGCTGACAGA	88	XM_026265784.1
		TTAGAGGCCTCGGGTCGAT		
Endoplasmic reticulum oxidoreductase 1 alpha	*ero1α*	ATGCCCAACACAAGCAACAC	129	XM_026242578.1
		TGACAACAGCGACCGAAAGT		
Microtubule-associated proteins 1A/1B light chain 3B	*lc3b*	CTACGAGCGCGAGAGAGATG	81	XM_026238789.1
		TGAGGACACGCAGTTCCAAA		
Beclin-1	*beclin1*	TGGAGAACTTGAGTCGCAGG	129	XM_026249455.1
		GCTGAGTGTCCAGATGGTCG		
Autophagy protein 5	*atg5*	GCTCTTCCGACCAGTGTCTC	188	XM_026284696.1
		AGTTGTCTGGGTGGCTCAAG		
Autophagy protein 12	*atg12*	GCTGTTGAAAGCAGTAGGTGATG	170	XM_026284438.1
		GGTCTGGTGATGGAGCAAATGAC		
Apoptosis regulator Bcl-2	*bcl2*	AAAGGATGTACCAGCGCGAA	83	XM_026237836.1
		GGCTAAGAATCTGCGTTGCG		
BCL2 associated X, apoptosis regulator	*bax*	ACCCCAGCCATAAACGTCTTGCG	214	XM_026262399.1
		GCCTTGATGACAAGCCGACAC		
Caspase 3	*casp3*	ATCATGACCAGGGTCAACCA	119	XM_026266756.1
		TACATCTCTTTGGTGAGCAT		
Caspase 9	*casp9*	ATCACAAACTACCTCAACGG	80	XM_026241892.1
		CCTCCACAGGCCTGGATGAA		

2.7. Statistical Analysis

Results are presented as means ± standard errors. Normality and homoscedasticity of the data were assessed by Shapiro–Wilk and Levene tests. Two-way analysis of variance (ANOVA) was conducted with SPSS 26.0 (Chicago, IL, USA), and $p < 0.05$ was considered as a significant difference. Independent t-tests were conducted to examine the differences between pre- and post-challenge test groups. Gene expression heatmap of genes related to antioxidation, ER stress, autophagy, and apoptosis were created using heatmapper (http://www.heatmapper.ca/ accessed on 4 July 2022).

3. Results

3.1. Growth Performance

No significant differences in final body weight (FBW) or specific growth rate (SGR) were observed in the two strains of gibel carp fed diets with taurine supplementation (Figure 2). However, dietary taurine supplementation significantly decreased the feed efficiency (FE) and increased the feed conversion ratio (FCR) in both strains. The F strain presented significantly higher FBW, SGR, and FE and lower FCR than the A strain ($p < 0.05$). During the experiment, the survival rate of fish was 100%.

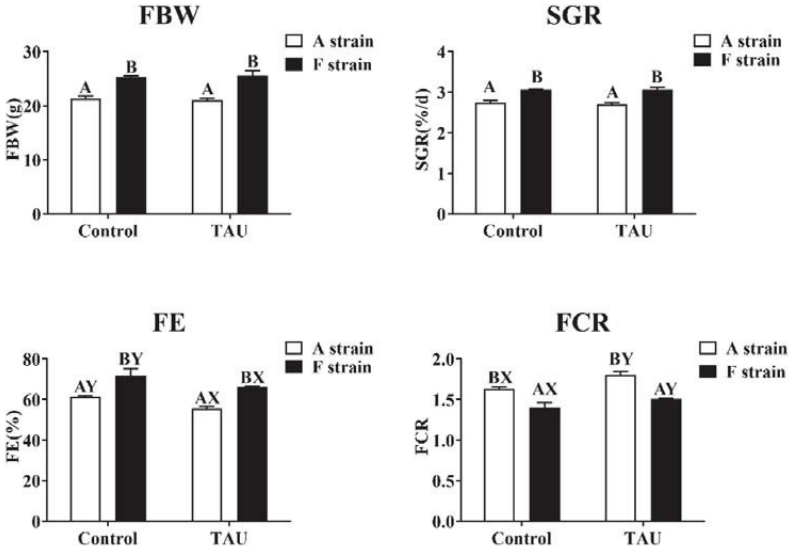

Figure 2. Specific growth rate and feed efficiency of two gibel carp strains fed the control diet and diet supplemented with taurine. Control: control diet, white bars; TAU: diet supplemented with taurine, black bars. FBW: final body weight; SGR: specific growth rate (%/d) = 100 × [ln (final weight) − ln (initial weight)]/day; FE: feeding efficiency (%) = (100 × body weight gain)/dry feed intake; FCR: feed conversion ratio = (100 × dry feed intake)/body weight gain. Bars with different uppercase letters (A, B) represent significant differences between the A and F strains ($p < 0.05$). Bars with different upper-case letters (X, Y) represent significant differences between the control diet group and the taurine diet group ($p < 0.05$).

3.2. Histological Observation

Ultrastructural images of the liver in the two gibel carp strains exposed to Cd are shown in Figure 3. Cd exposure induced ultrastructural alterations in the two gibel carp strains, as shown by the degenerated cristae and swelling of mitochondria. Meanwhile, irregular parallel stacked endoplasmic reticulum and plaque accumulation within hepatocytes were detected by transmission electron microscopy.

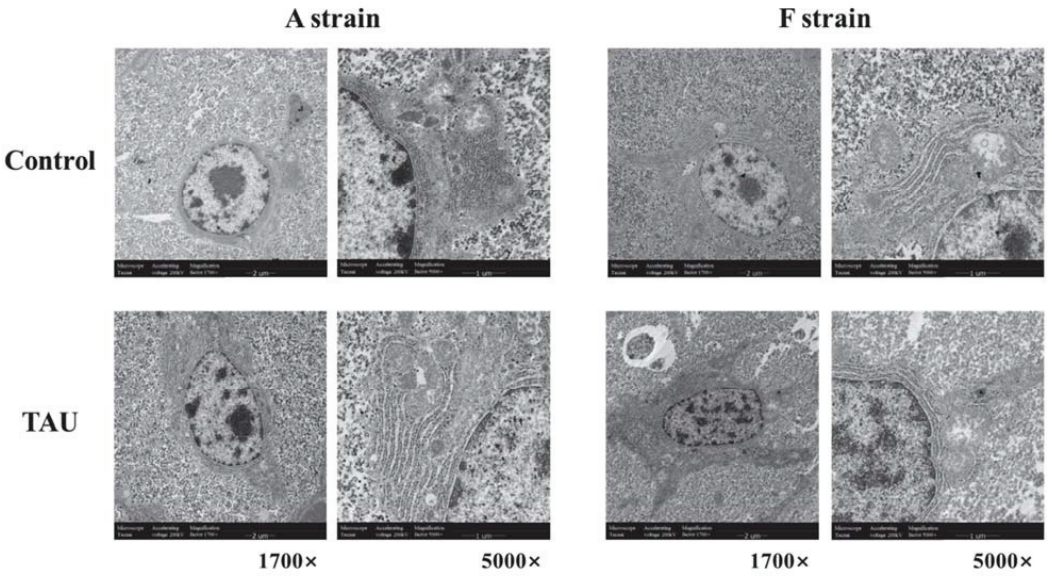

Figure 3. Representative histological transmission electron microscopy (TEM) images of gibel carp (A and F strains) after 96 h cadmium exposure. Control: control diet; TAU: diet supplemented with taurine.

A terminal deoxynucleotidyl transferase dUTP nick end labeling assay (TUNEL) was conducted to assess the apoptosis index in the livers of gibel carp (Figure 4). The results showed that apoptosis signals increased significantly after Cd exposure ($p < 0.05$), while dietary taurine supplementation decreased the apoptosis index compared with the control group. Moreover, the apoptosis index in the A strain fed the control diet was the highest ($p < 0.05$).

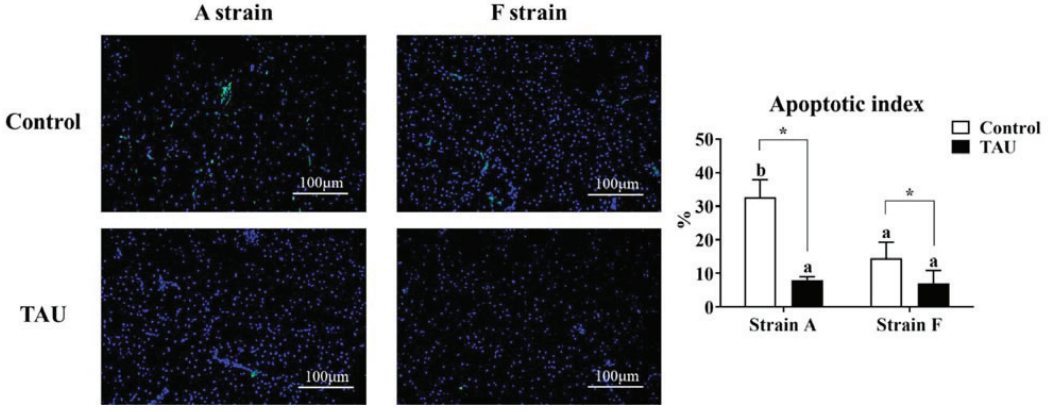

Figure 4. Representative DAPI and TUNEL double staining and image quantification results from the livers of gibel carp (A and F strains) after 96 h cadmium exposure. Positive apoptotic cells appear in green, and normal nuclei appear in blue. Control: control diet, white bars; TAU: diet supplemented with taurine, black bars. Bars with different lowercase letters (a, b) indicate the interaction effect and represent significant differences among groups ($p < 0.05$). Bars with * indicate significant changes between diets in the same strain ($p < 0.05$). The magnification factor is 200×, and the scale bar is 100 μm.

3.3. Activities of the Antioxidant and Caspase Enzymes

Before Cd exposure, the enzyme activities of T-AOC, SOD, GSH-Px, Casp3, and contents of GSH showed no significant variation among treatments (Figure 5). Dietary taurine supplementation significantly enhanced the activities of CAT in the A strain compared to other groups ($p < 0.05$), while MDA contents were significantly lower in the F strain than in the A strain ($p < 0.05$). After Cd exposure, no significant differences were found among groups in the activities of T-AOC, SOD, or Casp3 or in GSH content. The A strain had significantly higher GSH-Px activities and MDA contents than the F strain ($p < 0.05$). For the diet effects, dietary taurine supplementation elevated the CAT activities, whereas taurine decreased the MDA content after Cd exposure in both strains.

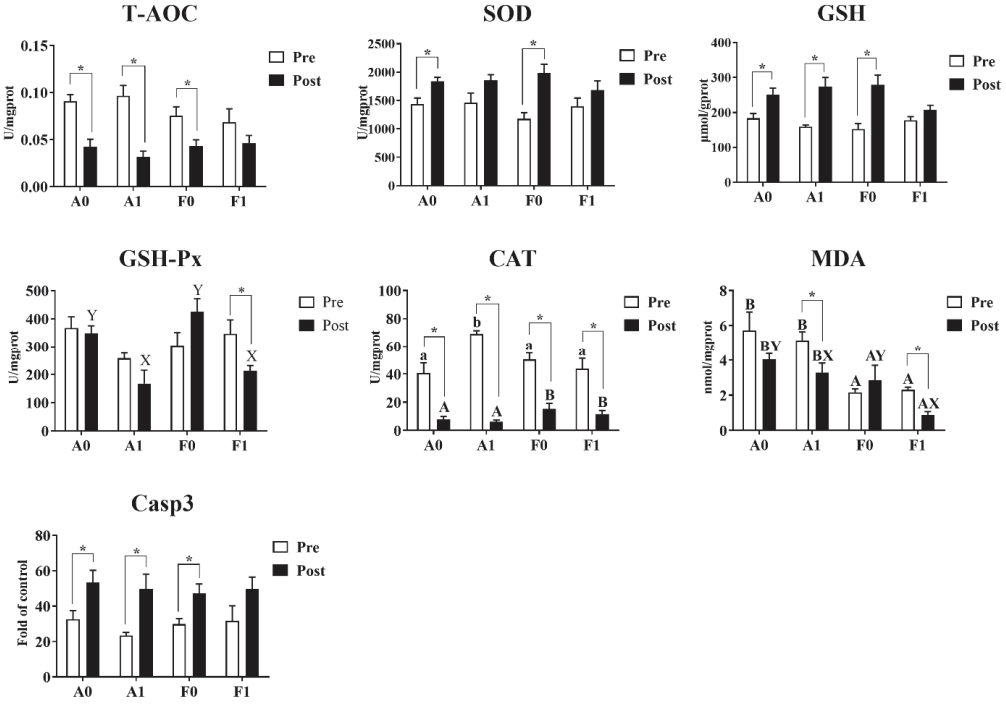

Figure 5. Antioxidant indices and Casp3 activity in the livers of gibel carp (A and F strains) before cadmium exposure (white bars) and after cadmium exposure (black bars). A0: A strain fed the control diet; A1: A strain fed a diet supplemented with taurine; F0: A strain fed the control diet; F1: A strain fed a diet supplemented with taurine. Bars with different uppercase letters (A, B) represent significant differences between the A and F strains ($p < 0.05$). Bars with different uppercase letters (X, Y) represent significant differences between the control diet group and the taurine diet group ($p < 0.05$). Bars with different lowercase letters (a, b) indicate the interaction effect and represent significant differences among all groups ($p < 0.05$). Bars with * indicate significant changes between before and after cadmium exposure ($p < 0.05$).

Cd exposure significantly inhibited the activities of CAT in both strains of gibel carp and reduced the content of MDA in the F strain. For both gibel carp strains, Cd exposure suppressed the activity of T-AOC, whereas the activity of Casp3 and the contents of GSH were elevated. However, the F strain fed the diet with taurine supplementation did not show significant differences in the activities of T-AOC or Casp3 or in GSH content. Among all groups, only the F strain given dietary taurine supplementation showed significant reduction in the activity of GSH-Px ($p < 0.05$).

3.4. Antioxidant Pathways and Metallothionein Levels

The expression levels of antioxidant genes and metallothionein are shown in Figure 6. Prior to Cd exposure, the gene expression levels of *prx2*, *hsp70*, and *mt* showed no significant differences among groups ($p > 0.05$). Dietary taurine supplementation significantly upregulated the expression of *bach1* and *nrf2* in both strains compared to the control group ($p < 0.05$). The F strain showed significantly higher mRNA levels of *keap1* than the A strain ($p < 0.05$).

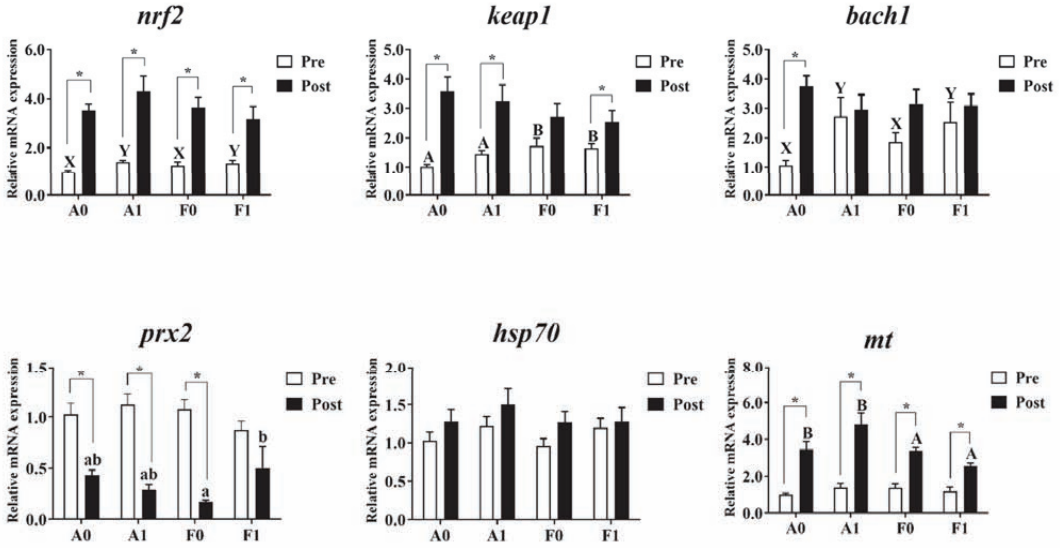

Figure 6. Expression levels of genes related to antioxidation and metallothionein (*mt*) in the livers of gibel carp (A and F strains) before cadmium exposure (white bars) and after cadmium exposure (black bars). A0: A strain fed the control diet; A1: A strain fed a diet supplemented with taurine; F0: A strain fed the control diet; F1: A strain fed a diet supplemented with taurine. Bars with different uppercase letters (A, B) represent significant differences between the A and F strains ($p < 0.05$). Bars with different uppercase letters (X, Y) represent significant differences between the control diet group and the taurine diet groups ($p < 0.05$). Bars with different lowercase letters (a, b) indicate a significant interaction effect and represent the differences among all the groups ($p < 0.05$). Bars with * indicate significant changes between before and after cadmium exposure ($p < 0.05$).

After Cd exposure, no significant variation was observed in the mRNA levels of *bach1*, *keap1*, *nrf2*, or *hsp70* among all groups ($p > 0.05$). The A strain showed significantly higher mt mRNA levels than the F strain ($p < 0.05$). Interactions were identified in the expression of *prx2*, with the highest levels found in the F strain given dietary taurine supplementation ($p < 0.05$). Cd exposure enhanced the expression levels of *nrf2* and *mt* in both strains, while the A strain showed significant elevation of the mRNA level of *bach1* ($p < 0.05$). The expression of *prx2* was significantly upregulated after Cd exposure ($p < 0.05$), while no significant differences were observed in the F strains ($p > 0.05$). The expression of *keap1* was significantly higher after Cd exposure ($p < 0.05$), except for the F strain fed with the control diet.

3.5. ER Stress

As shown in Figure 7, no significant differences were observed in the expression of *xbp1* or *eif2a* among all groups before Cd exposure ($p > 0.05$). Dietary taurine supplementation significantly upregulated the mRNA levels of *ire1*, *perk*, and *chop* in the livers of both strains compared to the control group. The F strain had markedly higher levels of *atf6* than the A

strain ($p < 0.05$). Diets interacted with strains to affect the expression of *atf4* in the livers of gibel carp, with the F strain showed the highest levels among all groups ($p < 0.05$).

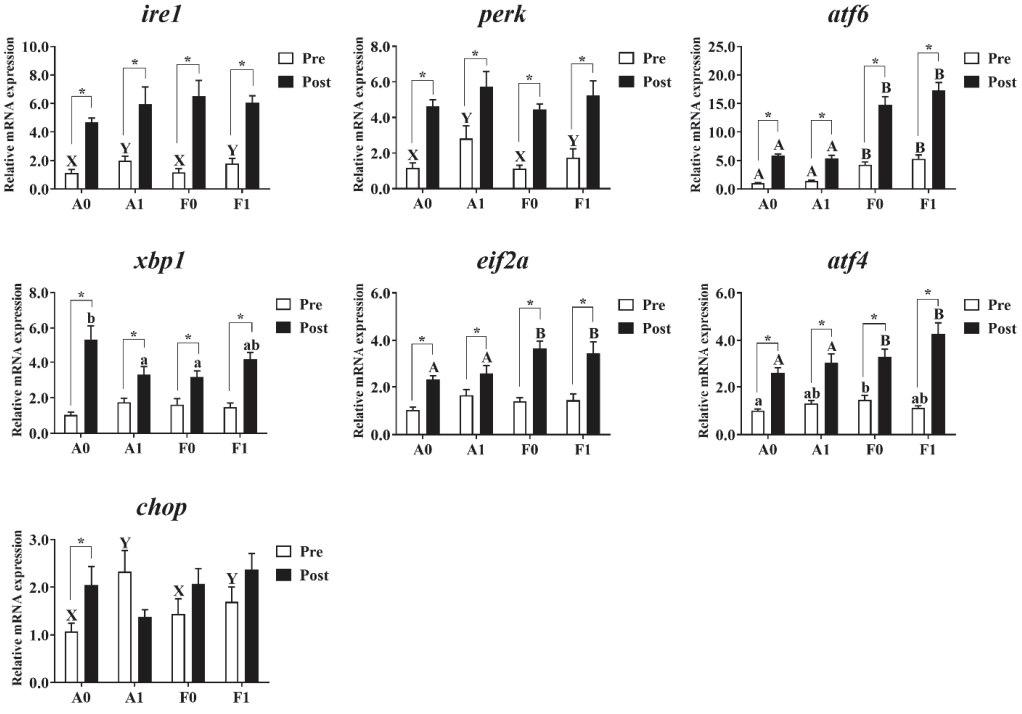

Figure 7. Expression levels of genes related to ER stress in the livers of gibel carp (A and F strains) before cadmium exposure (white bars) and after cadmium exposure (black bars). A0: A strain fed the control diet; A1: A strain fed a diet supplemented with taurine; F0: A strain fed the control diet; F1: A strain fed a diet supplemented with taurine. Bars with different uppercase letters (A, B) represent significant differences between the A and F strains ($p < 0.05$). Bars with different uppercase letters (X, Y) represent significant differences between the control diet and taurine diet groups ($p < 0.05$). Bars with different lowercase letters (a, b) indicate the interaction effect and represent the differences among all groups ($p < 0.05$). Bars with * indicate significant changes between before and after cadmium exposure ($p < 0.05$).

After Cd exposure, no significant variation was observed in the expression of *ire1*, *perk*, or *chop* among all groups ($p > 0.05$). The F strain showed significantly higher expression levels of *atf6*, *eif2a*, and *atf4* than the A strain ($p < 0.05$). Interactions were observed in the mRNA level of *xbp1*, with the highest level found in the A strain fed the control diet ($p < 0.05$). Cd exposure significantly induced higher mRNA levels of *ire1*, *perk*, *atf6*, *xbp1*, *eif2a*, and *atf4* in the livers of both strains, whereas the A strain fed the control diet had the higher *chop* mRNA levels ($p < 0.05$).

3.6. Autophagy and Apoptosis

Hepatic mRNA levels related to autophagy and apoptosis were investigated in both strains (Figure 8). Prior to Cd exposure, no significant differences were found in the expression of *atg12*, *atg5*, *beclin1*, or *bcl2* ($p > 0.05$). The mRNA levels of *lc3b* in the A strain were significantly lower than in the F strain among all groups ($p < 0.05$). Dietary taurine supplementation elevated the expression of *ero1α* and *bax* ($p < 0.05$). The diets and strains interacted to affect the expression of *casp9* and *casp3*, with the highest levels found in the A strain fed the taurine diet ($p < 0.05$).

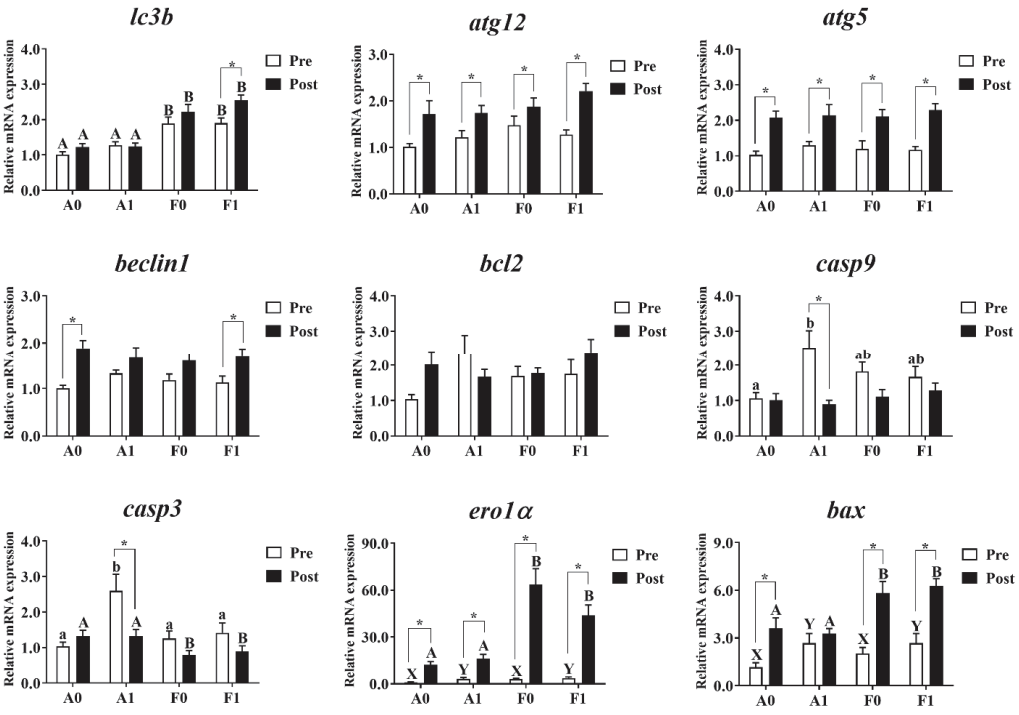

Figure 8. Expression levels of genes related to autophagy and apoptosis in the livers of gibel carp (A and F strains) before cadmium exposure (white bars) and after cadmium exposure (black bars). A0: A strain fed the control diet; A1: A strain fed a diet supplemented with taurine; F0: A strain fed the control diet; F1: A strain fed a diet supplemented with taurine. Bars with different uppercase letters (A, B) represent significant differences between A and F strains ($p < 0.05$). Bars with different upper-case letters (X, Y) represent significant differences between the control diet group and the taurine diet group ($p < 0.05$). Bars with different lowercase letters (a, b) indicate the interaction effect and represent the differences among all groups ($p < 0.05$). Bars with * mean significant changes between before and after cadmium exposure ($p < 0.05$).

After Cd exposure, the expression of *atg12*, *atg5*, *beclin1*, *bcl2*, and *casp9* showed no significant differences among all groups ($p > 0.05$). The A strain showed significantly higher levels of *lc3b*, *ero1α*, and *bax* and significantly lower levels of *casp9* than the F strain ($p < 0.05$). Cd exposure significantly upregulated the mRNA levels of *atg12*, *atg5*, and *ero1α* in the livers of both strains. However, the upregulated levels of *lc3b* were only found in the F strain fed the taurine diet. The increased expression of *beclin1* was found in the A strain fed the control diet and the F strain fed the taurine diet ($p < 0.05$). The A strain subjected to the taurine diet had significantly higher hepatic mRNA levels of *casp3* and *casp9*. Cd exposure induced significant upregulation of the expression of *bax* among all groups ($p < 0.05$) except for the A strain fed the diet with taurine supplementation ($p > 0.05$).

3.7. Heatmap Cluster Analysis

The mean values of molecular (gene expression) signatures of all treatments are presented in the clustering heatmap (Figure 9). Obvious differences were observed in the two strains before or after Cd exposure. Molecular expression of genes involved in antioxidant response, ER stress, and autophagy in the F strain after Cd exposure was not in a cluster with other treatments, especially in the F strain fed the taurine diet.

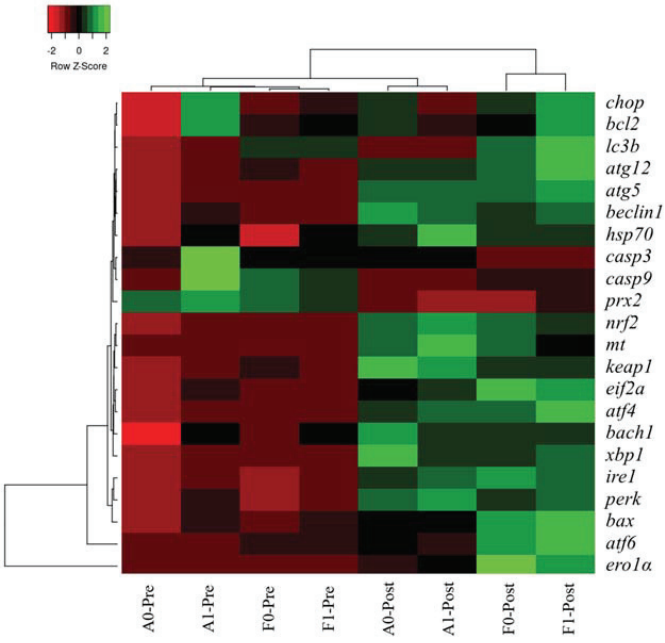

Figure 9. Gene expression heatmap of genes related to antioxidation, ER stress, autophagy, and apoptosis in the livers of gibel carp.

4. Discussion

Taurine has been reported to have beneficial effects on the growth performance of aquatic animals fed low fish meal diets in species such as black carp and white shrimp [30,31]. In the Phase 1 period of the present study, no significant effects on FBW or SGR were observed in either strain of gibel carp subjected to 8 weeks of taurine supplementation. Consistent with our results, the positive effects of dietary taurine supplementation (0, 0.5, 1.0, 1.5, and 2.0%) on growth improvement in yellowtail disappeared after six weeks of feeding, although higher final body weight was observed in fish fed a taurine diet for three weeks [32]. Dietary taurine supplementation significantly decreased FE and increased FCR in both strains. When the dietary taurine level exceeds the basic nutritional requirement, this can lead to feed intake reduction, as has been reported in Nile tilapia [33]. Therefore, the effects of dietary taurine supplement on growth of aquatic animals may be dose or time dependent.

As a semi-essential amino acid, taurine has physiological functions in the antioxidant and anti-apoptosis responses. Being a non-essential heavy metal, Cd exerts its effects and causes damage to tissues primarily through peroxidation and apoptosis [34]. Reports have shown that dietary taurine supplementation could mitigate Cd toxicity in catfish and red sea bream [16,24]. In the present study, histological observations showed that 96 h Cd exposure caused degenerated cristae, swelling of mitochondria, and irregular parallel stacked endoplasmic reticulum, and plaques in the cytoplasm of hepatocytes of both strains, suggesting that Cd damaged the mitochondria and endoplasmic reticulum in the liver cells of gibel carp. Meanwhile, Cd triggered apoptosis signals, as shown by the TUNEL results. Nevertheless, the apoptosis index was significantly lower in both strains fed diets with taurine supplementation compared to the control groups. Therefore, dietary taurine supplementation could apparently mitigate Cd-induced hepatic damage in gibel carp as in catfish and red sea bream [16,24]. Metallothionein (mt) is considered as a biomarker in the Cd detoxification process, as it can combine with Cd to form a Cd-MT complex [35]. In the present study, hepatic mRNA levels of *mt* increased significantly after Cd exposure,

indicating that Cd triggered the protective proteins to counteract the damage to the liver. To further elucidate the potential protective effects of taurine in gibel carp against Cd toxicity, we investigated the antioxidant response, ER stress, autophagy, and apoptosis.

Induction of oxidative stress is one of the toxicological mechanisms involved in heavy metal stress in fish, where the production of ROS (reactive oxygen species) causes oxidative damage to cells. Previous studies have shown that the hepatic enzyme activity of SOD increased significantly in rainbow trout after 7 days of waterborne Cd exposure [36]. Meanwhile, 21 days of waterborne Cd exposure enhanced the hepatic enzyme activity of SOD in catfish [37]. In the present study, Cd exposure elevated the SOD activity in gibel carp fed the control diet. However, no significant differences were found in hepatic SOD activities in fish fed diets with taurine supplementation, implying the protective role of taurine against Cd exposure in gibel carp. MDA is considered as a biomarker of the lipid peroxidation level under oxidative stress [38]. Dietary taurine supplementation significantly decreased MDA levels in the liver, which is consistent with the results for hepatic SOD activity. Cd exposure suppressed the enzyme activity of CAT in the livers of both strains, but the F strain showed higher levels than the A strain. Moreover, Cd exposure inhibited the activities of T-AOC while elevating the activity of Casp3 and the contents of GSH. However, no significant differences were observed in the activities of T-AOC or Casp3 or in the content of GSH in the F strain fed the taurine diet. Additionally, even though the activity of GSH-Px showed no variation among groups, the lowest level was found in the F strain fed the diet with taurine supplementation. Overall, taurine may exert its protective function against Cd poisoning more efficiently in the F strain than in the A strain.

Nuclear factor erythroid 2-related factor 2 (nrf2) is a key transcriptional factor involved in the regulation of the cellular antioxidant response [39]. Nrf2 regulates downstream antioxidant-related genes such as *keap1*, *prx2*, *bach1*, and *hsp70* to alleviate oxidative stress in organisms [40]. In the present study, the nrf2 signaling pathway was activated, as indicated by upregulation of *nrf2* mRNA levels in both strains fed the taurine supplemented diet. In zebrafish, the nrf2 pathway demonstrated protective effects by mitigating Cd-induced cellular oxidative damage [41]. Before Cd exposure, the expression levels of *nrf2* and *bach1* were significantly higher in both strains fed diets with taurine supplementation than in the control groups, indicating that dietary taurine could enhance the antioxidant potential of gibel carp, while such beneficial effects were not observed after the Cd exposure. Moreover, Cd exposure downregulated the expression levels of *prx2*, except in the F strain fed the diet with taurine supplementation. Taken together, the results suggest that taurine had a protective role against Cd-induced damage in both strains, especially in the F strain.

The endoplasmic reticulum is a dynamic organelle that is responsible for folding and assembly of proteins [42]. ER stress and its downstream signaling pathways play a crucial regulatory role in response to heavy-metal-induced toxic effects [43]. Previous studies had indicated that Cd waterborne could induce ER stress in both strains of gibel carp [25]. In the present study, the expression levels of the ER-stress-related genes *ire1*, *perk*, *atf6*, *xbp1*, *eif2α*, and *atf4* were increased after Cd exposure. In other words, all branches of the regulatory pathways of PERK-eIF2a-ATF4, IRE1-XBP1, and ER stress transducers ATF6 were induced after Cd exposure, suggesting the occurrence of ER stress in gibel carp exposed to Cd. The phosphorylation dependence of PERK induces dissociation of Nrf2/Keap1 complexes, thereby triggering the transcription of downstream genes involved in antioxidant pathways [44]. The expression level of *perk* had a variation trend similar to that of *nrf2*. Meanwhile, hepatic histological alterations such as swelling of mitochondria and irregular parallel stacks of ER were triggered by Cd exposure, observations that confirmed the ER stress in gibel carp.

Autophagy refers to a catabolic process in which cytoplasmic constituents and organelles in the lysosome are degraded to maintain homeostasis as an adaptative response to stressful conditions [45]. Autophagic pathways can be triggered through induction of ER sensors under long-lasting ER stress [46]. It has been reported that Cd exposure could cause

such a stress response, eliciting ER-stress-mediated autophagic and apoptosis processes in both strains of gibel carp [9,25]. Moreover, the formation of autophagosomes requires two ubiquitin-like conjugation pathways: one involves the formation of the multimeric complex of ATG5-ATG12-ATG16 conjugation; the other results in the conjugation of phosphatidylethanolamine (PE) to LC3b for the expansion of autophagic membranes [45,47]. In the present study, Cd exposure upregulated the hepatic mRNA levels of *atg5* and *atg12* in both strains regardless of the diet effect, suggesting that autophagic processes may be triggered by the increasing level of the ATG5-ATG12 complex. The mRNA levels of *lc3b* were only elevated in the F strain fed with the taurine diet, implying that more conjugation pathways were stimulated in the F strain. Thus, stronger autophagy may have been triggered in the F strain fed the taurine diet. Furthermore, Beclin-1 is a critical regulator of autophagy, because it participates in the formation of autophagosomes [48]. The transcriptional levels of *beclin1* were increased in the A strain fed the control diet and the F strain fed the taurine diet. Taken together, the results suggest that Cd exposure induced the autophagic process, and stronger autophagy responses were observed in the F strain fed the taurine diet.

Autophagy may play a protective role in cell survival, and extensive autophagy may trigger apoptosis as an independent pathway of cell death [49]. Apoptosis is also known as a cellular biomarker of metal-induced physiological alterations in aquatic animals [50]. Cd exposure was reported to induce apoptosis in topsmelt, purse red common carp, and gibel carp [25,51,52]. Apoptosis can be triggered by three main pathways, one of which is upstream caspase activation and includes the enzymes Caspase 9 and Caspase 3 [53]. In the present study, the transcriptional levels of *casp9* and *casp3* were inhibited in the A strain fed the diet supplemented with taurine. The mRNA levels of *casp3* were not consistent with the Casp3 activities, possibly due to a feedback response; a similar result has been reported in *Litopenaeus vannamei* [54]. Meanwhile, the apoptotic index in the A strain after Cd exposure was higher than in other groups as shown by the TUNEL results, suggesting that Cd exposure caused higher levels of apoptosis, and dietary taurine supplementation manifested its antioxidant effects through the regulation of the caspase gene in the A strain. In the apoptotic process, bcl2 is a member of the anti-apoptosis protein family, while bax and ero1α have opposite functions [47,55]. In the present study, no significant variation in *bcl2* expression was found after exposure to Cd, while the expression of *ero1α* was significantly elevated, indicating that apoptosis was induced by Cd exposure. The mRNA levels of *bax* increased after Cd exposure in all groups, but unaltered mRNA levels of *bax* were found in the A strain fed taurine, implying that dietary taurine supplementation alleviated the Cd toxicity by attenuating apoptosis in the A strain compared to the F strain.

Hierarchy cluster heatmap analysis showed that significant differences were observed in the two strains before or after Cd exposure, which verified the effects induced by Cd exposure as mentioned above. Expression levels of genes involved in antioxidant response, ER stress, and autophagy in the F strain post Cd exposure was not in cluster with other treatments, especially in the F strain fed the taurine diet, which was in line with previous results. Differential responses between the A and F strains of gibel carp were investigated in our previous studies owing to their genetic differences produced by selection [9,25]. The A strain was produced from eggs of gibel carp D strain and the sperm of gibel carp A strain, while the F strain was produced by the eggs of gibel carp E strain via stimulation with blunt snout bream sperm [56,57]. Therefore, a partial genome from the blunt snout bream may have been introduced into the genome of the F strain; this may have caused genetic differences between the A and F strains that led to differential genomic expression between the two strains upon Cd exposure. In the present study, even the growth performance was not significantly improved by dietary taurine supplement, but the detoxication of taurine might help to increase the survival rate of fish and raise fish quality, thereby improving the economic benefits.

5. Conclusions

Our study found that Cd exposure induced damage and oxidative stress in the livers of both strains of gibel carp, thereby triggering the occurrence of ER stress and the downstream responses of autophagy and apoptosis. Dietary taurine supplementation had no significant effect on the growth performance of gibel carp but did alleviate the Cd toxicity in both strains via specific genetic pathways. Dietary taurine played a protective role in mitigating Cd toxicity in the F strain through the antioxidant response, ER stress response, and autophagy, while in the A strain taurine alleviated cadmium toxicity by attenuation of apoptosis. In conclusion, the present study has provided evidence for the use of taurine in intervention or therapy for Cd poisoning in fish; thus, providing useful information for selective breeding in aquaculture.

Author Contributions: Conceptualization, investigation, methodology, validation, visualization, writing—review and editing, funding acquisition, W.X.; Conceptualization, data curation, methodology, formal analysis, writing—original draft, H.L. (Hongyan Li); Data curation, L.W.; Conceptualization, funding acquisition, project administration, supervision, writing—review and editing, J.J.; Supervision, D.H., X.Z., Y.Y. and H.L. (Haokun Liu); Funding acquisition, investigation, supervision, S.X. All authors have read and agreed to the published version of the manuscript.

Funding: This work was financially supported by the China Agriculture Research System of MOF and MARA (CARS-45-09), the National Natural Science Foundation of China (32122089; U19A2041; 32102811; 31972805), the National Key R&D Program of China (2018YFD0900605; 2019YFD0900200) and the Strategic Priority Research Program of Chinese Academy of Sciences (XDA24010206).

Institutional Review Board Statement: All animal care and experimental procedures were approved by the Experimental Animal Ethics Committee of Institute of Hydrobiology, Chinese Academy of Sciences (approval ID: IHB20140724).

Informed Consent Statement: Not applicable.

Data Availability Statement: Data are contained within the article.

Acknowledgments: The authors thank Guanghan Nie for his technical support with the research system.

Conflicts of Interest: The authors declare no conflict of interest.

References

1. Patra, R.C.; Rautray, A.K.; Swarup, D. Oxidative Stress in Lead and Cadmium Toxicity and Its Amelioration. *Vet. Med. Int.* **2011**, *2011*, 457327. [CrossRef] [PubMed]
2. Ninkov, M.; Popov Aleksandrov, A.; Demenesku, J.; Mirkov, I.; Mileusnic, D.; Petrovic, A.; Grigorov, A.; Zolotarevski, L.; Tolinacki, M.; Kataranovski, D.; et al. Toxicity of oral cadmium intake: Impact on gut im-munity. *Toxicol. Lett.* **2015**, *237*, 89–99. [CrossRef] [PubMed]
3. Wright, D.A.; Welbourn, P.M. Cadmium in the aquatic environment: A review of ecological, physiological, and toxicological effects on biota. *Environ. Rev.* **1994**, *2*, 187–214. [CrossRef]
4. Deforest, D.K.; Meyer, J.S. Critical review: Toxicity of dietborne metals to aquatic organisms. *Crit. Rev. Environ. Sci. Technol.* **2015**, *45*, 1176–1241. [CrossRef]
5. Driessnack, M.K.; Jamwal, A.; Niyogi, S. Effects of chronic waterborne cadmium and zinc interactions on tissue-specific metal accumulation and reproduction in fathead minnow (*Pimephales promelas*). *Ecotoxicol. Environ. Saf.* **2017**, *140*, 65–75. [CrossRef]
6. Basha, P.S.; Rani, A.U. Cadmium-induced antioxidant defense mechanism in freshwater teleost *Oreochromis mossambicus* (Tilapia). *Ecotoxicol. Environ. Saf.* **2003**, *56*, 218–221. [CrossRef]
7. Defo, M.A.; Bernatchez, L.; Campbell, P.G.C.; Couture, P. Waterborne cadmium and nickel impact oxidative stress responses and retinoid metabolism in yellow perch. *Aquat. Toxicol.* **2014**, *154*, 207–220. [CrossRef]
8. Isani, G.; Andreani, G.; Cocchioni, F.; Fedeli, D.; Carpené, E.; Falcioni, G. Cadmium accumulation and biochemical responses in Sparus aurata following sub-lethal Cd exposure. *Ecotoxicol. Environ. Saf.* **2009**, *72*, 224–230. [CrossRef]
9. Li, H.; Xu, W.; Wu, L.; Dong, B.; Jin, J.; Han, D.; Zhu, X.; Yang, Y.; Liu, H.; Xie, S. Distinct dietary cadmium toxic effects and defense strategies in two strains of gibel carp (*Carassius gibelio*) revealed by a comprehensive perspective. *Chemosphere* **2020**, *261*, 127597. [CrossRef]
10. Méndez-Armenta, M.; Ríos, C. Cadmium neurotoxicity. *Environ. Toxicol. Pharmacol.* **2007**, *23*, 350–358. [CrossRef]
11. Lawal, A.O.; Ellis, E.M. The chemopreventive effects of aged garlic extract against cadmium-induced toxicity. *Environ. Toxicol. Pharmacol.* **2011**, *32*, 266–274. [CrossRef] [PubMed]

12. Obioha, U.E.; Suru, S.M.; Ola-Mudathir, K.F.; Faremi, T.Y. Hepatoprotective Potentials of Onion and Garlic Extracts on Cadmium-Induced Oxidative Damage in Rats. *Biol. Trace Elem. Res.* **2008**, *129*, 143. [CrossRef] [PubMed]
13. Cuypers, A.; Plusquin, M.; Remans, T.; Jozefczak, M.; Keunen, E.; Gielen, H.; Opdenakker, K.; Nair, A.R.; Munters, E.; Artois, T.J.; et al. Cadmium stress: An oxidative challenge. *BioMetals* **2010**, *23*, 927–940. [CrossRef] [PubMed]
14. Lucia, M.; André, J.-M.; Gonzalez, P.; Baudrimont, M.; Bernadet, M.-D.; Gontier, K.; Maury-Brachet, R.; Guy, G.; Davail, S. Effect of dietary cadmium on lipid metabolism and storage of aquatic bird *Cairina moschata*. *Ecotoxicology* **2009**, *19*, 163. [CrossRef] [PubMed]
15. El-Sayed, Y.S.; El-Gazzar, A.M.; El-Nahas, A.F.; Ashry, K.M. Vitamin C modulates cadmium-induced hepatic antioxidants' gene transcripts and toxicopathic changes in Nile tilapia, *Oreochromis niloticus*. *Environ. Sci. Pollut. Res.* **2016**, *23*, 1664–1670. [CrossRef]
16. Hano, T.; Ito, K.; Kono, K.; Ito, M.; Ohkubo, N.; Mochida, K. Effect of taurine supplementation on hepatic metabolism and alleviation of cadmium toxicity and bioaccumulation in a marine teleost, red sea bream, *Pagrus major*. *Fish Physiol. Biochem.* **2017**, *43*, 137–152. [CrossRef]
17. Sampath, W.W.H.A.; Rathnayake, R.M.D.S.; Yang, M.; Zhang, W.; Mai, K. Roles of dietary taurine in fish nutrition. *Mar. Life Sci. Technol.* **2020**, *2*, 360–375. [CrossRef]
18. Jong, C.J.; Azuma, J.; Schaffer, S. Mechanism underlying the antioxidant activity of taurine: Prevention of mitochondrial oxidant production. *Amino Acids* **2012**, *42*, 2223–2232. [CrossRef]
19. Takeuchi, T. Progress on larval and juvenile nutrition to improve the quality and health of seawater fish: A review. *Fish. Sci.* **2014**, *80*, 389–403. [CrossRef]
20. Yu, X.; Chen, K.; Wei, N.; Zhang, Q.; Liu, J.; Mi, M. Dietary taurine reduces retinal damage produced by photochemical stress via antioxidant and anti-apoptotic mechanisms in Sprague-Dawley rats. *Br. J. Nutr.* **2007**, *98*, 711–719. [CrossRef]
21. El-Sayed, W.M.; Al-Kahtani, M.A.; Abdel-Moneim, A.M. Prophylactic and therapeutic effects of taurine against aluminum-induced acute hepatotoxicity in mice. *J. Hazard. Mater.* **2011**, *192*, 880–886. [CrossRef] [PubMed]
22. Hwang, D.F.; Wang, L.C.; Cheng, H.M. Effect of taurine on toxicity of copper in rats. *Food Chem. Toxicol.* **1998**, *36*, 239–244. [CrossRef]
23. Hwang, D.F.; Wang, L.C. Effect of taurine on toxicity of cadmium in rats. *Toxicology* **2001**, *167*, 173–180. [CrossRef]
24. Kumar, P.; Prasad, Y.; Patra, A.K.; Ranjan, R.; Swarup, D.; Patra, R.C.; Pal, S. Ascorbic acid, garlic extract and taurine alleviate cadmium-induced oxidative stress in freshwater catfish (*Clarias batrachus*). *Sci. Total Environ.* **2009**, *407*, 5024–5030. [CrossRef]
25. Li, H.; Xu, W.; Wu, L.; Dong, B.; Jin, J.; Han, D.; Zhu, X.; Yang, Y.; Liu, H.; Xie, S. Differential regulation of endoplasmic reticulum stress-induced autophagy and apoptosis in two strains of gibel carp (*Carassius gibelio*) exposed to acute waterborne cadmium. *Aquat. Toxicol.* **2021**, *231*, 105721. [CrossRef] [PubMed]
26. Andres, S.; Ribeyre, F.; Tourencq, J.-N.; Boudou, A. Interspecific comparison of cadmium and zinc contamination in the organs of four fish species along a polymetallic pollution gradient (Lot River, France). *Sci. Total Environ.* **2000**, *248*, 11–25. [CrossRef]
27. Potter, B. Liver-Intermediary Metabolism. In *xPharm: The Comprehensive Pharmacology Reference*; Enna, S.J., Bylund, D.B., Eds.; Elsevier: New York, NY, USA, 2007; pp. 1–6.
28. Li, H.; Xu, W.; Jin, J.; Zhu, X.; Yang, Y.; Han, D.; Liu, H.; Xie, S. Effects of dietary carbohydrate and lipid concentrations on growth performance, feed utilization, glucose, and lipid metabolism in two strains of gibel carp. *Front. Vet. Sci.* **2019**, *6*, 165. [CrossRef]
29. Pfaffl, M.W. A new mathematical model for relative quantification in real-time RT-PCR. *Nucleic Acids Res.* **2001**, *29*, e45. [CrossRef]
30. Yue, Y.; Liu, Y.; Tian, L.; Gan, L.; Yang, H.; Liang, G.; He, J. The effect of dietary taurine supplementation on growth performance, feed utilization and taurine contents in tissues of juvenile white shrimp (*Litopenaeus vannamei*, Boone, 1931) fed with low-fishmeal diets. *Aquac. Res.* **2013**, *44*, 1317–1325. [CrossRef]
31. Zhang, J.; Hu, Y.; Ai, Q.; Mao, P.; Tian, Q.; Zhong, L.; Xiao, T.; Chu, W. Effect of dietary taurine supplementation on growth performance, digestive enzyme activities and antioxidant status of juvenile black carp (*Mylopharyngodon piceus*) fed with low fish meal diet. *Aquac. Res.* **2018**, *49*, 3187–3195. [CrossRef]
32. Matsunari, H.; Takeuchi, T.; Takahashi, M.; Mushiake, K. Effect of dietary taurine supplementation on growth performance of yellowtail juveniles *Seriola quinqueradiata*. *Fish. Sci.* **2005**, *71*, 1131–1135. [CrossRef]
33. Al-Feky, S.S.A.; El-Sayed, A.-F.M.; Ezzat, A.A. Dietary taurine enhances growth and feed utilization in larval Nile tilapia (*Oreochromis niloticus*) fed soybean meal-based diets. *Aquac. Nutr.* **2016**, *22*, 457–464. [CrossRef]
34. Stohs, S.J.; Bagchi, D. Oxidative mechanisms in the toxicity of metal ions. *Free Radic. Biol. Med.* **1995**, *18*, 321–336. [CrossRef]
35. Dang, F.; Wang, W.X. Assessment of tissue-specific accumulation and effects of cadmium in a marine fish fed contaminated commercially produced diet. *Aquat. Toxicol.* **2009**, *95*, 248–255. [CrossRef] [PubMed]
36. Hisar, O.; Yildirim, S.; Sönmez, A.Y.; Aras, H.N.; Gultepe, N. Changes in liver and kidney antioxidant enzyme activities in the rainbow trout (*Oncorhynchus mykiss*) exposed cadmium. *Asian J. Chem.* **2009**, *21*, 3133–3139.
37. Asagba, S.O.; Eriyamremu, G.E.; Igberaese, M.E. Bioaccumulation of cadmium and its biochemical effect on selected tissues of the catfish (*Clarias gariepinus*). *Fish Physiol. Biochem.* **2008**, *34*, 61–69. [CrossRef] [PubMed]
38. Liu, X.-J.; Luo, Z.; Li, C.-H.; Xiong, B.-X.; Zhao, Y.-H.; Li, X.-D. Antioxidant responses, hepatic intermediary metabolism, histology and ultrastructure in *Synechogobius hasta* exposed to waterborne cadmium. *Ecotoxicol. Environ. Saf.* **2011**, *74*, 1156–1163. [CrossRef] [PubMed]
39. Wu, K.C.; Liu, J.J.; Klaassen, C.D. Nrf2 activation prevents cadmium-induced acute liver injury. *Toxicol. Appl. Pharmacol.* **2012**, *263*, 14–20. [CrossRef]

40. Mizunoe, Y.; Kobayashi, M.; Sudo, Y.; Watanabe, S.; Yasukawa, H.; Natori, D.; Hoshino, A.; Negishi, A.; Okita, N.; Komatsu, M.; et al. Trehalose protects against oxidative stress by regulating the Keap1–Nrf2 and autophagy pathways. *Redox Biol.* **2018**, *15*, 115–124. [CrossRef]
41. Wang, L.; Gallagher, E.P. Role of Nrf2 antioxidant defense in mitigating cadmium-induced oxidative stress in the olfactory system of zebrafish. *Toxicol. Appl. Pharmacol.* **2013**, *266*, 177–186. [CrossRef]
42. Cao, S.S.; Kaufman, R.J. Endoplasmic Reticulum Stress and Oxidative Stress in Cell Fate Decision and Human Disease. *Antioxid. Redox Signal.* **2014**, *21*, 396–413. [CrossRef] [PubMed]
43. Wu, K.; Luo, Z.; Hogstrand, C.; Chen, G.; Wei, C.; Li, D. Zn Stimulates the phospholipids biosynthesis via the pathways of oxidative and endoplasmic reticulum stress in the intestine of freshwater teleost yellow catfish. *Environ. Sci. Technol.* **2018**, *52*, 9206–9214. [CrossRef]
44. Cullinan, S.B.; Zhang, D.; Hannink, M.; Arvisais, E.; Kaufman, R.J.; Diehl, J.A. Nrf2 Is a Direct PERK Substrate and Effector of PERK-Dependent Cell Survival. *Mol. Cell. Biol.* **2003**, *23*, 7198–7209. [CrossRef] [PubMed]
45. Kaur, J.; Debnath, J. Autophagy at the crossroads of catabolism and anabolism. *Nat. Rev. Mol. Cell Biol.* **2015**, *16*, 461–472. [CrossRef]
46. Ogata, M.; Hino, S.-I.; Saito, A.; Morikawa, K.; Kondo, S.; Kanemoto, S.; Murakami, T.; Taniguchi, M.; Tanii, I.; Yoshinaga, K.; et al. Autophagy Is Activated for Cell Survival after Endoplasmic ReticulumStress. *Am. Soc. Microbiol.* **2006**, *26*, 9220–9231. [CrossRef] [PubMed]
47. Zhang, L.; Xia, Q.; Zhou, Y.; Li, J. Endoplasmic reticulum stress and autophagy contribute to cadmium-induced cytotoxicity in retinal pigment epithelial cells. *Toxicol. Lett.* **2019**, *311*, 105–113. [CrossRef]
48. Wang, M.; Wang, X.; Li, Y.; Chen, N.; Fan, Y.; Huang, W.; Hu, S.; Rao, M.; Zhang, Y.; Su, P. Cross-talk between autophagy and apoptosis regulates testicular injury/recovery induced by cadmium via PI3K with mTOR-independent pathway. *Cell Death Dis.* **2020**, *11*, 46. [CrossRef]
49. Agnello, M.; Roccheri, M.C. Apoptosis: Focus on sea urchin development. *Apoptosis* **2010**, *15*, 322–330. [CrossRef]
50. Capaldo, A.; Gay, F.; Scudiero, R.; Trinchella, F.; Caputo, I.; Lepretti, M.; Marabotti, A.; Esposito, C.; Laforgia, V. Histological changes, apoptosis and metallothionein levels in *Triturus carnifex* (Amphibia, Urodela) exposed to environmental cadmium concentrations. *Aquat. Toxicol.* **2016**, *173*, 63–73. [CrossRef]
51. Gao, D.; Xu, Z.E.; Qiao, P.; Liu, S.; Zhang, L.; He, P.; Zhang, X.; Wang, Y.; Min, W. Cadmium induces liver cell apoptosis through caspase-3a activation in purse red common carp (*Cyprinus carpio*). *PLoS ONE* **2013**, *8*, e83423.
52. Rose, W.L.; Nisbet, R.M.; Green, P.G.; Norris, S.; Fan, T.; Smith, E.H.; Cherr, G.N.; Anderson, S.L. Using an integrated approach to link biomarker responses and physiological stress to growth impairment of cadmium-exposed larval topsmelt. *Aquat. Toxicol.* **2006**, *80*, 298–308. [CrossRef]
53. Redza-Dutordoir, M.; Averill-Bates, D.A. Activation of apoptosis signalling pathways by reactive oxygen species. *Biochim. Biophys. Acta Mol. Cell Res.* **2016**, *1863*, 2977–2992. [CrossRef]
54. Chang, C.; Yeh, M.; Lin, H.; Cheng, W. The effect of Vibrio alginolyticus infection on caspase-3 expression and activity in white shrimp *Litopenaeus vannamei*. *Fish Shellfish. Immunol.* **2008**, *25*, 672–678. [CrossRef]
55. Song, S.; Tan, J.; Miao, Y.; Li, M.; Zhang, Q. Crosstalk of autophagy and apoptosis: Involvement of the dual role of autophagy under ER stress. *J. Cell. Physiol.* **2017**, *232*, 2977–2984. [CrossRef]
56. Gao, F.-X.; Wang, Y.; Zhang, Q.-Y.; Mou, C.-Y.; Li, Z.; Deng, Y.-S.; Zhou, L.; Gui, J.-F. Distinct herpesvirus resistances and immune responses of three gynogenetic clones of gibel carp revealed by comprehensive transcriptomes. *BMC Genom.* **2017**, *18*, 561. [CrossRef]
57. Chen, F.; Li, X.-Y.; Zhou, L.; Yu, P.; Wang, Z.-W.; Li, Z.; Zhang, X.-J.; Wang, Y.; Gui, J.-F. Stable Genome Incorporation of Sperm-derived DNA Fragments in Gynogenetic Clone of Gibel Carp. *Mar. Biotechnol.* **2020**, *22*, 54–66. [CrossRef]

antioxidants

MDPI

Article

A Novel Disease (Water Bubble Disease) of the Giant Freshwater Prawn *Macrobrachium rosenbergii* Caused by *Citrobacter freundii*: Antibiotic Treatment and Effects on the Antioxidant Enzyme Activity and Immune Responses

Caiyuan Zhao [1], Huagen Wen [2], Shengsheng Huang [2], Shaoping Weng [2] and Jianguo He [1,2,*]

[1] State Key Laboratory for Biocontrol, School of Marine Sciences, Sun Yat-sen University, No.132 Waihuan Dong Road, Higher Education Mega Center, Guangzhou 510006, China; zhaocy5@mail.sysu.edu.cn

[2] Southtern Marine Science and Engineering Guangdong Laboratory (Zhuhai), School of Life Science, Sun Yat-sen University, No.132 Waihuan Dong Road, Higher Education Mega Center, Guangzhou 510006, China; wenhg3@mail2.sysu.edu.cn (H.W.); huangshsh29@mail2.sysu.edu.cn (S.H.); lsswsp@mail.sysu.edu.cn (S.W.)

* Correspondence: lsshjg@mail.sysu.edu.cn; Tel.: +86-20-3933-2988; Fax: +86-20-3933-2849

Abstract: The giant freshwater prawn, *Macrobrachium rosenbergii*, is an important and economical aquaculture species widely farmed in tropical and subtropical areas of the world. A new disease, "water bubble disease (WBD)", has emerged and resulted in a large loss of *M. rosenbergii* cultured in China. A water bubble with a diameter of about 7 mm under the carapace represents the main clinical sign of diseased prawns. In the present study, *Citrobacter freundii* was isolated and identified from the water bubble. The optimum temperature, pH, and salinity of the *C. freundii* were 32 °C, 6, and 1%, respectively. A challenging experiment showed that *C. freundii* caused the same typical signs of WBD in prawns. Median lethal dose of the *C. freundii* to prawn was $10^{4.94}$ CFU/g. According to the antibiogram tests of *C. freundii*, florfenicol and ofloxacin were selected to evaluate their therapeutic effects against *C. freundii* in prawn. After the challenge with *C. freundii*, 86.67% and 72.22% survival of protective effects against *C. freundii* were evaluated in the oral florfenicol pellets and oral ofloxacin pellets feding prawns, respectively, whereas the mortality of prawns without fed antibiotics was 93%. After antibiotic treatment and *C. freundii* infection, the activities of superoxide dismutase (SOD), catalase (CAT), glutathione peroxidase (GPx), glutathione S-transferase (GST), malondialdehyde (MDA), acid phosphatase (ACP), alkaline phosphatase (ALP), and lysozyme (LZM) in the hemolymph and hepatopancreas of the prawns and the immune-related gene expression levels of Cu/Zn-SOD, CAT, GPx, GST, LZM, ACP, anti-lipopolysaccharide factor, crustin, cyclophilin A, and C-type lectin in hepatopancreas were all significantly changed, indicating that innate immune responses were induced by *C. freundii*. These results can be beneficial for the prevention and control of *C. freundii* in prawns.

Keywords: *Macrobrachium rosenbergii*; water bubble disease; *Citrobacter freundii*; antibiotic treatment; antioxidant enzyme activity

Citation: Zhao, C.; Wen, H.; Huang, S.; Weng, S.; He, J. A Novel Disease (Water Bubble Disease) of the Giant Freshwater Prawn *Macrobrachium rosenbergii* Caused by *Citrobacter freundii*: Antibiotic Treatment and Effects on the Antioxidant Enzyme Activity and Immune Responses. *Antioxidants* **2022**, *11*, 1491. https://doi.org/10.3390/antiox11081491

Academic Editors: Bo Liu, Changyou Song and Cunxin Sun

Received: 14 June 2022
Accepted: 26 July 2022
Published: 29 July 2022

1. Introduction

The giant freshwater prawn, *Macrobrachium rosenbergii*, is a member of arthropods, belonging to genus *Macrobrachium*, which is the largest freshwater and the most favored prawn for aquaculture in tropical and subtropical areas of the world [1–3], with annual yields of 290,708 metric tons [4]. *M. rosenbergii* has already been developed into an important economically aquaculture species in China [5–8]. The outbreaks of bacterial diseases in *M. rosenbergii* aquaculture have been reported, such as muscle necrosis disease caused by *Enterococcus* or *Pseudomonas aeruginosa* [9–11], *Aeromonas* species (*A. veronii* and *A. caviae*) and *Vibrio* species (*V. alginolyticus* and *V. parahaemolyticus*) [12,13] caused high-mortality

diseases. A new epidemic disease, referred to as "water bubble disease" (WBD), recently occurred in cultured *M. rosenbergii* in China, and it caused a mortality of over 30% in diseased prawns.

As *M. rosenbergii* is an invertebrate, it lacks the typical acquired immunity of vertebrates and entirely relies on its innate immunity system to resist infection by various pathogens [14]. Enhanced knowledge about the immune system of *M. rosenbergii* is crucial for disease management [15]. The innate immune system provides defense against invading bacteria through AMPs, enzymes, and cellular components [16]. Antiproteases, myeloperoxidase, and lysozyme (LZM) have been used to learn about and determine the innate immune status of an organism [17]. During pathogen invasion, host cells produce abundant reactive oxygen species (ROS) to kill the invading pathogens. However, a considerably high level of ROS in the body will cause the destruction and damage of DNA and other biological macromolecules [18]. Several major antioxidant enzymes include glutathione peroxidase (GPx), glutathione S-transferase (GST), catalase (CAT), malondialdehyde (MDA), and superoxide dismutase (SOD), which play important roles in anti-oxidization damage and related coping mechanisms [19,20]. Acid phosphatase (ACP), and alkaline phosphatase (ALP) are symbols of macrophage activation, important components of the lysosome system, and play important roles in the innate immune system by engulfing antigens and LZM intracellularly [21]. C-Type lectin (CTL), cyclophilin A (CypA), and AMPs, such as anti-lipopolysaccharide factor (ALF) and crustins, play important roles in the innate immunity for the recognition of effector molecules and clearance of bacteria, fungi, and viruses [22–29]. Antibiotics are commonly used in aquaculture to control the diseases caused by bacteria [30]. Antibiotics at therapeutic levels are mainly administered for short periods of time via the oral route (the most common route for the delivery occurs by mixing the antibiotic with commercial feed) to groups of prawn. Antibiotics legally used in aquaculture must be authorized by Food and Drug Administration (FDA), and abide by the rules for antibiotic use, comprising permissible routes of delivery, dose forms, withdrawal times, tolerances, and dose rates and limitations of specific species. In Norway, antibiotics were sold in pharmacies or in feed plants approved by the Norwegian Medicines Agency, and the amount of antibiotics used and retain records in prescriptions of veterinarian were mandatory to report [31].

In the present study, we aimed to isolate and identify the pathogen associated with WBD in *M. rosenbergii* using challenge experiments, molecular methods and antibiotic treatment. The activities of antioxidant enzymes (i.e., SOD, CAT, GPx, GST, and MDA), ACP, ALP, and LZM and the immune-related gene expression levels of Cu/Zn-SOD, CAT, GPx, GST, LZM, ACP, ALF, crustin, CypA, and CTL in *M. rosenbergii* after *C. freundii* challenge were investigated. The results of the present study will expound the pathogenesis of bacteria in *M. rosenbergii* and facilitate the further prevention and control of *C. freundii* in *M. rosenbergii*.

2. Materials and Methods

2.1. Strain Isolation and Identification

In November 2019, 30 *M. rosenbergii* (mean body weight 13.5 ± 2.3 g, body length 13.1 ± 1.2 cm) with WBD were collected in Zhaoqing, Guangdong, China. The water bubble diseased *M. rosenbergii* were dissected aseptically, and liquid sample of the water bubble was streaked onto a Luria-Bertani (LB) agarose plate (tryptone 10 g/L, yeast extract 5 g/L, NaCl 10 g/L, agarose powder 15 g/L, pH 7.4) (Sangon Biotech, Shanghai, China). The inoculated plates were incubated for 48 h at 28 °C, and single colonies were obtained and labeled GDZQ201912. After incubation in liquid LB culture (tryptone 10 g/L, yeast extract 5 g/L, NaCl 10 g/L, pH 7.4) for 24 h, the bacteria were collected and stored at −80 °C in 50% glycerol (*v*/*v*).

Biochemical characterization of the isolated strain was identified by Gram staining, shape, and motility, followed by biochemical tests and carbohydrate utilization test. The biochemical tests were performed with GEN III MicroPlate on BIOLOGY (Biology, Vacaville,

CA, USA). Transmission electron microscopy (TEM) (JEOL JEM-1400, JEOL, Tokyo, Japan) was used to observe the isolated strain at 120 kV.

2.2. Gene Sequencing and Phylogenetic Analysis

Genomic DNA of the bacterial isolate was extracted by using FastPure Cell/Tissue DNA Isolation Mini Kit (Vazyme, Nanjing, China). The 16S rRNA gene of the bacterium was amplified for polymerase chain reaction (PCR) analysis in accordance with the method of Lee et al. [32]. The following amplification primers were used: F (5′-AGAGTTTGATCCTGGCTCAG-3′) and R (5′-CGGTTACCTTGTTACGACTT-3′) (NR_176804.1). The PCR program was carried out as follows: denaturation at 95 °C for 10 min, 30 cycles of denaturation at 95 °C for 30 s, annealing at 53 °C for 30 s, extension at 72 °C for 80 s, and a final extension at 72 °C for 10 min. PCR products were run on a TBE-agarose gel, and the DNA was purified using a TaKaRa MiniBEST Universal Genomic DNA Extraction Kit (Takara, Kusatsu, Japan) and sub-cloned into the pMD19-T Easy Vector (Takara, Japan) for sequencing.

The 1416 bp PCR product was sequenced and blast analyzed. The 16S rRNA gene sequence of GDZQ201912 was aligned with the 16S rRNA gene sequences of other *Citrobacter* (KC210829.1, FN997639.1, MG011554.1, AP022399.1, AP022486.1, and AP022513.1), *Edwardsiella* (FJ405305.1, EF467289.1, GQ180182.1, FJ405309.1, GQ180181.1, and KC309472.1), *Vibrio* (MT071600.1, MT269596.1, MT307282.1, and MT505697.1), and *Aeromonas* species (EU770272.1, KF358430.1, MK182872.1, and MK182893.1) retrieved from the National Center for Biotechnology Information database. The phylogenetic tree based on 16S rRNA gene sequences of the bacteria cells was constructed via the neighbor-joining (NJ) method with the MEGA program (version 7) using a maximum composite likelihood model. The robustness of the NJ tree was assessed using the approximate likelihood-ratio test and bootstrapping with 1000 replicates. Bootstrap values were shown at each node.

2.3. Effects of Temperature, pH, and Salinity on the Growth of Citrobacter freundii

The isolated strain was inoculated into the LB liquid medium and homogenized. Different temperatures (24 °C, 28 °C, 32 °C, and 42 °C) were used to test their effects on the growth of *C. freundii* at pH 7.0 and salinity 1%. Different pH (3.0, 4.0, 5.0, 6.0, 7.0, 8.0, 9.0, and 10.0) were used to test their effects on the growth of *C. freundii* at 28 °C temperature and 1% salinity. Different salinities (0%, 1%, 2.0%, 3%, 4%, 5%, 6%, and 7%) were used to test their effects on the growth of *C. freundii* at 28 °C temperature and pH 7.0. A 210 µL LB liquid medium containing the isolated strain (10^2 CFU/mL) of different temperatures, pH, and salinities was added to each well of 96-well plates. Then, the bacteria were sampled regularly in triplicate to determine the optical density at a wavelength of 600 nm (OD_{600}) per 30 min and cultured for 24 h.

2.4. Antibiotic Susceptibility Test

The antibiotic susceptibility test was performed using 10^6 CFU/mL isolated strain in the disk diffusion method as described by Lalitha [33]. The isolated strain was tested following the antimicrobial agents (disk content indicated in parentheses): penicillin (10 µg), doxycycline (30 µg), florfenicol (30 µg), norfloxacin (10 µg), ofloxacin (5 µg), amoxicillin (20 µg), ampicillin (10 µg), cefepime (30 µg), ceftriaxone (30 µg), neomycin (30 µg), gentamicin (10 µg), streptomycin (10 µg), clindamycin (2 µg), lincomycin (2 µg), tetracycline (30 µg), novobiocin (30 µg), polymyxin B (300 µg), and rifampin (5 µg) (HANGWEI, Beijing, China). The sizes of the inhibition zones were measured and recorded triplicately. The experimental results were judged in accordance with the clinical and laboratory standards institute standards [34].

2.5. Experimental Challenge

Prawns were obtained from an aquaculture farm in Guandong and acclimated in a recirculating-water aquarium system filled with aerated freshwater for a week. The prawns were fed twice per day with commercial pellet feed (Table 1). Water was maintained

at 28 ± 1 °C using a water heater. Healthy prawns (11.00 ± 1.38 g) were used in the following challenge tests. The challenge tests included two groups: a control group, in which 30 prawns were injected intramuscularly with 100 μL phosphate-buffered saline (PBS) at the junction between the 3rd and 4th abdominal segments, and an infected group, in which 30 prawns were injected with 100 μL bacteria inocula ($10^{6.76}$ CFU/g) at the same junction. The 30 prawns of the normal or infected group were stocked in three 36 L aquaria (10 animals per aquarium). The survival rates and clinical signs of the infected and control groups were recorded daily.

Table 1. Ingredient composition and proximate analysis of commercial feed used for *M. rosenbergii*.

Ingredient	Dry Weight (%)
Rice bran	30.0
Soybean meal (44%)	25.0
Wheat midds	17.75
Menhaden meal (72%)	16.0
Meat, bone, and blood meal	11.0
Mineral premix [a]	0.1
Vitamin premix [b]	0.1
Choline	0.05
Proximate analysis (%)	
Moisture	12.3
Crude protein	36.2
Crude fat [c]	6.3
Crude fiber	4.4
Ash	10.7
Nitrogen free extract (by difference)	30.1

[a] Mineral premix contains: Mn, 11.0%; Zn, 10.0%; Fe, 8.0%; I, 0.36%; Co, 0.10%; Ca (carrier). [b] Vitamin premix contains: vitamin B1, 1.63%; riboflavin, 1.72%; pyridoxine, 1.2%; nicotinic acid, 9.97%; folie acid, 0.34%; vitamin B12, 0.003%; pantotbenic acid, 3.89%; ascorbic acid, 43.69%; vitamin A, 1700 IU/kg; vitamin D3 1200 IU/kg; vitamin E, 66.138 IU/kg; etboxyquin, 0.66%. [c] Acid hydrolysis.

2.6. Median Lethal Dose Determination

In total, 240 healthy prawns (8.00 ± 0.79 g) were used and stocked in 36 L aquaria (10 animals per aquarium). The *C. freundii* ($10^{8.01}$ cells/g) were used for the challenge experiments. For each trial, 10 animals were injected intramuscularly with the *C. freundii* (100 μL) at 10-fold serial dilutions (10^{0}–10^{-6}). Animals serving as negative controls were injected with the same volume of PBS. Each treatment was carried out in triplicate. The inoculum and PBS were injected at the junction between the third and fourth abdominal segments. Dead, moribund animals, and clinical signs in each treatment group were recorded and observed at 24 h intervals and examined by the method described in Section 2.1 to ensure the accuracy of the median lethal dose (LD_{50}). The LD_{50} was calculated using the Behrens-Kärber method [35].

2.7. Antibiotic Treatment

Based on the results of drug sensitivity tests on GDZQ201912, florfenicol and ofloxacin were selected for the evaluation of their therapeutic effects against *C. freundii* in *M. rosenbergii* by common oral pellets containing antibiotics. Florfenicol and ofloxacin were mixed in the pellets based on the 20.0 mg/kg prawn body weight dosage. All of the pellets were coated on the surface feed using edible oil. In total, 360 healthy prawns (7.00 ± 1.03 g) were used and stocked in 36 L aquaria (10 animals per aquarium). The experiment was divided into two groups depending on the different oral antibiotic mixed pellets and time. Group I prawns was treated with antibiotic pellets at the same time with *C. freundii* injection to evaluate their therapeutic effects against *C. freundii*, and group II was treated with antibiotic pellets at the time of typical signs appear after the challenge with *C. freundii* to evaluate the therapeutic effects of the pellets against *C. freundii*. Each group underwent six trials: feeding with common pellets after *C. freundii* injection, feeding with florfenicol mixed pellets after

C. freundii injection, feeding with ofloxacin mixed pellets after *C. freundii* injection, feeding with common pellets after PBS injection, feeding with florfenicol mixed pellets after PBS injection, and feeding with ofloxacin mixed pellets after PBS injection. Each treatment included 10 prawns and had 3 replicates, and the experimental observation period was 14 days. The concentration of *C. freundii* used to injected prawns was 100-fold LD_{50} of *C. freundii* in *M. rosenbergii* and the same volume described in Section 2.6. The prawns of PBS injection trials were injected with the same volume of PBS. The relative percent survival (RPS) of each trial was counted by the formula: (1% immunized mortality/% control mortality) × 100% [36].

2.8. Immune and Anti-Oxidization Parameter Changes in Hemolymph and Hepatopancreas

The hemolymph and hepatopancreas were also collected from group I in the treatment with antibiotics at 1-, 3-, 5-, 7-, 9-, 11-, and 14-days for the following immune enzyme activity assay. The determination of ACP, ALP, CAT, GPx, GST, LZM, MDA, and SOD activities in the hemolymph and hepatopancreas was performed following the protocols of the commercial kits from Nanjing Jiancheng Bioengineering Institute (Nanjing, China).

2.9. Expressions of Immune-Related Genes in Hepatopancreas

The total RNA of hepatopancreas was extracted using a high-purity total RNA Rapid Extraction Kit (Promega, Madison, WI, USA), in accordance with the manufacturer's protocol. The final RNA was resuspended in 50 mL diethyl pyrocarbonate water and stored at −80 °C. Easy Script One-Step gDNA Removal and cDNA Synthesis SuperMix (AccurateBiology, Changsha, China) were used to synthesize first-strand cDNA following the manufacturer's instructions. Quantitative PCR (qPCR) was operated on a LightCycler 480 (Roche Applied Science, Basel, Switzerland) with a final 10 µL reaction volume including 0.5 µL of each primer (10 mM), 5 µL SYBR® Green Realtime PCR Master Mix (AccurateBiology, China), 1 µL cDNA, and 3 µL DNase/RNase-free water. The immune-related gene expression levels of ACP, ALF, CAT, crustin, CTL, Cu/Zn-SOD, CypA, GPx, GST, and LZM were evaluated using qPCR to determine the changes after *C. freundii* infection in prawns, with β-actin acting as the house-keeping gene. The PCR cycling conditions and calculation of the relative expression of each gene were performed as described elsewhere [37]. Table 2 shows the primers used to amplify the above genes.

Table 2. Primers used for quantitative real-time PCR (qRT-PCR).

Target Genes	Sequences (5′–3′)	Accessions
β-actin	Forward: GAGACCTTCAACACCCCCGC Reverse: TAGGTGGTCTCGTGGATGCC	AF221096.1
ALF	Forward: ATCTGGCGTCGTTACCAAAAC Reverse: GAAATGAAACCTGATGATCGTC	JQ364961.1
Crustin	Forward: AACGACTTCAAGTGCTTCGGGTCT Reverse: AAGCTTAGTGGTTTGCAGACGTGC	JQ413342.1
CTL	Forward: ATGTTGACCTTAATGGCCAC Reverse: CTTTTCTGTGGGCGTTTCTTC	KX495215.1
Cu/Zn-SOD	Forward: TCGCCTAACGAGGAGGTTC Reverse: CGGCTTCATCAGGATTTTGAG	DQ121374.1
CypA	Forward: CTAATGCTGGACCCAACACC Reverse: CCTCCACT CCAAT TCTAGCTGTAA	EL696406.1

Table 2. *Cont.*

Target Genes	Sequences (5′–3′)	Accessions
LZM	Forward: TGCCATCAACCACCACAACT Reverse: CCCCTTTCCCTTCCACTTCT	AY257549.2
CAT	Forward: AGCGAGATTGGCAAGAAGACACC Reverse: AAGGATGGTGACCTGGTGCGTGG	HQ668089.1
GPx	Forward: TTCGCCCAGGGAACAATTT Reverse: CCTTTTCACTGAGAATTACCCAG	EL696567.1
GST	Forward: GTTGTGCAGCATTGAGGTTTAT Reverse: GTATCCTACACCATGTGCTCTG	HF570114.1
ACP	Forward: GTTTACACTCGCCTTATCCTCCG Reverse: CTTTGTGCATGAACATGACCCTG	JX975267.1

2.10. Statistical Analysis

All data were statistically analyzed using SPSS 21.0 software (IBM, New York, NY, USA), and the mean ± standard deviation was determined. p-value < 0.05 and <0.01 was considered significant after each measured datum was subjected to Least-significant Difference test. Different graphemes meant significant differences, and the same graphemes meant no significant difference. All columns in this study were drawn with GraphPad Prism 6.0 (San Diego, CA, USA).

3. Results

3.1. Clinical Symptoms of WBD in M. rosenbergii

A total of 30 infected *M. rosenbergii* and 30 healthy *M. rosenbergii* were used to examine the clinical signs of *C. freundii* infection. Compared with normal prawns, *C. freundii*-infected prawns showed a 7 mm-diameter bubble under the carapace of the diseased prawn (Figure 1), loss of appetite, inactivity, and weight loss. The 30 infected prawns all had a water bubble under the carapace. *C. freundii* infection caused mass mortality of the infected prawns after the onset of clinical symptoms and the rapid spread of the disease between prawns.

Figure 1. *Macrobrachium rosenbergii* infected with *Citrobacter freundii* showing typical signs of WBD under the carapace (red arrow).

3.2. Molecular Identification and Biochemical Characterization

The *C. freundii* strain GDZQ201912 was a motile, rod shaped, Gram-negative bacterium (Figure 2A). *C. freundii* was rod-shaped with blunt edges at both ends by TEM (Figure 2B). Ten individuals were randomly measured. The width and length of the bacteria were 0.67–0.76 and 1.88–2.07 µm, respectively.

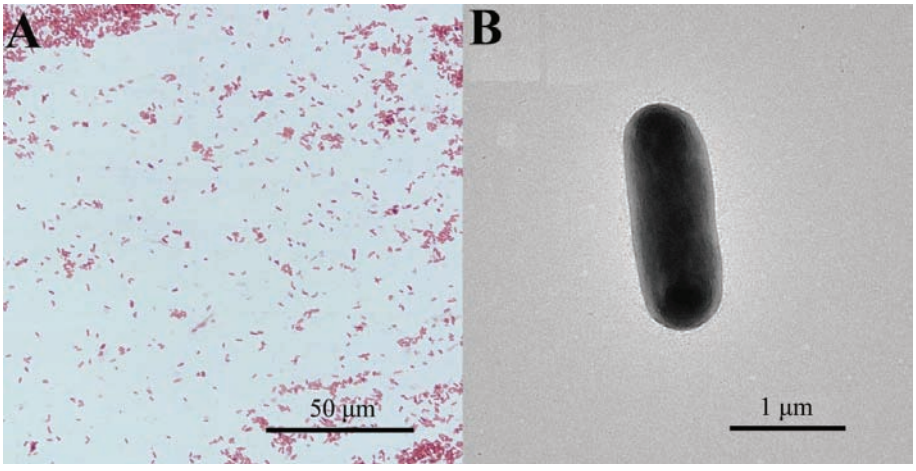

Figure 2. Morphological characteristics and TEM observation of *C. freundii* strain GDZQ201912. (**A**) Gram-stained strain GDZQ201912 observed by light micrograph (1000×). Scale bar 50 µm. (**B**) TEM observation of strain GDZQ201912. Scale bar 1 µm.

The 16S rRNA gene amplified from strain GDZQ201912 was sequenced and BLAST analyzed against the non-redundant database, which showed 99.66% identity with *C. freundii* (GenBank Accession Number: CP060662.1). Tables 3 and 4 present the physiological and biochemical characteristics of strain GDZQ201912, respectively. The molecular sequence and biochemical analyses revealed that the isolated bacterium was *C. freundii*.

Table 3. Morphological properties and conventional tests of strain GDZQ201912 isolated from *Macrobrachium rosenbergii*.

Characteristics	Strain GDZQ201912	*Citrobacter freundii* *
Gram reaction	−	−
Shape	Rod	Rod
Motility	+	+
Indole	−	V
Citrate	+	V
Methyl red	+	+
H_2S	+	V
Ornithine	−	−
Malonate	−	V
Sucrose	+	+
Melibiose	+	+
Raffinose	+	V
Dulcitol	+	V
Adonitol	−	−

"+" positive reaction, "−" negative reaction; "V" variable (positive or negative reaction). * Reference strain data compiled from Bergey's manual [38].

Table 4. Carbon source utilization reactions of strain GDZQ201912.

Characteristics	Strain GDZQ201912	*Citrobacter freundii* *
cis-Aconitate	+	+
trans-Aconitate	+	+
Adonitol	−	−
L-alanine	+	+
γ-Aminobutyrate	+	+
D-arabitol	−	−
Benzoate	−	−
Caprate	−	−
D-cellobiose	+	+
Dulcitol	+	+
D-galactose	+	+
N-acetyl-β-D-galactosamine	+	+
D-galacturonic acid	+	+
L-galactose	+	+
Esculin	−	−
D-fucose	+	+
D-glucose	+	+
Gentiobiose	+	+
Gentisate	+	+
L-glutamate	+	+
Glycerol	+	+
Inositol	+	+
L-lactate	+	+
Lactose	+	+
Lactulose	+	+
Maltitol	+	+
Melibiose	+	+
Phenylacetate	−	+
L-proline	+	+
Putrescine	−	+
Raffinose	+	+
D-sorbitol	+	+
Sucrose	+	+
D-turanose	−	−
L-tyrosine	−	+
Stachyose	−	−
D-fructose	−	−
L-fructose	+	+
D-mannose	+	+
L-rhamnose monohydrate	+	+
dextrin	−	−
D-glucosamic acid	+	+
D-salicin	+	+
N-acetylglucosamine	+	+
D-mannitol	+	+
N-acetylneuraminic acid	+	+
D-glucuronamide	−	−
D-serine	+	+
D-aspartic acid	+	+
L-arginine	−	−
Methyl pyruvate	+	+
Methyl D3phenyllactate	−	−
D-malic acid	+	+
L-malic acid	+	+

(+) positive and (−) negative. * Reference strain data compiled from Bergey's manual [38].

3.3. Phylogenetic Analysis

A phylogenetic tree was constructed using the NJ method by the MEGA 7 software based on the 16S rRNA gene sequences of strain GDZQ201912, and the phylogenetic tree revealed the relationship of strain GDZQ201912 with other *Citrobacter* and pathogenic bacterium species. Bootstrap values above 50% are shown at the nodes. The 16S rRNA gene sequence of strain GDZQ201912 was found to be evolutionarily close to *C. freundii* with the highest bootstrap value (Figure 3).

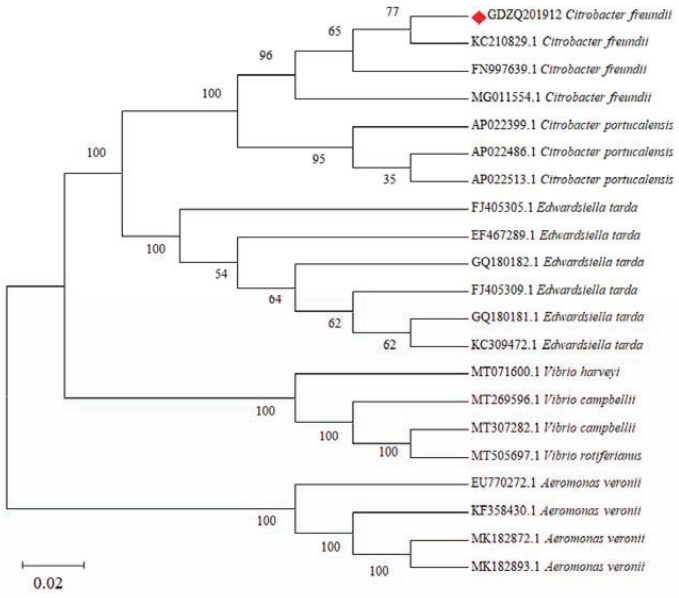

Figure 3. Phylogenetic tree analysis of *Citrobacter* sp. and other pathogenic bacterium species based on 16S rRNA nucleotide sequences. The tree was generated using NJ method by the MEGA 7 software. Bootstrap values above 50% are shown at the nodes. The isolate strain GDZQ201912 identified in this study is indicated by the red shaded diamond.

3.4. Effects of Temperature, pH, and Salinity on the Growth of C. freundii

Figure 4 shows the effects of temperature, pH, and salinity on the growth of *C. freundii*. *C. freundii* exhibits a wide adaptability to temperature. It can grow well in a range from 24 °C to 42 °C (Figure 4A). The optimum temperature was 32 °C. *C. freundii* has a wide pH range and can grow normally at pH 4–9, whose optimal value was around pH 6 (Figure 4B). The maximum salt tolerance of *C. freundii* was 6%, whose optimum value was 1% (Figure 4C). Our results indicated that *C. freundii* has a wide range of temperature, pH, and salinity tolerance.

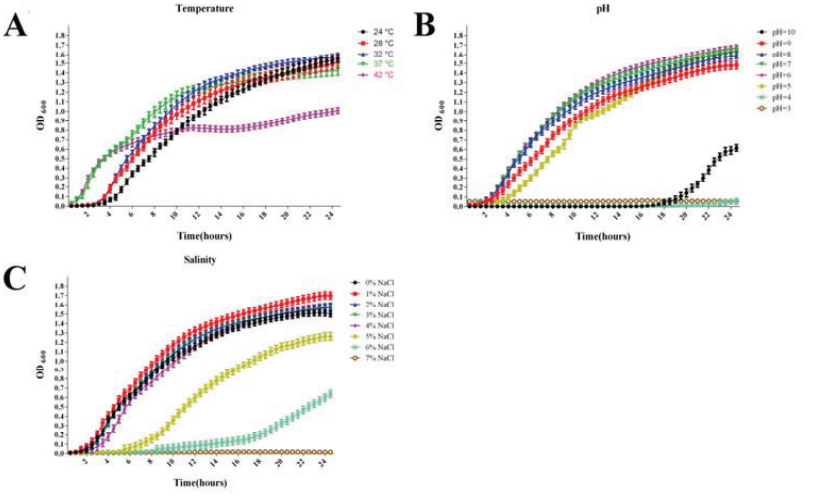

Figure 4. Growth (OD_{600}) of strain GDZQ201912 at different temperatures (**A**), pH (**B**), and salinities (**C**).

3.5. Experimental Challenge

Prawns challenged with strain GDZQ201912 died from the third day post-injection (dpi), and no death occurred in the control groups (Figure 5). The challenged prawns exhibited the typical signs of WBD as described previously. The diseased prawns were similar to those observed in naturally infected prawns in 2019. The bacteria re-isolated from the water bubble of challenged prawns and were reconfirmed as *C. freundii*.

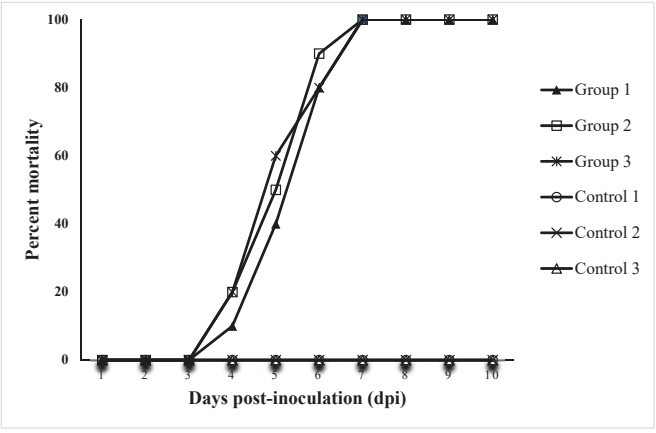

Figure 5. Cumulative mortality curves of the experimentally infected *M. rosenbergii* with strain GDZQ201912. Controls 1, 2, 3, and three replicates of healthy prawns injected with PBS; Groups 1, 2, 3, and three replicates of healthy prawns injected with bacterial inoculum. Each trial contained 10 animals.

3.6. LD_{50} of Strain GDZQ201912 in M. rosenbergii

Figure 6 shows the cumulative mortality rate of *M. rosenbergii* after post-infection with *C. freundii*. For each trial, 10 prawns were injected with bacteria inoculum at 10^0–10^{-6} dilutions, and the control group was injected with same volume of PBS. The control prawns showed no mortality during the experimental challenge. Among *M. rosenbergii* injected with serial dilutions of *C. freundii*, prawns injected with 10^0, 10^{-1}, and 10^{-2} dilutions showed disease signs from 2, 3, and 4 dpi, respectively. Prawns injected with 10^{-3} and 10^{-4} dilutions exhibited disease symptoms from 5 dpi, whereas no death occurred among those injected with 10^{-5} and 10^{-6} dilution during the experimental challenge. The LD_{50} of *C. freundii* was $10^{4.94}$ CFU/g (Figure 6).

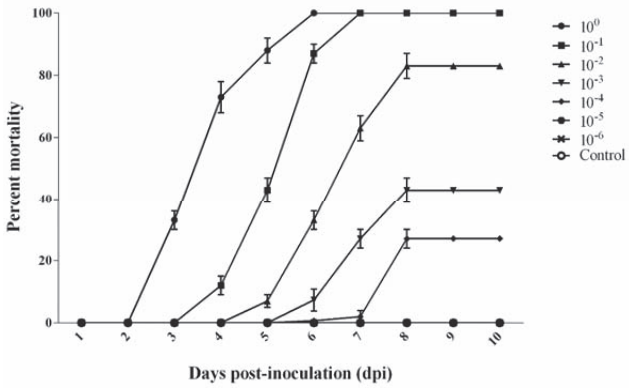

Figure 6. Cumulative mortality curves for the determination of LD_{50} in *M. rosenbergii* challenged with *C. freundii* at different concentrations.

3.7. Antibiogram Tests of Strain GDZQ201912

Antibiogram tests of strain GDZQ201912 revealed its resistance to different antibiotics, such as penicillin, ampicillin, clindamycin, lincomycin, and novobiocin, whereas it showed sensitivity to doxycycline, florfenicol, norfloxacin, ofloxacin, amoxicillin, cefepime, ceftriaxone, neomycin, gentamicin, streptomycin, tetracycline, polymyxin B, and rifampin (Table 5). Among the 13 sensitive antibiotics, strain GDZQ201912 was the most sensitive to cefepime, followed ceftriaxone, ofloxacin, and florfenicol in fourth.

Table 5. Antimicrobial susceptibility analysis of *C. freundii* isolates from *M. rosenbergii* (strain GDZQ201912).

Number	Antibiotics	Drug Content (μg/Pill)	Diameter of Inhibition Zone	Results
1	penicillin	10	6.00 ± 0.00	±
2	doxycycline	30	18.36 ± 0.16	+ +
3	florfenicol	30	28.57 ± 0.19	+ + +
4	norfloxacin	10	28.85 ± 0.21	+ + +
5	ofloxacin	5	29.91 ± 0.13	+ + +
6	amoxicillin	20	14.23 ± 0.11	+ +
7	ampicillin	10	6.00 ± 0.00	±
8	cefepime	30	41.12 ± 0.23	+ + +
9	ceftriaxone	30	36.78 ± 0.15	+ + +
10	neomycin	30	19.63 ± 0.12	+ + +
11	gentamicin	10	17.51 ± 0.18	+ + +
12	streptomycin	10	10.03 ± 0.10	+ +
13	clindamycin	2	6.00 ± 0.00	±
14	lincomycin	2	6.00 ± 0.00	±
15	tetracycline	30	26.56 ± 0.17	+ + +
16	novobiocin	30	6.00 ± 0.00	±
17	Polymyxin B	300	19.21 ± 0.14	+ + +
18	rifampin	5	10.11 ± 0.12	+ +

"+ + +": Highly sensitive; "+ +": Moderately sensitive; "±": Drug resistance.

3.8. Antibiotic Treatment

The *M. rosenbergii* mortalities caused by florfenicol and ofloxacin treatment at different time points after the intramuscular challenge with *C. freundii* or PBS were monitored for 14 days (Figure 7). Prawns fed with common pellets after *C. freundii* infection died from 5 dpi, and the death reached the maximum on 8 dpi with mortalities of 93.0%. In Group I, prawns fed with florfenicol mixed pellets after *C. freundii* infection died from 8 dpi, and the death reached the maximum on 8 dpi with mortalities of 19.40%; prawns fed with ofloxacin mixed pellets after *C. freundii* infection died from 7 dpi, and death reached the maximum on 8 dpi with mortalities of 32.83%. In Group II, prawns fed with florfenicol and ofloxacin mixed pellets after *C. freundii* infection all died from 5 dpi, and the death reached the maximum on 7 dpi with mortalities of 35.67% and 57.47%, respectively. No death was observed among prawns fed with common pellets and mixed pellets of florfenicol and ofloxacin after PBS injection. The evaluation of the therapeutic effects of antibiotic pellets revealed that the RPS of florfenicol and ofloxacin in group I against *C. freundii* in prawns were 86.67% and 72.22%, respectively (Figure 7A). The RPS of florfenicol and ofloxacin in Group II against *C. freundii* in prawns were 69.17% and 47.53%, respectively (Figure 7B). Both florfenicol and ofloxacin initially showed effective protection for *M. rosenbergii* against *C. freundii* (and especially florfenicol).

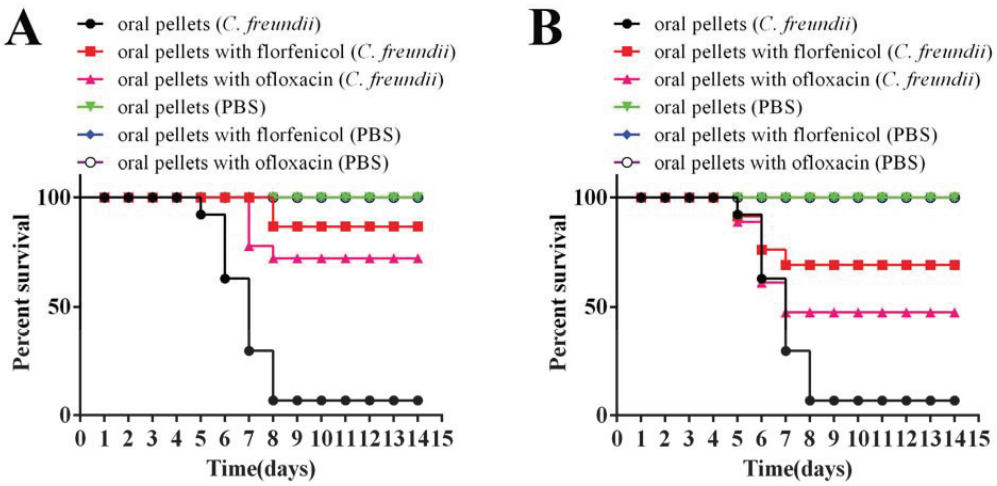

Figure 7. RPS of florfenicol and ofloxacin treatment at different time points after the challenge intramuscular with 100-fold LD_{50} *C. freundii* strain GDZQ201912 for 14 days. (**A**) RPS of prawns treated with antibiotic pellets at the same time with *C. freundii* challenge. (**B**) RPS of prawns treated with antibiotic pellets after death occurred post *C. freundii* challenge.

3.9. Immune and Antioxidant Enzyme Activity Changes in Hemolymph

The enzymatic activities of SOD, CAT, GPx, GST, MDA, ACP, ALP, and LZM of *M. rosenbergii* were measured at 1-, 3-, 5-, 7-, 9-, 11-, and 14-days after the *C. freundii* strain GDZQ201912 and florfenicol challenge. In hemolymph, the results revealed that the SOD activity in the groups fed with common and florfenicol mixed pellets significantly increased from three days post *C. freundii* infection, rapidly declined at five and seven days ($p < 0.05$, Figure 8A), and increased again to normal levels at 9-, 11-, and 14- days compared with the PBS control (fed with common pellets) group ($p > 0.05$, Figure 8A). No significant differences were observed between the SOD activities in the PBS control (fed with common pellets) groups ($p > 0.05$, Figure 8A).

The CAT activity in *M. rosenbergii* fed with common pellets significantly increased from three-, five-, and nine-days post *C. freundii* infection and reached the peak value at 5 dpi compared with the PBS control (fed with common pellets) group ($p < 0.05$, Figure 8B). This value significantly reduced to the lowest at 7-dpi. During this period, the CAT activity of prawns fed with florfenicol mixed pellets significantly increased from three and five days post *C. freundii* infection and reached the peak value at 5-dpi compared with the PBS control (fed with common pellets) group ($p < 0.05$, Figure 8B). No significant differences were observed between the CAT activities in the PBS control (fed with common pellets) groups ($p > 0.05$, Figure 8B).

The GPx activity in *M. rosenbergii* fed with common pellets significantly increased at 3-, 5-, 7-, 9-, 11-, and 14-days post *C. freundii* infection and reached the peak value at 5-dpi compared with the PBS control (fed with common pellets) group ($p < 0.01$, Figure 8C). During this period, the groups fed with florfenicol mixed pellets (*C. freundii* infection) presented similar trend levels of enzymatic activity, which were lower than that observed for the group fed with common pellets (*C. freundii* infection) and reached the peak value at 5 dpi compared with the PBS control (fed with common pellets) group ($p < 0.01$, Figure 8C). No significant differences were observed between the GPx activities in the PBS control (fed with common pellets) groups ($p > 0.05$, Figure 8C).

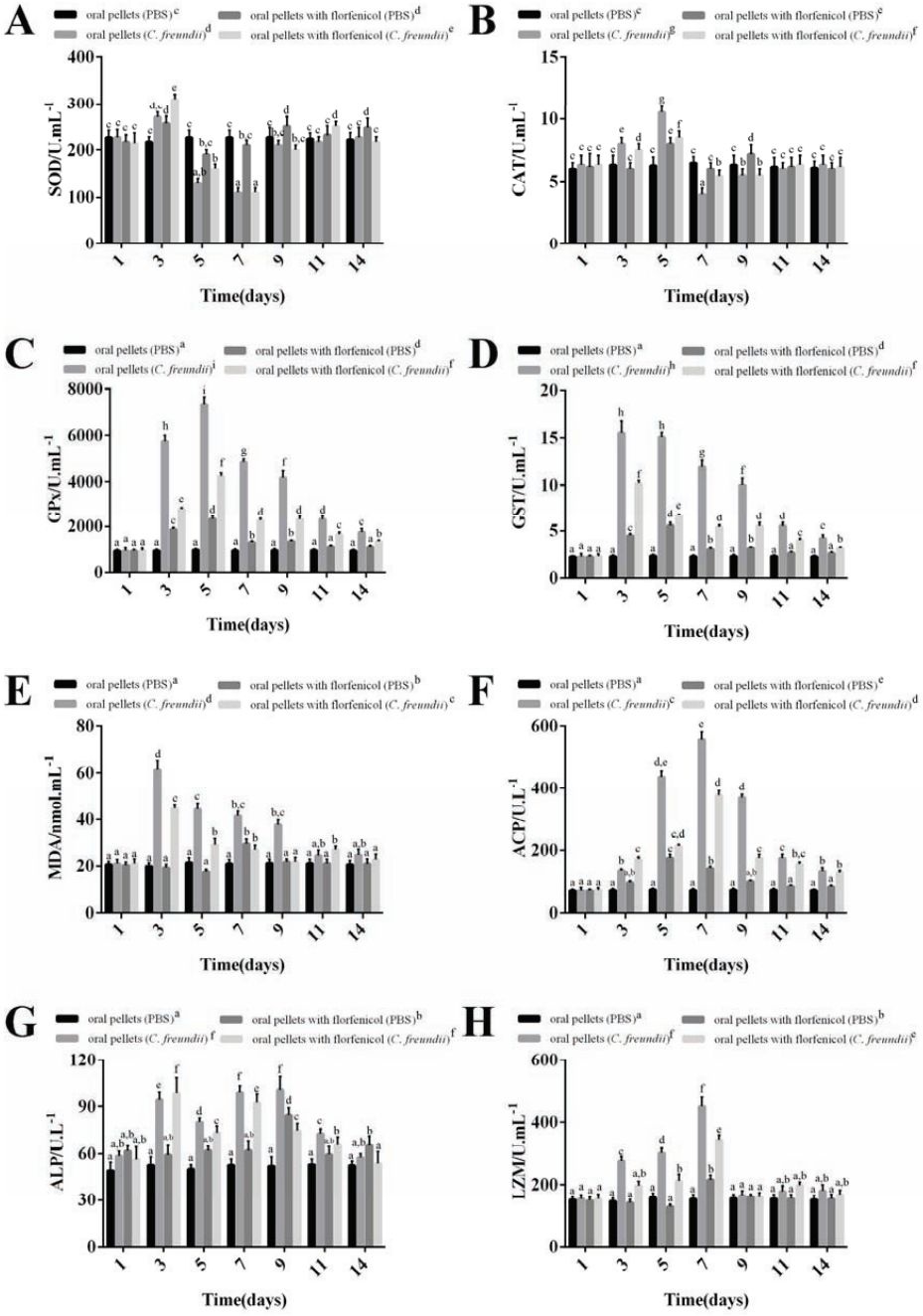

Figure 8. Changes in non-specific immune parameters of *M. rosenbergii* hemolymph at 1-, 3-, 5-, 7-, 9-, 11-, and 14-days after *C. freundii* infection. (**A**) SOD, (**B**) CAT, (**C**) GPx, (**D**) GST, (**E**) MDA, (**F**) ACP, (**G**) ALP, and (**H**) LZM activities. Data are presented as mean ± standard error of the mean (SEM) ($n = 3$); different graphemes (a, b, c, d, e, f, g, h and i) indicate significant difference values of non-specific immune parameters at $p < 0.05$.

The GST activity of prawns fed with common mixed pellets significantly increased at 3-, 5-, 7-, 9-, 11-, and 14-days post *C. freundii* infection and reached the peak value at 3 dpi compared with the PBS control (fed with common pellets) group ($p < 0.01$, Figure 8D). During this period, the groups fed with florfenicol mixed pellets (*C. freundii* infection) presented similar trend levels of enzymatic activity, which were lower than that observed for the group fed with common pellets (*C. freundii* infection) and reached the peak value at 3-dpi compared with the PBS control (fed with common pellets) group ($p < 0.01$, Figure 8D). No significant differences were observed between the GST activities in the PBS control (fed with common pellets) groups ($p > 0.05$, Figure 8D).

The MDA activity of prawns fed with common mixed pellets significantly increased at three, five, seven, and nine days post *C. freundii* infection and reached the peak value at 3-dpi compared with the PBS control (fed with common pellets) group ($p < 0.01$, Figure 8E). During this period, the groups fed with florfenicol mixed pellets (*C. freundii* infection) presented similar trend levels of enzymatic activity, which were lower than that observed for the group fed with common pellets (*C. freundii* infection) and reached the peak value at 3-dpi, compared with the PBS control (fed with common pellets) group ($p < 0.05$, Figure 8E). No significant differences were observed between the MDA activity in the PBS control (fed with common pellets) groups ($p > 0.05$, Figure 8E).

The ACP activity in *M. rosenbergii* fed with common pellets significantly increased from 3-days post *C. freundii* infection and peaked at 7-dpi (556.34 U/L) compared with the PBS control (fed with common pellets) group ($p < 0.01$, Figure 8F). Subsequently, this value declined at 9-, 11-, and 14-days. During this period, the two groups fed with florfenicol pellets (PBS and *C. freundii* infected) presented similar trend levels of enzymatic activity, which were lower than that observed for the group fed with common pellets and reached the peak values of 177.67 and 376.34 U/L on 5- and 7- dpi, respectively ($p < 0.01$). No significant differences were observed in this parameter in the PBS control (fed with common pellets) group ($p > 0.05$, Figure 8F).

The ALP activity of prawns fed with common and florfenicol mixed pellets significantly increased at three-, five-, seven-, and nine-days after *C. freundii* infection, with peak values of 98.67 and 64.67 U/L, respectively, at three and seven days compared with the PBS control (fed with common pellets) group ($p < 0.01$, Figure 8G). No significant differences were observed between ALP activities in the PBS control (fed with common pellets) group ($p > 0.05$, Figure 8G).

The LZM activity in *M. rosenbergii* fed with common pellets significantly increased from 3-, 5-, 7-, 11-, and 14-days post *C. freundii* infection and peaked 450.00 U/mL at 7 days compared with the PBS control (fed with common pellets) group ($p < 0.01$, Figure 8H). This value declined to normal level at 9-dpi ($p > 0.05$, Figure 8H). During this period, the groups fed with florfenicol mixed pellets (*C. freundii* infection) presented similar trend levels of enzymatic activity, which were lower than that observed for the group fed with common pellets and reached the peak value at seven days ($p < 0.05$, Figure 8H). No significant differences were observed between the LZM activities in the PBS control (fed with common pellets) groups ($p > 0.05$, Figure 8H).

3.10. Immune and Antioxidant Enzyme Activity Changes in Hepatopancreas

The results revealed that the SOD activity in *M. rosenbergii* (fed with common and florfenicol mixed pellets) significantly increased at 3-days, decreased at 5- and 7-days post *C. freundii* infection ($p < 0.05$, Figure 9A), and increased again to normal levels at 11 and 14 days compared with the PBS control (fed with common pellets) group ($p > 0.05$, Figure 9A). No significant differences were observed between the SOD activities in the PBS control (fed with common pellets) groups ($p > 0.05$, Figure 9A).

The CAT activity in *M. rosenbergii* (fed with common and florfenicol mixed pellets) significantly increased at three and five days and reached the peak value at 3- and 5-dpi, respectively, while prawns fed with common pellets decreased at seven days post *C. freundii* injection compared with the PBS control (fed with common pellets) group

($p < 0.05$, Figure 9B). No significant differences were observed between the CAT activities in the PBS control (fed with common pellets) groups ($p > 0.05$, Figure 9B).

The GPx activity in *M. rosenbergii* (fed with common and florfenicol mixed pellets) significantly increased at 3-, 5-, 7-, 9-, and 11-days post *C. freundii* injection and both reached the peak value at 5-dpi compared with the PBS control (fed with common pellets) group ($p < 0.01$, Figure 9C). No significant differences were observed between the GPx activities in the PBS control (fed with common pellets) group ($p > 0.05$, Figure 9C).

The GST activity of prawns (fed with common and florfenicol mixed pellets) significantly decreased at 3-, 5-, 7-, 9-, and 11-days post *C. freundii* injection, compared with the PBS control (fed with common pellets) group ($p < 0.05$, Figure 9D). No significant differences were observed between the GST activities in the PBS control (fed with common pellets) and *C. freundii* infection groups (fed with florfenicol mixed pellets) ($p > 0.05$, Figure 9D).

The MDA activity of prawns (fed with common and florfenicol mixed pellets) significantly increased at 3-, 5-, and 7-days post *C. freundii* injection, compared with the PBS control (fed with common pellets) group ($p < 0.05$, Figure 9E). No significant differences were observed between the MDA activities in the PBS control (fed with common and florfenicol mixed pellets) groups ($p > 0.05$, Figure 9E).

The ACP activity in the hepatopancreas of *M. rosenbergii* fed with common and florfenicol mixed pellets significantly increased at 3-, 5-, 7-, 9-, 11-, and 14-days post *C. freundii* infection and reached the peak value at 5- and 7-dpi, respectively, compared with the PBS control (fed with common pellets) group ($p < 0.05$, Figure 9F). No significant differences were observed between the ACP activities in the PBS control (fed with common pellets and florfenicol mixed pellets) groups ($p > 0.05$, Figure 9F).

The ALP activity of prawns (fed with common and florfenicol mixed pellets) significantly increased at three- and five-days post *C. freundii* injection, compared with the PBS control (fed with common pellets) group ($p < 0.05$, Figure 9G). No significant differences were observed between the ALP activities in the PBS control (fed with common and florfenicol mixed pellets) groups ($p > 0.05$, Figure 9G).

The LZM activity in *M. rosenbergii* fed with common pellets significantly increased at three-, five-, and seven-days post *C. freundii* infection and reached the peak value at 5-dpi compared with the PBS control (fed with common pellets) group ($p < 0.01$, Figure 9H). This value declined to normal levels at 9-, 11-, and 14-dpi. During this period, the groups fed with florfenicol mixed pellets (*C. freundii* infection) presented similar trend levels of enzymatic activity, which were lower than that observed for the prawns fed with common pellets and reached the peak value at 7-days ($p < 0.05$, Figure 9H). No significant differences were observed between the LZM activities in the PBS control (fed with common and florfenicol mixed pellets) groups ($p > 0.05$, Figure 9H).

3.11. Expression of Immune-Related Genes in Hepatopancreas after the Challenge with C. freundii

Immunity-related genes (Cu/Zn-SOD, CAT, GPx, GST, LZM, ACP, ALF, crustin, CypA and CTL) mRNA expressions were determined in the hepatopancreas of *M. rosenbergii* at 1-, 3-, 5-, 7-, 9-, 11-, and 14-days after the challenge with *C. freundii* (Figure 10). These genes were up-regulated at different levels following the challenge with *C. freundii* in the groups fed with common and florfenicol mixed pellets compared with the PBS control groups (fed with common and florfenicol mixed pellets). The mRNA expressions of several genes (CAT, GPx, GST, LZM, ACP, ALF, and CypA) in *M. rosenbergii* fed with common pellets reached their peak at five days after the challenged with *C. freundii* (Figure 10B–G,I), whereas the mRNA expressions of crustin (Figure 10H) and CTL (Figure 10J) peaked at 3- and 7-dpi, respectively. The mRNA expressions of several genes (CAT, GPx, GST, crustin and CTL) in *M. rosenbergii* fed with florfenicol mixed pellets reached their peak at 5-dpi (Figure 10B–D,H,J, respectively). Meanwhile, the mRNA expressions of LZM, ACP, ALF and CypA genes peaked at 7-dpi (Figure 10E–G,I, respectively). In addition, the mRNA expression of Cu/ZnSOD in prawns (fed with common and florfenicol mixed pellets) were

up-regulated at 3-dpi and down-regulated at 5- and 7-dpi, with the lowest peak value observed at 7-dpi (Figure 10A). No evident difference was reported between the PBS control groups (fed with common pellets).

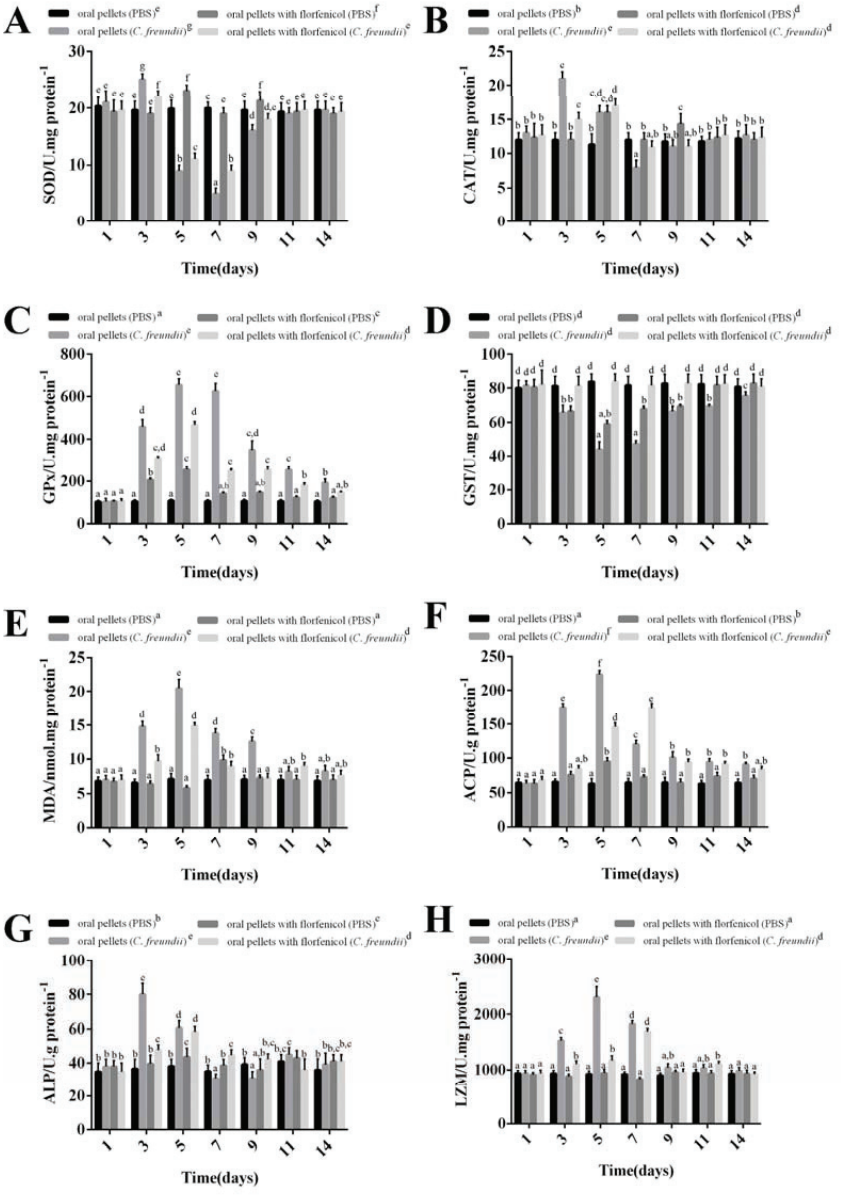

Figure 9. Changes in non-specific immune parameters of *M. rosenbergii* hepatopancreas at 1-, 3-, 5-, 7-, 9-, 11-, and 14-days after *C. freundii* infection. (**A**) SOD, (**B**) CAT, (**C**) GPx, (**D**) GST, (**E**) MDA, (**F**) ACP, (**G**) ALP, and (**H**) LZM activities. Data are presented as mean ± SEM ($n = 3$); different graphemes (a–g) indicate significant difference values of non-specific immune parameters at $p < 0.05$.

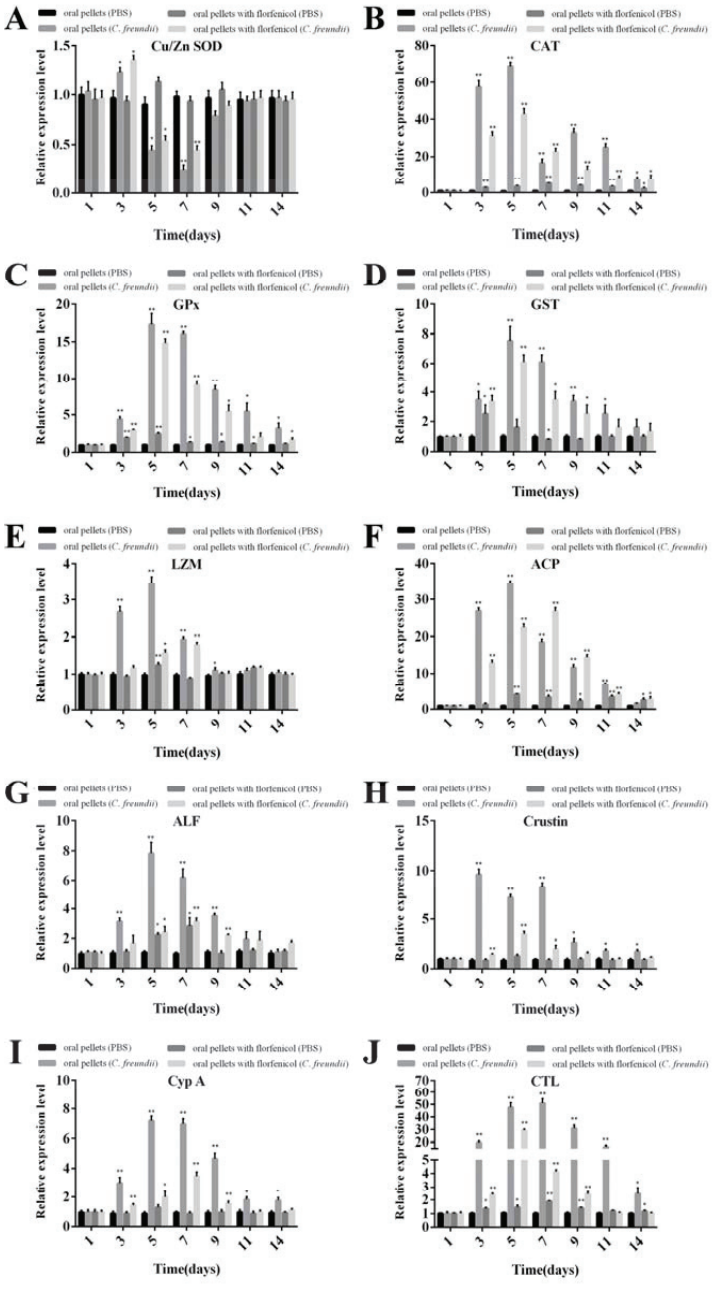

Figure 10. Analysis of immune-related gene expressions in hepatopancreas of *M. rosenbergii* in response to *C. freundii* challenge by RT-PCR at 1-, 3-, 5-, 7-, 9-, 11-, and 14-dpi. (**A**) Cu/ZnSOD, (**B**) CAT, (**C**) GPx, (**D**) GST, (**E**) LZM, (**F**) ACP, (**G**) ALF, (**H**) Crustin, (I) Cyp A, and (J) CTL gene expression levels of immune-related genes were measured by qRT-PCR, and measurement was performed in triplicate for each sample. Expression values were normalized to those of β-actin using the Livak ($2^{-\Delta\Delta CT}$) method, and the expression level detected at 1 day was set as 1.0. Data are presented as mean ± SEM ($n = 3$); * $p < 0.05$, ** $p < 0.01$.

4. Discussion

Diseases are a major constraint in the sustainable development of aquaculture all over the world. The outbreak and spread of bacterial infections in aquaculture farms pose a major concern. *C. freundii* is an opportunistic pathogen that is commonly found in water, soil, animals and has been reported to cause numerous diseases in aquaculture [39–41]. In recent years, an increasing number of studies reported *C. freundii* causing diseases and serious mass deaths in various aquatic products, such as Chinese mitten-handed crab [42], red swamp crayfish [14], grass carp [24], and crucian carp [43]. In addition, *C. freundii* can cause infections in amphibians, reptiles, birds, and mammals [36,44–48]. In the present study, *C. freundii* isolated from diseased *M. rosenbergii* was confirmed to be the cause contributing to prawn mortality, with the typical signs of water bubble under the carapace.

Phylogenetic analysis revealed that our isolated strain GDZQ201912 showed a very close association with other strains of *C. freundii* submitted from China and UK and formed separate clades with other *Citrobacter* sp., such as *C. portucalensis* (AP022399.1, AP022486.1, and AP022513.1). The physiological and biochemical profiles of strain GDZQ201912 were similar to those of other isolates reported by earlier works [49,50]. Variations in the biochemical test, such as those of tyrosine, putrescine [38], indole, citrate, H_2S, malonate, raffinose, and dulcitol, were also described by earlier studies [17,49].

In the case of pathogenic bacteria, such as *C. freundii*, multidrug resistance is one of the most prominent problems [50]. In this study, the isolated strain was resistant to four different β-lactam antibiotics, including ampicillin, clindamycin, lincomycin, and penicillin. Numerous studies demonstrated the existence of β-lactamase in *C. freundii* [51–54]. The resistant feature against β-lactam antibiotics of our strain indicated the existence of β-lactamase gene, which benefits the strain. The *C. freundii* resistant to tetracycline and oxytetracycline has been isolated from mammals, poikilothermic hosts, poultry, catfish, and rainbow trout [55–60].

The innate immune system defense against invading pathogens relies on AMPs, enzymes, and cellular components [16]. During this process, host cells will produce abundant ROS, such as superoxide anion ($O_2^{\bullet -}$), hydrogen peroxide (H_2O_2), hydroxyl radicals ($^{\bullet}OH$), and singlet oxygen ($^1O_2$), and reactive oxygen intermediates to kill the invading pathogens; however, excessive levels of ROS in the body will also cause the destruction and damage of DNA and other biological macromolecules [18]. Crustaceans can rely on complex enzymatic antioxidant systems to alleviate and restore the oxidative damage, SOD, GPx, GST, CAT, MDA, and so on [61]. SODs conduct the first step in eliminating the oxidative damage caused by ROS from cells. The SOD activity first increased at 1.5 h but decreased significantly at 12–48 h in the hepatopancreas of *P. monodon* after *V. parahaemolyticus* infection [62]. In *L. vannamei*, the SOD activity showed remarkable decreases in the hemolymph after 6–96 h and recovery after 96 h post-*V. alginolyticus* injection [63]. The SOD activity was also significantly reduced in *Probopyrus ringueleti*-infected *Palaemontes argentinus* [64]. In addition, the Cu/ZnSOD showed an up-regulated expression in the hemocytes of *M. rosenbergii* at 3 and 6 h after *Lactococcus garvieae* infection, whereas down-regulation was observed in the hepatopancreas at 3 h after *L. garvieae* infection [65]. In *M. nipponense*, the ecCuZnSOD mRNA expression level showed a drastic decrease at 12 h after *A. hydrophila* injection [66]. In *M. rosenbergii*, the cytMn-SOD transcript also decreased in the hepatopancreas at 3 h after *L. garvieae* injection [67]. The expression of icCu/Zn-SOD decreased in the first 8–16 h and then recovered after the challenge with *Listonella anguillarum* and *Micrococcus luteus* in *Chlamys farreri* [68]. The relative expression level of icCu/Zn-SOD mRNA increased rapidly at 6 h post infection with *Vibrio anguillarum* in *Venerupis philippinarum*, followed by a remarkable decrease, and then increased again [69]. In the present study, a similar expression profile was found in the hepatopancreas of *M. rosenbergii* after *C. freundii* infection, in which the relative expression level of Cu/ZnSOD mRNA was up-regulated first and then decrease extremely. Then, the expression level recovered, and SOD activities in hepatopancreas and hemolymph were restored. CAT plays an important role in the antioxidant enzyme defense system to alleviate ROS. The CAT activity in the hepatopancreas of *M. rosenbergii* and CAT mRNA expression increased

markedly at 6 and 24 h post injection with *V. parahaemolyticus* [70]. The CAT activity exhibited a significant rise at the early stage of white spot syndrome virus infection in *P. monodon* [71]. The CAT activity in the hepatopancreas of *M. rosenbergii* significantly decreased at 5 days after spiroplasma MR-1008 infection and showed a recovery at 15 days; however, the mRNA expression level was up-regulated and peaked at 12 days [72]. Similar trends were observed in the CAT activity and mRNA expression level in the present study. GST and GPx are involved in different mechanisms for the host defense against oxidative damage [73]. In *Fenneropenaeus chinensis*, the mRNA expression levels of *Fc*Theta*GST*, *Fc*Mu*GST*, and *Fc*GPx in the hepatopancreas were up-regulated after the challenge with *V. anguillarum* for 24 h, whereas the GST activity decreased [74]. In *L. vannamei*, the GPx activity and mRNA transcription increased significantly at 12 h after the challenge with *V. anguillarum* [75]. In *P. monodon*, the GPx activity of hepatopancreas increased significantly at 6 h and reached the peak level at 12 h after the *V. parahaemolyticus* challenge; the MDA activity significantly increased from 6 h to 24 h with a peak at 6 h, whereas the GST activity decreased significantly at 3 h [62]. The GPx activity in the gill of *F. chinensis* increased at 6 h and remained at high levels up to 24 h [74]. In addition, the results of increased mRNA expression levels and activities (GPx, GST, CAT, and MDA) during *C. freundii* infection in *M. rosenbergii* were in agreement with the histopathological damage in hepatopancreas.

LZM is an important enzyme of the innate immune defense system against bacterial infection, and it can cause bacterial cell disintegration by hydrolyzing the bacterial cell wall [76,77]. Lysosomal enzymes, which are produced by phagocytes from crayfish *Procambarus clarkii*, can efficiently degrade and eliminate foreign materials, as had been demonstrated by Franchini and Ottaviani [78]. In *P. monodon* and *M. rosenbergii*, the lysosomal activity showed a significant increase after *V. vulnificus* infection and increased in *L. vannamei* infected with *Micrococcus lysodeikticus* [79,80]. ACP and ALP are symbols of macrophage activation, important components of the lysosome system, and play important roles in the innate immune system to engulf antigens intracellularly [21]. The ACP activity increased substantially within 48 h in the hemolymph of *C. farreri* after the treatment with *V. anguillarum* [81]. In *L. vannamei*, the ACP and ALP activities significantly increased with *V. parahaemolyticus* and *M. lysodeikticus* infections, respectively [82]. In addition, the ACP and ALP activities in *M. rosenbergii* were significantly enhanced after the challenge with a novel pathogen spiroplasma MR-1008 [72]. In the present study, the enzyme activities of ACP, ALP, and LZM in the hepatopancreas and hemolymph were all enhanced after *M. rosenbergii* infection with *C. freundii*; the enzyme activities all increased significantly in the hepatopancreas after *T. chinensis* infection in *M. nipponense* [83].

AMPs are the main effector molecules in the innate immunity of crustaceans, and they act as frontline effectors to defend against invading bacteria, fungi, and viruses [26,27,84]. The major AMPs, such as penaeidins, crustins, and ALF, have been identified in shrimp [29]. In *P. monodon*, the mRNA expression level of crustin-like peptide significantly increased at 24 h post-infection with *V. harveyi* and recovered at 72 h [85]. The mortality of crustin-depleted *L. vannamei* by RNA interference (RNAi) had a remarkable increase within 48 h post-infection with *V. penaeicida* [86]. In *Marsupenaeus japonicus*, *Mj*Cru I-1 can enhance the hemocyte phagocytosis, increase shrimp survival rate with *V. anguillarum* and *Staphylococcus aureus* infection, and weaken the bacterial clearance by knockdown of *Mj*Cru I-1 [84]. In *L. vannamei*, *Lv*CrustinB was up-regulated with *V. parahaemolyticus* infection, and the knockdown of *Lv*CrustinB can increase the shrimp mortality rate [87]. The expression level of *Fc*ALF2 in *Fenneropenaeus chinensis* significantly increased after the injection with *M. lysodeikticus* and *V. anguillarum* [88]. The in vivo function of *Lv*ALF1 in response to *V. penaeicida* and *Fusarium oxysporum* infections was measured by RNAi; the *Lv*ALF1-depleted *L. vannamei* caused a significant increase in the mortality of infected shrimps [89]. With *C. freundii* infection, the ALF mRNA expression significantly increased in crayfish *P. clarkii* [14]. The expressions of ALF and crustin increased in the hepatopancreas of *M. rosenbergii* after *C. freundii* infection in the present study; in addition, the ALF expression significantly increased in *L. vannamei* after the *V. anguillarum* and *M. lysodeikticus* challenge [90].

CypA acts as the receptor for the immunosuppressive agent cyclosporin A and belongs to the superfamily of peptidyl-prolyl cis-trans isomerases [91]. The mRNA expression of *bts*CypA was up-regulated in the hepatopancreas of *P. monodon* after stimulation by lipopolysaccharide [92]. After *V. anguillarum* challenge, the expression level of *Cf*CypA was up-regulated in the gonads of *C. farreri* and reached the peak at 4 h post-injection [93]. The mRNA expression level of *Es*CypA increased in the fungal *Pichia pastoris*-infected *E. sinensis* [24]. The significantly up-regulated *Vp*CypA2 mRNA expression level was observed in the hemocytes of *V. philippinarum* after the challenge with *L. anguillarum* [94]. The expression of CypA increased in the hepatopancreas of *M. rosenbergii* after *C. freundii* infection in the present study; the CypA mRNA expression level was significantly up-regulated in the hepatopancreas of *P. clarkii* after the challenge with *C. freundii* [14].

CTLs are key recognition proteins and play important roles in shrimp innate immunity for the recognition and clearance of pathogens [22–25]. *Pm*CL1 expression was significantly upregulated in the hepatopancreas and gill of *P. monodon* after the infection with *V. harveyi* and *V. anguillarum*, respectively [95]. The expressions of hepatopancreas-specific CTL (*Fc-hs*L) and CTLs (*Fc*lectin, *Fc*Lec3 and *Fc*Lec4) from *F. chinensis* were up-regulated following the challenge of shrimp with *V. anguillarum* or *S. aureus* [96–99]. In *L. vannamei*, the expressions of *Lv*CTL3 and *Lv*PLP (the perlucin-like protein, a typical CTL) were up-regulated after *V. parahaemolyticus* infection; two CTLs (*Lv*Lectin-1 and *Lv*Lectin-2) showed significantly increased expressions after the *L. anguillarum* challenge [100–102]. Two novel lectins (*Mn*CTLDcp2 and *Mn*CTLDcp3) from *M. nipponense* were up-regulated in the heart after the challenge with *A. hydrophila* [103]. The expression of CTL increased in the hepatopancreas of *M. rosenbergii* after *C. freundii* infection in the present study, and a significantly up-regulated CTL mRNA expression level was observed in the hepatopancreas of *P. clarkii* after the challenge with *C. freundii* [14].

In general, when *M. rosenbergii* was infected with *C. freundii*, CTL, as one of pattern-recognition receptor, immediately recognized the non-self material that had entered the prawn body. With *C. freundii* infection, enzymes involved in the antioxidant antibacterial system (SOD, CAT, GPx, GST, and MDA) were synthesized rapidly in the hepatopancreas and hemolymph, and the phosphatase enzymes (ACP and ALP) and LZM also actively participated in this immune response. In addition, the expressions of immune-related genes (Cu/Zn-SOD, CAT, GPx, GST, LZM, ACP, ALF, crustin, CypA, and CTL) in the hepatopancreas were significantly up- or down- regulated, which suggested that the immediate immune response system in *M. rosenbergii* offers defense against *C. freundii* infection. The results of this study indicated that all of these antioxidant enzymes and genes play important roles in the *M. rosenbergii* immune responses. Furthermore, the hepatopancreas are important immune tissues in the defense against *C. freundii*.

Antibiotics are natural or synthetic compounds and have become the main means for the prevention and treatment of infectious diseases due to their low cost, good curative effect, and simple operation [104,105]. Florfenicol, oxytetracycline, oxytetracycline hydrochloride, ormetoprim, and sulfamethazine were the five antibiotics approved by the FDA [106]. In the present study, florfenicol and ofloxacin were selected to evaluate their therapeutic effects against *C. freundii* in *M. rosenbergii*. Ofloxacin was forbidden in aquaculture and its use in the present study was just for scientific research. Florfenicol is a broad-spectrum and effective antibacterial, belonging to a part of the chloramphenicol family of drugs, that is widely used to control susceptible bacterial diseases in fish and shrimp farming [107–111]. Florfenicol and ofloxacin can stop bacteria from multiplying by interfering with bacterial protein production and DNA replication, respectively [31]. The increasd immune and antioxidant responses in *M. rosenbergii* after *C. freundii* challenge were results of *C. freundii* activated the host's innate immune system. With antibiotics feeding, *C. freundii* in *M. rosenbergii* cannot multiplying well owing to the protein production or DNA replication interfering. Then, the innate immune system of *C. freundii* infected *M. rosenbergii* was more efficient against bacteria with the higher survival rate, immune and antioxidant responses. *C. freundii* can break the innate immune system of *M. rosenbergii* treated with-

out antibiotics, damage the capital functional organs and cause death. Florfenicol was effective in the treatment of pseudotuberculosis in Yellowtail *Seriola quinqueradiata* [112], vibriosis in Goldfish *Carassius auratus* [113], and furunculosis in Atlantic Salmon *Salmo salar* [114], *V. anguillarum* infection in Atlantic cod *Gadus morhua* [106], vibriosis in Black Tiger Shrimps *P. monodon* [111], *V. harveyi* infection in *L. vannamei* [110]. Due to the adverse environmental consequences, alternatives to antibiotics have been developed, including probiotics, phage therapy, essential oils (EOs), and Chinese herbal medicine [31]. *Pseudomonas synxantha* and *Pseudomonas aeruginosa*-fed *Penaeus latisulcatus* showed a higher tolerance to the *V. harveyi* challenge [115]. Four phages that had lytic activity against *V. harveyi* were isolated, and were demonstrated to be effective in controlling the population of *V. harveyi* in hatchery systems and improved the survival of *P. monodon* [116]. The usage of EOs from *Cinnamosma fragrans* enhanced the survival of *P. monodon* larvae with *Vibrio penaeicidae* and *Vibrio splendidus* challenge and decreased bacterial concentration [117]. For the WBD in *M. rosenbergii*, we also conducted alternatives therapies, such as Chinese herbal medicine. We found strain GDZQ201912 was sensitive to *Terminalia chebula Retz*, *Scutellaria baicalensis Georgi*, *Caesalpinia sappan Linn*, *Rhus chinensis Mill*, and *Schisandra chinensis* as well as the evaluations of their therapies of WBD, survival rate, immune and antioxidant responses of *M. rosenbergii* (Unpublished data).

5. Conclusions

Overall, in the present study, the pathogenic bacterium *C. freundii* was isolated from WBD *M. rosenbergii* with a mass mortality, and the cause of WBD in *M. rosenbergii* was identified with the typical sign under the carapace. The TEM observation, physiological and biochemical characteristics, LD_{50}, and antimicrobial susceptibility of the *C. freundii* isolate were studied. The therapeutic effects of antibiotics against WBD were also evaluated, and florfenicol was the most efficient antibiotic to defend against *C. freundii*. In addition, the results of the present study provide insights into the histopathological changes, antioxidant enzymatic activity, and changes in the expressions of immune-related genes of *M. rosenbergii* challenged with *C. freundii*, revealing the antibacterial immune responses in giant river prawn. These results will facilitate the development of therapies and management of the disease caused by this pathogen in aquaculture systems.

Author Contributions: Conceptualization, J.H.; methodology, C.Z.; software, H.W.; validation, C.Z., H.W. and S.H.; formal analysis, C.Z.; investigation, S.W.; resources, J.H.; data curation, C.Z.; writing—original draft preparation, C.Z.; writing—review and editing, J.H.; visualization, C.Z.; supervision, J.H. and C.Z.; project administration, S.W.; funding acquisition, J.H. All authors have read and agreed to the published version of the manuscript.

Funding: This work was funded by the National Key Research and Development Program of China (2018YFD0900501), Key-Area Research and Development Program of Guangdong Province (2019B020217001) and Supported by the earmarked fund for CARS-48.

Institutional Review Board Statement: Not applicable.

Informed Consent Statement: Not applicable.

Data Availability Statement: The data presented in this study are available in the article.

Conflicts of Interest: The authors declare no conflict of interest.

References

1. Nhan, D.T.; Wille, M.; Sorgeloos, P. Comparison of reproductive performance and offspring quality of giant freshwater prawn (*Macrobrachium rosenbergii*) broodstock from different regions. *Aquaculture* **2009**, *298*, 36–42. [CrossRef]
2. New, M. Freshwater prawn farming: Global status, recent research and a glance at the future. *Aquac. Res.* **2005**, *36*, 210–230. [CrossRef]
3. Kumaresan, V.; Palanisamy, R.; Pasupuleti, M.; Arockiaraj, J. Impacts of environmental and biological stressors on immune system of *Macrobrachium rosenbergii*. *Rev. Aquacult.* **2017**, *9*, 283–307. [CrossRef]

4. FAO Data form "Fisheries and Aquaculture Software Fishstatj-Software for Fishery and Aquaculture Statistical Time Series". FAO Fisheries Division 2021, Rome, Italy. Available online: http://www.fao.org/fishery/statistics/software/fishstatj/en (accessed on 18 November 2021).
5. Tiruvayipati, S.; Bhassu, S. Host, pathogen and the environment: The case of *Macrobrachium rosenbergii*, *Vibrio parahaemolyticus* and magnesium. *Gut. Pathog.* **2016**, *8*, 15. [CrossRef] [PubMed]
6. Gao, X.J.; Miao, Z.; Li, X.X.; Chen, N.; Gu, W.W.; Liu, X.D.; Yang, H.; Wei, W.H.; Zhang, X.J. Pathogenicity of non-O1/O139 *Vibrio cholerae* and its induced immune response in *Macrobrachium rosenbergii*. *Fish. Shellfish. Immunol.* **2019**, *92*, 300–307. [CrossRef] [PubMed]
7. Zhang, Y.Y.; Wang, L.F.; Zhuang, H.; Li, X.X.; Gao, X.J.; An, Z.H.; Liu, X.D.; Yang, H.; Wei, W.Z.; Zhang, X.J. Excessive use of enrofloxacin leads to growth inhibition of juvenile giant freshwater prawn *Macrobrachium rosenbergii*. *Ecotoxicol. Environ. Saf.* **2019**, *169*, 344–352. [CrossRef] [PubMed]
8. Zhu, X.J.; Yang, X.Q.; He, W.R.; Xiong, Y.A.; Liu, J.; Dai, Z.M. Involvement of tetraspanin 8 in the innate immune response of the giant prawn, *Macrobrachium rosenbergii*. *Fish. Shellfish. Immunol.* **2019**, *86*, 459–464. [CrossRef] [PubMed]
9. Tao, B.H.; Shi, H.R.; Huang, J.W.; Wang, G. Studied on yellow and black gills of *Macrobrachium rosenbergii* caused by *Pseudoonas*. *Acta Sci. Nat. Univ. Sunyatseni* **2000**, *1*, 255–259.
10. Cheng, W.; Chen, J. Isolation and characterization of an Enterococcus-like bacterium causing muscle necrosis and mortality in *Macrobrachium rosenbergii* in Taiwan. *Dis. Aquat. Organ.* **1998**, *34*, 93. [CrossRef] [PubMed]
11. Ramalingam, K.; Ramarani, S. Effect of *Pseudomonas aeruginosa* on the giant freshwater prawn, *Macrobrachium rosenbergii* histopathological and electron microscopic study. *J. Environ. Biol.* **2007**, *28*, 627–635. [PubMed]
12. Jayaprakash, N.S.; Rejish, K.V.J.; Philip, R.; Bright, S.I.S. Vibrios associated with *Macrobrachium rosenbergii* (De Man, 1879) larvae from three hatcheries on the Indian southwest coast. *Aquac. Res.* **2006**, *37*, 351–358. [CrossRef]
13. Sung, H.H.; Hwang, S.F.; Tasi, F.M. Responses of giant freshwater prawn (*Macrobrachium rosenbergii*) to challenge by two strains of *Aeromonas* spp. *J. Invertebr. Pathol.* **2000**, *76*, 278–284. [CrossRef] [PubMed]
14. Liu, X.; He, X.; An, Z.; Sun, W.; Chen, N.; Gao, X.; Li, X.X.; Zhang, X. *Citrobacter freundii* infection in red swamp crayfish (*Procambarus clarkii*) and host immune-related gene expression profiles. *Aquaculture* **2020**, *515*, 734499. [CrossRef]
15. Li, Y.; Zhan, F.; Li, F.; Lu, Z.; Shi, F.; Xu, Z.; Yang, Y.C.; Zhao, L.J.; Qin, Z.D.; Lin, L. Immune function of cytosolic manganese superoxide dismutase from *Macrobrachium rosenbergii* in response to bacterial infection. *Aquaculture* **2021**, *541*, 736771. [CrossRef]
16. Butprom, S.; Phumkhachorn, P.; Rattanachaikunsopon, P. Effect of Lactobacillus plantarum C014 on innate immune response and disease resistance against *Aeromonas hydrophila* in hybrid catfish. *Sci. World. J.* **2013**, *2013*, 392523. [CrossRef] [PubMed]
17. Behera, B.K.; Paria, P.; Das, A.; Das, B.K. Molecular identification and pathogenicity study of virulent *Citrobacter freundii* associated with mortality of farmed *Labeo rohita* (Hamilton 1822), in India. *Aquaculture* **2022**, *547*, 737437. [CrossRef]
18. Li, Y.; Yan, L.; Kong, X.; Chen, J.; Zhang, H. Cloning, expression, and characterization of a novel superoxide dismutase from deep-sea sea cucumber. *Int. J. Bio. Macromol.* **2020**, *163*, 1875–1883. [CrossRef] [PubMed]
19. Cetinkale, O.; Belce, A.; Konukoglu, D.; Senyuva, C.; Gumustas, M.K.; Tas, T. Evaluation of lipid peroxidation and total antioxidant status in plasma of rats following thermal injury. *Burns* **1997**, *23*, 114–116. [CrossRef]
20. Lopes, P.A.; Pinheiro, T.; Santos, M.C.; da Luz Mathias, M.; Collares-Pereira, M.J.; Viegas-Crespo, A.M. Response of antioxidant enzymes in freshwater fish populations (*Leuciscus alburnoides* complex) to inorganic pollutants exposure. *Sci. Total Environ.* **2001**, *280*, 153–163. [CrossRef]
21. Yin, F.; Gong, H.; Ke, Q.; Li, A. Stress, antioxidant defence and mucosal immune responses of the large yellow croaker *Pseudosciaena crocea* challenged with *Cryptocaryon irritans*. *Fish. Shellfish. Immunol.* **2015**, *47*, 344–351. [CrossRef] [PubMed]
22. Zhang, X.W.; Xu, W.T.; Wang, X.W.; Mu, Y.; Zhao, X.F.; Yu, X.Q.; Wang, J.X. A novel C-type lectin with two CRD domains from Chinese shrimp *Fenneropenaeus chinensis* functions as a pattern recognition protein. *Mol. Immunol.* **2009**, *46*, 1626–1637. [CrossRef] [PubMed]
23. Zhang, Y.X.; Zhang, M.L.; Wang, X.W. C-Type Lectin Maintains the Homeostasis of Intestinal Microbiota and Mediates Biofilm Formation by Intestinal Bacteria in Shrimp. *J. Immunol.* **2021**, *206*, 1140–1150. [CrossRef] [PubMed]
24. Wang, M.; Zhang, D.; Wang, L.; Gai, Y.; Zhou, Z.; Zhang, H.; Song, L. The molecular characterization of a cyclophilin A from Chinese mitten crab *Eriocheir sinensis* and the antifungal activity of its recombinant protein. *Electron. J. Biotechn.* **2013**, *16*, 2. [CrossRef]
25. Wang, X.W.; Vasta, G.R.; Wang, J.X. The functional relevance of shrimp C-type lectins in host-pathogen interactions. *Dev. Comp. Immunol.* **2020**, *109*, 103708. [CrossRef] [PubMed]
26. Brown, K.L.; Hancock, R.E. Cationic host defense (antimicrobial) peptides. *Curr. Opin. Immunol.* **2006**, *18*, 24–30. [CrossRef] [PubMed]
27. Hancock, R.E.; Brown, K.L.; Mookherjee, N. Host defence peptides from invertebrates-emerging antimicrobial strategies. *Immunobiology* **2006**, *211*, 315–322. [CrossRef]
28. Tassanakajon, A.; Amparyup, P.; Somboonwiwat, K.; Supungul, P. Cationic antimicrobial peptides in penaeid shrimp. *Mar. Biotechnol.* **2011**, *13*, 639–657. [CrossRef] [PubMed]
29. Destoumieux, D.; Munoz, M.; Bulet, P.; Bachere, E. Penaeidins, a family of antimicrobial peptides from penaeid shrimp (Crustacea, Decapoda). *Cell. Mol. Life. Sci.* **2000**, *57*, 1260–1271. [CrossRef]

30. Liu, B.; Ge, X.; He, Y.; Xie, J.; Xu, P.; He, Y.; Zhaou, Q.; Pan, L.; Chen, R. Effects of anthraquinones extracted from Rheum officinale Bail on the growth, non-specific immune response of *Macrobrachium rosenbergii*. *Aquaculture* **2010**, *310*, 13–19. [CrossRef]
31. Romero, J.; Feijoó, C.G.; Navarrete, P. Antibiotics in aquaculture-use, abuse and alternatives. *HEV. Aquacult.* **2012**, *159*, 159–198.
32. Lee, I.M.; Hammond, R.W.; Davis, R.E.; Gundersen, D.E. Universal amplification and analysis of pathogen 16S rDNA for classification and identification of mycoplasmalike organisms. *Phytopathology* **1993**, *83*, 834–842. [CrossRef]
33. Lalitha, M.K. Manual on antimicrobial susceptibility testing. In *Performance Standards for Antimicrobial Testing: Twelfth Informational Supplement*; Clinical and Laboratory Standards Institute: Wayne, PA, USA, 2004; Volume 56238, pp. 454–456.
34. Wayne, P.A. Clinical and laboratory standards institute. Performance standards for antimicrobial susceptibility testing. *Inf. Suppl.* **2011**, *31*, 100–121.
35. Kärber, G. Beitrag zur kollektiven Behandlung pharmakologischer Reihenversuche. *Arch. Exptl. Pathol. Pharmakol.* **1931**, *162*, 480–483. [CrossRef]
36. Pan, L.; Yang, Y.; Peng, Y.; Li, D.; Khan, T.A.; Chen, P.; Yan, P.; Hu, S.B.; Ding, X.Z.; Sun, Y.J.; et al. The novel pathogenic *Citrobacter freundii* (CFC202) isolated from diseased crucian carp (*Carassius auratus*) and its ghost vaccine as a new prophylactic strategy against infection. *Aquaculture* **2021**, *533*, 736190. [CrossRef]
37. Chen, M.; Chen, X.Q.; Tian, L.X.; Liu, Y.J.; Niu, J. Improvement of growth, intestinal short-chain fatty acids, non-specific immunity and ammonia resistance in Pacific white shrimp (*Litopenaeus vannamei*) fed dietary water-soluble chitosan and mixed probiotics. *Comp. Biochem. Physiol. C Toxicol. Pharmacol.* **2020**, *236*, 108791. [CrossRef]
38. Frederiksen, W. Citrobacter. In *Bergey's Manual of Systematics of Archaea and Bacteria*; Wiley: Hoboken, NJ, USA, 2015; pp. 1–23.
39. Baldissera, M.D.; Souza, C.F.; Junior, G.B.; Moreira, K.L.S.; da Veiga, M.L.; da Rocha, M.; Baldisserotto, B. *Citrobacter freundii* impairs the phosphoryl transfer network in the gills of *Rhamdia quelen*: Impairment of bioenergetics homeostasis. *Microb. Pathog.* **2018**, *117*, 157–161. [CrossRef] [PubMed]
40. Lü, A.; Hu, X.; Xue, J.; Zhu, J.; Wang, Y.; Zhou, G. Gene expression profiling in the skin of zebrafish infected with *Citrobacter freundii*. *Fish. Shellfish. Immunol.* **2012**, *32*, 273–283. [CrossRef]
41. Sun, H.Y.; Cao, X.H.; Jiang, Y.F.; Ni, L.Y.; Mo, Z.Q.; Qin, Q.W.; Li, Y.W.; Dan, X.M. Outbreak of a novel disease associated with *Citrobacter freundii* infection in freshwater cultured stingray, *Potamotrygon motoro*. *Aquaculture* **2018**, *492*, 35–39. [CrossRef]
42. Huang, X.D.; Zhou, H.H.; An, J.; Yang, X.L.; Cao, H.P. Isolation, identification and antibiotic susceptibility of pathogenic *Citrobacter freundii* from *Eriocheir sinensis*. *J. South. Agric.* **2019**, *50*, 1613–1619.
43. Xiong, F.; Qin, L.; Hao, Y.T.; Zhao, D.; Li, W.X.; Zou, H.; Li, M.; Wu, S.G.; Wang, G.T. Gut microbiota modulation and immunity response induced by *Citrobacter freundii* strain GC01 in grass carp (*Ctenopharyngodon idellus*). *Aquaculture* **2020**, *521*, 735015. [CrossRef]
44. Mauel, M.J.; Miller, D.L.; Frazier, K.S.; Hines, M.E. Bacterial pathogens isolated from cultured bullfrogs (*Rana Castesbeiana*). *J. Vet. Diag. Inv.* **2002**, *14*, 431–433. [CrossRef] [PubMed]
45. Novak, S.S.; Seigel, R.A. Gram-negative septicemia in American alligators (*Alligator mississippiensis*). *J. Wildl. Dis.* **1986**, *22*, 484–487. [CrossRef] [PubMed]
46. Bover-Cid, S.; Holzapfel, W.H. Improved screening procedure for biogenic amine production by lactic acid bacteria. *Int. J. Food. Microbiol.* **1999**, *53*, 33–41. [CrossRef]
47. Chuang, Y.M.; Tseng, S.P.; Teng, L.J.; Ho, Y.C.; Hsueh, P.R. Emergence of cefotaxime resistance in *Citrobacter freundii* causing necrotizing fasciitis and osteomyelitis. *J. Inf.* **2006**, *53*, e161–e163. [CrossRef] [PubMed]
48. Brock, T.D. *Robert Koch: A Life in Medicine and Bacteriology*; Zondervan: Grand Rapids, MI, USA, 1999.
49. Lü, A.; Hu, X.; Zheng, L.; Zhu, A.; Cao, C.; Jiang, J. Isolation and characterization of *Citrobacter* spp. from the intestine of grass carp Ctenopharyngodon idellus. *Aquaculture* **2011**, *313*, 156–160. [CrossRef]
50. Kumar, P.; Meghvansi, M.K.; Kamboj, D.V. Phenotypic characterization and whole-genome analysis of a novel bacteriophage HCF1 infecting *Citrobacter amalonaticus* and *C. freundii*. *Front. Microbiol.* **2021**, *12*, 15. [CrossRef] [PubMed]
51. Tajima, M.; Takenouchi, Y.; Sugawara, S.; Inoue, M.; Mitsuhashi, S. Purification and properties of chromosomally mediated β-lactamase from *Citrobacter freundii* GN7391. *Microbiology* **1980**, *121*, 449–456. [CrossRef] [PubMed]
52. Almeida, M.V.A.D.; Cangussú, Í.M.; Carvalho, A.L.S.D.; Brito, I.L.P.; Costa, R.A. Drug resistance, AmpC-β-lactamase and extended-spectrum β-lactamase-producing *Enterobacteriaceae* isolated from fish and shrimp. *Rev. Inst. Med. Trop.* **2017**, *59*, e70. [CrossRef] [PubMed]
53. Chen, C.M.; Huang, M.; Wu, H.J.; Guo, M.K.; Wu, L.T. Identification of CFE-2, a new plasmid-encoded AmpC β-lactamase from a clinical isolate of *Citrobacter freundii*. *Int. J. Antimicrob. Ag.* **2018**, *52*, 421–424. [CrossRef] [PubMed]
54. Hasan, M.S.; Sultana, M.; Hossain, M.A. Complete genome arrangement revealed the emergence of a poultry origin superbug *Citrobacter portucalensis* strain NR-12. *J. Glob. Antimicrob. Resist.* **2019**, *18*, 126–129. [CrossRef] [PubMed]
55. Toranzo, A.E.; Cutrin, J.M.; Roberson, B.S.; Nunez, S.; Abell, J.M.; Hetrick, F.M.; Baya, A.M. Comparison of the taxonomy, serology, drug resistance transfer, and virulence of *Citrobacter freundii* strains from mammals and poikilothermic hosts. *App. Eenviron. Microb.* **1994**, *60*, 1789–1797. [CrossRef] [PubMed]
56. Duman, M.; Saticioglu, I.B.; Buyukekiz, A.G.; Balta, F.; Altun, S. Molecular characterization and antimicrobial resistance profile of atypical *Citrobacter gillenii* and *Citrobacter* sp. isolated from diseased rainbow trout (*Oncorhynchus mykiss*). *J. Glob. Antimicrob. Resist.* **2017**, *10*, 136–142. [CrossRef] [PubMed]

57. Ture, M.; Kutlu, I. Isolation of *Citrobacter freundii* from Rainbow Trout (*Oncorhynchus mykiss*) in Freshwater Cage. *J. Limnol. Freshw. Fish. Res.* **2018**, *4*, 85–89. [CrossRef]
58. Zhao, C.Y.; Fu, H.T.; Sun, S.M.; Qiao, H.; Zhang, W.Y.; Jin, S.B.; Gong, Y.S. Experimental inoculation of oriental river prawn *Macrobrachium nipponense* with white spot syndrome virus (WSSV). *Dis. Aquat. Organ.* **2017**, *126*, 125–134. [CrossRef]
59. Jiravanichpaisal, P.; Roos, S.; Edsman, L.; Liu, H.; Söderhäll, K. A highly virulent pathogen, *Aeromonas hydrophila*, from the freshwater crayfish *Pacifastacus leniusculus*. *J. Invertebr. Pathol.* **2009**, *101*, 56–66. [CrossRef] [PubMed]
60. Khimmakthong, U.; Sukkarun, P. The spread of *Vibrio parahaemolyticus* in tissues of the Pacific white shrimp *Litopenaeus vannamei* analyzed by PCR and histopathology. *Microb. Pathog.* **2017**, *113*, 107–112. [CrossRef] [PubMed]
61. Jiang, Q.; Jiang, Z.; Ao, S.; Gao, X.; Zhu, X.; Zhang, Z.; Zhang, X. Multi-biomarker assessment in the giant freshwater prawn *Macrobrachium rosenbergii* after deltamethrin exposure. *Ecotoxicol. Environ. Saf.* **2021**, *214*, 112067. [CrossRef] [PubMed]
62. Duan, Y.; Zhang, J.; Dong, H.; Wang, Y.; Liu, Q.; Li, H. Oxidative stress response of the black tiger shrimp *Penaeus monodon* to *Vibrio parahaemolyticus* challenge. *Fish. Shellfish. Immunol.* **2015**, *46*, 354–365. [CrossRef] [PubMed]
63. Li, C.C.; Yeh, S.T.; Chen, J.C. The immune response of white shrimp *Litopenaeus vannamei* following *Vibrio alginolyticus* injection. *Fish. Shellfish. Immunol.* **2008**, *25*, 853–860. [CrossRef]
64. Neves, C.A.; Santos, E.A.; Bainy, A.C.D. Reduced superoxide dismutase activity in *Palaemonetes argentinus* (Decapoda, Palemonidae) infected by *Probopyrus ringueleti* (Isopoda, Bopyridae). *Dis. Aquat. Organ.* **2000**, *39*, 155–158. [CrossRef]
65. Cheng, W.; Tung, Y.H.; Liu, C.H.; Chen, J.C. Molecular cloning and characterisation of copper/zinc superoxide dismutase (Cu, Zn-SOD) from the giant freshwater prawn *Macrobrachium rosenbergii*. *Fish. Shellfish. Immunol.* **2006**, *21*, 102–112. [CrossRef]
66. Xiu, Y.; Wu, T.; Du, J.; Yao, W.; Li, W.; Ding, Z.; Ren, Q.; Gu, W.; Meng, Q.; Wang, W. Molecular characterization and expression analysis of extracellular copper/zinc superoxide dismutase (ecCuZnSOD) from oriental river prawn, *Macrobrachium nipponense*. *Aquaculture* **2013**, *380*, 23–28. [CrossRef]
67. Cheng, W.; Tung, Y.H.; Liu, C.H.; Chen, J.C. Molecular cloning and characterisation of cytosolic manganese superoxide dismutase (cytMn-SOD) from the giant freshwater prawn *Macrobrachium rosenbergii*. *Fish. Shellfish. Immunol.* **2006**, *20*, 438–449. [CrossRef] [PubMed]
68. Ni, D.; Song, L.; Gao, Q.; Wu, L.; Yu, Y.; Zhao, J.; Qiu, L.; Zhang, H.; Shi, F. The cDNA cloning and mRNA expression of cytoplasmic Cu, Zn superoxide dismutase (SOD) gene in scallop *Chlamys farreri*. *Fish. Shellfish. Immunol.* **2007**, *23*, 1032–1042. [CrossRef] [PubMed]
69. Li, C.; Sun, H.; Chen, A.; Ning, X.; Wu, H.; Qin, S.; Xue, Q.; Zhao, J. Identification and characterization of an intracellular Cu, Zn-superoxide dismutase (icCu/Zn-SOD) gene from clam *Venerupis philippinarum*. *Fish. Shellfish. Immunol.* **2010**, *28*, 499–503. [CrossRef] [PubMed]
70. Du, J.; Zhu, H.; Ye, M.; Ma, Y. *Macrobrachium rosenbergii* Cu/Zn superoxide dismutase (Cu/Zn SOD) expressed in *Saccharomyces cerevisiae* and evaluation of the immune function to *Vibrio parahaemolyticus*. *Fish. Shellfish. Immunol.* **2019**, *90*, 363–375. [CrossRef]
71. Mathew, S.; Kumar, K.A.; Anandan, R.; Nair, P.G.V.; Devadasan, K. Changes in tissue defence system in white spot syndrome virus (WSSV) infected *Penaeus monodon*. *Comp. Biochem. Physiol. C Toxicol. Pharmacol.* **2007**, *145*, 315–320. [CrossRef] [PubMed]
72. Du, J.; Zhu, H.; Liu, P.; Chen, J.; Xiu, Y.; Yao, W.; Wu, T.; Ren, Q.; Meng, Q.; Gu, W.; et al. Immune responses and gene expression in hepatopancreas from *Macrobrachium rosenbergii* challenged by a novel pathogen spiroplasma MR-1008. *Fish. Shellfish. Immunol.* **2013**, *34*, 315–323. [CrossRef] [PubMed]
73. Kim, M.; Ahn, I.Y.; Cheon, J.; Park, H. Molecular cloning and thermal stress-induced expression of a pi-class glutathione S-transferase (GST) in the Antarctic bivalve Laternula elliptica. *Comp. Biochem. Physiol. Part A Mol. Integr. Physiol.* **2009**, *152*, 207–213. [CrossRef] [PubMed]
74. Ren, Q.; Sun, R.R.; Zhao, X.F.; Wang, J.X. A selenium-dependent glutathione peroxidase (Se-GPx) and two glutathione S-transferases (GSTs) from Chinese shrimp (*Fenneropenaeus chinensis*). *Comp. Biochem. Physiol. C Toxicol. Pharmacol.* **2009**, *149*, 613–623. [CrossRef]
75. Liu, C.H.; Tseng, M.C.; Cheng, W. Identification and cloning of the antioxidant enzyme, glutathione peroxidase, of white shrimp, *Litopenaeus vannamei*, and its expression following *Vibrio alginolyticus* infection. *Fish. Shellfish. Immunol.* **2007**, *23*, 34–45. [CrossRef]
76. Hikima, S.; Hikima, J.I.; Rojtinnakorn, J.; Hirono, I.; Aoki, T. Characterization and function of kuruma shrimp lysozyme possessing lytic activity against *Vibrio* species. *Gene* **2003**, *316*, 187–195. [CrossRef]
77. Sotelo-Mundo, R.R.; Islas-Osuna, M.A.; De-la-Re-Vega, E.; Hernández-López, J.; Vargas-Albores, F.; Yepiz-Plascencia, G. cDNA cloning of the lysozyme of the white shrimp *Penaeus vannamei*. *Fish. Shellfish. Immunol.* **2003**, *15*, 325–331. [CrossRef]
78. Franchini, A.; Ottaviani, E. Fine structure and acid phosphatase localization of hemocytes in the freshwater snail *Viviparus ater* (Gastropoda, Prosobranchia). *J. Invertebr. Pathol.* **1990**, *55*, 28–34. [CrossRef]
79. Sung, H.H.; Sun, R.Y.A.N. Intrahaemocytic activity of lysosomal enzymes in *Penaeus monodon* and *Macrobrachium rosenbergii*. *Fish. Shellfish. Immunol.* **1999**, *9*, 505. [CrossRef]
80. Sun, C.B.; Wang, G.; Chan, S.F. Effects of artificial infection of *Litopenaeus vannamei* by *Micrococcus lysodeikticus* and WSSV on the activity of immunity related enzymes. *Fish. Shellfish. Immunol.* **2015**, *46*, 778–786. [CrossRef]
81. Wang, X.; Wang, L.; Zhang, H.; Ji, Q.; Song, L.; Qiu, L.; Zhou, Z.; Wang, M.Q.; Wang, L. Immune response and energy metabolism of *Chlamys farreri* under *Vibrio anguillarum* challenge and high temperature exposure. *Fish. Shellfish. Immunol.* **2012**, *33*, 1016–1026. [CrossRef] [PubMed]

82. Pang, H.; Wang, G.; Zhou, S.; Wang, J.; Zhao, J.; Hoare, R.; Monaghan, S.J.; Wang, Z.L.; Sun, C.B. Survival and immune response of white shrimp *Litopenaeus vannamei* following single and concurrent infections with WSSV and *Vibrio parahaemolyticus*. *Fish. Shellfish. Immunol.* **2019**, *92*, 712–718. [CrossRef]
83. Li, Y.; Han, Z.; Xu, W.; Li, X.; Zhao, Y.; Wei, H.; Li, X.; Chen, Q. Antioxidant and immune responses of the Oriental river prawn *Macrobrachium nipponense* to the isopod parasite *Tachaea chinensis*. *Fish. Shellfish. Immunol.* **2020**, *101*, 78–87. [CrossRef] [PubMed]
84. Liu, N.; Lan, J.F.; Sun, J.J.; Jia, W.M.; Zhao, X.F.; Wang, J.X. A novel crustin from *Marsupenaeus japonicus* promotes hemocyte phagocytosis. *Dev. Comp. Immunol.* **2015**, *49*, 313–322. [CrossRef]
85. Amparyup, P.; Kondo, H.; Hirono, I.; Aoki, T.; Tassanakajon, A. Molecular cloning, genomic organisation and recombinant expression of a crustin like antimicrobial peptide from black tiger shrimp *Penaeus monodon*. *Mol. Immunol.* **2008**, *45*, 1085–1093. [CrossRef]
86. Shockey, J.E.; O'Leary, N.A.; de la Vega, E.; Browdy, C.L.; Baatz, J.E.; Gross, P.S. The role of crustins in *Litopenaeus vannamei* in response to infection with shrimp pathogens: An in vivo approach. *Dev. Comp. Immunol.* **2009**, *33*, 668–673. [CrossRef] [PubMed]
87. Li, M.; Ma, C.; Zhu, P.; Yang, Y.; Lei, A.; Chen, X.; Liang, W.; Chen, M.; Xiong, J.; Li, C. A new crustin is involved in the innate immune response of shrimp *Litopenaeus vannamei*. *Fish. Shellfish. Immunol.* **2019**, *94*, 398–406. [CrossRef]
88. Li, S.; Guo, S.; Li, F.; Xiang, J. Characterization and function analysis of an anti-lipopolysaccharide factor (ALF) from the Chinese shrimp *Fenneropenaeus chinensis*. *Dev. Comp. Immunol.* **2014**, *46*, 349–355. [CrossRef] [PubMed]
89. De la Vega, E.; O'Leary, N.A.; Shockey, J.E.; Robalino, J.; Payne, C.; Browdy, C.L.; Warr, G.W.; Gross, P.S. Anti-lipopolysaccharide factor in *Litopenaeus vannamei* (*Lv*ALF): A broad spectrum antimicrobial peptide essential for shrimp immunity against bacterial and fungal infection. *Mol. Immunol.* **2008**, *45*, 1916–1925. [CrossRef]
90. Liu, Y.; Song, L.; Sun, Y.; Liu, T.; Hou, F.; Liu, X. Comparison of immune response in Pacific white shrimp, *Litopenaeus vannamei*, after knock down of Toll and IMD gene in vivo. *Dev. Comp. Immunol.* **2016**, *60*, 41–52. [CrossRef]
91. Muhammad, F.; Zhi-Feng, Z.; Ming-Yu, S.; Shafi, M. cDNA Cloning and expression of cyclophilin A (*Lv*CypA) in white leg shrimp, *Litopenaeus vannamei*. *Pak. J. Zoöl.* **2017**, *49*, 935–941. [CrossRef]
92. Qiu, L.; Jiang, S.; Huang, J.; Wang, W.; Zhu, C.; Su, T. Molecular cloning and mRNA expression of cyclophilin A gene in black tiger shrimp (*Penaeus monodon*). *Fish. Shellfish. Immunol.* **2009**, *26*, 115–121. [CrossRef]
93. Song, X.; Wang, L.; Song, L.; Zhao, J.; Zhang, H.; Zheng, P.; Qiu, L.; Liu, X.; Wu, L. A cyclophilin A inducible expressed in gonad of zhikong scallop *Chlamys farreri*. *Mol. Biol. Rep.* **2009**, *36*, 1637–1645. [CrossRef] [PubMed]
94. Chen, L.; Mu, C.; Zhao, J.; Wang, C. Molecular cloning and characterization of two isoforms of cyclophilin A gene from *Venerupis philippinarum*. *Fish. Shellfish. Immunol.* **2011**, *31*, 1218–1223. [CrossRef] [PubMed]
95. Qin, Y.; Jiang, S.; Huang, J.; Zhou, F.; Yang, Q.; Jiang, S.; Yang, L. C-type lectin response to bacterial infection and ammonia nitrogen stress in tiger shrimp (*Penaeus monodon*). *Fish. Shellfish. Immunol.* **2019**, *90*, 188–198. [CrossRef]
96. Liu, Y.C.; Li, F.H.; Dong, B.; Wang, B.; Luan, W.; Zhang, X.J.; Zhang, L.S.; Xiang, J.H. Molecular cloning, characterization and expression analysis of a putative C-type lectin (*Fc*lectin) gene in Chinese shrimp *Fenneropenaeus chinensis*. *Mol. Immunol.* **2007**, *44*, 598–607. [CrossRef] [PubMed]
97. Sun, Y.D.; Fu, L.D.; Jia, Y.P.; Du, X.J.; Wang, Q.; Wang, Y.H.; Zhao, X.F.; Yu, X.Q.; Wang, J.X. A hepatopancreas-specific C-type lectin from the Chinese shrimp *Fenneropenaeus chinensis* exhibits antimicrobial activity. *Mol. Immunol.* **2008**, *45*, 348–361. [CrossRef]
98. Wang, X.W.; Zhang, X.W.; Xu, W.T.; Zhao, X.F.; Wang, J.X. A novel C-type lectin (*Fc*Lec4) facilitates the clearance of *Vibrio anguillarum* in vivo in Chinese white shrimp. *Dev. Comp. Immunol.* **2009**, *33*, 1039–1047. [CrossRef] [PubMed]
99. Wang, X.W.; Xu, W.T.; Zhang, X.W.; Zhao, X.F.; Yu, X.Q.; Wang, J.X. A C-type lectin is involved in the innate immune response of Chinese white shrimp. *Fish. Shellfish. Immunol.* **2009**, *27*, 556–562. [CrossRef]
100. Wei, X.; Liu, X.; Yang, J.; Fang, J.; Qiao, H.; Zhang, Y.; Yang, J. Two C-type lectins from shrimp *Litopenaeus vannamei* that might be involved in immune response against bacteria and virus. *Fish. Shellfish. Immunol.* **2012**, *32*, 132–140. [CrossRef]
101. Li, M.; Li, C.; Ma, C.; Li, H.; Zuo, H.; Weng, S.; Chen, X.; Zeng, D.; He, J.; Xu, X. Identification of a C-type lectin with antiviral and antibacterial activity from pacific white shrimp *Litopenaeus vannamei*. *Dev. Comp. Immunol.* **2014**, *46*, 231–240. [CrossRef]
102. Bi, J.; Ning, M.; Xie, X.; Fan, W.; Huang, Y.; Gu, W.; Wang, W.; Wang, L.; Meng, Q. A typical C-type lectin, perlucin-like protein, is involved in the innate immune defense of whiteleg shrimp *Litopenaeus vannamei*. *Fish. Shellfish. Immunol.* **2020**, *103*, 293–301. [CrossRef] [PubMed]
103. Xiu, Y.; Hou, L.; Liu, X.; Wang, Y.; Gu, W.; Meng, Q.; Wang, W. Isolation and characterization of two novel C-type lectins from the oriental river prawn, *Macrobrachium nipponense*. *Fish. Shellfish. Immunol.* **2015**, *46*, 603–611. [CrossRef] [PubMed]
104. Feng, Y.; Zhai, Q.; Wang, J.; Li, J.; Li, J. Comparison of florfenicol pharmacokinetics in *Exopalaemon carinicauda* at different temperatures and administration routes. *J. Vet. Pharmacol. Ther.* **2019**, *42*, 230–238. [CrossRef]
105. Barani, A.; Fallah, A.A. Occurrence of tetracyclines, sulfonamides, fluoroquinolones and florfenicol in farmed rainbow trout in Iran. *Food. Agr. Immunol.* **2015**, *26*, 420–429. [CrossRef]
106. Caipang, C.M.A.; Lazado, C.C.; Brinchmann, M.F.; Berg, I.; Kiron, V. In vivo modulation of immune response and antioxidant defense in Atlantic cod, *Gadus morhua* following oral administration of oxolinic acid and florfenicol. *Comp. Biochem. Physi. C* **2009**, *150*, 459–464. [CrossRef]
107. Van de Riet, J.M.; Potter, R.A.; Christie-Fougere, M.; Burns, B.G. Simultaneous determination of residues of chloramphenicol, thiamphenicol, florfenicol, and florfenicol amine in farmed aquatic species by liquid chromatography/mass spectrometry. *J. AOAC. Int.* **2003**, *86*, 510–514. [CrossRef] [PubMed]

108. Fang, W.; Li, G.; Zhou, S.; Li, X.; Hu, L.; Zhou, J. Pharmacokinetics and Tissue Distribution of Thiamphenicol and Florfenicol in Pacific White Shrimp *Litopenaeus vannameiin* Freshwater following Oral Administration. *J. Aqua. Anim. Health.* **2013**, *25*, 83–89. [CrossRef] [PubMed]
109. Burridge, L.; Weis, J.S.; Cabello, F.; Pizarro, J.; Bostick, K. Chemical use in salmon aquaculture: A review of current practices and possible environmental effects. *Aquaculture* **2010**, *306*, 7–23. [CrossRef]
110. Parmar, P.; Yusufzai, S.K.; Parmar, H.V.; Nanjiyani, R.P.; Chavda, V.M. Therapeutic potentiality of florfenicol against vibriosis in *Litopenaeus vannamei*. *J. Entomol. Zool. Stud.* **2018**, *6*, 463–467.
111. Tipmongkolsilp, N.; Limpanon, Y.; Patamalai, B.; Lusanandana, P.; Wongtavatchai, J. Oral medication with florfenicol for black tiger shrimps *Penaeus monodon*. *Thai J. Vet. Med.* **2006**, *36*, 39–47.
112. Yasunaga, N.; Yasumoto, S. Therapeutic effect of florfenicol on experimentally induced pseudotuberculosis in Yellowtail. *Fish. Pathol.* **1988**, *23*, 1–5. [CrossRef]
113. Fukui, H.; Fujihara, Y.; Kano, T. In vitro and in vivo antibacterial activities of florfenicol, a new fluorinated analog of thiamphenicol, against fish pathogens. *Fish. Pathol.* **1987**, *22*, 201–207. [CrossRef]
114. Inglis, V.; Richards, R.H.; Varma, K.J.; Sutherland, I.H.; Brokken, E.S. Florfenicol in Atlantic salmon, *Salmo salar* L., parr: Tolerance and assessment of efficacy against furunculosis. *J. Fish Dis.* **1991**, *14*, 343–351. [CrossRef]
115. Van Hai, N.; Buller, N.; Fotedar, R. The use of customised probiotics in the cultivation of western king prawns (*Penaeus latisulcatus* Kishinouye, 1896). *Fish. Shellfish. Immunol.* **2009**, *27*, 100–104. [CrossRef] [PubMed]
116. Shivu, M.M.; Rajeeva, B.C.; Girisha, S.K.; Karunasagar, I.; Krohne, G.; Karunasagar, I. Molecular characterization of *Vibrio harveyi* bacteriophages isolated from aquaculture environments along the coast of India. *Environ. Microbiol.* **2007**, *9*, 322–331. [CrossRef] [PubMed]
117. Randrianarivelo, R.; Danthu, P.; Benoit, C.; Ruez, P.; Raherimandimby, M.; Sarter, S. Novel alternative to antibiotics in shrimp hatchery: Effects of the essential oil of *Cinnamosma fragrans* on survival and bacterial concentration of *Penaeus monodon* larvae. *J. Appl. Microbiol.* **2010**, *109*, 642–650. [CrossRef] [PubMed]

antioxidants

MDPI

Article

The Assessment of Dietary Organic Zinc on Zinc Homeostasis, Antioxidant Capacity, Immune Response, Glycolysis and Intestinal Microbiota in White Shrimp (*Litopenaeus vannamei* Boone, 1931)

Jinzhu Yang [1], Tiantian Wang [1], Gang Lin [2], Mingzhu Li [3], Yanjiao Zhang [1,*] and Kangsen Mai [1]

[1] The Key Laboratory of Aquaculture Nutrition and Feed (Ministry of Agriculture), The Key Laboratory of Mariculture (Ministry of Education), Ocean University of China, Qingdao 266003, China; yangjinzhu@stu.ouc.edu.cn (J.Y.); 21180511037@stu.ouc.edu.cn (T.W.); kmai@ouc.edu.cn (K.M.)
[2] Institute of Quality Standards and Testing Technology for Agricultural Products, Chinese Academy of Agricultural Sciences, Beijing 100081, China; lingang@caas.cn
[3] College of Agriculture, Ludong University, Yantai 264025, China; 2982@ldu.edu.cn
* Correspondence: yanjiaozhang@ouc.edu.cn; Tel.: +86-532-8203-1627

Abstract: This study aimed to assess dietary organic zinc on zinc homeostasis, antioxidant capacity, immune response, glycolysis and intestinal microbiota in white shrimp (*Litopenaeus vannamei* Boone, 1931). Six experimental diets were formulated: Control, zinc free; S120, 120 mg·kg^{-1} zinc from $ZnSO_4 \cdot 7H_2O$ added into control diet; O30, O60, O90 and O120, 30, 60, 90 and 120 mg·kg^{-1} zinc from Zn-proteinate added into control diet, respectively. The results showed that organic zinc significantly promoted zinc content and gene expression of ZnT1, ZIP11 and MT in the hepatopancreas and enhanced antioxidant capacity and immunity (in terms of increased activities of T-SOD, Cu/Zn SOD, PO, LZM, decreased content of MDA, upregulated expressions of GST, G6PDH, ProPO, LZM and Hemo, and increased resistance to *Vibrio parahaemolyticus*). Organic zinc significantly upregulated GluT1 expression in the intestine, increased glucose content of plasma and GCK, PFK and PDH activities of hepatopancreas, and decreased pyruvate content of hepatopancreas. Organic zinc improved intestinal microbiota communities, increased the abundance of potentially beneficial bacteria and decreased the abundance of potential pathogens. Inorganic zinc (S120) also had positive effects, but organic zinc (as low as O60) could achieve better effects. Overall, organic zinc had a higher bioavailability and was a more beneficial zinc resource than inorganic zinc in shrimp feeds.

Keywords: organic zinc; zinc homeostasis; antioxidants; immunity; glycolysis; intestinal microbiota; *Litopenaeus vannamei* Boone, 1931

Citation: Yang, J.; Wang, T.; Lin, G.; Li, M.; Zhang, Y.; Mai, K. The Assessment of Dietary Organic Zinc on Zinc Homeostasis, Antioxidant Capacity, Immune Response, Glycolysis and Intestinal Microbiota in White Shrimp (*Litopenaeus vannamei* Boone, 1931). *Antioxidants* **2022**, *11*, 1492. https://doi.org/10.3390/antiox11081492

Academic Editors: Bo Liu, Changyou Song and Cunxin Sun

Received: 13 June 2022
Accepted: 28 July 2022
Published: 29 July 2022

1. Introduction

As an essential microelement for animals, zinc is well known for its key role in various physiological processes such as organism growth and metabolism of proteins, carbohydrates and lipids [1,2]. Zinc is also a cofactor or component of various enzymes related to antioxidants, immune response and regulation, such as alkaline phosphatase (AKP), metallothionein (MT), superoxide dismutase (SOD) and copper/zinc superoxide dismutase (Cu/Zn SOD) [3]. In aquafeeds, zinc sulfate is traditionally used to meet the demand of aquatic animals due to its lower price and easy accessibility [4,5]. However, the disadvantages of zinc sulfate have been noticed with its low bioavailability and potential environmental problems. On the one hand, plant-based ingredients have been widely used in aquafeeds [6–8]. It is known that plant-based ingredients contain antinutritional factors that reduce the bioavailability of minerals [9,10]; for example, phytate is easily chelated to Zn^{2+}, forming stable chelates that are not absorbed intestinally [3,9]. Thus, overdosage of

zinc addition is common in aquafeeds [11,12], which increases the risk of water pollution in intensive aquaculture zones and their surroundings. On the other hand, sulfate salts are a common type of inorganic mineral (e.g., $ZnSO_4$, $CuSO_4$, $MnSO_4$) in feed addition [13]. The high concentration of SO_4^{2-} is toxic to aquatic organisms. SO_4^{2-} can be reduced into sulfide under anaerobic conditions, which is toxic to a number of aquatic organisms as well [14,15].

Organic zinc, formed by the chelation of Zn^{2+} with amino acids (e.g., glycine, methionine) and/or partially hydrolyzed proteins, provides a new option for zinc supplementation in aquafeeds [16]. It has been reported that organic zinc is more easily absorbed by the intestinal epithelium than inorganic zinc [17,18], and it can prevent the chelation of Zn^{2+} with phytate and protect the micronutrients (e.g., vitamins, fatty acids) from oxidation by Zn^{2+} [19]. In channel catfish (*Ictalurus punctatus*), organic zinc had over 3 times the potency of inorganic zinc in improving growth and increased resistance to *Edwardsiella ictaluri* [20,21]. Similarly, there was also a higher bioavailability of organic zinc than inorganic zinc in beluga sturgeon (*Huso huso*) [22], pangasius catfish (*Pangasianodon hypophthalmus*) [23] and juvenile abalone (*Haliotis discus hannai* Ino.) [24]. In triploid rainbow trout (*Oncorhynchus mykiss*), organic zinc reduced the zinc requirement and enhanced antioxidant capacity compared to inorganic zinc [25,26]. In white shrimp (*Litopenaeus vannamei* Boone, 1931), compared to inorganic zinc, organic zinc promoted growth performance and enhanced immunity and resistance to *Vibrio harveyi* better [27–29]. Glycolysis is a cellular process that breaks down glucose into pyruvate. Pyruvate can enter the tricarboxylic acid cycle (TAC) for further ATP production. Glycolysis is also an important method to metabolize glucose in most organisms. Previous studies have described that zinc plays a role in stimulating glycolysis in mice [30] and rats [31,32]; however, in aquaculture, relevant information is limited. The intestinal microbiota plays key roles in host health, nutrition metabolism and immune response. Studies have found zinc could increase the abundance of potential probiotics in weanling pigs [33] and improve the microbial population of broiler chickens [34]. However, information on the effect of zinc on the intestinal microbiota of aquatic animals is also limited.

White shrimp is a major species in aquaculture around the world and has great economic value due to its great texture, rapid growth rate and good adaptability to the environment [35]. At present, the increasing farming density and scale pose a challenge to the health and disease resistance of shrimp [36]. Organic zinc is considered to have immune-enhancing effects, which is beneficial for shrimp health. Most previous studies of organic zinc have focused on growth performance and biochemical parameters. This study aimed to assess dietary organic zinc (Zn-proteinate) on zinc homeostasis, antioxidant capacity, immune response, glycolysis, intestinal microbiota and resistance to *V. parahaemolyticus* in white shrimp, which will provide a comprehensive assessment of organic zinc application in shrimp culture.

2. Materials and Methods

2.1. Experimental Diets

Six isonitrogenous and isolipidic experimental diets were formulated to contain different dosage forms of zinc, resulting in the following six dietary treatments: Control, dietary Zn free; S120, dietary 120 mg·kg^{-1} zinc from $ZnSO_4 \cdot 7H_2O$ added into control diet; O30, O60, O90, O120, dietary 30, 60, 90, 120 mg·kg^{-1} zinc from Zn-proteinate added into control diet, respectively. All the ingredients were thoroughly mixed and pelleted with an approximate diameter of 2 mm. After that, feeds were dried until constant weight at 55 °C in a ventilated oven. Feeds were then stored at −20 °C until use. The formulation, chemical composition and zinc content in feeds are shown in Table 1.

Table 1. Formulation and proximate compositions of experimental diets.

Ingredients (%)	Diets					
	Control	**S120**	**O30**	**O60**	**O90**	**O120**
Fish meal [1]	15.00	15.00	15.00	15.00	15.00	15.00
Shrimp shell meal [1]	5.00	5.00	5.00	5.00	5.00	5.00
Brewer yeast [1]	5.00	5.00	5.00	5.00	5.00	5.00
Soybean meal [1]	30.00	30.00	30.00	30.00	30.00	30.00
Cottonseed protein [1]	5.00	5.00	5.00	5.00	5.00	5.00
Peanut meal [1]	10.00	10.00	10.00	10.00	10.00	10.00
Wheat flour [1]	22.00	22.00	22.00	22.00	22.00	22.00
Fish oil [1]	1.00	1.00	1.00	1.00	1.00	1.00
Soybean oil [1]	1.00	1.00	1.00	1.00	1.00	1.00
Phospholipid [1]	1.00	1.00	1.00	1.00	1.00	1.00
Monocalcium phosphate [1]	1.00	1.00	1.00	1.00	1.00	1.00
Choline chloride [2]	0.20	0.20	0.20	0.20	0.20	0.20
Vitamin mix [3]	1.00	1.00	1.00	1.00	1.00	1.00
Mineral mix (Zn Free) [3]	1.00	1.00	1.00	1.00	1.00	1.00
Lysine hydrochloride [1]	0.10	0.10	0.10	0.10	0.10	0.10
Methionine [2]	0.10	0.10	0.10	0.10	0.10	0.10
Threonine [2]	0.05	0.05	0.05	0.05	0.05	0.05
Vitamin C-35 phosphate [1]	0.20	0.20	0.20	0.20	0.20	0.20
$ZnSO_4 \cdot 7H_2O$ (22.74%) [2]	-	0.0528	-	-	-	-
Bioplex Zn® (15%) [4]	-	-	0.02	0.04	0.06	0.08
Astaxanthin (10%) [1]	0.10	0.10	0.10	0.10	0.10	0.10
Y_2O_3 [2]	0.01	0.01	0.01	0.01	0.01	0.01
Carrier [1]	1.24	1.1872	1.22	1.20	1.18	1.16
Analyzed Nutrient Compositions (% Dry Matter)						
Crude protein	45.70	45.76	45.96	46.22	45.89	46.46
Crude lipid	4.32	4.48	4.41	4.41	4.72	4.67
Ash	8.92	9.16	9.36	9.13	9.23	9.25
Zinc Analysis ($mg \cdot kg^{-1}$)						
Zn (formulated value)	0	120	30	60	90	120
Zn (analyzed value)	53	133	86	106	138	171

[1] Fish meal, shrimp shell meal, brewer yeast, etc., were purchased from Qingdao Great-seven Nutr-tech Co., Ltd., Qingdao, China. [2] Choline chloride, amino acid, $ZnSO_4 \cdot 7H_2O$ and Y_2O_3 were purchased from Shanghai Macklin Biochemical Co., Ltd., Shanghai, China. [3] Vitamin premix and mineral premix were purchased from Qingdao Master Biotech Co., Ltd., Qingdao, China. Vitamin premix contains (kg^{-1}): vitamin A acetate, 714,000 IU; vitamin D3, 266,000 IU; DL-α-tocopherol acetate, 8.6 g; menadione, 1.0 g; thiamine mononitrate, 1.0 g; riboflavin, 1.4 g; pyridoxine hydrochloride, 1.2 g; cyanocobalamin, 0.004 g; D-calcium pantothenate, 4.0 g; nicotinamide, 6.8 g; folic acid, 0.28 g; D-biotin, 0.012 g; inositol, 7.6 g; L-ascorbic acid-2-phosphate, 16.6 g; mineral premix contains (kg^{-1}): Mg, 12.5 g; Fe, 4.0 g; Mn, 2.0 g; Cu, 1.25 g; Co, 0.05 g; Se, 0.015 g; I, 0.05 g. [4] Bioplex Zn® was provided by Beijing Alltech Biological Products (China) Co., Ltd., Beijing, China.

Analysis of the chemical compositions of feeds was performed following standard protocols [37]. Dry matter was measured by drying samples to a constant weight at 105 °C, crude protein was determined by measuring nitrogen (N × 6.25) using the Kjeldahl method (FOSS 8400, Denmark, Sweden), crude lipid was determined by mineral ether extraction using the Soxhlet method (BUCHI 36880, Flawil, Switzerland) and ash content was determined by incineration of samples at 550 °C in a muffle furnace.

The moisture was calculated with the following equation:

$$\text{Moisture (\%)} = 100 \times (W_1 - W_2)/W_1, \quad (1)$$

W_1: Wet weight of matter; W_2: Dry weight of matter.

The ash content was calculated with the following equation:

$$\text{Ash (\%)} = 100 \times W_3/W_4, \quad (2)$$

W_3: Ash weight after incineration; W_4: Dry weight before incineration.

2.2. Feeding Trial and Sample Collection

The feeding trial was carried out at Huanghai Aquaculture Co., Ltd., Shandong, China. White shrimp were purchased from a local farm. Before the feeding trial, shrimp were acclimated to a commercial diet for 2 weeks with flowing water. Shrimp were then fasted for 24 h and weighted. A total of 960 shrimp (initial body weight of 2.37 ± 0.01 g) were randomly distributed to 24 cylindrical fiberglass tanks (with 200 L of seawater) in an indoor rearing system with flow-through seawater. A total of 40 shrimp were cultured in each tank. The six diets were randomly assigned to tanks (4 replications each group). During the feeding trial, shrimp were fed 4 times daily (05:30, 11:00, 16:30 and 21:30). The daily feeding quantity was at 4–6% of body weight and adjusted according to previous feeding responses. Two-thirds of seawater was exchanged twice daily. The water condition was detected once a week, and the results were as follows: temperature was 26.4–28.0 °C; salinity was 31–33‰; pH was 8.2–8.4; dissolved oxygen was higher than 7 mg·L^{-1}; nitrite was lower than 0.005 mg·L^{-1}; nitrate was lower than 15 mg·L^{-1}; ammonia was lower than 0.02 mg·L^{-1}.

After 8 weeks of feeding, shrimp were fasted for 24 h; all surviving shrimp were collected, and then the body length and weight of each shrimp were measured. After that, 12 shrimp of similar size from each tank were randomly selected. The hemolymph was collected from the caudal vein using 1 mL syringes and diluted immediately at a hemolymph-to-anticoagulant ratio of 1:1.5 (10 mmol·L^{-1} EDTA-Na_2, 450 mmol·L^{-1} NaCl, 10 mmol·L^{-1} KCl, 10 mmol·L^{-1} HEPES, pH 7.3) [38]. Approximately 50 μL of hemolymph was used for the hemocyte count using a hemocytometer (XB-K-25, Yuhuan County Qiujing Medical Instrument Factory, Zhejiang, China). The rest was centrifuged at 4 °C, 500 g·min^{-1} for 10 min. The supernatant was then collected into 0.2 mL PCR tubes (Cat. No.: PCR02C, Axygen™, Union City, CA, USA) and stored at −80 °C for biochemical analysis. After that, the hepatopancreas was quickly removed and then transferred to 1.8 mL sterile RNase-free cryogenic tubes (Cat. No.: 377267, Nunc™, Rochester, NY, USA), frozen in liquid nitrogen and stored at −80 °C for analysis of enzyme activity and gene expression. Intestines were then removed and transferred to 1.8 mL sterile RNase-free cryogenic tubes (Cat. No.: 377267, Nunc™, Rochester, NY, USA), frozen in liquid nitrogen and stored at −80 °C, of which 6 were used for gene expression analysis and the other 6 for microbiota analysis. The muscle and carapace of 2 shrimp were randomly selected and stored at −20 °C for zinc concentration analysis.

2.3. Vibrio Parahaemolyticus Challenge

After the feeding trial, 30 shrimp of each group were randomly selected and separated into 3 tanks (with 50 L of seawater). Each shrimp was injected intramuscularly with 0.1 mL of *Vibrio parahaemolyticus* (5×10^6 CFU/mL). Based on pre-experiments, mortality was recorded for 7 days. During the challenging trial, temperature was 26.4–28.0 °C, salinity was 31–33‰, pH was 8.2–8.4, dissolved oxygen was higher than 7 mg·L^{-1}, nitrite was lower than 0.005 mg·L^{-1}, nitrate was lower than 15 mg·L^{-1} and ammonia was lower than 0.02 mg·L^{-1}.

2.4. Growth Performance and Hemocyte Count

Growth performance was calculated by using the following equation:

$$\text{Weight gain rate (WGR,\%)} = 100 \times (\text{final body weight} - \text{initial body weight})/\text{initial body weight} \quad (3)$$

$$\text{Specific growth rate (SGR,\%·day}^{-1}\text{)} = 100 \times (\text{Ln final body weight} - \text{Ln initial body weight})/\text{days} \quad (4)$$

$$\text{Feed intake (FI,\%·day}^{-1}\text{)} = 100 \times \text{feed intake}/[(\text{initial body weight} + \text{final body weight})/2]/\text{days} \quad (5)$$

$$\text{Feed efficiency (FE)} = (\text{final body weight} - \text{initial body weight})/\text{feeds consumed} \quad (6)$$

$$\text{Condition factor (CF, 100 g·cm}^{-3}\text{)} = 100 \times \text{final body weight/finial body length}^3 \quad (7)$$

Hemocyte count was measured with a hemocytometer under a light microscope (Nikon, E 600, Tokyo, Japan). The number of blood cells per mL of hemolymph was calculated according to the formula below:

$$\text{Hemocyte count in 1 mL hemolymph} = A/5 \times 25 \times 10000 \times B \quad (8)$$

A: the total hemocyte count in 5 medium squares; *B*: dilution ratio of the sample.

2.5. Zinc Accumulation Analysis

Zinc concentrations in the diets, muscle and carapace were analyzed by an inductively coupled plasma optical emission spectrometer (ICP-OES, PE 2100DV, Perkin Elmer, Boston, MA, USA). This analysis was completed by the Beijing ZKGX Research Institute of Chemical Technology (Material Lab, Beijing, China). Zinc concentrations in the plasma and hepatopancreas were determined with a commercial assay kit (E011-1-1; Nanjing Jiancheng Bioengineering Institute, Nanjing, China).

2.6. Biochemical Analysis

Plasma of shrimp was used for biochemical analysis directly. The hepatopancreas was weighted, thawed and homogenized (1:9) in ice-cold 0.9% NaCl solution. After centrifugation (2500 rpm, 15 min, 4 °C), the supernatant was collected for biochemical analysis. The activities of acid phosphatase (ACP, A060-2-1), AKP (A059-2-2), catalase (CAT, A007-1-1), phenoloxidase (PO, H247), total antioxidant capacity (T-AOC, A015-2-1) and the contents of glucose (Glu, A154-1-1), malondialdehyde (MDA, A003-1-2) of plasma were determined with commercial assay kits (Nanjing Jiancheng Bioengineering Institute, Nanjing, China). The content of pyruvate (A081-1-1) and the activities of glucokinase (GCK, H439-1), phosphofructokinase (PFK, H244), pyruvate dehydrogenase (PDH, H262-1-2) of hepatopancreas were determined with commercial assay kits (Nanjing Jiancheng Bioengineering Institute, Nanjing, China). The activities of total superoxide dismutase (T-SOD, S0101M) and Cu/Zn SOD (S0103) of plasma and hepatopancreas and the content of total protein (P0012) of hepatopancreas were determined with commercial assay kits (Beyotime Biotechnology, Shanghai, China). The activity of lysozyme (LZM) of plasma was determined by using commercial Shrimp ELISA kits and following the manufacturer's instructions (CK-E94755, Shanghai Elisa Biotech Co., Ltd., Shanghai, China).

2.7. RNA Extraction and qPCR

The total RNA of hepatopancreas and intestine were extracted using the MolPure® Cell/Tissue Total RNA Kit (19221ES50; Yeasen Biotechnology (Shanghai) Co., Ltd., Shanghai, China). The concentration and quality of RNA were assessed with NanoDrop™ 2000 spectrophotometers (Thermo Scientific™, Waltham, MA, USA). The integrity of extracted RNA was determined by electrophoresis on a 1.2% (*w*/*v*) agarose gel. Reverse transcription of 1000 ng of RNA was conducted using Hifair® III 1st Strand cDNA Synthesis SuperMix for qPCR (11141ES60; Yeasen, Shanghai, China).

The qPCR was performed in a 20 μL volume: 1 μL of cDNA template (≤50 ng); 0.4 μL of forward primer (10 μM); 0.4 μL of reverse primer (10 μM); 8.2 μL of RNase-free ddH_2O (P071-01, Vazyme Biotech Co., Ltd., Nanjing, China); 10 μL of SYBR® Green Premix Pro Taq HS qPCR Kit (AG11701, Accurate Biotechnology (Hunan) Co., Ltd., Hunan, China). A two-step qPCR program was used: 95 °C for 30 s, followed by 40 cycles of 95 °C for 5 s and 60 °C for 30 s. Finally, melting curve analysis was used to ensure the specification of the PCR product. Specific gene primers were designed in NCBI, synthesized by Sangon Biotech (Shanghai) Co., Ltd., Shanghai, China. The specificity and amplification efficiency of primers were assessed (Table S1). β-Actin, 18S ribosomal RNA and elongation factor 1-alpha were selected as candidate housekeeping genes. BestKeeper [39] and

NormFinder [40] tools were used to assess the most stable expression gene. Finally, β-actin was assessed as the best housekeeping gene in the present experiment (Tables S2 and S3).

All qPCR analyses were performed in CFX96 Touch Real-Time PCR Detection System (Bio-Rad, Hercules, CA, USA). Moreover, a no-template control (NTC) (0 μL of cDNA template, 0.4 μL of forward primer (10 μM); 0.4 μL of reverse primer (10 μM); 9.2 μL of RNase-free ddH_2O; 10 μL of SYBR® Green Premix Pro Taq HS qPCR Kit) was set in each qPCR plate reaction to ensure no extraneous nucleic acid contamination. The gene expression levels were normalized using the relative quantitative method ($2^{-\Delta\Delta Cq}$) referencing β-actin of shrimp [41].

2.8. Intestinal Microbiota DNA Extraction and Sequencing

Genomic DNA of intestinal microbiota was extracted using the QIAamp PowerFecal® Pro DNA Kit (51804, Qiagen, Hilden, Germany) on a super-clean bench following the manual. Primer 515F/806R was used to amplify the V4 region of the 16S rRNA gene. PCR reaction and quality control were performed by Novogene Genomics Technology Co., Ltd., Beijing, China. Sequencing was conducted on an Illumina NovaSeq platform provided by Novogene Genomics Technology Co., Ltd., Beijing, China. After sequencing, raw data were merged with Fast Length Adjustment of SHort reads (FLASH) [42] and then assigned to each sample with unique barcodes. To obtain effective reads for further analysis, Cutadapter was used to cut adapter, barcode and primer sequences and filter low-quality reads [43], and the UCHIME algorithm was used to detect and remove chimeric sequences [44]. After dereplication, abundance sort and discarding singleton reads, sequences were clustered to operational taxonomic units (OTUs) with ≥97% similarity using UPARSE [45]. The representative sequence for each OUT was screened for further annotation using the Silva Database (version 138) based on the Ribosomal Database Project (RDP) classifier [46]. Alpha diversity (OTUs, Chao1, ACE, Shannon, Simpson and PD whole tree) and beta diversity (principal coordinates analysis (PCoA) and unweighted pair group method with arithmetic mean (UPGMA) clustering) were calculated with Quantitative Insights Into Microbial Ecology (QIIME) and displayed with R software (version 4.1.0) [47].

2.9. Statistical Analysis

Statistical software SPSS 22.0 for Windows (IBM SPSS Corporation, Chicago, IL, USA) was used for the data analysis. Results were analyzed by one-way analysis of variance (ANOVA). Tukey's multiple-range test was used for the multiple comparisons of group means. Differences were regarded as significant when $p < 0.05$.

Microbiota sequence data analysis proceeded on the NovoMagic cloud platform provided by Novogene Genomics Technology Co., Ltd., Beijing, China. An analysis of molecular variance (AMOVA) test was employed to assess the difference of microbiota composition within or between groups using the adegenet package in R software (version 4.1.0). MetaStat analysis was used to identify the differential abundant taxa between groups. The *p*-value was adjusted by the Benjamini-Hochberg false discovery rate (FDR), and differences were regarded as significant when $Q < 0.05$ (Q, adjusted p-value) [48].

3. Results

3.1. Growth Performance

As shown in Table 2, the FBW, WGR and SGR of shrimp fed the O60 diet were significantly higher than those of shrimp fed the control diet ($p < 0.05$). S120, O30, O90 and O120 were intermediate in the FBW, WGR and SGR, with no significant differences observed ($p > 0.05$). No significant differences were observed in the FI, FE, CF and total hemocyte number of shrimp among all groups ($p > 0.05$).

Table 2. Effects of organic and inorganic zinc on growth performance of *Litopenaeus vannamei* Boone, 1931 *.

Diets	Control	S120	O30	O60	O90	O120
IBW (g)	2.34 ± 0.02	2.38 ± 0.02	2.38 ± 0.03	2.36 ± 0.02	2.35 ± 0.02	2.38 ± 0.01
FBW (g)	10.02 ± 0.32 ^{a}	11.25 ± 0.43 ^{ab}	10.56 ± 0.18 ^{ab}	12.41 ± 0.83 ^{b}	10.50 ± 0.32 ^{ab}	10.73 ± 0.39 ^{ab}
WGR (%)	328.3 ± 13.1 ^{a}	374.0 ± 20.1 ^{ab}	343.9 ± 12.0 ^{ab}	427.2 ± 36.2 ^{b}	348.0 ± 16.2 ^{ab}	351.6 ± 16.0 ^{ab}
SGR (%·day^{-1})	2.59 ± 0.06 ^{a}	2.77 ± 0.08 ^{ab}	2.66 ± 0.05 ^{ab}	2.96 ± 0.12 ^{b}	2.67 ± 0.07 ^{ab}	2.69 ± 0.06 ^{ab}
FI (%·day^{-1})	1.56 ± 0.04	1.43 ± 0.05	1.47 ± 0.04	1.33 ± 0.07	1.44 ± 0.09	1.54 ± 0.08
FE	0.357 ± 0.014	0.409 ± 0.022	0.384 ± 0.013	0.463 ± 0.040	0.399 ± 0.029	0.372 ± 0.024
CF (100 g·cm^{-3})	0.652 ± 0.004	0.658 ± 0.010	0.650 ± 0.007	0.650 ± 0.003	0.648 ± 0.007	0.637 ± 0.011
Total hemocyte ($\times 10^{6}$)	27.14 ± 1.35	24.18 ± 1.90	26.25 ± 2.02	28.64 ± 2.11	24.42 ± 2.26	22.51 ± 2.42

* Values represent are means ± S.E. of 4 replicate tanks. IBW, initial body weight, FBW, final body weight, WGR, weight gain rate, SGR, specific growth rate, FI, feed intake, FE, feed efficiency, CF, condition factor. ^{a,b} Different superscript letters within a row denote significant differences as evaluated by Tukey's test ($p < 0.05$).

3.2. Zinc Accumulation and Zinc Transport

As shown in Figure 1A, no significant differences were observed in the zinc concentrations of shrimp muscle and carapace among all groups ($p > 0.05$). The zinc concentrations in the hepatopancreas and plasma of the control group were lower than in all other diets ($p < 0.05$). The zinc concentrations in the hepatopancreas and plasma of shrimp fed the S120 diet were significantly lower than those of shrimp fed the O60, O90 and O120 diets ($p < 0.05$). The zinc concentration in plasma was the highest in the O120 group ($p < 0.05$).

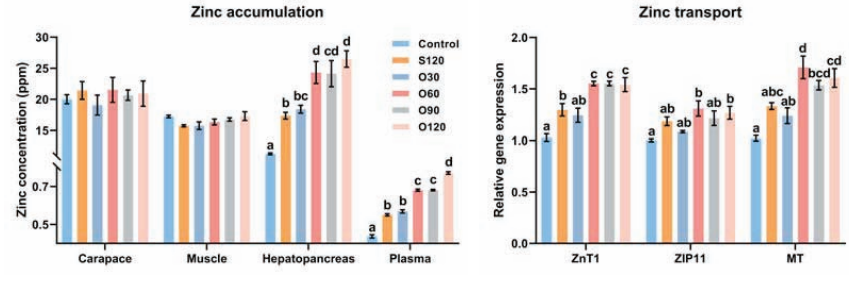

(**A**) (**B**)

Figure 1. Effects of organic and inorganic zinc on zinc accumulation of *Litopenaeus vannamei* Boone, 1931 tissues (**A**) and gene expressions of zinc transport in hepatopancreas of *L. vannamei* (**B**). ZnT1, zinc transporter 1; ZIP11, zinc transporter ZIP11, MT, metallothionein. Values represented are means ± S.E. of 4 replicate tanks. ^{a,b,c,d} Value bars not sharing the same superscript letter are significantly different ($p < 0.05$).

The zinc-transport-related gene expressions in the hepatopancreas (Figure 1B) showed that, compared with the control diet, the expression of ZnT1, ZIP11 and MT was significantly upregulated by the S120, O60, O90 and O120 diets, the O60 and O120 diets, and the O60, O90 and O120 diets, respectively ($p < 0.05$). Compared with the S120 diet, the expression of ZnT1 and MT was significantly upregulated by the O60, O90 and O120 diets and the O60 diet, respectively ($p < 0.05$).

3.3. Antioxidant Capacity

In plasma, as shown in Figure 2A, the activities of T-SOD, Cu/Zn SOD, CAT and T-AOC of shrimp fed the O60, O90 and O120 diets were significantly higher than those of shrimp fed the control diet ($p < 0.05$). The activities of T-SOD, Cu/Zn SOD and CAT of shrimp fed the O90 and O120 diets were significantly higher than those of shrimp fed the S120 diet ($p < 0.05$). The activities of T-SOD, Cu/Zn SOD and T-AOC of shrimp fed the control diet were significantly lower than those of shrimp fed the S120 diet ($p < 0.05$). The

MDA content of the control group was the highest among all groups ($p < 0.05$). The MDA contents of the O90 and O120 groups were significantly lower than those of the S120 group ($p < 0.05$). In the hepatopancreas, as shown in Figure 2B, the activities of T-SOD and Cu/Zn SOD of shrimp fed the S120, O60, O90 and O120 diets were significantly higher than those of shrimp fed the control diet ($p < 0.05$). The activity of T-SOD of the O120 group was the highest among all groups ($p < 0.05$).

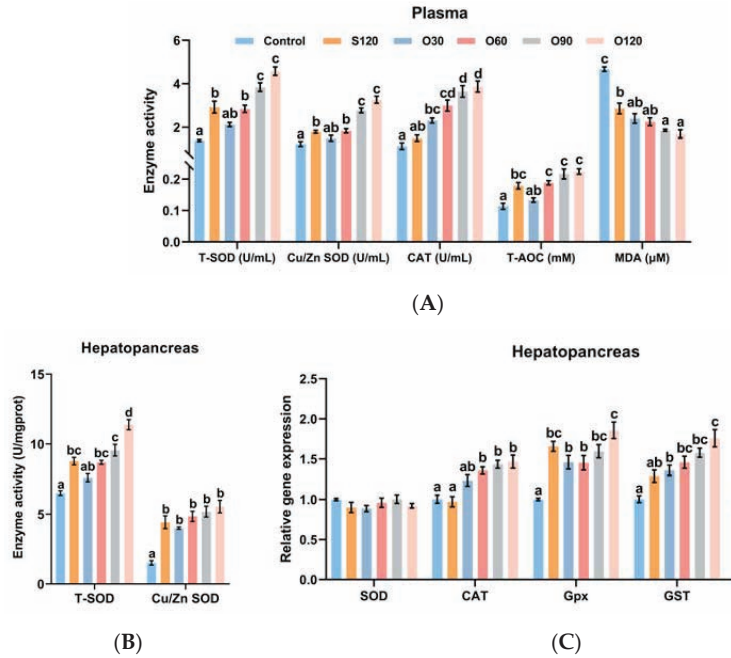

Figure 2. Effects of organic and inorganic zinc on antioxidant capacity of *L. vannamei*. (**A**) enzyme activities of plasma; (**B**) enzyme activities of hepatopancreas; (**C**) gene expressions of hepatopancreas. SOD, super dismutase; CAT, catalase; T-AOC, total antioxidant capacity; MDA, malondialdehyde; Gpx, glutathione peroxidase; GST, glutathione S-transferase; G6PDH, glucose-6-phosphate dehydrogenase. Values represented are means ± S.E. of 4 replicate tanks. ^{a,b,c,d,e} Value bars not sharing the same superscript letter are significantly different ($p < 0.05$).

The antioxidant-related gene expressions (Figure 2C) showed that the expressions of CAT, Gpx, GST and G6PDH of shrimp fed the O60, O90 and O120 diets were significantly higher than those of shrimp fed the control diet ($p < 0.05$). The expressions of Gpx and G6PDH of shrimp fed the S120 and O30 diets were significantly higher than those of shrimp fed the control diet ($p < 0.05$). When compared with the S120 diet, the expression of CAT was significantly upregulated by the O60, O90 and O120 diets, the expression of GST was significantly upregulated by the O120 diet, and the expression of G6PDH was significantly upregulated by the O60, O90 and O120 diets ($p < 0.05$). The expression of G6PDH of the O120 group was the highest among all groups ($p < 0.05$). No significant difference was observed in the expression of SOD among all groups ($p > 0.05$).

3.4. Immunity

In plasma, as shown in Figure 3A, the activities of ACP and LZM in the control group was the lowest among all groups ($p < 0.05$) and no significant difference was observed among S120, O30, O60 and O120 groups ($p > 0.05$). The activities of AKP and PO of shrimp fed the O60 and O120 diets were significantly higher than those of shrimp fed the control diet ($p < 0.05$). The activity of AKP of shrimp fed the S120 diet was significantly higher

than those of shrimp fed the control diet ($p < 0.05$). The activity of PO of shrimp fed the O120 diet was significantly higher than those of shrimp fed the S120 diet ($p < 0.05$).

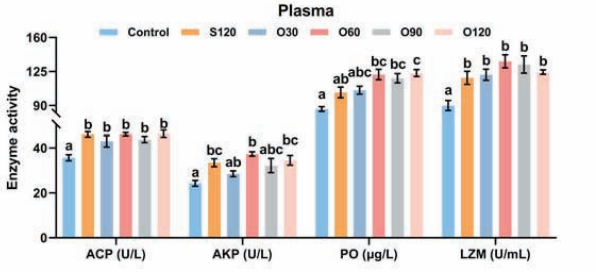

(**A**)

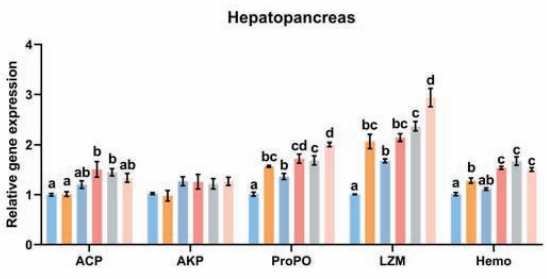

(**B**)

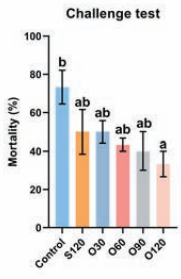

(**C**)

Figure 3. Effects of organic and inorganic zinc on immunity of *L. vannamei*. (**A**) enzyme activities of plasma; (**B**) gene expressions of hepatopancreas. (**C**) *Vibrio parahaemolyticus* challenge test of shrimp. ACP, acid phosphatase; AKP, alkaline phosphatase; PO, phenoloxidase; LZM: lysozyme; ProPO, pro-phenoloxidase; Hemo, hemocyanin. Values represented by A and B are means ± S.E. of 4 replicate tanks. Values represented by C are means ± S.E. of 3 replicate tanks. ^{a,b,c,d} Value bars not sharing the same superscript letter are significantly different ($p < 0.05$).

The immunity-related gene expressions of hepatopancreas (Figure 3B) showed that the expression of ACP of shrimp fed the O60 and O90 diets was significantly higher than those of shrimp fed the control and S120 diets ($p < 0.05$). The expressions of ProPO, LZM and Hemo of shrimp fed the S120, O60, O90 and O120 diets were significantly higher than those of shrimp fed the control diet ($p < 0.05$). When compared with the S120 diet, the expression of ProPO and was significantly upregulated by the O120 diet, the expression of LZM was significantly upregulated by the O120 diet, and the expression of Hemo was significantly upregulated by the O60, O90 and O120 diets ($p < 0.05$). No significant difference was observed in the expression of AKP among all groups ($p > 0.05$).

The challenge test showed lower mortality of shrimp fed with supplementary dietary zinc after 7-day stress of *V. parahaemolyticus*. The mortality of shrimp fed the S120, O30, O60, O90 and O120 diets was decreased by 31.82%, 31.82%, 40.91%, 45.45% and 54.55% compared to the control, respectively, and the mortality in the O120 group was significantly lower than that of the control group (Figure 3C) ($p < 0.05$).

3.5. Glucose Transport and Glycolysis

As shown in Figure 4A, the expression of GluT1 in the intestine of shrimp fed the O30, O60, O90 and O120 diets was significantly higher than that of shrimp fed the control and S120 diets ($p < 0.05$). As shown in Figure 4B, the content of Glu in plasma of the control group was the lowest ($p < 0.05$). The content of Glu in plasma of the S120 group was significantly lower than the O30, O60 and O120 groups ($p < 0.05$). As shown in Figure 4C,

the activities of GCK, PFK and PDH of shrimp fed the O60, O90 and O120 diets were significantly higher than those of shrimp fed the control diet ($p < 0.05$). When compared with the S120 diet, the activities of GCK, PFK and PDH of shrimp fed the O120 diet were significantly increased by the O60, O90 and O120 diets, the O120 diet, and the O30, O60, O90 and O120 diets, respectively ($p < 0.05$). The contents of pyruvate in the control and S120 groups were significantly higher than the other groups ($p < 0.05$).

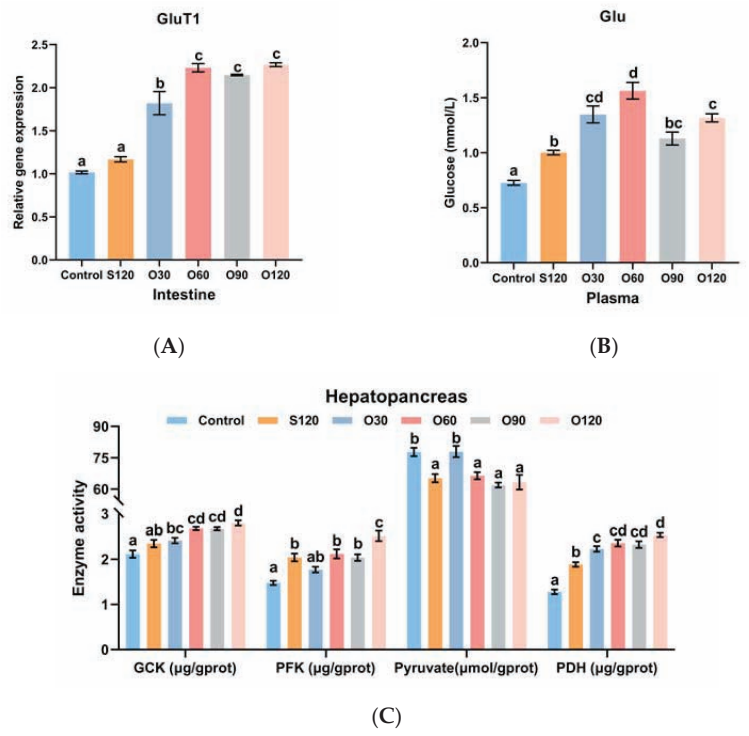

Figure 4. Effects of organic and inorganic zinc on transport and glycolysis of *L. vannamei*. (**A**) GluT1 expression of intestine; (**B**) Glu content of plasma; (**C**) enzyme activities of hepatopancreas. Glu, glucose; GluT1, glucose transporter 1; GCK, glucokinase; PFK, phosphofructokinase; PDH, pyruvate dehydrogenase. Values represented are means ± S.E. of 4 replicate tanks. ^{a,b,c,d} Value bars not sharing the same superscript letter are significantly different ($p < 0.05$).

3.6. Intestinal Microbiota

A total of 3,105,865 effective reads were obtained, and after annotation, 24 phyla, 42 classes, 109 orders, 204 families, 402 genera and 1454 OTUs were identified. Rank abundance, rarefaction curves and species accumulation boxplot showed that all samples reached the saturation phase, indicating adequate sequencing depth (Figure S1). At the phylum level, Firmicutes, Proteobacteria and Bacteroidota were the predominant bacterial phyla in the intestine among all groups (Figure 5A). At the genus level, *Candidatus_Bacilloplasma*, *Vibrio* and *Spongiimonas* were the predominant bacterial genera in the intestine among all groups (Figure 5B). As alpha diversity indices (OTUs, Chao1, ACE, Shannon, Simpson, PD whole tree) shown in Table 3, Chao1 and ACE indices in the O30 group were significantly higher than that in the O90 group ($p < 0.05$). Simpson index in the O120 group was significantly higher than that in the control and O90 groups ($p < 0.05$). No significant difference was observed in OTUs, Shannon index and PD whole tree among all groups ($p > 0.05$).

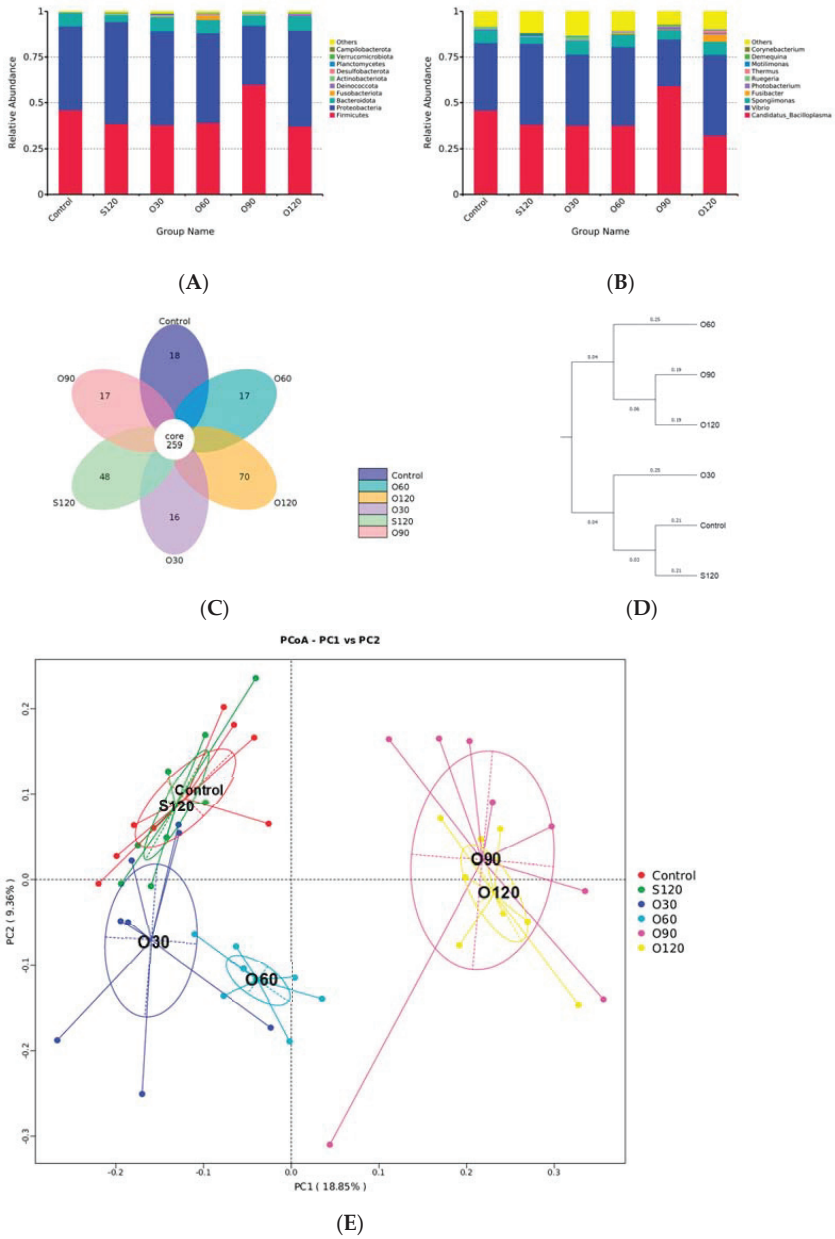

Figure 5. Effects of organic and inorganic zinc on intestinal microbiota of *L. vannamei*. Taxonomy classification of reads at phylum (**A**) and genus (**B**) levels. Only top 10 most abundant (based on relative abundance) bacterial phyla and genera were shown in the figures, other phyla and genera were all assigned as 'Others'. Flower diagram of intestinal microbiota among all groups (**C**). UPGMA clustering trees in groups (**D**) and principal coordinate analysis (PCoA) plot in samples (**E**) based on unweighted UniFrac distances among all groups.

Table 3. Richness and diversity indices of intestinal microbiota of *L. vannamei*. *.

Diets	Control	S120	O30	O60	O90	O120
OTUs	281 ± 25	346 ± 33	386 ± 47	336 ± 17	253 ± 39	281 ± 21
Chao1	310.7 ± 22.9 ^{ab}	385.4 ± 35.7 ^{ab}	422.0 ± 48.2 ^{b}	379.1 ± 16.9 ^{ab}	278.1 ± 40.0 ^{a}	303.1 ± 21.4 ^{ab}
ACE	332.8 ± 21.3 ^{ab}	404.8 ± 36.7 ^{ab}	445.7 ± 47.5 ^{b}	403.5 ± 15.7 ^{ab}	292.6 ± 41.3 ^{a}	319.8 ± 21.0 ^{ab}
Shannon	2.66 ± 0.18	3.05 ± 0.20	3.35 ± 0.30	2.99 ± 0.10	2.70 ± 0.16	3.24 ± 0.10
Simpson	0.693 ± 0.045 ^{a}	0.757 ± 0.026 ^{ab}	0.801 ± 0.023 ^{ab}	0.768 ± 0.016 ^{ab}	0.695 ± 0.028 ^{a}	0.812 ± 0.012 ^{b}
PD whole tree	18.61 ± 1.00	22.64 ± 1.45	24.10 ± 1.89	22.60 ± 0.81	19.07 ± 2.33	20.67 ± 1.00

* Values represent are means ± S.E. of 4 replicate tanks. ^{a,b} Different superscript letters within a row denote significant differences as evaluated by Tukey's test ($p < 0.05$).

The flower diagram showed that all groups shared 259 OTUs, and the control, S120, O30, O60, O90 and O120 groups had 18, 48, 16, 17, 17 and 70 unique OTUs, respectively (Figure 5C). The AMOVA test confirmed the difference between groups was greater than the differences within groups (Table S4). UPGMA (Figure 5D) and PCoA (Figure 5E) clusters based on the unweighted UniFrac distance showed that the microbiota community was related to the dosage of organic zinc. Briefly, the community between the control group and the S120 group and between the O90 group and the O120 group were similar, respectively. The microbiota community of the O30 group was slightly farther from the control and S120 groups. The O60 group had a farther distance from the control and S120 groups. The O90 and O120 groups together had the furthest distance from the control and S120 groups.

MetaStat analysis (Figure 6 and Table S5) showed that forty-two significantly changed genera were obtained among the control, S120, O60 and O120 groups, of which 21 genera might be beneficial to the host (Figure 6A–D) (e.g., *Aeromicrobium*, *Arthrobacter*, *Butyrivibrio*, *Kocuria* and *Sphingomonas*), and of which 21 genera might be pathogenic to the host (Figure 6E–H) (e.g., *Corynebacterium*, *Escherichia-Shigella*, *Flavobacterium*, *Sva0081_sediment_group* and *Rubripirellula*). Briefly, the genera in Figure 6A,B were potential probiotics for the host. The genera in Figure 6C produce organic acid (e.g., short-chain fatty acid, lactic acid). The genera in Figure 6D produce antibiotics or have antibacterial activity. The genera in Figure 6E–G are potential pathogens for the host or cause diseases. The genera in Figure 6H reduce sulfate into hydrogen sulfide. According to the result, compared with the control diet, the abundance of the majority of potential beneficial genera were significantly increased by the O60 (13 of 21) and O120 (16 of 21) diets (Table S6) ($Q < 0.05$). Compared with the S120 diet, O120 diet significantly increased the abundance of most potential beneficial genera (16 of 21) and decreased the abundance of many potential harmful genera (16 of 21) (Table S6) ($Q < 0.05$).

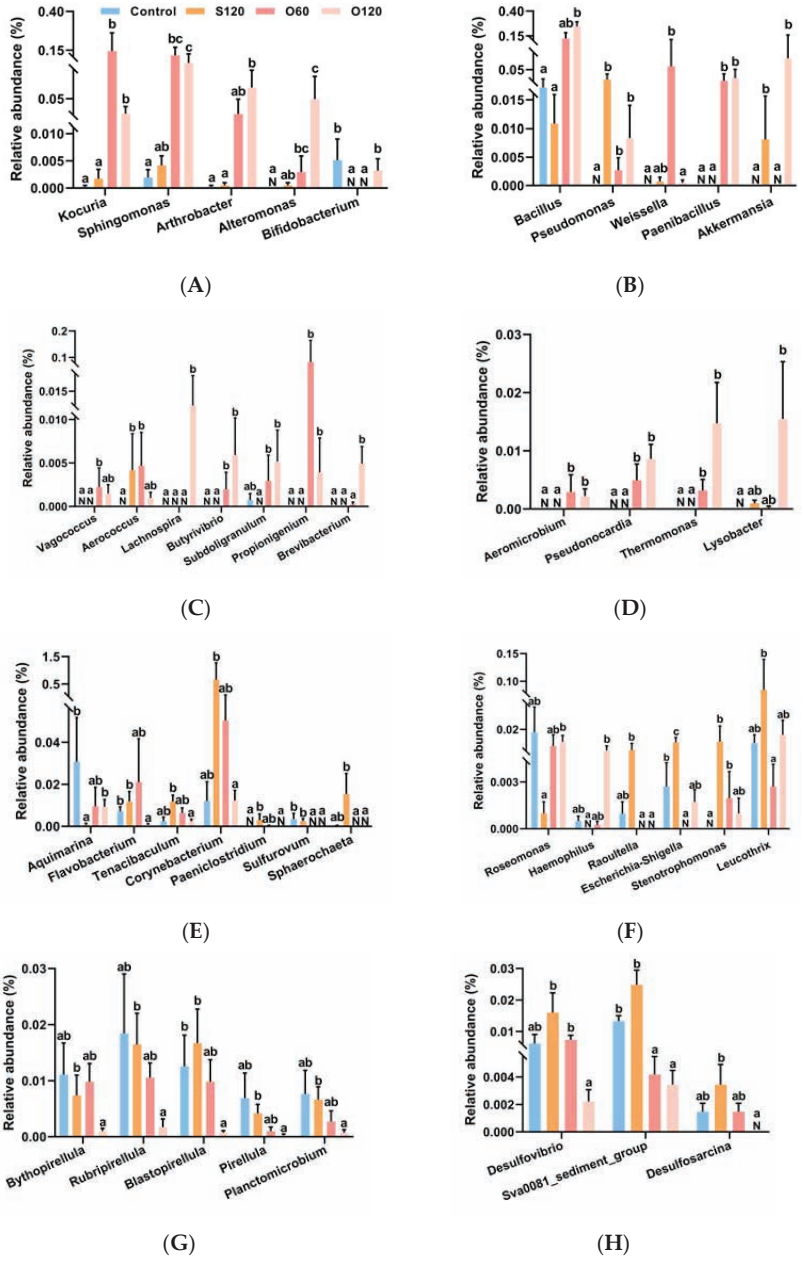

Figure 6. MetaStat analysis of intestinal microbiota communities at genus level of shrimp among control, S120, O60 and O120 groups. (**A**–**D**) potentially beneficial bacteria of shrimp intestine; (**E**–**H**) potentially pathogens of shrimp intestine. ^{a,b,c} Value bars not sharing the same superscript letter are significantly different ($Q < 0.05$). "N" means the abundance of genus is too low to get a value at a certain number or the genus does not exist.

4. Discussion

Some studies in channel catfish [20], pangasius catfish [23], juvenile abalone [24] and white shrimp [27] have shown benefits of organic zinc on growth. However, in the present study, white shrimp fed either organic or inorganic zinc had similar growth performance, concurrent with previous studies in beluga sturgeon [22], rainbow trout [49], Atlantic salmon (*Salmo salar*) [50] and European sea bass (*Dicentrarchus labrax*) [51]. The inconsistent results might be related to different species, developmental stages, diet formulation, culture condition and culture duration.

Investigations on zinc accumulation and transport accumulation have suggested that organic zinc has higher facilitation effects than inorganic zinc. In the present study, zinc concentrations of muscle and carapace were not affected. However, zinc concentrations of hepatopancreas and plasma were significantly higher with dietary zinc. Moreover, organic zinc showed significantly higher levels of zinc concentrations of hepatopancreas and plasma compared with inorganic zinc. This was similar to a previous study on white shrimp, where hepatopancreatic zinc was affected by dietary zinc and phytic acid, while carapace zinc was not [11]. This might also be related to the essential role of zinc in regulating antioxidant defense systems and immune responses, as well as in maintaining nutrient metabolism and transport, since the hepatopancreas and hemolymph are the main sites where these biological processes occur [3]. Additionally, zinc concentration regulation is closely related to two zinc transporter proteins: ZnTs (Slc30a family), which regulate the efflux of zinc from the cytoplasm [52,53], and ZIPs (Slc39a family), which regulate the influx of zinc into the cytoplasm [54]. MT is a cysteine-rich intracellular metal-binding protein that is inducible by Zn^{2+} [55]. By binding and releasing Zn^{2+}, MT regulates intracellular Zn^{2+} homeostasis to prevent the cytotoxicity of excess Zn^{2+} [56]. In the present study, organic zinc resulted in greater promotion of ZnT1, ZIP11 and MT expressions in the hepatopancreas than inorganic zinc, which was consistent with the changes in zinc concentrations of the hepatopancreas and plasma, suggesting that organic zinc could increase the intracellular concentration and transport of Zn^{2+} and maintain Zn^{2+} homeostasis. Moreover, zinc homeostasis, in which ZnTs, ZIPs and MT are involved, contributes to a range of physiological functions, including antioxidant capacity and immunity [57,58].

The role of zinc in enhancing antioxidant capacity has been widely summarized [2,4,59–61]. Previous studies have also demonstrated improved antioxidant capacity of zinc in beluga sturgeon [22], pangasius catfish [23], triploid trout [25] and white shrimp [29]. Antioxidant reactions are important for cells to prevent damage from free radicals, and the primary enzymatic systems include SOD (Cu/Zn SOD is the most prominent), CAT and Gpx [61]. SOD converts oxygen radicals into H_2O_2, which in turn is catalyzed by CAT or Gpx into H_2O and O_2 [61,62]. SOD is the most important and powerful oxidative defense enzyme and requires zinc as a cofactor for its activity [61]. T-AOC is defined as the capacity of inhibition of lipid oxidative degradation, which is important for inhibiting free radical production or maintaining antioxidant activity [63]. Moreover, it has been reported that zinc can decrease MDA content in cells [59]. On the other hand, MT releases Zn^{2+}, which in turn activates metal-responsive transcription factor-1 intracellularly and subsequently upregulates the expressions of a variety of antioxidant genes, including Gpx, GST, G6PDH and MT [60]. This is consistent with the present study, in which dietary zinc enhanced the antioxidant capacity of shrimp plasma and hepatopancreas, as evidenced by increased activities of T-SOD, Cu/Zn SOD, CAT and T-AOC, upregulated CAT, Gpx, GST and G6PDH expressions, and decreased MDA content. However, organic zinc, especially in the O60, O90 and O120 groups, had better efficacy. The present study revealed that organic zinc was better than inorganic zinc in enhancing antioxidant capacity, which might be related to the improved Zn^{2+} homeostasis.

Zinc is well known for its important role in immune response [64]. ACP and AKP are typically used to assess the immune status of invertebrates [65]. PO, LZM and Hemo are crucial innate immune defense molecules for shrimp and take part in various immune responses, including against pathogens [66–69]. Some studies have reported the advan-

tages of organic zinc in improving immunity in channel catfish [21], beluga sturgeon [22], pangasius catfish [23] and white shrimp [27,29]. In the present study, increased activities (ACP, AKP, PO and LZM) and expressions (ACP, ProPO, LZM and Hemo) demonstrated beneficial changes in the immune system with organic zinc, which were also consistent with lower mortality during the *V. parahaemolyticus* challenge. The mechanism might be that a strengthened intracellular zinc homeostasis status allows Zn^{2+} to regulate distinct signaling pathways in immune systems more positively to influence cellular activities such as immune cells [70].

Zinc can also stimulate glucose transport [71] and glycolysis [72]. Glucose is absorbed from the intestinal lumen into the hemolymph via glucose transporter (GluT) and transported to the hepatopancreas via the open circulatory system [73]. In the hepatopancreas, Glu is converted into pyruvate via glycolysis [74], and then pyruvate enters the TAC via the PDH complex for further energy production [75]. GCK and PFK are rate-limiting and key regulatory enzymes of glycolysis reactions [74,76]. The increased GluT1 expression, Glu content, GCK and PFK activities of the present results revealed that organic zinc supported energy production from glucose to a greater degree than inorganic zinc. Changes in glucose transport and glycolysis might be related to the fact that zinc is involved in the secretion of insulin and glucagon [77]. The decreased pyruvate content might be due to the increased PDH activity that facilitates the entry of pyruvate into the tricarboxylic acid cycle for further energy production [75]. Similarly, previous studies in rats and mice have also reported the role of zinc in stimulating glycolysis [30,31,78]. However, the specific mechanism by which zinc regulates glucose metabolism in white shrimp needs further study.

The intestinal microbiota community of shrimp is tightly associated with its health [79]. Few studies have reported the effects of zinc on intestinal microbiota in shrimp. The present study found that Firmicutes, Proteobacteria and Bacteroidota were the predominant phyla, and *Candidatus_Bacilloplasma*, *Vibrio* and *Spongiimonas* were the predominant genera, which is consistent with previous results in shrimp [80,81]. Moreover, the cluster results showed that the microbiota community was migrated by the dosage of organic zinc, especially in the O60, O90 and O120 groups, since the top 10 bacteria were similar among all groups and alpha diversity did not differ greatly. The migration might be caused by changes in the abundance of non-predominant bacteria. Forty-two significantly different genera were observed by MetaStat analysis. When compared with the control group, only 7 genera were observed in the S120 group, while about 20 genera were observed in the O60 or O120 groups. When compared with inorganic zinc (S120), organic zinc (O60 and O120)-supplemented shrimp had a significantly higher abundance of potentially beneficial bacteria yet lower abundance of potentially pathogenic bacteria. Among these genera, some probiotics have been used in aquaculture such as *Kocuria*, *Sphingomonas*, *Arthrobacter*, *Alteromonas*, *Bifidobacterium*, *Bacillus*, *Pseudomonas*, *Weissella* and *Paenibacillus* [82–84]. Some probiotics include lactic acid producers (*Akkermansia*, *Vagococcus*, *Aerococcus*) [85,86] and short-chain fatty acid producers (*Lachnospira*, *Butyrivibrio*, *Subdoligranulum*, *Propionigenium*, *Brevibacterium*) [87–91]. The presence of these probiotics in the present study may be beneficial to the nutrient availability, antioxidant and immune response of white shrimp [91]. Increased *Aeromicrobium*, *Pseudonocardia*, *Thermomonas* and *Lysobacter*, which could produce secondary metabolites and have antibacterial properties, may protect shrimp from pathogens [92–95]. Moreover, the bacteria *Aquimarina*, *Tenacibaculum*, *Flavobacterium*, *Paeniclostridium*, *Escherichia-Shigella*, *Sulfurovum* and *Leucothrix* are opportunistic or true pathogens that cause diseases of aquatic animals and egg mortality [96–99]. Some species in *Corynebacterium*, *Sphaerochaeta*, *Roseomonas*, *Haemophilus*, *Raoultella* and *Stenotrophomonas* are also potentially pathogenic agents of the host [100–104]. *Bythopirellula*, *Rubripirellula*, *Blastopirellula*, *Pirellula* and *Planctomicrobium* are related to host diseases and resistant to a variety of antibiotics [105]. *Desulfovibrio*, *Sva0081_sediment_group* and *Desulfosarcina* are sulfate-reducing bacteria that reduce sulfate into hydrogen sulfide [106–108]. The high concentration of hydrogen sulfide is toxic to intestinal microbiota and lowers intestinal pH [108]. This also prompts us to be concerned about the potential risks in the application

of sulfate mineral elements. Overall, the present study suggested that organic zinc-fed shrimp had a higher abundance of potentially beneficial genera and lower abundance of potential pathogens in intestinal samples of white shrimp. Taken in combination with other findings of this study, it is possible that the shrimp might have evolved a mechanism to regulate intestinal microbiota balance by utilizing zinc homeostasis [109]. On the one hand, dietary zinc is used by the host to inhibit the proliferation of pathogens and regulate interspecies competition of intestinal microbiota [110]. On the other hand, dietary zinc can enhance intestinal mucosal barrier function, which is beneficial for the colonization of probiotics and defense against pathogens [111,112]. The organic zinc supplementation benefited zinc homeostasis of white shrimp, which was crucial for enhancing the healthy balance of host and intestinal microbes [113].

5. Conclusions

The present results showed that both inorganic zinc and organic zinc could benefit the antioxidant capacity and immune response of shrimp. However, compared with inorganic zinc, organic zinc could further support zinc accumulation and transport, enhance antioxidant capacity and immune response, stimulate glucose transport and glycolysis and strengthen the resistance to disease of shrimp. Moreover, organic zinc resulted in beneficial shifts in the intestinal microbiota community, with a higher abundance of various potentially beneficial bacteria and a lower abundance of several potentially harmful bacteria. Overall, shrimp fed 60 $mg \cdot kg^{-1}$ zinc from Zn-proteinate achieved better effects than those fed 120 $mg \cdot kg^{-1}$ zinc from $ZnSO_4 \cdot 7H_2O$. The mechanism of organic zinc in these effects might be related to the improving zinc homeostasis of shrimp, which indicated that organic zinc has higher bioavailability than inorganic zinc in shrimp feeds.

Supplementary Materials: The following supporting information can be downloaded at: https://www.mdpi.com/article/10.3390/antiox11081492/s1, Figure S1. Rank abundance (A), rarefaction curves (B) and species accumulation boxplot (C) for all the intestinal microbiota samples; Table S1. Primers used in qPCR and amplification information; Table S2. Descriptive statistics of 3 candidate housekeeping genes (HKG) based on their cycle quantification (Cq) values; Table S3. Stability analysis of 3 candidate HKG based on their Cq values; Table S4. AMOVA analysis based on unweighted UniFrac distance of microbial community structure of *Litopenaeus vannamei* Boone, 1931; Table S5. The genus level classification information of MetaStat analysis showed in Figure 6; Table S6. The genera abundance changes of *L. vannamei* based on MetaStat analysis.

Author Contributions: Conceptualization, Y.Z., K.M. and G.L.; methodology, Y.Z., J.Y. and T.W.; formal analysis, Y.Z., J.Y. and T.W.; investigation, J.Y. and T.W.; data curation, J.Y. and T.W.; writing—original draft preparation, J.Y. and T.W.; writing—review and editing, Y.Z., J.Y., G.L. and M.L.; supervision, Y.Z. and K.M.; project administration, K.M. and Y.Z.; funding acquisition, K.M. and Y.Z. All authors have read and agreed to the published version of the manuscript.

Funding: This research was funded by the National Key R&D Program of China (2019YFD0900104), the National Natural Science Foundation of China (No. 31872577) and China Agriculture Research System (Grant No.: CARS 47-G10).

Institutional Review Board Statement: Not applicable.

Informed Consent Statement: Not applicable.

Data Availability Statement: The data of 16S rRNA sequence presented in the study are deposited in https://www.ncbi.nlm.nih.gov/sra (accessed on 3 May 2022), under Accession Number PRJNA834576.

Acknowledgments: The authors would like to thank Jihong Dai, Weihao Ou, Guijuan Yu, Xiuhua Ma, Yaoyao Kong, Zhonghao Zhang, Sihui Li and Jingjing Zhao for their support during this study.

Conflicts of Interest: The authors declare no conflict of interest.

References

1. Dawood, M.A.O.; Alagawany, M.; Sewilam, H. The role of zinc microelement in aquaculture: A review. *Biol. Trace Elem. Res.* **2021**, *200*, 3841–3853. [CrossRef] [PubMed]
2. Sloup, V.; Jankovská, I.; Nechybová, S.; Peřinková, P.; Langrová, I. Zinc in the animal organism: A review. *Sci. Agric. Bohem.* **2017**, *48*, 13–21. [CrossRef]
3. Wu, G.Y. *Principles of Animal Nutrition*; CRC Press: Boca Raton, FL, USA, 2017.
4. Reilly, C. Zinc. In *The Nutritional Trace Metals*; Blackwell Publishing Ltd.: Oxford, UK, 2004; pp. 82–117.
5. Gibson, R.S. Zinc nutrition in developing countries. *Nutr. Res. Rev.* **1994**, *7*, 151–173. [CrossRef]
6. Daniel, D. A review on replacing fish meal in aqua feeds using plant protein sources. *Int. J. Fish. Aquat. Stud.* **2018**, *6*, 164–179.
7. Oliva-Teles, A.; Enes, P.; Peres, H. Replacing fishmeal and fish oil in industrial aquafeeds for carnivorous fish. In *Feed and Feeding Practices in Aquaculture*; Davis., D.A., Ed.; Woodhead Publishing: Oxford, UK, 2015; pp. 203–233.
8. Gasco, L.; Gai, F.; Maricchiolo, G.; Genovese, L.; Ragonese, S.; Bottari, T.; Caruso, G. *Feeds for the Aquaculture Sector*; Springer International Publishing: Cham, Switzerland, 2018.
9. Lall, S.P.; Kaushik, S.J. Nutrition and metabolism of minerals in fish. *Animals* **2021**, *11*, 2711. [CrossRef] [PubMed]
10. Francis, G.; Makkar, H.P.S.; Becker, K. Antinutritional factors present in plant-derived alternate fish feed ingredients and their effects in fish. *Aquaculture* **2001**, *199*, 197–227. [CrossRef]
11. Davis, D.A.; Lawrence, A.L.; Gatlin, D.M. Evaluation of the dietary zinc requirement of *Penaeus vannamei* and effects of phytic acid on zinc and phosphorus bioavailability. *J. World Aquac. Soc.* **1993**, *24*, 40–47. [CrossRef]
12. Bharadwaj, A.S.; Patnaik, S.; Browdy, C.L.; Lawrence, A.L. Availability of dietary zinc sources and effects on performance of pacific white shrimp *Litopenaeus vannamei* (Boone). *Int. J. Recirc. Aquac.* **2017**, *13*, 1–10. [CrossRef]
13. Zak, D.; Hupfer, M.; Cabezas, A.; Jurasinski, G.; Audet, J.; Kleeberg, A.; McInnes, R.; Kristiansen, S.M.; Petersen, R.J.; Liu, H.; et al. Sulphate in freshwater ecosystems: A review of sources, biogeochemical cycles, ecotoxicological effects and bioremediation. *Earth-Sci. Rev.* **2021**, *212*, 103446. [CrossRef]
14. Wang, F.; Chapman, P.M. Biological implications of sulfide in sediment-a review focusing on sediment toxicity. *Environ. Toxicol. Chem.* **1999**, *18*, 2526–2532.
15. Lamers, L.P.M.; Govers, L.L.; Janssen, I.C.J.M.; Geurts, J.J.M.; Van der Welle, M.E.W.; Van Katwijk, M.M.; Van der Heide, T.; Roelofs, J.G.M.; Smolders, A.J.P. Sulfide as a soil phytotoxin–A review. *Front. Plant. Sci.* **2013**, *4*, 268. [CrossRef] [PubMed]
16. Alagawany, M.; Elnesr, S.S.; Farag, M.R.; Tiwari, R.; Yatoo, M.I.; Karthik, K.; Michalak, I.; Dhama, K. Nutritional significance of amino acids, vitamins and minerals as nutraceuticals in poultry production and health—A comprehensive review. *Vet. Q.* **2020**, *41*, 1–29. [CrossRef] [PubMed]
17. Glover, C.N.; Hogstrand, C. Amino acid modulation of in vivo intestinal zinc absorption in freshwater rainbow trout. *J. Exp. Biol.* **2002**, *205*, 151–158. [CrossRef] [PubMed]
18. Antony Jesu Prabhu, P.; Stewart, T.; Silva, M.; Amlund, H.; Ørnsrud, R.; Lock, E.-J.; Waagbo, R.; Hogstrand, C. Zinc uptake in fish intestinal epithelial model RTgutGC: Impact of media ion composition and methionine chelation. *J. Trace Elem. Med. Biol.* **2018**, *50*, 377–383. [CrossRef] [PubMed]
19. Lu, W.B.; Kuang, Y.G.; Ma, Z.X.; Liu, Y.G. The effect of feeding broiler with inorganic, organic, and coated trace minerals on performance, economics, and retention of copper and zinc. *J. Appl. Poult. Res.* **2020**, *29*, 1084–1090. [CrossRef]
20. Paripatananont, T.; Lovell, R.T. Chelated zinc reduces the dietary zinc requirement of channel catfish, *Ictalurus punctatus*. *Aquaculture* **1995**, *133*, 73–82. [CrossRef]
21. Paripatananont, T.; Lovell, R.T. Responses of channel catfish fed organic and inorganic sources of zinc to *Edwardsiella ictaluri* challenge. *J. Aquat. Anim. Health* **1995**, *7*, 147–154. [CrossRef]
22. Mohseni, M.; Hamidoghli, A.; Bai, S.C. Organic and inorganic dietary zinc in beluga sturgeon (*Huso huso*): Effects on growth, hematology, tissue concertation and oxidative capacity. *Aquaculture* **2021**, *539*, 736672. [CrossRef]
23. Jintasataporn, O.; Ward, T.; Kattakdad, S. The efficacy of organic zinc amino acid complex (Availazn®) on growth performance and immunity of pangasius catfish (*Pangasianodon hypophthalmus*). *Aquac. Indones.* **2015**, *15*, 94–97. [CrossRef]
24. Tan, B.; Mai, K. Zinc methionine and zinc sulfate as sources of dietary zinc for juvenile abalone, *Haliotis discus hannai* Ino. *Aquaculture* **2001**, *192*, 67–84. [CrossRef]
25. Meiler, K.A.; Cleveland, B.; Radler, L.; Kumar, V. Oxidative stress-related gene expression in diploid and triploid rainbow trout (*Oncorhynchus mykiss*) fed diets with organic and inorganic zinc. *Aquaculture* **2021**, *533*, 736149. [CrossRef]
26. Meiler, K.A.; Kumar, V. Organic and inorganic zinc in the diet of a commercial strain of diploid and triploid rainbow trout (*Oncorhynchus mykiss*): Effects on performance and mineral retention. *Aquaculture* **2021**, *545*, 737126. [CrossRef]
27. Lin, S.; Lin, X.; Yang, Y.; Li, F.; Luo, L. Comparison of chelated zinc and zinc sulfate as zinc sources for growth and immune response of shrimp (*Litopenaeus vannamei*). *Aquaculture* **2013**, *406–407*, 79–84. [CrossRef]
28. Katya, K.; Lee, S.; Yun, H.; Dagoberto, S.; Browdy, C.L.; Vazquez-Anon, M.; Bai, S.C. Efficacy of inorganic and chelated trace minerals (Cu, Zn and Mn) premix sources in Pacific white shrimp, *Litopenaeus vannamei* (Boone) fed plant protein based diets. *Aquaculture* **2016**, *459*, 117–123. [CrossRef]
29. Yuan, Y.; Luo, J.; Zhu, T.; Jin, M.; Jiao, L.; Sun, P.; Ward, T.L.; Ji, F.; Xu, G.; Zhou, Q. Alteration of growth performance, meat quality, antioxidant and immune capacity of juvenile *Litopenaeus vannamei* in response to different dietary dosage forms of zinc: Comparative advantages of zinc amino acid complex. *Aquaculture* **2020**, *522*, 735120. [CrossRef]

30. Zhang, Z.; Yu, J.; Xie, J.; Liu, D.; Fan, Y.; Ma, H.; Wang, C.; Hong, Z. Improvement roles of zinc supplementation in low dose lead induced testicular damage and glycolytic inhibition in mice. *Toxicology* **2021**, *462*, 152933. [CrossRef]
31. Tamaki, N.; Ikeda, T.; Funatsuka, A. Zinc as activating cation for muscle glycolysis. *J. Nutr. Sci. Vitaminol.* **1983**, *29*, 655–662. [CrossRef]
32. Brand, I.A.; Kleineke, J. Intracellular zinc movement and its effect on the carbohydrate metabolism of isolated rat hepatocytes. *J. Biol. Chem.* **1996**, *271*, 1941–1949. [CrossRef]
33. Villagómez-Estrada, S.; Pérez, J.F.; Darwich, L.; Vidal, A.; van Kuijk, S.; Melo-Durán, D.; Solà-Oriol, D. Effects of copper and zinc sources and inclusion levels of copper on weanling pig performance and intestinal microbiota. *J. Anim. Sci.* **2020**, *98*, skaa117. [CrossRef]
34. Khajeh Bami, M.; Afsharmanesh, M.; Ebrahimnejad, H. Effect of dietary *Bacillus coagulans* and different forms of zinc on performance, intestinal microbiota, carcass and meat quality of broiler chickens. *Probiotics Antimicrob. Proteins* **2020**, *12*, 461–472. [CrossRef]
35. Aktas, M.; Ciger, O.; Genc, E.; Genc, M.A.; Cavdar, N. Effects of mannan oligosaccharide and serotonin on molting, growth, body composition and hepatopancreas histology of white leg shrimp *Litopenaeus vannamei* (Boone 1931). *Turk. J. Fish Aquat. Sci.* **2014**, *14*, 205–211. [CrossRef]
36. Patil, P.K.; Muralidhar, M.; Solanki, H.G.; Patel, P.P.; Patel, K.; Gopla, C. Effect of culture intensity and probiotics application on microbiological and environmental parameters in *Litopenaeus vannamei* culture ponds. *J. Environ. Biol.* **2016**, *37*, 21–29.
37. AOAC. *Official Methods of Analysis of AOAC International*, 16th ed.; Association of Official Analytical Chemists: Washington, DC, USA, 1995.
38. Vargas-Albores, F.; Guzmán, M.-A.; Ochoa, J.-L. An anticoagulant solution for haemolymph collection and prophenoloxidase studies of penaeid shrimp (*Penaeus californiensis*). *Comp. Biochem. Physiol. Part A Physiol.* **1993**, *106*, 299–303. [CrossRef]
39. Pfaffl, M.W.; Tichopad, A.; Prgomet, C.; Neuvians, T.P. Determination of stable housekeeping genes, differentially regulated target genes and sample integrity: BestKeeper—Excel-based tool using pair-wise correlations. *Biotechnol. Lett.* **2004**, *26*, 509–515. [CrossRef]
40. Andersen, C.L.; Jensen, J.L.; Ørntoft, T.F. Normalization of real-time quantitative reverse transcription-pcr data: A model-based variance estimation approach to identify genes suited for normalization, applied to bladder and colon cancer data sets. *Cancer Res.* **2004**, *64*, 5245–5250. [CrossRef]
41. Livak, K.J.; Schmittgen, T.D. Analysis of relative gene expression data using real-time quantitative PCR and the $2^{-\Delta\Delta CT}$ method. *Methods* **2001**, *25*, 402–408. [CrossRef]
42. Magoč, T.; Salzberg, S.L. FLASH: Fast length adjustment of short reads to improve genome assemblies. *Bioinformatics* **2011**, *27*, 2957–2963. [CrossRef]
43. Martin, M. Cutadapt removes adapter sequences from high-throughput sequencing reads. *EMBnet.J.* **2011**, *17*, 10. [CrossRef]
44. Edgar, R.C.; Haas, B.J.; Clemente, J.C.; Quince, C.; Knight, R. UCHIME improves sensitivity and speed of chimera detection. *Bioinformatics* **2011**, *27*, 2194–2200. [CrossRef]
45. Edgar, R.C. UPARSE: Highly accurate OTU sequences from microbial amplicon reads. *Nat. Methods* **2013**, *10*, 996–998. [CrossRef]
46. Wang, Q.; Garrity, G.M.; Tiedje, J.M.; Cole, J.R. Naïve Bayesian classifier for rapid assignment of rRNA sequences into the new bacterial taxonomy. *Appl. Environ. Microbiol.* **2007**, *73*, 5261–5267. [CrossRef] [PubMed]
47. Caporaso, J.G.; Kuczynski, J.; Stombaugh, J.; Bittinger, K.; Bushman, F.D.; Costello, E.K.; Fierer, N.; Peña, A.G.; Goodrich, J.K.; Gordon, J.I.; et al. QIIME allows analysis of high-throughput community sequencing data. *Nat. Methods* **2010**, *7*, 335–336. [CrossRef] [PubMed]
48. White, J.R.; Nagarajan, N.; Pop, M. Statistical methods for detecting differentially abundant features in clinical metagenomic samples. *PLoS Comput. Biol.* **2009**, *5*, e1000352. [CrossRef] [PubMed]
49. Shahpar, Z.; Johari, S.A. Effects of dietary organic, inorganic, and nanoparticulate zinc on rainbow trout, *Oncorhynchus mykiss* larvae. *Biol. Trace Elem. Res.* **2019**, *190*, 535–540. [CrossRef]
50. Maage, A.; Julshamn, K.; Berge, G.E. Zinc gluconate and zinc sulphate as dietary zinc sources for *Atlantic salmon*. *Aquac. Nutr.* **2001**, *7*, 183–187. [CrossRef]
51. Fountoulaki, E.; Morgane, H.; Rigos, G.; Antigoni, V.; Mente, E.; Sweetman, J.; Nengas, I. Evaluation of zinc supplementation in European sea bass (*Dicentrarchus labrax*) juvenile diets. *Aquac. Res.* **2010**, *41*, 208–216. [CrossRef]
52. Sekler, I.; Sensi, S.L.; Hershfinkel, M.; Silverman, W.F. Mechanism and regulation of cellular zinc transport. *Mol. Med.* **2007**, *13*, 337–343. [CrossRef]
53. Kambe, T. An overview of a wide range of functions of ZnT and Zip zinc transporters in the secretory pathway. *Biosci. Biotechnol. Biochem.* **2011**, *75*, 1036–1043. [CrossRef]
54. Jeong, J.; Eide, D.J. The SLC39 family of zinc transporters. *Mol. Asp. Med.* **2013**, *34*, 612–619. [CrossRef]
55. Hamer, D.H. Metallothionein. *Annu. Rev. Biochem.* **1986**, *55*, 913–951. [CrossRef]
56. Pourang, N.; Dennis, J.H. Distribution of trace elements in tissues of two shrimp species from the Persian Gulf and roles of metallothionein in their redistribution. *Environ. Int.* **2005**, *31*, 325–341. [CrossRef] [PubMed]
57. Kambe, T.; Tsuji, T.; Hashimoto, A.; Itsumura, N. The physiological, biochemical, and molecular roles of zinc transporters in zinc homeostasis and metabolism. *Physiol. Rev.* **2015**, *95*, 749–784. [CrossRef] [PubMed]

58. Fukada, T.; Kambe, T. Molecular and genetic features of zinc transporters in physiology and pathogenesis. *Metallomics* **2011**, *3*, 662–674. [CrossRef]
59. Bray, T.M.; Bettger, W.J. The physiological role of zinc as an antioxidant. *Free Radic. Biol. Med.* **1990**, *8*, 281–291. [CrossRef]
60. Hogstrand, C. Zinc. In *Fish Physiology*; Wood, C.M., Farrell, A.P., Brauner, C.J., Eds.; Academic Press: Waltham, MA, USA, 2011; pp. 135–200.
61. Francenia Santos-Sánchez, N.; Salas-Coronado, R.; Villanueva-Cañongo, C.; Hernández-Carlos, B. Antioxidant compounds and their antioxidant mechanism. In *Antioxidants*; Shalaby, E., Ed.; IntechOpen: London, UK, 2019; p. 13.
62. Weydert, C.J.; Cullen, J.J. Measurement of superoxide dismutase, catalase and glutathione peroxidase in cultured cells and tissue. *Nat. Protoc.* **2010**, *5*, 51–66. [CrossRef] [PubMed]
63. Roginsky, V.; Lissi, E.A. Review of methods to determine chain-breaking antioxidant activity in food. *Food Chem.* **2005**, *92*, 235–254. [CrossRef]
64. Bonaventura, P.; Benedetti, G.; Albarède, F.; Miossec, P. Zinc and its role in immunity and inflammation. *Autoimmun. Rev.* **2015**, *14*, 277–285. [CrossRef] [PubMed]
65. Pang, H.; Wang, G.; Zhou, S.; Wang, J.; Zhao, J.; Hoare, R.; Monaghan, S.J.; Wang, Z.; Sun, C. Survival and immune response of white shrimp *Litopenaeus vannamei* following single and concurrent infections with WSSV and *Vibrio parahaemolyticus*. *Fish Shellfish Immunol.* **2019**, *92*, 712–718. [CrossRef]
66. Amparyup, P.; Charoensapsri, W.; Tassanakajon, A. Prophenoloxidase system and its role in shrimp immune responses against major pathogens. *Fish Shellfish Immunol.* **2013**, *34*, 990–1001. [CrossRef]
67. Boonchuen, P.; Jaree, P.; Somboonviwat, K.; Somboonwiwat, K. Regulation of shrimp prophenoloxidase activating system by lva-miR-4850 during bacterial infection. *Sci. Rep.* **2021**, *11*, 3821. [CrossRef]
68. De-la-Re-Vega, E.; García-Galaz, A.; Díaz-Cinco, M.E.; Sotelo-Mundo, R.R. White shrimp (*Litopenaeus vannamei*) recombinant lysozyme has antibacterial activity against Gram negative bacteria: *Vibrio alginolyticus*, *Vibrio parahemolyticus* and *Vibrio cholerae*. *Fish Shellfish Immunol.* **2006**, *20*, 405–408. [CrossRef] [PubMed]
69. Zhang, Y.; Yan, F.; Hu, Z.; Zhao, X.; Min, S.; Du, Z.; Zhao, S.; Ye, X.; Li, Y. Hemocyanin from shrimp *Litopenaeus vannamei* shows hemolytic activity. *Fish Shellfish Immunol.* **2009**, *27*, 330–335. [CrossRef] [PubMed]
70. Hojyo, S.; Fukada, T. Roles of zinc signaling in the immune system. *J. Immunol. Res.* **2016**, *2016*, 6762343. [CrossRef]
71. Ezaki, O. IIb group metal ions (Zn^{2+}, Cd^{2+}, Hg^{2+}) stimulate glucose transport activity by post-insulin receptor kinase mechanism in rat adipocytes. *J. Biol. Chem.* **1989**, *264*, 16118–16122. [CrossRef]
72. Ranasinghe, P.; Pigera, S.; Galappatthy, P.; Katulanda, P.; Constantine, G.R. Zinc and diabetes mellitus: Understanding molecular mechanisms and clinical implications. *Daru* **2015**, *23*, 44. [CrossRef] [PubMed]
73. Martínez-Quintana, J.A.; Yepiz-Plascencia, G. Glucose and other hexoses transporters in marine invertebrates: A mini review. *Electron. J. Biotechnol.* **2012**, *15*, 16.
74. Kumari, A. Glycolysis. In *Sweet Biochemistry*; Academic Press: Waltham, MA, USA, 2018; pp. 1–5.
75. Yetkin-Arik, B.; Vogels, I.M.C.; Nowak-Sliwinska, P.; Weiss, A.; Houtkooper, R.H.; Van Noorden, C.J.F.; Klaassen, I.; Schlingemann, R.O. The role of glycolysis and mitochondrial respiration in the formation and functioning of endothelial tip cells during angiogenesis. *Sci. Rep.* **2019**, *9*, 12608. [CrossRef]
76. McKerrecher, D.; Waring, M.J. Property-based design in the optimisation of benzamide glucokinase activators. In *Progress in Medicinal Chemistry*; Lawton, G., Witty, D.R., Eds.; Elsevier: Oxford, UK, 2013; pp. 1–43.
77. Olechnowicz, J.; Tinkov, A.; Skalny, A.; Suliburska, J. Zinc status is associated with inflammation, oxidative stress, lipid, and glucose metabolism. *J. Physiol. Sci.* **2018**, *68*, 19–31. [CrossRef]
78. Kechrid, Z.; Demýr, N.; Abdennour, C.; Bouzerna, N. Effect of low dietary zinc intake and experimental diabetes on the zinc and carbohydrate metabolism in rats. *Turk. J. Med. Sci.* **2002**, *32*, 101–105.
79. Xiong, J.; Wang, K.; Wu, J.; Qiuqian, L.; Yang, K.; Qian, Y.; Zhang, D. Changes in intestinal bacterial communities are closely associated with shrimp disease severity. *Appl. Microbiol. Biotechnol.* **2015**, *99*, 6911–6919. [CrossRef]
80. Wang, T.; Yang, J.; Lin, G.; Li, M.; Zhu, R.; Zhang, Y.; Mai, K. Effects of dietary mannan oligosaccharides on non-specific immunity, intestinal health, and antibiotic resistance genes in pacific white shrimp *Litopenaeus vannamei*. *Front. Immunol.* **2021**, *12*, 772570. [CrossRef] [PubMed]
81. Holt, C.C.; Bass, D.; Stentiford, G.D.; van der Giezen, M. Understanding the role of the shrimp gut microbiome in health and disease. *J. Invertebr. Pathol.* **2021**, *186*, 107387. [CrossRef] [PubMed]
82. Chaudhary, A.; Qazi, J.I. Probiotic antagonism of *Sphingomonas* sp. against *Vibrio anguillarum* exposed *Labeo rohita* fingerlings. *Adv. Life Sci.* **2014**, *4*, 156–165.
83. Ringø, E. Probiotics in shellfish aquaculture. *Aquac. Fish* **2020**, *5*, 1–27. [CrossRef]
84. Chauhan, A.; Singh, R. Probiotics in aquaculture: A promising emerging alternative approach. *Symbiosis* **2019**, *77*, 99–113. [CrossRef]
85. Farzanfar, A. The use of probiotics in shrimp aquaculture. *FEMS Immunol. Med. Microbiol.* **2006**, *48*, 149–158. [CrossRef]
86. Kong, C.; Gao, R.; Yan, X.; Huang, L.; Qin, H. Probiotics improve gut microbiota dysbiosis in obese mice fed a high-fat or high-sucrose diet. *Nutrition* **2019**, *60*, 175–184. [CrossRef] [PubMed]
87. Tungland, B. Short-chain fatty acid production and functional aspects on host metabolism. In *Human Microbiota in Health and Disease*; Tungland, B., Ed.; Academic Press: Waltham, MA, USA, 2018; pp. 37–106.

88. Ramakrishna, B.S. Role of the gut microbiota in human nutrition and metabolism. *J. Gastroenterol. Hepatol.* **2013**, *28* (Suppl. 4), 9–17. [CrossRef]
89. Brown, C.T.; Davis-Richardson, A.G.; Giongo, A.; Gano, K.A.; Crabb, D.B.; Mukherjee, N.; Casella, G.; Drew, J.C.; Ilonen, J.; Knip, M.; et al. Gut microbiome metagenomics analysis suggests a functional model for the development of autoimmunity for type 1 diabetes. *PLoS ONE* **2011**, *6*, e25792. [CrossRef] [PubMed]
90. Schink, B.; Pfennig, N. *Propionigenium modestum* gen. nov. sp. nov. a new strictly anaerobic, nonsporing bacterium growing on succinate. *Arch. Microbiol.* **1982**, *133*, 209–216. [CrossRef]
91. Madhana, S.; Kanimozhi, G.; Panneerselvam, A. Probiotics in shrimp aquaculture. In *Advances in Probiotics*; Dhanasekaran, D., Sankaranarayanan, A., Eds.; Academic Press: Waltham, MA, USA, 2021; pp. 309–325.
92. Panthee, S.; Hamamoto, H.; Paudel, A.; Sekimizu, K. *Lysobacter* species: A potential source of novel antibiotics. *Arch. Microbiol.* **2016**, *198*, 839–845. [CrossRef] [PubMed]
93. Brescia, F.; Pertot, I.; Puopolo, G. Lysobacter. In *Benef Microbes Agro-Ecology*; Amaresan, N., Kumar, M.S., Annapurna, K., Kumar, K., Sankaranarayanan, A., Eds.; Academic Press: Waltham, MA, USA, 2020; pp. 313–338.
94. Al-Daghistani, H.I.; Mohammad, B.T.; Kurniawan, T.A.; Singh, D.; Rabadi, A.D.; Xue, W.; Avtar, R.; Othman, M.H.D.; Shirazian, S. Characterization and applications of *Thermomonas hydrothermalis* isolated from Jordan's hot springs for biotechnological and medical purposes. *Process. Biochem.* **2021**, *104*, 171–181. [CrossRef]
95. Hazarika, S.N.; Thakur, D. Actinobacteria. In *Beneficial Microbes in Agro-Ecology*; Amaresan, N., Kumar, M.S., Annapurna, K., Kumar, K., Sankaranarayanan, A., Eds.; Academic Press: Waltham, MA, USA, 2020; pp. 443–476.
96. Waśkiewicz, A.; Irzykowska, L. Flavobacterium spp.—Characteristics, occurrence, and toxicity. In *Encyclopedia of Food Microbiology*, 2nd ed.; Batt, C.A., Tortorello, M.L., Eds.; Academic Press: Waltham, MA, USA, 2014; pp. 938–942.
97. Wu, Z.; Zhang, Q.; Lin, Y.; Hao, J.; Wang, S.; Zhang, J.; Li, A. Taxonomic and functional characteristics of the gill and gastrointestinal microbiota and its correlation with intestinal metabolites in NEW GIFT strain of farmed adult nile tilapia (*Oreochromis niloticus*). *Microorganisms* **2021**, *9*, 617. [CrossRef] [PubMed]
98. Lee, W.; Juniper, S.K.; Perez, M.; Ju, S.; Kim, S. Diversity and characterization of bacterial communities of five co-occurring species at a hydrothermal vent on the Tonga Arc. *Ecol. Evol.* **2021**, *11*, 4481–4493. [CrossRef] [PubMed]
99. Shields, J.D. The impact of pathogens on exploited populations of decapod crustaceans. *J. Invertebr. Pathol.* **2012**, *110*, 211–224. [CrossRef] [PubMed]
100. Berman, J.J. Actinobacteria. In *Taxonomic Guide to Infectious Diseases*; Berman, J.J., Ed.; Academic Press: Waltham, MA, USA, 2012; pp. 77–84.
101. Coretti, L.; Cuomo, M.; Florio, E.; Palumbo, D.; Keller, S.; Pero, R.; Chiariotti, L.; Lembo, F.; Cafiero, C. Subgingival dysbiosis in smoker and non-smoker patients with chronic periodontitis. *Mol. Med. Rep.* **2017**, *15*, 2007–2014. [CrossRef] [PubMed]
102. Berman, J.J. Gamma Proteobacteria. In *Taxonomic Guide to Infectious Diseases*; Berman, J.J., Ed.; Academic Press: Waltham, MA, USA, 2012; pp. 37–47.
103. Sękowska, A. *Raoultella* spp.—Clinical significance, infections and susceptibility to antibiotics. *Folia Microbiol.* **2017**, *62*, 221–227. [CrossRef]
104. Ghosh, R.; Chatterjee, S.; Mandal, N.C. Stenotrophomonas. In *Beneficial Microbes in Agro-Ecology*; Amaresan, N., Kumar, M.S., Annapurna, K., Kumar, K., Sankaranarayanan, A., Eds.; Academic Press: Waltham, MA, USA, 2020; pp. 427–442.
105. Mori, F.; Umezawa, Y.; Kondo, R.; Wada, M. Dynamics of sulfate-reducing bacteria community structure in surface sediment of a seasonally hypoxic enclosed bay. *Microbes Environ.* **2018**, *33*, 378–384. [CrossRef] [PubMed]
106. Drancourt, M.; Prebet, T.; Aghnatios, R.; Edouard, S.; Cayrou, C.; Henry, M.; Blaise, D.; Raoult, D. Planctomycetes DNA in febrile aplastic patients with leukemia, rash, diarrhea, and micronodular pneumonia. *J. Clin. Microbiol.* **2014**, *52*, 3453–3455. [CrossRef] [PubMed]
107. Loubinoux, J.; Bronowicki, J.P.; Pereira, I.A.C.; Mougenel, J.L.; Le Faou, A.E. Sulfate-reducing bacteria in human feces and their association with inflammatory bowel diseases. *FEMS Microbiol. Ecol.* **2002**, *40*, 107–112. [CrossRef]
108. Dordević, D.; Jančíková, S.; Vítězová, M.; Kushkevych, I. Hydrogen sulfide toxicity in the gut environment: Meta-analysis of sulfate-reducing and lactic acid bacteria in inflammatory processes. *J. Adv. Res.* **2021**, *27*, 55–69. [CrossRef] [PubMed]
109. Hood, M.I.; Skaar, E.P. Nutritional immunity: Transition metals at the pathogen-host interface. *Nat. Rev. Microbiol.* **2012**, *10*, 525–537. [CrossRef]
110. Chen, L.; Wang, Z.; Wang, P.; Yu, X.; Ding, H.; Wang, Z.; Feng, J. Effect of long-term and short-term imbalanced Zn manipulation on gut microbiota and screening for microbial markers sensitive to zinc status. *Microbiol. Spectr.* **2021**, *9*, e0048321. [CrossRef] [PubMed]
111. Shao, Y.; Wolf, P.G.; Guo, S.; Guo, Y.; Gaskins, H.R.; Zhang, B. Zinc enhances intestinal epithelial barrier function through the PI3K/AKT/mTOR signaling pathway in Caco-2 cells. *J. Nutr. Biochem.* **2017**, *43*, 18–26. [CrossRef] [PubMed]
112. Paone, P.; Cani, P.D. Mucus barrier, mucins and gut microbiota: The expected slimy partners? *Gut* **2020**, *69*, 2232–2243. [CrossRef] [PubMed]
113. Xia, P.; Lian, S.; Wu, Y.; Yan, L.; Quan, G.; Zhu, G. Zinc is an important inter-kingdom signal between the host and microbe. *Vet. Res.* **2021**, *52*, 39. [CrossRef] [PubMed]

antioxidants

MDPI

Article

Tolerance Assessment of *Atractylodes macrocephala* Polysaccharide in the Diet of Largemouth Bass (*Micropterus salmoides*)

Bo Dong [1,2], Liyun Wu [1,2], Qiaozhen Chen [1,2], Wenjie Xu [1], Dinggang Li [3], Dong Han [1,2], Xiaoming Zhu [1], Haokun Liu [1], Yunxia Yang [1], Shouqi Xie [1,2,4] and Junyan Jin [1,*]

[1] State Key Laboratory of Freshwater Ecology and Biotechnology, Institute of Hydrobiology, Chinese Academy of Sciences, Wuhan 430072, China
[2] University of Chinese Academy of Sciences, Beijing 100049, China
[3] Baoding Jizhong Pharmaceutical Co., Ltd., Baoding 071100, China
[4] The Innovative Academy of Seed Design, Chinese Academy of Sciences, Beijing 100101, China
* Correspondence: jinjunyan@ihb.ac.cn

Abstract: *Atractylodes macrocephala* polysaccharide (AMP) can enhance antioxidant defense and anti-inflammation, as the tolerance levels of AMP in aquaculture is important for additive utilization. However, the tolerance dose of AMP is unknown. We assess the tolerance levels of AMP in juvenile largemouth bass (3.38 ± 0.11 g) by feeding them a 0, 400, 4000, or 8000 mg/kg AMP supplemented diet for 10 weeks. The 400 mg/kg AMP dose increased growth performance. The Nrf2/Keap1 signaling pathway was activated, as indicated by Keap1 and Nrf2 protein levels in the liver. Enhanced activity of antioxidant enzymes (SOD, GPx), together with increased mRNA levels of antioxidant genes (*sod*, *gpx*) and decreased accumulation of reactive oxygen species (ROS) and MDA, was found in the liver, implying the antioxidant effect of AMP. Nutrient absorption was enhanced by AMP, as reflected by the increased length of intestinal villi and microvilli. However, 4000 and 8000 mg/kg AMP induced oxidant stress, as indicated by increased plasma ALT and AST content and decreased mRNA levels of antioxidant genes (*sod*, *gpx*) in the liver and intestinal tissues. Inflammatory reactions were also induced by high doses of AMP, as reflected by enhanced levels of pro-inflammatory cytokines (*tnfα*, *nfκb*) in the liver, intestinal, and kidney tissues and inhibited levels of anti-inflammatory cytokines (*tgfβ*, *iκb*). Histological analysis reveals inflammatory cell infiltration and tissue damage. Thus, the safe tolerance margin of AMP supplement for largemouth bass was 400–4000 mg/kg.

Keywords: AMP; Nrf2/Keap1 signaling pathway; antioxidant defense; inflammation; tolerance

Citation: Dong, B.; Wu, L.; Chen, Q.; Xu, W.; Li, D.; Han, D.; Zhu, X.; Liu, H.; Yang, Y.; Xie, S.; et al. Tolerance Assessment of *Atractylodes macrocephala* Polysaccharide in the Diet of Largemouth Bass (*Micropterus salmoides*). *Antioxidants* **2022**, *11*, 1581. https://doi.org/10.3390/antiox11081581

Academic Editors: Bo Liu, Changyou Song and Cunxin Sun

Received: 23 June 2022
Accepted: 12 August 2022
Published: 15 August 2022

1. Introduction

Aquaculture production, worldwide, reached 114.5 million tons in 2018 [1]. However, aquaculture problems, induced by the rapid increase and high-density production of fish and other aquaculture animals, include increased disease prevalence [2]. Feed additives are added in small amounts to aquafeed for specific purposes [3]. Plant-derived feed additives, such as polysaccharides, can enhance fish growth, intestinal health, disease resistance, and stress resistance [4,5]. *Astragalus* polysaccharide supplementation enhances the immune response of *Litopenaeus vannamei* by increasing superoxide dismutase (SOD) activity and inhibiting maleic dialdehyde (MDA) content in the hemolymph [6]. HP-02 polysaccharide from honeysuckle flowers has immunomodulatory effects on on-growing common carp by reducing the expression of pro-inflammatory cytokines, such as tumor necrosis factor α (*tnfα*), and increasing the expression of anti-inflammatory cytokines, such as transforming growth factor β (*tgfβ*) [7]. *Atractylodes macrocephala* polysaccharide (AMP), the main component extracted and purified from the Chinese herbal medicine *Atractylodes macrocephala*, is studied because of its anti-tumor effect [8,9]. AMP is widely used as an additive in animal

formulation for its growth-promoting effect and antioxidant effect [10]. AMP can reduce inflammatory damage and oxidative stress via the NF-κB signaling pathway [11,12]. AMP can also enhance antioxidant defense capacity by promoting the expression of glutathione peroxidase (GPx) and SOD [13,14], which are related to the Nrf2 signaling pathway [15]. However, few studies report the effects of AMP on aquatic animals.

The effects of feed additives on ingestion, growth, and the immune system are normally dose-dependent in omnivores [16–20]. The growth of on-growing crucian carp was increased by 40 g/kg *Enteromorpha prolifera* polysaccharide supplementation, while the opposite result was observed at a higher dose [16]. High doses of feed additives might affect intestine, liver, and kidney health. Mild damage was found in the intestinal tissues of juvenile Nile tilapia when organic trace mineral doses exceeded 50% [17]. Overdose of olaquindox, a growth-promoting feed additive, led to an increasing level of alanine aminotransferase (ALT) and aspartate aminotransferase (AST) in blood, as well as cell damage to the liver of on-growing common carp [18]. Similarly, an increase in plasma ALT and AST activities occurred when dietary *Coriolus versicolor* polysaccharides exceeded 2 g/kg in on-growing crucian carp [19]. An increase in phagocytic activity in hemocytes was only observed in *Litopenaeus vannamei* when they were fed diet supplemented with *Astragalus* polysaccharides in amounts less than 1.0 g/kg [6]. High doses of pectin and cellulose caused damage and dysfunction to the liver and intestine of juvenile yellow catfish [20]. These data show that tolerance assessment of aquatic animals to feed additives is important for the safe use of additives.

Largemouth bass (*Micropterus salmoides*) is a fast-growing aquaculture species in China, with production exceeding 0.61 million tons in 2020 [21]. However, disease is currently a major factor restricting the development of largemouth bass culture [22,23]. Functional additives are an effective way to promote growth and increase antioxidant defense in largemouth bass. Extracts of *Foeniculum vulgare* and *Artemisia annua* can enhance the specific growth rate (SGR) and the enzyme activity of SOD but decrease the MDA content [24]. Chlorogenic acid can regulate inflammatory reactions by reducing mRNA expression levels of *tnfα* [25]. Dietary sodium butyrate can improve intestinal morphology by increasing the villus width and villus height [26]. Because AMP can promote growth, antioxidant activity, and disease resistance [8,9,11–15], it could be used as a feed additive in largemouth bass culture. The optimal supplemental level of AMP as a feed additive for largemouth bass was determined to be 400 mg/kg without negative effects (data unpublished). However, since the maximum tolerated levels of AMP are unknown, we assessed the tolerance level of AMP supplementation in largemouth bass.

2. Materials and Methods

2.1. Experimental Diets

Atractylodes macrocephala polysaccharide was supplied by Baoding Jizhong Biotechnology Co., Ltd. (Hebei, China). The raw medicinal herb *Atractylodes macrocephala* was boiled three times with distilled water (1:12, *w*/*v*) for 2 h. The obtained filtrate was centrifuged. Then, the condensed filtrate was boiled with 1.0% activated carbon for 20 min, followed by standing for 12 h. The filtrate was condensed at 60 °C. After spray drying, the AMP power was obtained. The carbohydrate content of AMP was 75.0%. The content of crude protein, crude lipid, and moisture was 10.0%, 5.0%, and 5.0%, respectively. The main component of AMP was dextran. In addition, D-fructose, D-glucose, and L-arabinose were also included. Four isonitrogenous and isoenergetic diets were prepared by adding 0, 400, 4000, and 8000 mg/kg AMP to the basal diet formula of largemouth bass. The formulation and basic chemical composition are shown in Table 1. All ingredients were mixed well. After mixing with water, granular feeds with a diameter of 3 mm were prepared by a pelletizer (SLR-45, Fishery Machinery Research Institute, Chinese Academy of Fishery Sciences, Shanghai, China). The diets were dried in an oven at 70 °C for 1 h and then stored at 4 °C.

Table 1. Formulation and composition of experimental diets (dry matter, %).

Ingredients	A0	A400	A4000	A8000
Fish meal [a]	40	40	40	40
Wheat gluten	6.5	6.5	6.5	6.5
Casein	18.5	18.5	18.5	18.5
Flour	5	5	5	5
Cassava starch	10	10	10	10
Fish oil	6	6	6	6
Vitamin & mineral premix [b]	1	1	1	1
Monocalcium phosphate	1.50	1.50	1.50	1.50
Choline chloride	0.10	0.10	0.10	0.10
Bentonite	11.40	11.36	11.00	10.60
AMP (mg/kg) [c]	0	400	4000	8000
Chemical composition				
Moisture	7.91	7.97	7.16	7.28
Crude protein	52.07	52.14	51.29	51.70
Crude lipid	9.50	9.06	9.04	9.35

[a] Fish meal: From Superprime, TASA Fish Product Co., Ltd., Lima, Peru. [b] Vitamin & mineral premix: P301 1% perch compound premixed feed, Yinghuier Biotechnology Co., Ltd., Beijing, China. [c] AMP: From Baoding Jizhong Biotechnology Co., Ltd., Hebei, China.

2.2. Feeding Trial and Sampling

The largemouth bass were obtained from Ezhou Zhenghao Fry Co., Ltd. (Ezhou, Hubei, China), and were acclimated in a recirculating aquaculture system for 2 weeks with commercial feed. Fish (3.38 ± 0.11 g) were starved for 24 h before the experiment. A total of 720 healthy fish were assigned to 24 tanks (water volume: 140 L), with six tanks for each treatment. The water temperature was kept at 25–26 °C at a pH of 7–8, dissolved oxygen > 6.8 mg/L, and NH_4-N < 0.07 mg/L, with continuous aeration for 24 h. The fish were fed to apparent satiation twice a day (9:00 and 16:00). The experiment duration was 10 weeks.

At the end of the experiment, all fish in each tank were lightly anaesthetized with 60 mg/L MS-222 (Sigma, St. Louis, MO, USA) and weighed after starving for 12 h. Then, two fish were randomly selected from each tank for body composition analysis. Blood was taken from the caudal vein by using a syringe soaked with heparin sodium from the other two fish. The supernatant plasma was taken after a $3000\times g$ centrifugation. Then, the liver, intestine, and kidney tissue samples were stored at −80 °C prior to analyses. The liver, intestine, and kidney tissues were fixed in 4% paraformaldehyde for histological analysis. The experimental protocol was approved by the ethics committee of the Institute of Hydrobiology, Chinese Academy of Sciences (approval ID: IHB20140724).

2.3. Chemical Composition Analysis

All chemical compositions, including moisture, crude protein, crude lipid, and ash, were analyzed according to standard methods [27]. The moisture content was determined by baking at 105 °C and then using the weight loss method for calculation. Crude protein was measured by Kjeltec Auto Analyzer 4800 (FOSS Tecator, Hoganas, Sweden). Crude lipid was determined by soxhlet extraction (Soxtec System HT Tecator, Hoganas, Sweden) with ether as a solvent. The ash content was measured after full incineration at 550 °C in a muffle furnace (Jianli Electric Furnace Factory, Hubei, China).

2.4. Biochemical Analysis

The biochemical analysis was conducted based on reported methods [28]. The ALT and AST in plasma and the MDA, SOD, and GPx in the liver were determined using assay kits (Nanjing Jiancheng Bioengineering Institute; Catalog: C009-2-1, C010-2-1, A003-1, A001-3, and A005-1, Jiangsu, China). The liver ROS content was also determined using an assay kit (MSKBIO Co., Ltd. Wuhan, China; Catalog: 69-86537). All the above parameters were determined according to manufacturer protocols.

2.5. Histological Analysis

The liver, intestine, and kidney tissues were dehydrated before paraffin embedding. They were then cut into 4-μm sections with a slicer (RM2016, Leica Instruments Co., Ltd., Shanghai, China). The sections were dyed with hematoxylin and eosin (H&E) to stain the nuclei blue and the cytoplasm red. The intestine was fixed overnight in 2.5% glutaraldehyde in 0.1 M phosphate buffer (pH = 7.4) at 4 °C and post-fixed in 1% OsO_4 at 4 °C for 2.5 h [29]. The sections were dehydrated using graded ethanol (30, 50, 70, 90, and 100%), processed with a mixed solution of ethanol and acetone, infiltrated in a mixture of acetone and epoxy resin (1:1 for 3.5 h, and then 1:2 overnight), and finally embedded using SPI-PON 812 at 60 °C for 48 h. Ultrathin sections (74 nm) were obtained using a Leica EM UC7 ultramicrotome. The ultrathin sections were stained with 3% uranyl acetate and lead citrate and then observed and photographed with an HT7700 transmission electron microscope (Hitachi High-Tech, Tokyo, Japan). Quantitative analysis of intestinal villi was performed using Image-pro plus 6.0 software, and the microvilli were measured using Image J software.

2.6. RNA Extraction and Real-Time Quantitative PCR

The total RNA of the liver, intestine, and kidney tissues was extracted with TRIzol reagent (Invitrogen, Carlsbad, CA, USA). The integrity of RNA was evaluated by agarose electrophoresis. The concentration of RNA was spectrophotometrically quantified with Nanodrop 2000 (Thermo Fisher Scientific, Waltham, MA, USA). Then, the RNA was reverse transcribed into cDNA by M-MLV according to the manufacturer's instructions. Real-time qPCR was performed on a LightCycle® 480 II (Roche, Diagnostics, Basel, Switzerland) instrument with SYBR Green I Master Mix (Roche Diagnostics, Carlsbad, CA, USA). β-actin was selected as the housekeeping gene owing to its stable expression in the liver, intestine, and kidney tissues. The relative levels of target genes were calculated by the method described by Pfaffl [30]. The primers used in this experiment are listed in Table 2.

Table 2. Primers used in this experiment.

Gene Name	Sense and Antisense Primer (5′-3′)	Accession No.	Product Length (bp)
Transforming growth factor β (*tgfβ*)	ACAGTGGGCAATGTAAGCGGTA TGTCTGGTGGGCTCTCGGTCTG	XM_038693206.1	232
Tumor necrosis factor α (*tnfα*)	CAAGTGTCAAACCCAGTTCCAA ATTTGCCTCAATGTGTGACGAT	XM_038723994.1	154
Superoxide dismutase (*sod*)	CAGTTACCAGTGTGTCGGCTCT CTCCAGGGCACCATAGTCGTAG	XM_038727054.1	180
Glutathione peroxidase (*gpx*)	CAGCAGACATTTCCTCACCATT CAGTGGCAGAGTCAGCCTTTTA	XM_038697220.1	250
Inhibitory protein of nuclear factor-kappa B (*nfκb*)	GCCAGAAGACAACCATACGCAT GGACACCAGGAGACGCTCACAC	XM_038729519.1	164
Nuclear factor-kappa B (*iκb*)	CACACTCGGTGATGATAACTGG CTCCAGTAACGAGTAGTATGTA	XM_038699792.1	182
β-actin	CTTTCCTCGGTATGGAGTCTTG CAGTCGTTTGGGTTTGTAGCAG	MH018565.1	386

2.7. Western Blot

Western blot analysis of the liver tissues was performed according to the method described by Wu [31]. The primary antibodies were anti-Nrf2 (A1244, ABclonal, Wuhan, China), anti-Keap1 (A1820, ABclonal, Wuhan, China), and anti-GAPDH (ab70699, Abcam, Cambridge, UK). The bands were acquired using ImageQuant LAS 4000 mini (GE Healthcare Life Sciences, Wuxi, China) and quantified using Image J software (National Institutes of Health, Bethesda, MD, USA).

2.8. Statistical Analysis

All data are presented as mean ± standard error and analyzed by one-way ANOVA using SPSS Statistics 25 (International Business Machines Corp., Armonk, NY, USA). The differences were considered to be significant when $p < 0.05$.

3. Results

3.1. Growth Performance and Body Composition

The growth performance of largemouth bass is shown in Table 3. Compared with the A0 group, significantly higher FBW, WGR, SGR, and FE were found only in the A400 group. However, no significant difference was found in body composition among any of the groups.

Table 3. Effects of dietary AMP on growth performance.

	A0	A400	A4000	A8000
	Growth performance			
IBW (%)	3.33 ± 0.06	3.40 ± 0.05	3.43 ± 0.06	3.37 ± 0.07
FBW (g)	38.47 ± 0.54 [a]	48.62 ± 1.51 [b]	36.76 ± 0.72 [a]	37.64 ± 0.77 [a]
WGR (%) [a]	946.87 ± 60.51 [a]	1287.39 ± 36.07 [b]	903.13 ± 49.14 [a]	895.64 ± 51.55 [a]
SGR (%/d) [b]	3.53 ± 0.02 [a]	3.85 ± 0.05 [b]	3.43 ± 0.03 [a]	3.49 ± 0.03 [a]
FE (%)[c]	119.35 ± 7.5 [a]	146.89 ± 3.16 [b]	114.20 ± 5.45 [a]	112.17 ± 4.57 [a]
	Composition of whole fish			
Moisture	72.16 ± 0.17	72.09 ± 0.26	71.36 ± 1.23	72.42 ± 0.23
Ash	3.54 ± 0.05	3.60 ± 0.02	3.70 ± 0.15	3.64 ± 0.04
Crude lipid	6.87 ± 0.29	6.97 ± 0.30	7.14 ± 0.30	6.54 ± 0.17
Crude protein	16.45 ± 0.08	16.38 ± 0.08	16.89 ± 0.78	16.17 ± 0.11

The data are expressed as mean ± SEM, and the superscripts (a or b) of different letters in the same row indicate significant differences ($p < 0.05$). [a] WGR (weight gain rate, %) = 100 × (final total weight−initial total weight)/initial total weight. [b] SGR (specific growth rate, %/d) = 100 × [Ln (final body weight) − Ln (initial body weight)]/days. [c] FE (feed efficiency, %) = 100 × (final total weight−initial total weight)/feed intake in dry matter.

3.2. Plasma Metabolites

The levels of ALT and AST in the plasma are shown in Figure 1. The enzyme activities of ALT and AST were significantly increased only in the A8000 group, compared to the A0 group.

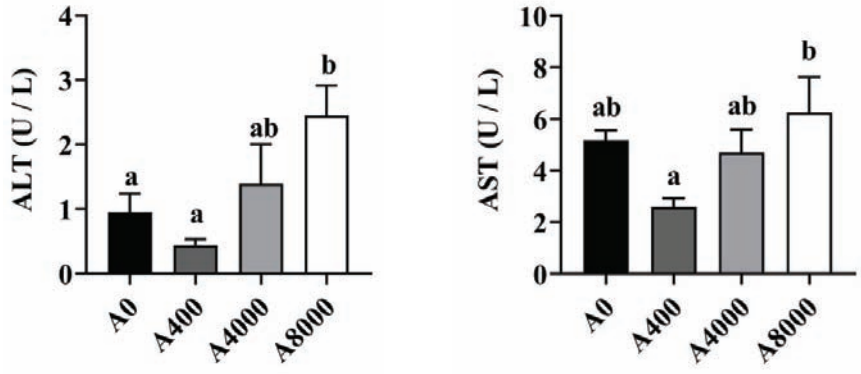

Figure 1. Plasma Effects of dietary *Atractylodes macrocephala* polysaccharide (AMP) on plasma ALT and AST. ALT: Alanine aminotransferase; ALT: Aspartate aminotransferase. Data are shown as mean ± SEM ($n = 6$). Different lowercase letters represent significant differences among all groups ($p < 0.05$).

3.3. Nrf2/Keap1 Signaling Pathway and Antioxidant-Related Genes in the Liver and Intestine

To investigate the effect of AMP on antioxidant defense, the protein levels of Nrf2/Keap1 were determined. As shown in Figure 2, The protein levels of Keap1 in the liver were significantly inhibited by 400 mg/kg AMP supplementation; however, the opposite result was found in the 8000 mg/kg AMP supplement group. Correspondingly, Nrf2 protein expression was significantly enhanced in the A400 group compared to the A0 group. Unaltered protein levels of Nrf2 were found in both the A4000 group and the A8000 group. The expression levels of *gpx* and *sod* in both the liver and intestine were significantly induced by 400 mg/kg AMP (Figure 3A,B).

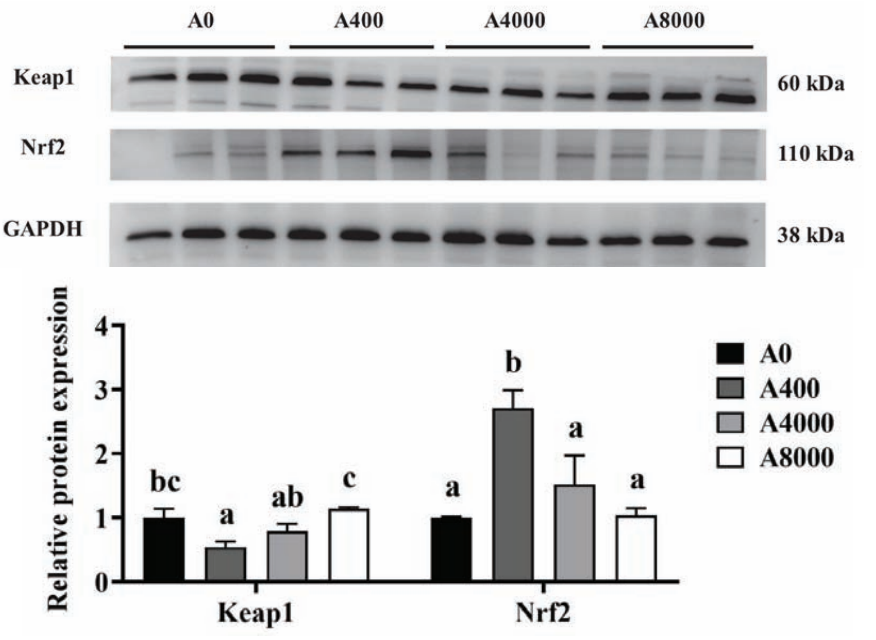

Figure 2. Effects of dietary AMP on protein expression and transcript levels of Keap1 and Nrf2. Keap1: Kelch-like ECH-associated protein 1; Nrf2: Nuclear factor erythroid 2-related factor 2. Data are shown as mean ± SEM (n = 6). Different lowercase letters represent significant differences among all groups ($p < 0.05$).

3.4. Activities of Antioxidant Enzymes in the Liver

The activities of antioxidant enzymes in the liver are shown in Figure 4. The activity of SOD was increased significantly in the AMP supplemented groups, irrespective of dosage. No change of GPx was found in any group. ROS and MDA levels were significantly inhibited by 400 mg/kg AMP supplementation. However, no significant difference was found between the A0 group and the A8000 group.

3.5. Expression of Inflammatory-Related Genes in the Liver, Intestine, and Kidney

Changes of the inflammation-related genes in the liver, intestine, and kidney are shown in Figure 5. The gene expression levels of *tnfα* and *nfκb* were significantly increased in the liver and kidney of the A4000 and A8000 groups, compared with the A0 group. Significantly enhanced expression of *tnfα* and *nfκb* was also found in the intestine of the A8000 group. The transcription levels of *tgfβ* and *ikb* were significantly decreased in the liver, intestine, and kidney of the A4000 and A8000 groups.

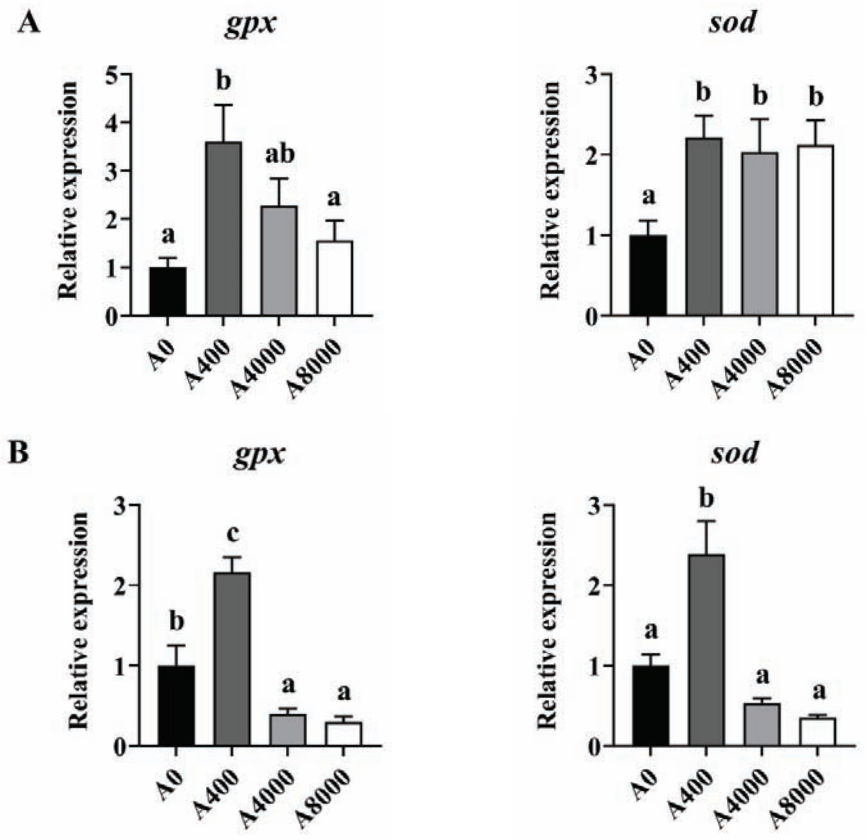

Figure 3. Effects of dietary AMP on expression of antioxidant-related genes in the liver (**A**) and intestine (**B**). *gpx*: glutathione peroxidase gene; *sod*: superoxide dismutase gene. Data are shown as mean ± SEM ($n = 6$). Different lowercase letters represent significant differences among all groups ($p < 0.05$).

3.6. Histological Analysis of the Liver, Intestine, and Kidney

The cell morphology of the liver is shown in Figure 6A. Compared with A0, no change was found in A400. However, cell edema, nucleus disappearance, and cytoplasmic vacuolation were observed in A4000. Cytoplasmic vacuolation accompanied by inflammatory cell infiltration was observed in A8000.

Figure 6B shows the intestinal morphology. A0 and A400 were relatively intact, and the goblet cells of A400 were significantly increased compared to A0. Intestinal villi in A4000 were damaged and were accompanied by inflammatory cell infiltration. Severe intestinal abnormalities and inflammatory cell infiltration were found in A8000. Compared with A0, the length of villi in A400 was significantly increased, whereas significantly decreased villi were found in A4000 and A8000. Transmission electron microscope images of villi are shown in Figure 6C. The tight junction of epithelial cells in A4000 was weakened, and the microvilli were significantly shrunken and reduced. In A8000, the intestinal wall was damaged, the tight junctions of intestinal epithelial cells were destroyed, the microvilli were wrinkled and shed, and their number was sparse. Microvillus length was significantly increased in A400 compared to A0 and was significantly decreased in A4000 compared to A0. A more severe change compared to A4000 was found in the A8000 group.

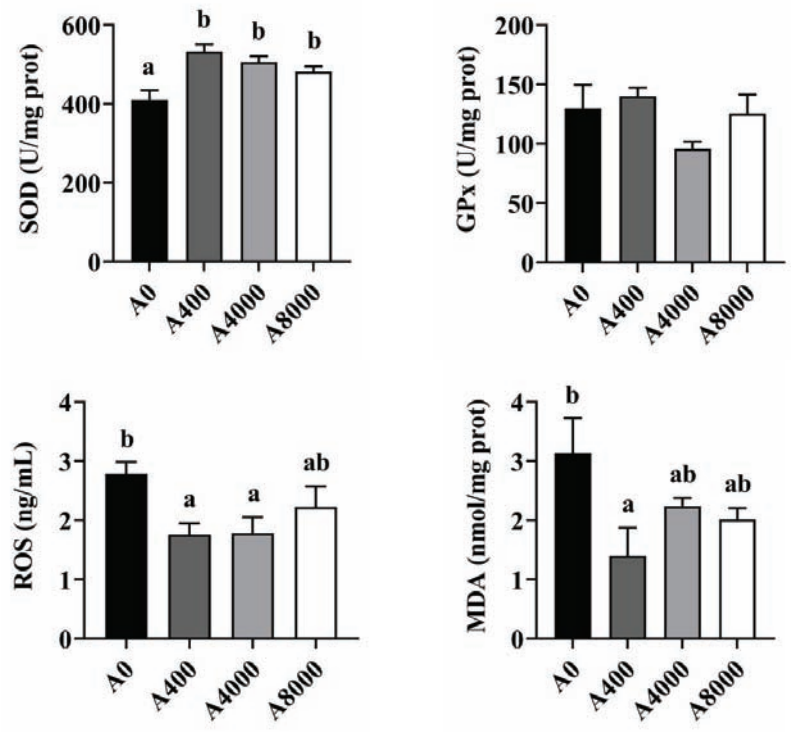

Figure 4. Effects of dietary AMP on activities of antioxidant enzymes in the liver (n = 6). SOD: superoxide dismutase; GPx: Glutathione peroxidase; ROS: Reactive oxygen species; MDA: Malondialdehyde. Data are shown as mean ± SEM (n = 6). Different lowercase letters represent significant differences among all groups ($p < 0.05$).

No abnormal histologic morphology was found in the kidneys of A0 and A400 (Figure 6D). A large number of inflammatory cell infiltrations were observed in the A4000 group. The renal tissue structure of A8000 was visibly abnormal, with the internal structure of glomerulus scattered and renal tubule edema accompanied by inflammatory cell infiltration.

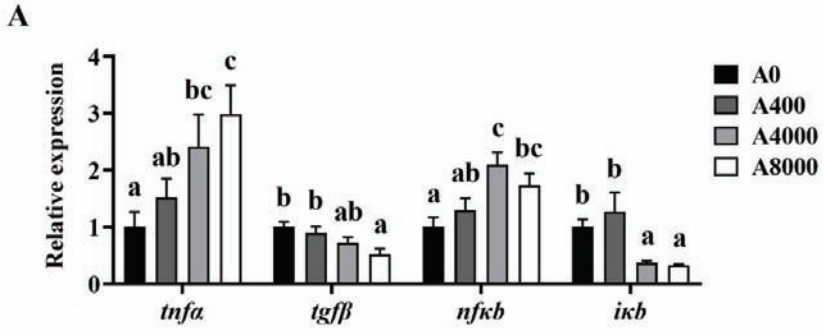

Figure 5. *Cont*.

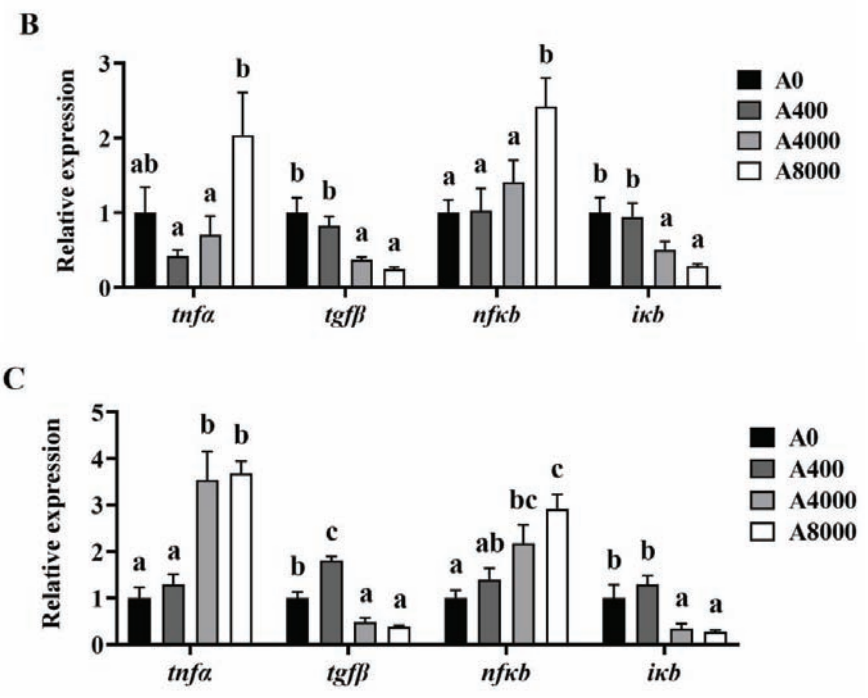

Figure 5. Effects of dietary AMP on expression of inflammatory-related genes in the liver (**A**), intestine (**B**), and kidney (**C**). *tnfα*: Tumor necrosis factor α; *tgfβ*: Transforming growth factor β; *nfκb*: Nuclear factor-kappa B; *iκb*: Inhibitory protein of nuclear factor-kappa B. Data are shown as mean ± SEM ($n = 6$). Different lowercase letters represent significant differences among all groups ($p < 0.05$).

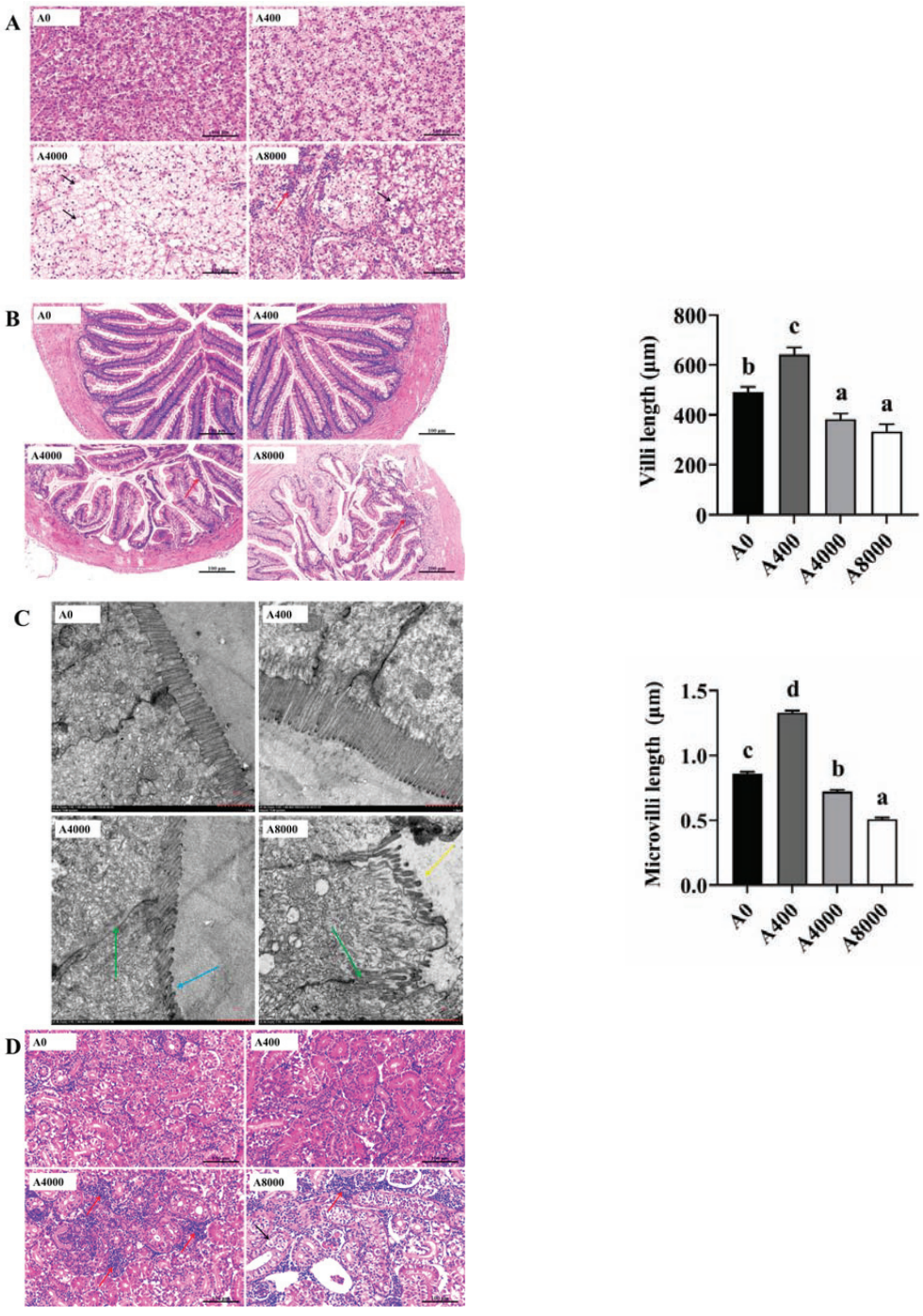

Figure 6. Effects of dietary AMP on histologic morphology of the liver (**A**), intestine (**B**,**C**), and kidney (**D**). Red row: inflammatory cell infiltration; black row: cell edema; green row: tight junctions; blue row: microvilli shrunk; yellow row: microvilli shed. Data are shown as mean ± SEM (n = 6). Different lowercase letters represent significant differences among all groups ($p < 0.05$).

4. Discussion

AMP is widely used for its antioxidant, anti-inflammatory, anti-tumor, immunopotentiator, and intestinal health maintenance benefits [8,9,11–15]. In the present study, 400 mg/kg AMP significantly promoted WGR, SGR, and FE. A similar growth promotion effect of polysaccharide additives was previously reported in tilapia [32], turbot [33], grey mullet [34], large yellow croaker [35], Asian seabass [36], and shrimp [37]. However, in this study, no significant difference in growth was found between fish with dietary AMP levels of 4000 mg/kg and 8000 mg/kg. These results are consistent with those on *Aloe vera* polysaccharide supplementation in African catfish [38], which might be due to higher feed additive levels affecting intestinal morphology, feed digestibility, and absorption [39,40].

ROS are active oxidants or free radicals produced by molecular oxygen gain electrons [41]. ROS can cause oxidative stress and damage to fish tissues, while antioxidant enzymes, such as SOD and GPx, can reduce ROS to protect the tissues from injury [42,43]. In the present study, 400 mg/kg dietary AMP increased the SOD activity and reduced the content of MDA and ROS in the liver. This indicates that AMP supplementation at a dosage of 400 mg/kg could increase antioxidant defense in largemouth bass. These results are consistent with those on other polysaccharide additives including *Astragalus* polysaccharide [44], *Porphyra yezoensis* polysaccharide [45], and fucoidan [46] supplementation in fish. Nrf2 can promote the expression of antioxidant-related genes after entering the nucleus, while Keap1 is a negative regulator of Nrf2 through ubiquitination and degradation and prevents Nrf2 from entering the nucleus [47]. The Nrf2 signaling pathway can regulate the expression of antioxidant-related genes and affect the antioxidant defense ability of shrimp and fish [48,49]. In this study, 400 mg/kg AMP supplementation significantly increased the expression of Nrf2 in the liver while inhibiting the expression of Keap1. Correspondingly, *sod* and *gpx* gene expression was also enhanced by 400 mg/kg AMP. Similarly, polysaccharide additives can enhance antioxidant defense in carp and tilapia by activating the Nrf2 signaling pathway [50,51]. However, the Nrf2 decreased in fish fed a diet supplemented with 4000 and 8000 mg/kg AMP, accompanied with a decrease in *sod* and *gpx* gene expression compared to 400 mg/kg AMP supplementation group. Consistent with this, the gene expression levels of nuclear factor erythroid 2-related factor 2 (*nrf2*), *sod*, and *gpx* were decreased in *Labeo rohita* fed diets supplemented with 100 mg/kg ulvan [52].

Histological analysis can reveal the functional mechanism of aquatic additives [53,54]. Here, the liver tissue was intact in the 400 mg/kg AMP supplementation group, while cell edema, nucleus disappearance, and cytoplasmic vacuolation accompanied by inflammatory cell infiltration occurred in the 4000 and 8000 mg/kg AMP supplementation groups. These results indicate that high dose (4000 and 8000 mg/kg) AMP causes severe liver injury in largemouth bass, consistent with the liver damage induced by ahigh dose of additives in common carp [18] and tilapia [55]. ALT and AST in plasma are considered as an index of liver injury in fish, which can indicate the function of the liver [56]. We found a significant increase in plasma AST and ALT in the 8000 mg/kg AMP supplementation group, which indicates that liver damage was induced by a high dose of AMP. Consistent with this, high levels of dietary histamine increased the plasma ALT and AST as well as caused hepatic injuries in yellow catfish [57]. In zebrafish (*Danio rerio*), increased villi length and surface area promote nutrient absorption [58]. Polysaccharides can also promote intestinal cell proliferation [59]. Increased length and width of intestinal microvilli promote feed digestion and absorption in Nile tilapia [60]. In the present study, the length of villi and microvilli was significantly increased in the 400 mg/kg AMP supplementation group, and this implies that nutrient absorption was increased. Supported by studies on Nile tilapia [61] and banana shrimp [62], the villus surface area and villus length and width as well as growth performance can be promoted by polysaccharide additive supplementation. However, damage to the intestinal wall and tight junctions, as well as the shrinkage and reduction in villi and microvilli, in the 4000 and 8000 mg/kg AMP supplementation groups indicates the toxic effects caused by the high concentrations of AMP on largemouth bass. Similar damaged intestinal histological morphology induced by a high dose of additives

was also observed in Nile tilapia and Pacific white shrimp [17,63]. The excessive use of additives can be harmful to the kidney of fish [64,65]. Consistent with the results in the liver and intestine, tissue damage in the kidney accompanied by inflammatory cell infiltration occurred when dietary AMP levels exceeded 4000 mg/kg. These results indicate that damaged tissue integrity induced by a high dose of AMP might be the reason for reduced feed utilization and unaltered growth in these groups [66].

Inflammation occurs when innate immune cells detect infection or tissue injury [67,68]. The pro-inflammatory cytokine *tnfα* is mainly secreted by macrophages that can stimulate the secretion of interleukin-1 [69]. The anti-inflammatory cytokine *tgfβ* can inhibit the secretion of *tnfα* [70]. NF-κB (the protein translated by *nfκb* gene) activation usually induces inflammatory cytokines and adhesion molecules, which leads to the recruitment of leukocytes to inflammation sites. I-κB (the protein translated by *iκb* gene) is an inhibitor of NF-κB that promotes the degradation of NF-κB [71]. In the 400 mg/kg AMP supplementation group, the anti-inflammatory cytokine *tgfβ* was significantly increased, suggesting that AMP could enhance an anti-inflammatory response in largemouth bass. Other polysaccharides, such as *Astragalus* polysaccharide [72], *Rehmannia glutinosa* polysaccharide [73], and sulphated polysaccharide [74], also exert anti-inflammatory effects on fish. However, the expression levels of *tnfα* and *nfκb* in the liver were increased by 4000 and 8000 mg/kg AMP supplementation, while the *iκb* and *tgfβ* mRNA levels were decreased in the present study. This indicates that an inflammatory response was induced by a high dose of AMP. A similar result was found in carp [7]. Expression of pro-inflammatory cytokines, such as *tnfα*, can be promoted by high levels of HP-02 polysaccharide and induce an inflammatory response. The expression of pro-inflammatory cytokines (*tnfα*, *nfκb*) was increased and that of anti-inflammatory cytokines (*tgfβ*, *iκb*) was decreased in the intestine and kidney of fish fed with diet supplemented with 4000 or 8000 mg/kg AMP. The inflammatory cell infiltrations found in the liver, intestine, and kidney of fish fed with diet supplemented with 4000 and 8000 mg/kg AMP imply that inflammation was induced by a high dose of AMP in largemouth bass.

5. Conclusions

Dietary supplementation with 400 mg/kg AMP could promote the growth performance, antioxidant capacity, and intestinal health of largemouth bass. However, high doses (4000 mg/kg and 8000 mg/kg) of AMP led to decreases in antioxidant-related gene (*sod*, *gpx*) expression, accumulation of oxidative stress metabolites (ROS, MDA), inflammation inducement (upregulated pro-inflammatory cytokines *tnfα* and *nfκb*; downregulated anti-inflammatory cytokines *tgfβ* and *iκb*), and tissue damages. Villi and microvilli shrank in the intestine and cell edema occurred in the liver and kidney. Thus, the safe tolerance margin of AMP supplement for largemouth bass was 400–4000 mg/kg. This study provides valuable information for possible AMP use in aquaculture.

Author Contributions: Methodology, Validation, Writing-original draft, B.D.; Data curation, Formal analysis, L.W., Q.C. and W.X.; Investigation, D.L.; Supervision, D.H., H.L. and X.Z.; Methodology, Y.Y.; Funding acquisition, Supervision, S.X.; Conceptualization, Funding acquisition, Supervision, Writing-review & editing, J.J. All authors have read and agreed to the published version of the manuscript.

Funding: This work was financially supported by the National Natural Science Foundation of China (32122089; U19A2041; 31972805), the National Key R&D Program of China (2018YFD0900605; 2019YFD0900200), the Strategic Priority Research Program of Chinese Academy of Sciences (XDA24010206) and the China Agriculture Research System of MOF and MARA (CARS-45-09).

Institutional Review Board Statement: All animal care and experimental procedures were approved by the Experimental Animal Ethics Committee of Institute of Hydrobiology, Chinese Academy of Sciences (approval ID: IHB20140724, approval date: 24 July 2014).

Informed Consent Statement: Not applicable.

Data Availability Statement: Data are contained within the article.

Acknowledgments: The authors thank Guanghan Nie for his technical support with the research system.

Conflicts of Interest: The authors declare no conflict of interest. Dinggang Li belongs to Baoding Jizhong Pharmaceutical Co., Ltd. The company had no role in the design of the study; in the collection, analyses, or interpretation of data; in the writing of the manuscript, or in the decision to publish the results.

References

1. FAO (Food and Agriculture Organization of the United Nations). *The State of World Fisheries and Aquaculture*; FAO Fisheries and Aquaculture Department: Rome, Italy, 2020.
2. Vazquez-Salgado, L.; Olveira, J.; Dopazo, C.; Bandin, I. Effect of rearing density on nervous necrosis virus infection in Senegalese sole (*Solea senegalensis*). *J. Fish Dis.* **2021**, *44*, 2003–2012. [CrossRef] [PubMed]
3. Yadav, M.; Khati, A.; Chauhan, R.; Arya, P.; Semwal, A. A review on feed additives used in fish diet. *Int. J. Environ. Agric. Biotechnol.* **2021**, *6*, 2. [CrossRef]
4. Yin, G.; Li, W.; Lin, Q.; Lin, X.; Lin, J.; Zhu, Q.; Jiang, H.; Huang, Z. Dietary administration of laminarin improves the growth performance and immune responses in *Epinephelus coioides*. *Fish Shellfish. Immunol.* **2014**, *41*, 402–406. [CrossRef]
5. Chen, G.; Liu, B.; Chen, J.; Liu, H.; Tan, B.; Dong, X.; Yang, Q.; Chi, S.; Zhang, S.; Yao, M. Supplementing sulfate-based alginate polysaccharide improves pacific white shrimp (*Litopenaeus vannamei*) fed fishmeal replacement with cottonseed protein concentrate: Effects on growth, intestinal health, and disease resistance. *Aquac. Nutr.* **2022**, *2022*, 7132362. [CrossRef]
6. Chang, Z.; Ge, Q.; Sun, M.; Wang, Q.; Lv, H.; Li, J. Immune responses by dietary supplement with *Astragalus* polysaccharides in the pacific white shrimp, *Litopenaeus vannamei*. *Aquac. Nutr.* **2018**, *24*, 702–711. [CrossRef]
7. Feng, J.; Chang, X.; Zhang, Y.; Lu, R.; Meng, X.; Song, D.; Yan, X.; Zhang, J.; Nie, G. Characterization of a polysaccharide HP-02 from honeysuckle flowers and its immunoregulatory and anti-*Aeromonas hydrophila* effects in *Cyprinus carpio* L. *Int. J. Biol. Macromol.* **2019**, *140*, 477–483. [CrossRef] [PubMed]
8. Feng, Y.; Ji, H.; Dong, X.; Liu, A. An alcohol-soluble polysaccharide from *Atractylodes macrocephala* Koidz induces apoptosis of Eca-109 cells. *Carbohydr. Polym.* **2019**, *226*, 115136. [CrossRef]
9. Feng, Y.; Ji, H.; Dong, X.; Yu, J.; Liu, A. Polysaccharide extracted from *Atractylodes macrocephala* Koidz (PAMK) induce apoptosis in transplanted H22 cells in mice. *Int. J. Biol. Macromol.* **2019**, *137*, 604–611. [CrossRef]
10. Yang, L.; Yu, H.; Hou, A.; Man, W.; Wang, S.; Zhang, J.; Wang, X.; Zheng, S.; Jiang, H.; Kuang, H. A review of the ethnopharmacology, phytochemistry, pharmacology, application, quality control, processing, toxicology, and pharmacokinetics of the dried rhizome of *Atractylodes macrocephala*. *Front. Pharmacol.* **2021**, *12*, 727154. [CrossRef]
11. Li, B.; Li, W.; Tian, Y.; Guo, S.; Huang, Y.; Xu, D.; Cao, N. Polysaccharide of *Atractylodes macrocephala* Koidz enhances cytokine secretion by stimulating the TLR4-MyD88-NF-κB signaling pathway in the mouse spleen. *J. Med. Food* **2019**, *22*, 937–943. [CrossRef]
12. Guo, S.; Li, W.; Chen, F.; Yang, S.; Huang, Y.; Tian, Y.; Xu, D.; Cao, N. Polysaccharide of *Atractylodes macrocephala* Koidz regulates LPS-mediated mouse hepatitis through the TLR4-MyD88-NFκB signaling pathway. *Int. Immunopharmacol.* **2021**, *98*, 107692. [CrossRef] [PubMed]
13. Li, W.; Zhou, X.; Xu, S.; Cao, N.; Li, B.; Chen, W.; Yang, B.; Yuan, M.; Xu, D. Lipopolysaccharide-induced splenic ferroptosis in goslings was alleviated by polysaccharide of *Atractylodes macrocephala* Koidz associated with pro-inflammatory factors. *Poult. Sci.* **2022**, *101*, 101725. [CrossRef] [PubMed]
14. Hou, R.; Li, Q.; Liu, J.; Hu, Y. Selenylation modification of *Atractylodes macrocephala* polysaccharide and evaluation of antioxidant activity. *Adv. Polym. Technol.* **2019**, *2019*, 8191385. [CrossRef]
15. Wang, P.; Zhao, Y.; Xu, R.; Zhang, X.; Sun, Y.; Feng, Q.; Li, Z.; Xu, J.; Xie, Z.; Zhang, Z.; et al. Sesquiterpene lactams and lactones with antioxidant potentials from *Atractylodes macrocephala* discovered by molecular networking strategy. *Front. Nutr.* **2022**, *9*, 865257. [CrossRef] [PubMed]
16. Zhou, Z.; Pan, S.; Wu, S. Modulation of the growth performance, body composition and nonspecific immunity of crucian carp *Carassius auratus* upon *Enteromorpha prolifera* polysaccharide. *Int. J. Biol. Macromol.* **2020**, *147*, 29–33. [CrossRef]
17. Pierri, B.; Silva, A.; Cadorin, D.; Ferreira, T.; Mourino, J.; Filer, K.; Pettigrew, J.; Fracalossi, D. Different levels of organic trace minerals in diets for Nile tilapia juveniles alter gut characteristics and body composition, but not growth. *Aquac. Nutr.* **2021**, *27*, 176–186. [CrossRef]
18. Ye, C.; Wang, E.; He, S.; Wang, K.; Geng, Y.; He, Q.; Yang, Q.; Liu, T.; Xie, H. Subchronic toxicity and hepatocyte apoptosis of dietary olaquindox in common carp (*Cyprinus carpio*). *Ecotoxicol. Environ. Saf.* **2018**, *164*, 131–139. [CrossRef]
19. Wu, Z.; Pang, S.; Chen, X.; Yu, Y.; Zhou, J.; Chen, X.; Pang, L. Effect of *Coriolus versicolor* polysaccharides on the hematological and biochemical parameters and protection against *Aeromonas hydrophila* in allogynogenetic crucian carp (*Carassius auratus gibelio*). *Fish Physiol. Biochem.* **2013**, *39*, 181–190. [CrossRef]
20. Ren, S.; Cai, C.; Cui, G.; Ni, Q.; Jiang, R.; Su, X.; Wang, Q.; Chen, W.; Zhang, J.; Wu, P. High dosages of pectin and cellulose cause different degrees of damage to the livers and intestines of *Pelteobagrus fulvidraco*. *Aquaculture* **2020**, *514*, 734445. [CrossRef]
21. Bureau MOAA. *2021 China Fishery Statistical Yearbook*; China Agriculture Press: Beijing, China, 2021.

22. Poudyal, S.; Pulpipat, T.; Wang, P.; Chen, S. Comparison of the pathogenicity of Francisella orientalis in Nile tilapia (*Oreochromis niloticus*), Asian seabass (*Lates calcarifer*) and largemouth bass (*Micropterus salmoides*) through experimental intraperitoneal infection. *J. Fish Dis.* **2020**, *43*, 1097–1106. [CrossRef]
23. Yi, W.; Zhang, X.; Zeng, K.; Xie, D.; Song, C.; Tam, K.; Liu, Z.; Zhou, T.; Li, W. Construction of a DNA vaccine and its protective effect on largemouth bass (*Micropterus salmoides*) challenged with largemouth bass virus (LMBV). *Fish Shellfish Immunol.* **2020**, *106*, 103–109. [CrossRef] [PubMed]
24. He, G.; Sun, H.; Liao, R.; Wei, Y.; Zhang, T.; Chen, Y.; Lin, S. Effects of herbal extracts (*Foeniculum vulgare* and *Artemisia annua*) on growth, liver antioxidant capacity, intestinal morphology and microorganism of juvenile largemouth bass, *Micropterus salmoides*. *Aquac. Rep.* **2022**, *23*, 101081. [CrossRef]
25. Yin, P.; Xie, S.; Zhuang, Z.; Fang, H.; Tian, L.; Liu, Y.; Niu, J. Chlorogenic acid improves health in juvenile largemouth bass (*Micropterus salmoides*) fed high-fat diets: Involvement of lipid metabolism, antioxidant ability, inflammatory response, and intestinal integrity. *Aquaculture* **2021**, *545*, 737169. [CrossRef]
26. Chen, W.; Chang, K.; Chen, J.; Zhao, X.; Gao, S. Dietary sodium butyrate supplementation attenuates intestinal inflammatory response and improves gut microbiota composition in largemouth bass (*Micropterus salmoides*) fed with a high soybean meal diet. *Fish Physiol. Biochem.* **2021**, *47*, 1805–1819. [CrossRef] [PubMed]
27. AOAC, Association of Official Analytical Chemists. Official Methods of Analysis. *AOAC* **2006**, *16*, 0066-0961X.
28. Wu, L.; Xu, W.; Li, H.; Dong, B.; Geng, H.; Jin, J.; Han, D.; Liu, H.; Zhu, X.; Yang, Y. Vitamin C attenuates oxidative stress, inflammation, and apoptosis induced by acute hypoxia through the Nrf2/Keap1 signaling pathway in gibel carp (*Carassius gibelio*). *Antioxidants* **2022**, *11*, 935. [CrossRef]
29. Farnese, F.; Oliveira, J.; Paiva, E.; Menezes-Silva, P.; da Sliva, A.; Campos, F.; Ribeiro, C. The involvement of nitric oxide in integration of plant physiological and ultrastructural adjustments in response to arsenic. *J. Front. Plant Sci.* **2017**, *8*, 516. [CrossRef]
30. Pfaffl, M. A new mathematical model for relative quantification in real-time RT–PCR. *Nucleic Acids Res.* **2001**, *29*, e45. [CrossRef]
31. Wu, L.; Li, H.; Xu, W.; Dong, B.; Jin, J.; Han, D.; Zhu, X.; Yang, Y.; Liu, H.; Xie, S. Dissimilar regulation of glucose and lipid metabolism by leptin in two strains of gibel carp (*Carassius gibelio*). *Br. J. Nutr.* **2021**, *125*, 1215–1229. [CrossRef]
32. Van Doan, H.; Tapingkae, W.; Moonmanee, T.; Seepai, A. Effects of low molecular weight sodium alginate on growth performance, immunity, and disease resistance of tilapia, *Oreochromis niloticus*. *Fish Shellfish Immunol.* **2016**, *55*, 186–194. [CrossRef]
33. Cui, L.; Xu, W.; Ai, Q.; Wang, D.; Mai, K. Effects of dietary chitosan oligosaccharide complex with rare earth on growth performance and innate immune response of turbot, *Scophthalmus maximus* L. *Aquac. Res.* **2013**, *44*, 683–690. [CrossRef]
34. Akbary, P.; Aminikhoei, Z. Effect of water-soluble polysaccharide extract from the green alga *Ulva rigida* on growth performance, antioxidant enzyme activity, and immune stimulation of grey mullet *Mugil cephalus*. *J. Appl. Phycol.* **2018**, *30*, 1345–1353. [CrossRef]
35. Liu, Y.; Miao, Y.; Xu, N.; Ding, T.; Cui, K.; Chen, Q.; Zhang, J.; Fang, W.; Mai, K.; Ai, Q. Effects of dietary *Astragalus* polysaccharides (APS) on survival, growth performance, activities of digestive enzyme, antioxidant responses and intestinal development of large yellow croaker (*Larimichthys crocea*) larvae. *Aquaculture* **2020**, *517*, 734752. [CrossRef]
36. Yu, W.; Yang, Y.; Zhou, Q.; Huang, X.; Huang, Z.; Li, T.; Wu, Q.; Zhou, C.; Ma, Z.; Lin, H. Effects of dietary *Astragalus* polysaccharides on growth, health and resistance to *Vibrio harveyi* of *Lates calcarifer*. *Int. J. Biol. Macromol.* **2022**, *207*, 850–858. [CrossRef] [PubMed]
37. Traifalgar, R.; Kira, H.; Tung, H.; Michael, F.; Laining, A.; Yokoyama, S.; Ishikawa, M.; Koshio, S.; Serrano, A.; Corre, V. Influence of dietary fucoidan supplementation on growth and immunological response of juvenile *Marsupenaeus japonicus*. *J. World Aquac. Soc.* **2010**, *41*, 235–244. [CrossRef]
38. Gabriel, N.; Wilhelm, M.; Habte-Tsion, H.; Chimwamurombe, P.; Omoregie, E.; Iipinge, L.; Shimooshili, K. Effect of dietary *Aloe vera* polysaccharides supplementation on growth performance, feed utilization, hemato-biochemical parameters, and survival at low pH in African catfish (*Clarias gariepinus*) fingerlings. *Int. Aquat. Res.* **2019**, *11*, 57–72. [CrossRef]
39. Gabriel, N.; Qiang, J.; Ma, X.; Xu, P.; Nakwaya, D. Effects of dietary *Aloe vera* crude extracts on digestive enzyme activities and muscle proximate composition of GIFT tilapia juveniles. *South Afr. J. Anim. Sci.* **2017**, *47*, 904–913. [CrossRef]
40. Heidarieh, M.; Mirvaghefi, A.; Sepahi, A.; Sheikhzadeh, N.; Alishahbazfar, A.; Akbari, M. Effects of dietary *Aloe vera* on growth performance, skin and gastrointestine morphology in rainbow trout (*Oncorhynchus mykiss*). *Turk. J. Fish. Aquat. Sci.* **2013**, *13*, 367–373. [CrossRef]
41. Bal, A.; Panda, F.; Pati, S.; Das, K.; Agrawal, P.; Paital, B. Modulation of physiological oxidative stress and antioxidant status by abiotic factors especially salinity in aquatic organisms. *Comp. Biochem. Physiol. Part C Toxicol. Pharmacol.* **2021**, *241*, 108971. [CrossRef]
42. Loro, V.; Jorge, M.; da Silva, K.; Wood, C. Oxidative stress parameters and antioxidant response to sublethal waterborne zinc in a euryhaline teleost *Fundulus heteroclitus*: Protective effects of salinity. *Aquat. Toxicol.* **2012**, *110*, 187–193. [CrossRef]
43. Liu, W.; Zhao, C.; Wang, P.; Wang, S.; Lin, H.; Qiu, L. The response of glutathione peroxidase 1 and glutathione peroxidase 7 under different oxidative stresses in black tiger shrimp, *Penaeus monodon*. *Comp. Biochem. Physiol. Part B Biochem. Mol. Biol.* **2018**, *217*, 1–13. [CrossRef] [PubMed]
44. Zahran, E.; Risha, E.; AbdelHamid, F.; Mahgoub, H.; Ibrahim, T. Effects of dietary *Astragalus* polysaccharides (APS) on growth performance, immunological parameters, digestive enzymes, and intestinal morphology of Nile tilapia (*Oreochromis niloticus*). *Fish Shellfish Immunol.* **2014**, *38*, 149–157. [CrossRef] [PubMed]

45. Chen, L.; Zhang, Y. The growth performance and nonspecific immunity of juvenile grass carp (*Ctenopharyngodon idella*) affected by dietary *Porphyra yezoensis* polysaccharide supplementation. *Fish Shellfish. Immunol.* **2019**, *87*, 615–619. [CrossRef] [PubMed]
46. Yang, Q.; Yang, R.; Li, M.; Zhou, Q.; Liang, X.; Elmada, Z. Effects of dietary fucoidan on the blood constituents, anti-oxidation and innate immunity of juvenile yellow catfish (*Pelteobagrus fulvidraco*). *Fish Shellfish Immunol.* **2014**, *41*, 264–270. [CrossRef]
47. Kobayashi, M.; Yamamoto, M. Molecular mechanisms activating the Nrf2-Keap1 pathway of antioxidant gene regulation. *Antioxid. Redox Signal.* **2005**, *7*, 385–394. [CrossRef]
48. Huang, Y.; Li, Q.; Yuan, Y.; Zhang, Z.; Jiang, B.; Yang, S.; Jian, J. Silencing of Nrf2 in *Litopenaeus vannamei*, decreased the antioxidant capacity, and increased apoptosis and autophagy. *Fish Shellfish Immunol.* **2022**, *122*, 257–267. [CrossRef]
49. Yu, X.; Wu, Y.; Deng, M.; Liu, Y.; Wang, S.; He, X.; Allaire-Leung, M.; Wan, J.; Zou, Y.; Yang, C. Tetracycline antibiotics as PI3K inhibitors in the Nrf2-mediated regulation of antioxidative stress in zebrafish larvae. *Chemosphere* **2019**, *226*, 696–703. [CrossRef]
50. Yu, Z.; Zhao, L.; Zhao, J.; Xu, W.; Guo, Z.; Zhang, A.; Li, M. Dietary *Taraxacum mongolicum* polysaccharide ameliorates the growth, immune response, and antioxidant status in association with NF-κB, Nrf2 and TOR in Jian carp (*Cyprinus carpio* var. Jian). *Aquaculture* **2022**, *547*, 737522. [CrossRef]
51. Mohammadi, G.; Karimi, A.; Hafezieh, M.; Dawood, M.; Abo-Al-Ela, H. Pistachio hull polysaccharide protects Nile tilapia against LPS-induced excessive inflammatory responses and oxidative stress, possibly via TLR2 and Nrf2 signaling pathways. *Fish Shellfish Immunol.* **2022**, *121*, 276–284. [CrossRef]
52. Harikrishnan, R.; Devi, G.; Van Doan, H.; Balasundaram, C.; Arockiaraj, J.; Jagruthi, C. Efficacy of ulvan on immune response and immuno-antioxidant gene modulation in *Labeo rohita* against columnaris disease. *Fish Shellfish Immunol.* **2021**, *117*, 262–273. [CrossRef]
53. Brum, A.; Cardoso, L.; Chagas, E.; Chaves, F.; Mourino, J.; Martins, M. Histological changes in nile tilapia fed essential oils of clove basil and ginger after challenge with *Streptococcus agalactiae*. *Aquac.* **2018**, *490*, 98–107. [CrossRef]
54. Kracizy, R.; Brazao, C.; Viott, A.; Ribeiro, K.; Koppenol, A.; Dos Santos, A.; Ballester, E. Evaluation of aflatoxin and fumonisin in the diet of pacific white shrimp (*Litopenaeus vannamei*) on their performance and health. *Aquaculture* **2021**, *544*, 737051. [CrossRef]
55. Qiang, J.; Khamis, O.; Jiang, H.; Cao, Z.; He, J.; Tao, Y.; Xu, P.; Bao, J. Effects of dietary supplementation with apple peel powder on the growth, blood and liver parameters, and transcriptome of genetically improved farmed tilapia (GIFT, *Oreochromis niloticus*). *PLoS ONE* **2019**, *14*, e0224995. [CrossRef]
56. Miandare, H.; Niknejad, M.; Shabani, A.; Safari, R. Exposure of Persian sturgeon (*Acipenser persicus*) to cadmium results in biochemical, histological and transcriptional alterations. *Comp. Biochem. Physiol. Part C Toxicol. Pharmacol.* **2016**, *181*, 1–8. [CrossRef] [PubMed]
57. Li, W.; Pan, X.; Cheng, W.; Cheng, Y.; Yin, Y.; Chen, J.; Xu, G.; Xie, L. Serum biochemistry, histology and transcriptomic profile analysis reflect liver inflammation and damage following dietary histamine supplementation in yellow catfish (*Pelteobagrus fulvidraco*). *Fish Shellfish Immunol.* **2018**, *77*, 83–90. [CrossRef]
58. Molinari, G.; Wojno, M.; McCracken, V.; Kwasek, K. The use of dipeptide supplementation as a means of mitigating the negative effects of dietary soybean meal on zebrafish *Danio rerio*. *Comp. Biochem. Physiol. Part A Mol. Integr. Physiol.* **2021**, *257*, 110958. [CrossRef]
59. Qiu, H.; Veeraperumal, S.; Lv, J.; Wu, T.; Zhang, Z.; Zeng, Q.; Liu, Y.; Chen, X.; Aweya, J.; Cheong, K. Physicochemical properties and potential beneficial effects of porphyran from *Porphyra haitanensis* on intestinal epithelial cells. *Carbohydr. Polym.* **2020**, *246*, 116626. [CrossRef]
60. El-Sayed, A.; Tammam, M.; Makled, S. Lecithin-containing bioemulsifier boosts growth performance, feed digestion and absorption and immune response of adult nile tilapia (*Oreochromis niloticus*). *Aquac. Nutr.* **2021**, *27*, 757–770. [CrossRef]
61. Mahgoub, H.; El-Adl, M.; Ghanem, H.; Martyniuk, C. The effect of fucoidan or potassium permanganate on growth performance, intestinal pathology, and antioxidant status in Nile tilapia (*Oreochromis niloticus*). *Fish Physiol. Biochem.* **2020**, *46*, 2109–2131. [CrossRef]
62. Liu, W.; Zhou, S.; Balasubramanian, B.; Zeng, F.; Sun, C.; Pang, H. Dietary seaweed (*Enteromorpha*) polysaccharides improves growth performance involved in regulation of immune responses, intestinal morphology and microbial community in banana shrimp *Fenneropenaeus merguiensis*. *Fish Shellfish Immunol.* **2020**, *104*, 202–212. [CrossRef]
63. Xie, S.; Zheng, L.; Wan, M.; Niu, J.; Liu, Y.; Tian, L. Effect of deoxynivalenol on growth performance, histological morphology, anti-oxidative ability and immune response of juvenile pacific white shrimp, *Litopenaeus vannamei*. *Fish Shellfish Immunol.* **2018**, *82*, 442–452. [CrossRef] [PubMed]
64. Umamaheswari, S.; Karthika, P.; Suvenitha, K.; Kadirvelu, K.; Ramesh, M. Dose-dependent molecular responses of *Labeo rohita* to triphenyl phosphate. *Chem. Res. Toxicol.* **2021**, *34*, 2500–2511. [CrossRef] [PubMed]
65. Berntssen, M.; Betancor, M.; Caballero, M.; Hillestad, M.; Rasinger, J.; Hamre, K.; Sele, V.; Amlund, H.; Ornsrud, R. Safe limits of selenomethionine and selenite supplementation to plant-based Atlantic salmon feeds. *Aquaculture* **2018**, *495*, 617–630. [CrossRef]
66. Gan, L.; Wu, P.; Feng, L.; Jiang, W.; Liu, Y.; Jiang, J.; Kuang, S.; Tang, L.; Zhou, X. Erucic acid inhibits growth performance and disrupts intestinal structural integrity of on-growing grass carp (*Ctenopharyngodon idella*). *Aquaculture* **2019**, *513*, 734437. [CrossRef]
67. Newton, K.; Dixit, V. Signaling in innate immunity and inflammation. *Cold Spring Harb. Perspect. Biol.* **2012**, *4*, a006049. [CrossRef]
68. Kotas, M.; Medzhitov, R. Homeostasis, inflammation, and disease susceptibility. *Cell* **2015**, *160*, 816–827. [CrossRef]

69. Wang, T.; He, C. Pro-inflammatory cytokines: The link between obesity and osteoarthritis. *Cytokine Growth Factor Rev.* **2018**, *44*, 38–50. [CrossRef]
70. Shah, R.; Hurley, C.; Posch, P. A molecular mechanism for the differential regulation of TGF-β1 expression due to the common SNP− 509C-T (c.− 1347C> T). *Hum. Genet.* **2006**, *120*, 461–469. [CrossRef]
71. Hoesel, B.; Schmid, J. The complexity of NF-κB signaling in inflammation and cancer. *Mol. Cancer* **2013**, *12*, 1–15. [CrossRef]
72. Sun, Y.; Wang, X.; Zhou, H.; Mai, K.; He, G. Dietary *Astragalus* polysaccharides ameliorates the growth performance, antioxidant capacity and immune responses in turbot (*Scophthalmus maximus* L.). *Fish Shellfish Immunol.* **2020**, *99*, 603–608. [CrossRef]
73. Feng, J.; Cai, Z.; Zhang, X.; Chen, Y.; Chang, X.; Wang, X.; Qin, C.; Yan, X.; Ma, X.; Zhang, J. The Effects of oral *Rehmannia glutinosa* polysaccharide administration on immune responses, antioxidant activity and resistance against *Aeromonas hydrophila* in the common carp, *Cyprinus carpio* L. *Front. Immunol.* **2020**, *11*, 904. [CrossRef] [PubMed]
74. Zhao, W.; Fang, H.H.; Liu, Z.Z.; Chen, J.M.; Zhang, C.W.; Gao, B.Y.; Niu, J. Responses in growth performance, enzymatic activity, immune function and liver health after dietary supplementation of *Porphyridium* sp. in juvenile golden pompano (*Trachinotus ovatus*). *Aquac. Nutr.* **2021**, *27*, 679–690. [CrossRef]

antioxidants

MDPI

Article

Hypothermia-Mediated Apoptosis and Inflammation Contribute to Antioxidant and Immune Adaption in Freshwater Drum, *Aplodinotus grunniens*

Jianxiang Chen [1,2], Hongxia Li [1,2], Pao Xu [1,2], Yongkai Tang [1,2], Shenyan Su [1,2], Guangxiang Liu [1], Ningyuan Wu [1], Miaomiao Xue [1], Fan Yu [1,2], Wenrong Feng [1,2], Changyou Song [1,2,*] and Haibo Wen [1,2,*]

[1] Wuxi Fisheries College, Nanjing Agricultural University, Wuxi 214081, China
[2] Key Laboratory of Freshwater Fisheries and Germplasm Resources Utilization, Ministry of Agriculture and Rural Affairs, Freshwater Fisheries Research Center, Chinese Academy of Fishery Sciences, Wuxi 214081, China
* Correspondence: songchangyou@ffrc.cn (C.S.); wenhb@ffrc.cn (H.W.)

Abstract: Hypothermia-exposure-induced oxidative stress dysregulates cell fate and perturbs cellular homeostasis and function, thereby disturbing fish health. To evaluate the impact of hypothermia on the freshwater drum (*Aplodinotus grunniens*), an 8-day experiment was conducted at 25 °C (control group, Con), 18 °C (LT18), and 10 °C (LT10) for 0 h, 8 h, 1 d, 2 d, and 8 d. Antioxidant and non-specific immune parameters reveal hypothermia induced oxidative stress and immunosuppression. Liver ultrastructure alterations indicate hypothermia induced mitochondrial enlargement, nucleoli aggregation, and lipid droplet accumulation under hypothermia exposure. With the analysis of the transcriptome, differentially expressed genes (DEGs) induced by hypothermia were mainly involved in metabolism, immunity and inflammation, programmed cell death, and disease. Furthermore, the inflammatory response and apoptosis were evoked by hypothermia exposure in different immune organs. Interactively, apoptosis and inflammation in immune organs were correlated with antioxidation and immunity suppression induced by hypothermia exposure. In conclusion, these results suggest hypothermia-induced inflammation and apoptosis, which might be the adaptive mechanism of antioxidation and immunity in the freshwater drum. These findings contribute to helping us better understand how freshwater drum adjust to hypothermia stress.

Keywords: hypothermia; oxidative stress; immunity; inflammation; apoptosis; freshwater drum

Citation: Chen, J.; Li, H.; Xu, P.; Tang, Y.; Su, S.; Liu, G.; Wu, N.; Xue, M.; Yu, F.; Feng, W.; et al. Hypothermia-Mediated Apoptosis and Inflammation Contribute to Antioxidant and Immune Adaption in Freshwater Drum, *Aplodinotus grunniens*. *Antioxidants* **2022**, *11*, 1657. https://doi.org/10.3390/antiox11091657

Academic Editor: Erchao Li

Received: 19 July 2022
Accepted: 23 August 2022
Published: 26 August 2022

1. Introduction

Water temperature is one of the essential external factors for aquatic animals [1]. Temperature fluctuations beyond the optimum range can trigger a variety of stress reactions in aquatic species, including metabolic problems, physiological malfunction, organ and cell damage, and even death [2,3]. In regard to global climate change and variations in seasonal temperatures, the effect of temperature fluctuations on biological systems is a crucial topic. Due to an increase in climate unpredictability, cold snaps are occurring more frequently and with greater severity [4,5]. Furthermore, the seasonal differences in water temperatures that fish experience during a year might be very substantial. The water temperature in China changes a lot from season to season. For example, the water in Wuxi may get as hot as 30 °C in the summer and as cold as almost 0 °C in the winter. Each year, this has led to a significant economic loss for the aquaculture industry. Therefore, investigating the mechanism of the fish's responses to low temperatures can contribute to the development of aquaculture.

Since fish are poikilothermic vertebrates, hypothermia exposure can affect their body temperature, which causes a variety of physiological reactions. Hypothermia exposure can result in increases in endogenous reactive oxygen species (ROS) [6]. The imbalance between

ROS accumulation and antioxidation defense induces oxidative stress [7]. Oxidative stress leads to physiological disorders, oxidative modification of the biological macromolecules, inflammation, immunosuppression, cellular death including apoptosis, and various pathological conditions as the foundation of many diseases [8–10]. Previous studies found that both acute and chronic cold stress could induce oxidative stress in fish tissues [11,12]. It has been reported that acute cold exposure induced high oxidative stress in zebrafish liver, which may lead to mortality [13], and long-term cold exposure also caused oxidative stress in tissues of *Hoplosternum littorale* [14]. Meanwhile, antioxidant defense mechanisms have developed in aquatic animals to cope with hypothermia exposure. The antioxidant enzymes including superoxide dismutase (SOD), catalase (CAT), and glutathione peroxidase (GSH-Px) make up the majority of this system and are crucial for regulating the redox status of cells [15]. Besides the antioxidant system, immune processes are crucial for fish to adjust to hypothermia exposure [16]. Alcorn et al. suggested that the immune apparatus of sockeye salmon reared at 8 °C relied more heavily on the innate immune response [17]. The innate immune system is the first boundary of host defense and plays a vital role in protecting organisms from pathogens and maintaining a physiological steady state under adverse stress conditions [18]. Hypothermia exposure suppresses the innate immune system of fish, thereby increasing susceptibility to infection [19]. Furthermore, many studies have demonstrated that fish tissues have inflammatory reactions as a result of hypothermia [20]. Under hypothermia exposure, inflammatory reactions in tilapia seem tissue specific. The liver showed inconsistent expression of the pro-inflammatory genes such as tumor necrosis factor-α (TNF-α) and interleukin-1 (IL-1β). In addition, hypothermia exposure impairs fish defense mechanisms, causing cellular damage and elevating levels of apoptosis [21]. Apoptosis also plays a key role in the body's immune response by controlling the number of immune cells, which helps to maintain cellular homeostasis [22].

Freshwater drum (*Aplodinotus grunniens*) is one of the most widely distributed freshwater fish in North and Central America. It is the only species in the genus of *Aplodinotus* that perpetually inhabits freshwater [23]. It is characterized by its abundant nutritional value, scrumptious meat quality, non-intermuscular fishbones, and so on [24]. Therefore, the future of freshwater drum culture seems promising. With these prospects, we imported the freshwater drum larvae from the USA in 2016 and achieved a milestone in artificial farming and breeding in 2019, which provided a breakthrough for aquaculture [24]. According to past studies, freshwater drum is adaptive to water temperatures between 7 and 30 °C [25]. Moreover, as the water temperature dropped to 1 °C or lower, the mortality of juveniles rose [26]. In light of our preliminary research, as a warm-water fish, the optimum temperature range for freshwater drum should be between 18 and 26 °C. However, the winter water temperature in East-Central China is typically below 10 °C. Therefore, this experiment was conducted at 25 °C (as the control group), 18 °C, and 10 °C for 8 days to investigate the mechanism of the hypothermia response of freshwater drum by transcriptomics. To our knowledge, this study is the first to evaluate potential mechanisms of the freshwater drum response to hypothermia exposure based on alterations in antioxidants, non-specific immunity, inflammation, and apoptosis. These studies provide novel insights into how fish respond to hypothermic stress, which could contribute to the risk assessment of hypothermia in the aquatic environment.

2. Materials and Methods

2.1. Ethics Statement

This study was approved by the Animal Care and Use Committee of Nanjing Agricultural University (Nanjing, China) (WXFC 2021-0006). All animal procedures were performed according to the Guideline for the Care and Use of Laboratory Animals in China.

2.2. Experimental Animals and Rearing Conditions

The hypothermia experiment was conducted at Wuxi Fisheries College of Nanjing Agricultural University. Laboratory fish were the first-generation larvae of freshwater drum

introduced from the United States by the Freshwater Fisheries Research Center, Chinese Academy of Fishery Sciences. Freshwater drums were reared in chamber temperature-adjustable circulating water systems (specifications for φ 820 × 700 mm) consisting of 12 tanks (300 L each). Freshwater drum averaging 20.88 ± 2.75 g were randomly assigned into 9 tanks (3 tanks per group, 40 fish per tank) and were fed with fresh shrimp (3–5% of their body weight) twice a day (8:00 and 16:00). Prior to the experiment, fish were acclimated in the tanks fed at 25 °C for 30 days. In the experiment, 25 °C was set as the control group (Con), 18 °C, and 10 °C were set as the hypothermia treatments for 8 days. During the experiment, the temperature was gradually decreased from 25 °C to 18 and 10 °C at a rate of 1 °C/h. The room temperature was stabilized at 8 °C. We reduced heat dissipation by covering the mouth of the barrels with cling film. During the 8-day experiment, we cleaned up food scraps and feces daily. Throughout the experiment, dissolved oxygen was kept at >6 mg L^{-1}, pH 7.2–7.8, and NH_3 < 0.05 mg L^{-1}.

2.3. Sample Collection

Experimental samples were collected at 0 h, 8 h, 1 d, 2 d, 4 d, and 8 d. Fish from each tank were randomly sampled and anesthetized with MS-222 (100 mg L^{-1}) at each time point. Blood samples were obtained from the caudal vein and put into anticoagulation tubes. These samples were centrifuged at 5000 rpm at 4 °C for 10 min to extract the plasma. The plasma samples were stored at −80 °C for antioxidant and immune parameter measurements. Meanwhile, the sampled fish were dissected to collect the liver, gut, spleen, head kidney, and caudal kidney on ice, frozen in liquid nitrogen immediately, and stored at −80 °C for subsequent analysis.

2.4. Plasma Antioxidant Parameters and Innate Immune Index Analysis

Plasma samples of three fish from each tank were used to measure parameters including total superoxide dismutase (T-SOD), malondialdehyde (MDA), catalase (CAT), glutathione (GSH), glutathione peroxidase (GSH-Px), alkaline phosphatase (AKP), acid phosphatase (ACP), aspartate aminotransferase (AST), and alanine aminotransferase (ALT) according to the manufacturer's instructions. In detail, T-SOD was determined by the hydroxylamine method (Category No: A001-1-2), MDA was detected by the TBA method (Category No: A003-1-2), GSH was determined by a microplate method (Category No: A006-2-1), GSH-Px was determined by a colorimetric method (Category No: A005-1-2), AKP and ACP were determined by the microenzyme conjugate method (Category No: A059-2 and A060-2), and AST and ALT were determined by the Reitman method (Category No: C010-2-1 and C009-2-1). All the assay kits were purchased from Nanjing Jiancheng Bioengineering Institute, Nanjing, China.

2.5. Transmission Electron Microscopy (TEM) Observation

The livers of three fish in each group were cut into small portions (1 mm × 1 mm × 1 mm) separately and then fixed with 2.5% glutaraldehyde for 24 h before transferring to the phosphate buffer (pH 7.4, 4 °C). Then, the tissue portions were fixed in 2% osmium tetroxide in a 0.1 M phosphate buffer (4 °C) for 1.5 h before being dehydrated in ethanol with a series of different concentrations (50, 70, 90, 95, and 100%) for 15 min each and acetone for 15 min. Then, the samples were embedded in epoxy resin (Epoxy Embedding Medium Kit, Sigma) and were cut to ultra-thin sections (70 nm) using the Leica Ultra-cut UCT25 ultramicrotome. Ultra-thin sections were stained with lead citrate and uranyl acetate and then observed using a Hitachi HT7700 transmission electron microscope (Hitachi, Tokyo, Japan). Ten images were saved for each group.

2.6. Transcriptome Assembly, Functional Annotation, and Differentially Expressed Genes (DEGs) Analysis

In each group, nine liver tissues were selected to conduct the high-throughput sequence, wherein three fish in each group were randomly mixed and three biological

replicates were finally applied for RNA-seq on the Illumina Hiseq6000 platform (Majorbio Bio-pharm Technology Co., Ltd., Shanghai, China). All sequences after quality control generated contig and singleton through de novo assembly were finally connected to obtain transcripts. All transcripts were compared with seven databases including NR (NCBI non-redundant protein sequences), Nt (NCBI non-redundant nucleotide sequences), Pfam (protein families), COG (clusters of orthologous groups of proteins), Swiss-Prot (a manually annotated and reviewed protein sequence database), GO (Gene Ontology), and KEGG (Kyoto Encyclopedia of Genes and Genomes) to obtain functional annotation information. The transcriptome was quantified by RNA-Seq by expectation-maximization (RSEM) to estimate expression abundance. The differentially expressed genes (DEGs) were identified based on the fragments per kilobase of exon model per million mapped reads (FPKM). Because the sequencing depth of samples differs from each other, the absolute gene expression was normalized to the FPKM value, which made the FKPM to be the expression quantity of genes. Deseq2 was used to analyze the variation in DEGs. The criteria for screening DEGs were $p \leq 0.05$ and a difference in fold change of $\geq$2 GO and KEGG enrichments were conducted to analyze DEGs.

2.7. Validation of Differentially Expressed Genes Obtained from RNA-seq

RNA extraction analysis was conducted according to our previously established methods [27]. Total liver, spleen, gut, head kidney, and caudal kidney RNA of each group were extracted using TRIzol Reagent according to protocols (Takara, Dalian, China). Meanwhile, real-time quantitative PCR (RT-PCR) was also conducted according to our previously established methods [27] to validate the expressions of key genes involved in inflammation and apoptosis. The mRNA sequences for each gene were obtained from the freshwater drum liver transcriptome sequencing database. β-Actin was applied as an internal reference. All the primers were synthesized in Shanghai Generay Biotech Co., Ltd. (Shanghai, China). Details of primers are listed in Table 1. The primers used were designed according to the cds sequences of the genes sequenced from the transcriptome (Table S1 cDNA sequence for the genes refered in manuscript). RT-PCR was performed with SYBR Green (Takara, Dalian, China) on a Takara 800 Fast Real-Time PCR system according to the manufacturer's protocol.

Table 1. Primers and sequences referred to in the experiment.

	Primer	Sequence (5′ → 3′)	Amplification Size (bp)
TLR5	F	CGACCTCGGAGCCCAGAAT	139
	R	CAAACCAGACAATCCCACAA	
TLR2	F	GGAGAAACCAGTGGGTCAAG	103
	R	CAACAGAATGGCGACAAATAG	
TCR	F	ATCTTCCGTCTTCCAAACCA	182
	R	AGCCATTCACTCACTGCCTC	
NF-κB	F	GTGGGAGGAGGAGTTTGA	113
	R	TATCGCAGCCCATCTATG	
MHC-II	F	ATCAGCTTCTCCCTCCTCTTC	179
	R	AATCCAACAAACTTTCCCACA	
TNF-α	F	ATCGGCGTGCTGTTCAA	219
	R	GCGACCGTGGGATTTAG	
IL-1	F	GTTCTCGGCGTCTGATTGTG	193
	R	GTGAGGCGGTGCTGGTGTTC	
IL-6	F	GCCCAGGGAAGCCTGAGAAT	112
	R	GGGACATCCGTGGTTTGACG	
BH3	F	CCCAAGACGGGTTGTGAT	125
	R	CCATATTGCCCTGCAAGTAG	
Casp8	F	GGAGAACCGACTGGAGGAA	134
	R	TGTAGATGGAGCCTGTGGAAG	
Bcl2	F	CGGGTCAATAGTTGCTCCTC	224

Table 1. *Cont.*

	Primer	Sequence (5′ → 3′)	Amplification Size (bp)
	R	CCGTGGTGGAGGTGAGATAC	
Bax	F	GAGGTGGTGGAACATCTGCT	209
	R	TTGGTGGTCAGTGCCTTGTA	
Casp3	F	CTGCTACGCCTCGTTTGTCT	240
	R	TCAGCTTCCACAGGGATCTT	
β-Actin	F	AAATCGTGCGTGGACATCA	127
	R	CCGTCAGGGCAGCTCATAG	

Note: The mRNA sequences for each gene were obtained from the freshwater drum liver transcriptome sequencing database which was preserved in the lab. The primers used were designed according to the cds sequences of the genes sequenced from the transcriptome (Table S1). Primers for RT-PCR were designed using primer premier 5.0.

2.8. Correlation Analysis

Pearson's correlation test was performed to analyze the correlations between parameters or key genes. The significance threshold was set at a p-value < 0.05.

2.9. Statistical Analysis

The data of immune and antioxidative parameters were analyzed with one-way ANOVA and students' t-test by SPSS 23.0. Relative RNA expression was calculated using the $2^{-\Delta\Delta CT}$ comparative CT method, one-way ANOVA was applied to compare the statistical difference by SPSS 23.0 (IBM SPSS Statistics, Version 23.0, Armonk, NY, USA).

3. Results

3.1. Hypothermia Exposure Suppressed Antioxidant and Innate Immunity

It is universally acknowledged that hypothermia inevitably induces oxidative stress and immunosuppression. Therefore, antioxidant and innate immune parameters were measured to evaluate the effect of hypothermia exposure on the freshwater drum. In this experiment, antioxidant and innate immune parameters apart from T-SOD exhibited no significant difference at 25 °C and 18 °C with continued exposure ($p > 0.05$) (Figure 1). However, hypothermia at 10 °C dramatically impacted the antioxidant and immune capacity of the freshwater drum. Evidently, the contents of MDA and CAT remarkedly increased with the duration of hypothermia exposure and were significantly higher than the 25 °C and 18 °C groups ($p < 0.05$) (Figure 1A,D). The activity of GSH dramatically declined in the 8 h treatment group ($p < 0.05$), but subsequently elevated significantly reaching a maximum at 2 d ($p < 0.01$), and thereafter decreased to a level that did not differ significantly with the values for the 0 h group ($p > 0.05$) (Figure 1B). In addition, the levels of GSH-Px and T-SOD decreased noticeably at 10 °C and considerably dropped at 2 d in comparison with the 25 °C group ($p < 0.05$) (Figure 1C,E).

In addition, ACP and AKP were found to be significant immunological parameters. As exposure time at 10 °C increased, the levels of AKP and ACP dropped significantly ($p < 0.05$) (Figure 1F,G). Specifically, under 10 °C treatment, AKP activity decreased significantly from 2 d and was significantly lower than the 25 °C group at 8 d ($p < 0.05$) (Figure 1F). Similarly, under the 10 °C treatment, the ACP content was significantly lower than 25 °C and significantly lower than 18 °C from 2 d ($p < 0.05$) (Figure 1G).

The liver is one of the most vulnerable organs to changes in the environment. To further investigate the effect of hypothermia exposure, AST and ALT content, regarded as considerably important indicators of liver function, was measured. Unexpectedly, the activities of ALT and AST did not differ significantly but tended to decrease at 10 °C ($p > 0.05$) (Figure 1H,I).

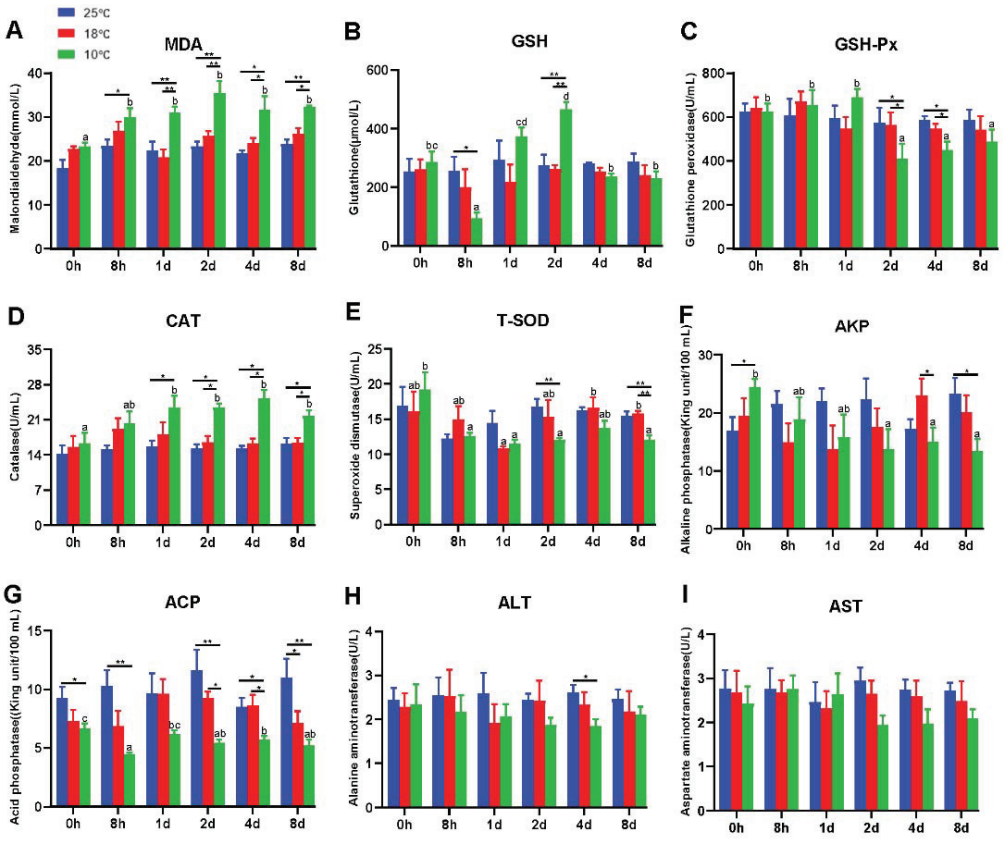

Figure 1. Hypothermia exposure suppressed antioxidant and innate immunity. (**A**), Malondialdehyde, MDA; (**B**), Glutathione, GSH; (**C**), Glutathione peroxidase, GSH-Px; (**D**), Catalase, CAT; (**E**), Total superoxide dismutase, T-SOD; (**F**), Alkaline phosphatase, AKP; (**G**), Acid phosphatase, ACP; (**H**), Alanine aminotransferase, ALT; (**I**), Aspartate aminotransferase, AST. Intra-group data were calculated by one-way ANOVA analysis with SPSS 23.0. Different superscript letters (a, b, c, d) represent the statistical difference inter-group ($p < 0.05$). Inter-group data were calculated by Students' *t*-test with SPSS 23.0. Asterisks represent the statistical differences inter-group (*, $p < 0.05$; **, $p < 0.01$). Results are expressed as mean ± SEM, $n = 9$.

3.2. Morphological Alterations in the Liver of Freshwater Drum Triggered by Hypothermia Exposure

Based on the findings of antioxidant and immunological parameters, we used transmission electron microscopy (TEM) to examine the ultrastructural alterations of the hepatocytes in the treatment groups at 10 °C for 2 and 8 days (LT10-2d and LT10-8d). Compared with the control group, the structure of mitochondria was damaged (Figure 2B). With continuous hypothermic exposure, mitochondria swelled (Figure 2C). In addition, hypothermia induced the accumulation of lipid droplets (Figure 2B), and the aggregation and enlargement of the nucleolus (Figure 2C). These results suggest that hypothermia exposure impaired liver tissue and induced cell fate dysregulation in the liver.

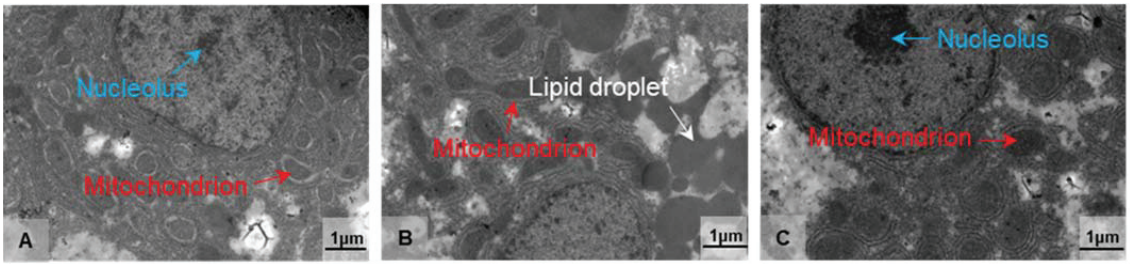

Figure 2. Morphological alterations in the liver of freshwater drum triggered by hypothermia exposure. Morphology and structure of (**A**) Con, (**B**) LT10-2d, and (**C**) LT10-8d, $n = 3$. Arrows in white represent the lipid droplets, in red represent the mitochondria, and in blue represent the nucleolus.

3.3. Transcriptome Profiling of DEGs Induced by Hypothermia Exposure in Freshwater Drum

To profoundly explain the impact of hypothermia exposure on the molecular mechanism of the liver, the transcriptomes were performed. The differentially expressed genes (DEGs) induced by hypothermia were analyzed by DESeq2 software. According to the sequenced results, DEGs between the control group (Con) and treatment groups (LT10-2d, LT10-8d) were identified. Results of the Venn diagrams displayed only 465 DEGs were overlapped in the pairwise comparison (Figure 3A). With the analysis of transcriptome sequencing, a total of 7794 and 5259 DEGs were identified in LT10-2d and LT10-8d, respectively, of which 3410 and 2434 were upregulated and 4384 and 2825 were downregulated, respectively (Figure 3B). Moreover, a total of 6227 DEGs were counted between LT10-2d and LT10-8d, including 3261 upregulated and 2966 downregulated (Figure 3B).

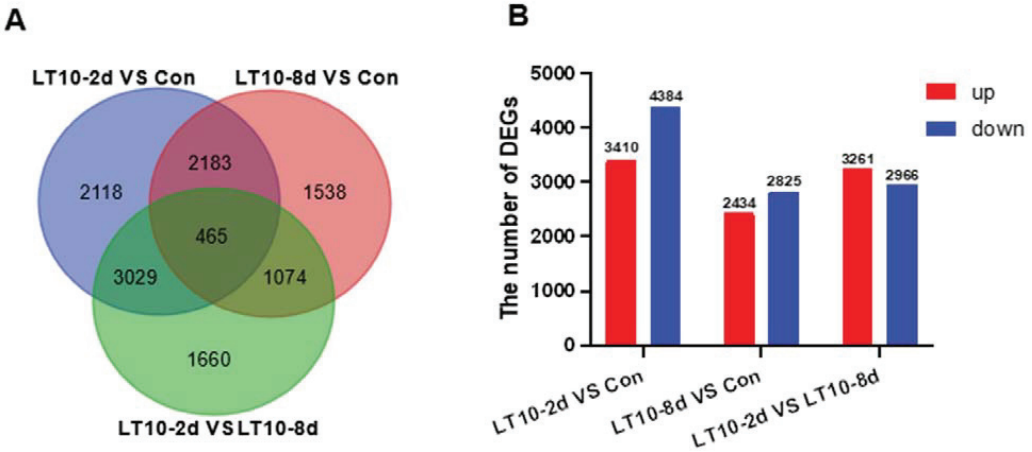

Figure 3. Transcriptome profiling of DEGs induced by hypothermia in freshwater drum. (**A**), Venn diagrams showing the overlap of DEGs among LT10-2d vs. Con (blue), LT10-8d vs. Con (red), and LT10-2d vs. LT10-8d (green). (**B**), Bar chart of DEGs.

3.4. GO and KEGG Enrichments of DEGs Induced by Hypothermia in Freshwater Drum

In order to better explore the functional relevance of DEGs, GO and KEGG enrichment analyses were performed by corresponding annotations of genes. According to the GO enrichment of LT10-2d, biosynthetic and metabolic processes were the most enriched categories, such as protein metabolic process (GO: 0019538), peptide metabolic process (GO: 0006518), celluar macromolecule biosynthetic process (GO: 0034645) macromolecule biosynthetic process (GO: 0009059), and organic substance biosynthetic process (GO: 1901576) (Figure 4A, Table S2A). Similarly, KEGG enrichment shows that DEGs

were mainly enriched in metabolism (tryptophan metabolism, retinol metabolism, lysine degradation, valine, leucine and isoleucine degradation, steroid hormone biosynthesis, glycerolipid metabolism, protein digestion and absorption, ascorbate and aldarate metabolism, and linoleic acid metabolism) and apoptosis ($p < 0.05$) (Figure 4B, Table S3A). However, immunity-related GO terms were significantly enriched in LT10-8d, such as immune system process (GO: 0002376), immune response (GO: 0006955), antigen processing and presentation (GO: 0019882) via MHC protein complex (GO: 0042611), and MHC class II protein complex (GO: 0042613) ($p < 0.05$) (Figure 4C, Table S2B). Meanwhile, according to KEGG enrichment in LT10-8d, the DEGs were mainly involved in metabolism (drug metabolism-cytochrome P450, phenylalanine metabolism, fructose and mannose metabolism, and glycolysis/gluconeogenesis), immunity (antigen processing and presentation, intestinal immune network for IgA production, and Th1 and Th2 cell differentiation), disease (graft-versus-host disease, autoimmune thyroid disease, inflammatory bowel disease (IBD), malaria, and pertussis) ($p < 0.05$) (Figure 4D, Table S3B). Thus, in the comparison of LT10-2d with LT10-8d, the DEGs were mainly enriched in immune- and metabolism-related GO items including humoral immune response (GO: 0006959), immune effector process (GO: 0002252), protein activation cascade (GO: 0072376), peptide metabolic process (GO: 0006518), peptide biosynthetic process (GO: 0043043) ($p < 0.05$) (Figure 4E, Table S2C). Similarly, metabolic- and disease-related pathways were significantly enriched in KEGG including non-alcoholic fatty liver disease (NAFLD), oxidative phosphorylation, fat digestion and absorption, Parkinson disease, Huntington disease, herpes simplex virus 1 infection, Chagas disease (American trypanosomiasis), and long-term depression ($p < 0.05$) (Figure 4F, Table S3C).

3.5. Relative Expression of Inflammation-and Apoptosis-Related Genes in Liver Based on RNA-seq under Hypothermia

Based on the transcriptome results, we selected key genes related to inflammation and apoptosis to be validated in the liver. According to the results of the validation, there was a significant change in gene expression levels regarding inflammation. The gene expression levels of toll-like receptor 2 (TLR2), toll-like receptor (TLR5), major histocompatibility complex II (MHC-II), and TCR (T cell receptor) were significantly downregulated at 10 °C ($p < 0.05$), whereas nuclear factor kappa B (NF-κB), TNF-α, IL-1β, and interleukin-6 (IL-6) were remarkedly upregulated ($p < 0.05$) (Figure 5B). Meanwhile, apoptosis was activated in liver by hypothermia exposure. At 10 °C, the gene expression levels of bcl-2 homolog 3 (BH3), bcl-2 associated X (Bax), caspase 3 (Casp3), and caspase 8 (Casp8) showed remarkable increases ($p < 0.05$), whereas B cell lymphoma-2 (Bcl2) was significantly inhibited at 10 °C ($p < 0.05$) (Figure 5D). Deservedly, the results of validation were consistent with ones in the transcriptome (Figure 5A,C).

3.6. Expression of Inflammation-and Apoptosis-Related Genes in Different Immune Organs of the Freshwater Drum under Hypothermia

In order to more comprehensively study hypothermia suppressed immunity, inflammation- and apoptosis-related genes were also validated in other immune organs. Although hypothermia induced inflammatory and apoptotic responses in different immune organs, there were differences in the expression of the associated genes. Specifically, in the gut the mRNA levels of inflammation-related genes (TNF-α) and apoptosis-related genes (Casp3, Casp8) were significantly higher than controls under hypothermia exposure ($p < 0.05$) (Figure 6A). In addition, the gene expression of Bax and BH3 were elevated only in the LT10-2d group. ($p < 0.05$) (Figure 6A). Meanwhile, the 8-day hypothermia exposure activated the gene expression of TLR2, NF-κB, IL-6, and Bcl2. ($p < 0.05$) (Figure 6A). However, the mRNA levels of TLR5 decreased rapidly ($p < 0.05$) (Figure 6A).

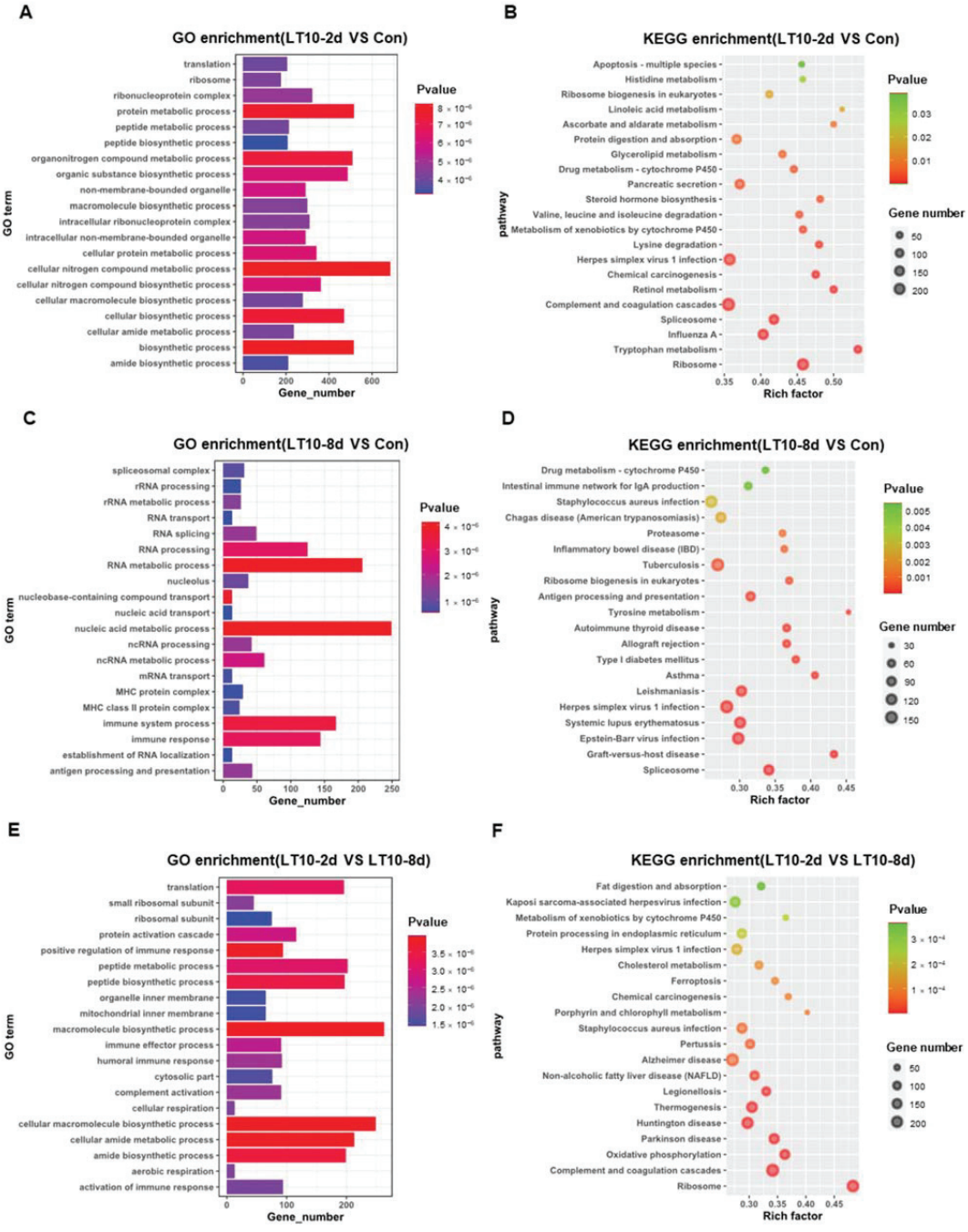

Figure 4. GO and KEGG enrichments of DEGs induced by hypothermia in freshwater drum. (**A**), GO enrichments of DEGs LT10-2d vs. Con; (**B**), KEGG enrichments of DEGs LT10-2d vs. Con; (**C**), GO enrichments of DEGs LT10-8d vs. Con; (**D**), KEGG enrichments of DEGs LT10-8d vs. Con; (**E**), GO enrichments of DEGs LT10-2d vs. LT10-8d; (**F**), KEGG enrichments of DEGs LT10-2d vs. LT10-8d.

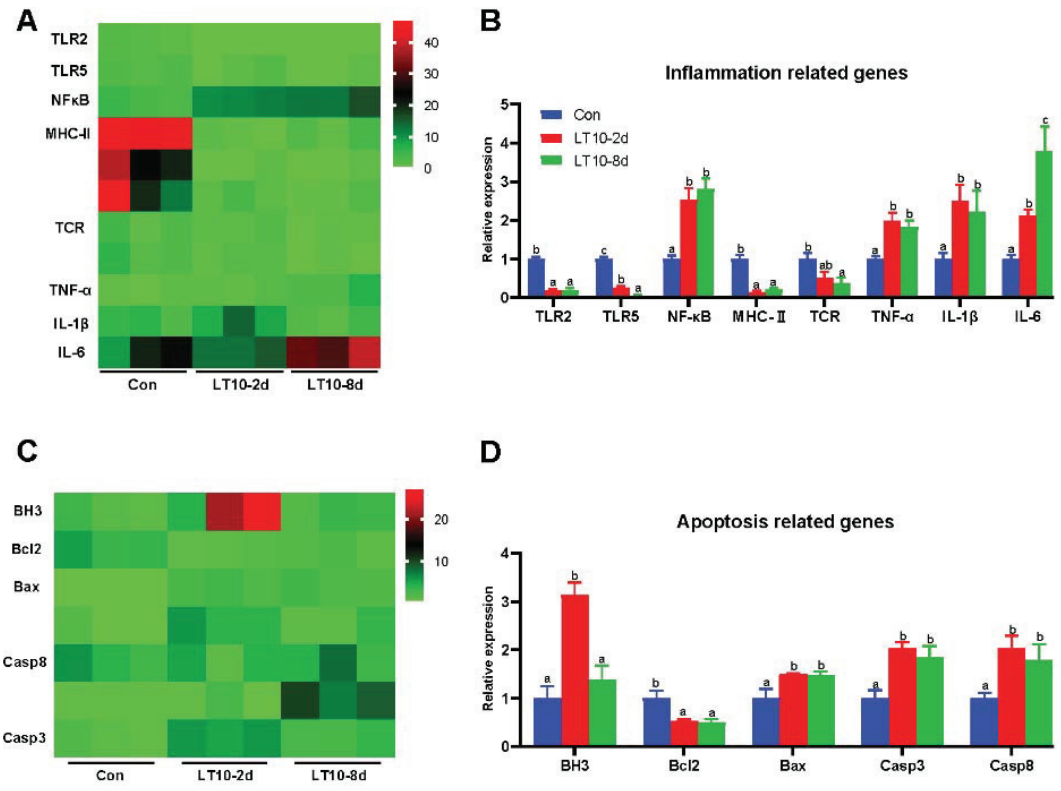

Figure 5. Relative expression of inflammation- and apoptosis-related genes in liver based on RNA-seq under hypothermia. (**A**), Heatmap of expression of inflammation-related genes in transcriptome; (**B**), transcriptional expression of inflammation-related genes in the liver; (**C**), heatmap of expression of apoptosis-related genes in transcriptome; (**D**), transcriptional expression of apoptosis-related genes in the liver. Data were calculated by one-way ANOVA analysis with SPSS 23.0. Different superscript letters (a, b, c) represent the statistical difference ($p < 0.05$). Results are expressed as mean ± SEM, $n = 9$.

In the spleen, hypothermia exposure induced a strong upregulation of the mRNA levels of inflammation-related genes (TLR5, NF-κB, IL-1β) and apoptosis-related genes (Casp3 and Bax) compared with Con ($p < 0.05$) (Figure 6B). The gene expression of IL-6 and BH3 was significantly higher than those of the control group with increasing time. ($p < 0.05$) (Figure 6B). Furthermore, surprisingly, the gene expression of TLR2 was significantly suppressed at 10 °C ($p < 0.05$) (Figure 6B).

In the head kidney, the transcript levels of NF-κB, IL-1β, IL-6, Bax, and BH3 were strongly enhanced during hypothermia exposure ($p < 0.05$) (Figure 6C). Additionally, TNF-α, Casp8, and Bcl2 were highly expressed only in LT10-8d ($p < 0.05$) (Figure 6C).

In the caudal kidney, the expression levels of NF-κB, IL-6, and Bax were promoted significantly in LT10-2d and LT10-8d groups ($p < 0.05$) (Figure 6D). Moreover, the mRNA levels of TNF-α, IL-1β, and Casp3 displayed significant upregulation only in LT10-8d ($p < 0.05$) (Figure 6D). However, the gene expression levels of TLR2 and Bcl2 showed a significant decrease under hypothermia exposure.

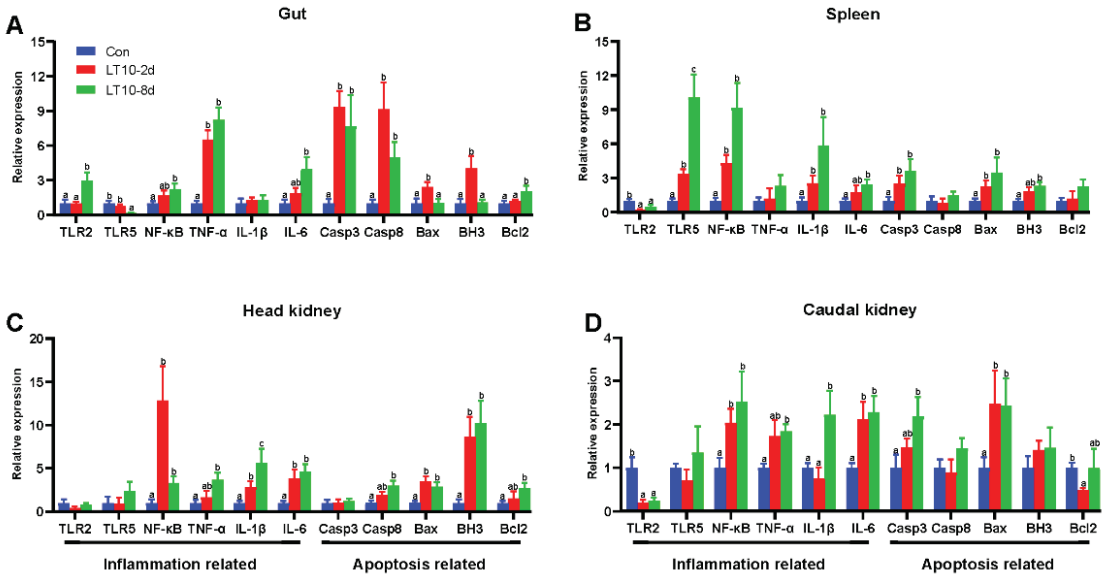

Figure 6. Expression of inflammation- and apoptosis-related genes in different immune organs of the freshwater drum under hypothermia. (**A**), Inflammation- and apoptosis-related genes in the gut; (**B**), inflammation- and apoptosis-related genes in the spleen; (**C**), inflammation- and apoptosis-related genes in the head kidney; (**D**), inflammation- and apoptosis-related genes in the caudal kidney. Data were calculated by one-way ANOVA analysis with SPSS 23.0. Different superscript letters (a, b, c) represent the statistical difference ($p < 0.05$). Results are expressed as mean ± SEM, $n = 9$.

3.7. Apoptosis and Inflammation Were Co-Related with Antioxidant and Immunity under Hypothermia in Freshwater Drum

Based on the aforementioned information, a Pearson correlation analysis was carried out to investigate the changes brought about by hypothermia exposure. The analysis aimed to better understand the relationship between the expression of inflammation and apoptosis-related genes and antioxidant and innate immune parameters. We discovered that exposure to hypothermia mostly affected the tissues of the liver and spleen (Figure 7A,C), with no discernible association increase seen in the gut, head kidney, or caudal kidney (Figure 7B,D,E). Eight days of hypothermia exposure led to an increase in oxidative stress and inflammation in the liver and spleen tissues (Figure 7A,C). Also, chronic hypothermia induced an increase in the correlation between oxidative stress and apoptosis in the spleen (Figure 7C). In addition, a significant correlation between apoptosis and immunity was found only in the liver under 2 d of hypothermia exposure (Figure 7A).

3.8. Hypothermia-Mediated Apoptosis and Inflammation Contributing to Antioxidant and Immune Adaptation in Freshwater Drum

We provide a possible schematic of hypothermia reactions in freshwater drum based on the aforementioned findings (Figure 8). The oxidative stress induced by hypothermic exposure impaired antioxidant and immune capacity and triggered inflammation and apoptosis. Meanwhile, there exist relationships between antioxidative, immunological, inflammatory, and apoptotic responses. Hypothermia-mediated inflammation and apoptosis contribute to antioxidant and immune adaption in the freshwater drum.

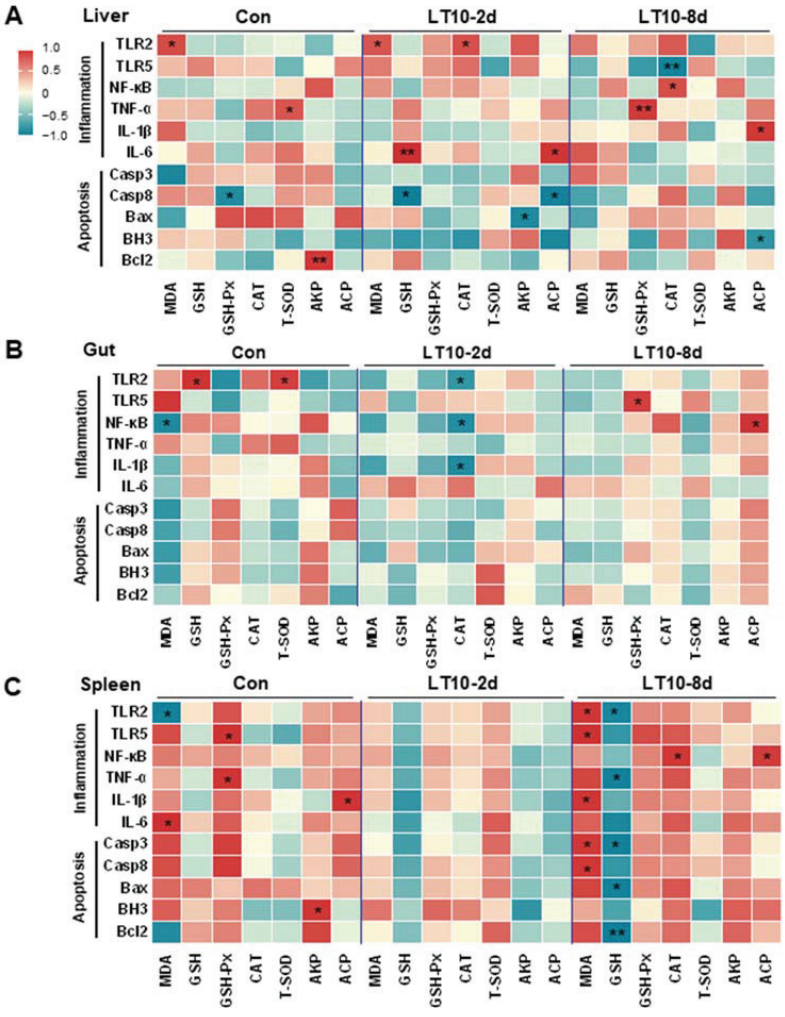

Figure 7. *Cont.*

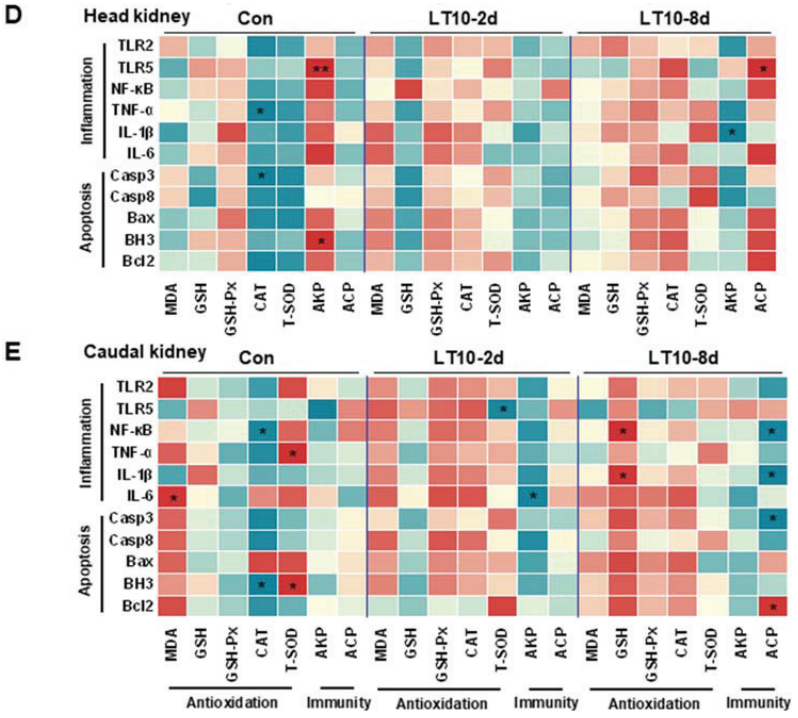

Figure 7. Apoptosis and inflammation were co-related with antioxidant and immunity under hypothermia in freshwater drum. (**A**), Correlation analysis in the liver; (**B**), correlation analysis in the gut; (**C**), correlation analysis in the spleen; (**D**), correlation analysis in the head kidney; and (**E**), correlation analysis in caudal kidney were retrieved from Pearson analysis with SPSS 23.0. * and ** represent the statistical difference (*, $p < 0.05$; **, $p < 0.01$).

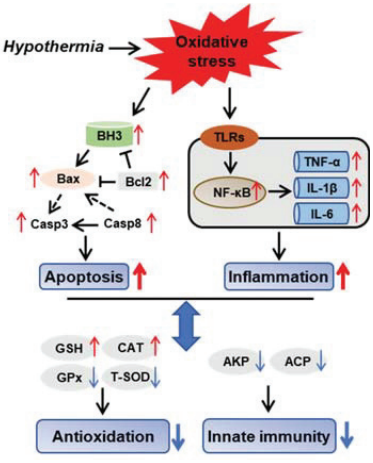

Figure 8. Hypothermia-mediated apoptosis and inflammation contributing to antioxidant and immune adaptation in freshwater drum. Hypothetical regulation of hypothermia on innate immunity, antioxidation, inflammation, and apoptosis was raised based on the results of this study. Solid red arrows represent upregulation. Solid blue arrows represent downregulation. Solid black arrows represent direct impacts, whereas dashed-dotted arrows represent indirect impacts.

4. Discussion

As one of the most important environmental factors for poikilotherm, changes in water temperature have been investigated to induce a variety of physiological regulation regulations in numerous aquatic species [28,29]. The physiology metabolism process unavoidably leads to the production of reactive oxygen species (ROS) in mitochondria [30]. The excessive production of ROS overwhelms the antioxidant system, which leads to lipid peroxidation resulting in generating a large quantity of MDA [31]. Therefore, MDA content is a biomarker commonly used to assess oxidative stress [32]. In this present study, the MDA content significantly increased with the duration of the hypothermia exposure, suggesting lipid peroxidation was induced on the cytomembrane [33]. Oxidative stress caused by hypothermia exposure may lead to cellular damage, alternations in cell fate, and affects normal physiological functions.

Animals respond to hypothermia-induced oxidative stress through antioxidants. GSH removes ROS in the body, playing an important role in protecting cells from damage [34]. As a peroxidase, GSH-Px can convert peroxides into harmless hydroxy compounds and water to prevent them from oxidizing and forming dangerous free radicals [35]. This study found that the synthesis of GSH increased dramatically in the freshwater drum in the initial phase of hypothermia exposure, indicating that the fish were quickly stressed and the synthesis of GSH increased to remove ROS from the environment [15]. The reduction of GSH content to normal levels at 4 d may be due to the conversion of GSH to oxidized glutathione (GSSG) to reduce GSH-Px to hydrogen peroxide, thereby maintaining the balance of GSH/GSH-Px. Meanwhile, the content of GSH-Px decreased remarkably with prolonged hypothermia exposure. Hypothermia-exposure-induced excess ROS cannot be eliminated by the antioxidant system and, in turn, may reduce enzyme activity. Additionally, antioxidant enzymes CAT and T-SOD are generally considered to be the first line of defense against oxidative stress [36]. T-SOD reduces the superoxide radicals into hydrogen peroxide, which is then decomposed into water and oxygen by CAT. Diverse aquatic species have varying antioxidant capacities when subjected to the same hypothermia exposure. It has been shown that the SOD content of brown noble scallops decreased significantly at 6 h whereas in golden scallops it increased greatly at low temperatures [37]. In the present study, the activity of CAT significantly increased at 10 °C whereas T-SOD decreased markedly, which was similar to the decrease in GSH-Px content. Partly, an antioxidant system would protect the freshwater drum from the oxidative stress induced by hypothermia exposure. However, the production of oxidizing substances that cannot be completely eliminated by the antioxidant system led to the inhibition of antioxidation [38].

In fish, the innate immune system is essential for preserving a complex physiological steady state under stressful circumstances [18]. AKP and ACP are important hydrolases that are involved in intrinsic immune defense and are commonly influenced by environmental stress in fish [39]. The activities of AKP and ACP are indicators to measure immune function and body state, reflecting the defense ability against exogenous microbial infection [40]. Under environmental stress, both the increased and decreased activities of ACP and AKP have been reported in fish [41,42]. In the present study, the levels of AKP and ACP decreased significantly under hypothermia exposure, suggesting hypothermia exposure suppressed the immune response and weakened disease resistance in the freshwater drum.

The liver is an important organ of metabolism and immunity in aquatic animals [43] and it is sensitive to external environmental changes, accompanied by ultrastructural alterations [44]. The nucleus, which is the largest and most significant component of eukaryotic cells, serves as the primary location for the storage, replication, and transcription of genetic material within the cell. By preserving gene integrity and managing cellular processes, it controls gene expression [45]. The mitochondrion is the dominant organelle to produce energy and is concurrently involved in cell differentiation, cell messaging, apoptosis, and cell growth and cycle regulation. In the present study, there were slight distortions in mitochondria and nuclei under hypothermia exposure, which were consistent with the results of Collins [46]. ROS produced non-specific damage to lipids, proteins, and

DNA, resulting in altered cell destiny, as evidenced by nucleus damage and mitochondrial swelling [47]. Apoptosis-related gene expression provides proof of this. In addition, mitochondria dysmorphology might be the reason for the increase in the number of lipid droplets. Mitochondrial abnormality inhibited lipid decomposition and impacts fatty acid β-oxidation. As a consequence, lipid droplets in the liver accumulated under hypothermia exposure. Furthermore, some studies indicate that lipid droplets are associated closely with inflammatory responses [48]. These alterations on organelles led to cellular damage and inevitably affected the normal function of the liver. Meanwhile, the variations in AST and ALT levels served as additional support for this. In this investigation, the levels of AST and ALT tended to decrease at 10 °C, demonstrating that exposure to hypothermia suppressed hepatic function.

Transcriptomics refers to a discipline on gene transcription and regulation in cells that analyzes gene expression at the RNA level. The utilization of transcriptomics will reveal the hypothermia response mechanism on freshwater drum more comprehensively and profoundly. In the present study, the DEGs were mainly involved in metabolism, immunity, inflammation, programmed cell death, and disease. It is well known that the regulation of metabolism is an important part of the temperature response in fish [49]. Hypothermia responses consume a lot of energy, therefore, the DEGs were significantly enriched in protein digestion and absorption, glycolysis/gluconeogenesis, and fat digestion and absorption. Hypothermia exposure promoted oxidative stress in a chronic manner. Persisting oxidative stress caused damage to substances in cells such as lipids and proteins and finally led to apoptosis in the freshwater drum [50]. Furthermore, hypothermia exposure limited antigen processing and presentation and affected Th1 and Th2 cell differentiation synchronously, thereby causing immunosuppression in the body [51]. In addition, oxidative stress activated a large range of inflammation-related transcription factors. Subsequently, these transcription factors induced the expression of many cytokines and chemokines, leading to chronic inflammation in the liver under hypothermia exposure. Finally, with the accumulation of various adverse responses to hypothermia exposure, the outbreak of endogenous and exogenous diseases in the freshwater drum may affect the body health and even cause death.

Immune organs play an important role in producing or storing immune cells. In fish, the organs of the immune system include the gills, thymus, spleen, head kidney, caudal kidney, liver, and gut [52,53]. However, there are relatively few studies on the effects of hypothermia exposure on immune organs. This study investigated the effects of oxidative stress induced by hypothermia exposure on immune organs from the perspective of inflammatory and apoptotic responses. The inflammatory response is a common consequence in fish under adverse environments, which usually was associated with oxidative stress. In recent years, accumulating evidence highlighted the role of TLRs/NF-κB signaling in inflammation caused by the antioxidative response, including the upstream and the downstream regulators [54,55]. As a specific pathogen recognition receptor, TLRs are regarded as pivotal regulators linking oxidative stress to inflammation [56,57] that can induce activation of NF-κB. In addition, MHC–peptide complexes play an important role in adaptive immunity. MHC-II is mainly involved in the presentation of exogenous antigens and is capable of endogenous antigen presentation under some conditions [58]. The treated antigen fragment is presented to TCRs during the initial phase of the immune response [59], which could eventually exhibit inflammatory functions via NF-κB signaling [60]. Furthermore, activation of NF-κB induces gene expression of inflammatory factors such as TNF-α, IL-1 β, and IL-6 [61]. In the present study, upregulated gene expression of NF-κB and inflammatory factors indicate hypothermia exposure promoted inflammatory responses in different organs. However, gene expression of TLRs in different organs showed different trends, suggesting the inflammatory response to hypothermia exposure showed a tissue-specific difference [15]. The underlying reasons for this are unclear. We hypothesized that TLR-mediated signal transmission may be independent of NF-κB. Moreover, mRNA levels of MHC-II and TCR in the liver were suppressed under

hypothermia exposure. The suppression of immunity by low temperature was confirmed again. Meanwhile, correlation analysis reveals the closer association between antioxidative response and inflammatory response under hypothermia exposure was enhanced in the liver and spleen. Inflammation caused by oxidative stress was further confirmed. The liver and spleen may be the important target organs for inflammatory responses induced by oxidative stress under hypothermia exposure. Apoptosis can remove the unnecessary or abnormal cells in multicellular organisms to maintain normal physiological functions. In the extrinsic pathway, caspase-8 can cause the following cascade reaction. In the intrinsic pathway, Bcl-2 and Bax mediate caspase-9. Activated caspase-9 further initiates caspase-3 to accomplish apoptosis. In this study, apoptosis-related genes were activated in different organs, indicating apoptosis was the extensive and key response mechanism to maintain homeostasis under hypothermia exposure and further demonstrated the molecular mechanism induced by hypothermia in the freshwater drum. Through correlation analysis among antioxidants, immunity, and apoptosis, we found there was a significant correlation between antioxidants and apoptosis in the spleen during hypothermia treatment, suggesting apoptosis was associated with oxidative stress. Inhibition of antioxidant capacity might promote the apoptotic response [62,63]. Meanwhile, the correlation between immunity and apoptosis in liver was also found. The accelerated apoptosis induced by hypothermia exposure can control the death of immune cells in immune organs and thereby affects the immune function in the body.

5. Conclusions

In conclusion, hypothermia induced oxidative stress and suppressed antioxidant and innate immunity in the freshwater drum. Inflammation and apoptosis were activated in response to hypothermia exposure, which might contribute to the antioxidant and innate immunity adaption. These alternations reveal the underlying mechanisms of hypothermia responses in the freshwater drum.

Supplementary Materials: The following supporting information can be downloaded at: https://www.mdpi.com/article/10.3390/antiox11091657/s1, Table S1: cDNA sequence for the genes referred in the experiment; Table S2: GO enrichment analysis statistical table; Table S3: KEGG enrichment analysis statistical table.

Author Contributions: J.C., conceptualization, methodology, validation, investigation, writing—review and editing; H.L., validation, investigation, and data curation; P.X., resources and formal analysis; Y.T., software and formal analysis; S.S., software; G.L., investigation; N.W., software and investigation; M.X., validation; F.Y., investigation and formal analysis; W.F., software and validation; C.S., methodology, writing—review and editing, supervision and funding acquisition; H.W., resources, supervision and project administration. All authors have read and agreed to the published version of the manuscript.

Funding: This work was supported by the Central Public-interest Scientific Institution Basal Research Fund, Freshwater Fisheries Research Center, CAFS (2020JBFR03, 2020JBMF02 and 2021JBFM13); the Innovation Project of Jiangsu Agricultural Science and Technology (CX(20)2025); the Central Public-interest Scientific Institution Basal Research Fund, CAFS(2020TD62); the Science and Technology Development Fund of Wuxi City (N20203008).

Institutional Review Board Statement: This study was approved by the Animal Care and Use Committee of Nanjing Agricultural University (Nanjing, China) (WXFC 2021-0006). All animal procedures were performed according to the Guideline for the Care and Use of Laboratory Animals in China.

Informed Consent Statement: Not applicable.

Data Availability Statement: The data are contained within the article and Supplementary Materials.

Acknowledgments: The authors gratefully acknowledge Xueyan Ma, Guohua Lv and Liang Zhang from Freshwater Fisheries Research Center, Chinese Academy of Fishery Sciences for their assistance during the experimental period. The authors would like to express sincere thanks to the personnel of Freshwater Fisheries Research Center, Chinese Academy of Fishery Sciences for their kind assistance.

Conflicts of Interest: The authors declare no conflict of interest.

References

1. Song, C.; Cui, Y.; Liu, B.; Xie, J.; Ge, X.; Xu, P.; Lin, Y. HSP60 and HSP90β from blunt snout bream, *Megalobrama amblycephala*: Molecular cloning, characterization, and comparative response to intermittent thermal stress and *Aeromonas hydrophila* infection. *Fish Shellfish. Immunol.* **2018**, *74*, 119–132. [CrossRef]
2. Snyder, R.J.; Hennessey, T.M. Cold tolerance and homeoviscous adaptation in freshwater alewives (*Alosa pseudoharengus*). *Fish Physiol. Biochem.* **2003**, *29*, 117–126. [CrossRef]
3. Song, C.; Liu, B.; Jiang, S.; Xiong, Y.; Sun, C.; Zhou, Q.; Jiang, Z.; Liu, B.; Zhang, H. Anthraquinone extract from *Rheum officinale* Bail improves growth performance and Toll–Relish signaling-regulated immunity and hyperthermia tolerance in freshwater prawn *Macrobrachium nipponense*. *3 Biotech.* **2020**, *10*, 526. [CrossRef]
4. Tingley, M.P.; Huybers, P. Recent temperature extremes at high northern latitudes unprecedented in the past 600 years. *Nature* **2013**, *496*, 201–205.
5. Pirhalla, D.E.; Sheridan, S.C.; Ransibrahmanakul, V.; Lee, C.C. Assessing cold-snap and mortality events in south Florida coastal ecosystems: Development of a biological cold stress index using satellite SST and weather pattern forcing. *Estuar. Coast.* **2015**, *38*, 2310–2322.
6. Blagojevic, D.P.; Grubor-Lajsic, G.N.; Spasic, M.B. Cold defence responses: The role of oxidative stress. *Front. Biosci.* **2011**, *3*, 416–427. [CrossRef]
7. Newsholme, P.; Cruzat, V.F.; Keane, K.N.; Carlessi, R.; Bittencourt, P.D. Molecular mechanisms of Ros production and oxidative stress in diabetes. *Biochem. J.* **2016**, *473*, 4527–4550. [CrossRef]
8. Song, C.; Liu, B.; Ge, X.; Li, H.; Liu, B.; Xu, P. miR-34a/Notch1b mediated autophagy and apoptosis contributes to oxidative stress amelioration by emodin in the intestine of teleost *Megalobrama amblycephala*. *Aquaculture* **2022**, *547*, 737441. [CrossRef]
9. Sindhi, V.; Gupta, V.; Sharma, K.; Bhatnagar, S.; Kumari, R.; Dhaka, N. Potential applications of antioxidants—A review. *J. Pharm. Res.* **2013**, *7*, 828–835. [CrossRef]
10. Apak, R.; Özyürek, M.; Guclu, K.; Capanoglu, E. Antioxidant activity/capacity measurement. III. reactive oxygen and nitrogen species (Ros/Rns) scavenging assays, oxidative stress biomarkers, and chromatographic/chemometric assays. *J. Agric. Food Chem.* **2016**, *64*, 1046–1070. [CrossRef]
11. Vinagre, C.; Madeira, D.; Narciso, L.; Cabral, H.N.; Diniz, M. Effect of temperature on oxidative stress in fish: Lipid peroxidation and catalase activity in the muscle of juvenile seabass, Dicentrarchus labrax. *Ecol. Indic.* **2012**, *23*, 274–279. [CrossRef]
12. Tseng, Y.C.; Chen, R.D.; Lucassen, M.; Schmidt, M.M.; Dringen, R.; Abele, D.; Hwang, P.P. Exploring uncoupling proteins and antioxidant mechanisms under acute cold exposure in brains of fish. *PLoS ONE* **2011**, *6*, e18180. [CrossRef]
13. Lu, D.; Ma, Q.; Sun, S.; Zhang, H.; Chen, L.; Zhang, M.; Du, Z. Reduced oxidative stress increases acute cold stress tolerance in zebrafish. *Comp. Biochem. Pysiol. A Mol. Integr. Physiol.* **2019**, *235*, 166–173. [CrossRef]
14. Rossi, A.; Bacchetta, C.; Cazenave, J. Effect of thermal stress on metabolic and oxidative stress biomarkers of *Hoplosternum littorale* (*Teleostei, Callichthyidae*). *Ecol. Indic.* **2017**, *79*, 361–370.
15. Chen, Y.; Liu, E.; Li, C.; Pan, C.; Zhao, X.; Wang, Y.; Ling, Q. Effects of heat stress on histopathology, antioxidant enzymes, and transcriptomic profiles in gills of pikeperch *Sander lucioperca*. *Aquaculture* **2020**, *534*, 736277. [CrossRef]
16. Cui, Y.; Hou, Z.; Ren, Y.; Men, X.; Zheng, B.; Liu, P.; Xia, B. Effects of aerial exposure on oxidative stress, antioxidant and non-specific immune responses of juvenile sea cucumber *Apostichopus japonicus* under low temperature. *Fish Shellfish. Immunol.* **2020**, *101*, 58–65. [CrossRef]
17. Alcorn, S.; Murray, A.; Pascho, R. Effects of rearing temperature on immune functions in sockeye salmon (*Oncorhynchus nerka*). *Fish Shellfish. Immun.* **2002**, *12*, 303–334.
18. Magnadóttir, B. Innate immunity of fish (overview). *Fish Shellfish. Immunol.* **2006**, *20*, 137–151. [CrossRef]
19. Song, H.; Xu, D.; Tian, L.; Chen, R.; Wang, L.; Tan, P.; You, Q. Overwinter mortality in yellow drum (*Nibea albiflora*): Insights from growth and immune responses to cold and starvation stress. *Fish Shellfish Immun.* **2019**, *92*, 341–347.
20. Dellagostin, E.N.; Martins, A.W.S.; Blödorn, E.B.; Silveira, T.L.R.; Komninou, E.R.; Junior, A.S.V.; Corcini, C.D.; Nunes, L.S.; Remião, M.H.; Collares, G.L.; et al. Chronic cold exposure modulates genes related to feeding and immune system in Nile tilapia (*Oreochromis niloticus*). *Fish Shellfish Immun.* **2022**, *128*, 269–278.
21. Cheng, C.; Ye, C.; Guo, Z.; Wang, A. Immune and physiological responses of pufferfish (*Takifugu obscurus*) under cold stress. *Fish Shellfish Immun.* **2017**, *64*, 137–145.
22. Miest, J.J. Apoptosis and Its Association with Immunomodulation and Disease in Common Carp (*Cyprinus carpio* L.). Ph.D. Dissertation, Keele University, Keele, UK, 2013.

23. Hernández-Gómez, R.E.; Contreras-Sánchez, W.M.; Hernández-Franyutti, A.; Perera-García, M.A.; Torres-Martínez, A. Testicular structure and development of the male germinal epithelium in the freshwater drum *Aplodinotus grunniens* (*Perci-formes: Sciaenidae*) from the Usumacinta River, Southern Mexico. *Acta Zool.* **2021**, *00*, 1–19.
24. Song, C.; Wen, H.; Liu, G.; Ma, X.; Lv, G.; Wu, N.; Chen, J.; Xue, M.; Li, H.; Xu, P. Gut Microbes Reveal Pseudomonas Medicates Ingestion Preference via Protein Utilization and Cellular Homeostasis Under Feed Domestication in Freshwater Drum, *Aplodinotus grunniens*. *Front. Microbiol.* **2022**, *13*, 861705. [CrossRef]
25. William, B.W. Life history aspects of smallmouth buffalo and freshwater drum in wheeler reservoir, Alabama. *Proc. Annu. Conf. Southeast. Assoc. Game Fish Comm.* **1968**, *22*, 479–495.
26. Bodensteiner, L.S.; Lewis, W.M. Role of Temperature, Dissolved Oxygen, and Backwaters in the Winter Survival of Freshwater Drum (Aplodinotus grunniens) in the Mississippi River. *Can. J. Fish. Aquat. Sci.* **1992**, *49*, 173–184.
27. Li, H.; Qiang, J.; Song, C.; Xu, P. Transcriptome profiling reveal *Acanthopanax senticosus* improves growth performance, immunity and antioxidant capacity by regulating lipid metabolism in GIFT (*Oreochromis niloticus*). *Comp. Biochem. Physiol. Part D Genom. Proteom.* **2020**, *37*, 100784. [CrossRef]
28. Jiang, S.; Zhou, F.; Yang, Q.; Huang, J.; Yang, L.; Jiang, S. Impact of temperature stress on oxygen and energy metabolism in the hepatopancreas of the black tiger Shrimp, *Penaeus monodon (Crustacea: Decapoda: Penaeidae*). *Pak. J. Zool.* **2019**, *51*, 141–148. [CrossRef]
29. Fan, L.; Wang, L.; Wang, Z. Proteomic characterization of the hepatopancreas in the Pacific white shrimp *Litopenaeus vannamei* under cold stress: Revealing the organism homeostasis mechanism. *Fish Shellfish. Immunol.* **2019**, *92*, 438–449. [CrossRef]
30. Apel, K.; Hirt, H. Reactive oxygen species: Metabolism, oxidative stress, and signal transduction. *Annu. Rev. Plant Biol.* **2004**, *55*, 373–399. [CrossRef]
31. Lykkesfeldt, J.; Svendsen, O. Oxidants and antioxidants in disease: Oxidative stress in farm animals. *Vet. J.* **2007**, *173*, 502–511. [CrossRef]
32. Tsikas, D. Assessment of lipid peroxidation by measuring malondialdehyde (MDA) and relatives in biological samples: Analytical and biological challenges. *Analytical. Biochem.* **2017**, *524*, 13–30. [CrossRef]
33. Géret, F.; Jouan, A.; Turpin, V.; Bebianno, M.J.; Cosson, R.P. Influence of metal exposure on metallothionein synthesis and lipid peroxidation in two bivalve mollusks: The oyster (*Crassostrea gigas*) and the mussel (*Mytilus edulis*). *Aquat. Living Resour.* **2002**, *15*, 61–66. [CrossRef]
34. Kosower, N.S.; Kosower, E.M. The glutathione status of cells. *Int. Rev. Cytol.* **1978**, *54*, 109–160. [CrossRef]
35. Imai, H.; Nakagawa, Y. Biological significance of phospholipid hydroperoxide glutathione peroxidase (PHGPx, GPx4) in mammalian cells. *Free. Radic. Biol. Med.* **2003**, *34*, 145–169. [CrossRef]
36. Ojha, A.; Yaduvanshi, S.K.; Srivastava, N. Effect of combined exposure of commonly used organophosphate pesticides on lipid peroxidation and antioxidant enzymes in rat tissues. *Pestic. Biochem. Physiol.* **2010**, *99*, 148–156. [CrossRef]
37. Tan, K.; Zhang, B.; Ma, H.; Li, S.; Zheng, H. Oxidative stress responses of golden and brown noble scallops *Chlamys nobilis* to acute cold stress. *Fish Shellfish Immun.* **2019**, *95*, 349–356.
38. Wei, H.; Zhang, R.; Su, Y.; Bi, Y.; Li, X.; Zhang, X.; Bao, J. Effects of Acute Cold Stress After Long-Term Cold Stimulation on Antioxidant Status, Heat Shock Proteins, Inflammation and Immune Cytokines in Broiler Heart. *Front. Physiol.* **2018**, *9*, 1–12. [CrossRef]
39. Hong, Y.; Huang, Y.; Yan, G.; Pan, C.; Zhang, J. Antioxidative status, immunological responses, and heat shock protein expression in hepatopancreas of Chinese mitten crab, *Eriocheir sinensis* under the exposure of glyphosate. *Fish Shellfish. Immunol.* **2018**, *86*, 840–845. [CrossRef]
40. Broeg, K. The activity of macrophage aggregates in the liver of flounder (*Platichthys flesus*) and wrasse (*Symphodus melops*) is associated with tissue damage. *Mar. Environ. Res.* **2010**, *69* (Suppl. S1), S14–S16. [CrossRef]
41. Jia, R.; Du, J.; Cao, L.; Feng, W.; He, Q.; Xu, P.; Yin, G. Immune, inflammatory, autophagic and DNA damage responses to long-term H_2O_2 exposure in different tissues of common carp (*Cyprinus carpio*). *Sci. Total Environ.* **2020**, *757*, 143831. [CrossRef]
42. Majumder, R.; Kaviraj, A. Acute and sublethal effects of organophosphate insecticide chlorpyrifos on freshwater fish *Oreochromis niloticus*. *Drug Chem. Toxicol.* **2019**, *42*, 487–495.
43. Meszaros, A.; Weidinger, A.; Dumitrescu, S.; Müllebner, A.V.; Duvigneau, J.C.; Kozlov, A.V. The Impact of Pro-inflammatory Cytokines on ROS Mediated Liver Damage. *Free. Radic. Biol. Med.* **2017**, *112*, 206. [CrossRef]
44. Xu, Z.; Regenstein, J.M.; Xie, D.; Lu, W.; Ren, X.; Yuan, J.; Mao, L. The oxidative stress and antioxidant responses of *Litopenaeus vannamei* to low temperature and air exposure. *Fish Shellfish. Immunol.* **2018**, *72*, 564–571. [CrossRef]
45. Shen, W.; Balajee, A.; Wang, J.; Wu, H.; Eng, C.; Pandolfi, P.P.; Yin, Y. Essential Role for Nuclear PTEN in Maintaining Chromosomal Integrity. *Cell* **2007**, *128*, 157–170. [CrossRef]
46. Collins, P. Environmental stress upon hepatopancreatic cells of freshwater prawns (*Decapoda: Caridea*) from the floodplain of Paraná River. *Nat. Sci.* **2010**, *2*, 748–759. [CrossRef]
47. Zhao, K.; Zhao, G.; Wu, D.; Soong, Y.; Birk, A.V.; Schiller, P.W.; Szeto, H.H. Cell-permeable Peptide Antioxidants Targeted to Inner Mitochondrial Membrane inhibit Mitochondrial Swelling, Oxidative Cell Death, and Reperfusion Injury. *J. Biol. Chem.* **2004**, *279*, 34682–34690. [CrossRef]
48. Melo, R.C.N.; Dvorak, A.M. Lipid Body-Phagosome Interaction in Macrophages during Infectious Diseases: Host Defense or Pathogen Survival Strategy? *PLoS Pathog.* **2012**, *8*, 6. [CrossRef]

49. Vornanen, M.; Hassinen, M.; Koskinen, H.; Krasnov, A. Steady-state effects of temperature acclimation on the transcriptome of the rainbow trout heart. *Am. J. Physiol. Regul. Integr. Comp. Physiol.* **2005**, *289*, 1177–1184. [CrossRef]
50. Liao, Z.; Lin, D.; Jia, J.; Cai, R.; Yu, Y.; Li, W. Innate Immune Response to Fasting and Refeeding in the Zebrafish Kidney. *Biomolecules* **2021**, *11*, 825. [CrossRef]
51. Gein, S.V.; Sharav'eva, I.L. Immunomodulating Effects of Cold Stress. *Biol. Bull. Rev.* **2018**, *8*, 482–488.
52. Whyte, S.K. The innate immune response of finfish—A review of current knowledge. *Fish Shellfish. Immunol.* **2007**, *23*, 1127–1151. [CrossRef]
53. Novoa, B.; Figueras, A. Zebrafish: Model for the Study of Inflammation and the Innate Immune Response to Infectious Diseases. *Curr. Top. Innate Immun. II* **2012**, *946*, 253–275.
54. Kane, L.P.; Shapiro, V.S.; Stokoe, D.; Weiss, A. Induction of NF-kappa B by the Akt PKB kinase. *Curr. Biol.* **1999**, *9*, 601–604. [CrossRef]
55. Thome, M.; Tschopp, J. TCR-induced NF-κB activation: A crucial role for Carma1, Bcl10 and MALT1. *Trends Immunol.* **2003**, *24*, 419–424. [CrossRef]
56. West, A.P.; Brodsky, I.E.; Rahner, C.; Woo, D.K.; Erdjument-Bromage, H.; Tempst, P.; Ghosh, S. TLR signaling augments macrophage bactericidal activity through mitochondrial ROS. *Nature* **2011**, *472*, 476–480. [CrossRef]
57. Jiang, X.; Fang, L.; Wu, H.; Mei, X.; He, F.; Ding, P.; Liu, R. TLR2 Regulates Allergic Airway Inflammation and Autophagy Through PI3K/Akt Signaling Pathway. *Inflammation* **2017**, *40*, 1382–1392. [CrossRef]
58. Dengjel, J.; Schoor, O.; Fischer, R.; Reich, M.; Kraus, M.; Müller, M.; Stevanovic, S. Autophagy promotes MHC class II presentation of peptides from intracellular source proteins. *Proc. Natl. Acad. Sci. USA* **2005**, *102*, 7922–7927. [CrossRef]
59. Birnbaum, M.E.; Mendoza, J.L.; Sethi, D.K.; Dong, S.; Glanville, J.; Dobbins, J.; Garcia, K.C. Deconstructing the peptide-MHC specificity of t cell recognition. *Cell* **2014**, *157*, 1073–1087. [CrossRef]
60. dos Santos, N.R.; Ghezzo, M.N.; da Silva, R.C.; Fernandes, M.T. NF-κB in T-cell acute lymphoblastic leukemia: Oncogenic functions in leukemic and in microenvironmental cells. *Cancers* **2010**, *2*, 1838–1860. [CrossRef]
61. Gribar, S.C.; Anand, R.J.; Sodhi, C.P.; Hackam, D.J. The role of epithelial toll-like receptor signaling in the pathogenesis of intestinal inflammation. *J. Leukoc. Biol.* **2008**, *83*, 493–498. [CrossRef]
62. Murakawa, M.; Jung, S.-K.; Lijima, K.; Yonehara, S. Apoptosis-inducing protein, AIP, from parasite-infected fish induces apoptosis in mammalian cells by two different molecular mechanisms. *Cell Death Differ.* **2001**, *8*, 298–307.
63. Woo, A.H.; Park, L.; Park, M.; Lee, H.; Lee, S.; Chun, Y.; Lee, S.; Hong, S.; Rhee, C.H. Arsenic trioxide induces apoptosis through a reactive oxygen species-dependent pathway and loss of mitochondrial membrane potential in HeLa cells. *Int. J. Oncol.* **2002**, *21*, 57–63.

antioxidants

MDPI

Article

ROS Induced by *Streptococcus agalactiae* Activate Inflammatory Responses via the TNF-α/NF-κB Signaling Pathway in Golden Pompano *Trachinotus ovatus* (Linnaeus, 1758)

Jie Gao [1,2,3], Mingjian Liu [1,3], Huayang Guo [1,3], Kecheng Zhu [1,3], Bo Liu [1,3], Baosuo Liu [1,3], Nan Zhang [1,3] and Dianchang Zhang [1,3,4,*]

1 Key Laboratory of South China Sea Fishery Resources Exploitation and Utilization, Chinese Academy of Fishery Sciences, South China Sea Fisheries Research Institute, Ministry of Agriculture and Rural Affairs, Guangzhou 510300, China
2 Ocean College, Hebei Agricultural University, Qinhuangdao 066000, China
3 Sanya Tropical Fisheries Research Institute, Sanya 572019, China
4 Guangdong Provincial Engineer Technology Research Center of Marine Biological Seed Industry, Guangzhou 510300, China
* Correspondence: zhangdch@scsfri.ac.cn; Tel.: +86-20-8910-8316; Fax: +86-20-8445-1442

Abstract: *Streptococcus agalactiae* is common pathogenic bacteria in aquaculture and can cause mass mortality after fish infection. This study aimed to investigate the effects of *S. agalactiae* infection on the immune and antioxidant regulatory mechanisms of golden pompano (*Trachinotus ovatus*). Serum and liver samples were obtained at 0, 6, 12, 24, 48, 96, and 120 h after golden pompano infection with *S. agalactiae* for enzyme activity and gene expression analyses. After infection with *S. agalactiae*, the content of reactive oxygen species (ROS) in serum was significantly increased ($p < 0.05$). Serum levels of glucose (GLU), alanine aminotransferase (ALT), aspartate aminotransferase (AST), and malondialdehyde (MDA) increased and then decreased ($p < 0.05$), reaching a maximum at 6 h. Serum antioxidant enzyme (LZM) activity increased significantly ($p < 0.05$) and reached a maximum at 120 h. In addition, the mRNA expression levels of antioxidant genes (*SOD*, *CAT*, and *GPx*) in the liver increased and then decreased, reaching the maximum at 24 h, 48 h, and 24 h, respectively. During the experimental period, the mRNA expression levels of NF-κB-related genes of the inflammatory signaling pathway inhibitory κB (*IκB*) showed an overall decreasing trend ($p < 0.05$) and the lowest expression at 120 h, whereas the mRNA expression levels of tumor necrosis factor α (*TNF-α*), interleukin-1β (*IL-1β*), IκB kinase (*IKK*), and nuclear factor NF-κB increased significantly ($p < 0.05$) and the highest expression was at 120 h. In conclusion, these results showed that *S. agalactiae* could activate internal regulatory signaling in the liver of golden pompano to induce defense and immune responses. This study is expected to lay a foundation to develop the healthy aquaculture of golden pompano and promote a more comprehensive understanding of its disease resistance mechanisms.

Keywords: *Trachinotus ovatus*; pathogenic bacterial infection; histopathology; immune-related genes; inflammatory response

Citation: Gao, J.; Liu, M.; Guo, H.; Zhu, K.; Liu, B.; Liu, B.; Zhang, N.; Zhang, D. ROS Induced by *Streptococcus agalactiae* Activate Inflammatory Responses via the TNF-α/NF-κB Signaling Pathway in Golden Pompano *Trachinotus ovatus* (Linnaeus, 1758). *Antioxidants* **2022**, *11*, 1809. https://doi.org/10.3390/antiox11091809

Academic Editor: Erchao Li

Received: 9 August 2022
Accepted: 8 September 2022
Published: 14 September 2022

Publisher's Note: MDPI stays neutral with regard to jurisdictional claims in published maps and institutional affiliations.

1. Introduction

Golden pompano (*Trachinotus ovatus*) is an economically important fish in China. It is mainly cultivated in deep-water cages along the southeastern coast of China. Due to its delicious meat and fast growth, it has become an essential fish in southern China [1,2]. In recent years, a large number of golden pompano have died due to *Streptococcus agalactiae* infection, causing severe economic losses to farmers [3]. There are no effective measures to prevent and treat *S. agalactiae* infection in golden pompano.

S. agalactiae is a Gram-positive parthenogenic anaerobic and often known as group B *Streptococcus* (GBS), which can cause inflammatory disorders in animal commensals. The

high pathogenicity and pathogenesis of *S. agalactiae* have been extensively studied in a range of species, including humans, rats, cows, horses, etc. [4]. It is highly pathogenic not only to terrestrial animals but also to aquatic animals. In many fish, *S. agalactiae* infection can cause multifunctional disorders and lead to high mortality. As a result, this species is of global concern as a significant pathogen in farmed fish [5]. Although scholars have reported on the pathogenesis of fish infected with *S. agalactiae*, the systematic studies of host factors in response to its infection are limited.

Serum parameters are critical indicators to measure the physiological status of the whole organism. When an organism is invaded by exogenous microorganisms, its health status can be determined by biochemical indicators in the serum [6]. Serum glucose (GLU) levels are often induced by environmental stress and are produced through glycolytic and gluconeogenic pathways to provide the energy required to combat stress [7,8]. In addition, alanine aminotransferase (ALT), aspartate aminotransferase (AST), and malondialdehyde (MDA), as sensitive indicators of the extent of oxidative damage to cells, are also commonly regulated by environmental factors [9]. Therefore, understanding changes in serum parameters is important for understanding the health status of an organism.

The invasion of pathogenic bacteria induces the production of reactive oxygen species (ROS) in the organism [2]. Excessive ROS accumulation can lead to oxidative damage to tissues and organs. As a vital antioxidant defense organ, the liver has established a complete antioxidant defense system, such as superoxide dismutase (SOD), catalase (CAT), and glutathione peroxidase (GPx) [10,11]. Therefore, the degree of oxidative damage to organisms by pathogenic bacteria can be judged by detecting the activity of antioxidant enzymes in the liver.

In addition, pathogenic infections can activate or control TNF-α/NF-κB-mediated signaling pathways [12,13]. Tumor necrosis factor α (TNF-α) and interleukin-1β (IL-1β) are the primary transcriptional regulators involved in the pathogenic invasion. Additionally, TNF-α and IL-1β function by nuclear factor-κB (NF-κB) regulatory genes through activation of classical NF-κB signaling [14]. NF-κB is a crucial regulator of cellular events and is involved in immune regulation and inflammatory and anti-apoptotic responses [15]. It is a heterodimer composed of P50 and P65 and chelated into inactive complexes under normal physiological conditions through interactions with inhibitory κB (IκB) family members [16]. When exogenous microorganisms stimulate cells, they can activate IκB kinase (IKK) through a signaling cascade [17]. IKK activates the NF-κB-IκB complex through phosphorylation of IκB and leads to ubiquitin-dependent degradation of IκB and release of NF-κB dimers from the inhibitory complex [18]. Activating NF-κB-related signaling pathways promotes nuclear translocation and transcription of NF-κB target genes, regulating proliferation, differentiation, and apoptosis or inflammation in various cell types [19,20]. In addition, IL-1β can enhance the inflammatory response by inducing NF-κB expression, creating a vicious cycle [21]. IL-1β can promote TNF-α secretion by broadly pan-activating T cells, B cells, and natural killer (NK) cells. TNF-α can promote gene transcription and exacerbate the inflammatory response by increasing the release of inflammatory factors such as IL-1β [22]. Based on the central regulation of the NF-κB pathway, the interaction of NF-κB with IL-1β and TNF-α can exacerbate inflammatory responses and lead to soft tissue contusion. Therefore, profoundly studying the immune defense mechanism of the TNF-α/NF-κB signaling pathway is necessary.

Therefore, this study assessed the effects of *S. agalactiae* infection on golden pompano by analysing serum parameters, histopathology, and the expression of genes related to the TNF-α/NF-κB signaling pathway. This study contributes to understanding the immune and defense mechanisms of *S. agalactiae* infection in golden pompano and provides a theoretical basis for its healthy breeding.

2. Materials and Methods

2.1. Ethical Statement

Animal research was approved by the Committee of the South China Sea Fisheries Research Institute, Chinese Academy of Fisheries Sciences (no. SCSFRI96-253) and performed in accordance with the applicable standards.

2.2. Experimental Fish and Bacteria Preparation

Golden pompano (average weight of 31.15 g) used in this experiment were healthy and energetic, obtained from the Shenzhen Experimental Base of the South China Sea Fisheries Research Institute of the Chinese Academy of Aquatic Sciences. The water temperature, salinity, dissolved oxygen, and pH range were 27 ± 2 °C, 25 ± 2%, >5.5 mg/L, and 7.8 ± 0.5, respectively. The fish were fed twice a day (9:00 am and 4:00 pm), and the feeding amount per feeding was approximately 4% of their organism mass. The strain of *S. agalactiae* was isolated from the sick golden pompano at the Shenzhen Base of the South China Sea Fisheries Research Institute in 2021. After purification and identification, it was then stored at −80 °C. The bacteria were inoculated into brain heart infusion (BHI) liquid medium and incubated at 140× *g*, 28 °C shakers for 24 h prior to the experiment. The precipitate was recovered after centrifuging the BHI liquid culture at 6200× *g* for 8 min. The pellet was then rinsed four times with sterile phosphate-buffered saline (PBS), and five concentration gradients (1.0×10^{10}, 1.0×10^{9}, 1.0×10^{8}, 1.0×10^{7}, 1.0×10^{6} colony-forming units [CFU]/mL) were established. A 120-h pre-experiment was then performed: one control group (PBS) and five experimental groups were included. Three replicates were set up for each group, with each replicate containing 30 fish (for a total of 540 fish). Each experimental group was injected with 200 μL of the corresponding concentration of bacterial solution for each fish, and the control group was injected with 200 μL of PBS per fish. During this period, the behavioral changes of fish were observed and recorded, and the relationship between mortality and time under different infection concentrations was studied. According to the pre-experimental results, the final 120 h half-lethal concentration (120 h LD50) of 2.0×10^{7} CFU/fish was obtained by multiplying the dilution of the PBS solution.

2.3. Experimental Infection and Sampling

Formal experiments were performed in six 150 L (140 L water) aquariums. Three hundred healthy golden pompano were selected and randomly divided equally into one control group and one infection group, each group of three parallels. Each fish in the infection group was injected with 200 μL bacteria solution at a concentration of 2.0×10^{7} CFU/fish. The control group was injected with 200 μL sterile PBS. Samples were collected at 0, 6, 12, 24, 48, 72, 96, and 120 h after infection. Nine fish were randomly selected at each time point in each group, and every three fish were mixed as one sample (fish were anesthetized with eugenol (40 mg/L) before sampling) [23]. The organism was sterilized with alcohol according to the previously described method [24]. Blood was collected from the caudal vein with a 1.0 mL sterile syringe and stored in a 1.5 mL centrifuge tube. After being silenced at 4 °C for 5 h, 100× *g*, 20 min centrifugation was performed to separate serum samples from blood. Serum samples from every three fish were combined into one mixed sample to obtain three, which were used for blood parameter analysis. Similarly, three fresh liver tissues were taken and immediately frozen in liquid nitrogen for enzyme activity assay and gene expression analysis. Subsequently, all samples were stored in a refrigerator at −80 °C. In addition, at 120 h, nine fish were randomly selected from the control and experimental groups, respectively. Their liver tissues were collected in sampling bottles containing 4% paraformaldehyde fixative for histological examination.

2.4. Histological Examination

In this experiment, liver tissue from the infection and control groups was sectioned separately by slightly modifying the protocol described by Tanaka et al. [25]. Liver tissue fixed in paraformaldehyde was first washed in 70% ethanol, dehydrated, and then em-

bedded in paraffin using conventional techniques. Sections were cut to 5 μm, fixed on slides, and stained with hematoxylin-eosin. Images of the sections were obtained using a microscope (NIKON ECLIPSE C1) according to a previous method [26].

2.5. Detection of Biochemical Parameters in Serum

The contents of ROS in serum were measured using a dichloro-dihydro-fluorescein diacetate (DCFH-DA) probe according to a chemical fluorescence method. The activities of LZM, AST, and ALT were determined by the test-tube turbidimetric method. Serum levels of GLU and MDA were measured by colorimetric immunoassay and enzyme immunoassay, respectively. All the assays were performed according to the kit instructions of the Nanjing Jiancheng Bioengineering Institute (Nanjing, China).

2.6. Detection of Antioxidant Enzyme Activity in Liver

The activities of several important antioxidant enzymes, including SOD, CAT, and GPx, in the liver were determined using a colorimetric method according to commercial colorimetric kits (Nanjing Jiancheng Bioengineering Institute, Nanjing, China).

2.7. RNA Extraction and First Strand cDNA Synthesis

Total RNA was extracted from the livers of the experimental and control groups using TRIzol reagent (Cat. No. DP424, Tiangen, Beijing, China), respectively. The spectrophotometer was used to measure the absorption values of the extracted samples at 260 nm and 280 nm and an optical density (OD) ratio of 260/280. The sample 260/280 OD ratio was 1.8−2.0, indicating that the RNA concentration was in line with the requirements and could be used for subsequent experiments [27]. cDNA was synthesized according to the manufacturer's instructions of the Prime Script™ RT reagent kit with gDNA Eraser (Accurate Biotechnology Co., Ltd., Shanghai, China). The reactions were carried out at 37 °C for 15 min and heated at 85 °C for 5 s. All cDNA samples obtained were stored at −20 °C until quantitative polymerase chain reaction (qPCR) detection.

2.8. Real-Time qPCR

The target gene expression was determined by qPCR using a Roche LightCycler 480 II (Roche Diagnostics, Shanghai, China). The reaction volume of qPCR was 12.5 μL. Melting curve analysis was performed based on a denaturation step at 95 °C for 30 s followed by 40 cycles at 95 °C for 5 s and 60 °C for 30 s. The experiment was repeated thrice for each sample to ensure accuracy (technical repetition) [10,28]. The primers are listed in Table 1, and the amplification efficiency was greater than 90%. *EF-1a* was chosen as the internal reference gene because it was not affected by *S. agalactiae* infection in our study. The relative expression levels of target genes relative to the control group were calculated using the $2^{-\Delta\Delta CT}$ method [29].

Table 1. Primers used for amplification and mRNA expression analysis.

Primer Name	Primer Sequences (5′−3′)	Amplification Target	Reference
SOD-F	CCTCATCCCCCTGCTTGGTA	qPCR	[2]
SOD-R	CCAGGGAGGGATGAGAGGTG		
CAT-F	GGATGGACAGCCTTCAAGTTCTCG	qPCR	[2]
CAT-R	TGGACCGTTACAACAGTGCAGATG		
GPx-F	GCTGAGAGGCTGGTGCAAGTG	qPCR	[2]
GPx-R	TTCAAGCGTTACAGCAGGAGGTTC		
IKK-F	CCTGGAGAACTGCTGTGGAATGAG	qPCR	[30]
IKK-R	ATGGAGGTAGGTCAGAGCCGAAG		
IκB-F	GCTGGTCCATTGCCTCCTGAAC	qPCR	[30]
IκB-R	GTGCCGTCTTCTCGTACAACTGG		
NF-κB-F	TGCGACAAAGTCCAGAAAGAT	qPCR	[31]
NF-κB-R	CTGAGGGTGGTAGGTGAAGGG		

Table 1. *Cont.*

Primer Name	Primer Sequences (5′−3′)	Amplification Target	Reference
IL-1β-F	CGGACTCGAACGTGGTCACATTC	qPCR	[32]
IL-1β-R	AATATGGAAGGCAACCGTGCTCAG		
TNF-α-F	GCTCCTCACCCACACCATCA	qPCR	[10]
TNF-α-R	CCAAAGTAGACCTGCCCAGACT		
EF-1α-F	AAGCCAGGTATGGTTGTCAACTTT	qPCR	[10]
EF-1α-R	CGTGGTGCATCTCCACAGACT		

2.9. Statistical Analyses

The data obtained from the experiments were analyzed by SPSS statistical software (26.0, IBM SPSS Inc., Chicago, IL, USA). All data were expressed as the means ± standard errors (SEs). Statistically significant differences between the group means were analyzed using one-way analysis of variance (ANOVA) and Tukey's multiple comparison test, and differences were considered statistically significant at $p < 0.05$ [10].

3. Results

3.1. Toxicology of Different Concentrations of S. agalactiae on Golden Pompano

The statistical results of the death of golden pompano infected with different concentrations of *S. agalactiae* are shown in Table 2. After 120 h of infection, the survival rate of the infection group injected with doses of 2.0×10^9 and 2.0×10^8 CFU/fish was zero. The survival rate of the infection group with an injected dose of 2.0×10^7 CFU/fish was 47 ± 3.5%, whereas no deaths were observed in the infection group with injected doses of 2.0×10^6 and 2.0×10^5 CFU/fish. The half-lethal time was 116 ± 5.5 h at a 2.0×10^7 CFU/fish dose.

Table 2. Survival rate of golden pompano induced by intraperitoneal injection of *S. agalactiae* and the survival time corresponding to each treatment.

Dosage (CFU/fish)	Survival Rate at 120 h (%)	Half-Lethal Time (LT_{50}, h)	Survival Time (h)
2.0×10^9	0	17 ± 1.0	16~19
2.0×10^8	0	37 ± 3.0	36~70
2.0×10^7	47 ± 3.5	116 ± 5.5	95~125
2.0×10^6	100	130 ± 2.5	130~150
2.0×10^5	100	>160	>160

3.2. Examination of Liver Histopathological

At 120 h, the hepatocytes of the control group of golden pompano were slightly rounded polygonal cells. The cells were closely arranged, regular, and orderly with a clear structure, and blood cells were contained in blood vessels, as shown in Figure 1A. After 120 h of infection, the histopathology of three of the fish is shown in Figure 1B–D. Infected golden pompano liver cells were ill-defined. Their nuclei were enlarged, translucent, and severely shifted. The cells around the hepatic blood sinusoids exhibited amyloid degeneration. The eosinophilic staining of the cytoplasm was cloudy, and the cell membranes disintegrated, resulting in a double-nucleated artifact. Focal necrosis and the sporadic appearance of enlarged basophilic cells in the cytoplasm were observed in the livers of infected fish.

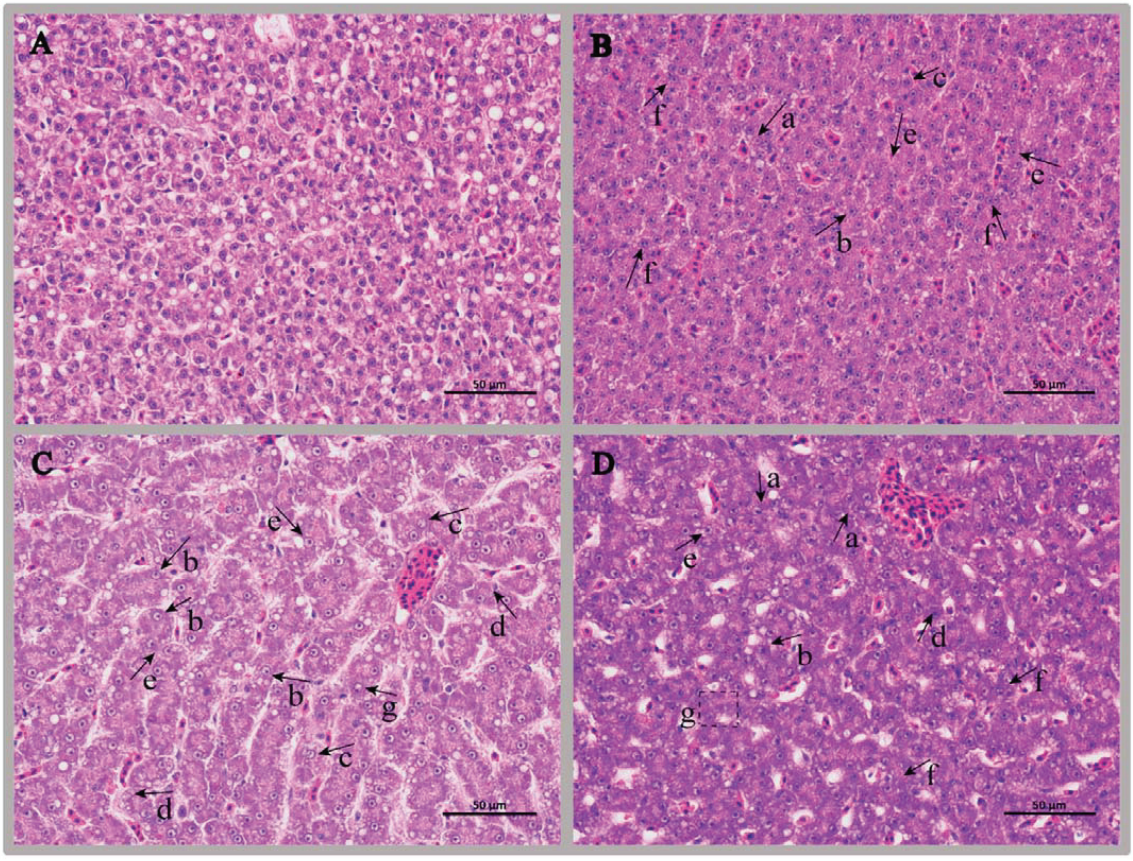

Figure 1. Histopathological examination of the livers of golden pompano infected with *S. agalactiae*. Notes: (**A**) represents a normal liver tissue section, HE, bar = 50 μm; (**B**–**D**) Representative liver tissue sections from three fish at 120 h of infection, respectively, HE, bar = 50 μm. a, liver sample in which liver cell boundaries were not well defined; b, liver sample with enlarged and severely displaced cells; c, liver sample exhibiting hepatic cytoplasmic lysis; d, liver sample exhibiting amyloidosis in the cells surrounding the hepatic sinusoids and cloudy eosinophilic staining of the cytoplasm; e–f, liver sample in which the cell membrane was disintegrated and the cells joined together, creating the illusion of binucleation; g, liver sample exhibiting multifocal necrosis.

3.3. Analysis of Serum Parameters

The serum parameters that changed in golden pompano after *S. agalactiae* infection are shown in Figure 2. The results showed that the serum ROS, GLU, and MDA contents showed similar trends; they all trended upwards and then downwards, and they reached a maximum at 6 h after infection (772.96 fluorescence intensity/mL, 16.30 nmol/L, and 3.64 nmol/L). However, only the GLU was significantly lower than the control group after 24 h of infection ($p < 0.05$). The LZM activity gradually increased after 6 h of infection ($p < 0.05$) and peaked at 120 h (376.22 nmol/mL). ALT and AST activity tended to increase and then decrease, and they reached a maximum at 6 h after infection (4.52 U/L, 62.07 U/L).

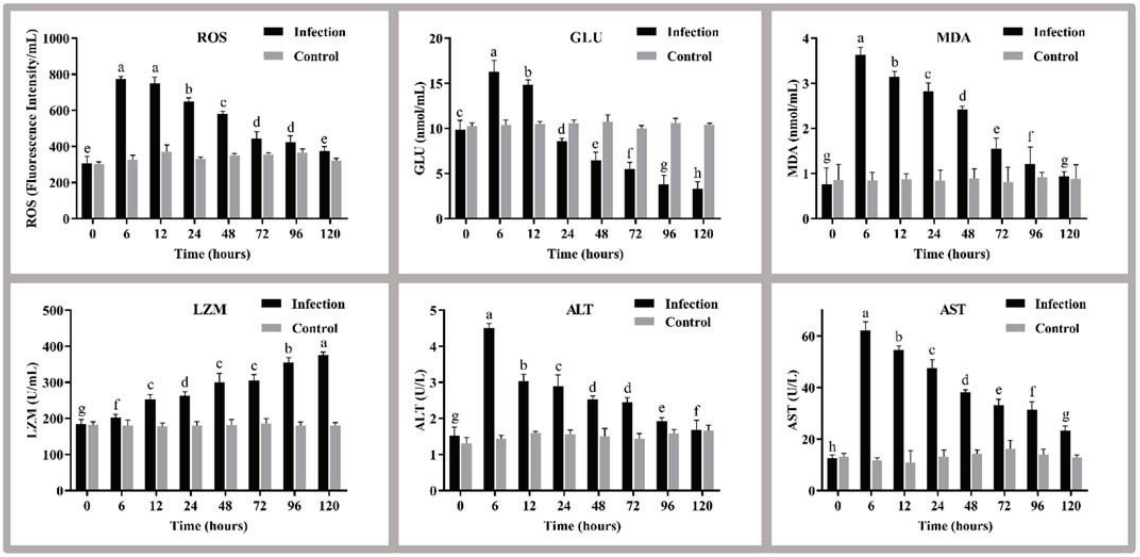

Figure 2. The levels of ROS, GLU, MDA, LZM, ALT, and AST in plasma at different times before and after the challenge. Different letters indicate significant differences between the stress groups ($p < 0.05$). Values are the means ± SEs ($n = 3$). The grey bars represent the indicators of fish before the challenge, and the black bars represent the indicators of fish after the challenge. ROS, reactive oxygen species; GLU, glucose; MDA; malondialdehyde, LZM, lysozyme; ALT, alanine aminotransferase; AST, aspartate aminotransferase.

3.4. Analysis of Liver Enzyme Activity

After *S. agalactiae* infection, the enzyme activities of SOD, CAT, and GPx in the liver all changed significantly. The activities of these enzymes decreased to the lowest level at 6 h after infection ($p < 0.05$), gradually increased, and reached normal levels (Figure 3).

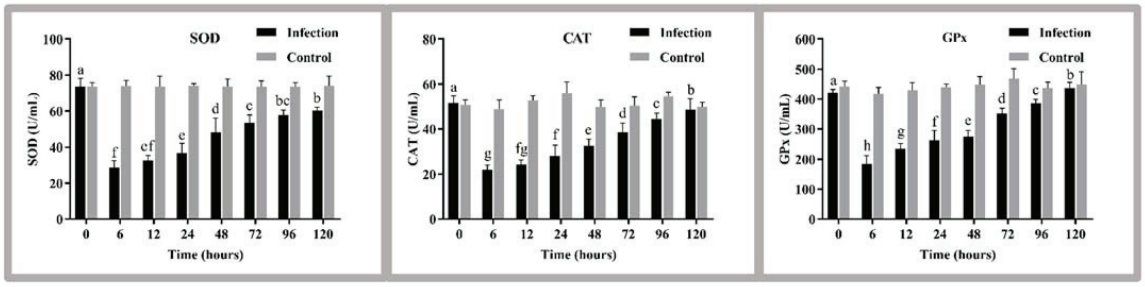

Figure 3. The liver antioxidant capacity of golden pompano before and after the challenge. Different letters indicate significant differences between the stress groups ($p < 0.05$). The values are the means ± SEs ($n = 3$). The grey bars represent the indicators of fish before the challenge, and the black bars represent the indicators of fish after the challenge. SOD, superoxide dismutase; CAT, catalase; GPx, glutathione peroxidase.

3.5. Expression of Antioxidant Markers and Signaling Pathway Genes in the Liver

The expression levels of antioxidant genes (*SOD*, *CAT*, *GPx*) and NF-κB pathway genes (*NF-κB*, *IKK*, *IKB*) in the liver were detected by qPCR after golden pompano was infected with *S. agalactiae* (Figure 4). Specifically, the expression of the antioxidant genes *SOD*, *CAT*, and *GPx* showed a trend of first increasing and then decreasing ($p < 0.05$),

reaching the maximum values at 24 h, 48 h, and 24 h, respectively. The pathway genes IKK and NF-κB were significantly upregulated at 12 h and 24 h post-infection, respectively ($p < 0.05$), whereas IκB mRNA expression showed the opposite trend. IL-1β and TNF-α mRNA expression levels gradually increased under *S. agalactiae* stimulation ($p < 0.05$), reaching the maximum at 120 h.

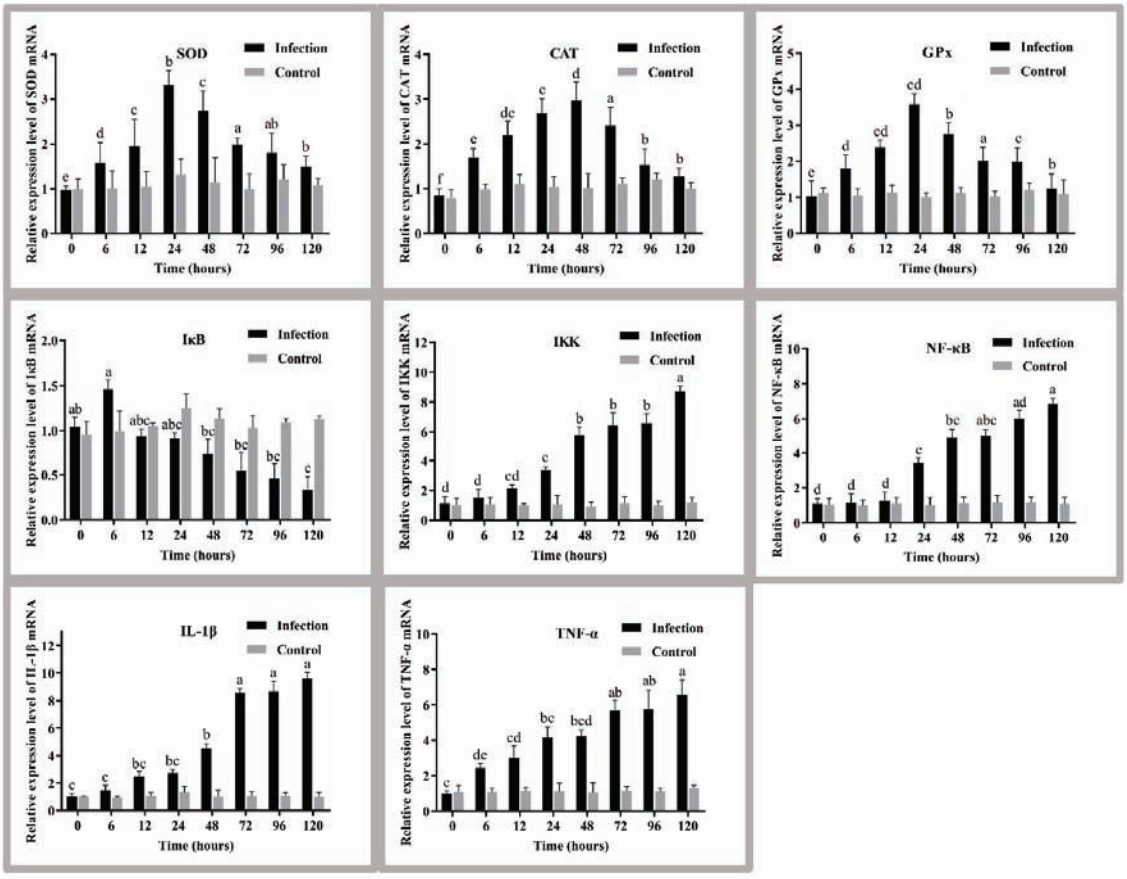

Figure 4. Liver antioxidant capacity and pathway genes of golden pompano before and after the challenge. Different letters indicate significant differences between the stress groups ($p < 0.05$). The values are the means ± SEs ($n = 3$). The grey bars represent the indicators of fish before the challenge, and the black bars represent indicators of fish after the challenge. IKK, inhibitor of kappa-B kinase; *IKB*, NF-kappa-B inhibitor; NF-κB, nuclear factor kappa-B; TNF-α, tumour necrosis factor α; IL-1β, interleukin 1β.

4. Discussion

In recent years, *S. agalactiae* infection has led to massive mortality of golden pompano, causing huge economic losses to the farming industry [3]. However, to date, no effective method has been found to prevent and treat this disease. Therefore, elucidating the pathological features of golden pompano after *S. agalactiae* infection from both the macro and micro perspectives is essential for its healthy farming.

4.1. Survival Rate and Histopathological Analysis

Survival analysis showed an inverse relationship between golden pompano survival time and *S. agalactiae* injection dose. The higher the injection dose of *S. agalactiae*, the

shorter the survival time of the golden pompano. The results are consistent with studies following injection of zebrafish [33] and Nile tilapia [34] via the same pathogenic bacteria, with deaths starting at 48 h post-infection. Furthermore, previous studies have shown that *S. agalactiae* infection can invade various tissues of the host [35]. It attacks the liver tissue of the host, resulting in cell rupture and bacterial cell adhesion, and then invades the inner sinusoidal wall and the sinus cavity [35,36]. In this study, it was observed that 120 h after *S. agalactiae* infection, the cell membrane was disintegrated in the hepatocytes, and the nucleus was translucent and severely displaced. Our study showed the similar histopathological changes in hepatocytes, indicating that the model of infection with *S. agalactiae* was successfully constructed and can be used for subsequent analysis.

4.2. Analysis of Serum Parameter

Hematological parameters, as the main indicators of fish health status, are sensitive to bacterial infections [37]. Bacterial infections can adversely affect the oxygen-carrying capacity of the blood and the electrolyte balance of the blood, leading to extravasation of red blood cells and changes in cell size [38]. Therefore, hematological parameters are often used as important indicators to assess the health status of fish after exposure to bacterial infections and various other environmental stresses [38,39]. ROS, GLU, MDA, LZM, ALT, and AST are common serum examination parameters [39]. ROS (O, O_2^-, -OH, H_2O_2, etc.) are associated with the occurrence and development of several bacterial infectious diseases [40]. A rapid increase in ROS contents of the host in response to pathogenic bacterial stimulation can enhance the antioxidant capacity of the organism [40]. Therefore, the higher ROS contents detected in the serum of the infected group in this study compared to the control group may be due to oxidative stress caused by the invasion of *S. agalactiae* into the fish. In general, pathogenic bacteria invading the mucosal system of fish can activate LZM and trigger an immune response against pathogenic bacteria [41]. LZM activity in serum is often elevated by pathogenic bacterial stimulation [42]. Thus, the infected fish in this study showed higher LZM activity than the uninfected fish, and this activity increased over time. It is consistent with the results of LZM changes following infection of *Cherax quadricarinatus* with *Aeromonas veronii* [22]. Significant changes in GLU levels were observed in infected golden pompano, probably due to impaired hepatic glucose metabolism caused by pathogenic bacterial infection, affecting insulin resistance and glucose metabolism [43]. Serum MDA levels reflect the degree of damage after a large number of free radicals have attacked the organism. The higher its level, the greater the degree of intracellular lipid peroxidation damage [44,45]. Therefore, the persistent elevation of serum MDA levels in infected golden pompano may be related to increased lipid oxidative damage after *S. agalactiae* attack the organism. In addition, serum ALT and AST levels are also often considered important indicators for assessing the health of the liver [46]. Once liver tissue is damaged or stressed by the surrounding environment, the porosity of the plasma membrane increases, and these two enzymes in serum levels increase rapidly [47]. Therefore, this study's elevated activities of ALT and AST may be associated with damage to hepatocytes in golden pompano.

4.3. Analysis of Liver Antioxidant Enzyme Parameters

Previous studies have shown that ROS do not usually cause direct damage to organisms, but rather play a role in mediating the organism's response to various stimuli. Excess ROS can lead to an increase in free radicals (O^{2-}, -OH) in the cells of the organism, which can cause oxidative damage to the organism, thereby weakening its immune defense system [22]. Fish prevent oxidative damage caused by ROS production from exposure to various environmental stress by increasing antioxidant enzyme activity. SOD can scavenge superoxide radicals (O^{2-}) in organisms through disproportionation reactions, converting them to H_2O_2 and O_2 [48,49]; CAT further decomposes H_2O_2 into H_2O and O_2, thereby reducing oxidative damage to the organism by free radicals [50]. In addition, the organism can be protected from ROS damage by GPx catalyzing the oxidation of GSH by H_2O_2 to

produce oxidized glutathione (GSSG), which reduces H_2O_2 to non-toxic hydroxyl compounds [51]. In general, the higher the environmental stress, the greater the resistance of the organism to oxidative damage and the higher the activity of antioxidant enzymes such as SOD, CAT and GPx [52]. However, exogenous infection may also lead to a decrease in antioxidant enzyme activity due to energy expenditure during the fight against oxidative stress [53]. Therefore, an acute decrease in SOD, CAT, and GPx at the beginning of *S. agalactiae* infection in this study may be related to the rapid energy depletion of the organism at the beginning of the infection. However, with prolonged infection time, ROS accumulated excessively, and the organisms gradually increased the activities of SOD, CAT, and GPx can alleviate the damage caused by ROS.

4.4. Analysis of Antioxidant Markers and Signaling Pathway Genes in the Liver

This study on liver enzyme activity has confirmed that the antioxidant enzymes SOD, CAT, and GPx play an essential role in resistance to *S. agalactiae* infection. To better understand the molecular mechanisms of immunity in golden pompano against *S. agalactiae* infection, the relative expression levels of its endogenous antioxidant enzyme genes in the liver were examined first. *SOD*, *CAT*, and *GPx* gene expression levels in the liver were significantly upregulated compared to the control group. These results were similar to *SOD*, *CAT*, and *GPx* gene expression in the liver after *Aeromonas hydrophila* attacked *Channa striata* [54], suggesting that *S. agalactiae* infection affects liver antioxidant gene expression. In addition, this study indicates that the level of enzyme activity is influenced by the expression of the corresponding genes in cells. However, our study did not observe a complete agreement between the level of antioxidant enzyme activity and its gene expression level. Researchers have reported that there is no strictly linear relationship between them [55]. Therefore, further studies are needed regarding the regulatory relationship between enzyme activity and genes.

Secondly, we analysed the effect of *S. agalactiae* infection on the expression of pro-inflammatory and anti-inflammatory genes in golden pompano. It has been established that a corresponding inflammatory response is triggered when ROS accumulates to a certain level. For example, the inflammatory response activated during spring viremia of carp virus infection carp is associated with ROS accumulation [56]. As a critical transcription factor in initiating and regulating inflammation, NF-κB gene plays an essential role in the development of inflammatory response. Meanwhile, NF-κB-mediated signaling pathways are classical signaling pathways that regulate the inflammatory response [57]. This study explored the expression of NF-κB blockers and several commonly induced genes. The results showed that the expression of IKK and NF-κB increased over time in the liver of infected golden pompano, whereas the expression of IκB gradually decreased and was lower than that of the control group. It is due to pathogenic bacteria invasion resulting in the inactivation of IκB and increased NF-κB dimer activity. NF-κB dimers are activated and transferred to the nucleus through post-translational modifications to induce the expression of multiple genes, producing multiple cytokines associated with inflammation [58,59]. Furthermore, NF-κB, a central regulator of the inflammatory response, plays a central role in inducting and encoding pro-inflammatory cytokines IL-1β and TNF-α [59,60]. Thus, IL-1β and TNF-α, as stress-inducible genes, are consistently upregulated in expression during infection [58].

5. Conclusions

In this study, serum biochemical indices, histopathology, and expression of TNF-α/NF-κB pathway genes after infection with *S. agalactiae* were investigated using golden pompano as experimental subjects. This study shows that serum biochemicals could be used to indicate the healthy status of golden pompano after infection with *S. agalactiae*. TNF-α/NF-κB has an essential immunomodulatory role in the resistance to *S. agalactiae* infection in golden pompano. In conclusion, our results may provide a theoretical basis for disease prevention and treatment of golden pompano.

Author Contributions: D.Z.: Writing—review and editing, Funding acquisition. J.G.: Writing—original draft. H.G.: Formal analysis. K.Z.: Data curation. B.L. (Bo Liu): Supervision. N.Z.: Visualization, Investigation. M.L.: Methodology, Software. B.L. (Baosuo Liu): Software, Validation. All authors have read and agreed to the published version of the manuscript.

Funding: This study was supported by the Key Projects of Joint Fund for Regional Innovation and Development of NSFC (U20A2064), the Central Public-interest Scientific Institution Basal Research Fund CAFS (No. 2020TD29), the Supported by the earmarked fund for CARS-47 (CARS-47), the Central Public-Interest Scientific Institution Basal Research Fund of South China Sea Fisheries Research Institute, the CAFS (2021SD12), and the Guangdong Provincial Special Fund for Modern Agriculture Industry Technology Innovation Teams (2019KJ143).

Institutional Review Board Statement: All experimental protocols and methods in this study were approved by the Animal Care and Use Ethics Committee in the South China Sea Fisheries Research Institute (SCSFRI96-253, 15 September 2021).

Informed Consent Statement: Not applicable.

Data Availability Statement: Data are contained within the article.

Conflicts of Interest: The authors declare no conflict of interest.

References

1. Yang, Q.; Guo, L.; Liu, B.S.; Guo, H.Y.; Zhu, K.C.; Zhang, N.; Jiang, S.G.; Zhang, D.C. Effects of stocking density on the growth performance, serum biochemistry, muscle composition and HSP70 gene expression of juvenile golden pompano *Trachinotus ovatus* (Linnaeus, 1758). *Aquaculture* **2020**, *518*, 734841. [CrossRef]
2. Liu, M.J.; Guo, H.Y.; Zhu, K.C.; Liu, B.S.; Liu, B.; Guo, L.; Zhang, N.; Yang, J.W.; Jiang, S.G.; Zhang, D.C. Effects of acute ammonia exposure and recovery on the antioxidant response and expression of genes in the Nrf2-Keap1 signaling pathway in the juvenile golden pompano (*Trachinotus ovatus*). *Aquat. Toxicol.* **2021**, *240*, 105969. [CrossRef] [PubMed]
3. Guo, S.; Mo, Z.; Wang, Z.; Xu, J.; Li, Y.; Dan, X.; Li, A. Isolation and pathogenicity of *Streptococcus iniae* in offshore cage-cultured *Trachinotus ovatus* in China. *Aquaculture* **2018**, *492*, 247–252. [CrossRef]
4. Johri, A.K.; Paoletti, L.C.; Glaser, P.; Dua, M.; Sharma, P.K.; Grandi, G.; Rappuoli RGroup, B. *Streptococcus*: Global incidence and vaccine development. *Nat. Rev. Microbiol.* **2006**, *4*, 932–942. [CrossRef] [PubMed]
5. Delannoy, C.M.J.; Samai, H.; Labrie, L. *Streptococcus agalactiae* serotype IV in farmed tilapia. *Aquaculture* **2021**, *544*, 737033. [CrossRef]
6. Fazio, F. Fish hematology analysis as an important tool of aquaculture: A review. *Aquaculture* **2019**, *500*, 237–242. [CrossRef]
7. Fuller, G.G.; Kim, J.K. Compartmentalization and metabolic regulation of glycolysis. *J. Cell Sci.* **2021**, *134*, 20. [CrossRef]
8. Uma, A.; Philominal, P.; Prabu, E.; Musthafa, M.S. Dietary Bougainvillea glabra leaf meal on growth, haemato-biochemical responses and disease resistance in Nile tilapia, *Oreochromis niloticus* against Enterococcus faecalis. *Aquaculture* **2022**, *549*, 737806. [CrossRef]
9. Abdel-Tawwab, M.; El-Araby, D.A. Immune and antioxidative effects of dietary licorice (*Glycyrrhiza glabra* L.) on performance of Nile tilapia, *Oreochromis niloticus* (L.) and its susceptibility to *Aeromonas hydrophila* infection. *Aquaculture* **2021**, *530*, 735828. [CrossRef]
10. Liu, M.J.; Guo, H.Y.; Liu, B.; Zhu, K.C.; Guo, L.; Liu, B.S.; Zhang, N.; Yang, J.W.; Jiang, S.G.; Zhang, D.C. Gill oxidative damage caused by acute ammonia infection was reduced through the HIF-1α/NF-κb signaling pathway in golden pompano (*Trachinotus ovatus*). *Ecotoxicol. Environ. Saf.* **2021**, *222*, 112504. [CrossRef]
11. Abdel-Tawwab, M.; Samir, F.; Abd El-Naby, A.S.; Monier, M.N. Antioxidative and immunostimulatory effect of dietary cinnamon nanoparticles on the performance of Nile tilapia, *Oreochromis niloticus* (L.) and its susceptibility to hypoxia infection and Aeromonas hydrophila infection. *Fish Shellfish. Immunol.* **2018**, *74*, 19–25. [CrossRef] [PubMed]
12. Senftleben, U.; Cao, Y.; Xiao, G.; Greten, F.R.; Krähn, G.; Bonizzi, G.; Chen, Y.; Hu, Y.; Fong, A.; Sun, S.C.; et al. Activation by IKKalpha of a second, evolutionary conserved, NF-kappa B signaling pathway. *Science* **2001**, *293*, 1495–1499. [CrossRef] [PubMed]
13. Hayden, M.S.; Ghosh, S. Regulation of NF-κB by TNF family cytokines. *Semin. Immunol.* **2014**, *26*, 253–266. [CrossRef] [PubMed]
14. Giri, S.S.; Sen, S.S.; Sukumaran, V. Pinocembrin attenuates lipopolysaccharide-induced inflammatory responses in *Labeo rohita* macrophages via the suppression of the NF-κB signaling pathway. *Fish Shellfish. Immunol.* **2016**, *56*, 459–466. [CrossRef] [PubMed]
15. Chu, Y.; Lv, X.; Zhang, L.; Fu, X.; Song, S.; Su, A.; Chen, D.; Xu, L.; Wang, Y.; Wu, Z.; et al. Wogonin inhibits in vitro herpes simplex virus type 1 and 2 infection by modulating cellular NF-κB and MAPK pathways. *BMC Microbiol.* **2020**, *20*, 2–11. [CrossRef]
16. Fujita, T.; Nolan, G.P.; Ghosh, S.; Baltimore, D. Independent modes of transcriptional activation by the p50 and p65 subunits of NF-KB. *Genes Dev.* **1992**, *6*, 775–787. [CrossRef]
17. Tacchi, L.; Casadei, E.; Bickerdike, R.; Secombes, C.J.; Martin, S.A.M. MULAN related gene (MRG): A potential novel ubiquitin ligase activator of NF-kB involved in immune response in Atlantic salmon (*Salmo salar*). *Dev. Comp. Immunol.* **2012**, *38*, 545–553. [CrossRef]

18. Deng, L.; Zeng, Q.; Wang, M.; Cheng, A.; Jia, R.; Chen, S.; Zhu, D.; Liu, M.; Yang, Q.; Wu, Y.; et al. Suppression of NF-κB activity: A viral immune evasion mechanism. *Viruses* **2018**, *10*, 409. [CrossRef]
19. Vlantis, K.; Wullaert, A.; Polykratis, A.; Kondylis, V.; Dannappel, M.; Schwarzer, R.; Welz, P.; Corona, T.; Walczak, H.; Weih, F.; et al. NEMO Prevents RIP Kinase 1-Mediated Epithelial Cell Death and Chronic Intestinal Inflammation by NF-κB-Dependent and -Independent Functions. *Immunity* **2016**, *44*, 553–567. [CrossRef]
20. Blackwell, K.; Zhang, L.; Workman, L.M.; Ting, A.T.; Iwai, K.; Habelhah, H. Two Coordinated Mechanisms Underlie Tumor Necrosis Factor Alpha-Induced Immediate and Delayed IκB Kinase Activation. *Mol. Cell. Biol.* **2013**, *33*, 1901–1915. [CrossRef]
21. Wang, J.X.; Li, X.M.; Bello, B.K.; Yu, G.L.; Yang, Q.K.; Yang, H.T.; Zhang, W.; Wang, L.; Dong, J.Q.; Liu, G.; et al. Activation of TLR2 heterodimers-mediated NF-κB, MAPK, AKT signaling pathways is responsible for *Vibrio alginolyticus* triggered inflammatory response in vitro. *Microb. Pathog.* **2022**, *162*, 105219. [CrossRef] [PubMed]
22. Guo, L.F.; Zhou, M.; Chen, D.D.; Yi, C.; Sun, B.; Wang, S.Q.; Ru, Y.Y.; Chen, H.J.; Wang, H. A new insight to characterize immunomodulation based on hepatopancreatic transcriptome and humoral immune factor analysis of the *Cherax quadricarinatus* infected with *Aeromonas veronii*. *Ecotoxicol. Environ. Saf.* **2021**, *219*, 112347. [CrossRef] [PubMed]
23. Roubach, R.; Gomes, L.C.; Leão Fonseca, F.A.; Val, A.L. Eugenol as an efficacious anaesthetic for tambaqui, *Colossoma macropomum* (Cuvier). *Aquac. Res.* **2005**, *36*, 1056–1061. [CrossRef]
24. Witeska, M.; Kondera, E.; Ługowska, K.; Bojarski, B. Hematological methods in fish-Not only for beginners. *Aquaculture* **2022**, *547*, 737498. [CrossRef]
25. Tanaka, N.; Izawa, T.; Kuwamura, M.; Higashiguchi, N.; Kezuka, C.; Kurata, O.; Wada, S.; Yamate, J. The first case of infectious spleen and kidney necrosis virus (ISKNV) infection in aquarium-maintained mandarin fish, *Siniperca chuatsi* (Basilewsky), in Japan. *J. Fish Dis.* **2014**, *37*, 401–405. [CrossRef]
26. Gerrits, P.O.; van Leeuwen, M.B. Glycol methacrylate embedding in histotechnology: The hematoxylin-eosin stain as a method for assessing the stability of glycol methacrylate sections. *Stain Technol.* **1987**, *62*, 181–190. [CrossRef]
27. Loureiro, S.; Amorim, A.; Cainé, L.; Silva, B.; Gomes, I. Evaluation of two DNA/RNA co-extraction methods for organism fluid identification in forensics. *Forensic Sci. Int. Genet. Suppl. Ser.* **2019**, *7*, 250–252. [CrossRef]
28. Ma, Q.W.; Guo, H.Y.; Zhu, K.C.; Guo, L.; Liu, B.S.; Zhang, N.; Liu, B.; Yang, J.W.; Jiang, S.G.; Zhang, D.C. Dietary taurine intake affects growth and taurine synthesis regulation in golden pompano, *Trachinotus ovatus* (Linnaeus 1758). *Aquaculture* **2021**, *530*, 735918. [CrossRef]
29. Livak, K.J.; Schmittgen, T.D. Analysis of relative gene expression data using real-time quantitative PCR and the $2^{-\Delta\Delta CT}$ Method. *Methods* **2001**, *25*, 402–408. [CrossRef]
30. Xie, J.J.; Fang, H.; He, X.; Liao, S.; Liu, Y.; Tian, L.; Niu, J. Study on mechanism of synthetic astaxanthin and *Haematococcus pluvialis* improving the growth performance and antioxidant capacity under acute hypoxia stress of golden pompano (*Trachinotus ovatus*) and enhancing anti-inflammatory by activating Nrf2-ARE pathway to antagonize the NF-κB pathway. *Aquaculture* **2020**, *518*, 734657. [CrossRef]
31. Xun, P.W.; Zhou, C.; Huang, X.; Huang, Z.; Yu, W.; Yang, Y.; Li, T.; Huang, J.; Wu, Y.; Lin, H. Effects of Dietary Sodium Acetate on Growth Performance, Fillet Quality, Plasma Biochemistry, and Immune Function of Juvenile Golden Pompano (*Trachinotus ovatus*). *Aquac. Nutr.* **2022**, *2022*, 9074549. [CrossRef]
32. Fang, H.H.; Xie, J.J.; Zhao, W.; Liu, Z.L.; Liu, Y.J.; Tian, L.X.; Niu, J. Study supplementation of astaxanthin in high-fat diet on growth performance, antioxidant ability, anti-inflammation, non-specific immunity and intestinal structure of juvenile *Trachinotus ovatus*. *Aquac. Nutr.* **2021**, *27*, 2575–2586. [CrossRef]
33. Wu, X.M.; Cao, L.; Hu, Y.W.; Chang, M.X. Transcriptomic characterization of adult zebrafish infected with *Streptococcus agalactiae*. *Fish Shellfish. Immunol.* **2019**, *94*, 355–372. [CrossRef] [PubMed]
34. Gallage, S.; Katagiri, T.; Endo, M.; Maita, M. Comprehensive evaluation of immunomodulation by moderate hypoxia in *S. agalactiae* vaccinated Nile tilapia. *Fish Shellfish. Immunol.* **2017**, *66*, 445–454. [CrossRef]
35. Cao, J.M.; Liu, Z.G.; Zhang, D.F.; Guo, F.Q.; Gao, F.Y.; Wang, M.; Yi, M.M.; Lu, M.X. Distribution and localization of *Streptococcus agalactiae* in different tissues of artificially infected tilapia (*Oreochromis niloticus*). *Aquaculture* **2022**, *546*, 737370. [CrossRef]
36. Soto, E.; Wang, R.; Wiles, J.; Green, C.; Plumb, J.; Hawke, J.; Soto, E. Characterization of isolates of *Streptococcus agalactiae* from diseased farmed and wild marine fish from the U.S. Gulf coast, Latin America, and Thailand. *J. Aquat. Anim. Health* **2015**, *27*, 123–134. [CrossRef]
37. Kim, J.H.; Sohn, S.; Kim, S.K.; Hur, Y.B. Effects on hematological parameters, antioxidant and immune responses, AChE, and stress indicators of olive flounders, *Paralichthys olivaceus*, raised in bio-floc and seawater challenged by *Edwardsiella tarda*. *Fish Shellfish. Immunol.* **2020**, *97*, 194–203. [CrossRef]
38. Bandeira Junior, G.; dos Santos, A.C.; de Freitas Souza, C.; Baldissera, M.D.; dos Santos Moreira , K.L.; da Veiga, M.L.; da Rocha, M.I.d.U.M.; de Vargas, A.P.C.; da Cunha, M.A.; Baldisserotto, B. *Citrobacter freundii* infection in silver catfish (*Rhamdia quelen*): Hematological and histological alterations. *Microb. Pathog.* **2018**, *125*, 276–280. [CrossRef]
39. Kim, J.H.; Yu, Y.B.; Choi, J.H. Toxic effects on bioaccumulation, hematological parameters, oxidative infection, immune responses and neurotoxicity in fish exposed to microplastics: A review. *J. Hazard. Mater.* **2021**, *413*, 125423. [CrossRef]
40. Rodríguez, I.; Novoa, B.; Figueras, A. Immune response of zebrafish (*Danio rerio*) against a newly isolated bacterial pathogen *Aeromonas hydrophila*. *Fish Shellfish. Immunol.* **2008**, *25*, 239–249. [CrossRef]

41. Zheng, X.; Jiang, W.D.; Feng, L.; Wu, P.; Liu, Y.; Jiang, J.; Kuang, S.Y.; Tang, L.; Zhou, X.Q. Effects of dietary pyridoxine on the skin immunity, tight junctions, antioxidants and apoptosis of grass carp (*Ctenopharyngodon idella*) infected with *Aeromonas hydrophila*. *Aquac. Res.* **2022**, *53*, 1582–1596. [CrossRef]
42. Xia, H.; Tang, Y.; Lu, F.; Luo, Y.; Yang, P.; Wang, W.; Jiang, J.; Li, N.; Han, Q.; Liu, F.; et al. The effect of *Aeromonas hydrophila* infection on the non-specific immunity of blunt snout bream (*Megalobrama amblycephala*). *Cent. Eur. J. Immunol.* **2017**, *42*, 239–243. [CrossRef] [PubMed]
43. Banaee, M.; Soltanian, S.; Sureda, A.; Gholamhosseini, A.; Haghi, B.N.; Akhlaghi, M.; Derikvandy, A. Evaluation of single and combined effects of cadmium and micro-plastic particles on biochemical and immunological parameters of common carp (*Cyprinus carpio*). *Chemosphere* **2019**, *236*, 124335. [CrossRef] [PubMed]
44. Tsikas, D. Assessment of lipid peroxidation by measuring malondialdehyde (MDA) and relatives in biological samples: Analytical and biological challenges. *Anal. Biochem.* **2017**, *524*, 13–30. [CrossRef]
45. Lang, X.; Wang, L.; Zhang, Z. Stability evaluation of reference genes for real-time PCR in zebrafish (*Danio rerio*) exposed to cadmium chloride and subsequently infected by bacteria *Aeromonas hydrophila*. *Aquat. Toxicol.* **2016**, *170*, 240–250. [CrossRef]
46. Chung, S.; Ribeiro, K.; Teixeira, D.V.; Copatti, C.E. Inclusion of essential oil from ginger in the diet improves physiological parameters of tambaqui juveniles (*Colossoma macropomum*). *Aquaculture* **2021**, *543*, 736934. [CrossRef]
47. Kong, Y.D.; Li, M.; Wu, X.Q.; Xia, C.G.; Liu, X.Y.; Wang, G.Q. Protective mechanism of homologous lactic acid bacteria against cholestatic liver injury in snakehead fish. *Aquaculture* **2022**, *550*, 737845. [CrossRef]
48. Aluta, U.P.; Aderolu, A.Z.; Lawal, M.O.; Olutola, A.A. Inclusion effect of onion peel powder in the diet of African catfish, *Clarias gariepinus*: Growth, blood chemistry, hepatic antioxidant enzymes activities and SOD mRNA responses. *Sci. Afr.* **2021**, *12*, e00780. [CrossRef]
49. Junior, G.B.; Baldisserotto, B. Fish infections associated with the genus *Aeromonas*: A review of the effects on oxidative status. *J. Appl. Microbiol.* **2021**, *131*, 1083–1101. [CrossRef]
50. Baruah, K.; Ranjan, J.; Sorgeloos, P.; MacRae, T.H.; Bossier, P. Priming the prophenoloxidase system of *Artemia franciscana* by heat shock proteins protects against *Vibrio campbellii* challenge. *Fish Shellfish. Immunol.* **2011**, *31*, 134–141. [CrossRef]
51. Muñoz-Peñuela, M.; Nostro, F.L.L.; Dal'Olio Gomes, A.; Tolussi, C.E.; Branco, G.S.; Pinheiro, J.P.S.; de Godoi, F.G.A.; Moreira, R.G. Diclofenac and caffeine inhibit hepatic antioxidant enzymes in the freshwater fish *Astyanax altiparanae* (Teleostei: Characiformes). *Comp. Biochem. Physiol. Part C Toxicol. Pharmacol.* **2021**, *240*, 108910. [CrossRef] [PubMed]
52. Lu, Y.P.; Zheng, P.H.; Zhang, X.X.; Wang, L.; Li, J.T.; Zhang, Z.L.; Xu JR Cao, Y.L.; Xian, J.A.; Wang, A.L.; Wang, D.M. Effects of dietary trehalose on growth, trehalose content, non-specific immunity, gene expression and desiccation resistance of juvenile red claw crayfish (*Cherax quadricarinatus*). *Fish Shellfish. Immunol.* **2021**, *119*, 524–532. [CrossRef] [PubMed]
53. Han, Y.; Liu, T.; Wang, J.; Wang, J.; Zhang, C.; Zhu, L. Genotoxicity and oxidative infection induced by the fungicide azoxystrobin in zebrafish (*Danio rerio*) livers. *Pestic. Biochem. Physiol.* **2016**, *133*, 13–19. [CrossRef] [PubMed]
54. Samayanpaulraj, V.; Velu, V.; Uthandakalaipandiyan, R. Determination of lethal dose of *Aeromonas hydrophila* Ah17 strain in snake head fish *Channa striata*. *Microb. Pathog.* **2019**, *127*, 7–11. [CrossRef]
55. Kim, C.H.; Kim, E.J.; Nam, Y.K. Superoxide dismutase multigene family from a primitive chondrostean sturgeon, acipenser baerii: Molecular characterization, evolution, and antioxidant defense during development and pathogen infection. *Antioxidants* **2021**, *10*, 232. [CrossRef]
56. Sun, J.; Wang, J.W.; Li, L.J.; Wu, Z.X.; Chen, X.X.; Yuan, J.F. ROS induced by spring viraemia of carp virus activate the inflammatory response via the MAPK/AP-1 and PI3K signaling pathways. *Fish Shellfish. Immunol.* **2020**, *101*, 216–224. [CrossRef]
57. Yang, F.; Sheng, X.; Huang, X.; Zhang, Y. Interactions between *Salmonella* and host macrophages—Dissecting NF-κB signaling pathway responses. *Microb. Pathog.* **2021**, *154*, 104846. [CrossRef]
58. Muto, A.; Ruland, J.; McAllister-Lucas, L.M.; Lucas, P.C.; Yamaoka, S.; Chen, F.F.; Lin, A.; Mak, T.W.; Núñez, G.; Inohara, N. Protein kinase C-associated kinase (PKK) mediates Bcl10-independent NF-κB activation induced by phorbol ester. *J. Biol. Chem.* **2002**, *277*, 31871–31876. [CrossRef]
59. Dong, W.J.; Gao, W.Y.; Yan, X.L.; Sun, Y.N.; Xu, T.J. microRNA-132 as a negative regulator in NF-κB signaling pathway via targeting IL-1β in miiuy croaker. *Dev. Comp. Immunol.* **2021**, *122*, 104113. [CrossRef]
60. Choi, J.H.; Ko, H.M.; Kim, J.W.; Lee, H.K.; Han, S.S.; Chun, S.B.; Im, S.Y. Platelet-activating factor-induced early activation of nf- b plays a crucial role for organ clearance of *Candida albicans*. *J. Immunol.* **2001**, *166*, 5139–5144. [CrossRef]

antioxidants

MDPI

Article

Expression Analysis of a Novel Oxidoreductase Glutaredoxin 2 in Black Tiger Shrimp, *Penaeus monodon*

Rui Fan [1,2], Yundong Li [1], Qibin Yang [1,3], Song Jiang [1], Jianhua Huang [1], Lishi Yang [1], Xu Chen [1,3], Falin Zhou [1,3,*] and Shigui Jiang [1,*]

[1] Key Laboratory of South China Sea Fishery Resources Exploitation and Utilization, Ministry of Agriculture and Rural Affairs, South China Sea Fisheries Research Institute, Chinese Academy of Fishery Sciences, Guangzhou 510300, China
[2] College of Fisheries and Life Science, Shanghai Ocean University, Shanghai 201306, China
[3] Tropical Fishery Research and Development Center, South China Sea Fisheries Research Institute, Chinese Academy of Fishery Sciences, Sanya 572018, China
* Correspondence: zhoufalin0925@163.com (F.Z.); jiangsg@21cn.com (S.J.)

Abstract: Glutaredoxin (Grx) is a glutathione-dependent oxidoreductase that is an important component of the redox system in organisms. However, there is a serious lack of sequence information and functional validation related to Grx in crustaceans. In this study, a novel Grx was identified in *Penaeus monodon* (*PmGrx2*). The full-length cDNA of *PmGrx2* is 998 bp, with an open reading frame (ORF) of 441 bp, encoding 119 amino acids. Sequence alignment showed that *PmGrx2* had the highest identity with Grx2 of *Penaeus vannamei* at 96.64% and clustered with Grx2 of other crustaceans. Quantitative real-time PCR (qRT-PCR) analysis showed that *PmGrx2* was expressed in all examined tissues, with higher expression levels in the stomach and testis. *PmGrx2* was continuously expressed during development and had the highest expression level in the zygote stage. Both ammonia-N stress and bacterial infection could differentially induce the expression of *PmGrx2* in hepatopancreas and gills. When *PmGrx2* was inhibited, the expression of antioxidant enzymes was suppressed, the degree of apoptosis increased, and the GSH content decreased with the prolongation of ammonia-N stress. Inhibition of *PmGrx2* resulted in shrimp being exposed to a greater risk of oxidative damage. In addition, an SNP locus was screened on the exons of *PmGrx2* that was significantly associated with an ammonia-N-stress-tolerance trait. This study suggests that *PmGrx2* is involved in redox regulation and plays an important role in shrimps' resistance to marine environmental stresses.

Keywords: glutaredoxin; *Penaeus monodon*; oxidative stress; SNPs

Citation: Fan, R.; Li, Y.; Yang, Q.; Jiang, S.; Huang, J.; Yang, L.; Chen, X.; Zhou, F.; Jiang, S. Expression Analysis of a Novel Oxidoreductase Glutaredoxin 2 in Black Tiger Shrimp, *Penaeus monodon*. *Antioxidants* **2022**, *11*, 1857. https://doi.org/10.3390/antiox11101857

Academic Editor: Stanley Omaye

Received: 23 August 2022
Accepted: 19 September 2022
Published: 20 September 2022

1. Introduction

Glutaredoxins (Grxs, also known as thioltransferase), as members of the thioredoxins (Trxs) superfamily, are oxidoreductases that are characterized by their thermal stability and small molecular weight [1,2]. Grxs are indispensable in the redox system of organisms [3]. Grxs were originally discovered in *Escherichia coli lacking* Trxs activity, in 1976 [4]. Typical Grxs fall into two categories according to active site motifs, the dithiol Grxs and the monothiol Grxs, whose active site motifs are Cys-X-X-Cys and Cys-Gly-Phe-Ser, respectively. In the monothiol Grxs, a single Cys residue is present at the n-terminal only. With the assistance of reduced glutathione (GSH), both types of Grxs can reduce disulfide bonds in proteins and convert GSH to oxidized glutathione (GSSH). The difference between the two is that both Cys-active sites of dithiol Grxs are involved in the reaction, whereas monothiol Grxs use only the N-terminal Cys for the reaction. This process is reversible, which implies the important role of Grxs in maintaining intracellular GSH/GSSG ratio homeostasis [5]. Many other types of Grxs are also observed, especially prokaryotes, owing to further research [6]. The Grxs of most types and quantities are currently found in plants, which exhibit a unique active site of Cys-Cys-X-X [7]. In addition, the involvement of Grxs in various physiological

and biochemical activities, such as iron–sulfur cluster coordination, resistance to oxidative stress, and cell growth and apoptosis, has been proved [8–10]. Instead, there exist numerous studies on prokaryotes, mammals, and plants, while studies on relevant sequences and the functional validation of Grxs in crustaceans are rare.

The black tiger shrimp (*Penaeus monodon*) is an economically promising mariculture crustacean, accounting for about 8% of the crustacean farming industry [11]. However, during the culture process, black tiger shrimps are exposed to oxidative stress damage from biotic or abiotic stressors, leading to high mortality rates from time to time and subsequent significant economic losses [12]. Studies on the expression responses of relevant genes in black tiger shrimps under environmental stress and pathogen infection can enhance shrimp culture management and fill the gap in crustacean-related research.

Therefore, this paper cloned the full-length cDNA of *P. monodon* Grx2 (*PmGrx2*) and elaborated its expression during development and in various tissues. In the hope of clarifying the involvement of *PmGrx2* in other physiological activities in shrimps, the authors selected the most common ammonia-N stress factor and various pathogenic bacteria in the aquatic survival environment and observed the expressions of *PmGrx2* in these conditions and the physiological changes in shrimps after *PmGrx2* was disrupted. Moreover, the SNPs loci of *PmGrx2* related to the ammonia-N-stress-tolerance trait were screened. The study contributes to the future exploration of *PmGrx2*'s role in the regulation of redox homeostasis in shrimp.

2. Materials and Methods

2.1. Materials

The authors obtained the shrimps from the experimental base of South China Sea Fisheries Research Institute, Shenzhen, Guangdong, China. Shrimps that were 7.01 ± 0.8 g in weight and 5.12 ± 0.69 cm in length underwent RNA interference. Shrimps that were 1.53 ± 0.36 g and 2.11 ± 0.24 cm were used for SNPs analysis. The indicators of the remaining were 15.08 ± 1.20 g and 12.37 ± 0.57 cm. The shrimps were stored in plastic cylinders with aerated filtered seawater for a week (salinity 29‰, temperature 26 ± 2 °C, and pH 7.5–7.8) and were fed once a day with compound feed in the temporary feeding period until 24 h before use.

2.2. Materials Collection

The *PmGrx2* expression test required fourteen tissues, while that of *PmGrx2* during development required samples collection under fourteen phases from oosperm to post-larvae [13]. The samples were kept in RNALater solution (Ambion, Austin, TX, USA) at 4 °C for one day and later at −80 °C till being used.

2.3. Ammonia-N Stress

As for the testing of *PmGrx2* expression under ammonia-N stress, an acute ammonia-N stress pre-experiment was utilized to study the 96 h median lethal concentration (96 h LC50) and safe concentration (SC) of 180 shrimps. Groups of 30 shrimps were preserved separately in 200 L of filtered seawater, which was aerated constantly through an air stone and refreshed daily. The NH_4Cl was applied to seawater of per cylinder to prepare ammonia-N in six concentrations, covering 0, 20, 40, 60, 80, and 100 mg/L. The pre-experiment recorded mortality every 3 h, and the 96 h LC50 and SC computed by Linear Regression after completion stood at 29.47 and 2.95 mg/L, respectively [14,15].

The actual experiment and pre-experiment conducted under similar conditions employed shrimps of alike size, which randomly fell into 3 groups (control, 96 h LC50, and SC), each having 3 subgroups consisting of 30 shrimps per. The survival of shrimps was recorded every 3 h without feed supply, and the dead were immediately removed from the container. Three were picked for duplication at different time points, and their hepatopancreas and gills were dissected and preserved in the RNALater solution (Ambion, USA) at 4 °C for one day and then at −80 °C till being used.

2.4. In Vivo Experiment

The *PmGrx2* expression test following the immune challenge randomly divided the samples into 4 groups, each having 3 subgroups consisting of 25 shrimps each. The bacteria mentioned were obtained from Key Laboratory of South China Sea Fishery Resources Extraction & Utilization. Samples of the control group were previously injected with 100 μL sterile phosphate buffer solution (PBS, pH 7.4), while those of other groups with 100 μL (1.0×10^8 CFU/mL) of corresponding bacterial solution, respectively [16]. All were intramuscularly injected at the second abdominal segment. Similarly, the survival was logged every 3 h, and the dead were immediately taken out of the container. Three were selected at different time points, and their hepatopancreas and gills were dissected and kept by RNALater solution (Ambion, USA) at 4 °C for one day and later at −80 °C till being used.

2.5. Extraction of RNA and Synthesis of cDNA

The HiPure Fibrous RNA Plus Kit (Magen, Guangzhou, China) was used to obtain the total RNA of the samples in quantification experiments, and the RNeasy Mini Kit (Qiagen, Hilden, Germany) was adopted to obtain the total RNA of the remaining samples. Moreover, a NanoDrop 2000 device (Thermo, Waltham, MA, USA) was utilized to explore the ultraviolet absorbance ratio at 260/280 nm, thus determining the purity and quantity of the total RNA, while 1 percent agarose gel electrophoresis was also taken to evaluate its integrity. The RNA was synthesized into the corresponding cDNA, which was stored under −80 °C until it was used.

2.6. Cloning the Full-Length cDNA of PmGrx2

PmGrx2 was screened for partial fragments and identified through the NCBI database BLAST in the cDNA library of *P. monodon* in the laboratory, upon which the primers were established through Premier 6.0. The PCR program, which facilitated the expansion of *PmGrx2* open reading frame (ORF), underwent three procedures: 95 °C (3 min), 35 cycles of 95 °C (15 s), 55 °C (15 s), 72 °C (15 s), and 72 °C (5 min). In addition, the PCR amplification was completed in 25 μL of reaction mixture made up of forward primer (1 μL), reverse primer (1 μL), cDNA template (1 μL), double-distilled water (12.5 μL), and 2 × Taq Plus Master Mix II (12.5 μL) (Vazyme, Nanjing, China). Nested PCR primers featuring 3′ and 5′ ends end were generated by Premier 6.0 based on *PmGrx2* ORF. The procedures of the PCR program referred to the literature [11].

All PCR products were cloned into pEASY®-T1 Cloning Vector (TransGen, Beijing, China), and a positive monoclonal colony was sequenced. RACE technology was taken to calculate the full-length cDNA of *PmGrx2*, while Ruibiotech (Guangzhou, China) was used for the synthesis of primers and the sequencing of PCR products. Supplementary Tables S1 and S2 list the primers above.

2.7. mRNA Expression by Quantitative Real-Time PCR (qRT-PCR) Analysis

This study employed qRT-PCR to detect the expression of *PmGrx2* and related genes of samples in the experiment, Premier 6.0. to construct the qRT-PCR primers, and Elongation factor 1α (EF-1α) to represent the reference gene. All primers were synthesized by Ruibiotech (Guangzhou, China) and are demonstrated in Supplementary Table S3. A Roche Light Cycler®480II contributed to the qRT-PCR, and the specific procedures referred to the literature [11].

2.8. Ammonia-N Stress on PmGrx2-Interfered Shrimps

The T7 RiboMAX Express RNAi kit (Promega, Madisonm, WI, USA) was taken to synthesize the double-stranded RNA (dsRNA) for *PmGrx2* (dsGrx2) and green fluorescent protein (GFP, as a non-specific negative control) gene (dsGFP). Supplementary Table S4 demonstrates the primers adopted for the synthetization. The ultraviolet absorbance ratio at 260/280 nm obtained through a NanoDrop 2000 device (Thermo, USA) promoted the

calculation of dsRNA's purity and quantity, while 1 percent agarose gel electrophoresis shed a light on its integrity. The dsRNA was kept under −80 °C until used.

The *PmGrx2* expression was initially explored by qRT-PCR to clarify the interference efficiency of dsGrx2. The dsRNA was diluted to 1 μg/μL through PBS buffer prior to in vivo injection. The samples were categorized into two groups of three replicates each, with five shrimps in each replicate. The second ventral segment was injected with dsGrx2 or dsGFP dilution (3 μg per gram of shrimp weight), with the former serving as the experimental group and the latter as the control group. Three of each replicate were picked 24 h after injection, and their hepatopancreas were gathered; then the same procedures as in Section 2.7 were followed.

Given dsRNA's significant interference efficiency, the shrimps were again categorized into two groups with three replicates of 40 shrimps each, and injections were conducted as above. Twenty-four hours after injection, shrimps injected with dsGrx2 or dsGFP experienced acute ammonia-N stress that lasted for 48 h, using 96 h LC50. Three shrimps of each replicate were taken at each time, and the hepatopancreas was gathered. One half was preserved in RNALater solution (Ambion, USA) at 4 °C for one day and later at −80 °C till being used, while the remaining was kept directly in liquid nitrogen till being used.

The steps in Sections 2.5 and 2.7 were conducted to explore the relative expression of related genes, whose primers are demonstrated in Supplementary Table S1. Given the identity of Grx2 as a glutathione-dependent oxidoreductase, shrimps directly preserved by liquid nitrogen were explored through a reduced glutathione (GSH) assay kit (Nanjing Jiancheng Bioengineering Institute, Nanjing, China), and three replicates of each shrimp were detected and statistically probed according to the instruction.

2.9. Correlation Analysis between the SNPs of PmGrx2 and Ammonia-N-Stress-Tolerance Trait

The ammonia-N-stress experiment adopted 400 healthy juvenile shrimps and followed the approach mentioned in Section 2.3. The first 40 shrimps that died belonged to the sensitive group, while the last 40 and those still alive were the resistant group. They were kept in ethanol for DNA extraction through MagPure Tissue/Blood DNA LQ Kit (Magen, Guangzhou, China).

The NCBI database was utilized to predict the exonic region of *PmGrx2*, upon which Premier 6.0 designed primers that spanned the exonic regions to amplify the samples' DNA order. The PCR reaction solution included forward primer (1 μL), reverse primer (1 μL), DNA template (2 μL), and mix green (21 μL) (Tsingke, Beijing, China). The three PCR procedures included 98 °C for 2 min, 35 cycles of 98 °C (10 s), 55 °C (15 s), 72 °C (1 min), and 72 °C (10 min). Tsingke Biotechnology undertook the synthesis of primers and the sequencing of PCR products (Guangzhou, China). The details are given in Supplementary Table S5.

DNAMAN and Chromas were adopted to elucidate DNA sequences of each shrimp, thus acknowledging the SNPs of *PmGrx2*. WPS office was used to calculate genetic parameters. An $\chi 2$ test was conducted with SPSS 26.0 to explore how the SNPs of *PmGrx2* are correlated to the ammonia-N-stress-tolerance trait, and $p < 0.05$ indicated a significant difference.

3. Results

3.1. Identification and Characterization of the PmGrx2 Nucleotide Sequence

The cDNA of *PmGrx2* (Supplementary Figure S1A; GenBank No. ON368189) is 998 bp in full length, covering 179 bp 5′-UTR, 459 bp 3′-UTR, a poly-A tail, and 360 bp ORF, as well as encoding a 119 amino acid putative protein. The putative *PmGrx2* protein, which was 12.87 kDa and covered only one Grx structural domain, had an isoelectric point of 8.51 theoretically. The active site motif of the *PmGrx2* domain was as typical as other known Grx2 proteins, C-P-Y-C (39–42 aa). All of these supported the inclusion of *PmGrx2* into the dithiol Grxs family. In the putative secondary structure, the α-helix, extended strand, β-turn, and random coil accounted for 42.02%, 15.97%, 8.40%, and 33.61%, respectively. Supplementary Figure S1B illustrates the tertiary structure.

The paper compared the amino acid sequences of Grx2 of seven crustacean species, most of which were conserved, and all had active site C-P-Y-C (Supplementary Figure S2). *PmGrx2* had the highest identity with Grx2 from *Penaeus vannamei* (96.64%). The homology parameters of Grx2 and PmGrx2 for the species involved in the comparison are shown in Supplementary Table S7. The amino acid sequences of fifty-four Grxs were chosen, and the minimal evolution of MEGA-X was employed to create a phylogenetic tree. Grx3 and Grx5 were clustered together, Grx2 from plants and bacteria was clustered separately, and Grx2 from the remaining species was clustered together (Supplementary Figure S3). Grx from crustaceans clustered closely, with *PmGrx2* being most closely related to Grx2 from *P. vannamei* and *Penaeus japonicus*. The scientific names and accession numbers of all the above species are shown in Supplementary Table S6.

Given the shortage of relevant sequence information and validation concerning crustaceans, the amino acid sequence of human Grx2 was selected for protein interaction analysis. The predicted results are shown in Figure 1. Among the proteins that have major interactions with Grx2, Grx3 and Grx5 belong to the same Grxs family as Grx2. Glutathione reductase (GSR) and glutathione peroxidase (GPX) are glutathione-dependent enzymes, and thioredoxin reductase 2 (TXNRD2) and thioredoxin (TXN) are key enzymes of the thioredoxin system. These proteins are important components of the eukaryotic antioxidant system, along with catalase (CAT). In addition, RNA-binding motif protein 28 (RBM28), isochorismatase 1 (ISOC1), and neural precursor-cell-expressed developmentally downregulated 8 (NEDD8) also interact closely with Grx2. The names and websites of the analysis software above are shown in Supplementary Table S8.

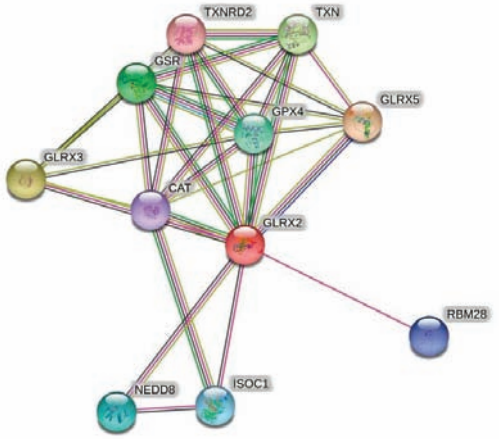

Figure 1. Grx2 protein interactions networks. The red dots represent the target protein Grx2. Other colored dots represent proteins that interact with Grx2. The names of all proteins are abbreviated to the top right of the dots.

3.2. mRNA Expression of PmGrx2 in Different Tissues and Developmental Stage

PmGrx2 was expressed in all 14 tissues of the shrimp and was significantly more abundant in the stomach and testis than in other tissues ($p < 0.05$). *PmGrx2* was less abundant in the ovary, brain, eyestalk nerves, and abdominal nerves (Figure 2).

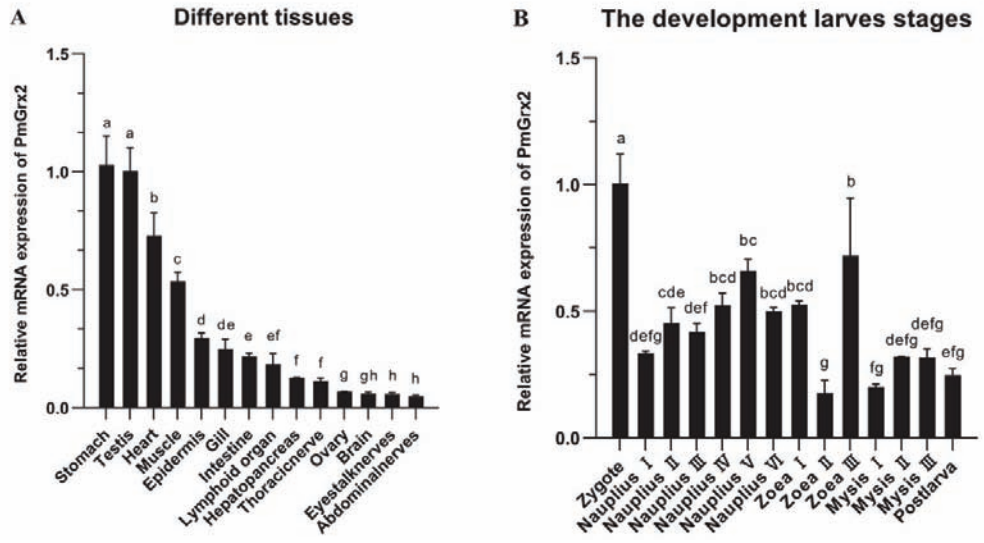

Figure 2. (**A**) mRNA expression levels of *PmGrx2* in different tissues. The data are presented as mean ± SD (n = 3). Different letters show significant differences ($p < 0.05$). (**B**) mRNA expression levels of PmGrx2 during the developmental period. The data are presented as mean ± SD (n = 3). Different letters are used to show significant differences ($p < 0.05$).

The expression of *PmGrx2* was constantly observed along the evolution of shrimp from zygote to post-larva, which obviously outnumbered in the zygote period compared with other periods ($p < 0.05$). As shrimp development progressed to the nauplius stage, the *PmGrx2* expression increased as a whole. In the zoea and mysis stages, the expression of *PmGrx2* decreased and fluctuated, and it only temporarily surged in zoea III (Figure 2B).

3.3. Exploration of PmGrx2 Transcription of Hepatopancreas and Gills on the Heels of Bacterial Challenge

Figure 3A validated the much higher expression of *PmGrx2* in the hepatopancreas compared with the control ($p < 0.05$) after the injection of *Staphylococcus aureus*, as well as its peak at 72 h after injection. Such expression, however, failed to jump after injection of two Gram-negative bacteria separately, especially *Vibrio anguillarum*. After injection of *Vibrio Harveyi*, it only picked up a certain amount at 24 h post-injection, followed by a decline. Figure 3B denies the exact similarity of PmGrx2's expression profiles between the gill and the hepatopancreas after bacterial injection. However, *S. aureus* still significantly elicited a response of *PmGrx2* in the gill ($p < 0.05$), just not as violently as *PmGrx2* in the hepatopancreas. After separate injections of the two Gram-negative bacteria, no jump of *PmGrx2* expression was observed in the gill compared to the control.

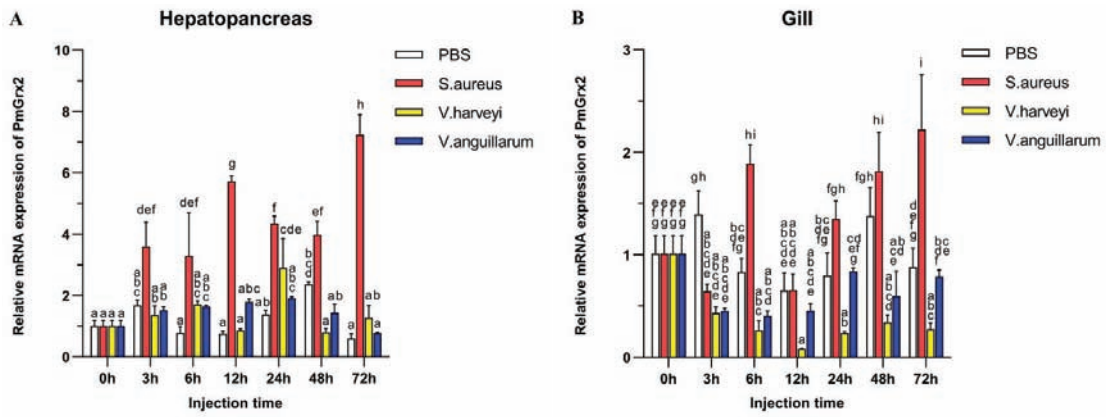

Figure 3. mRNA expression levels of *PmGrx2* in the hepatopancreas (**A**) and gill (**B**) at different time intervals after multiple pathogenic bacteria injections. The data are presented as mean ± SD (n = 3). Different letters are used to show significant differences ($p < 0.05$).

3.4. Exploration of PmGrx2 Transcription of Hepatopancreas and Gill under Ammonia-N Stress

Figure 4A confirms the similarity of the *PmGrx2′*s expression pattern in the two experimental groups under ammonia-N stress, and both peaked at 12 h ($p < 0.05$). No jump in the *PmGrx2′*s expression was observed in both experimental groups with increasing time compared with the control ($p < 0.05$), but its expression profile of the gill at 96 h following ammonia-N stress differed greatly from that in the hepatopancreas (Figure 4B). *PmGrx2′*s expression in the gill of the 96 h SC group outnumbered the control group within 12 h following the stress ($p < 0.05$), peaked at 6 h, and was not on par with the control group as the duration of ammonia-N stress prolonged. In contrast, its expression of the 96 h LC50 group never jumped ($p < 0.05$). *PmGrx2′*s expression was much lower compared with the control ($p < 0.05$) 12 h following stress.

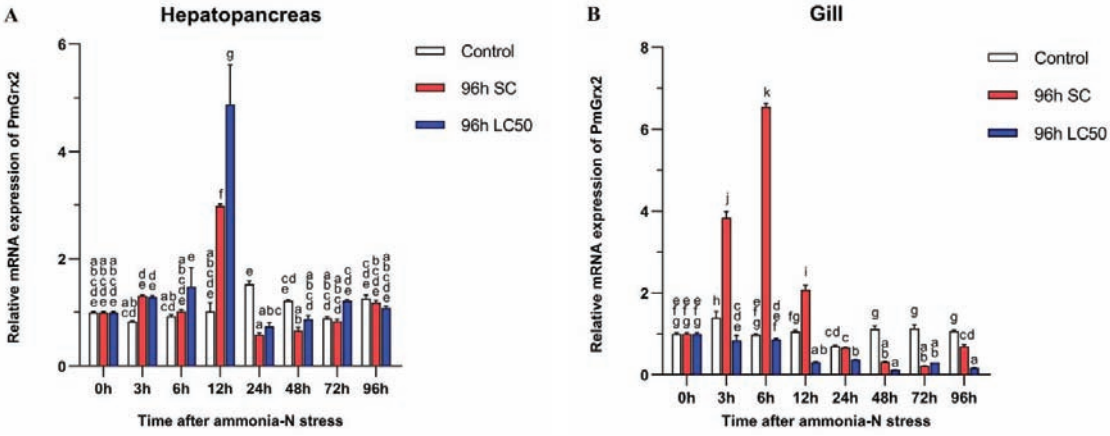

Figure 4. mRNA expression levels of *PmGrx2* in the hepatopancreas (**A**) and gill (**B**) at different time intervals, under different concentrations of ammonia-N stress. The data are presented as mean ± SD (n = 3). Different letters are used to show significant differences ($p < 0.05$).

3.5. The Interference Efficiency of dsGrx2 in the Hepatopancreas

Figure 5A proves dsGrx2's role in sharply decreasing *PmGrx2′*s expression in the hepatopancreas ($p < 0.05$). Figure 5B reveals the application of ammonia-N stress into both

groups 24 h following dsRNA injection. As to *PmGrx2*'s expression within 48 h following stress ($p < 0.05$), the dsGFP-injected group sharply outnumbered dsGrx2-injected group, indicating the powerful inhibitory effect of dsGrx2 within 72 h following injection.

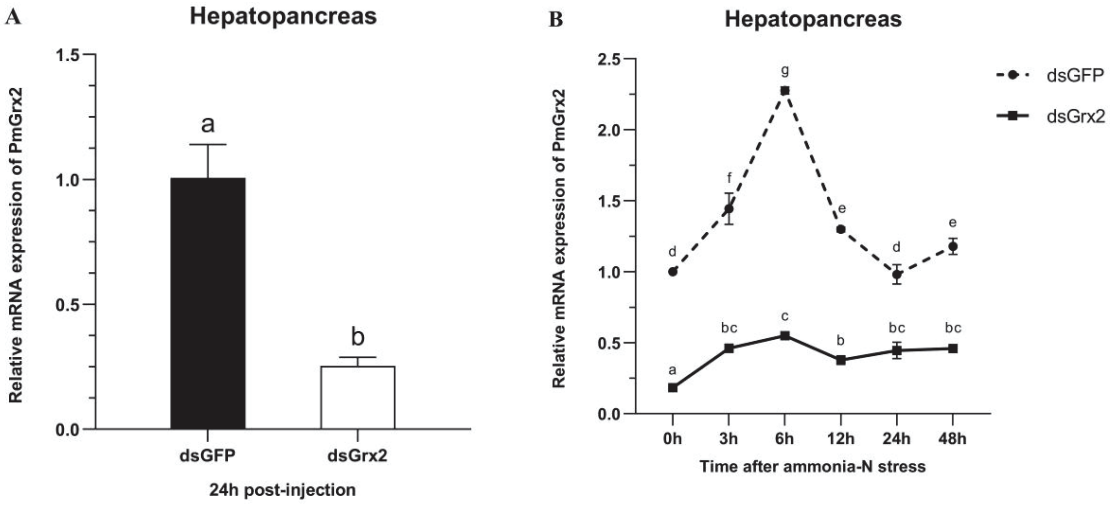

Figure 5. (**A**) mRNA expression levels of *PmGrx2* in the hepatopancreas at 24 h after dsRNA injection. (**B**) Expression profile of *PmGrx2* in the hepatopancreas of dsRNA-injected shrimps within 48 h under ammonia-N stress. The data are presented as mean ± SD (n = 3). Different letters show significant differences ($p < 0.05$).

3.6. GSH Content and mRNA Expression of Related Genes in the Hepatopancreas of dsRNA-Injected Shrimps under Ammonia-N Stress

Figure 6A demonstrates the gradual climb of *PmTrx*'s expression in the dsGFP-injected group, its peak at 12 h following ammonia-N stress, and the following gradual decrease. Such expression of the group injected with dsGrx2 also increased gradually and then decreased after a period of fluctuation. The expression of *PmTrx* in the dsGrx2-injected group outnumbered the dsGFP-injected counterpart at 6 h and 24 h following stress ($p < 0.05$).

In regard to *PmPrx1*'s expression, Figure 6B reveals its increase at 3 h under stress, and the following decrease and fluctuation at a similar level in the group injected with dsGFP. The one in the dsGrx2-injected group with the same stress, however, dramatically fluctuated and peaked at 6 h. The expression of *PmPrx1* of the two groups exhibited an opposite trend and differed significantly after 3 h, 6 h, and 24 h under the stress ($p < 0.05$).

Figure 6C validates both groups' similar expression tendency of *PmCAT* within 12 h after the stress, which first increased and then decreased. However, starting from 24 h, the dsGrx2-injected group presented a much lower expression ($p < 0.05$).

Figure 6D shows the similar expression tendency of *PmCYC* in both groups within 12 h following the stress, as well as the much higher expression in the dsGrx2-injected group ($p < 0.05$). One day later, the expression of the dsGrx2-injected group declined, and it decreased abruptly at 48 h ($p < 0.01$). In contrast, the expression of the dsGFP-injected counterpart gradually increased.

Figure 6E illustrates *PmIAP*'s irregularly fluctuated expression of the dsGFP-injected group within 48 h following the stress. The dsGrx2-injected group showed an increase and then a decrease in the expression of *PmIAP*, and then it reached a maximum at 6 h ($p < 0.05$).

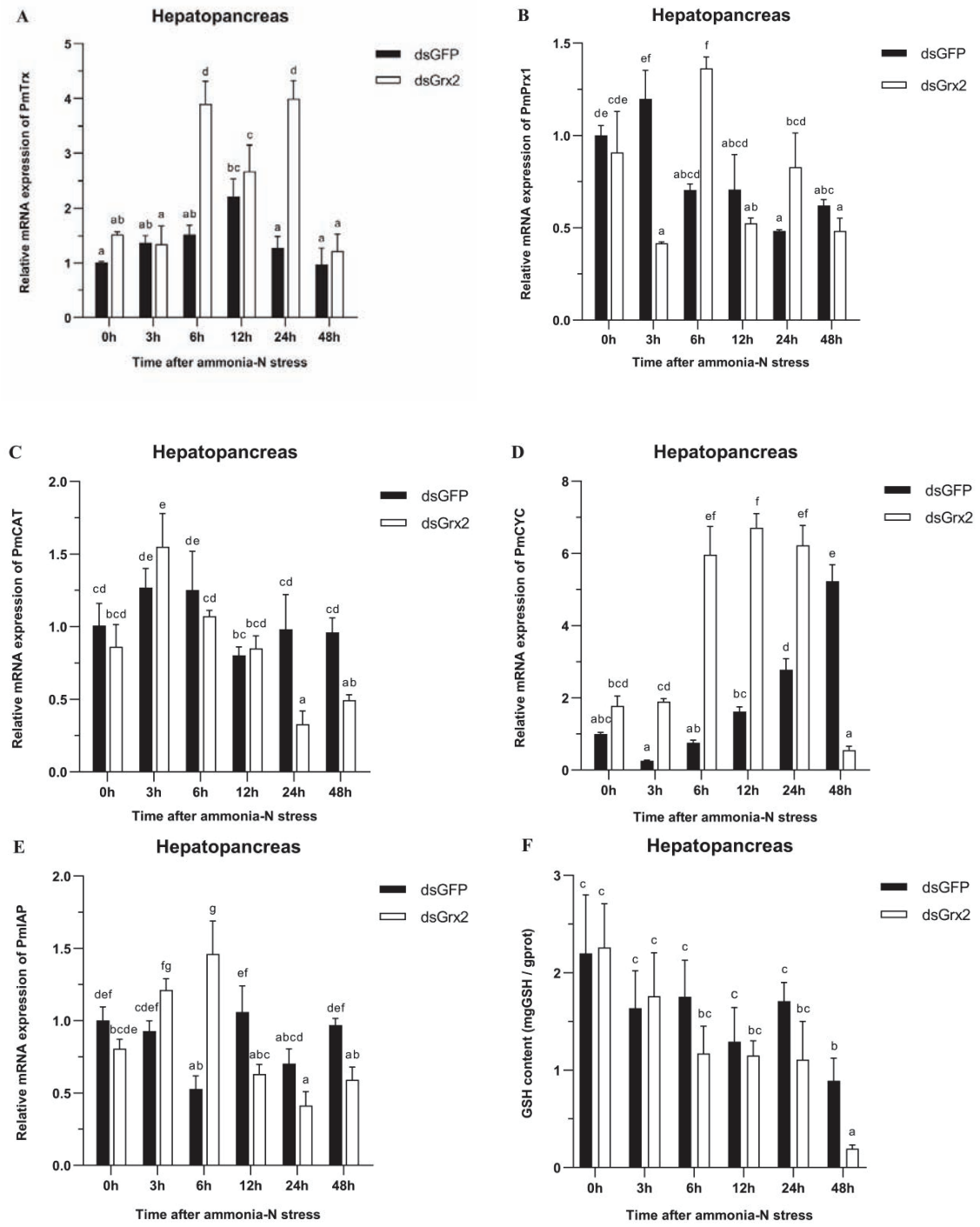

Figure 6. Expression profiles of five genes (*PmTrx* (**A**), *PmPrx1* (**B**), *PmCAT* (**C**), *PmCYC* (**D**), and *PmIAP* (**E**)) and changes in GSH content (**F**) in the hepatopancreas of dsRNA-injected shrimps under ammonia-N stress. The data are presented as mean ± SD (n = 3). Different letters show significant differences ($p < 0.05$).

Figure 6F illustrates the groups' similar trend of GSH content in 48 h following the stress in the hepatopancreas. The GSH content was the lowest in both groups at 48 h, while that of the dsGrx2-injected group was much lower compared to the group injected with dsGFP ($p < 0.05$).

3.7. Correlation Analysis between the SNPs of PmGrx2 and Ammonia-N-Stress-Tolerance Trait

This paper found two SNPs on the exons of *PmGrx2*, whose information and sequencing maps are demonstrated in Table 1 and Figure 7, respectively. According to Table 2, which reveals polymorphic parameters, *PmGrx2*-E3371 had a Ho of 0.0125, He of 0.0125, Ne of 1.0126, and MAF of 0.0063; the corresponding values for *PmGrx2*-E3398 were 0.0000, 0.0722, 1.0778, and 0.0375, respectively. Both *PmGrx2*-E3371 and *PmGrx2*-E3398 exhibited low polymorphism (PIC < 0.2500). The HWE results showed that *PmGrx2*-E3398 deviated significantly from HWE, while *PmGrx2*-E3371 did not. Table 3 displays the relation between the SNPs and ammonia-N-stress-tolerance trait. *PmGrx2*-E3398 was significantly correlated with the latter ($p < 0.05$), while *PmGrx2*-E3371 was not.

Table 1. Specific information of the SNPs of *PmGrx2*.

SNPs	Position	Type of Base Mutation	Type of Protein Mutation
PmGrx2-E3371	Exon 3 (371 bp)	c.192G > T	Mm p.Gln64His
PmGrx2-E3398	Exon 3 (398 bp)	c.219T > A	Sm p.Val73=

Mm, missense mutation; Sm, synonymous mutation; Meaning of the symbols in Table 2 [17].

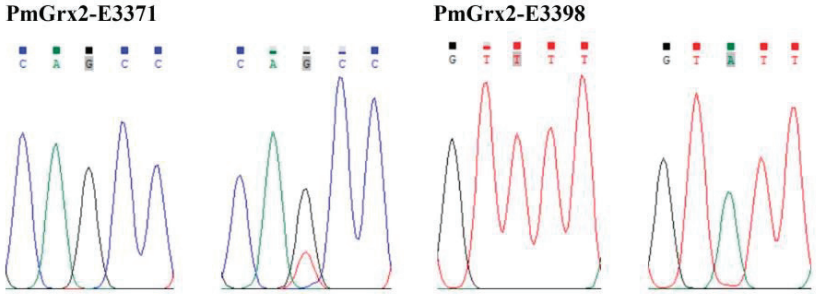

Figure 7. Sequencing maps of the SNPs of *PmGrx2*.

Table 2. Polymorphic parameters of the SNPs of *PmGrx2*.

SNPs	H_o	H_e	N_e	MAF	PIC	HWE
PmGrx2-E3371	0.0125	0.0124	1.0126	0.0063	0.0123	0.9984
PmGrx2-E3398	0.0000	0.0722	1.0778	0.0375	0.0696	0.0000

SNPs, single nucleotide polymorphisms; H_o, observed heterozygosity; H_e, expected heterozygosity; N_e, effective number; MAF, minimum allele frequency; PIC, polymorphism information content; HWE, Hardy–Weinberg equilibrium.

Table 3. Correlation analysis between the SNPs of *PmGrx2* and ammonia-N-stress-tolerance trait.

SNPs	Genotype	Genotype Frequencies		χ2 Value	*p*-Value
		Sensitivity	Resistance		
PmGrx2-E3371	GG	1.0000	0.9750	2.0006	0.1572
	TG	0.0000	0.0250		
PmGrx2-E3398	AA	0.0750	0.0000	6.0163	0.0142 *
	TT	0.9250	1.0000		

* Denotes significant correlation ($p < 0.05$).

4. Discussion

For the first time, the authors succeed in cloning the full-length cDNA of a new glutaredoxin, *PmGrx2*, in crustaceans. The only active site motif that is present among the predicted motifs was the Grx structural domain of C-P-Y-C, a typical dithiol Grx structural domain, which supported the inclusion of *PmGrx2* into the Grxs family [5]. This paper picked the amino acid sequences of Grx2 of seven crustacean species for multiple sequence alignment, and all of them had C-P-Y-C in their sequences. Phylogenetic analysis showed that the monothiol Grx3 and Grx5 clustered together, while the dithiol Grx2 clustered separately. Among them, *PmGrx2* converged to the one of crustacean Grx2. The above indicates that the Grx active sites are highly conserved among different species. However, Grxs are a large family with distinct segregation characteristics, both from a species-classification point of view and from a Grxs-classification point of view. For example, plants are known to possess dozens of Grxs, far more than other eukaryotes [18]. In recent years, new types of Grxs have been found in prokaryotes [6]. The abovementioned suggests that different types of Grxs may have distinct functions, and the taxonomic diversity they exhibit guides us to investigate and add new elements in different species.

Of the proteins predicted to interact with Grx2, most are core members of the eukaryotic redox system. This suggests that the fundamental role of Grx2 is to maintain redox homeostasis in the organism. In addition, RBM28 is an intracellular host factor that can interact directly with RNA viruses [19]. ISOC1 is involved in intracellular pathogen recognition and clearance [20]. NEDD8 is vital for the organism's defense mechanism against proteotoxicity [21]. The three proteins matter a lot in the organism's reaction to pathogen infection and immune activation. The predicted result that Grx2 interacts with them indicates the potential involvement of *PmGrx2* in the innate immune process in shrimp.

PmGrx2 was significantly more expressed in the stomach and testis than in other tissues. On the one hand, the stomach, as an important digestive organ of shrimp, undertakes functions such as grinding food, a process that consumes energy and generates a variety of oxygen metabolites [22]. On the other hand, the gastric epithelium acts as an external barrier to the digestive system, and it is crucial to maintain its redox homeostasis [23]. These may be the reasons for the elevated expression of *PmGrx2* in the stomach. Previous studies have shown that Grx2 expression levels are elevated during human sperm maturation. Moreover, Grx2b and Grx2c are testis-specific protein isoforms. It is hypothesized that Grx2 may be involved in the generation of disulfide bonds during sperm maturation [24]. In addition, a redox homeostatic system exists in reproductive tissues of animals, and the antioxidant mechanism is activated when stimulated by ROS, thus reducing the extent of oxidative damage to spermatozoa [25]. Therefore, *PmGrx2* may play the same role in the stomach and testis of shrimp.

PmGrx2 was expressed throughout the early growth of black tiger shrimps, which is complex and rapid, and employs mitochondria as feed [26]. In zebrafish, Grx2 was shown to participate in the coordination of intracellular iron–sulfur clusters [8]. Considering the vital role of the iron–sulfur cluster in the mitochondrial respiratory chain, *ZfGrx2* matters much as to the energy supply of mitochondria and is involved in regulating vascular, heart, and brain growth in zebrafish embryos [27–30]. All of these indicate *PmGrx2*'s similar function in driving their early development.

PmGrx2 in both hepatopancreas and gills responded strongly to *S. aureus* (Gram-positive bacteria) after injection with different species of bacteria. In contrast, both Gram-negative bacteria had almost no effect on the expression of *PmGrx2* compared to the control group. This indicates *PmGrx2*'s part in innate immune process of shrimp against pathogenic bacteria, but with different sensitivities to various species of pathogens. Since Gram-positive bacteria tend to produce exotoxins and do not have an outer membrane formed by lipopolysaccharides. Gram-negative bacteria tend to produce endotoxins and have capsules and mucus layers that cover the outer membrane, a characteristic that makes it easier for Gram-negative bacteria to invade organisms latently. In fact, it is often Gram-negative bacteria that cause mortality in aquatic animal populations during aquaculture.

Gram-negative bacteria do not elicit *PmGrx2*'s response in the gills, and this is one of the favorable conditions for their invasion of the organism. Meanwhile, the hepatopancreas was considered to be an immune organ of the highest significance in shrimp [31]. *PmGrx2*'s expression in the gills of the experimental group failed to be as strong as that in the hepatopancreas in comparison with the control, despite the higher expression of *PmGrx2*.

Ammonia-N refers to an ordinary environmental stressor in aquaculture processes. Excess ammonia-N induced excessive production of ROS/RNS, which caused oxidative damage and inflammatory effects in aquatic organisms [32–34]. *PmGrx2*'s expression in the 96 h SC group increased to different degrees following ammonia-N stress in comparison with the control group, and this was true for both hepatopancreas and gills. However, such expression in the 96 h LC50 group was only increased in the hepatopancreas, and in the gills, it was always lower compared with the control group. It is hypothesized that, since the gills are the first line of defense in contact with the aquatic environment, high concentrations of ammonia-N potentially undermine the gills in shrimp [15,35]. In *P. vannamei*, Grx2's expression of hepatopancreas and gills increased similarly following ammonia-N stress [36]. All of these suggest that *PmGrx2* participates in the resistance of shrimp to stress.

In regard to the part of *PmGrx2* in the resistance of shrimp to ammonia-N stress, dsRNA was employed to interfere *PmGrx2*'s expression, which supports its powerful interference role at least 72 h following injection. *PmTrx* and *PmPrx1*, also included in the Trx superfamily as *PmGrx2*, were picked for expression elaboration following the suppression of *PmGrx2*'s expression. In the hepatopancreas, *PmTrx*'s expression of the dsGrx2-injected group started to outnumber the dsGFP-injected group at 6 h following stress and was significant at 6 h and 24 h. *PmPrx1*'s expression in the dsGrx2-injected group, however, performed the opposite trend compared to the dsGFP-injected group under ammonia-N stress. Previously, it was shown that Grx could functionally supplement *E. coli* Trx mutant strains [4]. It is hypothesized that functionally similar enzymes in the same family complement each other, and the functional decline of one side surely causes the expression upregulation of the other side to compensate for the functional deficiency of the organism. This is the reason why Grx was originally called the Trx backup system [9]. With longer stress time, the dsGrx2-injected group presented much lower *PmCAT*'s expression compared with the dsGFP-injected group. *PmCAT* is a peroxidase, and the hike of its expression always oxidatively damages the organism [37]. As for *PmCYC*, an enzyme that was vital in apoptosis, its expression remained high in the dsGrx2-injected group compared to the dsGFP-injected group from 6 h to 24 h after stress [38]. IAP is an anti-apoptotic enzyme [39]. At the beginning of ammonia-N stress, *PmIAP*'s expression in the group with dsGrx2 gradually increased; however, from 12 h after stress, the expression was lower compared with the dsGFP-injected group. Meanwhile, the GSH content in hepatopancreas dropped. The abovementioned indicated the organism's upregulation of genes with alike functions to fight against ammonia-N stress in the presence of inhibited *PmGrx2*, some antioxidant enzymes' lower expression, and a higher degree of apoptosis. When *PmGrx2* was inhibited, the resistance of shrimp was weakened in the face of oxidative damage.

This study firstly adopted direct sequencing in *PmGrx2* for locus typing and obtained two SNPs loci, among which *PmGrx2*-E3398 significantly deviated from the Hardy–Weinberg equilibrium ($p < 0.05$). Allele frequency is swayed by manual selection, as well as extreme samples [11]. Both *PmGrx2*-E3371 and *PmGrx2*-E3398 are located on the ORF. Among them, *PmGrx2*-E3398 is a synonymous mutation, while *PmGrx2*-E3371 is a missense mutation, which would result in the mutation of glutamine (Gln) to histidine (His). Both Gln and His are polar amino acids. In the present study, *PmGrx2*-E3398 was highly related to the ammonia-N-stress-tolerance trait ($p < 0.05$). Since this mutation did not involve alteration of the encoded protein, the specific mode of its effect requires further investigation. Despite the long-standing neutral function of synonymous mutations, studies in recent years have demonstrated that synonymous mutations affect the efficiency and stability

of transcription and translation of genes [40–42]. *PmGrx2*-E3398 could be developed as a molecular marker for breeding shrimp tolerant to stress.

5. Conclusions

The cDNA of *PmGrx2* was cloned and included into Grxs family. *PmGrx2* was proved to express most in the stomach and testis of shrimp, and such an expression can be found in the early developmental stages. The expression of *PmGrx2* in the hepatopancreas and gills was induced owing to ammonia-N stress and bacterial infection, indicating the essential part of *PmGrx2* in the defense mechanism against environmental stress and pathogen infection. The inhibition of *PmGrx2* expression under the ammonia-N stress resulted in a greater risk of oxidative damage to shrimp. Moreover, this paper acknowledged SNPs in the exon region of *PmGrx2*, explored their relation to the ammonia-N-stress-tolerance trait, and successfully screened an SNP locus whose relationship with the ammonia-N-stress-tolerance trait was determined to be significant. This paper lays the foundation for studies on the involvement of Grx2 in crustacean resistance to oxidative stress.

Supplementary Materials: The following supporting information can be downloaded at https://www.mdpi.com/article/10.3390/antiox11101857/s1. Figure S1: The sequence of nucleotides, the deduced sequence of amino acids, and the putative secondary structure of *PmGrx2* (A). The putative tertiary structure of *PmGrx2* (B). Figure S2: Multiple sequence alignment of Grx2 from seven crustacean species. Figure S3: Phylogenetic tree of Grxs based on amino acid sequences. Tables S1–S5: Primers used in the study. Table S6: Accession numbers were used the alignment and phylogenic tree in this study. Table S7: Homology of *PmGrx2* with Grx2 of other species. Table S8: Names and Websites of the analysis software.

Author Contributions: Conceptualization, R.F., Y.L., F.Z. and S.J. (Shigui Jiang); methodology, R.F., Q.Y., S.J. (Song Jiang), J.H., L.Y. and X.C.; software, R.F.; validation, F.Z. and S.J. (Shigui Jiang); data curation, R.F. and F.Z.; writing—original draft preparation, R.F.; writing—review and editing, F.Z.; visualization, R.F.; supervision, S.J. (Shigui Jiang); project administration, S.J. (Shigui Jiang); funding acquisition, F.Z. and S.J. (Shigui Jiang). All authors have read and agreed to the published version of the manuscript.

Funding: This research was funded by Research and Development Projects in Key Areas of Guangdong Province, grant number 2021B0202003; China Agriculture Research System of MOF and MARA, grant number CARS-48; Central Public-interest Scientific Institution Basal Research Fund, CAFS, grant number No. 2020TD30; Financial Fund of Ministry of Agriculture and Rural affairs of Chin, grant number NHYYSWZZZYKZX2020; Central Public Interest Scientific Institution Basal Research Fund, South China Sea Fisheries Research Institute, CAFS, grant number NO.2021SD13; and Guangdong Basic and Applied Basic Research Foundation, grant number 2020A1515110200.

Institutional Review Board Statement: All experimental protocols and methods in this study were approved by the Animal Care and Use Ethics Committee in the South China Sea Fisheries Research Institute (20200826m).

Informed Consent Statement: Not applicable.

Data Availability Statement: The data presented in this study are available in the article and Supplementary Materials.

Conflicts of Interest: The authors declare no conflict of interest.

References

1. Holmgren, A.; Johansson, C.; Berndt, C.; Lönn, M.E.; Hudemann, C.; Lillig, C.H. Thiol redox control via thioredoxin and glutaredoxin systems. *Biochem. Soc. Trans.* **2005**, *33*, 1375–1377. [CrossRef] [PubMed]
2. Carvalho, A.P.; Fernandes, P.A.; Ramos, M.J. Similarities and differences in the thioredoxin superfamily. *Prog. Biophys. Mol. Biol.* **2006**, *91*, 229–248. [CrossRef]
3. Kapoor, D.; Sharma, R.; Handa, N.; Kaur, H.; Rattan, A.; Yadav, P.; Gautam, V.; Kaur, R.; Bhardwaj, R. Redox homeostasis in plants under abiotic stress: Role of electron carriers, energy metabolism mediators and proteinaceous thiols. *Front. Environ. Sci.* **2015**, *3*, 13. [CrossRef]
4. Holmgreen, A. Glutathione dependent synthesis of deoxyribonucleotides. *J. Biol. Chem.* **1979**, *254*, 3622–3638. [CrossRef]

5. Lillig, C.H.; Berndt, C.; Holmgren, A. Glutaredoxin systems. *Biochim. Biophys. Acta* **2008**, *1780*, 1304–1317. [CrossRef]
6. Mondal, S.; Kumar, V.; Singh, S.P. Phylogenetic distribution and structural analyses of cyanobacterial glutaredoxins (Grxs). *Comput. Biol. Chem.* **2020**, *84*, 107141. [CrossRef]
7. Yang, Y.; Xue, W.; Chen, P.; Yuan, X.; Li, X.; Zhang, T.; Chen, S. Identification and expression analyzes of CC-type glutaredoxin in cucumber (*Cucumis sativus* L.) under abiotic stress. *Sci. Hortic.* **2021**, *289*, 110417. [CrossRef]
8. Bräutigam, L.; Johansson, C.; Kubsch, B.; McDonough, M.A.; Bill, E.; Holmgren, A.; Berndt, C. An unusual mode of iron-sulfur-cluster coordination in a teleost glutaredoxin. *Biochem. Biophys. Res. Commun.* **2013**, *436*, 491–496. [CrossRef]
9. Fernandes, A.P.; Holmgren, A. Glutaredoxins: Glutathione-dependent redox enzymes with functions far beyond a simple thioredoxin backup system. *Antioxid. Redox Signal.* **2004**, *6*, 63–74. [CrossRef]
10. Murata, H.; Ihara, Y.; Nakamura, H.; Yodoi, J.; Sumikawa, K.; Kondo, T. Glutaredoxin Exerts an Antiapoptotic Effect by Regulating the Redox State of Akt. *J. Biol. Chem.* **2003**, *278*, 50226–50233. [CrossRef]
11. Fan, R.; Jiang, S.; Li, Y.; Yang, Q.; Jiang, S.; Huang, J.; Yang, L.; Chen, X.; Zhou, F. Molecular Characterization and Expression Analysis of Glutaredoxin 5 in Black Tiger Shrimp (*Penaeus monodon*) and Correlation Analysis Between the SNPs of PmGrx5 and Ammonia-N Stress Tolerance Trait. *Front. Mar. Sci.* **2022**, *9*, 909827. [CrossRef]
12. Li, Y.; Zhou, F.; Huang, J.; Yang, L.; Jiang, S.; Yang, Q.; He, J.; Jiang, S. Transcriptome reveals involvement of immune defense, oxidative imbalance, and apoptosis in ammonia-stress response of the black tiger shrimp (*Penaeus monodon*). *Fish Shellfish. Immunol.* **2018**, *83*, 162–170. [CrossRef] [PubMed]
13. Gürel, T. The Larval Development of *Penaeus semisulcatus* (de Hann, 1850) (Decapoda: *Penaeidae*). *J. Fish. Aquat. Sci.* **2005**, *22*, 195–199. [CrossRef]
14. Li, Y.; Yang, Q.; Su, T.; Zhou, F.; Yang, L.; Huang, J. The toxicity of ammonia-N on *Penaeus monodon* and immune parameters. *J. Shanghai Ocean. Univ.* **2012**, *21*, 358–362.
15. Zhou, K.; Zhou, F.; Huang, J.; Yang, Q.; Jiang, S.; Qiu, L.; Yang, L.; Zhu, C.; Jiang, S. Characterization and Expression Analysis of a Chitinase Gene (PmChi-4) From Black Tiger Shrimp (*Penaeus monodon*) Under Pathogen Infection and Ambient Ammonia Nitrogen Stress. *Fish Shellfish. Immunol.* **2017**, *62*, 31–40. [CrossRef]
16. Qin, Y.; Jiang, S.; Huang, J.; Zhou, F.; Yang, Q.; Jiang, S.; Yang, L. C-type lectin response to bacterial infection and ammonia nitrogen stress in tiger shrimp (*Penaeus monodon*). *Fish Shellfish. Immunol.* **2019**, *90*, 188–198. [CrossRef]
17. Dunnen, J.; Dalgleish, R.; Maglott, D.; Hart, R.; Greenblatt, M.; Jordan, J.; Roux, A.; Smith, T.; Antonarakis, S.; Taschner, P.E.M. HGVS Recommendations for the Description of Sequence Variants: 2016 Update. *Hum. Mutat.* **2016**, *37*, 564–569. [CrossRef]
18. Malik, W.A.; Wang, X.; Wang, X.; Shu, N.; Cui, R.; Chen, X.; Wang, D.; Lu, X.; Yin, Z.; Wang, J.; et al. Genome-wide expression analysis suggests glutaredoxin genes response to various stresses in cotton. *Int. J. Biol. Macromol.* **2020**, *153*, 470–491. [CrossRef]
19. Lisy, S.; Rothamel, K.; Ascano, M. RNA Binding Proteins as Pioneer Determinants of Infection: Protective, Proviral, or Both? *Viruses* **2021**, *13*, 2172. [CrossRef]
20. Wang, Y.; Zhang, K.; Shi, X.; Wang, C.; Wang, F.; Fan, J.; Shen, F.; Xu, J.; Bao, W.; Liu, M.; et al. Critical role of bacterial isochorismatase in the autophagic process induced by Acinetobacter baumannii in mammalian cells. *FASEB J.* **2016**, *30*, 3563–3577. [CrossRef]
21. Maghames, C.M.; Lobato-Gil, S.; Perrin, A.; Trauchessec, H.; Rodriguez, M.S.; Urbach, S.; Marin, P.; Xirodimas, D.P. NEDDylation promotes nuclear protein aggregation and protects the Ubiquitin Proteasome System upon proteotoxic stress. *Nat. Commun.* **2018**, *9*, 4376. [CrossRef] [PubMed]
22. Aviello, G.; Knaus, U.G. NADPH oxidases and ROS signaling in the gastrointestinal tract. *Mucosal Immunol.* **2018**, *11*, 1011–1023. [CrossRef] [PubMed]
23. Goroshinskaya, I.; Surikova, E.; Frantsiyants, E.; Neskubina, I.; Pogorelova, Y.; Medvedeva, D.; Maslov, A.; Kit, O. Redox forms of glutathione mark the aggressiveness of stomach cancer. *Ann. Oncol.* **2018**, *29*, v4. [CrossRef]
24. Lönn, M.E.; Hudemann, C.; Berndt, C.; Cherkasov, V.; Capani, F.; Holmgren, A.; Lillig, C.H. Expression pattern of human glutaredoxin 2 isoforms: Identification and characterization of two testis/cancer cell-specific isoforms. *Antioxid. Redox Signal.* **2008**, *10*, 547–557. [CrossRef]
25. Fujii, J.; Iuchi, Y.; Matsuki, S.; Ishii, T. Cooperative function of antioxidant and redox systems against oxidative stress in male reproductive tissues. *Asian J. Androl.* **2003**, *3*, 231–242.
26. Beinert, H. Iron-sulfur proteins: Ancient structures, still full of surprises. *J. Biol. Inorg. Chem.* **2000**, *5*, 2–15. [CrossRef]
27. Bräutigam, L.; Jensen, L.D.E.; Poschmann, G.; Nyström, S.; Bannenberg, S.; Dreij, K.; Lepka, K.; Prozorovski, T.; Montano, S.J.; Aktas, O.; et al. Glutaredoxin regulates vascular development by reversible glutathionylation of sirtuin 1. *Proc. Natl. Acad. Sci. USA* **2013**, *110*, 20057–20062. [CrossRef]
28. Berndt, C.; Poschmann, G.; Stühler, K.; Holmgren, A.; Bräutigam, L. Zebrafish heart development is regulated via glutaredoxin 2 dependent migration and survival of neural crest cells. *Redox Biol.* **2014**, *2*, 673–678. [CrossRef]
29. Mailloux, R.J.; Xuan, J.Y.; McBride, S.; Maharsy, W.; Thorn, S.; Holterman, C.E.; Kennedy, C.R.J.; Rippstein, P.; deKemp, R.; da Silva, J.; et al. Glutaredoxin-2 is required to control oxidative phosphorylation in cardiac muscle by mediating deglutathionylation reactions. *J. Biol. Chem.* **2014**, *289*, 14812–14828. [CrossRef]
30. Bräutigam, L.; Schütte, L.D.; Godoy, J.R.; Prozorovski, T.; Gellert, M.; Hauptmann, G.; Holmgren, A.; Lillig, C.H.; Berndt, C. Vertebrate-specific glutaredoxin is essential for brain development. *Proc. Natl. Acad. Sci. USA* **2011**, *108*, 20532–20537. [CrossRef]

31. Rőszer, T. The invertebrate midintestinal gland ("hepatopancreas") is an evolutionary forerunner in the integration of immunity and metabolism. *Cell Tissue Res.* **2014**, *358*, 685–695. [CrossRef] [PubMed]
32. Randall, D.J.; Tsui, T.K.N. Ammonia toxicity in fish. *Mar. Pollut. Bull.* **2002**, *45*, 17–23. [CrossRef]
33. Cheng, C.; Yang, F.; Ling, R.; Liao, S.; Miao, Y.; Ye, C.; Wang, A. Effects of ammonia exposure on apoptosis, oxidative stress and immune response in pufferfish (*Takifugu obscurus*). *Aquat. Toxicol.* **2015**, *164*, 61–71. [CrossRef] [PubMed]
34. Liu, M.; Guo, H.; Liu, B.; Zhu, K.; Guo, L.; Liu, B.; Zhang, N.; Yang, J.; Jiang, S.; Zhang, D. Gill oxidative damage caused by acute ammonia stress was reduced through the HIF-1α/NF-κb signaling pathway in golden pompano (*Trachinotus ovatus*). *Ecotoxicol. Environ. Saf.* **2021**, *222*, 112504. [CrossRef] [PubMed]
35. Shi, M.; Jiang, S.; Li, Y.; Yang, Q.; Jiang, S.; Yang, L.; Huang, J.; Zhou, F. Comprehensive expression analysis of the beta integrin from *Penaeus monodon* indicating its participation in innate immunity and ammonia nitrogen stress response. *Fish Shellfish. Immunol.* **2019**, *98*, 887–898. [CrossRef]
36. Zheng, P.; Wang, L.; Wang, A.; Zhang, X.; Ye, J.; Wang, D.; Sun, J.; Li, J.; Lu, Y.; Xian, J. cDNA cloning and expression analysis of glutaredoxin (Grx) 2 in the Pacific white shrimp *Litopenaeus vannamei*. *Fish Shellfish. Immunol.* **2018**, *86*, 662–671. [CrossRef]
37. Trenzado, C.; Hidalgo, M.C.; García-Gallego, M.; Morales, A.E.; Furné, M.; Domezain, A.; Domezain, J.; Sanz, A. Antioxidant enzymes and lipid peroxidation in sturgeon Acipenser naccarii and trout Oncorhynchus mykiss. A comparative study. *Aquaculture* **2005**, *254*, 758–767. [CrossRef]
38. Hu, W.; Yao, C. Molecular and immune response characterizations of a novel AIF and cytochrome c in *Litopenaeus vannamei* defending against WSSV infection. *Fish Shellfish. Immunol.* **2016**, *56*, 84–95. [CrossRef]
39. Zhu, J.; Du, R.; Liu, Q.; Luo, L.; Lin, S.; Zhang, H.; Chen, Y. Transcriptome analysis provides insights into the molecular mechanism of hepatocyte apoptosis in response to feeding restriction in juvenile largemouth bass Micropterus salmoides. *Aquaculture* **2022**, *548*, 737500. [CrossRef]
40. Chaney, J.L.; Clark, P.L. Roles for Synonymous Codon Usage in Protein Biogenesis. *Annu. Rev. Biophys.* **2015**, *44*, 143–166. [CrossRef]
41. Chen, K.; Guo, R.; Wei, C.C. Synonymous mutation rs2515641 affects CYP2E1 mRNA and protein expression and susceptibility to drug-induced liver injury. *Pharmacogenomics* **2020**, *21*, 459–470. [CrossRef] [PubMed]
42. Wang, S.Y.; Cheng, Y.Y.; Liu, S.C.; Xu, Y.X.; Gao, Y.; Wang, C.L.; Wang, Z.G.; Feng, T.Q.; Lu, G.H.; Song, J.; et al. A synonymous mutation in IGF-1 impacts the transcription and translation process of gene expression. *Mol. Ther.-Nucleic Acids* **2021**, *26*, 1446–1465. [CrossRef] [PubMed]

antioxidants

MDPI

Article

Effects of Copper Exposure on Oxidative Stress, Apoptosis, Endoplasmic Reticulum Stress, Autophagy and Immune Response in Different Tissues of Chinese Mitten Crab (*Eriocheir sinensis*)

Wenrong Feng [1], Shengyan Su [1], Changyou Song [1], Fan Yu [1], Jun Zhou [2], Jianlin Li [1], Rui Jia [1], Pao Xu [1] and Yongkai Tang [1,*]

[1] Key Laboratory of Freshwater Fisheries and Germplasm Resources Utilization, Ministry of Agriculture and Rural Affairs, Freshwater Fisheries Research Center, Chinese Academy of Fishery Sciences, Wuxi 214081, China
[2] Freshwater Fisheries Research Institute of Jiangsu Province, Nanjing 210017, China
* Correspondence: tangyk@ffrc.cn; Tel.: +86-051085554198

Abstract: High concentrations of copper (Cu^{2+}) pose a great threat to aquatic animals. However, the mechanisms underlying the response of crustaceans to Cu^{2+} exposure have not been well studied. Therefore, we investigated the alterations of physiological and molecular parameters in Chinese mitten crab (*Eriocheir sinensis*) after Cu^{2+} exposure. The crabs were exposed to 0 (control), 0.04, 0.18, and 0.70 mg/L of Cu^{2+} for 5 days, and the hemolymph, hepatopancreas, gills, and muscle were sampled. The results showed that Cu^{2+} exposure decreased the antioxidative capacity and promoted lipid peroxidation in different tissues. Apoptosis was induced by Cu^{2+} exposure, and this activation was associated with the mitochondrial and ERK pathways in the hepatopancreas. ER stress-related genes were upregulated in the hepatopancreas but downregulated in the gills at higher doses of Cu^{2+}. Autophagy was considerably influenced by Cu^{2+} exposure, as evidenced by the upregulation of autophagy-related genes in the hepatopancreas and gills. Cu^{2+} exposure also caused an immune response in different tissues, especially the hepatopancreas, where the TLR2-MyD88-NF-κB pathway was initiated to mediate the inflammatory response. Overall, our results suggest that Cu^{2+} exposure induces oxidative stress, ER stress, apoptosis, autophagy, and immune response in *E. sinensis*, and the toxicity may be implicated following the activation of the ERK, AMPK, and TLR2-MyD88-NF-κB pathways.

Keywords: copper; apoptosis; endoplasmic reticulum stress; oxidative stress; *Eriocheir sinensis*

Citation: Feng, W.; Su, S.; Song, C.; Yu, F.; Zhou, J.; Li, J.; Jia, R.; Xu, P.; Tang, Y. Effects of Copper Exposure on Oxidative Stress, Apoptosis, Endoplasmic Reticulum Stress, Autophagy and Immune Response in Different Tissues of Chinese Mitten Crab (*Eriocheir sinensis*). *Antioxidants* **2022**, *11*, 2029. https://doi.org/10.3390/antiox11102029

Academic Editor: Stefan W. Ryter

Received: 29 August 2022
Accepted: 11 October 2022
Published: 14 October 2022

1. Introduction

Copper (Cu) is an essential metal element for all living organisms and mainly exists in Cu^{2+} and Cu^{+} states. It is involved in a variety of physiological functions, such as electron transport, mitochondrial function, and free radical scavenging [1]. When present in excess, however, Cu becomes toxic and causes damage to cellular components [2]. It is also classified as a priority environmental pollutant [3]. Cu can accumulate in aquatic systems from both natural (e.g., erosion of rocks and soils, geological deposition) and anthropogenic sources (e.g., industrial, mining and agricultural activities, sewage discharge) [3,4]. In aquaculture, copper sulfate ($CuSO_4$) has been extensively used as a therapeutic agent to control skin lesions and gill diseases caused by parasites and pathogenic bacteria [5]. It is further used globally as an algicide to control harmful cyanobacterial blooms in freshwater [6]. The extensive use of Cu^{2+} may lead to its short-term and/or repeated accumulation in aquatic environments. High concentrations of Cu^{2+} (up to 100 mg/L) have further been detected in various aquatic ecosystems [7].

High concentrations of copper have been reported to be potentially toxic to aquatic animals in aquatic environment [8]. Liver and gills are the primary sites of Cu toxicity in freshwater fish, where accumulated Cu^{2+} disrupts regular Cu homeostasis and branchial ion regulation [9]. The tolerance to waterborne Cu^{2+} varies among aquatic animals, for example, 48 h LD_{50} 0.75 mg/L in *Oncorhynchus mykiss* [10] and 72 h LD_{50} 40.6 mg/L in *Oreochromis niloticus* [11]. In crustaceans, the safe concentration of Cu^{2+} is also variable, e.g., 0.02 mg/L in juvenile *Macrobrachium rosenbergii* [12], 0.375 mg/L in juvenile *procambarus clarkia* [13], and 0.008 mg/L in larval *Penaeus vannamei* [14]. Acute exposure (24–96 h) to Cu^{2+} (0.1–84.9 μM) decreases the rate of oxygen consumption and alters the swimming performance of fish [15,16]. Cu^{2+} also suppresses immune function by decreasing blood leukocytes in fish [17,18]. The toxicity of Cu^{2+} to crustaceans has also garnered attention. Long-term exposure to Cu^{2+} (0.1641 ppm, 30 days) suppresses the glutathione system in *Penaeus indicus* [19]. Furthermore, sub-lethal Cu^{2+} exposure leads to necrosis and the loss of regular structures in the gills and hepatopancreas of *Litopenaeus vannamei* [20]. However, the underlying mechanisms of Cu toxicity in crustaceans are not yet well understood; therefore, it is necessary to systematically examine the effects of Cu^{2+} exposure on crustaceans and its potential ecological risks in aquatic environments.

The Chinese mitten crab (*Eriocheir sinensis*) is one of the most commercially cultured aquatic species in China. When managing crab ponds, $CuSO_4$ is commonly used to eradicate filamentous algae and control parasites and pathogens, which may lead to Cu^{2+} accumulation in the ponds. High ambient Cu^{2+} is a significant threat to the health of *E. sinensis.* After 24 h of Cu^{2+} exposure, the metabolism and osmotic regulation in the gills of *E. sinensis* are altered [21], and after 96 h, its molting, growth, and survival are suppressed [22,23]. Although Cu^{2+} toxicity in *E. sinensis* has garnered much attention in recent years, the knowledge of its underlying molecular mechanisms remains limited. It is unclear whether endoplasmic reticulum (ER) stress and autophagy are involved in Cu^{2+} toxicity in *E. sinensis*; the key signaling pathways have rarely been evaluated in Cu^{2+}-induced inflammatory responses and apoptosis. In addition, it is important to determine whether there is tissue specificity in the response to Cu^{2+} toxicity.

In this study, we investigated the physiological and molecular responses of *E. sinensis* to Cu^{2+} and evaluated the potential molecular mechanisms. To this end, we exposed *E. sinensis* to different concentrations of Cu^{2+} for 5 days [24] and observed the changes in the redox state, apoptosis, ER stress, autophagy, immune response, and detoxification in different tissues. We also analyzed multiple key signaling pathways, including the inositol-requiring enzyme 1 (IRE1), mitogen-activated protein kinases (MAPKs), AMP-activated protein kinase (AMPK), and Toll-like receptor (TLR) pathways. Our findings provide new insights into the mechanisms underlying the toxicity of Cu^{2+} exposure in *E. sinensis*, which may contribute to the risk assessments of Cu^{2+} in aquatic environments.

2. Materials and Methods

2.1. Crab Rearing, Experimental Design, and Sample Collection

Healthy *E. sinensis* (120 ± 1.2 g) were obtained from the Freshwater Fisheries Research Center (Wuxi, China). The crabs were kept in indoor glass tanks (100 × 60 × 40 cm) for 7 days to acclimatize to the laboratory conditions (temperature, 25 ± 1 °C; dissolved oxygen > 5.0 mg/L; ammonia nitrogen < 0.1 mg/L; pH 8.0 ± 0.5). After acclimatizing, the crabs were randomly distributed into four groups and exposed to 0 (control), 0.04, 0.18, and 0.70 mg/L of copper for 5 days. Each group contained 36 crabs (pooled male and female, 1:1), and the experiment was performed in triplicate. The sub-lethal copper concentrations were chosen according to our previous study, where the 96 h LC_{50} of Cu^{2+} was 5.63 mg/L [24]. The Cu^{2+} concentrations were prepared and adjusted by adding $CuSO_4$ (Aladdin, Shanghai, China). During the experiment, the water was renewed every day, and the crabs were fed a commercial diet (crude protein 42.6%, crude lipid 8.0%, crude ash 16.2%; HIPORE Feed Co., Ltd., Taizhou, China) at 1% of their body weight daily to avoid the adverse effects caused by hunger.

After 5 days of exposure, eight crabs from each tank were sampled randomly, and the hemolymph, hepatopancreas, gills, and muscle were immediately collected after anesthetization with an ice bath. Tissues from four crabs were mixed into one sample (six samples in total). The hemolymph was centrifuged (4000× *g* for 10 min at 4 °C) to obtain the supernatant. All samples were stored at −80 °C for gene expression and biochemistry analyses. The use of the crabs in the experiment was approved by the Freshwater Fisheries Research Center, and all experimental procedures were performed according to the Animal Care Guidelines.

2.2. Biochemical Assay

The hepatopancreas, gills, and muscle were homogenized nine times (*v/w*) with ice-cold normal saline (0.86% NaCl). The homogenized mixture was centrifuged at 3600 rpm at 4 °C for 10 min to collect the supernatant, which was used for biochemical assays. The levels of glutathione (GSH), glutathione *S*-transferase (GST), superoxide dismutase (SOD), total antioxidant capacity (T-AOC), malondialdehyde (MDA), and total protein (TP) in the hemolymph, hepatopancreas, gills, and muscle were measured as described by Jia, et al. [25]. Commercial kits for GSH, GST, SOD, T-AOC, MDA, and TP were purchased from Nanjing Jiancheng Bioengineering Institute (Nanjing, China) and Beyotime Biotechnology (Nantong, China).

2.3. Quantitative Real-Time PCR Analysis

Total RNA from the hepatopancreas, gills, and muscle was isolated using the RNAiso Plus reagent (TaKaRa, Beijing, China) according to the manufacturer's instructions. The quality and quantity of total RNA were evaluated using OD_{260}, the ratio of OD_{260}/OD_{280}, and agarose gel electrophoresis. The isolated RNA was used to synthesize cDNA via reverse transcription PCR using the PrimeScript™ RT reagent (TaKaRa, No. RR047). In brief, the RNA (1 μg) was mixed with gDNA Eraser at 42 °C for 2 min to remove the genomic DNA. The mixture was then reacted with PrimeScript RT Enzyme Mix I (1 μL), RT Primer Mix (1 μL), 5× PrimeScript Buffer 2 (4 μL), and RNase-Free dH_2O (4 μL) for 15 min at 37 °C and 5 s at 85 °C.

The mRNA levels of the target genes were measured by quantitative real-time PCR (qPCR) on a CFX96 Real-Time PCR instrument (Bio-Rad, Hercules, CA, USA). During the qPCR amplification process, cDNA (2 μL), TB Green Premix Ex Taq II (TaKaRa; 12.5 μL), forward and reverse specific primers (1 μL), and RNase-free water (8.5 μL) were mixed. The mixture was incubated for 30 s at 95 °C and subjected to 40 cycles at 95 °C for 5 s and 59–61 °C for 1 min. The expression of the target genes was analyzed using the $2^{-\Delta\Delta Cq}$ method [26]. The primers used are listed in Table S1. The ubiquitin-conjugating enzyme E2b (UBE) and β-actin genes were used as internal references to normalize the quantification cycle (Cq) values [27].

2.4. Integrated Biomarker Response Analysis

The integrated biomarker response (IBR) analysis for the oxidative stress parameters of different tissues was conducted using the method described by Sanchez, et al. [28]. The control group (without Cu^{2+}) was used as the reference condition. The IBR_{v2} value per concentration is the sum of the absolute values of the biomarker deviation index (A). The reference deviation of each biomarker is represented by the A value. In the star plot, the values above and below zero reflect the induction and reduction of the biomarker, respectively.

2.5. Statistical Analysis

All statistical analyses were performed using SPSS 24.0 (SPSS, Chicago, IL, USA). The results are expressed as the mean ± standard error of the mean (SEM). The normal distribution and heterogeneity of variance were evaluated using the Shapiro–Wilk and Bartlett tests, respectively. For comparisons among different groups, a one-way analysis of variance (ANOVA) was performed, followed by an LSD post hoc test in cases of equal variance

or the Kruskal–Wallis test for unequal variance. Differences were considered statistically significant at $p < 0.05$ among the different groups.

3. Results

3.1. Alterations in the Redox State

There was a linear decrease in the levels of T-AOC, SOD, and GST and an increase in MDA after treatment with different concentrations of Cu^{2+} in the hemolymph (Figure 1A–E). Compared to the control group, the decreases in T-AOC, SOD, and GST were statistically significant in the 0.70 mg/L Cu^{2+}-exposed group ($p < 0.05$; Figure 1A–C), while the increase in MDA was statistically significant in the 0.18 and 0.70 mg/L Cu^{2+}-exposed groups ($p < 0.05$; Figure 1D). GSH was not influenced by Cu^{2+} exposure in the hemolymph ($p > 0.05$; Figure 1E).

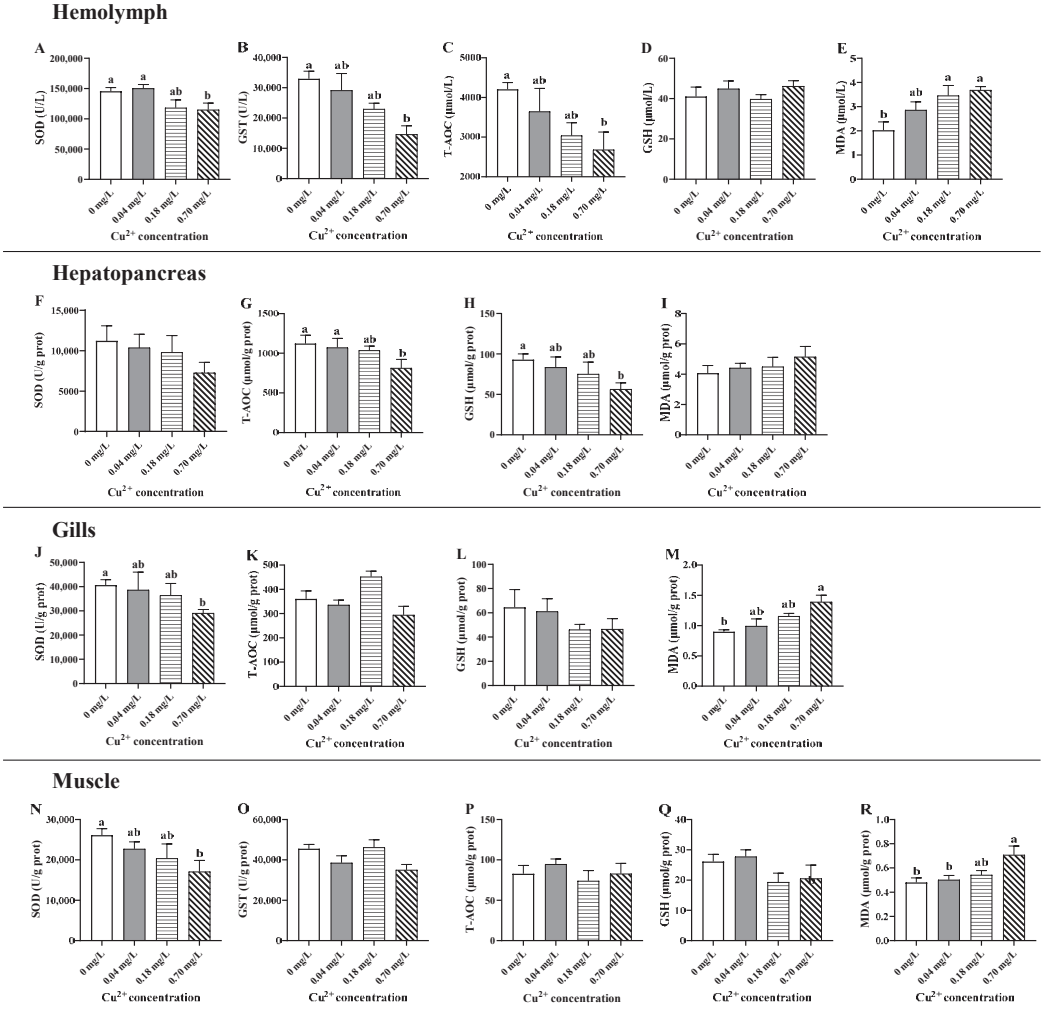

Figure 1. Changes in the oxidative stress parameters in different tissues of *E. sinensis* exposed to copper for 5 days. (**A**–**E**) hemolymph; (**F**–**I**) hepatopancreas; (**J**–**M**) gills; (**N**–**R**) muscle. The values are expressed the mean ± SEM ($n = 6$). Different letters denote significant differences among different groups ($p < 0.05$).

In the hepatopancreas, the level of T-AOC decreased with increasing Cu^{2+} concentrations, and the lowest value was observed after exposure to 0.70 mg/L of Cu^{2+} ($p < 0.05$; Figure 1G). Similarly, the level of GSH underwent a dose-dependent decrease, which was statistically significant in the 0.70 mg/L Cu^{2+}-exposed group ($p < 0.05$; Figure 1H). SOD activity and MDA content did not exhibit significant alterations in the hepatopancreas among the different Cu^{2+}-exposed groups ($p > 0.05$; Figure 1F,I).

In the gills, SOD activity showed a downward trend after Cu^{2+} exposure and was strongly decreased in crabs exposed to 0.70 mg/L of Cu^{2+} ($p < 0.05$; Figure 1J). Conversely, the MDA content exhibited a rising tendency and was enhanced in crabs exposed to 0.70 mg/L of Cu^{2+} ($p < 0.05$; Figure 1M). The levels of T-AOC and GSH showed a slight but non-significant alteration in the gills among the different groups ($p > 0.05$; Figure 1K,L).

In the muscle, exposure to 0.70 mg/L of Cu^{2+} markedly decreased SOD activity and enhanced MDA formation ($p < 0.05$; Figure 1N,R) but did not influence other parameters ($p > 0.05$; Figure 1O,P).

To compare the differences among the tissues and groups exposed to different concentrations of Cu^{2+}, four biomarkers related to the redox state were standardized and depicted in a star plot (Figure 2). The IBRv2 index increased with increasing Cu^{2+} concentrations and exhibited dose-dependent toxicity. Among the different tissues, the following order of average IBR_{v2} values was observed: hemolymph (5.64) > hepatopancreas (4.87) > gills (4.77) > muscle (4.53). In addition, after exposure to 0.70 mg/L of Cu^{2+}, the highest IBR_{v2} value was observed in the hepatopancreas (9.26).

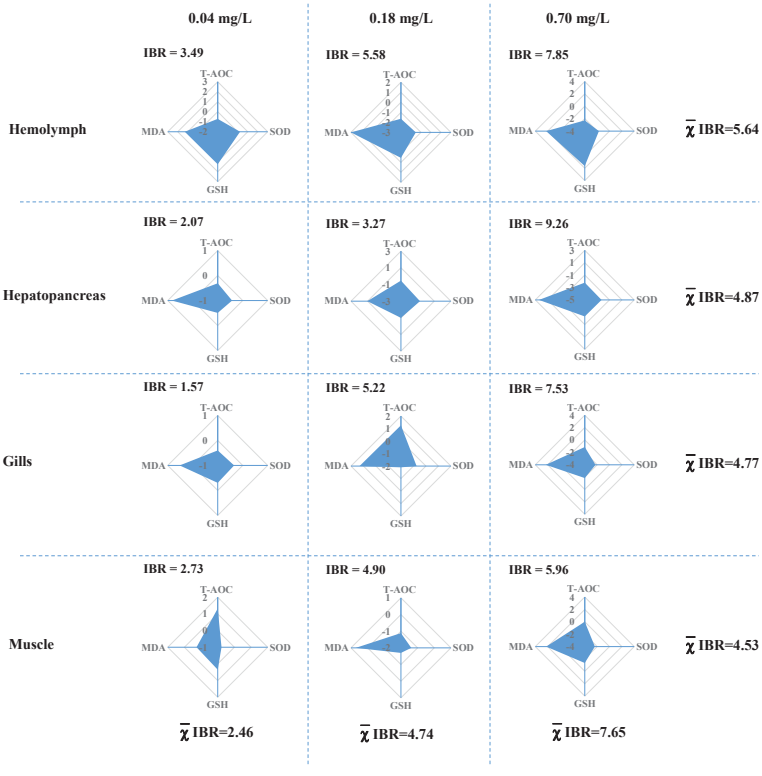

Figure 2. IBR index of the oxidative stress response to different concentrations of copper in the hemolymph, hepatopancreas, gills, and muscle. Biomarker values are represented in relation to the control group. The areas above zero reflect an increase in the biomarker, and the areas below zero reflect a decrease in the biomarker.

3.2. Alterations in the Expression of Apoptosis-Related Genes

To evaluate whether Cu^{2+} exposure could induce apoptosis, we measured the mRNA levels of apoptosis-related genes, including *caspase-3*, *caspase-8*, B-cell lymphoma 2 (*Bcl-2*), Bcl2 X protein (*Bax*), *p53*, and cytochrome c (*cytc1*) in the hepatopancreas, gills, and muscle (Figure 3). In the hepatopancreas, the mRNA levels of *caspase-3*, *caspase-8*, *Bax*, and *p53* showed an increasing tendency, and the highest value of the expression levels of the genes was observed in the group treated with 0.70 mg/L of Cu^{2+} ($p < 0.05$; Figure 3A).

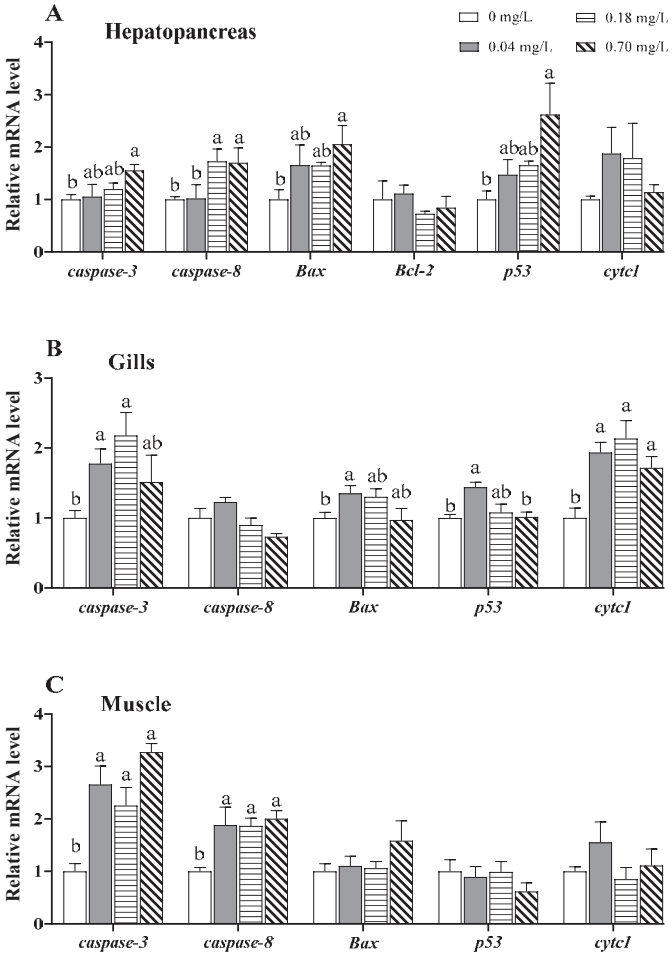

Figure 3. Expression of apoptosis-related genes in different tissues of *E. sinensis* exposed to copper for 5 days. (**A**) Hepatopancreas; (**B**) gills; (**C**) muscle. The values are expressed as the mean ± SEM ($n = 6$). Different letters denote significant differences among different groups ($p < 0.05$).

In the gills, the mRNA levels of *caspase-3*, *Bax*, *p53*, and *cytc1* increased in treatments with 0.04 and/or 0.18 mg/L of Cu^{2+} and then decreased to near normal values in treatment with 0.70 mg/L of Cu^{2+} (Figure 3B). The *caspase-3* and *cytc1* were markedly upregulated under exposure to 0.04 and 0.18 mg/L of Cu^{2+} ($p < 0.05$; Figure 3B) and gradually decreased under exposure to 0.70 mg/L of Cu^{2+}. Similarly, *Bax* and *p53* were upregulated after exposure to 0.04 mg/L of copper ($p < 0.05$) and gradually decreased with increasing Cu^{2+} concentrations (Figure 3B).

In the muscle, *caspase-3* and *caspase-8* transcription were significantly upregulated compared to the control group after 5 days of Cu^{2+} exposure ($p < 0.05$; Figure 3C). However, the mRNA levels of *Bax*, *p53*, and *cytc1* were not significantly altered after copper exposure.

3.3. Alterations in the Expression of MAPK Pathway-Related Genes

After Cu^{2+} exposure, the genes associated with the MAPK signaling pathway showed various degrees of change (Figure 4). In the hepatopancreas, the transcription of extracellular signal-regulated protein kinase (*erk*) was elevated in the groups exposed to 0.18 and 0.70 mg/L of Cu^{2+}, and *jun* (an AP-1 subunit) was elevated in the group exposed to 0.70 mg/L of Cu^{2+}, both compared to that in the control group ($p < 0.05$; Figure 4A).

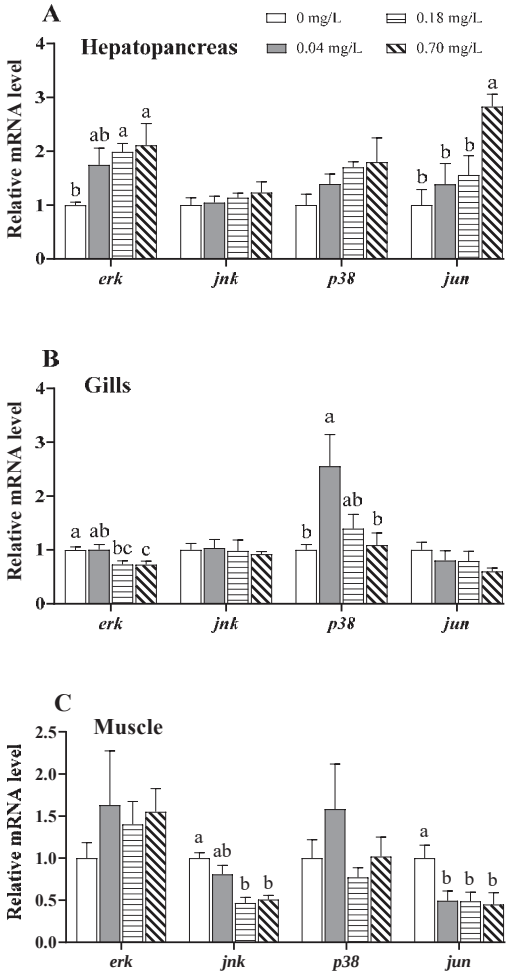

Figure 4. Expression of MAPK pathway-related genes in different tissues of *E. sinensis* exposed to copper for 5 days. (**A**) Hepatopancreas; (**B**) gills; (**C**) muscle. The values are expressed as the mean ± SEM ($n = 6$). Different letters denote significant differences among different groups ($p < 0.05$).

In the gills, *erk* expression was distinctly downregulated in the group exposed to 0.70 mg/L of Cu^{2+} compared to that in the control group ($p < 0.05$; Figure 4B), while *p38* expression was upregulated in the group exposed to 0.04 mg/L of Cu^{2+} and gradually downregulated under exposure to 0.18 and 0.70 mg/L of Cu^{2+} ($p < 0.05$; Figure 4B).

In the muscle, c-Jun N-terminal kinase (*jnk*) mRNA was downregulated in the groups exposed to 0.18 and 0.70 mg/L of Cu^{2+}, and *jun* mRNA was downregulated in the groups exposed to 0.04, 0.18, and 0.70 mg/L of Cu^{2+}, compared to those in the control group ($p < 0.05$; Figure 4C).

3.4. Alterations in the Expression of ER Stress-Related Genes

The mRNA levels of the ER stress-related genes showed irregular variations after Cu^{2+} exposure in the hepatopancreas, gills, and muscle (Figure 5). In the hepatopancreas, the mRNA levels of activating transcription factor 6 (*atf6*) and *atf4* exhibited a linear rising trend with increasing Cu^{2+} concentrations and were upregulated in the group treated with 0.70 mg/L of Cu^{2+} ($p < 0.05$; Figure 5A). Compared to those in the control group, exposure to 0.18 and 0.70 mg/L of Cu^{2+} upregulated the transcription of eukaryotic translation initiation factor 2 α (*eif2α*), and 0.70 mg/L of Cu^{2+} upregulated inositol-requiring enzyme 1 (*ire1*) transcription ($p < 0.05$; Figure 5A).

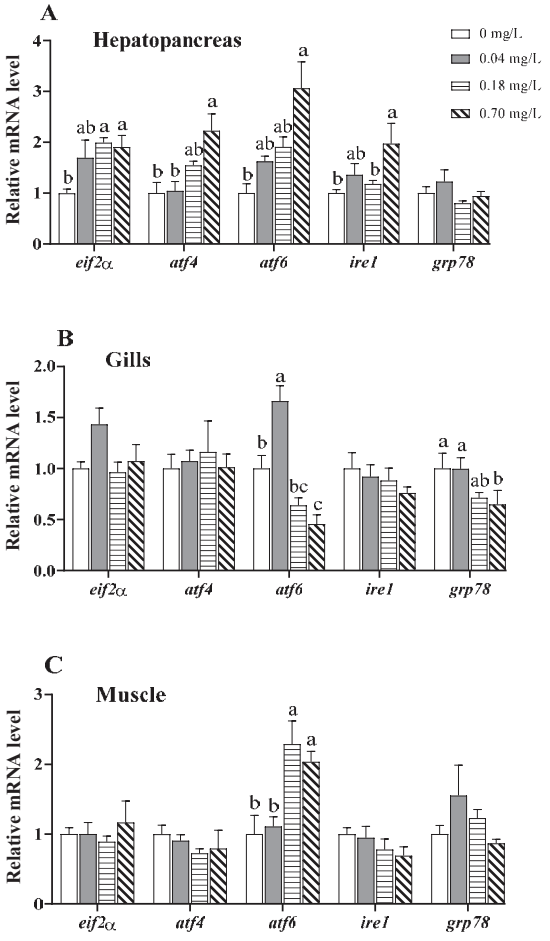

Figure 5. Expression of ER stress-related genes in different tissues of *E. sinensis* exposed to copper for 5 days. (**A**) Hepatopancreas; (**B**) gills; (**C**) muscle. The values are the mean ± SEM ($n = 6$). Different letters denote significant differences among different groups ($p < 0.05$).

In the gills, the mRNA levels of *atf6* exhibited an initial upregulation followed by a decreasing tendency, and a peak value was observed in the crabs exposed to 0.04 mg/L of

Cu^{2+} ($p < 0.05$; Figure 5B). The expression of *atf6* was downregulated under exposure to 0.70 mg/L of Cu^{2+} relative to that in the control group ($p < 0.05$; Figure 5B). In addition, exposure to 0.70 mg/L of Cu^{2+} decreased *grp78* transcription ($p < 0.05$; Figure 5B).

In the muscle, the mRNA level of *atf6* was significantly enhanced in the 0.18 and 0.70 mg/L Cu^{2+}-exposed groups compared to that in the control group ($p < 0.05$), but other genes were not significantly changed (Figure 5B).

3.5. Alterations in the Expression of Autophagy-Related Genes

Eight autophagy-related genes, including 5-AMP-activated protein kinase β (*ampkβ*), *beclin*, *p62*, microtubule-associated proteins 1A/1B light chain 3a (*lc3a*), *lc3c*, autophagy-related gene 7 (*atg7*), transcription factor EB (*tfeb*), and lysosome-associated membrane protein 1 (*lamp1*), were used to evaluate the autophagic response to Cu^{2+} exposure in the hepatopancreas, gills, and muscle (Figure 6). In the hepatopancreas, the mRNA levels of *atg7*, *tfeb*, *ampkβ*, *beclin*, *p62*, and *lc3a* increased with Cu^{2+} concentrations in a linear or non-linear manner, and they were significantly upregulated in the 0.70 mg/L Cu^{2+}-exposed group compared to the control group ($p < 0.05$; Figure 6A). A significant upregulation was also observed in *atg7* under exposure to 0.18 mg/L of Cu^{2+} and in *tfeb* and *p62* under exposure to 0.04 and 0.18 mg/L Cu^{2+} ($p < 0.05$; Figure 6A).

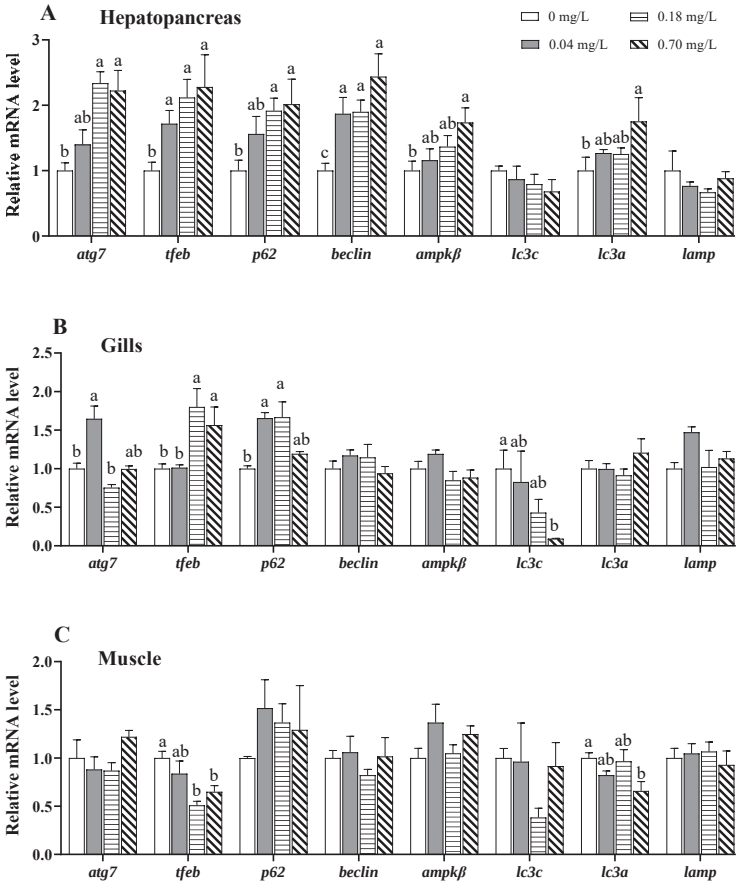

Figure 6. Expression of autophagy-related genes in different tissues of *E. sinensis* exposed to copper for 5 days. (**A**) Hepatopancreas; (**B**) gills; (**C**) muscle. The values are expressed as the mean ± SEM ($n = 6$). Different letters denote significant differences among different groups ($p < 0.05$).

In the gills, Cu^{2+} exposure caused a significant increase in the *atg7* mRNA level in the 0.04 mg/L Cu^{2+}-exposed group, *tfeb* in the 0.18 and 0.70 mg/L Cu^{2+}-exposed groups, and *p62* in the 0.04 and 0.18 mg/L Cu^{2+}-exposed groups compared with those in the control group ($p < 0.05$; Figure 6B). In contrast, Cu^{2+} exposure caused a significant decrease in *lc3c* mRNA in the 0.70 mg/L Cu^{2+}-exposed group ($p < 0.05$; Figure 6B).

In the muscle, only the transcription of *tfeb* and *lc3a* was significantly changed by Cu^{2+} exposure (Figure 6C). The transcription of *tfeb* was lower in the 0.18 and 0.70 mg/L Cu^{2+}-exposed groups than in the 0 mg/L Cu^{2+}-exposed group ($p < 0.05$; Figure 6C). Furthermore, the transcription of *lc3a* was lower in the 0.70 mg/L Cu^{2+}-exposed group than in the 0 mg/L Cu^{2+}-exposed group ($p < 0.05$; Figure 6C).

3.6. Alterations in the Expression of Immune Response-Related Genes

The immune response to Cu^{2+} exposure was assessed by determining the immune response-related genes in the hepatopancreas, gills, and muscle (Figure 7). In the hepatopancreas, the mRNA levels of Toll-like receptor 2 (*tlr2*), myeloid differentiation protein-88 (*myd88*), *relish*, interleukin-16 (*il-16*), lipopolysaccharide-induced TNF-α factor (*litaf*), and *pelle* were higher in the 0.70 mg/L Cu^{2+}-exposed group than in the control group ($p < 0.05$; Figure 7A). Higher mRNA levels of *tlr2* and *myd88* were also observed in the 0.18 mg/L Cu^{2+}-exposed group ($p < 0.05$; Figure 7A).

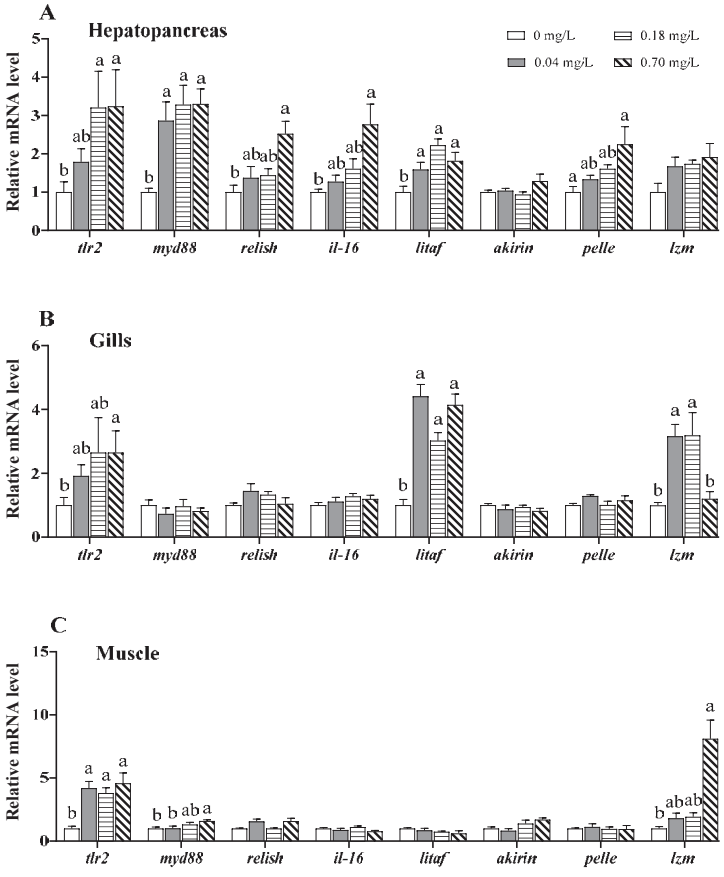

Figure 7. Expression of immune response-related genes in different tissues of *E. sinensis* exposed to copper for 5 days. (**A**) Hepatopancreas; (**B**) gills; (**C**) muscle. The values are expressed as the mean ± SEM ($n = 6$). Different letters denote significant differences among different groups ($p < 0.05$).

In the gills, the mRNA level of *tlr2* was strongly upregulated in the 0.70 mg/L Cu^{2+}-treated group compared to that in the control group ($p < 0.05$; Figure 7B). The *litaf* in the three Cu^{2+}-treated groups and lysozyme (*lzm*) in the 0.04 and 0.18 mg/L Cu^{2+}-treated groups were highly expressed ($p < 0.05$; Figure 7B).

In the muscle, the transcription of *tlr2* was upregulated in the three Cu^{2+}-treated groups compared to that in the control group ($p < 0.05$; Figure 7C). Likewise, the expression of *myd88* and *lzm* was upregulated in the 0.70 mg/L Cu^{2+}-treated group ($p < 0.05$; Figure 7C).

3.7. Alterations in the Expression of Stress- and Detoxification-Related Genes

In the hepatopancreas, the mRNA levels of shock protein 90 (*hsp90*), cytochrome P450 (*cyp*) 2b, and *cyp4* exhibited a linear rising trend with increasing Cu^{2+} concentrations, and upregulation was observed in the 0.70 mg/L Cu^{2+}-treated group ($p < 0.05$; Figure 8A). The mRNA levels of *hsp70* and metallothioneins (*mt*) were first upregulated and then downregulated with increasing Cu^{2+} concentrations, as evidenced by higher *hsp70* expression under exposure to 0.04 mg/L of Cu^{2+} and higher *mt* and *cyp2a* expression under exposure to 0.04 and 0.18 mg/L of Cu^{2+} ($p < 0.05$; Figure 8A).

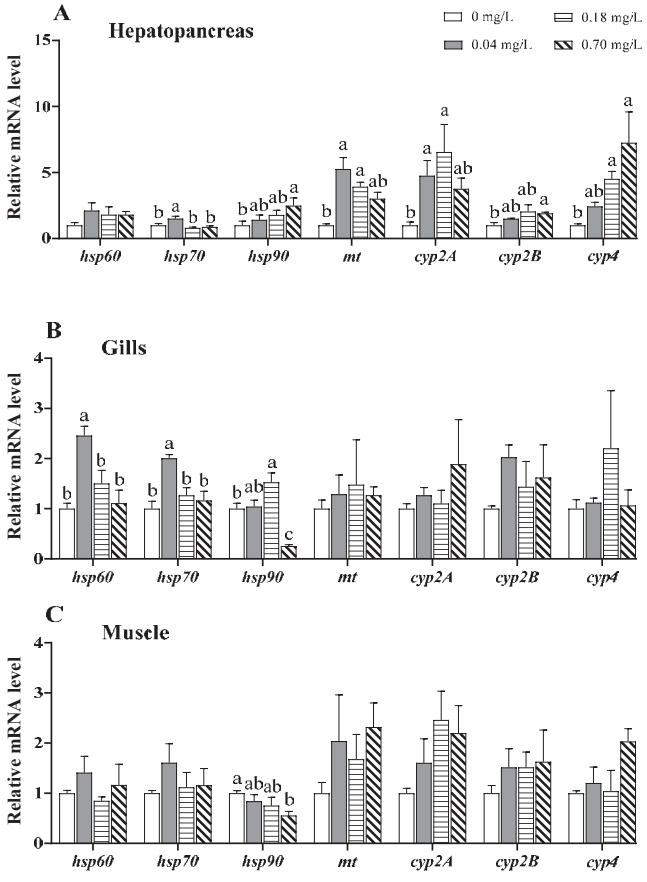

Figure 8. Expression of stress- and detoxification-related genes in different tissues of *E. sinensis* exposed to copper for 5 days. (**A**) Hepatopancreas; (**B**) gills; (**C**) muscle. The values are expressed as the mean ± SEM ($n = 6$). Different letters denote significant differences among different groups ($p < 0.05$).

In the gills, the mRNA levels of *hsp60* and *hsp70* were significantly upregulated under 0.04 mg/L Cu^{2+} exposure ($p < 0.05$; Figure 8B) but gradually reduced to the same level as that in the control group. Similarly, *hsp90* expression was upregulated in the group exposed to 0.18 mg/L of Cu^{2+} but downregulated in the group exposed to 0.70 mg/L of Cu^{2+} ($p < 0.05$; Figure 8B). Other genes were not markedly affected by Cu^{2+} exposure.

In the muscle, only *hsp90* expression was significantly reduced in the 0.70 mg/L Cu^{2+}-exposed group compared to that in the control group ($p < 0.05$; Figure 8C).

4. Discussion

Excess copper has been widely confirmed to be toxic to crustaceans, and the toxic effect is linked not only to concentration but also to exposure time. The median lethal concentration (24–96 h LC_{50}) of Cu^{2+} decreased with the extension of exposure time in crustaceans [12,13]. Exposure to 0.75 mg/L Cu^{2+} for 7 days resulted in abnormal gill tip structure of *M. rosenbergii* [29]. The stress biomarkers showed an increased tendency in a time-dependent manner (1–7 days) in *Macrobrachium scabriculum* exposed to Cu^{2+} at doses of 0.032–0.352 mg/L [30]. A study of 3–48 h of exposure showed that Cu^{2+} treatments (5–20 mg/L) began to negatively influence the immune ability of *L. vannamei* after 12 h [31]. Similar to previous studies, our data also exhibited that exposure to Cu^{2+} (0.04–0.70 mg/L) for 5 days had adverse effects on antioxidative status, apoptosis, ER stress, and immune response in *E. sinensis*. It is worth noting that the Cu^{2+} toxicity showed tissue-specificity, and hepatopancreas was more sensitive to Cu^{2+} exposure in *E. sinensis*. In invertebrates, metals, including copper, are commonly taken in via gills and accumulate in the hepatopancreas [32]. Yang et al. reported that the accumulation of copper in the hepatopancreas was higher than in other tissues in *E. sinensis* after Cu^{2+} exposure [33]. Meanwhile, the hepatopancreas is considered a primary organ of excretion and detoxification for metals in crustaceans [34]. Thus, it may be more susceptible to copper exposure.

4.1. Effects of Copper Exposure on Antioxidative Status

Oxidative stress is a physiological imbalance state in which the production of reactive oxygen species (ROS) overwhelms the cellular antioxidant defense capacity, eventually resulting in damage to cellular macromolecules, such as DNA, proteins, and lipids. Copper is known to participate in the formation of ROS, and its overload may result from repetitive radical formation via redox cycling [35,36]. Excessive ROS can induce oxidative stress and impair the antioxidant defense system. Indeed, strong evidence exists that acute or chronic Cu^{2+} exposure induces oxidative stress in different aquatic animals. For example, Cu^{2+} exposure enhances the activities of antioxidative enzymes such as SOD and glutathione peroxidase (Gpx) in hepatopancreas of *L. vannamei* [37] and *Callinectes sapidus* [38], and gills of *O. niloticus* [39], reflecting an occurrence of oxidative stress. In contrast, exposure to high levels of waterborne Cu^{2+} decreases enzymatic and non-enzymatic antioxidants and induces oxidative damage in the gills of *P. clarkia* [40], the hepatopancreas of *Minuca rapax* [41], and the brain of *Cyprinus carpio* [42]. Our study further showed that the antioxidant capacity in different tissues of *E. sinensis* decreased following exposure to 0.70 mg/L of Cu^{2+}, indicating that a higher level of Cu^{2+} exposure induces oxidative damage. In addition, our data showed a variable intensity of oxidative stress in different tissues after Cu^{2+} exposure, which was supported by a previous study in *Carassius auratus* [43], indicating the tissue specificity of Cu^{2+} toxicity.

Peroxidative damage to membrane lipids is another common consequence of excess Cu^{2+}. Lipid peroxy radicals formed during lipid peroxidation may change the fluidity and permeability of the cell membrane in injured cells [44]. MDA, a lipid peroxidation product, is a typical indicator used to evaluate lipid peroxidation. It is increased in multiple fish tissues after Cu^{2+} exposure [45–47]. Similarly, Cu^{2+}-overloaded *Procambarus clarkii* has a significantly increased MDA concentration in the hemolymph, hepatopancreas, and gills [40,48,49]. Our data also exhibited enhanced MDA content in the hemolymph, gills,

and muscle of *E. sinensis* after exposure to 0.70 mg/L of Cu^{2+}, indicating that high levels of Cu^{2+} exposure induce lipid peroxidation and augment oxidative damage.

It has been reported that the toxic effect of copper on redox state was related to cultured conditions, such as salinity, temperature, and pH, in aquatic animals. Moderate salinity levels increased GST activity to alleviate the lethal toxicity of Cu^{2+}, but high salinity levels worsen the Cu^{2+}-induced oxidative damage in *Danio rerio* embryos [50]. In *M. rapax*, the higher temperature (35 °C) significantly increased Cu^{2+}-induced oxidative stress [41]. Carvalho et al. (2015) suggested that the effect of Cu^{2+} on the response of antioxidant defense systems was determined by water pH in *Prochilodus lineatus* [51]. The evidence revealed that copper combined with other factors causes more significant toxicity in aquatic animals than copper alone. Thus, interactive effects between copper exposure and cultured conditions will be examined in future research.

4.2. Effects of Copper Exposure on Apoptosis

Apoptosis is considered a sensitive parameter for assessing the toxicity of environmental pollutants [52]. It has been reported that Cu, a common environmental pollutant, can induce apoptosis in aquatic animals. High concentrations of Cu^{2+} increase the incidence of TUNEL-positive cells (apoptosis) in the gills of *D. rerio* and *C. auratus* [53,54]. Acute exposure to Cu^{2+} increases the apoptotic hemocyte ratio and *caspase-3* gene expression in *L. vannamei* [55]. In our study, apoptosis-related genes such as *caspase-3*, *caspase-8*, *Bax*, *p53*, and *cytc* were upregulated in the hepatopancreas, gills, and/or muscle of *E. sinensis*, indicating that mitochondria-mediated apoptosis was activated by Cu^{2+} exposure. Cu^{2+}-induced apoptosis is likely elicited by the induction of ROS [56]. Our data support this view, given the strong oxidative stress that was found after Cu^{2+} exposure. Additionally, in *D. rerio*, the central nervous system and liver show higher sensitivity to apoptosis induced by Cu^{2+} exposure [57]. Similarly, Cu^{2+}-exposed *E. sinensis* exhibits stronger apoptosis in the hepatopancreas and gills. In the hepatopancreas, the activation of apoptosis was mainly observed under exposure to 0.7 mg/L of Cu^{2+}, while in the gills, it was mainly observed under exposure to 0.04 and 0.18 mg/L of Cu^{2+}. Thus, Cu-triggered apoptosis may occur in a tissue-specific manner.

MAPK signaling pathways, including ERK, JNK, and p38, play critical roles in apoptosis [58]. The ERK-AP-1 and JNK-AP-1 pathways have been reported to regulate oxidative stress-induced apoptosis [59]. A previous study reported that Cu^{2+} exposure causes apoptosis via the activation of ERK and p38 in the hepatocytes of *O. mykiss* [60]. Mitochondrial apoptosis induced by copper nanoparticles has been associated with the activation of the ERK signaling pathway in female mice [61]. In our study, the mRNA levels of *erk* and *jun* (a AP-1 subunit) were upregulated in the hepatopancreas after Cu^{2+} exposure and significantly associated with apoptosis, indicating that the ERK-AP-1 pathway may be involved in Cu^{2+}-induced apoptosis. In the gills, *p38* gene expression was upregulated in the 0.04 mg/L copper-exposed group, which implies that the p38 pathway may be activated to regulate apoptosis after exposure to lower dose of Cu^{2+}. In the muscle, however, the mRNA levels of *jnk* and *jun* were downregulated after Cu^{2+} exposure, although the underlying mechanisms remain unclear. We hypothesize that the downregulation may be related to tissue damage caused by Cu^{2+} exposure.

4.3. Effects of Copper Exposure on ER Stress

The ER is a pivotal organelle that is responsible for protein assembly, folding, and transportation. Protein misfolding and ER stress trigger a complex signaling process, known as the unfolded protein response (UPR), to restore ER homeostasis [62]. A triggered UPR is a protective mechanism to reinstate ER homeostasis, but persistent or severe ER stress can initiate cell death via mitochondrial pathways [63]. Environmental pollutants, such as Cu^{2+}, activate ER stress and impair mitochondrial function in aquatic animals [64]. Cu^{2+} exposure for 30 days leads to upregulated ER stress-related genes, such as *grp78*, *perk*, *eif2a*, *ire-1α*, and *atf6* in the liver of *Synechogobius hasta* and *Pelteobagrus fulvidraco* [65,66].

We also observed a marked upregulation of *eif2a*, *atf4*, *atf6*, and *ire1* in the hepatopancreas of *E. sinensis*, indicating that exposure to 0.7 mg/L of Cu^{2+} induced ER stress. In the gills, exposure to 0.04 mg/L of Cu^{2+} upregulated *atf6*, while 0.7 mg/L of Cu^{2+} downregulated *atf6* and *grp78*. We hypothesize that the downregulation of these genes was related to ER damage under exposure to higher concentrations of Cu^{2+}. Similar data have also been found in the liver of *S. hasta* exposed to a higher level (0.055 mg/L) of Cu^{2+} for 60 days [65]. In addition, increased ROS production under Cu^{2+} exposure can induce ER stress and activate the ATF6 and IRE1 signaling pathways, leading to apoptosis [67].

4.4. Effects of Copper Exposure on Autophagy

Autophagy is a crucial cell-clearing process that regulates the degradation of damaged organelles and unfolded proteins by fusion with lysosomes in cells. LC3 and p62 are widely used as markers of autophagy. In the later stages of autophagy, TFEB coordinates lysosomal activation and autophagosome–lysosome fusion [68]. A recent study reported that excess dietary copper induces oxidative stress and autophagy, as evidenced by the upregulated expression of *beclin1*, *lc3B*, and *p62* in *P. fulvidraco*, which then protected against copper-induced lipid accumulation [69]. Activated autophagy has also been reported in GC-1 cells [70], pig testes [71], and the hypothalamus of broilers [72] following Cu^{2+} exposure due to oxidative stress. In contrast, Cu^{2+} exposure has been found to downregulate the mRNA levels of *lc3* in *D. rerio* gills, indicating the impairment of macroautophagy [73]. Furthermore, the AMPK signaling pathway has been shown to regulate Cu^{2+}-induced autophagy [74,75]. In our study, the mRNA levels of autophagy-related genes, including *ampkβ*, *beclin*, *lc3a*, *tfeb*, *p62*, and *atg7*, were upregulated in the hepatopancreas, suggesting that Cu^{2+} exposure may activate autophagy via the AMPK-Beclin pathway. Unlike those in the hepatopancreas, the mRNA levels of *atg7* and *p62* in the gills were upregulated following exposure to lower doses of Cu^{2+} (0.04 and/or 0.18 mg/L) but returned to similar levels as those in the control group after being exposed to a higher dose of Cu^{2+} (0.7 mg/L). The expression of *lc3c* was even downregulated in the 0.7 mg/L Cu^{2+}-exposed gills. The findings suggest that a low dose of Cu^{2+} may initiate autophagy, but a high dose can impair the autophagic process in the gills. The detailed mechanisms require further study. The activation of autophagy may be linked to oxidative stress and ER stress induced by Cu^{2+} exposure [76].

4.5. Effects of Copper Exposure on the Immune Response

The immune response is a key mechanism following pollutant toxicity in aquatic organisms. TLRs, widely existing pattern-recognition receptors, are considered major regulators of the immune response [77]. Numerous studies have suggested that environmental pollutants, including heavy metals, can activate the TLRs to regulate immune response in animals. For example, Cr(VI) exposure upregulated *tlr2* and *myd88* expression in *Geloina erosa* gills [78], and microbiota-dependent TLR2 signaling reduced silver nanoparticle toxicity to *D. rerio* larvae [79]. Relish, an NF-κB transcription factor, also plays a key role in the innate immunity of crustaceans [80]. In crustaceans, the TLR2-MyD88 pathway regulates the immune response to pathogenic bacterial infections [81,82]. A transcriptomic analysis revealed that Cu^{2+} exposure significantly affects the TLR pathway in *Mizuhopecten yessoensis* [83]. In *L. vannamei*, the gene expression of TLRs was significantly increased in the 0.05 mg/L Cu^{2+}-treated group, but returned to the control level following treatments with higher doses of Cu^{2+} [37]. Aksakal and Ciltas [84] also reported that a low expression of immune-related genes such as *tlr4* and *tlr22* resulted in immunosuppression in *D. rerio* after exposure to copper oxide nanoparticles. In our study, the immune response to Cu^{2+} exposure was tissue-specific. In the hepatopancreas, a significant inflammatory response occurred via the TLR2-MyD88-NF-κB pathway after Cu^{2+} exposure. Despite the upregulation of *tlr2* and/or *myd88* in the gills and muscle, *relish* and *il-16* (an important pro-inflammatory cytokine in crabs) were not altered, which may indicate no obvious

inflammatory response in the two tissues, especially the muscle. In addition, the ERK pathway may also be involved in Cu^{2+}-induced inflammation in the hepatopancreas [85].

In addition to NF-κB, LITAF is a pivotal transcription factor in the inflammatory response and regulates the transcription of TNF-α and other cytokines [86]. Tang et al. [87] suggested that LITAF is a mediator from the NF-κB pathway in the lipopolysaccharide-induced inflammatory response. It has been reported that *litaf* is upregulated and involved in the immune response in *E. sinensis* after *Edwardsiella tarda* and *Vibrio anguillarum* infections [86]. Similarly, our data show that Cu^{2+} exposure upregulated the expression of *litaf* in the hepatopancreas, suggesting that the TLR2-MyD88-LITAF pathway may be triggered in response to Cu^{2+} toxicity.

4.6. Effects of Copper Exposure on the Stress Response and Detoxification

HSPs are molecular chaperones that play well-established roles in protein folding and transport. HSP60, HSP70, and HSP90 are well-studied HSPs that are abundantly induced under a variety of chemical exposures [88], which is a protective response to stressors [89]. A previous study reported that Cu^{2+} exposure upregulated the mRNA levels of *hsp60*, *hsp70*, and *hsp90* in the liver of *C. carpio* [90]. A study on freshwater prawns (*Macrobrachium malcolmsonii*) further showed that the synthesis of HSP70 appeared from the 1st to 24th hour in the gills under Cu^{2+} exposure but was not recorded after the 24-h mark [91]. We also observed that the mRNA levels of *hsp60*, *hsp70*, and *hsp90* exhibited an initial upregulation followed by a decreasing tendency in the gills. We therefore conjectured that Cu^{2+} exposure at lower doses triggered an HSP-mediated protective mechanism. In addition, the downregulation of *hsp90* may be interpreted as a result of the strong oxidative stress induced by higher doses of Cu^{2+} [92].

MT, a metal-binding protein with a high affinity for metals, is involved in the regulation of essential metal ion homeostasis and the detoxification of non-essential metal ions [93]. After 4 days of Cu^{2+} exposure, the MT level was found to increase in *Gasterosteus aculeatus* [94]. An increased MT level has also been reported after Cu^{2+} exposure in *Pacifastacus leniusculus* [95] and constitutes a protective response to Cu^{2+} accumulation. Similarly, our data show upregulated *mt* expression in the hepatopancreas after exposure to 0.04 and 0.18 mg/L of Cu^{2+}, indicating that a lower concentration of Cu^{2+} induces a positive response, but a higher concentration inhibits the response.

CYP enzymes have been implicated in the detoxification and metabolism of environmental pollutants, including heavy metals, in aquatic animals. The CYP 1–4 families are considered reliable biomarkers for monitoring environmental toxicants [96]. The induction of CYP enzymes may be an adaptive response to metal exposure, whereas their decrease inhibits detoxification [97]. In Cu^{2+}-exposed *Diaphanosoma celebensis*, CYP-related genes, including *cyp2* and *cyp4*, were found to be upregulated at an earlier exposure time (6 h) but downregulated at a later exposure time (24h) [98]. In *C. auratus*, Cu^{2+} exposure upregulated the expression of *cyp1a* and *cyp3a*, but combined treatment with Cu^{2+} and diclofenac decreased their expression [99]. In our study, the mRNA levels of *cyp2A*, *cyp2B*, and *cyp4* were markedly increased in the hepatopancreas, implying that CYP enzymes may be involved in the phase I detoxification of Cu^{2+} toxicity. In addition, our data revealed that detoxification predominantly occurred in the hepatopancreas but not in the gills or muscle.

Apart from acute toxicity, long-term Cu^{2+} exposure also causes its accumulation in different tissues of crustaceans. In *E. sinensis*, the copper accumulation was positively related to its level in water, and the hepatopancreas was the primary target organ [33]. The accumulation presents potential for bio-magnification through the food chain [100], which may pose a health risk to humans, since humans are the primary consumers of *E. sinensis* and other aquatic animals. In order to maintain cellular homeostasis, many organisms possess a purification ability of toxic elements. Boada et al. [101] reported that *Mugil curema* eliminated enriched copper for14 days after Cu^{2+} exposure. Similarly, the purification process in juvenile *Petenia kraussii* exposed to Cu^{2+} was achieved after 14 days [102]. In *P. clarkii*, enrichment of copper in hepatopancreas was completely eliminated after

7 days [103]. However, the depuration time of *E. sinensis* for excessive copper has not been reported until now, and will be further evaluated in our future research. Furthermore, the potential health risks of copper accumulation from aquatic food consumption should be investigated.

5. Conclusions

In this study, we examined the adverse effects of Cu^{2+} exposure on different tissues of *E. sinensis*. Cu^{2+} exposure suppressed antioxidative parameters and promoted lipid peroxidation in different tissues, resulting in oxidative damage. After Cu^{2+} exposure, apoptosis-related genes were upregulated, implying that apoptosis was activated, and the activation may be related to the upregulation of the MAPK pathway and ER stress. In the hepatopancreas and gills, the regulation of autophagy-related genes indicated that the autophagic response was involved in Cu^{2+} toxicity. In addition, Cu^{2+} exposure increased immune-related gene expression in different tissues, especially the hepatopancreas, where the TLR2-MyD88-NF-κB pathway may be initiated to mediate the inflammatory response. Furthermore, the upregulation of anti-stress and detoxification genes revealed that an adaptive mechanism was activated in different tissues following Cu^{2+} exposure. Overall, the toxicity response of Cu^{2+} in *E. sinensis* was associated with oxidative stress, apoptosis, ER stress, autophagy, and immune response. This study enriches our understanding of the potential toxicity response of Cu^{2+} in crustaceans, which may provide more reference data for the environmental risk assessments of Cu^{2+}.

Supplementary Materials: The following supporting information can be downloaded at: https://www.mdpi.com/article/10.3390/antiox11102029/s1, Table S1: Specific primer sequences for qPCR in the study.

Author Contributions: Conceptualization and writing—original draft preparation, W.F.; methodology, S.S.; formal analysis, C.S.; software, F.Y.; investigation, J.Z.; validation, J.L.; resources and data curation, R.J.; visualization and supervision, P.X.; writing—review and editing, project administration, and funding acquisition, Y.T. All authors have read and agreed to the published version of the manuscript.

Funding: This research was funded by the Central Public Interest Scientific Institution Basal Research Fund, Freshwater Fisheries Research Center, CAFS (no. 2021JBFM12; 2020TD36), the Key Project for Jiangsu Agricultural New Variety Innovation (no. PZCZ201749), and the Jiangsu Revitalization of Seed Industry (no. JBGS[2021]031).

Institutional Review Board Statement: Not applicable.

Informed Consent Statement: Not applicable.

Data Availability Statement: All data are included in the manuscript and Supplementary Materials.

Conflicts of Interest: The authors declare no conflict of interest.

References

1. Tapiero, H.; Townsend, D.á.; Tew, K. Trace elements in human physiology and pathology. Copper. *Biomed. Pharmacother.* **2003**, *57*, 386–398. [CrossRef]
2. Ugarte, M.; Osborne, N.N.; Brown, L.A.; Bishop, P.N. Iron, zinc, and copper in retinal physiology and disease. *Surv. Ophthalmol.* **2013**, *58*, 585–609. [CrossRef]
3. Rehman, M.; Liu, L.J.; Wang, Q.; Saleem, M.H.; Bashir, S.; Ullah, S.; Peng, D.X. Copper environmental toxicology, recent advances, and future outlook: A review. *Environ. Sci. Pollut. Res.* **2019**, *26*, 18003–18016. [CrossRef]
4. O'Gara, B.A.; Bohannon, V.K.; Teague, M.W.; Smeaton, M.B. Copper-induced changes in locomotor behaviors and neuronal physiology of the freshwater oligochaete, Lumbriculus variegatus. *Aquat. Toxicol.* **2004**, *69*, 51–66. [CrossRef]
5. Tavares-Dias, M. Toxic, physiological, histomorphological, growth performance and antiparasitic effects of copper sulphate in fish aquaculture. *Aquaculture* **2021**, *535*, 736350. [CrossRef]
6. Zhang, B.H.; Ding, Z.G.; Li, H.Q.; Mou, X.Z.; Zhang, Y.Q.; Yang, J.Y.; Zhou, E.M.; Li, W.J. Algicidal Activity of Streptomyces eurocidicus JXJ-0089 Metabolites and Their Effects on Microcystis Physiology. *Appl. Environ. Microbiol.* **2016**, *82*, 5132–5143. [CrossRef] [PubMed]

7. Chen, W.Y.; Ju, Y.R.; Lin, C.J.; Tsai, J.W.; Chen, S.C.; Liao, C.M. Environmental stochasticity promotes copper bioaccumulation and bioenergetic response in tilapia. *Stoch. Environ. Res. Risk Assess.* **2015**, *29*, 1545–1555. [CrossRef]
8. Zhang, F.; Li, D.; Yang, Y.; Zhang, H.; Zhu, J.; Liu, J.; Bu, X.; Li, E.; Qin, J.; Yu, N. Combined effects of polystyrene microplastics and copper on antioxidant capacity, immune response and intestinal microbiota of Nile tilapia (*Oreochromis niloticus*). *Sci. Total Environ.* **2022**, *808*, 152099. [CrossRef] [PubMed]
9. Daglish, R.W.; Nowak, B.F. Rainbow Trout Gills Are a Sensitive Biomarker of Short-Term Exposure to Waterborne Copper. *Arch. Environ. Contam. Toxicol.* **2002**, *43*, 98–102. [CrossRef] [PubMed]
10. Brown, V.; Dalton, R. The acute lethal toxicity to rainbow trout of mixtures of copper, phenol, zinc and nickel. *J. Fish Biol.* **1970**, *2*, 211–216. [CrossRef]
11. Mohamed, M.; El-Fiky, S.; Soheir, Y.; Abeer, A. Cytogenetic studies on the effect of copper sulfate and lead acetate. pollution on Oreochromis niloticus fish. *J. Cell Biol.* **2008**, *3*, 51–60. [CrossRef]
12. Dai, X.; Zang, W.; Yang, H.; Zhong, X.; Jiang, M.; Ke, X. The toxic effects of Cu^{2+},Zn^{2+},Cd^{2+} on giant freshwater prawn juvenile. *J. Shanghai Fish. Univ.* **2001**, *10*, 295–302. [CrossRef]
13. Dong, X.; Lv, L.; Wang, A.; Wang, L.; Miao, J. Study on the acute toxicity of Cu^{2+} and Cd^{2+} acting on Procambarus clarkii juvenile. *J. Hydroecology* **2010**, *3*, 90–93. [CrossRef]
14. Yao, Q.; Zang, W.l.; Dai, X.; Jiang, M.; Xu, G.; Ding, F. A acute toxic effects of copper, cadmium, dichlorvos and methamidophos on Penaeus vannamei larval shrimp and their interactions. *J. Shanghai Fish. Univ.* **2003**, *12*, 117–122.
15. Tilton, F.A.; Bammler, T.K.; Gallagher, E.P. Swimming impairment and acetylcholinesterase inhibition in zebrafish exposed to copper or chlorpyrifos separately, or as mixtures. *Comp. Biochem. Physiol. Part C Toxicol. Pharmacol.* **2011**, *153*, 9–16. [CrossRef] [PubMed]
16. Van Aardt, W.; Hough, M. Acute effects of Cu on oxygen consumption and 96 hr-LC50 values in the freshwater fish *Tilapia sparrmani* (Teleostei: Cichlidae) in Mooi River hard water, South Africa. *Afr. J. Aquat. Sci.* **2006**, *31*, 305–311. [CrossRef]
17. Rougier, F.; Troutaud, D.; Ndoye, A.; Deschaux, P. Non-specific immune response of Zebrafish, Brachydanio rerio (Hamilton-Buchanan) following copper and zinc exposure. *Fish Shellfish Immunol.* **1994**, *4*, 115–127. [CrossRef]
18. Hoseini, S.M.; Hoseinifar, S.H.; Doan, H.V. Effect of dietary eucalyptol on stress markers, enzyme activities and immune indicators in serum and haematological characteristics of common carp (*Cyprinus carpio*) exposed to toxic concentration of ambient copper. *Aquac. Res.* **2018**, *49*, 3045–3054. [CrossRef]
19. Vani Paila, R.; Rao Yallapragada, P.; Thatipaka, S.D.R. Response of glutathione system and carotenoids to sublethal copper in the postlarvae of Penaeus indicus. *Ecotoxicol. Environ. Saf.* **2012**, *75*, 127–133. [CrossRef] [PubMed]
20. Frías-Espericueta, M.G.; Castro-Longoria, R.; Barrón-Gallardo, G.J.; Osuna-López, J.I.; Abad-Rosales, S.M.; Páez-Osuna, F.; Voltolina, D. Histological changes and survival of Litopenaeus vannamei juveniles with different copper concentrations. *Aquaculture* **2008**, *278*, 97–100. [CrossRef]
21. Tang, D.; Liu, R.; Shi, X.; Shen, C.; Bai, Y.; Tang, B.; Wang, Z. Toxic effects of metal copper stress on immunity, metabolism and pathologic changes in Chinese mitten crab (*Eriocheir japonica sinensis*). *Ecotoxicology* **2021**, *30*, 632–642. [CrossRef] [PubMed]
22. Sun, S.; Ge, X.; Hu, J.; Yu, H.; Jiang, Z. Effects of water-borne copper on the survival, antioxidant status, metallothionein-I mRNA expression and physiological responses of the *Chinese mitten crab*, *Eriocheir sinensis* (Decapoda: Brachyura) larvae. *Sci. Mar.* **2014**, *78*, 91–97. [CrossRef]
23. Yang, Z.B.; Zhao, Y.L.; Zhou, Z.; Yang, J. Effects of water CuSO4 concentration on molting, growth and survival of eriocheir sinensis. *Acta Hydrobiol. Sin.* **2006**, *30*, 563–569.
24. Zhou, C. *Toxic Effects of Copper Ions on Eriocheir sinensis*; Nanjing Agricultural University: Nanjing, China, 2021.
25. Jia, R.; Du, J.; Cao, L.; Feng, W.; He, Q.; Xu, P.; Yin, G. Chronic exposure of hydrogen peroxide alters redox state, apoptosis and endoplasmic reticulum stress in common carp (*Cyprinus carpio*). *Aquat. Toxicol.* **2020**, *229*, 105657. [CrossRef] [PubMed]
26. Livak, K.; Schmittgen, T. Analysis of relative gene expression data using real-time quantitative PCR and the 2(-Delta Delta C(T)) Method. *Methods–A Companion Methods Enzymol.* **2001**, *25*, 402–408. [CrossRef] [PubMed]
27. Huang, S. *Study on Reciprocal Regulation Mechanism of MIH and Ec R Genes in the Molting Process of Chinese Mitten Crab, Eriocheir Sinensis*; Shanghai Ocean University: Shanghai, China, 2017.
28. Sanchez, W.; Burgeot, T.; Porcher, J.-M. A novel "Integrated Biomarker Response" calculation based on reference deviation concept. *Environ. Sci. Pollut. Res.* **2013**, *20*, 2721–2725. [CrossRef] [PubMed]
29. Asih, A.Y.P.; Irawan, B.; Soegianto, A. Effect of copper on survival, osmoregulation, and gill structures of freshwater prawn (Macrobrachium rosenbergii, de Man) at different development stages. *Mar. Freshw. Behav. Physiol.* **2013**, *46*, 75–88. [CrossRef]
30. Mukherjee, A. Experimental study of copper toxicity and some stress biomarkers in *Macrobrachium scabriculum* (Heller, 1862). *J. Appl. Aquac.* **2022**, *34*, 425–440. [CrossRef]
31. Yeh, S.T.; Liu, C.H.; Chen, J.C. Effect of copper sulfate on the immune response and susceptibility to *Vibrio alghiolyticus* in the white shrimp *Litopenaeus vannamei*. *Fish Shellfish Immunol.* **2004**, *17*, 437–446. [CrossRef]
32. Grosell, M.; Blanchard, J.; Brix, K.; Gerdes, R. Physiology is pivotal for interactions between salinity and acute copper toxicity to fish and invertebrates. *Aquat. Toxicol.* **2007**, *84*, 162–172. [CrossRef] [PubMed]
33. Yang, Z.; Zhao, Y.; Zhou, Z.; Zhou, X.; Yang, J. Effects of copper in water on distribution of copper and digestive enzymes activities in *Eriocheir sinensis*. *J. Fish. CHINA* **2005**, *29*, 496–501.

34. Gurkan, M. Effects of three different nanoparticles on bioaccumulation, oxidative stress, osmoregulatory, and immune responses of *Carcinus aestuarii*. *Toxicol. Environ. Chem.* **2018**, *100*, 693–716. [CrossRef]
35. Bremner, I. Manifestations of copper excess. *Am. J. Clin. Nutr.* **1998**, *67*, 1069S–1073S. [CrossRef] [PubMed]
36. Gaetke, L.M.; Chow, C.K. Copper toxicity, oxidative stress, and antioxidant nutrients. *Toxicology* **2003**, *189*, 147–163. [CrossRef]
37. Qian, D.; Xu, C.; Chen, C.; Qin, J.G.; Chen, L.; Li, E. Toxic effect of chronic waterborne copper exposure on growth, immunity, anti-oxidative capacity and gut microbiota of Pacific white shrimp *Litopenaeus vannamei*. *Fish Shellfish Immunol.* **2020**, *100*, 445–455. [CrossRef]
38. Brouwer, M.; Brouwer, T.H. Biochemical defense mechanisms against copper-induced oxidative damage in the blue crab, *Callinectes sapidus*. *Arch. Biochem. Biophys.* **1998**, *351*, 257–264. [CrossRef]
39. Ma'rifah, F.; Saputri, M.R.; Soegianto, A.; Irawan, B.; Putranto, T.W.C. The Change of Metallothionein and Oxidative Response in Gills of the *Oreochromis niloticus* after Exposure to Copper. *Animals* **2019**, *9*, 353. [CrossRef]
40. Wei, K.; Yang, J. Oxidative damage induced by copper and beta-cypermethrin in gill of the freshwater crayfish *Procambarus clarkii*. *Ecotoxicol. Environ. Saf.* **2015**, *113*, 446–453. [CrossRef]
41. Capparelli, M.V.; Bordon, I.C.; Araujo, G.; Gusso-Choueri, P.K.; de Souza Abessa, D.M.; McNamara, J.C. Combined effects of temperature and copper on oxygen consumption and antioxidant responses in the mudflat fiddler crab *Minuca rapax* (Brachyura, Ocypodidae). *Comp. Biochem. Physiol. Part C Toxicol. Pharmacol.* **2019**, *223*, 35–41. [CrossRef]
42. Jiang, W.-D.; Liu, Y.; Hu, K.; Jiang, J.; Li, S.-H.; Feng, L.; Zhou, X.-Q. Copper exposure induces oxidative injury, disturbs the antioxidant system and changes the Nrf2/ARE (CuZnSOD) signaling in the fish brain: Protective effects of myo-inositol. *Aquat. Toxicol.* **2014**, *155*, 301–313. [CrossRef]
43. Husak, V.V.; Mosiichuk, N.M.; Kubrak, O.I.; Matviishyn, T.M.; Storey, J.M.; Storey, K.B.; Lushchak, V.I. Acute exposure to copper induces variable intensity of oxidative stress in goldfish tissues. *Fish Physiol. Biochem.* **2018**, *44*, 841–852. [CrossRef] [PubMed]
44. Qian, Y.; Buettner, G.R. The EPR detection of lipid-dervied radicals during membrane lipid peroxidation of cells. *Free Radic. Biol. Med.* **1998**, *25*, S106. [CrossRef]
45. Rajabiesterabadi, H.; Hoseini, S.M.; Fazelan, Z.; Hoseinifar, S.H.; Hien Van, D. Effects of dietary turmeric administration on stress, immune, antioxidant and inflammatory responses of common carp (*Cyprinus carpio*) during copper exposure. *Aquac. Nutr.* **2020**, *26*, 1143–1153. [CrossRef]
46. Kong, X.; Jiang, H.; Wang, S.; Wu, X.; Fei, W.; Li, L.; Nie, G.; Li, X. Effects of copper exposure on the hatching status and antioxidant defense at different developmental stages of embryos and larvae of goldfish *Carassius auratus*. *Chemosphere* **2013**, *92*, 1458–1464. [CrossRef]
47. Kamunde, C.; MacPhail, R. Effect of humic acid during concurrent chronic waterborne exposure of rainbow trout (*Oncorhynchus mykiss*) to copper, cadmium and zinc. *Ecotoxicol. Environ. Saf.* **2011**, *74*, 259–269. [CrossRef]
48. Wei, K.; Yang, J. Copper-induced oxidative damage to the prophenoloxidase-activating system in the freshwater crayfish *Procambarus clarkii*. *Fish Shellfish Immunol.* **2016**, *52*, 221–229. [CrossRef]
49. Wei, K.; Yang, J. Oxidative damage of hepatopancreas induced by pollution depresses humoral immunity response in the freshwater crayfish *Procambarus clarkii*. *Fish Shellfish Immunol.* **2015**, *43*, 510–519. [CrossRef]
50. Santos, B.; Andrade, T.; Domingues, I.; Ribeiro, R.; Soares, A.M.V.M.; Lopes, I. Influence of salinity on the toxicity of copper and cadmium to *Zebrafish embryos*. *Aquat. Toxicol.* **2021**, *241*, 106003. [CrossRef]
51. Carvalho, C.d.S.; Bernusso, V.A.; Fernandes, M.N. Copper levels and changes in pH induce oxidative stress in the tissue of curimbata (*Prochilodus lineatus*). *Aquat. Toxicol.* **2015**, *167*, 220–227. [CrossRef]
52. AnvariFar, H.; Amirkolaie, A.K.; Jalali, A.M.; Miandare, H.K.; Sayed, A.H.; Üçüncü, S.İ.; Ouraji, H.; Ceci, M.; Romano, N. Environmental pollution and toxic substances: Cellular apoptosis as a key parameter in a sensible model like fish. *Aquat. Toxicol.* **2018**, *204*, 144–159. [CrossRef]
53. Vergolyas, M.R.; Veyalkina, N.N.; Goncharuk, V.V. Effect of copper ions on hematological and cytogenetic parameters of freshwater fishes *Carassius auratus gibelio*. *Cytol. Genet.* **2010**, *44*, 124–128. [CrossRef]
54. Luzio, A.; Monteiro, S.M.; Fontaínhas-Fernandes, A.; Pinto-Carnide, O.; Matos, M.; Coimbra, A.M. Copper induced upregulation of apoptosis related genes in zebrafish (*Danio rerio*) gill. *Aquat. Toxicol.* **2013**, *128*, 183–189. [CrossRef] [PubMed]
55. Guo, H.; Li, K.X.; Wang, W.; Wang, C.G.; Shen, Y.C. Effects of Copper on Hemocyte Apoptosis, ROS Production, and Gene Expression in White Shrimp *Litopenaeus vannamei*. *Biol. Trace Elem. Res.* **2017**, *179*, 318–326. [CrossRef] [PubMed]
56. Chandra, J.; Samali, A.; Orrenius, S. Triggering and modulation of apoptosis by oxidative stress. *Free Radic. Biol. Med.* **2000**, *29*, 323–333. [CrossRef]
57. Hernandez, P.P.; Undurraga, C.; Gallardo, V.E.; Mackenzie, N.; Allende, M.L.; Reyes, A.E. Sublethal concentrations of waterborne copper induce cellular stress and cell death in zebrafish embryos and larvae. *Biol. Res.* **2011**, *44*, 7–15. [CrossRef]
58. Junttila, M.R.; Li, S.-P.; Westermarck, J. Phosphatase-mediated crosstalk between MAPK signaling pathways in the regulation of cell survival. *FASEB J.* **2008**, *22*, 954–965. [CrossRef]
59. Hiramatsu, N.; Kasai, A.; Yao, J.; Meng, Y.; Takeda, M.; Maeda, S.; Kitamura, M. AP-1-independent sensitization to oxidative stress-induced apoptosis by proteasome inhibitors. *Biochem. Biophys. Res. Commun.* **2004**, *316*, 545–552. [CrossRef]
60. Nawaz, M.; Manzl, C.; Lacher, V.; Krumschnabel, G. Copper-induced stimulation of extracellular signal-regulated kinase in trout hepatocytes: The role of reactive oxygen species, $Ca^{(2+)}$, and cell energetics and the impact of extracellular signal-regulated kinase signaling on apoptosis and necrosis. *Toxicol. Sci.* **2006**, *92*, 464–475. [CrossRef]

61. Zhang, C.H.; Wang, Y.; Sun, Q.Q.; Xia, L.L.; Hu, J.D.; Cheng, K.; Wang, X.; Fu, X.X.; Gu, H. Copper Nanoparticles Show Obvious in vitro and in vivo Reproductive Toxicity via ERK Mediated Signaling Pathway in Female Mice. *Int. J. Biol. Sci.* **2018**, *14*, 1834–1844. [CrossRef]
62. Schröder, M.; Kaufman, R.J. ER stress and the unfolded protein response. *Mutat. Res. Fundam. Mol. Mech. Mutagen.* **2005**, *569*, 29–63. [CrossRef]
63. Kim, I.; Xu, W.; Reed, J.C. Cell death and endoplasmic reticulum stress: Disease relevance and therapeutic opportunities. *Nat. Rev. Drug Discov.* **2008**, *7*, 1013–1030. [CrossRef] [PubMed]
64. Xu, Y.-H.; Xu, Y.-C.; Hogstrand, C.; Zhao, T.; Wu, L.-X.; Zhuo, M.-Q.; Luo, Z. Waterborne copper exposure up-regulated lipid deposition through the methylation of GRP78 and PGC1α of grass carp *Ctenopharyngodon idella*. *Ecotoxicol. Environ. Saf.* **2020**, *205*, 111089. [CrossRef] [PubMed]
65. Song, Y.-F.; Huang, C.; Shi, X.; Pan, Y.-X.; Liu, X.; Luo, Z. Endoplasmic reticulum stress and dysregulation of calcium homeostasis mediate Cu-induced alteration in hepatic lipid metabolism of javelin goby Synechogobius hasta. *Aquat. Toxicol.* **2016**, *175*, 20–29. [CrossRef] [PubMed]
66. Song, Y.-F.; Luo, Z.; Zhang, L.-H.; Hogstrand, C.; Pan, Y.-X. Endoplasmic reticulum stress and disturbed calcium homeostasis are involved in copper-induced alteration in hepatic lipid metabolism in yellow catfish *Pelteobagrus fulvidraco*. *Chemosphere* **2016**, *144*, 2443–2453. [CrossRef]
67. Zhao, G.; Sun, H.; Zhang, T.; Liu, J.-X. Copper induce zebrafish retinal developmental defects via triggering stresses and apoptosis. *Cell Commun. Signal.* **2020**, *18*, 45. [CrossRef]
68. Settembre, C.; Di Malta, C.; Polito, V.A.; Arencibia, M.G.; Vetrini, F.; Erdin, S.; Erdin, S.U.; Huynh, T.; Medina, D.; Colella, P.; et al. TFEB Links Autophagy to Lysosomal Biogenesis. *Science* **2011**, *332*, 1429. [CrossRef]
69. Zhong, C.-C.; Zhao, T.; Hogstrand, C.; Chen, F.; Song, C.-C.; Luo, Z. Copper (Cu) induced changes of lipid metabolism through oxidative stress-mediated autophagy and Nrf2/PPARγ pathways. *J. Nutr. Biochem.* **2022**, *100*, 108883. [CrossRef]
70. Kang, Z.L.; Qiao, N.; Liu, G.Y.; Chen, H.M.; Tang, Z.X.; Li, Y. Copper-induced apoptosis and autophagy through oxidative stress-mediated mitochondrial dysfunction in male germ cells. *Toxicol. Vitr.* **2019**, *61*, 104639. [CrossRef]
71. Li, Y.L.; Chen, H.M.; Liao, J.Z.; Chen, K.L.; Javed, M.T.; Qiao, N.; Zeng, Q.W.; Liu, B.X.; Yi, J.N.; Tang, Z.X.; et al. Long-term copper exposure promotes apoptosis and autophagy by inducing oxidative stress in pig testis. *Environ. Sci. Pollut. Res.* **2021**, *28*, 55140–55153. [CrossRef]
72. Liao, J.Z.; Yang, F.; Chen, H.L.; Yu, W.L.; Han, Q.Y.; Li, Y.; Hu, L.M.; Guo, J.Y.; Pan, J.Q.; Liang, Z.P.; et al. Effects of copper on oxidative stress and autophagy in hypothalamus of broilers. *Ecotoxicol. Environ. Saf.* **2019**, *185*, 109710. [CrossRef]
73. Luzio, A.; Parra, S.; Costa, B.; Santos, D.; Álvaro, A.; Monteiro, S. Copper impair autophagy on zebrafish (*Danio rerio*) gill epithelium. *Environ. Toxicol. Pharmacol.* **2021**, *86*, 103674. [CrossRef] [PubMed]
74. Liao, J.Z.; Yang, F.; Yu, W.L.; Qiao, N.; Zhang, H.; Han, Q.Y.; Hu, L.M.; Li, Y.; Guo, J.Y.; Pan, J.Q.; et al. Copper induces energy metabolic dysfunction and AMPK-mTOR pathway-mediated autophagy in kidney of broiler chickens. *Ecotoxicol. Environ. Saf.* **2020**, *206*, 111366. [CrossRef]
75. Chen, H.L.; Wang, Y.Y.; Luo, J.; Kang, M.; Hou, J.; Tang, R.P.; Zhao, L.; Shi, F.; Ye, G.; He, X.L.; et al. Autophagy and apoptosis mediated nano-copper-induced testicular damage. *Ecotoxicol. Environ. Saf.* **2022**, *229*, 113039. [CrossRef] [PubMed]
76. Fornai, F.; Puglisi-Allegra, S. Autophagy status as a gateway for stress-induced catecholamine interplay in neurodegeneration. *Neurosci. Biobehav. Rev.* **2021**, *123*, 238–256. [CrossRef] [PubMed]
77. Fan, Z.-J.; Zou, P.-F.; Yao, C.-L. Toll-like receptors (tlr) and its signaling pathway in teleost. *Acta Hydrobiol. Sin.* **2015**, *39*, 173–184.
78. Wang, G.; Zhang, C.; Huang, B. Transcriptome analysis and histopathological observations of *Geloina erosa* gills upon Cr(VI) exposure. *Comp. Biochem. Physiol. Part C Toxicol. Pharmacol.* **2020**, *231*, 108706. [CrossRef] [PubMed]
79. Brinkmann, B.W.; Koch, B.E.V.; Peijnenburg, W.J.G.M.; Vijver, M.G. Microbiota-dependent TLR2 signaling reduces silver nanoparticle toxicity to zebrafish larvae. *Ecotoxicol. Environ. Saf.* **2022**, *237*, 113522. [CrossRef] [PubMed]
80. Zhu, F.; Sun, B.Z.; Wang, Z.Y. The crab Relish plays an important role in white spot syndrome virus and *Vibrio alginolyticus* infection. *Fish Shellfish Immunol.* **2019**, *87*, 297–306. [CrossRef] [PubMed]
81. Gao, Q.; Tang, Q.; Xia, Z.; Yi, S.; Cai, M.; Du, H.; Yang, J.; Li, J.; Xing, Q.; Luo, J.; et al. Molecular identification and functional analysis of MyD88 in giant freshwater prawn (*Macrobrachium rosenbergii*) and expression changes in response to bacterial challenge. *Int. J. Biol. Macromol.* **2021**, *178*, 492–503. [CrossRef] [PubMed]
82. Jiang, Z.; Li, X.; Gao, X.; Jiang, Q.; Chen, Q.; Zhang, S.; Tong, S.; Liu, X.; Zhu, J.; Zhang, X. Pathogenicity of Aeromonas hydrophila causing mass mortalities of *Procambarus clarkia* and its induced host immune response. *Microb. Pathog.* **2020**, *147*, 104376. [CrossRef] [PubMed]
83. Meng, X.L.; Tian, X.; Nie, G.X.; Wang, J.L.; Liu, M.; Jiang, K.Y.; Wang, B.J.; Guo, Q.Q.; Huang, J.R.; Wang, L. The transcriptomic response to copper exposure in the digestive gland of Japanese scallops (*Mizuhopecten yessoensis*). *Fish Shellfish Immunol.* **2015**, *46*, 161–167. [CrossRef] [PubMed]
84. Aksakal, F.I.; Ciltas, A. Impact of copper oxide nanoparticles (CuO NPs) exposure on embryo development and expression of genes related to the innate immune system of zebrafish (*Danio rerio*). *Comp. Biochem. Physiol. Part C Toxicol. Pharmacol.* **2019**, *223*, 78–87. [CrossRef]

85. Park, J.-Y.; Chung, T.-W.; Jeong, Y.-J.; Kwak, C.-H.; Ha, S.-H.; Kwon, K.-M.; Abekura, F.; Cho, S.-H.; Lee, Y.-C.; Ha, K.-T. Ascofuranone inhibits lipopolysaccharide–induced inflammatory response via NF-kappaB and AP-1, p-ERK, TNF-α, IL-6 and IL-1β in RAW 264.7 macrophages. *PLoS ONE* **2017**, *12*, e0171322. [CrossRef] [PubMed]
86. Li, S.; Jia, Z.; Li, X.; Geng, X.; Sun, J. Identification and expression analysis of lipopolysaccharide-induced TNF-alpha factor gene in Chinese mitten crab *Eriocheir sinensis*. *Fish Shellfish Immunol.* **2014**, *38*, 190–195. [CrossRef]
87. Tang, X.R.; Metzger, D.; Leeman, S.; Amar, S. LPS-induced TNF-alpha factor (LITAF)-deficient mice express reduced LPS-induced cytokine: Evidence for LITAF-dependent LPS signaling pathways. *Proc. Natl. Acad. Sci. USA* **2006**, *103*, 13777–13782. [CrossRef] [PubMed]
88. Gupta, S.C.; Sharma, A.; Mishra, M.; Mishra, R.K.; Chowdhuri, D.K. Heat shock proteins in toxicology: How close and how far? *Life Sci.* **2010**, *86*, 377–384. [CrossRef] [PubMed]
89. Singh, M.P.; Reddy, M.M.; Mathur, N.; Saxena, D.K.; Chowdhuri, D.K. Induction of hsp70, hsp60, hsp83 and hsp26 and oxidative stress markers in benzene, toluene and xylene exposed *Drosophila melanogaster*: Role of ROS generation. *Toxicol. Appl. Pharmacol.* **2009**, *235*, 226–243. [CrossRef] [PubMed]
90. Jiang, X.Y.; Guan, X.T.; Yao, L.L.; Zhang, H.; Jin, X.; Han, Y. Effects of Single and Joint Subacute Exposure of Copper and Cadmium on Heat Shock Proteins in Common Carp (*Cyprinus carpio*). *Biol. Trace Elem. Res.* **2016**, *169*, 374–381. [CrossRef]
91. Yamuna, A.; Kabila, V.; Geraldine, P. Expression of heat shock protein 70 in freshwater prawn *Macrobrachium malcolmsonii* (H. Milne Edwards) following exposure to Hg and Cu. *Indian J. Exp. Biol.* **2000**, *38*, 921–925.
92. Jia, R.; Du, J.; Cao, L.; Feng, W.; He, Q.; Xu, P.; Yin, G. Immune, inflammatory, autophagic and DNA damage responses to long-term H_2O_2 exposure in different tissues of common carp (*Cyprinus carpio*). *Sci. Total Environ.* **2021**, *757*, 143831. [CrossRef]
93. Amiard, J.C.; Amiard-Triquet, C.; Barka, S.; Pellerin, J.; Rainbow, P.S. Metallothioneins in aquatic invertebrates: Their role in metal detoxification and their use as biomarkers. *Aquat. Toxicol.* **2006**, *76*, 160–202. [CrossRef] [PubMed]
94. Santos, E.M.; Ball, J.S.; Williams, T.D.; Wu, H.; Ortega, F.; Van Aerle, R.; Katsiadaki, I.; Falciani, F.; Viant, M.R.; Chipman, J.K. Identifying health impacts of exposure to copper using transcriptomics and metabolomics in a fish model. *Environ. Sci. Technol.* **2010**, *44*, 820–826. [CrossRef] [PubMed]
95. Gunderson, M.P.; Boyd, H.M.; Kelly, C.I.; Lete, I.R.; McLaughlin, Q.R. Modulation of endogenous antioxidants by zinc and copper in signal crayfish (*Pacifastacus leniusculus*). *Chemosphere* **2021**, *275*, 129982. [CrossRef] [PubMed]
96. Uno, T.; Ishizuka, M.; Itakura, T. Cytochrome P450 (CYP) in fish. *Environ. Toxicol. Pharmacol.* **2012**, *34*, 1–13. [CrossRef] [PubMed]
97. Aziz, N.; Butt, A. Enzymatic and non-enzymatic detoxification in Lycosa terrestris and *Pardosa birmanica* exposed to single and binary mixture of copper and lead. *Environ. Toxicol. Pharmacol.* **2020**, *80*, 103500. [CrossRef] [PubMed]
98. Han, J.; Lee, K.-W. Identification and response of cytochrome P450 genes in the brackish water flea *Diaphanosoma celebensis* after exposure to benzo [α] pyrene and heavy metals. *Mol. Biol. Rep.* **2021**, *48*, 657–664. [CrossRef] [PubMed]
99. Xie, Z.; Luan, H.; Zhang, Y.; Wang, M.; Cao, D.; Yang, J.; Tang, J.; Fan, S.; Wu, X.; Hua, R. Interactive effects of diclofenac and copper on bioconcentration and multiple biomarkers in crucian carp (*Carassius auratus*). *Chemosphere* **2020**, *242*, 125141. [CrossRef] [PubMed]
100. Naqvi, S.; Devalraju, I.; Naqvi, N. Copper bioaccumulation and depuration by red swamp crayfish, *Procambarus clarkii*. *Bull. Environ. Contam. Toxicol.* **1998**, *61*, 65–71. [CrossRef] [PubMed]
101. Barron, M.G.; Adelman, I.R. Nucleic acid, protein content, and growth of larval fish sublethally exposed to various toxicants. *Can. J. Fish. Aquat. Sci.* **1984**, *41*, 141–150. [CrossRef]
102. Lemus, M.; Chung, K. Effect of Temperature on Copper Toxicity, Accumulation, and Purification in Tropical Fish Juveniles *Petenia kraussii* (Pisces: Cichlidae). *Caribb. J. Sci.* **1999**, *35*, 64–69.
103. Dan, Z.; Zhang, X.; Liu, D.; Ru, S. Cu accumulation, detoxification and tolerance in the red swamp crayfish *Procambarus clarkii*. *Ecotoxicol. Environ. Saf.* **2019**, *175*, 201–207. [CrossRef]

antioxidants

MDPI

Article

Tea Tree Oil Mediates Antioxidant Factors Relish and Nrf2-Autophagy Axis Regulating the Lipid Metabolism of *Macrobrachium rosenbergii*

Mingyang Liu [1,2,†], Xiaochuan Zheng [2,†], Cunxin Sun [2], Qunlan Zhou [2], Bo Liu [2,*] and Pao Xu [2,*]

[1] Wuxi Fisheries College, Nanjing Agricultural University, Wuxi 214081, China
[2] Key Laboratory of Aquatic Animal Nutrition and Health, Freshwater Fisheries Research Center, Chinese Academy of Fishery Science, Wuxi 214081, China
* Correspondence: liub@ffrc.cn (B.L.); xup@ffrc.cn (P.X.); Tel.: +86-0510-8555-6101 (P.X.)
† These authors contributed equally to this work.

Abstract: Both oxidative stress and autophagy refer to regulating fat metabolism, and the former affects autophagy, but the role and mechanism of the antioxidant–autophagy axis in regulating lipid metabolism remains unclear. As an antioxidant, tea tree oil (TTO) has little research on the regulatory mechanism of lipid metabolism in crustaceans. This study investigated whether TTO could alter hepatopancreatic lipid metabolism by affecting the antioxidant–autophagy axis. Feed *Macrobrachium rosenbergii* with three different levels of TTO diets for 8 weeks: CT (0 mg/kg TTO), 100TTO (100 mg/kg TTO), and 1000TTO (1000 mg/kg TTO). The results showed that 100TTO treatment reduced the hemolymph lipids level and hepatopancreatic lipid deposition compared to CT. In contrast, 1000TTO treatment increased hepatopancreatic lipid deposition, damaging both morphology and function in the hepatopancreas. The 100TTO treatment promoted lipolysis and reduced liposynthesis at the transcriptional level compared to the CT group. Meanwhile, it improved the hepatopancreas antioxidant capacity and maintained mitochondrial structural and ROS homeostasis. In addition, it simultaneously activated the expression of transcription factors *Keap1-Nrf2* and *Imd-Relish*. By contrast, the 1000TTO group significantly enhanced the ROS level, which considerably activated the *Keap1-Nrf2* signaling expression but had no significant effects on the expression of *Imd-Relish*. The 100TTO group supplementation significantly enhanced lipid droplet breakdown and autophagy-related genes and protein expression. On the contrary, the 1000TTO group significantly inhibited the expression of genes and proteins related to autophagy. Pearson analysis revealed that *Nrf2* has a positive correlation to lipid anabolism-related genes (*Fasn*, *Srebp1*, *Pparγ*) and autophagy regulators (*mtor*, *akt*, *p62*), and were negatively correlated with lipolysis-related genes (*Cpt1*, *Hsl*, *Ampkα*) and autophagy markers (*Ulk1*, *Lc3*). *Relish* was positively correlated with *Atgl*, *Cpt1*, *Ampkα*, *Ulk1*, and *Lc3*, and negatively correlated with *Pparγ* and *p62*. Moreover, *Keap1* and *Imd* were negatively correlated with *p62* and *mtor*, respectively. In sum, 100 mg/kg TTO enhanced antioxidant activity and increased autophagy intensity through the *Relish-Imd* pathway to enhance lipid droplet breakdown, while 1000 mg/kg TTO overexpressed *Nrf2*, thus inhibiting autophagy and ultimately causing excessive lipid deposition and peroxidation. Our study gives a fresh perspective for deciphering the bidirectional regulation mechanism of lipid metabolism by different doses of TTO based on the antioxidant–autophagy axis.

Keywords: tea tree oil; lipid metabolism; autophagy; Relish; Nrf2; *Macrobrachium rosenbergii*

Citation: Liu, M.; Zheng, X.; Sun, C.; Zhou, Q.; Liu, B.; Xu, P. Tea Tree Oil Mediates Antioxidant Factors Relish and Nrf2-Autophagy Axis Regulating the Lipid Metabolism of *Macrobrachium rosenbergii*. *Antioxidants* **2022**, *11*, 2260. https://doi.org/10.3390/antiox11112260

Academic Editor: Stanley Omaye

Received: 30 September 2022
Accepted: 14 November 2022
Published: 16 November 2022

1. Introduction

For quite some time, the ongoing evolution of feed standards has gradually enhanced the nutritional quality of aquatic feed and expanded the economic benefits of aquaculture [1]. However, high-frequency feeding and excessive nutrient intake (high fat and carbohydrate content in aquafeeds) derived from the pursuit of benefits lead to eutrophic diseases, such as lipid metabolism disorder [2].

The hepatopancreas is the crucial tissue for lipid anabolism and deposition to the crustacean. The hepatopancreas of crustaceans has similar functions to the pancreas, liver, and intestine in mammals [3], and it is more sensitive and intolerant to high lipid deposition than the liver of mammals [4]. The excessive deposition of lipids can lead to steatosis-like lesions of the hepatopancreas [5]. The pathological symptoms of lipid metabolism disorders in crustaceans are similar to that of mammalian nonalcoholic fatty liver disease, manifested by abnormal blood lipid parameters and the disordered expression of hepatic lipid synthesis and catabolism genes (*Acca*, *Fasn*, *Pparα*, *Cpt1*) [6,7].

Previous studies pointed out that lipid accumulation and metabolism were regulated by oxidative stress [8,9]. Abnormal lipid metabolism induced by oxidative stress is an essential reason for the occurrence of lipid metabolic diseases [10,11]. Notably, autophagy was found to be an important intermediate mechanism of oxidative stress involved in the regulation of lipid metabolism [12]. Normal cellular processes require appropriate ROS levels, but excessive ROS can induce oxidative stress and cause severe damage to cell structure and function [13,14]. Simultaneously, ROS can affect the essential regulatory pathway of autophagy Ampk/mTOR to induce autophagy [15]. Oxidative stress and ROS levels are not only regulated tightly by the Keap1 and Nrf2 proteins [16,17] but are also affected by the *NF-κB* immunity regulatory pathway [18]. Further, new reports found that these antioxidant genes combined with the Ampk-mTOR pathway could form a discontinuous adverse feedback pathway to affect autophagy [19,20].

Tea tree oil (TTO) is a typical essential oil of flora, also known as *Melaleuca alternatifolia* essential oil, which is obtained from distilled *Melaleuca alternatifolia* leaves [21], well known for its antioxidant and growth-promoting functions [22]. Our earlier study exhibited that plant essential oils could activate *NF-κB* and regulate oxidative stress [23]. Essential oils can regulate blood lipid levels and lipid peroxidation [24]. Additionally, study found that an excessive increase in ROS is a critical factor in lipid excess in the liver [25]. High levels of essential oils induce oxidative stress and increase LPO and ROS production [26,27]. Active ingredients of *Calocedrus formosana* essential oil have also been found to activate lipid autophagy by significantly increasing *Ampk* phosphorylation [28]. The impairment of lipid autophagy is direct to liver metabolic diseases, and the gene level is shown as the reduction in vital autophagic genes such as *atg5* or *atg7* [29]. Therefore, the up-regulation of autophagy is considered beneficial, and autophagy impairment is a phenotype of several liver diseases [30,31]. Few studies have been conducted based on the "antioxidant-autophagy-lipid metabolism" axis to explore the regulation mechanisms of lipid metabolism by tea tree oil, let alone explicitly targeting these two oxidative factor regulators (*NF-κB* and *Nrf2*).

Macrobrachium rosenbergii is a frequently used crustacean model animal for immunology, nutrition, and metabolism research. This study used *M. rosenbergii* as a model animal to explore whether different TTO levels regulate lipid metabolism through the "antioxidant-autophagy-lipid metabolism" axis and its key regulatory targets. It is essential for the development of therapeutic strategies for oxidative stress-type lipid metabolic diseases.

2. Materials and Methods

2.1. Ethical Statement

All experiments were conducted following the guidelines for scientific breeding and use of animals formulated by the IACUC under the Chinese Academy of Fishery Sciences. At the same time, it has followed the guidelines of the Institute of Animal Research of Nanjing Agricultural University on animal care and use.

2.2. Experimental Materials, Design, and Growth Evaluation

Dietary formulation and *M. rosenbergii* feeding were presented in Table 1. We formulated experimental diets containing three different levels of TTO at 0 ppm (diet without TTO, CT), 100 ppm (diet with 100 mg/kg TTO, 100 TTO), and 1000 ppm (diet with 1000 mg/kg TTO, 1000 TTO) (Table 1). Put 360 freshwater prawns (initial body weight: 0.15 ± 0.01 g) in 9 vats (R × H, 1.0 m × 1.5 m), randomly assigned to 3 groups with 3 replicates, each

with 40 prawns. During the domestication period, the prawns were fed with commercial feed provided by Fuyuda Food Products Co. LTD., Yangzhou, China for one week. The prawns were fed a day thrice at 8:00 am, 1:00 pm, and 6:00 pm. After 8 weeks of feeding, the survival rate and the weight of prawns in each group were recorded. Calculation methods of feed the conversion ratio (FCR), hepatosomatic index (HSI), specific growth rate (SGR), and weight gain rate (WGR) were listed as follows:

- WGR (%) = (Final weight − Initial weight)/initial weight × 100
- SGR(%/day) = (Ln final weight − Ln initial weight) × 100/days
- FCR = Dry feed intake (g)/weight gain (g)
- HSI (%) = (Hepatopancreas weight/ final weight) × 100

Table 1. The formulation and proximate composition of the experimental diet.

Ingredients (g kg^{-1})	CT	100TTO	1000TTO
Fish meal [1]	750.00	750.00	750.00
Chellocken meal [1]	150.00	150.00	150.00
Blood globulin powder [1]	60.00	60.00	60.00
Shrimp meal [1]	240.00	240.00	240.00
Soybean meal [2]	570.00	570.00	570
Repeseed meal [2]	300.00	300.00	300
Shrimp meal [1]	240.00	240.00	240.00
Squid extract [1]	90.00	90.00	90.00
Soybean oil [2]	60.00	60.00	60.00
Fish oil [2]	60.00	60.00	60.00
α-starch [1]	600.00	600.00	600.00
Soy lecithin oil [1]	30.00	30.00	30.00
Ecdysone [1]	0.30	0.30	0.30
MCP	60.00	60.00	60.00
Premix [3]	30.00	30.00	30.00
Choline chloride [4]	30.00	30.00	30.00
Bentonite [4]	29.70	29.40	26.70
10% Tea Tree Oil	0.00	3.00	30.00
Total	3000.00	3005.40	3054.00
Proximate analysis (%)			
Moisture	10.40	9.48	9.68
Crude protein	40.91	39.46	40.29
Crude lipid	9.76	9.06	9.54
Ash	17.43	16.52	16.87

Notes: [1] Obtained from Jiangsu Fuyuda Food Products Co., Ltd., Yangzhou, China; [2] Obtained from Hulunbeier Sanyuan Milk Co., Ltd., Inner Mongolia, China; [3] Premix supplied the following minerals (g kg^{-1}) and vitamins (IU or mg kg^{-1}): Pantothenate, 1000 mg; Folic acid, 165 mg; Vitamin A, 900,000 IU; Vitamin D, 200,000 IU; Vitamin E, 4500 mg; Vitamin K_3, 220 mg; Vitamin B_1, 320 mg; Vitamin B_2, 1090 mg; Vitamin B_5, 2000 mg; Vitamin B_6, 500 mg; Vitamin B_{12}, 1.6 mg; Vitamin C, 5000 mg; $CuSO_4 \cdot 5H_2O$, 2.0 g; $FeSO_4 \cdot 7H_2O$, 25 g; $ZnSO_4 \cdot 7H_2O$, 22 g; $MnSO_4 \cdot 4H_2O$, 7 g; Na_2SeO_3, 0.04 g; KI, 0.026 g; $CoCl_2 \cdot 6H_2O$, 0.1 g. Wuxi Hanove Animal Health Products Co., Ltd. provides mineral and Vitamin additives.[4] Obtained from Freshwater Fisheries Research Center, Chinese Academy of Fishery Sciences (CAFS).

2.3. Samples Collection

After 8 weeks of feeding, in order to avoid the influence of diet, the prawns were fasted for 12 h and then euthanized with MS-222 (Millipore Sigma, St. Louis, MO, USA). The hepatopancreases of 3 prawns were dissected from each vat for samples. The samples were put into cryogenic vials, thrown into liquid nitrogen for quick freezing, and finally, stored in a refrigerator at −80 °C for subsequent RNA and protein separation. In order to analyze the biochemical indexes of hemolymph, 3 prawns were randomly picked from each vat for sampling, the hemolymph and blood cells were separated at 4 °C for 4000 rpm and 10 min, and the supernatant was put into a 4 °C refrigerator with a 1.5 mL centrifuge tube [32]. In addition, the hepatopancreases of 3 prawns were taken for immunohisto-

chemical and ultrastructural analysis and put into 4% paraformaldehyde solution and 2.5% glutaraldehyde solution (Biosharp, Labgic, Technology Co., LTD., Hefei, China) with 5 mL centrifuge tubes, respectively. The remaining samples were stored in the refrigerator at −80 °C for standby.

2.4. Sample Analysis

2.4.1. Antioxidant, Peroxide, and Lipid Parameters Analysis

Catalase (CAT), glutathione peroxidase (GSH-Px), total antioxidant capacity (T-AOC), total superoxide dismutase (T-SOD) activities, protein carbonyl (OH), and triglyceride (TG) content used Nanjing Jiancheng Institute of Bioengineering kits for measuring. The general measurement method is to suspend the hepatopancreas in 50 mM potassium phosphate buffer, which contains 0.5 mM EDTA, and the pH value is about 7.0. Use a handheld homogenizer to homogenize the hepatopancreas for 5 min in a 2.0 mL centrifuge tube. After homogenization, all samples were centrifuged at 4 °C for 15 min at 2000× *g*. The supernatant product was extracted for enzyme analysis, and the Spectra Max Plus spectrophotometer (Molecular Devices, Menlo Park, CA, USA) was used for full-package enzyme activity analysis. The content of malondialdehyde (MDA) in the hepatopancreas was determined by the thiobarbituric acid (TBA) test [33]. Nanjing Jiancheng Bioengineering Research Institute provided the determination kit. The malondialdehyde extraction of the supernatant for determination is similar to the enzyme method. All specific experimental methods are according to the manufacturer's instructions.

According to the manufacturer's instructions, the content of several lipid metabolism-related enzymes (Acetyl-CoA carboxylase, ACC; carnitine palmitoyltransferase 1, CPT1; fatty acid synthase, FAS) and peroxide (4-hydroxynonenal, 4-HNE; Lipid peroxidation, LPO) was determined by ELISA kits (Shanghai mlbio Biotechnology Co., Ltd., China) specific for freshwater shrimp. Briefly, the hepatopancreas supernatant was mixed with the reactants and recorded the absorbance corrected at 430 nm and 650 nm. The Spectra Max Plus spectrophotometer was used for all of Elisa's technical readings of optical density.

2.4.2. ROS Levels

Flow cytometry was used based on a previous study that analyzed ROS levels [34] in the fresh hemolymph cell of *M. rosenbergii*. Cells were washed three times by PBS (1000 rpm for 5 min), and the final concentration of the cell suspension was adjusted to 1×10^6/mL. Then, use the serum-free medium to dilute DCFH-DA to a concentration of 10 m at 1:1000, collect cells, suspend them in diluted DCFH-DA, and incubate them at 37 °C for 20 min. Then, mix them upside down for 3–5 min to let the probe and the cells fully contact. Next, the cells were washed three times using serum-free cell culture to remove DCFH-DA that does not fully enter cells. Finally, flow cytometry was used to detect (Ex = 488 nm; Em = 530 nm) ROS in cells.

2.4.3. Oil Red O Staining, H&E Stainings, and Transmission Electron Microscopy

Remove fixed hepatopancreas samples in 4% paraformaldehyde buffer. The samples were embedded in the optimum cutting temperature (OCT) medium and stored at −80 °C. For OCT embedding, 7 μ of the fat content of the m sections was detected by ORO (Sigma Aldrich, St. Louis, MO, USA) staining. Use and equip an Olympus UPlan Apo 200×. The objective lens of the Olympus BX51 optical microscope (Tokyo, Japan) was used to take pictures of randomly selected tissue sections. ImageJ software (National Institutes of Health, Bethesda, MD, USA) adapted from the ORO-staining section algorithm was used to analyze the lipid content of the ORO-staining section and expressed it as the % of the area of lipid-positive hepatopancreas tissue and finally determined its gray value. According to published methods, Hematoxylin-eosin (H&E) and transmission electron microscopy staining for hepatopancreas were conducted [32,35]. To calculate the relative area of the liver vesicles in the H&E stainings, 3 fields were analyzed randomly. Additionally, then, Image J software was used for quantification.

2.4.4. Haemolymph Biochemical Parameters

The levels of hemolymph alanine aminotransferase (ALT), aspartate aminotransferase (AST), albumin (ALB), and lactate dehydrogenase (LDH) were measured by an automatic hemolymph biochemical analyzer (Mindray BS-400, Shenzhen, China). The specific method is to put 200 μL hemolymph into a special colorimetric tube according to the manufacturer's instructions and use the corresponding commercial kit (Mindray Medical International Co., Ltd., Shenzhen, China).

2.5. Real-Time Quantitative PCR (qPCR)

According to the fragments obtained from the original hepatopancreas transcriptome determined initially in our laboratory and the ORF intercepted, primer 5.0 was used to design the gene primer for qRT PCR analysis (see Supplementary Table S1). Because the expression of *β-actin* is stable [23], choosing *β-actin* mRNA serves as an internal reference. Shanghai Sangong Biotechnology Co., Ltd. synthesized PCR primers.

The total RNA of the hepatopancreas in the three experimental groups (3 samples for each repetition) was extracted with RNAiso Plus (TaKaRa, Japan). Then, the concentration was determined with Nanodrop 2000 (Thermo Fisher Scientific, Waltham, Massachusetts, USA). The RNA concentration of each sample was diluted to 500 ng/mL. Use Two-Step SYBR® Prime Script® Plus RT-PCR Kit (TaKaRa, Japan) for 2 μg quantitative analysis of total RNA; the total system of sample loading was 20 μL. Based on Liu et al. [36], an ABI 7500 Real-time PCR system was used for real-time quantitative PCR (RT-PCR), and the $2^{-\Delta\Delta CT}$ method was used to calculate the relative gene expression.

2.6. Western Blot Analysis

We performed Western blot analysis with reference to Dai et al. [37]. Simply put, the protein was extracted from hepatopancreas tissue with a high-fat protein extraction kit (BB3162, Bestbio Biotechnology Co., LTD., Shanghai, China) and we performed Western blot by the manufacturer's guidelines (Bio/Rad, Hercules, CA, USA). The final strip was used for imaging. Enhanced chemiluminescent substrate reagents (CW0049-S, Cwbio Biotechnology Co., LTD, Shanghai, China) were used to detect immune complexes, visualization by a luminous image analyzer (ChemiDoc XRS+, Bio/Rad, USA) according to the manufacturer's instructions. In the experiment, the GAPDH antibody (1:10,000, Proteintech, Chicago, IL, USA, 66009-1-Ig), Relish/NF-kB (1:1000, Abcam, ab183559), Nrf2 (1:2500, Proteintech, 16396-1-AP), Beclin 1 antibody (1:5000, Proteintech, 11306-1-AP), Ulk 1 antibody (1:4000, Cell Signaling Technology, Danvers, MA, USA, #8054S), and Lc3 antibody (1:2000, Abcam, ab128025) were used. Image J software (NIH, Bethesda, MD, USA) was used for gray-scale analysis to evaluate protein band intensities.

2.7. Data Analysis

After Levene tested the homogeneity of variance, the data were subjected to a two-way ANOVA analysis to investigate the evaluation of growth, enzyme activity, hemolymph index, and relative gene and protein expression. Suppose the difference is significant ($p < 0.05$), the Duncan multi-interval test is used to rank the mean. Pearson correlation analysis was used to analyze the correlation between the two variables that conform to the normality and used the following marks: one asterisk (*) indicated a significant difference ($p < 0.05$), and two asterisks (**) indicated an extremely significant difference ($p < 0.01$). All data were demonstrated as means ± S.E.M. (standard error of mean). All the above analysis methods use SPSS program v16.0 (SPSS Inc., Michigan Avenue, Chicago, IL, USA) on Windows 10.

3. Results

3.1. Growth Evaluation

Table 2 showed that the survival rate (SR) was lower for prawns fed the 1000 mg/kg TTO diet ($p < 0.05$). The 1000TTO group had a higher weight gain rate (WGR) and sig-

nificantly increased specific growth rate (SGR) and hepatosomatic index (HSI) than the other two groups ($p < 0.05$). The WGR and SGR in the 100TTO group were higher than the control but had no significant difference ($p > 0.05$). The feed conversion ratio (FCR) and HSI in the 100TTO group were lower than in the CT and 1000TTO group ($p < 0.05$).

Table 2. Effects of dietary TTO levels on growth evaluation of *M. rosenbergii*.

Index	Groups		
	CT	100TTO	1000TTO
Survival rate (%)	82.50 ^{b} ± 3.23	85.00 ^{b} ± 5.50	72.50 ^{a} ± 4.62
Initial weight (g)	0.14 ± 0.01	0.15 ± 0.01	0.15 ± 0.00
Final weight (g)	2.84 ± 0.10 ^{a}	3.05 ± 0.14 ^{ab}	3.44 ± 0.44 ^{b}
Weight gain rate (%)	1839.82 ± 51.39 ^{a}	1942.06 ± 117.08 ^{ab}	2130.23 ± 107.98 ^{b}
Specific growth rate (%/day)	6.18 ± 0.05 ^{a}	6.27 ± 0.12 ^{a}	6.42 ± 0.26 ^{b}
Feed conversion ratio	1.33 ± 0.04 ^{b}	1.15 ± 0.01 ^{a}	1.26 ± 0.04 ^{b}
Hepatopancreas index (%)	7.23 ± 1.06 ^{b}	5.73 ± 0.86 ^{a}	10.73 ± 0.42 ^{c}

Note: Data are expressed as means with SEM. Means in the same line with different superscripts (a, b and c) are significantly different ($p < 0.05$).

3.2. Morphological Characteristics of Hepatopancreas

Figure 1 showed that the dietary TTO levels considerably affected the hepatopancreatic morphology and lipid deposition. Prawns fed 100 mg/kg TTO diet significantly decreased the vacuolization degree in hepatopancreas than the CT ($p < 0.05$), and the 1000TTO group significantly increased the vacuolization degree ($p < 0.05$, Figure 1B). Compared with the CT and 1000TTO groups, the hepatopancreatic nuclei in the 100TTO group were more visible, and the cell boundary was more pronounced. The hepatopancreatic lipid droplet area of the 100TTO group was significantly decreased compared to the other two groups ($p < 0.05$, Figure 1C). The highest lipid droplet area was found in the 1000TTO group but without significant difference from the control ($p > 0.05$). Compared with the CT and 100TTO groups, the hepatopancreatic cells in the 1000TTO group were significantly swollen.

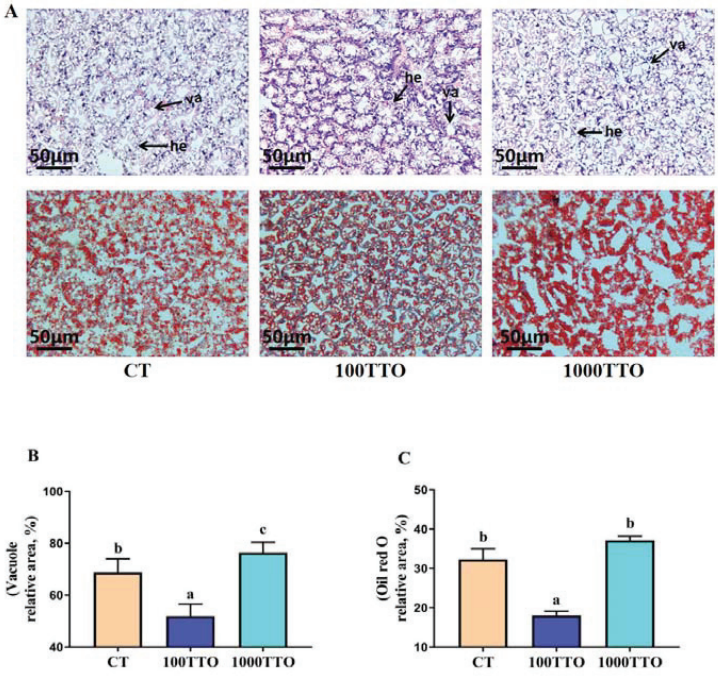

Figure 1. Effect of dietary TTO levels on morphology and lipid deposition in the hepatopancreas of

M. rosenbergii. (**A**) The representative micrographs of H&E and Oil Red O-stainings (200× magnification). Va, vacuole; He, Hepatopancreas cell. (**B**) The relative vacuole area of H&E staining and (**C**) Oil Red O-staining lipid droplets. The significant difference between the three TTO levels is characterized by different lowercase letters (a, b, c) ($p < 0.05$).

3.3. Hepatopancreatic Cell Function

As shown in Figure 2, dietary TTO levels significantly affected hepatopancreatic cell function. Compared to the control, 1000TTO induced significantly increased activity levels of hepatopancreatic function-related enzymes (AST, ALT, and LDH) and a significantly decreased ALB level ($p < 0.05$). There were no significant differences in the AST, ALT, ALB, and LDH levels between the 100TTO group and the control group ($p > 0.05$).

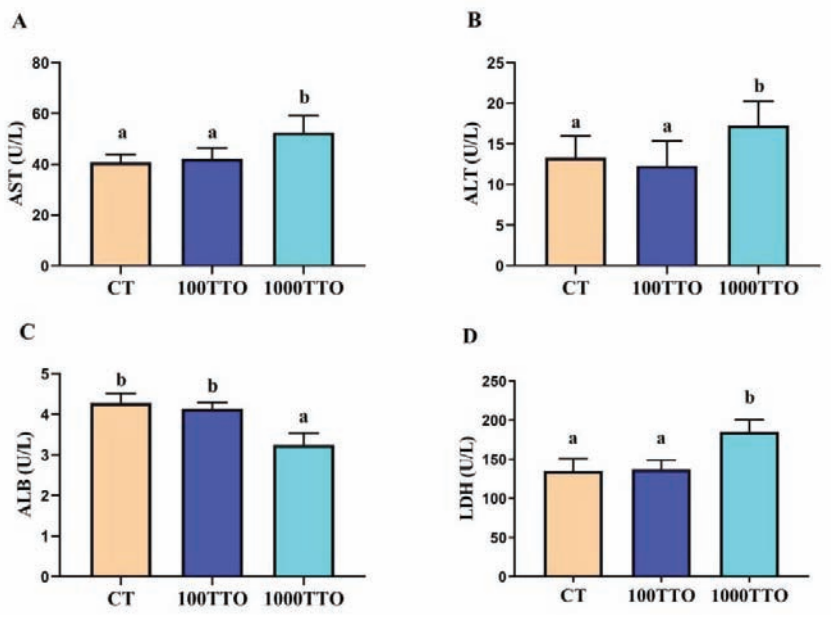

Figure 2. Effect of dietary TTO levels on hepatopancreatic function indicators of *M. rosenbergii*. (**A**) AST activity; (**B**) ALT activity (**C**) ALB activity; (**D**) LDH activity. The significant difference between the three TTO levels is characterized by different lowercase letters (a, b) ($p < 0.05$).

3.4. Lipid Contents in Hepatopancreas

Compared to the CT group, TG and LDL-C significantly decreased in the 100TTO group, while the TG content in the 1000TTO group significantly increased ($p < 0.05$, Figure 3A–C). In addition, although the TC content in the 100TTO group was lower than that in the control group, it had no consequential difference ($p > 0.05$). The 1000TTO group significantly increased TC and LDL-C compared to the 100TTO group ($p < 0.05$). At the same time, the 1000TTO group had a lower HDL-C level than the other two groups ($p < 0.05$, Figure 3D).

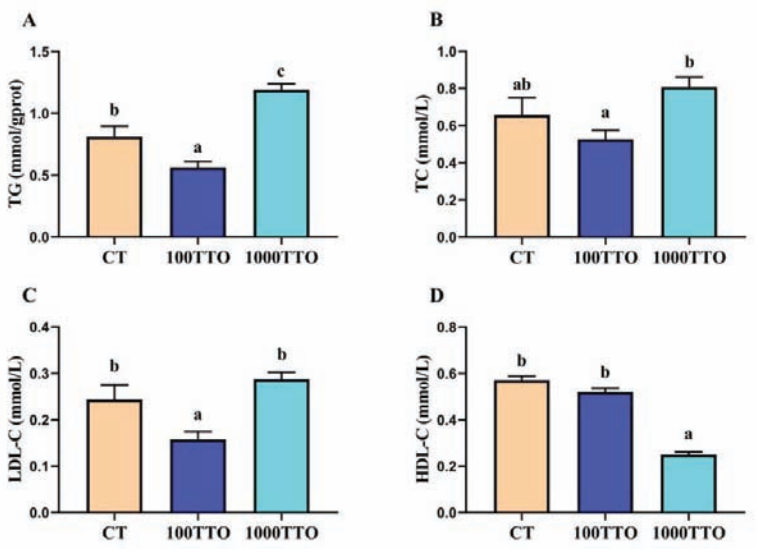

Figure 3. Effect of dietary TTO levels on lipid contents of *M. rosenbergii*. (**A**) TG content in hepatopancreas. (**B**–**D**) TC, LDL-C, HDL-C content in hemolymph. The significant difference between the three TTO levels is characterized by different lowercase letters (a, b, c) ($p < 0.05$).

3.5. Lipid Metabolism Enzymes Activities and Gene Expression

Dietary TTO levels significantly affected lipid metabolism enzymes in the hepatopancreas (Figure 4A–C). Compared to the CT group, the 100TTO group had significantly lower FAS and ACC levels and higher CPT1 levels ($p < 0.05$). The 1000TTO group had higher FAS and ACC contents than the control. CPT1 content showed no significant differences between the 1000TTO group and the control ($p > 0.05$).

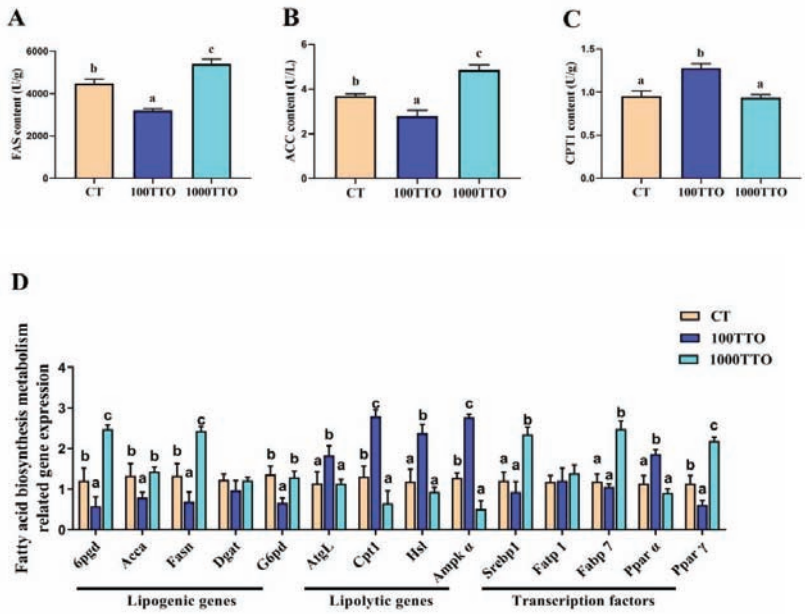

Figure 4. Effects of dietary TTO levels on hepatopancreatic lipid metabolism of M. rosenbergii. (**A**) FAS

content; (**B**) ACC content; (**C**) CPT1 content. (**D**) mRNA expression of lipid metabolism-related genes. The significant difference between the three TTO levels is characterized by different lowercase letters (a, b, c) ($p < 0.05$).

At the transcriptional level (Figure 4D), the 100TTO group had significantly lower mRNA abundances of lipogenic genes (*6pgd*, *Acca*, *Fasn*, and *G6pd*) and *Pparγ*, and higher lipolytic (*Cpt1*, *AtgL*, *Hsl*, *Ampkα*) and *Pparα* mRNA expression compared to the control ($p < 0.05$). At the same time, the 1000TTO group significantly increased the 6pgd, *Fasn*, *Srebp1*, *Fabp7*, and *Pparγ* mRNA expression, and decreased lipolytic gene expression (*Cpt1* and *Ampkα*) compared to the control ($p < 0.05$). *Dagt* and *Fatp1* mRNA abundances showed no significant differences among the three groups ($p > 0.05$).

3.6. Antioxidant Enzyme Activity and Peroxidase Levels in Hepatopancreas

The dietary TTO levels significantly changed the activities of antioxidant enzymes in the hepatopancreas (Figure 5). Compared to the CT group, the levels of CAT, T-SOD, GSH-PX, and T-AOC in the 100TTO group significantly increased, the content of MDA significantly decreased ($p < 0.05$), and the PCO activity had no significant difference between the two groups ($p > 0.05$). In the 1000TTO group, considerably increased MDA and PCO activities were found compared to the control ($p < 0.05$). Additionally, the levels of T-SOD in the 1000TTO group were significantly lower than in the control, and the CAT and T-AOC activities were lower than those in the control but had no significant distinction ($p < 0.05$).

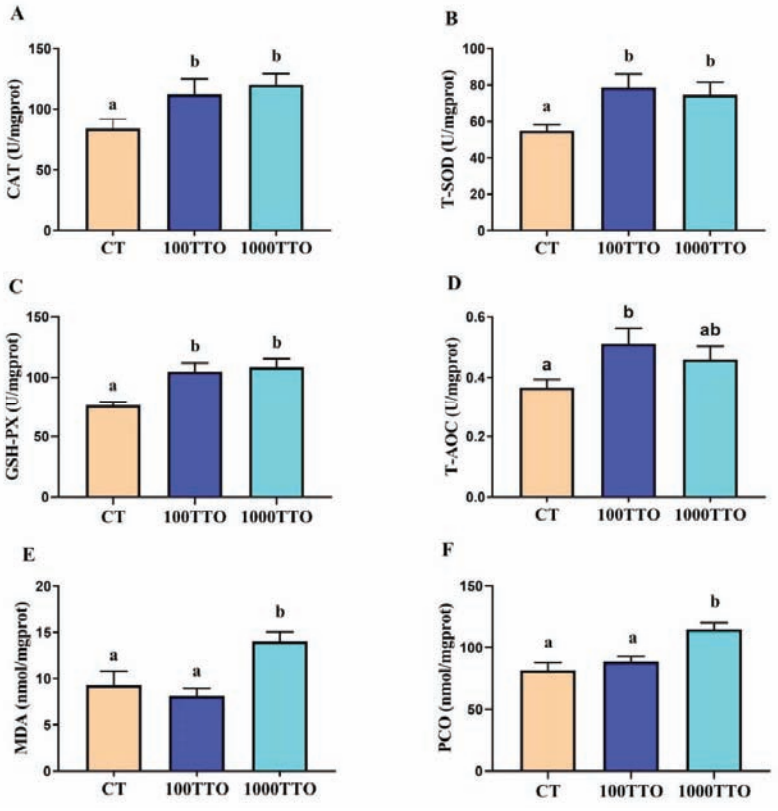

Figure 5. Effects of dietary TTO levels on the antioxidant level in the hepatopancreas of *M. rosenbergii*.

(**A**) CAT activity; (**B**) T-SOD activity; (**C**) GSH-PX activity; (**D**) T-AOC activity; (**E**) MDA content; (**F**) PCO content. The significant difference between the three TTO levels is characterized by different lowercase letters (a, b) ($p < 0.05$).

3.7. Different TTO Levels Affect Oxidative Stress in the Hepatopancreas

Ultrastructural changes in mitochondria were given in Figure 6A. In the CT and 100TTO group, mitochondria showed standard morphology under TEM. The double membrane and mitochondrial ridge of the nucleus were excellently visible. However, the mitochondria damage was found in the 1000TTO group, accompanied by the mitochondria turgidity, vacuolation, and the ridge broken. At the same time, the nuclear membrane of the 1000TTO group was blurred, and pyknosis deformity occurred.

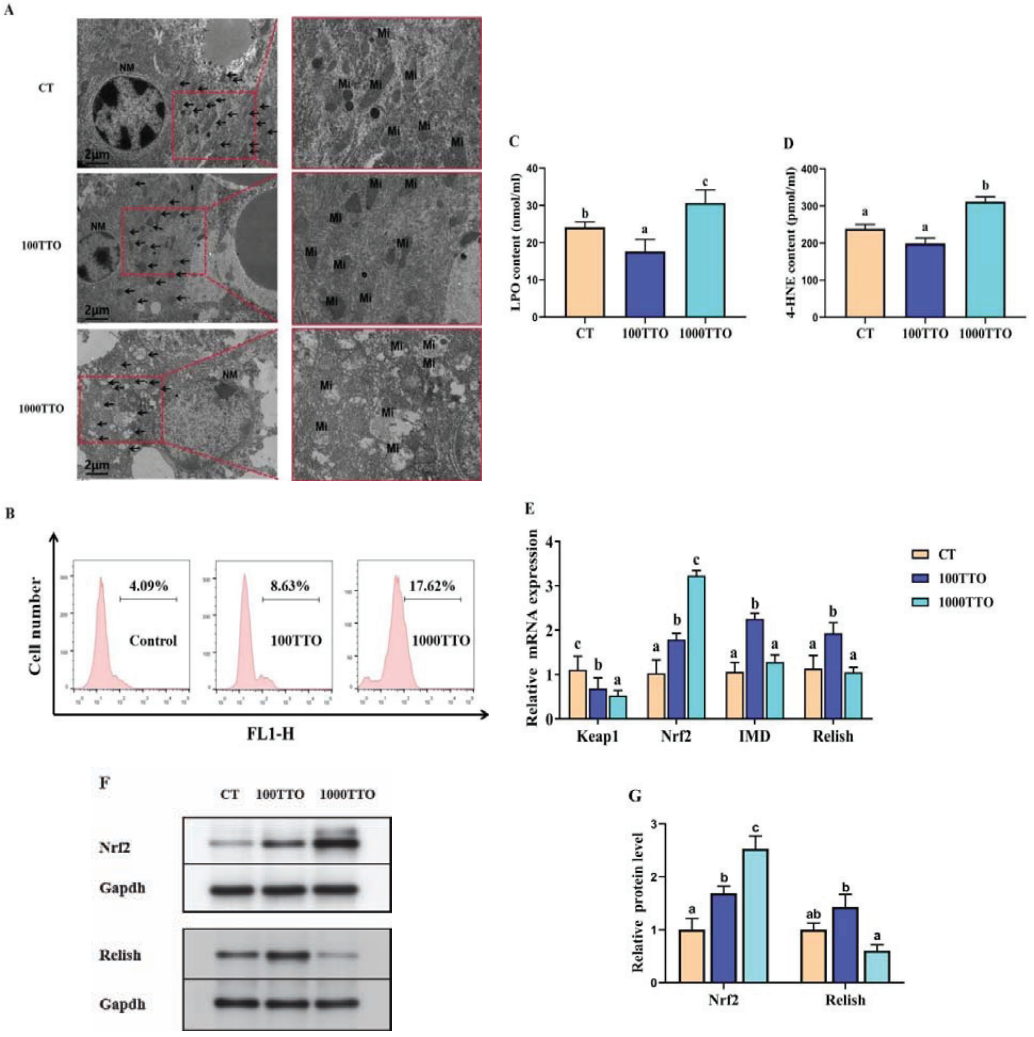

Figure 6. Effects of dietary TTO levels on hepatopancreatic oxidative stress of *M. rosenbergii*. (**A**) Characteristic TEM image. Arrow points to mitochondria; NM, nuclear membranes; Mi, mitochondria.

(**B**) Fluorescence intensity of ROS in hemolymph displayed by flow cytometry. (**C**) LPO content; (**D**) 4-HNE content. (**E**) mRNA levels of *Keap1*, *Nrf2*, *Imd* and *Relish*. (**F**) Nrf2 and Relish protein bands under Western blot analysis. (**G**) Relative quantification of Nrf2 and Relish protein expression. The significant difference between the three TTO levels is characterized by different lowercase letters (a, b, c) ($p < 0.05$).

The 1000TTO group significantly increased ROS levels more than the other two groups (Figure 6B). The ROS level of 100TTO increased slightly compared with the control group. At the same time, ELISA results showed that the 1000TTO increased the LPO and 4-HNE contents compared to the control and 100TTO groups ($p < 0.05$, Figure 6C,D). The LPO content of the 100TTO group was extremely lower than the control ($p < 0.05$).

mRNA expressions of significantly lower *Keap1* and higher *Nrf2*, *Imd*, and *Relish* were found in the 100TTO group compared to the CT ($p < 0.05$, Figure 6E). In addition, the 1000TTO group substantially decreased *Keap1* and increased *Nrf2* mRNA expression compared to the control ($p < 0.05$). It is worth noting that the 1000TTO group significantly decreased *Imd* and *Relish* mRNA expression more than the 100TTO group ($p < 0.05$). Figure 6F,G showed that the 100TTO group had higher Relish protein expression than the 1000TTO group and higher Nrf2 than the control ($p < 0.05$). The 1000TTO group had a higher Nrf2 protein expression diet than the other two groups.

3.8. Autophagy-Related Genes and EM Observation

The prominent display of the electron microscope (EM) pictures of the prawn hepatopancreas in each group can see the difference in the degree of autophagy (Figure 7A). The 100TTO group promoted the formation of autolysosomes and autophagosomes and hardly found large lipid droplets, while a small amount of autolysosome formation around some large lipid droplets was found in the control. Numerous large lipid droplets and thimbleful autophagosomes were found in the 1000TTO group. The quantification of autophagic vesicles by TEM confirmed that autophagic changes were in response to the level of TTO. To further analyze the effect of the TTO level on autophagy, we measured the autophagy-related genes.

As shown in Figure 7B, the 100TTO group significantly regulated the expression of autophagosome upstream regulatory genes (*Ampk* increased, *mtor* decreased) and autophagy markers (*Lc3* increased and *p62* decreased) compared to the control ($p < 0.05$). At the same time, the 100TTO group significantly up-regulated the expression of autophagosome membrane initiation (*Ulk1* and *Beclin1* increased) and autophagosome membrane expansion-related genes (*atg13*, *atg3*, *atg4b*, *atg5*, and *atg7* increased). The 1000TTO group significantly down-regulated *Ampk*, *Beclin1*, *atg13*, *atg5*, and *Lc3* expression and up-regulated *akt* and *mtor* expression compared to the control ($p < 0.05$). Meanwhile, the 1000TTO group significantly down-regulated the autophagy marker gene *Lc3* accompanied by significantly up-regulated autophagic flux gene *p62* ($p < 0.05$). Western blotting analysis showed that prawns fed the 100 mg/kg TTO diet had higher Beclin1, Ulk1, and Lc3 II protein expression than those in the control and the 1000TTO group ($p < 0.05$, Figure 7C,D). Additionally, the 1000TTO group had lower Beclin1 protein expression than the control group ($p < 0.05$).

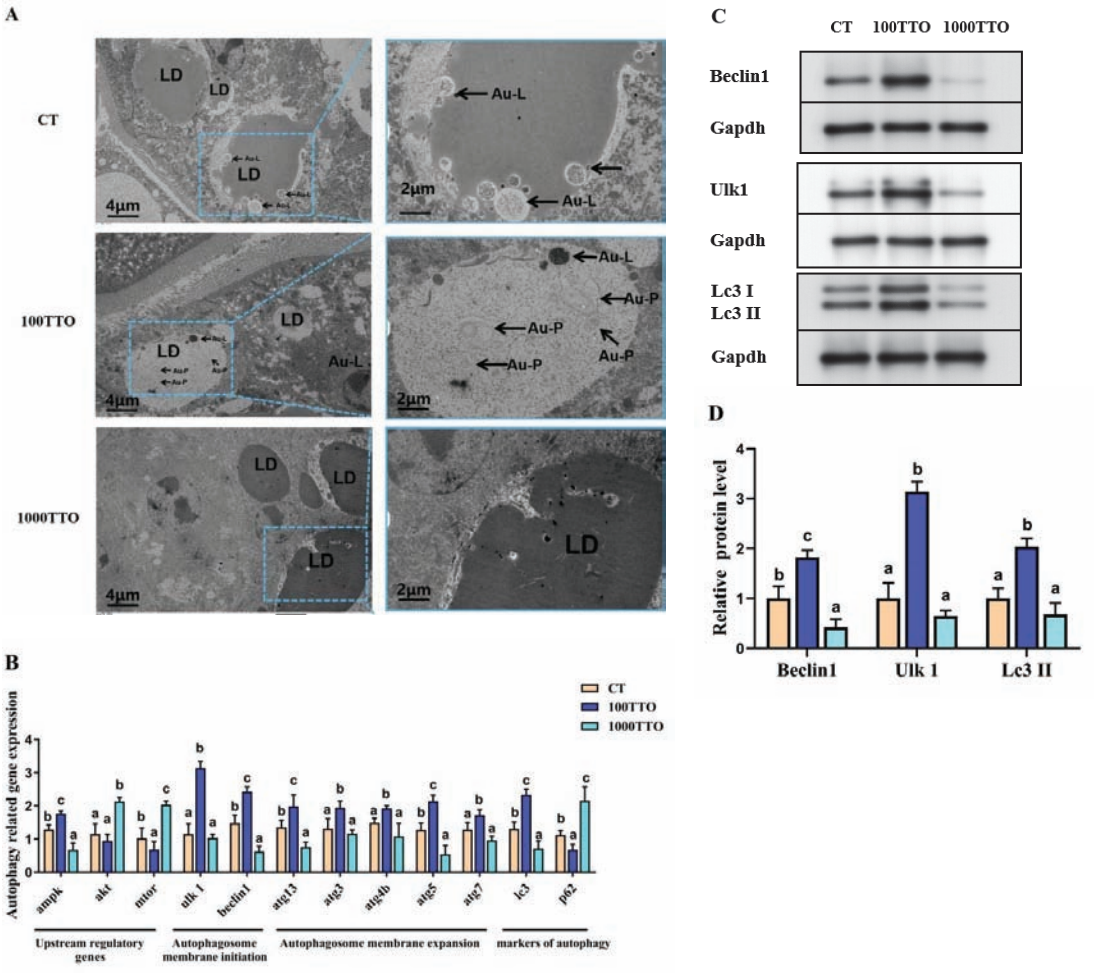

Figure 7. Effects of dietary TTO levels on autophagy formation in the hepatopancreas of *M. rosenbergii*. (**A**) Characteristic TEM image. Arrow points to autophagy. LD, lipid droplet; Au-P, autophagosome; Au-L, autolysosome. (**B**) mRNA levels of key autophagy-related genes. (**C**) Beclin1, Ulk1, and Lc3 protein bands under Western blot analysis. (**D**) Relative quantification of Beclin1, Ulk1, and Lc3 II protein expression. The significant difference between the three TTO levels is characterized by different lowercase letters (a, b, c) ($p < 0.05$).

3.9. Correlation Analysis

Figure 8 showed the Pearson correlation analysis of oxidative stress regulatory gene mRNA levels with lipid anabolism and autophagy genes. We found that the mRNA levels of *Fasn*, *Srebp1*, and *Pparγ* were positively correlated with *Nrf2*. The levels of *Cpt1*, *Hsl*, and *Ampkα* were negatively correlated with *Nrf2*. In addition, the mRNA expression of *Atgl*, *Cpt1*, and *Ampkα* were positively correlated with *Relish*, and *Pparγ* was negatively correlated with *Relish*.

Comparing oxidative stress and autophagy (Figure 8B), the *Nrf2* levels were positively correlated with *mtor*, *akt*, and *p62* and negatively correlated with *Beclin1* and *Lc3*. The *Relish* levels were positively correlated with *Ulk1* and *Lc3* and negatively correlated with *p62*. Meanwhile, *Keap1* and *Imd* were negatively correlated with *p62* and mtor, respectively.

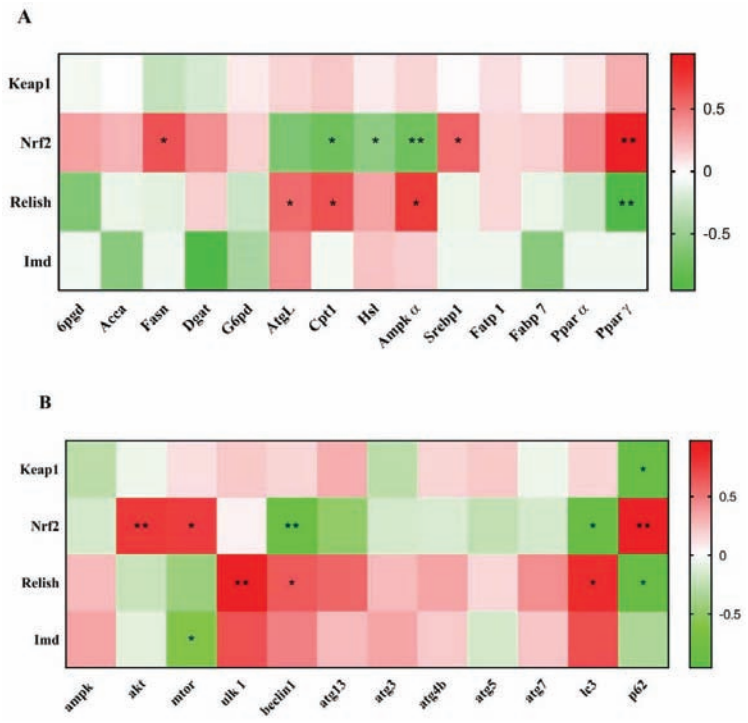

Figure 8. Correlation between oxidative stress with (**A**) lipid metabolism and (**B**) autophagy in mRNA levels. Note: Red represents positive correlation and green represents negative correlation. The stronger the correlation, the more intense the color. * $p < 0.05$, ** $p < 0.01$.

4. Discussion

In the present study, we found that different TTO levels significantly affected the growth performance of *M. rosenbergii*. The prawns fed with a 100 mg/kg TTO diet improved the growth indicators (WGR, SGR, FCR) while decreasing the HSI compared to the control. Decreased HSI may be associated with enhanced hepatic lipid energy metabolism and the energy used for the growth of other tissues [38]. Therefore, combined with our undisclosed results about muscles, we speculated that the 100 mg/kg TTO diet may promote the other tissues' growth (e.g., muscles) instead of the hepatopancreas. An important finding in our study is that the 1000TTO group significantly improved growth indicators (WGR, SGR) with a substantial increase in HSI compared to the control. This result indicated that the 1000TTO group may improve growth performance mainly by increasing hepatopancreas weight. However, the marked increase in HSI may be due to burgeoning lipid accumulation, often leading to metabolic disease [39]. At the same time, in crustaceans, the HSI surge also damages the tissue structure of the hepatopancreas [40], which verified that the survival rate of the 1000TTO group was significantly decreased compared to the other two groups (CT and 100TTO). The hepatopancreas is a vital metabolic organ of crustaceans, and its main component is lipids. Furthermore, excessive lipid deposition in the hepatopancreas not only leads to damage to the hepatopancreatic metabolic function and eventually leads to the lesions of the hepatopancreas but also impairs the antioxidant capacity [41,42]. Based on this premise, we speculate that 1000 mg/kg TTO causes a decreased survival rate and brings about lesions caused by superfluous lipid production in the hepatopancreas. However, 100 mg/kg TTO could reverse this phenomenon. Based on this speculation, we further measured the lipid deposition status in the hepatopancreas.

In the ORO staining results, we found significantly increased lipid droplet content and steatosis in the hepatopancreas in the 1000TTO group. Furthermore, we found the vacuolization of hepatopancreatic cells induced by 1000TTO supplementation through H&E analysis. Moreover, the nuclei of hepatopancreatic cells and the cell boundary were not obvious in the 1000TTO group. This phenotype was a classical manifestation of hepatopancreatic injury in previous studies [43]. In contrast, the 100TTO group had significantly lower lipid droplet content, less vacuolation, and a clearer nucleus. This proves the conclusion that the 1000TTO group will cause excessive fat accumulation and hepatopancreas tissue damage, while 100TTO treatment maintains lipid homeostasis and protects hepatopancreatic cells.

In addition, when there is excess fat deposition in the hepatopancreas and the organism hardly metabolizes the excess fat, it can lead to elevated blood lipids [44]. The present study found that the 100TTO group down-regulated blood lipid indicators while the 1000TTO group increased blood lipid contents. Therefore, we speculated that the dysfunction of the hepatopancreas in the 1000TTO group resulted in the inability to metabolize excess lipids. To assess its health status, we measured indicators reflecting hepatopancreatic function (AST, ALT, ALB, LDH). Compared with the control, 100TTO treatment had no adverse effect on hepatopancreatic function. However, the 1000TTO treatment may destroy hepatopancreatic function supported by up-regulated AST, ALT, and LDH levels and down-regulated ALB content in the hemolymph. The significantly elevated AST, ALT, and LDH in the hemolymph are markers of impaired hepatopancreatic function. When the hepatocytes are damaged, AST and ALT will enter the blood from the hepatocytes and cause their content to increase [45,46]. ALB is mainly synthesized in the hepatopancreas and is an important immune protein. Hepatopancreatic function damage will bring about a significant reduction in ALB levels [47]. Combined with AST, ALT, LDH, and ALB results, it was proved that 1000TTO causes hepatopancreas dysfunction. In summary, 100TTO treatment did reduce the fat content in the hepatopancreas and did not cause damage to the hepatopancreas. In contrast, the 1000TTO group increased fat deposition and disrupted hepatopancreas morphology and function.

In order to elucidate the mechanism of TTO influencing lipid deposition and metabolism, we further explored changes in lipid metabolism-related enzymes and genes in the hepatopancreas. Our ELISA results showed that the essential enzymes of fat synthesis (FAS and ACC) [48] observably decreased in the 100TTO group and increased in the 1000TTO group. In addition, CPT1 is a rate-limiting enzyme in fatty acid β-oxidation [49]; the significant increase in CPT1 in the 100TTO group indicated that the 100TTO treatment stimulated fatty acid β-oxidation and accelerated lipid breakdown. At the transcriptional level, we found that 100TTO up-regulated the expression of lipolysis-related genes and down-regulated the expression of fat synthesis-related genes in the hepatopancreas. The trends in the 1000TTO group are the opposite of the 100TTO group.

In terms of the transcription factor, our study found that the 1000TTO group increased the mRNA abundances of *Srebp1*, *Fatp1*, and *Pparγ*, which also confirmed its promotion of fat synthesis. Existing evidence shows that *Fatp1* is a crucial transcription factor for regulating lipid synthesis, responsible for fatty acid transport [50]. *Srebp1* and *Pparγ* are classical lipogenic regulators [51]. *Pparα* is the transcription factor regulating lipid metabolism and could activate *Cpt1* to improve steatosis induced by excess lipid deposition [52]. In this study, only the 100TTO group enhanced the *Pparα* levels. Our data suggest that the 100TTO group decreased lipid synthesis and promoted lipolysis and fatty acid β-oxidation. In contrast, the 1000TTO group promoted lipid production while inhibiting the breakdown of deposited lipids.

Autophagy is a physiological process of self-repair of cells and subcellular structures after being subjected to stress, injury, or free radicals and plays an important role in maintaining lipid metabolism homeostasis [53]. The inhibition of autophagy has been observed in some models of dyslipidemia or disorders [54]. At the same time, the principle of some lipid metabolism-modulating drugs and additives to regulate excessive lipid

deposition is to regulate autophagy [55,56]. In general, autophagy plays many important roles in regulating hepatocyte lipid metabolism. Lipid droplets can serve as substrates for the process of autophagy, so autophagy plays a role in regulating the lipolysis process [57]. Because of the vital role of autophagy in lipid metabolism, we further explored the effect of TTO on autophagy.

Through ultramicroscopic analysis, we hardly observed the phenotype of autophagy in the 1000TTO group, and the lipid droplet morphology was intact compared with a small number of autophagolysosomes existing in lipid droplets in the CT group. In sharp contrast, the 100TTO group had a large number of autophagosomes in lipid droplets accompanied by the breakdown of lipid droplets. These results showed that the 100TTO group enhanced autophagy, possibly decomposing lipids through autophagy, while the 1000TTO group inhibited autophagy and caused lipid deposition in the hepatopancreas. Degraded lipids by enhanced mitophagy and lipophagy were commonly found in other studies [58,59], but there was seldom research on essential oils affecting lipid metabolism by regulating autophagy.

Autophagy is a process by which a membrane derived from the organelle or lysosome surrounds the material for degradation to form an autophagosome [30]. At the molecular level, the mRNA results showed that 100 mg/kg TTO activates autophagy by initiating autophagic membrane phagocytosis and regulating autophagy-related gene expression. The 100 mg/kg TTO enhanced autophagosome membrane initiation and the expansion of mRNA expression, and 1000 mg/kg TTO inhibited the generation and expansion of autophagosome membrane mRNA expression. Meanwhile, the WB analysis showed that 100TTO intervention up-regulated the expression of two autophagy marker proteins (*Beclin1* and *Lc3*) and increased the expression level of autophagy initiation protein *Ulk1* and the degrading cell protein *atg7* [60]. In addition, we found that 100TTO increased the gene expression of the upstream activator proteins *Ulk1* and *Ampk*, and the 1000TTO group increased the expression of the upstream autophagy-inhibiting protein *mTOR* [61]. Moreover, a higher expression of *p62* was found in the 1000TTO group, indicating that the autophagy was suppressed, as the high intracellular expression of *p62* occurs when autophagy is blocked [62]. The above results indicated that the 100TTO treatment activated the autophagy upstream essential proteins to enhance the formation of the autophagy membrane. In contrast, the 1000TTO group down-regulated the expression of autophagy-related proteins to inhibit autophagy.

Studies have shown that oxidative stress could impair cell metabolic function to obtain abnormal liver lipid deposition, and the abnormal lipid deposition is accompanied by severe oxidative stress [8,63]. The study found that TTO levels have antioxidant properties [64]. In addition, consuming moderate levels of TTO may enhance host antioxidant capacity as a cofactor for antioxidant enzymes to increase defense against oxidative stress [23,65]. Based on these premises, we evaluated the oxidative stress status of each group. Our study found that the 100 mg/kg TTO diet enhances antioxidant enzyme activity and reduces peroxide production in the hepatopancreas compared to the control. On the contrary, 1000TTO did not improve the activity of antioxidant enzymes while it induced a significant increase in the levels of MDA and PCO, indicating that oxidative damage occurs as MDA and PCO are both marker products of oxidative damage [66]. The *Keap1-Nrf2* pathway has a central role in the defense against oxidative stress in vertebrates [67,68]. Studies in crustaceans have also found that oxidative stress activates the *Keap1-Nrf2*-mediated antioxidant pathway [69]. The activation of this pathway is mainly caused by ROS-stimulated *Nrf2* uncoupling from *Keap1* into the nucleus and binding to AREs to achieve antioxidant purposes. Our study found that the addition of 100TTO activated the *Keap1-Nrf2* pathway expression compared to the control group, and 1000TTO significantly increased the level of *Nrf2* expression compared to the 100TTO group. Moreover, 1000TTO enormously increased ROS production and caused mitochondrial damage accompanied by increased lipid peroxidation products (LPO and 4-HNE). This is consistent with previous findings that state that the sharp up-regulation of *Nrf2* always accompanies a vastly improved level of ROS, which may be compensatory stress [70]. Another study has

shown that oxidative stress disrupted the morphology and function of mitochondria [71]. In addition, the *NF-κB* signaling pathway was found to have bidirectional regulation effects on ROS regulation [72]. *Relish* was an *NF-κB* homologous protein in invertebrate animals and was found to have oxidative stress-regulating effects [73,74]. Our results showed that 100TTO significantly increased *Relish* and its downstream factor *Imd*, whereas 1000TTO did not activate *Relish-Imd* expression. The above results show that 100TTO improves the antioxidant capacity by activating the *Keap1-Nrf2* and *Relish-Imd* signaling pathways, while the 1000TTO group only activates *Keap1-Nrf2* but without activating the *Relish-Imd* antioxidant pathway, which may also cause oxidation stress finally. Therefore, we speculated that excess TTO levels stimulate ROS production and impair the antioxidant system, thereby inducing oxidative stress that mediates excess TTO-induced mitochondrial dysfunction. Similarly, other studies have shown that high levels of essential oils cause an increase in ROS, and excess ROS induce oxidative stress damage [75,76].

The above results suggest that different TTO levels simultaneously affected oxidative stress status, autophagy levels, and the lipid metabolism process. However, the concrete underlying molecular link among them is unclear. In view of this, Pearson correlation analysis was performed to explore the correlation between the expression levels of the two oxidative stress regulatory pathways *Keap1-Nrf2* and *Relish-Imd*, lipid metabolism regulatory factors, and autophagy indicators. Through Pearson correlation analysis, two key node factors are determined; one is *Nrf2*, and the other is *Relish*.

Firstly, we found that *Nrf2* and *Pparγ* were significantly positively correlated. Martinez-Lopez et al. [77] pointed out that *Nrf2* translocates to the nucleus and activates many genes via ARE transport following oxidative stress. Oxidative stress promoted the binding of *Nrf2* to the *Pparγ* promoter and increased *Pparγ*-mediated adipogenesis [78]. At the same time, *Nrf2* was also positively correlated with *Fasn* and *Srebp1* in this study; this is consistent with previous conclusions that the activation of *Nrf2* under oxidative stress promotes adipogenesis by activating *Srebp1*, and the increase in *Fasn* expression directly causes the increase in fat synthesis [79,80]. In addition, *Nrf2* was negatively correlated with lipolysis genes *Cpt1*, *Hsl*, and *Ampkα* in this study. Past studies have found that the inhibition of lipolysis promotes adipocyte lipid accumulation [81]. Therefore, it is demonstrated that the high expression of *Nrf2* leads to increased lipid synthesis. In terms of autophagy, *Nrf2* was found to be positively correlated with autophagy-related genes, including autophagy marker *p62* and upstream regulatory genes (*Akt* and *mtor*), and negatively correlated with *Beclin1* and *Lc3*. *Nrf2* hyperactivation leads to the accumulation of *p62* and the inhibition of autophagy [82]. *Nrf2* positively regulates *Akt* expression under oxidative stress [83], and the increase in *Akt* activates the *Akt-mtor* pathway expression [84]. The increase in *Akt* expression will induce the dephosphorylation of *Lc3* [85]. The activation of mtor inhibits autophagy and reduces marker *Beclin1* expression [62].

The above results demonstrate that *Nrf2* is an important node between oxidative stress, autophagy, and lipid metabolism, and affects lipid deposition in the hepatopancreas simultaneously through antioxidant and lipid droplet autophagy pathways. This also explains why the 1000TTO group caused liver cell damage and excessive lipid deposition, accompanied by the high expression of *Nrf2* and inhibited autophagy and lipolysis. In addition, the down-regulation of hepatic lipid deposition in the 100TTO group may be regulated by other factors.

In terms of the other key node factor, *Relish*, correlation analysis data found that *Relish* was positively correlated with key lipolytic genes *Atgl* and *Cpt1*. Although few studies have shown that *Relish* enhances lipolysis, one study found that *Relish* was inhibited when the body fat increased in shrimp [35]. In addition, *Relish* was positively correlated with *Ulk1*, *Beclin1*, and *Lc3*, and negatively correlated with *p62*. Research has shown that *Relish* increases the activation of *atg1*(*Ulk1*) and the level of autophagy, and an increase in marker *Lc3* inevitably accompanies the increased expression of *Relish* [86]. When autophagy is blocked, the *p62* protein accumulates in the cytoplasm, so the negative correlation between *Relish* and *p62* in this study means the activation of autophagy [87].

The Ampk-mtor pathway is critical for regulating autophagy [88]. *Imd* was found negatively correlated with *mtor*, and *Relish* was positively correlated with *Ampkα*. Studies have shown that *Imd* inhibits the expression of *mTOR* [89], and mtor acts as an upstream pathway of autophagy; its inhibition will activate autophagy. Moreover, *Ampkα* acts as an essential gene for lipolysis [90]. Therefore, the *Relish-Imd* signal may enhance lipolytic ability by regulating *Ampk-mtor* to stimulate autophagy activation. *Pparγ* as an essential fat synthesis gene was negatively correlated with *Relish* in this study. A similar study also found that increased expression of *Relish* downregulates lipid synthesis through the regulation of *Pparγ* [91]. Therefore, the 100TTO group may activate autophagy by increasing the expression of *Relish* to regulate the autophagy initiation factor and down-regulating *Pparγ* to promote lipolysis.

5. Conclusions

In conclusion, this study demonstrates that 100 mg/kg TTO enhances antioxidant activity and induces autophagy through the *Relish-Imd* pathway to enhance lipid droplet breakdown and maintain lipid homeostasis. However, 1000 mg/kg TTO treatment will overexpress *Nrf2*, thus inducing the transcriptional activation of *Pparγ* and other genes to promote fat synthesis and inhibit autophagy, eventually causing lipid peroxidation and oxidative stress. This putative mechanism that can explain our results is shown in Figure 9. Our study supplies a new perspective focus on *Nrf2*, *Relish*, and the "antioxidant-autophagy-lipid metabolism" axis to reveal the regulation mechanisms of lipid metabolism by tea tree oil. Next, we will design the agonists and inhibitors of *Nrf2* and *Relish* and verify the precise mechanism of TTO to regulate the lipid metabolism of crustaceans based on the "antioxidant-autophagy-lipid-metabolism" axis at the tissue or cell level in vitro.

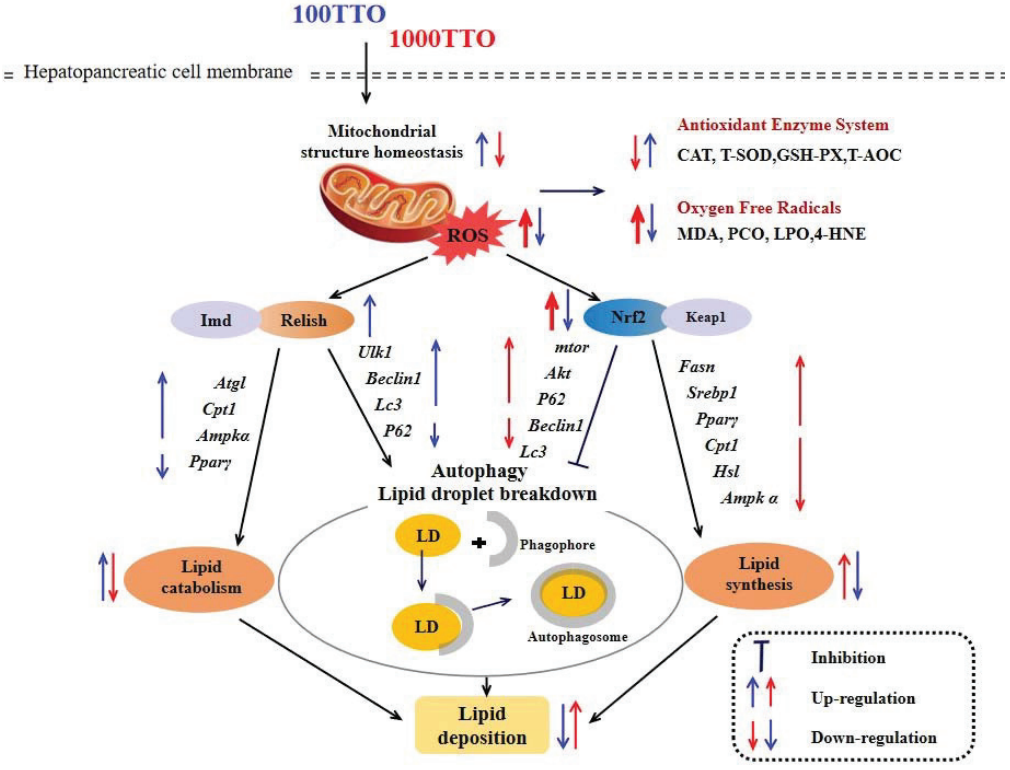

Figure 9. The mechanism of 100TTO and 1000TTO regulates lipid metabolism based on antioxidant

factors *Relish* and *Nrf2*-autophagy axis. The blue arrows indicate the regulation effects of 100TTO; the red arrows indicate the regulation effects of 1000TTO. Arrows up indicate significant up-regulation or improvement, and arrows down indicate significant down-regulation or inhibition. Thick arrows indicate extremely significant regulation.

Supplementary Materials: The following supporting information can be downloaded at: https://www.mdpi.com/article/10.3390/antiox11112260/s1. Table S1: Primers used in the study.

Author Contributions: M.L. contributed to the areas of experimental design, sampling, data analysis, and write-up; B.L. and P.X. contributed to the experimental design and manuscript review; C.S., Q.Z., B.L. and P.X. contributed to the feeding and cultivating of experimental prawns, sampling, and statistics, and X.Z. contributed to feed production, the feeding of prawns, and sampling. X.Z. was also responsible for language review and revision. All authors have read and agreed to the published version of the manuscript.

Funding: This work was supported by the Project of National Key R&D Program of China (2019YFD0900200), China Agriculture Research System of MOF and MARA (CARS-48), the National Natural Science Foundation of China (32002404), Central Public-interest Scientific Institution Basal Research Fund, and CAFS (2020TD59). The authors would like to express their sincere thanks to the personnel of these teams for their kind assistance.

Institutional Review Board Statement: The care and use of animals followed the Animal Research Institute Committee guidelines of Nanjing Agricultural University, China. This study has been approved by the Committee of the Animal Research Institute of Nanjing Agricultural University, China (SYXK (Su) 2019-0136, approved 21 May 2017).

Informed Consent Statement: Not applicable.

Data Availability Statement: Data are contained within the article.

Acknowledgments: The authors would like to express sincere thanks to the personnel of the Freshwater Fisheries Research Center, Chinese Academy of Fishery Sciences for their kind assistance.

Conflicts of Interest: The authors declare no conflict of interest.

References

1. Cao, L.; Naylor, R.; Henriksson, P.; Leadbitter, D.; Metian, M.; Troell, M.; Zhang, W.B. China's aquaculture and the world's wild fisheries. *Science* **2015**, *347*, 133–135. [CrossRef] [PubMed]
2. Catacutan, M.R.; Coloso, R.M. Growth of juvenile Asian seabass, Lates calcarifer, fed varying carbohydrate and lipid levels. *Aquaculture* **1997**, *149*, 137–144. [CrossRef]
3. Ruan, G.L.; Li, S.X.; He, N.J.; Liu, F.; Wang, Q. Short-term adaptability to non-hyperthermal stress: Antioxidant, immune and gut microbial responses in the red swamp crayfish, *Procambarus clarkii*. *Aquaculture* **2022**, *560*, 738497. [CrossRef]
4. Huang, Q.C.; You, J.F.; Wang, X.D.; Song, Y.; Zhang, C.; Du, Z.Y.; Shi, Q.C.; Qin, J.G.; Chen, L.Q. Effect of vitamin A supplement on the growth performance, antioxidant status, and lipid accumulation of Chinese mitten crab *Eriocheir Sinensis* fed different lipid levels. *Aquaculture* **2022**, *554*, 738123. [CrossRef]
5. Vogt, G. Synthesis of digestive enzymes, food processing, and nutrient absorption in decapod crustaceans: A comparison to the mammalian model of digestion. *Zoology* **2021**, *147*, 125945. [CrossRef]
6. Ishida, N.; Yamada, H.; Hirose, M. *Euphausia pacifica* (North Pacific Krill): Review of Chemical Features and Potential Benefits of 8-HEPE against Metabolic Syndrome, Dyslipidemia, NAFLD, and Atherosclerosis. *Nutrients* **2021**, *13*, 3765. [CrossRef]
7. Shi, B.; Lu, J.J.; Hu, X.Y.; Betancor, M.B.; Zhao, M.M.; Tocher, D.R. Dietary copper improves growth and regulates energy generation by mediating lipolysis and autophagy in hepatopancreas of Pacific white shrimp (*Litopenaeus vannamei*). *Aquaculture* **2021**, *537*, 736505. [CrossRef]
8. Yu, D.; Chen, G.; Pan, M.; Zhang, J.; He, W.; Liu, Y.; Nian, X.; Sheng, L.; Xu, B. High fat diet-induced oxidative stress blocks hepatocyte nuclear factor 4 alpha and leads to hepatic steatosis in mice. *J. Cell Physiol.* **2018**, *236*, 4770–4782. [CrossRef]
9. Zhao, T.; Wu, K.; Hogstrand, C.; Xu, Y.H.; Chen, G.H.; Wei, C.C.; Luo, Z. Lipophagy mediated carbohydrate-induced changes of lipid metabolism via oxidative stress, endoplasmic reticulum (ER) stress and ChREBP/PPARγ pathways. *Cell. Mol. Life Sci.* **2020**, *77*, 1987–2003. [CrossRef]
10. Gummersbach, C.; Hemmrich, K.; Kröncke, K.D.; Suschek, C.V.; Fehsel, K.; Pallua, N. New aspects of adipogenesis: Radicals and oxidative stress. *Differentiation* **2009**, *77*, 115–120. [CrossRef]
11. Lee, E.; Lim, Y.; Kwon, S.W.; Kwon, O. Pinitol consumption improves liver health status by reducing oxidative stress and fatty acid accumulation in subjects with non-alcoholic fatty liver disease: A randomized, double-blind, placebo–controlled trial. *J. Nutr. Biochem.* **2019**, *68*, 33–41. [CrossRef] [PubMed]

12. Kaushik, S.; Cuervo, A.M. Degradation of lipid droplet-associated proteins by chaperone-mediated autophagy facilitates lipolysis. *Nat. Cell Biol.* **2015**, *17*, 759–770. [CrossRef] [PubMed]
13. Rodrigo, R.; González, J.; Paoletto, F. The role of oxidative stress in the pathophysiology of hypertension. *Hypertens Res.* **2011**, *34*, 431. [CrossRef] [PubMed]
14. Zhou, G.; Meng, S.; Li, Y.; Ghebre, Y.T.; Cooke, J.P. Optimal ROS signaling is critical for nuclear reprogramming. *Cell Rep.* **2016**, *15*, 919. [CrossRef]
15. Kapuy, O.; Papp, D.; Vellai, T.; Bánhegyi, G.; Korcsmáros, T. Systems-Level Feedbacks of NRF2 Controlling Autophagy upon Oxidative Stress Response. *Antioxidants* **2018**, *7*, 39. [CrossRef]
16. Stewart, D.; Killeen, E.; Naquin, R.; Alam, S.; Alam, J. Degradation of transcription factor Nrf2 via the ubiquitin-proteasome pathway and stabilization by cadmium. *J. Biol. Chem.* **2003**, *278*, 2396–2402. [CrossRef]
17. Ma, Q. Role of Nrf2 in oxidative stress and toxicity. *Annu. Rev. Pharmacol. Toxicol.* **2013**, *53*, 401–426. [CrossRef]
18. Gao, Q.; Liu, B.; Shan, F.; Liu, B.; Gu, Z.M.; Song, C.Y.; Sun, C.X.; Zhou, Q.L. Effects of oxidized fish oil on digestive enzyme activity and antioxidant system in *Macrobrachium rosenbergii* post-larvae. *Aquacult. Rep.* **2022**, *23*, 101062. [CrossRef]
19. Huang, Y.X.; Li, Q.; Yuan, Y.H.; Zhang, Z.Q.; Jiang, B.J.; Yang, S.P.; Jian, J.C. Silencing of Nrf2 in *Litopenaeus vannamei*, decreased the antioxidant capacity, and increased apoptosis and autophagy. *Fish Shellfish Immunol.* **2022**, *122*, 257–267. [CrossRef]
20. Meng, H.M.; Song, J.; Fan, B.Q.; Li, Y.Q.; Zhang, J.J.; Yu, J.P.; Zheng, Y.; Wang, M. Monascus vinegar alleviates high-fat-diet-induced inflammation in rats by regulating the NF-KB and PI3K/AKT/mTOR pathways. *Food Sci. Hum. Wellness* **2022**, *11*, 943–953. [CrossRef]
21. Cox, S.D.; Mann, C.M.; Markham, J.L.; Bell, H.C.; Gustafson, J.E.; Warmington, J.R.; Wyllie, S.G. The mode of antimicrobial action of the essential oil of *Melaleuca alternifolia* (tea tree oil). *J. Appl. Microbiol.* **2010**, *88*, 170–175. [CrossRef] [PubMed]
22. An, P.P.; Yang, X.B.; Yu, J.; Qi, J.R.; Ren, X.Y.; Kong, Q.J. α-terpineol and terpene-4-ol, the critical components of tea tree oil, exert antifungal activities in vitro and in vivo against Aspergillus niger in grapes by inducing morphous damage and metabolic changes of fungus. *Food Control* **2019**, *98*, 42–53. [CrossRef]
23. Liu, M.Y.; Gao, Q.; Sun, C.; Liu, B.; Liu, X.; Zhou, Q.; Liu, B.; Xu, P. Effects of dietary tea tree oil on the growth, physiological and non-specific immunity response in the giant freshwater prawn (*Macrobrachium rosenbergii*) under high ammonia stress. *Fish Shellfish Immunol.* **2022**, *120*, 458–469. [CrossRef] [PubMed]
24. Wu, Y.; Huang, J.; Zuo, A.; Yao, L. Research on the Effects of Rosemary (*Rosmarinus officinalisL.*) on the Blood Lipids and Anti-lipid Peroxidation in Rats. *J. Essent. Oil Res.* **2011**, *23*, 26–34. [CrossRef]
25. Svegliati-Baroni, G.; Pierantonelli, I.; Torquato, P.; Marinelli, R.; Ferreri, C.; Chatgilialoglu, C.; Bartolini, D.; Galli, F. Lipidomic biomarkers and mechanisms of lipotoxicity in non-alcoholic fatty liver disease. *Free Radic. Biol. Med.* **2019**, *144*, 293–309. [CrossRef] [PubMed]
26. Rivera-Gomis, J.; Peres Rubio, C.; Martínez Conesa, C.; Otal Salaverri, J.; Cerón, J.J.; Tortosa, D.E.; Pablo, M.J.C. Effects of Dietary Supplementation of Garlic and Oregano Essential Oil on Biomarkers of Oxidative Status, Stress and Inflammation in Postweaning Piglets. *Animals* **2020**, *10*, 2093. [CrossRef] [PubMed]
27. Mo, K.; Li, J.; Liu, F.; Xu, Y.; Huang, X.; Ni, H. Superiority of Microencapsulated Essential Oils Compared With Common Essential Oils and Antibiotics: Effects on the Intestinal Health and Gut Microbiota of Weaning Piglet. *Front. Nutr.* **2022**, *8*, 808106. [CrossRef]
28. Lee, J.H.; Jeong, J.K.; Park, S.Y. AMPK Activation Mediated by Hinokitiol Inhibits Adipogenic Differentiation of Mesenchymal Stem Cells through Autophagy Flux. *Int. J. Endocrinol.* **2018**, *2018*, 2014192. [CrossRef]
29. Sarkar, S.; Carroll, B.; Buganim, Y.; Maetzel, D.; Ng, A.H.M.; Cassady, J.P.; Cohen, M.A.; Chakraborty, S.; Wang, H.Y.; Spooner, E.; et al. Impaired Autophagy in the Lipid-Storage Disorder Niemann-Pick Type C1 Disease. *Cell Rep.* **2013**, *5*, 1302–1315. [CrossRef]
30. Mizushima, N.; Levine, B.; Cuervo, A.M.; Klionsky, D.J. Autophagy fights disease through cellular self-digestion. *Nature* **2008**, *451*, 1069–1075. [CrossRef]
31. Rubinsztein, D.C.; Codogno, P.; Levine, B. Autophagy modulation as a potential therapeutic target for diverse diseases. *Nat. Rev. Drug Discov.* **2012**, *11*, 709–730. [CrossRef] [PubMed]
32. Liu, M.Y.; Sun, C.; Xu, P.; Liu, B.; Zheng, X.C.; Liu, B.; Zhou, Q.L. Effects of dietary tea tree (*Melaleuca alternifolia*) oil and feeding patterns on the zootechnical performance and nonspecific immune response of the giant freshwater prawn (*Macrobrachium rosenbergii*). *J. World Aquacult. Soc.* **2021**, *53*, 542–557. [CrossRef]
33. Satoh, K. Serum lipid peroxide in cerebrovascular disorders determined by a new colorimetric method. *Clin. Chim. Acta* **1978**, *90*, 37–43. [CrossRef] [PubMed]
34. Simon, H.U.; Haj-Yehia, A.; Levi-Schaffer, F. Role of reactive oxygen species (ROS) in apoptosis induction. *Apoptosis* **2000**, *5*, 415–418. [CrossRef]
35. Sun, C.X.; Shan, F.; Liu, M.Y.; Liu, B.; Zhou, Q.L.; Zheng, X.C.; Xu, X.D. High-Fat-Diet-Induced Oxidative Stress in Giant Freshwater Prawn (*Macrobrachium rosenbergii*) via NF-kappa B/NO Signal Pathway and the Amelioration of Vitamin E. *Antioxidants* **2022**, *11*, 228. [CrossRef]
36. Liu, M.Y.; Sun, C.X.; Zheng, X.C.; Zhou, Q.L.; Liu, B.; Zhou, Y.F.; Xu, P.; Liu, B. Comparative Proteomic Analysis Revealed the Mechanism of Tea Tree Oil Targeting Lipid Metabolism and Antioxidant System to Protect Hepatopancreatic Health in *Macrobrachium rosenbergii*. *Front. Immunol.* **2022**, *13*, 906435. [CrossRef]

37. Dai, Y.J.; Liu, W.B.; Abasubong, K.P.; Zhang, D.D.; Li, X.F.; Xiao, K.; Wang, X.; Jiang, G.Z. The Mechanism of Lipopolysaccharide Escaping the Intestinal Barrier in *Megalobrama amblycephala* Fed a High-Fat Diet. *Front. Nutr.* **2022**, *9*, 853409. [CrossRef]
38. Li, G.; Chang, L.; Zhang, G.; Song, Z.; Wan, D.; Xie, C.; Wang, H.; Fan, Z.Y. Oral administration of dibutyryl adenosine cyclophosphate improved growth performance in weaning piglets by enhancing lipid fatty acids metabolism. *Anim. Nutr.* **2018**, *4*, 260–264. [CrossRef]
39. Tripolino, C.; Irace, C.; Cutruzzolà, A.; Parise, M.; Barone, M.; Scicchitano, C.; Cortese, C.; Gnasso, A. Hepatic Steatosis Index Is Associated with Type 1 Diabetes Complications. *Diabetes Metab. Syndr. Obes.* **2019**, *12*, 2405–2410. [CrossRef]
40. Wang, Z.; Cai, C.; Cao, X.; Zhu, J.; He, J.; Wu, P.; Ye, Y. Supplementation of dietary astaxanthin alleviated oxidative damage induced by chronic high pH stress, and enhanced carapace astaxanthin concentration of Chinese mitten crab *Eriocheir sinensis*. *Aquaculture* **2018**, *483*, 230–237. [CrossRef]
41. Tian, J.; Lei, C.; Ji, H.; Kaneko, G.; Zhou, J.; Yu, H.; Li, Y.; Yu, E.M.; Xie, J. Comparative analysis of effects of dietary arachidonic acid and EPA on growth, tissue fatty acid composition, antioxidant response and lipid metabolism in juvenile grass carp, *Ctenopharyngodon idellus*. *Br. J. Nutr.* **2017**, *118*, 411–422. [CrossRef] [PubMed]
42. Fan, Z.; Li, J.N.; Zhang, Y.Y.; Wu, D.; Zheng, X.H.; Wang, C.; Wang, L.S. Excessive Dietary Lipid Affecting Growth Performance, Feed Utilization, Lipid Deposition, and Hepatopancreas Lipometabolism of Large-Sized Common Carp (*Cyprinus carpio*). *Front. Nutr.* **2021**, *8*, 694426. [CrossRef] [PubMed]
43. Nadella, R.K.; Prakash, R.R.; Dash, G.; Ramanathan, S.K.; Kuttanappilly, L.V.; Mothadaka, M.P. Histopathological changes in giant freshwater prawn *Macrobrachium rosenbergii* (de Man 1879) fed with probiotic Bacillus licheniformis upon challenge with Vibrio alginolyticus. *Aquac. Res.* **2017**, *49*, 81–92. [CrossRef]
44. Yao, J.; Hu, P.; Zhu, Y.; Xu, Y.; Tan, Q.; Liang, X. Lipid-Lowering Effects of Lotus Leaf Alcoholic Extract on Serum, Hepatopancreas, and Muscle of Juvenile Grass Carp via Gene Expression. *Front. Physiol.* **2020**, *11*, 584782. [CrossRef] [PubMed]
45. Dai, W.; Fu, L.; Du, H.; Jin, C.; Xu, Z. Changes in Growth Performance, Metabolic Enzyme Activities, and Content of Fe, Cu, and Zn in Liver and Kidney of Tilapia (*Oreochromis niloticus*) Exposed to Dietary Pb. *Biol. Trace Elem. Res.* **2008**, *128*, 176–183. [CrossRef]
46. Gao, X.; Liu, X.; Song, X.; Teng, P.; Ji, H.; Peng, L.; Qiu, Y.; Guo, D.; Jiang, S. Effect of maduramicin on crayfish (*Procambius clarkii*): Hematological parameters, oxidative stress, histopathological changes and stress response. *Ecotox. Environ. Saf.* **2021**, *211*, 111896. [CrossRef]
47. Vincent, J.L. Relevance of albumin in modern critical care medicine. *Best Pract. Res. Clin. Anaesthesiol.* **2009**, *23*, 183–191. [CrossRef]
48. Wilentz, R.E.; Witters, L.A.; Pizer, E.S. Lipogenic Enzymes Fatty Acid Synthase and Acetyl-Coenzyme A Carboxylase Are Coexpressed with Sterol Regulatory Element Binding Protein and Ki-67 in Fetal Tissues. *Pediatr. Devel. Pathol.* **2000**, *3*, 525–531. [CrossRef]
49. Schlaepfer, I.R.; Rider, L.; Rodrigues, L.U.; Gijon, M.A.; Pac, C.T.; Romero, L.; Cimic, A.; Sirintrapun, S.J.; Glode, L.M.; Eckel, R.H. Lipid Catabolism via CPT1 as a Therapeutic Target for Prostate Cancer. *Mol. Cancer Ther.* **2014**, *13*, 2361–2371. [CrossRef]
50. Martin, G.; Nemoto, M.; Gelman, L.; Geffroy, S.; Najib, J.; Fruchart, J.C. The Human Fatty Acid Transport Protein-1 (SLC27A1; FATP-1) cDNA and Gene: Organization, Chromosomal Localization, and Expression. *Genomics* **2000**, *66*, 296–304. [CrossRef]
51. Xu, W.F.; Hou, L.; Li, P.; Li, L. Effect of nicotinamide N-methyltransferase on lipid accumulation in 3T3-L1 adipocytes. *Bioengineered* **2022**, *13*, 12421–12434. [CrossRef] [PubMed]
52. Wang, T.; Chen, D.F. Effect of polyene phosphatidyl choline on hepatocyte steatosis via PPARalpha/CPT-1A pathway. *Chin. J. Hepatol.* **2016**, *24*, 291–296. [CrossRef]
53. Diskin, T.; Tal-Or, P.; Erlich, S.; Mizrachy, L.; Alexandrovich, A.; Shohami, E. Closed Head Injury Induces Upregulation of Beclin 1 at the Cortical Site of Injury. *J. Neurotraum.* **2005**, *22*, 750–762. [CrossRef] [PubMed]
54. Sparks, D.L.; Chatterjee, C. Purinergic Signaling, Dyslipidemia and Inflammatory Disease. *Cell. Physiol. Biochem.* **2012**, *30*, 1333–1339. [CrossRef]
55. Islam, M.T.; Ali, E.S.; Uddin, S.J.; Shaw, S.; Islam, M.A.; Ahmed, M.I.; Shill, M.C.; Karmakar, U.K.; Yarla, N.S.; Khan, I.N.; et al. Phytol: A review of biomedical activities. *Food Chem. Toxicol.* **2018**, *121*, 82–94. [CrossRef]
56. Signorelli, P.; Pivari, F.; Barcella, M.; Merelli, I.; Zulueta, A.; Dei Cas, M.; Rosso, L.; Ghidoni, R.; Caretti, A.; Paroni, R. Myriocin modulates the altered lipid metabolism and storage in cystic fibrosis. *Cell. Signal.* **2021**, *81*, 109928. [CrossRef]
57. Tatsumi, T.; Takayama, K.; Ishii, S.; Yamamoto, A.; Hara, T.; Minami, N.; Miyasaka, N.; Kubota, T.; Matsuura, A.; Itakura, E.; et al. Forced lipophagy reveals that lipid droplets are required for early embryonic development in mouse. *Development* **2018**, *145*, dev161893. [CrossRef]
58. Lu, Y.; Cederbaum, A. Autophagy Protects against CYP2E1/Chronic Ethanol-Induced Hepatotoxicity. *Biomolecules* **2015**, *5*, 2659–2674. [CrossRef]
59. Qiao, L.; Zhang, X.; Liu, M.; Liu, X.; Dong, M.; Cheng, J.; Zhang, X.Y.; Zhai, C.G.; Song, Y.; Lu, H.X.; et al. Corrigendum: Ginsenoside Rb1 Enhances Atherosclerotic Plaque Stability by Improving Autophagy and Lipid Metabolism in Macrophage Foam Cells. *Front. Pharmacol.* **2018**, *8*, 964. [CrossRef]
60. Allavena, G.; Boyd, C.; Oo, K.S.; Maellaro, E.; Zhivotovsky, B.; Kaminskyy, V.O. Suppressed translation and ULK1 degradation as potential mechanisms of autophagy limitation under prolonged starvation. *Autophagy* **2016**, *12*, 2085–2097. [CrossRef]

61. Zhang, Q.; Yang, Y.J.; Wang, H.; Dong, Q.T.; Wang, T.J.; Qian, H.Y.; Xu, H. Autophagy Activation: A Novel Mechanism of Atorvastatin to Protect Mesenchymal Stem Cells from Hypoxia and Serum Deprivation via AMP-Activated Protein Kinase/Mammalian Target of Rapamycin Pathway. *Stem Cells Devel.* **2012**, *21*, 1321–1332. [CrossRef] [PubMed]
62. Wang, L.; Kim, D.; Wise, J.T.F.; Shi, X.; Zhang, Z.; DiPaola, R.S. p62 as a therapeutic target for inhibition of autophagy in prostate cancer. *Prostate* **2018**, *78*, 390–400. [CrossRef] [PubMed]
63. Ge, C.X.; Xu, M.X.; Qin, Y.T.; Gu, T.T.; Feng, J.; Lv, J.X.; Wang, S.J.; Ma, Y.J.; Lou, D.S.; Li, Q.; et al. Loss of RIP3 initiates annihilation of high-fat diet initialized nonalcoholic hepatosteatosis: A mechanism involving Toll-like receptor 4 and oxidative stress. *Free Radical Biol. Med.* **2019**, *134*, 23–41. [CrossRef]
64. Kim, H.J.; Chen, F.; Wu, C.; Wang, X.; Chung, H.Y.; Jin, Z. Evaluation of antioxidant activity of Australian tea tree (*Melaleuca alternifolia*) oil and its components. *J. Agric. Food Chem.* **2004**, *52*, 2849–2854. [CrossRef]
65. Brand, C.; Ferrante, A.; Prager, R.H. The water-soluble components of the essential oil of *Melaleuca alternifolia* (tea tree oil) suppress the production of superoxide by human monocytes, but not neutrophils, activated in vitro. *Inflamm. Res.* **2001**, *50*, 213–219. [CrossRef]
66. Haribabu, A.; Reddy, V.S.; Pallavi, C.; Bitla, A.R.; Sachan, A.; Pullaiah, P.; Suresh, V.; Rao, P.; Suchitra, M.M. Evaluation of protein oxidation and its association with lipid peroxidation and thyrotropin levels in overt and subclinical hypothyroidism. *Endocrine* **2012**, *44*, 152–157. [CrossRef]
67. Kensler, T.W.; Wakabayashi, N.; Biswal, S. Cell Survival Responses to Environmental Stresses Via the Keap1-Nrf2-ARE Pathway. *Annu. Rev. Pharmacol.* **2007**, *47*, 89–116. [CrossRef]
68. Baird, L.; Dinkova-Kostova, A.T. The cytoprotective role of the Keap1-Nrf2 pathway. *Arch. Toxicol.* **2011**, *85*, 241–272. [CrossRef]
69. Chen, X.; Gao, C.; Du, X.; Yao, J.; He, F.; Niu, X.; Wang, G.Q.; Zhang, D.M. Effects of dietary astaxanthin on the growth, innate immunity and antioxidant defence system of Paramisgurnus dabryanus. *Aquacult. Nutr.* **2020**, *26*, 1453–1462. [CrossRef]
70. Kovac, S.; Angelova, P.R.; Holmström, K.M.; Zhang, Y.; Dinkova-Kostova, A.T.; Abramov, A.Y. Nrf2 regulates ROS production by mitochondria and NADPH oxidase. *BBA-Gen. Subj.* **2015**, *1850*, 794–801. [CrossRef]
71. Pan, Y.X.; Luo, Z.; Zhuo, M.Q.; Wei, C.C.; Chen, G.H.; Song, Y.F. Oxidative stress and mitochondrial dysfunction mediated Cd-induced hepatic lipid accumulation in zebrafish *Danio rerio*. *Aquat. Toxicol.* **2018**, *199*, 12–20. [CrossRef] [PubMed]
72. Morgan, M.J.; Liu, Z.G. Crosstalk of reactive oxygen species and NF-κB signaling. *Cell Res.* **2011**, *21*, 103–115. [CrossRef] [PubMed]
73. Jiang, Y.S.; Wu, X.Z. Characterization of a Rel\NF-κB homologue in a gastropod abalone, *Haliotis diversicolor supertexta*. *Dev. Comp. Immunol.* **2007**, *31*, 121–131. [CrossRef] [PubMed]
74. Li, F.; Wang, L.; Zhang, H.; Zheng, P.; Zhao, J.; Qiu, L.; Zhang, Y.; Song, L. Molecular cloning and expression of a Relish gene in Chinese mitten crab Eriocheir sinensis. *Int. J. Immunogenet.* **2010**, *37*, 499–508. [CrossRef] [PubMed]
75. Ferreira, F.; Fernandes-Ferreira, M.; Piper, P.; Sousa, M.J. Mentha piperitaessential oil induces apoptosis in yeast associated with both cytosolic and mitochondrial ROS-mediated damage. *FEMS Yeast Res.* **2014**, *14*, 1006–1014. [CrossRef] [PubMed]
76. Tapeinos, C.; Larrañaga, A.; Sarasua, J.R.; Pandit, A. Functionalised collagen spheres reduce H2O2 mediated apoptosis by scavenging overexpressed ROS. *Nanomed-Nanotechnol.* **2018**, *14*, 2397–2405. [CrossRef]
77. Martinez-Lopez, N.; Singh, R. Autophagy and lipid droplets in the liver. *Annu. Rev. Nutr.* **2015**, *35*, 215–237. [CrossRef]
78. Huang, J.; Tabbi-Anneni, I.; Gunda, V.; Wang, L. Transcription factor Nrf2 regulates SHP and lipogenic gene expression in hepatic lipid metabolism. *Am. J. Physiol. Gastrointest. Liver Physiol.* **2010**, *299*, G1211–G1221. [CrossRef]
79. Nigro, D.; Menotti, F.; Cento, A.S.; Serpe, L.; Chiazza, F.; Dal Bello, F.; Romaniello, F.; Medana, C.; Aragno, M. Chronic administration of saturated fats and fructose differently affect SREBP activity resulting in different modulation of Nrf2 and Nlrp3 inflammasome pathways in mice liver. *J. Nutr. Biochem.* **2017**, *42*, 160–171. [CrossRef]
80. Dong, L.; Han, X.; Tao, X.; Xu, L.; Xu, Y.; Fang, L.; Yin, L.H.; Qi, Y.; Li, H.; Peng, J.Y. Protection by the Total Flavonoids from Rosa laevigata Michx Fruit against Lipopolysaccharide-Induced Liver Injury in Mice via Modulation of FXR Signaling. *Foods* **2018**, *7*, 88. [CrossRef]
81. Wakai, E.; Aritake, K.; Urade, Y.; Fujimori, K. Prostaglandin D-2 enhances lipid accumulation through suppression of lipolysis via DP2 (CRTH2) receptors in adipocytes. *Biochem. Biophys. Res. Commun.* **2017**, *490*, 393–399. [CrossRef] [PubMed]
82. Fan, R.F.; Tang, K.K.; Wang, Z.Y.; Wang, L. Persistent activation of Nrf2 promotes a vicious cycle of oxidative stress and autophagy inhibition in cadmium-induced kidney injury. *Toxicology* **2021**, *464*, 152999. [CrossRef] [PubMed]
83. Ding, H.; Li, Z.Q.; Li, X.; Yang, X.R.; Zhao, J.; Guo, J.; Lu, W.F.; Liu, H.Y.; Wang, J. FTO Alleviates CdCl2-Induced Apoptosis and Oxidative Stress via the AKT/Nrf2 Pathway in Bovine Granulosa Cells. *Int. J. Mol. Sci.* **2022**, *23*, 4948. [CrossRef] [PubMed]
84. Zhao, Y.; Hu, X.; Liu, Y.; Dong, S.; Wen, Z.; He, W.; Zhang, S.Y.; Huang, Q.; Shi, M. ROS signaling under metabolic stress: Cross-talk between AMPK and AKT pathway. *Mol. Cancer* **2017**, *16*, 79. [CrossRef]
85. Yang, Y.H.; Chen, K.; Li, B.; Chen, J.W.; Zheng, X.F.; Wang, Y.R.; Jiang, S.D.; Jiang, L.S. Estradiol inhibits osteoblast apoptosis via promotion of autophagy through the ER–ERK–mTOR pathway. *Apoptosis* **2013**, *18*, 1363–1375. [CrossRef]
86. Nandy, A.; Lin, L.; Velentzas, P.D.; Wu, L.P.; Baehrecke, E.H.; Silverman, N. The NF-kappa B Factor Relish Regulates Atg1 Expression and Controls Autophagy. *Cell Rep.* **2018**, *25*, 2110. [CrossRef]
87. Vucicevic, L.; Misirkic-Marjanovic, M.; Paunovic, V.; Kravic-Stevovic, T.; Martinovic, T.; Ciric, D.; Maric, N.; Petricevic, S.; Harhaji-Trajkovic, L.; Bumbasirevic, V.; et al. Autophagy inhibition uncovers the neurotoxic action of the antipsychotic drug olanzapine. *Autophagy* **2014**, *10*, 2362–2378. [CrossRef]

88. Wan, Q.; Kang, W.Q.; Zhu, Q.; Zhang, P.J.; Liu, Y. Aging impairs insulin-stimulated glucose uptake in rat skeletal muscle via suppressing AMPKα. *Exp. Mol. Med.* **2007**, *39*, 535–543.
89. Feng, Y.M.; Pathria, G.; Heynen-Genel, S.; Jackson, M.; James, B.; Yin, J.; Scott, D.A.; Ronai, Z.A. Identification and Characterization of IMD-0354 as a Glutamine Carrier Protein Inhibitor in Melanoma. *Mol. Cancer Ther.* **2021**, *20*, 816–832. [CrossRef]
90. Jung, T.Y.; Ryu, J.E.; Jang, M.M.; Lee, S.Y.; Jin, G.R.; Kim, C.W.; Lee, C.Y.; Kim, H.; Kim, E.; Park, S.; et al. Naa20, the catalytic subunit of NatB complex, contributes to hepatocellular carcinoma by regulating the LKB1-AMPK-mTOR axis. *Exp. Mol. Med.* **2020**, *52*, 1831–1844. [CrossRef]
91. Gadang, V.; Gilbert, W.; Hettiararchchy, N.; Horax, R.; Katwa, L.; Devareddy, L. Dietary Bitter Melon Seed Increases Peroxisome Proliferator-Activated Receptor-γ Gene Expression in Adipose Tissue, Down-Regulates the Nuclear Factor-κB Expression, and Alleviates the Symptoms Associated with Metabolic Syndrome. *J. Med. Food* **2010**, *14*, 86–93. [CrossRef] [PubMed]

antioxidants

MDPI

Article

High Dietary Histamine Induces Digestive Tract Oxidative Damage in Juvenile Striped Catfish (*Pangasianodon hypophthalmus*)

Yu Liu [1,2,3,†], Xinlangji Fu [1,2,3,†], Huajing Huang [1,2,3], Jiongting Fan [1,2,3], Hang Zhou [1,2,3], Junming Deng [1,2,3,4,*] and Beiping Tan [1,2,3,4,*]

1 College of Fisheries, Guangdong Ocean University, Zhanjiang 524088, China
2 Aquatic Animals Precision Nutrition and High-Efficiency Feed Engineering Research Centre of Guangdong Province, Zhanjiang 524088, China
3 Key Laboratory of Aquatic, Livestock and Poultry Feed Science and Technology in South China, Ministry of Agriculture, Zhanjiang 524088, China
4 Laboratory of Aquatic Animal Nutrition and Feed, College of Fisheries, Guangdong Ocean University, Zhanjiang 524088, China
* Correspondence: jmdeng@stu.gdou.edu.cn (J.D.); tanbp@gdou.edu.cn (B.T.)
† These authors contributed equally to this work.

Abstract: A 56-day feeding trial investigated the effects of dietary histamine on the antioxidant capacity, gastric and intestinal barrier functions, and growth performance of striped catfish (*Pangasianodon hypophthalmus*). Seven isonitrogenous (34.0% crude protein) and isolipidic (10.5% crude lipid) diets were formulated with supplemental 0, 15, 30, 60, 120, 240, and 480 mg/kg of histamine, named H0, H15, H30, H60, H120, H240, and H480 group, respectively. Results showed that the weight gain rate, specific growth rate, relative intestinal length in the H240 and H480 groups, and the condition factors in the H480 group were significantly lower than those in the H0 group. Intestinal total antioxidant capacity, peroxidase, catalase, superoxide dismutase, glutathione peroxidase, and glutathione reductase activities in the H480 group were significantly lower than those in the H0 group, whereas intestinal malondialdehyde content exhibited the opposite trend. Intestinal complement 3, complement 4, immunoglobulin M, and Recombinant Mucin 2 in the H480 group were significantly lower than those in the H0 group, in contrast to intestinal lipopolysaccharide content. Intestinal *IL-10* gene expression in the H480 group was significantly lower than that in the H0 group, whereas the *TNF-α*, *IL-1*, *IL-6*, and *IL-8* gene expression exhibited opposite results. Scanning and transmission electron microscopic observation of the gastrointestinal tract revealed severe damage to the gastric mucosa and intestinal epithelium in the H480 group. The abundance of *Treponema* in the histamine groups was significantly higher than that in the H0 group. These results indicated that high dietary histamine decreases intestinal immunity and antioxidant capacity, inducing digestive tract oxidative damage and ultimately decreasing the growth of striped catfish.

Keywords: histamine; striped catfish; digestive tract; mucosal barrier; oxidative damage

Citation: Liu, Y.; Fu, X.; Huang, H.; Fan, J.; Zhou, H.; Deng, J.; Tan, B. High Dietary Histamine Induces Digestive Tract Oxidative Damage in Juvenile Striped Catfish (*Pangasianodon hypophthalmus*). *Antioxidants* **2022**, *11*, 2276. https://doi.org/10.3390/antiox11112276

Academic Editors: Bo Liu, Changyou Song and Cunxin Sun

Received: 12 October 2022
Accepted: 15 November 2022
Published: 17 November 2022

1. Introduction

The striped catfish (*Pangasianodon hypophthalmus*) is native to the Mekong and Chao Phraya River basins and is widely farmed in many Asian countries because of its fast growth, strong adaptability, and high disease resistance [1]. In Vietnam, exports of striped catfish already accounted for 23.2% of the national aquatic product exports in 2019 [2]. Due to its delicious meat quality, no intermuscular spines, and low price, striped fish is popular among consumers [3]. As a result, the culture scale of this species is still expanding. It is well known that reducing farming costs is one of the main strategies to improve farming economic efficiency [4]. In modern aquaculture, feed costs usually account for

more than 50% of total costs, since fish meal is increasingly expensive [5–7]. Currently, fish meal remains an integral part of commercial feed for striped catfish, remaining at 20–60% [8]. In Vietnam, stale fishmeal has been routinely used in catfish farming because of its local availability and it facilitates the control of feed costs [9]. However, fishmeal stored for long periods usually contains high doses of histamine due to the decarboxylation of histidine [10–12]. Moreover, striped catfish are cultivated commercially in subtropical and tropical regions where unfavorable storage conditions (humidity and heat) often lead to feed spoilage and produce large amounts of histamine [13]. Therefore, striped catfish may face dietary challenges with high doses of histamine.

Histamine is a low molecular weight organic nitrogen compound with the chemical formula of C5H9N3 [14], which extensively participated in numerous metabolic activities [15–17]. Excessive intake of histamine may cause human health disorders, poisoning, headaches, and even anaphylaxis [18–20]. Therefore, some regions and countries legislate to limit the histamine content in food; for the European Union, Australia, and South Africa, histamine content should be less than 100 mg/kg [21–23], and for the United States of America, below 50 mg/kg [24]. Recently, the effects of histamine on the growth, metabolism, and health of aquatic animals have attracted widespread attention [12,25–29], with results showing that dietary histamine interferes with normal metabolism, causes inflammatory responses, and reduces antioxidant capacity and growth in aquatic animals. Moreover, the toxic effects of dietary histamine can directly damage the morphology, physiology, and health of the digestive tract of aquatic animals [29–32] and disrupt the normal gut microbiota structure [28]. Thus, striped fish may suffer from the toxic effects of dietary histamine; however, limited information is available about this.

The digestive tract is the main nutrient intake place of fish, and its physiological function and health maintenance are closely related to antioxidant and immune status. Specifically, the antioxidant status usually depends on the activity of antioxidant enzyme systems, including peroxidase, catalase superoxide dismutase, glutathione peroxidase, and glutathione reductase; the immune status is determined by both the innate and acquired immune systems, with the innate immune system being the dominant type in fish [29], which consists of complement and immunoglobulins. To date, no studies have reported the effects of dietary histamine on the intestinal antioxidant and immune system of striped catfish. Therefore, this study evaluated the effects of dietary histamine on the antioxidant capacity, gastric and intestinal barrier functions, and growth performance of striped catfish. Our data will contribute to the healthy farming of striped fish.

2. Materials and Methods

2.1. Experimental Diets Preparation

Before making the test diet, we tested the histamine content of 22 commercial feeds for striped catfish (Table 1), and the results showed that the histamine contents ranged from 33.70–177.00 mg/kg. Among them, the histamine content exceeded 80 mg/kg in eight feeds, accounting for 36.36%. Subsequently, the histamine content of the experimental diet was designed based on these data.

Table 1. Histamine content of commercial feeds.

Manufacturer	Product Name	Production Date	Test Date	Crude Protein (%)	Crude Lipid (%)	Histamine (mg/kg)
CPP	783-③	2021/3/25	2021/8/5	26.60	6.98	58.60
CPP	781-②	2021/4/16	2022/2/7	32.56	8.02	89.00
CPP	781	2021/7/9	2022/2/7	33.72	7.60	40.00
Evergreen	102-3	2021/11/21	2022/2/7	32.80	8.20	107.00
Evergreen	102-3	2021/6/24	2022/2/7	32.56	7.09	40.90
Foshan Baiyang	BC-3	2020/11/30	2021/5/27	29.08	6.37	53.80
GLOBAL	SAFIR-3	2021/6/11	2022/2/7	31.29	8.34	44.60
Indonesia Evergreen	104-3	2021/3/29	2021/8/5	23.04	8.72	50.00

Table 1. *Cont.*

Manufacturer	Product Name	Production Date	Test Date	Crude Protein (%)	Crude Lipid (%)	Histamine (mg/kg)
Indonesia Evergreen	104-2	2021/6/19	2021/8/5	23.89	8.69	60.90
Indonesia Tongwei	168	2021/2/6	2021/8/5	32.03	7.92	67.80
Jiangmen Coral	3662	2021/1/25	2021/5/10	34.10	8.34	177.00
PT. CJ	AT-3	2021/3/28	2021/8/5	15.80	7.12	55.80
PT. SURITANI PEMUKA	SPM 4A	2021/4/5	2021/8/5	25.92	5.98	51.00
STP	LA 7K	2021/8/1	2022/2/7	29.69	7.21	33.70
Tongwei	8505	2021/7/18	2022/2/7	34.44	9.54	121.00
Yangjiang Dahai	3664	2020/9/27	2021/5/10	29.39	5.66	54.20
Yangjiang Dahai	3663	2021/8/2	2021/8/16	28.92	5.58	54.50
Yangjiang Dahai	3664	2021/9/3	2021/11/12	29.20	5.33	99.50
Yangjiang Dahai	3664	2021/9/4	2021/11/12	28.32	5.32	112.00
Yangjiang Dahai	4411	2021/10/10	2021/11/25	30.46	5.88	104.00
Zhanjiang Yuehua	3663	2021/5/9	2021/5/27	32.44	5.30	56.40
Zhanjiang Yuehua	3663	2021/5/29	2021/7/23	34.38	6.28	81.50

Seven isonitrogenous (34.0% crude protein) and isolipidic (10.5% crude lipid) diets were formulated with supplemental 0, 15, 30, 60, 120, 240, and 480 mg/kg of histamine, named H0, H15, H30, H60, H120, H240, and H480 groups, respectively. To reduce the histamine content in the basal diet, we used fresh white fish meal (PILENGA 2, histamine $\leq$ 40 mg/kg, purchased from fishing vessel IMO: 9120310). All ingredients were ground into meals and sifted out with a 60 μm sieve, and then accurately weighed and mixed with a V-mixer (M-256, South China University of Technology, Guangzhou, China). Subsequently, the soybean oil and pure water were supplemented to prepare a dough and then extruded with an extruder (School of Chemical Engineering, South China University of Technology, Guangzhou, China) to produce 2.0 mm diameter pellets. The moist pellets were dried in an air-conditioned room at 25 °C (dehumidification mode) and then collected in self-sealing bags and stored at −20 °C until use. Diet formulation and proximate composition are shown in Table 2.

Table 2. Ingredients and nutritional compositions of the experimental diets.

Ingredients	H0	H15	H30	H60	H120	H240	H480
White fish meal	150.00	150.00	150.00	150.00	150.00	150.00	150.00
Rapeseed meal	200.00	200.00	200.00	200.00	200.00	200.00	200.00
Soybean meal	200.00	200.00	200.00	200.00	200.00	200.00	200.00
Wheat flour	150.00	150.00	150.00	150.00	150.00	150.00	150.00
Rice bran meal	252.99	252.99	252.99	252.99	252.99	252.99	252.99
Soybean oil	20.00	20.00	20.00	20.00	20.00	20.00	20.00
$Ca(H_2PO_4)_2$	12.00	12.00	12.00	12.00	12.00	12.00	12.00
Choline chloride (50%)	4.00	4.00	4.00	4.00	4.00	4.00	4.00
Vitamin C	0.20	0.20	0.20	0.20	0.20	0.20	0.20
Compound premix [a]	10.00	10.00	10.00	10.00	10.00	10.00	10.00
Histamine dihydrochloride	0.00	0.025	0.050	0.101	0.203	0.406	0.811
Cellulose microcrystalline	0.81	0.785	0.760	0.709	0.607	0.404	0.00
Proximate composition [b] (dry matter, g/kg)							

Table 2. *Cont.*

Ingredients	H0	H15	H30	H60	H120	H240	H480
Moisture	104.76	109.79	105.13	104.49	105.47	97.18	105.76
Crude protein	338.00	342.94	342.44	338.50	347.50	353.81	348.88
Crude lipid	106.52	104.61	103.88	109.84	107.33	105.23	104.36
Ash	104.48	107.76	101.83	103.91	98.99	96.99	101.63
Gross energy (MJ/kg) [c]	18.33	18.18	18.34	18.42	18.50	18.67	18.39
Histamine (mg/kg)	8.47	23.60	38.59	68.49	128.71	248.87	488.75

[a] Compound premix (g/kg mixture): vitamin A, 0.20 g; vitamin D3, 0.003 g; vitamin E, 4.40 g; vitamin K3, 0.66 g; vitamin B1, 0.33 g; vitamin B2, 0.88 g; vitamin B6, 0.73 g; vitamin B12, 0.001 g; nicotinic acid, 2.89 g; calcium pantothenate, 1.64 g; folic acid, 0.07 g; biotin, 0.003 g; vitamin C, 10.01 g; $FeSO_4 \cdot 7H_2O$, 52.87 g; $H_3ClCu_2O_3$, 0.65 g; $ZnSO_4 \cdot 7H_2O$, 43.15 g; $MnSO_4 \cdot 7H_2O$, 31.56 g; $MgSO_4 \cdot H_2O$, 44.65 g; $Ca(IO_3)_2$, 0.42 g; Na_2SeO_3, 0.11 g; $CoCl_2 \cdot 6H_2O$, 0.14 g. [b] Measured values; GE, gross energy; CP, crude protein; CL, crude lipid; DM, dry matter; ASH, ash. [c] Gross energy.

2.2. Animal and Feeding Trial

A total of 630 striped catfish juveniles (body weight = 31.38 ± 0.09 g) were randomly assigned to 21 cages with 30 fish per cage (0.7 m × 0.7 m × 1 m). The feeding trial lasted 8 weeks, and the fish were fed twice daily at 7:00 and 17:30 h to apparent satiation during this period. The amount of feed fed to each net box was recorded daily and checked for fish mortality. This trial was conducted in the Freshwater Base of Guangdong Ocean University with the following water parameters: temperature keep at 29–32 °C, dissolved oxygen > 4.0 mg/L, ammonia nitrogen < 0.04 mg/L.

2.3. Sample Collection

At the end of the feeding trial, the fish were starved for 1 day, then weighed and counted. Subsequently, the fish were anesthetized with eugenol solution (1:10,000 dilution, Macklin, Shanghai, China) before starting the sampling. Four fish per cage were individually measured in terms of body weight and length, visceral weight, liver weight, intestinal length, and intestinal weight to calculate condition factors (CF), viscerosomatic index (VSI), hepatosomatic index (HSI), relative intestinal length (RIL) and relative intestinal weight (RIW). Four fish from each cage were selected for dissection, and the hindgut tissues were harvested and placed in an Eppendorf (EP) tube, then stored at −80 °C for enzyme activities analysis. Another four fish per cage were selected for dissection, and the hindgut was collected in an RNAlater-added EP tube for intestinal gene quantitative analysis, and the digesta in the hindgut was collected for intestinal flora analysis.

2.4. Gastrointestinal Tract Histomorphological Observation

One fish per cage from the H0, H60, and H480 groups was selected for dissection, and the stomach and hindgut were harvested and placed in an EP tube containing glutaraldehyde fixative (Wuhan Servicebio Technology Co., Ltd., Wuhan, China). Subsequently, the stomach tissue blocks were washed with 0.1 mol/L phosphoric acid buffer (PSB) solution 3 times, 15 min each, and then the tissue was transferred to PBS containing 1% OsO4 and left for 1–2 h at room temperature. Afterward, the tissue blocks were washed three times with PBS for 15 min each, followed by dehydration with an alcohol gradient. The tissues were placed in an isoamyl acetate solution and then dried with a critical point dryer (K850, Quorum, Nottingham, United Kingdom). Finally, the specimens were attached to metal stakes for 30 s using a carbon sticker and sputtering apparatus (MC1000, Hitachi, Tokyo, Japan) and then observed using a scanning electron microscope (SEM, SU8100, Hitachi, Japan).

Hindgut tissue was fixed and dehydrated according to the procedure of gastric tissue, and the treated hindgut tissue was placed in resin for permeabilization and embedding, followed by cutting into ultrathin sections (Leica UC7, Leica, Wetzlar, Germany). Subsequently, ultrathin sections were stained with 2% uranyl acetate and 2.6% lead citrate and observed using a transmission electron microscope (TEM, HT7800, HITACHI, Japan).

2.5. Intestinal Biochemical Parameters Analysis

Wet intestine samples were first accurately weighted, and then a ninefold volume (v/m) of phosphate buffer (pH 7.4) was added to prepare crude enzyme extract solution with the following method: homogenized evenly using a homogenizer (IKA Works Asia, Bhd, Kuala Lumpur, Malaysia) and then centrifuged at 875 g for 10 min at 4 °C; the supernatant was then removed for subsequent analysis. The total protein concentration of each intestine sample was measured by the bicinchoninic acid method (BCA) using the commercially available kit (No. A045-3-2, Nanjing Jiancheng Bioengineering Institute, Nanjing, China). Intestinal total antioxidant capacity (T-AOC, ABTS method, No. A015-2-1), peroxidase (POD, colorimetric method, No. A084-1-1), catalase (CAT, ultraviolet method, No. A007-2-1), superoxide dismutase (SOD, WST-1 method, No. A001-3-2), glutathione peroxidase (GPX, colorimetric method, No. A005-1-2), glutathione reductase (GR, ultraviolet method, No. A062-1-1), and lysozyme (LZM, turbidimetric method, A050-1-1) activities and intestinal malondialdehyde (MDA, TBA method, No. A003-1-2) content were determined by using commercial kits purchased from Nanjing Jiancheng Bioengineering Institute (Nanjing, China). Intestinal recombinant lipopolysaccharide (LPS, No. ml505648), complement 3 (C3, ml003460), complement 4 (C4, ml003461), and immunoglobulin M (IgM, No. ml326413) contents were determined by the ELISA method using commercial kits purchased from Shanghai Enzyme Link Biotechnology Co., Ltd. (Shanghai, China). The determination procedures of each parameter were performed in strict accordance with the corresponding instructions, and unit conversion was performed by dividing by the protein concentration of the corresponding sample.

2.6. Real-Time Quantitative PCR

Total intestinal RNA was extracted using the TRIzol™ Reagent kit (TransGenBiotech, Beijing, China), followed by concentration and integrity detection using a spectrophotometer (NanoDrop® ND-2000, Thermo, Waltham, MA, USA) and a 1.2% denatured agarose, respectively. Subsequently, the qualified samples (1 μg RNA) were used as reverse transcription templates to synthesize cDNA using commercial kits (Accurate Biology, Changsha, China). Real-Time Quantitative PCR analysis was performed under a 10 μL SYBR® Green Premix Pro Taq HS qPCR Kit II reaction system (Accurate Biology, China) using a quantitative PCR instrument (Roche LightCycler® 480) following the method described in a previous study [33]. Briefly, the 10 μL reaction system contains a 10 ng cDNA template, 0.4 μM forward primers, 0.4 μM reverse primers, 5 μL 2 × SYBR® Green Pro Taq HS Premix II, and the rest is RNase-free water. The PCR instrument was set up with a program of denaturation at 95 °C for 30 s, followed by 40 amplification cycles with denaturation at 95 °C for 5 s and annealing at 60 °C for 30 s. The primers used in this trial are shown in Table 3. The expression level or target genes were calculated by the $2^{-\Delta\Delta CT}$ method [34] and normalized with the expression level of β-actin in the H0 group.

Table 3. Primers pair sequences used for real-time PCR.

Target Gene	Primer Sequence	Product Size	Accession No.
TNF-α	F-TGTCTCGCTGGTCTGACTCCTATG R-CAGTGGGTTTGTTGCTCTTCAAGTG	97	XM_026942329.2
IL-10	F-TCTACTTGGAGACCGTGTTGCCTAG R-GATGGTGTCGATGGGAGTTCTGAAG	80	XM_026935649.2
IL-6	F-GACTGCGGGTCTGAGAGTTTACTTC R-GCAACACTGGGTCTGATCTGTCTG	142	XM_026922014.2
IL-8	F-GCTTAGGGAGGTGAGGGCTGAG R-TAGGTGTGGAGGTGGATGTGGTAAG	112	XM_027138229.2
IL-1β	F-TTCTTCAGAAACGGCACTGGTGAC R-GGAGGTGACTGGATTGCTGCTTAC	130	NM_001200219
β-actin	F-GGCTACTCCTTCACCACCACA R-ATTGAGTCGGCGTGAAGTGGTAAC	100	XM_026929614.2

TNF-α, tumor necrosis factor a; IL-10, interleukin-10; IL-6, interleukin-6; IL-8, interleukin-8; IL-1β, interleukin 1-beta.

2.7. Intestinal Microbiome Analysis

Intestinal microbiota total DNA was extracted by using the HiPure Soil DNA Extraction Kit (Magen, Guangzhou, China) according to the instructions, followed by a quality test with a UV spectrophotometer (Thermo, Waltham, MA, USA). Subsequently, the V3-V4 region of the 16SrRNA gene was amplified using a universal primer pair (341F/806R, CCTACGGGNGGCWGCAG/GGACTACHVGGGTATCTAAT) and a commercially available kit (New England Biolabs, MA, USA). The amplification conditions were set as follows: pre-denaturation at 95 °C for 5 min, followed by denaturation at 95 °C for 1 min, annealing at 60 °C for 1 min, extension at 72 °C for 1 min, and incubation at 72 °C for 7 min after performing 30 cycles. PCR amplification was performed using a 50 μL reaction system containing 10 μL of 5 × Q5@ Reaction Buffer, 10 μL 5 × Q5@ High GC Enhancer, 1.5 μL of 2.5 mM dNTPs, 1.5 μL of forward and reverse primers (10 μM), 0.2 μL of Q5@ High-Fidelity DNA Polymerase, and 50 ng of template DNA. Afterward, the amplification products are purified and quantified, and then a library is constructed before initiating the sequencing work (Illumina platform, Illumina, San Diego, CA, USA). Intestinal microbiome analysis was entrusted to Guangzhou Genedenovo Biotechnology Co., Ltd. (Guangzhou, China).

2.8. Statistical Analysis

The obtained data were subjected to one-way analysis of variance (ANOVA) by SPSS software (version 22, IBM, Chicago, IL, USA), followed by Duncan's multiple comparison test when p-value < 0.05. All data were expressed as mean ± standard error of measurement (SEM).

3. Results

3.1. Growth Performance and Morphologic Indexes

As shown in Table 4, the SR, VSI, and RIW were not significantly affected by experimental diets ($p > 0.05$). The FMW, WGR, SGR, and RIL in the H240 and H480 groups and the CF in the H480 group were significantly lower than those in the H0 group, whereas the FCR in the H240 and H480 groups exhibited an opposite result ($p < 0.05$). The HIS in the H0 group was significantly lower than that in the H60, H120, H240, and H480 groups ($p < 0.05$).

$$WGR(\%) = 100 \times (W_F - W_I)/W_I$$

$$SGR(\%/\text{day}) = 100 \times (\text{Ln}W_F - \text{Ln}W_I)/56$$

$$FCR(\%) = 100 \times W_{FI}/(W_F - W_I)$$

$$SR(\%) = 100 \times N_F/N_I$$

$$VSI(\%) = 100 \times W_V/W$$

$$HSI(\%) = 100 \times W_L/W$$

$$CF\left(g/cm^3\right) = W/L^3$$

$$RIL(\%) = 100 \times L_I/L$$

$$RIW(\%) = 100 \times W_I/W$$

where W_I, W_F, W_{FI}, N_I, and N_F are the initial body weight (g), final body weight (g), feed intake weight (g), initial fish numbers, and final fish numbers, respectively; W, W_V, W_L, W_I, L, and L_I are the body weight (g), visceral weight (g), liver weight (g), intestinal weight (g), body length (cm), and intestinal length (cm) of the same sampled fish.

Table 4. Effect of dietary histamine on growth performance and morphologic indexes of striped catfish.

Items	H0	H15	H30	H60	H120	H240	H480
IBW (g)	31.45 ± 0.01	31.40 ± 0.08	31.35 ± 0.03	31.32 ± 0.02	31.33 ± 0.04	31.36 ± 0.14	31.43 ± 0.12
FBW (g)	106.56 ± 1.80 ^{b}	107.68 ± 2.86 ^{b}	105.25 ± 1.60 ^{b}	105.00 ± 5.67 ^{b}	102.87 ± 2.21 ^{ab}	96.8 ± 5.69 ^{a}	96.31 ± 2.90 ^{a}
WGR (%)	2.39 ± 0.06 ^{c}	2.43 ± 0.08 ^{c}	2.36 ± 0.05 ^{c}	2.31 ± 0.12 ^{bc}	2.28 ± 0.08 ^{abc}	2.09 ± 0.19 ^{ab}	2.07 ± 0.08 ^{a}
FCR (%)	1.27 ± 0.05 ^{a}	1.26 ± 0.04 ^{a}	1.30 ± 0.03 ^{a}	1.33 ± 0.02 ^{ab}	1.34 ± 0.04 ^{ab}	1.48 ± 0.12 ^{bc}	1.43 ± 0.06 ^{c}
SGR (%/day)	2.18 ± 0.05 ^{b}	2.20 ± 0.04 ^{b}	2.16 ± 0.03 ^{b}	2.14 ± 0.02 ^{b}	2.12 ± 0.04 ^{b}	1.99 ± 0.11 ^{a}	2.00 ± 0.04 ^{a}
SR (%)	100	100	100	100	100	100	100
HSI (%)	1.63 ± 0.08 ^{a}	1.73 ± 0.20 ^{ab}	1.83 ± 0.16 ^{ab}	1.90 ± 0.19 ^{b}	1.91 ± 0.18 ^{b}	1.89 ± 0.18 ^{b}	1.96 ± 0.23 ^{b}
VSI (%)	11.19 ± 1.44	11.35 ± 1.94	11.03 ± 1.04	10.97 ± 1.67	11.41 ± 1.78	10.56 ± 1.79	10.74 ± 1.72
CF (g/cm^{3})	1.54 ± 0.05 ^{b}	1.52 ± 0.04 ^{b}	1.52 ± 0.06 ^{b}	1.51 ± 0.06 ^{ab}	1.50 ± 0.08 ^{ab}	1.46 ± 0.10 ^{ab}	1.43 ± 0.05 ^{a}
RIL (%)	213.43 ± 28.21 ^{b}	197.41 ± 9.7 ^{ab}	195.42 ± 12.97 ^{ab}	189.1 ± 19.91 ^{ab}	183.31 ± 40.77 ^{ab}	172.54 ± 29.43 ^{a}	165.81 ± 29.95 ^{a}
RIW (%)	1.71 ± 0.34	1.75 ± 0.25	1.91 ± 0.31	1.88 ± 0.31	1.74 ± 0.32	1.66 ± 0.28	1.64 ± 0.28

Data in the same row with different superscript letters indicate significant differences between groups (n = 3; $p < 0.05$).

3.2. Intestinal Antioxidant Capacity

As shown in Table 5, intestinal POD and SOD activities in the H480 groups, intestinal GR activity in the H240 and H480 groups, and intestinal T-AOC and GPX activities in the H120, H240, and H480 groups were significantly lower than those in the H0 group, whereas the intestinal MDA content in the H480 group exhibited an opposite result ($p < 0.05$). The intestinal CAT activity in the H30, H60, H120, H240, and H480 groups was significantly lower than that in the H0 group ($p < 0.05$).

Table 5. Effect of dietary histamine on the intestinal antioxidant ability of striped catfish.

Items	H0	H15	H30	H60	H120	H240	H480
T-AOC (U/mg prot)	0.80 ± 0.10 ^{b}	0.76 ± 0.02 ^{b}	0.77 ± 0.03 ^{b}	0.78 ± 0.04 ^{b}	0.60 ± 0.06 ^{a}	0.58 ± 0.03 ^{a}	0.53 ± 0.04 ^{a}
POD (U/g prot)	54.22 ± 13.01 ^{b}	50.69 ± 10.81 ^{b}	45.06 ± 9.33 ^{ab}	44.94 ± 7.64 ^{ab}	41.12 ± 9.17 ^{ab}	39.78 ± 5.97 ^{ab}	32.84 ± 9.80 ^{a}
CAT (U/g prot)	12.28 ± 1.19 ^{b}	10.44 ± 0.36 ^{ab}	9.62 ± 0.40 ^{a}	9.77 ± 0.06 ^{a}	9.56 ± 0.46 ^{a}	8.32 ± 1.24 ^{a}	8.05 ± 1.20 ^{a}
SOD (U/g prot)	33.17 ± 1.75 ^{b}	28.74 ± 2.13 ^{ab}	31.29 ± 2.27 ^{ab}	26.52 ± 5.91 ^{ab}	26.12 ± 2.28 ^{ab}	23.45 ± 4.24 ^{ab}	18.84 ± 1.84 ^{a}
GPX (U/g prot)	29.17 ± 2.44 ^{c}	27.67 ± 5.00 ^{bc}	25.73 ± 2.07 ^{bc}	24.94 ± 2.47 ^{bc}	22.20 ± 1.97 ^{ab}	18.31 ± 3.54 ^{a}	17.62 ± 6.23 ^{a}
GR (U/g prot)	24.79 ± 2.72 ^{b}	23.16 ± 5.13 ^{b}	22.40 ± 2.59 ^{b}	22.32 ± 2.51 ^{b}	19.81 ± 3.04 ^{b}	13.94 ± 2.23 ^{a}	14.07 ± 2.13 ^{a}
MDA (nmol/mg prot)	1.13 ± 0.65 ^{a}	1.44 ± 0.35 ^{a}	1.58 ± 0.32 ^{a}	1.71 ± 0.64 ^{a}	2.47 ± 0.39 ^{ab}	2.57 ± 0.87 ^{ab}	3.57 ± 1.40 ^{b}

Data in the same row with different superscript letters indicate significant differences between groups (n = 3; $p < 0.05$).

3.3. Intestinal Immune Status

As shown in Table 6, the intestinal LZM activity was not significantly affected by experimental diets ($p > 0.05$). The intestinal C3 content in the H240 and H480 groups and the IgM content in the H60, H120, H240, and H480 groups were significantly lower than those in the H0 group ($p < 0.05$). The intestinal C4 content in the H30, H60, H120, H240, and H480 groups was significantly lower than that in the H0 group, whereas the LPS content exhibited an opposite result ($p < 0.05$).

Table 6. Effect of dietary histamine on intestinal immunity of striped catfish.

Items	H0	H15	H30	H60	H120	H240	H480
LZM (U/g prot)	1.55 ± 0.25	1.44 ± 0.10	1.57 ± 0.12	1.86 ± 0.05	1.91 ± 0.48	2.10 ± 0.25	2.04 ± 0.31
C3 (mg/g prot)	20.37 ± 2.21 ^{b}	16.28 ± 4.40 ^{ab}	15.14 ± 5.21 ^{ab}	14.28 ± 3.93 ^{ab}	15.53 ± 2.33 ^{ab}	12.66 ± 1.89 ^{a}	11.48 ± 1.01 ^{a}
C4 (mg/g prot)	77.78 ± 4.90 ^{c}	66.44 ± 2.76 ^{bc}	54.89 ± 7.44 ^{ab}	51.08 ± 1.69 ^{ab}	45.95 ± 12.71 ^{a}	43.78 ± 4.66 ^{a}	39.81 ± 2.79 ^{a}
IgM (mg/g prot)	15.21 ± 1.80 ^{b}	13.93 ± 1.56 ^{ab}	13.99 ± 3.35 ^{ab}	10.82 ± 1.85 ^{a}	10.13 ± 0.67 ^{a}	10.47 ± 1.24 ^{a}	9.57 ± 0.04 ^{a}
LPS (ng/mg prot)	0.69 ± 0.14 ^{a}	0.84 ± 0.13 ^{ab}	0.95 ± 0.01 ^{bc}	1.18 ± 0.02 ^{c}	1.12 ± 0.17 ^{c}	1.15 ± 0.05 ^{c}	1.11 ± 0.09 ^{c}

Data in the same row with different superscript letters indicate significant differences between groups (n = 3; $p < 0.05$).

3.4. Intestinal Inflammatory Response

The intestinal IL-6 and IL-8 expressions in the H240 and H480 groups and the intestinal TNF-α and IL-1 expressions in the H120, H240, and H480 groups were significantly higher than those in the H0 group, whereas the IL-10 expression in the H60, H120, H240, and H480 groups was significantly lower than that in the H0 group ($p < 0.05$; Figure 1).

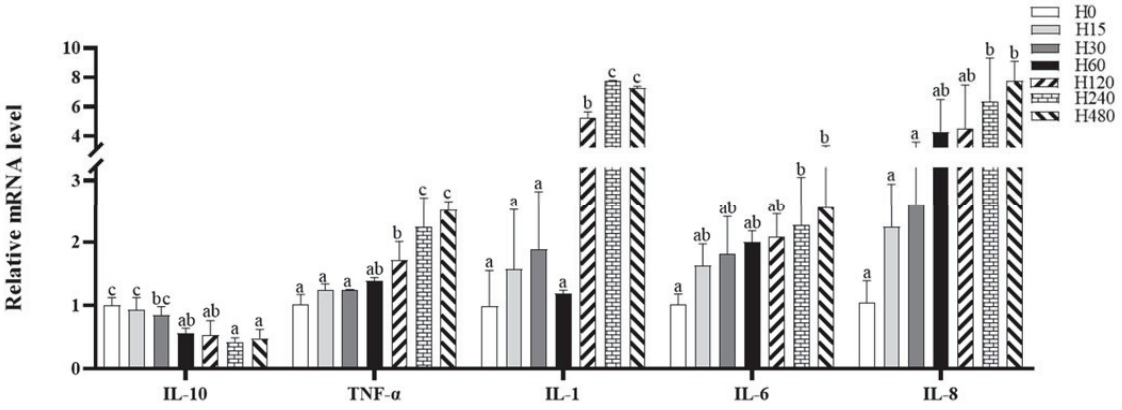

Figure 1. Intestinal inflammation-related gene expression of striped catfish fed with experimental diets. Values in each column with different superscripts represent significant differences ($p < 0.05$).

3.5. Gastric SEM and Intestinal TEM Observations

The gastric SEM and intestinal TEM observations are presented in Figure 2A,B, respectively. As shown in Figure 2A, the degree of gastric mucosal damage increased with increasing dietary histamine levels. Furthermore, as shown in Figure 2B, dietary histamine damaged intestinal epithelial cells, and organelle lysis was observed in the H480 group.

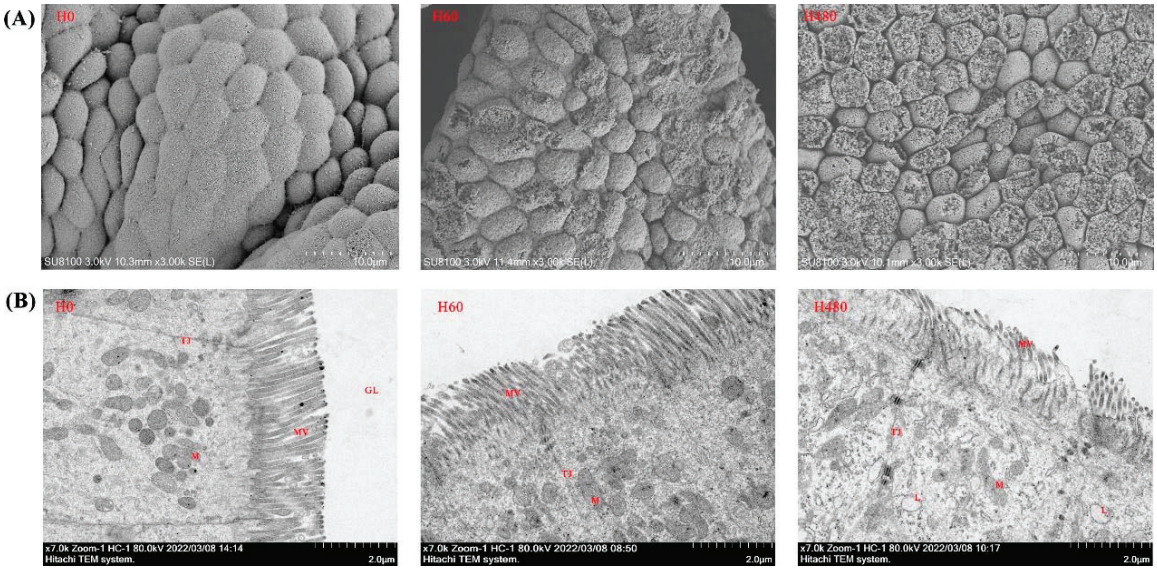

Figure 2. Gastric SEM and intestinal TEM observations of striped catfish fed with experimental diets. (**A**), gastric SEM observations; (**B**), intestinal TEM observations. M, mitochondria; TJ, tight junction; MV, microvillus; L, lysosome. Mitochondrial dissolution, lysosome volume increase, and microvilli damage were clearly observed in the H480 group.

3.6. Microbiota Structure

As shown in Table 7, the Goods coverage of all the groups was above 99%, indicating that the sequencing depth in this study was adequate. The Shannon, Simpson, Chao1, and ACE indices were not significantly affected by the experimental diets ($p > 0.05$). The

structural composition analysis of microbiota exhibited that Bacteroidetes, Firmicutes, Fusobacteria, and Spirochaetes were the dominant phyla of all groups (Figure 3A). The top 10 genera of all groups are shown in Figure 3B, and the *Bacteroides*, *Clostridium sensu stricto*, and *Cetobacterium* were the three dominant genera in all groups. As shown in Figure 3C, the abundance of *Bacteroides* in the H60 group, the abundance of Treponema2 in the H240 group, and the abundance of *Parabacteroides* in the H120 group were significantly higher than those in the H0 group, whereas the abundance of *Catobacterium* in the H480 group and the abundance of *Terrisporobacter* in the H240 group were significantly lower than those in the H0 group ($p < 0.05$).

Table 7. Effect of dietary histamine on microbiota α-diversity of striped catfish.

Items	H0	H15	H30	H60	H120	H240	H480
Goods coverage	0.99	0.99	0.99	0.99	0.99	0.99	0.99
Shannon	4.69 ± 0.21	4.35 ± 0.19	4.65 ± 0.11	4.29 ± 0.25	4.38 ± 0.15	4.64 ± 0.58	5.28 ± 0.09
Simpson	0.92 ± 0.01	0.88 ± 0.01	0.91 ± 0.03	0.89 ± 0.03	0.89 ± 0.00	0.89 ± 0.06	0.94 ± 0.02
Chao1	462.84 ± 112.71	503.1 ± 51.95	532.33 ± 42.14	511.99 ± 111.15	492.98 ± 19.82	531.99 ± 33.7	472.69 ± 17.32
Ace	467.86 ± 121.96	507.63 ± 54.8	537.84 ± 46.52	507.99 ± 115.19	499.28 ± 22.27	533.86 ± 30.56	465.54 ± 16.79

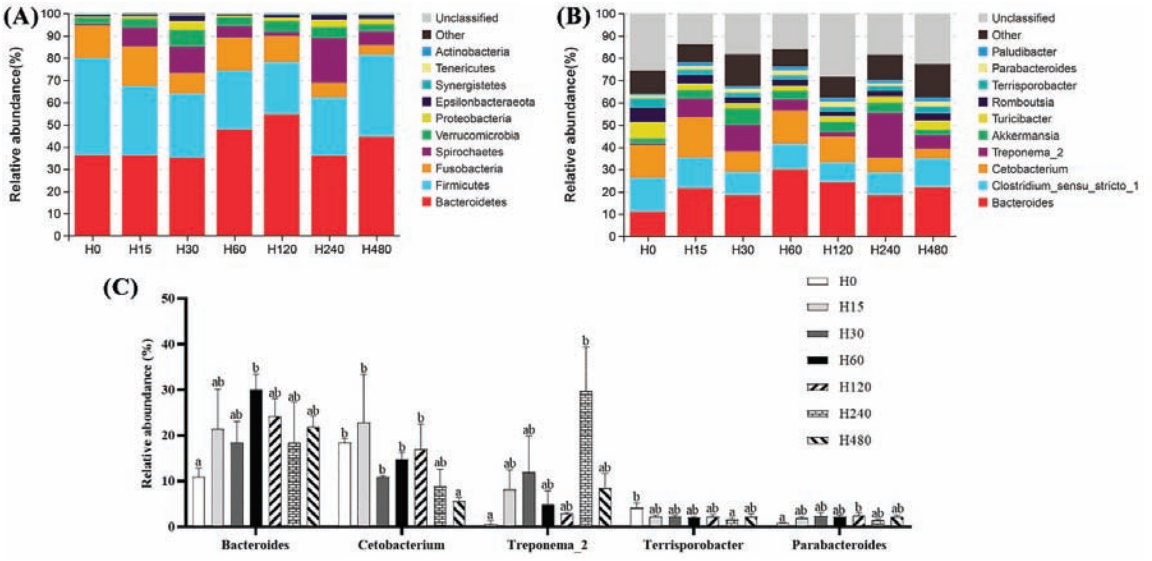

Figure 3. Intestinal flora composition of striped catfish fed with different experimental diets. (**A**), phylum level; (**B**), general level; (**C**), genera with significant differences. Values in each column with different superscripts represent significant differences ($p < 0.05$).

4. Discussion

This study first investigated the effects of dietary histamine on the antioxidant capacity, gastric and intestinal barrier functions, and growth performance of striped catfish. As a toxic dietary component, histamine has attracted much attention from aquatic animal nutritionists in recent years. Previous studies have shown that dietary histamine significantly decreased the growth performance of the juvenile group (*Epinephelus coioides*) [35], mysis (*Neomysis japonica Nakazawa*) [36,37], American eels (*Anguilla rostrata*) [38,39], yellow catfish (*Pelteobagrus fulvidraco*) [29], and rainbow trout (*Oncorhynchus mykiss*) [40]. In this study, our data exhibited that dietary histamine below 60 mg/kg has limited effects on the growth of striped catfish, whereas dietary histamine above 120 mg/kg significantly decreased the growth, suggesting that the growth-inhibiting effect of dietary histamine was

dose-dependent. Of note, the striped catfish in the H15 group showed better growth than in the H0 group. Similarly, He et al. (2018) [40] found that diets containing 18.0 mg/kg of histamine had a growth-promoting effect on yellow catfish. This evidence suggests that low-dose histamine may benefit the growth of fish. Conversely, diets containing 4000 mg/kg of histamine showed no detrimental effects on the performance of Chinese mitten crab (*Eriocheir sinensis*) [32], and high-dose dietary histamine (2400 mg/kg) even showed a growth-promoting effect on blue shrimp (*Litopenaeus stylirostris*) [41]. The difference in these results may be related to differences in the digestive physiology of different aquatic animals.

A healthy digestive tract is important for maintaining proper immunity and growth in fish, and the health of the digestive tract is regulated by dietary ingredients [42,43]. Oxidative damage is an unavoidable part of the physiological activity of aerobic organisms, due to the continuous production of oxygen radicals during their physiological metabolism [44]. The scavenging of oxygen radicals is accomplished by the antioxidant system, including antioxidant enzymes and antioxidant active substances [45]. Therefore, the antioxidant capacity is commonly used to evaluate the health status of fish. In this study, fish in the H480 group exhibited the lowest intestinal T-AOC, POD, CAT, SOD, GPX, and GR activities and the highest MDA content, suggesting that high dietary histamine is detrimental to the intestinal antioxidant capacity of striped catfish. Similarly, high-dose dietary histamine significantly decreased the antioxidant capability of grouper [35], American eel [38], and Pacific white shrimp (*Litopenaeus vannamei*) [12]. Liu et al. [35] concluded that the long-term intake of histamine disrupts the ability of fish to respond to reactive oxygen intermediates, thereby disrupting the antioxidant system and causing oxidative damage. However, considering that the intestinal antioxidant capacity of striped catfish fed low-dose dietary histamine (below 60 mg/kg) was not significantly reduced, we hypothesized that dietary histamine disrupts the intestinal antioxidant system in a dose-dependent manner.

Intestinal innate immunity plays an essential role in maintaining intestinal health, which constitutes the first line of defense against colonization by disease-causing microorganisms [46]. Intestinal immune activity is accomplished by the synergistic action of multiple immune enzymes and immunologically active substances, including immunoglobulins M (IgM), lysozyme, and the complement (C3, C4) [47,48]. In this study, dietary histamine (above 120 mg/kg) significantly decreased intestinal C3, C4, and IgM contents, suggesting that high-dose dietary histamine is detrimental to the innate immunity of striped catfish, thereby disrupting intestinal health. Besides, the complement system also plays an equally important role in regulating inflammation in fish [49]. The inflammatory response is usually regulated by a dynamic balance of pro- and anti-inflammatory factors [26,50]. In this study, dietary histamine (above 120 mg/kg) caused the downregulation of anti-inflammatory factors (e.g., IL-10 and NF-κB) and the upregulation of pro-inflammatory factors (e.g., IL-1, IL-6, IL-8, and TNF-α), suggesting that high doses of histamine may cause intestinal inflammation in striped catfish. Similarly, dietary histamine also induced inflammation in Pacific white shrimp and Perciformes [12,51]. Galindo-Villegas et al. [51] suggested that dietary histamine regulates the inflammatory response by acting directly with macrophages. Therefore, this evidence suggests that high doses of dietary histamine may trigger an inflammatory response mediated by macrophages, thereby impairing intestinal health.

Dong et al. [52] suggested that inflammation usually occurs when immune cells are infected or tissues are damaged. In this study, the intestinal TEM observation exhibited that high-dose dietary histamine (480 mg/kg) severely damaged the structure and morphology of intestinal epithelial cells, including an increase in the number of lysosomes and swelling of mitochondria and endoplasmic reticulum. Moreover, the gastric SEM observation also showed that high-dose dietary histamine severely damaged the mucosal layer. Combined with the poor intestinal antioxidant capacity and upregulated inflammation levels, these results sufficiently suggest that high-dose dietary histamine disrupts the intestinal antioxidant system, causing oxidative damage to intestinal tissues and inducing inflammation in striped catfish. More importantly, the morphology of the digestive tract is closely related

to its physiological function [53]. Thus, the poor digestive tract morphology also plausibly explains the reduced intestinal immune function and growth performance of striped catfish [54]. Similar results were observed in grouper [35] and yellow catfish [29]. This evidence suggests that high-dose dietary histamine may reduce fish growth by disrupting digestive tract health and function.

As a component of the intestinal mucosal layer, the intestinal flora is also critical to intestinal health and function [55,56]. Meanwhile, the structure of the intestinal flora is easily affected by dietary ingredients [57,58]. In this study, Firmicutes, Fusobacteria, Bacteroidetes, and Spirochaetes were the four dominant phyla of all groups, which was highly consistent with a previous study reported by Hieu et al. [59]. These results indicate that these phyla may constitute the core flora of striped catfish and are essential for maintaining intestinal health and function [60]. In this study, dietary histamine altered the relative abundance of individual phyla, although it did not change the species of the core flora, suggesting that dietary histamine may induce the migration of intestinal function.

In this study, Fusobacteria, mainly *Cetobacterium* genera, have been reported to produce vitamin B_{12}, acetate, and propionate through their fermentation process [61,62]. These metabolites extensively participate in the regulation of energy metabolism, gut health, and gut microecology [62,63]. Therefore, a decrease in the abundance of *Cetobacterium* in the H480 group suggests that high-dose dietary histamine is detrimental to the intestinal physiological function and health of striped catfish. *Bacteroidetes* mainly consist of Bacteroides and Parabacteroides in this trial. *Bacteroidetes* are considered to be the main catabolite of polysaccharides in the intestine, producing large amounts of short-chain fatty acids that contribute to improved intestinal health [64]. *Parabacteroides* are a butyrate producer with equally positive effects on improving intestinal health [65,66]. Thus, an increase in the abundance of *Bacteroides* and *Parabacteroides* may suggest that low-dose dietary histamine has an ameliorative effect on intestinal health. Nevertheless, this degree of ameliorative effect did not effectively mitigate the toxic effects of dietary histamine, and therefore, dietary histamine ultimately impaired the intestinal health of striped catfish. Moreover, considering that dietary histamine caused a significant decrease in intestinal maltase activity in striped catfish (Table S1) and that both *Bacteroides* and *Parabacteroides* usually use carbohydrates as the carbon source, we speculate that the increase in the abundance of these two genera caused by dietary histamine may be related to poor carbohydrate utilization efficiency. Firmicutes mainly consist of *Terrisporobacter* genera in this study. *Terrisporobacter* is an acetate-producing bacterium that is positively correlated with host health [67,68]. *Treponema_2* genera are the dominant genera of Spirochaetes in this study, which has been reported as pathogenic bacteria [69]. Therefore, a decrease in the abundance of *Terrisporobacter* and a decrease in the abundance of *Treponema_2* in the H240 group suggests that high-dose dietary histamine is detrimental to the intestinal health of striped catfish. Moreover, the colonization of pathogenic microorganisms indicates a decrease in the immune viability of the intestinal mucosa and an imbalance in the balance of the microbial community. Combined with the poor intestinal immunity, decreased intestinal antioxidant capacity, and increased oxidative stress in the H240 group, the increased abundance of pathogenic microorganisms in the H240 group suggests that a high dose of dietary histamine disrupts intestinal antioxidant and immune defenses, leading to colonization by pathogenic microorganisms.

5. Conclusions

In conclusion, high-dose dietary histamine decreased intestinal antioxidant capacity, thereby inducing intestinal oxidative damage and decreasing the growth of striped catfish. In addition, high-dose dietary histamine reduces intestinal immunity, induces the colonization of pathogenic microorganisms and intestinal inflammation, and impairs intestinal health. High-dose dietary histamine severely damaged the mucosal layer of the digestive tract in striped catfish. More importantly, our data confirmed that histamine is a toxic

dietary component for aquatic animals and that increases in histamine levels should be prevented during aquafeed production and storage.

Supplementary Materials: The following supporting information can be downloaded at: https://www.mdpi.com/article/10.3390/antiox11112276/s1, Table S1: Intestinal digestive enzyme activities of striped catfish fed with different experimental diets.

Author Contributions: Y.L. and X.F.: Formal analysis, Data curation, Writing—original draft, Writing—review and editing; H.H., J.F. and H.Z.: Formal analysis, Data curation; J.D. and B.T.: Conceptualization, Methodology, Writing—original draft, Writing—review and editing, Supervision, and Funding acquisition. All authors have read and agreed to the published version of the manuscript.

Funding: This work was financially supported by the National Key R&D Program of China (2019YFD0900200), the Program for Scientific Research Startup Funds of Guangdong Ocean University (060302022007), the Foundation of Tongwei Co., Ltd. (TA2019A003), National Natural Science Foundation of China (31760761), and the Natural Science Foundation of Yunnan Province (2018FA018).

Institutional Review Board Statement: The striped catfish juveniles used in this study were provided by Guangdong Evergreen Feed Industry Co., Ltd. The procurement of test fish was approved by the Animal Research and Ethics Committee of Guangdong Ocean University (Zhanjiang, China; approval ID: GDOU-IACUC-2021-A2220, approval date: 8 September 2021), and all experimental procedures were carried out in strict accordance with its guidelines.

Informed Consent Statement: Not applicable.

Data Availability Statement: Data is contained within the article and in the Supplementary Material.

Acknowledgments: The authors would like to thank Yixiong Cao, Yumeng Zhang, and Xiaomei Dou for their help during the experiments.

Conflicts of Interest: The authors declare that no conflict of interest could be perceived as prejudicing the impartiality of the research reported.

References

1. Gao, Z.; You, X.; Zhang, X.; Chen, J.; Xu, T.; Huang, Y.; Lin, X.; Xu, J.; Bian, C.; Shi, Q. A chromosome-level genome assembly of the striped catfish (*Pangasianodon hypophthalmus*). *Genomics* **2021**, *113*, 3349–3356. [CrossRef]
2. Dang, T.H.O.; Xuan, T.T.T.; Duyen, L.T.M.; Le, N.P.; Hoang, H.A. Protective efficacy of phage pvn02 against haemorrhagic septicaemia in striped catfish *Pangasianodon hypophthalmus* via oral administration. *J. Fish Dis.* **2021**, *44*, 1255–1263. [CrossRef] [PubMed]
3. Wang, D.; Hsieh, Y.-H.P. The use of imported pangasius fish in local restaurants. *Food Control* **2016**, *65*, 136–142. [CrossRef]
4. Glencross, B.; Hien, T.T.T.; Phuong, N.T.; Cam Tu, T.L. A factorial approach to defining the energy and protein requirements of tra catfish, pangasianodon hypothalamus. *Aquac. Nutr.* **2011**, *17*, e396–e405. [CrossRef]
5. Zhang, Y.; Chen, P.; Liang, X.F.; Han, J.; Wu, X.F.; Yang, Y.H.; Xue, M. Metabolic disorder induces fatty liver in japanese seabass, *Lateolabrax japonicas* fed a full plant protein diet and regulated by camp-jnk/nf-kb-caspase signal pathway. *Fish Shellfish Immunol.* **2019**, *90*, 223–234. [CrossRef]
6. Medard, G.; Ouattara, N.G.; Bamba, Y.; Mamadou, O.; Ouattara, A.; Kouakou, Y.A.O. Substitution of the fish meal by the earthworm and maggot meal in the feed of nile tilapia oreochromis niloticus reared in freshwater. *Int. J. Fish. Aquac.* **2018**, *10*, 77–85. [CrossRef]
7. Kotzamanis, Y.; Kouroupakis, E.; Ilia, V.; Haralabous, J.; Papaioannou, N.; Papanna, K.; Richards, R.; Gisbert, E. Effects of high-level fishmeal replacement by plant proteins supplemented with different levels of lysine on growth performance and incidence of systemic noninfectious granulomatosis in meagre (*Argyrosomus regius*). *Aquac. Nutr.* **2018**, *24*, 1738–1751. [CrossRef]
8. Allam, B.W.; Khalil, H.S.; Mansour, A.T.; Srour, T.M.; Omar, E.A.; Nour, A.A.M. Impact of substitution of fish meal by high protein distillers dried grains on growth performance, plasma protein and economic benefit of striped catfish (*Pangasianodon hypophthalmus*). *Aquaculture* **2020**, *517*, 734792. [CrossRef]
9. Edwards, P.; Anh Tuan, H.; Allan, G. *A Survey of Marine Trash Fish and Fish Meal as Aquaculture Feed Ingredients in Vietnam*; Working Paper; Australian Centre for International Agricultural Research: Canberra, Australia, 2004; p. 57.
10. Eitenmiller, R.R.; Wallis, J.W.; Orr, J.H.; Phillips, R.D. Production of histidine decarboxylase and histamine by *Proteus morganii*. *J. Food Prot.* **1981**, *44*, 815–820. [CrossRef]
11. Moniente, M.; García-Gonzalo, D.; Llamas-Arriba, M.G.; Virto, R.; Ontañón, I.; Pagán, R.; Botello-Morte, L. Potential of histamine-degrading microorganisms and diamine oxidase (dao) for the reduction of histamine accumulation along the cheese ripening process. *Food Res. Int.* **2022**, *160*, 111735. [CrossRef]

12. Lin, C.; Yan, P.; Lou, Z.; Shi, X.; Zhao, Q.; Li, E. Effects of histamine on the neuroendocrine-immune regulatory network in the pacific white shrimp, *Litopenaeus vannamei*. *Aquaculture* **2022**, *554*, 738156. [CrossRef]
13. Jaw, Y.M.; Chen, Y.Y.; Lee, Y.C.; Lee, P.H.; Jiang, C.M.; Tsai, Y.H. Histamine content and isolation of histamine-forming bacteria in fish meal and fish soluble concentrate. *Fish. Sci.* **2012**, *78*, 155–162. [CrossRef]
14. Chu, B.; Lin, L.; Yu, K.-Q. Rapid determination of histamine concentration in fish (*Miichthys miiuy*) by surface-enhanced raman spectroscopy and density functional theory. *Int. J. Agric. Biol. Eng.* **2017**, *10*, 252–258. [CrossRef]
15. Yılmaz, C.; Gökmen, V. Neuroactive compounds in foods: Occurrence, mechanism and potential health effects. *Food Res. Int.* **2020**, *128*, 108744. [CrossRef]
16. Wang, K.; Sun, Z.; Li, Y.; Liu, M.; Loor, J.J.; Jiang, Q.; Liu, G.; Wang, Z.; Song, Y.; Li, X. Histamine promotes adhesion of neutrophils by inhibition of autophagy in dairy cows with subacute ruminal acidosis. *J. Dairy Sci.* **2022**, *105*, 7600–7614. [CrossRef]
17. Barik, B.; Mohapatra, S. Selective visual detection of histamine and ascorbic acid through the rapid gel-sol transition of luminescent alginate hydrogel. *Sens. Actuators B Chem.* **2022**, *367*, 132128. [CrossRef]
18. Maintz, L.; Novak, N. Histamine and histamine intolerance. *Am. J. Clin. Nutr.* **2007**, *85*, 1185–1196. [CrossRef]
19. Efsa Efsa panel on biological hazards (biohaz): Scientific opinion on risk-based control of biogenic amine formation in fermented foods. *EFSA J.* **2011**, *9*, 2393. [CrossRef]
20. Schnedl, W.J.; Schenk, M.; Lackner, S.; Enko, D.; Mangge, H.; Forster, F. Diamine oxidase supplementation improves symptoms in patients with histamine intolerance. *Food Sci Bio.* **2019**, *28*, 1779–1784. [CrossRef]
21. Union, E. Commission regulation no. 2073/2005 of 15 november 2005 on microbiological criteria for foodstuffs. *Off. J. Eur. Union* **2005**, *48*, 1–26.
22. Food Standards Australia New Zealand. *Imported Food Risk Statement Fish and Fish Products from the Families Specified and Histamine*; Food Standards Australia New Zealand: Majura, Australia; Wellington, New Zealand, 2016.
23. South African Bureau of Standards. *Regulations Governing Microbiological Standards for Foodstuffs and Related Matters*; Government Notice No. R 490; South African Bureau of Standards: Pretoria, South Africa, 2001.
24. Food and Drug Administration. *Fish and Fishery Products Hazards and Controls Guidance*; Food and Drug Administration: Silver Spring, MD, USA, 2011.
25. Li, W.; Pan, X.; Cheng, W.; Cheng, Y.; Yin, Y.; Chen, J.; Xu, G.; Xie, L. Serum biochemistry, histology and transcriptomic profile analysis reflect liver inflammation and damage following dietary histamine supplementation in yellow catfish (*Pelteobagrus fulvidraco*). *Fish Shellfish Immunol.* **2018**, *77*, 83–90. [CrossRef]
26. Li, W.; Liu, B.; Liu, Z.; Yin, Y.; Xu, G.; Han, M.; Xie, L. Effect of dietary histamine on intestinal morphology, inflammatory status, and gut microbiota in yellow catfish (*Pelteobagrus fulvidraco*). *Fish Shellfish Immunol.* **2021**, *117*, 95–103. [CrossRef]
27. García-García, E.; Gómez-González, N.E.; García-Ayala, A.; Mulero, V. The possible role of histamine as a modulator in inflammation in the tunicate styela plicata. *Fish Shellfish Immunol.* **2013**, *34*, 1652. [CrossRef]
28. Xu, Q. Preliminary Study of Toxic Effects of Dietary Histamine on American Eel (*Anguilla rostrata*) Juveniles. Master's thesis, Jimei University, Xiamen, China, 2019.
29. He, J.; Wu, D.; Ye, Y.; Cai, C.; Wu, P.; Luo, Q.; Pu, Q. Effects of dietary histamine level on growth performance, serum biochemical indexes and gastrointestinal mucosa structure of yellow catfish (*Pelteobagrus fulvidraco*). *Chin. J. Anim. Nutr.* **2018**, *30*, 2581–2593. [CrossRef]
30. Watanabe, T.; Takeuchi, T.; Satoh, S.; Toyama, K.; Okuzumi, M. Effect of dietary histidine or histamine on growth and development of stomach erosion in rainbow trout. *Nippon Suisan Gakkaishi* **1987**, *53*, 1207–1214. [CrossRef]
31. Fairgrieve, W.T.; Dong, F.M.; Hardy, R.W. Histamine effects feed acceptability but not protein utilization by juvenile rainbow trout (*Oncorhynchus mykiss*). In Proceedings of the VIII International Symposium on Nutrition and Feeding of fish & Crustacean Nutrition, Las Palmas de Gran Canaria, Spain, 1–4 June 1998.
32. Zhao, L.; Yang, X.; Cheng, Y.; Yang, S. Effect of dietary histamine supplementation on growth, digestive enzyme activities and morphology of intestine and hepatopancreas in the Chinese mitten crab *Eriocheir sinensis*. *Springerplus* **2016**, *5*, 552. [CrossRef]
33. Chen, Y.; Chi, S.; Zhang, S.; Dong, X.; Yang, Q.; Liu, H.; Zhang, W.; Deng, J.; Tan, B.; Xie, S. Replacement of fish meal with methanotroph (methylococcus capsulatus, bath) bacteria meal in the diets of pacific white shrimp (*Litopenaeus vannamei*). *Aquaculture* **2021**, *541*, 736801. [CrossRef]
34. Livak, K.J.; Schmittgen, T.D. Analysis of relative gene expression data using real-time quantitative pcr and the $2^{-\Delta\Delta ct}$ method. *Methods* **2001**, *25*, 402–408. [CrossRef]
35. Liu, Z.-Y.; Yang, H.-L.; Hu, L.-H.; Yang, W.; Ai, C.-X.; Sun, Y.-Z. Dose-dependent effects of histamine on growth, immunity and intestinal health in juvenile grouper (*Epinephelus coioides*). *Front. Mar. Sci.* **2021**, *8*, 650. [CrossRef]
36. Yang, X.; Wang, J.; Fan, P.; Zhao, L.; Cheng, Y.; Wu, X.; Zeng, C. Survival, growth, sexual maturity and tissue histamine accumulation of the mysis, neomysis awatschensis and n. Japonica nakazawa, fed histamine supplemented diets. *Aquaculture* **2010**, *302*, 256–260. [CrossRef]
37. Yang, X.; Wang, J.; Zhao, L.; Fan, P.; Wu, X.; Cheng, Y.; Zeng, C. Effects of elevated ambient histamine level on survival, growth, sexual maturity and tissue histamine accumulation of the mysis neomysis awatschensis and neomysis japonica nakazawa. *Aquac. Int.* **2012**, *20*, 347–356. [CrossRef]
38. Ma, D.; Cai, P.; Zhai, S.; Cheng, X. Effect of dietary histamine on growth performance, digestive enzyme activities and antioxidant indices in intestine of juvenile american eels (*Anguilla rostrata*). *Feed Res.* **2020**, 42–45. [CrossRef]

39. Zhai, S.; Wang, Y.; He, Y.; Chen, X. Oligomeric proanthocyanidins counteracts the negative effects of high level of dietary histamine on american eel (*Anguilla rostrata*). *Front. Mar. Sci.* **2020**, *7*, 549145. [CrossRef]
40. Moghaddam, M.R.M.; Janmohammadi, H.; Sheikhzade, N.; Moghanloo, K.S.J.I.J.o.B. The effect of histamine resulted from decarboxylase corruption of the diets on non-specific immune response, growth performance and hepatic index of rainbow trout (*Oncorhynchus mykiss*). *Int. J. Biosci.* **2015**, *6*, 243–251.
41. Tapia-Salazar, M.; Smith, T.K.; Harris, A.; Ricque-Marie, D.; Cruz-Suarez, L.-E. Effect of dietary histamine supplementation on growth and tissue amine concentrations in blue shrimp *Litopenaeus stylirostris*. *Aquaculture* **2001**, *193*, 281–289. [CrossRef]
42. Liu, H.; Wang, F.; Zhang, S.; Li, C.; Ma, Y. Effect of chinese herbal compound on immune protection of rainbow trout (*Oncorhynchus mykiss*). *J. Guangdong Ocean Univ.* **2022**, *42*, 7–12. [CrossRef]
43. Willora, F.P.; Vatsos, I.N.; Mallioris, P.; Bordignon, F.; Keizer, S.; Martınez-Llorens, S.; Sørensen, M.; Hagen, Ø. Replacement of fishmeal with plant protein in the diets of juvenile lumpfish (*Cyclopterus lumpus*, L. 1758): Effects on digestive enzymes and microscopic structure of the digestive tract. *Aquaculture* **2022**, *561*, 738601. [CrossRef]
44. Liu, Y.; Zhou, H.; Fan, J.; Huang, H.; Deng, J.; Tan, B. Assessing effects of guar gum viscosity on the growth, intestinal flora, and intestinal health of micropterus salmoides. *Int. J. Biol. Macromol.* **2022**, *222*, 1037–1047. [CrossRef]
45. Pan, S.; Yan, X.; Dong, X.; Li, T.; Suo, X.; Tan, B.; Zhang, S.; Li, Z.; Yang, Y.; Zhang, H. The positive effects of dietary inositol on juvenile hybrid grouper (♀*Epinephelus fuscoguttatus* × ♂*E. Lanceolatu*) fed high-lipid diets: Growthperformance, antioxidant capacity and immunity. *Fish Shellfish Immunol.* **2022**, *126*, 84–95. [CrossRef]
46. Zheng, W.; Sun, L.; Yang, L.; Xu, T. The circular rna circbcl2l1 regulates innate immune responses via microrna-mediated downregulation of traf6 in teleost fish. *J. Biol. Chem.* **2021**, *297*, 101199. [CrossRef]
47. Meng, X.; Shen, Y.; Wang, S.; Xu, X.; Dang, Y.; Zhang, M.; Li, L.; Zhang, J.; Wang, R.; Li, J. Complement component 3 (c3): An important role in grass carp (*Ctenopharyngodon idella*) experimentally exposed to aeromonas hydrophila. *Fish Shellfish Immunol.* **2019**, *88*, 189–197. [CrossRef]
48. Hu, Y.; Zhang, J.; Xue, J.; Chu, W.; Hu, Y. Effects of dietary soy isoflavone and soy saponin on growth performance, intestinal structure, intestinal immunity and gut microbiota community on rice field eel (*Monopterus albus*). *Aquaculture* **2021**, *537*, 736506. [CrossRef]
49. Copenhaver, M.; Yu, C.Y.; Hoffman, R.P. Complement components, c3 and c4, and the metabolic syndrome. *Curr. Diabetes Rev.* **2019**, *15*, 44–48. [CrossRef]
50. Lin, S.M.; Zhou, X.M.; Zhou, Y.L.; Kuang, W.M.; Chen, Y.J.; Luo, L.; Dai, F.Y. Intestinal morphology, immunity and microbiota response to dietary fibers in largemouth bass, micropterus salmoide. *Fish Shellfish Immunol.* **2020**, *103*, 135–142. [CrossRef]
51. Galindo-Villegas, J.; Garcia-Garcia, E.; Mulero, V. Role of histamine in the regulation of intestinal immunity in fish. *Develop. Compar. Immunol.* **2016**, *64*, 178–186. [CrossRef]
52. Dong, B.; Wu, L.; Chen, Q.; Xu, W.; Li, D.; Han, D.; Zhu, X.; Liu, H.; Yang, Y.; Xie, S.; et al. Tolerance assessment of atractylodes macrocephala polysaccharide in the diet of largemouth bass (*Micropterus salmoides*). *Antioxidants* **2022**, *11*, 1581. [CrossRef]
53. Fang, H.; Xie, J.; Liao, S.; Guo, T.; Xie, S.; Liu, Y.; Tian, L.; Niu, J. Effects of dietary inclusion of shrimp paste on growth performance, digestive enzymes activities, antioxidant and immunological status and intestinal morphology of hybrid snakehead (*Channa maculata* ♀× *Channa argus* ♂). *Front. Physiol.* **2019**, *10*, 1027. [CrossRef]
54. Li, J.; Wang, C.; Zhang, Y.; Wu, D.; Fan, Z.; Wang, L. Effect of arginine supplementation in high starch diets on intestinal digestive enzyme activities and intestinal morphology of songpu mirror carp (*Cyprinus carpio* L.). *J. Guangdong Ocean Univ.* **2020**, *41*, 39–46. [CrossRef]
55. Liu, Y.; Deng, J.; Tan, B.; Xie, S.; Zhang, W. Effects of soluble and insoluble non-starch polysaccharides on growth performance, digestive enzyme activity, antioxidant capacity, and intestinal flora of juvenile genetic of improvement of farmed tilapia (*Oreochromis niloticus*). *Front. Mar. Sci.* **2022**, *9*, 872577. [CrossRef]
56. Nayak, S.K. Role of gastrointestinal microbiota in fish. *Aquac. Res.* **2010**, *41*, 1553–1573. [CrossRef]
57. Han, F.; Xu, C.; Qi, C.; Lin, Z.; Li, E.; Wang, C.; Wang, X.; Qin, J.G.; Chen, L. Sodium butyrate can improve intestinal integrity and immunity in juvenile chinese mitten crab (*Eriocheir sinensis*) fed glycinin. *Fish Shellfish Immunol.* **2020**, *102*, 400–411. [CrossRef]
58. He, Y.; Chi, S.Y.; Tan, B.; Zhang, H.; Dong, X.H.; Yang, Q.; Liu, H.Y.; Zhang, S. Effect of yeast culture on intestinal microbiota of *litopenaeus vannamei*. *J. Guangdong Ocean Univ.* **2017**, *37*, 21–27. [CrossRef]
59. Hieu, D.Q.; Hang, B.T.B.; Lokesh, J.; Garigliany, M.M.; Huong, D.T.T.; Yen, D.T.; Liem, P.T.; Tam, B.M.; Hai, D.M.; Son, V.N.; et al. Salinity significantly affects intestinal microbiota and gene expression in striped catfish juveniles. *Appl Microb. Biotech.* **2022**, *106*, 3245–3264. [CrossRef]
60. Ghanbari, M.; Kneifel, W.; Domig, K.J. A new view of the fish gut microbiome: Advances from next-generation sequencing. *Aquaculture* **2015**, *448*, 464–475. [CrossRef]
61. Tsuchiya, C.; Sakata, T.; Sugita, H. Novel ecological niche of cetobacterium somerae, an anaerobic bacterium in the intestinal tracts of freshwater fish. *Lett. Appl. Microbiol.* **2008**, *46*, 43–48. [CrossRef]
62. Degnan, P.H.; Taga, M.E.; Goodman, A.L. Vitamin b_{12} as a modulator of gut microbial ecology. *Cell Metab.* **2014**, *20*, 769–778. [CrossRef]
63. Lin, M.; Zeng, C.X.; Jia, X.Q.; Zhai, S.W.; Li, Z.Q.; Ma, Y. The composition and structure of the intestinal microflora of anguilla marmorata at different growth rates: A deep sequencing study. *J. Appl. Microbiol.* **2019**, *126*, 1340–1352. [CrossRef]

64. Cheng, J.; Hu, J.; Geng, F.; Nie, S. Bacteroides utilization for dietary polysaccharides and their beneficial effects on gut health. *Food Sci. Human Well.* **2022**, *11*, 1101–1110. [CrossRef]
65. Zhang, S.; Wu, P.; Tian, Y.; Liu, B.; Huang, L.; Liu, Z.; Lin, N.; Xu, N.; Ruan, Y.; Zhang, Z.; et al. Gut microbiota serves a predictable outcome of short-term low-carbohydrate diet (lcd) intervention for patients with obesity. *Microb. Spectr.* **2021**, *9*, e0022321. [CrossRef]
66. Biagi, E.; Nylund, L.; Candela, M.; Ostan, R.; Bucci, L.; Pini, E.; Nikkïla, J.; Monti, D.; Satokari, R.; Franceschi, C.; et al. Through ageing, and beyond: Gut microbiota and inflammatory status in seniors and centenarians. *PLoS ONE* **2010**, *5*, e10667. [CrossRef]
67. Wang, X.; Shang, Y.; Wei, Q.; Wu, X.; Dou, H.; Zhang, H.; Zhou, S.; Sha, W.; Sun, G.; Ma, S.; et al. Comparative analyses of the gut microbiome of two fox species, the red fox (vulpes vulpes) and corsac fox (vulpes corsac), that occupy different ecological niches. *Microb. Ecol.* **2022**, *83*, 753–765. [CrossRef]
68. Deng, Y.; Guo, X.; Wang, Y.; He, M.; Ma, K.; Wang, H.; Chen, X.; Kong, D.; Yang, Z.; Ruan, Z. *Terrisporobacter petrolearius* sp. Nov., isolated from an oilfield petroleum reservoir. *Int. J. Syst. Evol. Microbiol.* **2015**, *65*, 3522–3526. [CrossRef]
69. Sampedro, A.; de Asís Ramirez, F. Leptospira, borrelia and treponema. *Encycl. Infect. Immun.* **2022**, *1*, 719–729. [CrossRef]

antioxidants

MDPI

Article

Effects of Different Dietary β-Glucan Levels on Antioxidant Capacity and Immunity, Gut Microbiota and Transcriptome Responses of White Shrimp (*Litopenaeus vannamei*) under Low Salinity

Yanbing Qiao, Li Zhou, Yayu Qu, Kunyu Lu, Fenglu Han * and Erchao Li *

Key Laboratory of Tropical Hydrobiology and Biotechnology of Hainan Province, Hainan Aquaculture Breeding Engineering Research Center, College of Marine Sciences, Hainan University, Haikou 570228, China

* Correspondence: flhan@hainanu.edu.cn (F.H.); ecli@bio.ecnu.edu.cn (E.L.)

Abstract: β-Glucan could significantly improve the antioxidant capacity of aquatic animals. The effects of different dietary levels (0 (control), 0.05, 0.1, 0.2 or 0.4%) of β-glucan on the growth, survival, antioxidant capacity, immunity, intestinal microbiota and transcriptional responses of *Litopenaeus vannamei* under low salinity (≤3) were investigated. The dietary growth trial lasted 35 days (initial shrimp 0.26 ± 0.01 g). The results indicated that the growth performance of the 0.1% and 0.2% groups was significantly better than that of the control group. A second-order polynomial regression analysis of growth performance against dietary β-glucan indicated that the optimal dietary β-glucan level was 0.2% of dry matter. The digestive enzyme activity of the hepatopancreas was enhanced with increasing β-glucan levels. The antioxidant and nonspecific immunity capacities of the hepatopancreas were also enhanced in the 0.1% group. The α-diversity index analysis of the intestinal microbiota showed that the intestinal microbial richness of *L. vannamei* increased in the 0.1% group. The relative abundance of Proteobacteria decreased in the 0.1% group compared with the control group. The transcriptome results indicate that the prebiotic mechanisms of β-glucan include upregulating the expression of nonspecific immune genes and osmoregulation genes and activating KEGG pathways associated with carbohydrate metabolism under low-salinity stress. These results suggested that dietary supplementation with β-glucan markedly increased growth performance and alleviated the negative effects of low-salinity stress by contributing to the activity of biochemical enzymes and enriching carbohydrate metabolism in *L. vannamei*.

Keywords: *Litopenaeus vannamei*; aquaculture; low salinity; β-glucan; transcriptome

Citation: Qiao, Y.; Zhou, L.; Qu, Y.; Lu, K.; Han, F.; Li, E. Effects of Different Dietary β-Glucan Levels on Antioxidant Capacity and Immunity, Gut Microbiota and Transcriptome Responses of White Shrimp (*Litopenaeus vannamei*) under Low Salinity. *Antioxidants* **2022**, *11*, 2282. https://doi.org/10.3390/antiox11112282

Academic Editors: Bo Liu, Changyou Song and Cunxin Sun

Received: 22 October 2022
Accepted: 16 November 2022
Published: 18 November 2022

1. Introduction

White shrimp (*Litopenaeus vannamei*) can tolerate salinities ranging from 0.5 to 50 due to its strong ability to maintain osmosis and ion regulation, making it a widely farmed shrimp worldwide [1,2]. In 2021, freshwater aquatic animal production in China reached 665,202 t, with the freshwater production of *L. vannamei* accounting for 35% of the total production [3]. Although *L. vannamei* can be cultured on a large scale in freshwater, this factor does not mean that white shrimp can produce an optimal physiological response. Shrimp reared at low salinity can experience passive effects, including low survival (53.3%), which was observed at a salinity of 5, and increases in oxygen consumption and feed coefficients were reported [4,5]. Some research also documented that low salinity could reduce innate immune parameters [6,7], increase the toxicity of ammonia (NH_3) and nitrite (NO_2^-) [8,9], decrease resistance against pathogens [7,10] and even destroy the structure of the intestinal microbiota during aquatic animal culture [11,12]. These negative effects ultimately lead to the poor aquaculture production of *L. vannamei*. Therefore, the

exploitation of novel strategies to overcome the above problems is particularly important for the rapid development of the *L. vannamei* aquaculture industry. Nutritive regulation is an effective strategy to alleviate the adverse effects of low-salt stress. Previous studies have documented that dietary mineral supplements, proteins and prebiotics can improve growth performance [12–16] and enhance the antistress ability and immune defense ability of *L. vannamei* to alleviate the unfavorable effects of low salinity.

Prebiotics are commonly added to feed to improve the immune activity of white shrimp to environmental stress [13,17–19]. Among the many prebiotics, β-glucan is commonly used as an immunostimulant in the aquaculture industry [20]. β-Glucan is a complex polysaccharide present in grains, seaweeds, mushrooms, yeast and certain bacteria, distinguished by the presence of pathogen-associated molecular patterns (PAMPs) in molecules with immunomodulatory activity [21]. β-Glucan can improve the immunity and disease resistance of crustaceans, including tiger shrimp (*Penaeus monodon*) [22] and banana shrimp (*Penaeus merguiensis*) [23]. Feeding *L. vannamei* 0.2% β-glucan has positive effects on growth performance [24]. Dietary 0.05–0.20% β-glucan can improve the tolerance of Golden Pompano (*Trachinotus ovatus*) to low-salt stress [25]. Dietary β-glucans could alter the dominance of the intestinal microbiota structure in *L. vannamei* [26,27] and turbot (*Scophthalmus maximus*) [28]. Although studies have confirmed that β-glucan could promote nonspecific immune defense and improve low-salt adaptation [13], previous research involving the optimal dosage of β-glucan has not presented consistent results for *L. vannamei* under environmental stress. In addition, the effects of prebiotics on aquaculture are primarily focused on their growth and physiological and biochemical functions, but little is known about the prebiotic mechanism of prebiotics at the molecular level in shrimp under low salinity.

This study aimed to explore the optimal supplementation level of β-glucan as a prebiotic under low salinity. This study examined the effects on the growth, antioxidant capacity, immunity and intestinal microflora of *L. vannamei* under low salinity ($\leq$3). The results of transcriptome and microbiology techniques further reveal the prebiotic mechanism of β-glucan in alleviating the unfavorable effects of low salinity.

2. Materials and Methods

2.1. Experimental Diets

The basic feed formula and nutrients are displayed in Table 1. The basic diet was formulated according to the nutritional requirements of *L. vannamei* and previous research [13]. The diet was supplemented with isonitrogenous and isolipids containing different levels (0, 0.05, 0.1, 0.2 or 0.4%) of β-glucan. Yeast (1,3)-(1,6)-β-glucan with a purity of 88% was the experimental β-glucan source. The diet material was ground with a grinder and filtered with a 60-mesh screen. All single raw materials were thoroughly mixed, and distilled water was added to make a dough, which was extruded into 2 mm diameter pellets by an extruder (CD4-1TS extruder, Guangzhou Huagongguang Electromechanical Technology Co., Ltd., Guangzhou, China). The prepared pellets were air-dried. After drying, the pellets were classified into different sizes with the most suitable sieve (12, 14, 16 and 20 mm) to ensure effective feeding and stored at −20 °C.

2.2. Experimental Design and Breeding

Larvae of *L. vannamei* (P5) were purchased from a commercial shrimp farm (Wenchang, China). During the acclimation period, larvae were fed a commercial diet (Alpha feed Co., Ltd., Protein 48%, Shenzhen, China) at 4% of their body weight per day. All shrimp were acclimated to a salinity of 3 at a rate of 2% reduction per day by adding fresh water. Fresh water was adequately aerated prior to adjusting the salinity of the seawater.

After finishing acclimation, shrimp (0.26 ± 0.01 g) were randomly separated into five groups: 0% β-glucan (control), 0.05% β-glucan (0.05%), 0.1% β-glucan (0.1%), 0.2% β-glucan (0.2%) and 0.4% β-glucan (0.4%), divided into five groups in 20 tanks (60 × 30 × 36 cm) with 20 shrimp, each with four replicates (October to November 2020). During the five-week experiment, daily water exchange was carried out at a rate of 1/2 the culture water volume

using low-salinity (≤3) water, and residual food and feces were removed. The temperature (27 ± 2 °C), pH (7.5–8.0), total nitrogen concentration (<0.03 mg/L) and dissolved oxygen (≥7 mg/L) were maintained and checked twice a week throughout the experimental session. Shrimp were fed three times a day (7:00, 12:00 and 18:00).

Table 1. Dietary formulations and proximate composition of the experimental diets (% dry matter).

Ingredients (%)	Dietary β-Glucan Concentrations				
	0	**0.05%**	**0.1%**	**0.2%**	**0.4%**
Fish meal	26	26	26	26	26
Soybean meal	28	28	28	28	28
Com starch	23	23	23	23	23
Shrimp meal	4	4	4	4	4
Calcium dihydrogen phosphate	1.5	1.5	1.5	1.5	1.5
Vitamin premix [a]	2	2	2	2	2
Mineral premix [b]	2	2	2	2	2
Choline chloride	1	1	1	1	1
Fish oil	2.5	2.5	2.5	2.5	2.5
Soybean oil	2.5	2.5	2.5	2.5	2.5
Soybean lecithin	1	1	1	1	1
Cholesterol	0.5	0.5	0.5	0.5	0.5
Carboxymethylcellulose (CMC)	3	3	3	3	3
Butylated hydroxytoluene (BHT)	0.1	0.1	0.1	0.1	0.1
Microcrystalline cellulose	2.9	2.85	2.8	2.7	2.5
β-1,3-Glucan [c]	0	0.05	0.1	0.2	0. 4
Total	100	100	100	100	100
Nutrient levels (%)					
Crude protein	35.2	35.4	35.5	35.5	35.4
Crude lipid	7.6	7.6	7.6	7.6	7.6
Ash	10.3	10.4	10.7	10.7	10.6
Moisture	9.2	9.2	9.2	9.2	9.3

[a] Vitamin premix (g/kg premix): vitamin A acetate (500,000 IU/g), 0.960; L-ascorbyl-2-polyphosphate 35% Active C, 71.420; folic acid, 0.360; biotin, 5.000; riboflavin, 6.000; DL Ca-pantothenate, 10.000; pyridoxine HCl, 2.000; 1% vitamin B12, 0.400; thiamin HCl, 1.000; Menadione, 4.000; DL-alpha-tocopheryl acetate (250 IU/g), 16.000; nicotinic acid, 10.000; vitamin D (500,000 IU/g), 1.600; defatted rice bran, 871.260. [b] Mineral premix (g/kg premix): zinc sulfate monohydrate, 20.585; calcium iodate, 0.117; cupric sulfate pentahydrate, 0.625; manganous sulfate monohydrate, 1.625; magnesium sulfate monohydrate, 39.860; cobalt chloride, 0.010; ferrous sulfate monohydrate, 11.179; sodium selenite, 0.025; calcium hydrogen phosphate dihydrate, 166.442; defatted rice bran, 759.532. [c] β-Glucan was purchased from Xi'an Ruilin Biotechnology Co., Ltd., Xi'an, China.

2.3. Sampling and Growth Performance

After completing the 35-day dietary trial, all shrimp fasted for 24 h before sampling. Before sampling began, the shrimp were counted, and then they were anesthetized in an ice-water bath. The body length and body weight were randomly measured. The middle intestines and whole hepatopancreas were aseptically dissected and placed into a 1.5 mL sterile centrifuge tube, and the two tissues were prepared for the biochemical and multiomics analyses. All tube samples were immediately stored in liquid nitrogen and transferred to −80 °C for storage until further analyses. Three intestine samples were pooled into one sample per tank for microbiota analysis. Hepatopancreas samples were examined for digestive enzyme, antioxidant and immune enzyme activities. Growth-related indicators were evaluated using the following formulas:

$$\text{Survival (\%)} = (\text{final shrimp number}/\text{initial shrimp number}) \times 100$$

$$\text{Weight gain (WG, \%)} = (\text{final weight} - \text{initial weight})/\text{initial weight} \times 100$$

$$\text{Specific growth rate (SGR, \% day)} = 100\ (\text{Ln final weight} - \text{Ln initial weight})/\text{number of days}$$

2.4. Biochemical Assay

Eight samples of the hepatopancreas (1 g) from two shrimp per tank per treatment were accurately weighed, transferred to sterile centrifuge tubes and homogenized in a cold 0.86 saline solution (1:9, w/v) using a tissue grinder (Shanghai Jingxin, Shanghai, China) (60 Hz, 30 s) and centrifuged at 1500× g (4 °C/15 min, 3–18 KS, Sigma, Osterode, Germany). After centrifugation, the supernatant was collected to determine the total protein concentration, digestive enzymes (protease, amylase and lipase), total antioxidant capacity (T-AOC), catalase (CAT), malondialdehyde content (MDA), superoxide dismutase (SOD), acid phosphatase (ACP) and alkaline phosphatase (AKP). These biochemical enzyme activities in the hepatopancreas were measured according to procedures described in [29,30]. All hepatopancreatic biochemical indices were determined using commercial assay kits (Nanjing Jiancheng Bioengineering Institute, Nanjing, China), and the operating procedures were used according to the manufacturer's instructions.

2.5. Intestinal Microbiota Analysis

Total genomic DNA was extracted from intestinal samples using the TAB/SDS method. DNA quality was measured using a NanoDrop spectrophotometer (Thermo, Wilmington, DE, USA). Generation sequencing was performed on an Illumina HiSeq system according to the protocol of Majorbio Biopharm Technology Co., Ltd. (Shanghai, China). The hypervariable V3–V4 region of the 16S rRNA gene was amplified by using primers 338 (forward 5-ACTCCTACGGGAGGCAGCA-3) and 806 (reverse 5-GGACTACHVGGGTWTCTAAT-3). A TruSeq® DNA PCR-free Sample Preparation Kit (Illumina, CA, USA) was used to construct the library, and index codes were added. Finally, the libraries were carried out on an Illumina HiSeq 2500 platform. All statistical analyses of the results were performed using the R package software (version 2.11 http://sourceforge.net/projects/rdp-classifier/; accessed on 10 January 2021). Alpha-diversity indices (ACE, Chao1, Simpson, Shannon and Observed_species) were determined using QIIME software (http://www.mothur.org/wiki/Calculators; accessed on 10 January 2021), and statistical analyses were performed using one-way analysis of variance (ANOVA) (SPSS 23.0). The raw sequences of intestinal microbiota in this study were submitted to Sequence ReadArchive (SRA) under GenBank database number PRJNA842883.

2.6. Transcriptomic Analysis

Total RNA was extracted from the hepatopancreas of individual shrimp (three samples per treatment) using TRIzol Reagent (Ambion, CA, USA). The quality and concentration of the RNA were determined using a 1% agarose gel on a 2100 Bioanalyzer (Agilent Technologies, Palo Alto, CA, USA) and ND-2000 (Thermo, Wilmington, DE, USA). One microgram of total RNA per sample was used to construct a sequencing library using a TruSeq RNA sample preparation kit from Illumina (San Diego, CA, USA). The prepared cDNA libraries were sequenced on the Illumina HiSeq™ 4000 platform at Majorbio Bio-Pharm Technology Co., Ltd. (Shanghai, China). Raw paired-end reads were quality-checked with default parameters. Clean reads were individually screened using Trimmomatic software (http://www.usadellab.org/cms/uploads/supplementary/Trimmomatic; accessed on 13 January 2021). Further, total clean reads were separately aligned to the reference *L. vannamei* genome in orientation mode using TopHat (http://tophat.cbcb.umd.edu; accessed on 13 January 2021). The expression levels of unigenes were calculated according to the fragments per kilobase of transcripts per million reads (TPM) to identify differentially expressed genes (DEGs) between different samples. RSEM was used to estimate gene abundances (http://deweylab.biostat.wisc.edu/rsem/; accessed on 10 January 2021). Essentially, differential expression analysis was performed using DESeq2/DEGseq/EdgeR with a Q value of 0.05. DEGs with $|\log2FC| > 1$ and Q value ≤ 0.05 (DESeq2 or EdgeR)/Q value ≤ 0.001 (DEGseq) were considered DEGs. Kyoto Encyclopedia of Genes and Genomics (KEGG) pathway analysis of the DEGs was performed using KOBAS software (http://kobas.cbi.pku.edu.cn/home.do; accessed on 10 January 2021). In addition, KEGG

enrichment analyses were conducted with Bonferroni-corrected p values < 0.05. A false discovery rate < 0.01 and FC > 2 were considered for the significance analysis. The RNA-seq data were deposited in the NCBI SRA database (PRJNA846923).

2.7. Statistical Analysis

To clarify the mechanism of dietary β-glucan on growth, biochemical and omics analyses were performed. SPSS 23 software (IBM, New York, NY, USA) was used to carry out all statistical analyses. The data are expressed as the mean ± standard error (mean ± SE). One-way ANOVA was chosen to determine the significant effects among different groups, followed by multiple comparisons by Duncan's multiple comparison test. The statistical significance level was set at $p < 0.05$. In addition, to determine whether the effect was quadratic, a follow-up trend analysis using the method of orthogonal polynomial contrasts was performed using SPSS 23. The assumptions of normality and homoscedasticity were confirmed before conducting any statistical analyses. The relationship between WG, SGR and dietary β-glucan was estimated through second-order polynomial regression [31], and the optimal dietary β-glucan requirement was also evaluated.

3. Results

3.1. Growth Performance

The growth performance results of the 35-day trial are shown in Table 2. There was no significant difference in survival among the groups ($p > 0.05$). The growth performance of shrimp was the highest in the 0.2% group, which was significantly higher than that of the other groups ($p < 0.05$) but not significantly different from that of the 0.1% group ($p > 0.05$). Furthermore, a second-order polynomial regression analysis of WG and SGR against dietary β-glucan indicated that the ideal dietary β-glucan level was 0.2–0.23% of dry matter (Figure 1).

Table 2. Regression analysis of the growth performance of Juvenile *L. vannamei* fed different dietary β-glucan levels for 5 weeks.

Dietary β-Glucan Levels (%) [a]	IW (g)	FW (g)	WG (%)	SGR (% Day^{-1})	Survival (%)
0	0.27	1.91 ± 0.07 ^{a}	634.08 ± 35.42 ^{a}	5.68 ± 0.14 ^{a}	90 ± 4.56
0.05	0.27	2.01 ± 0.09 ^{a}	663.15 ± 26.37 ^{ab}	5.80 ± 0.10 ^{ab}	90 ± 2.04
0.1	0.26	2.23 ± 0.09 ^{b}	756.20 ± 43.09 ^{bc}	6.12 ± 0.15 ^{bc}	95 ± 3.54
0.2	0.25	2.36 ± 0.04 ^{b}	845.86 ± 22.82 ^{c}	6.42 ± 0.07 ^{c}	90 ± 1.44
0.4	0.25	1.92 ± 0.02 ^{a}	710.36 ± 21.32 ^{ab}	5.98 ± 0.07 ^{ab}	92.5 ± 1.25
ANOVA (p value)	0.533	0.001	0.002	0.003	0.444
SOP (n = 4)					
Adj. R^2		0.6423	0.5365	0.0257	
p Value		<0.001	<0.001	<0.001	

Note: [a] Values represent the means of four replicate tanks (n = 4). Different superscript lowercase letters within a column indicate significant differences ($p < 0.05$). IW, initial weight; FW, final weight; WG, weight gain; SGR, specific growth rate; SOP, second-order polynomial; Adj. R^2, adjusted R-squared.

3.2. Hepatopancreatic Digestive Enzyme Activity

The hepatopancreatic digestive enzyme activities are shown in Figure 2 and Table 3. Hepatopancreas protease and lipase activities were significantly higher in the 0.1%, 0.2% and 0.4% groups than in the control group ($p < 0.05$) (Figure 2A,B). The hepatopancreas amylase activity was also significantly increased with the addition of β-glucan compared with the control group ($p < 0.05$) (Figure 2C).

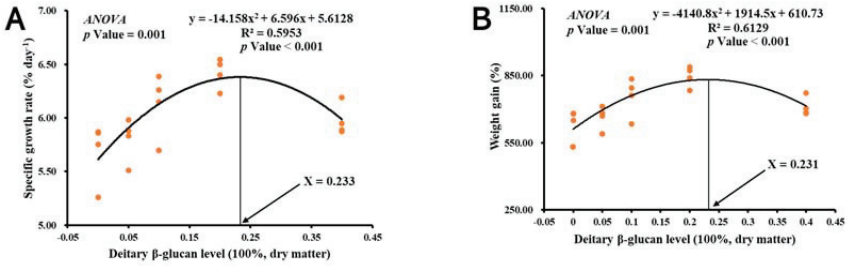

Figure 1. Relationships of (**A**) specific growth rate and (**B**) weight gain with dietary β-glucan levels based on second−order polynomial regression analysis of Juvenile *L. vannamei*, where Xopt represents the dietary β-glucan level (n = 4).

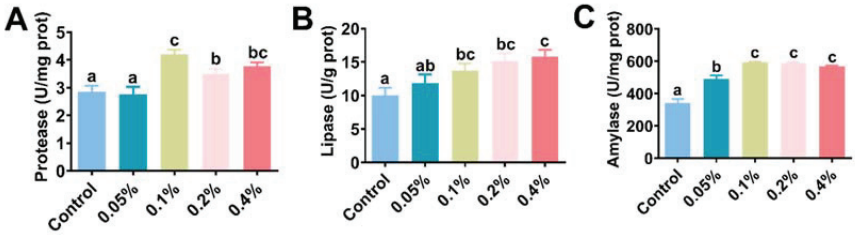

Figure 2. Effects of different doses of β-glucan on the (**A**) protease, (**B**) lipase and (**C**) amylase enzyme activities in Juvenile *L. vannamei*. Different letters indicate significant differences ($p < 0.05$) among groups. All data are expressed as the mean ± SE (n = 4).

Table 3. Regression analysis of biochemical assays in the hepatopancreas of Juvenile *L. vannamei* fed different dietary β-glucan levels.

Enzyme [a]	Regression Analysis (n = 4) [b]		Enzyme	Regression Analysis (n = 4)	
	SOP			SOP	
	Adj. R^2	p Value		Adj. R^2	p Value
T-AOC	0.3935	0.046	Protease	0.326	0.035
SOD	0.3979	0.695	Lipase	0.5556	0.002
CAT	0.056	0.567	Amylase	0.8093	0.005
MDA	0.2971	0.023			
ACP	0.7077	0.765			
AKP	0.2194	0.193			

Note: [a] T-AOC, total antioxidant capacity; SOD, superoxide dismutase; CAT, catalase; MDA, malondialdehyde content; ACP, acid phosphatase; AKP, alkaline phosphatase. [b] SOP, second-order polynomial; Adj. R^2, adjusted R-squared.

3.3. Antioxidant Capacity and Immunity

The hepatopancreatic antioxidant performance and nonspecific immune response results are shown in Figure 3 and Table 3. The T-AOC enzyme activity in the hepatopancreas of shrimp in the 0.1%, 0.2% and 0.4% groups was significantly higher than that in the control group ($p < 0.05$) (Figure 3A). The SOD enzyme activity in the hepatopancreas of shrimp in the 0.1% group was significantly higher than that in the other groups ($p < 0.05$) (Figure 3B). The CAT enzyme activity in the hepatopancreas of shrimp in the 0.1% group was significantly lower than that in the other groups ($p < 0.05$) but not significantly different from that in the 0.4% group ($p > 0.05$) (Figure 3C). The MDA content of the hepatopancreas in shrimp in the 0.2% group was significantly increased compared with that in shrimp in the other groups ($p < 0.05$) but was not significantly different from that in shrimp in the 0.4% group ($p > 0.05$) (Figure 3D). The ACP enzyme activity in the hepatopancreas of shrimp in the 0.1% and 0.2% groups was significantly higher than that in the other groups

($p < 0.05$) (Figure 3E). The AKP enzyme activity in the hepatopancreas of shrimp in the 0.05% and 0.1% groups was significantly higher than that in the other groups ($p < 0.05$) (Figure 3F).

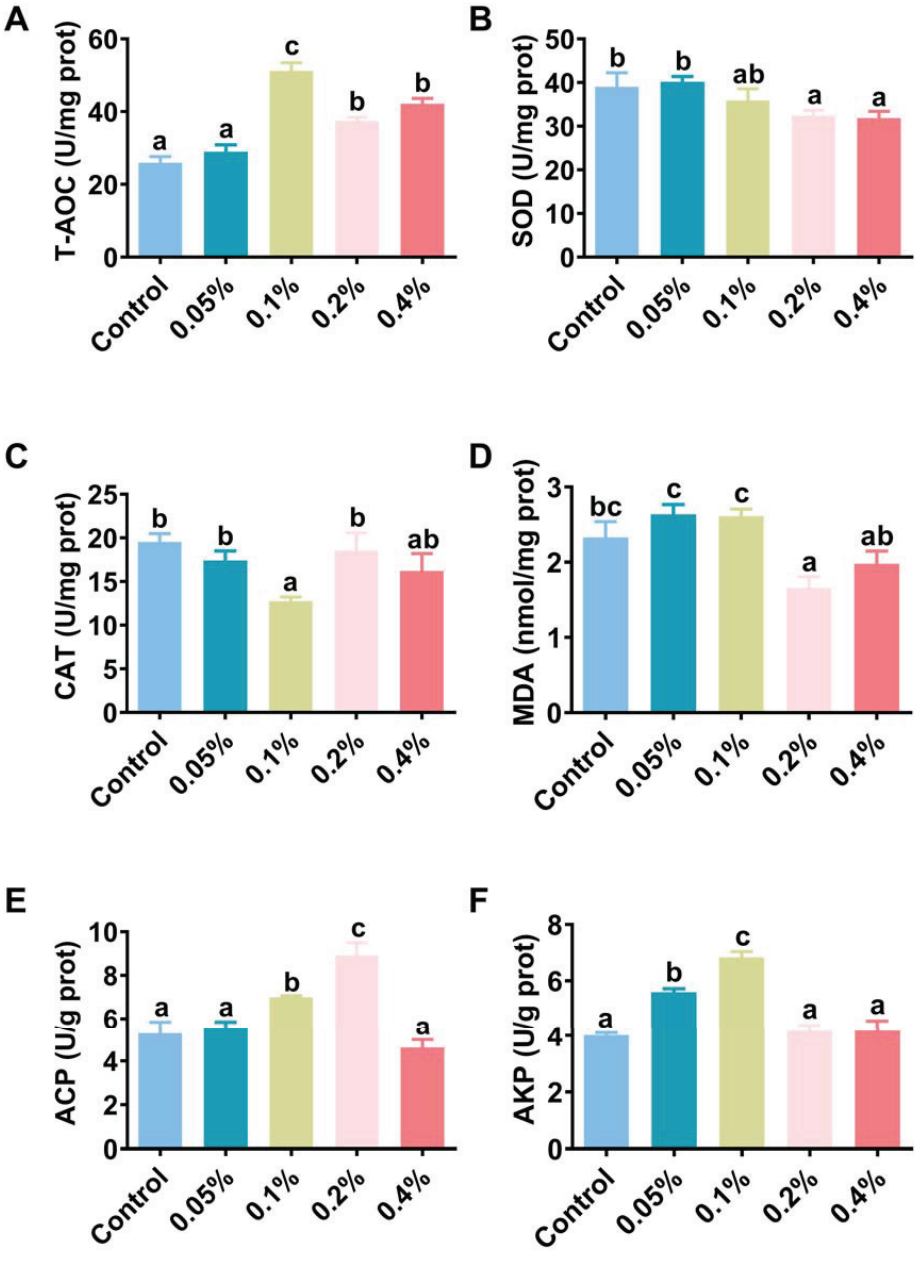

Figure 3. Effects of different doses of β-glucan on the (**A**) total antioxidant capacity, (**B**) superoxide dismutase, (**C**) catalase, (**D**) malondialdehyde content, (**E**) acid phosphatase and (**F**) alkaline phosphatase of Juvenile *L. vannamei*. Different letters indicate significant differences ($p < 0.05$) among groups. All data are expressed as the mean ± SE ($n = 4$).

3.4. Intestinal Microbiota Analysis

In this study, the analysis of the intestinal microflora showed that a total of 2,384,213 high-quality sequences were acquired in all samples. Each sample had an average of 99,342 sequences. The observed species ranged from 338.00 to 828.25. Supplementation with 0.1% β-glucan significantly increased the alpha-diversity indices (Shannon and Observed_species) compared with those of the other groups ($p < 0.05$), as shown in Figure 4 and Table S1. At the phylum level, the most dominant phylum was Proteobacteria, followed by Firmicutes, Actinobacteriota and Bacteroidota in all samples (Figure 5A,B), and Firmicutes and Actinobacteriota were dominant in the 0.1% group (Figure 5C and Table S1). Supplementation with 0.1% significantly induced an increase in the relative abundance of intestinal microbial species compared with those of the other groups of *L. vannamei* ($p < 0.05$). At the genus level, the relative abundances of Vibrio, Rheinheimera and Demequina in the 0.1% group were significantly lower than those in the other groups, but the relative abundance of Lacrobacillus in the 0.1% group was significantly higher than those in the other groups (Figure 5D–F and Table S1). In addition, the principal coordinate analysis (PCoA) cluster analysis indicated that the overall structure of the intestinal microflora in the 0.1% group was significantly different compared with the control group (Figure 6).

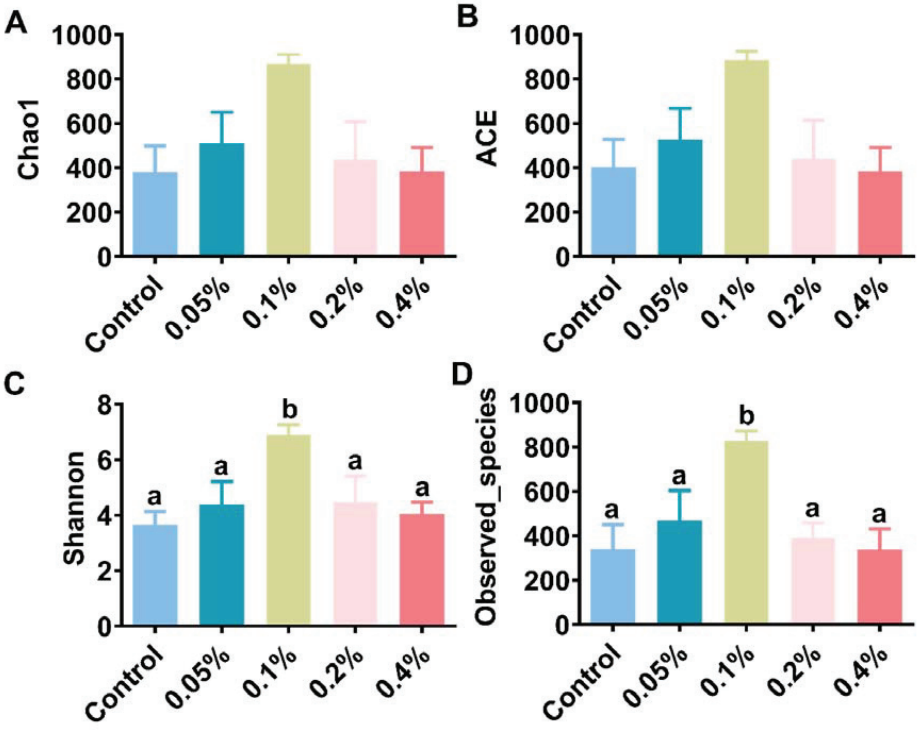

Figure 4. Effects of different doses of β-glucan on the alpha-diversity using (**A**) Chao1 estimator, (**B**) ACE estimator, (**C**) Shannon estimator and (**D**) observed species in gut microbiota in Juvenile *L. vannamei*. Different letters indicate significant differences ($p < 0.05$) among groups. All data are expressed as the mean ± SE ($n = 4$).

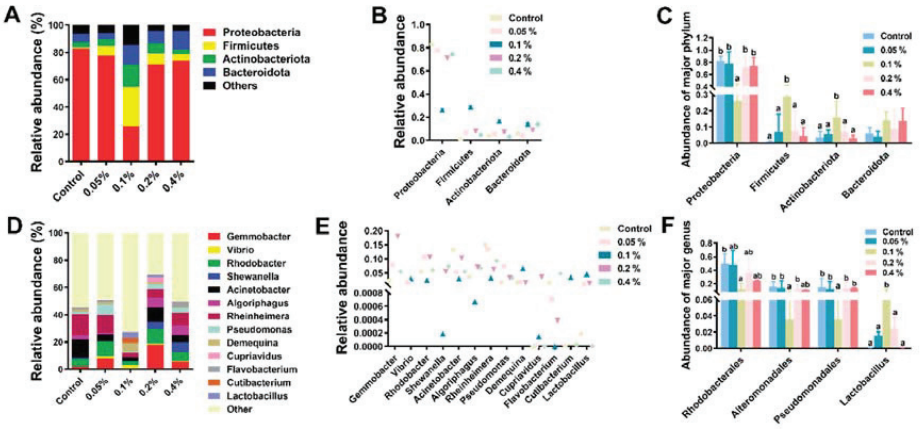

Figure 5. Effects of different doses of β-glucan on the gut microbiota composition of Juvenile *L. vannamei* at the phylum and genus levels. (**A**) Microbiota composition at the phylum level with the relative abundance of the top four. (**B**) Relative abundance of gut microbiota at the phylum level. (**C**) Differences in the relative abundance of phylum taxa among groups. (**D**) Microbiota composition at the genus level with the relative abundance of the top thirteen. (**E**) Relative abundance of gut microbiota at the genus level. (**F**) Differences in the relative abundance of genus taxa among groups. Different letters indicate significant differences ($p < 0.05$) among groups. All data are expressed as the mean ± SE ($n = 4$).

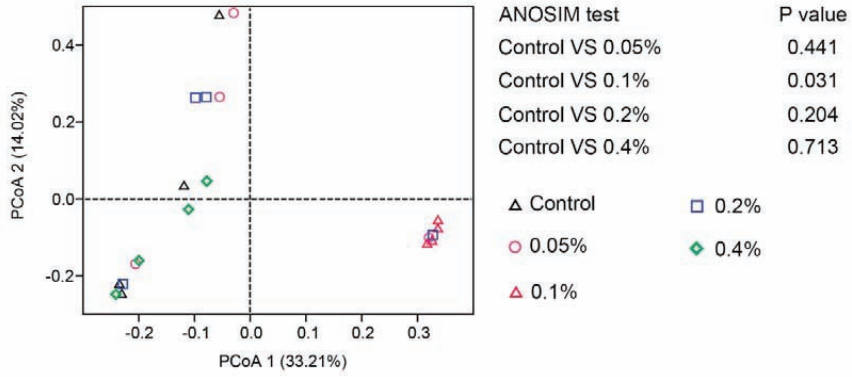

Figure 6. Effects of different doses of β-glucan on the β−diversity of gut microbiota in Juvenile *L. vannamei*. PCoA of the microbiota at the OTU level based on Jaccard distances. Analysis of similarity (ANOSIM) was performed to evaluate the overall differences in bacterial community structure based on Jaccard distance ($n = 4$).

3.5. Transcriptome Analysis

Among the five treatment groups, 2354 differentially expressed genes (DEGs) were identified. As shown in Figure 7, a total of 27 DEGs were shared among the treatment groups, while 32, 23, 300 and 1114 DEGs were significantly expressed only in the control vs. 0.05% group, control vs. 0.1% group, control vs. 0.2% group and control vs. 0.4% group, respectively (Figure 7A,B). A total of 183 DEGs were found in the control vs. 0.05% group, including 94 upregulated and 89 downregulated genes; 134 DEGs were found in the control vs. 0.1% group, including 68 upregulated and 66 downregulated genes; 902 DEGs were found in the control vs. 0.2% group, including 467 upregulated and 435 downregulated genes; and 1801 DEGs were found in the control vs. 0.4% group, including 808 upregulated and 993 downregulated genes (Figure 7C). Compared with the control group, there were

27 differentially expressed genes treated with different doses of β-glucan. Specific information on these 27 common DEGs is shown in Table S2. Significant DEGs were studied using KEGG pathway enrichment statistics to study the important functional pathways of DEGs (Table S3). The phenoloxidase gene, antimicrobial peptide gene and $Na^+/K^+/2Cl^-$ cotransporter gene expression levels were significantly upregulated in the β-glucan addition group. The KEGG analyses of DEGs showed that dietary β-glucan under low salinity also regulated signal transduction pathways (RIG-I-like receptor, PPAR, JAK-STAT, prolactin, neurotrophic factor, AMPK, Toll-like receptor, TNF and sphingolipid) and activated KEGG pathways associated with carbohydrate metabolism (starch and sucrose metabolism, carbohydrate digestion and absorption and galactose metabolism).

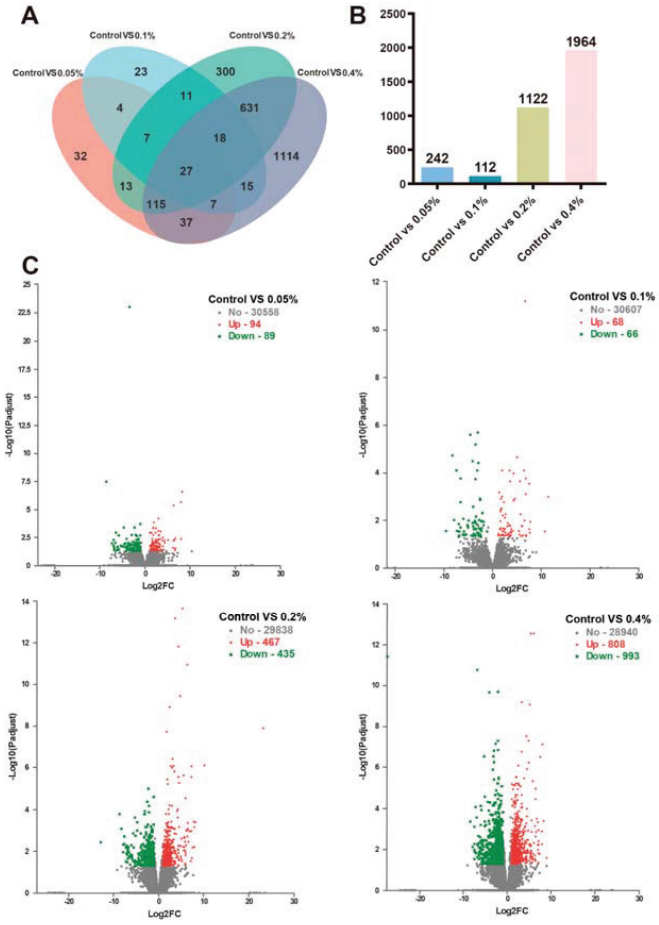

Figure 7. Changes in transcriptome levels of differentially expressed genes with different doses of β-glucan in Juvenile *L. vannamei*. (**A**,**B**) The Venn diagram shows the number of common or unique differential genes among groups (0.05%, 0.1%, 0.2% and 0.4%) compared with the control group. (**C**) Volcano map showing the number of upregulated and downregulated genes in the control vs. 0.05%, control vs. 0.1%, control vs. 0.2% and control vs. 0.4% groups; the *X*-axis is represented by log2 (fold change), and the larger the variation, the wider the distribution; the *Y*-axis is represented by −log10 (Padj), a negative logarithm of the adjusted *p*-value; the green dots represent downregulated genes, the red dots represent upregulated genes, and the gray dots represent genes that do not differ significantly ($n = 4$).

4. Discussion

L. vannamei can adapt to extensive environmental salinity fluctuations; its optimal growth rate occurs at ≥20 salinity [11], and it faces hyposaline stress under low salinity [32]. Various prebiotics have been proven to alleviate hyposaline stress; for instance, inulin can cope with low-salinity stress in shrimp [19]. Dietary β-glucan significantly increased the WG, SGR and PO activity of Pacific white shrimp [27] and post-larval *P. monodon* [33]. This study revealed that 0.1% and 0.2% β-glucan increased the growth performance, protease activity, lipase activity and amylase activity of *L. vannamei* under low-salinity stress. β-Glucan could improve the growth of *L. vannamei*, which could be due to the increased digestive capacity and the absorption and accumulation of nutrients. As with almost all functional substances, β-glucan is often underutilized in practical farming due to a lack of scientific strategies for its use, but this study showed that β-glucan improved growth performance at low salinity, suggesting that β-glucan has superior production applications. Similar results showed that the addition of 0.02% β-glucan (0.04%) increased the weight gain of *L. vannamei* [13]. Prebiotic xylooligosaccharides fed to crucian carp (*Carassius auratus*) caused an increase in digestive enzymes [34], while mannanoligosaccharides significantly enhanced digestive enzymes in *Pangasianodon hypophthalmus* [35]. Multiple stressors, such as low salinity, nitrite and ammonia, can produce excess reactive oxygen species (ROS) that damage the organism [36,37]. SOD and CAT enzymes, as antioxidant enzymes, can remove excess ROS, and GPx also has an efficient antioxidant capacity [38]. This study demonstrated that the antioxidant enzyme activity was increased due to supplementation with β-glucan compared with the control. Similarly, this research showed that 0.02% and 0.04% β-glucan could have a positive effect on SOD and GPX enzyme activities in *L. vannamei* [13]. Dietary β-glucan enhanced the SOD activity in *Penaeus monodon* [27,39], and similar results were found with the addition of inulin in Pacific white shrimp [19]. These results suggest that dietary β-glucan could reduce oxidative damage caused by low-salinity stress by increasing the activities of antioxidant enzymes. In addition, this experiment showed that 0.1% β-glucan helped to increase the ACP and AKP activities in *L. vannamei*. ACP and AKP are capable of assisting, modulating and accelerating phagocytosis [40]. A previous study also showed that the oral administration of β-glucan enhanced ACP activity [41]. In this study, the significant activation of SOD, ACP and AKP activities clearly illustrates that β-glucan can be used as an immunostimulatory agent in Pacific white shrimp, which is beneficial for improving the immunity of shrimp in a low-salinity environment.

The effects of prebiotics are closely related to the dosage in aquatic animals [17–19]. In this study, the growth performance of *L. vannamei* increased with the additive dose (0–0.2%) but started to decrease when β-glucan was 0.4%. This indicated that there was no linear relationship between the growth-promoting effect of prebiotics on *L. vannamei* and the additive dose. In addition to the growth performance indicators, other indicators, such as digestive enzyme activity, total antioxidant capacity, malondialdehyde content, AKP, ACP activity and so on, all showed the same phenomenon. A previous study found that the addition of 0.064% β-glucan improved the weight gain of *L. vannamei* [42]. Moreover, 0.02% dietary β-glucan showed higher levels of immune gene expression in *L. vannamei* [13]. In this study, based on the growth performance, oxidation resistance and immune indices, it was speculated that the optimal β-glucan additive level in the diet of *L. vannamei* in low-salinity culture conditions was 0.1%. It should be noted that the most appropriate prebiotic dose may vary depending on the species of aquatic animal, the type of prebiotic, the structure and dietary conditions, so there is no simple linear relationship.

The intestine not only plays a vital role in nutrient absorption and metabolic activity but also improves environmental stress and provides a defense against pathogens [43]. Intestinal microorganisms and their metabolites can directly or indirectly affect the physiological functions of animals, including metabolism and immunity [44]. Recently, most research on Pacific white shrimp has paid more attention to the relationships between shrimp health and intestinal microbiota [45,46]. Dietary prebiotics can modulate the microbial population in the intestine of the host [47]. This study showed that adding 0.1%

β-glucan significantly increased the intestinal microflora values of α-diversity indices. The effect of prebiotics on the α-diversity of intestinal flora in aquatic animals is still controversial. Some studies have shown that inulin and β-glucan have no effect on the α-diversity of intestinal flora in white shrimp [13,19]. However, some studies have documented that prebiotics increase the α-diversity of intestinal flora [48]. Some results suggested that prebiotics enhanced immunity in the host by stimulating the growth of probiotics such as *Lactobacillus* and *Bacillus* [49,50]. This study showed that the dominant phylum and genus in the intestine were significantly changed by the addition of β-glucan. The addition of 0.1% β-glucan could affect the bacterial community in the intestine of *L. vannamei* by increasing the relative abundance of *Lactobacillus*, thereby maintaining a more stable intestinal environment and resisting the invasion of pathogens [45]. The vast majority of *Lactobacillus* species are considered probiotics for aquatic animals [51]. Therefore, dietary β-glucan could have beneficial effects by promoting the occupancy of these intestinal probiotics in the host. Furthermore, we hypothesize that the practical value of β-glucan in aquaculture is mainly through intestinal microbiota and physiological changes that synergistically improve the physiological health of farmed shrimp.

Transcriptome sequencing technology is a significant approach for quantifying transcriptional expression in nonmodel species [52,53]. This strategy has been used in the environmental stress response, such as different salinities [54] and temperatures in *L. vannamei* [55]. In this study, differential gene expression analysis revealed that there were 27 common differential gene changes between the β-glucan groups at different doses and the control group, and these differential gene changes ranged from 1 to 3. The number of upregulated DEGs was much larger than that of downregulated DEGs. This result indicated that β-glucan alleviated low-salinity stress mainly by activating gene expression levels in *L. vannamei*. The expression levels of phenoloxidase genes and antimicrobial peptide genes were significantly upregulated with β-glucan addition. Phenol oxidase activity has a positive correlation with disease [56]. Shrimp encode and produce antimicrobial peptides (AMPs) as part of their innate immune response [57]. These results suggest that dietary β-glucan could enhance the nonspecific immune function of white shrimp under low salinity by enhancing the expression of immune-related genes, thus producing a probiotic effect on the host. In addition, compared with the control group, the expression level of the $Na^+/K^+/2Cl^-$ cotransporter gene was significantly upregulated in the β-glucan group at different doses and was closely related to osmotic pressure regulation [58]. Similar results were found in a previous study, where prebiotic inulin significantly upregulated metabolic pathways related to osmotic pressure regulation (aldosterone-mediated sodium reuptake metabolic pathway) in *L. vannamei* under low-salinity stress [19]. These results suggest that the prebiotic effect of prebiotics on the host may be mediated by regulating osmotic pressure at low salinity. However, there is limited information on the effect of prebiotics on osmotic regulation, and more research is needed. In the present study, transcriptome analyses were performed in *L. vannamei* receiving dietary β-glucan to investigate how β-glucan plays an active role. KEGG analyses of DEGs showed that β-glucan has significant effects on pathways related to energy metabolism and immune defense. Low-salinity stress may affect the metabolism and immune system of *L. vannamei*. It was speculated that β-glucan could exert its probiotic effect on the host by regulating these signaling pathways. Osmotic regulation requires a certain amount of energy in crustaceans to ensure normal metabolism [2]. Many enzymes and transporters are relevant to iono- and osmoregulatory processes, which consume large amounts of energy [59]. In this study, KEGG pathways related to carbohydrate metabolism, such as starch and sucrose metabolism, carbohydrate digestion and absorption, and galactose metabolism, were significantly enriched under low salinity by adding β-glucan. To date, dietary supplementation with xylooligosaccharides (XOS) has been demonstrated to be effective in improving blood glucose [60]. A previous study showed that the prebiotic inulin enriches different metabolic pathways, including glycolysis and gluconeogenesis [61], consistent with this study. These results indicate that dietary β-glucan addition can improve immune defense and energy metabolism disor-

ders under low-salinity stress. Furthermore, the prebiotic β-glucan could meet energy requirements under low salinity by activating KEGG pathways related to carbohydrate metabolism, thus producing a probiotic effect on the host.

5. Conclusions

The addition of β-glucan could improve the antioxidant capacity of *L. vannamei* by enhancing the activities of T-AOC, SOD and CAT to relieve low-salinity stress (≤3). In addition, dietary β-glucan addition could enhance growth performance and effectively alleviate the physiological effects by enhancing biochemical indicators (digestive and nonspecific immune activity) and improving intestinal microbiota and carbohydrate metabolism (starch and sucrose metabolism, carbohydrate digestion and absorption, galactose metabolism, etc.). In addition, it is recommended that the β-glucan dose added to the diet be 0.1–0.2% to improve growth performance and relieve low-salinity stress (≤3). These results can provide a reference for the practical application value and farming costs of β-glucan in aquaculture, which will set a model for subsequent research on functional substances in *L. vannamei* and contribute to the green, healthy and sustainable development of the global aquaculture industry.

Supplementary Materials: The following supporting information can be downloaded at: https://www.mdpi.com/article/10.3390/antiox11112282/s1. Table S1: Regression analysis of the gut microbiota composition in *L. vannamei* fed different dietary β-glucan levels; Table S2: Shared differentially expressed genes between the control, 0.05%, 0.1%, 0.2% and 0.4% groups; Table S3: KEGG pathway enrichment of the differentially expressed genes between control, 0.05%, 0.1%, 0.2% and 0.4%.

Author Contributions: Y.Q. (Yanbing Qiao) was responsible for feeding management, data analysis and the writing of the original manuscript. Y.Q. (Yayu Qu) and K.L. were responsible for feeding management and validation of the data. Y.Q. (Yanbing Qiao), F.H., L.Z. and E.L. were responsible for the research investigation and experimental design. F.H. and E.L. were responsible for reviewing and revising the article. E.L. was responsible for the overall planning of funds and review of the manuscript. All authors have read and agreed to the published version of the manuscript.

Funding: This study was co-sponsored by the National Natural Science Foundation of China (grant number 32060832), the Research and Development Program Projects in Key Areas of Guangdong Province (grant number 2020B0202010001) and the initial fund from Hainan University for R & D (grant number KYQD(ZR)21091).

Institutional Review Board Statement: The animal experiments in this study were reviewed and approved by the Committee on the Ethics of Animal Experiments of Hainan University (HNUAUCC-2021-00119).

Informed Consent Statement: Not applicable.

Data Availability Statement: The data provided in this study have been uploaded to the NCBI database. The accession numbers are PRJNA842883 and PRJNA846923, and the links are https://www.ncbi.nlm.nih.gov/sra/PRJNA842883 (accessed on 23 May 2022) and https://submit.ncbi.nlm.nih.gov/subs/PRJN-A846923 (accessed on 23 May 2022).

Acknowledgments: The authors would acknowledge Hainan Blue Ocean Biotechnology Co., Ltd., for the contribution of experimental sites and experimental materials, the Beijing Novogene Co., Ltd., for assistance in microbial 16S bioinformatics analysis, and Shanghai Majorbio Co., Ltd., for assistance in the transcriptome analysis of hepatopancreas.

Conflicts of Interest: The authors declare no conflict of interest.

References

1. Saoud, I.; Davis, D.; Rouse, D. Suitability studies of inland well waters for *Litopenaeus vannamei* culture. *Aquaculture* **2003**, *217*, 373–383. [CrossRef]
2. Romano, N.; Zeng, C. Osmoregulation in decapod crustaceans: Implications to aquaculture productivity, methods for potential improvement and interactions with elevated ammonia exposure. *Aquaculture* **2012**, *334–337*, 12–23. [CrossRef]
3. Bureau of Fisheries, Ministry of Agriculture PRC. *China Fishery Statistical Yearbook*; China Agriculture Press: Beijing, China, 2020.

4. Ye, L.; Jiang, S.; Zhu, X.; Yang, Q.; Wen, W.; Wu, K. Effects of salinity on growth and energy budget of juvenile *Penaeus monodon*. *Aquaculture* **2009**, *290*, 140–144. [CrossRef]
5. Li, E.; Chen, L.; Zeng, C.; Chen, X.; Yu, N.; Lai, Q.; Qin, J. Growth, body composition, respiration and ambient ammonia nitrogen tolerance of the juvenile white shrimp, *Litopenaeus vannamei*, at different salinities. *Aquaculture* **2007**, *265*, 385–390. [CrossRef]
6. Esparza-Leal, H.; Ponce-Palafox, J.; Cervantes-Cervantes, C.; Valenzuela-Quiñónez, W.; Luna-González, A.; López-Álvarez, E.; Vázquez-Montoya, N.; López-Espinoza, M.; Gómez-Peraza, R. Effects of low salinity exposure on immunological, physiological and growth performance in *Litopenaeus vannamei*. *Aquac. Res.* **2019**, *50*, 944–950. [CrossRef]
7. Lin, Y.; Chen, J.; Li, C.; Morni, W.; Suhaili, A.; Kuo, Y.; Chang, Y.; Chen, L.; Tsui, W.; Chen, Y.; et al. Modulation of the innate immune system in white shrimp *Litopenaeus vannamei* following long-term low salinity exposure. *Fish Shellfish Immunol.* **2012**, *33*, 324–331. [CrossRef]
8. Lin, Y.; Chen, J. Acute toxicity of nitrite on *Litopenaeus vannamei* (Boone) juveniles at different salinity levels. *Aquaculture* **2003**, *224*, 193–201. [CrossRef]
9. Lin, Y.; Chen, J. Acute toxicity of ammonia on *Litopenaeus vannamei* Boone juveniles at different salinity levels. *J. Exp. Mar. Biol. Ecol.* **2001**, *259*, 109–119. [CrossRef]
10. Ramos-Carreño, S.; Valencia-Yáñez, R.; Correa-Sandoval, F.; Ruíz-García, N.; Díaz-Herrera, F.; Giffard-Mena, I. White spot syndrome virus (WSSV) infection in shrimp (*Litopenaeus vannamei*) exposed to low and high salinity. *Arch. Virol.* **2014**, *159*, 2213–2222. [CrossRef]
11. Chaiyapechara, S.; Uengwetwanit, T.; Arayamethakorn, S.; Bunphimpapha, P.; Phromson, M.; Jangsutthivorawat, W.; Tala, S.; Karoonuthaisiri, N.; Rungrassamee, W. Understanding the host-microbe-environment interactions: Intestinal microbiota and transcriptomes of black tiger shrimp *Penaeus monodon* at different salinity levels. *Aquaculture* **2022**, *546*, 737371. [CrossRef]
12. Tian, L.; Tan, P.; Yang, L.; Zhu, W.; Xu, D. Effects of salinity on the growth, plasma ion concentrations, osmoregulation, non-specific immunity, and intestinal microbiota of the yellow drum (*Nibea albiflora*). *Aquaculture* **2020**, *528*, 735470. [CrossRef]
13. Li, H.; Xu, C.; Zhou, L.; Dong, Y.; Li, E. Beneficial effects of dietary β-glucan on growth and health status of Pacific white shrimp *Litopenaeus vannamei* at low salinity. *Fish Shellfish Immunol.* **2019**, *91*, 315–324. [CrossRef] [PubMed]
14. Meena, D.; Das, P.; Kumar, S.; Mandal, S.; Prusty, A.; Singh, S.; Akhtar, M.; Behera, B.; Kumar, K.; Pal, A. Beta-glucan: An ideal immunostimulant in aquaculture (a review). *Fish Physiol. Biochem.* **2013**, *39*, 431–457. [CrossRef]
15. Yoshida, K.; Hirano, R.; Sakai, Y.; Choi, M.; Sakanaka, M.; Kurihara, S.; Iino, H.; Xiao, J.; Katayama, T.; Odamaki, T. Bifidobacterium response to lactulose ingestion in the gut relies on a solute-binding protein-dependent ABC transporter. *Commun. Biol.* **2021**, *4*, 541. [CrossRef]
16. Xie, S.; Wei, D.; Yin, P.; Zheng, L.; Guo, T.; Liu, Y.; Tian, L.; Niu, J. Dietary replacement of fish-meal impaired protein synthesis and immune response of juvenile Pacific white shrimp, *Litopenaeus vannamei* at low salinity. *Comp. Biochem. Physiol. B Biochem. Mol. Biol.* **2019**, *228*, 26–33. [CrossRef]
17. Abdel-Latif, H.; El-Ashram, S.; Yilmaz, S.; Naiel, M.; Abdul Kari, Z.; Hamid, N.; Dawood, M.; Nowosad, J.; Kucharczyk, D. The effectiveness of Arthrospira platensis and microalgae in relieving stressful conditions affecting finfish and shellfish species: An overview. *Aquac. Rep.* **2022**, *24*, 101135. [CrossRef]
18. Tang, S.; Han, F.; Zhou, L.; Liu, S.; Xu, C.; Chen, L.; Li, E. Regulation of mannan oligosaccharide on growth, health and intestinal microbiota of *Litopenaeus vannamei* at low salinity. *J. Fish China* **2021**, *45*, 2044–2060.
19. Kuo, H.; Chang, C.; Cheng, W. Synbiotic combination of prebiotic, cacao pod husk pectin and probiotic, Lactobacillus plantarum, improve the immunocompetence and growth of *Litopenaeus vannamei*. *Fish Shellfish Immunol.* **2021**, *118*, 333–342. [CrossRef]
20. Dawood, M.; Koshio, S.; Ishikawa, M.; Yokoyama, S.; El Basuini, M.; Hossain, M.; Nhu, T.; Moss, A.; Dossou, S.; Wei, H. Dietary supplementation of β-glucan improves growth performance, the innate immune response and stress resistance of red sea bream, *Pagrus major*. *Aquac. Nutr.* **2017**, *23*, 148–159. [CrossRef]
21. Mohan, K.; Ravichandran, S.; Muralisankar, T.; Uthayakumar, V.; Chandirasekar, R.; Seedevi, P.; Rajan, D. Potential uses of fungal polysaccharides as immunostimulants in fish and shrimp aquaculture: A review. *Aquaculture* **2019**, *500*, 250–263. [CrossRef]
22. Luan, L.; Vu, N.; Nghia, N.; Thao, N. Synergic degradation of yeast β-glucan with a potential of immunostimulant and growth promotor for tiger shrimp. *Aquac. Rep.* **2021**, *21*, 100858. [CrossRef]
23. Pooljun, C.; Jariyapong, P.; Wongtawan, T.; Hirono, I.; Wuthisuthimethavee, S. Effect of feeding different types of β-glucans derived from two marine diatoms (Chaetoceros muelleri and Thalassiosira weissflogii) on growth performance and immunity of banana shrimp (*Penaeus merguiensis*). *Fish Shellfish Immunol.* **2022**, *130*, 512–519. [CrossRef] [PubMed]
24. Murthy, H.; Li, P.; Lawrence, A.; Gatlin, D. Dietary β-glucan and nucleotide effects on growth, survival and immune responses of pacific white shrimp, *Litopenaeus vannamei*. *J. Appl. Aquac.* **2009**, *21*, 160–168. [CrossRef]
25. Do Huu, H.; Sang, H.; Thuy, N. Dietary β-glucan improved growth performance, Vibrio counts, haematological parameters and stress resistance of pompano fish, *Trachinotus ovatus Linnaeus*, 1758. *Fish Shellfish Immunol.* **2016**, *54*, 402–410. [CrossRef]
26. da Silva, B.; do Nascimento Vieira, F.; Mouriño, J.; Ferreira, G.; Seiffert, W. Salts of organic acids selection by multiple characteristics for marine shrimp nutrition. *Aquaculture* **2013**, *384*, 104–110. [CrossRef]
27. Wongsasak, U.; Chaijamrus, S.; Kumkhong, S.; Boonanuntanasarn, S. Effects of dietary supplementation with β-glucan and synbiotics on immune gene expression and immune parameters under ammonia stress in Pacific white shrimp (*Litopenaeus vannamei*). *Aquaculture* **2015**, *436*, 179–187. [CrossRef]

28. Miest, J.; Arndt, C.; Adamek, M.; Steinhagen, D.; Reusch, T. Dietary β-glucan (MacroGard®) enhances survival of first feeding turbot (*Scophthalmus maximus*) larvae by altering immunity, metabolism and microbiota. *Fish Shellfish Immunol.* **2016**, *48*, 94–104. [CrossRef]
29. Xu, Z.; Wang, Y.; Gul, Y.; Li, Q.; Song, J.; Hu, M. Effects of copper supplement on the immune function and blood-chemistry in adult Chinese horseshoe crab *Tachypleus tridentatus*. *Aquaculture* **2020**, *515*, 734576. [CrossRef]
30. Yu, Q.; Fu, Z.; Huang, M.; Xu, C.; Wang, X.; Qin, J.; Chen, L.; Han, F.; Li, E. Growth, physiological, biochemical, and molecular responses of Pacific white shrimp *Litopenaeus vannamei* fed different levels of dietary selenium. *Aquaculture* **2021**, *535*, 736393. [CrossRef]
31. Davis, M. Contrast Coding in Multiple Regression Analysis: Strengths, Weaknesses, and Utility of Popular Coding Structures. *J. Dairy Sci.* **2010**, *8*, 61–73. [CrossRef]
32. Chen, K.; Li, E.; Xu, C.; Wang, X.; Lin, H.; Qin, J.; Chen, L. Evaluation of different lipid sources in diet of pacific white shrimp *Litopenaeus vannamei* at low salinity. *Aquac. Rep.* **2015**, *2*, 163–168. [CrossRef]
33. Felix, N.; Jeyaseelan, M.; Kirubakaran, C. Growth improvement and enhanced disease resistance against Vibrio alginolyticus using-glucan as a dietary supplement for *Penaeus monodon* (Fabricius). *Indian J. Fish* **2008**, *55*, 247–250.
34. Xu, B.; Wang, Y.; Li, J.; Lin, Q. Effect of prebiotic xylooligosaccharides on growth performances and digestive enzyme activities of allogynogenetic crucian carp (*Carassius auratus gibelio*). *Fish Physiol. Biochem.* **2009**, *35*, 351–357. [CrossRef]
35. Akter, M.; Sutriana, A.; Talpur, A.; Hashim, R. Dietary supplementation with mannan oligosaccharide influences growth, digestive enzymes, gut morphology, and microbiota in juvenile striped catfish, *Pangasianodon hypophthalmus*. *Aquac. Int.* **2016**, *24*, 127–144. [CrossRef]
36. Li, E.; Wang, X.; Chen, K.; Xu, C.; Qin, J.; Chen, L. Physiological change and nutritional requirement of Pacific white shrimp *Litopenaeus vannamei* at low salinity. *Rev. Aquac.* **2017**, *9*, 57–75. [CrossRef]
37. Liu, Y.; Wang, W.; Wang, A.; Wang, J.; Sun, R. Effects of dietary vitamin E supplementation on antioxidant enzyme activities in *Litopenaeus vannamei* (Boone, 1931) exposed to acute salinity changes. *Aquaculture* **2007**, *265*, 351–358. [CrossRef]
38. Köhrle, J. The deiodinase family: Selenoenzymes regulating thyroid hormone availability and action. *Cell Mol. Life Sci.* **2000**, *57*, 1853–1863. [CrossRef]
39. Chang, C.; Su, M.; Chen, H.; Liao, I. Dietary β-1, 3-glucan effectively improves immunity and survival of *Penaeus monodon* challenged with white spot syndrome virus. *Fish Shellfish Immunol.* **2003**, *15*, 297–310. [CrossRef]
40. Xing, J.; Lin, T.; Zhan, W. Variations of enzyme activities in the haemocytes of scallop Chlamys farreri after infection with the acute virus necrobiotic virus (AVNV). *Fish Shellfish Immunol.* **2008**, *25*, 847–852. [CrossRef]
41. Chang, C.; Huang, S.; Chen, S.; Chen, S. Innate immune responses and efficacy of using mushroom beta-glucan mixture (MBG) on orange-spotted grouper, *Epinephelus coioides*, aquaculture. *Fish Shellfish Immunol.* **2013**, *35*, 115–125. [CrossRef]
42. Xu, B.; Zhang, G.; Wang, L.; Sagada, G.; Zhang, J.; Shao, Q. The influence of dietary β-1, 3-glucan on growth performance, feed utilization, antioxidative and immune status of Pacific white shrimp, *Litopenaeus vannamei*. *Aquac. Nutr.* **2021**, *27*, 1590–1601. [CrossRef]
43. Sonnenburg, E.; Sonnenburg, J.; Manchester, J.; Hansen, E.; Chiang, H.; Gordon, J. A hybrid two-component system protein of a prominent human gut symbiont couples glycan sensing in vivo to carbohydrate metabolism. *Proc. Natl. Acad. Sci. USA* **2006**, *103*, 8834–8839. [CrossRef] [PubMed]
44. De Vadder, F.; Mithieux, G. Gut-brain signaling in energy homeostasis: The unexpected role of microbiota-derived succinate. *J. Endocrinol.* **2018**, *236*, R105–R108. [CrossRef] [PubMed]
45. Li, E.; Xu, C.; Wang, X.; Wang, S.; Zhao, Q.; Zhang, M.; Qin, J.; Chen, L. Gut microbiota and its modulation for healthy farming of Pacific white shrimp *Litopenaeus vannamei*. *Rev. Fish Sci. Aquac.* **2018**, *26*, 381–399. [CrossRef]
46. Pinoargote, G.; Flores, G.; Cooper, K.; Ravishankar, S. Effects on survival and bacterial community composition of the aquaculture water and gastrointestinal tract of shrimp (*Litopenaeus vannamei*) exposed to probiotic treatments after an induced infection of acute hepatopancreatic necrosis disease. *Aquac. Res.* **2018**, *49*, 3270–3288. [CrossRef]
47. Boonanuntanasarn, S.; Wongsasak, U.; Pitaksong, T.; Chaijamrus, S. Effects of dietary supplementation with β-glucan and synbiotics on growth, haemolymph chemistry, and intestinal microbiota and morphology in the Pacific white shrimp (*Litopenaeus vannamei*). *Aquac. Nutr.* **2016**, *22*, 837–845. [CrossRef]
48. Zhang, X.; Chen, S.; Duan, F.; Liu, A.; Li, S.; Zhong, W.; Sheng, W.; Chen, J.; Xu, J.; Xiao, S. Prebiotics enhance the biotransformation and bioavailability of ginsenosides in rats by modulating gut microbiota. *J. Ginseng Res.* **2021**, *45*, 334–343. [CrossRef]
49. Nie, L.; Zhou, Q.; Qiao, Y.; Chen, J. Interplay between the gut microbiota and immune responses of ayu (*Plecoglossus altivelis*) during Vibrio anguillarum infection. *Fish Shellfish Immunol.* **2017**, *68*, 479–487. [CrossRef]
50. Siriyappagouder, P.; Galindo, J.; Lokesh, J.; Mulero, V.; Fernandes, J.; Kiron, V. Exposure to yeast shapes the intestinal bacterial community assembly in zebrafish larvae. *Front. Microbiol.* **2018**, *9*, 1868. [CrossRef]
51. Ringø, E.; Olsen, R.; Gifstad, T.; Dalmo, R.; Amlund, H.; Hemre, G.; Bakke, A. Prebiotics in aquaculture: A review. *Aquac. Nutr.* **2010**, *16*, 117–136. [CrossRef]
52. Hornett, E.; Wheat, C. Quantitative RNA-Seq analysis in non-model species: Assessing transcriptome assemblies as a scaffold and the utility of evolutionary divergent genomic reference species. *BMC Genom.* **2012**, *13*, 361. [CrossRef] [PubMed]
53. Ma, D.; Yang, H.; Sun, L.; Chen, M. Transcription profiling using RNA-Seq demonstrates expression differences in the body walls of juvenile albino and normal sea cucumbers *Apostichopus japonicus*. *China J. Oceanol. Limnol.* **2014**, *32*, 34–46. [CrossRef]

54. Wang, X.; Wang, S.; Li, C.; Chen, K.; Qin, J.; Chen, L.; Li, E. Molecular pathway and gene responses of the pacific white shrimp *Litopenaeus vannamei* to acute low salinity stress. *J. Shellfish Res.* **2015**, *34*, 1037–1048. [CrossRef]
55. Zhuo, X.; Qin, Y.; He, P.; Wei, P.; Zhang, B.; Chen, X.; Peng, J. Transcriptomic analysis of *Litopenaeus vannamei* hepatopancreas under cold stress in cold-tolerant and cold-sensitive cultivars. *Gene* **2021**, *764*, 145090. [CrossRef]
56. Nappi, A.; Vass, E.; Frey, F.; Carton, Y. Superoxide anion generation in Drosophila during melanotic encapsulation of parasites. *Eur. J. Cell Biol.* **1995**, *68*, 450–456.
57. Tassanakajon, A.; Rimphanitchayakit, V.; Visetnan, S.; Amparyup, P.; Somboonwiwat, K.; Charoensapsri, W.; Tang, S. Shrimp humoral responses against pathogens: Antimicrobial peptides and melanization. *Dev. Comp. Immunol.* **2018**, *80*, 81–93. [CrossRef]
58. Zhao, C.; Guo, H.; Zhu, K.; Guo, L.; Zhang, N.; Liu, B.; Yang, J.; Liu, B.; Jiang, S.; Zhang, D. Molecular characterization of $Na^+/K^+/2Cl^-$ cotransporter 1 alpha from *Trachinotus ovatus* (Linnaeus, 1758) and its expression responses to acute salinity stress. *Comp. Biochem. Physiol. B Biochem. Mol. Biol.* **2018**, *223*, 29–38. [CrossRef]
59. Lee, J.; Cho, B.; Park, J. Transcriptomic analysis of brine shrimp Artemia franciscana across a wide range of salinities. *Mar. Genom.* **2022**, *61*, 100919. [CrossRef]
60. Gobinath, D.; Madhu, A.; Prashant, G.; Srinivasan, K.; Prapulla, S. Beneficial effect of xylo-oligosaccharides and fructo-oligosaccharides in streptozotocin-induced diabetic rats. *Br. J. Nutr.* **2010**, *104*, 40–47. [CrossRef]
61. Lokesh, J.; Ghislain, M.; Reyrolle, M.; Bechec, M.; Pigot, T.; Terrier, F.; Roy, J.; Panserat, S.; Ricaud, K. Prebiotics modify host metabolism in rainbow trout (*Oncorhynchus mykiss*) fed with a total plant-based diet: Potential implications for microbiome-mediated diet optimization. *Aquaculture* **2022**, *561*, 738699. [CrossRef]

antioxidants

MDPI

Article

Berberine Regulation of Cellular Oxidative Stress, Apoptosis and Autophagy by Modulation of m^{6}A mRNA Methylation through Targeting the *Camk1db*/ERK Pathway in Zebrafish-Hepatocytes

Meijuan Zhang [1], Jin Liu [1], Chengbing Yu [1], Shangshang Tang [1], Guangzhen Jiang [2], Jing Zhang [1], Hongcai Zhang [1], Jianxiong Xu [1] and Weina Xu [1,*]

[1] Shanghai Key Laboratory for Veterinary and Biotechnology, School of Agriculture and Biology, Shanghai Jiao Tong University, No. 800 Jiangchuan Road, Shanghai 200240, China
[2] Key Laboratory of Aquatic Nutrition and Feed Science of Jiangsu Province, College of Animal Science and Technology, Nanjing Agricultural University, No. 1 Weigang Road, Nanjing 210095, China
* Correspondence: xuweina@sjtu.edu.cn

Abstract: Berberine (BBR) ameliorates cellular oxidative stress, apoptosis and autophagy induced by lipid metabolism disorder, however, the molecular mechanism associated with it is not well known. To study the mechanism, we started with m^{6}A methylation modification to investigate its role in lipid deposition zebrafish hepatocytes (ZFL). The results showed that BBR could change the cellular m^{6}A RNA methylation level, increase m^{6}A levels of *Camk1db* gene transcript and alter *Camk1db* gene mRNA expression. Via knockdown of the *Camk1db* gene, *Camk1db* could promote cellular ERK phosphorylation levels. Berberine regulated the expression level of *Camk1db* mRNA by altering the M^{6}A RNA methylation of the Camk1db gene, which further affected the synthesis of calmodulin-dependent protein kinase and activated ERK signaling pathway resulting in changes in downstream physiological indicators including ROS production, cell proliferation, apoptosis and autophagy. In conclusion, berberine could regulate cellular oxidative stress, apoptosis and autophagy by mediating *Camk1db* m^{6}A methylation through the targeting of the *Camk1db*/ERK pathway in zebrafish-hepatocyte.

Keywords: berberine; m^{6}A methylation; *Camk1db*; ERK; zebrafish hepatocytes (ZFL)

Citation: Zhang, M.; Liu, J.; Yu, C.; Tang, S.; Jiang, G.; Zhang, J.; Zhang, H.; Xu, J.; Xu, W. Berberine Regulation of Cellular Oxidative Stress, Apoptosis and Autophagy by Modulation of m^{6}A mRNA Methylation through Targeting the *Camk1db*/ERK Pathway in Zebrafish-Hepatocytes. *Antioxidants* **2022**, *11*, 2370. https://doi.org/10.3390/antiox11122370

Academic Editors: Zhihui Feng and Mark G. Clemens

Received: 30 September 2022
Accepted: 28 November 2022
Published: 30 November 2022

1. Introduction

The long-term excessive exposure to a high-fat diet results in lipid metabolism disorders and over-production of reactive oxygen species (ROS), which triggers oxidative stress and cell damage at the cellular and molecular levels [1]. Studies have demonstrated cell damage biochemical mechanisms involved in the cellular signaling pathways [2] and the interaction between genes and protein expression changes at the transcriptional level [3,4]. Gene RNA is a key linking DNA to protein in the transmission of genetic information, but the level of synthesized protein does not necessarily correlate positively with the level of mRNA, suggesting the importance of post-transcriptional RNA modifications. There are more than 100 known post-transcriptional modifications of RNA. Among these, m^{6}A methylation is the most common type [5], and also the most widely studied dynamic modification method of RNA. M^{6}A RNA methylation, the sixth methylation modification of adenine on nitrogen atoms, is an evolutionarily-conserved RNA modification that is present in most organisms from bacteria to mammals [6,7]. M^{6}A RNA methylation is also a reversible epigenetic RNA modification that exists at the transcriptional level of the nitrogen or oxygen atom of S-adenosylmethionine, and regulates mRNA stability, splicing, export, localization, and translation [8–10]. M^{6}A RNA methylation can affect most aspects of gene

expression. Recent studies have identified m^6A RNA methylation modifications plays an important role in regulating cell biological function, controlling cell proliferation and differentiation [11], cellular oxidative stress response [12,13], DNA damage response [14], and lipid metabolism [15–18]. Now, biological functions for this m^6A modification are emerging through more mechanistic analyses.

The Chinese medicine berberine (BBR, chemical formula $C_{20}H_{18}NO_4$) is an isoquinoline quaternary alkaloid isolated from several medicinal plants, including *Berberis aristata* and *Coptis chinensis* [19,20]. Berberine can inactivate highly active molecules such as $O_2^{\bullet -}$, $HO^{\bullet}$, NO and $OONO^-$, so as to facilitate the ability to remove reactive oxygen species clusters (ROS) directly [21]. In addition, modern pharmacological studies have shown that berberine exhibits hepatoprotective, anti-inflammatory, antioxidant, hypoglycemic, hypolipidemic properties [22,23], and reduces obesity in mammals [24]. Our previous studies showed berberine-supplemented diets could attenuate oxidative stress, improve the function of the mitochondrial respiratory chain, reduce apoptosis and inhibit the inflammation response as well as modulate the intestinal microflora profile caused by high-fat and high-carbohydrate diets in fish in vitro and vivo [25–28]. However, the molecular mechanism of berberine's role in oxidative stress, apoptosis, and autophagy is still limited. In this paper, we investigated whether berberine could regulate cellular oxidative stress, apoptosis and autophagy by changing the methylation level of cell gene m6A RNA.

Zebrafish (*Danio rerio*, Cyprinidae) is an important vertebrate model organism for development, genetics, and reproduction [29]. The liver is the main organ for fat synthesis, and about 90% of the fat in fish is synthesized in the liver [30], which plays an important role in maintaining the metabolic balance of carbohydrates, amino acids, and fatty acids [31]. There were many studies using Zebrafish hepatocytes (ZFLs) to study fat deposition in vitro. Therefore, in this study, we selected ZFL as model system for the study of metabolic syndrome combined with oxidative stress to investigated the roles of m^6A RNA methylation modification in lipid-deposition ZFL treated with berberine in vitro. The results may have implications for a molecular theoretical basis for the research and development of hepatoprotective herbal treatments in fish farming.

2. Materials and Methods

2.1. Materials

Zebrafish hepatocytes (ZFL, CRL-2643) were purchased from the American Tissue Culture Collection (ATCC, Manassas, VA, USA). Other materials and reagents purchased included the following: DMEM-F12 medium, DMEM medium, L-15 medium, fetal bovine serum (Gibco, Waltham, MA, USA); penicillin, murine epithelial growth factor, insulin, DPBS and 0.25% trypsin (Thermo Fisher, Shanghai, China); total RNA extraction kit (OMEGA, Cambridge, MA, USA); reverse transcription kit, and fluorescent quantitative PCR kit (Takara, Beijing, China); the targeted antibody (ERK, P-ERK, P62, LC3-B) and the internal antibody tubulin (because the size of the antibody protein of interest is between 10 and 70 kDa, in order to ensure that the target internal reference is on a membrane, and our sample is a whole cell protein, the loading amount is 30 micrograms, using ripa lysate, so for comprehensive consideration, tubulin was selected as the internal reference protein) are purchased from CST (Parsons, KS, USA). Instrumentation included the following: high-speed frozen centrifuge (Eppendorf, Hamburg, Germany, 5804 R, Shanghai, China); real-time fluorescence quantitative PCR instrument (Applied Biosystems, StepOnePlus™, Waltham, MA, USA); inverted microscope (Nikon Corporation, Hong Kong, China); multifunctional enzyme labeling instrument (SYNERGY 2 BioTek, Waltham, MA, USA). Oil Red O staining solution, sodium palmitate, and berberine, were purchased from Sigma-Aldrich (Shanghai, China) Trading Co. CCK-8 cell activity assay kit, BCA protein assay kit, triglyceride assay kit, ROS, MDA, and T-AOC assay kits, were purchased from Nanjing Jiancheng Institute of Biological Engineering. Total RNA extraction kit was purchased from OMEGA (Cambridge, MA, USA). Primers were synthesized by Thermo Fisher Scientific China Ltd (Shanghai, China). The reverse transcription kit PrimeScript RT reagent Kit (Perfect Real

Time) and its matching fluorescent quantitative PCR kit TB Green™ Premix Ex Taq™ (Tli RNaseH Plus) were purchased from Takara Corporation (Beijing, China).

2.2. Lipid Accumulation Injury Treatment and Berberine Repair Treatment in ZFL

2.2.1. Lipid Accumulation Injury Treatment in ZFL

Mixed media was composed of 50% L-15, 30% DMEM/F12, and 20% DMEM (containing 5% fetal bovine serum, 1% penicillin, 1% insulin and 50 ng/mL murine epithelial growth factor). ZFL cells were cultured to 70–80% fusion with a mixed culture base at 28°C and 5% CO_2. Cells were collected after treatment with sodium palmitate (SP) culture solution at a concentration of 0.25 mmol/L for 24 h, thus establishing a validated model of hepatocyte fat deposition [32].

2.2.2. Berberine Repair Treatment in ZFL

ZFL cells were treated with SP culture solution at a concentration of 0.25 mmol/L for 24 h and then collected. The cells were then treated with BBR working solution (solvent 0.1% DMSO) at a concentration of 25 μmol/L for 6 h and then collected, thus establishing an effective model of hepatocyte fat deposition repair [32].

2.3. Oxidative Stress Indicator Test

2.3.1. ROS Content Detection

The intracellular ROS (reactive oxygen species) content was detected using a DCFH-DA probe. After each group of cells was treated, cells were rinsed with DPBS three times, incubated with DCFH-DA probe for 30 min, and rinsed with DPBS three times, and ROS fluorescence photographs were taken with fluorescence microscopy. Cells received the same treatment as above, with a microplate reader to determine the fluorescence intensity at an excitation wavelength of 488 nm and an emission wavelength of 525 nm. The calculation formula is as follows:

$$\text{ROS content} = \left(\frac{\text{Fluorescence intensity of the treatment group} - \text{Fluorescence intensity of blank group}}{\text{Fluorescence intensity of the control group} - \text{Fluorescence intensity of blank group}} \right) \div \text{Cell density} \times 100\%$$

2.3.2. MDA and T-AOC Contents Measurement

After the cell culture treatment, cells were placed on ice. The cell culture medium was discarded, rinsed 3 times with DPBS, and then 200 μL of cell lysate was added to each well for lysis. The cell lysate was collected, and the intracellular MDA and T-AOC contents were measured separately according to the method of the kit (Nanjing Jiancheng Institute of Biological Engineering).

2.4. Cell Apoptosis

Apoptotic cells were detected by Annexin V/FITC as described previously [33]. Each group of cells was collected in a centrifuge tube and centrifuged at 1000× *g* for 5 min. Supernatant was discarded and 195 μL of membrane linked protein V-FITC binding solution was added to gently suspend the cells. Next, 5 μL of Annexin V-FITC were added and mixed well before further adding 10 μL of propyl iodide solution. The mixture was incubated at room temperature for 10–20 min on ice, protected from light. Apoptosis was detected using flow cytometry counting, where the apoptosis rate (%) = number of apoptotic cells/total number of cells × 100%.

2.5. Western Blot

Cells were collected by centrifugation, lysed on ice for 30 min with RIPA cell lysis solution, and the total protein concentration was determined by BCA method. Each well was sampled with 30 μg of protein and separated by 10% polyacrylamide gel electrophoresis. The separated proteins were electro transferred (200 mA current for 2 h) to PVDF membrane. ERK (cst, 9102), P-ERK (cst, 9101), P62 (cst, 5114), LC3-B (cst, 2775) (1:1000 volume dilution) were taken from the primary antibody rabbit, and the internal reference primary antibody tubulin (cst, 2146) (1:2000 volume dilution) was taken, and incubated

overnight at 4 °C. The next day, the membranes were washed three times with TBST for 10 min each time, followed by the addition of secondary antibodies against rabbit anti-IgG (1:2000 v/v) for 2–4 h at room temperature, and then washed three times with TBST for 10 min each time, and developed according to the instructions of the ECL kit. The grayscale values of the protein bands were analyzed using the LK5100 electrochemiluminescence analysis system.

2.6. Cellular Microstructure Detection

A sufficient number of cells were cultured in a 10 cm dish. Cells grown in the petri dish were scraped off directly and the cell suspension was transferred to the centrifuge tube. Cells were centrifuged at 1000–3000 rpm, the supernatant was discarded, and PBS was added to transfer the cells to a 1.5 mL centrifuge tube. After centrifugation, supernatant was discarded. PBS was added to repeat the above steps, and 2.5% glutaraldehyde fixative for tissue and cell electron microscopy was added at 4 °C overnight. Samples were then sent to Wuhan Max Bio-Technology Co., Ltd. (Wuhan, China) the next day for subsequent electron microscopy detection.

2.7. m^6A Methylation and Transcriptome Merip-Seq Sequencing

The RNA of the total samples was isolated and purified using TRizol, and the amount and purity of the total RNA was tested for quality control and integrity, while the protocol was verified by agar electrophoresis. Magnetic beads with Poly adenylic acid were used to specifically capture the mRNA. Fragmentation was performed with a magnesium ion interruption kit, and the fragmented RNA was pre-mixed with immunomagnetic beads with m^6A antibody, and subjected to IP. The IP product was subjected to duplex synthesis, converting the DNA and RNA duplexes into DNA duplexes, and complementing the ends. Base A was added at each end, ligated to the end with base T, and purified by screening with magnetic beads. After digestion of the duplexes, PCR was pre-denatured at 95 °C for 3 min, denatured at 98 °C for 15 s, cycled 8 times, annealed at 60 °C for 15 s, extended at 72 °C for 30 s, and held at 72 °C for 5 min to obtain fragments of approximately 300 bp size. Finally, it was sequenced using Illumina NovaSeq TM 6000 according to the sequencing mode PE150.

2.8. Methylation Level Detection

RNA samples were fragmented and immunoprecipitated magnetic beads were prepared, immunoprecipitated reaction was performed. Then, the obtained RNA samples were eluted and purified. The MeRIP RNA was analyzed together with the corresponding Input RNA by quantitative RT-PCR, or constructed using standard library building kits for RNA-seq library construction and identification of RNA methylation regions within the transcriptome by deep sequencing.

2.9. SiRNA Transfection

For the study, 1×10^6 cells were inoculated into 6-well plates so that the cell density during transfection could reach 30~50%. After 24 h, samples were washed twice with DPBS, then 2 mL of the configured mixed reagent were added to each well. After 6 h, this was replaced with normal culture medium until the end of the corresponding transfection time when cells were collected for subsequent assay tests. To configure the mixed reagent, 10 μL of lipo2000 were added to 190 μL of serum-free culture medium, which was then gently mixed for 5 min. Next, 5 nmol of siRNA (sequence shown in Table 1) was added to 250 μL of DEPC water, i.e., dry powdered siRNA was configured into a 20 nmol/mL solution. Then, 5 μL of the prepared solution was combined with 195 μL of serum-free culture medium, and gently mixed for 5 min. The two liquid solutions described above were then mixed 1:1 and incubated for 15 min at room temperature to prepare the transfection complex. The complete culture medium was supplemented to 2 mL, which is the required transfection mixture for one well.

Table 1. SiRNA sequence of target genes.

Target Gene	Accession Number	siRNA Sequence
camk1db	NC_007136.7	CTGCAAGAACATCCACGAA

2.10. Cell Activity Assay

The CCK-8 colorimetric assay was used to determine cell activity [34]. Cells were inoculated on 96-well plates at an inoculation density of 1×10^4/mL. After incubation with SP or BBR, 10 μL of CCK-8 solution was added to each well in a humidified incubator with 5% CO_2 at 28 °C for 2 h. The absorbance value (OD) of each well was measured using ELISA (single wavelength, 450 nm).

2.11. Cellular TG Content Assay

Cells were inoculated into 96-well plates. The original cell culture medium was discarded after each group of cells was treated, followed by rinsing three times with DPBS. Next, 100 μL of cell lysis solution was added to each well and oscillated to fully lyse the cells. Intracellular TG level was measured with GPO-POD method using Triglyceride Colorimetric Assay Kit (Nanjing, Jiangsu, China). The content of protein in each sample was determined by BCA Protein Assay Kit (Nanjing, Jiangsu, China).

2.12. Total RNA Extraction, Reverse Transcription and Real-Time PCR

Total cellular RNA was extracted and reverse transcribed, and the expression level of *Camk1db* in each group of cells was detected by real-time fluorescence quantitative PCR. Real-time quantitative primer sequences for the genes to be tested were designed by Primer Premier 5.0 software and synthesized by Inweigeki (Table 2). The reaction solution was prepared on ice, mixed thoroughly, and the configured mixture was divided into reaction tubes of 18 μL each. Next, cDNA was added to the samples, which were then centrifuged thoroughly for the amplification reaction. The specific reaction conditions were as follows: 95 °C for 30 s; 95 °C for 5 s, 60 °C for 34 s, 40 cycles and 95 °C for 15 s; 60 °C for 60 s, 95 °C for 15 s. The relative expression of the genes to be tested in the samples was calculated using the $2^{-\Delta\Delta CT}$ method [35].

Table 2. Nucleotide sequences of primers of target genes.

Target Gene	Accession Number	Forward Primer (5′-3′)	Reverse Primer (5′-3′)
camk1db	NC_007136.7	GCGTGACGGATGGAGAAA	AGGCCACAGTAAACAGGAATAT

2.13. Statistical Analysis

All results are shown as mean ± standard error (X ± SEM) and one-way ANOVA, and Duncan's multiple range test were performed using SPSS 20.0. The significance level was $p < 0.05$, which was considered statistically significant.

3. Results

3.1. Modulation of Oxidative Stress, Apoptosis and Autophagy in Palmitic Acid-Induced Fat-Deposited Zebrafish Hepatocytes by Berberine

3.1.1. Berberine on Sodium Palmitate-Induced Oxidative Stress in Zebrafish Hepatocytes

To detect the oxidative stress status of cells, the intracellular ROS (reactive oxygen species) content, MDA (malondialdehyde) content, and T-AOC (total antioxidant capacity), were measured. Excess ROS causes cellular damage, and MDA is an important marker of ROS-induced oxidative damage [36]. High levels of T-AOC can effectively protect cells from reactive oxygen species [37]. Four groups were created for the experiment: a control group (Control), a lipid accumulation group (SP), a berberine group (BBR), and a lipid accumulation + berberine group (SP + BBR), respectively. As seen in Figure 1A, the intracellular MDA content was significantly higher in the lipid accumulation group

compared with the control group, but there was no significant change in the MDA content in the berberine group or the lipid accumulation + berberine group, and the MDA content in the lipid accumulation + berberine group was significantly reduced compared with the lipid accumulation group ($p < 0.05$). As seen in Figure 1B, the intracellular T-AOC (total antioxidant capacity) was significantly lower in the lipid accumulation group compared with the control group; there was no significant change in the T-AOC in the berberine group and the lipid accumulation + berberine group; and the T-AOC in the lipid accumulation + berberine group was significantly higher compared with the lipid accumulation group ($p < 0.05$). As seen in Figure 1C, the intracellular ROS (reactive oxygen species) content was significantly higher in the lipid accumulation group compared with the control group; there was no significant change in the berberine group; and the ROS content was significantly higher in the lipid accumulation + berberine group ($p < 0.05$). In addition, we also examined the ROS fluorescence graph, in which the brightness of the green spot represented the level of intracellular ROS content, and the brighter fluorescence indicated higher intracellular ROS concentration (red arrows). This can be seen from the luminescence trend compared with the control group, as the fluorescence intensity of all other groups was significantly higher, with the lipid accumulation + berberine group having the highest fluorescence intensity, which was consistent with the results in Figure 1D. These data indicated that lipid accumulation treatment caused oxidative stress in cells, and the total antioxidant capacity was reduced. Conversely, the addition of appropriate amounts of berberine were found to effectively alleviate the level of oxidative stress in cells, and improve the lipotoxicity caused by lipid accumulation.

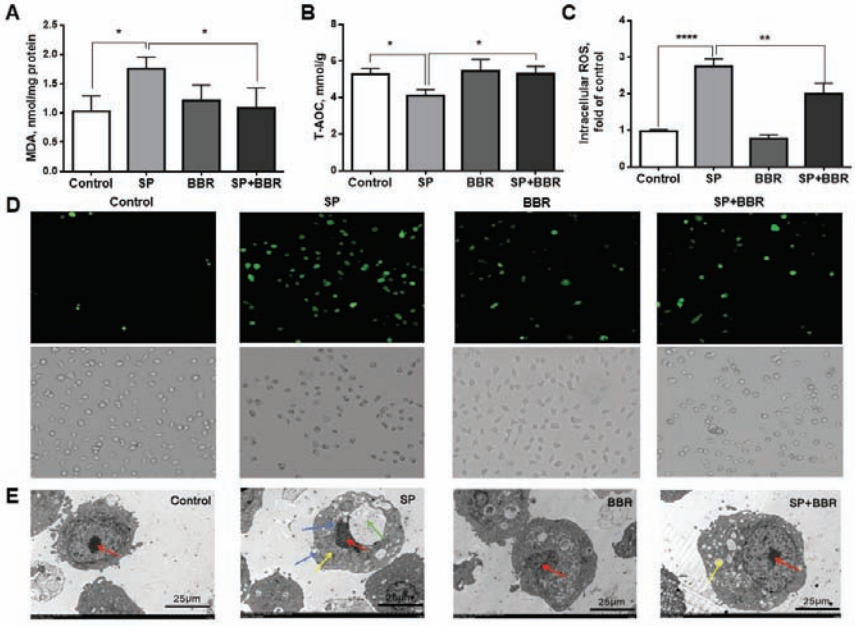

Figure 1. Indicators of oxidative stress in different treatment groups within ZFL and transmission electron microscopy pictures of ZFL. (**A**) is MDA (malondialdehyde). (**B**) is T-AOC (total antioxidant capacity). (**C**) is the relative expression of ROS. (**D**) is the ROS fluorescence microscope picture. The red arrow is the fluorescence of ROS in zebrafish liver cells. The higher the ROS content, the stronger the fluorescence intensity. Dates were presented as mean ± SEM ($n = 3$). * $p < 0.05$, ** $p < 0.01$, and **** $p < 0.0001$. (**E**) shows transmission electron microscopy pictures of ZFL. The red arrow is the nucleus, the blue arrow is the lipid drop, and the yellow arrow is the mitochondria, the green arrow is bubbles.

3.1.2. Berberine on Sodium Palmitate-Induced Hepatocyte Apoptosis and Autophagy

To investigate changes of the apoptosis rates in each treatment group, flow cytometry was applied (Figure 2A), and the data were counted in Figure 2B plots ($p < 0.05$). Results indicated that the apoptosis rate in the lipid accumulation group was significantly higher than the control group, and the apoptosis rate in the berberine group was significantly lower, while the apoptosis rate in the lipid accumulation + berberine group was significantly lower than the lipid accumulation group. Among all groups, the apoptosis rate was lowest in the berberine group, followed by the control group and the lipid accumulation + berberine group, while the apoptosis rate was highest in the lipid accumulation group. To detect changes in the level of cellular autophagy in each group, Western blotting was applied to detect the expression of proteins associated with cellular autophagy in each group (Figure 2C). The relative content of P62 protein, which was calculated as shown in gray in Figure 2D, was significantly lower in the lipid accumulation group compared with the control group, significantly higher in the berberine group, and significantly higher in the lipid accumulation + berberine group, compared with the lipid accumulation group ($p < 0.05$). The relative content of LC3-B protein is presented in Figure 2E, indicating that LC3-B protein content was significantly higher in the lipid accumulation group compared with the control group, significantly lower in the berberine group, and significantly lower in the lipid accumulation + berberine group, compared with the lipid accumulation group ($p < 0.05$). The expression of P62 protein was negatively correlated with the level of cellular autophagy, and the expression of LC3-B protein was positively correlated with the level of cellular autophagy. The P62 and LC3-B protein expression levels indicated that the autophagy levels in the lipid accumulation group was significantly higher than in the control group, and that the autophagy level in the lipid accumulation + berberine group was significantly lower than in the lipid accumulation group, while the autophagy level in the berberine group was the lowest, and the autophagy level in the lipid accumulation group was the highest.

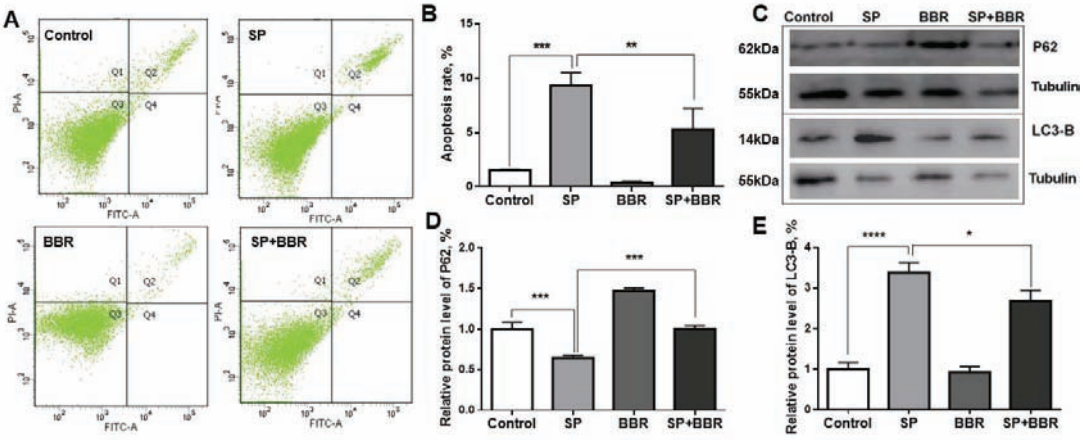

Figure 2. Berberine on sodium palmitate-induced hepatocyte apoptosis and autophagy. (**A**) is flow cytometry to detect ZFL apoptosis, each group has a cell count of 10,000. (**B**) is apoptosis and apoptosis rate of ZFL. (**C**) is WB diagram of P62 protein and LC3-B protein. (**D**) is relative expression level of P62 protein. (**E**) is relative expression level of LC3-B protein. Dates were presented as mean ± SEM ($n = 3$). * $p < 0.05$, ** $p < 0.01$, and *** $p < 0.001$, **** $p < 0.0001$.

3.1.3. Berberine on the Morphology of Zebrafish Hepatocytes Induced by Sodium Palmitate

As seen in Figure 1E, transmission electron micrographs of the cells were taken. The cells in the control group were morphologically intact, with round and regular shaped nuclei (red arrow), clear nuclear membranes, and normal endoplasmic reticulum and

mitochondrial morphology. The morphology of the cells in the lipid accumulation group was significantly changed. The cells were severely vacuolated (green arrow); the nucleoli were extruded and deformed; the intracellular mitochondria were swollen (yellow arrow); and a large number of obvious lipid droplets appeared (blue arrow), indicating that the lipid accumulation treatment induced by sodium palmitate had an adverse effect on the cell morphology. In contrast, after the addition of an appropriate amount of berberine, there was a significant trend of cell morphology recovery compared with the lipid accumulation group, but there were still small amounts of swollen mitochondria and lipid droplets compared with the control group.

3.2. Effect of Berberine on Palmitic Acid-Induced m^{6}A Methylation and Transcription Levels in Zebrafish Hepatocytes

3.2.1. m^{6}A Methylation Analysis

Cells were collected from four experimental groups: control group (Control), lipid accumulation group (SP), berberine group (BBR), and lipid accumulation + berberine group (SP + BBR), and methylation analysis was conducted by Merip-seq high-throughput sequencing to investigate the effect of berberine on lipid accumulation-induced m^{6}A methylation in zebrafish cells. As seen in Table 3, in terms of the number of methylation sites, the highest number was detected in the berberine group, followed by the lipid accumulation + berberine group and the control group, with the least number of methylation sites detected in the lipid accumulation group. Results indicated that the addition of either lipid accumulation or berberine affected the number of m^{6}A methylation sites in zebrafish hepatocytes.

Table 3. Number of methylation sites.

Group	Number of Methylation Sites
Control	23,182
SP	20,859
BBR	26,152
SP + BBR	25,432

To study the distribution of m^{6}A sites on mRNA, m^{6}A peaks were then divided into four parts according to their position on the transcript: 5′ untranslated region (5′UTR); 3′ untranslated region (3′UTR), 1st Exon (1st Exon), and Other Exon (Other Exon). Table S1 and Figure 3 summarize the distribution of m^{6}A sites in each group, with most peaks located in the 3′ untranslated region, followed by the 5′ untranslated region and other exon regions. Compared with the control group, there was a significant increase in the proportion of m^{6}A peaks in the 3′ and 5′ untranslated regions in the lipid accumulation group, while the proportion within the 3′ untranslated region was significantly reduced and the proportion within 5′ untranslated region was further increased after the addition of berberine. M^{6}A peaks possessed a higher enrichment ploidy. This indicated that lipid accumulation-induced zebrafish hepatocytes possessed different m^{6}A methylation patterns, and the addition of appropriate amounts of berberine changed these m^{6}A methylation patterns.

The methylation and demethylation process of RNA requires binding proteins to the motifs of methylation sites. The analysis software HOMER was used to look for motifs with high feasibility in the peak region, as seen in Figure 4A, for the four groups of samples with motif prediction results. Motifs with multiple occurrences and high similarity in the four groups revealed potential motifs of zebrafish methylation sites. Results indicated that all four different treatment groups contained the "RRACH" motif, which indicated that zebrafish also conformed to the general pattern of other species, and confirmed that the results of this experiment were reliable and could be used for subsequent analysis.

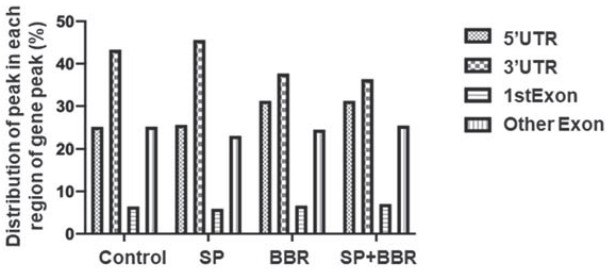

Figure 3. Distribution of m6A peaks of each group within ZFL.

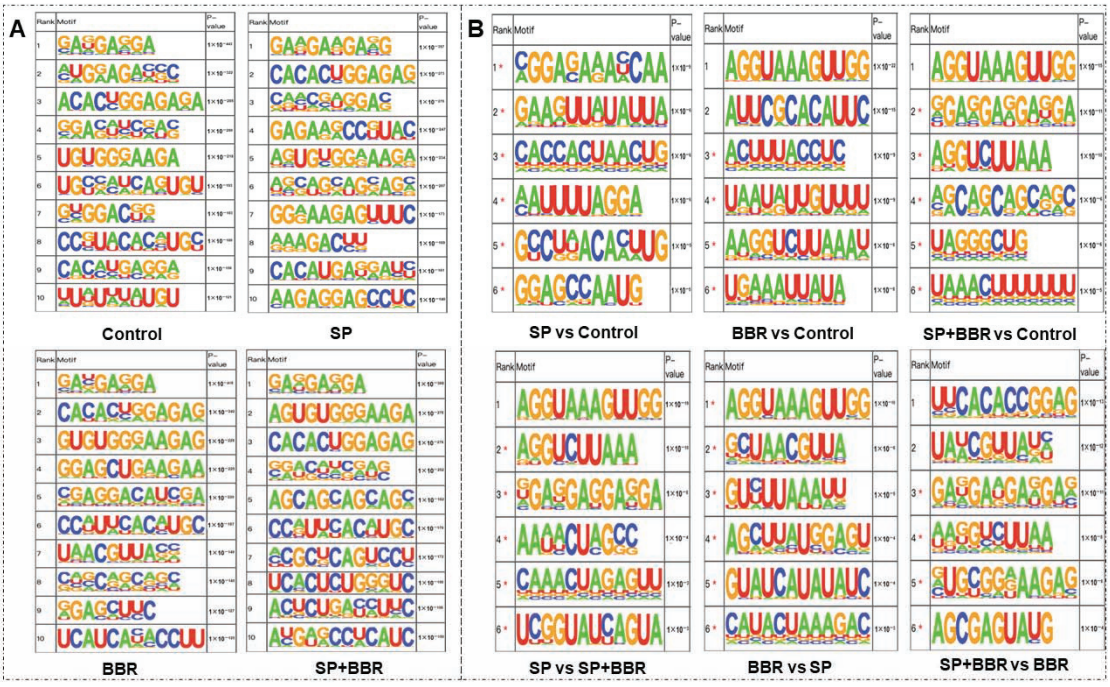

Figure 4. M^{6}A methylation analysis. (**A**) is top ten motif analysis for different treatment groups within ZFL. (**B**) is top six motif analysis of each comparison group. *—possible false positive.

Table S2 illustrates the significant changes in methylation levels in each comparison group. The number of genes with significant methylation differences was 231 in the lipid accumulation group compared with the control group; 488 in the berberine group compared with the control group; 107 in the lipid accumulation + berberine group compared with the lipid accumulation group; and 441 in the lipid accumulation + berberine group compared with the berberine group. This indicated that the effect of the treatment with berberine on methylation levels was more significant compared to the lipid accumulation treatment. The distribution of the screened differentially methylated gene peaks was further counted, and data in Table S3 demonstrates that most of the differentially m^{6}A methylated loci in each group was located in the 3′ untranslated region, followed by distribution in the 5′ untranslated region, then other exons, and finally, the first exon region. From the table, it can be seen that the proportion of m^{6}A peaks in the 3′ and 5′ untranslated regions was significantly increased in the lipid accumulation versus control group, while the proportion of the 3′ untranslated region was significantly decreased and the proportion

of the 5′ untranslated region was significantly increased in the berberine-repaired lipid accumulation group versus the control group. The addition of an appropriate amount of berberine was observed to change the m^6A methylation pattern of differential genes in lipid accumulation-induced zebrafish hepatocytes, with a decrease in the proportion of the 3′ untranslated region and an increase in the proportion of the 5′ untranslated region. The differentially methylated peaks screened for each comparison group were subjected to motif analysis, and the top six ranked differentially methylated motifs of lipid accumulation versus control are listed in Figure 4B. From the figure, we can find that lipid accumulation treatment affected m^6A methylation at these loci, and the m^6A methylation occurring at these loci was also associated with berberine treatment. Similarly, these motifs contained multiple "RRACH" sequences, which verified the reliability of the results.

3.2.2. Transcriptome Analysis

Cells were collected for transcriptomic analysis from four experimental setup groups: control (Control), lipid accumulation group (SP), berberine group (BBR), and lipid accumulation + berberine group (SP + BBR). Significant changes in transcript levels in each comparison group are summarized in Table S4. In terms of up- and down-regulation of transcript levels, the number of genes up-regulated by methylation was greater than the number of genes down-regulated by methylation in all comparison groups, except for the lipid accumulation + berberine group, where the number of genes up-regulated by methylation was smaller than the number of genes down-regulated by methylation compared with the lipid accumulation group.

The results of KEGG pathway enrichment analysis with significant differences in transcript levels are shown in Figure 5. Compared with the control group, the significantly differentially expressed genes in the lipid accumulation group were mainly involved in PPAR signaling pathway, phenylalanine, tyrosine and tryptophan biosynthesis, steroid biosynthesis, necroptosis, herpes simplex virus 1 infection, fructose and mannose metabolism, amino sugar and nucleotide sugar metabolism. Compared with the control group, the significantly differentially expressed genes in the berberine group were mainly involved in the TGF−beta signaling pathway, sphingolipid metabolism, selenocompound metabolism, primary bile acid biosynthesis, PPAR signaling pathway, FoxO signaling pathway, focal adhesion, arginine and proline metabolism, arachidonic acid metabolism, and the AGE−RAGE signaling pathway in diabetic complications. Compared with the control group, the significantly differentially expressed genes in the lipid accumulation + berberine group were mainly involved in the TGF−beta signaling pathway, terpenoid backbone biosynthesis, steroid biosynthesis, fatty acid elongation, cytokine−cytokine receptor interaction, biosynthesis of unsaturated fatty acids, and the AGE−RAGE signaling pathway in diabetic complications. Compared with the lipid accumulation + berberine group, the significantly differentially expressed genes in the lipid accumulation group were mainly involved in the TGF−beta signaling pathway, steroid biosynthesis, notch signaling pathway, MAPK signaling pathway, fatty acid elongation, biosynthesis of unsaturated fatty acids, and the AGE−RAGE signaling pathway in diabetic complications. Compared with the berberine group, the significantly differentially expressed genes in the lipid accumulation group were mainly involved in the sphingolipid metabolism, PPAR signaling pathway, FoxO signaling pathway, fatty acid degradation, cytokine−cytokine receptor interaction, biosynthesis of unsaturated fatty acids, and the AGE−RAGE signaling pathway in diabetic complications. Compared with the lipid accumulation + berberine group, the differentially expressed genes in the berberine group were mainly involved in the TGF−beta signaling pathway, steroid biosynthesis, taurine and hypotaurine metabolism, MAPK signaling pathway, linoleic acid metabolism, glycerolipid metabolism, cytokine−cytokine receptor interaction, and arachidonic acid metabolism. From the above results of the analysis of KEGG, the addition of high-fat and berberine significantly differentiates the transcriptional expression of genes in zebrafish liver cells, which in turn regulates related signaling pathways, mainly manifested as pathways related to lipid metabolism (PPAR signaling pathway,

MAPK signaling pathway, glyceril lipid metabolism, etc.), and pathways related to oxidative stress (FoxO signaling pathway, TGF-beta signaling pathway, etc.). This indicates that lipid deposition and berberine treatment have obvious effects on lipid metabolism and oxidative stress in zebrafish hepatocytes.

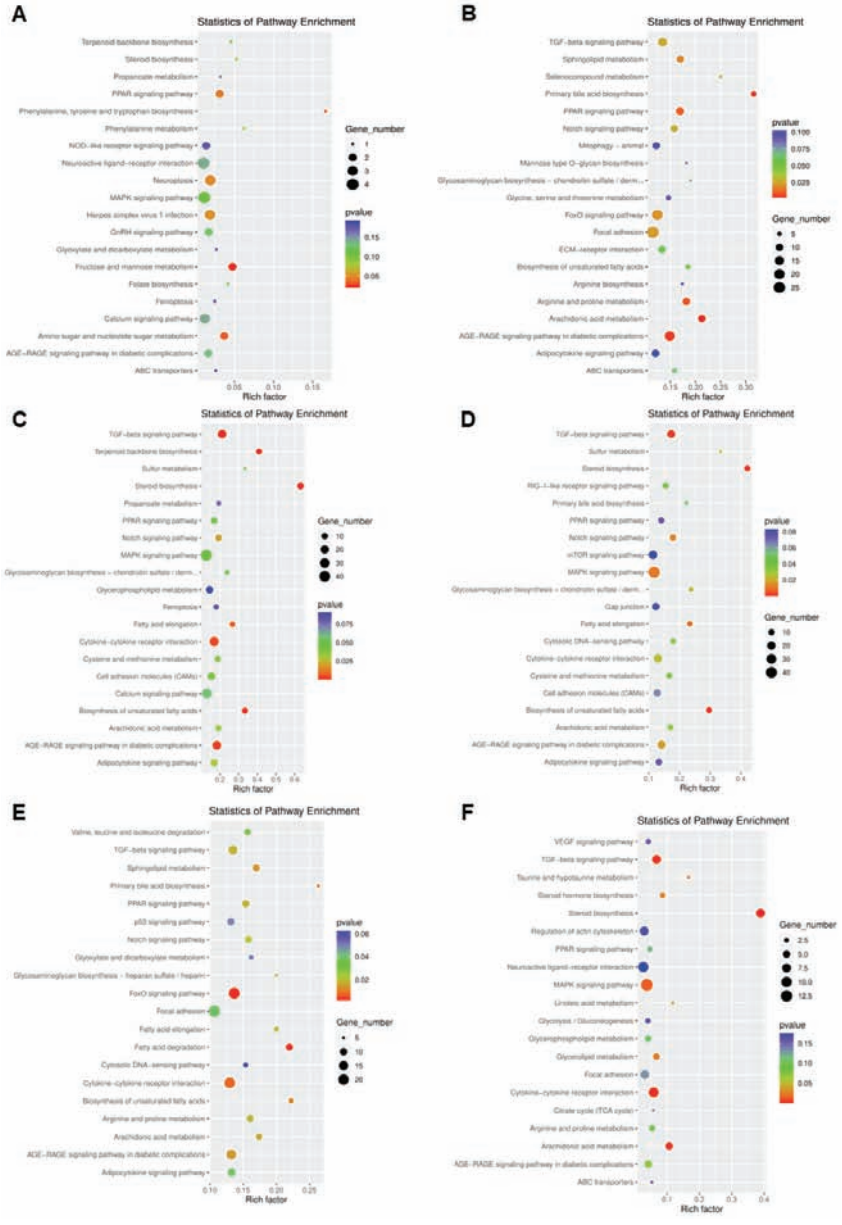

Figure 5. KEGG enrichment analysis of transcriptional differential genes in each comparison group. (**A**) is the comparison group of SP and Control. (**B**) is the comparison group of BBR and Control. (**C**) is the comparison group of SP + BBR and Control. (**D**) is the comparison group of SP + BBR and SP. (**E**) is the comparison group of BBR and SP. (**F**) is the comparison group of SP + BBR and BBR comparison group.

3.2.3. Analysis of m^{6}A Methylation and Transcriptome Association

For the correlation analysis of transcription levels and methylation levels, we counted the number of genes with changes in methylation and transcription levels, respectively, and the number of genes with significant differences in methylation and transcription levels at the same time in each comparison group, as seen in Table S5. We also analyzed the KEGG pathway for genes with significant differences in methylation and transcription together (Figure 6). Compared with the control group, the significantly differentially expressed genes in the lipid accumulation group were mainly involved in adrenergic signaling in cardiomyocytes. Compared with the control group, the significantly differentially expressed genes in the berberine group were mainly involved in PPAR signaling pathway, DNA replication, and arachidonic acid metabolism. Compared with the control group, the significantly differentially expressed genes in the lipid accumulation + berberine group were mainly involved in terpenoid backbone biosynthesis, synthesis and degradation of ketone bodies, ABC transporters, glycosaminoglycan biosynthesis − chondroitin sulfate/dermatan sulfate. Compared with the lipid accumulation + berberine group, the significantly differentially expressed genes in the lipid accumulation group were mainly involved in glycosaminoglycan biosynthesis − heparan sulfate/heparin, glycosaminoglycan biosynthesis − chondroitin sulfate/dermatan sulfate, beta−alanine metabolism, arginine biosynthesis, arginine and proline metabolism, and ABC transporters. Compared with the berberine group, the significantly differentially expressed genes in the lipid accumulation group were mainly involved in purine metabolism, PPAR signaling pathway, p53 signaling pathway, fatty acid degradation, arginine and proline metabolism, alanine, aspartate and glutamate metabolism, and N−Glycan biosynthesis. Compared with the lipid accumulation + berberine group, the differentially expressed genes in the berberine group were mainly involved in VEGF signaling pathway, tyrosine metabolism, sphingolipid metabolism, regulation of actin cytoskeleton, PPAR signaling pathway, MAPK signaling pathway, glycosaminoglycan biosynthesis − keratan sulfate, focal adhesion, adherens junction, and autophagy—other. From the above results of KEGG analysis of differentially methylated coding genes, it can be speculated that some genes related to lipid metabolism and translation regulation in zebrafish hepatocytes were differentially modified by m^{6}A methylation under lipid accumulation and berberine treatment, and thus their expression was regulated, which in turn affected the phenotype.

3.2.4. Screening of Target Genes

The screening process for methylation-transcription level association analysis focused on genes that showed significant changes in methylation levels and also showed significant differences in transcript levels ($p < 0.05$) (Fc $\geq$ 2). From these, the *Camk1db* gene of zebrafish was screened as the key gene for the next study. Trends are summarized in Table S6. The M^{6}A RNA methylation of the *Camk1db* gene was significantly lower in the lipid accumulation group compared with the control group, and the transcript level was reduced but not significantly different. The methylation levels and transcript levels were significantly higher in the berberine group compared to the lipid accumulation group. Methylation levels and transcript levels were also significantly increased in the lipid accumulation + berberine group compared to the lipid accumulation group.

3.3. Validation of Camk1db Gene Methylation and Its Regulation of Cellular Homeostasis in ZFL

3.3.1. Validation of m^{6}A Methylation Level and Transcription Level of Camk1db Gene

Changes in m^{6}A methylation levels and gene expression levels occurring in the *Camk1db* gene in each treatment group were also evaluated at a low throughput level. Merip PCR was used to detect the m^{6}A methylation level of the *Camk1db* gene (Figure 7A), and q-PCR was applied to detect the mRNA expression of the *Camk1db* gene (Figure 7B). Compared with the control group, the methylation and mRNA expression levels of *Camk1db* gene were significantly lower in the lipid accumulation group, and significantly higher in the berberine and lipid accumulation + berberine groups. Compared with the lipid accumulation group, the *Camk1db* gene methylation and mRNA expression levels were

significantly higher in the lipid accumulation + berberine group. The trends in each set are basically consistent with the previous Merip-seq high-throughput sequencing results.

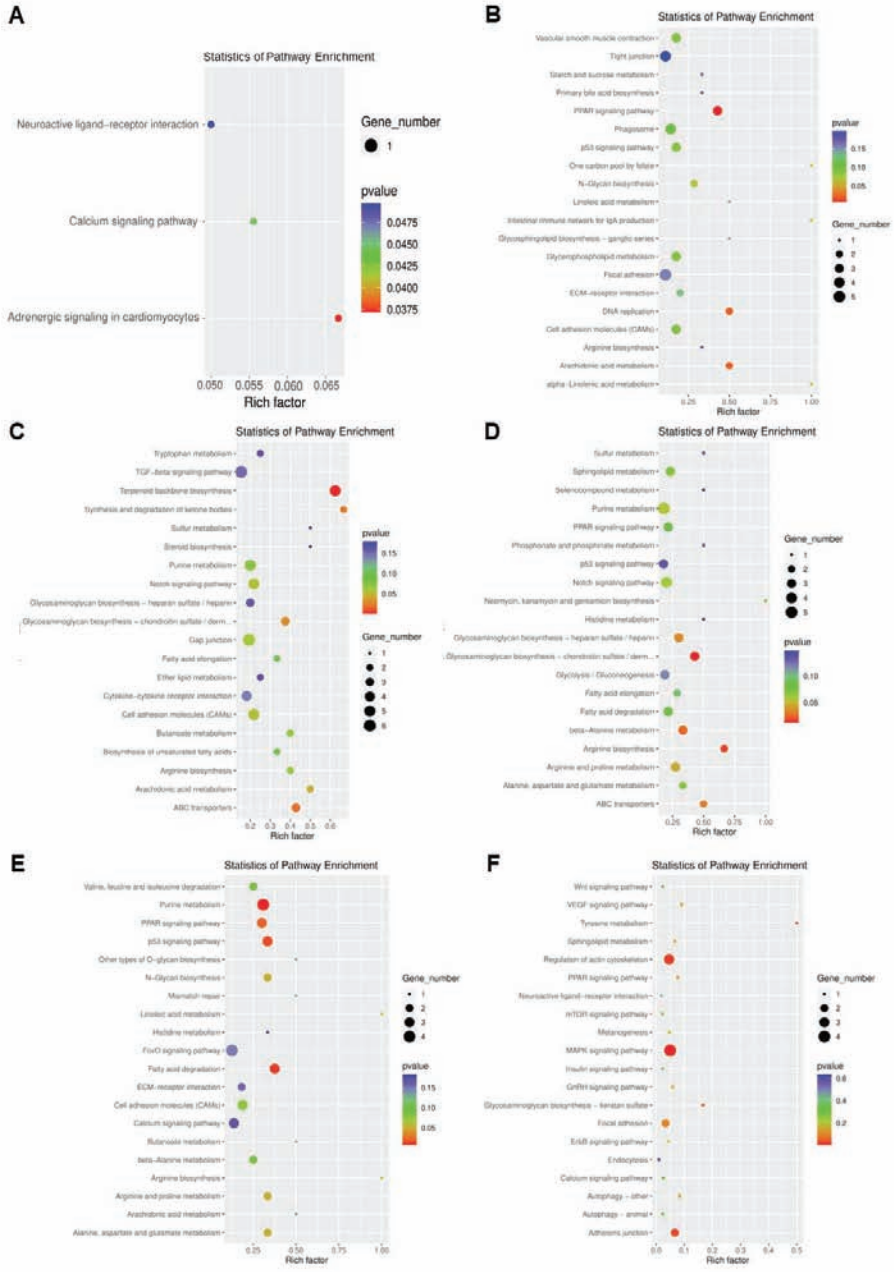

Figure 6. KEGG enrichment analysis of genes with significant differences in methylation and transcription levels in each comparison group. (**A**) is the comparison group of SP and Control. (**B**) is the comparison group of BBR and Control. (**C**) is the comparison group of SP + BBR and Control. (**D**) is the comparison group of SP + BBR and SP. (**E**) is the comparison group of BBR and SP. (**F**) is the comparison group of SP + BBR and BBR comparison group.

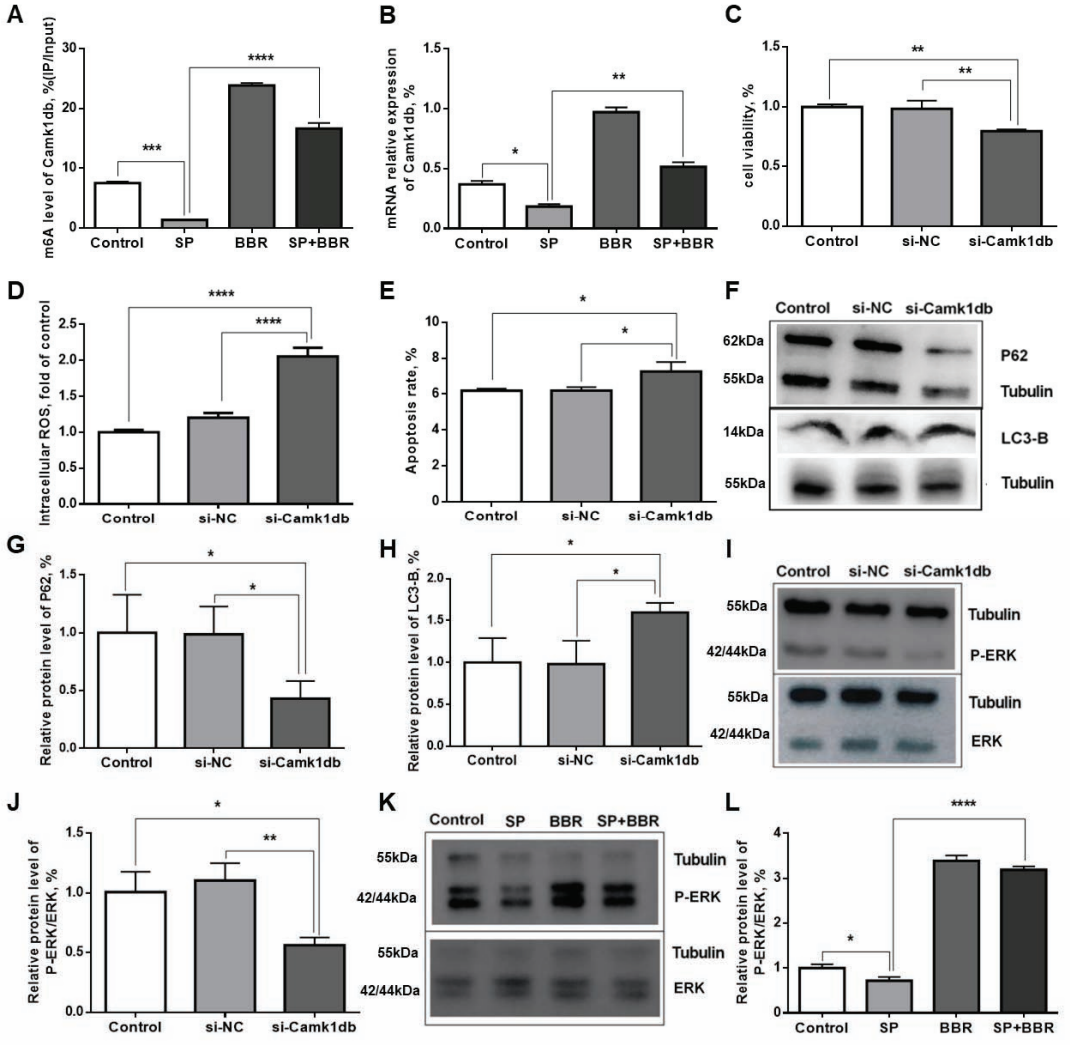

Figure 7. Validation of *Camk1db* gene methylation and its regulation of cellular homeostasis in ZFL by *Camk1db*. (**A**) is m^6A methylation level of *Camk1db* gene in ZFL. (**B**) is relative mRNA expression of *Camk1db* gene in ZFL. (**C**) is liver cell activity. (**D**) is the relative expression of intracellular ROS. (**E**) is apoptosis rate. (**F**) is the WB map of LC3-B and P62 protein. (**G**) are relative content of P62 protein. (**H**) are relative content of LC3-B protein. (**I**,**J**) are the WB map and relative level of P-ERK/ERK protein before and after transfection. (**K**,**L**) are different treatment groups (Control, SP, BBR, SP + BBR) P-ERK/ERK WB map and relative expression of protein. Dates were presented as mean ± SEM ($n = 3$). * $p < 0.05$, ** $p < 0.01$, and *** $p < 0.001$, **** $p < 0.0001$.

3.3.2. Regulation of Biological Functions of ZFL by Camk1db

To investigate the physiological function of *Camk1db* gene in zebrafish hepatocytes, siRNA transfection was used to silence *Camk1db* gene, and three groups were set up for the experiment: Control (control group), NC (non-specific control group), and Si-*Camk1db* (transfection group). First, we measured zebrafish physiological functions, including: cell activity, intracellular ROS content, apoptosis, and autophagy, before and after *Camk1db* gene silencing. As seen in Figure 7C, there was no significant change in cell activity in

the NC group compared with the control group, while there was a significant decrease in cell activity after transfection with siRNA to silence the *Camk1db* gene, indicating that the expression of the *Camk1db* gene was related to cell activity. Combined with the analysis from the previous experimental results, the lipid accumulation treatment may have reduced the cell activity by inhibiting the expression of *Camk1db* gene. Berberine treatment may have enhanced the cell activity by promoting the expression of *Camk1db* gene. As seen in Figures 7D and S1, no significant changes in intracellular ROS content were observed in the NC group compared with the control group, while there was a significant increase in intracellular ROS content after transfection with siRNA to silence the *Camk1db* gene, indicating that the expression of the *Camk1db* gene was negatively correlated with ROS. Combined with the analysis from the previous experimental results, lipid accumulation treatment promoted ROS by inhibiting the expression of the *Camk1db* gene. Berberine treatment increased the expression of *Camk1db* gene, which in turn inhibited the occurrence of ROS. As seen in Figure 7E and Figure S2, the apoptosis rate did not change significantly in the NC group compared with the control group, while there was a significant increase in the apoptosis rate after transfection with siRNA to silence the *Camk1db* gene, indicating that the expression of the *Camk1db* gene was negatively correlated with apoptosis. Combined with the analysis from the previous experimental results, lipid accumulation treatment promoted apoptosis by inhibiting the expression of the *Camk1db* gene. Berberine treatment increased the expression of *Camk1db* gene, which in turn inhibited the occurrence of apoptosis. To investigate changes in the level of autophagy occurring in the cells after transfection, the levels of P62 and LC3-B proteins in the cells before and after transfection were measured by Western blot. As seen in Figure 7F–H), there was a significant decrease in P62 protein content and a significant increase in LC3-B protein content in cells transfected with siRNA-silenced *Camk1db* gene compared with the control group. While P62 content was negatively correlated with the autophagy level of the cells, LC3-B content was positively correlated with the autophagy level of the cells. Therefore, the expression of *Camk1db* gene was inhibited and the level of cellular autophagy was increased. Combined with the analysis from the previous experimental results, these results indicated that lipid accumulation treatment inhibited the expression of *Camk1db* gene, which in turn increased the level of cellular autophagy. Berberine treatment increased the expression of *Camk1db* gene, which in turn inhibited the occurrence of autophagy in cells.

3.3.3. Exploration of the Signaling Pathway Acting by Camk1db

The protein encoded by *Camk1db*, a calmodulin-dependent protein kinase, can be activated by Ca^{2+} and calmodulin binding in cells, which in turn activates certain intracellular signaling pathways, including the ERK (extracellular regulated protein kinases) pathway, by inducing cell depolarization. Michelle et al. reported that increased expression of CaMKII could activate the extracellular signal-regulated kinase ERK signaling pathway and increase the level of ERK phosphorylation [38]. The ERK signaling pathway is an important member of the cellular signaling pathway, which mediates different cellular functions, including cell proliferation, migration, differentiation, and survival. This is consistent with the function of *Camk1db* gene discussed above. Therefore, to further investigate whether the *Camk1db* gene affects downstream physiological indicators through the ERK pathway, Western blot was used to detect the levels of ERK and P-ERK protein in the cells before and after transfection, and the relative levels of P-ERK/ERK were further calculated to measure the activation level of the ERK pathway. Results are presented in Figure 7I,J. Compared with the control group, the relative levels of P-ERK/ERK did not change significantly in the NC group, while there was a significant decrease in the relative levels of P-ERK/ERK in cells transfected with siRNA to silence the Camk1db gene. To investigate whether lipid accumulation and berberine treatment could mediate the effect of *Camk1db* gene on the activation of the ERK pathway, the relative level of P-ERK/ERK in the four treatment groups (Control, SP, BBR, SP + BBR) identified above. Results are summarized in Figure 7K,L. Compared with the control group, the level of P-ERK/ERK was

significantly lower in the lipid accumulation group and significantly higher in the berberine group, while the level of P-ERK/ERK was significantly higher in the lipid accumulation + berberine group compared with the lipid accumulation group. Taken together, these results suggested that lipid accumulation treatment can further inhibit the activation of the ERK pathway by suppressing the expression of *Camk1db* gene, and that berberine treatment could further promote the activation of ERK pathway by promoting the expression of *Camk1db* gene.

4. Discussion

M^6A RNA methylation was important for dietary regulation of downstream genes and physiological indicators. In our study, berberine alleviated cellular oxidative stress by reducing the high levels of apoptosis and autophagy caused by lipid accumulations, and was firstly found to change the cellular m^6A RNA methylation level. Berberine may increase the expression level of *Camk1db* mRNA by altering *Camk1db* m6A RNA methylation, and could regulate oxidative stress, apoptosis and autophagy through mediating the ERK1/2 signaling pathway activated by *Camk1db* in zebrafish-hepatocyte, which in turn affects cellular function, as shown in Figure 8.

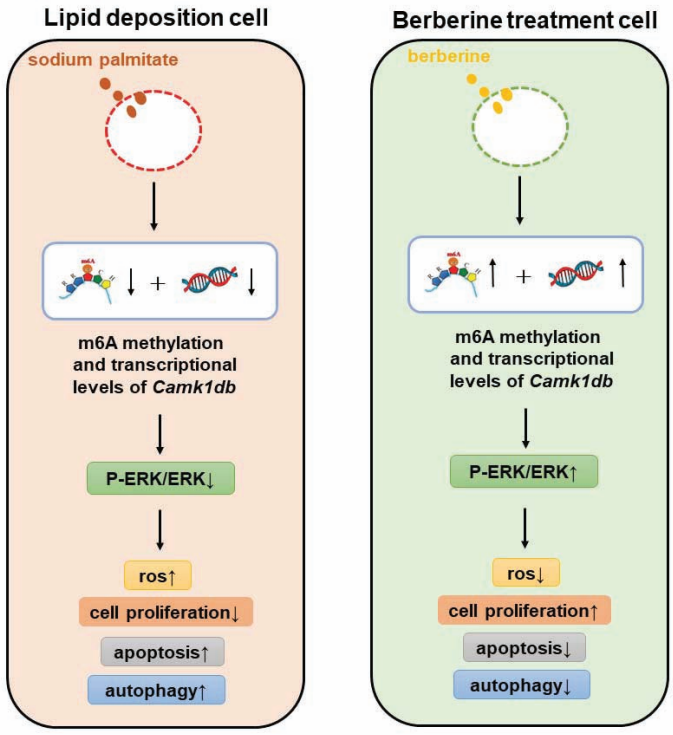

Figure 8. Berberine mediates the mechanism of *Camk1db*/ERK1/2 signaling pathway.

Under normal conditions, the oxidative and reductive systems in the cell are in organic equilibrium, maintaining normal cellular function. Once the oxidative and reductive systems are out of balance, homeostasis of the cellular redox environment ceases to exist, exhibiting stress and functional abnormalities, and continued imbalance will lead to abnormal cellular function. The free radical aging doctrine states that when oxidative damage dominates in cells, biomolecular functions will be disrupted, leading to the onset of aging [39]. It has been noted that excess palmitic acid can induce oxidative stress in hepatocytes [40]. In this study, berberine could effectively alleviate the oxidative stress, including ROS and

MDA contents, of ZFL cells induced by lipid accumulation. Numerous studies have shown that ROS levels are closely associated with apoptosis and autophagy. Fat deposition leads to an increase in intracellular ROS content, which triggers endoplasmic reticulum stress and further causes apoptosis [41]. ROS can be involved in cell proliferation, differentiation, apoptosis and other physiological functions, especially mitochondria-derived ROS, which are closely involved in the regulation of cellular autophagy. Under oxidative stress, autophagy can, on the one hand, restore cells to normal function by removing damaged organelles, while conversely, it can also directly induce the death of oxidized cells [42]. In this experiment, we examined the changes of apoptosis and autophagy levels in each treatment group. The combined indices showed that the lipid accumulation treatment significantly elevated the apoptosis rate and autophagy level of cells compared with the control group, while the addition of berberine could alleviate the high level of apoptosis and autophagy induced by lipid accumulation. Therefore, the alleviating effect of berberine on the high levels of apoptosis and autophagy induced by lipid accumulation may be related to the oxidative stress status of the cells. Lipid accumulation treatment induces cellular oxidative stress and increases apoptosis and autophagy levels. Berberine may alleviate oxidative stress by reducing high levels of apoptosis and autophagy caused by lipid accumulation.

When cells are under different environments, m^6A methylation can dynamically regulate the cellular response to the environment [43]. Several studies have shown that m^6A methylation plays a crucial role in regulating oxidative stress and cell damage. For example, in the mouse renal tubular epithelial cell model treated with colistin [44] and the mouse model of hepatic ischemia-reperfusion [45], the oxidative stress response was altered with the down-regulation or overexpression of METTL3 or FTO. Mettl3-mediated modification of m^6A is involved in PM2.5-induced apoptosis and autophagy [46]. METTL3 and FTO-mediated modification of m^6A jointly participate in the oxidative stress process induced by cadmium sulfate and cause cell apoptosis [47]. This study was designed to estimate whether dietary factors or herb regulates cell proliferation by m^6A methylation. We investigated the effect of berberine on lipid accumulation-induced m^6A methylation in ZFL cells by Merip-seq high-throughput sequencing, and the results showed that m^6A methylation was a dynamic and reversible modification occurring on RNA through changes in methylation sites and numbers, and that berberine treatment increased the overall m^6A methylation level in zebrafish hepatocytes, while the methylation level of m^6A decreased in cells under strong oxidative stress and cell damage after lipid accumulation treatment. This result is consistent with results reported by Sun [48]. Additionally, Andres et al. reported that the modification of m6A methylation in the 5′UTR increased during a state of oxidative stress, and that m6A methylation in the 5′UTR promoted the process of translation initiation of transcripts generated due to the stress state [49]. In this experiment, lipid accumulation treatment triggered the oxidative stress state of the cells. From the distribution observed, m6A methylation in the lipid accumulation group increased at the 5′UTR, and this proportion further increased after the addition of berberine, presumably related to the oxidative stress state. Berberine alleviated the oxidative stress state produced by lipid accumulation induced by increasing cellular m6A methylation modification in the 5′UTR. To investigate the gene function of the significantly altered m^6A methylation, the differentially methylated genes KEGG pathway was enriched. The enrichment results showed that differentially methylated genes were involved in several pathways related to oxidative stress, including: TGF-beta signaling pathway, MAPK signaling pathway, FOXO signaling pathway, PPAR signaling pathway, and VEGF signaling pathway. It should be noted that the effect of berberine on lipid accumulation-induced m^6A methylation production in ZFL cells was closely related to cellular oxidative stress, and m^6A methylation modification regulated oxidative stress-related signaling pathways, thereby regulating the level of oxidative stress in cells and thus affecting cell proliferation phenotype.

To further investigate the mechanism of m^6A methylation in the regulation of lipid accumulation-induced ZFL cells by berberine, a correlation analysis of methylation and

transcript level data was performed, and results screened for differential genes with significant differential changes at both levels for *Camk1db*. The protein encoding the zebrafish *Camk1db* gene is CaMKID (calmodulin-dependent protein kinase ID), which is generally inactive, and its activation is closely related to Ca^{2+} and calmodulin activity within the cell. Ca^{2+}, as a second messenger, is an important signaling ion that binds to receptors and proteins to participate in several physiological responses in the cell [50], particularly the protein CaM (calmodulin) [51]. When bound by Ca^{2+}, CaM enters an activated state, allowing it to bind to the target protein, calmodulin-dependent protein kinase (CaMK), to exert physiological effects. CaMKI kinase is known to be widely present in the cytoplasm of many animal tissues and can promote cell proliferation by regulating cell cycle proteins [52]. The activated state of CaMKI can induce cell depolarization, which in turn activates the ERK (extracellular regulated protein kinases) pathway [53]. In this study, the effect of *Camk1db* gene silencing on the level of P-ERK/ERK was examined using siRNA silencing target gene combined with Western blotting. The results showed that the level of P-ERK/ERK was significantly reduced in the *Camk1db* gene silencing group, confirming the aforementioned findings that CaMKI can activate the ERK pathway. In addition, *Camk1db* gene silencing significantly reduced cell viability and elevated cellular oxidative stress, apoptosis and autophagy levels. It is hypothesized that the effect of *Camk1db* on the ERK pathway is closely related to the alteration of these physiological functions.

ERK is an extracellular signal-regulated protein kinase, which belongs to one of the MAPKs (mitogen-activated protein kinases) and is involved in several physiological processes such as cell growth, division, development, and death [54]. It has been shown that the ERK pathway is also involved in the process of oxidative stress, especially the reperfusion injury caused by hemorrhagic shock resuscitation is closely related to the ERK signaling pathway. The ERK signaling pathway is an important signaling pathway for post-ischemic drug treatment to play a protective role in tissue and organ ischemia-reperfusion injury. The activation of ERK can effectively improve ischemia-reperfusion injury [55]. ERK can promote survival by inhibiting the activation of pro-apoptotic BCL-2 family proteins (e.g., BAX and BIM) and thereby inducing the expression of anti-apoptotic members of the BCL-2 family (e.g., BCL-2, BCL-XL and MCL-1) [56]. In HT-29 cells, ERK can be inhibited by penicillin to up-regulate the expression of autophagy signature protein LC3 and promote the occurrence of autophagy [57]. In summary, phosphorylation of ERK1/2 activates the ERK pathway, promotes cell proliferation, inhibits oxidative stress and apoptosis, increases the autophagy level of cells, which is consistent with the results of this experiment. In addition, this study also found that the ERK phosphorylation level was reduced in the lipid accumulation group compared with the control group, and the ERK pathway was inhibited, while the treatment with berberine significantly increased the ERK phosphorylation level and activated the ERK pathway in ZFL cells. Combined with the effects of berberine on the methylation of lipid accumulation-induced ZFL cells and on the expression of *Camk1db* gene, it was hypothesized that berberine could regulate the expression level of mRNA by altering the M^6A RNA methylation of the *Camk1db*, which further affected the synthesis of calmodulin-dependent protein kinase and thus the activation of the ERK pathway, resulting in changes in downstream physiological indicators.

5. Conclusions

In conclusion, this study explored the effects of berberine on the biological functions of oxidative stress, apoptosis, and autophagy in ZFL induced by sodium palmitate, while identified a new direction of m^6A methylation of cellular RNA and screening the key differential gene *Camk1db*. However, there are still some unresolved questions. It will be necessary to elucidate the role of m^6A methylation in the regulation of oxidative stress processes in vivo.

Supplementary Materials: The following supporting information can be downloaded at: https://www.mdpi.com/article/10.3390/antiox11122370/s1, Figure S1: ROS fluorescence microscope picture; Figure S2: Flow cytometry detection graphs; Table S1: Distribution of m6A peaks; Table S2: Statistics of the number of differentially methylated genes; Table S3: Peaks distribution statistics of differentially methylated genes; Table S4: Transcription level change statistics; Table S5: Statistics of changes in methylation level and transcription level; Table S6: Changes in the methylation level and transcription level of Camk1db gene.

Author Contributions: W.X., M.Z. and J.L. conceived and designed the experiments. M.Z. and J.L. performed most of the experiments. S.T. and C.Y. provided technical assistance. W.X. and M.Z. wrote the article. G.J., J.Z., H.Z., J.X. and W.X. were responsible for the funding acquisition. All authors have read and agreed to the published version of the manuscript.

Funding: This research was funded by the National Natural Science Foundation of China (NSFC) (31472292), Agri-X (2017003) and the Natural Science Foundation of Jiangsu Province (BK20201325).

Institutional Review Board Statement: Not applicable.

Informed Consent Statement: Not applicable.

Data Availability Statement: All of the data is contained within the article and the Supplementary Materials.

Acknowledgments: This work was jointly supported by grants from the School of Agriculture and Biology, Shanghai Jiao Tong University and College of Animal Science and Technology, Nanjing Agricultural University.

Conflicts of Interest: The authors declare no competing interest.

References

1. Trindade de Paula, M.; Poetini Silva, M.R.; Machado Araujo, S.; Cardoso Bortolotto, V.; Barreto Meichtry, L.; Zemolin, A.P.; Wallau, G.L.; Jesse, C.R.; Franco, J.L.; Posser, T.; et al. High-Fat Diet Induces Oxidative Stress and MPK2 and HSP83 Gene Expression in Drosophila melanogaster. *Oxidative Med. Cell. Longev.* **2016**, *2016*, 4018157. [CrossRef] [PubMed]
2. Zhou, X.; He, L.; Zuo, S.; Zhang, Y.; Wan, D.; Long, C.; Huang, P.; Wu, X.; Wu, C.; Liu, G.; et al. Serine prevented high-fat diet-induced oxidative stress by activating AMPK and epigenetically modulating the expression of glutathione synthesis-related genes. *Biochim. Biophys. Acta (BBA)-Mol. Basis Dis.* **2018**, *1864*, 488–498. [CrossRef] [PubMed]
3. Oldham, S.; Hafen, E. Insulin/IGF and target of rapamycin signaling: A TOR de force in growth control. *Trends Cell Biol.* **2003**, *13*, 79–85. [CrossRef] [PubMed]
4. Perez, C.L.; Van Gilst, M.R. A 13C isotope labeling strategy reveals the influence of insulin signaling on lipogenesis in *C. elegans*. *Cell Metab.* **2008**, *8*, 266–274. [CrossRef]
5. Pan, Y.; Ma, P.; Liu, Y.; Li, W.; Shu, Y. Multiple functions of m6A RNA methylation in cancer. *J. Hematol. Oncol.* **2018**, *11*, 48. [CrossRef]
6. Deng, X.; Chen, K.; Luo, G.Z.; Weng, X.; Ji, Q.; Zhou, T.; He, C. Widespread occurrence of N6-methyladenosine in bacterial mRNA. *Nucleic Acids Res* **2015**, *43*, 6557–6567. [CrossRef]
7. Ma, S.; Chen, C.; Ji, X.; Liu, J.; Zhou, Q.; Wang, G.; Yuan, W.; Kan, Q.; Sun, Z. The interplay between m6A RNA methylation and noncoding RNA in cancer. *J. Hematol. Oncol.* **2019**, *12*, 121. [CrossRef]
8. Liu, N.; Dai, Q.; Zheng, G.; He, C.; Parisien, M.; Pan, T. N6-methyladenosine-dependent RNA structural switches regulate RNA–protein interactions. *Nature* **2015**, *518*, 560–564. [CrossRef]
9. Wang, X.; Zhao, B.S.; Roundtree, I.A.; Lu, Z.; Han, D.; Ma, H.; Weng, X.; Chen, K.; Shi, H.; He, C. N6-methyladenosine Modulates Messenger RNA Translation Efficiency. *Cell* **2015**, *161*, 1388–1399. [CrossRef]
10. Roundtree, I.A.; Luo, G.Z.; Zhang, Z.; Wang, X.; Zhou, T.; Cui, Y.; Sha, J.; Huang, X.; Guerrero, L.; Xie, P.; et al. YTHDC1 mediates nuclear export of N(6)-methyladenosine methylated mRNAs. *eLife* **2017**, *6*, e31311. [CrossRef] [PubMed]
11. Klungland, A.; Dahl, J.A.; Greggains, G.; Fedorcsak, P.; Filipczyk, A. Reversible RNA modifications in meiosis and pluripotency. *Nat. Methods* **2017**, *14*, 18–22. [CrossRef]
12. Zhou, J.; Wan, J.; Gao, X.; Zhang, X.; Jaffrey, S.R.; Qian, S.B. Dynamic m(6)A mRNA methylation directs translational control of heat shock response. *Nature* **2015**, *526*, 591–594. [CrossRef] [PubMed]
13. Wang, S.; Tan, B.; Xiao, L.; Zhao, X.; Zeng, J.; Hong, L.; Yang, J.; Cai, G.; Zheng, E.; Wu, Z.; et al. Comprehensive Analysis of Long Noncoding RNA Modified by m(6)A Methylation in Oxidative and Glycolytic Skeletal Muscles. *Int. J. Mol. Sci.* **2022**, *23*, 4600. [CrossRef]
14. Xiang, Y.; Laurent, B.; Hsu, C.H.; Nachtergaele, S.; Lu, Z.; Sheng, W.; Xu, C.; Chen, H.; Ouyang, J.; Wang, S.; et al. RNA m(6)A methylation regulates the ultraviolet-induced DNA damage response. *Nature* **2017**, *543*, 573–576. [CrossRef] [PubMed]

15. Zhou, X.; Chen, J.; Chen, J.; Wu, W.; Wang, X.; Wang, Y. The beneficial effects of betaine on dysfunctional adipose tissue and N6-methyladenosine mRNA methylation requires the AMP-activated protein kinase alpha 1 subunit. *J. Nutr. Biochem.* **2015**, *26*, 1678–1684. [CrossRef] [PubMed]
16. Zhao, X.; Yang, Y.; Sun, B.F.; Shi, Y.; Yang, X.; Xiao, W.; Hao, Y.J.; Ping, X.L.; Chen, Y.S.; Wang, W.J.; et al. FTO-dependent demethylation of N6-methyladenosine regulates mRNA splicing and is required for adipogenesis. *Cell Res.* **2014**, *24*, 1403–1419. [CrossRef]
17. Wu, W.; Feng, J.; Jiang, D.; Zhou, X.; Jiang, Q.; Cai, M.; Wang, X.; Shan, T.; Wang, Y. AMPK regulates lipid accumulation in skeletal muscle cells through FTO-dependent demethylation of N6-methyladenosine. *Sci. Rep.* **2017**, *7*, 41606. [CrossRef]
18. Zhong, X.; Yu, J.; Frazier, K.; Weng, X.; Li, Y.; Cham, C.M.; Dolan, K.; Zhu, X.; Hubert, N.; Tao, Y.; et al. Circadian Clock Regulation of Hepatic Lipid Metabolism by Modulation of m6A mRNA Methylation. *Cell Rep.* **2018**, *25*, 1816–1828.e4. [CrossRef]
19. Chen, X.W.; Di, M.Y.; Zhang, J.; Zhou, Z.W.; Li, C.G.; Zhou, S.F. Interaction of herbal compounds with biological targets: A case study with berberine. *Sci. World J.* **2012**, *2012*, 708292. [CrossRef]
20. Tillhon, M.; Guamán Ortiz, L.M.; Lombardi, P.; Scovassi, A.I. Berberine: New perspectives for old remedies. *Biochem. Pharmacol.* **2012**, *84*, 1260–1267. [CrossRef]
21. Katsuyama, M. NOX/NADPH Oxidase, the Superoxide-Generating Enzyme: Its Transcriptional Regulation and Physiological Roles. *J. Pharmacol. Sci.* **2010**, *114*, 134–146. [CrossRef] [PubMed]
22. Huang, C.H.; Huang, Z.W.; Ho, F.M.; Chan, W.H. Berberine impairs embryonic development in vitro and in vivo through oxidative stress-mediated apoptotic processes. *Environ. Toxicol.* **2018**, *33*, 280–294. [CrossRef] [PubMed]
23. Mo, C.; Wang, L.; Zhang, J.; Numazawa, S.; Tang, H.; Tang, X.; Han, X.; Li, J.; Yang, M.; Wang, Z.; et al. The crosstalk between Nrf2 and AMPK signal pathways is important for the anti-inflammatory effect of berberine in LPS-stimulated macrophages and endotoxin-shocked mice. *Antioxid. Redox Signal.* **2014**, *20*, 574–588. [CrossRef] [PubMed]
24. Kong, W.; Wei, J.; Abidi, P.; Lin, M.; Inaba, S.; Li, C.; Wang, Y.; Wang, Z.; Si, S.; Pan, H.; et al. Berberine is a novel cholesterol-lowering drug working through a unique mechanism distinct from statins. *Nat. Med.* **2004**, *10*, 1344–1351. [CrossRef]
25. Yu, C.; Zhang, J.; Qin, Q.; Liu, J.; Xu, J.; Xu, W. Berberine improved intestinal barrier function by modulating the intestinal microbiota in blunt snout bream (Megalobrama amblycephala) under dietary high-fat and high-carbohydrate stress. *Fish Shellfish Immunol.* **2020**, *102*, 336–349. [CrossRef]
26. Chen, Q.Q.; Liu, W.B.; Zhou, M.; Dai, Y.J.; Xu, C.; Tian, H.Y.; Xu, W.N. Effects of berberine on the growth and immune performance in response to ammonia stress and high-fat dietary in blunt snout bream Megalobrama amblycephala. *Fish Shellfish Immunol.* **2016**, *55*, 165–172. [CrossRef]
27. Yang, S.S.; Yu, C.B.; Luo, Z.; Luo, W.L.; Zhang, J.; Xu, J.X.; Xu, W.N. Berberine attenuates sodium palmitate-induced lipid accumulation, oxidative stress and apoptosis in grass carp(Ctenopharyngodon idella)hepatocyte in vitro. *Fish Shellfish Immunol.* **2019**, *88*, 518–527. [CrossRef]
28. Lu, K.L.; Wang, L.N.; Zhang, D.D.; Liu, W.B.; Xu, W.N. Berberine attenuates oxidative stress and hepatocytes apoptosis via protecting mitochondria in blunt snout bream Megalobrama amblycephala fed high-fat diets. *Fish Physiol. Biochem.* **2017**, *43*, 65–76. [CrossRef] [PubMed]
29. Dahm, R.; Geisler, R.; Nüsslein-Volhard, C. Zebrafish (*Danio rerio*) Genome and Genetics. In *Reviews in Cell Biology and Molecular Medicine*; Wiley Online Library: Hoboken, NJ, USA, 2006; pp. 593–626. [CrossRef]
30. Ceni, E.; Mello, T.; Galli, A. Pathogenesis of alcoholic liver disease:Role of oxidative metabolism. *World J. Gastroenterol.* **2014**, *20*, 17756–17772. [CrossRef]
31. Abdel-Misih, S.R.; Bloomston, M. Liver anatomy. *Surg. Clin. N. Am.* **2010**, *90*, 643–653. [CrossRef] [PubMed]
32. Liu, J.; Zhang, M.J.; Yu, C.B.; Yang, S.S.; Zhang, J.; Xu, J.X.; Xu, W.N. Effects of berberine on lipid metabolism of Danio rerio liver cells induced by high fat. *J. Fish. China* **2021**, *46*, 1473–1486. (In Chinese) [CrossRef]
33. Ren, L.; Li, Z.; Dai, C.; Zhao, D.; Wang, Y.; Ma, C.; Liu, C. Chrysophanol inhibits proliferation and induces apoptosis through NF-κB/cyclin D1 and NF-κB/Bcl-2 signaling cascade in breast cancer cell lines. *Mol. Med. Rep.* **2018**, *17*, 4376–4382. [CrossRef]
34. Yoshimura, K.; Tanimoto, A.; Abe, T.; Ogawa, M.; Yutsudo, T.; Kashimura, M.; Yoshida, S. Shiga toxin 1 and 2 induce apoptosis in the amniotic cell line WISH. *J. Soc. Gynecol. Investig.* **2002**, *9*, 22–26. [CrossRef]
35. Livak, K.J.; Schmittgen, T.D. Analysis of relative gene expression data using real-time quantitative PCR and the 2(-Delta Delta C(T)) Method. *Methods* **2001**, *25*, 402–408. [CrossRef]
36. Surapon, T. Oxidative stress, insulin resistance, dyslipidemia and type 2 diabetes mellitus. *World J. Diabetes* **2015**, *6*, 456–480. [CrossRef]
37. Ruszkiewicz, J.; Albrecht, J. Changes of the thioredoxin system, glutathione peroxidase activity and total antioxidant capacity in rat brain cortex during acute liver failure: Modulation by L-histidine. *Neurochem. Res.* **2015**, *40*, 293–300. [CrossRef] [PubMed]
38. Melgarejo da Rosa, M.; Yuanxiang, P.; Brambilla, R.; Kreutz, M.R.; Karpova, A. Synaptic GluN2B/CaMKII-α Signaling Induces Synapto-Nuclear Transport of ERK and Jacob. *Front. Mol. Neurosci.* **2016**, *9*, 66. [CrossRef]
39. Barbouti, A.; Lagopati, N.; Veroutis, D.; Goulas, V.; Evangelou, K.; Kanavaros, P.; Gorgoulis, V.G.; Galaris, D. Implication of Dietary Iron-Chelating Bioactive Compounds in Molecular Mechanisms of Oxidative Stress-Induced Cell Ageing. *Antioxidants* **2021**, *10*, 491. [CrossRef]

40. Shan, X.; Miao, Y.; Fan, R.; Song, C.; Wu, G.; Wan, Z.; Zhu, J.; Sun, G.; Zha, W.; Mu, X.; et al. Suppression of Grb2 expression improved hepatic steatosis, oxidative stress, and apoptosis induced by palmitic acid in vitro partly through insulin signaling alteration. *In Vitro Cell. Dev. Biol. Anim.* **2013**, *49*, 576–582. [CrossRef]
41. Raza, M.H.; Siraj, S.; Arshad, A.; Waheed, U.; Aldakheel, F.; Alduraywish, S.; Arshad, M. ROS-modulated therapeutic approaches in cancer treatment. *J. Cancer Res. Clin. Oncol.* **2017**, *143*, 1789–1809. [CrossRef] [PubMed]
42. Wu, Z.; Wang, H.; Fang, S.; Xu, C. Roles of endoplasmic reticulum stress and autophagy on H_2O_2-induced oxidative stress injury in HepG2 cells. *Mol. Med. Rep.* **2018**, *18*, 4163–4174. [CrossRef] [PubMed]
43. Jia, G.; Fu, Y.; Zhao, X.; Dai, Q.; Zheng, G.; Yang, Y.; Yi, C.; Lindahl, T.; Pan, T.; Yang, Y.G.; et al. N6-methyladenosine in nuclear RNA is a major substrate of the obesity-associated FTO. *Nat. Chem. Biol.* **2011**, *7*, 885–887. [CrossRef] [PubMed]
44. Wang, J.; Ishfaq, M.; Xu, L.; Xia, C.; Chen, C.; Li, J. METTL3/m(6)A/miRNA-873-5p Attenuated Oxidative Stress and Apoptosis in Colistin-Induced Kidney Injury by Modulating Keap1/Nrf2 Pathway. *Front. Pharm.* **2019**, *10*, 517. [CrossRef]
45. Du, Y.D.; Guo, W.Y.; Han, C.H.; Wang, Y.; Chen, X.S.; Li, D.W.; Liu, J.L.; Zhang, M.; Zhu, N.; Wang, X. N6-methyladenosine demethylase FTO impairs hepatic ischemia-reperfusion injury via inhibiting Drp1-mediated mitochondrial fragmentation. *Cell Death Dis.* **2021**, *12*, 442. [CrossRef]
46. Yuan, Q.; Zhu, H.; Liu, H.; Wang, M.; Chu, H.; Zhang, Z. METTL3 regulates PM(2.5)-induced cell injury by targeting OSGIN1 in human airway epithelial cells. *J. Hazard. Mater.* **2021**, *415*, 125573. [CrossRef]
47. Reyfman, P.A.; Walter, J.M.; Joshi, N.; Anekalla, K.R.; McQuattie-Pimentel, A.C.; Chiu, S.; Fernandez, R.; Akbarpour, M.; Chen, C.I.; Ren, Z.; et al. Single-Cell Transcriptomic Analysis of Human Lung Provides Insights into the Pathobiology of Pulmonary Fibrosis. *Am. J. Respir. Crit. Care Med.* **2019**, *199*, 1517–1536. [CrossRef] [PubMed]
48. Sun, M.; Zhang, X. Epigenetic regulation of N6-methyladenosine modifications in obesity. *J. Diabetes Investig.* **2021**, *12*, 1306–1315. [CrossRef]
49. Anders, M.; Chelysheva, I.; Goebel, I.; Trenkner, T.; Zhou, J.; Mao, Y.; Verzini, S.; Qian, S.B.; Ignatova, Z. Dynamic m^6A methylation facilitates mRNA triaging to stress granules. *Life Sci. Alliance* **2018**, *1*, e201800113. [CrossRef]
50. Buchholz, J.N.; Behringer, E.J.; Brzozowski, T. *Calcium and Signal Transduction*; IntechOpen: London, UK, 2018; Volume 36.
51. O'Day, D.H.; Eshak, K.; Myre, M.A. Calmodulin Binding Proteins and Alzheimer's Disease. *J. Alzheimer's Dis.* **2015**, *46*, 553–569. [CrossRef] [PubMed]
52. Mallampalli, R.K.; Kaercher, L.; Snavely, C.; Pulijala, R.; Chen, B.B.; Coon, T.; Zhao, J.; Agassandian, M. Fbxl12 triggers G1 arrest by mediating degradation of calmodulin kinase I. *Cell. Signal.* **2013**, *25*, 2047–2059. [CrossRef] [PubMed]
53. Schmitt, J.M.; Wayman, G.A.; Nozaki, N.; Soderling, T.R. Calcium activation of ERK mediated by calmodulin kinase I. *J. Biol. Chem.* **2004**, *279*, 24064–24072. [CrossRef] [PubMed]
54. Burotto, M.; Chiou, V.L.; Lee, J.M.; Kohn, E.C. The MAPK pathway across different malignancies: A new perspective. *Cancer* **2014**, *120*, 3446–3456. [CrossRef]
55. Kim, M.J.; Park, I.J.; Yun, H.; Kang, I.; Choe, W.; Kim, S.S.; Ha, J. Correction: AMP-activated protein kinase antagonizes pro-apoptotic extracellular signal-regulated kinase activation by inducing dual-specificity protein phosphatases in response to glucose deprivation in HCT116 carcinoma. *J. Biol. Chem.* **2018**, *293*, 18012. [CrossRef] [PubMed]
56. Yue, J.; López, J.M. Understanding MAPK Signaling Pathways in Apoptosis. *Int. J. Mol. Sci.* **2020**, *21*, 2346. [CrossRef]
57. Zhao, Y.; Chen, H.; Shang, Z.; Jiao, B.; Yuan, B.; Sun, W.; Wang, B.; Miao, M.; Huang, C. SD118-xanthocillin X(1), a novel marine agent extracted from Penicillium commune, induces autophagy through the inhibition of the MEK/ERK pathway. *Mar. Drugs* **2012**, *10*, 1345–1359. [CrossRef]

antioxidants

MDPI

Article

Transcriptome and 16S rRNA Analyses Reveal That Hypoxic Stress Affects the Antioxidant Capacity of Largemouth Bass (*Micropterus salmoides*), Resulting in Intestinal Tissue Damage and Structural Changes in Microflora

Zhuo Song [1,†], Wei Ye [1,2,†], Yifan Tao [2], Tao Zheng [1], Jun Qiang [1,2,*], Yan Li [2], Wenting Liu [2] and Pao Xu [1,2,*]

[1] Wuxi Fisheries College, Nanjing Agricultural University, Wuxi 214081, China
[2] Key Laboratory of Freshwater Fisheries and Germplasm Resources Utilization, Ministry of Agriculture and Rural Affairs, Freshwater Fisheries Research Center, Chinese Academy of Fishery Sciences, Wuxi 214081, China
* Correspondence: qiangj@ffrc.cn (J.Q.); xup@ffrc.cn (P.X.)
† These authors contributed equally to this study.

Abstract: Dissolved oxygen (DO) is a key factor affecting the health of aquatic organisms in an intensive aquaculture environment. In this study, largemouth bass (*Micropterus salmoides*) were subjected to acute hypoxic stress for 96 h (DO: 1.00 mg/L) followed by recovery under sufficient DO conditions (DO: 7.50 mg/L) for 96 h. Serum biochemical indices, intestinal histomorphology, the transcriptome, and intestinal microbiota were compared between hypoxia-treated fish and those in a control group. The results showed that hypoxia caused oxidative stress, exfoliation of the intestinal villus epithelium and villus rupture, and increased cell apoptosis. Transcriptome analyses revealed that antioxidant-, inflammation-, and apoptosis-related pathways were activated, and that the MAPK signaling pathway played an important role under hypoxic stress. In addition, 16S rRNA sequencing analyses revealed that hypoxic stress significantly decreased bacterial richness and identified the dominant phyla (Proteobacteria, Firmicutes) and genera (*Mycoplasma*, unclassified *Enterobacterales*, *Cetobacterium*) involved in the intestinal inflammatory response of largemouth bass. Pearson's correlation analyses showed that differentially expressed genes in the MAPK signaling pathway were significantly correlated with some microflora. The results of this study will help to develop strategies to reduce damage caused by hypoxic stress in aquacultured fish.

Keywords: dissolved oxygen; *Micropterus salmoides*; transcriptome; 16S rDNA; intestine

Citation: Song, Z.; Ye, W.; Tao, Y.; Zheng, T.; Qiang, J.; Li, Y.; Liu, W.; Xu, P. Transcriptome and 16S rRNA Analyses Reveal That Hypoxic Stress Affects the Antioxidant Capacity of Largemouth Bass (*Micropterus salmoides*), Resulting in Intestinal Tissue Damage and Structural Changes in Microflora. *Antioxidants* **2023**, *12*, 1. https://doi.org/10.3390/antiox12010001

Academic Editor: Erchao Li

Received: 19 November 2022
Revised: 9 December 2022
Accepted: 14 December 2022
Published: 20 December 2022

1. Introduction

Dissolved oxygen (DO) is an important environmental factor affecting the growth and development of aquatic organisms. In the process of fish farming, especially in overcast and rainy weather in summer and autumn, acute hypoxia can readily occur. Prolonged low DO levels (below 1–2 mg/L) adversely affect fish [1]. Low DO not only affects fish behavior, immunity, and metabolism [2] but also leads to oxidative stress [3] and even death [4]. Thus, hypoxia seriously restricts the sustainable development of intensive aquaculture.

Previous studies have revealed the effects of the duration of hypoxia on oxidative stress, inflammation, and apoptosis, in aquatic organisms. For example, culturing large yellow croaker (*Larimichthys crocea*) in water with a DO level of 2 mg/L for 96 h can cause oxidative stress, affect the balance of the redox system, and lead to gill tissue damage [5]. A study on hybrid yellow catfish (*Pelteobagrus fulvidraco* ♀× *Pelteobagrus vachelli* ♂) found that oxidative stress, respiratory metabolism, and apoptosis were affected when the DO level reached 0.7 ± 0.05 mg/L and was maintained at that level for 6.5 h [6]. The contents of serum metabolites (glucose and lactic acid) in mrigal (*Cirrhinus mrigala*) also changed significantly upon 24 h of exposure to water with a DO level of 0.5 ± 0.04 mg/L [7]. In

common carp (*Cyprinus carpio*), hypoxia led to an inflammation response, and then the reintroduction of oxygen into anoxic tissue caused oxidative stress and immune damage to fish tissue [8].

The intestine is not only an important part of the digestive and absorption system of fish but also an important immune organ. Under hypoxic stress, the intestinal mucosal immune system is activated and drives the adaptation to hypoxia by upregulating the expression of several metabolic enzymes and vasoactive factors and disrupting barrier function, growth, and apoptosis [9,10]. The disruption of the oxygen gradient is responsible for many intestinal diseases [11]. Several studies have shown that hypoxic stress significantly affects the intestinal structure of fish. Dong et al. found that intermittent hypoxia for 7 days led to the exfoliation of intestinal epithelial cells and a significant decrease in the length of intestinal villi [12]; Yang et al. found that the height and width of intestinal villi and the thickness of the muscle layer decreased significantly after 28 days of hypoxic stress [13]. Hypoxia also affects the immune system of fish, and was shown to affect neutrophils and cause inflammation in the intestinal mucosa of *Salmo salar* [9] and increase oxidative stress and apoptosis-related factors in the intestine of *Lateolabrax maculatus* [14]. Therefore, exposure to hypoxia can severely affect the intestinal health of fish.

The rapid development of second-generation sequencing technologies and bioinformatic analysis methods has allowed for effective and rapid analyses of the molecular mechanisms underlying responses of various tissues and organs to environmental conditions [15]. Using these techniques, researchers have unraveled a series of molecular changes in fish under hypoxic stress. It has been reported that in channel catfish (*Ictalurus punctatus*) [16] and blunt snout bream (*Megalobrama amblycephala*) [17], the pathways significantly enriched with differentially expressed genes (DEGs) under hypoxic stress are HIF-1, MAPK, and PI3K-Akt. The environmental stress caused by hypoxia reduces the oxygen transfer to the surrounding tissues. Previous analyses have shown that hypoxic stress also reduces the abundance of beneficial bacteria and increases the abundance of opportunistic pathogens in *Pelteobagrus vachelli* [18], thus leading to a higher incidence of gastrointestinal and intestinal inflammation. Studies on oriental river prawn (*Macrobrachium nipponense*) showed that intestinal microorganisms had important effects on physiological homeostasis under hypoxia [19]. Intestinal microbes and hosts can interact with each other [20,21]. We have confirmed this in hybrid yellow catfish (*Tachysurus fulvidraco* ♀× *Pseudobagrus vachellii* ♂) [22]. To determine whether a similar phenomenon would occur under hypoxic conditions, it is necessary to study the correlation between the gut microbiota and the transcriptome. The Largemouth bass (*Micropterus salmoides*) is popular because of its delicious meat, lack of intermuscular spines, and high nutritional value. In the study of hypoxia, 6 and 96 h are common stress times [23,24]. To observe the dynamic physiology of largemouth bass under hypoxic stress, we set several time points in multiples of four to determine the characteristics of stress response in largemouth bass. We identified changes in intestinal molecular indices by transcriptome sequencing and analyzed the intestinal histomorphology, serum antioxidant capacity, and intestinal microbial composition under acute hypoxic stress followed by reoxygenation. These results contribute to a comprehensive understanding of how these fish adapt to hypoxia, and will be useful to devise strategies to reduce the damage caused by hypoxic stress in cultured fish.

2. Materials and Methods

2.1. Fish Maintenance

The fish used in the experiment were healthy largemouth bass that were free of disease and injuries from the Yixing Base of Freshwater Fisheries Center, Chinese Academy of Fishery Sciences (Wuxi, China). Before the experiment, the fish were temporarily reared for 15 days in a 400 L indoor tank (water temperature 27 °C ± 1 °C, DO > 7.5 mg/L, ammonia nitrogen and nitrite < 0.01 mg/L, pH 7.6 ± 0.2). They were fed a commercial diet at 3% of their bodyweight (46% crude protein, 6% crude fat) at 8:00 and 16:00, respectively.

2.2. Determination of 96h-LH50

According to our previous research [25], fish (average weight, 8.27 ± 1.20 g) were subjected to DO at five different levels (0.15, 0.3, 0.6, 1.2, 2.4 mg/L) for 96 h to determine the median lethal hypoxia (96h-LH_{50}). The preliminary experiment was carried out in a 400 L indoor tank (20 fish per tank, with a total of 300 fish). Each inflatable tank was filled with 150 L tap water, and the oxygen concentration was measured with a DO meter (LD0101 probe, range: 0.1–20.0 mg/L, Hach, Loveland, LVLD, USA). Before the start of the experiment, the DO was adjusted to the specified level using nitrogen. The fish were observed every half hour. At each observation time, the dead fish were counted and removed. The mortality of largemouth bass was recorded at 24 h, 48 h, 72 h, and 96 h, and the cumulative mortality in each treatment during 96 h was calculated. Finally, the 96h-LH_{50} of largemouth bass was obtained by linear interpolation.

2.3. Sample Collection

The hypoxic stress experiments were carried out on the basis of 96h-LH50 for 96 h. The control group (DO: 7.50 mg/L) and the hypoxia group (DO: 1.00 mg/L) were set up with three parallel experiments per treatment group. The experiment was carried out in six 400 L culture tanks, each one containing 60 uniform and healthy largemouth bass (8.27 ± 0.22 g). In the hypoxia groups, the DO level was maintained at 1.00 mg/L for 96 h by adding nitrogen along with oxygen through the inlet valve. At the end of 96 h, oxygen was supplied through the valve to quickly return the DO to the normal level (DO: 7.50 mg/L), and these conditions were maintained for a further 96 h. During the experiment, the fish were fed normally.

Samples were taken at 0 h, 6 h, 24 h, 96 h under hypoxic stress (DO: 1.00 mg/L) and after 96 h of recovery under sufficient DO conditions (DO: 7.50 mg/L). At each sampling time, 12 fish were randomly selected from each of the three parallel groups in the hypoxia group and the control group for tail vein blood collection and foregut extraction. The blood was collected by caudal vein drawing. As described by Ma et al., [26], the serum was immediately centrifuged (4 °C, 3000× *g*) and frozen at −20 °C. These serum samples were used to analyze biochemical parameters. The foregut samples were fixed in 4% paraformaldehyde solution for pathological observations and apoptotic cell detection. Another 12 fish were taken from each of three parallel groups: 0 h group (Ctrl), 96 h group (Hyp), and 96 h recovery group (Rec). Foregut tissue samples were collected and frozen in liquid nitrogen and stored at −80 °C. The foregut of each fish was divided into three parts, which were used for 16S rRNA sequencing, transcriptome sequencing, and qRT-PCR verification, respectively.

2.4. Determination of Serum Biochemical Indices

The serum supernatant was used to analyze the contents of glucose, lactic acid (LAC), and malondialdehyde (MDA) and the activity of superoxide dismutase (SOD) and catalase (CAT). All these analyses were conducted using kits from the Shanghai Langton Biology Co., Ltd. (Shanghai, China) [25]. The absorbance values of the reaction mixtures were determined using an Epoch™ Microplate Spectrophotometer (BioTek Instruments, Inc., Winooski, VT, USA).

2.5. Histopathological Analysis of Intestine Samples

Paraffin sections were prepared as described previously [27]. The intestinal samples were fixed in 4% paraformaldehyde solution for 24 h, dehydrated in an ethanol gradient, then cleared in a mixture of xylene:anhydrous ethanol = 1:1 and xylene. The transparent samples were embedded in wax blocks using a Leica EG1150H embedding machine (leica, Germany), and the wax blocks were cut into thin slices (7 μm thickness) using a Leica RM2255 slicer (leica, Germany). After spreading, drying, and baking, the paraffin slices were dewaxed in xylene and ethanol solutions, and then stained with hematoxylin–eosin (HE). Finally, the slices were sealed with neutral gum and observed and photographed

under a Nikon Eclipse Ci microscope (Nikon, Tokyo, Japan) equipped with a Nikon digital sight DS-FI2 imaging system. The length and width of villi and the thickness of the muscle layer in each slice were measured using Image-Pro Plus 6.0 software (media cybernetics, Silver Spring, MD, USA).

2.6. Detection of Intestinal Cell Apoptosis in Largemouth Bass

Intestinal cell apoptosis was detected using a TUNEL (terminal dUTP nick-end labeling) kit (Yanjin Biotechnology Co., Ltd. Shanghai, China). After the paraffin sections were prepared as described above, they were immersed in xylene I (20 min), xylene II (20 min), and ethanol (100, 100, 85, 75%; 5 min at each concentration), and then washed with water for 2 min. The tissues were covered with DNase-free proteinase K (20 μg/mL), incubated at 37 °C for 25 min, and washed with PBS three times for 5 min each time. Tissue samples were placed in a wet box, covered with TUNEL reaction solution, and incubated at 37 °C for 1 h. After incubating with 3,3-diaminobenzidine (DAB) for 5 min, sections were restained with hematoxylin for 12 s. The sections were observed and photographed under a Nikon Eclipse Ci microscope equipped with a Nikon DS-U3 imaging system. The nuclei of normal nonapoptotic cells were stained blue by hematoxylin, while the nuclei of positive apoptotic cells were stained brownish-green by DAB. Image-Pro Plus 6.0 were used to calculate the number of apoptotic cells.

2.7. Sequencing and Analysis of Intestinal Transcriptome

2.7.1. Construction and Sequencing of mRNA Libraries

Total RNA was extracted from intestinal samples of the Ctrl, Hyp, and Rec groups (n = 12) using a TRIzol kit (Invitrogen, Carlsbad, CA, USA). The quantity and purity of total RNA were determined using a NanoDrop ND-1000 instrument (NanoDrop, Wilmington, DE, USA) and the integrity of RNA was tested using a Bioanalyzer 2100 instrument (Agilent, Palo Alto, CA, USA). Equal amounts of RNA were extracted from the Ctrl group, Hyp group, and Rec group and mixed for sequencing. There were three replicates in each group, and a total of nine samples were prepared (Ctrl1, Ctrl2, Ctrl3, Hyp1, Hyp2, Hyp3, Rec1, Rec2, Rec3). The mRNA with polyA (polyadenylate) was specifically captured using Dynabeads Oligo magnetic beads (Dynabeads Oligo (dT), cat.25-61005, Thermo Fisher, Waltham, MA, USA) through two rounds of purification, and then RNA-Seq libraries were constructed using the mRNA-Seq sample preparation kit (Illumina, San Diego, CA, USA) [28]. Finally, libraries were sequenced on the Illumina Novaseq sequence 6000 platform (LC Bio Technology Co., Ltd. Hangzhou, China) in the PE150 sequencing mode.

2.7.2. Data Filtering, Read Mapping and Detection of Differentially Expressed Genes

Cutadapt [29] was used to remove sequencing connectors and low-quality sequencing data, and Hisat2 [30] was used to compare the preprocessed effective data (clean data) with the reference genome of the largemouth bass (https://www.ncbi.nlm.nih.gov/genome/?term=Micropterus+salmoides%5Borgn%5D (accessed on 21 October 2021)). According to the alignment results, the transcripts were reconstructed using Stringtie [31] and the expression levels of all genes in each sample were calculated. The FPKM value [32] (fragments per kilobase million) was used as the measurement index of gene expression to calculate gene expression in different samples. T-tests were used to detect significant differences in gene expression between pairs of samples. Differentially expressed genes were screened using the following criteria: $|\log2FOLDCHANGE| >= 1$ & $p < 0.05$. Gene ontology (http://geneontology.org/, accessed on 20 November 2021, GO) and Kyoto Encyclopedia of Genes and Genomes (http://www.kegg.jp/, accessed on 20 November 2021, KEGG) enrichment analyses were used to determine the function and related metabolic pathways of DEGs, respectively.

2.7.3. Identification of DEGs in Intestines by qRT-PCR

Total RNA was extracted from intestines of Ctrl, Hyp, and Rec groups using an RNAiso Plus kit (TaKaRa, Dalian, China). The mass and concentration of RNA were determined by measuring the absorbance values of 260 nm and 280 nm (A260/A280 ratio, 1.9–2.1). A Prime Script template RT Master Mix (Takara) (Dalian, China) kit was used to synthesize the template cDNA by reverse transcription.

All the primers (Table S1) used to amplify differentially expressed genes were synthesized by the Genewiz Biotechnology Co., Ltd. (Suzhou, China). Using the known *β-actin* gene of largemouth bass as the internal reference [33], real-time fluorescence quantitative PCR analyses were performed using the SYBR ®Premix Ex Taq assay (Takara, Dalian, China) kit. The composition of the qRT-PCR reaction system was as follows: 2 × SYBR Premix Ex Taq™ 12.5 μL, 1 μL each of the forward and reverse primers, 50 × ROX reference Dye II 0.5 μL, 2 μL cDNA template, and RNase-free dH_2O to complete the volume to 25 μL. The thermal cycling conditions were as follows: 95 °C for 30 s; 95 °C for 5 s; 60 °C for 30 s (40 cycles). To confirm the specificity of primers, the amplification curve and melting curve of PCR were confirmed at the end of each operation. According to the Ct value measured by fluorescence quantitative PCR, the relative gene transcript level was calculated by the $2^{-\Delta\Delta Ct}$ method [34].

2.8. Sequencing and Analysis of Intestinal Microorganisms in 16S rRNA

2.8.1. DNA Extraction and Sequencing

DNA was extracted from the foregut of the Ctrl, Hyp, and Rec groups using an EZNA ® Stool DNA Kit (D4015, Omega Inc., Norcross, GA, USA). Ten samples with good DNA quality were selected from each group for follow-up experiments. The V4 and V3 variable regions of the bacterial 16s rRNA gene (400–450 bp) were selected for PCR amplification. The PCR thermal cycling program was as follows: 98 °C initial denaturation for 30 s, then 98 °C for 10 s (denaturation), 54 °C for 30 s, then 35 cycles of 72 °C for 45 s (annealing), and final extension for 10 min at 72 °C. The PCR products were purified using AMPure XT beads (Beckman Coulter Genomics, Danvers, MA, USA) and quantified by Qubit (Invitrogen, Carlsbad, CA, USA). The PCR amplification products were detected by 2% w/v agarose gel electrophoresis and recovered using AMPure XT beads recovery reagent. The purified PCR products were evaluated using an Agilent 2100 Bioanalyzer (Agilent, CA, USA) and an Illumina (Kapa Biosciences, Woburn, MA, USA) library quantification kit. Qualified library concentrations were higher than 2 nM. After gradient dilution of the qualified sequencing libraries, the libraries were mixed according to the required sequencing quantity and denatured into single strands by NaOH for sequencing. Double-ended sequencing of 2 × 250 bp was carried out using a NovaSeq 6000 sequencer (LC Bio Technology Co., Ltd. Hangzhou, China), with reagents of the NovaSeq 6000 SP Reagent Kit (500 cycles).

2.8.2. Statistical and Bioinformatic Analysis

After sequencing, the raw double-terminal data were spliced by overlapping, and then quality-control steps and chimera filtering were conducted to obtain high-quality clean data. Then, we used the concept of ASVs (amplicon sequence variants) to construct the OTUs (operational taxonomic units) table, and obtained the final ASV feature table and feature sequences for further analyses. QIIME (v.1.8.0) was used to calculate goods coverage, observed species, Chao1, and Shannon's and Simpson's indices to evaluate the alpha diversity of samples and to determine differences in species composition among samples. SILVA (release 138, https://www.arb-silva.de/documentation/release-138 (accessed on 1 November 2021)) and the NT-16S database were used to classify species and compare abundance ratios. The results are shown as a stacked bar chart. The linear discriminant analysis (LDA) effect magnitude (LEfSe) method was used to detect differences in bacterial group abundance among the Ctrl, Hyp, and Rec groups. PICRUSt2 analysis was used to predict the function of intestinal flora by KEGG functional annotation.

2.9. Transcriptome and Intestinal Microorganism Correlation Analyses

To detect correlations between intestinal bacteria and the MAPK signaling pathway, Pearson's correlation analysis was carried out using OmicStudio tool (https://www.omicstudio.cn (accessed on 15 August 2022)) [22]. The p value was corrected for multiple comparisons using R (version 3.6.1); $p < 0.05$ was considered to be statistically significant, $p < 0.01$ was very significant, and $p < 0.001$ was extremely significant.

2.10. Statistical Analysis

Data for 96h-LH_{50}, serum biochemical parameters, and qRT-PCR were analyzed using SPSS 23.0 (SPSS Inc., Chicago, IL, USA) and are expressed as means ± standard error. Shapiro–Wilk and Levene median tests were used to test for variance normality and homogeneity of data. One-way analysis of variance (ANOVA) and Tukey's test were used to detect significant differences in biochemical indices and gene transcript levels among different sampling times. The Kruskal–Wallis method was used to detect significant differences in alpha and beta diversity indices among different samples.

3. Results

3.1. Determination of 96h-LH_{50} in Largemouth Bass

As shown in Table 1, as the DO level decreased, the mortality of largemouth bass increased significantly. Taking the 96 h DO level and mortality as independent and dependent variables, respectively, the regression equation was obtained: $Y = -47.73x + 99.72$ ($r = 0.905$, $p < 0.0001$). The 96h-LH_{50} determined by linear interpolation was 1.04 mg/L (Figure 1). Therefore, 1.00 mg/L was selected as the 96h-LH_{50} of largemouth bass for further experiments.

Table 1. Effects of different low DO levels on 96 h mortality (%) of largemouth bass.

Time (h)	Dissolved Oxygen Levels (mg/L)				
	2.4	**1.2**	**0.6**	**0.3**	**0.15**
0	0	0	0	0	0
24	0	0	20	31.7	50
48	0	0	46.7	58.3	73.3
72	0	0	68.3	78.3	100
96	0	6.7	78.3	91.7	100

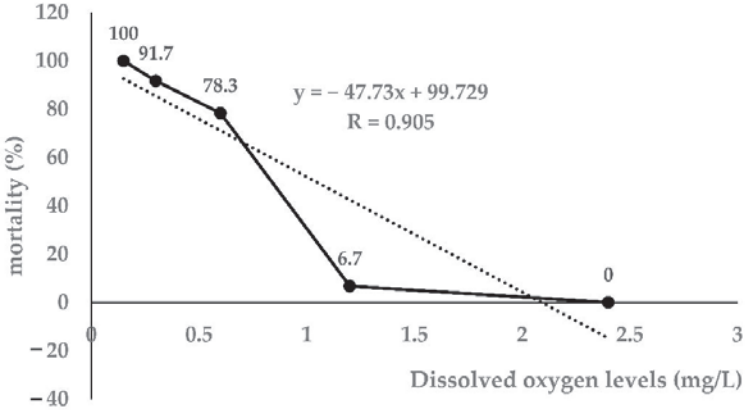

Figure 1. Linear interpolation graph for 96h-LH_{50} ($n = 20$).

3.2. Determination of Antioxidant Capacity of Largemouth Bass under Hypoxic Stress and Reoxygenation

As shown in Figure 2, the serum glucose content in largemouth bass reached the lowest level at 96 h under hypoxic stress, and then increased somewhat after 96 h of recovery under sufficient DO conditions (Figure 2A). In contrast, the LAC and MDA contents peaked at 96 h of hypoxic stress, and then decreased significantly by 96 h of recovery under sufficient DO conditions (Figure 2B,C). The activities of SOD and CAT reached the lowest values at 96 h of hypoxic stress, but significantly increased after 96 h of recovery under sufficient DO conditions (Figure 2D,E). All of these indices showed significant differences between the control group and the hypoxia group at 96 h ($p < 0.05$).

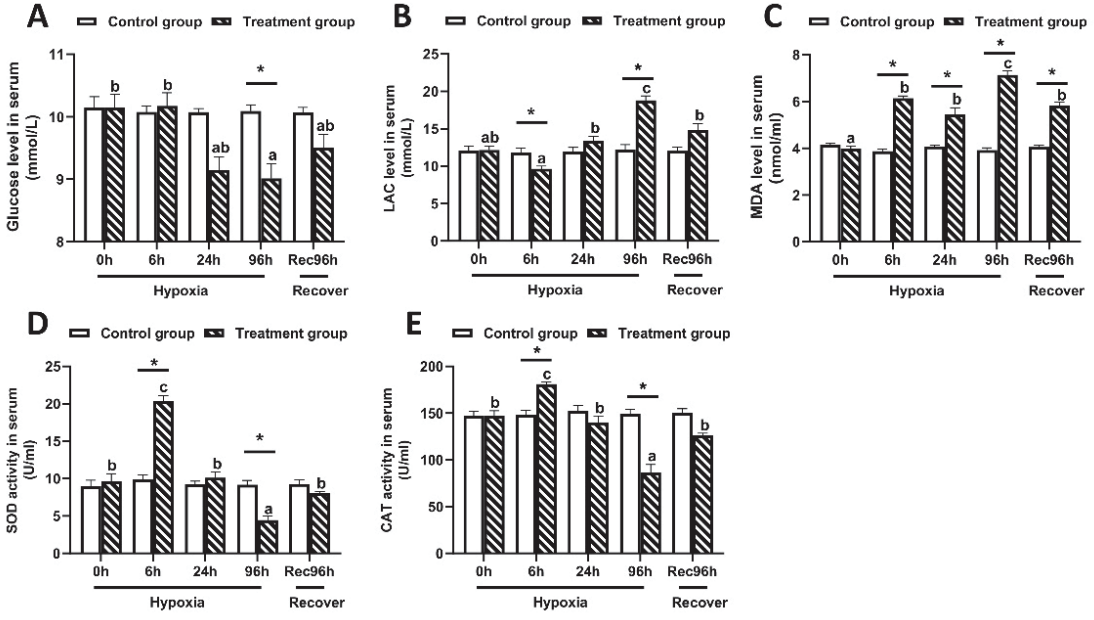

Figure 2. Serum biochemical indices of largemouth bass under 96 h of hypoxic stress and recovery for 96 h ($n = 12$). (**A**): Glucose concentration. (**B**): Lactic acid concentration. (**C**): Malondialdehyde (MDA) content. (**D**): Superoxide dismutase (SOD) activity. (**E**): Catalase (CAT) activity. Different letters above bars indicate significant differences among sampling times. Asterisks indicate significant difference between control group and hypoxia treated group at each time point.

3.3. Intestinal Histological Structure of Largemouth Bass under Hypoxic Stress and Reoxygenation

As shown in Figure 3, compared with fish at 0 h, those exposed to hypoxic stress for 24 h and 96 h showed obvious tissue damage, including exfoliation of the chorionic epithelium, rupture of chorionic villi, and decreased thickness of the intestinal muscle layer ($p < 0.05$) (Table 2). The morphology of the intestine recovered somewhat after 96 h of recovery under sufficient DO conditions. The length and width of villi were not significantly affected by the hypoxia treatment in this experiment ($p > 0.05$).

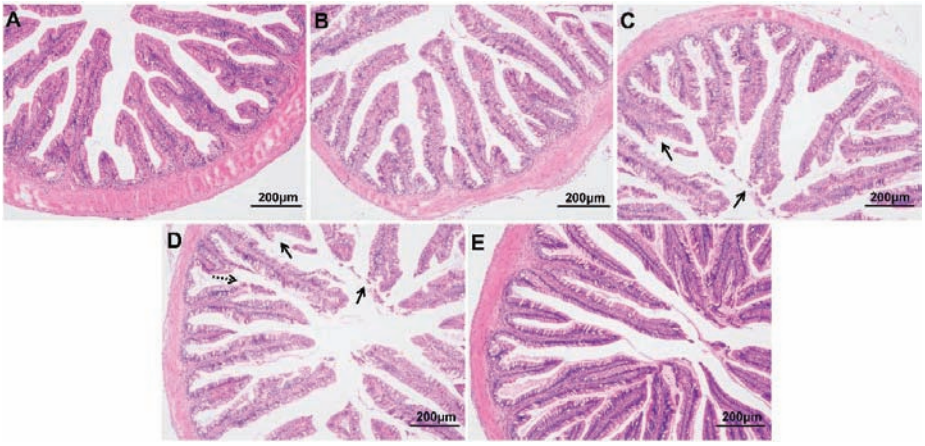

Figure 3. Intestinal morphology of largemouth bass under hypoxic stress for 0 h (**A**), 6 h (**B**), 24 h (**C**), 96 h (**D**) and 96 h of recovery under sufficient DO conditions (**E**) (n = 12). Solid arrow: intestinal epithelial injury; dotted arrow: ruptured intestinal villus.

Table 2. Morphological indices of largemouth bass under hypoxic stress followed by 96 h of recovery.

	Hyp_0 h	Hyp_6 h	Hyp_24 h	Hyp_96 h	Rec_96 h
Villi Length (μm)	654.85 ± 54.48	630.65 ± 42.79	452.70 ± 52.72	498.94 ± 61.55	518.87 ± 94.61
Villi Thickness (μm)	93.37 ± 6.48	89.14 ± 7.11	75.05 ± 2.36	76.77 ± 1.45	78.80 ± 5.6
Muscle Layer Thickness (μm)	83.34 ± 3.37 ^{a}	67.09 ± 7.46 ^{ab}	53.87 ± 4.90 ^{bc}	42.01 ± 3.91 ^{c}	64.04 ± 4.62 ^{abc}

$^{a, b, c}$ Within each row, different letters indicate significant differences among groups.

3.4. Intestinal Cell Apoptosis in Largemouth Bass under Hypoxic Stress and Recovery

The TUNEL staining results showed that the number of apoptotic cells in the intestine of largemouth bass increased during exposure to hypoxia compared with the control group (Figure 4A–D, Table 3) and then decreased during recovery under sufficient DO conditions (Figure 4E, Table 3).

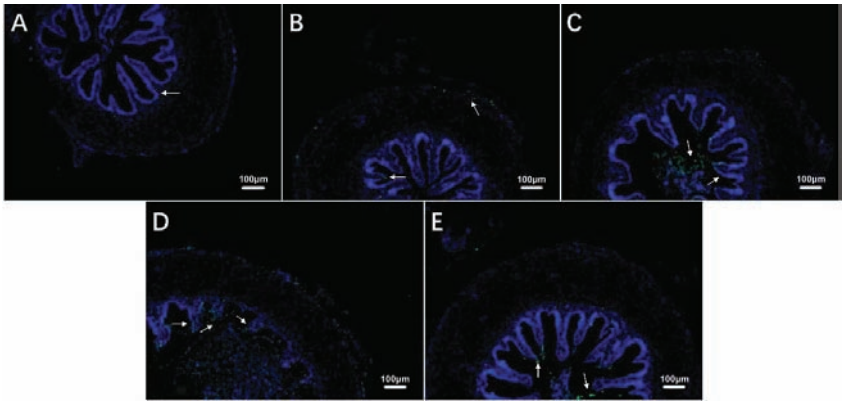

Figure 4. Effects of hypoxic stress (0 h (**A**), 6 h (**B**), 24 h (**C**), 96 h (**D**)) and reoxygenation (96 h (**E**)) on intestinal cell apoptosis in largemouth bass (n = 12). White arrows indicate apoptotic cells.

Table 3. Number of intestinal apoptotic cells of largemouth bass under hypoxic stress followed by 96 h of recovery.

	Hyp_0 h	Hyp_6 h	Hyp_24 h	Hyp_96 h	Rec_96 h
Number of Apoptotic Cells	18.42 ± 4.09 [a]	75.33 ± 12.45 [a]	291.58 ± 35.16 [b]	978.08 ± 237.68 [c]	333.08 ± 31.99 [b]

[a, b, c] Within each row, different letters indicate significant differences among groups.

3.5. Transcriptome Analysis of Largemouth Bass under Hypoxic Stress and Reoxygenation

Nine libraries (Ctrl1, Ctrl2, Ctrl3, Hyp1, Hyp2, Hyp3, Rec1, Rec2, Rec3) were constructed from mRNA extracted from intestinal tissues of fish in the Ctrl (0 h), Hyp (96 h of hypoxic stress), and Rec (96 h recovery after hypoxic stress) groups. A total of 36,223,342–5,000,644 reads were obtained by sequencing. After quality-control steps to remove low-quality sequences, as shown in Table S2, the number of reads in each library ranged from 31,738,670 to 46,246,716 (Q20 value, 99.96–99.97%; Q30 value, 98.09–98.26%). The GC content was 47–49%, indicating that the sequencing data were of sufficient quality for subsequent analyses.

We detected 3300 upregulated DEGs and 1548 downregulated DEGs between the Ctrl group and the Hyp group (Figure 5); 1372 upregulated DEGs and 2540 downregulated DEGs between the Hyp group and the Rec group; and 1372 upregulated DEGs and 2540 downregulated DEGs between the Ctrl group and the Rec group (Figure 5A–D). The Venn diagram shows the number of DEGs between and among the different groups (Figure 5E).

The results of GO functional annotation analyses showed how hypoxic stress affected different subcategories of genes within the "biological process" (BP), "cellular component" (CC), and "molecular function" (MF) categories in largemouth bass (Figure S1). Compared with the Ctrl group, the Hyp group showed significant enrichment of DEGs in signal transduction, G-protein-coupled receptor signaling pathway, and oxidation-reduction process subcategories in the BP category; integral component of membrane, membrane, and cytoplasm subcategories in the CC category; and transferase activity, metal ion binding, and ATP-binding subcategories in the MF category. Compared with the Rec group, the Hyp group showed significant enrichment of DEGs in the regulation of transcription, DNA-template, and oxidation-reduction process subcategories in the BP category; membrane, integral component of membrane, and nucleus subcategories in the CC category; and metal ion binding, ATP binding, and transferase activity in the MF category. Compared with the Ctrl group, the Rec group showed significant enrichment of DEGs in the signal transduction, regulation of transcription, DNA-template, and proteolysis subcategories in the BP category; membrane, integral component of membrane, and cytoplasm subcategories in the CC category; and metal ion binding, ATP-binding, and nucleotide-binding subcategories in the MF category.

KEGG enrichment analysis showed that 114, 36, and 25 signaling pathways were enriched with DEGs in the Ctrl vs. Hyp, Hyp vs. Rec, and Ctrl vs. Rec comparisons, respectively. The oxidative stress pathways (HIF-1 signaling, MAPK signaling), inflammation pathways (MAPK signaling, NF-kappa B signaling, PI3K-Akt signaling), and apoptosis pathways (MAPK signaling, apoptosis, p 53 signaling) were significantly enriched with DEGs under hypoxia ($p < 0.05$) (Figure 6).

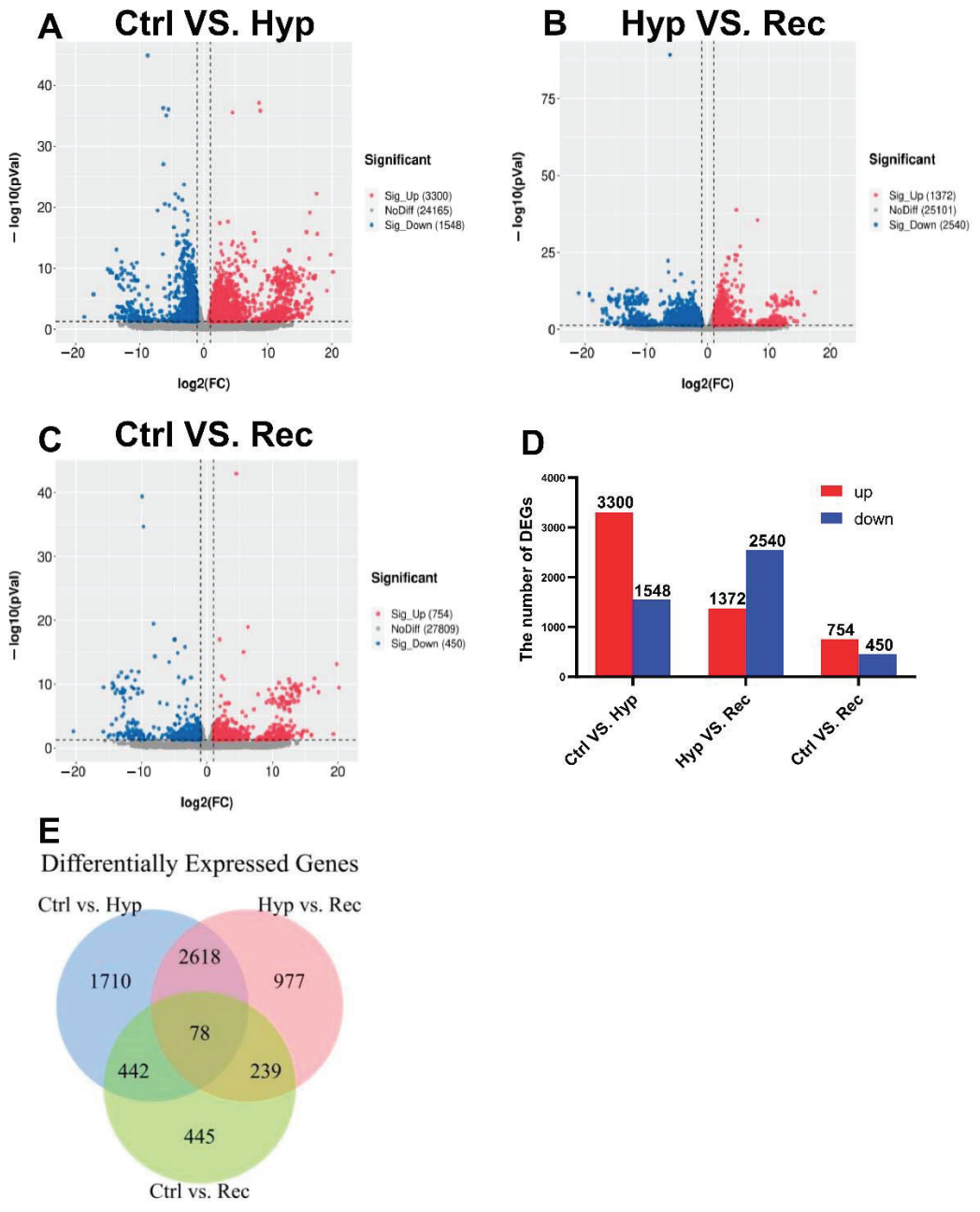

Figure 5. (**A**): Volcanic diagram of differentially expressed genes (DEGs) in Ctrl vs. Hyp groups (n = 3). (**B**): Volcanic map of DEGs in Hyp vs. Rec groups (n = 3). (**C**): Volcanic map of DEGs in Ctrl vs. Rec groups (n = 3). Grey dots represent genes with no significant difference in transcript levels between groups; red dots and blue dots represent significantly upregulated and downregulated DEGs, respectively. (**D**): Transcriptome analysis of DEGs quantity and expression (n = 3). (**E**): Venn diagram showing number of DEGs between and among groups (n = 3).

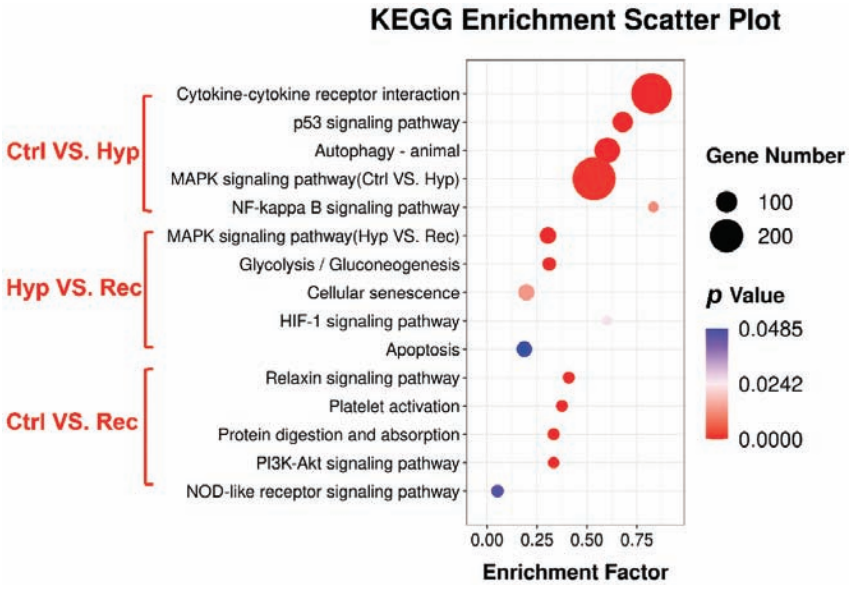

Figure 6. KEGG pathway enrichment analysis of DEGs in the intestine of largemouth bass under acute hypoxic stress (n = 3).

The MAPK signaling pathway was significantly enriched with DEGs in the Ctrl vs. Hyp and the Hyp vs. Rec comparisons. To verify these results concerning the immune and inflammatory responses of largemouth bass to hypoxic stress, several MAPK signaling pathway genes were selected for qRT-PCR analysis. The changes in gene transcript levels detected by qRT-PCR were consistent those detected from the sequencing results (Figure 7). Compared with the Ctrl group, the Hyp group showed significantly decreased transcript levels of *mapk11*, *elk-1*, and *map2k4b*. After 96 h of recovery under sufficient DO conditions, the transcript level of *mapk11* had increased, but the transcript level of *map2k4b* was still lower than that in the Hyp group. Compared with the Ctrl and Rec groups, the Hyp group showed significantly increased transcript levels of *atf2*, *tnfrsf1a*, *tgf-β2*, and *dusp5*.

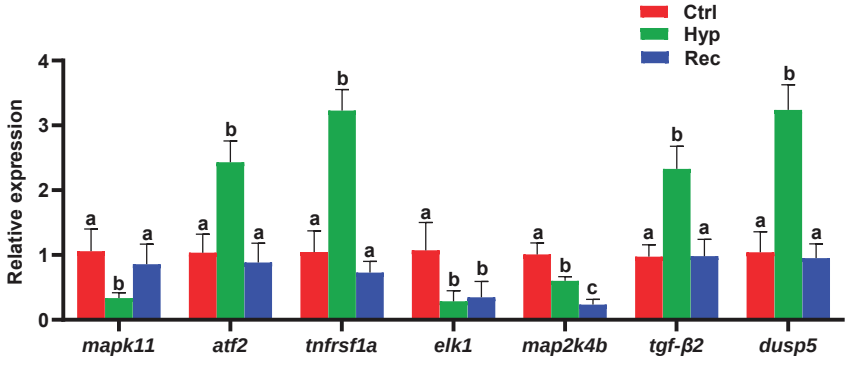

Figure 7. qRT-PCR analysis of differentially expressed genes in Ctrl group, Hyp group, and Rec group (n = 12). Different letters indicate significant differences in gene transcript levels among groups.

3.6. Sequencing and Analysis of Intestinal 16S rRNA of Largemouth Bass under Hypoxic Stress and Reoxygenation

Alpha diversity is mainly used to reflect species richness and evenness as well as sequencing depth. Among the indices, Chao1 and observed OTUs mainly estimate the number of species in the community, while Shannon's and Simpson's indices reflect the diversity of the community. The results showed that the observed OTU index and Chao1 index were significantly lower in the Hyp group than in the Ctrl group ($p < 0.05$) (Figure 8A,D). The observed OTU index, Shannon's index, and Chao1 index were significantly lower in the Rec group than in the Ctrl group ($p < 0.05$) (Figure 8A,B,D).

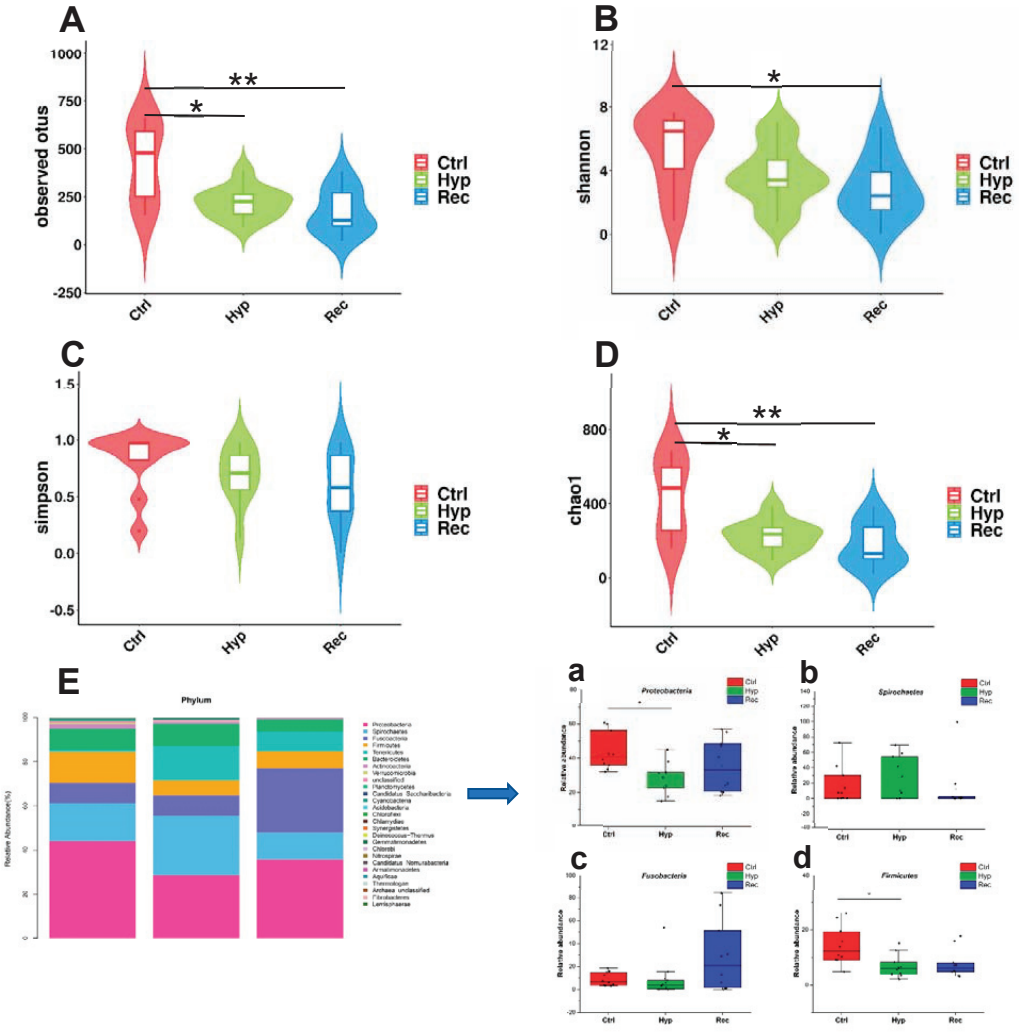

Figure 8. Intestinal alpha diversity of largemouth bass under hypoxic stress. (**A**): Observed operational taxonomic units (OTUs) index (alpha) ($n = 10$). (**B**): Shannon's index (alpha) ($n = 10$), (**C**): Simpson's index (alpha) ($n = 10$). (**D**): Chao1 index (alpha), * and ** indicate significant differences in abundance among different groups (Kruskal–Wallis test, *: $p < 0.05$, **: $p < 0.01$) ($n = 10$). (**E**): Relative abundance of main taxa of intestinal microflora in Ctrl group, Hyp group, and Rec group (**a**–**d**) ($n = 10$). Each bar represents relative abundance in each sample, and shows 27 most abundant taxa.

A PCoA analysis based on weighted UniFrac and unweighted UniFrac was used to describe the beta diversity of intestinal flora (Figure S2). The results indicated that there were significant differences in beta diversity among the Ctrl group, the Hyp group, and the Rec group ($p < 0.05$).

Proteobacteria, Spirochaetes, Fusobacteria, and Firmicutes were the dominant phyla in the intestinal microflora (Figure 8E). Under hypoxic stress, the abundance of Proteobacteria and Firmicutes decreased significantly in the Hyp group ($p < 0.05$) (Figure 8E(a,d)), while the abundance of Spirochaetes and Fusobacteria showed no significant differences among the three groups (Figure 8E(b,c)).

The LEfSe method was used to compare the abundance of all detected bacterial groups among the Ctrl, Hyp, and Rec groups (Figure S3). To determine which bacteria responded to differences in DO levels, we calculated the relative abundance of selected bacteria. The genera showing large differences in relative abundance among the three groups were Mycoplasma, Cetobacterium, unclassified Enterobacterales, and unclassified Betaproteobacteria. The relative abundance of Mycoplasma was significantly higher in the Hyp group than in the Ctrl and Rec groups (Figure 9B(a)). The relative abundance of Cetobacterium in the Hyp group was significantly lower than that in the Ctrl group ($p < 0.05$), but not significantly different from that in the Rec group ($p > 0.05$) (Figure 9B(b)). Enterobacteriaceae were more abundant in the Rec group than in the Ctrl and Hyp groups (Figure 9B(c)), while Betaproteobacteria were less abundant in the Rec group than in the Ctrl and Hyp groups (Figure 9B(d)).

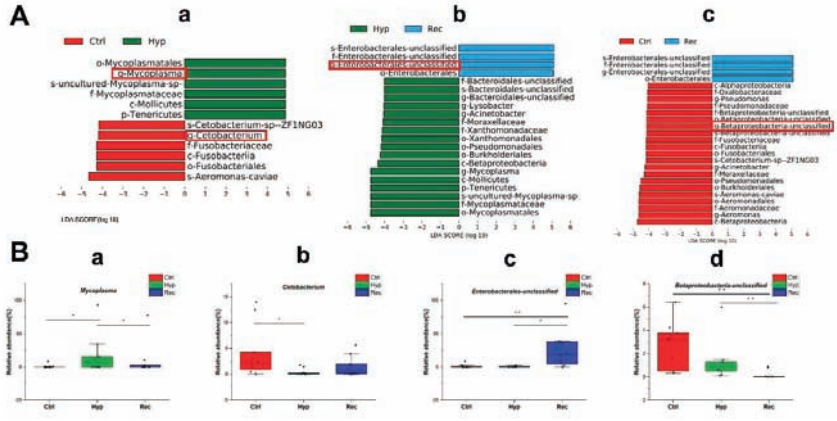

Figure 9. (**A**): Taxa shown in histogram were determined to differ significantly in abundance among Ctrl, Hyp, and Rec groups by Kruskal–Wallis test (($p < 0.05$, LDA score > 4, (**a**): Ctrl vs. Hyp; (**b**): Hyp vs. Rec; (**c**): Ctrl vs. Rec) ($n = 10$). (**B**): Abundance of major bacteria (**a**–**d**) in Ctrl, Str, and Rec groups (*, $p < 0.05$; **, $p < 0.01$) ($n = 10$).

As shown in Figure 10A, the Ctrl, Hyp, and Rec groups shared 237 OTUs. Compared with the Ctrl group, the Hyp group had 748 unique OTUs and the Rec group had 774 unique OTUs. The main functions of the intestinal microorganisms at KEGG level 2 are shown in Figure 10B. The main functions of the intestinal microorganisms across the Ctrl, Hyp, and Rec groups were "membrane transport", "replication and repair", and "translation".

3.7. Correlations between Intestinal Microorganisms and DEGS

Pearson's correlation analyses were conducted to detect relationships between DEGs and intestinal microorganisms at the genus level (Figure 11). We detected positive correlations between *igf2b* and *g-Zoogloea* and *g-Cetobacterium*; and between *rac2* and *g-Asticcacaulis*, *g-Zoogloea*, and *g-Cetobacterium*; and detected negative correlations between *mapk8b* and *g-Asticcacaulis*, *g-Zoogloea*, and *g-Cetobacterium*. *map2k4b* was positively correlated with *g-Devosia* and *g-Pseudorhodoferax* and negatively correlated with *g-Eisenbergiella*, *g-Moraxellaceae*,

g-Lacibacterium, *g-Microbacteriaceae*, *g-Propionibacterium*, and *g-Edwardsiella*. The relationships between *efna1b*, *cacnb2a*, *mknk2b* and these flora were opposite to that of *map2k4b*. *cacnb2a* and *mknk2b* were positively correlated with *g-Lysobacter*. *kras* was positively correlated with *g-Pseudorhodoferax* and *g-Empedobacter*, and negatively correlated with *g-Edwardsiella*. *pak2b* and *fgf18a* were positively correlated with *g-Empedobacter*, *g-Devosia*, and *g-Pseudorhodoferax*. *krt222*, *areg*, and *rac1b* were significantly positively correlated with *g-Empedobacter* and *g-Dyadobacter*, while *hsc70* and *erbb3b* were significantly negatively correlated with *g-Empedobacter* and *g-Dyadobacter*. *hsc70* was negatively correlated with *g-Pseudorhodoferax*. *tradd* and *casp3a* were positively correlated with *g-Dyadobacter*, while *fgf20b* and *hspb1* were negatively correlated with *g-Dyadobacter*. *map2k6* was negatively correlated with *g-Mycoplasma*, and positively correlated with *g-Sphingobacterium*. *rasgrf2b* and *map2k2b* were also positively correlated with *g-Sphingobacterium*.

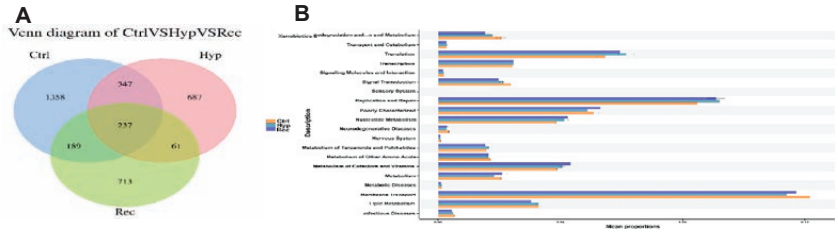

Figure 10. (**A**): Venn diagram showing number of OTUs shared between and among Ctrl, Hyp, and Rec groups (n = 10). (**B**): Abundance ratio of intestinal microflora in Ctrl, Hyp, and Rec groups with predicted level 2 functions (n = 10).

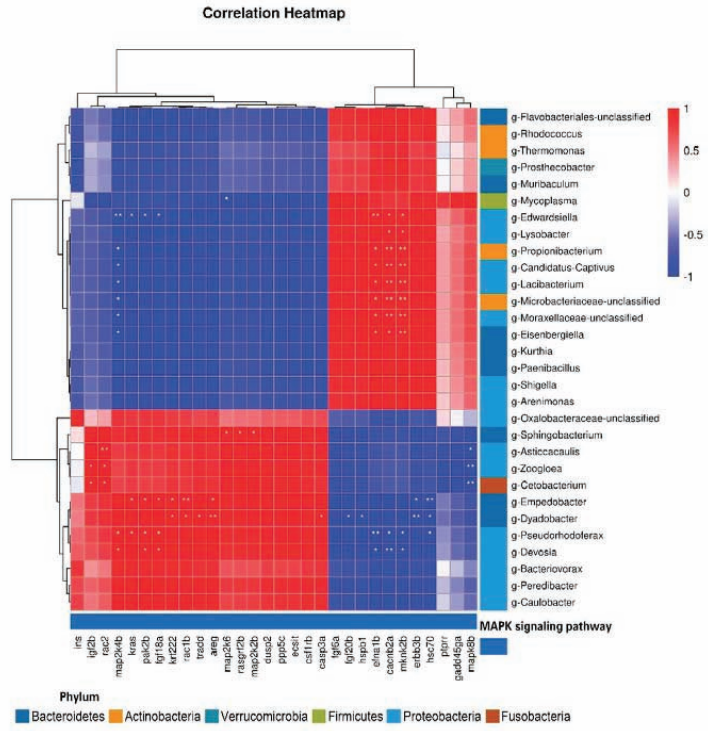

Figure 11. Correlation between DEGs and intestinal microflora at the genus level (*, $p < 0.05$; **, $p < 0.01$).

4. Discussion

The physiological state of fish is readily affected by water quality. The DO level is an important indicator of whether the water is suitable for fish survival or not. Hypoxic conditions affect the survival of fish and disrupt their normal physiological functions. Therefore, low DO is one of the main factors causing economic losses in the aquaculture industry [35]. In this study, the effects of hypoxic stress on the antioxidant system, immunity responses, and intestinal microflora of largemouth bass were studied through comprehensive analyses of serum, the intestine, and the intestinal microbiota.

Fish adapt to hypoxic stress via a series of complex physiological and biochemical changes [1]. The concentrations of glucose and lactic acid in serum are readily affected by external pressure. Hypoxia leads to stress in fish: there is a change from aerobic metabolism to anaerobic metabolism, and anaerobic glycolysis increases, resulting in the accumulation of lactic acid in serum [36,37]. In the present study, we found that blood glucose levels were lower in the hypoxia-treated group than in the control group. It may be that fish consume more endogenous substances such as glucose during the response to hypoxic stress, leading to a lack of energy. When fish lack energy, their ability to resist stress may be diminished. Many studies have shown that reactive oxygen species (ROS) are overproduced in fish under hypoxic conditions. The superoxide anion radical can be decomposed into H_2O_2, which is less harmful, via the activity of SOD, and then CAT decomposes H_2O_2 into H_2O and O_2 through the cellular antioxidant pathway [38]. Therefore, the activities of CAT and SOD reflect the defense function of the antioxidant system to some extent. Lipid peroxidation is one of the main forms of damage caused by oxidative stress, and the extent of lipid peroxidation is reflected by the content of MDA, the final product of this reaction. High levels of MDA can lead to further lipid peroxidation in the cell membranes and cell damage [39]. Studies on Nile tilapia (*Oreochromis niloticus*) and Chinese sea bass (*Lateolabrax maculatus*) subjected to hypoxic conditions for 24 h detected signs of oxidative stress in their intestines, gills, and liver, including increased activities of SOD and CAT [40]. After exposure to hypoxic conditions for 48 h, the activities of SOD and CAT decreased and the content of MDA increased [14]. Recovery under sufficient DO conditions restored the activity of SOD and CAT. Our findings suggest that hypoxic stress can lead to oxidative stress. More specifically, short-term hypoxia activates the antioxidant system, while long-term hypoxia leads to metabolic dysfunction and a decreased antioxidant capacity.

Previous studies have shown that oxidative stress can lead to excessive ROS production, damage to intestinal structure [41], cell apoptosis [42], and impaired function of the intestinal barrier [43]. Intestinal villus morphology and muscle thickness are important indices to measure the function of the intestinal barrier [13]. Previous studies have shown that hypoxia can significantly affect the morphology and thickness of the intestinal muscle layer [12,44]. The decreased muscle thickness observed in our study may indicate that hypoxia led to a loosening of the dense connective tissue of the muscle. We observed that the intestinal villous epithelium sloughed off, the villi broke, and the thickness of muscle layer decreased in fish under hypoxic stress. All of these results indicate that the function of the intestinal barrier in largemouth bass was impaired under hypoxic stress. Such extensive tissue damage may lead to intestinal inflammation and the invasion of opportunistic bacteria. Studies have shown that excessive accumulation of H_2O_2 under oxidative stress can induce cell apoptosis and lead to tissue damage [45]. In our study, the number of apoptotic intestinal cells had increased by 96 h of hypoxic stress, and this may have been related to the decrease in CAT activity under prolonged hypoxic conditions.

To explore the mechanisms underlying these biochemical and physiological changes in largemouth bass, we carried out transcriptome analyses. High-throughput sequencing revealed which regulatory pathways and key genes involved in those pathways were affected under hypoxic stress [46]. The response of cells to oxidative stress is guided by signal transduction pathways. The cascade of MAPK family members plays an important role in regulating cell survival and the immune response [47]. The transcriptome analysis showed that the MAPK signaling pathway was significantly enriched with DEGs under hypoxic

stress. The MAPK signaling pathway is sensitive to extracellular stimulation. *mapk11* encodes p38β, which is one of the four members of the p38 subfamily, while *tgf-β2* and *map2k4b* are upstream and downstream genes of the MAPK pathway, respectively. Under external stimulation, both *tgf-β2* and *map2k4b* can rapidly activate JNK/p38 [48,49]. The targets of JNK/p38 include Ets-like transcription factor-1 (*elk-1*) and activating transcription factor 2 (*atf2*), and so the transcript levels of these genes change in response to the phosphorylation of JNK/p38 during the stress response. The product of *elk-1* inhibits apoptosis in the cytoplasm [50], while upregulation of *atf2* regulates the immune response [51] and protects the intestine from excessive damage caused by the destructive stimulus [52]. In this study, the downregulation of *elk-1* and the upregulation of *atf2* may be indicative of a self-protective response in fish to activate the immune system under hypoxic stress. The tumor necrosis factor receptor superfamily (*tnfrsf1*) can be divided into type I (*tnfrsf1a*) and type II (*tnfrsf1b*) family members. The product of *tnfrsf1a* mainly triggers apoptosis or inflammation [53]. Under hypoxic conditions, the overexpression of *tnfrsf1a* can promote the activation of the NF-κB signal pathway and induce inflammation [54]. Another study showed that during tissue inflammation, *dusp5* can specifically inhibit the phosphorylation of ERK1/2, thereby downregulating the expression of the proinflammatory gene *tnf-α*, whose expression pattern is parallel with that of *dusp5* [55]. Our results show that there is a similar phenomenon between *dusp5* and *tnfrsf1a* under hypoxic stress, suggesting that *dusp5* may reduce inflammation and cell apoptosis by simultaneously affecting *tnf-α* and its receptors.

Under stress conditions, fish intestinal flora can be used as a biomarker of the stress response [56]. The intestinal microflora inhabit the gastrointestinal tract and play an important role in maintaining the function of the intestinal mucosal barrier. The microflora can regulate homeostasis of the internal environment of fish, especially that of the intestinal tract, and are closely related to the antioxidant response, immune response, and pathogenic reactions of fish [57,58]. Under oxidative stress, mitochondrial and bacterial DNA are inserted into the nuclear genome, resulting in changes in cellular gene expression [59]. Previous studies have shown that hypoxic stress significantly affects fish gut microflora [60] and that gut microflora is associated with hypoxia tolerance [61]. In this study, we found that hypoxic stress affected the number of species, species richness, community composition in the intestinal microflora of largemouth bass [18,62], and this may have been related to the high level of ROS in the intestine of fish under oxidative stress [63]. A high ROS level is indicative of intestinal inflammation [64]. After 96 h of recovery under sufficient DO conditions, the number of anaerobes was greatly decreased, and the specific species of bacteria differed significantly from those in the Hyp group.

In this study, Proteobacteria, Spirochaetes, Fusobacteria, and Firmicutes were the dominant intestinal bacteria in the three groups. These results, combined with the results of the alpha and beta diversity analyses, show that hypoxia changed the structure of intestinal microflora communities in largemouth bass, but did not change the dominant species. Proteobacteria and Firmicutes showed significant changes in abundance under hypoxic stress.

Proteobacteria are Gram-negative bacteria that are very sensitive to environmental factors. Previous studies have shown that the expansion of Proteobacteria under stress is the main feature of intestinal inflammation [65]. However, in zebrafish (*Danio rerio*), hypoxia led to a significant decrease in the abundance of Proteobacteria [66], and this was related to inflammation [67]. We speculate that the subordinate flora of Proteobacteria are more obviously affected by oxygen concentration. In short, the imbalance of Proteobacteria in the intestinal tract sends a danger signal. Firmicutes is the main taxon in the intestinal flora of most vertebrates [68]. Members of this family are spherical or rod-shaped, with cell walls, and many of them are beneficial bacteria. Some studies have shown that Firmicutes contribute to the absorption of fatty acids in the intestine [69] and energy metabolism [70]. To some extent, a decrease in the abundance of Firmicutes reflects the imbalance of intestinal metabolism under hypoxic stress.

Mycoplasma and *Enterobacterales* are common pathogens in humans and animals [71], and they can strongly induce an inflammatory response in the intestine [72,73]. The increased abundance of these taxa in the Hyp and Rec groups suggests an increased risk of intestinal disease in largemouth bass under hypoxic stress, although there is usually a lag time before such disease outbreaks occur under stress conditions [22]. *Cetobacterium* is classified as a Fusobacterium. This bacterium was found to improve glucose homeostasis through parasympathetic activation in zebrafish [74]. As a probiotic, *Cetobacterium* was found to improve intestinal health and enhance resistance to pathogens in tilapia [75]. Previous studies have also shown that the abundance of *Cetobacterium* is significantly affected under hypoxic stress [66]. Overall, our results show that the abundance of beneficial intestinal bacteria decreases and the abundance of opportunistic pathogens increases under hypoxic stress. Thus, hypoxic stress may cause intestinal inflammation via disruption of the intestinal flora.

We detected differences in microbial community structure among the Ctrl, Hyp, and Rec groups, indicating that the host genome interacted with the microbiome to select for certain microbial taxa [20]. The combined results of intestinal microflora and transcriptome analyses revealed relationships between some microorganisms and DEGs in the MAPK signaling pathway. *Edwardsiella* is an opportunistic pathogen in the gut. A significant increase in the abundance of *Edwardsiella* was detected in the intestine of zebrafish with enteritis [76]. In this study, *Edwardsiella* was significantly associated with several genes with different functions, which indicates the complexity of the response of largemouth bass to hypoxic stress. We also detected a significant correlation between Proteobacteria and MAPK pathway genes, indicating that intestinal flora respond to acute host immune activation by rapidly changing gene transcription when the host undergoes pathological changes [77]. In conclusion, our results show that the intestinal inflammatory response of largemouth bass under hypoxic stress may be mediated by the MAPK signaling pathway, and this may be related to the disruption of the intestinal microflora.

5. Conclusions

Hypoxic stress caused oxidative stress, decreased antioxidant capacity, induced inflammatory and apoptotic responses in the intestine, activated the MAPK signaling pathway, and disrupted the intestinal microflora of largemouth bass. Ultimately, these changes resulted in impaired function of the intestinal barrier. The results of this study provide new insights into how fish adapt to hypoxic stress.

Supplementary Materials: The following supporting information can be downloaded at: https://www.mdpi.com/article/10.3390/antiox12010001/s1, Table S1. Sequences of primers used for qRT-PCR; Table S2. Overview of transcriptome sequencing reads and quality filtering of largemouth bass; Figure S1. GO classification of Ctrl, Hyp and Rec DEGs; Figure S2. Btea diversity was analyzed based on weighted UniFrac(A) and unweighted UniFrac(B) PCOA analysis; Figure S3. Taxonomic cladistics derived from Lefse analysis. Red, green, and blue represent Ctrl, Hyp, and Rec groups, respectively. The brightness is proportional to the abundance of taxa.

Author Contributions: Conceptualization, Z.S., Y.T., W.Y. and J.Q.; methodology, Z.S., Y.T., W.Y. and J.Q.; validation, Z.S.; formal analysis, Y.T. and T.Z.; investigation, Z.S., Y.L. and W.L.; resources, J.Q.; data curation, J.Q.; writing—original draft preparation, Z.S.; writing—review and editing, Z.S.; supervision, P.X.; project administration, P.X.; funding acquisition, P.X. and J.Q. All authors have read and agreed to the published version of the manuscript.

Funding: This research was funded by the project of seed industry revitalization in Jiangsu province, China (grant JBGS (2021) 130), and Suzhou Science and Technology Project (grant SNG2021009).

Institutional Review Board Statement: All experiments in this study were approved by the Bioethics Committee of the Freshwater Fisheries Research Center (FFRC), Chinese Academy of Fishery Sciences (2013863BCE). Experiments were conducted according to the *Guide for the Care and Use of Laboratory Animals*—Chinese version.

Informed Consent Statement: Not applicable.

Data Availability Statement: The data are contained within the article and Supplementary Materials.

Acknowledgments: We thank Jennifer Smith for editing the English text of a draft of this manuscript.

Conflicts of Interest: The authors declare no conflict of interest.

References

1. Abdel-Tawwab, M.; Monier, M.N.; Hoseinifar, S.H.; Faggio, C. Fish response to hypoxia stress: Growth, physiological, and immunological biomarkers. *Fish Physiol. Biochem.* **2019**, *45*, 997–1013. [CrossRef] [PubMed]
2. Zhao, L.L.; Cui, C.; Liu, C.; Sun, J.L.; He, K.; Adam, A.A.; Luo, J.; Li, Z.Q.; Wang, Y.; Yang, S. Combined exposure to hypoxia and ammonia aggravated biological effects on glucose metabolism, oxidative stress, inflammation and apoptosis in largemouth bass (*Micropterus salmoides*). *Aquat. Toxicol.* **2020**, *224*, 105514. [CrossRef] [PubMed]
3. Leyva-López, N.; Lizárraga-Velázquez, C.E.; Hernández, C.; Sánchez-Gutiérrez, E.Y. Exploitation of Agro-Industrial Waste as Potential Source of Bioactive Compounds for Aquaculture. *Foods* **2020**, *9*, 843. [CrossRef] [PubMed]
4. Mattiasen, E.G.; Kashef, N.S.; Stafford, D.M.; Logan, C.A.; Sogard, S.M.; Bjorkstedt, E.P.; Hamilton, S.L. Effects of hypoxia on the behavior and physiology of kelp forest fishes. *Glob. Change Biol.* **2020**, *26*, 3498–3511. [CrossRef] [PubMed]
5. Luo, S.Y.; Liu, C.; Ding, J.; Gao, X.M.; Wang, J.Q.; Zhang, Y.B.; Du, C.; Hou, C.C.; Zhu, J.Q.; Lou, B.; et al. Scavenging reactive oxygen species is a potential strategy to protect *Larimichthys crocea* against environmental hypoxia by mitigating oxidative stress. *Zool. Res.* **2021**, *42*, 592–605. [CrossRef]
6. Pei, X.Y.; Chu, M.X.; Tang, P.; Zhang, H.Y.; Zhang, X.Y.; Zheng, X.; Li, J.; Mei, J.; Wang, T.; Yin, S.W. Effects of acute hypoxia and reoxygenation on oxygen sensors, respiratory metabolism, oxidative stress, and apoptosis in hybrid yellow catfish "Huangyou-1". *Fish Physiol. Biochem.* **2021**, *47*, 1429–1448. [CrossRef]
7. Varghese, T.; Mishal, P.; Gupta, G.; Kumar, M.; Pal, A.K.; Dasgupta, S. Temporal changes in behavioural responses and serum metabolites of *Cirrhinus mrigala* exposed to acute hypoxia. *J. Environ. Biol.* **2019**, *40*, 641–647. [CrossRef]
8. Lushchak, V.I.; Bagnyukova, T.V.; Lushchak, O.V.; Storey, J.M.; Storey, K.B. Hypoxia and recovery perturb free radical processes and antioxidant potential in common carp (*Cyprinus carpio*) tissues. *Int. J. Biochem. Cell Biol.* **2005**, *37*, 1319–1330. [CrossRef]
9. Niklasson, L.; Sundh, H.; Fridell, F.; Taranger, G.L.; Sundell, K. Disturbance of the intestinal mucosal immune system of farmed Atlantic salmon (*Salmo salar*), in response to long-term hypoxic conditions. *Fish Shellfish Immunol.* **2011**, *31*, 1072–1080. [CrossRef]
10. Fagundes, R.R.; Taylor, C.T. Determinants of hypoxia-inducible factor activity in the intestinal mucosa. *J. Appl. Physiol. (1985)* **2017**, *123*, 1328–1334. [CrossRef]
11. Colgan, S.P. Targeting hypoxia in inflammatory bowel disease. *J. Investig. Med.* **2016**, *64*, 364–368. [CrossRef] [PubMed]
12. Dong, H.B.; Sun, Y.X.; Duan, Y.F.; Li, H.; Li, Y.; Liu, Q.S.; Wang, W.H.; Zhang, J.S. The effect of teprenone on the intestinal morphology and microbial community of Chinese sea bass (*Lateolabrax maculatus*) under intermittent hypoxic stress. *Fish Physiol. Biochem.* **2020**, *5*, 1873–1882. [CrossRef] [PubMed]
13. Yang, E.J.; Zhang, J.D.; Yang, L.T. Effects of hypoxia stress on digestive enzyme activities, intestinal structure and the expression of tight junction proteins coding genes in juvenile cobia (*Rachycentron canadum*). *Aquac. Res.* **2021**, *52*, 5630–5641. [CrossRef]
14. Sun, Y.X.; Dong, H.B.; Zhan, A.J.; Wang, W.H.; Duan, Y.F.; Xie, M.J.; Liu, Q.S.; Li, H.; Zhang, J.S. Protection of teprenone against hypoxia and reoxygenation stress in stomach and intestine of *Lateolabrax maculatus*. *Fish Physiol. Biochem.* **2020**, *46*, 575–584. [CrossRef] [PubMed]
15. Xu, W.H.; Guo, H.H.; Chen, S.J.; Wang, Y.Z.; Lin, Z.H.; Huang, X.D.; Tang, H.J.; He, Y.H.; Sun, J.J.; Gan, L. Transcriptome analysis revealed changes of multiple genes involved in muscle hardness in grass carp (*Ctenopharyngodon idellus*) fed with faba bean meal. *Food Chem.* **2020**, *314*, 126205. [CrossRef]
16. Yang, Y.J.; Fu, Q.; Wang, X.Z.; Liu, Y.; Zeng, Q.F.; Li, Y.; Gao, S.; Bao, L.S.; Liu, S.K.; Gao, D.Y.; et al. Comparative transcriptome analysis of the swimbladder reveals expression signatures in response to low oxygen stress in channel catfish, *Ictalurus punctatus*. *Physiol. Genom.* **2018**, *50*, 636–647. [CrossRef]
17. Zhao, S.S.; Su, X.L.; Pan, R.J.; Lu, L.Q.; Zheng, G.D.; Zou, S.M. The transcriptomic responses of blunt snout bream (*Megalobrama amblycephala*) to acute hypoxia stress alone, and in combination with bortezomib. *BMC Genom.* **2022**, *23*, 162. [CrossRef]
18. Zheng, X.; Fu, D.Y.; Cheng, J.H.; Tang, R.; Chu, M.X.; Chu, P.; Wang, T.; Yin, S.W. Effects of hypoxic stress and recovery on oxidative stress, apoptosis, and intestinal microorganisms in *Pelteobagrus vachelli*. *Aquaculture* **2021**, *543*, 736945. [CrossRef]
19. Sun, S.M.; Yang, M.; Fu, H.T.; Ge, X.P.; Zou, J. Altered intestinal microbiota induced by chronic hypoxia drives the effects on lipid metabolism and the immune response of oriental river prawn *Macrobrachium nipponense*. *Aquaculture* **2020**, *526*, 735431. [CrossRef]
20. Levy, M.; Thaiss, C.A.; Elinav, E. Metagenomic cross-talk: The regulatory interplay between immunogenomics and the microbiome. *Genome Med.* **2015**, *7*, 120. [CrossRef]
21. Wahlström, A.; Sayin, S.I.; Marschall, H.U.; Bäckhed, F. Intestinal Crosstalk between Bile Acids and Microbiota and Its Impact on Host Metabolism. *Cell Metab.* **2016**, *24*, 41–50. [CrossRef] [PubMed]
22. Zheng, T.; Tao, Y.F.; Lu, S.Q.; Qiang, J.; Xu, P. Integrated Transcriptome and 16S rDNA Analyses Reveal That Transport Stress Induces Oxidative Stress and Immune and Metabolic Disorders in the Intestine of Hybrid Yellow Catfish (*Tachysurus fulvidraco* ♀× *Pseudobagrus vachellii* ♂). *Antioxidants* **2022**, *11*, 1737. [CrossRef] [PubMed]

23. Florindo, L.H.; Leite, C.A.C.; Kalinin, A.L.; Reid, S.G.; Milsom, W.K.; Rantin, F.T. The role of branchial and orobranchial O2 chemoreceptors in the control of aquatic surface respiration in the neotropical fish tambaqui (*Colossoma macropomum*): Progressive responses to prolonged hypoxia. *J. Exp. Biol* **2006**, *209*, 1709–1715. [CrossRef] [PubMed]
24. Plante, S.; Chabot, D.; Dutil, J.D. Hypoxia tolerance in Atlantic cod. *J. Fish Biol.* **1998**, *53*, 1342–1356. [CrossRef]
25. Ma, J.L.; Qiang, J.; Tao, Y.F.; Bao, J.W.; Zhu, H.J.; Li, L.G.; Xu, P. Multi-omics analysis reveals the glycolipid metabolism response mechanism in the liver of genetically improved farmed Tilapia (GIFT, *Oreochromis niloticus*) under hypoxia stress. *BMC Genom.* **2021**, *22*, 105. [CrossRef]
26. Ma, X.Y.; Qiang, J.; He, J. Changes in the physiological parameters, fatty acid metabolism, and SCD activity and expression in juvenile GIFT tilapia (*Oreochromis niloticus*) reared at three different temperatures. *Fish Physiol. Biochem.* **2015**, *41*, 937–950. [CrossRef]
27. Zheng, T.; Song, Z.; Qiang, J.; Tao, Y.F.; Zhu, H.J.; Ma, J.L.; Xu, P. Transport Stress Induces Skin Innate Immunity Response in Hybrid Yellow Catfish (*Tachysurus fulvidraco* ♀× *Pseudobagrus vachellii* ♂) Through TLR/NLR Signaling Pathways and Regulation of Mucus Secretion. *Front. Immunol.* **2021**, *12*, 430. [CrossRef]
28. Qiang, J.; Bao, J.W.; Tao, Y.F.; He, J.; Li, H.X.; Xu, P.; Sun, L.Y. The expression profiles of miRNA–mRNA of early response in genetically improved farmed tilapia (*Oreochromis niloticus*) liver by acute heat stress. *Sci. Rep.* **2017**, *7*, 8705. [CrossRef]
29. Kechin, A.; Boyarskikh, U.; Kel, A.; Filipenko, M. cutPrimers: A New Tool for Accurate Cutting of Primers from Reads of Targeted Next Generation Sequencing. *J. Comput. Biol.* **2017**, *24*, 1138–1143. [CrossRef]
30. Kim, D.; Paggi, J.M.; Park, C.; Bennett, C.; Salzberg, S.L. Graph-based genome alignment and genotyping with HISAT2 and HISAT-genotype. *Nat. Biotechnol.* **2019**, *37*, 907–915. [CrossRef]
31. Kovaka, S.; Zimin, A.V.; Pertea, G.M.; Razaghi, R.; Salzberg, S.L.; Pertea, M. Transcriptome assembly from long-read RNA-seq alignments with StringTie2. *Genome Biol.* **2019**, *20*, 278. [CrossRef] [PubMed]
32. Wang, Z.Y.; Leushkin, E.; Liechti, A.; Ovchinnikova, S.; Mößinger, K.; Brüning, T.; Rummel, C.; Grützner, F.; Cardoso-Moreira, M.; Janich, P.; et al. Transcriptome and translatome co-evolution in mammals. *Nature* **2020**, *588*, 642–647. [CrossRef] [PubMed]
33. Wang, Y.Y.; Ni, J.J.; Nie, Z.J.; Gao, J.C.; Sun, Y.; Shao, N.L.; Li, Q.J.; Hu, J.W.; Xu, P.; Xu, G.C. Effects of stocking density on growth, serum parameters, antioxidant status, liver and intestine histology and gene expression of largemouth bass (*Micropterus salmoides*) farmed in the in-pond raceway system. *Aquac. Res.* **2020**, *51*, 5228–5240. [CrossRef]
34. Livak, K.J.; Schmittgen, T.D. Analysis of Relative Gene Expression Data Using Real-Time Quantitative PCR and the $2^{-\Delta\Delta CT}$ Method. *Methods* **2001**, *25*, 402–408. [CrossRef] [PubMed]
35. Tao, Y.F.; Qiang, J.; Dagoudo, M.; Zhu, H.J.; Bao, J.W.; Ma, J.L.; Li, M.X.; Xu, P. Transcriptome profiling reveals differential expression of immune-related genes in gills of hybrid yellow catfish (*Tachysurus fulvidraco* ♀× *Pseudobagrus vachellii* ♂) under hypoxic stress: Potential NLR-mediated immune response. *Fish Shellfish Immunol.* **2021**, *119*, 409–419. [CrossRef]
36. Yang, S.; Wu, H.; He, K.; Yan, T.; Zhou, J.; Zhao, L.L.; Sun, J.L.; Lian, W.Q.; Zhang, D.M.; Du, Z.J.; et al. Response of AMP-activated protein kinase and lactate metabolism of largemouth bass (*Micropterus salmoides*) under acute hypoxic stress. *Sci. Total Environ.* **2019**, *666*, 1071–1079. [CrossRef]
37. Wu, L.Y.; Xu, W.J.; Li, H.Y.; Dong, B.; Geng, H.C.; Jin, J.Y.; Han, D.; Liu, H.K.; Zhu, X.M.; Yang, Y.X.; et al. Vitamin C Attenuates Oxidative Stress, Inflammation, and Apoptosis Induced by Acute Hypoxia through the Nrf2/Keap1 Signaling Pathway in Gibel Carp (*Carassius gibelio*). *Antioxidants* **2022**, *11*, 935. [CrossRef]
38. Jimenez, A.G.; Braun, E.; Tobin, K. How does chronic temperature exposure affect hypoxia tolerance in sheepshead minnows' (*Cyprinodon variegatus variegatus*) ability to tolerate oxidative stress? *Fish Physiol. Biochem.* **2019**, *45*, 499–510. [CrossRef]
39. Liu, B.H.; Wen, H.S.; Li, X.H.; Yang, J.; Li, G.L.; Zhang, M.Z.; Li, J.F.; He, F. Acute hypoxia effects on Keap1/Nrf2 (Mafs)-GST pathway related oxidative metabolism in muscle of Japanese flounder (*Paralichthys olivaceus*). *Sci. Total Environ.* **2021**, *795*, 148646. [CrossRef]
40. Dawood, M.A.O.; Noreldin, A.E.; Sewilam, H. Long term salinity disrupts the hepatic function, intestinal health, and gills antioxidative status in Nile tilapia stressed with hypoxia. *Ecotoxicol. Environ. Saf.* **2021**, *220*, 112412. [CrossRef]
41. Kong, Y.D.; Li, M.; Shan, X.F.; Wang, G.Q.; Han, G.H. Effects of deltamethrin subacute exposure in snakehead fish, *Channa argus*: Biochemicals, antioxidants and immune responses. *Ecotoxicol. Environ. Saf.* **2021**, *209*, 111821. [CrossRef] [PubMed]
42. Dvorakova, K.; Waltmire, C.N.; Payne, C.M.; Tome, M.E.; Briehl, M.M.; Dorr, R.T. Induction of mitochondrial changes in myeloma cells by imexon. *Blood* **2001**, *97*, 3544–3551. [CrossRef] [PubMed]
43. Huang, X.L.; Zhong, L.; Kang, Q.; Liu, S.; Feng, Y.; Geng, Y.; Chen, D.F.; OuYang, P.; Yang, S.Y.; Yin, L.Z.; et al. A High Starch Diet Alters the Composition of the Intestinal Microbiota of Largemouth Bass *Micropterus salmoides*, Which May Be Associated with the Development of Enteritis. *Front. Microbiol.* **2021**, *12*, 696588. [CrossRef]
44. Sharma, R.K.; Oliveira, A.C.; Yang, T.; Karas, M.M.; Li, J.; Lobaton, G.O.; Aquino, V.P.; Robles-Vera, I.; Kloet, A.D.D.; Krause, E.G.; et al. Gut Pathology and Its Rescue by ACE2 (Angiotensin-Converting Enzyme 2) in Hypoxia-Induced Pulmonary Hypertension. *Hypertension* **2020**, *76*, 206–216. [CrossRef]
45. Wang, Z.Y.; Sun, R.M.; Wang, G.Z.; Chen, Z.; Li, Y.; Zhao, Y.; Liu, D.S.; Zhao, H.Y.; Zhang, F.; Yao, J.H.; et al. SIRT3-mediated deacetylation of PRDX3 alleviates mitochondrial oxidative damage and apoptosis induced by intestinal ischemia/reperfusion injury. *Redox Biol.* **2020**, *28*, 101343. [CrossRef] [PubMed]

46. Qiang, J.; Khamis, O.M.A.; Jiang, H.J.; Cao, Z.M.; He, J.; Tao, Y.F.; Xu, P.; Bao, J.W. Effects of dietary supplementation with apple peel powder on the growth, blood and liver parameters, and transcriptome of genetically improved farmed tilapia (GIFT, *Oreochromis niloticus*). *PLoS ONE* **2019**, *14*, e0224995. [CrossRef] [PubMed]
47. Runchel, C.; Matsuzawa, A.; Ichijo, H. Mitogen-Activated Protein Kinases in Mammalian Oxidative Stress Responses. *Antioxid. Redox Signal.* **2011**, *15*, 25–218. [CrossRef]
48. Tzavlaki, K.; Moustakas, A. TGF-β Signaling. *Biomolecules* **2020**, *10*, 487. [CrossRef]
49. Liu, S.; Huang, J.; Zhang, Y.W.; Liu, Y.Y.; Zuo, S.; Li, R. MAP2K4 interacts with Vimentin to activate the PI3K/AKT pathway and promotes breast cancer pathogenesis. *Aging* **2019**, *11*, 10697–10710. [CrossRef]
50. Besnard, A.; Galan-Rodriguez, B.; Vanhoutte, P.; Caboche, J. Elk-1 a Transcription Factor with Multiple Facets in the Brain. *Front. Neurosci.* **2011**, *5*, 35. [CrossRef]
51. Hommes, D.W.; Peppelenbosch, M.P.; van Deventer, S.J.H. Mitogen activated protein (MAP) kinase signal transduction pathways and novel anti-inflammatory targets. *Gut* **2003**, *52*, 144–151. [CrossRef] [PubMed]
52. Meijer, B.J.; Giugliano, F.P.; Baan, B.; Meer, J.H.M.V.D.; Meisner, S.; Roest, M.V.; Koelink, P.J.; Boer, R.J.D.; Jones, N.; Breitwieser, W.; et al. ATF2 and ATF7 Are Critical Mediators of Intestinal Epithelial Repair. *Cell. Mol. Gastroenterol. Hepatol.* **2020**, *10*, 23–42. [CrossRef] [PubMed]
53. Aggarwal, B.B. Signalling pathways of the TNF superfamily: A double-edged sword. *Nat. Rev. Immunol.* **2003**, *3*, 745–756. [CrossRef] [PubMed]
54. Gao, X.Z.; Zhang, Z.X.; Han, G.L. MiR-29a-3p Enhances the Viability of Rat Neuronal Cells that Injured by Oxygen-Glucose Deprivation/Reoxygenation Treatment Through Targeting TNFRSF1A and Regulating NF-κB Signaling Pathway. *J. Stroke Cerebrovasc. Dis.* **2020**, *29*, 105210. [CrossRef] [PubMed]
55. Habibian, J.S.; Jefic, M.; Bagchi, R.A.; Lane, R.H.; McKnight, R.A.; McKinsey, T.A.; Morrison, R.F.; Ferguson, B.S. DUSP5 functions as a feedback regulator of TNFα-induced ERK1/2 dephosphorylation and inflammatory gene expression in adipocytes. *Sci. Rep.* **2017**, *7*, 12879. [CrossRef]
56. Llewellyn, M.S.; Boutin, S.; Hoseinifar, S.H.; Derome, N. Teleost microbiomes: The state of the art in their characterization, manipulation and importance in aquaculture and fisheries. *Front. Microbiol.* **2014**, *5*, 207. [CrossRef]
57. Talwar, C.; Nagar, S.; Lal, R.; Negi, R.K. Fish Gut Microbiome: Current Approaches and Future Perspectives. *Indian J. Microbiol.* **2018**, *58*, 397–414. [CrossRef]
58. Li, F.L.; Tang, Y.; Wei, L.X.; Yang, M.X.; Lu, Z.J.; Shi, F.; Zhan, F.B.; Li, Y.N.; Liao, W.C.; Lin, L.; et al. Alginate oligosaccharide modulates immune response, fat metabolism, and the gut bacterial community in grass carp (*Ctenopharyngodon idellus*). *Fish Shellfish Immunol.* **2022**, *130*, 103–113. [CrossRef]
59. Marciano, F.; Vajro, P. *Oxidative Stress and Gut Microbiota*; Academic Press: Cambridge, MA, USA, 2017; pp. 113–123.
60. Fan, S.; Li, H.; Zhao, R. Effects of normoxic and hypoxic conditions on the immune response and gut microbiota of Bostrichthys sinensis. *Aquaculture* **2020**, *525*, 735336. [CrossRef]
61. Gatesoupe, F.; Huelvan, C.; Bayon, N.L.; Delliou, H.L.; Madec, L.; Mouchel, O.; Quazuguel, P.; Mazurais, D.; Zambonino-Infante, J. The highly variable microbiota associated to intestinal mucosa correlates with growth and hypoxia resistance of sea bass, *Dicentrarchus labrax*, submitted to different nutritional histories. *BMC Microbiol.* **2016**, *16*, 266.
62. Khan, F.U.; Shang, Y.Y.; Chang, X.Q.; Kong, H.; Zuberi, A.; Fang, J.K.H.; Liu, W.; Peng, J.X.; Zhang, X.Z.; Hu, M.H.; et al. Effects of Ocean Acidification, Hypoxia, and Warming on the Gut Microbiota of the Thick Shell Mussel *Mytilus coruscus* Through 16S rRNA Gene Sequencing. *Front. Mar. Sci.* **2021**, *7*, 736338. [CrossRef]
63. Yang, H.T.; Yang, M.C.; Sun, J.J.; Guo, F.; Lan, J.F.; Wang, X.W.; Zhao, X.F.; Wang, J.X. Catalase eliminates reactive oxygen species and influences the intestinal microbiota of shrimp. *Fish Shellfish Immunol.* **2015**, *47*, 63–73. [CrossRef] [PubMed]
64. Swidsinski, A.; Loening-Baucke, V.; Theissig, F.; Engelhardt, H.; Bengmark, S.; Koch, S.; Lochs, H.; Dörffel, Y. Comparative study of the intestinal mucus barrier in normal and inflamed colon. *Gut* **2007**, *56*, 343–350. [CrossRef] [PubMed]
65. Shin, N.R.; Whon, T.W.; Bae, J.W. Proteobacteria: Microbial signature of dysbiosis in gut microbiota. *Trends Biotechnol.* **2015**, *33*, 496–503. [CrossRef] [PubMed]
66. Ma, Q.; Wang, X.; Li, L.Y.; Qiao, F.; Zhang, M.L.; Du, Z.Y. High protein intake promotes the adaptation to chronic hypoxia in zebrafish (*Danio rerio*). *Aquaculture* **2021**, *535*, 736356. [CrossRef]
67. Qiao, R.X.; Sheng, C.; Lu, Y.F.; Zhang, Y.; Ren, H.Q.; Lemos, B. Microplastics induce intestinal inflammation, oxidative stress, and disorders of metabolome and microbiome in zebrafish. *Sci. Total Environ.* **2019**, *662*, 246–253. [CrossRef]
68. Ringø, E.; Birkbeck, T.H.; Munro, P.O.; Vadstein, O.; Hjelmeland, K. The effect of early exposure to Vibrio pelagius on the aerobic bacterial flora of turbot, *Scophthalmus maximus* (L.) larvae. *J. Appl. Bacteriol.* **1996**, *81*, 207–211. [CrossRef]
69. Machate, D.J.; Figueiredo, P.S.; Marcelino, G.; Guimarães, R.D.C.A.; Hiane, P.A.; Bogo, D.; Pinheiro, V.A.Z.; Oliveira, L.C.S.D.; Pott, A. Fatty Acid Diets: Regulation of Gut Microbiota Composition and Obesity and Its Related Metabolic Dysbiosis. *Int. J. Mol. Sci.* **2020**, *21*, 4093. [CrossRef]
70. Stojanov, S.; Berlec, A.; Štrukelj, B. The Influence of Probiotics on the Firmicutes/Bacteroidetes Ratio in the Treatment of Obesity and Inflammatory Bowel disease. *Microorganisms* **2020**, *8*, 1715. [CrossRef]
71. Zakrzewski, A.J.; Zarzecka, U.; Chajęcka-Wierzchowska, W.; Zadernowska, A. A Comparison of Methods for Identifying Enterobacterales Isolates from Fish and Prawns. *Pathogens* **2022**, *11*, 410. [CrossRef]
72. Shimizu, T. Analysis of pathogenic factors of Mycoplasma. *Nihon Saikingaku Zasshi* **2015**, *70*, 369–374. [CrossRef] [PubMed]

73. Cevallos, S.A.; Lee, J.Y.; Velazquez, E.M.; Foegeding, N.J.; Shelton, C.D.; Tiffany, C.R.; Parry, B.H.; Stull-Lane, A.R.; Olsan, E.E.; Savage, H.P.; et al. 5-Aminosalicylic Acid Ameliorates Colitis and Checks Dysbiotic Escherichia coli Expansion by Activating PPAR-gamma Signaling in the Intestinal Epithelium. *mBio* **2021**, *12*, e03227. [CrossRef] [PubMed]
74. Wang, A.R.; Zhang, Z.; Ding, Q.W.; Yang, Y.L.; Bindelle, J.; Ran, C.; Zhou, Z.G. Intestinal Cetobacterium and acetate modify glucose homeostasis via parasympathetic activation in zebrafish. *Gut Microbes* **2021**, *13*, 1–15. [CrossRef] [PubMed]
75. Zhou, W.; Xie, M.X.; Xie, Y.D.; Liang, H.; Li, M.; Ran, C.; Zhou, Z.G. Effect of dietary supplementation of Cetobacterium somerae XMX-1 fermentation product on gut and liver health and resistance against bacterial infection of the genetically improved farmed tilapia (GIFT, *Oreochromis niloticus*). *Fish Shellfish Immunol.* **2022**, *124*, 332–342. [CrossRef] [PubMed]
76. Liu, X.H.; Chang, X.Y.; Wu, H.Z.; Xiao, J.F.; Gao, Y.; Zhang, Y.X. Role of intestinal inflammation in predisposition of Edwardsiella tarda infection in zebrafish (*Danio rerio*). *Fish Shellfish Immunol.* **2014**, *41*, 271–278. [CrossRef] [PubMed]
77. Becattini, S.; Sorbara, M.T.; Kim, S.G.; Littmann, E.L.; Dong, Q.W.; Walsh, G.; Wright, R.; Amoretti, L.; Fontana, E.; Hohl, T.M.; et al. Rapid transcriptional and metabolic adaptation of intestinal microbes to host immune activation. *Cell Host Microbe* **2021**, *29*, 378–393.e5. [CrossRef]

antioxidants

MDPI

Article

Dietary Supplementation of *Sophora flavescens* Root Extract Improved the Growth Performance, Antioxidant Capacity, Innate Immunity, and Disease Resistance against *Edwardsiella tarda* Challenge in Turbot (*Scophthalmus maximus*)

Yuqing Hou [1], Xuezheng Gao [1], Xueying Shi [1], Na Dong [1,2], Tongtong Yue [1], Peiyu Zhang [1,2,3] and Haiyan Liu [1,2,3,*]

[1] Laboratory of Aquatic Animal Nutrition and Ecology, College of Life Sciences, Hebei Normal University, Shijiazhuang 050024, China
[2] Hebei Key Laboratory of Animal Physiology, Biochemistry and Molecular Biology, Shijiazhuang 050024, China
[3] Hebei Collaborative Innovation Center for Eco-Environment, Shijiazhuang 050024, China
* Correspondence: liuhaiyan@hebtu.edu.cn; Tel.: +86-311-8078-7598

Abstract: The impacts of dietary supplementation with graded levels of *Sophora flavescens* root extract (SFE) on growth performance, antioxidant capacity, immune status, and resistance against *Edwardsiella tarda* challenge in *Scophthalus maximus* were investigated in this study. In all, 600 turbot (initial body weight: 8.38 ± 0.07 g) were randomly distributed in 12 tanks with 50 fish per tank and fed four experimental diets supplemented with 0, 0.05%, 0.1%, or 0.2% SFE (named as: SFE0, SFE0.05, SFE0.1, and SFE0.2, respectively), for 56 days. The results showed that 0.1% and 0.2% SFE supplementation have significantly increased the FBW, WGR, SGR, and PER of turbot, while decreased the FCR of turbot ($p < 0.05$). Dietary SFE supplementations have significantly increased the activities of plasma SOD, CAT, GPx, T-AOC, GST and LZM, decreased plasma MDA contents in turbot under normal or challenge condition ($p < 0.05$). Meanwhile, SFE addition dramatically enhanced the hepatic mRNA expression of antioxidant parameters (including Nrf2, Keap1, SOD, CAT, Trx2, GST and GR) during the normal condition. mRNA levels of NF-κB p65, IκBα, TNF-α, TGF-β, and IL-10 in the liver of fish were notably up-regulated by SFE treatment during normal condition ($p < 0.05$), while the transcription of IL-1β was down-regulated by SFE whenever under normal or challenge condition. 0.1% and 0.2% SFE administration have significantly increased the survival rate of turbot against *E. tarda* challenge ($p < 0.05$). In conclusion, dietary SFE supplementation improved the growth performance, antioxidant activity and disease resistance of turbot, and SFE could be a potential feed additive for turbot.

Keywords: turbot; *Sophora flavescens* root extract; growth performance; antioxidant capacity; disease resistance

Citation: Hou, Y.; Gao, X.; Shi, X.; Dong, N.; Yue, T.; Zhang, P.; Liu, H. Dietary Supplementation of *Sophora flavescens* Root Extract Improved the Growth Performance, Antioxidant Capacity, Innate Immunity, and Disease Resistance against *Edwardsiella tarda* Challenge in Turbot (*Scophthalmus maximus*). *Antioxidants* **2023**, *12*, 69. https://doi.org/10.3390/antiox12010069

Academic Editors: Bo Liu, Changyou Song, Cunxin Sun and Erchao Li

Received: 24 November 2022
Revised: 25 December 2022
Accepted: 26 December 2022
Published: 29 December 2022

1. Introduction

Nowadays, aquaculture is faced with great challenges due to intensive culture modes, and fish are more susceptible to oxidative stress and infectious diseases [1]. Turbot, *Scophthalmus maximus* L., is an important industrial mariculture species in Northern China, with an annual output of about 60,000 tons, and has a good culture prospect. However, the high-density intensive culture usually led to disease out-breaking in turbot culture. Antibiotics are used to prevent bacterial pathogens and reduce the economic loss of aquaculture [2]. The indiscriminate use of antibiotics can be hazardous to the environment and aid in the evolution of antimicrobial-resistant genes [3–5], which has also become a

major problem hindering the sustainable development of turbot aquaculture. Hence, more attention has been drawn to search for safe, practical, and effective immunostimulants or antioxidants to protect and improve the health of fish in the aquaculture industry.

Herbs have been used as immunostimulants in traditional medicine for thousands of years [6]. Many medicinal plants including Cornelian cherry (*Cornus mas* L.), *Bougainvillea glabra* leaf meal, dandelion extract are proved useful in controlling diseases in aquatic organisms and in boosting host immune responses [7–9]. It is believed that herbs have a great development prospect to replace the use of antibiotics [10,11]. Herbs contain various bioactive compounds, such as flavonoids, polysaccharides, alkaloids, and volatile oils, which work alone or in combination with other feed additives [12,13]. These bioactive compounds could promote growth performance, immunity, digestive enzyme activities, antioxidant status, disease resistance, and stress management of fish [14,15]. Therefore, using herbs as immunostimulants for aquatic animals might be a promising approach to dealing with disease outbreaks in aquaculture.

Sophora flavescens root is a kind of traditional medicinal herbs and has a long history in the traditional medicine of many countries, such as China, Japan, Korea, India, and some countries in Europe. More than 200 compounds are isolated from *S. flavescens* root, the main bioactive components are alkaloids and flavonoids [16]. Previous studies on human medicine demonstrated that *S. flavescens* had a wide range of biological properties, such as anti-inflammatory, antioxidant, antibacterial, antiviral, antitumor, and hepatoprotective actions [17,18]. However, few researches on *S. flavescens* were reported in aquatic animals except for tilapia and flounder. *S. flavescens* could increase the activities of non-specific immune enzymes in tilapia (*Oreochromis niloticus*) and improve the survival rate of tilapia infected with *Streptococcus agalactia* [19]. It can also improve the lysozyme activity and phagocytic activity of flounder (*Paralichthys olivaceus*), and enhance the disease resistance to *Edwardsiella tarda* [20]. There is an urgent need for more researches on *S. flavescens* in aquatic animals.

Nrf2 (nuclear factor erythroid 2-related factor 2) and NF-κB (nuclear factor kappa B) signaling pathways play a major role in the regulation of oxidative stress as well as immune response in aquatic animals [21–23]. Nrf2 transcription factor regulates the oxidative stress response and also suppresses the inflammatory response [24], after that the NF-κB immunity regulatory pathway could affect oxidative stress and ROS levels [25]. It is proved that *S. flavescens* had a strong role in improving antioxidant capacity and innate immunity by regulating Nrf2 and NF-κB signal pathway in mammals [26]. *S. flavescens* promoted Nrf2 translocation to the nucleus with subsequently up-regulating antioxidative enzyme protein expression, and then enhanced antioxidant capacity [27]; it could also suppress the phosphorylation of inhibitor of κBα (IκBα), interfere with the translocation of NF-κB from cytoplasm to nucleus, and affect the expression of downstream inflammatory factors, so as to enhance the body immunity of mammals [28]. Therefore, we hypothesized that *S. flavescens* root extract has the potential to enhance the antioxidant capacity and disease resistance of turbot by activating the Nrf2 and NF-κB signaling pathways.

The objective of the current study was to investigate the effects of dietary administration of *S. flavescens* root extract on the growth performance, antioxidant activity, innate immune response, disease resistance, and the expression of genes associated with the Nrf2 and NF-κB signaling pathways.

2. Materials and Methods

2.1. Experimental Diets

Sophora flavescens root extract (SFE) was purchased from Xi'an Shengqing Biological Technology Co. Ltd. (Xian, China), and it is the ethanolic extract of *S. flavescens* root. (Including: 97.35 mg matrine/kg and: 97.82 mg oxymatrine/kg, determined by HPLC). Four iso-nitrogenous and iso-energetic experimental diets with 0, 0.05%, 0.1% or 0.2% SFE (named as: SFE0, SFE0.05, SFE0.1, and SFE0.2, respectively), were prepared. The

experimental diets used white fish meal and chicken meal as primary protein sources, fish oil as chief lipid sources, α-starch as the main carbohydrate source.

The feed ingredients were mixed and ground sufficiently through a 178 μm mesh sieve. Then, the fish oil was added to the powder and mix the ingredients. All ingredients were supplemented the distilled water and mixed adequately to form into 2 mm pellets by extruded pelletizer (EL-260, Youyi Machinery Factory, Weihai, Shandong, China), which were placed in a ventilated place to dry at room temperature for 30 min. The prepared diets were stored at −20 °C for further use. The dietary formulation and proximate compositions are shown in Table 1.

Table 1. Formulation and nutrient composition of experimental diets (dry weight basis, %).

Ingredients	SFE 0	SFE 0.05	SFE 0.1	SFE 0.2
White fish meal	40.00	40.00	40.00	40.00
Chicken meal	17.50	17.50	17.50	17.50
Dried squid liver meal	5.00	5.00	5.00	5.00
Wheat gluten	5.00	5.00	5.00	5.00
Yeast powder	4.00	4.00	4.00	4.00
α-starch	18.00	17.95	17.90	17.80
Fish oil	4.00	4.00	4.00	4.00
Sophora flavescens root extract	0.00	0.05	0.10	0.20
CaHPO4	3.00	3.00	3.00	3.00
Zeolite powder	1.30	1.30	1.30	1.30
Choline chloride	0.20	0.20	0.20	0.20
Premix	2.00	2.00	2.00	2.00
		Nutrient composition		
Crude protein	48.61	48.54	48.52	48.58
Crude lipid	10.53	10.54	10.56	10.51
Crude ash	16.58	16.60	16.62	16.68
Gross energy (MJ/kg)	19.54	19.59	19.60	19.56

Premix: According to Zhang et al. (2023) [29].

2.2. Fish and Growth Trial

Turbots were obtained from a commercial aqua-farm (Tianjin, China). All fish are acclimated to the laboratory conditions and fed the prepared basal diet for 2 weeks. After acclimatization period, 600 fish (average weight: 8.38 ± 0.07 g) were assigned to twelve tanks (capacity: 560 L) with three replicates per treatment and 50 fish per tank. Fish were hand-fed the corresponding diets twice a day (8:00 and 18:00) to apparent satiation. The feeding trial was conducted for 56 days. During the feeding trial, water temperature was maintained at 16–18 °C, salinity at 15–20‰, ammonia nitrogen lower than 0.05 mg/L and dissolved oxygen higher than 6.0 mg/L.

2.3. Sample Collection

At the end of feeding trial, all fish were anesthetized with 100 mg/L MS-222 solutions (Sigma-Aldrich, St. Louis, MO, USA) and batch weighed. Four fish per tank were dissected and stripped to calculate VSI and HSI. Two fish per tank were used for chemical analysis and gene expression. The blood of fish was collected from the tail vein of the syringe moistened by heparin sodium and centrifuged with 3000× *g* 15 min to measure the plasma non-specific immune and antioxidant indexes. The liver was stripped to analyze the mRNA expression. All the samples were immediately frozen in liquid nitrogen and stored in the refrigerator at −80 °C until use.

After feeding trial, 20 fish per tank were exposed to bacteria challenge test. *Edwardsiella tarda* was provided from Fish Disease Laboratory of Hebei Agricultural University. The bacteria were inoculated into TSA solid medium and cultured at 30 °C for 12 h. Then the single

bacteria were selected in the aseptic beef soup liquid medium, cultured in 200 rpm shaker at 30 °C for 24 h, 4000 rpm centrifugation 10 min, remove the supernatant, rinse with 3.5% aseptic salt water and dilute the precipitated bacteria. The fish in 12 tanks were injected intraperitoneally with 3×10^8 CFU/mL *E. tarda* solution 0.3 mL (the injection concentration and dose were determined by the pre-experiment). Mortality was observed for 7 days, the dead fish was counted every 6 h and the survival rate was calculated. The plasma and liver of turbot were sampled for further analysis after 72 h challenge as the process described above.

2.4. Chemical Analysis

The proximate compositions of diets were analyzed according to standard methods, as previously described [29]. Moisture was determined by oven drying at 105 °C to constant weight. Crude protein (N × 6.25) was measured by Kjeldahl method using a 4800 Kjeltec Analyzer Unit (FOSS Tecator, Haganas, Sweden). Crude lipids were detected by petroleum ether extraction using the Soxhlet method. Crude ash was determined by combustion in a muffle furnace at 550 °C for 12 h. Gross energy was evaluated by an oxygen calorimeter (Parr 6300, Parr Instrument Company, Houston, TX, USA).

Plasma parameters, including lysozyme (LZM), complement 3 (C3), immunoglobulin (IgM), catalase (CAT), superoxide dismutase (SOD), glutathione peroxidase (GPx), total antioxidant capacity (T-AOC), glutathione-S-transferase (GST) activities, glutathione reductase (GR) and malondialdehyde (MDA)content were measured using commercial kits (Jiancheng Bioengineering Ltd., Nanjing, China). The determination method and calculation follow its instructions. The LZM, complement 3 and IgM activity were measured by turbidimetric assay. The activity of CAT was measured according to visible light spectrophotometry. The activity of SOD activity was evaluated according to hydroxylamine method. The T-AOC present in plasma was measured according to ABTS method. The MDA activity in the plasma was measured by means of a TBA method. These parameters were analyzed using a microplate reader (BioTek Instruments, Inc., Winooski, VT, USA) to determine the contents. Activities of GPx and GR were determined by recording the colorimetry through TU-1810 spectrophotometer (Beijing Purkinje General Instrument Co., Ltd., Beijing, China).

2.5. Real-Time Quantitative PCR Analysis

Total RNA of liver was extracted with Trizol reagent (Shanghai Generay, Shanghai, China). The RNA concentration and purity were evaluated with a Nano-Drop ND-2000 spectrophotometer (Thermo Scientific, Wilmington, DE, USA). The quality of RNA was assessed by 1.2% (*w/v*) agarose gel electrophoresis. Complementary DNA (cDNA) was synthesised using the cDNA synthesis kit (RevertAid First Strand cDNA Synthesis Kit, Thermo Scientific, Wilmington, DE, USA). Ribosomal protein S4 (RPS4) was applied as housekeeping gene, Real-time quantitative PCR analyses were performed using the CFX96 Real-Time PCR system (Bio-Rad, Hercules, CA, USA) following standard protocols. Reaction mixtures of 20 μL (0.4 μL forward primer, 0.4 μL reverse primer (10 μM), 10μL 2× TransStart® Top Green qPCR SuperMix (TransGen Biotech, Beijing, China), 2 μL cDNA (200 ng/μL) and 7.2 μL RNase-free water) were amplified for 30 s at 94 °C followed by 45 cycles of 5 s at 94 °C, annealing for 30 s, finally, 30 s at 72 °C. The primers used for qRT-PCR were listed in Table 2. The amplification efficiencies of all primers were verified to be approximately 100%. The relative expression levels of the target gene were calculated by $2^{-\Delta\Delta Ct}$ methods [30]. Six samples were employed for each treatment and each sample was tested in duplicate.

Table 2. Primer sequences for RT- qPCR.

Target Gene	Primer Sequence	Annealing Temperature (°C)	Product Size (bp)	Accession Number
NF-κB p65	F:ACTCACCCAGCCATCAAG R:AAGCAAAGCCGAACTGAA	58	314	XM_035627239.1
IκBα	F:AGAAAGCAGGAAATCAACTAAG R:TTGCGACTGACGATAAGG	58	205	XM_035649251.1
TNF-α	F:TGGAGATGGGTCTTGAGG R:TGGCATTGCTGCTGATTT	55	249	XM_035629860.2
IL-1β	F:ATGGTGCGATTTCTGTTCTAC R:TTCCACTTTGGGTCGTCTT	50	204	XM_035640817.2
TGF-β	F:TCAGCATTCCAGATGTAGGTG R:GGAGAGTGGCTTCAGTTTTTC	54	312	XM_035623668.2
IL-10	F:CCACGCCATGAACAGCATCCT R:ACATCGGACTTGAGCTCGTCGAA	60	141	XM_035632547.1
Nrf2	F:GGCAAGAACAAAGTGGCT R:GCAGACGCTCTTTCTCATC	59	106	XM_035651303.1
Keap1	F:TTGCCGAGCAGATTGGTT R:AGCGGACAGCCTGGAGTA	58	249	XM_035636756.1
Trx2	F:GGCTCACAGGCTGCTCGTA R:GGGCAGTTCGCTGTTGAT	60	253	XM_035616077.1
TrxR2	F:GAGGCTGTTCACAACCACG R:CCACCTGAGGCGATTACG	60	182	XM_035640386.1
GPx	F:CCCTGATGACTGACCCAAAG R:GCACAAGGCTGAGGAGTTTC	57	174	XM_035632618.1
GR	F:GTCTCCTCTGGGCTATTGG R:CGTGATACATCGGAGTGAAA	55	375	XM_035650249
GST	F:TGGATTACTTCACTGGACCTT R:TTTACCTATGAGTCGTCGTTC	53	272	XM_035636617
SOD	F:AAACAATCTGCCAAACCTCTG R:CAGGAGAACAGTAAAGCATGG	58	165	MG253620.1
CAT	F:TCCCGTCCTTCATTCACT R:AATAGCATAATCTGGGTTGGT	57	205	MG253621.1
RPS4	F:CAACATCTTCGTCATCGGCAAGG R:ATTGAACCAGCCTCAGTGTTTAGC	60	143	XM_035608277.1

NF-κB p65, nuclear factor kappa B–p65; IκBα, inhibitor of κBα; TNF-α, tumor necrosis factor-alpha; IL-1β, interleukin-1 beta; TGF-β, transforming growth factor beta; IL-10, interleukin -10; Nrf2, nuclear factor erythroid 2-related factor 2; Keap1, kelch-like ECH-associated protein 1; Trx2, thioredoxin 2; TrxR2, thioredoxin reductase 2; GPx, glutathione peroxidase; GR, glutathione reductase; GST, glutathione S-transferase; SOD, superoxide dismutase; CAT, catalase; RPS4, ribosomal protein S4.

2.6. Statistical Analysis

All data were presented as mean values and standard deviation (S.D.). Statistical analyses were performed using the STATISTICA 10.0 (StatSoft Inc., Tulsa, OK, USA) software, the normality and variance homogeneity of data were tested. The parameters of growth (including FBW, FR, WGR, SGR, FCR, PER, SR) and morphology (containing CF, VSI, HSI) were analyzed by one-way ANOVA. Two-way ANOVA was employed in plasma biochemistry indexes (including LZM, Complement C3, IgM, CAT, SOD, T-AOC, GPx, GST, GR, and MDA) and gene expression parameters. Duncan multiple comparisons were used when there was a significant difference in ANOVA analysis, and $p < 0.05$ was considered statistically significant.

3. Results

3.1. Growth Performance

The effects of *S. flavescens* root extract (SFE) on the growth performance and morphometric parameters of turbot are presented in Table 3. No significant differences were observed in SR, FR, VSI and HSI ($p > 0.05$). The FBW, WGR, SGR and PER in SFE 0.1 and SFE 0.2 treatments were significantly higher than that in SEF 0 group ($p < 0.05$). Dietary

SFE supplementation significantly reduced the FCR values in SFE 0.1 and SFE 0.2 groups ($p < 0.05$), the lowest value was at SFE 0.1 group. CF was significantly highest in the SFE 0.1 group compared to other groups ($p < 0.05$).

Table 3. Effects of dietary SFE on growth performance and morphometric parameters of turbot.

Indices	SFE0	SFE0.05	SFE0.1	SFE0.2	*p* Value
IBW (g)	8.40 ± 0.10	8.40 ± 0.00	8.37 ± 0.06	8.37 ± 0.12	0.916
FBW (g)	25.31 ± 1.03 ^{a}	26.45 ± 0.42 ^{ab}	30.00 ± 0.90 ^{c}	27.67 ± 0.87 ^{b}	<0.001
FR (%/d)	1.38 ± 0.06	1.39 ± 0.04	1.36 ± 0.04	1.32 ± 0.04	0.310
WGR (%)	201.41 ± 15.74 ^{a}	214.83 ± 5.01 ^{ab}	258.60 ± 9.26 ^{c}	230.65 ± 7.83 ^{b}	<0.001
SGR (%/d)	1.97 ± 0.09 ^{a}	2.05 ± 0.03 ^{ab}	2.28 ± 0.05 ^{c}	2.14 ± 0.04 ^{b}	0.001
FCR	0.77 ± 0.02 ^{b}	0.75 ± 0.03 ^{b}	0.68 ± 0.01 ^{a}	0.69 ± 0.03 ^{a}	0.002
PER	2.66 ± 0.09 ^{a}	2.73 ± 0.09 ^{a}	3.00 ± 0.06 ^{b}	2.99 ± 0.11 ^{b}	0.003
SR (%)	99.33 ± 1.15	99.33 ± 1.15	98.67 ± 1.15	100.00 ± 0.00	0.487
CF (%)	3.15 ± 0.23 ^{a}	3.19 ± 0.24 ^{a}	3.41 ± 0.23 ^{b}	3.21 ± 0.21 ^{a}	0.040
VSI (%)	6.83 ± 0.52	6.78 ± 0.31	6.74 ± 0.44	6.67 ± 0.31	0.814
HSI (%)	2.55 ± 0.43	2.66 ± 0.50	2.64 ± 0.49	2.42 ± 0.43	0.593

Values (mean ± S.D.) in the same line with different superscript letters were significantly different from each other ($p < 0.05$). IBW, initial body weight; FBW, final body weight; Weight gain rate (WGR,%) = ((FBW–IBW)/IBW) × 100; Specific growth rate (SGR, %/d) = ((LnFBW–LnIBW)/days) × 100; Feeding rate (FR, %/d) = 100 × feed intake/(days× (FBW+IBW)/2); Feed conversion ratio (FCR) = (total dry feed intake (g) /wet weight gain (g)); Survival rate (SR, %) = (Final number of fish/Initial number of fish) × 100; Protein efficiency ratio (PER, %) = wet weight gain (g)/protein intake (g); Hepatosomatic index (HSI, %) = (liver weight (g)/body weight (g) × 100; Viscerosomatic index (VSI, %) = (visceral weight (g)/body weight (g) × 100; Condition factor (CF) = 100 × (body weight (g)/body length $(cm)^3$).

3.2. Plasma Antioxidant and Lipid Peroxidation Parameters

Table 4 showed the effects of dietary SFE supplementation on the plasma antioxidant parameters. SFE supplementations have significantly increased the activities of plasma SOD, CAT, GPx, T-AOC, and GST of turbot under normal or challenge condition ($p < 0.05$). The highest levels existed in SFE 0.1 group except for CAT and GPx under challenge condition, which were highest in SFE 0.05 group. The plasma MDA contents were dramatically decreased by SFE addition, and the lowest concentration was in SFE 0.1 treatment under normal and challenge condition ($p < 0.05$). No significant effect of SFE on plasma GR activities were observed in this study ($p > 0.05$).

Table 4. Effects of dietary SFE on plasma antioxidant indices of turbot.

Index		Group				Two-Way ANOVA (*p* Value)		
		SFE0	SFE0.05	SFE0.1	SFE0.2	SFE	Challenge	SFE × Challenge
SOD(U/mL)	Normal	59.58 ± 1.94 ^{a}	60.13 ± 1.95 ^{a}	67.63 ± 1.32 ^{c}	63.97 ± 3.62 ^{b}	<0.001	<0.001	0.002
	Challenge	73.69 ± 7.01 ^{ab}	77.79 ± 1.21 ^{bc}	80.14 ± 2.30 ^{c}	72.50 ± 1.24 ^{a}			
CAT(U/mL)	Normal	5.13 ± 1.16 ^{a}	6.07 ± 1.45 ^{ab}	7.14 ± 1.31 ^{b}	6.55 ± 1.07 ^{b}	<0.001	<0.001	<0.001
	Challenge	10.96 ± 4.19 ^{a}	30.56 ± 11.73 ^{b}	14.32 ± 5.17 ^{a}	17.29 ± 4.05 ^{a}			
GPx (U/mL)	Normal	30.76 ± 6.21 ^{a}	42.72 ± 6.43 ^{b}	45.90 ± 12.94 ^{b}	41.18 ± 11.88 ^{b}	<0.001	<0.001	<0.001
	Challenge	240.67 ± 20.00 ^{a}	331.33 ± 11.60 ^{b}	243.33 ± 11.18 ^{a}	247.33 ± 27.05 ^{a}			
T-AOC (mM)	Normal	0.93 ± 0.08 ^{a}	0.98 ± 0.08 ^{ab}	1.06 ± 0.05 ^{c}	1.00 ± 0.05 ^{b}	<0.001	0.022	0.036
	Challenge	0.87 ± 0.01 ^{a}	0.92 ± 0.02 ^{b}	1.05 ± 0.05 ^{c}	1.03 ± 0.03 ^{c}			
GST (U/mL)	Normal	17.82 ± 5.14 ^{a}	24.43 ± 1.66 ^{a}	40.96 ± 16.82 ^{b}	17.96 ± 2.75 ^{a}	<0.001	0.001	0.104
	Challenge	63.06 ± 5.88 ^{a}	51.53 ± 21.79 ^{a}	95.29 ± 3.55 ^{b}	46.59 ± 17.92 ^{a}			
GR (U/L)	Normal	30.55 ± 7.01	35.37 ± 9.78	20.90 ± 12.56	28.62 ± 13.90	0.347	0.012	0.651
	Challenge	21.57 ± 6.71	20.19 ± 10.28	17.68 ± 8.57	19.65 ± 8.12			
MDA (nmol/mL)	Normal	30.38 ± 1.32 ^{c}	23.96 ± 1.49 ^{b}	19.68 ± 0.88 ^{a}	19.68 ± 0.74 ^{a}	<0.001	<0.001	<0.001
	Challenge	32.37 ± 6.73 ^{b}	26.31 ± 2.71 ^{a}	25.43 ± 3.84 ^{a}	34.89 ± 4.40 ^{b}			

Values (mean ± S.D.) ($n = 6$) in the same line with different superscript letters were significantly different from each other ($p < 0.05$). SOD, superoxide dismutase; CAT, catalase; GPx, glutathione peroxidase; T-AOC, total antioxidant capacity; GST, glutathione S-transferase; GR, glutathione reductase; MDA, malondialdehyde.

3.3. Plasma Immune Indexes

Dietary supplementation with SFE positively influenced the plasma LZM ($p < 0.05$). The LZM was highest in the SFE 0.1 group compared with that in other groups. However, no significant difference was observed in plasma complement C3 and IgM levels among all groups ($p > 0.05$) (Table 5).

Table 5. Effects of SFE supplementation on plasma nonspecific immune indices of turbot.

Index	SFE0	SFE0.05	SFE0.1	SFE0.2	*p* Value
LZM (μg/mL)	3.89 ± 0.26^{a}	4.00 ± 0.25^{b}	4.17 ± 0.21^{c}	4.02 ± 0.29^{b}	0.027
Complement C3 (g/L)	3.70 ± 0.09	3.70 ± 0.07	3.71 ± 0.09	3.69 ± 0.08	0.978
IgM (μg/mL)	54.60 ± 7.79	63.81 ± 10.88	64.25 ± 11.33	61.65 ± 16.91	0.200

Values (mean ± S.D.) ($n = 6$) in the same line with different superscript letters were significantly different from each other ($p < 0.05$). LZM, lysozyme; IgM, immunoglobulin M.

3.4. Antioxidant-Related Gene Expression

As seen from Figure 1, SFE treatment has significantly affected the Nrf2 signaling pathway and its downstream genes expression. In the normal condition, SFE has dramatically enhanced the mRNA levels of Nrf2 and Keap1 expect for Nrf2 in SFE 0.1 group ($p < 0.05$), the Nrf2 gene expression increased with the increasing of dietary SFE levels after pathogen challenge, it is significantly higher in SFE 0.2 than in SFE 0 group ($p < 0.05$). The SFE additions have significantly increased the mRNA levels of CAT and SOD during the normal condition. When exposed to pathogen challenge, the gene expressions of CAT, SOD in SFE 0.05 group were significantly lower than that in other treatments ($p < 0.05$).

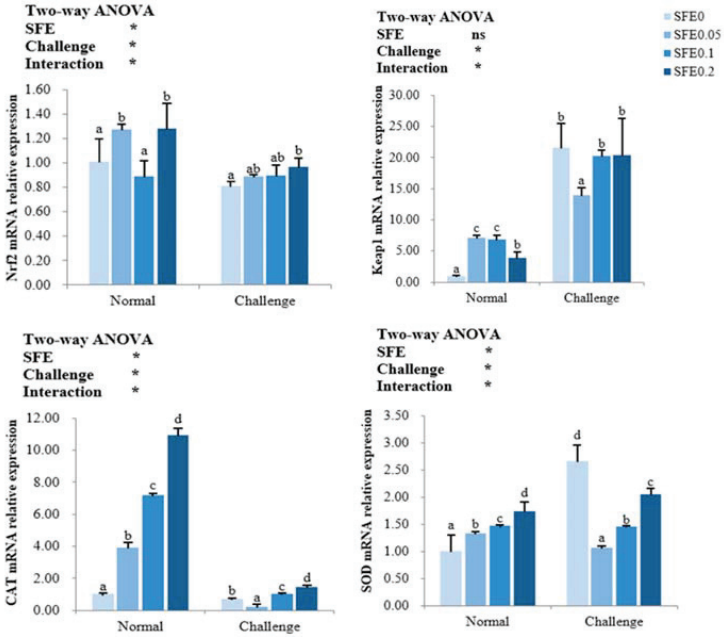

Figure 1. This relative transcription of nuclear factor erythroid 2-related factor 2 (Nrf2), kelch-like ECH-associated protein 1 (Keap1), catalase (CAT), superoxide dismutase (SOD) of turbot fed varied levels of SFE for 8 weeks. Normal refers to the parameters of the breeding group, and Challenge refers to the parameters of the challenge group. Values represent the mean ± S.D. ($n = 6$). Different letters indicate a significant difference between the groups fed different SFE diets ($p < 0.05$). ns: $p > 0.05$, *: $p < 0.05$.

The transcription levels of the thioredoxin regulatory system and glutathione antioxidant regulatory system related genes are presented in Figure 2. The gene expression of GPx was not affected by SFE treatment ($p > 0.05$), while SFE additions have significantly increased the mRNA levels of Trx2, GST and GR during the normal condition, the highest transcription levels of Trx2 and TrxR2 was in SFE 0.1 group, the highest mRNA expressions of GST and GR were observed in SFE 0.2 group. When exposed to pathogen challenge, the gene expressions of TrxR2, Trx2, GST and GR in SFE 0.05 group were significantly lower than that in other treatments ($p < 0.05$).

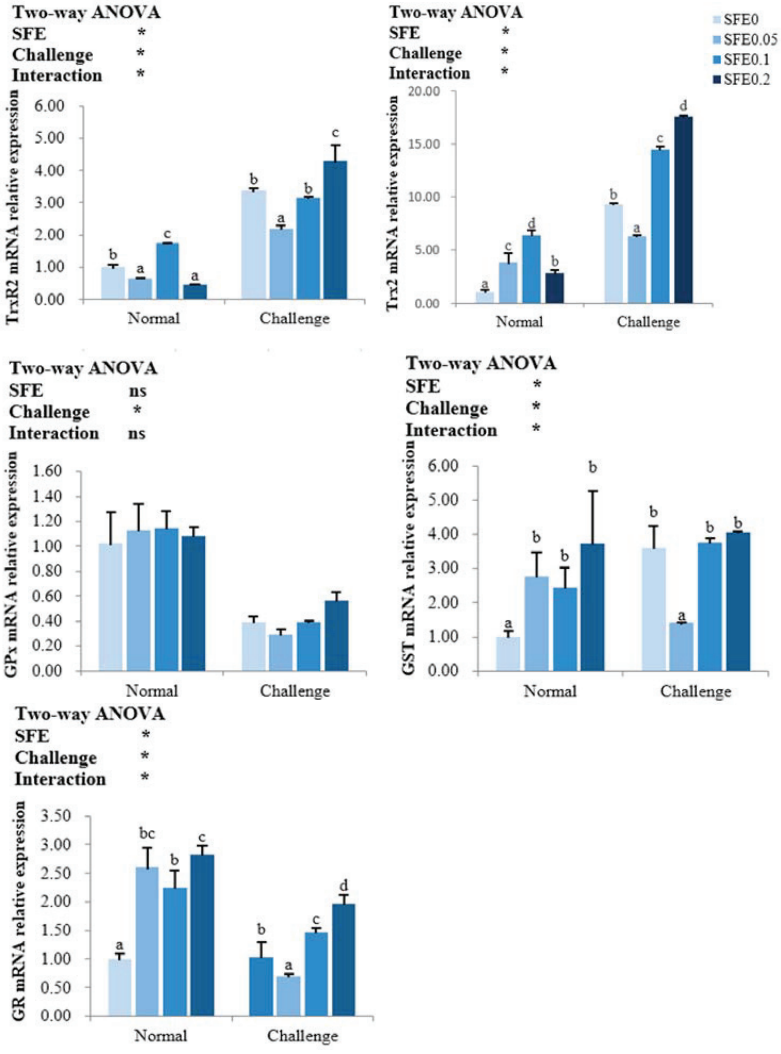

Figure 2. Relative transcription of thioredoxin reductase 2 (TrxR2), thioredoxin 2 (Trx2), glutathione peroxidase (GPx), glutathione S-transferase (GST), glutathione reductase (GR) of turbot fed varied levels of SFE for 8 weeks. Normal refers to the parameters of the breeding group, and Challenge refers to the parameters of the challenge group. Values represent the mean ± S.D. ($n = 6$). Different letters indicate a significant difference between the groups fed different SFE diets ($p < 0.05$). ns: $p > 0.05$, *: $p < 0.05$.

3.5. Inflammation-Related Gene Expression

SFE treatment significantly regulated the key regulators NF-κB p65 and IκBα in the NF-κB signaling pathway, and their downstream pro-inflammatory factors TNF-α and IL-1β, anti-inflammatory factors TGF-β and IL-10 ($p < 0.05$) (Figure 3). Under normal condition, mRNA levels of NF-κB p65, IκBα, TNF-α, TGF-β and IL-10 in the liver of fish were notably increased by SFE treatment ($p < 0.05$), NF-κB p65, IκBα, TNF-α, and IL-10 increased first and then decreased, and reached the highest value in the SFE 0.1 group ($p < 0.05$). Anti-inflammatory cytokine TGF-β expression was the highest in SFE 0.2 group. Dietary SFE significantly decreased the transcription levels of pro-inflammatory cytokines IL-1β ($p > 0.05$) whenever under normal or challenge condition. After pathogen challenge, the mRNA levels of NF-κB p65 were significantly increased in SFE 0.1 and SFE 0.2 groups. Pro-inflammatory cytokines TNF-α was down-regulated in the SFE 0.05 and SFE 0.2 groups. Anti-inflammatory cytokine IL-10 were down-regulated in all SFE treatment groups ($p < 0.05$).

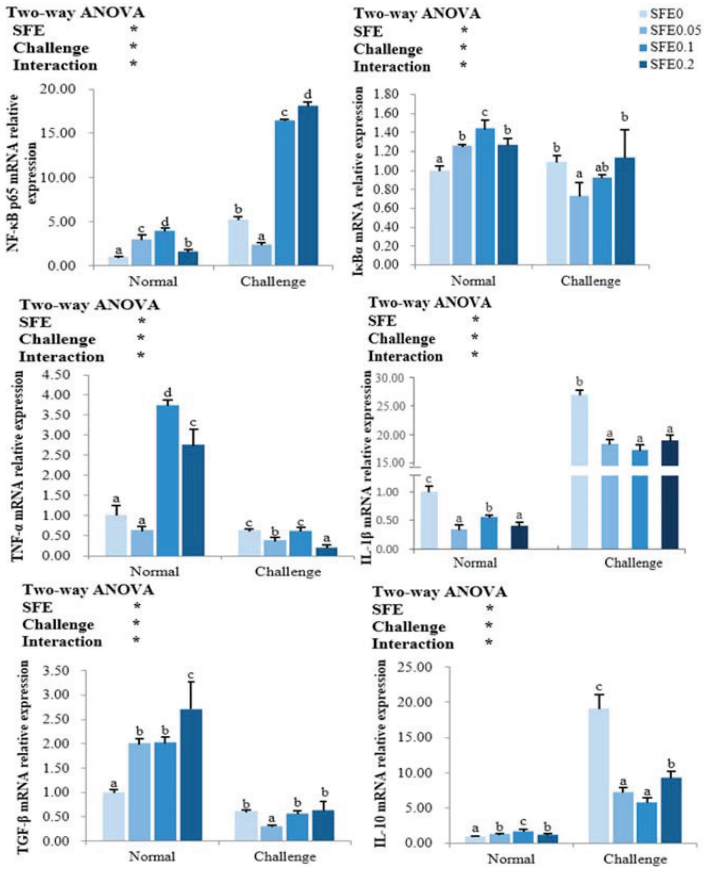

Figure 3. Relative transcription of nuclear factor kappa B–p65 (NF-κB p65), inhibitor of κBα (IκBα), tumor necrosis factor-alpha (TNF-α), interleukin-1 beta (IL-1β), transforming growth factor beta (TGF-β), interleukin -10 (IL-10) of turbot fed varied levels of SFE for 8 weeks. Normal refers to the parameters of the breeding group, and Challenge refers to the parameters of the challenge group. Values represent the mean ± S.D. ($n = 6$). Different letters indicate a significant difference between the groups fed different SFE diets ($p < 0.05$). ns: $p > 0.05$, *: $p < 0.05$.

3.6. Disease Resistance

After pathogen challenge, dead of turbot was observed firstly in SFE 0 group, and then the mortality was dramatically increased during 2–6 days post challenge. Dietary supplementation with SFE increased the survival rate of turbot exposed to pathogen challenge (Figure 4). The survival rates in SFE 0 and SFE 0.05 were significantly lower than that in SFE 0.1 and SFE 0.2 groups ($p < 0.05$).

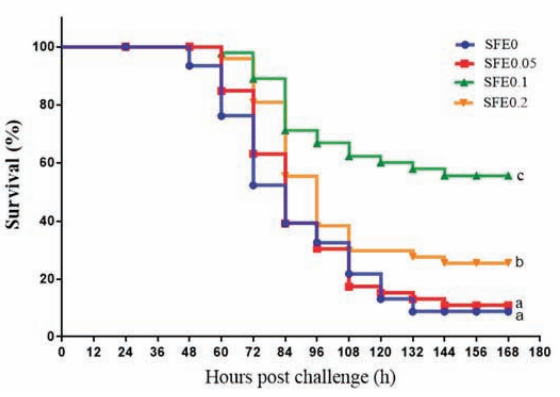

Figure 4. The survival rate of turbot fed varied levels of SFE when exposed to *Edwardsiella tarda* challenge for 7 days. Values are presented as means ± S.D. Different letters indicate significant differences among all treatments ($p < 0.05$).

4. Discussion

Many herbs or their compounds have been used as supplements and additive in animals as well as human diets because of their numerous beneficial properties such as growth promotion, anti-cancer, anti-pathogenic, anti-inflammatory, immunomodulatory, and antioxidant properties [13]. In recent years, there has been increasing interest in using natural plant extract as functional compounds to enhance the immunity of fish in aquaculture. The root extracts of *S. flavescens*, a kind of traditional Chinese herbal medicine, has a wide range of medicinal values, such as antibacterial and anti-inflammatory [16]. However, little information was available about the functions and regulating mechanism of *S. flavescens* in fish. This study demonstrated that *S. flavescens* root extract enhanced the growth performance, antioxidant capacity, immunity, and disease resistance of turbot.

4.1. SFE improved the Growth Performance and Feed Utilization of Fish

In this study, 0.1% and 0.2% dietary SFE supplementation significantly increased the growth performance and feed utilization of fish, which is similar with previous studies of plant herbs extract. It is reported that *Radix glycyrrhizae* extract, *Panaxnotoginseng* extract and tea tree oil have increased the WGR, SGR of yellow catfish (*Pelteobagrus fulvidraco*), grouper (*Epinephelussp*) and prawn (*Macrobrachium rosenbergii*) [31–33], respectively. This is probably related to the bioactive compounds isolated from these herbs. It is proved that the bioactive substances contained in Chinese herbal medicine are the main factors to promote the rapid growth of aquatic animals [15]. Many studies have shown that alkaloids (such as berberine), flavonoids, triterpenes (such as hesperidin) and polysaccharides (such as Astragalus polysacharin) extracted from Chinese herbal medicine can significantly increase fish FBW, WGR and SGR, and reduce FCR [34–37]. The composition of *S. flavescens* extract is complex, more than 200 compounds are isolated from *S. flavescens* root, and the main bioactive components are alkaloids and flavonoids [16]. It might be ascribed to these bioactive components from SFE improved the antioxidant capacity and non-specific immune responses, which in turn boosts turbot growth performance.

4.2. SFE Enhanced the Antioxidant Capacity of Fish

Antioxidant enzymes are indicative biomarkers of health and the reaction in oxidative stress response when the reactive oxygen species (ROS) and free radicals production were uncontrolled [38], and MDA is regarded as a bio-indicator of oxidative stress [39]. In the current study, the activities of plasma CAT, SOD, T-AOC, GPx, GST, and GR were significantly increased, and plasma MDA contents were decreased in fish fed *S. flavescens* diets. The results of this study indicated that *S. flavescens* extract could improve the antioxidant capacity of juvenile turbot. Previous research has confirmed that *S. flavescens* can trigger the antioxidant defense system of mammals [40]. Similarly, antioxidant enzymes activity increased significantly in fish with dietary administration of grape seed proanthocyanidin extract [41] or curcumin [42], and decreased the MDA levels in the fish. The current results proved that *S. flavescens* extract improved the antioxidant system of turbot and reduced oxidative stress. This may be because the bioactive components in *S. flavescens* extract can activate the antioxidant related pathway Nrf2 and thus lead to the change of enzyme activity level. As we know, the increased enzyme activity is caused by the increased synthesis of enzyme protein, which largely relies on its gene transcription and translation [43]. Therefore, in order to further confirm whether the change of antioxidant enzyme activity is caused by the change of mRNA level of related genes in Nrf2 signaling pathway, this study determined the influence of *S. flavescens* extract on the expression level of antioxidation-related genes.

A number of reports have demonstrated the importance of the Nrf2- Keap1 signaling pathway against oxidative stress in the body. The nuclear transcription factor Nrf2 is widely expressed in an extensive range of cell and tissue types and regulates antioxidant defense [44,45]. Nrf2 transcriptional activity can be inhibited by Keap1-controlled ubiquitination-proteasomal degradation [46]. Nrf2 translocates into the nucleus and binds ARE to regulate and code are involved in redox regulation (CAT, SOD and Trx), and enzymes related to glutathione synthesis metabolism, such as GST, GR, GPx, etc., to regulate oxidation in the body [47]. In this study, *S. flavescens* extract supplementation activated Nrf2/Keap1 signaling pathway under normal condition, thus increased the expression of downstream related antioxidant genes, the mRNA expression results were consistent with the results of their enzyme activities under normal condition, which revealed that dietary SFE could strengthen antioxidant activity associated with decreased MDA content of turbot. Similar to our research, dietary supplementations of *P. tectorius* in *C. carpio* [48], emodin in *M. amblycephala* [49], curcumin in *C. argus* [42] regulated the expression of Nrf2, Keap1 and its downstream regulated genes such as SOD, CAT, GPx and GST to improve the antioxidant activity in fish. To date, no reports have investigated the potential effects of *S. flavescens* on the thioredoxin regulatory system of fish. The thioredoxin system is one of the major redox systems in cells and is an important regulator of eliminating ROS accumulation, the main components are thioredoxin (Trx) and thioredoxin reductase (TrxR) [50,51]. In the current study, the expressions of hepatic Trx2 and TrxR2 were significantly up-regulated in turbot fed an *S. flavescens* extract diet. *S. flavescens* extract increases the expression of thioredoxin and its related reductases by activating the Nrf2/Keap1 signaling pathway, and further improves the antioxidant capacity of turbot, so that it can quickly eliminate excessive ROS to protect the body. Furthermore, it is interestingly found in this study that the expression of SOD was down-regulated in SFE groups compared to control after 72 h pathogen challenge. There probably exists the negative feedback suppression. The activities and mRNA expression of SOD in SFE treatments were all at higher levels during normal condition, which showed there are enough SOD activities in SFE treatments to defense the bacterial invasion to maintain the body homeostasis, no need to activate the genes to produce more enzymes. Hence, in this study, the transcriptional levels of SOD in SFE groups were not significantly increased by *E. tarda* challenge, while the level in SFE 0 significantly increased, which revealed that dietary SFE supplementation could protect turbot from pathogen persecution. Based on the results of antioxidant parameters determined in this study, a dietary supplement of SFE improved the antioxidant capacity

of turbot by activating the Nrf2 pathway and enhancing antioxidant systems including SOD, CAT, GPx, GST and Trx and protected lipids from peroxidation.

4.3. SFE Enhanced the Innate Immunity and Disease Resistance of Fish

Lysozyme, the first line of protection against pathogen invasion, plays a key role in non-specific immune response in fish. It can cleave bacteria by hydrolyzing the β-1,4 glycosidic bond of peptidoglycan layer of the bacterial cell wall [52]. In this study, *S. flavescens* exerted its antibacterial effect by increasing the activity of plasma LZM and enhancing immunity in juvenile turbot. This is consistent with the results in tilapia and flounder [19,20]. Similarly, dietary *Eucommia ulmoides* Oliver and Astragalus polysaccharides increased LZM in turbot [37,53]. *Allium mongolicum* Regel significantly improved LZM in *Channa argus* [35]. This indicated that the bioactive substances in the extracts of Chinese herbal medicine could improve the activity of LZM, and then improve the immunity of fish.

Moreover, the transcription levels of immune-related genes were analyzed in this study to further evaluate the effects of SFE on immune responses of turbot. NF-κB pathway is involved in the initiation, amplification and regression of inflammation and is activated by different stimuli [54,55]. Cytokines play a vital role in the immune system by binding to specific receptors and setting off a cascade of immunological events [56]. Pro-inflammatory cytokines (IL-1β, TNF-α) regulate multiple aspects of the immune response in fish [57]. TGF-β and IL-10, anti-inflammatory cytokine, suppresses the production of pro-inflammatory cytokines [58]. In this study, SFE treatment activated the expression of NF-κB p65 and IκBα in the normal condition, then up-regulated the mRNA expression of anti-inflammatory cytokine (TGF-β and IL-10), and down-regulated the mRNA expression of pro-inflammatory cytokines (IL-1β). Similar results were found in other plant extract studies, such as turmeric in *Cyprinus carpio* [59], *Allium mongolicum Regel* in *Channa argus* [35]. However, in the present study, the transcription of TNF-α, another anti-inflammatory cytokine, were up-regulated sharply in SFE 0.1 and SFE 0.2 groups. TNF-α is a pro-inflammatory cytokine secreted from activated macrophages, vital in regulating innate immune functions and inflammatory responses [60]. In previous studies, dietary *P. tectorius* extract and *Agaricus bisporus* polysaccharides up-regulated TNF-α expression in the fish [61,62], while dietary turmeric significantly decreased the expression of TNF-α in *Cyprinus carpio* [59]. The difference of gene expression results may be due to the difference of the type and dose of plant immune stimulants, feeding time and fish species. Under challenge condition, the gene expressions of NF- κB p65 and IκBα in SFE0 group were up-regulated compared with normal condition, and the mRNA levels of IL-1β and IL-10 increased sharply, which means that excessive inflammatory response occurred in turbot after *E. tarda* infection. Meanwhile, dietary SFE administration significantly decreased the mRNA levels of IL-1β and IL-10, which suggested that dietary supplementation of SFE could inhibit the inflammatory response of turbot infected by *E. tarda* to protect the body from excessive inflammatory reaction.

Due to the prevalence of industrialized intensive farming, fish usually face greater risks of antioxidant stress and pathogen attack. *E. tarda*, a causative infectious agent of disease in aquaculture, caused mass mortalities and considerable economic losses, particularly in turbot [63]. Bacterial challenge test is often used as an effective indicator of fish immunity and health status. In this study, after the challenge, turbot in SFE 0 treatment firstly displayed the clinical symptoms of *E. tarda* infection: red bleeding plaques in the head and muscles, dark red mucus in the gills, blood spots on the fins, anal congestion, and protrusion. Then, the first dead turbot was observed in the SFE 0 group on the second day, the mortality lasted to the sixth day after challenge. Further, 0.1% SFE administration significantly relieved the symptoms and increased the survival rate of turbot. The survival rates of SFE administration groups were higher than that of SFE 0 group. Therefore, the elevation of disease resistance against *E. tarda* is contributed to the regulation of immune response and antioxidant capacity by SFE administration. That is to say, SFE could affect mRNA levels of immune-related genes by activating Nrf2/Keap 1 and NF-κB signaling

pathways, and then improved the antioxidant capacity and immunity of turbot, which also improved the ability of juvenile fish to resist *E. tarda* infection. It also suggests that antioxidant capacity, immunity, and disease resistance are inextricably linked.

5. Conclusions

Overall (Figure 5), the present study was apparently the first report that dietary SFE supplementation for 56 days promoted the immunity and antioxidant capacity through activating Nrf2/Keap1 and NF-κB signal pathways, thus improving the growth performance and disease resistance against *E. tarda*. SFE could be a potential feed additive for turbot.

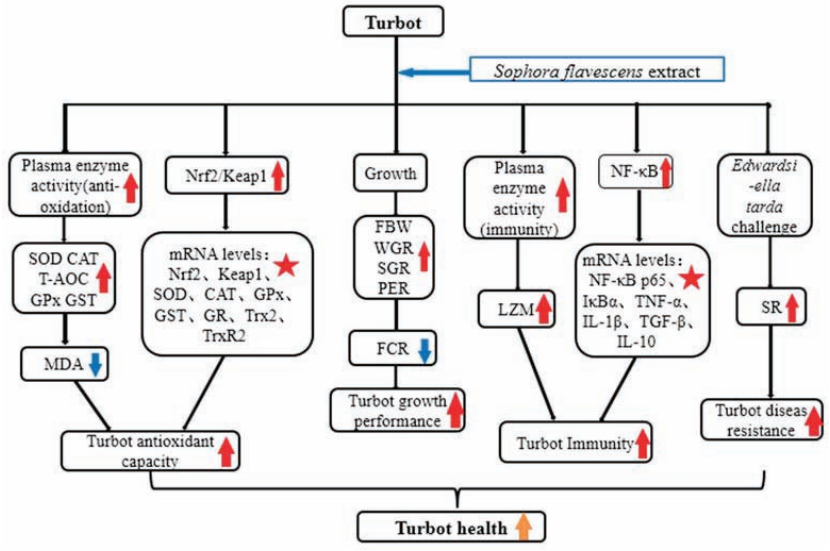

Figure 5. General summary for the beneficial effects and potential mechanisms of SFE on the health of turbot. (★: indicates a significant impact. The red arrow indicates the promoting effect, the blue arrow indicates the inhibitory effect, and the orange arrow indicates a positive effect on fish health).

Author Contributions: Conceptualization, H.L.; methodology, H.L., X.G. and Y.H.; software, X.G. and Y.H.; validation, X.S., N.D. and T.Y.; formal analysis, X.G. and Y.H.; investigation, X.G. and Y.H.; resources, H.L.; data curation, X.G. and Y.H.; writing—original draft preparation, Y.H.; writing—review and editing, H.L. and P.Z.; visualization, Y.H.; supervision, H.L.; project administration, H.L.; funding acquisition, H.L. All authors have read and agreed to the published version of the manuscript.

Funding: This research was funded by S &T Program of Hebei (19226705D, C2021205020), and Modern Agro-industry Technology Research Team of Hebei (HBCT2018170205).

Institutional Review Board Statement: The animal study protocol was approved by the Ethics Committee of Hebei Normal University (protocol code is 208007; approval date is 15 July 2020).

Informed Consent Statement: Not applicable.

Data Availability Statement: Data is contained within the article.

Conflicts of Interest: The authors declare no conflict of interest.

Abbreviations

IBW, initial body weight; FBW, final body weight; WGR, Weight gain rate; SGR, Specific growth rate; FR, Feeding rate; FCR, Feed conversion ratio; SR, Survival rate; PER, Protein efficiency ratio; HIS, Hepatosomatic index; VSI, Viscerosomatic index; CF, Condition factor; NF-κB p65, nuclear factor kappa B–p65; IκBα, inhibitor of κBα; TNF-α,

tumor necrosis factor-alpha; IL-1β, interleukin-1 beta; TGF-β, transforming growth factor beta; IL-10, interleukin -10; Nrf2, nuclear factor erythroid 2-related factor 2; Keap1, kelch-like ECH-associated protein 1; Trx2, thioredoxin 2; TrxR2, thioredoxin reductase 2; GPx, glutathione peroxidase; GR, glutathione reductase; GST, glutathione S-transferase; SOD, superoxide dismutase; CAT, catalase; RPS4, ribosomal protein S4.

References

1. Leung, T.L.F.; Bates, A.E. More rapid and severe disease outbreaks for aquaculture at the tropics: Implications for food security. *J. Appl. Ecol.* **2013**, *50*, 215–222. [CrossRef]
2. Schar, D.; Klein, E.Y.; Laxminarayan, R.; Gilbert, M.; Van Boeckel, T.P. Global trends in antimicrobial use in aquaculture. *Sci. Rep.* **2020**, *10*, 21878. [CrossRef] [PubMed]
3. Chen, C.Q.; Zheng, L.; Zhou, J.L.; Zhao, H. Persistence and risk of antibiotic residues and antibiotic resistance genes in major mariculture sites in Southeast China. *Sci. Total Environ.* **2017**, *580*, 1175–1184. [CrossRef] [PubMed]
4. Du, J.; Zhao, H.; Wang, Y.; Xie, H.; Zhu, M.; Chen, J. Presence and environmental risk assessment of selected antibiotics in coastal water adjacent to mariculture areas in the Bohai Sea. *Ecotoxicol. Environ. Saf.* **2019**, *177*, 117–123. [CrossRef]
5. Zhang, R.; Pei, J.; Zhang, R.; Wang, S.; Zeng, W.; Huang, D.; Wang, Y.; Zhang, Y.; Wang, Y.; Yu, K. Occurrence and distribution of antibiotics in mariculture farms, estuaries and the coast of the Beibu Gulf, China: Bioconcentration and diet safety of seafood. *Ecotoxicol. Environ. Saf.* **2018**, *154*, 27–35. [CrossRef]
6. Stratev, D.; Zhelyazkov, G.; Noundou, X.S.; Krause, R.W.M. Beneficial effects of medicinal plants in fish diseases. *Aquac. Int.* **2017**, *26*, 289–308. [CrossRef]
7. Ahmadifar, E.; Mohammadzadeh, S.; Kalhor, N.; Yousefi, M.; Moghadam, M.S.; Naraballobh, W.; Ahmadifar, M.; Hoseinifar, S.H.; Van Doan, H. Cornelian cherry (*Cornus mas* L.) fruit extract improves growth performance, disease resistance, and serum immune-and antioxidant-related gene expression of common carp (*Cyprinus carpio*). *Aquaculture* **2022**, *558*, 738372.
8. Uma, A.; Philominal, P.; Prabu, E.; Musthafa, M.S. Dietary *Bougainvillea glabra* leaf meal on growth, haemato-biochemical responses and disease resistance in Nile tilapia, *Oreochromis niloticus* against *Enterococcus faecalis*. *Aquaculture* **2022**, *549*, 737806. [CrossRef]
9. Sun, Z.; Tan, X.; Wei, Z.; Liu, Q.; Mai, H.; Liu, Y.; Liu, B.; Zhuang, Y.; Zou, D.; Zhang, W.; et al. Effects of dietary dandelion extract on the growth performance, serum biochemical parameters, liver histology, and immune and apoptosis-related genes expression of hybrid grouper (*Epinephelus lanceolatus* ♂× *Epinephelus fuscoguttatus* ♀) at different feeding period. *Fish Shellfish Immunol.* **2022**, *120*, 280–286.
10. Dawood, M.A.O.; Koshio, S.; Esteban, M.Á. Beneficial roles of feed additives as immunostimulants in aquaculture: A review. *Rev. Aquac.* **2018**, *10*, 950–974. [CrossRef]
11. Reverter, M.; Bontemps, N.; Lecchini, D.; Banaigs, B.; Sasal, P. Use of plant extracts in fish aquaculture as an alternative to chemotherapy: Current status and future perspectives. *Aquaculture* **2014**, *433*, 50–61. [CrossRef]
12. Van Hai, N. The use of medicinal plants as immunostimulants in aquaculture: A review. *Aquaculture* **2015**, *446*, 88–96. [CrossRef]
13. Zhu, F. A review on the application of herbal medicines in the disease control of aquatic animals. *Aquaculture* **2020**, *526*, 735422. [CrossRef]
14. He, Q.; Xiao, S.; Zhang, C.; Zhang, Y.; Shi, H.; Zhang, H.; Lin, F.; Liu, X.; Yang, H.; Wang, Q.; et al. Modulation of the growth performance, biochemical parameters, and non-specific immune responses of the hybrid grouper (*Epinephelus fuscoguttatus* ♀× *E lanceolatus* ♂) by two kinds of Chinese herb. *Aquac. Rep.* **2021**, *19*, 100604.
15. Pu, H.; Li, X.; Du, Q.; Cui, H.; Xu, Y. Research Progress in the Application of Chinese Herbal Medicines in Aquaculture: A Review. *Engineering* **2017**, *3*, 731–737. [CrossRef]
16. He, X.; Fang, J.; Huang, L.; Wang, J.; Huang, X. *Sophora flavescens* Ait.: Traditional usage, phytochemistry and pharmacology of an important traditional Chinese medicine. *J. Ethnopharmacol.* **2015**, *172*, 10–29.
17. Ma, H.; Huang, Q.; Qu, W.; Li, L.; Wang, M.; Li, S.; Chu, F. In vivo and in vitro anti-inflammatory effects of *Sophora flavescens* residues. *J. Ethnopharmacol.* **2018**, *224*, 497–503. [CrossRef]
18. Weng, Z.; Guo, S.; Qian, D.; Zhu, Z.; Zhang, S.; Li, A.; Lei, Z.; Duan, J. *Sophora flavescens* Seed as a promising high potential by-product: Phytochemical characterization and bioactivity evaluation. *Ind. Crops Prod.* **2017**, *109*, 19–26. [CrossRef]
19. Wu, Y.R.; Gong, Q.F.; Fang, H.; Liang, W.W.; Chen, M.; He, R.J. Effect of *Sophora flavescens* on non-specific immune response of tilapia (GIFT *Oreochromis niloticus*) and disease resistance against *Streptococcus agalactiae*. *Fish Shellfish Immunol.* **2013**, *34*, 220–227. [CrossRef]
20. Seo, J.-S.; Jeon, E.-J.; Kwon, M.-G.; Hwang, J.-Y.; Kim, J.-D.; Jung, S.-H.; Kim, N.-Y.; Jee, B.-Y.; Park, M.-A. Effect of Disease Resistance on Oral Administration of Lightyellow *Sophora* Extract in *Olive flounder*. *J. Fish. Mar. Sci. Educ.* **2015**, *27*, 1656–1664.
21. Wen, L.M.; Feng, L.; Jiang, W.D.; Liu, Y.; Wu, P.; Zhao, J.; Jiang, J.; Kuang, S.Y.; Tang, L.; Tang, W.N.; et al. Thiamin deficiency induces impaired fish gill immune responses, tight junction protein expression and antioxidant capacity: Roles of the NF-kappaB, TOR, p38 MAPK and Nrf2 signaling molecules. *Fish Shellfish Immunol.* **2016**, *51*, 373–383. [CrossRef] [PubMed]

22. Jiang, W.D.; Tang, R.J.; Liu, Y.; Wu, P.; Kuang, S.Y.; Jiang, J.; Tang, L.; Tang, W.N.; Zhang, Y.A.; Zhou, X.Q.; et al. Impairment of gill structural integrity by manganese deficiency or excess related to induction of oxidative damage, apoptosis and dysfunction of the physical barrier as regulated by NF-kappaB, caspase and Nrf2 signaling in fish. *Fish Shellfish Immunol.* **2017**, *70*, 280–292. [CrossRef] [PubMed]
23. Jiang, W.D.; Feng, L.; Qu, B.; Wu, P.; Kuang, S.Y.; Jiang, J.; Tang, L.; Tang, W.N.; Zhang, Y.A.; Zhou, X.Q.; et al. Changes in integrity of the gill during histidine deficiency or excess due to depression of cellular anti-oxidative ability, induction of apoptosis, inflammation and impair of cell-cell tight junctions related to Nrf2, TOR and NF-kappaB signaling in fish. *Fish Shellfish Immunol.* **2016**, *56*, 111–122. [CrossRef] [PubMed]
24. Kobayashi, E.H.; Suzuki, T.; Funayama, R.; Nagashima, T.; Hayashi, M.; Sekine, H.; Tanaka, N.; Moriguchi, T.; Motohashi, H.; Nakayama, K.; et al. Nrf2 suppresses macrophage inflammatory response by blocking proinflammatory cytokine transcription. *Nat. Commun.* **2016**, *7*, 11624. [CrossRef] [PubMed]
25. Gao, Q.; Liu, B.; Shan, F.; Liu, B.; Gu, Z.; Song, C.; Sun, C.; Zhou, Q. Effects of oxidized fish oil on digestive enzyme activity and antioxidant system in *Macrobrachium rosenbergii* post-larvae. *Aquac. Rep.* **2022**, *23*, 101062. [CrossRef]
26. Gong, S.S.; Li, Y.X.; Zhang, M.T.; Du, J.; Ma, P.S.; Yao, W.X.; Zhou, R.; Niu, Y.; Sun, T.; Yu, J.Q. Neuroprotective Effect of Matrine in Mouse Model of Vincristine-Induced Neuropathic Pain. *Neurochem. Res.* **2016**, *41*, 3147–3159. [CrossRef]
27. Zhang, H.F.; Shi, L.J.; Song, G.Y.; Cai, Z.G.; Wang, C.; An, R.J. Protective effects of matrine against progression of high-fructose diet-induced steatohepatitis by enhancing antioxidant and anti-inflammatory defences involving Nrf2 translocation. *Food Chem. Toxicol.* **2013**, *55*, 70–77. [CrossRef]
28. Sun, P.; Sun, N.; Yin, W.; Sun, Y.; Fan, K.; Guo, J.; Khan, A.; He, Y.; Li, H. Matrine inhibits IL-1beta secretion in primary porcine alveolar macrophages through the MyD88/NF-kappaB pathway and NLRP3 inflammasome. *Vet. Res.* **2019**, *50*, 53. [CrossRef]
29. Zhang, Y.; Yang, P.; Sun, H.; Hou, Y.; Zhang, Y.; Liu, H. Evaluation of extruded full-fat soybean as the substitution for fish meal in diets for juvenile *Scophthalmus maximus* based on growth performance, intestinal microbiota, and aquaculture water quality. *Aquaculture* **2023**, *562*, 738734. [CrossRef]
30. Livak, K.J.; Schmittgen, T.D. Analysis of relative gene expression data using real-time quantitative PCR and the 2(-Delta Delta C(T)) Method. *Methods* **2001**, *25*, 402–408. [CrossRef]
31. Sun, Z.; Tan, X.; Ye, H.; Zou, C.; Ye, C.; Wang, A. Effects of dietary *Panax notoginseng* extract on growth performance, fish composition, immune responses, intestinal histology and immune related genes expression of hybrid grouper (*Epinephelus lanceolatus* ♂× *Epinephelus fuscoguttatus* ♀) fed high lipid diets. *Fish Shellfish Immunol.* **2018**, *73*, 234–244. [PubMed]
32. Wang, Q.; Shen, J.; Yan, Z.; Xiang, X.; Mu, R.; Zhu, P.; Yao, Y.; Zhu, F.; Chen, K.; Chi, S.; et al. Dietary *Glycyrrhiza uralensis* extracts supplementation elevated growth performance, immune responses and disease resistance against *Flavobacterium columnare* in yellow catfish (*Pelteobagrus fulvidraco*). *Fish Shellfish Immunol.* **2020**, *97*, 153–164. [CrossRef] [PubMed]
33. Liu, M.; Gao, Q.; Sun, C.; Liu, B.; Liu, X.; Zhou, Q.; Zheng, X.; Xu, P.; Liu, B. Effects of dietary tea tree oil on the growth, physiological and non-specific immunity response in the giant freshwater prawn (*Macrobrachium rosenbergii*) under high ammonia stress. *Fish Shellfish Immunol.* **2022**, *120*, 458–469. [CrossRef] [PubMed]
34. Doan, H.V.; Hoseinifar, S.H.; Jaturasitha, S.; Dawood, M.A.O.; Harikrishnan, R. The effects of berberine powder supplementation on growth performance, skin mucus immune response, serum immunity, and disease resistance of Nile tilapia (*Oreochromis niloticus*) fingerlings. *Aquaculture* **2020**, *520*, 734927. [CrossRef]
35. Li, M.; Zhu, X.; Tian, J.; Liu, M.; Wang, G. Dietary flavonoids from *Allium mongolicum Regel* promotes growth, improves immune, antioxidant status, immune-related signaling molecules and disease resistance in juvenile northern snakehead fish (*Channa argus*). *Aquaculture* **2019**, *501*, 473–481. [CrossRef]
36. Liu, F.; Geng, C.; Qu, Y.; Cheng, B.; Zhang, Y.; Wang, A.; Zhang, J.H.; Liu, B.; Tian, H.; Yang, W.; et al. The feeding of dietary *Codonopsis pilosula* polysaccharide enhances the immune responses, the expression of immune-related genes and the growth performance of red swamp crayfish (*Procambarus clarkii*). *Fish Shellfish Immunol.* **2020**, *103*, 321–331. [CrossRef] [PubMed]
37. Sun, Y.; Wang, X.; Zhou, H.; Mai, K.; He, G. Dietary Astragalus polysaccharides ameliorates the growth performance, antioxidant capacity and immune responses in turbot (*Scophthalmus maximus* L.). *Fish Shellfish Immunol.* **2020**, *99*, 603–608. [CrossRef]
38. Lushchak, V.I. Environmentally induced oxidative stress in aquatic animals. *Aquat. Toxicol.* **2011**, *101*, 13–30. [CrossRef]
39. Schupp, T.; Allmendinger, H.; Bossuyt, B.T.A.; Hidding, B.; Tury, B.; West, R.J. Review of the Ecotoxicological Properties of the Methylenedianiline Substances. *Rev. Environ. Contam. Toxicol.* **2017**, *241*, 39–72.
40. Zhao, P.; Zhou, R.; Li, H.N.; Yao, W.X.; Qiao, H.Q.; Wang, S.J.; Niu, Y.; Sun, T.; Li, Y.X.; Yu, J.Q. Oxymatrine attenuated hypoxic-ischemic brain damage in neonatal rats via improving antioxidant enzyme activities and inhibiting cell death. *Neurochem. Int.* **2015**, *89*, 17–27. [CrossRef]
41. Mohammadi, Y.; Bahrami Kamangar, B.; Zarei, M.A. Effects of diets containing grape seed proanthocyanidin extract on the growth and oxidative capacity of common carp (*Cyprinus carpio*). *Aquaculture* **2021**, *540*, 736689. [CrossRef]
42. Kong, Y.; Li, M.; Guo, G.; Yu, L.; Sun, L.; Yin, Z.; Li, R.; Chen, X.; Wang, G. Effects of dietary curcumin inhibit deltamethrin-induced oxidative stress, inflammation and cell apoptosis in *Channa argus* via Nrf2 and NF-κB signaling pathways. *Aquaculture* **2021**, *540*, 736744. [CrossRef]
43. Zhao, J.; Liu, Y.; Jiang, J.; Wu, P.; Chen, G.; Jiang, W.; Li, S.; Tang, L.; Kuang, S.; Feng, L. Effects of dietary isoleucine on growth, the digestion and absorption capacity and gene expression in hepatopancreas and intestine of juvenile Jian carp (*Cyprinus carpio* var. *Jian). Aquaculture* **2012**, *368*, 117–128. [CrossRef]

44. Copple, I.M.; Goldring, C.E.; Kitteringham, N.R.; Park, B.K. The Nrf2-Keap1 defence pathway: Role in protection against drug-induced toxicity. *Toxicology* **2008**, *246*, 24–33. [CrossRef]
45. Jaiswal, A.K. Nrf2 signaling in coordinated activation of antioxidant gene expression. *Free Radic. Biol. Med.* **2004**, *36*, 1199–1207. [CrossRef] [PubMed]
46. Itoh, K.; Wakabayashi, N.; Katoh, Y.; Ishii, T.; Igarashi, K.; Engel, J.D.; Yamamoto, M. Keap1 represses nuclear activation of antioxidant responsive elements by Nrf2 through binding to the amino-terminal Neh2 domain. *Genes Dev.* **1999**, *13*, 76–86. [CrossRef] [PubMed]
47. Calkins, M.J.; Johnson, D.A.; Townsend, J.A.; Vargas, M.R.; Dowell, J.A.; Williamson, T.P.; Kraft, A.D.; Lee, J.-M.; Li, J.; Johnson, J.A. The Nrf2/ARE pathway as a potential therapeutic target in neurodegenerative disease. *Antioxid. Redox Signal.* **2009**, *11*, 497–508. [CrossRef]
48. Cheng, C.; Park, S.C.; Giri, S.S. Effect of *Pandanus tectorius* extract as food additive on oxidative stress, immune status, and disease resistance in *Cyprinus carpio*. *Fish Shellfish Immunol.* **2022**, *120*, 287–294. [CrossRef]
49. Song, C.; Liu, B.; Li, H.; Tang, Y.; Ge, X.; Liu, B.; Xu, P. Protective Effects of Emodin on Oxidized Fish Oil-Induced Metabolic Disorder and Oxidative Stress through Notch-Nrf2 Crosstalk in the Liver of Teleost *Megalobrama amblycephala*. *Antioxidants* **2022**, *11*, 1179. [CrossRef]
50. Pacitti, D.; Wang, T.; Martin, S.A.; Sweetman, J.; Secombes, C.J. Insights into the fish thioredoxin system: Expression profile of thioredoxin and thioredoxin reductase in rainbow trout (*Oncorhynchus mykiss*) during infection and in vitro stimulation. *Dev. Comp. Immunol.* **2014**, *42*, 261–277. [CrossRef]
51. Kugapreethan, R.; Umasuthan, N.; Wan, Q.; Thulasitha, W.S.; Kim, C.; Lee, J. Comparative analysis of two thioredoxin-like genes in black rockfish *Sebastes schlegelii* and their possible involvement in redox homeostasis and innate immune responses. *Dev. Comp. Immunol.* **2017**, *67*, 43–56. [CrossRef] [PubMed]
52. Saurabh, S.; Sahoo, P. Lysozyme: An important defence molecule of fish innate immune system. *Aquac. Res.* **2008**, *39*, 223–239. [CrossRef]
53. Zhang, B.; Li, C.; Wang, X.; Zhou, H.; Mai, K.; He, G. The effects of dietary Eucommia ulmoides Oliver on growth, feed utilization, antioxidant activity and immune responses of turbot (*Scophthalmus maximus* L.). *Aquac. Nutr.* **2019**, *25*, 367–376. [CrossRef]
54. Ghosh, S.; Hayden, M.S. New regulators of NF-κB in inflammation. *Nat. Rev. Immunol.* **2008**, *8*, 837–848. [CrossRef]
55. Hayden, M.S.; Ghosh, S. NF-kappaB in immunobiology. *Cell Res.* **2011**, *21*, 223–244. [CrossRef] [PubMed]
56. Bols, N.C.; Brubacher, J.L.; Ganassin, R.C.; Lee, L.E. Ecotoxicology and innate immunity in fish. *Dev. Comp. Immunol.* **2001**, *25*, 853–873. [CrossRef] [PubMed]
57. Fast, M.D.; Johnson, S.C.; Jones, S.R. Differential expression of the pro-inflammatory cytokines IL-1beta-1, TNFalpha-1 and IL-8 in vaccinated pink (*Oncorhynchus gorbuscha*) and chum (*Oncorhynchus keta*) salmon juveniles. *Fish Shellfish Immunol.* **2007**, *22*, 403–407. [CrossRef]
58. Chen, G.; Liu, Y.; Jiang, J.; Jiang, W.; Kuang, S.; Tang, L.; Tang, W.; Zhang, Y.A.; Zhou, X.; Feng, L. Effect of dietary arginine on the immune response and gene expression in head kidney and spleen following infection of Jian carp with *Aeromonas hydrophila*. *Fish Shellfish Immunol.* **2015**, *44*, 195–202. [CrossRef]
59. Giri, S.S.; Sukumaran, V.; Park, S.C. Effects of bioactive substance from turmeric on growth, skin mucosal immunity and antioxidant factors in common carp, *Cyprinus carpio*. *Fish Shellfish Immunol.* **2019**, *92*, 612–620. [CrossRef]
60. Denis, F.; Archambault, D. Molecular cloning and characterization of beluga whale (*Delphinapterus leucas*) interleukin-1beta and tumor necrosis factor-alpha. *Can. J. Vet. Res.* **2001**, *65*, 233.
61. Awad, E.; Austin, D.; Lyndon, A.; Awaad, A. Possible effect of hala extract (*Pandanus tectorius*) on immune status, anti-tumour and resistance to Yersinia ruckeri infection in rainbow trout (*Oncorhynchus mykiss*). *Fish Shellfish Immunol.* **2019**, *87*, 620–626. [CrossRef] [PubMed]
62. Harikrishnan, R.; Devi, G.; Van Doan, H.; Balasundaram, C.; Thamizharasan, S.; Hoseinifar, S.H.; Abdel-Tawwab, M. Effect of diet enriched with *Agaricus bisporus polysaccharides* (ABPs) on antioxidant property, innate-adaptive immune response and pro-anti inflammatory genes expression in *Ctenopharyngodon idella* against *Aeromonas hydrophila*. *Fish Shellfish Immunol.* **2021**, *114*, 238–252. [CrossRef] [PubMed]
63. Cui, H.; Cong, C.; Wang, L.; Li, X.; Li, J.; Yang, H.; Li, S.; Xu, Y. Control of *Edwardsiella tarda* infection in turbot *Scophthalmus maximus* (L.) using phage vB_EtaM_ET-ABTNL-9. *Aquac. Res.* **2022**, *53*, 3010–3024.

antioxidants

MDPI

Article

Molecular Cloning and Functional Characterization of Catalase in Stress Physiology, Innate Immunity, Testicular Development, Metamorphosis, and Cryopreserved Sperm of Pacific Abalone

Shaharior Hossen [1], Zahid Parvez Sukhan [1], Soo Cheol Kim [2], Md. Abu Hanif [1], Il-Keun Kong [3] and Kang Hee Kho [1,*]

[1] Department of Fisheries Science, College of Fisheries and Ocean Sciences, Chonnam National University, 50 Daehak-ro, Yeosu 59626, Republic of Korea
[2] South Sea Fisheries Research Institute, National Institute of Fisheries Science, Yeosu 59780, Republic of Korea
[3] Department of Animal Science, Division of Applied Life Science (BK21 Four), Gyeongsang National University, Jinju 52828, Republic of Korea
* Correspondence: kkh@chonnam.ac.kr; Tel.: +82-616-597-168; Fax: +82-616-597-169

Abstract: Catalase is a crucial enzyme of the antioxidant defense system responsible for the maintenance of cellular redox homeostasis. The aim of the present study was to evaluate the molecular regulation of catalase (*Hdh-CAT*) in stress physiology, innate immunity, testicular development, metamorphosis, and cryopreserved sperm of Pacific abalone. *Hdh-CAT* gene was cloned from the digestive gland (DG) of Pacific abalone. The 2894 bp sequence of *Hdh-CAT* had an open reading frame of 1506 bp encoding 501 deduced amino acids. Fluorescence *in situ* hybridization confirmed *Hdh-CAT* localization in the digestive tubules of the DG. *Hdh-CAT* was induced by different types of stress including thermal stress, H_2O_2 induction, and starvation. Immune challenges with *Vibrio*, lipopolysaccharides, and polyinosinic–polycytidylic acid sodium salt also upregulated *Hdh-CAT* mRNA expression and catalase activity. *Hdh-CAT* responded to cadmium induced-toxicity by increasing mRNA expression and catalase activity. Elevated seasonal temperature also altered *Hdh-CAT* mRNA expression. *Hdh-CAT* mRNA expression was relatively higher at the trochophore larvae stage of metamorphosis. Cryopreserved sperm showed significantly lower *Hdh-CAT* mRNA expression levels compared with fresh sperm. *Hdh-CAT* mRNA expression showed a relationship with the production of ROS. These results suggest that *Hdh-CAT* might play a role in stress physiology, innate immunity, testicular development, metamorphosis, and sperm cryo-tolerance of Pacific abalone.

Keywords: catalase; innate immunity; stress physiology; starvation; metamorphosis; cryopreserved sperm; Pacific abalone

Citation: Hossen, S.; Sukhan, Z.P.; Kim, S.C.; Hanif, M.A.; Kong, I.-K.; Kho, K.H. Molecular Cloning and Functional Characterization of Catalase in Stress Physiology, Innate Immunity, Testicular Development, Metamorphosis, and Cryopreserved Sperm of Pacific Abalone. *Antioxidants* **2023**, *12*, 109. https://doi.org/10.3390/antiox12010109

Academic Editors: Bo Liu, Changyou Song and Cunxin Sun

Received: 22 November 2022
Revised: 29 December 2022
Accepted: 29 December 2022
Published: 1 January 2023

1. Introduction

Catalase (CAT) is the most frequently used biomarker of oxidative stress in animals of aquatic environments [1,2]. Catalase is a vital antioxidant enzyme that can balance the redox system by regulating antioxidant defenses against oxidative stress [3,4]. This antioxidant enzyme responds to the adverse effects of environmental pollution on organisms [1]. CAT is a part of the reactive oxygen species (ROS) network and plays a central role in balancing hydrogen peroxide (H_2O_2) levels in cells [5–7]. The key biological mechanism of CAT is to scavenge the excessive level of ROS by directly breaking down H_2O_2 into water and oxygen [8–11]. H_2O_2 is a highly reactive ROS [12] and a secondary key performer of mitochondrial ROS production [13]. Excessive H_2O_2 lead to infertility whereas CAT restored fertility [14]. H_2O_2 challenges induce CAT expression in mollusks [3,15]. Whereas heat stress induces H_2O_2 production [16,17] that ultimately increases CAT expression [18–20]. Heat stress also induces CAT activity and increases its mRNA expression in a marine mollusk, *Scapharca subcrenata* [21]. Cold stress imbalances CAT activity and expression in scallop,

Chlamys nobilis [4]. CAT neutralizes the effects of ROS production during starvation [22]. Starvation induces CAT activity and mRNA expression in fish [22,23].

CAT also plays an important role in the innate host defense mechanism against environmental stress and pathogen infection [24]. CAT is a reliable biomarker for detecting a variety of pollutants [25]. It can defend against metal-oriented stress [26]. Cadmium (Cd) is a bioaccumulation environmental pollutant able to induce ROS [27] and finally damage the physiological function of organs [26]. Antioxidant activity of CAT has been previously detected in Cd exposed-aquatic organisms [26]. *Vibrios* are categorized as the main infected pathogenic bacteria of abalone [28]. Bacterial challenges of disk abalone can induce CAT expression [28], which proves that CAT might play a role in the immune defense mechanism against pathogens [15]. Viral challenge also alters *CAT* mRNA expression in disc abalone [28].

The antioxidant defense system of CAT is altered seasonally in response to several types of environmental factors [29,30]. Elevated temperature modulates the activity and expression of CAT in the gill and digestive glands of American oyster [31].

CAT also plays a potential role in sperm physiology, which is essential for normal sperm function and spermatogenesis. CAT is a molecular marker to determine fertility [14]. Higher activity and abundance of CAT have been found in aquatic organisms during early embryogenesis [32–34].

Cryopreservation of sperm is responsible for excessive ROS generation that causes an imbalance of the natural antioxidant defense system of sperm [35]. CAT activity and mRNA abundance have been found to be antioxidant indicators of cryopreserved sperm and ovary [35,36].

Abalone are high-priced marine bioresources found worldwide in tropical and temperate waters [37]. Abalone are key components of the marine ecosystem as well as the aquaculture industry [38]. Dynamic environmental and pathogenic conditions of the intertidal zone create various environmental stresses [39]. These adverse environmental conditions lead to a decrease in the survivability of abalone [38,39]. Abalone are vital bio-indicators of the marine ecosystem [39] due to their innate responses against viruses, bacteria, and toxic substances [28]. Of various abalone species, Pacific abalone *Haliotis discus hannai* is the most demanded seafood in Korea, Taiwan, China, and Japan, because it contains bioactive molecules [40]. It is also known as the "emperor of shellfish" in Korea [41] and recognized worldwide as the "soft gold" of the Ocean [42,43]. Among abalone, to date, CAT has been reported in disk abalone, *H. discus discus* [3]. CAT is highly expressed in the DG and gill of disk abalone, *H. discus discus* [3]. The DG, gill, and blood are important immune organs of abalone [44]. Moreover, the DG (hepatopancreas) is the main metabolic organ of Pacific abalone. The DG act as the major site for the accumulation of bacteria and toxic metals, playing a vital role against oxidative stress by eliminating excessive ROS [44]. However, molecular characterization of CAT in Pacific abalone is unknown. Thus, the objective of this study was to obtain the full-length cDNA of CAT from Pacific abalone and apply this sequence to understand the molecular characterization of CAT in stress physiology, immune response, elevated seasonal temperature, testicular development, metamorphosis, and cryopreserved sperm of Pacific abalone. Furthermore, the localization of CAT was determined using fluorescence *in situ* hybridization.

2. Materials and Methods

2.1. Ethics Statement

The experimental protocols were approved by the Institutional Animal Care and Use Committee (IACUC) of Chonnam National University (CNU IACUC-YS-2020-5). All experiments were conducted following the Guidelines for the Care and Use of Laboratory Animals of the National Institutes of Health.

2.2. Experimental Abalone Collection

Biologically matured three years old Pacific abalone were collected from sea cages of Wando-gun, Republic of Korea. A total of 512 Pacific abalone having a mean body weight of 134.8 ± 14.3 g were used in the experiments.

2.3. Tissue Collection for Gene Cloning

Abalone (n = 10) were euthanized for collecting digestive gland (DG) tissue samples. The samples were washed using 0.1M phosphate-buffered saline (PBS) and subsequently snap-frozen in liquid nitrogen (LN_2). Samples were then stored at −80 °C until total ribonucleic acid (tRNA) extraction.

2.4. Tissue Collection of Different Organs of Pacific Abalone

Abalone including digestive gland (DG), testis (TE), ovary (OV), muscle (MUS), mantle (MA), gill (G), heart (HRT), hemocyte (HCY), cerebral ganglion (CG), and pleuropedal ganglion (PPG) were collected to check the tissue distribution of catalase.

2.5. Fluorescence In Situ Hybridization (FISH) to Localize Hdh-CAT in Digestive Gland Tissue of Pacific Abalone

2.5.1. Tissue Collection for Fluorescence In Situ Hybridization

Abalone digestive gland tissues (n = 6) were collected after performing anesthesia with 5% $MgCl_2$. Samples were washed with pre-chilled 0.1 M PBS and fixed with 4% paraformaldehyde (PFA) for in situ hybridization.

2.5.2. Riboprobe Synthesis

Riboprobe synthesis was performed using the method described previously [45], with slight modifications. Briefly, sense and antisense mRNA probes were prepared from 714 bp fragments of the catalase domain of *Hdh-CAT* that had been amplified using a pair of primers (Table S1). Sense and anti-sense riboprobes were separately labeled with fluorescein-12-UTP (Roche, Grenzach-Wyhlen, Germany) using SP6 or T7 RNA polymerase (Promega, Medison, WI, USA). A total 20 µL working solution including 1 µg plasmid DNA, 2.0 µL SP6 or T7 RNA polymerase, 4 µL 5X optimized transcription buffer, 2 µL DTT (100 mM), 2 µL RNase inhibitor, 2 µL fluorescein RNA labeling mix, and 7 µL RNase-free water was prepared and incubated for 2 h at 37 °C. Then, the samples were digested with 2.0 µL DNase I and 0.5 µL RNase-OUT at 37 °C for 15 min. Finally, riboprobes were purified using ethanol precipitation with 1 µL yeast tRNA (10 mg/mL, Sigma-Aldrich, St. Louis, MO, USA). The probes were stored at −80 °C until use.

2.5.3. Preparation of Tissue Sections

Paraformaldehyde-fixed digestive gland samples of Pacific abalone were infiltrated using a 30% sucrose solution. Tissue samples were embedded in optimum cutting temperature compounds (FSC 222, Leica Biosystems, Wetzlar, Germany). Transverse-oriented tissues were then sectioned at 8 µM in thickness using a cryostat device (CM 3050, Leica, Wetzlar, Germany) and mounted on electrostatically charged glass slides (SuperFrost Plus, Radnor, PA, USA). Slides were air-dried for 30 min and stored at −20 °C until use. Consecutive slides were prepared with alternative sections for the hybridization of *Hdh-CAT* mRNA using sense and antisense riboprobes.

2.5.4. Fluorescence In Situ Hybridization (FISH)

FISH was performed following a previously described protocol [45] and DIG in situ hybridization manual with minor modifications. Briefly, a total of 50 mL hybridization buffer (HB) was prepared using deionized formamide (25 mL), 20X saline sodium citrate (SSC, 12.5 mL), 0.1% Tween-20 (0.5 mL), 1M citric acid (0.46 mL), and DEPC-treated water (11.54 mL). Yeast tRNA was mixed with HB at a ratio of 1:9 to prepare HB mix. Digestive gland tissue sections were prehybridized with HB mix for 2 h at 65 °C, fol-

lowed by hybridization with fluorescein-12-UTP-labeled RNA probe (200 ng/mL, diluted with HB mix) at 65 °C overnight. Samples were subsequently washed with degraded series (75%, 50%, and 25% volume) of hybridization mix with 2X SSC for 10 min each at 65 °C. Samples were then washed with SSC (2X and 0.2X) for 15 min. Then, the tissue sections were sequentially cleaned with degraded series of 0.2X SSC (75%, 50%, and 25% volume) mixed with PBST for 5 min and washed with PBST for 5 min. Tissue sections were then incubated with calf serum (10%) for 1 h at 25 °C and then incorporated with Fab fragments antibody (anti-digoxigenin-fluorescein) for 1 h at 25 °C. Samples were then washed three times (10 min each) with PBST, followed by three times of wash with alkaline-tris buffer for 5 min each. Finally, hybridized tissue samples were counterstained and mounted using VECTASHIELD® antifade mounting medium with DAPI (Vector Laboratories, Burlingame, CA, USA). Fluorescence catalase signals were visualized and captured using a confocal microscope with Airyscan2 (LSM 900, ZEISS, Oberkochen, Germany). Images were processed on ZEISS ZEN 3.2 (Blue 268 edition, Oberkochen, Germany) software.

2.6. Thermal Stress Experiments

2.6.1. Cold Stress of Pacific Abalone at 15 °C

Cold temperature stress (15 °C) was carried out by transferring abalone into experimental tanks. Water temperature was reduced from 20 °C to 15 °C with a temperature reduction rate of 1 °C/h until it reached 15 °C. Cold temperature (15 °C) was maintained using an electric cooling unit (SunCool, DA-3000C, DAEIL, Busan, Republic of Korea). Abalone reared at 20 °C were sampled as a control, and the cold stressed at 15 °C were sampled at 1 h, 6 h, 12 h, 24 h, 48 h, and 72 h, respectively. Before sampling, abalone were anesthetized with 5% $MgCl_2$. Digestive gland and gill tissue samples (n = 6) were collected and washed with 0.1 M PBS. Hemolymph samples were collected and plasma samples were separated for catalase activity assay. Samples were snap-frozen in LN_2 and stored at −80 °C until tRNA extraction and catalase activity assay.

2.6.2. Heat Stress of Pacific Abalone at 25 °C and 30 °C

Abalone were transferred into experimental tanks and acclimatized before conducting the thermal stress experiment. Water temperature was gradually increased from 20 °C to 25 °C and 20 °C to 30 °C at 1 °C/h until it reached 25 °C or 30 °C. Abalone reared at 20 °C were used as control, and the heat-stressed abalone at 25 °C and 25 °C were sampled at 1 h, 6 h, 12 h, 24 h, 48 h, and 72 h. Digestive gland and gill tissue samples (n = 6) were collected and washed with 0.1 M PBS. Hemolymph samples were collected and plasma samples were separated for catalase activity assay. Samples were snap-frozen in LN_2 and stored at −80 °C until tRNA extraction and catalase activity assay.

2.7. Seasonal Sample Collection

To detect *Hdh-CAT* mRNA levels in seasonal samples, abalone were collected in different seasons including winter, summer, autumn, and spring (Wando-gun, Republic of Korea), and transported to Molecular Physiology Laboratory, Chonnam National University. After anesthetizing, digestive gland and gill sample (n = 10) were collected and stored at −80 °C until tRNA extraction.

2.8. H_2O_2 Induction Treatments

Abalone were transferred into experimental tanks and acclimatized one week before the H_2O_2 induction experiment. Abalone were reared in seawater-supplied tanks with continuous aeration. Abalones (n = 6) were intramuscularly injected with 50 μL (0.3 mg/mL) of H_2O_2 and an equal volume of PBS was injected into control abalone. Digestive gland and gill samples (n = 6) were collected at 3 h, 6 h, 12 h, 24 h, and 48 h. A blood sample was collected and separated the plasma for catalase activity. Samples were immediately snap-frozen in LN_2 and stored at −80 °C until tRNA extraction and catalase activity assay.

2.9. $CdCl_2$ Exposed Treatments

Acclimatized abalone were transferred to a 50 L aquarium to conduct $CdCl_2$ (Sigma-Aldrich, St. Louis, MO, USA) exposed treatments of Pacific abalone. The Cd^{2+} at concentrations of 1.5 mgL^{-1}, 3 mgL^{-1}, 6 mgL^{-1}, and 12 mgL^{-1} were selected to conduct this experiment. Abalone were exposed to different concentrations of Cd^{2+} and the samples (digestive gland and gill) were collected at 3 h, 6 h, 12 h, 24 h, and 48 h. A blood sample was collected and separated the plasma for catalase activity assay. Samples were immediately snap-frozen in LN_2 and stored at −80 °C until tRNA extraction and catalase activity assay.

2.10. Tissue Collection of Starved Pacific Abalone

Experimental abalone were starved for 21 days and re-fed for 7 days. Abalone were reared in the experimental aquarium (50 L). Digestive gland, gill, and hemolymph samples (n = 6) were collected from 7 days (st-7 d), 14 days (st-14 d), 21 days (st-21 d) starved, and 7 days re-fed (ref-7 d) abalones. Samples were immediately snap-frozen in LN_2 and stored at −80 °C until tRNA extraction and catalase activity assay.

2.11. Immune Challenges of Pacific Abalone to Check the Hdh-CAT Activity and mRNA Abundance

Lipopolysaccharides from *Escherichia coli* O55:B5 (LPS, Sigma-Aldrich, Saint Louis, MO, USA), polyinosinic–polycytidylic acid sodium salt (PIC, Sigma-Aldrich, Saint Louis, MO, USA), and *Vibrio parahaemolyticus* (ATCC 17802, Koram Biotech Corp., Seoul, Republic of Korea) were used to conduct the immune challenge experiments. LPS and PIC were separately injected into the adductor muscle at a concentration of 10 µg/g-BW. *V. parahaemolyticus* were cultured in Luria-Bertani broth (Becton, Dickinson and Company, Sparks, MD, USA) and injected in the adductor muscle at a previously recommended dose [46]. Control abalone were injected with an equal volume of PBS. Digestive gland, gill, and hemolymph samples (n = 6) were collected 3 h, 6 h, 12 h, 24 h, and 48 h after the injection. Samples were immediately snap-frozen in LN_2 and stored at −80 °C until tRNA extraction and catalase activity assay.

2.12. Tissue Collection of Testicular Developmental Stages

Testis tissue samples (n = 10) were collected during gonadal development stages including the degenerative stage (DS), active stage (AS), ripening stage (RS), and spent stage (SS) as described previously [47].

2.13. Sperm Cryopreservation of Pacific Abalone

To determine *Hdh-CAT* mRNA levels in cryopreserved sperm samples, Pacific abalone sperm samples were cryopreserved according to the protocol described previously [48]. Different types of penetrating cryoprotectants namely 8% dimethyl sulfoxide (8% DMSO), 2% glycerol (2% GLY), 8% ethylene glycol (8% EG), 6% propylene glycol (6% PG), and 2% methanol (2% MeOH), with or without antifreeze protein (AFPIII) were used as reported previously [41,48]. Briefly, stripped sperm over 90% motility was used for sperm cryopreservation. Sperm were diluted with filtered seawater at a ratio of 1:10 (v/v). Diluted sperm samples were then mixed with cryoprotectant solution (8% DMSO + AFPIII, 2% GLY + AFPIII, 8% EG + AFPIII, 6% PG + AFPIII, and 2% MeOH + AFPIII) at a ratio of 1:1 (v/v). Sperm were then transferred into 0.50 mL straws. The straws were then placed at a 5 cm rack height of LN_2 for 10 min and subsequently submerged into LN2. Straws were thawed at 60 °C for 5 s in a seawater bath (JISICO Lab & Scientific Instrument, Seoul, Republic of Korea). After thawing, the sperm samples were prepared as previously described [48].

2.14. Samples Collection of Metamorphosis Stages of Pacific Abalone

Experimental samples during metamorphosis stages including unfertilized egg (UF), 2-cell (2-CL), 4-cell (4-CL), morula (MO), blastula (BL), trochophore (TR), veliger (VEL), shell formed (SHF), and juvenile (JUV) were collected during peak reproductive season

(May). Samples were immediately snap-frozen in LN_2 and stored at −80 °C until tRNA extraction and catalase activity.

2.15. Total RNA Extraction and cDNA Synthesis

Total RNA of all collected samples was extracted using an ISOSPIN Cell & Tissue RNA kit (Nippon Gene, Tokyo, Japan). Total RNA concentration was measured using a spectrophotometer (Nanodrop ACTGene ASP-2680, Piscataway, NJ, USA). cDNA synthesis was accomplished by reverse transcribing the tRNA using a Superscript®III First-Strand synthesis kit (Invitrogen, Carlsbad, CA, USA) following the manufacturer's procedures.

2.16. Molecular Cloning and Sequencing of Catalase Gene (Hdh-CAT) in Haliotis discus hannai

2.16.1. Cloning of a Partial *Hdh-CAT* Sequence

To obtain a partial *Hdh-CAT* sequence, cDNA synthesized from the digestive gland was reverse transcribed using reverse transcription (RT) primers (Table S1) designed from known catalase sequence of *H. discus discus* (GenBank accession no. DQ821496.1). Reverse transcription polymerase chain (RT-PCR) reaction mixture (20 µL) was prepared using a 1 µL cDNA template, 1 µL of each sense and antisense primers (20 pmol), 4 µL of HF buffer, 2 µL of dNTP mix, 0.5 µL of DNA polymerase, and 10.5 µL sterile distilled water (dH_2O). The RT-PCR was conducted in a thermal cycler with the following conditions: an initial denaturation at 94 °C for 3 min; 35 cycles of denaturation at 94 °C for 30 s; annealing at 58 °C for 30 s; and extension at 72 °C for 30 s; with a final dissociation step of 5 min at 72 °C. The PCR products were separated on 1.2% agarose gel and purified using a gel extraction kit (Promega, Madison, WI, USA). Purified DNA was ligated to a pTOP Blunt V2 vector (Enzynomics, Daejeon, Republic of Korea) and transformed into Escherichia coli DHα competent cells (Enzynomics, Daejeon, Republic of Korea). Plasmid DNA was extracted from positive clones using a Hybrid-QTM Plasmid Rapidprep mini kit (GeneAll, Seoul, Republic of Korea). Sequencing was performed using the Macrogen Online Sequencing System (Macrogen, Seoul, Republic of Korea).

2.16.2. Cloning of the Full-Length *Hdh-CAT* Sequence

To obtain full-length *Hdh-CAT* sequence, gene-specific primers (GSP) were designed (Table S1) from a partial sequence, including a 15 bp overlap with the 5′ end of GSP sequences. Rapid amplification of cDNA ends (RACE) PCR was conducted using 50 µL volume of PCR mixture containing 2.5 µL of first-strand cDNA from the digestive gland, 5 µL of universal primer mix, 25 µL of SeqAMP buffer, 1 µL of SeqAMP DNA polymerase, and 15.5 µL pf PCR grade water. Touchdown PCR was performed with 25 cycles for rapid amplification of 3′ cDNA ends (3′-RACE) and 5′-RACE PCR following the manufacturer's protocol. PCR products were purified from 1.2 % agarose gel using a NucleoSpin® Gel and PCR Clean-up kit (MARCHERY-NAGEL GmbH & Co. KG, Düren, Germany). Purified products were cloned into a linearized pRACE vector (Clontech Laboratories, Inc., Mountain View, CA, USA) and transformed into Stellar competent cells. Plasmid DNA extraction and sequencing were performed as the method described in the "Cloning of partial *Hdh-CAT* sequence" section. Finally, the sequences were combined by overlapping with the initial cloned fragment to obtain the full-length sequence of *Hdh-CAT*.

2.17. Sequence Analysis

A series of bioinformatics tools were used for the sequence analysis of Hdh-CAT. The protein sequence of Hdh-CAT was predicted using ORFfinder, a National Center for Biotechnology Information (NCBI) tool (https://www.ncbi.nlm.nih.gov/orffinder/, accessed on 8 November 2021). The protein homology of Hdh-CAT was performed using the Basic Local Alignment Search Tool (BLASTP) (https://blast.ncbi.nlm.nih.gov/Blast.cgi, accessed on 8 November 2021). Identification and annotation of CAT domain architecture were performed using the simple modular architecture research tool (SMART) (http://smart.embl-heidelberg.de/, accessed on 8 November 2021). The molecular weight and theoretical

isoelectric point (PI) of Hdh-CAT were determined using ProtParam (https://web.expasy.org/protparam/, accessed on 4 February 2022). Motif scan analysis was performed using a motif scan program (https://myhits.sib.swiss/cgi-bin/motif_scan, accessed on 4 February 2022). The conserved motifs in the Hdh-CAT amino acid sequence were analyzed using Multiple Em for Motif Elicitation (MEME) online tools (http://meme-suite.org/tools/meme, accessed on 4 February 2022). Multiple protein sequences were aligned using Clustal Omega (https://www.ebi.ac.uk/Tools/msa/clustalo/, accessed on 5 February 2022). The multiple sequence alignments were edited and visualized using Jalview Java alignment editor version 2.11.1.7. Gene ontology of Hdh-CAT was predicted using Contact-guided Iterative Threading ASSEmbly Refinement (C-I-TASSER) protein structure prediction server (https://zhanggroup.org/C-I-TASSER/, accessed on 2 February 2022).

2.18. Phylogenetic Analysis

Catalase protein sequences of different organisms were retrieved from the NCBI database and selected to construct the phylogenetic tree. Protein sequences were aligned using the Clustal Omega program. Phylogenetic and molecular evolutionary analyses were performed using MEGA 11 (https://www.megasoftware.net/, accessed on 5 February 2022) with the neighbor-joining algorithm following 1000 bootstrap replicates.

2.19. The Three-Dimensional Protein Structure of Hdh-CAT

The three-dimensional (3D) protein structure of Hdh-CAT was generated using an online protein structure and function prediction program, Iterative Threading ASSEmbly Refinement (I-TASSER; https://zhanggroup.org/I-TASSER/, accessed on 4 February 2022). Chimera software (https://www.cgl.ucsf.edu/chimera/, accessed on 6 February 2022) was used to analyze and visualize the predicted 3D structure of Hdh-CAT. Heme binding and NADPH binding sites were detected using an online program, SWISS-MODEL (https://swissmodel.expasy.org/, accessed on 7 February 2022).

2.20. Quantitative Real-Time PCR (qRT-PCR) Analysis

qRT-PCR analysis was performed to quantify *Hdh-CAT* mRNA expression in different types of tissue samples. qRT-PCR was conducted on a LightCycler® 96 system (Roche, Grenzach-Wyhlen, Germany) using a 2× qPCRBIO SyGreen Mix Lo-Rox kit (PCR Biosystems, Ltd., London, UK) as described previously [49]. Gene-specific sense and antisense primers (Table S1) were designed to quantify *Hdh-CAT* mRNA in different tissues. PCR was performed using a 20 µL volume of reaction mix containing 1 µL of cDNA, 1 µL of each sense and antisense primer, 10 µL of SyGreen Mix, and 7 µL of dH_2O. The following melting temperature was used as default settings: 95 °C for 10 s, 65 °C for 1 min, and 97 °C for 1 min. The relative *Hdh-CAT* mRNA expression was quantified using the $2^{-\Delta\Delta ct}$ method [50]. Expression levels were normalized by amplifying a housekeeping Pacific abalone *β-actin* gene.

2.21. Catalase Activity

Catalase activity in hemolymph samples was determined using a catalase colorimetric activity kit (Invitrogen, Frederick, MD, USA) according to the manufacturer's instructions. Catalase concentration (U/mL) at 560 nm was measured (n = 3) using an Epoch™ Microplate Spectrophotometer (Epoch 2, BioTek, Winooski, VT, USA).

2.22. Fluorescent Technique to Detect ROS in DG Tissue Samples of Pacific Abalone

Thermal stress (15 °C and 30 °C), H_2O_2 induced, starved, Cd-exposed (12 mgL^{-1}) and *V. parahaemolyticus*-challenged digestive glands were used to conduct this experiment. Tissue samples were selected based on higher *Hdh-CAT* mRNA abundance levels (Heat stressed abalone: 48 h; starved abalone: st-21 d; H_2O_2-induced abalone: 12 h; vibrio challenged abalone: 12 h; and Cadmium-exposed abalone: 6 h), and the samples of the experimental peak time point (Heat stressed abalone: 72 h; re-fed abalone: ref-7 d; H_2O_2-induced abalone: 48 h; vibrio-

challenged abalone: 48 h; and Cadmium-exposed abalone: 48 h). Reactive oxygen species (ROS: $O_2^{\bullet -}$ production) were detected using a DHE (dihydroethidium) assay kit (Invitrogen Molecular Probes, Eugene, OR, USA) according to the method described previously [51], with minor modifications. Briefly, digestive gland tissue samples were homogenized and washed using 0.1M PBS. Tissue samples were stained with 10 μM DHE and incubated for 30 min at 10 °C in the dark. DHE-stained cells were visualized under a fluorescence microscope (red filter: 510–560 nm, Eclipse E600, Nikon, Tokyo, Japan) with a 20× objective lens. Gray values of 200 cells in each treatment were measured using ImageJ software version 1.8.0_172 (https://imagej.nih.gov/ij/download.html, accessed on 13 April 2022).

2.23. Statistical Analysis

Changes of *Hdh-CAT* mRNA expression levels were analyzed by GraphPad Prism 9.3.1 software (GraphPad Software, San Diego, CA, USA) following nonparametric one-way analysis of variance (ANOVA). Tukey's post hoc test was performed to calculate statistically significant differences among different experimental tissues of Pacific abalone. Data from qRT-PCR are expressed as the mean ± SD. Differences were considered as significant at $p < 0.05$. GraphPad Prism 9.3.1 software was used to generate graphs.

3. Results

3.1. Cloning and Bioinformatic Analysis of H. discus hannai Catalase (Hdh-CAT) Sequence

The complete sequence of *H. discus hannai* catalase was cloned from digestive gland samples by 5′-RACE and 3′-RACE PCR and named Hdh-CAT (Figure 1A). The full-length sequence of *Hdh-CAT* (GenBank: OK042347.1) was 2894 bp in length, including a 148 bp 5′-untranslated region (UTR) and a 1240-bp 3′-UTR with a canonical polyadenylation signal sequence (AATAAA) located 12 bp upstream of the poly-A tail. The open reading frame (ORF) of Hdh-CAT had a length of 1506 bp, encoding 501 deduced amino acids (GenBank: UFT26656.1).

The molecular weight and theoretical isoelectric point (pI) of Hdh-CAT protein were predicted to be 56.46 KDa and 8.81, respectively. Glycine was the most abundant amino acid (7.8%), while tryptophan was the least abundant (1.2%) in the deduced protein sequence. Motif scan and conserved domain analysis revealed that Hdh-CAT has a catalase domain at position 25–410 amino acid residues with an E-value of 5.01E-280. The Hdh-CAT deduced amino acid sequence covered a highly conserved catalytic site motif, [F/I]-X-[R]-XXXX-[ER]-XX-[H]-XX-[G/A/S]-[G/A/S/T/F/Y]-[G/A/S/T], at the positions 61–77 (FNRERIPERVVHAKGAG). The proximal heme-ligand signature motif (RLYSYSDT) was detected at amino acid positions 351–358. Heme-binding site residues were identified at eight positions (R_{69}, H_{72}, R_{109}, N_{145}, F_{150}, R_{351}, Y_{355}, and R_{362}).

Additionally, the catalytic residue of histidine (H) at position 72 was identified as a proper binding, and peroxide reduction site. Three amidation sites were found at amino acid positions of 32–35 (VGRK), 100–103 (VGKK), and 486–489 (FGRR). Two N-glycosylation sites were found at amino acid positions of 241–244 (NLTG) and 436–439 (NFSQ). Four N-myristoylation sites were found at amino acid positions of 29–34 (GAPVGR), 114–119 (GGEKGS), 201–206 (GTPDGY), and 396–401 (GGAPNY).

Phosphorylation site analysis showed six protein kinase C phosphorylation sites, [T/S]-X-[K/R], at amino acid positions of 122–124 (TAR), 164–166 (TQK), 184–186 (TLR), 198–200 (SNR), 216–218 (TFK), and 358–360 (THR). Casein kinase II phosphorylation site was detected at the positions of 122–125 (TARD), 338–341 (TGIE), 354–357 (SYSD), and 430–433 (STED). A tyrosine kinase phosphorylation site, [K/R]-XXX- [E/D]-XXX-[Y], was detected at amino acid positions 421–429 (KLSGDVARY). Catalase-related immune-responsive sites were found at amino acid positions 418–495 with an E-value of 1.5E-33.

Gene ontology (GO) term analysis predicts that Hdh-CAT had catalase activity with a heme-binding ability (Figure S1A) in molecular function (GO: 0003674), hydrogen peroxidase catabolic process (Figure S1B) in biological process (GO:0008150), and located in peroxisome (Figure S1C) of cellular component (GO:0005575).

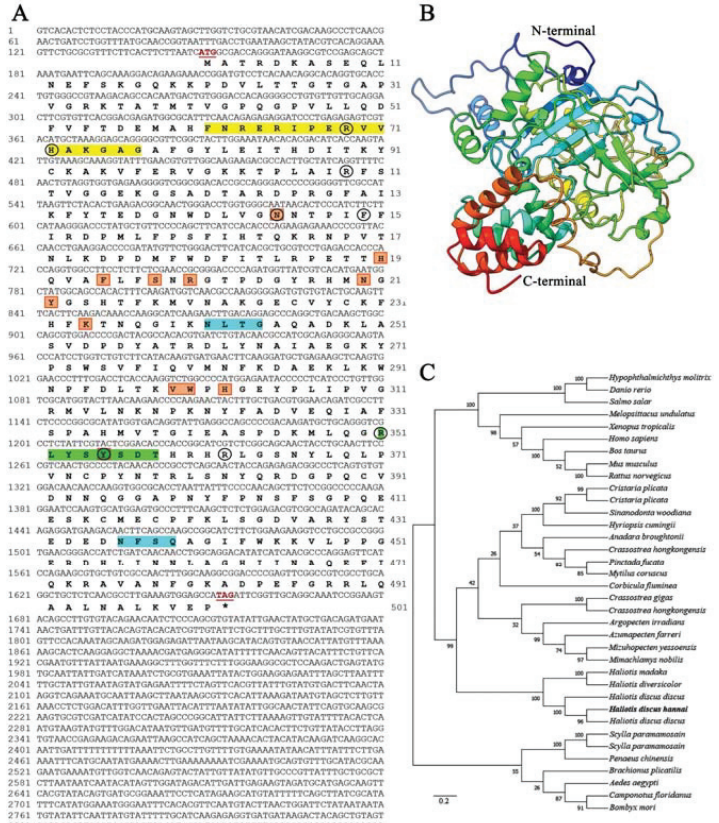

Figure 1. Sequence analysis of catalase (*Hdh-CAT*) in Pacific abalone, *H. discus hannai*. (**A**) The full-length nucleotide (GenBank: OK042347.1) and deduced amino acid sequences (GenBank: UFT26656.1). Numbers on the left and right columns indicate nucleotide and amino acid positions in the sequence, respectively. The initiation (ATG) and termination (TAG) codons of nucleotide sequence are marked as bold red color and underlined. The stop codon of nucleotide sequence was indicated using *. *Hdh-CAT* active site motif and heme-ligand signature motif are highlighted using yellow and light green colors, respectively. Heme-binding site residues are pointed using circle. Two putative *N*-glycosylation sites are indicated using light sky color. The putative NADPH binding residues are pointed using box. The polyadenylation signal (AATAAA) is indicated in boldface. (**B**) Three-dimensional (3D) homology modeling of Hdh-CAT. (**C**) Phylogenetic tree of catalase protein sequences from vertebrates and invertebrates. GenBank accession number of all sequences of phylogenetic tree are as follows: *Hypophthalmichthys molitrix* (ADJ67807.1), *Danio rerio* (NP_570987.2), *Salmo salar* (ACN11170.1), *Melopsittacus undulatus* (AAO72713.1), *Xenopus tropicalis* (AAH90377.1), *Homo sapiens* (NP_001743.1), *Bos taurus* (3NWL_A), *Mus musculus* (P24270.4), *Rattus norvegicus* (NP_036652.1), *Cristaria plicata* (ADM64337.1), *C. plicata* (AEL31245.1), *Sinanodonta woodiana* (AMO00631.1), *Hyriopsis cumingii* (ADL14588.1), *Anadara broughtonii* (ALZ42087.1), *Crassostrea hongkongensis* (ADZ76134.1), *Pinctada fucata* (ADW08700.1), *Mytilus coruscus* (AQY56552.1), *Corbicula fluminea* (APX42721.1), *C. gigas* (ABS18267.1), *C. hongkongensis* (ADZ93495.1), *Argopecten irradians* (ADD71945.1), *Azumapecten farreri* (ABI64115.1), *Mizuhopecten yessoensis* (AKV63251.1), *Mimachlamys nobilis* (AHX22599.1), *H. madaka* (ALU63753.1), *H. diversicolor* (AEP83810.1), *H. discus discus* (ABF67505.1), *H. discus hannai* (UFT26656.1), *H. discus discus* (ABQ60044.1, ABF67505.1), *Scylla paramamosain* (QNT61282.1), *S. paramamosain* (ACX46120.1), *Penaeus chinensis* (ABW82155.1), *Brachionus plicatilis* (BAH28837.1), *Aedes aegypti* (EAT34333.1), *Camponotus floridanus* (EFN66292.1), *Bombyx mori* (NP_001036912.1).

Multiple alignments of catalase homologs from selected amino acid sequences of vertebrate and invertebrate are shown in Figure S2. Active site motif and heme-ligand signature motif were well conserved in aligned amino acid sequences of *H. discus discus*, *H. diversicolor*, *Danio rerio,* and *Homo sapiens*. Multiple alignment revealed 12 NADPH binding site residues (N_{145}, H_{191}, F_{195}, S_{198}, R_{200}, N_{210}, Y_{212}, K_{234}, V_{299}, W_{300}, H_{302}, and Y_{355}). Hdh-CAT shared the highest sequence identities (99.38%) with CAT of *H. discus discus*.

3.2. Homology Modeling of Hdh-CAT

Three-dimensional structures of *Hdh-CAT* exhibited four basic domains including an N-terminal domain, an eight-stranded β-barrel domain, a wrapping loop-formed connection domain, and a helical C-terminal domain (Figure 1B).

3.3. Phylogenetic Analysis

A phylogenetic tree was constructed using the neighbor-joining method to show the possible evolutionary linkage of *Hdh-CAT* with other catalase proteins. The phylogenetic tree showed three major groups where *Hdh-CAT* was positioned in the mollusk group (Figure 1C). *Hdh-CAT* was closely positioned with *H. discus discus* catalase.

3.4. Tissue Distribution Analysis of Hdh-CAT

Hdh-CAT mRNA expression levels in different tissue samples are shown in Figure S3. The expression levels of *Hdh-CAT* mRNA were significantly higher in the digestive gland (DG) tissue samples than in other examined tissue samples.

3.5. Fluorescence In Situ Hybridization

Fluorescence *in situ* hybridization (FISH) revealed that *Hdh-CAT* was localized in the digestive tubules of the digestive gland of Pacific abalone. The antisense probe of FISH showed positive signals (green fluorescent) in the digestive tubules of the digestive gland (Figure 2). Blue fluorescent (DAPI-stained) counter-stained the positive signal of *Hdh-CAT*. Confocal laser scanning image confirmed that the *Hdh-CAT* localized in the Pacific abalone digestive gland (Figure 2).

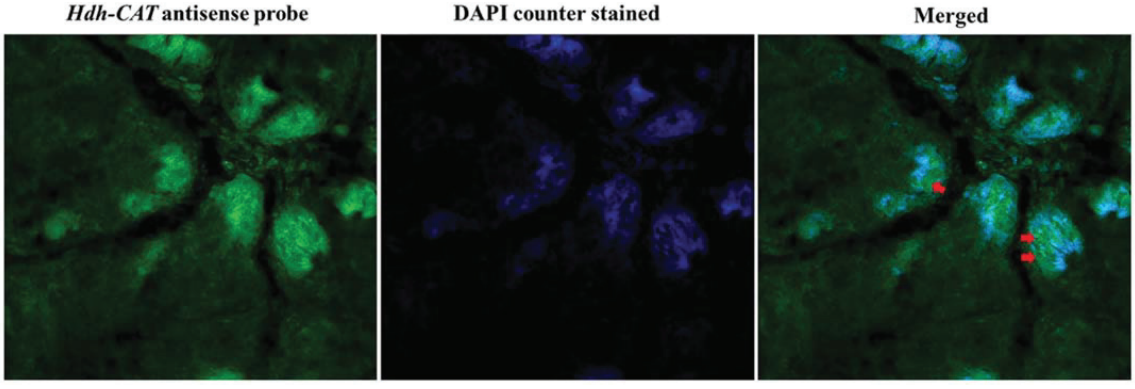

Figure 2. Confocal laser scanning microscopic observation after fluorescence in situ hybridization of *Hdh-CAT* mRNA in digestive gland tissue of Pacific abalone. The positive signals of *Hdh-CAT* mRNA were indicated using arrows. Scale bar: 50 μm.

3.6. Hdh-CAT mRNA Expression in Thermal Stressed Tissue Samples of Pacific Abalone

Expression levels of *Hdh-CAT* mRNA in gill and digestive gland (DG) tissues of thermal-stressed Pacific abalone are shown in Figure 3.

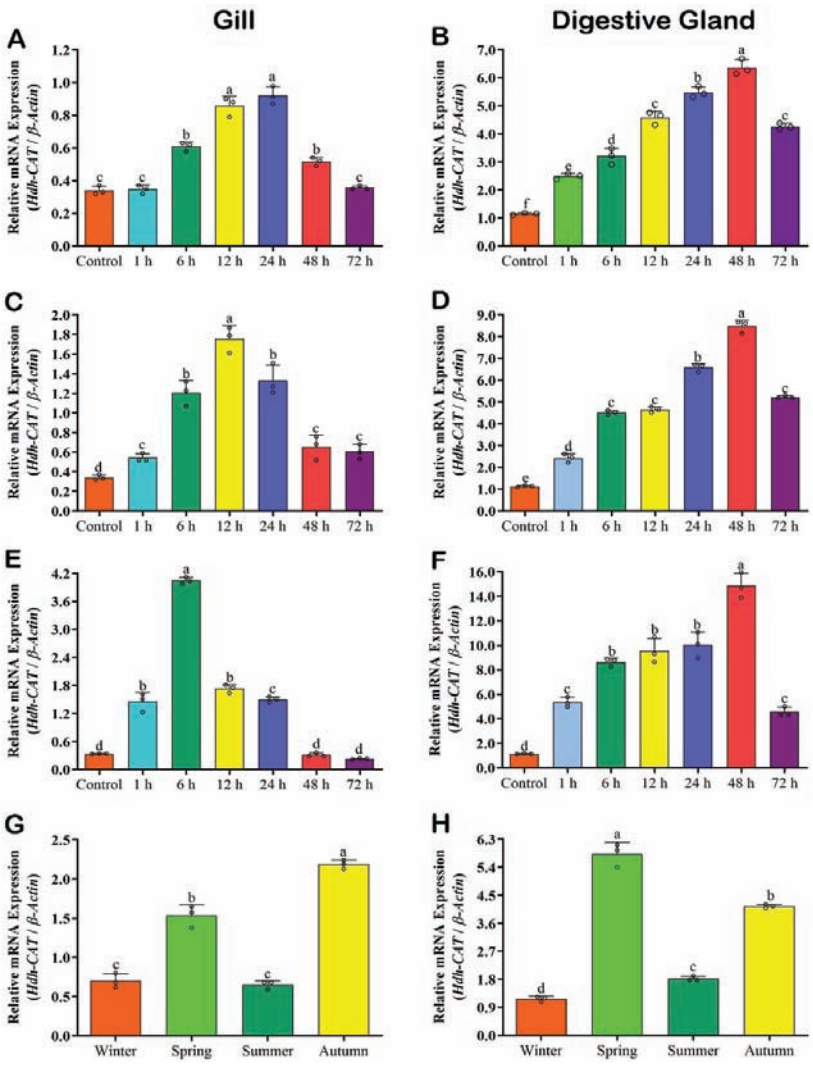

Figure 3. *Hdh-CAT* mRNA expression levels in thermal stressed and during elevated seasonal temperatures of Pacific abalone at different time points. (**A**) Cold-stressed (15 °C) gill samples. (**B**) Cold-stressed digestive gland (DG) samples. (**C**) Heat-stressed (25 °C) gill samples. (**D**) Heat-stressed (25 °C) DG samples. (**E**) Heat-stressed (30 °C) gill samples. (**F**) Heat-stressed (30 °C) DG samples. (**G**) *Hdh-CAT* mRNA expression level in gill during elevated seasonal temperatures. (**H**) *Hdh-CAT* mRNA expression level in DG during elevated seasonal temperatures. Different letters above the bars indicate significant differences ($p < 0.05$).

3.6.1. *Hdh-CAT* mRNA Expression in Cold Stressed (15 °C) Samples

The mRNA expression level of *Hdh-CAT* reached its peak at time points of 24 h in the gill (Figure 3A), and 48 h in the DG (Figure 3B) of Pacific abalone.

3.6.2. *Hdh-CAT* mRNA Expression in Heat Stressed (25 °C) Samples

Hdh-CAT mRNA expression level was significantly highest at time points of 12 h in the gill (Figure 3C), and 48 h in the DG (Figure 3D). However, in gill samples, the expression level was neutralized at time points of 48 h to 72 h.

3.6.3. *Hdh-CAT* mRNA Expression in Heat Stressed (30 °C) Samples

The mRNA expression level of *Hdh-CAT* in gill samples of heat-stressed Pacific abalone was significantly ($p < 0.05$) higher at time points of 6 h (Figure 3E). DG samples showed a significantly ($p < 0.05$) higher expression level of *Hdh-CAT* mRNA at time points of 48 h (Figure 3F).

3.7. Hdh-CAT mRNA Expression in Seasonal Samples

Hdh-CAT mRNA expression levels in gill were significantly ($p < 0.05$) higher in autumn (Figure 3G) compared to other seasons. Whereas DG samples showed significantly ($p < 0.05$) higher *Hdh-CAT* mRNA expression levels in spring (Figure 3H).

3.8. Hdh-CAT mRNA Expression in H_2O_2 Induced Tissue Samples of Pacific Abalone

The mRNA expression level of *Hdh-CAT* reached its peak at time points of 24 h in the gill (Figure 4A), and 12 h in the DG (Figure 4B) of H_2O_2-induced Pacific abalone.

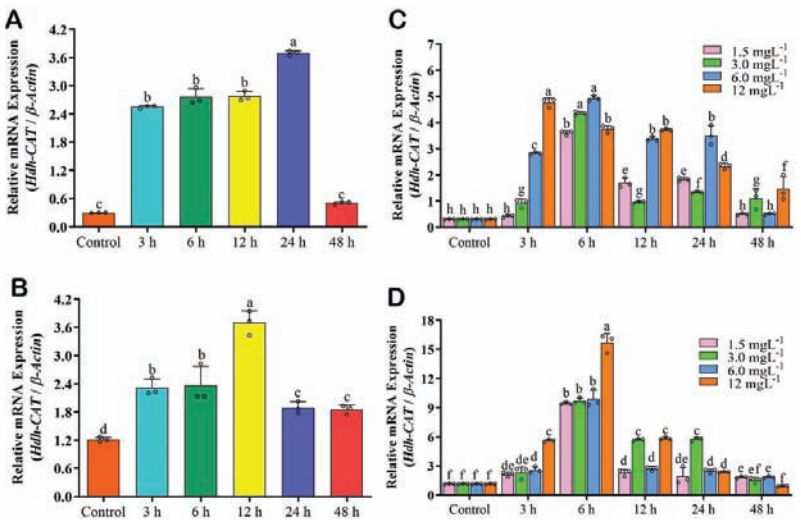

Figure 4. *Hdh-CAT* mRNA expression levels in H_2O_2 induced and cadmium (Cd) exposed (1.5 mgL^{-1}, 3.0 mgL^{-1}, 6.0 mgL^{-1}, and 12.0 mgL^{-1}) Pacific abalone at different time points. (**A**) *Hdh-CAT* mRNA expression level in gill of H_2O_2 induced Pacific abalone. (**B**) *Hdh-CAT* mRNA expression level in digestive gland (DG) of H_2O_2-induced Pacific abalone. (**C**) *Hdh-CAT* mRNA expression level in gill of Cd-exposed Pacific abalone. (**D**) *Hdh-CAT* mRNA expression level in DG of Cd-exposed Pacific abalone. Different letters above the bars indicate significant differences ($p < 0.05$).

3.9. Hdh-CAT mRNA Expression in $CdCl_2$ Exposed Tissues of Pacific Abalone

The expression levels of *Hdh-CAT* mRNA in different concentrations of $CdCl_2$ exposed tissue samples are presented in Figure 4C,D. *Hdh-CAT* mRNA expression levels were significantly ($p < 0.05$) different in different concentrations of $CdCl_2$ exposed gill and DG samples, compared to the control. In gill samples, higher *Hdh-CAT* mRNA expression levels were shown at the time points of 3 h in the 12 mgL^{-1} $CdCl_2$, 6 h in the 3 mgL^{-1}, and 6 mgL^{-1} $CdCl_2$, respectively (Figure 4C). DG tissue samples showed significantly higher *Hdh-CAT* mRNA at the time points of 6 h in the 12 mgL^{-1} $CdCl_2$-exposed abalone (Figure 4D).

3.10. Hdh-CAT mRNA Expression in Starved Tissue Samples of Pacific Abalone

Hdh-CAT mRNA expression levels were significantly ($p < 0.05$) higher in Pacific abalone gill at 14 days after starvation (st-14 d) (Figure 5A). DG samples showed significantly ($p < 0.05$) higher *Hdh-CAT* mRNA expression levels at 21 days after starvation (st-21 d)

(Figure 5A) of Pacific abalone. After re-feeding for seven days, *Hdh-CAT* mRNA expression levels in DG of starved samples were similar to those in control samples without starvation (Figure 5B).

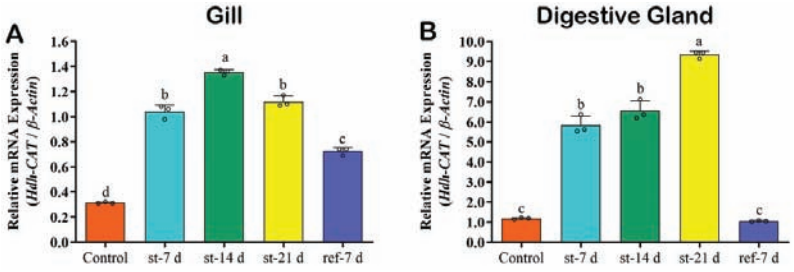

Figure 5. *Hdh-CAT* mRNA expression levels in starved and re-fed Pacific abalone at different time points. (**A**) *Hdh-CAT* mRNA expression level in gill of starved Pacific abalone. (**B**) *Hdh-CAT* mRNA expression level in DG of starved Pacific abalone. Different letters above the bars indicate significant differences ($p < 0.05$).

3.11. Hdh-CAT mRNA Expression in Immune Challenged Tissues of Pacific Abalone

3.11.1. *Hdh-CAT* Expression in *Vibrio parahaemolyticus* Challenged Samples

The mRNA expression level of *Hdh-CAT* reached its peak in the gill at 6 h after *V. parahaemolyticus* challenge (Figure 6A) and in the DG at 12 h after *V. parahaemolyticus* challenge (Figure 6B). Expression levels were stabilized in both tissue samples at 24 h and 48 h after *V. parahaemolyticus* challenge (Figure 6A,B).

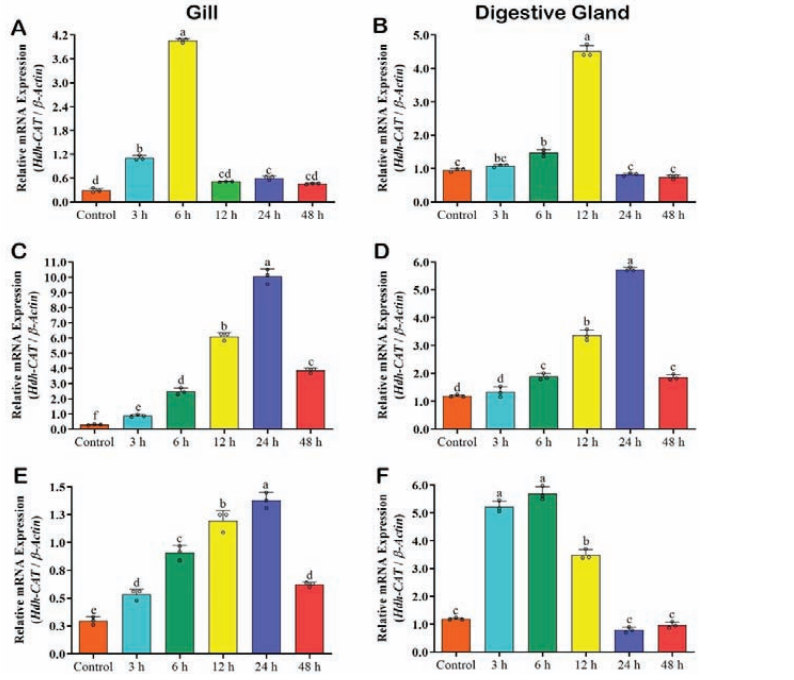

Figure 6. *Hdh-CAT* mRNA expression levels in immune-challenged Pacific abalone at different time points. (**A**) *V. parahaemolyticus*-challenged gill samples. (**B**) *V. parahaemolyticus*-challenged DG samples. (**C**) Lipopolysaccharides (LPS)-challenged gill (GIL) samples. (**D**) LPS-challenged digestive gland (DG) samples. (**E**) Polyinosinic–polycytidylic acid sodium salt (PIC)-challenged gill samples. (**F**) PIC-challenged DG samples. Different letters above the bars indicate significant differences ($p < 0.05$).

3.11.2. *Hdh-CAT* Expression in Lipopolysaccharides (LPS) Challenged Samples

The mRNA expression level of *Hdh-CAT* reached its peak at time points of 24 h in the gill (Figure 6C), and DG (Figure 6D) of LPS-challenged Pacific abalone.

3.11.3. *Hdh-CAT* Expression in Poly I:C Challenged Samples

The mRNA expression level of *Hdh-CAT* reached its peak at time points of 24 h in the gill (Figure 6E), and 6 h in the DG (Figure 6F) of PIC-challenged Pacific abalone.

3.12. Hdh-CAT mRNA Expression in Testicular Developmental Stages

Hdh-CAT mRNA expression levels during different testicular developmental stages are given in Figure 7A. Ripening stage showed significantly ($p < 0.05$) higher *Hdh-CAT* mRNA expression levels compared to other stages (Figure 7A).

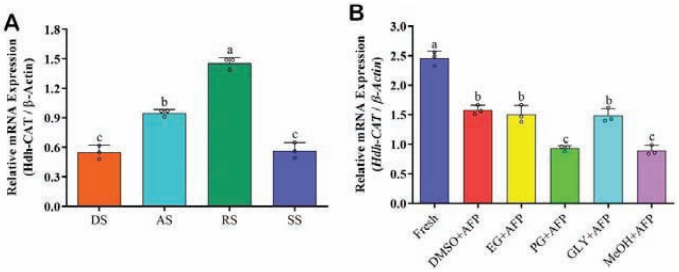

Figure 7. *Hdh-CAT* mRNA expression levels at different testicular developmental stages and in cryopreserved sperm samples of Pacific abalone. (**A**) *Hdh-CAT* mRNA expression level in different testicular developmental stages. (**B**) *Hdh-CAT* mRNA expression levels at cryopreserved sperm samples. DS, degenerative stage; AS, active stage; RS, ripening stage; SS, spent stage; DMSO + AFP, 8% dimethyl sulfoxide + antifreeze protein; EG + AFP, 8% ethylene glycol + antifreeze protein; PG + AFP, 6% propylene glycol + antifreeze protein; GLY + AFP, 2% glycerol + antifreeze protein; and MeOH + AFP, 2% methanol + antifreeze protein. Different letters above the bars indicate significant differences ($p < 0.05$).

3.13. Hdh-CAT mRNA Expression in Cryopreserved Sperm

Hdh-CAT mRNA expression levels in fresh sperm and different types of cryopreserved sperm samples are shown in Figure 7B. *Hdh-CAT* mRNA expression levels in cryopreserved sperm samples were significantly lower than those in fresh sperm (Figure 7B).

3.14. Hdh-CAT mRNA Expression in Embryonic and Larval Developmental Stages

Hdh-CAT mRNA expression levels during embryogenesis are shown in Figure 8. Blastula (BL) and trochophore (TRO) larvae showed significantly ($p < 0.05$) higher *Hdh-CAT* mRNA expression levels compared to other stages.

3.15. Catalase (CAT) Activity in the Hemolymph

CAT activities in hemolymph samples of cold (15 °C), heat-stressed (25 °C and 30 °C), H_2O_2-induced, starved, immune-challenged, and Cd-exposed abalone are summarized in Figure 9. Cold-stressed abalone showed significantly ($p < 0.05$) higher CAT activity at 6 h after cold stress (Figure 9A), whereas abalone with heat stress (25 °C and 30 °C) showed higher CAT activities at 48 h after heat stress (Figure 9B,C). H_2O_2-induced abalone showed higher CAT activity at the time point 3 h (Figure 9D), significantly similar to the time point of 6 h post-induction. Starved abalone showed significantly higher CAT activities at st-14 d (Figure 9E). However, re-fed (ref-7 d) abalone showed similar ($p > 0.05$) CAT activity to the control. LPS-challenged abalone showed significantly ($p < 0.05$) higher CAT activity at 12 h after LPS challenge (Figure 9F). PIC (Figure 9G) and *V. parahaemolyticus* (Figure 9H)-challenged abalone showed significantly higher CAT activity at 6 h after challenge. Cd exposure increased CAT activity in a dose-dependent manner (Figure 9I). After exposure to 6 mgL^{-1} of Cd, CAT activity was significantly higher at 6 h after exposure (Figure 9I).

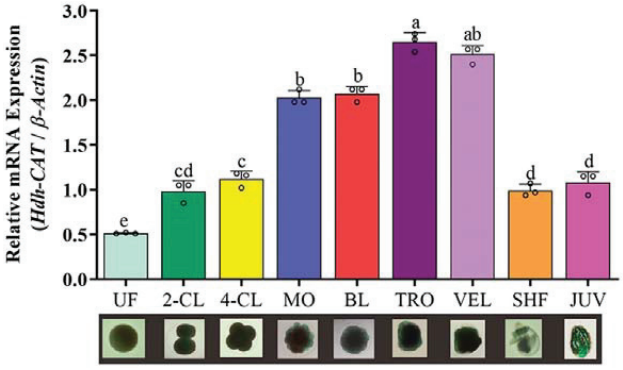

Figure 8. *Hdh-CAT* mRNA expression levels during metamorphosis of Pacific abalone. UF; unfertilized egg, 2-CL; 2-cell, 4-CL; 4-cell, MO; morula, BL; blastula, TRO; trochophore larvae, VEL; veliger larvae, SHF; shell formed larvae, JUV; juvenile. Different letters above the bars indicate significant differences ($p < 0.05$).

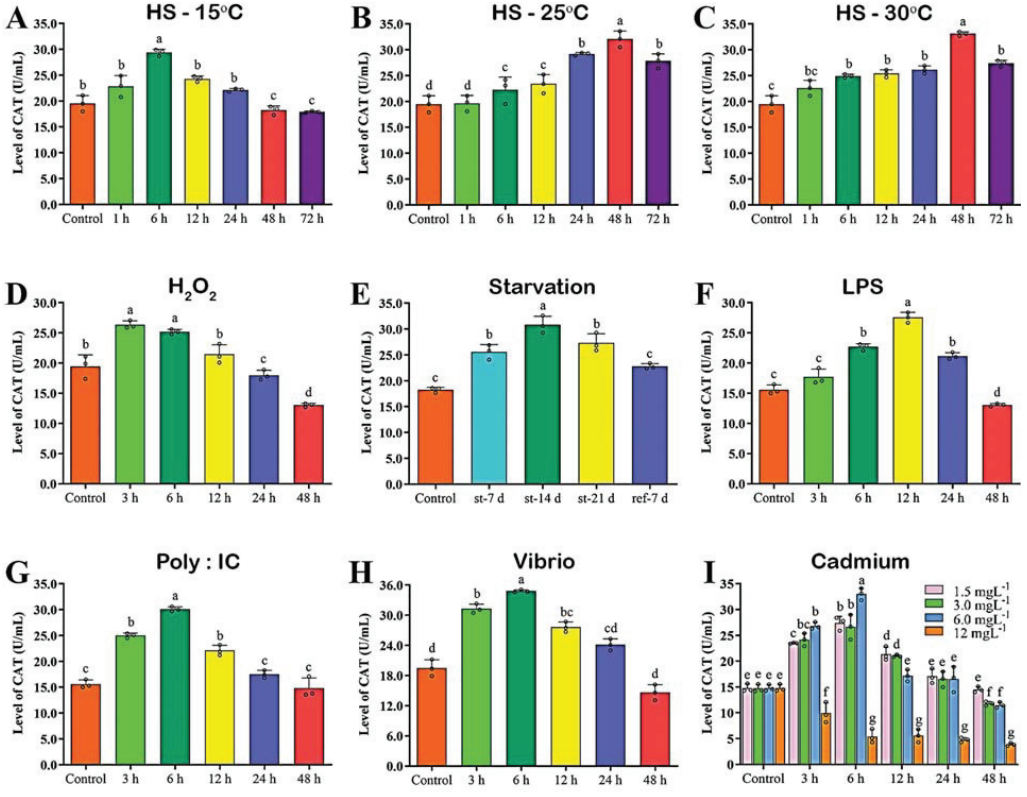

Figure 9. Catalase (CAT) activity in the different types of stress and immune-challenged plasma of Pacific abalone. (**A**) CAT activity in cold-stressed (15 °C) abalone, (**B**) CAT activity in heat-stressed (25 °C) abalone, (**C**) CAT activity in heat-stressed (30 °C) abalone, (**D**) CAT activity in H_2O_2-induced abalone, (**E**) CAT activity in starved abalone, (**F**) CAT activity in LPS-challenged abalone, (**G**) CAT activity in poly: (IC)-challenged abalone, (**H**) CAT activity in *V. parahaemolyticus*-challenged abalone, (**I**) CAT activity in cadmium-exposed abalone. Significantly different levels ($p < 0.05$) are denoted by different letters.

3.16. ROS in DG Tissue Samples of Pacific Abalone

The results of ROS production in response to thermal stress (15 °C and 30 °C), starvation, H_2O_2 induction, *Vibrio* challenged, and Cd-exposed toxicity are presented in Figure 10. Heat-induced (30 °C) abalone showed higher ROS production at 72 h (Figure 10A,B). H_2O_2-induced, Vibrio-challenged, and Cd-exposed abalone showed higher ROS production at 48 h (Figure 10A,B). However, re-feed abalone showed reduced ROS production (Figure 10A,B).

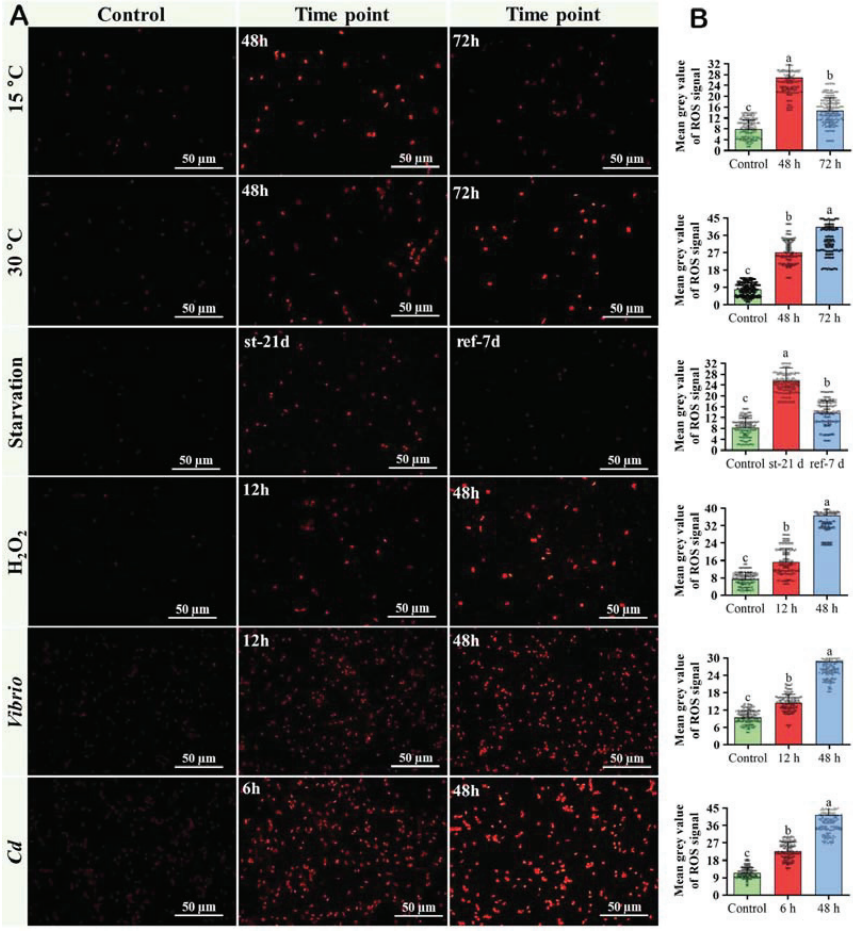

Figure 10. Detection of reactive oxygen species (ROS) in thermal-stressed, starved, H_2O_2-induced, bacterial-challenged, and Cd-exposed Pacific abalone. (**A**) Fluorescent images of dihydroethidium (DHE) stained digestive gland tissue samples. (**B**) Level of ROS production was analyzed by measuring mean grey values of DHE signal. Significantly different levels ($p < 0.05$) are denoted by different letters.

4. Discussion

The aim of the present study was to isolate catalase and detect its molecular regulation in stress physiology, innate immunity, testicular development, elevated seasonal temperature, metamorphosis, and cryopreserved sperm of Pacific abalone. The full-length cDNA of Pacific abalone catalase (*Hdh-CAT*) was isolated for the first time, and its expression in digestive gland tissue was characterized. The architecture of *Hdh-CAT* showed key features of a catalase gene, including a proximal heme-ligand signature motif, a proximal active site signature, and heme-binding site residues. These features are common in most catalases [3].

Fluorescence *in situ* hybridization confirmed the localization of *Hdh-CAT* mRNA in the digestive tubules of the digestive gland (DG). Previous studies have reported that CAT is immunolocalized in the digestive tubules of different mollusks including oyster, and mussel [52]. CAT is also immunolocalized in the digestive tubules of crab, and the liver of mullet [52]. Molluscan DG has combined functions of the liver, pancreas, and intestine of vertebrates [53]. The liver is the predominant source of peroxisomes where CAT is exclusively located [54,55]. Tissue distribution analysis also revealed that *Hdh-CAT* mRNA was highly expressed in DG tissue samples, consistent with findings of CAT in disk abalone [3].

Temperature is a vital abiotic factor that can significantly affect the physiology of marine organisms [21]. In recent decades, seawater temperature has been rising with the acceleration of climate change [21,56]. Temperature changes are known to influence ROS production and activate antioxidant enzymes in mollusk [57]. Marine invertebrates have strong antioxidant defense systems including CAT to normalize ROS accumulation and physiological function [58]. An elevated activity of CAT is essential to counteract thermal stress-induced oxidative damage [59]. In the present study, induced CAT activity and higher *Hdh-CAT* mRNA expression levels were observed in response to thermal stress. Similar findings have been previously reported for CAT in scallop [4], ark shell [21], Mediterranean mussel [60], and Pacific oyster [61]. The present study also found elevated ROS levels in thermal-stressed abalone, consistent with previous findings of American oyster [31]. It has been reported that both heat and cold stress lead to excessive ROS production [13]. Present findings suggest that thermal stress can increase the CAT activity of Pacific abalone which may have a relationship with ROS production since it has been described that the overproduction of ROS is associated with the dysfunction of the antioxidant defense system. The antioxidant defense system consists of five vital antioxidant genes including catalase, Cu/Zn-superoxide dismutase, manganese superoxide dismutase, glutathione peroxidase, and glutathione reductase [62].

H_2O_2 is ubiquitously distributed in the surface seawater [63]. H_2O_2 can affects the survivability, growth, and metabolism of aquatic organisms [64]. In the present study, H_2O_2-injected Pacific abalone showed upregulated *Hdh-CAT* mRNA expression in gill and DG. Similar phenomena have been reported in *H. discus discus* [3]. Induced CAT activity was detected in the hemolymph of H_2O_2-injected Pacific abalone. A lower concentration of CAT could not eliminate H_2O_2 which might accumulate excessive H_2O_2. Accumulated H_2O_2 might accelerate the downregulation of CAT [15]. The fluorescence technique detected higher ROS in DG at 48 h after H_2O_2 induction, which might be the reason for the lower CAT mRNA abundance and activity. Similar phenomena have been previously reported for CAT in American oyster [31]. Present findings suggest that Hdh-CAT might play a role in the antioxidant defensive mechanism against ROS generation induced by H_2O_2. Another antioxidant, SOD, has been previously recommended as an antioxidant defender against H_2O_2-induced damage in Pacific abalone [4].

Cd exposure increased *Hdh-CAT* mRNA expression levels in the gill and DG of Pacific abalone in a dose-dependent manner. Similar findings have been previously reported for CAT in the gill of Pacific oyster after Cd exposure [65]. Higher CAT mRNA expression levels could protect Pacific oyster against Cd exposure-induced oxidative stress [65]. The present study detected higher ROS in Cd-exposed DG using a fluorescent technique, although induced ROS production in Cd-exposed tissue samples of abalone has been previously reported with a colorimetric method [66]. In this study, hemolymph of Cd-exposed abalone showed induced CAT activity. Similar findings have been previously reported for marine invertebrate after exposure to toxic chemicals [67]. Induced H_2O_2 activity in the hemolymph of Cd-exposed Pacific oyster has been reported previously [65] since CAT is a main scavenger of H_2O_2. Taken together, present findings hypothesize that CAT could protect Pacific abalone against ROS induced by exposure to Cd, a heavy metal pollutant.

The present study showed higher *Hdh-CAT* mRNA expression levels in gill at two weeks and in DG of abalone at three weeks of starved abalone compared to the control. After two weeks of starvation, the gill sample showed gradually decreased *Hdh-CAT*

mRNA expression levels in prolonged periods and re-feeding. However, DG showed gradually increased *Hdh-CAT* mRNA expression levels until three weeks of starvation. The re-fed sample showed an expression level of *Hdh-CAT* mRNA similar to the control. Similar phenomena have previously been reported from fish [68,69]. Starvation stimulates oxidative stress-oriented energy deficiencies [68]. When the starvation period is prolonged, cells produce ROS and gradually accumulate. In this circumstance, stored antioxidants cannot be supplied in vivo resulting in gradually decreased antioxidant capacity [23]. The present study also reported similar phenomena in the case of ROS production.

Gill and DG are important immune organs of Pacific abalone [44]. In this study, *V. parahaemolyticus* influenced the mRNA expression level of *Hdh-CAT* in gill and DG. Gill showed an earlier response (6 h) than DG (12 h) against *Vibrio* by showing higher *Hdh-CAT* mRNA abundance. A possible explanation for this time variation in different tissues might be the species- and tissue-specific nature of pathogen. *Vibrio*-infected abalone produced a significant amount of ROS; higher CAT mRNA might eliminate the excessive ROS generation. In mollusk, antioxidant response and ROS production show wide variations depending on tissue type, pathogen, and host [28]. *Vibrio* challenges also induced mRNA expression of catalase in the digestive gland and gill of *Mytilus galloprovincialis* and *H. discus discus* [28,70]. The present findings suggest that *Hdh-CAT* might play a role in the innate immune response of Pacific abalone against *V. parahaemolyticus*.

Lipopolysaccharide (LPS) is a well-recognized pathogen-associated immune stimulant [44]. In the present study, *Hdh-CAT* mRNA expression levels were quantified from gill and DG in response to LPS challenge at different time points. Upregulated *Hdh-CAT* mRNA expression was determined in both the gill and DG of LPS-challenged Pacific abalone. The expression of superoxide dismutase (SOD), an antioxidant gene, has been previously reported to be upregulated in the gill and DG of Pacific abalone [44]. CAT is activated immediately after the activation of SOD in the oxidative defense system. LPS challenge can also upregulate CAT expression level in the hepatopancreases or DG of *Scylla paramamosain* [71].

Poly I:C (PIC) is a synthetic viral mimic extensively used in viral infection experiments [72]. In the present study, PIC induced *Hdh-CAT* mRNA expression levels in the gill and DG tissues of Pacific abalone. PIC can also induce mRNA expression of CAT in the liver (DG) of *Bostrychus sinensis* [73]. Upregulated mRNA expression of CAT in viral challenged gill of *H. discus discus* has been previously reported [28]. Results of the present study suggest that PIC challenge might activate the immune response in DG more than in gill since DG is a key metabolic organ of mollusk [74].

Sperm have multiple antioxidants including CAT which can be altered during cryopreservation [75]. The present study found that cryopreserved sperm had significantly lower *Hdh-CAT* mRNA abundance than fresh sperm. Similar findings have been previously reported for cryopreserved rooster sperm [35]. Results of the present study suggest that *Hdh-CAT* might be considered as a biomarker of cryopreserved sperm of Pacific abalone.

The present study showed higher *Hdh-CAT* mRNA expression levels in trochophore (TRO) and veliger (VEL) larvae stages of embryogenesis. In abalone, trochophore larvae are considered as hatching steps and veliger larvae are considered as hatched larvae of embryogenesis [76]. Similar findings have been previously observed in Atlantic bluefin tuna [32] and Seabass [77]. The present findings suggest that *Hdh-CAT* might be involved in hatching succession in the embryogenesis process of Pacific abalone.

5. Conclusions

Hdh-CAT was for the first time cloned from the digestive gland of Pacific abalone, *H. discus hannai*. *Hdh-CAT* was localized in the digestive tubules of the digestive gland. Catalase activity and mRNA expression analysis indicated that *Hdh-CAT* might regulate the antioxidant defense system against thermal stress, viral infection, bacterial infection, starvation, and cadmium-induced toxicity. *Hdh-CAT* might have a potential role in testicular development and metamorphosis. Our findings also suggest that *Hdh-CAT* may have

a defensive role against excessive ROS production. Expression levels of *Hdh-CAT* in cryopreserved sperm suggest that *Hdh-CAT* might be used as an indicator of cryotolerance of Pacific abalone sperm. Taken together, the present findings suggest that Hdh-CAT might be used as a stress and toxicity indicator.

Supplementary Materials: The following supporting information can be downloaded at: https://www.mdpi.com/article/10.3390/antiox12010109/s1, Figure S1: Functional activity analysis of Hdh-CAT amino acid sequence of Pacific abalone, *H. discus hannai*. (**A**) Molecular function, (**B**) Biological process, (**C**) Cellular component; Figure S2: Multiple sequence alignment of deduced amino acid sequences of different catalase (CAT) from *H. discus hannai* (UFT26656.1), *H. discus discus* (ABQ60044.1), *H. madaka* (ALU63753.1), *H. diversicolor* (AEP83810.1), *Danio rerio* (NP_570987.2), and *Homo sapiens* (NP_001743.1). CAT active site motif and heme-ligand binding site motif are indicated by blacked lined box. Conserved NADPH binding site residues are pointed using a symbol on the top of each residue; Figure S3: Expression of *Hdh-CAT* mRNA in different tissue of Pacific abalone, *Haliotis discus hannai*. GIL; gill, DG; digestive gland, MNT; mantle, MUS; muscle, TE; testis, OV; ovary, HCY; hemocyte, HRT; heart, PPG; pleuropedal ganglion, CG; cerebral ganglion. Different letters above the bar indicate significance difference ($p < 0.05$); Table S1: List of primers used for cDNA cloning, tissue distribution, and expression analysis of *Hdh-CAT* in Pacific abalone.

Author Contributions: K.H.K. and S.H. conceptualized, designed the experiments, and wrote the manuscript; S.H., Z.P.S., S.C.K., M.A.H. and K.H.K. conducted the experiments; S.H. performed data curation, and visualization; S.H. and Z.P.S. performed software analysis; S.H., Z.P.S., S.C.K., and M.A.H. performed formal analysis; S.H. and K.H.K. performed investigation; I.-K.K. performed review and editing; K.H.K., S.H., I.-K.K. performed validation; K.H.K. performed supervision, project administration, and fund acquisition. All authors have read and agreed to the published version of the manuscript.

Funding: This research was a component of a project entitled "Development of technology for abalone aquaculture using sperm cryopreservation", funded by the Ministry of Oceans and Fisheries, Republic of Korea, Grant No. 20180375.

Institutional Review Board Statement: The present study was performed in accordance with guidelines of the Institutional Animal Care and Use Committee of Chonnam National University (CNU IACUC) under an approval number of CNU IACUC-YS-2022-8 and according to the 14th Article of Korean Animal Protection Law of the Korean government.

Informed Consent Statement: Not applicable.

Data Availability Statement: All data generated in this study are included in this published article and its supplementary information files.

Acknowledgments: The authors acknowledge the staff at the Chonnam Center for Research Facilities (CCRF) of Chonnam National University (CNU), Yeosu campus for their support in confocal microscopy.

Conflicts of Interest: The authors have no conflict of interest relevant to this study to disclose.

References

1. Vidal-Liñán, L.; Bellas, J.; Campillo, J.A.; Beiras, R. Integrated use of antioxidant enzymes in mussels, *Mytilus galloprovincialis*, for monitoring pollution in highly productive coastal areas of Galicia (NW Spain). *Chemosphere* **2010**, *78*, 265–272. [CrossRef] [PubMed]
2. Karadag, H.; Fırat, Ö.; Fırat, Ö. Use of oxidative stress biomarkers in *Cyprinus carpio* L. for the evaluation of water pollution in Ataturk Dam Lake (Adiyaman, Turkey). *Bull. Environ. Contam. Toxicol.* **2014**, *92*, 289–293. [CrossRef]
3. Ekanayake, P.M.; De Zoysa, M.; Kang, H.S.; Wan, Q.; Jee, Y.; Lee, Y.H.; Kim, S.J.; Lee, J. Cloning, characterization and tissue expression of disk abalone (*Haliotis discus discus*) catalase. *Fish Shellfish Immunol.* **2008**, *24*, 267–278. [CrossRef] [PubMed]
4. Zhang, H.; Tan, K.; Zheng, H. Characterization of a novel catalase gene and its response to low temperature stress in noble scallop *Chlamys nobilis* with different total carotenoids content. *Aquac. Res.* **2021**, *52*, 6179–6188. [CrossRef]
5. Vetrano, A.M.; Heck, D.E.; Mariano, T.M.; Mishin, V.; Laskin, D.L.; Laskin, J.D. Characterization of the oxidase activity in mammalian catalase. *J. Biol. Chem.* **2005**, *280*, 35372–35381. [CrossRef]
6. Sellaththurai, S.; Priyathilaka, T.T.; Lee, J. Molecular cloning, characterization, and expression level analysis of a marine teleost homolog of catalase from big belly seahorse (*Hippocampus abdominalis*). *Fish Shellfish Immunol.* **2019**, *89*, 647–659. [CrossRef]

7. Yuan, H.; Jin, C.; Pei, H.; Zhao, L.; Li, X.; Li, J.; Huang, W.; Fan, R.; Liu, W.; Shen, Q.H. The powdery mildew effector CSEP0027 interacts with barley catalase to regulate host immunity. *Front. Plant Sci.* **2021**, *12*, 733237. [CrossRef]
8. Li, C.; Ni, D.; Song, L.; Zhao, J.; Zhang, H.; Li, L. Molecular cloning and characterization of a catalase gene from Zhikong scallop *Chlamys farreri*. *Fish Shellfish Immunol.* **2008**, *24*, 26–34. [CrossRef]
9. Shaeer, A.; Aslam, M.; Rashid, N. Structural and functional analyses of a novel manganese-catalase from *Bacillus subtilis* R5. *Int. J. Biol. Macromol.* **2021**, *180*, 222–233. [CrossRef]
10. Galasso, M.; Gambino, S.; Romanelli, M.G.; Donadelli, M.; Scupoli, M.T. Browsing the oldest antioxidant enzyme: Catalase and its multiple regulation in cancer. *Free Radic. Biol. Med.* **2021**, *172*, 264–272. [CrossRef]
11. Chakravarty, D.; Bihani, S.C.; Banerjee, M.; Kalwani, P.; Ballal, A. Unique functional insights into the antioxidant response of the cyanobacterial Mn-catalase (KatB). *Free Radic. Biol. Med.* **2021**, *179*, 266–276. [CrossRef] [PubMed]
12. Yu, L.; Wan, F.; Dutta, S.; Welsh, S.; Liu, Z.; Freundt, E.; Baehrecke, E.H.; Lenardo, E. Autophagic programmed cell death by selective catalase degradation. *Proc. Natl. Acad. Sci. USA* **2006**, *103*, 4952–4957. [CrossRef]
13. Slimen, I.B.; Najar, T.; Ghram, A.; Dabbebi, H.; Ben Mrad, M.; Abdrabbah, M. Reactive oxygen species, heat stress and oxidative-induced mitochondrial damage. A review. *Int. J. Hyperth.* **2014**, *30*, 513–523. [CrossRef] [PubMed]
14. Rubio-Riquelme, N.; Huerta-Retamal, N.; Gómez-Torres, M.J.; Martínez-Espinosa, R.M. Catalase as a molecular target for male infertility diagnosis and monitoring: An overview. *Antioxidants* **2020**, *9*, 78. [CrossRef] [PubMed]
15. Wang, C.; Yue, X.; Lu, X.; Liu, B. The role of catalase in the immune response to oxidative stress and pathogen challenge in the clam *Meretrix meretrix*. *Fish Shellfish Immunol.* **2013**, *34*, 91–99. [CrossRef] [PubMed]
16. Zhao, Q.L.; Fujiwara, Y.; Kondo, T. Mechanism of cell death induction by nitroxide and hyperthermia. *Free Radic. Biol. Med.* **2006**, *40*, 1131–1143. [CrossRef] [PubMed]
17. Kikusato, M.; Toyomizu, M. Crucial role of membrane potential in heat stress-induced overproduction of reactive oxygen species in avian skeletal muscle mitochondria. *PLoS ONE* **2013**, *8*, e64412. [CrossRef]
18. Yu, H.; Deng, W.; Zhang, D.; Gao, Y.; Yang, Z.; Shi, X.; Sun, J.; Zhou, J.; Ji, H. Antioxidant defenses of *Onychostoma macrolepis* in response to thermal stress: Insight from mRNA expression and activity of superoxide dismutase and catalase. *Fish Shellfish Immunol.* **2017**, *66*, 50–61. [CrossRef]
19. Bai, H.; Ukita, H.; Kawahara, M.; Mitani, T.; Furukawa, E.; Yanagawa, Y.; Yabuuchi, N.; Kim, H.; Takahashi, M. Effect of summer heat stress on gene expression in bovine uterine endometrial tissues. *Anim. Sci. J.* **2020**, *91*, e13474. [CrossRef]
20. Miao, Z.Q.; Tu, Y.Q.; Guo, P.Y.; He, W.; Jing, T.X.; Wang, J.J.; Wei, D.D. Antioxidant enzymes and heat shock protein genes from *Liposcelis bostrychophila* are involved in stress defense upon heat shock. *Insects* **2020**, *11*, 839. [CrossRef]
21. Zou, D.; Ning, J.; Lu, X.; Wang, X.; Chen, M.; Liu, B.; Fang, J.; Wang, C. Physiological and Transcriptional Responses to Acute and Chronic Thermal Stress in the Ark Shell *Scapharca subcrenata*. *Front. Mar. Sci.* **2021**, *8*, 739662. [CrossRef]
22. Dar, S.A.; Srivastava, P.P.; Varghese, T.; Nazir, M.I.; Gupta, S.; Krishna, G. Temporal changes in superoxide dismutase, catalase, and heat shock protein 70 gene expression, cortisol and antioxidant enzymes activity of *Labeo rohita* fingerlings subjected to starvation and refeeding. *Gene* **2019**, *692*, 94–101. [CrossRef] [PubMed]
23. Wu, P.; Wang, A.; Cheng, J.; Chen, L.; Pan, Y.; Li, H.; Zhang, Q.; Zhang, J.; Chu, W.; Zhang, J. Effects of starvation on antioxidant-related signaling molecules, oxidative stress, and autophagy in juvenile Chinese perch skeletal muscle. *Mar. Biotechnol.* **2020**, *22*, 81–93. [CrossRef] [PubMed]
24. Zhang, H.C.; Ma, K.X.; Yang, Y.J.; Shi, C.Y.; Chen, G.W.; Liu, D.Z. Molecular cloning, characterization, expression and enzyme activity of catalase from planarian *Dugesia japonica* in response to environmental pollutants. *Ecotoxicol. Environ. Saf.* **2018**, *165*, 88–95. [CrossRef]
25. Wang, X.; Li, P.; He, S.; Xing, S.; Cao, Z.; Cao, X.; Liu, B.; Li, Z.H. Effects of tralopyril on histological, biochemical and molecular impacts in Pacific oyster, *Crassostrea gigas*. *Chemosphere* **2022**, *289*, 133157. [CrossRef]
26. Zhao, Y.Q.; Liu, G.D.; Hou, C.C.; Han, Y.L.; Zhu, J.Q. Effect of cadmium exposure on antioxidant enzyme catalase in different tissues of *Acrossocheilus fasciatus*. *Mol. Cell Toxicol.* **2016**, *12*, 255–263. [CrossRef]
27. Wang, J.; Zhu, X.; Huang, X.; Gu, L.; Chen, Y.; Yang, Z. Combined effects of cadmium and salinity on juvenile *Takifugu obscurus*: Cadmium moderates salinity tolerance; salinity decreases the toxicity of cadmium. *Sci. Rep.* **2016**, *6*, 30968. [CrossRef]
28. Zoysa, M.D.; Whang, I.; Nikapitiya, C.; Oh, C.; Choi, C.Y.; Lee, J. Transcriptional analysis of disk abalone (*Haliotis discus discus*) antioxidant enzymes against marine bacteria and virus challenge. *Fish Shellfish Immunol.* **2011**, *31*, 155–160. [CrossRef]
29. Chainy, G.B.N.; Paital, B.; Dandapat, J. An overview of seasonal changes in oxidative stress and antioxidant defence parameters in some invertebrate and vertebrate species. *Scientifica* **2016**, *2016*, 6126570. [CrossRef]
30. Oliveira, M.R.; Braghirolli, F.M.; Lanés, L.E.K.; Verrastro, L.; Oliveira, G.T. Evaluation of the seasonal variation of parameters of oxidative status of *Tropidurus catalanensis* Gudynas and Skuk, 1983. *S. Am. J. Herpetol.* **2021**, *19*, 12–21. [CrossRef]
31. Nash, S.; Rahman, M.S. Short-term heat stress impairs testicular functions in the American oyster, *Crassostrea virginica*: Molecular mechanisms and induction of oxidative stress and apoptosis in spermatogenic cells. *Mol. Reprod. Dev.* **2019**, *86*, 1444–1458. [CrossRef] [PubMed]
32. Mazurais, D.; Covès, D.; Papandroulakis, N.; Ortega, A.; Desbruyeres, E.; Huelvan, C.; Le Gall, M.M.; De La Gándara, F.; Cahu, C.L. Gene expression pattern of digestive and antioxidant enzymes during the larval development of reared Atlantic bluefin tuna (ABFT), *Thunnus thynnus* L. *Aquac. Res.* **2015**, *46*, 2323–2331. [CrossRef]

33. Zengin, H.; Yılmaz, Ö.; Demir, E.; Gökçe, Z. Antioxidant enzymatic defences during embryogenesis of rainbow trout *Oncorhynchus mykiss* (Walbaum 1792). *Turk. J. Fish. Aquat. Sci.* **2015**, *15*, 443–452. [CrossRef]
34. Rampon, C.; Volovitch, M.; Joliot, A.; Vriz, S. Hydrogen peroxide and redox regulation of developments. *Antioxidants* **2018**, *7*, 159. [CrossRef]
35. Mirzaei, A.H.; Deldar, H.; Pirsaraei, Z.A.; Shohreh, B. Royal jelly may improve sperm characteristics during preservation of rooster semen: Gene expression of antioxidant enzymes. *Reprod. Domest. Anim.* **2021**, *56*, 658–666. [CrossRef]
36. Gale, S.L.; Burritt, D.J.; Tervit, H.R.; Adams, S.L.; McGowan, L.T. An investigation of oxidative stress and antioxidant biomarkers during Greenshell mussel (*Perna canaliculus*) oocyte cryopreservation. *Theriogenology* **2014**, *82*, 779–789. [CrossRef]
37. Sharker, M.; Kim, S.C.; Hossen, S.; Kho, K.H. Characterization of insulin-like growth factor binding Protein-5 (IGFBP-5) gene and its potential roles in ontogenesis in the Pacific Abalone, *Haliotis discus hannai*. *Biology* **2020**, *9*, 216. [CrossRef]
38. Sandamalika, W.G.; Priyathilaka, T.T.; Liyanage, D.S.; Lee, S.; Lim, H.K.; Lee, J. Molecular characterization of kappa class glutathione S-transferase from the disk abalone (*Haliotis discus discus*) and changes in expression following immune and stress challenges. *Fish Shellfish Immunol.* **2018**, *77*, 252–263. [CrossRef]
39. Elvitigala, D.A.S.; Jayasooriya, R.G.P.T.; Lee, J. First report on the gastropod proapoptotic AIF3 counterpart from disk abalone (*Haliotis discus discus*) deciphering its transcriptional modulation by induced pathogenic stress. *Fish Shellfish Immunol.* **2015**, *47*, 697–705. [CrossRef]
40. Hossen, S.; Sukhan, Z.P.; Cho, Y.; Kho, K.H. Effects of cryopreservation on gene expression and post thaw sperm quality of Pacific abalone, *Haliotis discus hannai*. *Front. Mar. Sci.* **2021**, *8*, 652390. [CrossRef]
41. Kim, S.C.; Hossen, S.; Kho, K.H. Cryopreservation of sperm from farmed Pacific abalone, *Haliotis discus hannai*. *Cryobiology* **2020**, *94*, 49–56. [CrossRef] [PubMed]
42. Kong, N.; Li, H.; Yang, W.; Fu, Q.; Gong, C.; Wang, L.; Song, L. The effects of protein kinase a catalytic subunit on sperm motility regulation in Pacific abalone *Haliotis discus hannai*. *Aquac. Res.* **2020**, *51*, 2525–2534. [CrossRef]
43. Hossen, S.; Sukhan, Z.P.; Cho, Y.; Lee, W.K.; Kho, K.H. Antioxidant Activity and Oxidative Stress-Oriented Apoptosis Pathway in Saccharides Supplemented Cryopreserved Sperm of Pacific Abalone, *Haliotis discus hannai*. *Antioxidants* **2022**, *11*, 1303. [CrossRef] [PubMed]
44. Qiao, K.; Fang, C.; Chen, B.; Liu, Z.; Pan, N.; Peng, H.; Hao, H.; Xu, M.; Wu, J.; Liu, S. Molecular characterization, purification, and antioxidant activity of recombinant superoxide dismutase from the Pacific abalone *Haliotis discus hannai Ino*. *World J. Microbiol. Biotechnol.* **2020**, *36*, 1–14. [CrossRef] [PubMed]
45. Sukhan, Z.P.; Hossen, S.; Cho, Y.; Lee, W.K.; Kho, K.H. Hdh-Tektin-4 Regulates Motility of Fresh and Cryopreserved Sperm in Pacific Abalone, *Haliotis discus hannai*. *Front. Cell Dev. Biol.* **2022**, *10*, 870743. [CrossRef]
46. Silva-Aciares, F.; Moraga, D.; Auffret, M.; Tanguy, A.; Riquelme, C. Transcriptomic and cellular response to bacterial challenge (pathogenic *Vibrio parahaemolyticus*) in farmed juvenile *Haliotis rufescens* fed with or without probiotic diet. *J. Invertebr. Pathol.* **2013**, *113*, 163–176. [CrossRef]
47. Sukhan, Z.P.; Cho, Y.; Sharker, M.R.; Hossen, S.; Rha, S.J.; Kho, K.H. Effective accumulative temperature affects gonadal maturation by controlling expression of GnRH, GnRH receptor, serotonin receptor and APGWamide gene in Pacific abalone, *Haliotis discus hannai* during broodstock conditioning in hatcheries. *J. Therm. Biol.* **2021**, *100*, 103037. [CrossRef]
48. Hossen, S.; Sharker, M.; Cho, Y.; Sukhan, Z.P.; Kho, K.H. Effects of antifreeze protein III on sperm cryopreservation of Pacific abalone, *Haliotis discus hannai*. *Int. J. Mol. Sci.* **2021**, *22*, 3917. [CrossRef]
49. Sharker, M.R.; Hossen, S.; Nou, I.S.; Kho, K.H. Characterization of insulin-like growth factor binding protein 7 (igfbp7) and its potential involvement in shell formation and metamorphosis of Pacific abalone, *Haliotis discus hannai*. *Int. J. Mol. Sci.* **2020**, *21*, 6529. [CrossRef]
50. Livak, K.J.; Schmittgen, T.D. Analysis of relative gene expression data using real-time quantitative PCR and the $2^{-\Delta\Delta CT}$ method. *Methods* **2001**, *25*, 402–408. [CrossRef]
51. Bankoglu, E.E.; Tschopp, O.; Schmitt, J.; Burkard, P.; Jahn, D.; Geier, A.; Stopper, H. Role of PTEN in oxidative stress and DNA damage in the liver of whole-body Pten haplodeficient mice. *PLoS ONE* **2016**, *11*, e0166956. [CrossRef] [PubMed]
52. Orbea, A.; Dariush, H.F.; Cajaraville, M.P. Immunolocalization of four antioxidant enzymes in digestive glands of mollusks and crustaceans and fish liver. *Histochem. Cell Biol.* **2000**, *114*, 393–404. [CrossRef] [PubMed]
53. Zarai, Z.; Boulais, N.; Marcorelles, P.; Gobin, E.; Bezzine, S.; Mejdoub, H.; Gargouri, Y. Immunohistochemical localization of hepatopancreatic phospholipase in gastropods mollusc, *Littorina littorea* and *Buccinum undatum* digestive cells. *Lipids Health Dis.* **2011**, *10*, 1–10. [CrossRef] [PubMed]
54. Gronemeyer, T.; Wiese, S.; Ofman, R.; Bunse, C.; Pawlas, M.; Hayen, H.; Eisenacher, M.; Stephan, C.; Meyer, H.E.; Waterham, H.R.; et al. The proteome of human liver peroxisomes: Identification of five new peroxisomal constituents by a label-free quantitative proteomics survey. *PLoS ONE* **2013**, *8*, e57395. [CrossRef]
55. Marín-García, J. Oxidative stress and cell death in cardiovascular disease. In *Post-Genomic Cardiology*; Elsevier: Amsterdam, The Netherlands, 2014; pp. 471–498.
56. Hoegh-Guldberg, O.; Mumby, P.J.; Hooten, A.J.; Steneck, R.S.; Greenfield, P.; Gomez, E.; Harvell, C.D.; Sale, P.F.; Edwards, A.J.; Caldeira, K.; et al. Coral reefs under rapid climate change and ocean acidification. *Science* **2007**, *318*, 1737–1742. [CrossRef] [PubMed]

57. Abele, D.; Heise, K.; Pörtner, H.O.; Puntarulo, S. Temperature-dependence of mitochondrial function and production of reactive oxygen species in the intertidal mud clam *Mya arenaria*. *J. Exp. Biol.* **2002**, *205*, 1831–1841. [CrossRef]
58. Soldatov, A.A.; Gostyukhina, O.L.; Golovina, I.V. Antioxidant enzyme complex of tissues of the bivalve *Mytilus galloprovincialis* Lam. Under normal and oxidative-stress conditions: A review. *Appl. Biochem. Microbiol.* **2007**, *43*, 556–562. [CrossRef]
59. Cheng, C.H.; Guo, Z.X.; Luo, S.W.; Wang, A.L. Effects of high temperature on biochemical parameters, oxidative stress, DNA damage and apoptosis of pufferfish (Takifugu obscurus). *Ecotox. Environ. Safe* **2018**, *150*, 190–198. [CrossRef]
60. Wang, J.; Ren, R.M.; Yao, C.L. Oxidative stress responses of *Mytilus galloprovincialis* to acute cold and heat during air exposure. *J. Molluscan Stud.* **2018**, *84*, 285–292. [CrossRef]
61. Ding, F.F.; Li, A.; Cong, R.H.; Wang, X.X.; Wang, W.; Que, H.Y.; Zhang, G.; Li, l. The phenotypic and the genetic response to the extreme high temperature provides new insight into thermal tolerance for the pacific oyster *Crassostrea gigas*. *Front. Mar. Sci.* **2020**, *7*, 399. [CrossRef]
62. Nita, M.; Grzybowski, A. The role of the reactive oxygen species and oxidative stress in the pathomechanism of the age-related ocular diseases and other pathologies of the anterior and posterior eye segments in adults. *Oxid. Med. Cell. Longev.* **2016**, *2016*, 3164734. [CrossRef] [PubMed]
63. Hopwood, M.J.; Rapp, I.; Schlosser, C.; Achterberg, E.P. Hydrogen peroxide in deep waters from the Mediterranean Sea, South Atlantic and South Pacific oceans. *Sci. Rep.* **2017**, *7*, 43436. [CrossRef] [PubMed]
64. Alam, M.R.; Ehiguese, F.O.; Vitale, D.; Martín-Díaz, M.L. Oxidative stress response to hydrogen peroxide exposure of *Mytilus galloprovincialis* and *Ruditapes philippinarum*: Reduced embryogenesis success and altered biochemical response of sentinel marine bivalve species. *J. Environ. Chem. Ecotoxicol.* **2022**, *4*, 97–105. [CrossRef]
65. Jo, P.G.; Choi, Y.K.; Choi, C.Y. Cloning and mRNA expression of antioxidant enzymes in the Pacific oyster, *Crassostrea gigas* in response to cadmium exposure. *Comp. Biochem. Physiol. Part-C Toxicol. Pharmacol.* **2008**, *147*, 460–469. [CrossRef]
66. Qi, Z.; Wang, Q.; Song, S.; Wang, H.; Tan, M. Enhanced cytotoxicity of cadmium by a sulfated polysaccharide from abalone. *J. Agric. Food Chem.* **2020**, *68*, 14996–15004. [CrossRef]
67. Peng, Y.Q.; Wang, M.J.; Chen, H.G.; Chen, J.H.; Gao, H.; Huang, H.H. Immunological responses in haemolymph and histologic changes in the hepatopancreas of *Charybdis japonica* (A. Milne-Edwards, 1861) (Decapoda: Brachyura: Portunidae) exposed to bisphenol A. *J. Crustac. Biol.* **2018**, *38*, 489–496. [CrossRef]
68. Sakyi, M.E.; Cai, J.; Tang, J.; Abarike, E.D.; Xia, L.; Li, P.; Kuebutornye, F.K.A.; Zou, Z.; Liang, Z.; Jian, J. Effects of starvation and subsequent re-feeding on intestinal microbiota, and metabolic responses in Nile tilapia, *Oreochromis niloticus*. *Aquac. Rep.* **2020**, *17*, 100370. [CrossRef]
69. Shi, Q.; Xiong, X.; Wen, Z.; Qin, C.; Li, R.; Zhang, Z.; Gong, Q.; Wu, X. Cu/Zn Superoxide Dismutase and Catalase of Yangtze Sturgeon, Acipenser dabryanus: Molecular Cloning, Tissue Distribution and Response to Fasting and Refeeding. *Fishes* **2022**, *7*, 35. [CrossRef]
70. Canesi, L.; Barmo, C.; Fabbri, R.; Ciacci, C.; Vergani, L.; Roch, P.; Gallo, G. Effects of vibrio challenge on digestive gland biomarkers and antioxidant gene expression in *Mytilus galloprovincialis*. *Comp. Biochem. Physio.* **2010**, *152*, 399e406. [CrossRef]
71. Liu, H.P.; Chen, F.Y.; Gopalakrishnan, S.; Qiao, K.; Bo, J.; Wang, K.J. Antioxidant enzymes from the crab *Scylla paramamosain*: Gene cloning and gene/protein expression profiles against LPS challenge. *Fish Shellfish Immunol.* **2010**, *28*, 862–871. [CrossRef]
72. Priyathilaka, T.T.; Bathige, S.D.N.K.; Lee, S.; Yang, H.; Jeong, T.; Lee, S.; Lee, J. Structural and functional analysis of three Iκb kinases (IKK) in disk abalone (*Haliotis discus discus*): Investigating their role in the innate immune responses. *Fish Shellfish Immunol.* **2020**, *103*, 111–125. [CrossRef] [PubMed]
73. Shen, B.; Wei, K.; Ding, Y.; Zhang, J. Molecular cloning, mRNA expression and functional characterization of a catalase from Chinese black sleeper (*Bostrychus sinensis*). *Fish Shellfish Immunol.* **2020**, *103*, 310–320. [CrossRef] [PubMed]
74. Lobo-da-Cunha, A.; Alves, Â.; Oliveira, E.; Guimarães, F.; Calado, G. Endocytosis, lysosomes, calcium storage and other features of digestive-gland cells in cephalaspidean gastropods (*Euopisthobranchia*). *J. Molluscan Stud.* **2018**, *84*, 451–462. [CrossRef]
75. Figueroa, E.; Farias, J.G.; Lee-Estevez, M.; Valdebenito, I.; Risopatrón, J.; Magnotti, C.; Romero, J.; Watanabe, I.S.; Oliveira, R.P.S. Sperm cryopreservation with supplementation of α-tocopherol and ascorbic acid in freezing media increase sperm function and fertility rate in Atlantic salmon (*Salmo salar*). *Aquaculture* **2018**, *493*, 1–8. [CrossRef]
76. De Viçose, G.C.; Viera, M.P.; Bilbao, A.; Izquierdo, M.S. Embryonic and larval development of Haliotis tuberculata coccinea Reeve: An indexed micro-photographic sequence. *J. Shellfish. Res.* **2007**, *26*, 847–854. [CrossRef]
77. Kalaimani, N.; Chakravarthy, N.; Shanmugham, R.; Thirunavukkarasu, A.R.; Alavandi, S.V.; Santiago, T.C. Antioxidant status in embryonic, post-hatch and larval stages of Asian seabass (*Lates calcarifer*). *Fish Physiol. Biochem.* **2008**, *34*, 151–158. [CrossRef]

antioxidants

MDPI

Article

Transport Stress Induces Oxidative Stress and Immune Response in Juvenile Largemouth Bass (*Micropterus salmoides*): Analysis of Oxidative and Immunological Parameters and the Gut Microbiome

Qingchun Wang [1,†], Wei Ye [2,†], Yifan Tao [2], Yan Li [2,*], Siqi Lu [2], Pao Xu [1,2] and Jun Qiang [1,2,*]

[1] Wuxi Fisheries College, Nanjing Agricultural University, Wuxi 214081, China
[2] Key Laboratory of Freshwater Fisheries and Germplasm Resources Utilization, Ministry of Agriculture and Rural Affairs, Freshwater Fisheries Research Center, Chinese Academy of Fishery Sciences, Wuxi 214081, China
* Correspondence: liyan@ffrc.cn (Y.L.); qiangj@ffrc.cn (J.Q.)
† These authors contributed equally to this study.

Abstract: Transport is essential in cross-regional culturing of juvenile fish. Largemouth bass (*Micropterus salmoides*) often exhibit decreased vitality and are susceptible to disease after transportation. To study the effects of transport stress on juvenile largemouth bass, juveniles (average length: 8.42 ± 0.44 cm, average weight 10.26 ± 0.32 g) were subjected to a 12 h simulated transport, then subsequently, allowed to recover for 5 d. Liver and intestinal tissues were collected at 0, 6 and 12 h after transport stress and after 5 d of recovery. Oxidative and immunological parameters and the gut microbiome were analyzed. Hepatocytic vacuolization and shortened intestinal villi in the bass indicated liver and intestinal damage due to transport stress. Superoxide dismutase, lysozyme and complement C3 activities were significantly increased during transport stress ($p < 0.05$), indicating that transport stress resulted in oxidative stress and altered innate immune responses in the bass. With the transport stress, the malondialdehyde content first increased, then significantly decreased ($p < 0.05$) and showed an increasing trend in the recovery group. 16S rDNA analysis revealed that transport stress strongly affected the gut microbial compositions, mainly among Proteobacteria, Firmicutes, Cyanobacteria and Spirochaetes. The Proteobacteria abundance increased significantly after transport. The Kyoto Encyclopedia of Genes and Genomes functional analysis revealed that most gut microbes played roles in membrane transport, cell replication and repair. Correlation analyses demonstrated that the dominant genera varied significantly and participated in the measured physiological parameter changes. With 5 days of recovery after 12 h of transport stress, the physiological parameters and gut microbiome differed significantly between the experimental and control groups. These results provide a reference and basis for studying transport-stress-induced oxidative and immune mechanisms in juvenile largemouth bass to help optimize juvenile largemouth bass transportation.

Keywords: largemouth bass; transport stress; gut microbiome; oxidative stress; innate immunity response

Citation: Wang, Q.; Ye, W.; Tao, Y.; Li, Y.; Lu, S.; Xu, P.; Qiang, J. Transport Stress Induces Oxidative Stress and Immune Response in Juvenile Largemouth Bass (*Micropterus salmoides*): Analysis of Oxidative and Immunological Parameters and the Gut Microbiome. *Antioxidants* **2023**, *12*, 157. https://doi.org/10.3390/antiox12010157

Academic Editor: Stanley Omaye

Received: 19 December 2022
Revised: 5 January 2023
Accepted: 6 January 2023
Published: 9 January 2023

1. Introduction

Transportation is important in cross-regional fingerling cultures. However, the fish often showed decreased vitality, loss of appetite, and low resistance after long-distance transportation, which adversely affects healthy breeding and limits rapid development in the aquaculture industry. Many reasons, such as water quality changes, fish body bruising, starvation and so on, may cause transport stress. Increases in ammonia-nitrogen and nitrite concentrations in the water caused by fish metabolites during transportation is often considered as one of the important factors causing transport stress [1] and increased mortality

in the fish after transport [2]. Transport stress can cause irregular oxidation in the aerobic metabolic pathway, resulting in oxidative stress in transported fish [3,4]. Mechanical damage caused by turbulence and congestion during transport can lead to immune injury, making fish susceptible to pathogenic infection [5]. Transport stress significantly affected glycogen, superoxide dismutase (SOD) and malondialdehyde (MDA) contents in hybrid snapper (*Pagrus major*♀× *Acanthopagrus schlegelii*♂) livers, with significantly increased mortality in these fish after transport [6]. One study found that liver lysozyme and IgM activity increased significantly in hybrid *Pelteobagrus fulvidraco* (*Tachysurus fulvidraco*♀× *Pseudobagrus vachelliii*♂) after transport stress [7]. Another study found that alkaline phosphatase, acid phosphatase, SOD activity and total antioxidant capacity (T-AOC) in the gills first increased, then decreased [8]. Additionally, short-distance transport stress significantly decreased the SOD and T-AOC activities in liver tissue from *Oncorhynchus mykiss* [9]. T-AOC, CAT and MDA levels first increased, then decreased during transport in *Ictalurus punctatus* [2], and T-AOC, lysozyme and complement C3 activities increased significantly in blunt snout bream (*Megalobrama amblycephala*) after transport [10].

The intestines are important for digestion and absorption in fish, and the gut microbiome participates in metabolism and synthesis of proteins, amino acids and other substances [11], which is important in physiological metabolism and immunity. Gut microbiome stability is important for maintaining host health [12]. Environmental stress can change the gut microbiome structure [13]. Crowding stress significantly changed the gut microbial abundances in blunt snout bream (*Megalobrama amblycephala*) at the genus level, with a significant correlation between intestinal microorganisms and 13 metabolites [14]. In *Penaeus vannamei*, stress from high ammonia-nitrogen concentrations significantly decreased the gut microbial abundances and reshaped the genus-level community structure of the gut microbiome [15]. Additionally, transport stress changed the intestinal microbial diversity of hybrid yellow catfish (*Tachysurus fulvidraco*♀× *Pseudobagrus vachelliii*♂) and affected host microbial functions [16].

Largemouth bass (*Micropterus salmoides*) are native to freshwater basins in North America and are now widely farmed throughout China. This species is economically important owing to its fast growth and strong disease resistance [17,18]. However, breeding largemouth bass seedlings is concentrated in Jiangsu and Guangdong, and the fingerling often need to be transported long distances, which can lead to decreased vitality and sometimes death, which adversely affects healthy breeding and limits rapid development in the aquaculture industry. This study was conducted to observe the effects of transport stress on liver and intestinal tissue structures in largemouth bass by simulating long-distance transport. We also analyzed the effects of transport stress on antioxidant and immune abilities in largemouth bass and clarified the differences in gut microbiome compositions before and after transport stress. The results provide a reference for optimizing transportation of juvenile largemouth bass.

2. Materials and Methods

2.1. Experimental Materials

Largemouth bass (50 days of age with average body length 8.42 ± 0.44 cm, average weight 10.26 ± 0.32 g) were selected from the Yixing Base of Freshwater Fisheries Center, Chinese Academy of Fishery Sciences (Wuxi, China). The bass were cultured in a recirculating aquaculture system consist of 26 cylindrical circulation barrels with a diameter of 1.0 m, height of 1.2 m, and the water used for aquaculture was filtered pond water. The bass were fed commercial feed (crude protein 46.0% and crude fat 6%) at 2% of their body weight twice daily (8:00 am and 16:00 pm) in a recirculating aquaculture system with density of 1.3 g/L at 24.0 ± 0.3 °C, ammonia-nitrogen <0.01 mg/L, and dissolved oxygen >6 mg/L before the experiment. The culture conditions were applied to the control and recovery groups. The fish was fasted 24 h immediately after last feeding, then used for experiment.

2.2. Experimental Design

The experiment was divided into treatment groups: 0-h, 6-h, and 12 h transport stress; 5 d recovery after a 12 h simulated transport, and a control group. Three parallels were set per group. The bass that remained in the recirculating aquaculture system were used as controls. Twelve double-layered plastic bags (40 × 80 cm) containing one-third water and two-third oxygen were placed on an automated shaker (Mince instrument, Changzhou, China) to simulate the actual transport. The vibration frequency was set at 100 rpm [6,16], and each bag contained 15 fish. The air conditioning temperature was set to 22 degrees to ensure that the ring temperature was constant during the simulated transportation, and avoided all light in the process. Nine bags were used for sampling at 0, 6, and 12 h of transportation. The other three bags were placed in the recirculating aquaculture system for recovery after 12 h of transport stress, then sampled after 5 d of recovery. The recovery conditions were the same with the control group.

2.3. Sample Collection

Three bags were randomly selected for sampling at each time point, water samples were taken, 15 fish were randomly selected and 5 of the 15 fish were sampled from each of the 3 bags. Control water and fish were obtained from the recirculating aquaculture system at the corresponding time points. The fish were anesthetized via 200 mg/L MS-222 before sampling. The livers and posterior section of the intestines were collected from three fish and fixed with 4% paraformaldehyde solution for histological analysis. The livers and intestines from the remaining 12 fish were homogenized and mixed with precooled phosphate-buffered saline, then centrifuged for 15 min at 12,000× *g* at 4 °C. The supernatant was aspirated and stored at −80 °C for physiological parameter analysis. The hindguts were collected from five fish each from the control, 12 h transport and recovery groups, immediately frozen in liquid nitrogen, and stored in a −80 °C freezer for gut microbiome analysis.

2.4. Water Quality Detection

The dissolved oxygen was measured using an oxygen-dissolving meter (Hach, Loveland, CO, USA), and the total ammonia-nitrogen and nitrite-nitrogen contents were determined via spectrophotometry [7].

2.5. Histological Analysis of the Liver and Intestinal Tissues

The tissues were immersed in 4% paraformaldehyde for 24 h, then routinely processed, embedded in paraffin, and sectioned. The sections were dewaxed in xylene for 2–5 min, then washed continuously in 100%, 96%, 80%, and 70% ethanol for 1 min. Sections were then stained with hematoxylin for 7 min, rinsed with distilled water for 2 min, rinsed with 0.1% hydrochloric acid and 50% ethanol for 2–5 s, rinsed with tap water for 5–7 min, stained with eosin for 2–4 min, rinsed with distilled water for 1 min, dehydrated with 95% and 100% ethanol for 1 min each and finally rinsed with xylene (2–5 min) [19]. The sections were then air-dried, and the slides were covered and observed under a light microscope. Hematoxylin stained the normal nuclei blue. The liver tissue size and cavitation ratio (cavitation ratio [%] = cell vacuolar area/section area×100) were measured using Image-Pro Plus 6.0 [20].

2.6. Liver and Intestinal Biochemical Analyses

Liver SOD, MDA, lysozyme, complement C3, intestinal SOD and MDA activities were detected using commercial kits (Jiancheng Institute, Nanjing, China) following the manufacturer's instructions [16].

2.7. Determination of the Gut Microbiome

The E.Z.N.A.® Stool DNA Kit (D4015, Omega Inc., Norcross, GA, USA) was used to extract microbial DNA from the intestinal samples, and the DNA sample quality was detected via 1% agarose gel electrophoresis and quantified using an ultraviolet spectrophotometer.

Samples with correct target bands were regarded as qualified samples. PCR was performed using universal primers: v3-v4 region [21]: 341F: 5′-CCTACGGGNGGCWGCAG-3′ and 805R: 5′-GACTACHVGGGTATCTAATCC-3′. The PCR reaction system consisted of 50 ng template DNA, 12.5 μL of PCR Premix, 2.5 μL each of forward and reverse primers and ddH2O added to 25 μL. The PCR amplification reaction was 98 °C predenaturation for 30 s, 35 cycles of 98 °C denaturation for 10 s, 54 °C annealing for 30 s, and a 72 °C extension for 45 s. Extension was continued at 72 °C for 10 min at the end of the cycle, and finally, preserved at 4 °C. The product quality was detected via 1% agarose gel electrophoresis. Correctly sized target bands with 700 bp were considered qualified samples. PCR products were purified using AMPure XT beads (Beckman Coulter Genomics, Danvers, MA, USA) and quantified using Qubit (Invitrogen, Carlsbad, CA, USA). The sequencing libraries were prepared by Pacific Biosciences SMRTbell™ Template Prep kit 1.0 (Kapa Biosciences, Woburn, MA, USA). The size and number of amplicon libraries were assessed using a library quantification kit from Illumina (Kapa Biosciences, Woburn, MA, USA) and an Agilent 2100 Bioanalyzer (Agilent, Santa Clara, CA, USA).

Eligible libraries were sequenced on the Illumina NovaSeq platform and read by FLASH merge matching ends. Under specific filtering conditions, fqtrim (v0.94) was used to quality-filter the raw read data to obtain high-quality clean labels. Chimeric sequences were filtered with the Vsearch (v2.3.4) software. The feature table and sequence were obtained by demodulation using DADA2. Observed species, Chao1, Shannon and Simpson indices were used to evaluate alpha diversity. Beta-diversity indexes were used to evaluate species composition differences among samples. The alpha and beta diversity were calculated using QIIME2. Species with significantly different abundances between groups were analyzed with the nonparametric factor Kruskal–Wallis rank-sum test. The PICRUSt2 software was used for Kyoto Encyclopedia of Genes and Genomes (KEGG) enrichment analysis.

2.8. Statistical Analysis

Data were analyzed and processed using SPSS 26.0 (SPSS Inc., Chicago, IL, USA). Shapiro–Wilk and Levene tests were used to analyze the normality and variance homogeneity of the data, and single factor analysis of variance (one-way ANOVA) was used to analyze significant differences among groups by Duncan's multiple comparisons. The control and treatment groups were compared using independent sample t-tests. The Kruskal–Wallis method was used to analyze the significant differences in alpha diversity indexes among samples, and correlations between the gut microbiome and physiological parameters were analyzed via Spearman's correlation analyses. Box plots were drawn using origin software; all other pictures were constructed in R [22]. $p < 0.05$ was considered significant, and all data were expressed as means ± standard error of the mean.

3. Results

3.1. Water Quality during Transport

The total ammonia-nitrogen and nitrite-nitrogen concentrations increased significantly as the transportation time increased ($p < 0.05$, Figure 1A,B). After 12 h of transportation, the total ammonia-nitrogen concentration reached 0.723 ± 0.009 mg/L, which was significantly higher than that of its control group (0.0163 ± 0.002 mg/L), and the nitrite-nitrogen concentration was 0.129 ± 0.008 mg/L, which was significantly higher than that of its control group (0.009 ± 0.002 mg/L). The dissolved oxygen was kept above 20 mg/L during transport (Figure 1C).

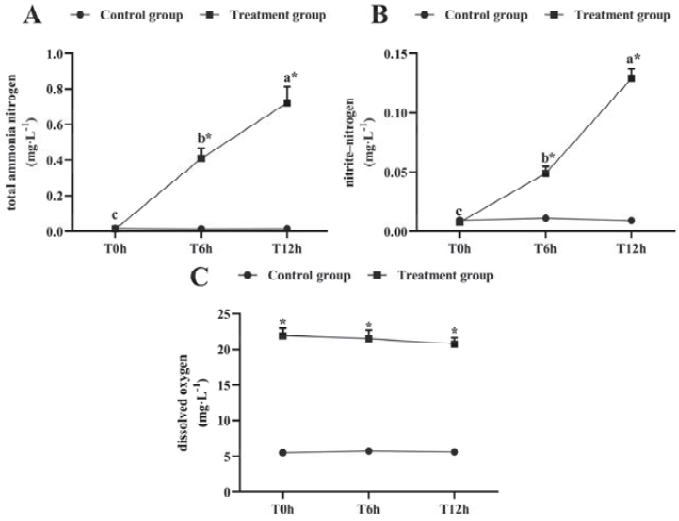

Figure 1. Changes in total ammonia-nitrogen (**A**) nitrite-nitrogen (**B**) and dissolved oxygen (**C**) levels during transport. T0h: transport stress at 0 h; T6h: transport stress at 6 h; T12h: transport stress at 12 h. * significant difference between control and treatment groups (paired samples *t*-test, *: $p < 0.05$). Lowercase letters indicate significant differences ($p < 0.05$) between treatments (Duncan's multiple range test).

3.2. Histological Analysis of the Liver and Intestinal Tissues

After 0 h of transport stress, liver cells from the juvenile largemouth bass were undamaged, and the cells exhibited obvious boundaries (Figure 2(Aa)). After 6 h of transport stress, vacuoles appeared in the liver cells, at proportions reaching 22.60% (Figure 2(Ab); Table 1). After 12 h of transport stress, the liver cells showed severe vacuolization (Figure 2(Ac)), with proportions reaching 60.34%, which was significantly higher than that after 6 h of transport stress ($p < 0.01$), and the healthy hepatocytes were squeezed as the vacuoles expanded. After 5 days of recovery, the vacuolar area remained significantly larger than that of the control group (37.06%; $p < 0.05$; Figure 2(Ad)).

Hematoxylin-eosin staining showed that the intestinal muscle layer thickness increased and the intestinal villus length decreased under transport stress (Figure 2B). The intestinal muscle layer thickness did not significantly differ among groups at 0, 6 and 12 h of transport ($p > 0.05$). However, the thickness in the recovery group was significantly greater than those at 0 and 6 h of transport stress ($p < 0.05$) and did not significantly differ from that at 12 h of transport stress ($p > 0.05$). The villus length decreased as the transport time increased and remained significantly shorter after 5 days of recovery ($p < 0.05$; Table 1). No fish died during transport.

Table 1. Changes in liver vacuolar area, intestinal muscular thickness and villus length in juvenile largemouth bass under transport stress.

Items	Groups							
	T0h	Ctrl	T6h	Ctrl	T12h	Ctrl	R5d	Ctrl
Liver vacuolar area (%)	0.81 ± 0.02^{d}	0.37 ± 0.04	23 ± 0^{c}	1.04 ± 0.10	60 ± 1^{a}	0.97 ± 0.07	37 ± 1^{b}	1.36 ± 0.47
Muscularis thickness (μm)	39 ± 5^{b}	37 ± 4	39 ± 3^{b}	40 ± 2	50 ± 7^{ab}	34 ± 4	56 ± 2^{a}	37 ± 8
The length of intestinal villus (μm)	391 ± 7^{a}	378 ± 10	316 ± 21^{b}	415 ± 18	272 ± 16^{c}	420 ± 13	193 ± 11^{d}	381 ± 4

T0h: transport stress at 0 h; T6h: transport stress at 6 h; T12h: transport stress at 12 h; R5d: 5-day recovery after transport stress; Ctrl: control group at the corresponding time points. Lowercase letters indicate significance differences ($p < 0.05$).

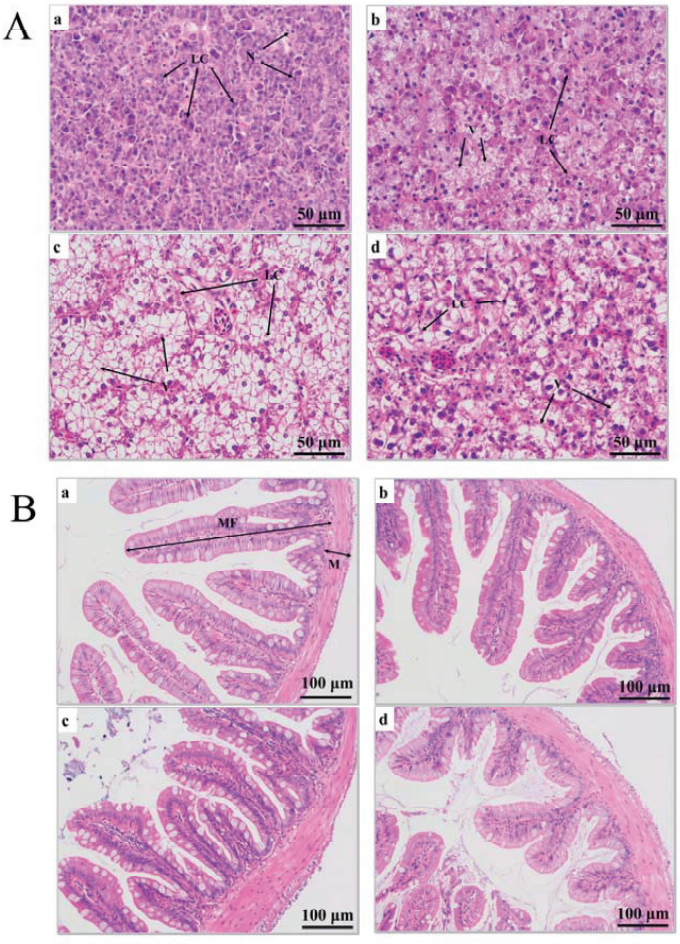

Figure 2. (**A**) Histopathological sections of juvenile largemouth bass livers under transport stress. LC: liver cells; N: nucleus; V: vacuoles. Scale 1:400. (**B**) Histopathological sections of juvenile largemouth bass intestines under transport stress. MF: intestinal villi; M: muscular layer. Scale 1:200. Sections under transport stress at 0 h (**a**), 6 h (**b**), 12 h (**c**) and after 5 d of recovery (**d**) after transportation.

3.3. Oxidative and Immunological Parameters

None of the measured physiological parameters differed significantly in the control group (Figure 2). However, SOD activity in the livers and intestines of the juvenile largemouth bass increased significantly as the transport time increased ($p < 0.05$), and the SOD activity peaked after 5 days of recovery, which was significantly higher than that after 12 h of transport stress (Figure 3A,E; $p < 0.05$). MDA concentrations in the livers and intestines peaked after 6 h of transportation, decreased significantly after 12 h of transport ($p < 0.05$), then increased significantly after 5 days of recovery (Figure 3B,F; $p < 0.05$). Lysozyme activity increased as the transport stress time increased ($p < 0.05$), with the highest activity at 12 h of transport stress. No significant difference was noted in the recovery group (Figure 3C). Complement C3 levels increased rapidly from 6 to 12 h of transport stress (Figure 3D; $p < 0.05$), with no significant difference between the 12 h transport group and the recovery group. The SOD, MDA, lysozyme and complement C3 levels differed markedly between the recovery and control groups.

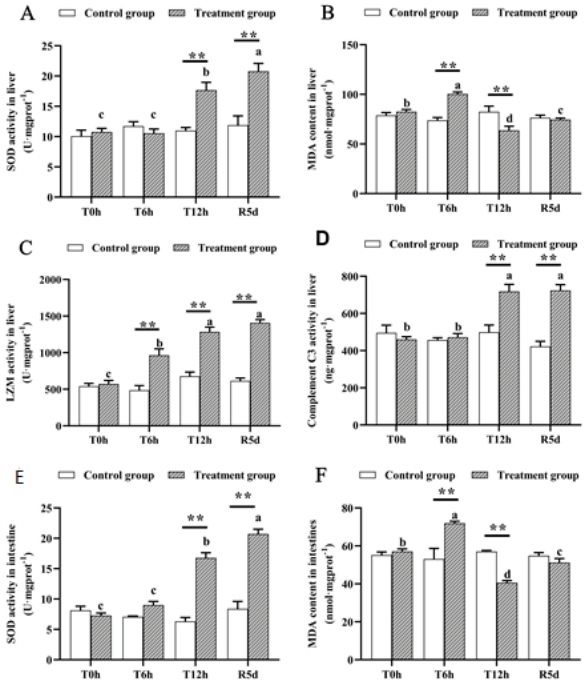

Figure 3. Antioxidant- and immune-related physiological parameters in the livers and intestines of juvenile largemouth bass under transport stress. Superoxide dismutase, SOD; malondialdehyde, MDA; lysozyme, LZM (**A**) liver SOD; (**B**) liver MDA; (**C**) liver LZM; (**D**) liver complement C3; (**E**) intestinal SOD; (**F**) intestinal MDA. T0h: transport stress at 0 h; T6h: transport stress at 6 h; T12h: transport stress at 12 h; R5d: recovery for 5 d. **: significant difference between the control and treatment groups (paired samples *t*-test, **: $p < 0.01$). Lowercase letters indicate significant differences ($p < 0.05$) between treatments (Duncan's multiple-range test).

3.4. Transport Stress Effects on the Gut Microbiome

To investigate the effects of transport stress and recovery on the gut microbiomes of juvenile largemouth bass, the gut microbiomes of the control, 12 h transport stress and 5 d recovery groups were analyzed. High-throughput sequencing yielded 3207 characteristic data points of which 157 were shared by the three groups. The recovery group had the least characteristic data (Figure 4A). Alpha diversity indexes (i.e., observed species, Shannon, Simpson, and Chao1 indexes) were used to assess the richness and evenness of the intestinal microbiotas (Figure 4B), which did not significantly differ among the groups ($p > 0.05$).

Principal coordinates analysis based on weighted and unweighted UniFrac distances was used to describe the beta diversity of the intestinal flora to quantify the microbial community compositions in each group (Figure 4C). The samples in each group were clustered together. The distance between the control and treatment groups was long, and the overlap between the 12 h transport and recovery groups was large.

The gut microbiome compositions of the juvenile largemouth bass were analyzed at the phylum and genus levels. At the phylum level (Figure 5A), Proteobacteria, Firmicutes, Cyanobacteria and Spirochaetes were predominant. The box plots describe their abundance changes (Figure 5B). The Proteobacteria abundance increased significantly after transport stress ($p < 0.05$), with no significant difference between the 12 h transport and recovery groups. Firmicutes increased in abundance after transport stress, but did not significantly differ among the groups. The relative abundances of Cyanobacteria and Spirochetes

were higher in the control group, but decreased significantly after 12 h of transport stress ($p < 0.05$). The abundance was maintained in the recovery group.

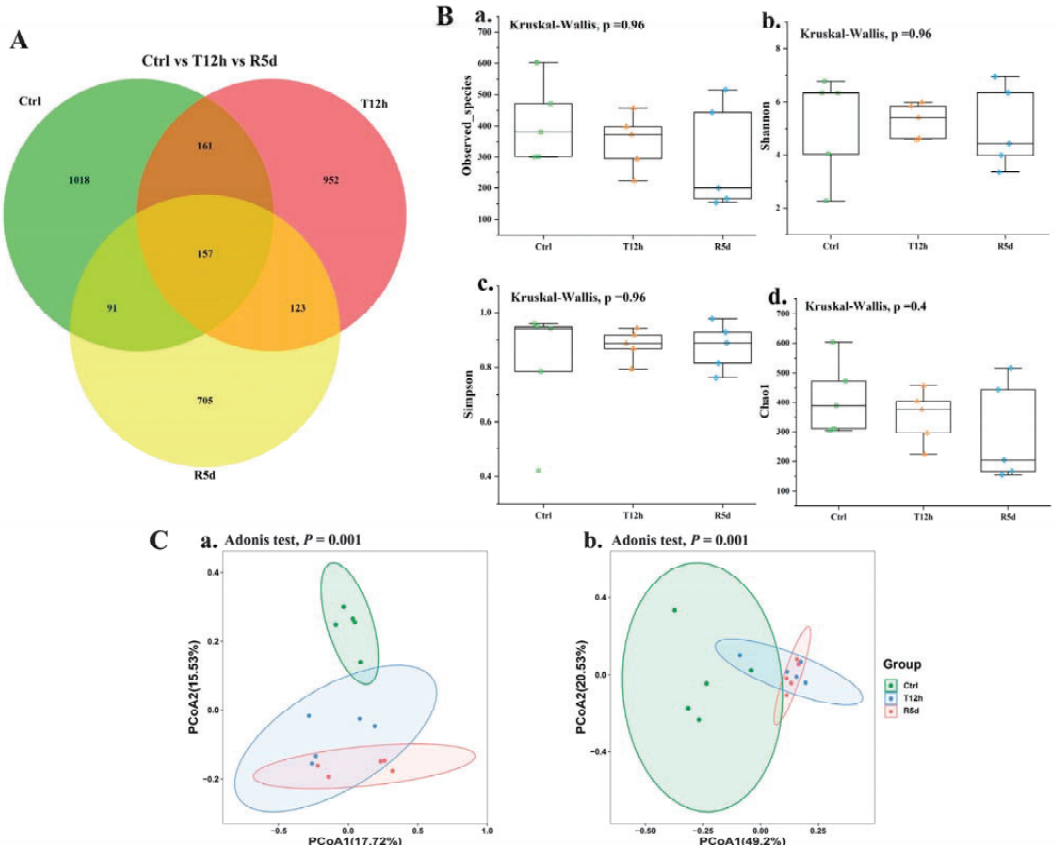

Figure 4. (**A**) Common and unique operational taxonomic units (OTUs) displayed by Venn diagram in the control, 12 h transport and recovery groups. The overlap indicates shared OTUs (**B**) and alpha and beta diversity of the gut microbiomes of juvenile largemouth bass under transport stress. Measures of alpha diversity included: (**a**) Observed species; (**b**) Shannon index; (**c**) Simpson index; (**d**) Chao1 index. (**C**) Beta diversity analysis based on principal coordinates analysis of unweighted UniFrac (**a**) and weighted UniFrac (**b**) distances. Ctrl: control group; T12h: transport stress for 12 h; R5d: recovery for 5 d.

Linear discriminant analysis results (Figure 6A,B) showed significant differences in the abundances of *Plesiomonas*, *Cyanobium_PCC_6307*, *Firmicutes_unclassified*, *Brevinema Clostridium_sensu_stricto_1* and *Cetobacterium*. The *Plesiomonas* abundance increased significantly after transport stress, and was maintained in the recovery group (Figure 6(Ca)). The relative abundances of *Cyanobium_PCC_6307* and *Brevinema* were significantly higher in the control group than in the 12 h transport stress and 5 d recovery groups (Figure 6(Cb,Cd); $p < 0.05$). The relative abundances of *Clostridium_sensu_stricto_1* and *Firmicutes_unclassified* were significantly higher in the 5 d recovery group than in the control and 12 h transport groups (Figure 6(Cc,Cf); $p < 0.05$). The relative abundance of *Cetobacterium* was significantly higher in the 12 h transport group than in the control group but was similar to that of the recovery group (Figure 6(Ce)).

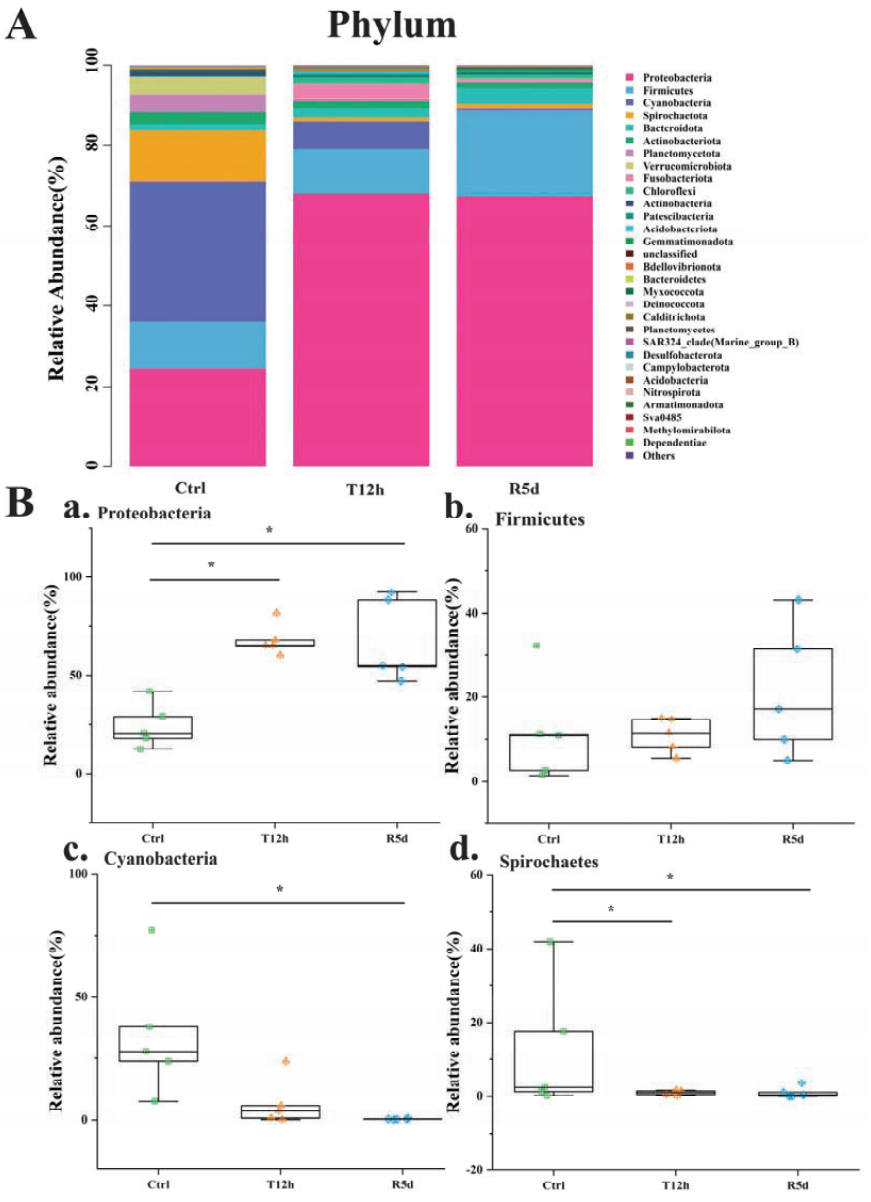

Figure 5. (**A**) Relative abundances of dominant phylum-level taxa in the control (Ctrl), 12 h transport (T12h) and recovery (R5d) groups. Species with lower abundances were classified as "others". (**B**) Relative abundances of the dominant phylum-level bacteria (**a**–**d**) in the Ctrl, T12h and R5d groups. * significant difference between the control and treatment groups (Kruskal-Wallis H test, *: $p < 0.05$).

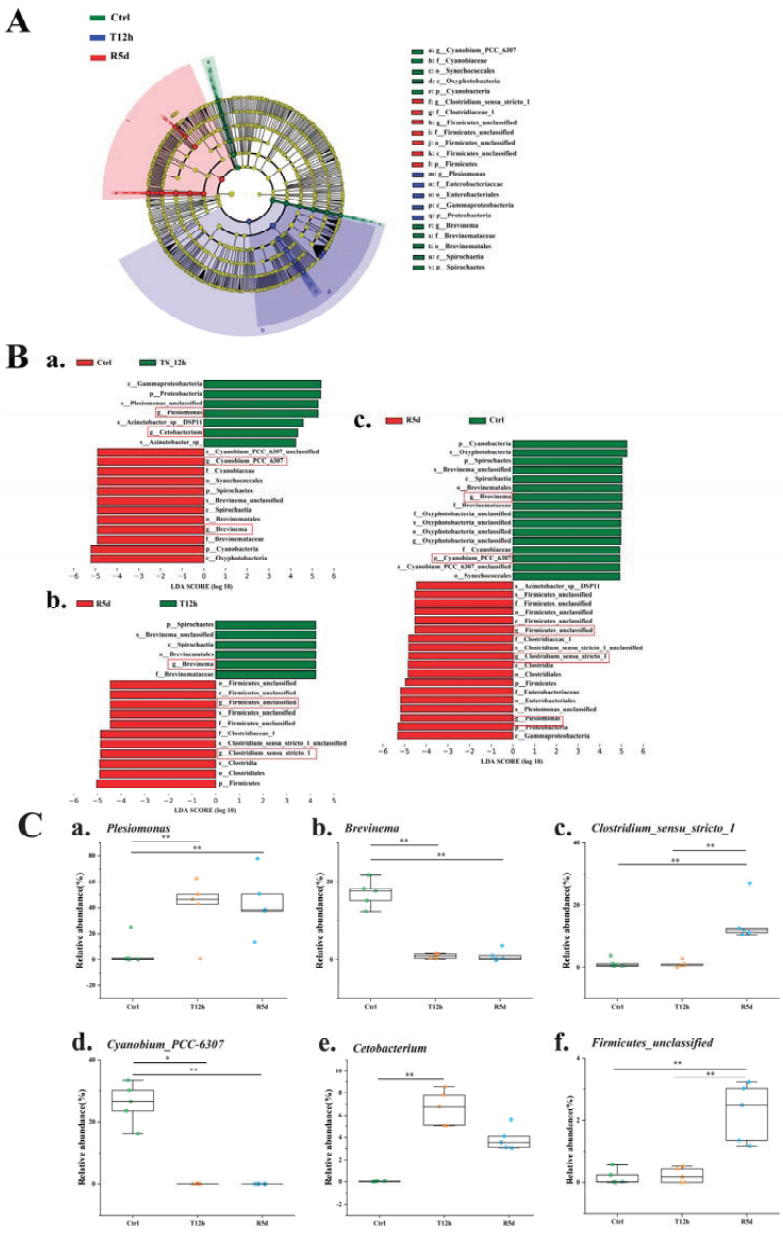

Figure 6. Linear discriminant analysis effect size (LEfSe) analysis comparing abundances of bacterial taxa in the control (Ctrl), 12 h transport (T12h) and recovery (R5d) groups. The LDA score >4. (**A**) Cladogram based on LEfSe analysis. Green, blue and red represent taxa enriched in the Ctrl, T12h and R5d groups. (**B**) Bacterial taxa with different abundances among groups. (**a**) Ctrl vs. T12h, (**b**) Ctrl vs. R5d, (**c**) T12h vs. R5, and (**d**) by Kruskal–Wallis test. (**C**) Relative abundances of dominant bacteria at the genus level (**a**–**f**) in the Ctrl, T12h and R5d groups. *, **: significant differences between the control and treatment groups (Kruskal–Wallis H test, *: $p < 0.05$, **: $p < 0.01$).

Bacteria with significant changes in abundance were used to analyze the correlations with intestinal SOD, MDA, villus length and muscle layer thickness. The measured in-

testinal parameters were strongly correlated with the gut microbiome at the genus level (Figure 7A). The MDA content was correlated with all bacterial genera, the intestinal villus length and muscle layer thickness were correlated with five genera, and the SOD content was correlated with four genera.

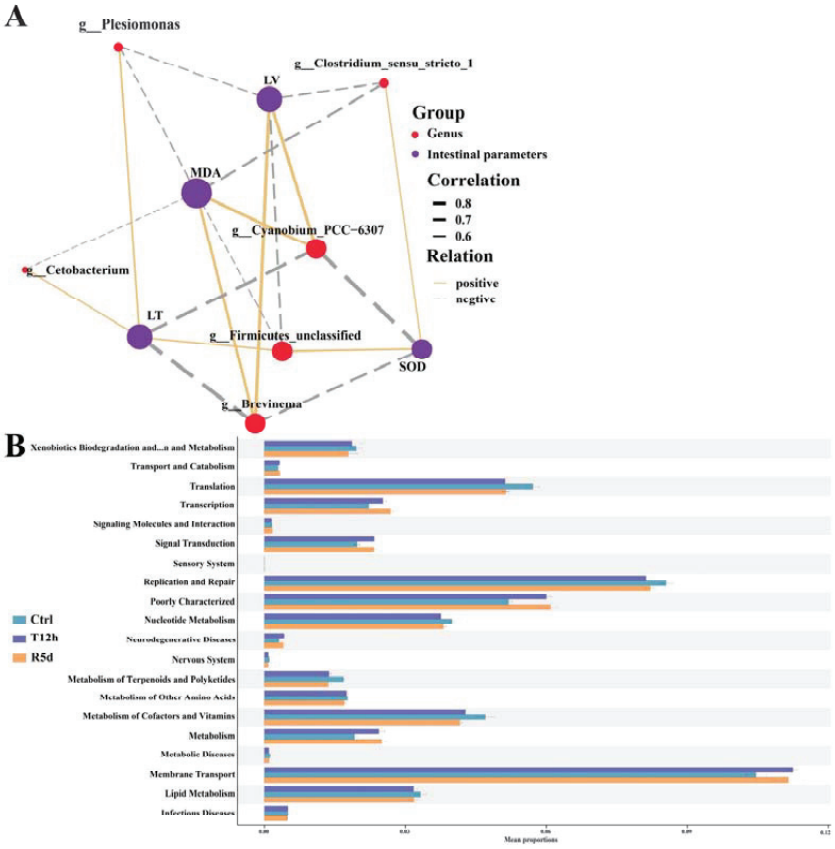

Figure 7. (**A**) Correlation network showing connections between gut microbial genera and intestinal parameters. Line thickness indicates the magnitude of the correlation. LV: intestinal villus length; LT: muscular thickness. (**B**) Functional analysis of the gut microbiota predicted at Level 2 for the control, 12 h transport and recovery groups.

KEGG functional analysis showed that that gut microbiome was mostly enriched in membrane transport, replication and repair, and translation (Figure 7B). Compared with the control group, fewer gut microbes were involved in replication and repair and translation, and more functional bacteria were involved in membrane transport in the 12 h transport and 5 d recovery groups.

4. Discussion

4.1. Water Quality Parameters during Transport Stress

Many factors, such as water quality changes, fish body bruising, starvation and so on, may cause transport stress during fish transportation. The total ammonia-nitrogen, nitrite-nitrogen and oxygen concentrations are the important factors causing transport stress in fish [1]. Studies have shown that increased ammonia-nitrogen concentrations can destroy the osmotic pressure balance and cause oxidative stress [3], while increased nitrite-nitrogen

concentrations can poison fish and inhibit nonspecific immunity [23]. In this experiment, while the ammonia-nitrogen and nitrite-nitrogen concentrations increased significantly (ammonia-nitrogen concentrations from 0.01 ± 0.00 mg/L to 0.72 ± 0.09 mg/L and nitrite-nitrogen concentrations from 0.01 ± 0.00 mg/L to 0.13 ± 0.02 mg/L) as the transport time increased, the detected N levels were still ~20-fold below those considered to be harmful to wild fish [24]. Even so, elevated aquatic N levels may have increased the transport stress incurred by the largemouth bass, possibly owing to increases in fish metabolites. This variation tendency is consistent with previous studies [6,7]. Increased ammonia-nitrogen and nitrite concentrations during transport stress have been shown to cause oxidative stress responses in channel catfish and nonspecifically damage hybrid yellow catfish [4,7]. This may be due to the increased ammonia-nitrite concentration accelerating reactive oxygen species (ROS) production, thus causing oxidative stress during transport. Additionally, deteriorated water quality can cause pathogen proliferation and damage nonspecific immunity among largemouth bass. In our study, the oxygen concentration (about 20 mg/L) remained relatively stable but four times higher than the control group under transport stress, possibly because the transport bags contained two-thirds oxygen, which caused hyperoxia to fish. Rainbow trout exposed to intermittent hyperoxia showed significant oxidative stress [25]. Hyperoxia results in transient oxidative stress and alters antioxidant enzymes in goldfish [26]. Tristan et al. [27] believe that hyperoxia can affect the level of ROS in fish and give rise to oxidative stress. So, hyperoxia may be one of the reasons for the changes in the antioxidant enzyme activities in this study.

4.2. Effects of Transport Stress on Liver and Intestinal Structure in Juvenile Largemouth Bass

The liver is involved in the synthesis and decomposition of various substances in fish. Vacuolation, edema and necrosis of liver cells are all signs of damage to fish livers under environmental stress [28]. Safahieh et al. [29] believe that liver cell vacuolization indicates degeneration before cell necrosis. In this study, as the transport stress increased, the liver cell volume and number of vacuoles increased, possibly related to energy metabolism increases in largemouth bass to maintain homeostasis during transport, resulting in an altered liver glycogen content, leading to liver cell vacuolization [30]. Severe vacuolization in the liver tissue persisted even after the 5-day recovery, indicating that the liver damage caused by transport stress could not be recovered within 5 days.

Villus length, villus width and muscle thickness enable evaluating the intestinal health of fish [31]. In this experiment, the intestinal villus length was significantly shortened after transport stress, suggesting intestinal damage and likely affected nutrient digestion and absorption in juvenile largemouth bass [32]. Additionally, transport stress significantly increased the intestinal muscle layer thickness, possibly because it induced intestinal inflammation. Studies have shown that the shortened intestinal villus length and altered muscle layer thickness may be related to intestinal inflammation [31,33].

4.3. Effects of Transport Stress and Recovery on Antioxidant and Immune Enzyme Activities in Juvenile Largemouth Bass

SOD is cells' first-line defense against toxic free radicals can remove excessive ROS in fish [34]. In this study, the SOD activity increased significantly under transport stress, likely due to the increased ammonia-nitrogen and nitrite concentrations and the long crowding conditions, leading to excessive ROS production in transported fish [35]. Meanwhile, the hyperoxia environment also could be the underlying cause for enzyme activity changes or increased levels of ROS [27]. ROS are harmful substances produced by metabolic activities in fish, which can cause oxidative stress. Increased SOD activity accelerates ROS removal. Additionally, increased activity of SOD may be related to the accelerated generation of ROS. A study on hybrid snapper also showed that SOD activity increases under transport stress [6]. Free radicals and ROS can damage fish livers [36] by damaging the liver cell biofilm through lipid peroxidation (LPO), resulting in liver cell damage [37]. Oxidative stress caused by transport stress may have been one reason for the liver damage in this

study. Biofilm oxidation by ROS leads to LPO, and MDA, the final product of LPO, is an important indicator of antioxidant capacity in fish [6]. Previous studies have shown that oxidative stress caused by transport stress significantly increased MDA contents in fish [2,6], and the significant increase in MDA content after 6 h of transport stress indicated oxidative stress caused by transportation. However, the MDA content decreased significantly in the 12 h transport group, possibly owing to accelerated MDA metabolism under high-oxygen conditions (dissolved oxygen >20 mg/L). Fish can regulate enzymatic and nonenzymatic antioxidant defense systems to accelerate MDA clearance under hyperoxic conditions [38]. Additionally, oxidative stress can reduce polyunsaturated fatty acid contents by damaging cell membrane structures, which can be oxidized and produce MDA, thus reducing MDA concentrations [39].

The lysozyme activity and complement C3 concentration increased significantly after transport stress. Lysozyme is an important component of fish's nonspecific immunity and can lyse bacterial cell walls and effectively resist pathogen invasion [9,40]. Complement comprises the plasma protein family and is the core component of innate immunity [41]. Complement C3 helps fish recognize invading microorganisms, mark damaged host cells, and help phagocytes eliminate pathogenic bacteria and damaged cells [42]. Under environmental stress, fish activate homeostatic regulatory mechanisms to affect the body's immune response [43]. The increased lysozyme and complement C3 activity indicate an enhanced immune response in fish. Transport stress experiments with *Pelteobagrus fulvidraco* and *Piaractus mesopotamicus* showed increased lysozyme and complement C3 contents [7,44], possibly because the transport stress impaired part of the immune capacity of the largemouth bass, combined with the deteriorated water quality accelerating pathogen proliferation, which exacerbated bacterial infection in the fish, thus activating the lysozyme and complement C3.

The lysozyme and complement C3 activities were significantly higher in the recovery group than in the 0 h transport group. Studies on transport stress in *Lateolabrax maculatus* and *Piaractus mesopotamicus* have also reported this phenomenon [42,43], possibly due to the susceptibility of the fish after transport stress, sustaining the immune response. There is a study that shows that transport stress can damage the immune system of transported fish [44], making them vulnerable to bacterial infection. Studies have shown that pathogen infection often leads to excessive ROS production in animals [45], resulting in oxidative stress, which may be why the SOD activity in the recovery group was significantly higher than that of the 12 h transport stress without recovery. Therefore, we suspect that the infectibility of the largemouth bass after transportation caused their inability to recover.

4.4. Effects of Transport Stress on Gut Microbial Diversity and Structure in Juvenile Largemouth Bass

In this experiment, alpha diversity did not significantly differ among the groups, possibly owing to individual factors in largemouth bass. Yan et al. [46] suggested that the influence of the fish itself on its gut microbiome was much greater than that of the environment. Sullam et al. [47] studied *Poecilia reticulata* and proposed that its core flora was strongly correlated with the host genotype, which does not easily fluctuate when affected by the external environment. Largemouth bass are carnivorous; their gut microbiome may be stable even with different treatments, and no significant differences were noted in their gut microbiome alpha diversity [48,49]. Therefore, largemouth bass gut microbiomes may be associated with their own genes, and their alpha diversity is not significantly altered under transport stress. However, significant differences were observed in beta diversity, suggesting that transport stress did not alter the gut microbial richness or evenness but significantly affected the gut microbial composition and distribution in juvenile largemouth bass. Changing community structures can easily cause abnormal host physiological functions [50], thus affecting nutrient digestion and absorption [51]. Additionally, correlation analysis results showed a significant correlation between gut microbes at the genus level

and the measured intestinal parameters; however, the connection between these bacteria and intestinal parameters during transport stress requires further study.

Gut microbes perform diverse functions within the host's gut and are closely related to host health [50]. Proteobacteria are the largest branch of prokaryotes and include pathogens such as *Escherichia coli*, *Salmonella*, *Vibrio*, and *Helicobacter pylori* [52]. Increased numbers of Proteobacteria are a potential marker of fish infection [53]. In this study, the Proteobacteria abundance increased markedly after transport stress, which may have increased the susceptibility to infectious diseases in juvenile largemouth bass. *Plesiomonas*, the dominant genus in this study, is a Gram-negative bacterium of the Enterobacteriaceae family. *Shigella* is also related to outbreaks of fish disease [54]. We found that the abundance of *Plesiomonas* in the 12 h transport group was significantly higher than that of the control group, which might indicate the infectivity of juvenile largemouth bass after transport stress. Therefore, juvenile largemouth bass may be more susceptible to disease after long-distance transportation. The high abundance of Proteobacteria in the 5 d recovery group showed that largemouth bass remained susceptible to bacteria after 5 days, which is consistent with the results for the antioxidant and immune enzyme activities. KEGG functional analysis showed that few gut microbes were enriched in metabolic diseases; therefore, we suspect that increased abundances of Proteobacteria may be a marker of susceptibility to infection in juvenile largemouth bass and that Proteobacteria are not directly pathogenic to largemouth bass.

Firmicutes play roles in physiological processes such as polysaccharide degradation [52,55]. Smriga et al. [56] found that Firmicutes played a role in host digestion. Studies have shown that Firmicutes are related to lipid metabolism in animals [57] and can accelerate the metabolism of the precursor of MDA: total polyunsaturated fatty acids, which might decrease MDA contents. Firmicutes abundances did not significantly differ among groups. However, the abundances of *Clostridium_sensu_stricto_1* and *Firmicutes_unclassified* were significantly increased under transport stress. Therefore, transport stress likely significantly affected only some Firmicutes. *Clostridium* can enhance glucose metabolism, promote fish growth [58], and increase energy metabolism levels in fish. Changes in the ammonia-nitrogen concentration between transportation and recovery can activate osmotic mechanisms and activate osmotic regulation [59]. KEGG functional analysis also showed that intestinal microorganisms were mainly enriched in membrane transport, which may enhance energy metabolism after transport. This may have increased the abundances of *Clostridium_sensu_stricto_1* and *Firmicutes_unclassified*. When more energy is used to defend against pathogens and regulate the osmotic balance, glucose metabolism occurs via glycolysis under hormone regulation, resulting in large amounts of liver glycogen being stored in the liver and may, therefore, lead to liver cell swelling and vacuolization [28,60].

In this study, the Spirochetes abundance was significantly higher in the control group than in the 12 h transport and 5 d recovery groups. Spirochetes are endosymbionts with some arthropods and mollusks and participate in lignocellulose decomposition and nitrogen fixation in termite intestines [61]. Spirochetes may play roles in host nutrient metabolism [62], and decreased Spirochetes abundances may indicate physiological damage in largemouth bass. Cyanophyta is a primitive green autotrophic plant group, and its physiological functions remain unclear. It can pass into the gut combined with feed, and showed high abundance in the control group. It may be passed out of the gut with the increase in fasting time. Whether Cyanophyta plays a role in antioxidant and physiological immune functions in largemouth bass requires further study. It is worth noting that Cyanophyta abundance was markedly lower in the 5 d recovery groups than in the control group, which may arise from a vitality decrease and eating less after transport stress.

5. Conclusions

Deterioration of water quality caused by transport stress can cause oxidative stress and activate immune responses in largemouth bass. Changes in the intestinal microbial community revealed that the gut microbiotas of largemouth bass are involved in adaptation

to transport stress. These variations manifested as changes in the liver and intestinal structure. Additionally, juvenile largemouth bass required more than 5 days to recover after 12 h of transportation due to increased infection susceptibility. These results may provide a theoretical basis and support for clarifying the transport stress-induced oxidative and immune mechanisms of juvenile largemouth bass.

Author Contributions: Conceptualization, Q.W., W.Y., Y.T. and J.Q.; methodology, Q.W., W.Y., Y.T. and J.Q.; software, Q.W.; validation, Q.W.; formal analysis, Q.W., Y.T. and J.Q.; investigation, Q.W. and Y.L.; resources, J.Q.; data curation, J.Q.; writing—original draft preparation, Q.W.; writing—review and editing, Q.W.; visualization, Q.W. and W.Y.; supervision, P.X. and S.L.; project administration, J.Q.; funding acquisition, J.Q. All authors have read and agreed to the published version of the manuscript.

Funding: This research was funded by the Project of Seed Industry Revitalization in Jiangsu Province, China (Grant No. JBGS [2021] 130) and the Suzhou Science and Technology Project (Grant No. SNG2021009).

Institutional Review Board Statement: All experiments in this study were approved by the Bioethical Committee of the Freshwater Fisheries Research Center, Chinese Academy of Fishery Sciences (2013863BCE). Experiments were conducted according to the Guidelines for the Care and Use of Laboratory Animals in China.

Informed Consent Statement: Not applicable.

Data Availability Statement: The 16S rRNA datasets are under accession number PRJNA853451. The raw data supporting the conclusions of this article will be made available by the authors without undue reservation. Requests to access these datasets should be directed to qiangj@ffrc.cn.

Acknowledgments: We thank Jennifer Smith, and Traci Raley, from Liwen Bianji (Edanz) (www.liwenbianji.cn/) for editing the English text of drafts of this manuscript.

Conflicts of Interest: The authors declare no conflict of interest.

References

1. Dhanasiri, A.K.S.; Kiron, V.; Fernandes, J.M.O.; Bergh, Ø.; Powell, M.D. Novel application of nitrifying bacterial consortia to ease ammonia toxicity in ornamental fish transport units: Trials with zebrafish. *J. Appl. Microbiol.* **2011**, *111*, 278–292. [CrossRef] [PubMed]
2. Refaey, M.M.; Li, D. Transport stress changes blood biochemistry, antioxidant defense system, and hepatic HSPs mRNA expressions of channel catfish ictalurus punctatus. *Front. Physiol.* **2018**, *9*, 01628. [CrossRef] [PubMed]
3. Lushchak, V.I. Environmentally induced oxidative stress in aquatic animals. *Aquat. Toxicol.* **2006**, *101*, 13–30. [CrossRef]
4. Sun, H.; Wang, W.; Li, J.; Yang, Z. Growth oxidative stress responses, and gene transcription of juvenile bighead carp (*Hypophthalmichthys nobilis*) under chronic-term exposure of ammonia. *Environ. Toxicol. Chem.* **2014**, *33*, 1726–1731. [CrossRef] [PubMed]
5. Wang, J.; Xiong, G.; Bai, C.; Liao, T. Anesthetic efficacy of two plant phenolics and the physiological response of juvenile *Ictalurus punctatus* to simulated transport. *Aquaculture* **2021**, *538*, 736566. [CrossRef]
6. Qiang, J.; Zhang, Z.; Yu, J.; Xu, J.; Liu, H.; Zhang, Z.; Xu, P. Water quality and physiological response of F1hybrid seabream (*Pagrus major* female × *Acanthopagrus schlegelii* male) to transport stress at different densities. *Aquac. Res.* **2017**, *49*, 767–775. [CrossRef]
7. Zheng, T.; Song, Z.; Qiang, J.; Tao, Y.; Zhu, H.; Ma, J.; Xu, P. Transport Stress Induces Skin Innate Immunity Response in Hybrid Yellow Catfish (*Tachysurus fulvidraco* female × *P. vachellii* male) Through TLR/NLR Signaling Pathways and Regulation of Mucus Secretion. *Front. Immunol.* **2021**, *12*, 740359. [CrossRef]
8. Zheng, T.; Song, Z.; Tao, Y.; Qiang, J.; Ma, J.; Lu, S.; Xu, P. Transport stress induces innate immunity responses through TLR and NLR signaling pathways and increases mucus cell number in gills of hybrid yellow catfish (*Tachysurus fulvidraco* ♀× *Pseudobagrus vachellii* ♂). *Fish Shellfish Immunol.* **2022**, *127*, 166–175. [CrossRef]
9. Wu, Y.; You, X.; Sun, W.; Xiong, G.; Shi, L.; Qiao, Y.; Wu, W.; Li, X.; Wang, J.; Ding, A.; et al. Insight into acute heat stress on meat qualities of rainbow trout (*Oncorhynchus mykiss*) during short-time transportation. *Aquaculture* **2021**, *543*, 737013. [CrossRef]
10. Zhang, R.; Jiang, Y.; Liu, W.; Zhou, Y. Evaluation of zinc-bearing palygorskite effects on the growth, immunity, antioxidant capability, and resistance to transport stress in blunt snout bream (*Megalobrama amblycephala*). *Aquaculture* **2021**, *532*, 735963. [CrossRef]
11. Chen, C.; Li, P.; Liu, L.; Li, Z. Exploring the interactions between the gut microbiome and the shifting surrounding aquatic environment in fisheries and aquaculture: A review. *Environ. Res.* **2022**, *214*, 114202. [CrossRef] [PubMed]
12. Björkstén, B. The gut microbiota: A complex ecosystem. *Clin. Exp. Allergy* **2006**, *36*, 1215–1217. [CrossRef] [PubMed]
13. Bagi, A.; Riiser, E.; Molland, H.; Star, B.; Haverkamp, T.; Sydnes, M.; Pampanin, D. Gastrointestinal microbial community changes in Atlantic cod (*Gadus morhua*) exposed to crude oil. *BMC Microbiol.* **2018**, *18*, 25. [CrossRef]
14. Du, F.; Li, Y.; Tang, Y.; Su, S.; Yu, J.; Yu, F.; Li, J.; Li, H.; Wang, M.; Xu, P. Response of the gut microbiome of *Megalobrama amblycephala* to crowding stress. *Aquaculture* **2019**, *500*, 586–596. [CrossRef]

15. Jiang, L.; Feng, J.; Ying, R.; Yin, F.; Pei, S.; Lu, J.; Cao, Y.; Guo, J.; Li, Z. Individual and combined effects of ammonia-N and sulfide on the immune function and intestinal microbiota of Pacific white shrimp *Litopenaeus vannamei*. *Fish Shellfish Immunol.* **2019**, *92*, 230–240. [CrossRef]
16. Zheng, T.; Tao, Y.; Lu, S.; Qiang, J.; Xu, P. Integrated Transcriptome and 16S rDNA Analyses Reveal That Transport Stress Induces Oxidative Stress and Immune and Metabolic Disorders in the Intestine of Hybrid Yellow Catfish (*Tachysurus fulvidraco*♀× *Pseudobagrus vachelliii*♂). *Antioxidants* **2022**, *11*, 1737. [CrossRef]
17. Ouyang, J.; Zhu, Y.; Hao, W.; Wang, X.; Yang, H.; Deng, X.; Feng, T.; Huang, Y.; Yu, H.; Wang, Y. Three naturally occurring host defense peptides protect largemouth bass (*Micropterus salmoides*) against bacterial infections. *Aquaculture* **2022**, *546*, 737383. [CrossRef]
18. Middaugh, C.R.; Alfermann, T.; Strickland, P.A.; Nguyen, P. A regional evaluation of suwannee bass and largemouth bass exploitation in north florida rivers. *N. Am. J. Fsih Manag.* **2016**, *35*, 958–963. [CrossRef]
19. Lee, Y.; Wada, S.; Kurata, O. Cellular inflammatory response on marbled rockfish Sebastiscus marmoratus experimentally infected with *Ochroconis humicola*. *Fish Shellfish Immunol.* **2019**, *91*, 419. [CrossRef]
20. Hu, Y.; Yu, J.; Cui, X.; Zhang, Z.; Li, Q.; Guo, W.; Zhao, C.; Chen, X.; Meng, M.; Li, Y.; et al. Combination usage of AdipoCount and Image-Pro Plus/ImageJ software for quantification of adipocyte sizes. *Front. Endocrinol.* **2021**, *12*, 642000. [CrossRef]
21. François, T.; Simon, M.D.; Maéva, B.; Nolwen, L.D.; Gwenn, T.; Catherine, L.; Angélique, G. Evaluation of a new primer combination to minimize plastid contamination in 16S rDNA metabarcoding analyses of alga-associated bacterial communities. *Environ. Microbiol. Rep.* **2020**, *12*, 30–37.
22. R Core Team. *R: A Language and Environment for Statistical Computing*; R Foundation for Statistical Computing: Vienna, Austria, 2016; Available online: https://www.R-project.org/ (accessed on 7 November 2022).
23. Helen, E.R.; Brian, P.; Weber, E.S. Bacterial and parasitic diseases of pet fish. *Vet. Clin. N. Am. Exot. Anim. Pract.* **2009**, *12*, 609–638.
24. Nordin, R.N. Water Quality Guidelines for Nitrogen (Nitrate, Nitrite, and Ammonia). Available online: https://www2.gov.bc.ca/assets/gov/environment/air-land-water/water/waterquality/water-quality-guidelines/approved-wqgs/bc_env_nitrate_waterqualityguideline_overview.pdf (accessed on 14 October 2009).
25. Kalinowski, C.T.; Larroquet, L.; Véron, V.; Robaina, L.; Izquierdo, M.S.; Panserat, S.; Kaushik, S.; Fontagné-Dicharry, S. Influence of dietary astaxanthin on the hepatic oxidative stress response caused by episodic hyperoxia in rainbow trout. *Antioxidants* **2019**, *8*, 626. [CrossRef] [PubMed]
26. Volodymyr, I.L.; Tetyana, V.B.; Victor, V.H.; Lidiya, I.L.; Oleh, V.L.; Kenneth, B.S. Hyperoxia results in transient oxidative stress and an adaptive response by antioxidant enzymes in goldfish tissues. *Int. J. Biochem. Cell B* **2005**, *37*, 1670–1680.
27. Tristan, J.M.; Erik, S.; Neill, A.H. Fish and hyperoxia—From cardiorespiratory and biochemical adjustments to aquaculture and ecophysiology implications. *Fish Fish.* **2021**, *22*, 324–355.
28. Hargreaves, J.A.; Kucuk, S. Effects of diel un-ionized ammonia fluctuation on juvenile hybrid striped bass, channel catfish, and blue tilapia. *Aquaculture* **2001**, *195*, 163–181. [CrossRef]
29. Safahieh, A.; Hedayati, A.; Savari, A.; Movahedinia, A. Effect of sublethal dose of mercury toxicity on liver cells and tissue of yellowfin seabream. *Toxicol. Ind. Health* **2012**, *10*, 583–592. [CrossRef]
30. Chang, C.; Huang, J.; Yeh, C.; Tang, C.; Hwang, L.; Lee, T. Salinity effects on strategies of glycogen utilization in livers of euryhaline milkfish (*Chanos chanos*) under hypothermal stress. *Front. Physiol.* **2018**, *9*, 00081. [CrossRef]
31. Li, X.; Rahimnejad, S.; Wang, L.; Lu, K.; Song, K.; Zhang, C. Substituting fish meal with housefly (*Musca domestica*) maggot meal in diets for bullfrog Rana (Lithobates) catesbeiana: Effects on growth, digestive enzymes activity, antioxidant capacity and gut health. *Aquaculture* **2019**, *499*, 295–305. [CrossRef]
32. Yu, L.; Wen, H.; Jiang, M.; Wu, F.; Tian, J.; Lu, X.; Xiao, J.; Liu, W. Effects of ferulic acid on intestinal enzyme activities, morphology, microbiome composition of genetically improved farmed tilapia (*Oreochromis niloticus*) fed oxidized fish oil. *Aquaculture* **2020**, *528*, 735543. [CrossRef]
33. Zhang, C.; Rahimnejad, S.; Wang, Y.R.; Lu, K.; Kai, S.; Ling, W.; Mai, K. Substituting fish meal with soybean meal in diets for Japanese seabass (*Lateolabrax japonicus*): Effects on growth, digestive enzymes activity, gut histology, and expression of gut inflammatory and transporter genes. *Aquaculture* **2018**, *483*, 173–182. [CrossRef]
34. Qiang, J.; Tao, Y.; He, J.; Xu, P.; Bao, J.; Sun, Y. miR-122 promotes hepatic antioxidant defense of genetically improved farmed tilapia (GIFT, *Oreochromis niloticus*) exposed to cadmium by directly targeting a metallothionein gene. *Aquat. Toxicol.* **2017**, *182*, 39–48. [CrossRef] [PubMed]
35. Volodymyr, I.L.; Tetyana, V.B. Temperature increase results in oxidative stress in goldfish tissues. 1. Indices of oxidative stress. *Comp. Biochem. Phys. C* **2006**, *143*, 30–35.
36. Lin, S.Y.; Xu, D.; Du, X.X.; Ran, C.L.; Xu, L.; Ren, S.J.; Tang, Z.T.; Yin, L.Z.; He, C.L.; Yuan, Z.X.; et al. Protective Effects of Salidroside against Carbon Tetrachloride (CCl_4)-Induced Liver Injury by Initiating Mitochondria to Resist Oxidative Stress in Mice. *Int. J. Mol. Sci.* **2019**, *20*, 3187. [CrossRef] [PubMed]
37. Du, J.; Cao, L.; Jia, R.; Gu, Z.; He, Q.; Xu, P.; Galina, J.; Ma, Y.; Yin, G. Analysis of Streptococcus agalactiae-induced liver injury in tilapia (*Oreochromis niloticus*). *Aquac. Res.* **2020**, *51*, 1398–1405. [CrossRef]
38. Wu, S.; Tseng, Y.; Lin, J.; Bonnie, S.P. Mitigation of stress and water deterioration with a root extract of Glycine tomentella during simulated transport of orange-spotted grouper (*Epinephelus coioides*). *Aquaculture* **2020**, *514*, 734485. [CrossRef]
39. Dong, W.; Sun, H.; Zhang, Y.; Lin, H.; Chen, J.; Hong, H. Impact on growth, oxidative stress, and apoptosis-related gene transcription of zebrafish after exposure to low concentration of arsenite. *Chemosphere* **2018**, *211*, 648–652. [CrossRef]

40. Saurabh, S.; Sahoo, P.K. Lysozyme: An important defence molecule of fish innate immune system. *Aquac. Res.* **2008**, *39*, 223–239. [CrossRef]
41. Chen, D.; Li, J.; Yao, Y.; Zhang, Y. Aeromonas hydrophila suppresses complement pathways via degradation of complement C3 in bony fish by metalloprotease. *Fish Shellfish Immun.* **2019**, *94*, 739–745. [CrossRef]
42. Fábio, S.Z.; Rafael, E.S.; Luz, N.F.M.; Gisele, F.; Elisabeth, C.U. Aloe vera enhances the innate immune response of pacu (*Piaractus mesopotamicus*) after transport stress and combined heat killed *Aeromonas hydrophila* infection. *Fish Shellfish Immun.* **2017**, *65*, 198–205.
43. Wang, Q.; Mei, J.; Cao, J.; Xie, J. Effects of Melissa officinalis L. Essential Oil in Comparison with Anaesthetics on Gill Tissue Damage, Liver Metabolism and Immune Parameters in Sea Bass (*Lateolabrax maculatus*) during Simulated Live Transport. *Biology* **2022**, *11*, 11. [CrossRef] [PubMed]
44. Tan, J.; Sun, X.; Gao, F.; Sun, H.; Chen, A.; Gai, C.; Yan, J. Immune responses of the sea cucumber *Apostichopus japonicus* to stress in two different transport systems. *Aquac. Res.* **2016**, *47*, 2114–2122. [CrossRef]
45. Deng, S.; Yu, K.; Wu, Q.; Li, Y.; Zhang, X.; Zhang, B.; Liu, G.; Liu, Y.; Lia, Z. Interplay between oxidative stress and metabolism in signalling and disease. *Oxid. Med. Cell. Longev.* **2016**, *2016*, 9151290. [PubMed]
46. Yan, Q.; Li, J.; Yu, Y.; Wang, J.; He, Z.; Joy, D.V.N.; Megan, L.K.; Wu, L.; Wang, Y.; Liao, L.; et al. Environmental filtering decreases with fish development for the assembly of gut microbiota. *Environ. Microbiol.* **2016**, *18*, 4739–4754. [CrossRef]
47. Sullam, K.; Rubin, B.; Dalton, C.; Susan, S.K.; Alexander, S.F.; Jacob, A.R. Divergence across diet, time and populations rules out parallel evolution in the gut microbiomes of *Trinidadian guppies*. *ISME J.* **2015**, *9*, 1508–1522. [CrossRef]
48. Karolina, K.; Michal, W.; Samuel, P.; Frank, O.; Chrissy, C.; Lee, J.P. The effect of first feeding exposure of larval largemouth bass to a formulated soybean meal-based or soy saponin-supplemented diet on fish growth performance and gut microbiom. *N. Am. J. Aquacult.* **2021**, *83*, 312–326.
49. Wang, S.; Han, Z.; Turchini, G.M.; Wang, X.; Fang, Z.; Chen, N.; Xie, R.; Zhang, H.; Li, S. Effects of dietary phospholipids on growth performance, digestive enzymes activity and intestinal health of largemouth bass (*Micropterus salmoides*) larvae. *Front. Immunol.* **2022**, *12*, 827946. [CrossRef]
50. Hassenrück, C.; Reinwald, H.; Kunzmann, A.; Tiedemann, I.; Gärdes, A. Effects of Thermal Stress on the Gut Microbiome of Juvenile Milkfish (*Chanos chanos*). *Microorganisms* **2021**, *9*, 5. [CrossRef]
51. Phillip, J.A.; Stephanie, D.G.; Xie, Y.; Abigail, D.; Alana, W.; Markus, B.; Vince, P.P.; Karsten, L.; Markus, H.; David, M.J.; et al. Effects of in situ experimental selenium exposure on finescale dace (*Phoxinus neogaeus*) gut microbiome. *Environ. Res.* **2022**, *212*, 113151.
52. Zhu, H.; Qiang, J.; Tao, Y.; Tlou, K.N.; Bao, J.; Chen, D.; Xu, P. Physiological and gut microbiome changes associated with low dietary protein level in genetically improved farmed tilapia (GIFT, *Oreochromis niloticus*) determined by 16S rRNA sequence analysis. *MicrobiologyOpen* **2020**, *9*, e1000. [CrossRef]
53. Shin, N.; Tae, W.W.; Bae, J. Proteobacteria: Microbial signature of dysbiosis in gut microbiota. *Trends Biotechnol.* **2015**, *33*, 496–503. [CrossRef] [PubMed]
54. Wang, H.; Gu, Y.; Zhou, H.; Chen, J.; Wang, M.; Jiang, H.; Cao, H. *Plesiomonas shigelloides*, a potential pathogen of enteritis in *Ictalurus punctatus*. *Isr. J. Aquacult.-Bamid.* **2020**, *72*, 1–11. [CrossRef]
55. Flint, H.J.; Bayer, E.A.; Rincon, M.T.; Lamed, R.; White, B.A. Polysaccharide utilization by gut bacteria: Potential for new insights from genomic analysis. *Nat. Rev. Microbiol.* **2008**, *6*, 121–131. [CrossRef] [PubMed]
56. Steven, S.; Stuart, A.S.; Farooq, A. Abundance, diversity, and activity of microbial assemblages associated with coral reef fish guts and feces. *FEMS Microbiol. Ecol.* **2010**, *73*, 31–42.
57. Bradlow, H.L. Obesity and the gut microbiome: Pathophysiological aspects. *Horm. Mol. Biol. Clin. Investig.* **2014**, *17*, 53–61. [CrossRef]
58. Larsen, A.M.; Mohammed, H.H.; Arias, C.R. Characterization of the gut microbiota of three commercially valuable warmwater fish species. *J. Appl. Microbiol.* **2014**, *116*, 1396–1404. [CrossRef]
59. Yang, W.; Xiang, F.; Sun, H.; Chen, Y.; Minter, E.; Yang, Z. Changes in the selected hematological parameters and gill Na+/K+ ATPase activity of juvenile crucian carp Carassius auratus during elevated ammonia exposure and the post-exposure recovery. *Biochem. Syst. Ecol.* **2010**, *38*, 557–562. [CrossRef]
60. Yang, Y.; Yu, W.; Lin, H.; Shu, H.; Huang, X.; Li, T.; Huang, Z.; Wang, P.; Huang, Q.; Xun, P. Effects of acute low salinity stress on the liver structure, physiology and biochemistry of juvenile Chinese sea bass (*Lateolabrax maculatus*). *Isr. J. Aquacult.-Bamid.* **2021**, *73*, 1–13. [CrossRef]
61. Yang, G.; Tao, Z.; Xiao, J.; Tu, G.; Kumar, V.; Wen, C. Characterization of the gastrointestinal microbiota in paddlefish (*Polyodon spathula*). *Aquac. Rep.* **2020**, *17*, 100402. [CrossRef]
62. van de Water, J.A.; Melkonian, R.; Junca, H.; Voolstra, C.R.; Reynaud, S.; Allemand, D.; Ferrier-Pagès, C. Spirochaetes dominate the microbial community associated with the red coral *Corallium rubrum* on a broad geographic scale. *Sci. Rep.* **2016**, *6*, 27277. [CrossRef] [PubMed]

antioxidants

MDPI

Article

Aflatoxin B1 Induced Oxidative Stress and Gut Microbiota Disorder to Increase the Infection of Cyprinid Herpesvirus 2 in Gibel Carp (*Carassius auratus gibelio*)

Mingyang Xue [1,†], Miao Fu [2,†], Mengwei Zhang [1,3], Chen Xu [1], Yan Meng [1], Nan Jiang [1], Yiqun Li [1], Wenzhi Liu [1], Yuding Fan [1] and Yong Zhou [1,*]

[1] Yangtze River Fisheries Research Institute, Chinese Academy of Fishery Sciences, Wuhan 430223, China
[2] Department of Ophthalmology, Renmin Hospital of Wuhan University, Wuhan 430060, China
[3] Department of Aquatic Animal Medicine, College of Fisheries, Huazhong Agricultural University, Wuhan 430070, China
* Correspondence: zhouy@yfi.ac.cn
† These authors contributed equally to this work.

Abstract: Aflatoxin contamination of food and water is a serious problem worldwide. This study investigated the defensive ability of gibel carp exposed to aflatoxin B1 (AFB1) by challenging it with cyprinid herpesvirus 2 (CyHV-2) infection. The data showed that AFB1 exposure significantly increased the mortality of CyHV-2-infected gibel carp, and enhanced the viral load in the fish liver, kidney, and spleen. The oxidative-antioxidant balance suggested that AFB1 induced severe oxidative stress, including increased reactive oxygen species (ROS) and malondialdehyde (MDA) levels in the AFB1 exposed group, and the reduced activity of superoxide dismutase (SOD), glutathione-S-transferase (GST) and catalase (CAT) in the AFB1 exposed group. Meanwhile, the related expression of nuclear factor erythroid 2-related factor 2 (Nrf2), interferon regulatory factor 3 (IRF3) and the type 1 interferon (IFN1) were noticeably down-regulated, but caspase-1 was up-regulated, after exposure to AFB1, demonstrating that fish are unable to avoid the virus infection. It should be noted that the intestinal microbiota diversity and richness were lower in the AFB1 exposed group, and the composition of intestinal microbiota was affected by AFB1, resulting in the higher abundance of bacteria (such as *Aeromonas* and *Bacteroides*) and the lower abundance of potentially beneficial bacteria (such as *Cetobacterium* and *Clostridium*) in the AFB1 exposed group. This research provides insight into the possibility that AFB1 may increase the susceptibility of *C. gibelio* to CyHV-2 infection, and thus amplify the viral outbreak to endanger ecological safety in aquatic environment.

Keywords: aflatoxin B1; oxidative stress; intestinal microbiota; cyprinid herpesvirus 2; *Carassius auratus gibelio*; susceptibility

Citation: Xue, M.; Fu, M.; Zhang, M.; Xu, C.; Meng, Y.; Jiang, N.; Li, Y.; Liu, W.; Fan, Y.; Zhou, Y. Aflatoxin B1 Induced Oxidative Stress and Gut Microbiota Disorder to Increase the Infection of Cyprinid Herpesvirus 2 in Gibel Carp (*Carassius auratus gibelio*). *Antioxidants* **2023**, *12*, 306. https://doi.org/10.3390/antiox12020306

Academic Editors: Bo Liu, Changyou Song, Cunxin Sun and Alessandra Napolitano

Received: 6 December 2022
Revised: 19 January 2023
Accepted: 24 January 2023
Published: 28 January 2023

1. Introduction

In recent years, the rapid growth of the aquaculture industry worldwide, without an accompanying increase in fishmeal, has stimulated an increased use of plant ingredients as a source of protein in commercial aquaculture feeds [1]. Consequently, the potential risk of mycotoxin contamination in fish has increased due to the high amount of mycotoxin contamination in plant sources [2]. Mycotoxin, such as aflatoxin, exposure in fish causes growth inhibition, bioaccumulation, immunosuppression, and increased susceptibility to opportunistic pathogens [3]. Although certain precautions are taken at the feed production stage, mycotoxin contamination during transport and storage may be difficult to avoid [4]. Therefore, it is crucial to study the toxicity mechanism of mycotoxin on fish and find effective strategies to alleviate the adverse effects caused by mycotoxin.

Aflatoxins (AFs) are highly toxic, carcinogenic, teratogenic, and mutagenic secondary metabolites secreted primarily by conidial fungi of the genus *Aspergillus*, specifically *Aspergillus flavus* and *Aspergillus parasiticus* [5]. Aflatoxin has five main analogs: aflatoxin B1, G1,

M1, B2, and G2 (AFB1, AFG1, AFM1, AFB2, and AFG2) [6]. These compounds are serious contaminants of food, water, aquafeeds, and aquaculture systems, causing health hazards in humans and animals [7]. The International Agency for Research on Cancer (IARC) classifies AFB1 and AFM1 as the most toxic and carcinogenic among different types of AFs [8]. Several studies around the world have reported that AFB1 has been detected at a ratio of 60–70% in aquaculture feeds [9–12]. Previous studies have reported that AFB1 causes internal organ dysfunction, including induction of hepatotoxicity, teratogenicity, and immunosuppression in fish [13,14]. AFB1 exposure could activate oxidative stress and the endoplasmic reticulum stress pathway, inducing apoptosis and inflammation in northern snakehead (*Channa argus*) [15]. Hepatic and intestinal histopathological damages were found in common carp (*Cyprinus carpio*) fed with an aflatoxin-contaminated diet [16]. Dietary aflatoxin B1 could decrease growth performance and damage the structural integrity of immune organs in juvenile grass carp (*Ctenopharyngodon idella*) [4]. Thus, an aflatoxin-contaminated diet may reduce the growth performance of fish and render them more susceptible to opportunistic pathogens frequently found in aquaculture systems [17].

The balance of pro-oxidation and anti-oxidation in the internal environment plays a key role in maintaining the immunity and metabolism function. The previous study demonstrated that AFB1 induced excessive production of reactive oxygen species (ROS) and hydrogen peroxide (H_2O_2) in the liver, and caused oxidative stress to aggravate liver damage [18]. DNA virus-induced ROS accumulation in the host could trigger the negative change of cyclic GMP-AMP (cGAMP) synthase (cGAS) and nuclear factor erythroid 2-related factor 2 (Nrf2), which is associated with type-I interferon regulatory factor 3 (IRF3) activation, and ultimately affect the secretion of type I IFNs needed to achieve viral immune escape [19–21]. Therefore, the immune organ damage caused by AFB1 may be related to the reduction of the antioxidant capacity [4].

Intestinal bacteria play an important role in host health owing to the critical effect on metabolism and immune function [22]. Cumulative evidence demonstrates that the intestinal microbiota can modulate IFN responses, indirectly affecting viral infections [23–25]. External factors may change the structure of gut microbiota, which in turn affect intestinal physiological function [26]. Previous studies have reported that AFB1 could reduce the diversity of the composition of the intestinal microbiota community and severely affect the gut microbiota metabolome in rats [27]. However, research on the effects of aflatoxin on the intestinal flora in aquatic animals is lacking.

Gibel carp, *Carassius auratus gibelio*, is one of the most important cultivated freshwater fish species in China [28]. Crucian carp hematopoietic necrosis is an acute and contagious hemorrhagic disease in crucian carp caused by cyprinid herpesvirus 2 (CyHV-2) [29]. In recent years, CyHV-2 has spread rapidly in many provinces of China and resulted in huge losses for the crucian carp farming industry [30].

In the present study, we characterized the defensive capacities of gibel carp exposed to AFB1 and subsequently challenged them with CyHV-2 infection. To comprehensively evaluate the threat of AFB1 to aquaculture, the oxidative stress, gut microbiota, and related gene expression were assessed.

2. Materials and Methods

2.1. Fish Specimens

Healthy gibel carp specimens (15 $\pm$ 2 g, 12 $\pm$ 1 cm) with no history of disease were obtained from the gibel carp breeding base in Wuhan, China. The fish were maintained in recirculating aquaria (300 L) for 14 days to acclimatize to laboratory conditions. During the acclimatization period, the fish were fed with commercial feed (Tongwei, Chengdu, China) twice a day, the water temperature was 25 °C $\pm$ 1 °C and the water was renewed daily, approximately 30%. All animal experimental procedures were conducted according to the Animal Experimental Ethical Inspection (Ethical protocol code: YFI2022-zhouyong-09).

2.2. Diet Preparation and Sampling

AFB1 (purity > 98%) was purchased from Sigma–Aldrich (Sigma–Aldrich, St. Louis, MI, USA). The fish were randomly selected and divided into three groups: Group 1 (control diet, C), Group 2 (control diet + 50 μg/kg AFB1, T1), and Group 3 (control diet + 100 μg/kg AFB1, T2). There were three replicates in each group, with 60 fish in each replicate.

On days 14 and 28 of feeding, three fish from each tank were randomly collected and anesthetized with 100 mg/L MS222 (Sigma Aldrich, St. Louis, MI, USA). Over the 28-day period, excluding sampled fish, the survival rate of the control, T1, and T2 fish was 98.8%, 97.2%, and 95.6%, respectively. The liver tissues were removed and divided into three parts. One part was fixed in neutral 4% paraformaldehyde and subsequently used for immunofluorescence, one part was placed in RNase-free centrifuge tubes containing 200 μL TRIzol reagent (Invitrogen, Carlsbad, CA, USA) and subsequently used to analyze related genes expression, and the third part was placed in sterile tubes and stored at −80 °C to be used to determine the liver antioxidant index. During the 28 days of feeding, intestinal tissue was flash-frozen in liquid nitrogen and stored at −80 °C for Illumina sequencing.

2.3. Immunofluorescence

Liver tissues were fixed in 4% paraformaldehyde for 24 h and dehydrated in a sequential ethanol series. Tissue blocks were sectioned on a freezing microtome (Olympus, Tokyo, Japan). The tissue sections were blocked in 5% bovine serum albumin with normal serum in 0.1% Triton X-100, washed, and incubated with primary antibodies (CAT, 1:1000, ABCAM, Cambridge, MA, USA; GSTT1, 1:1000). The tissue sections were further incubated with secondary antibodies (Alexa Fluor 555-conjugated antibodies and Alexa Fluor 488-conjugated antibodies, 1:500, Invitrogen). Cell nuclei were stained with DAPI solution (blue). Images were obtained using fluorescence microscopy (Olympus BX41).

2.4. Changes in Antioxidant and Antiviral Related Genes Expression

The TRIzol reagent (Invitrogen, Carlsbad, CA, USA) was used to extract total RNA from tissues of gibel carp. The quality and purity of RNA were assessed by nanodrop (Thermo, Waltham, MA, USA). The cDNA was synthesized using random primers (TaKaRa, Dalian, China) following the manufacturer's instructions. Then, the cDNA was used as the template for real-time quantitative PCR by real-time PCR Kit (TaKaRa, Dalian, China). The β-actin gene was performed as an internal reference. The specific primers are listed in Table 1. Each PCR reaction was performed in triplicate. The relative quantification of gene expression was conducted using the $2^{-\Delta\Delta CT}$ method [31].

Table 1. Primer sequences used in this study.

Gene	Primer Sequence (5′-3′)	Accession Numbers	References
β-actin	F: CATCTACGAGGGTTACGCCC R: AACCACACGTCGGCTTGTTA	NC068418.1	[32]
GST	F: CCTGAAAACAAACCGGCACA R: AAAAGGAGGTGGCTCAACACG	NC068386.1	[32]
CAT	F: ATC TTACAGGAAACAACACCC R: CGATTCAGGACGCAAACT	NC056596.1	[33]
Nrf2	F: GCGAGCGTAGCTCCAGTCTGA R: AAGGCTTGCCGTGCTCGTCT	MG759384.1	[34]
IRF3	F: TCCAGGCCAAGCATACGAA R: CCATTTGCAACAGCCATCAT	NC056583.1	[35]
Caspase-1	F: AAACCCAAGATCATCATCATCCA R: CAGGGCATCAGCCTCTAAGTTGT	NW024042261.1	[36]
IFN1	F: GTCAATGCTCTGCTTGCGAAT R: CAAGAAACTTCACCTGGTCCT	NC007114.7	[37]
CyHV-2	F: TCGGTTGGACTCGGTTTGTG R: CTCGGTCTTGATGCGTTTCTTG	AY939863.1	[38]
CyHV-2 probe	FAM-CCGCTTCCAGTCTGGGCCACTACC-BHQ1		

2.5. Liver Antioxidant Index

Liver tissues were homogenized in phosphate-buffered saline at a ratio of 1:9 (*w*/*v*) using a glass homogenizer at 4 °C. The homogenate was centrifuged at 5000× *g* for 20 min at 4 °C to remove tissue debris. The supernatant was used to determine the superoxide dismutase (SOD) activity, malondialdehyde (MDA) levels, and reactive oxygen species (ROS) levels using appropriate kits according to the manufacturer's instructions (Jiancheng, Nanjing, China).

2.6. Illumina miSeq Sequencing and Bioinformatics Analysis

The total bacterial genomic DNA of the intestinal content was extracted using a Bacterial DNA Kit (Omega, Norcross, GA, USA) following the manufacturer's instructions. The DNA was quantified using NanoDrop 2000 spectrometer (Thermo Fisher Scientific, Waltham, MA, USA), diluted to a concentration of 1 ng/μL, and stored at −20 °C. The V3–V4 region of the bacterial 16S rRNA gene was amplified by PCR using specific primers 338F (5′-ACTCCTACGGGAGGCAGCA-3′) and 806R (5′-GGACTACHVGGGTWTCTAAT-3′) with barcodes in 50 μL reactions. The following thermal cycling conditions were used: initial denaturation at 95 °C for 1 min; followed by 30 cycles at 95 °C for 30 s, 55 °C for 30 s, and 72 °C for 45 s; and a final extension at 72 °C for 10 min. PCR amplicons were isolated from 2% agarose gels and purified using the DNA Gel Extraction Kit (Omega, Norcross, USA). Subsequently, amplicons were sequenced on an Illumina MiSeq PE250 high-throughput sequencing platform. All sequence reads were quality filtered and assembled using the Mothur software package [39]. Reads were clustered into operational taxonomic units (OTUs) at 97% identity [40]. Representative reads were selected from each OTU using QIIME package. Annotated taxonomic classification was performed using the RDP Classifier algorithm (http://rdp.cme.msu.edu/ accessed on 20 August 2022) against the Silva database version 123 (16S rDNA) [41].

Alpha diversity analyses (abundance-based coverage estimator [ACE], Chao, Shannon, and Simpson index) were performed using Mothur (version v.1.30) [42]. Beta diversity was estimated by computing the Bray-Curtis distance based on the abundances of microbes at the genus level and visualized using principal coordinate analyses (PCoA) and Unweighted Pair Group Method with Arithmetic Mean (UPGMA) clustering. Other analyses were performed using the R software.

2.7. Challenge Tests and Viral Load in Liver, Kidney, and Spleen of Gibel Carp

After 28 days of the feeding trial, a challenge test was performed in each group with CyHV-2 purified by sucrose gradient ultracentrifugation in our laboratory. Fish in each group were intraperitoneally injected with 0.2 mL CyHV-2 ($10^{6.3}$ $TCID_{50}$/mL). Infected fish were observed daily, and mortality was recorded for 14 days. At 2, 7, and 14 days post injection (dpi), three fish were randomly selected to investigate the viral load. Liver, kidney, and spleen tissues were collected from the fish. Total DNA was extracted from each tissue type using a Viral DNA Kit (Omega, Norcross, GA, USA). Viral DNA was quantified using droplet digital PCR (ddPCR, Bio-Rad, Hercules, CA, USA) with the primers CyHV2-F, CyHV2-R, and CyHV2-probe (Table 1) [29]. The viral load was determined as the number of viral copies per microgram of total tissue.

2.8. Statistical Analysis

Data were analyzed by one-way analysis of variance (ANOVA) and expressed as the arithmetic mean ± standard deviation (SD). Survival curves were estimated by the Kaplan–Meier method. Differences were determined by Tukey's test in SPSS statistical software (SPSS Inc., Chicago, IL, USA), with p-values < 0.05 indicating statistical significance.

3. Results

3.1. Oxidative Stress in the Liver

As shown in Figure 1, the 50 μg/kg AFB1 and 100 μg/kg AFB1 exposed groups showed significantly higher ROS and MDA levels and significantly lower SOD levels in

the liver than those in the control group (C; $p < 0.05$; Figure 2A–C). At day 28, the ROS and MDA levels in the 100 μg/kg AFB1 exposed group were about 45% and 189% higher, respectively, and the mean SOD levels in the 100 μg/kg AFB1-exposed group were 45% of the control group. There were no significant differences between the 50 μg/kg AFB1 and 100 μg/kg AFB1 exposed groups on day 28 ($p > 0.05$).

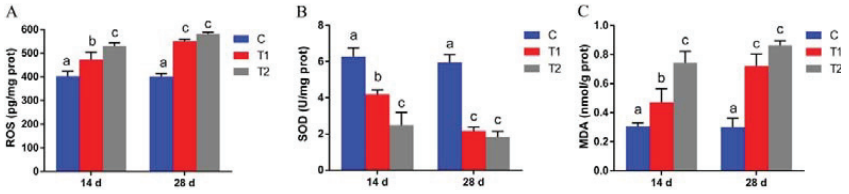

Figure 1. Reactive oxygen species (ROS; (**A**)), superoxide dismutase (SOD; (**B**)), and malondialdehyde (MDA; (**C**)) activity in gibel carp liver after exposure to aflatoxin B1 (AFB1) for 14 and 28 days. C: control diet, T1: 50 μg/kg AFB1, T2: 100 μg/kg AFB1. Results are presented as mean ± standard deviation (SD). Dissimilar superscript letters represent statistically significant differences between different treatment groups ($p < 0.05$).

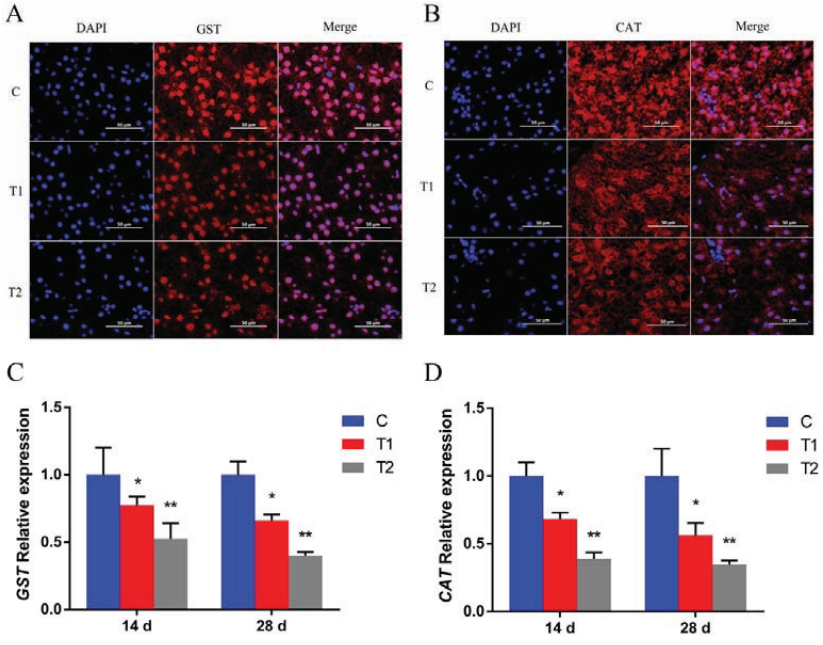

Figure 2. Effects of aflatoxin B1 (AFB1) on glutathione-S-transferase (GST) and catalase (CAT) levels in the liver of gibel carp. (**A**,**B**) Immunofluorescence of GST and CAT in the liver of gibel carp. (**C**,**D**) mRNA expression levels of the *GST* and *CAT* in the liver of gibel carp. C: control diet, T1: 50 μg/kg AFB1, T2: 100 μg/kg AFB1.Data are presented as mean ± standard deviation (SD; * $p < 0.05$; ** $p < 0.01$).

3.2. Effects of Aflatoxin B1 on Antioxidant Enzymes in the Liver

Liver tissue obtained from the AFB1 exposed groups on day 28 showed a lower intensity of red fluorescence (Figure 2A,B) than the control group, indicating lower GST and CAT levels in hepatocytes. Moreover, the fluorescence intensity was lower in 100 μg/kg AFB1 exposed group than in 50 μg/kg AFB1 group. The GST and CAT mRNA expression levels in the liver were significantly lower in the 50 μg/kg AFB1 and 100 μg/kg AFB1 exposed groups than in the control group on days 14 and 28 ($p < 0.05$; Figure 2C,D).

3.3. Effects of Aflatoxin B1 on Related Genes Expression

The mRNA expressions of Nrf2, IRF3, and IFN1 were significantly lower in the AFB1 exposed groups on day 28 ($p < 0.01$) (Figure 3A,C,D), and at day 28, the mRNA expressions of apoptosis related gene (Caspase-1) were significantly higher in the AFB1 treatment groups than in the control group ($p < 0.01$) (Figure 3B).

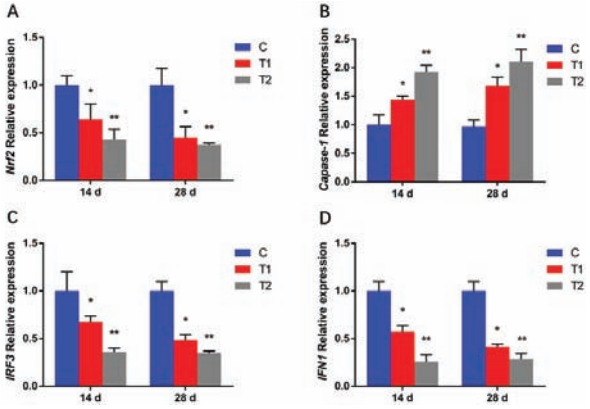

Figure 3. Effects of AFB1 on the mRNA levels of Nrf2(**A**), Caspase-1(**B**), IRF3(**C**), and IFN1(**D**) in gibel carp. C: control diet, T1: 50 μg/kg AFB1, T2: 100 μg/kg AFB1. Data represent the means ± SD (* $p < 0.05$, ** $p < 0.01$).

3.4. Characteristics of 16S rDNA Sequencing

After quality filtering and assignment, 990,671 valid read sequences were obtained from the nine samples belonging to three groups. The rarefaction curves and rank abundance curve demonstrated that sufficient sequencing depth, richness, and evenness were achieved for each sample (Figure 4A,C).

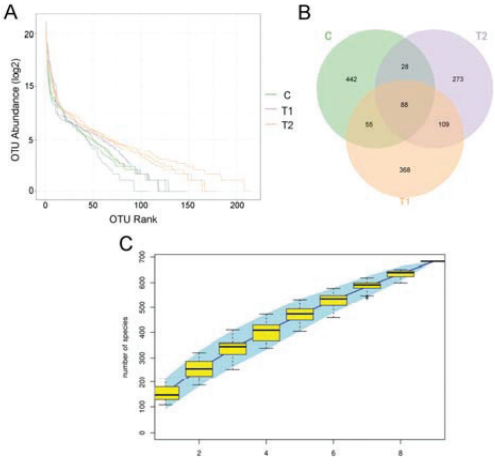

Figure 4. Rarefaction curves, Venn diagram, and rank abundance curve of different treatment groups of gibel carp exposed to aflatoxin B1 for 28 days. (**A**) Rarefaction curves. (**B**) Venn diagram representing the operational taxonomic units (OTUs) shared among treatment groups. (**C**) Rank abundance curve. C: control diet, T1: 50 μg/kg AFB1, T2: 100 μg/kg AFB1.

On the basis of 97% nucleotide sequence identity, these high-quality sequences were clustered into 1363 OTUs in total. The OTU distribution in different groups is depicted in a

Venn diagram in Figure 4B. The number of OTUs in the control group was higher than that in the treatment groups. Meanwhile, 88 core OTUs were observed in all collected samples. Furthermore, the number of OTUs in the 100 μg/kg AFB1 exposed group was the lowest.

3.5. Effects of Aflatoxin B1 on Alpha Diversity of Intestinal Microbiota

ACE and Chao1 indices were used to quantify species richness. The ACE index ranged from 0.34 to 0.44, and the Chao1 index ranged from 37 to 198. The ACE index and Chao1 index were significantly lower in the AFB1 exposed groups than in the control group (C; $p < 0.05$; Figure 5A,B). The alpha diversity of each sample was calculated via the Shannon index and Simpson index. The Shannon index ranged from 2.2 to 2.8, and the Simpson index ranged from 0.43 to 0.79. The AFB1 exposed groups showed a significantly lower Shannon index and a significantly higher Simpson index than the control group (Figure 5C,D). The richness and diversity of bacterial communities in the treatment groups were lower than those in control group. The average Good's coverage was 0.999913 (values ranged from 0.999870 to 0.99936), indicating that the sequences identified represented the majority of the bacteria in each sample (Figure 5E).

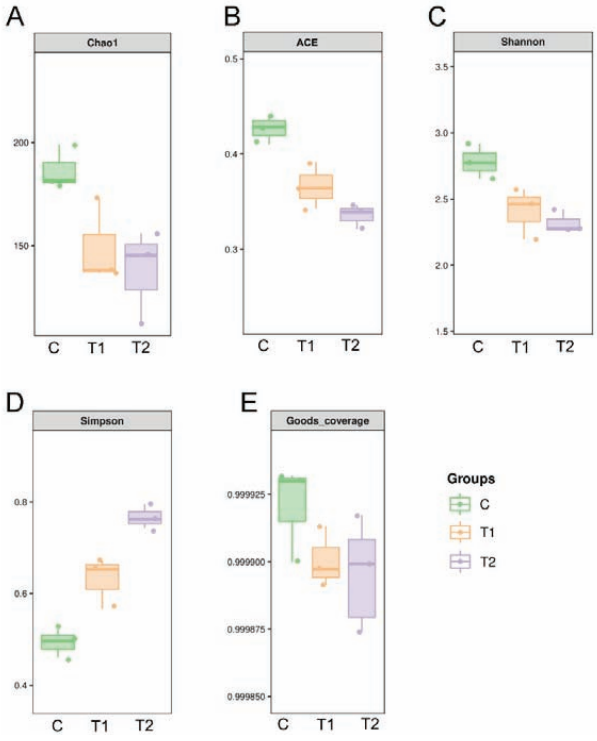

Figure 5. Richness and diversity indices of bacterial communities in different treatment groups of gibel carp exposed to aflatoxin B1 for 28 days. (**A**) Chao1 index, (**B**) abundance-based coverage estimator (ACE), (**C**) Shannon index, and (**D**) Simpson index of operational taxonomic unit (OTU) level. (**E**) The average Good's coverage of treatment groups. C: control diet, T1: 50 μg/kg AFB1, T2: 100 μg/kg AFB1.

3.6. Microbial Community Composition

A total of 19 phyla were identified in all samples, and five phyla were identified at an abundance >1%. As shown in Figure 6A, the dominant phyla in the control group were Fusobacteria, Proteobacteria, Firmicutes, and Actinobacteria, accounting for over 98% of the bacterial sequences from control group samples. In the treatment groups, the

dominant bacterial phyla were Fusobacteria, Proteobacteria, Bacteroidetes, and Firmicutes, accounting for over 99% of the total reads from treatment group. At the phylum level, the AFB1 exposed groups showed a significantly higher abundance of Proteobacteria and Bacteroidetes ($p < 0.05$; Figure 6C,D) and a significantly lower abundance of Fusobacteria and Firmicutes ($p < 0.05$; Figure 6B,E) than the control group.

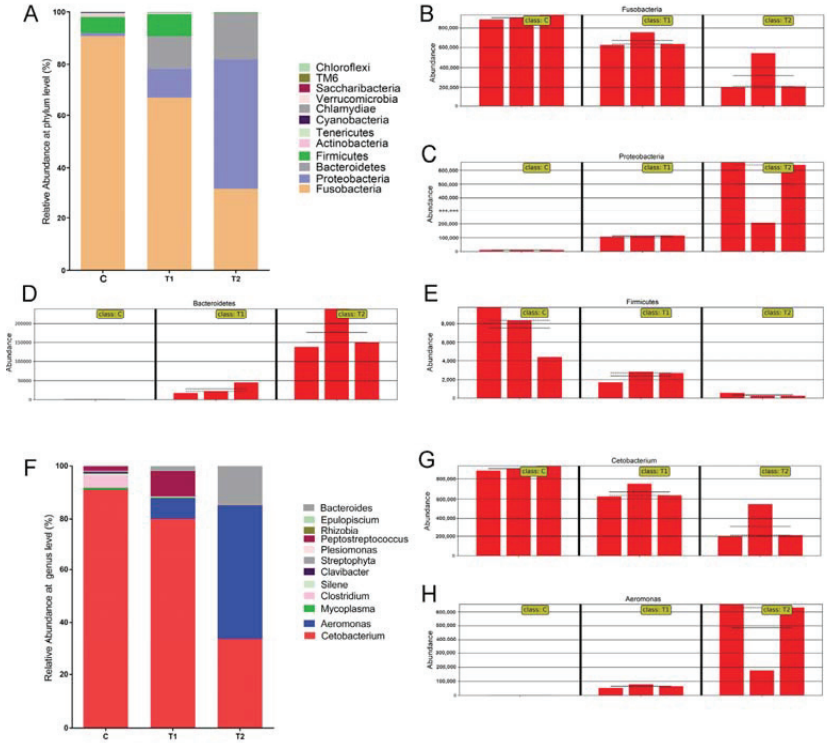

Figure 6. Gut microbiota composition at the phylum level (**A**) and at the genus level (**F**) in gibel carp exposed to aflatoxin B1 for 28 days. (**B**–**E**) Partial phyla with significant changes in relative abundance among treatment groups. (**G**,**H**) Partial genera with significant changes in relative abundance among treatment groups. C: control diet, T1: 50 μg/kg AFB1, T2: 100 μg/kg AFB1.

A total of 198 genera were detected across all nine samples. In the control group, the dominant genera were *Cetobacterium*, *Clostridium*, *Peptostreptococcus*, and *Mycoplasma* (Figure 6F). In the treatment groups, the dominant genera were *Cetobacterium*, *Aeromonas*, *Bacteroides*, and *Peptostreptococcus*. The relative abundance of dominant genera of intestinal bacteria was significantly different between the control and the treatment groups. At the genus level, the AFB1 exposed groups showed a significantly higher abundance of *Aeromonas* ($p < 0.05$; Figure 6C,D), and a significantly lower abundance of *Cetobacterium* ($p < 0.05$; Figure 6B,E) than the control group.

3.7. Beta Diversity of Intestinal Microbiota

PCoA and unweighted pair group method with arithmetic mean (UPGMA) clustering were conducted to evaluate beta diversity. As shown in Figure 7, the intestinal microbiomes of the control group and treatment group were separated into different clusters. In addition, the individual differences in gut microflora in the AFB1 exposed groups were less than those in the control group. Overall, the PCoA and UPGMA clustering results showed that AFB1 exposure markedly altered the intestinal microbial community structure in gibel carp.

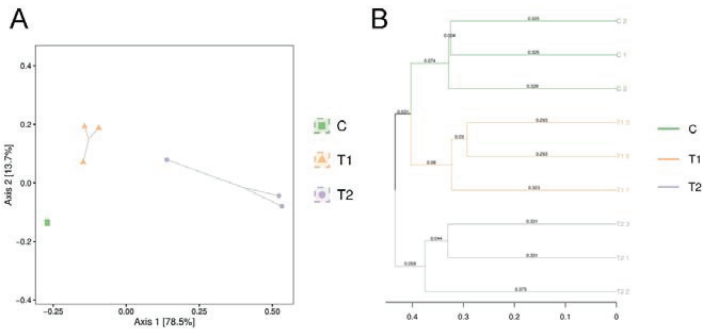

Figure 7. Beta diversity of the gut microbiota among different groups of gibel carp exposed to aflatoxin B1. (**A**) The principal co-ordinate analysis (PCoA) of the bacterial community at the operational taxonomic unit (OTU) level. (**B**) The hierarchical clustering tree was calculated using the unweighted pair group method with arithmetic mean (UPGMA) method. C: control diet, T1: 50 μg/kg AFB1, T2: 100 μg/kg AFB1.

3.8. Effect of AFB1 on CyHV-2 Infection and Viral Load in Tissues in Gibel Carp

The cumulative survival rate of *C. gibelio* challenged with CyHV-2 for 14 days is shown in Figure 8A. The cumulative mortality of CyHV-2-infected gibel carp in the control group was 40%, and the cumulative mortality in the T2 group reached 83% at 14 dpi. At 14 dpi, the cumulative survival rate of fish exposed to AFB1 was significantly less than in the control group ($p < 0.05$). Moreover, the 100 μg/kg AFB1 exposed group of gibel carp showed significantly higher mortality than the 50 μg/kg AFB1 exposed group. Regarding viral load, the AFB1 exposed groups showed a significantly higher number of copies of CyHV-2 in the liver, kidney, and spleen than the control group ($p < 0.05$; Figure 8B–D).

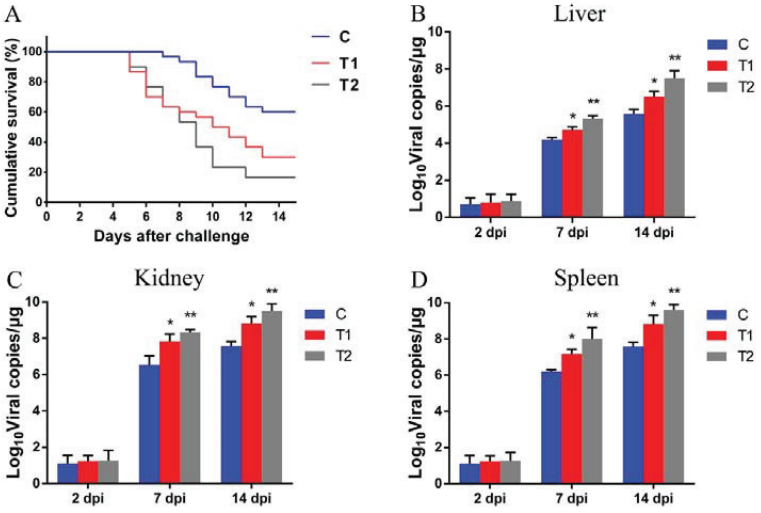

Figure 8. Effects of AFB1 on cyprinid herpesvirus 2 (CyHV-2) infection in gibel carp and viral load in tissues of gibel carp. (**A**) Cumulative survivorship curves of gibel carp intraperitoneally injected with CyHV-2 in different treatment groups. (**B**–**D**) CyHV-2 viral load in the liver, kidney, and spleen of gibel carp in different treatment groups at 2, 7, and 14 days post infection (dpi). C: control diet, T1: 50 μg/kg AFB1, T2: 100 μg/kg AFB1. Data are presented as mean ± standard deviation (SD; * $p < 0.05$; ** $p < 0.01$).

4. Discussion

Fisheries provide a large amount of high-quality protein to meet the nutritional requirements of the increasing human population (Food and Agriculture Organization [FAO], Rome, Italy, 2018). The rapid expansion of fish farming has led to an increased use of plant protein sources in aquaculture feeds [13]. AFB1 could be a latent threat to the health of aquatic organisms when fishmeal ingredients are replaced with plant-based materials in aquafeeds [43]. The present study reveals that AFB1 causes oxidative stress, changes in intestinal microbiota and exacerbates CyHV-2 infection in *C. gibelio*.

Oxidative stress under exposure to extreme conditions induces ROS and MDA production, which may lead to protein, lipid, and DNA damage [44]. In the present study, changes in the levels of antioxidant enzymes and oxidative stress markers were observed in the AFB1 exposed groups. The lower SOD levels, and the higher ROS and MDA levels were observed in the AFB1 exposed groups. The immunofluorescence and mRNA expression levels of GST and CAT showed that the quantity of antioxidant enzymes was lower in the AFB1 exposed groups. These results suggest that AFB1 induces oxidative stress. Moreover, the oxidative stress increased with the increase in AFB1 concentration. Similarly, previous studies have reported that AFB1 significantly reduced the activity of antioxidant enzymes by down-regulating the expression of Nrf2, and increased the levels of ROS and MDA in Nile tilapia [45] and gibel carp [46]. Previous research showed that ROS accumulation could promote the replication of CyHV-2, while antioxidants could inhibit the amplification of CyHV-2 by activating Nrf2 signaling pathway [19]. In this study, we found that the expression of Nrf2 was inhibited significantly by AFB1. Thus, we believe that the oxidative stress induced by AFB1 could promote CyHV-2 proliferation.

Recently, it has been reported that ROS accumulation could limit the virus DNA induced cGAS-STING activation by activating caspase-1 [20]. STING is involved in the activation of IRF3. Activated IRF3 induces inflammation through generating IFN1 [21]. Our study demonstrated that the expression of caspase-1 was higher, and the expressions of IRF3 and IFN1 were lower, in the AFB1 exposed group. Based on the challenge test, we found that AFB1 exposure increased the mortality of gibelio carp infected with CyHV-2 and enhanced the viral load in liver, kidney and spleen of gibelio carp. We believe that AFB1 promoted the amplification of CyHV-2 by inducing the oxidative stress and suppressing the IFN1 response (Figure 9). Similarly, it has been found that azoxystrobin enhance the spring viremia of carp virus (SVCV) replication by regulated the MAPK-Nrf2 signaling pathway to suppress HO-1-mediated IFN expression [47].

Intestinal microbiota is crucial to host health owing to its significant influence on metabolism and immune function [48]. The gut microbiome can influence ROS levels, immune response and host health [49–51]. Changes in the intestinal flora are highly correlated with physiological, pathological, and environmental conditions [52]. An increasing number of studies have focused on the relationship between environmental pollution and gut microbiota to understand the toxicological response [53]. Bioaccumulation of benzophenone-3 in *Carassius auratus* can affect the structure and diversity of intestinal flora [54]. Another study showed that the intestinal microbiota of freshwater crayfish (*Procambarus clarkii*) was significantly altered by microcystin [55]. In the present study, the results demonstrated that AFB1 exposure disrupts the intestinal microbiota of gibel carp. The PCoA and UPGMA clustering analysis showed that AFB1 exposure markedly altered the intestinal microbial community structure of gibel carp. The AFB1 exposed groups showed significantly lower richness and diversity of the gut microbiota than the control group. The lower intestinal bacterial richness and diversity reduced the stability of intestinal microbial communities of gibel carp. Previous research suggests that viral infection, toxin exposure, and unfavorable environment reduce the richness and diversity of gut flora in animals [48,56,57]. In the present study, the intestinal microbiota composition of gibel carp was examined and compared to identify common flora that showed significant difference after AFB1 exposure. At the phylum level, the higher relative abundances of Proteobacteria and Bacteroidetes and the lower relative abundances of Fusobacteria and Firmicutes were observed

in AFB1 exposed group. Some members of Proteobacteria and Bacteroidetes are opportunistic pathogens and facilitate inflammation or disrupt the intestinal mucosal barrier [58]. Fan et al. (2019) showed that increased relative abundance of phylum Proteobacteria in the intestine is associated with slow growth and disease in shrimp [59]. Previous studies have demonstrated that members of Fusobacteria regulate the transepithelial transport, thus strengthening the mucosal barrier and improving the oxidative and inflammatory status of the intestinal mucosa [60]. At the genus level, the abundance of *Aeromonas* was significantly higher and that of *Cetobacterium* was significantly lower in the AFB1 exposed groups than in the control group. Members of *Aeromonas* are ubiquitous opportunistic pathogens in the intestinal tracts of aquatic animals and aquaculture waters, and some of these species cause infections in humans [61]. *Cetobacterium* has been observed to be the dominant genus in the intestinal microbiota of different freshwater fishes; it has been shown to improve digestion and produce large quantities of vitamin B [62]. Several studies pointed to the role of the intestinal microbiota in modulating the systemic immunity and providing a competitive barrier to bacterial, viral, and fungal pathogens [23,63]. In murine models of lymphocytic choriomeningitis virus (LCMV) or influenza infection, disorder of the gut microbiota results in an unresponsive reaction to the virus [64]. Feeding with *Clostridium butyricum* improved the host immune responses and the survival rate of gibel carp against *Carassius auratus* herpesvirus (CaHV) infection [65]. Our data demonstrated that the changes in intestinal microbiota caused by AFB1 might weaken the immunity and antioxidant capacity of gibel carp.

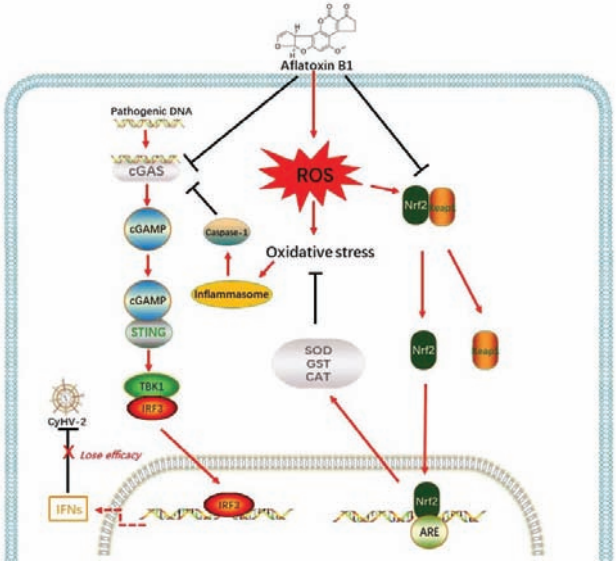

Figure 9. Proposed model for AFB1 inducing the oxidative stress and promoting CyHV-2 proliferation through suppressing the IFNs response [19,20,66].

5. Conclusions

In summary, our study is the first, to our knowledge, to report that AFB1 exacerbates viral infection in aquatic animals. We found that AFB1 exposure increased the mortality and enhanced the viral load of gibelio carp infected with CyHV-2. The cCAS-STING pathway and the expression of IFN1 was significantly suppressed by AFB1, which might be associated with severe oxidative stress and intestinal microbiota disorder induced by AFB1. This research provides new understanding of the threat that AFB1 may increase CyHV-2 susceptibility in *C. gibelio*.

Author Contributions: Conceptualization, M.X., M.F. and Y.Z.; methodology, M.X., M.F. and Y.Z.; software, M.F., M.Z. and W.L.; validation, C.X., Y.M. and N.J.; formal analysis, N.J. and W.L.; investigation, M.Z., N.J., Y.M. and Y.L.; resources, M.X.; data curation, M.X. and W.L.; writing—original draft preparation, M.X.; writing—review and editing, M.X., M.F., Y.M., M.Z., C.X., Y.L. and Y.F.; visualization, C.X. and Y.L.; supervision, Y.F. and Y.Z.; project administration, Y.F.; funding acquisition, Y.F. and Y.Z. All authors have read and agreed to the published version of the manuscript.

Funding: This work was supported by the Earmarked Fund for China Agriculture Research System [grant number CARS-45-19]; and the Central Public-interest Scientific Institution Basal Research Fund [grant number 2020TD44].

Institutional Review Board Statement: The study was conducted in accordance with the guidelines of the Animal Experimental Ethical Inspection of Laboratory Animal Centre, and approved by the Institutional Review Board of the Yangtze River Fisheries Research Institute, Chinese Academy of Fishery Sciences (ID Number: YFI2022-zhouyong-09).

Informed Consent Statement: Not applicable.

Data Availability Statement: The data presented in this study are available on request from the corresponding author.

Acknowledgments: We would like to thank Wuhan Dynamic Life Science Co., Ltd. for their support in carrying out this study.

Conflicts of Interest: The authors declare that they have no known competing financial interest or personal relationships that may have appeared to influence the work reported in this paper. The authors declare no conflict of interest.

References

1. Bu, X.; Chen, A.; Lian, X.; Chen, F.; Zhang, Y.; Muhammad, I.; Ge, X.; Yang, Y. An evaluation of replacing fish meal with cottonseed meal in the diet of juvenile Ussuri catfish Pseudobagrus ussuriensis: Growth, antioxidant capacity, nonspecific immunity and resistance to Aeromonas hydrophila. *Aquaculture* **2017**, *479*, 829–837. [CrossRef]
2. Matejova, I.; Svobodova, Z.; Vakula, J.; Mares, J.; Modra, H. Impact of Mycotoxins on Aquaculture Fish Species: A Review. *J. World Aquac. Soc.* **2017**, *48*, 186–200. [CrossRef]
3. Barany, A.; Guilloto, M.; Cosano, J.; Boevre, M.d.; Oliva, M.; Saeger, S.D.; Fuentes, J.; Martinez-Rodriguez, G.; Mancera, J.M. Dietary aflatoxin B1 (AFB1) reduces growth performance, impacting growth axis, metabolism, and tissue integrity in juvenile gilthead sea bream (*Sparus aurata*). *Aquaculture* **2021**, *536*, 736510. [CrossRef]
4. Zeng, Z.-Z.; Jiang, W.-D.; Wu, P.; Liu, Y.; Zeng, Y.-Y.; Jiang, J.; Kuang, S.-Y.; Tang, L.; Zhou, X.-Q.; Feng, L. Dietary aflatoxin B1 decreases growth performance and damages the structural integrity of immune organs in juvenile grass carp (*Ctenopharyngodon idella*). *Aquaculture* **2019**, *500*, 1–17. [CrossRef]
5. Alshannaq, A.F.; Gibbons, J.G.; Lee, M.K.; Han, K.H.; Yu, J.H. Controlling aflatoxin contamination and propagation of Aspergillus flavus by a soy-fermenting Aspergillus oryzae strain. *Sci. Rep.* **2018**, *8*, 16871. [CrossRef] [PubMed]
6. Yoshida, S.; Zhang, H.; Takahashi, R.; Yoshida, S.; Abiko, Y.; Toriba, A. Identification and removal of aflatoxin coprecipitates derived from plant samples on immunoaffinity chromatographic purification. *J. Chromatogr. A* **2022**, *1678*, 463382. [CrossRef] [PubMed]
7. Gell, R.M.; Carbone, I. HPLC quantitation of aflatoxin B 1 from fungal mycelium culture. *J. Microbiol. Methods* **2019**, *158*, 14–17. [CrossRef] [PubMed]
8. Silvia, M.; Andrea, P.; Andrea, A.; Salvatore, V.; Susan, C.; Lorella, S. Aflatoxin B1 and M1: Biological Properties and Their Involvement in Cancer Development. *Toxins* **2018**, *10*, 214. [CrossRef]
9. Rodrigues, I.; Handl, J.; Binder, E.M. Mycotoxin occurrence in commodities, feeds and feed ingredients sourced in the Middle East and Africa. *Food Addit. Contam. Part B Surveill.* **2011**, *4*, 168–179. [CrossRef] [PubMed]
10. Barbosa, T.S.; Pereyra, C.M.; Soleiro, C.A.; Dias, E.O.; Oliveira, A.A.; Keller, K.M.; Silva, P.P.; Cavaglieri, L.R.; Rosa, C.A. Mycobiota and mycotoxins present in finished fish feeds from farms in the Rio de Janeiro State, Brazil. *Int. Aquat. Res.* **2013**, *5*, 3. [CrossRef]
11. Fallah, A.A.; Pirali-Kheirabadi, E.; Rahnama, M.; Saei-Dehkordi, S.S.; Pirali-Kheirabadi, K. Mycoflora, aflatoxigenic strains of Aspergillus section Flavi and aflatoxins in fish feed. *Qual. Assur. Saf. Crops Foods* **2014**, *6*, 419–424. [CrossRef]
12. Dey, D.K.; Kang, S.C. Aflatoxin B1 induces reactive oxygen species-dependent caspase-mediated apoptosis in normal human cells, inhibits Allium cepa root cell division, and triggers inflammatory response in zebrafish larvae. *Sci. Total Environ.* **2020**, *737*, 139704. [CrossRef] [PubMed]
13. Hassaan, M.S.; Nssar, K.M.; Mohammady, E.Y.; Amin, A.; Tayel, S.I.; El-Haroun, E.R. Nano-zeolite efficiency to mitigate the aflatoxin B1 (AFB1) toxicity: Effects on growth, digestive enzymes, antioxidant, DNA damage and bioaccumulation of AFB1 residues in Nile tilapia (*Oreochromis niloticus*). *Aquaculture* **2020**, *523*, 735123. [CrossRef]

14. Abdelhiee, E.Y.; Elbialy, Z.I.; Saad, A.H.; Dawood, M.; Fadl, S.E. The impact of Moringa oleifera on the health status of Nile tilapia exposed to aflatoxicosis. *Aquaculture* **2020**, *533*, 736110. [CrossRef]
15. Li, M.; Kong, Y.; Guo, W.; Wu, X.; Zhang, J.; Lai, Y.; Kong, Y.; Niu, X.; Wang, G. Dietary aflatoxin B1 caused the growth inhibition, and activated oxidative stress and endoplasmic reticulum stress pathway, inducing apoptosis and inflammation in the liver of northern snakehead (*Channa argus*). *Sci. Total Environ.* **2022**, *850*, 157997. [CrossRef]
16. Ht, A.; Ai, A.; Ksm, A.; Nn, A.; Mo, B. Aflatoxicosis in fingerling common carp (*Cyprinus carpio*) and protective effect of rosemary and thyme powder: Growth performance and digestive status. *Aquaculture* **2020**, *527*, 735437. [CrossRef]
17. Ayyat, M.S.; Ayyat, A.M.N.; Al-Sagheer, A.A.; El-Hais, A.E.-A.M. Effect of some safe feed additives on growth performance, blood biochemistry, and bioaccumulation of aflatoxin residues of Nile tilapia fed aflatoxin-B1 contaminated diet. *Aquaculture* **2018**, *495*, 27–34. [CrossRef]
18. Wu, J.; Gan, Z.; Zhuo, R.; Zhang, L.; Zhong, X. Resveratrol Attenuates Aflatoxin B1-Induced ROS Formation and Increase of m6A RNA Methylation. *Animals* **2020**, *10*, 677. [CrossRef]
19. Lu, C.; Tang, R.; Su, M.; Zou, J.; Lu, L. Induction of Reactive Oxygen Species Is Necessary for Efficient Onset of Cyprinid Herpesvirus 2 Replication: Implications for Novel Antiviral Strategy With Antioxidants. *Front. Microbiol.* **2022**, *12*, 792655. [CrossRef]
20. Wang, Y.; Ning, X.; Gao, P.; Wu, S.; Sha, M.; Lv, M.; Zhou, X.; Gao, J.; Fang, R.; Meng, G.; et al. Inflammasome Activation Triggers Caspase-1-Mediated Cleavage of cGAS to Regulate Responses to DNA Virus Infection. *Immunity* **2017**, *46*, 393–404. [CrossRef]
21. Yilmaz, I.C.; Dunuroglu, E.; Ayanoglu, I.C.; Ipekoglu, E.M.; Yildirim, M.; Girginkardesler, N.; Ozbel, Y.; Toz, S.; Ozbilgin, A.; Aykut, G.; et al. Leishmania kinetoplast DNA contributes to parasite burden in infected macrophages: Critical role of the cGAS-STING-TBK1 signaling pathway in macrophage parasitemia. *Front. Immunol.* **2022**, *13*, 1007070. [CrossRef] [PubMed]
22. Xu, Y.; Li, Y.; Xue, M.; Xiao, Z.; Fan, Y.; Zeng, L.; Zhou, Y. Effects of Dietary Enterococcus faecalis YFI-G720 on the Growth, Immunity, Serum Biochemical, Intestinal Morphology, Intestinal Microbiota, and Disease Resistance of Crucian Carp (*Carassius auratus*). *Fishes* **2022**, *7*, 18. [CrossRef]
23. Wirusanti, N.I.; Baldridge, M.T.; Harris, V.C. Microbiota regulation of viral infections through interferon signaling. *Trends Microbiol.* **2022**, *30*, 778–792. [CrossRef] [PubMed]
24. Antunes, K.H.; Fachi, J.L.; de Paula, R.; da Silva, E.F.; Pral, L.P.; Dos Santos, A.A.; Dias, G.B.M.; Vargas, J.E.; Puga, R.; Mayer, F.Q.; et al. Microbiota-derived acetate protects against respiratory syncytial virus infection through a GPR43-type 1 interferon response. *Nat. Commun.* **2019**, *10*, 3273. [CrossRef] [PubMed]
25. Schaupp, L.; Muth, S.; Rogell, L.; Kofoed-Branzk, M.; Melchior, F.; Lienenklaus, S.; Ganal-Vonarburg, S.C.; Klein, M.; Guendel, F.; Hain, T.; et al. Microbiota-Induced Type I Interferons Instruct a Poised Basal State of Dendritic Cells. *Cell* **2020**, *181*, 1080–1096. [CrossRef] [PubMed]
26. Van Winkle, J.A.; Peterson, S.T.; Kennedy, E.A.; Wheadon, M.J.; Ingle, H.; Desai, C.; Rodgers, R.; Constant, D.A.; Wright, A.P.; Li, L.; et al. Homeostatic interferon-lambda response to bacterial microbiota stimulates preemptive antiviral defense within discrete pockets of intestinal epithelium. *Elife* **2022**, *11*, e74072. [CrossRef]
27. Wang, J.; Tang, L.; Glenn, T.C.; Wang, J.S. Aflatoxin B1 Induced Compositional Changes in Gut Microbial Communities of Male F344 Rats. *Toxicol. Sci.* **2016**, *150*, 54–63. [CrossRef]
28. Noor-Ul, H.; Haokun, L.; Junyan, J.; Xiaoming, Z.; Dong, H.; Yunxia, Y.; Shouqi, X. Dietary supplementation of Geotrichum candidum improves growth, gut microbiota, immune-related gene expression and disease resistance in gibel carp CAS (*Carassius auratus gibelio*). *Fish Shellfish Immunol.* **2020**, *99*, 144–153. [CrossRef]
29. Xiao, Z.; Xue, M.; Xu, C.; Jiang, N.; Luo, X.; Li, Y.; Fan, Y.; Meng, Y.; Liu, W.; Zeng, L.; et al. First report of cyprinid herpesvirus 2 isolated from the golden crucian carp in China. *Aquaculture* **2022**, *558*, 738043. [CrossRef]
30. Zhao, R.; Geng, Y.; Yu, Z.; Wang, K.; Lai, W. New detection of Cyprinid herpesvirus 2 associated with mass mortality in colour crucian carp (*Carassius auratus*), in China. *Aquac. Res.* **2019**, *50*, 1705–1709. [CrossRef]
31. Livak, K.J.; Schmittgen, T.D. Analysis of relative gene expression data using real-time quantitative PCR and the 2(-Delta Delta C(T)) method. *Methods* **2013**, *25*, 402–408. [CrossRef] [PubMed]
32. Zhang, C.; Wang, J.; Qi, Q.; Yang, L.; Sun, P.; Yuan, X. Modulatory effect of fructooligosaccharide against triphenyltin-induced oxidative stress and immune suppression in goldfish (*Carassius auratus*). *Ecotoxicol. Environ. Saf.* **2021**, *212*, 111966. [CrossRef]
33. Li, Z.; Song, J.A.; Choi, C. Oxidative Stress and Apoptosis in Goldfish (*Carassius auratus*) Caused by Exposure to Different Concentrations of Micro-polystyrene. *Ocean. Polar Res.* **2021**, *43*, 141–148. [CrossRef]
34. Yang, G.; Shen, K.; Yu, R.; Wu, Q.; Yan, Q.; Chen, W.; Ding, L.; Kumar, V.; Wen, C.; Peng, M. Probiotic (*Bacillus cereus*) enhanced growth of Pengze crucian carp concurrent with modulating the antioxidant defense response and exerting beneficial impacts on inflammatory response via Nrf2 activation. *Aquaculture* **2020**, *529*, 735691. [CrossRef]
35. Sun, F.; Zhang, Y.B.; Liu, T.K.; Gan, L.; Yu, F.F.; Liu, Y.; Gui, J.F. Characterization of fish IRF3 as an IFN-inducible protein reveals evolving regulation of IFN response in vertebrates. *J. Immunol.* **2010**, *185*, 7573–7582. [CrossRef] [PubMed]
36. Zhang, X.; Liu, Z.; Li, C.; Zhang, Y.; Wang, L.; Wei, J.; Qin, Q. Characterization of orange-spotted grouper (*Epinephelus coioides*) ASC and caspase-1 involved in extracellular ATP-mediated immune signaling in fish. *Fish Shellfish Immunol.* **2020**, *97*, 58–71. [CrossRef] [PubMed]
37. Zhou, Y.; Lu, L.F.; Lu, X.B.; Li, S.; Zhang, Y.A. Grass carp cGASL negatively regulates fish IFN response by targeting MITA. *Fish Shellfish Immunol.* **2019**, *94*, 871–879. [CrossRef]

38. Goodwin, A.E.; Merry, G.E.; Sadler, J. Detection of the herpesviral hematopoietic necrosis disease agent (*Cyprinid herpesvirus* 2) in moribund and healthy goldfish: Validation of a quantitative PCR diagnostic method. *Dis. Aquat. Org.* **2006**, *69*, 137–143. [CrossRef]
39. Schloss, P.D.; Westcott, S.L.; Ryabin, T.; Hall, J.R.; Hartmann, M.; Hollister, E.B.; Lesniewski, R.A.; Oakley, B.B.; Parks, D.H.; Robinson, C.J. Introducing mothur: Open-Source, Platform-Independent, Community-Supported Software for Describing and Comparing Microbial Communities. *Appl. Environ. Microbiol.* **2009**, *75*, 7537–7541. [CrossRef]
40. Edgar, R.C. UPARSE: Highly accurate OTU sequences from microbial amplicon reads. *Nat. Methods* **2013**, *10*, 996–998. [CrossRef]
41. Wang, Q.; Garrity, G.M.; Tiedje, J.M.; Cole, J.R. Naive Bayesian classifier for rapid assignment of rRNA sequences into the new bacterial taxonomy. *Appl. Environ. Microbiol.* **2007**, *73*, 5261–5267. [CrossRef] [PubMed]
42. Grice, E.A.; Kong, H.H.; Conlan, S.; Deming, C.B.; Davis, J.; Young, A.C.; NISC Comparative Sequencing Program; Bouffard, G.G.; Blakesley, R.W.; Murray, P.R.; et al. Topographical and temporal diversity of the human skin microbiome. *Science* **2009**, *324*, 1190–1192. [CrossRef] [PubMed]
43. Gonçalves, R.A.; Schatzmayr, D.; Albalat, A.; Mackenzie, S. Mycotoxins in aquaculture: Feed and food. *Rev. Aquac.* **2020**, *12*, 145–175. [CrossRef]
44. Xu, Z.; Regenstein, J.M.; Xie, D.; Lu, W.; Ren, X.; Yuan, J.; Mao, L. The oxidative stress and antioxidant responses of Litopenaeus vannamei to low temperature and air exposure. *Fish Shellfish Immunol.* **2018**, *72*, 564–571. [CrossRef] [PubMed]
45. El-Barbary, M.I. Detoxification and antioxidant effects of garlic and curcumin in Oreochromis niloticus injected with aflatoxin B-1 with reference to gene expression of glutathione peroxidase (GPx) by RT-PCR. *Fish Physiol. Biochem.* **2016**, *42*, 617–629. [CrossRef] [PubMed]
46. Huang, Y.; Han, D.; Zhu, X.; Yang, Y.; Jin, J.; Chen, Y.; Xie, S. Response and recovery of gibel carp from subchronic oral administration of aflatoxin B1. *Aquaculture* **2011**, *319*, 89–97. [CrossRef]
47. Liu, L.; Wang, H.; Xu, M.; Qiu, T.-X.; Chen, J. Azoxystrobin increases the infection of spring viraemia of carp virus in fish. *Chemosphere* **2021**, *285*, 131465. [CrossRef]
48. Xue, M.; Jiang, N.; Fan, Y.; Yang, T.; Li, M.; Liu, W.; Li, Y.; Li, B.; Zeng, L.; Zhou, Y. White spot syndrome virus (WSSV) infection alters gut histopathology and microbiota composition in crayfish (*Procambarus clarkii*). *Aquac. Rep.* **2022**, *22*, 101006. [CrossRef]
49. Ballard, J.W.O.; Towarnicki, S.G. Mitochondria, the gut microbiome and ROS. *Cell. Signal.* **2020**, *75*, 109737. [CrossRef]
50. Backhed, F.; Ley, R.E.; Sonnenburg, J.L.; Peterson, D.A.; Gordon, J.I. Host-bacterial mutualism in the human intestine. *Science* **2005**, *307*, 1915–1920. [CrossRef]
51. Wang, Y.; Zhang, Z.; Li, B.; He, B.; Li, L.; Nice, E.C.; Zhang, W.; Xu, J. New Insights into the Gut Microbiota in Neurodegenerative Diseases from the Perspective of Redox Homeostasis. *Antioxidants* **2022**, *11*, 2287. [CrossRef]
52. Feng, Q.Q.; Chen, W.D.; Wang, Y.D. Gut Microbiota: An Integral Moderator in Health and Disease. *Front. Microbiol.* **2018**, *9*, 151. [CrossRef] [PubMed]
53. Sun, R.; Xu, K.; Ji, S.; Pu, Y.; Man, Z.; Ji, J.; Chen, M.; Yin, L.; Zhang, J.; Pu, Y. Benzene exposure induces gut microbiota dysbiosis and metabolic disorder in mice. *Sci. Total Environ.* **2020**, *705*, 135879. [CrossRef]
54. Zhang, P.; Lu, G.; Liu, J.; Yan, Z.; Wang, Y. Toxicological responses of Carassius auratus induced by benzophenone-3 exposure and the association with alteration of gut microbiota. *Sci. Total Environ.* **2020**, *747*, 141255. [CrossRef] [PubMed]
55. Zhang, Y.; Li, Z.; Kholodkevich, S.; Sharov, A.; Feng, Y.; Ren, N.; Sun, K. Microcystin-LR-induced changes of hepatopancreatic transcriptome, intestinal microbiota, and histopathology of freshwater crayfish (*Procambarus clarkii*). *Sci. Total Environ.* **2020**, *711*, 134549. [CrossRef]
56. She, R.; Li, T.T.; Luo, D.; Li, J.B.; Yin, L.Y.; Li, H.; Liu, Y.M.; Li, X.Z.; Yan, Q.G. Changes in the Intestinal Microbiota of Gibel Carp (*Carassius gibelio*) Associated with Cyprinid herpesvirus 2 (CyHV-2) Infection. *Curr. Microbiol.* **2017**, *74*, 1130–1136. [CrossRef]
57. Wang, B.; Liu, J.; Lei, R.; Xue, B.; Li, Y.; Tian, X.; Zhang, K.; Luo, B. Cold exposure, gut microbiota, and hypertension: A mechanistic study. *Sci. Total Environ.* **2022**, *833*, 155199. [CrossRef]
58. Shin, N.R.; Whon, T.W.; Bae, J.W. Proteobacteria: Microbial signature of dysbiosis in gut microbiota. *Trends Biotechnol.* **2015**, *33*, 496–503. [CrossRef] [PubMed]
59. Fan, L.; Li, Q.X. Characteristics of intestinal microbiota in the Pacific white shrimp Litopenaeus vannamei differing growth performances in the marine cultured environment. *Aquaculture* **2019**, *505*, 450–461. [CrossRef]
60. Sossai, P. Butyric acid: What is the future for this old substance? *Swiss Med. Wkly.* **2012**, *142*, w13596. [CrossRef]
61. Dallagassa, C.B.; Surek, M.; Vizzotto, B.S.; Prediger, K.C.; Moriel, B.; Wolf, S.; Weiss, V.; Cruz, L.M.; Assis, F.E.A.; Paludo, K.S.; et al. Characteristics of an Aeromonas trota strain isolated from cerebrospinal fluid. *Microb. Pathog.* **2018**, *116*, 109–112. [CrossRef]
62. Tsuchiya, C.; Sakata, T.; Sugita, H. Novel ecological niche of Cetobacterium somerae, an anaerobic bacterium in the intestinal tracts of freshwater fish. *Lett. Appl. Microbiol.* **2008**, *46*, 43–48. [CrossRef]
63. Erttmann, S.F.; Swacha, P.; Aung, K.M.; Brindefalk, B.; Jiang, H.; Hartlova, A.; Uhlin, B.E.; Wai, S.N.; Gekara, N.O. The gut microbiota prime systemic antiviral immunity via the cGAS-STING-IFN-I axis. *Immunity* **2022**, *55*, 847–861.e810. [CrossRef]
64. Abt, M.C.; Osborne, L.C.; Monticelli, L.A.; Doering, T.A.; Alenghat, T.; Sonnenberg, G.F.; Paley, M.A.; Antenus, M.; Williams, K.L.; Erikson, J.; et al. Commensal Bacteria Calibrate the Activation Threshold of Innate Antiviral Immunity. *Immunity* **2012**, *37*, 158–170. [CrossRef] [PubMed]

65. Li, T.; Ke, F.; Gui, J.-F.; Zhou, L.; Zhang, X.-J.; Zhang, Q.-Y. Protective effect of Clostridium butyricum against Carassius auratus herpesvirus in gibel carp. *Aquac. Int.* **2019**, *27*, 905–914. [CrossRef]
66. Mishra, S.R.; Mahapatra, K.K.; Behera, B.P.; Patra, S.; Bhol, C.S.; Panigrahi, D.P.; Praharaj, P.P.; Singh, A.; Patil, S.; Dhiman, R.; et al. Mitochondrial dysfunction as a driver of NLRP3 inflammasome activation and its modulation through mitophagy for potential therapeutics. *Int. J. Biochem. Cell Biol.* **2021**, *136*, 106013. [CrossRef]

antioxidants

MDPI

Article

Dietary Histamine Impairs the Digestive Physiology Function and Muscle Quality of Hybrid Grouper (*Epinephelus fuscoguttatus*♀ × *Epinephelus lanceolatus*♂)

Yumeng Zhang [1,2,3], Hang Zhou [1,2,3], Yu Liu [1,2,3], Lulu Zhu [1,2,3], Jiongting Fan [1,2,3], Huajing Huang [1,2,3], Wen Jiang [1,2,3], Junming Deng [1,2,3,*] and Beiping Tan [1,2,3,*]

[1] College of Fisheries, Guangdong Ocean University, Zhanjiang 524088, China
[2] Aquatic Animals Precision Nutrition and High Efficiency Feed Engineering Research Centre of Guangdong Province, Zhanjiang 524088, China
[3] Key Laboratory of Aquatic, Livestock and Poultry Feed Science and Technology in South China, Ministry of Agriculture, Zhanjiang 524088, China
* Correspondence: jmdeng@stu.gdou.edu.cn (J.D.); tanbp@gdou.edu.cn (B.T.)

Abstract: An 8-week feeding experiment was conducted to investigate the effect of dietary histamine on growth performance, digestive physiology function and muscle quality in a hybrid grouper (*Epinephelus fuscoguttatus*♀ × *Epinephelus lanceolatus*♂). Seven isoproteic (50%) and isolipidic (11%) diets were prepared with various histamine inclusion levels of 0, 30, 60, 120, 240, 480 and 960 mg/kg in diets (actual contents were 72.33, 99.56, 138.60, 225.35, 404.12, 662.12 and 1245.38 mg/kg), respectively. Each diet was randomly assigned to triplicates of 30 juveniles (average body weight 14.78 g) per tank in a flow-through mariculture system. The increase in the dietary histamine level up to 1245.38 mg/kg made no significant difference on the growth rate and feed utilization of the grouper. However, the increased histamine content linearly decreased the activities of digestive enzymes, while no differences were observed in groups with low levels of histamine (≤404.12 mg/kg). Similarly, high levels of histamine (≥404.12 mg/kg) significantly damaged the gastric and intestinal mucosa, disrupted the intestinal tight junction structure, and raised the serum diamine oxidase activity and endotoxin level. Meanwhile, high doses of histamine (≥662.12 mg/kg) significantly reduced the activities of antioxidant enzymes, upregulated the relative expression of Kelch-like ECH-associated protein 1, and hardened and yellowed the dorsal muscle of grouper. These results showed that dietary histamine was detrimental to the digestive physiology function and muscle quality of the grouper, although it did compromise its growth performance.

Keywords: histamine; hybrid grouper; growth performance; antioxidant response; digestive physiology function; muscle texture

Citation: Zhang, Y.; Zhou, H.; Liu, Y.; Zhu, L.; Fan, J.; Huang, H.; Jiang, W.; Deng, J.; Tan, B. Dietary Histamine Impairs the Digestive Physiology Function and Muscle Quality of Hybrid Grouper (*Epinephelus fuscoguttatus*♀ × *Epinephelus lanceolatus*♂). *Antioxidants* **2023**, *12*, 502. https://doi.org/10.3390/antiox12020502

Academic Editors: Bo Liu, Changyou Song and Cunxin Sun

Received: 28 November 2022
Revised: 9 February 2023
Accepted: 14 February 2023
Published: 16 February 2023

1. Introduction

As the main protein source of aquafeed, fishmeal is widely used in the feed of carnivorous fish. Thus, the quality of fishmeal has attracted considerable attention in the aquaculture industry [1–3]. During the processing and storage of fishmeal, a hazardous level of histamine is easily produced by the microbial decarboxylation of free histidine present in fishmeal [4,5]. Thus, histamine is regarded as a good indication of the quality of fishmeal [6,7]. Meanwhile, histamine can cause the poisoning of animals, including fish [8]. Previous studies have shown that high levels of histamine in diets can reduce the growth rate and increase the mortality rate of chickens, as well as cause stomach erosion [9,10]. However, dietary histamine has different effects on the growth of various fish species. Dietary histamine inhibited the growth of American eel (*Anguilla rostrata*) [11], damaged the gastrointestinal tract structure of yellow catfish (*Pelteobagrus fulvidraco*) [12] and rainbow trout (*Oncorhynchus mykiss*) [13], and reduced the antioxidant capacity and immunity of

American eel [14]. Conversely, dietary histamine had no negative impact [15,16] and even improved the growth performance of other fish species [12,17]. Therefore, the potential effects of dietary histamine on the growth and health of fish need to be further clarified.

The hybrid grouper (*Epinephelus fuscoguttatus*♀ × *E. polyphekadion*♂) has a bright future because of its fast growth and delicate flesh [18], and is widely farmed in China and Southeast Asia [19,20]. The hybrid grouper, as a typical carnivorous fish, has a high protein requirement (about 45–50%) in compound feed, with a high level of fishmeal [21]. In addition, the hybrid grouper is mostly farmed in high temperature and high humidity environments, and the diets are easily deteriorated to produce a large amount of histamine. However, the effects of dietary histamine on the growth performance and digestive physiology function of the hybrid grouper have been less reported. Thus, the present study was conducted to clarify the effects of dietary histamine on growth performance, digestive enzyme activities, the structure and function of the gastrointestinal tract, and the dorsal muscle texture and color, and thereby determine the tolerance level of the hybrid grouper to dietary histamine.

2. Materials and Methods

2.1. Experimental Feed

Fish meal, soy protein concentrate and soybean meal were used as the main protein sources, and soybean oil and soybean lecithin were used as the main lipid sources. Histamine dihydrochloride (purity ≥ 98%, Macklin Biochemical Co., Ltd., Shanghai, China) was selected as the source of histamine (Table 1). Our preliminary investigation showed that the histamine content in 130 commercial grouper diets ranged from 59 to 1120 mg/kg (Table S1). Seven isoproteic and isolipidic diets (named H0, H3, H6, H12, H24, H48 and H96) were prepared with histamine inclusion levels of 0, 30, 60, 120, 240, 480 and 960 mg/kg; the actual histamine contents were 72.33, 99.56, 138.60, 225.35, 404.12, 662.12 and 1245.38 mg/kg diets. All materials (expect for lipid sources) were crushed and passed through a sieve with a 60-mesh diameter, and then weighed according to the feed formula and mixed evenly. Soybean oil and soybean phospholipid were then added to the mixture and re-blended. Finally, approximately 25% distilled water was added to make a dough, and the dough was squeezed into 2.5 mm pellets by a double helix extrusion mechanism (F-26 type; South China University of Technology, Guangzhou, China). The feeds were placed in the shade to dry naturally for two days and then stored at −20 °C.

Table 1. Ingredients and chemical composition of the experimental diets (% dry matter).

Ingredients (%)	Diets						
	H0	**H3**	**H6**	**H12**	**H24**	**H48**	**H96**
Fish meal	45.00	45.00	45.00	45.00	45.00	45.00	45.00
Soy protein concentrate	21.00	21.00	21.00	21.00	21.00	21.00	21.00
Soybean meal	6.00	6.00	6.00	6.00	6.00	6.00	6.00
Wheat flour	17.91	17.91	17.91	17.91	17.91	17.91	17.91
Soybean oil	5.30	5.30	5.30	5.30	5.30	5.30	5.30
Soybean lecithin	2.00	2.00	2.00	2.00	2.00	2.00	2.00
$Ca(H_2PO_4)_2$	1.20	1.20	1.20	1.20	1.20	1.20	1.20
Choline chloride	0.40	0.40	0.40	0.40	0.40	0.40	0.40
Vitamin C	0.03	0.03	0.03	0.03	0.03	0.03	0.03
Vitamin and mineral premixes [1]	1.00	1.00	1.00	1.00	1.00	1.00	1.00
Histamine dihydrochloride (mg/kg) [2]	0.00	50.70	101.39	202.78	405.56	811.13	1622.25
Cellulose microcrystalline (mg/kg)	1622.25	1571.55	1520.86	1419.47	1216.69	811.12	0.00
Proximate composition							
Dry matter (DM, %)	92.34	92.28	92.30	92.30	92.35	92.40	92.36
Crude protein (% DM)	49.50	50.20	48.97	49.18	49.23	50.11	49.79
Crude lipid (% DM)	11.27	11.30	11.28	11.28	11.28	11.27	11.26
Histamine (mg/kg DM)	72.33	99.56	138.60	225.35	404.12	662.12	1245.38

[1] Supplied by Beijing Enhalor Biotechnology Co., Ltd., Beijing, China. [2] Supplied by Macklin Biochemical Co., Ltd., Shanghai, China; purity ≥ 98%.

2.2. Fish and Experimental Conditions

Experimental fish were purchased from a commercial fish farm (Zhanjiang, China). A total of 630 healthy and uniform juveniles (initial body weight 14.78 ± 0.01 g) were randomly assigned into 7 groups with triplicates of 30 juveniles per tank (0.3 m^3). Fish were fed twice daily at 8:00 and 17:00 for 8 weeks, and a siphon tube was used to remove feces from the tank daily to ensure the water quality in the flow-through mariculture system. During the experimental period, all tanks were kept under natural light conditions, with the water temperature at 26–30 °C and the dissolved oxygen level above 6 mg/L.

2.3. Sample Collection and Pre-Treatment

After the feeding trial, all fish were fasted for a day. The fish from each tank were weighed and counted to calculate the growth index, then anesthetized with eugenol solution. Four fish per tank were randomly selected, weighed or measured by body length, body weight, visceral mass weight and liver weight for the calculation of morphological indices.

Blood samples were removed from four fish per tank with a 1 mL syringe and placed at 4 °C for 12 h, and the serum was collected and stored at −80 °C. The stomach, foregut (one third of the intestinal segment near the stomach end) and hindgut (one third of the intestinal segment near the excretory opening) of six fish per tank were quickly put into liquid nitrogen for temporary storage and then stored at −80 °C for enzyme activity analyses. The hindguts of another four fish per tank were harvested and placed in an Eppendorf tube with RNA, which were later stored at 4 °C for a day and then put in a −80 °C refrigerator for an analysis of the relative mRNA expression.

In addition, the hindgut of four fish per tank were placed in 2.5% glutaraldehyde fixation solution and 4% paraformaldehyde solution, and the stomach was placed in 2.5% glutaraldehyde fixation solution for histological observation, respectively. The dorsal muscles were stripped and cut to the size of 3 cm × 3 cm × 1 cm for the analysis of textural characteristics and coloration.

2.4. Chemical Composition Analysis

The chemical composition of the experimental diets was determined with reference to the AOAC standard methods [22]. The moisture was dried at 105 °C to constant weight; crude protein was determined by an automatic Kjeldahl apparatus (Kjeltec™ 8400; Foss, Hoganas, Sweden); crude lipid was extracted with petroleum ether by the Soxhlet method; and crude ash was incinerated at 550 °C for 6 h. The content of histamine in the diet was determined by an enzyme-linked immunosorbent assay (ELISA) kit (Shanghai Enzyme Linked Biotechnology Co., Ltd., Shanghai, China).

2.5. Biochemical Indexes Analyses

In total, a 0.1 g sample of stomach/foregut/hindgut and a ninefold volume ice-cold saline solution was mixed and homogenized using a homogenizer (T 25 digital ULTRA-TURRAX®, IKA, Staufen, Germany), and the supernatant was collected after centrifugation at 3500 rpm/min for 10 min at 4 °C. The total antioxidant capacity (TAC), catalase (CAT), and superoxide dismutase (SOD) activities, as well as the malondialdehyde (MDA) content in the serum and hindgut, and the activities of lipase, maltase and amylase in the foregut, were measured by commercial kits (Nanjing Jiancheng Bioengineering Institute, Nanjing, China) according to the kit's instructions. The activity of pepsin in the stomach, the content of endotoxin and the activities of peroxidase (POD), glutathione peroxidase (GPx), glutathione reductases (GR) and diamine oxidase (DAO) in the serum and hindgut, and the activities of trypsin, Na^+/K^+-ATPase and Ca^{2+}/Mg^{2+}-ATPase in the foregut were measured using commercial kits (Shanghai Enzyme Linked Biotechnology Co., Ltd., Shanghai, China), according to the kit's instructions.

2.6. Histological Observation

The hindgut was soaked in a 4% formaldehyde solution for one day and then transferred to 70% ethanol for preservation. The hindgut was dehydrated in different concentrations of ethanol (70%, 80%, 90%, 95%, 100%), immersed in xylene solution to make it transparent and then embedded in paraffin. It was cut into sections of 5–7 μm thickness, stained by hematoxylin and eosin (H&E) and sealed with neutral gum. The slides were observed in a fluorescent inverted microscope (Nikon Eclipse Ni-U; Nikon, Tokyo, Japan), and ten folds per section were randomly selected to measure the fold height, fold width and muscle thickness by image acquisition software (CellSens Standard 1.8, Pooher Optoelectronics (Shanghai) Technology Co., Ltd., Shanghai, China). The hindgut and stomach were placed in a 2.5% glutaraldehyde fixed solution for 24 h; the production of intestinal transmission electron microscopy (TEM) sections was performed with reference to Huang's method [23]. The scanning electron microscopy (SEM) sections of the stomach were made with reference to Chen's method [24].

2.7. Extraction of RNA and Real-Time Quantitative PCR Analysis

The total RNA from the hindgut was extracted using TransZol Up Plus RNA Kit (Beijing TransGen Biotech Co. Ltd., Beijing, China). The integrity of the total RNA was confirmed by 1% agarose gel electrophoresis, and the purity and concentration of the total RNA were evaluated spectrophotometrically (A260:280 nm). Then, the PrimeScript^{TM} RT eagent Kit (Takara, Tokyo, Japan) was used to reverse transcribe the RNA into cDNA according to the kit's instructions. Based on the sequences in Gen Bank, gene-specific primers were designed using Primer 5 software (Table 2), and β-action was selected as the reference gene. The relative expression levels of the target genes were calculated using the $2^{-\Delta\Delta CT}$ method [25]; H0 was the reference group.

Table 2. The forward and reverse primers used for real-time quantitative PCR analysis and accession numbers of gene sequences (GenBank).

Target Gene	Primer Sequence	GenBank Accession No.
claudin3	F-AGCCTTCATCGGCAGCAA R-GGATGCCTCGTCGTCAATG	EU714179.1
occludin	F-GGAGGAGAAACAGGGAATGAACT R-TCTGCTACAGCCTGGTATTTGG	KF861990.1
Keap1 [1]	F-TCCACAAACCCACCAAAGTAA R-TCCACCAACAGCGTAGAAAAG	XM_018665037.1
Nrf2 [2]	F-TATGGAGATGGGTCCTTTGGTG R-GCTTCTTTTCCTGCGTCTGTTG	KU892416.1
β-Actin	F-GGCTACTCCTTCACCACCACA R-TCTGGGCAACGGAACCTCT	AY510710.2

[1] Keap1, kelch-like ECH-associated protein 1. [2] Nrf2, nuclear factor erythroid 2-related factor 2.

2.8. Muscle Texture and Color Analysis

The textural characterization of the dorsal muscle was analyzed by the texture analyzer (TMS-PRO, Food Technology Corporation, Sterling, VA, USA). The color of the dorsal muscle was measured using a color colorimeter (Chroma Meter CR-400, Konica Minolta, Inc., Tokyo, Japan).

2.9. Calculations and Statistical Analysis

Formulas for growth performance and body index are as follows:
Weight gain (WG) = $(W_f - W_i)/W_i$;
Specific growth ratio (SGR, %/d) = $100 \times (\text{Ln } W_f - \text{Ln } W_i)/t$;
Voluntary feed intake (VFI, mg/MBW/d) = $FI/((W_i + W_f)/2)/t \times 1000$;
Feed conversion ratio (FCR) = $FI/(W_f - W_i)$;
Protein efficiency ratio (PER) = $(W_f - W_i)/(F \times CP)$;

Survival rate (SR, %) = $100 \times (N_f - N_i)/N_i$;
Hepatosomatic index (HSI, %) = $100 \times W_l/W_b$;
Viscerosomatic index (VSI, %) = $100 \times W_v/W_b$;
Condition factor (CF, g/cm^3) = $100 \times W_f/L^3$;

Where W_f and W_i are the final body weight (g) and initial body weight (g); t is feeding days (d); FI is feed intake per fish (g); CP is crude protein content of feed (%); N_f and N_i are final fish number and initial fish number; and W_b, W_v, W_l and L are body weight (g), viscera weight (g), liver weight (g) and body length (cm).

The data were analyzed by a one-way analysis of variance followed by Duncan's multiple range tests. A significant difference was set at the level of $p < 0.05$. For detecting the potential linear or quadratic effects of the dietary histamine level, all data were also subjected to polynomial orthogonal contrast analysis. Statistical analysis was performed using SPSS 21.0 (SPSS Inc., Chicago, IL, USA) for Windows.

3. Results

3.1. Growth Performance

After the 8-week feeding trial, the SR of the grouper ranged from 90.00% to 97.78%, and no significant difference was found among the dietary groups ($p > 0.05$, Table 3). Similarly, no significant differences were observed in the WG, SGR, VFI, FCR, PER, HSI, VSI and CF of the grouper among the dietary groups ($p > 0.05$). However, the SR, PER and CF showed negative linear ($p < 0.05$) and quadratic ($p < 0.05$) trends in response to the dietary histamine level, while the HSI and VSI exhibited a negative linear trend in response to the dietary histamine level ($p < 0.05$).

3.2. Digestive Enzyme Activity

The dietary histamine level did not affect the foregut maltase and Ca^{2+}/Mg^{2+}-ATPase activities ($p > 0.05$, Table 4). The activities of pepsin, foregut trypsin, lipase, amylase, and Na^+/K^+-ATPase showed significantly negative linear ($p < 0.01$) and quadratic ($p < 0.01$) trends in response to the dietary histamine content; meanwhile, no significant differences were observed in the pepsin and lipase activities among the H0, H3, H6, and H12 groups, in the trypsin and amylase activities among the H0, H3, and H6 groups, and in the Na^+/K^+-ATPase activity among the H0, H3, H6, H12, and H24 groups ($p > 0.05$).

3.3. Intestinal Permeability

The serum DAO activity and endotoxin level increased with the rising dietary histamine content (Figure 1). Thus, the DAO activity was significantly higher in the H96 group compared to the H0 group ($p < 0.05$), and the endotoxin level was significantly higher in the H48 and H96 groups compared to the H0, H3 and H6 groups ($p < 0.05$).

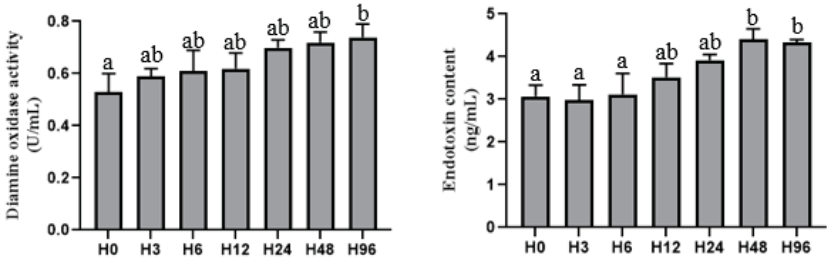

Figure 1. Effect of dietary histamine content on the intestinal permeability-related index in the serum of the hybrid grouper. Values are means ± SE of three replications. Different superscript letters in the bars indicate a significant difference among treatments by Tukey's test ($p < 0.05$).

Table 3. Effects of dietary histamine content on growth performance, feed utilization and body index of hybrid grouper.

	Diets							*p*-Value	
	H0	**H3**	**H6**	**H12**	**H24**	**H48**	**H96**	**Linear**	**Quadratic**
Initial body weight (g)	14.77 ± 0.01	14.80 ± 0.01	14.76 ± 0.01	14.81 ± 0.00	14.76 ± 0.05	14.76 ± 0.01	14.77 ± 0.01	0.486	0.581
Final body weight (g)	116.39 ± 0.25	117.19 ± 1.49	115.01 ± 1.84	114.62 ± 1.03	114.76 ± 1.53	114.18 ± 0.46	113.57 ± 0.70	0.080	0.159
Weight gain	6.88 ± 0.03	6.81 ± 0.02	6.79 ± 0.13	6.74 ± 0.07	6.78 ± 0.09	6.73 ± 0.03	6.69 ± 0.05	0.128	0.285
Specific growth ratio (%/d)	3.62 ± 0.01	3.60 ± 0.00	3.60 ± 0.03	3.59 ± 0.01	3.60 ± 0.02	3.59 ± 0.01	3.58 ± 0.01	0.131	0.291
Voluntary feed intake (mg/MBW/d)	23.62 ± 0.50	23.26 ± 0.23	23.47 ± 0.42	23.31 ± 0.46	23.86 ± 0.15	23.61 ± 0.09	23.73 ± 0.39	0.414	0.634
Feed conversion ratio	0.83 ± 0.01	0.87 ± 0.01	0.87 ± 0.04	0.89 ± 0.02	0.88 ± 0.03	0.89 ± 0.02	0.90 ± 0.02	0.059	0.110
Protein efficiency ratio	2.44 ± 0.03	2.38 ± 0.04	2.40 ± 0.07	2.37 ± 0.03	2.31 ± 0.03	2.32 ± 0.07	2.29 ± 0.02	0.021	0.041
Survival rate (%)	96.67 ± 0.00	97.78 ± 1.11	96.67 ± 3.33	93.33 ± 1.93	91.11 ± 2.94	90.00 ± 3.33	90.00 ± 3.33	0.007	0.003
Hepatosomatic index (%)	4.55 ± 0.12	4.46 ± 0.29	4.20 ± 0.22	4.09 ± 0.18	4.02 ± 0.29	3.94 ± 0.22	3.87 ± 0.25	0.043	0.056
Viscerosomatic index (%)	12.79 ± 0.35	12.51 ± 0.61	12.16 ± 0.32	11.97 ± 0.46	11.86 ± 0.31	11.67 ± 0.42	11.50 ± 0.49	0.041	0.061
Condition factor (g/cm^3)	3.01 ± 0.09	2.86 ± 0.12	2.82 ± 0.08	2.87 ± 0.10	2.74 ± 0.07	2.73 ± 0.05	2.73 ± 0.03	0.023	0.011

Values are means ± standard error (SE) of three replications. Different superscript letters in each row show significant differences among treatments by Tukey's test ($p < 0.05$).

Table 4. Effect of dietary histamine content on the digestive enzyme activity in the gastrointestinal tract of the hybrid grouper.

	Diets							*p*-Value	
	H0	**H3**	**H6**	**H12**	**H24**	**H48**	**H96**	**Linear**	**Quadratic**
Stomach									
Pepsin (U/mg protein)	56.05 ± 2.82 ^{bc}	58.39 ± 1.36 ^{c}	51.32 ± 4.41 ^{abc}	49.60 ± 3.32 ^{abc}	45.57 ± 3.18 ^{ab}	44.56 ± 3.72 ^{ab}	42.57 ± 1.70 ^{a}	0.009	0.008
Foregut									
Trypsin (U/μg protein)	0.25 ± 0.02 ^{c}	0.25 ± 0.02 ^{c}	0.22 ± 0.01 ^{bc}	0.19 ± 0.01 ^{ab}	0.19 ± 0.01 ^{ab}	0.17 ± 0.01 ^{a}	0.18 ± 0.01 ^{ab}	0.002	<0.001
Lipase (U/g protein)	1.65 ± 0.04 ^{c}	1.68 ± 0.06 ^{c}	1.49 ± 0.06 ^{abc}	1.54 ± 0.15 ^{bc}	1.37 ± 0.07 ^{ab}	1.26 ± 0.03 ^{a}	1.27 ± 0.09 ^{a}	<0.001	<0.001
Amylase (U/mg protein)	0.38 ± 0.00 ^{c}	0.33 ± 0.02 ^{bc}	0.31 ± 0.02 ^{abc}	0.26 ± 0.02 ^{ab}	0.29 ± 0.00 ^{ab}	0.25 ± 0.03 ^{ab}	0.25 ± 0.05 ^{a}	0.009	0.005
Maltase (U/mg protein)	13.93 ± 1.80	13.30 ± 0.56	12.88 ± 0.52	12.58 ± 1.49	11.49 ± 1.56	10.83 ± 0.74	10.72 ± 1.51	0.077	0.112
Na^+/K^+-ATPase (U/mg protein)	1.64 ± 0.12 ^{c}	1.63 ± 0.09 ^{c}	1.48 ± 0.06 ^{bc}	1.54 ± 0.08 ^{bc}	1.46 ± 0.09 ^{bc}	1.31 ± 0.03 ^{ab}	1.14 ± 0.02 ^{a}	<0.001	<0.001
Ca^{2+}/Mg^{2+}-ATPase (U/mg protein)	5.71 ± 0.49	5.73 ± 0.87	5.63 ± 0.43	5.52 ± 0.08	5.53 ± 0.74	5.12 ± 0.78	4.96 ± 0.07	0.213	0.450

Values are means ± standard error (SE) of three replications. Different superscript letters in each row show significant differences among treatments by Tukey's test ($p < 0.05$).

3.4. Gastrointestinal Tract Structure

3.4.1. SEM of Gastric Mucosa Cell

Damage to the gastric mucosal cells of the hybrid grouper was aggravated with the increasing dietary histamine content (Figure 2). In the H0 group, the gastric mucosa cells of the hybrid grouper were normal, with tightly arranged cells and clear borders; in the H24 group, some cells were ruptured and the rest were relatively intact; in the H96 group, most of the cells were severely damaged.

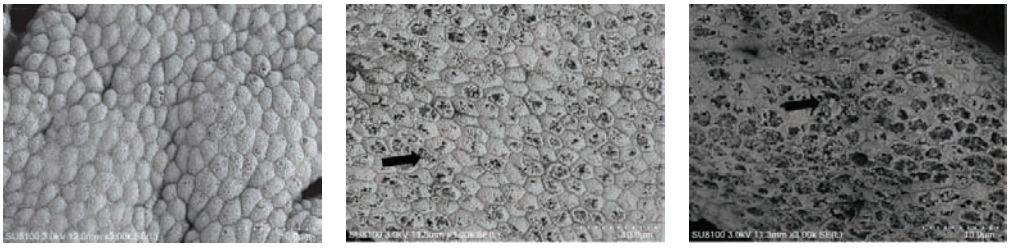

(**a**) (**b**) (**c**)

Figure 2. Scanning electron microscopy of gastric mucosa in the hybrid grouper fed with various dietary histamine levels. (**a**) indicates H0 group; (**b**) indicates H24 group; and (**c**) indicates H96 group. Arrows indicate cell damage. The cells of gastric mucosa cells in the H0 group were normal and tightly arranged; some cells in the H24 group were ruptured and the rest were relatively intact; most cells in the H96 group were severely damaged. The magnification was ×3.00 k, and the minimum scale (lower right) was 10.0 μm.

3.4.2. Intestinal Morphology

The dietary histamine content had no significant effect on the hindgut fold height and the muscular thickness of the grouper ($p > 0.05$, Table 5 and Figure 3). However, the hindgut fold width displayed the negative linear ($p < 0.01$) and quadratic ($p < 0.05$) trends in response to the dietary histamine level, which was significantly lower in the H96 group compared to the H0 group ($p < 0.05$).

Table 5. Effect of dietary histamine content on the intestinal histomorphology of the hybrid grouper.

	Diets							*p*-Value	
	H0	**H3**	**H6**	**H12**	**H24**	**H48**	**H96**	**Linear**	**Quadratic**
Fold height (μm)	643.16 ± 19.54	646.77 ± 17.25	647.34 ± 12.29	645.80 ± 19.92	637.39 ± 12.97	627.73 ± 7.95	617.98 ± 15.18	0.167	0.382
Fold width (μm)	82.28 ± 2.41 ^{b}	79.04 ± 3.21 ^{ab}	80.85 ± 3.14 ^{ab}	80.48 ± 2.77 ^{ab}	76.38 ± 3.16 ^{ab}	73.16 ± 3.05 ^{ab}	69.51 ± 2.63 ^{a}	0.008	0.025
Muscular thickness (μm)	147.27 ± 7.00	144.93 ± 9.01	145.42 ± 8.22	154.83 ± 6.98	155.31 ± 6.42	138.20 ± 6.71	142.61 ± 10.33	0.531	0.823

Values are means ± standard error (SE) of three replications. Different superscript letters in each row show significant differences among treatments by Tukey's test ($p < 0.05$).

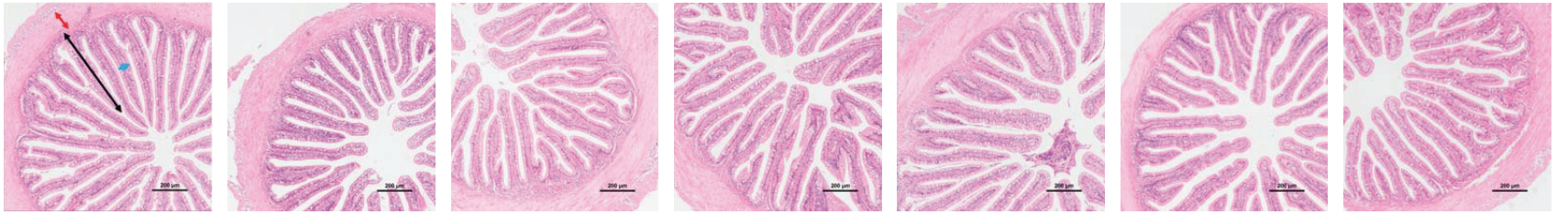

(**a**) (**b**) (**c**) (**d**) (**e**) (**f**) (**g**)

Figure 3. Effect of dietary histamine content on the hindgut histomorphology of the hybrid grouper. (**a**) indicates H0 group; (**b**) indicates H3 group; (**c**) indicates H6 group; (**d**) indicates H12 group; (**e**) indicates H24 group; (**f**) indicates H48 group; and (**g**) indicates H96 group. Black arrows: fold height (μm); blue arrows: fold width (μm); red arrows: muscular thickness (μm). The magnification was ×100, and the minimum scale (lower right) was 200 μm.

3.4.3. TEM of Intestinal Mucosal Cell

As shown in Figure 4, the linkage structure between the mucosal cells in the H0 group was tight and there were no gaps between the cells; meanwhile, in the H24 and H96 groups, gaps appeared at the microvilli end, indicating that the linkage structure between the mucosal cells was damaged.

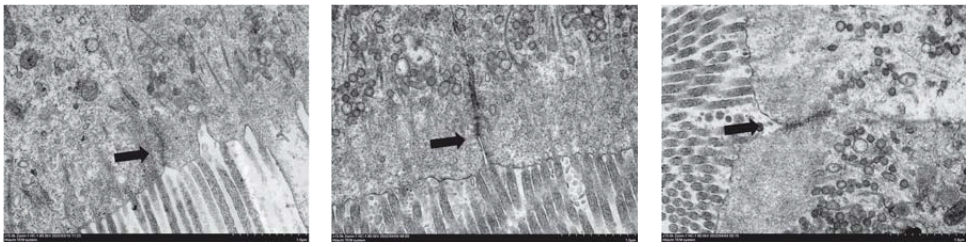

(**a**) (**b**) (**c**)

Figure 4. Transmission electron microscopy of intestinal mucosa in the hybrid grouper fed with various dietary histamine contents. (**a**) indicates H0 group; (**b**) indicates H24 group; and (**c**) indicates H96 group. Arrows indicate the junctions of the microvilli ends. The microvilli ends of intestinal mucosal cells in the H0 group were connected tightly between cells; in the H24 and H96 groups, gaps appeared between the microvilli ends of cells. The magnification was ×15.0 k, and the minimum scale (lower right) was 1.0 μm.

3.5. Antioxidant Index

Serum SOD, CAT, POD, GPx, GR, and TAC activities exhibited significantly negative linear ($p < 0.05$) and quadratic ($p < 0.05$) trends in response to the dietary histamine level (Table 6); meanwhile, no significant differences were found in the SOD and GPx activities among the H0, H3, H6 and H12 groups, in the CAT and GR activities among the H0, H3, H6, H12 and H24 groups, in the POD activity among the H0, H3, H6, H12, H24 and H48 groups, and in the TAC activity among the H0 and H3 groups ($p > 0.05$). Conversely, the serum MDA level showed significantly positive linear ($p < 0.001$) and quadratic ($p < 0.001$) trends in response to the dietary histamine level, which was significantly higher in the H12, H24, H48 and H96 groups compared to the H0, H3 and H6 groups ($p < 0.05$).

The dietary histamine content had no significant effect on the activities of SOD and POD in the hindgut of the grouper ($p > 0.05$, Table 7), but the POD activity displayed negative linear ($p < 0.05$) and quadratic ($p < 0.05$) trends in response to the dietary histamine level. A negative linear trend was observed in the hindgut CAT activity ($p < 0.05$), and was significantly lower in the H96 group compared to the H0, H3, H6 and H12 groups ($p < 0.05$). In addition, the activities of GPx, GR and TAC in the hindgut exhibited significantly negative linear ($p < 0.01$) and quadratic ($p < 0.05$) trends in response to the dietary histamine level; meanwhile, no significant differences were found in the GPx and GR activities among the H0, H3, H6 and H12 group, or in the TAC activity among the H0, H3, H6, H12, H24 and H48 groups ($p > 0.05$). Conversely, the hindgut MDA level showed a significantly positive linear ($p < 0.01$) and quadratic ($p < 0.01$) trend in response to the dietary histamine level, which was significantly higher in the H96 group compared to the H0 group ($p < 0.05$).

Table 6. Effect of dietary histamine content on the antioxidant-related index in the serum of the hybrid grouper.

	Diets							*p*-Value	
	H0	**H3**	**H6**	**H12**	**H24**	**H48**	**H96**	**Linear**	**Quadratic**
SOD (U/mL)	62.85 ± 2.26 ^{c}	61.64 ± 1.38 ^{bc}	56.76 ± 1.81 ^{abc}	56.70 ± 3.38 ^{abc}	54.90 ± 1.50 ^{ab}	55.35 ± 2.13 ^{a}	52.83 ± 1.65 ^{a}	0.003	0.002
CAT (U/mL)	9.71 ± 1.36 ^{b}	8.75 ± 1.19 ^{ab}	7.77 ± 0.37 ^{ab}	7.23 ± 0.52 ^{ab}	7.15 ± 0.79 ^{ab}	6.72 ± 1.04 ^{a}	6.10 ± 0.59 ^{a}	0.009	0.017
POD (U/mL)	0.34 ± 0.01 ^{b}	0.32 ± 0.02 ^{ab}	0.30 ± 0.03 ^{ab}	0.29 ± 0.01 ^{ab}	0.30 ± 0.01 ^{ab}	0.28 ± 0.02 ^{ab}	0.26 ± 0.02 ^{a}	0.004	0.014
GPx (U/mL)	0.17 ± 0.01 ^{b}	0.15 ± 0.01 ^{ab}	0.15 ± 0.01 ^{ab}	0.15 ± 0.01 ^{ab}	0.14 ± 0.00 ^{a}	0.13 ± 0.00 ^{a}	0.13 ± 0.01 ^{a}	0.012	0.005
GR (U/mL)	0.15 ± 0.01 ^{b}	0.15 ± 0.01 ^{b}	0.13 ± 0.01 ^{b}	0.13 ± 0.01 ^{b}	0.12 ± 0.00 ^{ab}	0.10 ± 0.00 ^{a}	0.10 ± 0.01 ^{a}	<0.001	<0.001
TAC (nmol/L)	1.83 ± 0.05 ^{c}	1.72 ± 0.05 ^{bc}	1.62 ± 0.03 ^{ab}	1.62 ± 0.00 ^{ab}	1.59 ± 0.04 ^{ab}	1.55 ± 0.06 ^{a}	1.53 ± 0.07 ^{a}	0.002	0.001
MDA (nmol/L)	3.30 ± 0.43 ^{a}	3.08 ± 0.24 ^{a}	3.27 ± 0.22 ^{a}	4.95 ± 0.44 ^{b}	6.03 ± 0.71 ^{b}	6.48 ± 0.47 ^{b}	6.43 ± 0.58 ^{b}	<0.001	<0.001

Values are means ± standard error (SE) of three replications. Different superscript letters in each row show significant differences among treatments by Tukey's test ($p < 0.05$).

Table 7. Effect of dietary histamine content on the antioxidant-related index in the hindgut of the hybrid grouper.

	Diets							*p*-Value	
	H0	**H3**	**H6**	**H12**	**H24**	**H48**	**H96**	**Linear**	**Quadratic**
SOD (U/μg protein)	0.60 ± 0.01	0.58 ± 0.02	0.59 ± 0.02	0.56 ± 0.02	0.62 ± 0.02	0.61 ± 0.01	0.60 ± 0.03	0.284	0.315
CAT (U/mg protein)	17.46 ± 0.91 ^{b}	17.51 ± 0.73 ^{b}	16.82 ± 1.84 ^{b}	16.85 ± 3.11 ^{b}	15.85 ± 1.07 ^{ab}	16.61 ± 0.85 ^{ab}	13.21 ± 0.50 ^{a}	0.047	0.139
POD (U/g protein)	27.13 ± 3.02	27.08 ± 0.57	25.57 ± 2.39	23.98 ± 3.43	22.16 ± 2.29	20.05 ± 3.16	18.69 ± 1.13	0.012	0.021
GPx (U/mg protein)	15.27 ± 1.31 ^{c}	16.08 ± 0.46 ^{c}	13.46 ± 0.57 ^{bc}	12.79 ± 0.97 ^{abc}	11.34 ± 0.84 ^{ab}	9.57 ± 1.22 ^{a}	9.64 ± 1.65 ^{a}	0.001	<0.001
GR (U/mg protein)	2.49 ± 0.21 ^{c}	2.62 ± 0.28 ^{c}	2.31 ± 0.09 ^{bc}	2.22 ± 0.15 ^{bc}	1.77 ± 0.11 ^{ab}	1.52 ± 0.21 ^{a}	1.67 ± 0.16 ^{a}	0.003	<0.001
TAC (mmol/g protein)	15.00 ± 2.64 ^{b}	13.66 ± 1.46 ^{ab}	13.07 ± 1.79 ^{ab}	12.97 ± 1.14 ^{ab}	10.57 ± 0.98 ^{ab}	10.32 ± 2.07 ^{ab}	8.75 ± 1.29 ^{a}	0.007	0.014
MDA (nmol/g protein)	22.87 ± 5.92 ^{a}	26.77 ± 5.08 ^{ab}	27.63 ± 3.34 ^{ab}	28.26 ± 2.36 ^{ab}	29.00 ± 2.61 ^{ab}	34.61 ± 6.42 ^{ab}	39.31 ± 2.50 ^{b}	0.001	0.004

Values are means ± standard error (SE) of three replications. Different superscript letters in each row show significant differences among treatments by Tukey's test ($p < 0.05$).

3.6. Dorsal Muscle Texture and Color

The dietary histamine content did not affect the adhesiveness, springiness and resilience of the dorsal muscle ($p > 0.05$; Table 8). The hardness, cohesiveness, gumminess, and chewiness of the dorsal muscle exhibited significantly positive linear ($p < 0.01$) and quadratic ($p < 0.01$) trends in response to the dietary histamine level; meanwhile, no significant differences were observed in the hardness and chewiness among the H0, H3, H6, H12, H24 and H48 groups, or in the cohesiveness and gumminess among the H0, H3, H6, H12 and H24 groups ($p < 0.05$).

The L* and a* values of the dorsal muscle were not affected by the dietary treatments ($p > 0.05$; Table 9). However, the b* value showed significantly positive linear ($p < 0.05$) and quadratic ($p < 0.05$) trends in response to the dietary histamine content, which was significantly higher in the H48 and H96 groups compared to the H0 group ($p < 0.05$).

3.7. The Relative mRNA Expression of Tight Junction Proteins and Oxidative Stress-Related Factors

There was no significant difference in the relative expression level of nuclear factor erythroid 2-related factor 2 (Nrf2) among the dietary groups ($p > 0.05$; Figure 5). The relative expression levels of intestinal claudin3 and occludin gradually decreased with the increase in dietary histamine content; meanwhile, no significant differences were observed in the relative expression level of claudin3 among the H0, H3, H6 and H12 groups, or in the relative expression level of occludin among the H0, H3, H6, H12 and H24 groups ($p < 0.05$). Conversely, the relative expression level of Kelch-like ECH-associated protein 1 (Keap1) increased with the rising dietary histamine content, which was significantly higher in the H96 groups compared to the H0 group ($p < 0.05$).

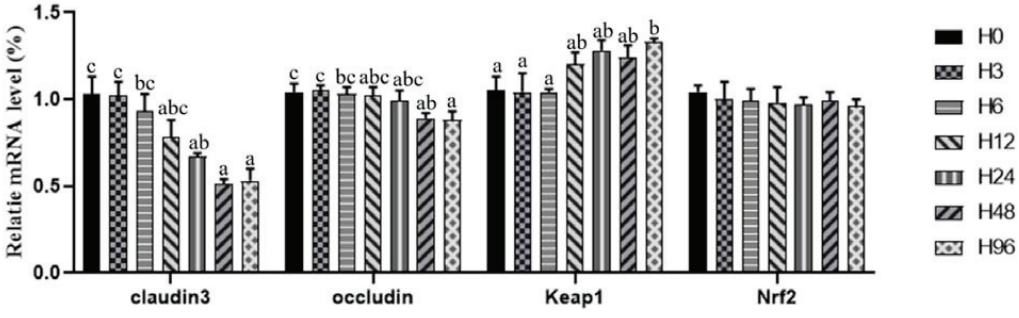

Figure 5. Effect of dietary histamine content on the relative mRNA expression of tight junction proteins and oxidative stress-related factors in the hindgut of the hybrid grouper. Keap1, Kelch-like ECH-associated protein 1; Nrf2, nuclear factor erythroid 2-related factor 2. Bars represent means ± SE of three replications. Different superscript letters in the bars indicate a significant difference among treatments by Tukey's test ($p < 0.05$).

Table 8. Effect of dietary histamine content on the dorsal muscle texture of the hybrid grouper.

	Diets							*p*-Value	
	H0	**H3**	**H6**	**H12**	**H24**	**H48**	**H96**	**Linear**	**Quadratic**
Hardness (kg)	0.95 ± 0.07 ^{a}	0.96 ± 0.08 ^{a}	1.06 ± 0.05 ^{ab}	1.08 ± 0.09 ^{ab}	1.16 ± 0.08 ^{ab}	1.15 ± 0.09 ^{ab}	1.25 ± 0.08 ^{b}	0.003	0.008
Adhesiveness (g.sec)	−11.29 ± 2.74	−9.13 ± 1.22	−10.33 ± 1.91	−8.35 ± 1.00	−11.03 ± 2.14	−10.97 ± 2.29	−10.50 ± 2.06	0.729	0.922
Springiness	0.23 ± 0.02	0.26 ± 0.06	0.22 ± 0.02	0.28 ± 0.04	0.23 ± 0.03	0.23 ± 0.04	0.24 ± 0.05	0.817	0.961
Cohesiveness	0.10 ± 0.00 ^{a}	0.09 ± 0.00 ^{a}	0.10 ± 0.01 ^{a}	0.12 ± 0.00 ^{ab}	0.11 ± 0.01 ^{ab}	0.13 ± 0.01 ^{bc}	0.15 ± 0.01 ^{c}	<0.001	<0.001
Gumminess	85.85 ± 13.39 ^{a}	86.86 ± 7.46 ^{a}	110.87 ± 13.44 ^{ab}	115.02 ± 13.15 ^{ab}	122.43 ± 3.75 ^{ab}	118.84 ± 11.89 ^{b}	113.67 ± 23.77 ^{b}	0.003	0.005
Chewiness	20.75 ± 0.75 ^{a}	19.94 ± 3.04 ^{a}	27.83 ± 4.67 ^{ab}	38.18 ± 5.83 ^{ab}	36.23 ± 7.67 ^{ab}	39.63 ± 8.51 ^{ab}	42.88 ± 7.39 ^{b}	0.008	0.008
Resilience	0.04 ± 0.00	0.04 ± 0.00	0.04 ± 0.00	0.04 ± 0.00	0.04 ± 0.00	0.04 ± 0.00	0.05 ± 0.01	0.123	0.262

Values are means ± standard error (SE) of three replications. Different superscript letters in each row show significant differences among treatments by Tukey's test ($p < 0.05$).

Table 9. Effect of dietary histamine content on the color of the dorsal muscle of the hybrid grouper.

	Diets							*p*-value	
	H0	**H3**	**H6**	**H12**	**H24**	**H48**	**H96**	**Linear**	**Quadratic**
L value [1]	59.52 ± 1.40	59.76 ± 1.43	59.71 ± 0.94	60.08 ± 0.84	60.10 ± 0.70	60.19 ± 1.73	59.34 ± 1.49	0.906	0.832
a value [2]	−3.94 ± 0.13	−3.63 ± 0.32	−3.19 ± 0.46	−3.75 ± 0.33	−3.87 ± 0.24	−3.92 ± 0.12	−3.72 ± 0.31	0.710	0.840
b value [3]	6.43 ± 0.29 ^{a}	7.54 ± 0.70 ^{ab}	7.59 ± 0.75 ^{ab}	6.93 ± 0.36 ^{ab}	7.77 ± 0.39 ^{ab}	8.42 ± 0.28 ^{b}	8.48 ± 0.28 ^{b}	0.010	0.021

[1] If the value is positive, the sample is brighter than the standard version; if it is negative, it is darker. [2] If the value is positive, the sample is redder than the standard version; if it is negative, it is greener. [3] If the value is positive, the sample is more yellow than the standard version; if it is negative, it is bluer. Values are means ± standard error (SE) of three replications. Different superscript letters in each row show significant differences among treatments by Tukey's test ($p < 0.05$).

4. Discussion

Dietary histamine is a toxin to some fish species [26,27] and has a negative impact on the growth of fish [15,16,28–30]. However, the effects of dietary histamine on the growth of fish vary with different fish species. It has been shown that a low level of dietary histamine does not affect the growth performance of yellow catfish [12,31], American eel [28] and rainbow trout [13], and even has a beneficial effect on the growth of yellow catfish [12] and Atlantic salmon (*Salmo salar* L.) [17]. In this study, the growth performance of the hybrid grouper was not affected by the dietary histamine content (72–1245 mg/kg), which is consistent with the results of previous studies with orange-spotted grouper (*Epinephelus coioides*, 158.7–2158.7 mg/kg) [3], yellow catfish (100–1000 mg/kg) [31] and American eel (67–414 mg/kg) [28]. Meanwhile, the SR and PER exhibited negative linear and quadratic trends in response to the dietary histamine level, suggesting that dietary histamine has a negative effect on the growth and health of the hybrid grouper. Liu et al. found that up to 2000 mg/kg of dietary histamine did not result in a remarkable reduction in growth, whereas 2500 mg/kg or more of dietary histamine could cause significant negative effects on the growth and health of the orange-spotted grouper [3]. Similar results were found in Atlantic Halibut (*Hippoglossus*) [32] and Atlantic Salmon (*Salmo Salar*) [17], where a low dose of dietary histamine had no significant effect on fish growth, but high levels of histamine (690 and 1742 mg/kg) reduced SGR significantly. Additionally, the growth performance of orange-spotted grouper was not statistically different among the dietary treatments at the initial feeding period (0–28 days), whereas dietary histamine suppressed the growth performance during the whole feeding period (0–56 days) [3]. Thus, the constant growth performance in this study may be attributed to the relative low content of dietary histamine and the relatively short-term feeding trial.

The gastrointestinal tract comprises the important digestive organs of fish and the main sites of digestion and absorption. The activities of digestive and absorptive enzymes reflect the digestive and absorptive capacity of fish [33], which is closely related to the growth and health of fish. Histamine regulates the secretion of gastric acid, and the intake of a certain amount of histamine by animals can promote gastric acid secretion, thereby affecting digestive enzyme activity [34]. Meanwhile, histamine intake can damage the structure and function of the fish intestine, and also inhibit digestive enzyme activities [14]. In this study, high doses of dietary histamine ($\geq$225 mg/kg) decreased the digestive enzyme (pepsin, trypsin, lipase and amylase) activities of the hybrid grouper, which was similar to the results found with Chinese mitten crab [26] and American eel [14]. Thus, dietary histamine may disrupt intestinal structure and function, and thereby depress the digestive enzyme activities of the hybrid grouper.

The normal development of the intestinal tract is associated with the health of fish [35]. The surface area of intestinal absorption is related to the height of mucosal folds, and the muscularis is related to the abilities of intestinal peristalsis [23,36]. In this study, the width of the intestinal folds decreased linearly with the increased dietary histamine content, indicating that dietary histamine impaired the structure of the intestine. It is generally believed that dietary histamine exerts its pathological effects through histamine receptors in the gastric and intestinal mucosa [37], and thereby affects the structure and function of the gastrointestinal tract of the hybrid grouper. Previous studies showed that 10,000 mg/kg of histamine in the diet caused the epithelial exfoliation and the atrophy of lamina propria in the stomach mucosa of rainbow trout [16], and that 103.5 mg/kg of histamine damaged the gastric mucosa of yellow catfish [12]. In this study, SEM of gastric mucosa showed that some gastric mucosal cells of the hybrid grouper were destroyed by the dietary histamine content up to 404 mg/kg. These results indicated that the tolerance to histamine of fish vary with different fish species.

The intestinal barrier prevents the invasion of toxins, antigens and pathogens [38]. An intact intestinal cell structure and intercellular junction structure are associated with intestinal health in fish. The intestinal mucosa allows nutrients to enter the body while blocking pathogens [39]. Serum DAO activity and endotoxin level can, to some extent,

reflect the degree of damage to the intestinal mucosa. Under normal conditions, DAO is mainly distributed inside the cells of the intestinal villi [40], and endotoxin is distributed in the intestinal lumen of the organism [41]. After damage to the intestinal mucosa, DAO and endotoxin enter the blood circulation through the intestinal mucosa, causing an increase in DAO activity [39] and endotoxin level [42]. In this study, serum DAO activity and endotoxin level increased with the increase in the dietary histamine content and damaged the connection structure between intestinal mucosal cells when the dietary histamine level exceeded 404 mg/kg. In addition, tight junction proteins (such as claudins and occludin) are a major part of the mechanical barrier of intestinal mucosa [43], which control the paracellular space between intestinal epithelial cells and prevent the spread of bacteria and antigens. In this study, the relative expressions of claudin 3 and occludin were markedly decreased by dietary histamine up to 404 mg/kg, indicating that a high dose of histamine increased the intestinal permeability and impaired the intercellular junctional structures of intestinal mucosa, leading to the entry of toxic substances into the bloodstream.

The antioxidant capacity of fish is mainly reflected by antioxidant enzymes, which protect the body from damage by removing the excessive accumulation of reactive oxygen species (ROS) [44]. Oxidative stress is a state of imbalance between oxidation and antioxidation that can have harmful effects on cellular organelles [45]. TAC is a comprehensive indicator of the reaction antioxidant capacity [46,47]. MDA is a main product of lipid peroxidation [48] and a sign of mucosal damage by ROS [49]. SOD, CAT, POD, GPx and GR are the main antioxidant enzymes in fish [50–53], which maintain the balance of oxidation and antioxidation [54]. High doses of dietary histamine increased the intestinal MDA level but decreased the intestinal TAC, SOD and CAT activities in American eel [14]. In this study, dietary histamine levels above 662 mg/kg decreased the antioxidant enzymes activities in the intestine of the hybrid grouper, but increased the MDA content. Nrf2-Keap1 is an important pathway that regulates oxidative stress [55,56], and Nrf2 is suppressed through Keap1-controlled ubiquitination-proteasomal degradation [57,58]. In this study, a high histamine level (1245 mg/kg) up-regulated the expression of Keap1 and thereby caused oxidative stress; there was an inability to scavenge oxygen radicals, which, in turn, led to the damage of the intestinal mucosa and intestinal epithelium.

Muscle texture can respond to the softness and elasticity of meat, which is an important indicator of meat consumption [59]; it not only affects the appearance of aquatic products, but also affects the taste [60]. Hardness reflects the internal binding force of meat to maintain its shape; cohesiveness reflects the magnitude of the intercellular binding force; and springiness and resilience reflect the biological resilience of fish [61]. In this study, the hardness, cohesiveness, gumminess and chewiness of the hybrid grouper were markedly increased when the dietary histamine level exceeded 662 mg/kg, indicating that high levels of histamine harden the muscle texture of the dorsal muscle and affect the taste of the hybrid grouper. In addition, the color of the meat is an indication of the quality of meat and an important factor affecting consumption [59,62]. The oxidation of muscle tissue lipids causes the meat to turn brown [63]. In this study, the b* value was markedly increased when the dietary histamine level reached 662 mg/kg. This may be due to the oxidation of the dorsal muscle, caused by a high dose of histamine, leading to the yellowing of the muscle color of the grouper.

In this study, although a high dose of dietary histamine depressed digestive enzyme activity, intestinal morphology and antioxidant capacity, resulting in a negative impact on intestinal health, it had no detrimental effect on the growth performance of the hybrid grouper. Similar situations were also observed in the research on yellow catfish [31], American eel [28] and rainbow trout [13]. The above phenomenon may be related to the short trial time, meaning that the damage to the organs was not yet visible in the organism. Furthermore, dietary 2500 mg/kg of histamine supplementation had no negative effect on the growth of the grouper in 28 days, whereas the SGR was significantly reduced in 56 days [3]. The above phenomenon can also be caused by the low content of histamine in the diet; its toxic effect was not sufficient to affect the growth of the hybrid grouper. Similar

to our hypothesis, stating that dietary histamine levels above 1742 mg significantly reduce the SGR of Atlantic salmon, a dietary low dose of histamine had no significant effect [17]. Additionally, a dietary high dose of histamine (517 mg/kg) supplementation had a negative effect on the immune capacity of American eels [11]. Therefore, a dietary high dose of histamine supplementation may also reduce the immunity of the hybrid grouper, and future related studies are warranted.

5. Conclusions

Under this experimental condition, a dietary histamine content of no more than 1245 mg/kg did not negatively affect the growth performance of the hybrid grouper. However, the dietary histamine content up to 404 mg/kg impaired the structure and function of the gastrointestinal tract, inhibited the intestinal digestive enzyme activities and antioxidant response, and resulted in muscle sclerosis and the yellowing of the hybrid grouper.

Supplementary Materials: The following are available online at https://www.mdpi.com/article/10.3390/antiox12020502/s1, Table S1: Histamine levels in partially commercial feeds.

Author Contributions: Y.Z.: Conceptualization, Formal analysis, Investigation, Writing-original draft. H.Z.: Conceptualization, Methodology, Investigation. Y.L., L.Z., J.F., H.H., W.J.: Methodology, Validation. J.D.: Methodology, Supervision, Writing-review and editing, Project administration, Funding acquisition. B.T.: Methodology, Supervision, Project administration, Funding acquisition. All authors have read and agreed to the published version of the manuscript.

Funding: This research was funded by China Agriculture Research System of MOF and MARA (CARS-47), the National Natural Science Foundation of China (32273152), the Program for Scientific Research Start-up Funds of Guangdong Ocean University (060302022007), the Special Project in Key Fields of Universities in Guangdong Province (2022ZDZX4013), the Zhanjiang Innovation and Entrepreneurship Team Cultivation "Pilot Program" Project (211207157080995).

Institutional Review Board Statement: The hybrid grouper juveniles used in this study were provided by a commercial fish farm (Zhanjiang, China). The procurement of test fish was approved by the Animal Research and Ethics Committee of Guangdong Ocean University (Zhanjiang, China; approval ID: GDOU-IACUC-2021-A2113, approval date: 25 August 2021), and all experimental procedures were carried out in strict accordance with its guidelines.

Informed Consent Statement: Not applicable.

Data Availability Statement: Data are contained within the article and supplementary materials.

Conflicts of Interest: The authors declare that they have no competing interest.

References

1. Oliva-Teles, A.; Enes, P.; Peres, H. Replacing Fishmeal and Fish Oil in Industrial Aquafeeds for Carnivorous Fish. *Feed. Feed. Pract. Aquac.* **2015**, 203–233. [CrossRef]
2. Ye, G.; Dong, X.; Yang, Q.; Chi, S.; Liu, H.; Zhang, H.; Tan, B.; Zhang, S. A formulated diet improved digestive capacity, immune function and intestinal microbiota structure of juvenile hybrid grouper (*Epinephelus fuscoguttatus* ♀× *Epinephelus lanceolatus* ♂) when compared with chilled trash fish. *Aquaculture* **2020**, *523*, 735230. [CrossRef]
3. Liu, Z.; Yang, H.; Hu, L.; Yang, W.; Ai, C.; Sun, Y. Dose-dependent effects of histamine on growth, immunity and intestinal health in juvenile grouper (*Epinephelus coioides*). *Front. Mar. Sci.* **2021**, *8*, 685720. [CrossRef]
4. Jaw, Y.-M.; Chen, Y.-Y.; Lee, Y.-C.; Lee, P.-H.; Jiang, C.-M.; Tsai, Y.-H. Histamine content and isolation of histamine-forming bacteria in fish meal and fish soluble concentrate. *Fish. Sci.* **2011**, *78*, 155–162. [CrossRef]
5. Köse, S.; Quantick, P.; Hall, G. Changes in the levels of histamine during processing and storage of fish meal. *Anim. Feed. Sci. Technol.* **2003**, *107*, 161–172. [CrossRef]
6. Vinci, G.; Antonelli, M. Biogenic amines: Quality index of freshness in red and white meat. *Food Control* **2002**, *13*, 519–524. [CrossRef]
7. Yang, X.; Wang, J.; Fan, P.; Zhao, L.; Cheng, Y.; Wu, X.; Zeng, C. Survival, growth, sexual maturity and tissue histamine accumulation of the mysis, Neomysis awatschensis and N. japonica Nakazawa, fed histamine supplemented diets. *Aquaculture* **2010**, *302*, 256–260. [CrossRef]
8. Li, W.; Liu, B.; Liu, Z.; Yin, Y.; Xu, G.; Han, M.; Xie, L. Effect of dietary histamine on intestinal morphology, inflammatory status, and gut microbiota in yellow catfish (*Pelteobagrus fulvidraco*). *Fish Shellfish. Immunol.* **2021**, *117*, 95–103. [CrossRef]

9. Shifrine, M.; Adler, H.E.; Ousterhout, L.E. The pathology of chicks fed histamine. *Avian Dis.* **1960**, *4*, 12–21. [CrossRef]
10. Barnes, D.M.; Kirby, Y.K.; Oliver, K.G. Effects of Biogenic Amines on Growth and The Incidence of Proventricular Lesions in Broiler Chickens. *Poult. Sci.* **2001**, *80*, 906–911. [CrossRef]
11. Zhai, S.; Wang, Y.; He, Y.; Chen, X. Oligomeric proanthocyanidins counteracts the negative effects of high level of dietary histamine on american eel (*Anguilla rostrata*). *Front. Mar. Sci.* **2020**, *7*, 549145. [CrossRef]
12. He, J.; Wu, D.; Ye, Y.; Cai, C.; Wu, P.; Luo, Q.; Pu, Q. Effects of dietary histamine level on growth performance, serum biochemical indexes and gastrointestinal mucosa Structure of yellow catfish (*Pelteobagrus fulvidraco*). *Chin. J. Anim. Nutr.* **2018**, *30*, 2581–2593. [CrossRef]
13. Watanabe, T.; Takeuchi, T.; Satoh, S.; Toyama, K.; Okuzumi, M. Effect of dietary histidine or histamine on growth and development of stomach erosion in rainbow trout. *Nippon. Suisan Gakkaishi* **1987**, *53*, 1207–1214. [CrossRef]
14. Ma, D.; Cai, P.; Zhai, S.; Chen, X. Effect of dietary histamine on growth performance, digestive enzyme activities and antioxidant indices in intestine of juvenile American eels (*Anguilla rostrata*). *Feed Res.* **2020**, *2*, 42–45. [CrossRef]
15. Cheng, Y.; Li, W.; Han, M.; Xu, G.; Xie, L.; Yin, Y.; Liang, J. The enterohepatic protection of *pelteobagrus fulvidraco* adding lactobacillus reuteri induced by histamine. *Acta. Hydrobiol. Sin.* **2019**, *43*, 94–101. [CrossRef]
16. Shiozaki, K.; Nakano, T.; Yamaguchi, T.; Sato, M.; Sato, N. The protective effect of stevia extract on the gastric mucosa of rainbow trout *Oncorhynchus mykiss* (Walbaum) fed dietary histamine. *Aquac. Res.* **2004**, *35*, 1421–1428. [CrossRef]
17. Opstvedt, J.; Mundheim, H.; Nygård, E.; Aase, H.; Pike, I.H. Reduced growth and feed consumption of Atlantic salmon (Salmo salar L.) fed fish meal made from stale fish is not due to increased content of biogenic amines. *Aquaculture* **2000**, *188*, 323–337. [CrossRef]
18. Fan, X.; Qin, X.; Zhang, C.; Chen, J.; Zhu, Q. Nutritional and volatile flavor components of dorsal and ventral muscle from hybrid grouper (*Epinephelus fuscoguttatus* ♀ × *E. lanceolatus* ♂). *J. GDOU* **2018**, *38*, 39–46.
19. Lu, Z.; Huang, H.; Huang, X.; Huang, W. Effects of hypoxic stress on antioxidant and energy metabolism of hybrid grouper (*Epinephelus fuscoguttatus*♀ × *Epinephelus lanceolatus* ♂). *J. GDOU* **2022**, *42*, 13–19. [CrossRef]
20. Boonyaratpalin, M. Nutrient requirements of marine food fish cultured in Southeast Asia. *Aquaculture* **1997**, *151*, 283–313. [CrossRef]
21. Zheng, C.; Cao, J.; Dong, X.; Chi, S.; Zhang, S.; Yang, Q.; Liu, H.; Deng, J.; Zhang, W.; Tan, B.; et al. Apparent digestibility coefficients of seven protein sources for juvenile hybrid grouper (*Epinephelus fuscoguttatus* ♀ × *Epinephelus lanceolatus* ♂). *Acta Hydrobiol. Sin.* **2022**, *47*, 1–12. [CrossRef]
22. AOAC. *Official Methods of Analysis of AOAC International*, 16th ed.; Association of Official Analytical Chemists: Arlington, TX, USA, 1995.
23. Huang, B.; Zhang, S.; Dong, X.; Chi, S.; Yang, Q.; Liu, H.; Tan, B.; Xie, S. Effects of fishmeal replacement by black soldier fly on growth performance, digestive enzyme activity, intestine morphology, intestinal flora and immune response of pearl gentian grouper (*Epinephelus fuscoguttatus* ♀ × *Epinephelus lanceolatus* ♂). *Fish Shellfish. Immunol.* **2021**, *120*, 497–506. [CrossRef]
24. Chen, K.; Ye, Y.; Cai, C.; Wu, P.; Huang, Y.; Wu, T.; Lin, X.; Luo, Q.; Zhang, B.; Xiao, P.; et al. Effects of MDA on the growth performance, structure and function of hepatopancreas and intestine of grass carp (*Ctenopharyngodon Idellus*). *Acta Hydrobiol. Sin.* **2016**, *40*, 779–792. [CrossRef]
25. Livak, K.J.; Schmittgen, T.D. Analysis of relative gene expression data using real-time quantitative PCR and the $2^{-\Delta\Delta CT}$ Method. *Methods* **2001**, *25*, 402–408. [CrossRef]
26. Zhao, L.; Yang, X.; Cheng, Y.; Yang, S. Effect of dietary histamine supplementation on growth, digestive enzyme activities and morphology of intestine and hepatopancreas in the Chinese mitten crab *Eriocheir sinensis*. *SpringerPlus* **2016**, *5*, 552. [CrossRef] [PubMed]
27. Lumsden, J.S.; Clark, P.; Hawthorn, S.; Minamikawa, M.; Fenwick, S.G.; Haycock, M.; Wybourne, B. Gastric dilation and air sacculitis in farmed chinook salmon, Oncorhynchus tshawytscha (Walbaum). *J. Fish Dis.* **2002**, *25*, 155–163. [CrossRef]
28. Hu, J.; Ma, D.; Chen, X.; Zhai, S. Effect of dietary histamine on growth performance and muscle quality of American eel (*Anguilla rostrata*). *Feed Res.* **2019**, *6*, 34–37. [CrossRef]
29. Reyes-Sosa, C.F.; Castellanos-Molina, R. Nutritional evaluation of gizzard erosion positive brown fish meal in starter diets for Nile tilapia, *Oreochromis niloticus*. *Aquaculture* **1995**, *138*, 323–329. [CrossRef]
30. Hu, L.; Yun, B.; Xue, M.; Wang, J.; Wu, X.; Zheng, Y.; Han, F. Effects of fish meal quality and fish meal substitution by animal protein blend on growth performance, flesh quality and liver histology of Japanese seabass (*Lateolabrax japonicus*). *Aquaculture* **2013**, *372*, 52–61. [CrossRef]
31. Zhang, L.; Xu, Y.; Cheng, W.; Li, W.; Chen, J.; Xie, L.; Xu, G. Effect of dietary histamine levels on growth performance and body pigmentation of *Pelteobagrus Fulvidraco*. *FW Fish.* **2017**, *47*, 79–84. [CrossRef]
32. Aksnes, A.; Mundheim, H. The impact of raw material freshness and processing temperature for fish meal on growth, feed efficiency and chemical composition of Atlantic halibut (*Hippoglossus*). *Aquaculture* **1997**, *149*, 87–106. [CrossRef]
33. Yang, E.; Zhang, J.; Yang, L.; Amenyogbe, E.; Wang, W.; Huang, J.; Chen, G. Effects of hypoxia stress on digestive enzyme activities, intestinal structure and the expression of tight junction proteins coding genes in juvenile cobia (*Rachycentron canadum*). *Aquac. Res.* **2021**, *52*, 5630–5641. [CrossRef]
34. Leng, X.; Wang, K.; Yang, F.; Duanmu, D.; Zhou, A. Effects of supplemental histamine on gastric acid secretion, digestive enzyme activities and intestinal microfloral of early weaned piglets. *SAS* **2003**, *36*, 324–328. [CrossRef]

35. Kamiya, S.; Nagino, M.; Kanazawa, H.; Komatsu, S.; Mayumi, T.; Takagi, K.; Asahara, T.; Nomoto, K.; Tanaka, R.; Nimura, Y. The value of bile replacement during external biliary drainage: An analysis of intestinal permeability, integrity, and microflora. *Ann. Surg.* **2004**, *239*, 510–517. [CrossRef]
36. Geda, F.; Rekecki, A.; Decostere, A.; Bossier, P.; Wuyts, B.; Kalmar, I.; Janssens, G. Changes in intestinal morphology and amino acid catabolism in common carp at mildly elevated temperature as affected by dietary mannanoligosaccharides. *Anim. Feed. Sci. Technol.* **2012**, *178*, 95–102. [CrossRef]
37. Simons, F.E.R.; Simons, K.J. Histamine and H1-antihistamines: Celebrating a century of progress. *J. Allergy Clin. Immunol.* **2011**, *128*, 1139–1150.e4. [CrossRef]
38. Zhang, H.; Zheng, Y.; Zha, X.; Ma, Y.; Liu, X.; Elsabagh, M.; Wang, H.; Wang, M. Dietary L-Arginine or N-Carbamylglutamate Alleviates Colonic Barrier Injury, Oxidative Stress, and Inflammation by Modulation of Intestinal Microbiota in Intrauterine Growth-Retarded Suckling Lambs. *Antioxidants* **2022**, *11*, 2251. [CrossRef]
39. Gu, M.; Jia, Q.; Zhang, Z.; Bai, N.; Xu, X.; Xu, B. Soya-saponins induce intestinal inflammation and barrier dysfunction in juvenile turbot (*Scophthalmus maximus*). *Fish Shellfish. Immunol.* **2018**, *77*, 264–272. [CrossRef]
40. Fukudome, I.; Kobayashi, M.; Dabanaka, K.; Maeda, H.; Okamoto, K.; Okabayashi, T.; Baba, R.; Kumagai, N.; Oba, K.; Fujita, M.; et al. Diamine oxidase as a marker of intestinal mucosal injury and the effect of soluble dietary fiber on gastrointestinal tract toxicity after intravenous 5-fluorouracil treatment in rats. *Med. Mol. Morphol.* **2013**, *47*, 100–107. [CrossRef]
41. Qiao, X.; Wu, H. Detection of D-lactic acid and endotoxin and effect of dietary fiber complex on intestinal mucosal barrier in rats with portal hypertension. *CHN Med. Herald* **2014**, *11*, 26–32.
42. Ding, L.-A.; Li, J.-S.; Li, Y.-S.; Zhu, N.-T.; Liu, F.-N.; Tan, L. Intestinal barrier damage caused by trauma and lipopolysaccharide. *World J. Gastroenterol.* **2004**, *10*, 2373–2378. [CrossRef] [PubMed]
43. Runkle, E.A.; Mu, D. Tight junction proteins: From barrier to tumorigenesis. *Cancer Lett.* **2013**, *337*, 41–48. [CrossRef] [PubMed]
44. Liang, X.-P.; Li, Y.; Hou, Y.-M.; Qiu, H.; Zhou, Q.-C. Effect of dietary vitamin C on the growth performance, antioxidant ability and innate immunity of juvenile yellow catfish (*Pelteobagrus fulvidraco* Richardson). *Aquac. Res.* **2015**, *48*, 149–160. [CrossRef]
45. Denning, T.L.; Takaishi, H.; Crowe, S.E.; Boldogh, I.; Jevnikar, A.; Ernst, P.B. Oxidative stress induces the expression of Fas and Fas ligand and apoptosis in murine intestinal epithelial cells. *Free. Radic. Biol. Med.* **2002**, *33*, 1641–1650. [CrossRef] [PubMed]
46. Mohammadi, G.; Rashidian, G.; Hoseinifar, S.H.; Naserabad, S.S.; Van Doan, H. Ginger (*Zingiber officinale*) extract affects growth performance, body composition, haematology, serum and mucosal immune parameters in common carp (*Cyprinus carpio*). *Fish Shellfish. Immunol.* **2020**, *99*, 267–273. [CrossRef]
47. Hu, B.; Song, L.; Mao, S.; Xu, P. Effects of four chinese herbal preparations on growth performance and antioxidant activity in juvenile *Micropterus salmoides*. *J. GDOU* **2019**, *39*, 101–107. [CrossRef]
48. An, W.; He, H.; Dong, X.; Tan, B.; Yang, Q.; Chi, S.; Zhang, S.; Liu, H.; Yang, Y. Regulation of growth, fatty acid profiles, hematological characteristics and hepatopancreatic histology by different dietary n-3 highly unsaturated fatty acids levels in the first stages of juvenile Pacific white shrimp (Litopenaeus vannamei). *Aquac. Rep.* **2020**, *17*, 100321. [CrossRef]
49. Kwiecień, S.; Brzozowski, T.; Konturek, S.J. Effects of reactive oxygen species action on gastric mucosa in various models of mucosal injury. *J. Physiol. Pharmacol.* **2002**, *53*, 39–50. [CrossRef]
50. Zhu, X.; Hao, R.; Zhang, J.; Tian, C.; Hong, Y.; Zhu, C.; Li, G. Dietary astaxanthin improves the antioxidant capacity, immunity and disease resistance of coral trout (*Plectropomus leopardus*). *Fish Shellfish. Immunol.* **2022**, *122*, 38–47. [CrossRef]
51. Wang, Y.; Li, Z.; Li, J.; Duan, Y.-F.; Niu, J.; Wang, J.; Huang, Z.; Lin, H.-Z. Effects of dietary chlorogenic acid on growth performance, antioxidant capacity of white shrimp Litopenaeus vannamei under normal condition and combined stress of low-salinity and nitrite. *Fish Shellfish. Immunol.* **2015**, *43*, 337–345. [CrossRef]
52. Tan, X.; Sun, Z.; Zhou, C.; Huang, Z.; Tan, L.; Xun, P.; Huang, Q.; Lin, H.; Ye, C.; Wang, A. Effects of dietary dandelion extract on intestinal morphology, antioxidant status, immune function and physical barrier function of juvenile golden pompano Trachinotus ovatus. *Fish Shellfish. Immunol.* **2017**, *73*, 197–206. [CrossRef] [PubMed]
53. Tang, X.; Xiong, K. Intrauterine growth retardation affects intestinal health of suckling piglets via altering intestinal antioxidant capacity, glucose uptake, tight junction, and immune responses. *Oxidative Med. Cell* **2022**, *2022*, 2644205. [CrossRef] [PubMed]
54. Xie, R.-T.; Amenyogbe, E.; Chen, G.; Huang, J.-S. Effects of feed fat level on growth performance, body composition and serum biochemical indices of hybrid grouper (*Epinephelus fuscoguttatus* × *Epinephelus polyphekadion*). *Aquaculture* **2020**, *530*, 735813. [CrossRef]
55. Zhou, Z.; Wu, X.; Li, X.; Dong, Y.; Wang, X.; Mu, W.; Gatlin, D.M.; Zhang, Y. The optimum dietary isoleucine requirement of juvenile hybrid grouper (*Epinephelus fuscoguttatus* ♀ × *Epinephelus lanceolatus* ♂). *Aquac. Nutr.* **2020**, *26*, 1295–1310. [CrossRef]
56. Zou, C.; Xu, M.; Chen, L.; Liu, Q.; Zhou, Y.; Sun, Z.; Ye, H.; Su, N.; Ye, C.; Wang, A. Xiaochaihu Decoction reduces hepatic steatosis and improves D-GalN/LPS-induced liver injury in hybrid grouper (Epinephelus lanceolatus ♂ × Epinephelus fuscoguttatus ♀). *Fish Shellfish. Immunol.* **2019**, *91*, 293–305. [CrossRef] [PubMed]
57. Ma, Q. Role of nrf2 in oxidative stress and toxicity. *Annu. Rev. Pharmacol.* **2013**, *53*, 401–426. [CrossRef]
58. Pyun, B.-J.; Jo, K.; Lee, J.Y.; Lee, A.; Jung, M.-A.; Hwang, Y.-H.; Jung, D.H.; Ji, K.-Y.; Choi, S.; Kim, Y.H.; et al. *Caesalpinia sappan* Linn. Ameliorates Allergic Nasal Inflammation by Upregulating the Keap1/Nrf2/HO-1 Pathway in an Allergic Rhinitis Mouse Model and Nasal Epithelial Cells. *Antioxidants* **2022**, *11*, 2256. [CrossRef]
59. Zhong, X.; Li, X.; Cai, W.; Xu, C.; Li, Q.; Huang, J.; Liu, W. Effects of fermented feed on growth performance, digestive enzyme activity, fillet quality and immunity of juvenile carp (*Cyprinus carpio*). *J. NJAU* **2018**, *41*, 154–162. [CrossRef]

60. Yang, X.; Song, Z.; Zhi, X.; Zhao, X.; Wang, G.; Chi, S.; Tan, B. Effects of replacing fish meal with enzyme-digested poultry by-product meal on muscle quality and expression of muscle growth-related factors of hybrid grouper (*Epinephelus fuscoguttatus* ♀ × *E.lanceolatus* ♂). *Chin. J. Anim. Nutr.* **2021**, *33*, 6999–7011. [CrossRef]
61. Wu, F.; Wen, H.; Jiang, M.; Liu, W.; Tian, J.; Yang, C.; Huang, F. Effect of dietary vitamin C on growth performance, flesh quality and antioxidant function in genetically improved farmed tilapia. *J. Fish Sci. CHN* **2015**, *22*, 79–87. [CrossRef]
62. Jiang, J.; Hu, Y.; Zhou, X.; Yin, L.; Feng, L.; Jiang, W.; Liu, Y.; Zhao, Y. Effects of replacement ratio of fish meal by soybean meal in extruded diets on muscle quality of jian carp (*Cyprinus carpio var. Jian*). *Chin. J. Anim. Nutr.* **2015**, *27*, 623–630. [CrossRef]
63. Greene, B.E.; Price, L.G. Oxidation-induced color and flavor changes in meat. *J. Agric. Food Chem.* **1975**, *23*, 164–167. [CrossRef]

MDPI
St. Alban-Anlage 66
4052 Basel
Switzerland
Tel. +41 61 683 77 34
Fax +41 61 302 89 18
www.mdpi.com

Antioxidants Editorial Office
E-mail: antioxidants@mdpi.com
www.mdpi.com/journal/antioxidants

Academic Open
Access Publishing

www.mdpi.com

ISBN 978-3-0365-8187-3